

THE JOURNAL OF
PHYSICAL
CHEMISTRY

Volume 72

MAY—AUGUST 1968

PAGES 1405—3072

FREDERICK T. WALL, *Editor*

MARILYN H. PERRIN AND ROBERT G. LINCK, *Assistant Editors*

EDITORIAL BOARD

R. BERSOHN
S. BRUNAUER
L. F. DAHL
J. R. FRESCO
G. J. HILLS
M. KASHA
C. KEMBALL

W. KLEMPERER
A. KUPPERMANN
F. A. LONG
R. A. MARCUS
W. J. MOORE
W. A. NOYES, JR.
B. S. RABINOVITCH

R. E. RICHARDS
F. S. ROWLAND
W. G. SCHNEIDER
R. L. SCOTT
R. SEIFERT
S. I. WEISSMAN
B. H. ZIMM

CHARLES R. BERTSCH, *Senior Production Editor*

JOSEPH H. KUNY
Director of Business Operations
Director of Publications Research

RICHARD L. KENYON
Director of Publications

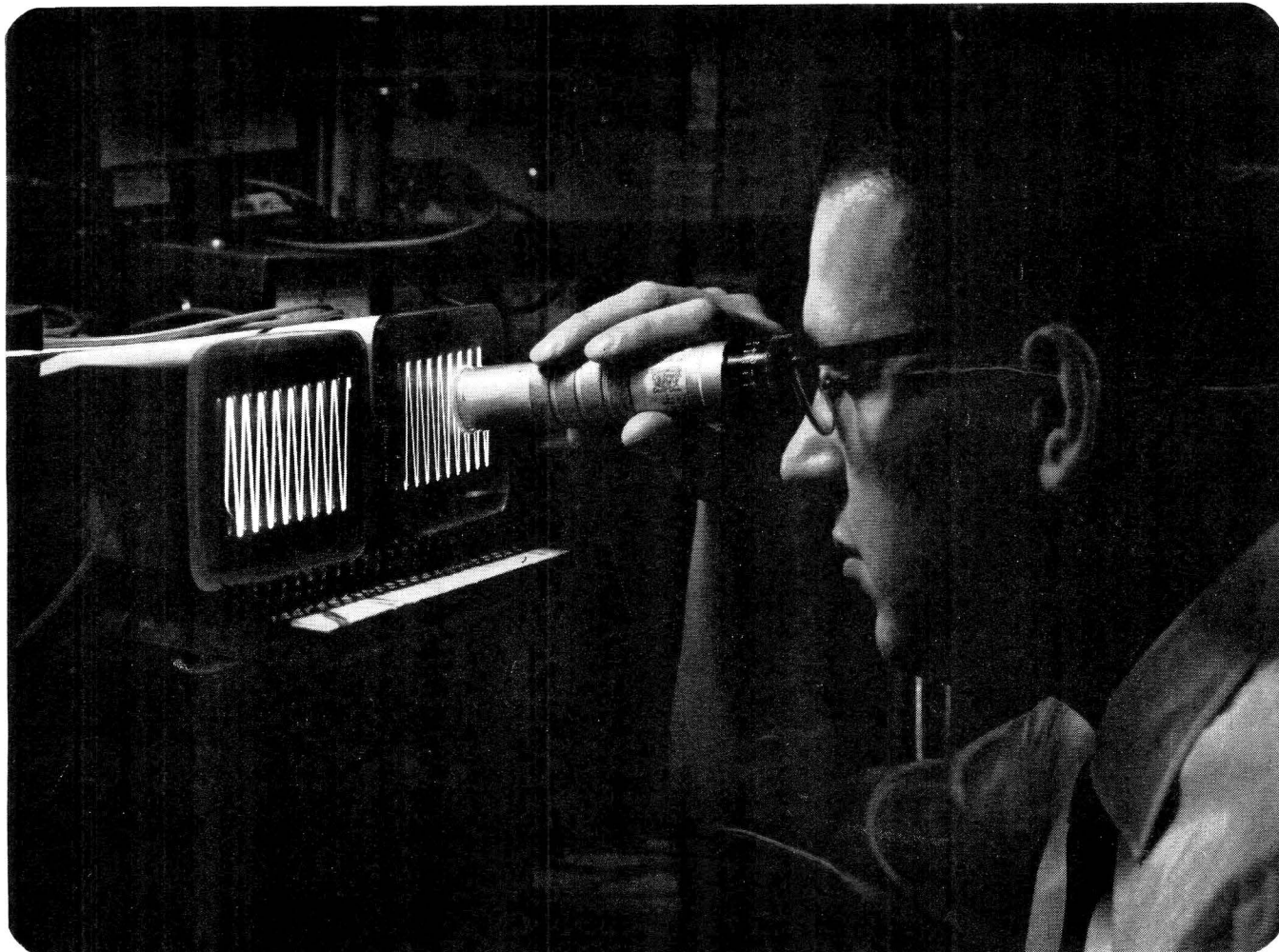
DAVID E. GUSHEE
Publication Manager, Journals

EASTON, PA.
MACK PRINTING COMPANY
1968

THE JOURNAL OF PHYSICAL CHEMISTRY

Volume 72, Number 5 May 1968

The Temperature Variation of the Dipole Moment of <i>o</i> -Dimethoxybenzene Louis M. DiBello, Helen M. McDevitt, and Dominic M. Roberti	1405
The Calculation of Cohesive and Adhesive Energies from Intermolecular Forces at a Surface J. F. Paddy and N. D. Uffindell	1407
The Semiempirical Method for the Calculation of Some Parameters for High-Resolution Nuclear Magnetic Resonance Spectra P. G. Maslov	1414
Sorption and Magnetic Susceptibility Studies on Metal-Free-Radical Systems: Nitric Oxide on Palladium Richard W. Zuehlke, Maurice Skibba, and Carl Gottlieb	1425
The Hg(¹ P ₁)-Photosensitized Decomposition of Cyclobutane E. G. Spittler and G. W. Klein	1432
A Study of the Solubility of Metals in Liquid Sodium. II. The System Sodium-Lead G. J. Lamprecht, L. Dicks, and P. Crowther	1439
Kinetics of Electrode Processes in Molten Salts. II. The Influence of Solvent Anions and Cations on the Molybdenum-Molybdenum(III) Electrode Sidney M. Selis	1442
Mean Amplitudes of Vibration of Comparatively Large Molecules. I. Isotopic Naphthalenes G. Hagen and S. J. Cyvin	1446
Tentatively Standardized Symmetry Coordinates for Vibrations of Polyatomic Molecules. VI. Naphthalene and Biphenyl Models G. Hagen and S. J. Cyvin	1451
γ -Radiation-Induced <i>cis-trans</i> Isomerization of Stilbenes in Liquid Naphthalene O. G. Malan, H. Güsten, and D. Schulte-Frohlinde	1457
Relationships between the Two Types of Frequency-Temperature Representation of Dielectric Relaxation Data M. E. Baird	1462
Pulse Radiolysis of Solutions of Amines of Low Ionization Potential T. J. Kemp, J. P. Roberts, G. A. Salmon, and G. F. Thompson	1464
Infrared Study of Benzene Adsorption on Aerosil Adriano Zecchina, Carlo Versino, Anna Appiano, and Giancarlo Occhiena	1471
Low-Conversion Radiolysis of Methane Containing Traces of Oxygen and Olefins D. C. Myers and F. Schmidt-Bleek	1475
Vicinal Effects on the Optical Activity of Some Adenine Nucleosides Daniel W. Miles, S. J. Hahn, Roland K. Robins, Morris J. Robins, and Henry Eyring	1483
Kinetics and Mechanism of the Reaction between Bromine Trifluoride Vapor and Uranium Tetrafluoride Tsutomu Sakurai and Matae Iwasaki	1491
Oxidation of Thiourea and Thioacetamide by Alkaline Hexacyanoferrate(III) M. C. Agrawal and S. P. Mushran	1497
Binding of Divalent Metal Ions by Cross-Linked Polyacrylic Acid Richard L. Gustafson and Joseph A. Lirio	1502
The Radiolysis of Aqueous Solutions of Cobalt Complexes Nicholas Zevos	1506
A Semiempirical Model for Simple Liquids F. Ciani, G. Cicogna, and M. Maestro	1510
Thermal Decomposition of Some Polynitroalkanes H. P. Marshall, F. G. Borgardt, and P. Noble, Jr.	1513
An Investigation of the Electrical Polarizations of Several Molecules Which Have Been Assigned Anomalous Dipole Moments Ernest N. Di Carlo, Thomas P. Logan, and Robert E. Stronski	1517
Complex Refractive Index of Colloidal Silver Bromide in the Near-Ultraviolet E. J. Meehan and Jerry K. Miller	1523



display devices for tomorrow ...

opportunities for Physical Scientists at Tektronix® today

If you have practical experience in Materials and Processes Development, Manufacturing Engineering, Cathode-Ray Tube Design; or if your education is in the disciplines of Physical Chemistry, Chemical Engineering, Physics or Metallurgy, Tektronix is interested in talking with you. Our commitment to progress in waveform measurement has produced significant contributions toward advancing the state-of-the-art in high-performance, storage and special-purpose oscilloscopes.

Tektronix provides an informal atmosphere, encouraging a free exchange of ideas between engineers and scientists of the many disciplines required for electronic instrument development.

While helping advance the state-of-the-measurement art, Tektronix engineers and scientists share in the financial success of the company through a merit-oriented salary plan and a substantial profit-sharing program. For the family, the Portland area offers excellent educational, cultural and recreational facilities. Abundant fishing, hunting and skiing are available nearby, with either the Cascade Mountains or the rugged Oregon beaches only 90 minutes away.

Please send the coupon or your resume to Professional Placement Manager, Tektronix, Inc., P. O. Box 500C, Beaverton, Oregon 97005. If you prefer, please call us at (503) 644-0161, Ext. 7346.

Tektronix, Inc.



Professional Placement Mgr., Tektronix, Inc.

P. O. Box 500C, Beaverton, Oregon 97005

My resume is enclosed. Please send an application.

Please send your booklet, "Tektronix."

NAME: _____

ADDRESS: _____

CITY: _____ STATE: _____ ZIP: _____

An equal opportunity employer

Thermodynamics of Binary Liquid Mixtures by Rayleigh Light Scattering Raymond L. Schmidt and H. Lawrence Clever	1529
The Independence of Isothermal Equilibria in Electrolyte Solutions on Changes in Dielectric Constant Arvin S. Quist and William L. Marshall	1536
Electrical Conductances of Aqueous Hydrogen Bromide Solutions from 0 to 800° and at Pressures to 4000 Bars Arvin S. Quist and William L. Marshall	1545
Free Radicals by Mass Spectrometry. XXXVII. The Ionization Potential and Heat of Formation of Dichlorocarbene J. S. Shapiro and F. P. Lossing	1552
Adsorption from Solution on a Free Liquid Surface and on an Inert Solid S. K. Suri and V. Ramakrishna	1555
The Crystal Structure of the Triphenylphosphine Sulfide-Iodine Addition Complex W. W. Schweikert and Edward A. Meyers	1561
Phenomenological Coefficients for Volume Flow across an Ion-Exchange Membrane A. S. Tombalakian	1566
Composition of Electrosorbed Methanol T. Biegler	1571
Radiation-Induced Solid-State Polymerization of Derivatives of Methacrylic Acid. IV. Electron Spin Resonance Spectra of Barium Methacrylate Dihydrate M. J. Bowden and J. H. O'Donnell	1577
Flash Photolysis and Time-Resolved Mass Spectrometry. II. Decomposition of Methyl Iodide and Reactivity of I(² P _{1/2}) Atoms Richard T. Meyer	1583
Pulse Radiolysis of Ammonia Gas—Rate of Disappearance of the NH ³ Σ Radical G. M. Meaburn and Sheffield Gordon	1592
Pulse Radiolytic Studies of the Competition H + H and H + Ferricyanide. The Absolute Rate Constants J. Rabani and D. Meyerstein	1599
The Photolysis of 1,3-Difluoro- and 1,1,3,3-Tetrafluoroacetone at Low Pressure G. O. Pritchard and J. T. Bryant	1603
Dissociation Energy of PN and Other Thermodynamic Properties for the Vaporization of P ₃ N ₅ O. Manuel Uy, Fred J. Kohl, and K. Douglas Carlson	1611
Solvation of Extracted Complex Metal Acids. IV. The HAuCl ₄ -Nitrobenzene System Stephen L. Law and R. L. McDonald	1617
The Photolysis of Cyclobutanone T. Howard McGee	1621
Dimerization of Nitrogen Dioxide in Solution: a Comparison of Solution Thermodynamics with the Gas Phase Thomas F. Redmond and Bradford B. Wayland	1626
Base Strengths of Amine-Amine Hydrochloride Systems in Toluene Robert R. Grinstead and James C. Davis	1630
The Reaction of Hydrogen Atoms with Hydrogen Iodide. Ralf D. Penzhorn and B. deB. Darwent	1639
Proton Nuclear Magnetic Resonance Spectra of Di- and Trisubstituted Pyrazines and Their Cations R. H. Cox and A. A. Bothner-By	1642
Proton Nuclear Magnetic Resonance Spectra of Monosubstituted Pyrazines. . . R. H. Cox and A. A. Bothner-By	1646
Influence of Double-Layer Charging in Chronopotentiometry Michael L. Olmstead and Richard S. Nicholson	1650
On the Analysis of Dielectric Dispersion Data into Two Relaxation Regions E. A. S. Cavell and P. C. Knight	1656
Mass Spectrometric Studies at High Temperatures. XXVII. The Reactions of Aluminum Vapor with S ₂ (g), Se ₂ (g), and Te ₂ (g) P. J. Ficalora, J. W. Hastie, and J. L. Margrave	1660
The Critical Temperature and Coexistence Curve for Aluminum Bromide J. W. Johnson, W. J. Silva, and Daniel Cubicciotti	1664
The Vapor Pressure and Enthalpy of Vaporization of Molten Aluminum Bromide to the Critical Point J. W. Johnson, W. J. Silva, and Daniel Cubicciotti	1669
The Kinetics of Hydrogen Isotope Exchange in Benzene Using a Homogeneous Platinum Catalyst R. J. Hodges and J. L. Garnett	1673
The Electronic Properties of Aluminum Oxide and the Chemisprion of Water, Hydrogen, and Oxygen S. Khoobiar, J. L. Carter, and P. J. Lucchesi	1682
Tracer Studies of the Isomerization of Cyclopropane over a Deuterated Zeolite Catalyst B. H. Bartley, H. W. Habgood, and Z. M. George	1689
The Vaporization of Ytterbium Dicarbide John M. Haschke and Harry A. Eick	1697
Radical Production by γ Irradiation of 3-Methylpentane, Methyltetrahydrofuran, and Methylcyclohexane Glasses at 77°K with and without Alkyl Halide Solutes Miriam Shirom and John E. Willard	1702

how do you get
the world's
most complete
thermal analysis
system?

begin
with the Mettler
starter set.

The Mettler Thermoanalyzer is a completely modular system that fits together into five running feet of laboratory floor space. It arrives on your doorstep accompanied by a Mettler thermo-engineer who will put it together and show you how to use it.

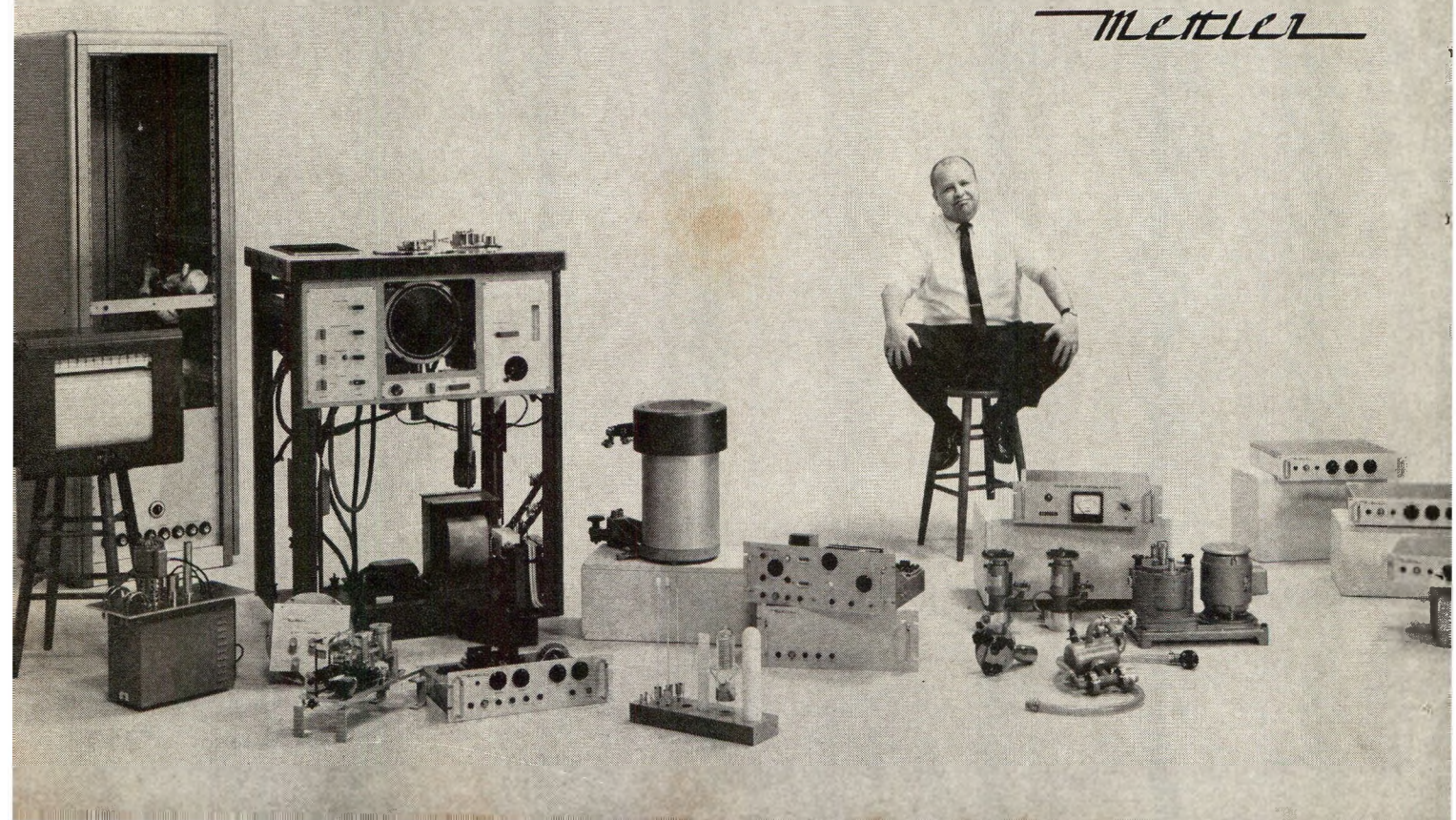
It is the only system that permits you to perform thermogravimetric analysis, derivative thermogravimetry, and differential thermal analysis...all simultaneously in controlled gas atmospheres and pressures. You can start with the basic Mettler TGA system, add modules and new capabilities at any time you like, and get the world's most versatile system for thermal analysis.

You can, for example, measure weight change, rate of weight change, and enthalpic change as a function of time or temperature up to 1600° C. The sample can be maintained in a dynamic atmosphere of almost any composition including wet and corrosive gases. Gas pressure can be controlled from atmospheric to a vacuum of 10⁻⁶ torr. You also can connect the system to other equipment and use it, for instance, for effluent gas analysis.

It is equally valuable for rapid survey work and for exacting quantitative studies. It offers far greater flexibility, reliability and working convenience than any other system for investigation of thermal phenomena.

For complete technical information, write Mettler Instrument Corporation, 20 Nassau Street, Princeton, New Jersey 08540.

METTLER



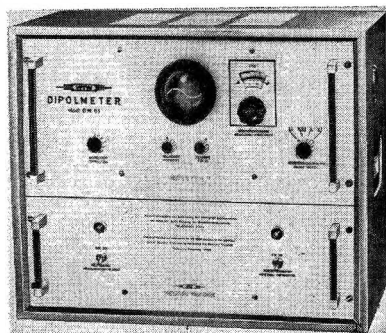
Intrinsic Mobilities and Independent Fluxes in Multicomponent Isothermal Diffusion. I. Simple Darken Systems	P. C. Carman	1707
Intrinsic Mobilities and Independent Fluxes in Multicomponent Isothermal Diffusion. II. Complex Darken Systems	P. C. Carman	1713
Electron Spin Resonance of Nitrogen Dioxide in Frozen Solutions	B. H. J. Bielski, J. J. Freeman, and J. M. Gebicki	1721
Energy Transfer in Thermal Methyl Isocyanide Isomerization. Dilution Effects at Low Pressure	Y. N. Lin and B. S. Rabinovitch	1726
Photodecomposition of Solid Metal Azides	V. R. Pai Verneker	1733
The Viscosity of Molten Bismuth-Bismuth Halide Solutions	Jordan D. Kellner	1737
Infrared Spectral Evidence for Trihalomethyl lithium and -sodium Compounds in Solid Argon	Lester Andrews and T. Granville Carver	1743
Dielectric Study of the Hydration of Cyclohexylamine in Benzene	M. Duane Gregory, Harold E. Afsprung, and Sherril D. Christian	1748
Studies of Membrane Phenomena. VI. Further Study of Volume Flow	Y. Kobatake, M. Yuasa, and H. Fujita	1752
Apparent Molal Volumes of Ammonium Chloride and Some Symmetrical Tetraalkylammonium Chlorides at Various Temperatures	Frank J. Millero and W. Drost-Hansen	1758
The Electrical Conductivity of Aqueous Tetraalkylammonium Halide Solutions under Hydrostatic Pressure	R. A. Horne and R. P. Young	1763
The Thermal Stability of Hydroxyl Groups in Decationated Zeolites X and Y	Jan B. Uytterhoeven, P. Jacobs, K. Makay, and R. Schoonheydt	1768
Spectrophotometric Identification of γ -Radiolytic Intermediates in a New Halogenic Glassy Matrix	A. Grimison and G. A. Simpson	1776
The Radiolysis of Cyclohexane in the Presence of Deuterated Olefins. The Involvement of the Olefins in Hydrogen Formation	M. G. Robinson and G. R. Freeman	1780
The Mechanism of Radiation-Induced Luminescence from Scintillators in Cyclohexane	Robert R. Hentz and Ronald J. Knight	1783
Recoil-Tritium Reactions in the Solid Phase: Absolute Yields and Phase Effects	Michael Menzinger and Richard Wolfgang	1789
Extension of the "Band Model" to the Inner-Sphere Mechanism of Electron-Transfer Reactions	I. Ruff	1792
Light-Induced Proton Ejection and Electron Transfer in the Zinc Tetraphenylporphyrin-Benzoquinone System	Kenneth P. Quinlan	1797
Flash Photolysis Study of Sulfite, Thiocyanate, and Thiosulfate Ions in Solution	L. Dogliotti and E. Hayon	1800

NOTES

Structural Features of Some Water <i>n</i> -Alkylamine Complexes	J. J. Fripiat, A. Léonard, and E. Mendelovici	1808
Isotopic Oxygen Exchange and Hydrolysis in Dialkylphosphonates	David Samuel and Brian L. Silver	1809
The Exchange Reaction of Pentafluoroethyl Iodide with Iodine	C. Grygorcewicz and G. S. Laurence	1811
The Rate of Reaction of Active Nitrogen with Perfluorobutene-2	N. Madhavan and W. E. Jones	1812
The Variation of Partial Molar Volume of Some Tetraalkylammonium Iodides with Temperature in Aqueous Solutions	Ram Gopal and Mohd. Aslam Siddiqi	1814
Temperature Coefficients of Protein Partial Volumes	Henry B. Bull and Keith Breese	1817
Studies of the Solvent Effects on the Chemical Shifts in Nuclear Magnetic Resonance Spectroscopy. V. A Model for the Benzene Solutions of Polar Molecules	Taku Matsuo	1819
On the Kihara Core Model for Polar Molecules	T. S. Storvick and T. H. Spurling	1821
Crystal Field Energy Levels for Various Symmetries	Steven T. Spees, Jr., Jayarama R. Perumareddi, and Arthur W. Adamson	1822
Estimation of the High-Temperature Entropy of Solids by the Entropy Correspondence Principle	J. G. Eberhart and E. N. Gruetter	1825
On the Reaction Complex of the $C_3H_6^+-C_3H_6$ Ion-Molecule Reaction	Fred P. Abramson and Jean H. Futrell	1826
Electron Paramagnetic Resonance Spectra of the Naphthacene Trianion and the 5,12-Naphthacenequinone Anion Radicals	Eddie T. Seo, John M. Fritsch, and Robert F. Nelson	1829

MORE AND MORE PEOPLE ARE USING

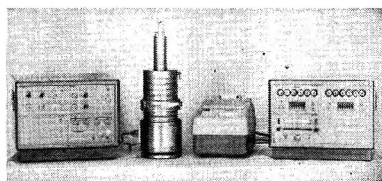
KAHLSICO INSTRUMENTS IN THEIR LAB



DIPOLMETER

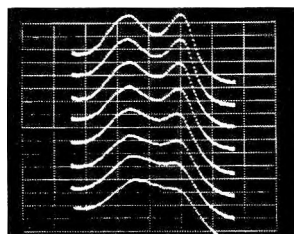
Precision, temperature stabilized, heterodyne beat, dielectric constant measuring bridge with CRT indicator and accessory sample holding cells. Sensitivity of $4 \cdot 10^{-5}$ with liquids assures reliable, molecular electrical dipole moment evaluations. Simple to operate with repeatable high accuracy. Designed for research and molecular structure confirmation.

Complete, automatic system with variable speed sample drive, shielded scintillation counting chamber, power supplies, digital pulse height spectrometer with printer, and recorder.



MÖSSBAUER EFFECT ANALYZER

Rapid, dual-beam spectroscopy permits absorptive or reflective measurements in 8.3 millisecond scan time over typical 350 to 700 nm spectrum with 1 to 5 nm resolution. Fixed wavelength determination available in 0.1 ms. CRT indicator can display 16 spectra for 1 hour. Solid state electronics and data handling permit operation at 100 spectral/sec. rates. Photosensor head



10 millisecond interval absorption spectra of blood film undergoing oxygenation

may be used vertically or horizontally and is offset to facilitate large specimen handling.

Also Variable Frequency Dielectric Constant and Dielectric Loss Instruments, Motorized Tensiometers, Gas Leak Apparatus, Precision Thermometers and Thermostats, Rate-meters, High Frequency Titrimeters, Sound Velocity-Elastic and Torsion Modulus-Meters, Nanosecond Light Sources.

Please contact us for details.

KAHL SCIENTIFIC INSTRUMENT CORP.

739 West Main St., El Cajon, Calif. 92022

PHONE (714) 444-2009

CABLE: KAHLSICO SANDIEGO

Eastern Office:

2425 Third Avenue, Bronx, N.Y. 10451

PHONE (212) 665-1605

TIP THE BALANCE IN YOUR FAVOR



with a subscription to **ANALYTICAL CHEMISTRY**

your best guide to analytical instrumentation and how to use it.

Each month—AC articles describe for you

- The most recent equipment
- The newest techniques
- The latest applications
- The newest chemicals and reagents.

You get 2 major bonuses as part of your AC subscription—

- 1 The special "Annual Reviews" issue, surveying analytical science in detail... and featuring *fundamental* developments one year... *applications* the next—
- 2 The annual "Laboratory Guide to Instruments, Equipment and Chemicals," containing over 20,000 separate entries... more than 1,000 manufacturers... over 600 different products.

ANALYTICAL CHEMISTRY will keep you current in *all* areas of analytical science. Enjoy both the monthly Journal and the 2 bonuses. Start your AC subscription... *today*.

Domestic and Canada Foreign

1 year: ACS members..... \$4.00 \$ 4.00
All others..... 5.00 15.00

Additional postage: Foreign \$3.50
PUAS and Canada \$2.50

ORDER FROM Dept. M

AMERICAN

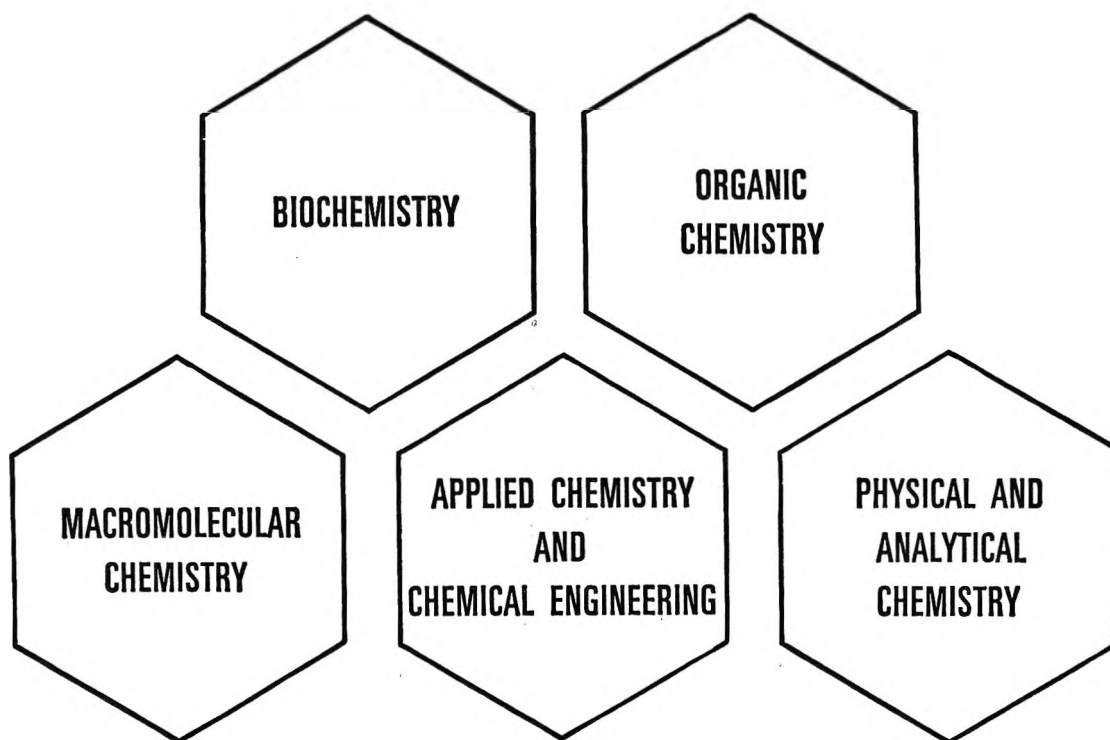
CHEMICAL SOCIETY

1155 Sixteenth Street, N.W.
Washington, D.C. 20036



COMMUNICATIONS TO THE EDITOR

Comment on "Electron Paramagnetic Resonance Spectra of the Naphthacene Trianion and the 5,12-Naphthacenequinone Anion Radicals"	K. Möbius and M. Plato 1830
The Complete Macroscopic Characteristic of Isothermal Diffusion in Binary Systems of Neutral Components	Bogdan Baranowski and Andrzej S. Cukrowski 1831
Electron Spin Resonance of Perfluorocyclobutanone Ketyl. Long-Range Fluorine Coupling	John L. Gerlock and Edward G. Janzen 1832
Comments on "Gibbs Equation for Polyelectrolyte Adsorption," by D. K. Chattoraj	I. R. Miller and M. A. Frommer 1834
Reply to the Comments on "Gibbs Equation for Polyelectrolyte Adsorption"	D. K. Chattoraj 1835
Hydrogen-Bonded Dimers and the 2.86- μ Band in Alcohols	R. M. Hammaker, Robert M. Clegg, Larry K. Patterson, Paul E. Rider, and Steven L. Rock 1837
The Alcohol Self-Association Dimer and the Absorption Band(s) near 1.53 μ m	Aaron N. Fletcher and Carl A. Heller 1839
A Criticism of the Term "Hydrophobic Bond"	Joel H. Hildebrand 1841
Comments on the Communication "A Criticism of the Term 'Hydrophobic Bond'" by Joel H. Hildebrand	George Némethy, Harold A. Scheraga, and Walter Kauzmann 1842
The Internal Pressure of Simple Liquids	R. N. Haward and B. M. Parker 1842
Comment on "Quantum Theoretical Treatment of Equilibrium Chemical Rate Processes"	B. A. Ridley, K. A. Quickert, and D. J. Le Roy 1844
Reply to "Comment on 'Quantum Theoretical Treatment of Equilibrium Chemical Rate Processes'"	S. J. Yao and B. J. Zwolinski 1845
The Primary Isotope Effect for the Replacement of H <i>vs.</i> D by Energetic Tritium Atoms	Thomas Smail and F. S. Rowland 1845
Bidimensional Condensation in Adsorbed Layers.	Y. Larher 1847



Look into CHEMICAL ABSTRACTS Section Groupings for efficient and economical coverage of specific interest areas.

Abstracts of the world's chemical literature published regularly in CHEMICAL ABSTRACTS are also published in separate issues or "Section Groupings" covering five general areas in the field of chemistry. These Section Groupings are published every other week and contain both the abstracts and a keyword index made up of significant terms selected from the abstracts. Taken together, the five Section Groupings include all abstracts published in CA.

The Section Groupings are extremely valuable as personal desk copies for immediate reference and for browsing in specific subject areas. If your individual interest or that of

your organization is limited to a particular phase of chemistry, a CA Section Grouping can provide you with a comprehensive and economical abstracting service.

Section Groupings can also be used as alerting tools in conjunction with the issue keyword indexes and as retrospective search tools in conjunction with the volume and collective indexes to CHEMICAL ABSTRACTS in your company or institution library.

Complete information on CHEMICAL ABSTRACTS Section Grouping subscriptions can be obtained by writing to: E. G. Johnson, Subscriber Information Dept. CASG.



CHEMICAL ABSTRACTS SERVICE

American Chemical Society
Columbus, Ohio 43216

AUTHOR INDEX

- Abramson, F. P., 1826
 Adamson, A. W., 1822
 Affsprung, H. E., 1748
 Agrawal, M. C., 1497
 Andrews, L., 1743
 Appiano, A., 1471

 Baird, M. E., 1462
 Baranowski, B., 1831
 Bartley, B. H., 1689
 Biegler, T., 1571
 Bielski, B. H. J., 1721
 Borgardt, F. G., 1513
 Bothner-By, A. A., 1642, 1646
 Bowden, M. J., 1577
 Breese, K., 1817
 Bryant, J. T., 1603
 Bull, H. B., 1817

 Carlson, K. D., 1611
 Carman, P. C., 1707, 1713
 Carter, J. L., 1682
 Carver, T. G., 1743
 Cavell, E. A. S., 1656
 Chattoraj, D. K., 1835
 Christian, S. D., 1748
 Ciani, F., 1510
 Cicogna, G., 1510
 Clegg, R. M., 1837
 Clever, H. L., 1529
 Cox, R. H., 1642, 1646
 Crowther, P., 1439
 Cubicciotti, D., 1664, 1669
 Cukrowski, A. S., 1831
 Cyvin, S. J., 1446, 1451

 Darwent, B. deB., 1639
 Davis, J. C., 1630
 DiBello, L. M., 1405
 Di Carlo, E. N., 1517
 Dicks, L., 1439
 Dogliotti, L., 1800
 Drost-Hansen, W., 1758

 Eberhart, J. G., 1825

 Eick, H. A., 1697
 Eyring, H., 1483

 Ficalora, P. F., 1660
 Fletcher, A. N., 1839
 Freeman, G. R., 1780
 Freeman, J. J., 1721
 Fripiat, J. J., 1808
 Fritsch, J. M., 1829
 Frommer, M. A., 1834
 Fujita, H., 1752
 Futrell, J. H., 1826

 Garnett, J. L., 1673
 Gebicki, J. M., 1721
 George, Z. M., 1689
 Gerlock, J. L., 1832
 Gopal, R., 1814
 Gordon, S., 1592
 Gottlieb, C., 1425
 Gregory, M. D., 1748
 Grimison, A., 1776
 Grinstead, R. R., 1630
 Gruetter, E. N., 1825
 Grygorcewicz, C., 1811
 Gustafson, R. L., 1502
 Güsten, H., 1457

 Habgood, H. W., 1689
 Hagen, G., 1446, 1451
 Hahn, S. J., 1483
 Hammaker, R. M., 1837
 Haschke, J. M., 1697
 Hastie, J. W., 1660
 Haward, R. N., 1842
 Hayon, E., 1800
 Heller, C. A., 1839
 Hentz, R. R., 1783
 Hildebrand, J. H., 1841
 Hodges, R. J., 1673
 Horne, R. A., 1763

 Iwasaki, M., 1491

 Jacobs, P., 1768
 Janzen, E. G., 1832
 Johnson, J. W., 1664, 1669

 Jones, W. E., 1812

 Kauzmann, W., 1842
 Kellner, J. D., 1737
 Kemp, T. J., 1464
 Khoobiar, S., 1682
 Klein, G. W., 1432
 Knight, P. C., 1656
 Knight, R. J., 1783
 Kobatake, Y., 1752
 Kohl, F. J., 1611

 Lamprecht, G. J., 1439
 Larher, Y., 1847
 Laurence, G. S., 1811
 Law, S. L., 1617
 Léonard, A., 1808
 Le Roy, D. J., 1844
 Lin, Y. N., 1726
 Lirio, J. A., 1502
 Logan, T. P., 1517
 Lossing, F. P., 1552
 Lucchesi, P. J., 1682

 Madhavan, N., 1812
 Maestro, M., 1510
 Makay, K., 1768
 Malan, O. G., 1457
 Margrave, J. L., 1660
 Marshall, H. P., 1513
 Marshall, W. L., 1536, 1545
 Maslov, P. G., 1414
 Matsuo, T., 1819
 McDevitt, H. M., 1405
 McDonald, R. L., 1617
 McGee, T. H., 1621
 Meaburn, G. M., 1592
 Meehan, E. J., 1523
 Mendelovici, E., 1808
 Menzinger, M., 1789
 Meyer, R. T., 1583
 Meyers, E. A., 1561
 Meyerstein, D., 1599
 Miles, D. W., 1483
 Miller, I. R., 1834
 Miller, J. K., 1523
 Miller, F. J., 1758

 Möbius, K., 1830
 Mushran, S. P., 1497
 Myers, D. C., 1475

 Nelson, R. F., 1829
 Némethy, G., 1842
 Nicholson, R. S., 1650
 Noble, P., Jr., 1513

 Occhiena, G., 1471
 O'Donnell, J. H., 1577
 Olmstead, M. L., 1650

 Padday, J. F., 1407
 Pai Verneker, V. R., 1733
 Parker, B. M., 1842
 Patterson, L. K., 1837
 Penzhorn, R. D., 1639
 Perumareddi, J. R., 1822
 Plato, M., 1830
 Pritchard, G. O., 1603

 Quickert, K. A., 1844
 Quinlan, K. P., 1797
 Quist, A. S., 1536, 1545

 Rabani, J., 1599
 Rabinovitch, B. S., 1726
 Ramakrishna, V., 1555
 Redmond, T. F., 1626
 Rider, P. E., 1837
 Ridley, B. A., 1844
 Roberti, D. M., 1405
 Roberts, J. P., 1464
 Robins, M. J., 1483
 Robins, R. K., 1483
 Robinson, M. G., 1780
 Rock, S. L., 1837
 Rowland, F. S., 1845
 Ruff, I., 1792

 Sakurai, T., 1491
 Salmon, G. A., 1464
 Samuel, D., 1809

 Scheraga, H. A., 1842
 Schmidt, R. L., 1529
 Schmidt-Bleek, F., 1475
 Schoonheydt, R., 1768
 Schulte-Frohlinde, D., 1457
 Schweikert, W. W., 1561
 Selis, S. M., 1442
 Seo, E. T., 1829
 Shapiro, J. S., 1552
 Shirom, M., 1702
 Siddiqi, M. A., 1814
 Silva, W. J., 1664, 1669
 Silver, B. L., 1809
 Simpson, G. A., 1776
 Skibba, M., 1425
 Smail, T., 1845
 Spees, S. T., Jr., 1822
 Spittler, E. G., 1432
 Spurling, T. H., 1821
 Storvick, T. S., 1821
 Stronski, R. E., 1517
 Suri, S. K., 1555

 Thompson, G. F., 1464
 Tombalakian, A. S., 1566

 Uffindell, N. D., 1407
 Uy, O. M., 1611
 Uytterhoeven, J. B., 1768

 Versino, C., 1471

 Wayland, B. B., 1626
 Willard, J. E., 1702
 Wolfgang, R., 1789

 Yao, S. J., 1845
 Young, R. P., 1763
 Yuasa, M., 1752

 Zecchina, A., 1471
 Zevos, N., 1506
 Zuehlke, R. W., 1425
 Zwolinski, B. J., 1845

1967-68 LABORATORY GUIDE

to Instruments, Equipment and Chemicals

1 Laboratory Supply Houses 11 LG

2 Product Classifications 25 LG


3 Instruments & Equipment 51 LG

4 Chemicals & Services 243 LG

5 Trade Names 313 LG

6 Books 355 LG

7 Company Directory 393 LG

 an American Chemical Society Publication

The beginning of a requisition

This is where laboratory chemists, life scientists, physicists and engineers turn first to find who sells what, to inquire about products, to locate sales offices, to consult vendors, to create lists of bidders, to place orders.

The definitive ACS LABORATORY GUIDE is issued annually in July to subscribers to the ACS Research Journals.

THE JOURNAL OF PHYSICAL CHEMISTRY

Volume 72, Number 6 June 1968

The Explosive Decomposition of Chlorine Dioxide	Edward T. McHale and Guenther von Elbe	1849
Thermal Decomposition of Azoethane	H. S. Sandhu	1857
The Biradical Mechanism in Small Ring Compound Reactions	H. E. O'Neal and S. W. Benson	1866
Densities of Several Proteins and L-Amino Acids in the Dry State	E. Berlin and M. J. Pallansch	1887
Molten Sulfur Chemistry. V. Kinetics of Chemical Equilibration in Pure Liquid Sulfur	T. K. Wiewiorowski, A. Parthasarathy, and B. L. Slaten	1890
Miscibility of Liquid Metals with Salts. VIII. Strontium-Strontium Halide and Barium-Barium Halide Systems	A. S. Dworkin, H. R. Bronstein, and M. A. Bredig	1892
A Semiempirical Treatment of Properties of Fluid Mixtures. II. Estimation of the Effects of Molecular Sizes in Fluids and Fluid Mixtures	Aleksander Kreglewski	1897
Ion-Molecule Reactions in Propyne and Allene	J. J. Myher and A. G. Harrison	1905
Thermodynamics of the Solubility of Mercury Metal. III. Dimethylcyclohexanes and Alcohols as Solvents	James N. Spencer and Adolf F. Voigt	1913
Viscosities of Some Organic Glasses Used as Trapping Matrices	A. Campbell Ling and John E. Willard	1918
Thermal Conductivity of Binary Mixtures of Gases. I. Hydrogen-Helium Mixtures	Clarke C. Minter	1924
Free-Radical Intermediates in the Reaction of the Hydroxyl Radical with Amino Acids	Hitoshi Taniguchi, Katsuji Fukui, Shun-ichi Ohnishi, Hiroyuki Hatano, Hideo Hasegawa, and Tetsuo Maruyama	1926
Energy Transfer in Thermal Methyl Isocyanide Isomerization. Incremental and Relative Cross Sections of Hydrocarbons	Y. N. Lin, S. C. Chan, and B. S. Rabinovitch	1932
Molar Excess Enthalpies and Volumes of Benzene-Isomeric Xylene Systems at 25°	Jaswant Singh, H. D. Pflug, and G. C. Benson	1939
Acid Dissociation Constant of Trifluoroacetic Acid in Water Measured by Differential Refractometry	Ernest Grunwald and James F. Haley, Jr.	1944
The Reaction of Thermal Hydrogen Atoms with Frozen Organic Substrates	A. K. E. Hagopian and R. H. Johnsen	1949
The Hill Equation for Adsorption on Uniform Surfaces	Conway Pierce	1955
The Electrical Conductance of Tetraethylammonium Perchlorate in Valeronitrile	John J. Banewicz, John A. Maguire, and Pong Su Shih	1960
Membrane Potentials and Ion Selectivity of Fused Silica in Molten Salts	Kurt H. Stern	1963
Self-Exchange Reaction of Deuterium in Monodeuteriotoluene Catalyzed by Nickel and Platinum	Kozo Hirota, Tomiko Ueda, Toyoki Kitayama, and Michiya Itoh	1976
A Fluorescence Study of Aminopyridines	A. Weisstuch and A. C. Testa	1982
The Effect of Radiation on the Reactions of Recoil Carbon-11 in the Nitrogen-Oxygen System	Hans J. Ache and Alfred P. Wolf	1988
Ionic Reactions in Unsaturated Compounds. III. Propylene and the Isomeric Butenes	Fred P. Abramson and J. H. Futrell	1994
pH Dependence of Electronic and Nuclear Magnetic Resonance Spectra of Isomeric Cyanine Dyes	L. H. Feldman, A. H. Herz, and T. H. Regan	2008
Surface Tension of Polymer Liquids	Ryong-Joon Roe	2013

Pulse Radiolysis of Aqueous Fluorescein	P. Cordier and L. I. Grossweiner	2018
The Kinetics of Formation of Nickel Malonate and Nickel Succinate Complexes	John L. Bear and Chin-Tung Lin	2026
Some Tensimetric Studies in the Mixed Ceria-Terbium System	J. Kordis and L. Eyring	2030
A Tensimetric Study of the Terbium and Praseodymium Systems and the Mixed Praseodymium-Terbium System	J. Kordis and L. Eyring	2044
Decomposition of Aqueous Perchlorates by Radiation	D. Katakis and J. Konstantatos	2054
Mesomorphic Phases. I. X-Ray Studies of the Dimethyldodecylamine Oxide-Deuterium Oxide System	K. D. Lawson, A. J. Mabis, and T. J. Flautt	2058
Mesomorphic Phases. II. Proton and Deuterium Magnetic Resonance Studies of the Dimethyldodecylamine Oxide-Deuterium Oxide System	K. D. Lawson and T. J. Flautt	2066
Coordination Disproportionation Equilibria in Solution. II. Cobaltous Chloride and Zinc Chloride in Acetonitrile	W. Libuś, D. Puchalska, and T. Szuchnicka	2075
Dissociation Constants of Piperazinium Ion and Related Thermodynamic Quantities from 0 to 50°	Hannah B. Hetzer, R. A. Robinson, and Roger G. Bates	2081
Thermodynamic Treatment and Electromotive Force Measurements of the Ternary Molten Salt Systems Silver Chloride-Sodium Chloride-Potassium Chloride and Silver Chloride-Sodium Chloride-Cesium Chloride	J. Guion, M. Blander, D. Hengstenberg, and K. Hagemark	2086
Heats of Immersion in the Thorium Oxide-Water System. IV. Variation of the Net Differential Heat of Adsorption with Specific Surface Area	H. F. Holmes, E. L. Fuller, Jr., and C. H. Secoy	2095
Electrical Conductances of Aqueous Sodium Bromide Solutions from 0 to 800° and at Pressures to 4000 Bars	Arvin S. Quist and William L. Marshall	2100
Thermodynamic Studies in the High-Conducting Solid Systems RbI-AgI, KI-AgI, and NH ₄ I-AgI	L. E. Topol and B. B. Owens	2106
Medium Effects in Nuclear Magnetic Resonance. V. Liquids Consisting of Nonpolar, Magnetically Isotropic Molecules	F. H. A. Rummens, W. T. Raynes, and H. J. Bernstein	2111
The Crystal and Molecular Structure of 1,2,3,4-Tetrabromo-1,2,3,4-diphthaloylcyclobutane	Gert J. Kruger and Jan C. A. Boeyens	2120
Transport Numbers and Ionic Conductances in Sulfolane at 30°	M. Della Monica, U. Lamanna, and L. Senatore	2124
The Surface Area of Silicate Minerals by the BET Method Using the Adsorption of Xenon at -78°	K. A. Kini, R. M. Manser, and A. S. Joy	2127
Molecular Complexes of Iodine with Tetramethylurea and Tetramethylthiourea	Robert P. Lang	2129
Proton Magnetic Resonance and Infrared Studies of the <i>cis</i> and <i>trans</i> Isomers of a Monosubstituted Formanilide	T. H. Siddall, III, W. E. Stewart, and A. L. Marston	2135
Surface Interactions of Zinc Oxide and Zinc Sulfide with Nitric Oxide.	Jack H. Lunsford	2141
Reactions of Thiyl Radicals. IV. Photolysis of Methanethiol	R. P. Steer and A. R. Knight	2145
Kinetics of the Chlorination of Mercuric Chloride in Acetone at a Solid Surface	L. Hellemans and C. Jonckheere	2154
Light-Scattering Measurements of Poly(α -methylstyrene). The Effect of Molecular Weight Heterogeneity on the Second Virial Coefficient	Tadaya Kato, Katsuhiko Miyaso, and Mitsuru Nagasawa	2161
Kinetics of Formation and Growth of Colloidal Silver Bromide Particles. III. Experiments at Short Reaction Times	E. J. Meehan and Jerry K. Miller	2168
Vibrational Intensities. XXI. Some Band Shapes and Intensities in Liquid Hexafluorobenzene	Tsunetake Fujiyama and Bryce Crawford, Jr.	2174
The Radiation Chemistry of Acetamide	K. Narayana Rao and A. O. Allen	2181
The Preexponential Factors for Solid-State Thermal Decomposition	Herman F. Cordes	2185
The Thermal Decomposition of Solid Alkali Perchlorates	Herman F. Cordes and S. Ruven Smith	2189
Ionic Membranes. I. Surface Sulfonic Acid Groups on Porous Glass: a Potentiometric Study	L. S. Hersh	2195
Hyperfiltration Studies. XI. Salt Rejection Properties of Dynamically Formed Hydrous Zirconium(IV) Oxide Membranes	A. J. Shor, K. A. Kraus, W. T. Smith, Jr., and James S. Johnson, Jr.	2200
The Spectrum of the Hexachloroiridium(IV) Ion.	Thomas P. Sleight and Curtis R. Hare	2207

Thiazolium Ions and Related Heteroaromatic Systems. II. The Acidity Constants of Thiazolium, Oxazolium, and Imidazolium Ions	Paul Haake and Larry P. Bausher	2213
Ideal Behavior of Sodium Alkyl Sulfates at Various Interfaces. Thermodynamics of Adsorption at the Air-Water Interface	William R. Gillap, Norman D. Weiner, and Milo Gibaldi	2218
Ideal Behavior of Sodium Alkyl Sulfates at Various Interfaces. Thermodynamics of Adsorption at the Oil-Water Interface	William R. Gillap, Norman D. Weiner, and Milo Gibaldi	2222
Ultrasonic Absorption Measurements in Aqueous Solutions of Glycine, Diglycine, and Triglycine	Gordon G. Hammes and C. Nick Pace	2227

NOTES

Vaporization, Thermodynamics, and Dissociation Energy of Lanthanum Monosulfide. II	E. David Cater and Ronald P. Steiger	2231
The Heat and Entropy of Dissociation of Carbonium Ion Pairs	N. Kalfoglou and M. Szwarc	2233
Elimination of Difluoromethylene from Chemically Activated 1,1,2,2-Tetrafluorocyclopropane	Norman C. Craig, Tai-na Hu, and Peter H. Martyn	2234
On the Reaction of Atomic Nitrogen with Carbon Dioxide	John T. Herron and Robert E. Huie	2235
The Reaction of Methylene with Carbon Monoxide	R. A. Cox and R. J. Cvetanović	2236
Electron Spin Resonance Spectra of Polyphenyl Anion Radicals	A. L. Allred and Lee W. Bush	2238
The Rate of Sublimation of Magnesium Nitride from Effusion Cells and from Free Surfaces <i>in Vacuo</i> and in Argon and Nitrogen Gases	Bette A. H. Blank and Alan W. Searcy	2241
The Measurement of the Vapor Pressures of Carbon-14-Labeled Dodecanoic Acid from 20 to 30° Using a Modified Knudsen Effusion Method	David P. Baccanari, Marguerite M. Yevitz, and Howard A. Swain, Jr.	2243
Ion-Pair Association of Strong Electrolytes in Binary Mixtures of Polar Solvents: Alkaline Perchlorates in Methanol-Methyl Cyanide Mixtures	Filippo Conti and Gianfranco Pistoia	2245
The Solubility of Fluorocarbon Gases in Cyclohexane	Keith W. Miller	2248
An Electron Spin Resonance Study of Intermediates Formed in Fe^{2+} - H_2O_2 and Ce^{4+} - H_2O_2 Systems in the Presence of Ti^{4+} Ions	M. S. Bains, Jett C. Arthur, Jr., and Oscar Hinojosa	2250
Relative Viscosity and Apparent Molal Volume of Aqueous Sodium Sulfate at Various Temperatures	Frank J. Millero, W. Drost-Hansen, and Lawrence Korson	2251
An Attempted Kinetic Study of Chemiluminescent Electron-Transfer Reactions	Robert Livingston and Horst R. Leonhardt	2254
Ion Diffusion into Fused Silica from Molten Salts	Kurt H. Stern	2256
The Relation of Rotation-Like Absorptions to Vibrational Band Contours of Molecules in Liquids	Gordon M. Barrow and Pabitra Datta	2259
Bond Dissociation Energies of <i>t</i> -Butyl Hypohalites	Cheves Walling and Christos G. Papaioannou	2260
The Reaction of Oxygen Difluoride and Sulfur Trioxide. Transfer of the OF Radical	I. J. Solomon, A. J. Kacmarek, and J. Raney	2262
On the Slope of the Liquidus and Solidus Curves at the Melting Point of a Congruently Melting Compound	Alan F. Berndt and Dennis J. Diestler	2263
Observed Phosphorescence Lifetimes and Glass Relaxation at 77°K	T. E. Martin and A. H. Kalantar	2265
Ultrasonic Relaxation in 3,3-Diethylpentane and Its Relation to That in Alkylammonium Ions	M. J. Blandamer, M. J. Foster, N. J. Hidden, and M. C. R. Symons	2268
Motional Properties of Polycrystalline Tetramethylammonium Bromide	D. J. Blears, S. S. Danyluk, and E. Bock	2269
Autoprotolysis of Constant of Acetonitrile	I. M. Kolthoff and M. K. Chantooni, Jr.	2270
Studies on Complexes. XIII. Another Spectrophotometric Equilibrium Equation, a Simple, Versatile Apparatus Designed for Its Use, and the Application to Some Charge-Transfer Interactions	P. R. Hammond	2272
The Electric Dipole Moment and Conformation of Acetyl Sulfide	J. Hodge Markgraf, George A. Lee, and James F. Skinner	2276
Rate of Hydrogen Diffusion in Room-Temperature Irradiated Quartz	John K. Garland and John W. Schroeder	2277

COMMUNICATIONS TO THE EDITOR

Comment on "Evidence for Nitrogen Trioxide in the Combustion of a Double-Base Propellant"	L. Phillips	2279
Activation Energy for the Mobility of the Hydrated Electron	B. Cercek	2279
On the Critical and Pseudocritical Pressure of Binary Mixtures	Aleksander Kreglewski	2280
The Thermal Decomposition of Lithium Azide	E. G. Prout and V. C. Liddiard	2281
Comments on "Temperature Dependence of Contact Angle and of Interfacial Free Energies in the Naphthalene-Water-Air System"	J. A. Lavelle	2283
Response to "Comments on Temperature Dependence of Contact Angle and of Interfacial Free Energies in the Naphthalene-Water-Air System"	Arthur W. Adamson	2284
Hydrogen-Deuterium Exchange of Propane on a Fuel-Cell Electrode	H. J. Barger, Jr., and A. J. Coleman	2285
Radical-Initiated Chain Dehalogenation of Alkyl Halides in Alkaline Alcoholic Solution	Warren V. Sherman	2287

AUTHOR INDEX

- Abramson, F. P., 1994
 Ache, H. J., 1988
 Adamson, A. W., 2284
 Allen, A. O., 2181
 Allred, A. L., 2238
 Arthur, J. C., Jr., 2250

 Baccanari, D. P., 2243
 Bains, M. S., 2250
 Banewicz, J. J., 1960
 Barger, H. J., Jr., 2285
 Barrow, G. M., 2259
 Bates, R. G., 2081
 Bausher, L. P., 2213
 Bear, J. L., 2026
 Benson, G. C., 1939
 Benson, S. W., 1866
 Berlin, E., 1887
 Berndt, A. F., 2263
 Bernstein, H. J., 2111
 Blandamer, M. J., 2268
 Blander, M., 2086
 Blank, B. A. H., 2241
 Blears, D. J., 2269
 Bock, E., 2269
 Boeyens, J. C. A., 2120
 Bredig, M. A., 1892
 Bronstein, H. R., 1892
 Bush, L. W., 2238

 Cater, E. D., 2231
 Cercek, B., 2279
 Chan, S. C., 1932
 Chantooni, M. K., Jr., 2270
 Coleman, A. J., 2285
 Conti, F., 2245
 Cordes, H. F., 2185, 2189
 Cordier, P., 2018
 Cox, R. A., 2236
 Craig, N. C., 2234
 Crawford, B., Jr., 2174
 Cvetanović, R. J., 2236

 Danyluk, S. S., 2269
 Datta, P., 2259
 Della Monica, M., 2124
 Diestler, D. J., 2263
 Drost-Hansen, W., 2251
 Dworkin, A. S., 1892

 Eyring, L., 2030, 2044

 Feldman, L. H., 2008
 Flautt, T. J., 2058, 2066
 Foster, M. J., 2268
 Fujiyama, T., 2174
 Fukui, K., 1926
 Fuller, E. L., Jr., 2095
 Futrell, J. H., 1994

 Garland, J. K., 2277
 Gibaldi, M., 2218, 2222
 Gillap, W. R., 2218, 2222
 Grossweiner, L. I., 2018
 Grunwald, E., 1944
 Guion, J., 2086

 Haake, P., 2213
 Hagemark, K., 2086
 Hagopian, A. K. E., 1949
 Haley, J. F., Jr., 1944
 Hammes, G. G., 2227
 Hammond, P. R., 2272
 Hare, C. R., 2207
 Harrison, A. G., 1905
 Hasegawa, H., 1926
 Hatano, H., 1926
 Hellemans, L., 2154
 Hengstenberg, D., 2086
 Herron, J. T., 2235
 Hersh, L. S., 2195
 Herz, A. H., 2008
 Hetzer, H. B., 2081
 Hidden, N. J., 2268
 Hinojosa, O., 2250
 Hirota, K., 1976

 Holmes, H. F., 2095
 Hu, T., 2234
 Huie, R. E., 2235

 Itoh, M., 1976

 Johnsen, R. H., 1949
 Johnson, J. S., Jr., 2200
 Jonckheere, C., 2154
 Joy, A. S., 2127

 Kacmarek, A. J., 2262
 Kalantar, A. H., 2265
 Kalfoglou, N., 2233
 Katakis, D., 2054
 Kato, T., 2161
 Kini, K. A., 2127
 Kitayama, T., 1976
 Knight, A. R., 2145
 Kolthoff, I. M., 2270
 Konstantatos, J., 2054
 Kordis, J., 2030, 2044
 Korson, L., 2251
 Kraus, K. A., 2200
 Kreglewski, A., 1897, 2280
 Kruger, G. J., 2120

 Lamanna, U., 2124
 Lang, R. P., 2129
 Lavelle, J. A., 2283
 Lawson, K. D., 2058, 2066
 Lee, G. A., 2276
 Leonhardt, H. R., 2254
 Libuś, W., 2075
 Liddiard, V. C., 2281
 Lin, C.-T., 2026
 Lin, Y. N., 1932
 Ling, A. C., 1918
 Livingston, R., 2254
 Lunsford, J. H., 2141

 Mabis, A. J., 2058
 Maguire, J. A., 1960

 Manser, R. M., 2127
 Markgraf, J. H., 2276
 Marshall, W. L., 2100
 Marston, A. L., 2135
 Martin, T. E., 2265
 Martyn, P. H., 2234
 Maruyama, T., 1926
 McHale, E. T., 1849
 Meehan, E. J., 2168
 Miller, J. K., 2168
 Miller, K. W., 2248
 Millero, F. J., 2251
 Minter, C. C., 1924
 Miyaso, K., 2161
 Myher, J. J., 1905

 Nagasawa, M., 2161

 Ohnishi, S., 1926
 O'Neal, H. E., 1866
 Owens, B. B., 2106

 Pace, C. N., 2227
 Pallansch, M. J., 1887
 Papaioannou, C. G., 2260
 Parthasarathy, A., 1890
 Pflug, H. D., 1939
 Phillips, L., 2279
 Pierce, C., 1955
 Pistoia, G., 2245
 Prout, E. G., 2281
 Puchalska, D., 2075

 Quist, A. S., 2100

 Rabinovitch, B. S., 1932
 Raney, J., 2262
 Rao, K. N., 2181
 Raynes, W. T., 2111
 Regan, T. H., 2008
 Robinson, R. A., 2081
 Roe, R.-J., 2013
 Rummens, F. H. A., 2111

 Sandhu, H. S., 1857
 Schroeder, J. W., 2277
 Searcy, A. W., 2241
 Secoy, C. H., 2095
 Senatore, L., 2124
 Sherman, W. V., 2287
 Shih, P. S., 1960
 Shor, A. J., 2200
 Siddall, T. H., III, 2135
 Singh, J., 1939
 Skinner, J. F., 2276
 Slaten, B. L., 1890
 Sleight, T. P., 2207
 Miyaso, K., 2161
 Smith, S. R., 2189
 Smith, W. T., Jr., 2200
 Solomon, I. J., 2262
 Spencer, J. N., 1913
 Steer, R. P., 2145
 Steiger, R. P., 2231
 Stern, K. H., 1963, 2256
 Stewart, W. E., 2135
 Swain, H. A., Jr., 2243
 Symons, M. C. R., 2268
 Szuchnicka, T., 2075
 Swarc, M., 2233

 Taniguchi, H., 1926
 Testa, A. C., 1982
 Topol, L. E., 2106

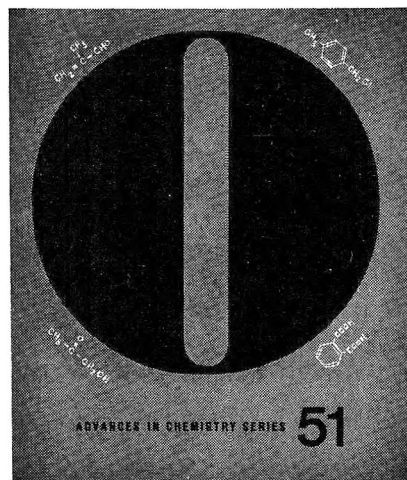
 Ueda, T., 1976

 Voigt, A. F., 1913
 von Elbe, G., 1849

 Walling, C., 2260
 Weiner, N. D., 2218, 2222
 Weisstuch, A., 1982
 Wiewiorowski, T. K., 1890
 Willard, J. E., 1918
 Wolf, A. P., 1988

 Yevitz, M. M., 2243

Do oxidation processes, products, and mechanisms interest you? "Selective Oxidation Processes" **ADVANCES IN CHEMISTRY SERIES No. 51** surveys a number of processes and details research on improving the range, selectivity, and mechanisms of such processes.



The book includes discussions of hydroxylating selected aromatics and olefins, pyrolysis of isobutylene—all of these by vapor phase processes. Among liquid phase processes are three general methods for oxidizing aromatics, sulfur dioxide as oxidant for a number of products, use of nitrogen dioxide catalyzed by selenium dioxide, and ozone as a selective oxidant. The last chapter is a broad survey of carbanion oxidation. The book is based on a symposium sponsored by the ACS Division of Petroleum Chemistry.

177 pages with index Cloth bound (1965) \$6.50

Other books in **ADVANCES IN CHEMISTRY SERIES** on topics of Industrial interest include:

No. 48 Plasticization and Plasticizer Processes. Seventeen papers survey recent studies on plasticizer action, properties, and production. Includes chapters on glass transition, plasticizer mobility, processes for phthalates and other plasticizers, and antiplasticizers.

200 pages with index Cloth bound (1965) \$7.00

No. 46 Patents for Chemical Inventions. What to do about your patentable idea before you call the attorney.

117 pages with index Cloth bound (1964) \$4.00

No. 38 Saline Water Conversion—II. Fourteen papers from two symposia; includes recovery of minerals from sea water, minimizing scale formation, wiped thin-film distillation, diffusion still, solar flash evaporation, osmosis, electrodialysis (3 papers), research in Israel, hydrate process.

199 pages Paper bound (1963) \$6.00

No. 34 Polymerization and Polycondensation Processes. An I&EC Division symposium with emphasis on unit processes. Twenty-one papers on addition polymerization, polycondensation reactions, commercial polymerization processes, and equipment design.

260 pages Paper bound (1962) \$8.00

No. 27 Saline Water Conversion. A Water and Waste Chemistry Division symposium; includes thermodynamics of desalting, solvent extraction, freezing, cen-

trifugal phase barrier recompression distillation, multi-stage flash evaporation, ion exchange, osmosis, and electrochemical demineralization.

246 pages Paper bound (1960) \$5.85

No. 24 Chemical Marketing in the Competitive Sixties. Twenty articles survey the challenge in marketing drugs, agricultural chemicals, industrial organics, inorganic and heavy chemicals, and plastics; the role of advertising; sales; delivering goods to the customer; monitoring sales performance; market research; technical service, and application research.

147 pages Paper bound (1959) \$3.50

No. 21 Ozone Chemistry and Technology. Sixty papers from the International Ozone Conference; includes ozone chemistry, high concentration ozone, ozone analysis and technology, formation in electrical discharge, toxicity, sterilization and water purification.

465 pages Cloth bound (1959) \$7.00

No. 19 Handling and Uses of Alkali Metals. Nineteen articles on the chemistry, manufacture, and use of the alkali metals; five are devoted solely or partly to lithium, two to potassium, the remainder to sodium.

177 pages Paper bound (1957) \$4.75

No. 10 Literature Resources for Chemical Process Industries. Information sources on market research (13 papers), resins and plastics (7 papers), textile chemistry (6 papers), food industry (10 papers), petroleum (10 papers), literature searching and language problems (13 papers).

582 pages with index Paper bound (1954) \$7.50

No. 5 Progress in Petroleum Technology. Survey of 25 years of progress at the ACS Diamond Jubilee. Thirty-two papers on all aspects of petroleum processing and products.

392 pages Cloth bound (1951) \$6.50

Order from Special Issues Sales, Dept. M
American Chemical Society
1155 Sixteenth St., N.W.
Washington, D. C. 20036

THE JOURNAL OF PHYSICAL CHEMISTRY

Volume 72, Number 7 July 1968

The Photolysis and Pyrolysis of Succinimide Vapor	G. Choudhary, A. M. Cameron, and R. A. Back	2289
Gravimetric Adsorption Studies of Thorium Oxide. III. Adsorption of Water on Porous and Nonporous Samples	H. F. Holmes, E. L. Fuller, Jr., and C. H. Secoy	2293
The Passivation of Mercury in Sulfide Ion Solutions	R. D. Armstrong, D. F. Porter, and H. R. Thirsk	2300
The Thermal Dissociation of Oxygen Difluoride. I. Incident Shock Waves	Jay A. Blauer and Wayne C. Solomon	2307
The Thermal Dissociation of Oxygen Difluoride. II. Static Reactor	W. C. Solomon, J. A. Blauer, and F. C. Jaye	2311
Thermodynamics of Ternary Systems. The Quasi-Chemical Approximation	K. Hagemark	2316
Electrolytic Oxidation of 9,10-Diphenylanthracene and Properties of Its Free Radical Cation and Anion	R. E. Sioda	2322
Radiolysis of Aqueous Chromium and Vanadium in Their +2 and +3 Oxidation States	P. A. P. Lykourazos, A. Kanellopoulos, and D. Katakis	2330
Analysis of Experimental Term Energies	Norman Padnos	2335
The Photochemistry of Gaseous Acetone	Henry Shaw and Sidney Toby	2337
Analysis of Proton Magnetic Resonance Spectra of <i>trans</i> -2,5-Dimethylpiperazine and Its Hydrochlorides. Effect of Amine Substituents on Chemical Shifts and Coupling Constants	J. L. Sudmeier	2344
Solutions of N-Substituted Amino Acids. III. The Influence of Solvent on the Tautomeric Equilibrium	David A. Horsma and Charles P. Nash	2351
Apparent and Partial Molal Volumes of Na-Kaolin and NaCl in Kaolin Suspensions	A. K. Helmy, F. F. Assaad, M. Naguib Hassan, and H. Sadek	2358
Transpiration Vapor Pressure Measurements for the Molten Salt Systems PbCl ₂ + CsCl and CdCl ₂ + CsCl	H. Bloom and J. W. Hastie	2361
A Multilayer Model for the Surface Transport of Adsorbed Gases	Weldon K. Bell and Lee F. Brown	2365
Infrared Spectrum, Surface Reaction, and Polymerization of Adsorbed Hydrogen Cyanide on Porous Glass	M. J. D. Low, N. Ramasubramanian, P. Ramamurthy, and A. V. Deo	2371
Interactions of Propionic and Acetic Acids with Germania	J. C. McManus and M. J. D. Low	2378
Lead Bromide Photochemistry: Reduction of Lead Ion and Oxidation of Leucocrystal Violet	H. E. Spencer and Jennifer O. Darlak	2384
The Heat and Products of Detonation of Cyclotetramethylenetetranitramine, 2,4,6-Trinitrotoluene, Nitromethane, and Bis[2,2-dinitro-2-fluoroethyl]formal	Donald L. Ornellas	2390
Studies in the Aqueous Radiation Chemistry of Cysteine. I. Deaerated Acidic Solutions	Adnan Al-Thannon, Richard M. Peterson, and Conrad N. Trumbore	2395
Conformational Properties of Optically Active Poly- α -olefins in Solution	P. L. Luisi and P. Pino	2400
Kinetic Analysis of Thermogravimetric Data	J. Zsákó	2406
The Wettability of Gold	Robert A. Erb	2412
Focused, Coherent Radiation (Laser)-Induced Degradation of Aromatic Compounds	Richard H. Wiley and P. Veeravagu	2417
Prediction of Heats of Formation.	W. Schotte	2422

Kinetic Isotope Effects in the Hydrogen Electrode Reaction	J. D. E. McIntyre and M. Salomon	2431
Vapor Pressure and Heats of Sublimation of Calcium Nitride	Roy C. Blair and Zuhair A. Munir	2434
The Reaction Products of γ -Picoline and Iodine.	I. Haque and J. L. Wood	2438
The n-Donor Complex Formation and Polymorphic Transformation of Zinc Phthalocyanine in Organic Suspension Media	Takashi Kobayashi, Natsu Uyeda, and Eiji Suito	2446
Infrared Evidence for FHF ⁻ in Annealed LiF-HX Films	R. L. Redington and T. E. Redington	2456
Electron Spin Resonance Study of Hydroperoxide on Zinc Oxide	M. Codell, H. Gisser, J. Weisberg, and R. D. Iyengar	2460
Hydration of N-Methylacetamide in Carbon Tetrachloride	R. D. Grigsby, S. D. Christian, and H. E. Affsprung	2465
Concentration Dependence of the Nuclear Magnetic Resonance Spectral Properties of Some N,N-Dimethylamides and -thioamides	Robert C. Neuman, Jr., William Snider, and Violet Jonas	2469
The Mean Activity Coefficient of Sodium Sulfate in Aqueous Sodium Sulfate-Sodium Chloride Electrolytes	John C. Synnott and James N. Butler	2474
Evidence for Trimerization in Aqueous Solutions of Methylene Blue	Emory Braswell	2477
The Oxidation of Sodium, Potassium, and Cesium in Flames.	R. Carabetta and W. E. Kaskan	2483
Application of the WKB Method to the Dynamics of Anharmonic Oscillators	Robert Dubrow, Douglas Hatzenbuehler, William Marx, Eva Zahorian, and David J. Wilson	2489
Divalent Transition Metal Complexes of Hydrolyzed Ethylene-Maleic Anhydride Copolymer	Betty J. Felber, Ernest M. Hodnett, and Neil Purdie	2496
Nuclear Quadrupole Resonance of Nitrogen-14 in Some Pyridine Derivatives	Ryuichi Ikeda, Shinzaburo Onda, Daiyu Nakamura, and Masaji Kubo	2501
Comparison of Electrical Transport Properties of Anionic Polyelectrolytes and Polysoaps	Raphael Varoqui and Ulrich P. Strauss	2507
Solute-Solvent Interactions in Aqueous Media	O. D. Bonner	2512
Nuclear Magnetic Resonance Study of Proton Exchange Involving Methyl-Substituted Pyridinium Salts in Methanol	Michael Cocivera	2515
Nuclear Magnetic Resonance Study of Proton Exchange Involving Methyl-Substituted Pyridinium Salts in Water	Michael Cocivera	2520
Standard Partial Molal Heat Capacities of Sodium Tetraphenylboron in Aqueous Solution from 0 to 90°. Effect of Water Structure and Hydrophobic Hydration	S. Subramanian and J. C. Ahluwalia	2525
Diffusion of Aromatic and Cycloparaffin Hydrocarbons in Water from 2 to 60°	L. Bonoli and P. A. Witherspoon	2532
Investigation of Liquid Palladium-Tin Alloys	J. R. Guadagno and M. J. Pool	2535
Arrhenius Parameters for the Reactions of Atomic Nitrogen with Some Olefins and Acetylenes	John T. Herron and Robert E. Huie	2538
Study on the Kinetics of Fast Electrode Processes with Pulse Technique and Electron Spin Resonance Methods	Ryo Hirasawa, Takashi Mukaibo, Hideo Hasegawa, Noboru Odan, and Tetsuo Maruyama	2541
New Forms of McKay-Perring Equations	Chai-fu Pan	2548
Nuclear Magnetic Resonance Spectra of Mono- and Disubstituted Benzenes Containing OH, SH, NH ₂ , and COOH	H. B. Evans, Jr., A. R. Tarpley, and J. H. Goldstein	2552
Thermodynamic Properties of Gases in Propellants. III. Equilibria in N ₂ H ₄ -1,1-N ₂ H ₂ (CH ₃) ₂ and He (or N ₂)-N ₂ H ₄ -1,1-N ₂ H ₂ (CH ₃) ₂ Systems	E. T. Chang and N. A. Gokcen	2556
Electron Spin Resonance of α -Chromia-Alumina Solid Solutions	Charles J. Carman and William J. Kroenke	2562
Quantum Deviations from the Principle of Corresponding States	R. M. Gibbons	2567
Simultaneous Electrochemical and Internal-Reflection Spectrometric Measurements Using Gold-Film Electrodes	Arnold Prostack, Harry B. Mark, Jr., and Wilford N. Hansen	2576
The Photoperoxidation of Unsaturated Organic Molecules. I. Relaxation and Oxygen-Quenching Parameters of the Sensitizer Singlet State	B. Stevens and B. E. Algar	2582
Potassium Chloride Conductance in Aqueous Solutions of a Structure-Forming Nonionic Solute, Hexamethylenetetramine	G. Barone, V. Crescenzi, and V. Vitagliano	2588
An Asymmetry-Potential Effect across Gradient Permselective Membranes	F. de Körösy	2591
Chemistry of Crystalline Aluminosilicates. V. Preparation of Aluminum-Deficient Faujasites	George T. Kerr	2594

Disulfide Ions Products in γ -Irradiated Organic Glasses at -196° . A Photochromism of the Anion Tadamasa Shida	2597
Kinetic Isotope Effects: Approximate Calculations Paul C. Chang and Carole R. Gatz	2602
Stepwise Formation of Cyanide Complexes of Copper(I) in Anion Exchangers J. S. Coleman, R. George, L. Allaman, and L. H. Jones	2605
An X-Ray Study of the Participation of the Bulk Phase of Cobalt Oxide in Oxidation Catalysis Richard M. Levy	2609
Low-Frequency Raman Spectra of Aqueous Solutions of Formates and Acetates L. A. Blatz and Peter Waldstein	2614
Carbon-13 Nuclear Magnetic Resonance Studies of 2-Substituted Pyridines H. L. Retcofsky and R. A. Friedel	2619
Evidence for Electron Migration during γ Irradiation of Silica Gel: Reactions of Adsorbed Electron Scavengers P. K. Wong and J. E. Willard	2623
Activation Energies and Rate Constants Computed for Reactions of Oxygen with Hydrocarbons S. W. Mayer and L. Schieler	2628
Reaction of Recoil Tritium with Methylsilanes Judith Witkin and Richard Wolfgang	2631
The Mechanism of Hydrogen Formation in the γ Radiolysis of 1,4-Dioxane and Its Mixtures with Water Robert R. Hentz and Warren V. Sherman	2635
The Oxidation of Chlorine Dioxide by Cobalt(III) in Perchlorate Solution Richard C. Thompson	2642
The Isotope Effect on the Vapor Pressures of $H_2O-C_2H_5OH$ and $D_2O-C_2H_5OD$ Mixtures C. U. Linderstrøm-Lang and Fred Vaslow	2645
Heat Capacity Changes in Ion-Exchange Reactions. The Exchange of Tetra- <i>n</i> -butylammonium with Sodium Ion in Cross-Linked Polystyrenesulfonate G. E. Boyd, Q. V. Larson, and S. Lindenbaum	2651
Absorption Spectra of the Alkali Metals in Hexamethylphosphoramide Jon M. Brooks and Robert R. Dewald	2655

NOTES

Direct Detection of the Hexaaquocobalt(II) Ion in Aqueous Solutions by Proton Magnetic Resonance Spectroscopy N. A. Matwiyoff and P. E. Darley	2659
Proton Magnetic Resonance Spectra of DL- and LL-Phenylalanylvalines Vito J. Morlino and R. Bruce Martin	2661
Viscosity of Mixtures of Electrolyte Solutions Y. C. Wu	2663
Ion Exchange with a Two-Phase Glass R. H. Doremus	2665
The Nuclear Magnetic Resonance Spectrum of Chloromethylphosphine H. Goldwhite and D. G. Rowsell	2666
Volumetric Behavior of Dilute Aqueous Solutions of Sodium Alkyl Sulfates F. Franks, M. J. Quickenden, J. R. Ravenhill, and H. T. Smith	2668
An Electron Paramagnetic Resonance Study of Cupric Ion Tetrahedrally Coordinated by Nitrogen Atoms Denis Forsner and Virgil W. Weiss	2669
Determination of Electron Affinities of Radicals and Bond Dissociation Energies by Electron-Attachment Studies at Thermal Energies—Electron Affinity of Acetate Radical W. E. Wentworth, Edward Chen, and Joe C. Steelhammer	2671
A Kinetic Study of the System $^{237}\text{Np(V)} \cdot \text{Cr(III)}-^{239}\text{Np(V)}$ James C. Sullivan and Mary J. Burkhart	2675
The Thermal Decomposition of Dimethyl Azodiformate A. Jones, E. R. Morris, and J. C. J. Thynne	2677
Some Observations on the Proton Magnetic Resonance Spectrum of Tetraethyl Ethylenebisphosphonate M. P. Williamson and C. E. Griffin	2678
2-Aminopyridine as a Standard for Low-Wavelength Spectrofluorimetry R. Rusakowicz and A. C. Testa	2680
Negative-Ion Mass Spectra of Some Boron Hydrides D. F. Munro, J. E. Ahnell, and W. S. Koski	2682
Photolysis of Methylene Blue by a Giant-Pulse Ruby Laser Ikuzo Tanaka, Yuji Mori, Yoshisato Minagawa, and Eiichi Okutsu	2684

COMMUNICATIONS TO THE EDITOR

The Kinetics of the Reaction of Trapped Hydrogen Atoms in Sulfuric Acid Glasses K. Vacek and D. Schulte-Frohlinde	2686
On the Purported Infrared Absorption at 21μ of Carbon Monoxide Adsorbed on Silica-Supported Platinum J. F. Ogilvie	2688
Infrared Absorption at 21μ of Carbon Monoxide Adsorbed on Silica-Supported Platinum J. K. A. Clarke, G. M. Farren, and H. E. Rubalcava	2688

The Nature of Sites Formed on Zeolites by Addition of Water	John W. Ward	2689
The Spectra of Polyene-Iodine Complexes	P. E. Blatz, N. Baumgartner, and S. Dewhurst	2690
The Existence of Homogeneous Oscillating Reactions	H. Degn and J. Higgins	2692
Homogeneous Periodic Reactions	D. H. Shaw and H. O. Pritchard	2693
Comment on "A Low-Temperature, High-Pressure Hydrate of <i>n</i> -Tetrabutylammonium Halides"	S. Subramanian	2694
The Pressure Dependence, Specific Volume, and Suggested Structure of Hydrophobic Hydration	R. A. Horne and R. P. Young	2694
The Pressure at the Maximum in Adsorption Isotherms at High Pressures	P. G. Menon	2695

AUTHOR INDEX

- Affsprung, H. E., 2465
 Ahluwalia, J. C., 2525
 Ahnell, J. E., 2682
 Algar, B. E., 2582
 Allaman, L., 2605
 Al-Thannon, A., 2395
 Armstrong, R. D., 2300
 Assaad, F. F., 2358
- Back, R. A., 2289
 Barone, G., 2588
 Baumgartner, N., 2690
 Bell, W. K., 2365
 Blair, R. C., 2434
 Blatz, L. A., 2614
 Blatz, P. E., 2690
 Blauer, J. A., 2307, 2311
 Bloom, H., 2361
 Bonner, O. D., 2512
 Bonoli, L., 2532
 Boyd, G. E., 2651
 Braswell, E., 2477
 Brooks, J. M., 2655
 Brown, L. F., 2365
 Burkhardt, M. J., 2675
 Butler, J. N., 2474
- Cameron, A. M., 2289
 Carabetta, R., 2483
 Carman, C. J., 2562
 Chang, E. T., 2556
 Chang, P. C., 2602
 Chen, E., 2671
 Choudhary, G., 2289
 Christian, S. D., 2465
 Clarke, J. K. A., 2688
 Cocivera, M., 2515, 2520
 Codell, M., 2460
 Coleman, J. S., 2605
 Crescenzi, V., 2588
- Darlak, J. O., 2384
 Darley, P. E., 2659
 Degn, H., 2692
 de Körösy, F., 2591
 Deo, A. V., 2371
- Dewald, R. R., 2655
 Dewhurst, S., 2690
 Doremus, R. H., 2665
 Dubrow, R., 2489
- Erb, R. A., 2412
 Evans, H. B., Jr., 2552
- Farren, G. M., 2688
 Felber, B. J., 2496
 Forster, D., 2669
 Franks, F., 2668
 Friedel, R. A., 2619
 Fuller, E. L., Jr., 2293
- Gatz, C. R., 2602
 George, R., 2605
 Gibbons, R. M., 2567
 Gisser, H., 2460
 Gokcen, N. A., 2556
 Goldstein, J. H., 2552
 Goldwhite, H., 2666
 Griffin, C. E., 2678
 Grigsby, R. D., 2465
 Guadagno, J. R., 2535
- Hagemark, K., 2316
 Hansen, W. N., 2576
 Haque, I., 2438
 Hasegawa, H., 2541
 Hassan, M. N., 2358
 Hastie, J. W., 2361
 Hatzenbuehler, D., 2489
 Helmy, A. K., 2358
 Hentz, R. R., 2635
 Herron, J. T., 2538
 Higgins, J., 2692
 Hirasawa, R., 2541
 Hodnett, E. M., 2496
 Holmes, H. F., 2293
 Horne, R. A., 2694
 Horsma, D. A., 2351
 Huie, R. E., 2538
- Ikeda, R., 2501
 Iyengar, R. D., 2460
- Jaye, F. C., 2311
- Jonas, V., 2469
 Jones, A., 2677
 Jones, L. H., 2605
- Kanellopoulos, A., 2330
 Kaskan, W. E., 2483
 Katakis, D., 2330
 Kerr, G. T., 2594
 Kobayashi, T., 2446
 Koski, W. S., 2682
 Kroenke, W. J., 2562
 Kubo, M., 2501
- Larson, Q. V., 2651
 Levy, R. M., 2609
 Lindenbaum, S., 2651
 Linderström-Lang, C. U., 2645
 Low, M. J. D., 2371, 2378
 Luisi, P. L., 2400
 Lykourazos, P. A. P., 2330
- Mark, H. B., Jr., 2576
 Martin, R. B., 2661
 Maruyama, T., 2541
 Marx, W., 2489
 Matwiyoff, N. A., 2659
 Mayer, S. W., 2628
 McIntyre, J. D. E., 2431
 McManus, J. C., 2378
 Menon, P. G., 2695
 Minagawa, Y., 2684
 Mori, Y., 2684
 Morlino, V. J., 2661
 Morris, E. R., 2677
 Mukaibo, T., 2541
 Munir, Z. A., 2434
 Munro, D. F., 2682
- Nakamura, D., 2501
 Nash, C. P., 2351
 Neuman, R. C., Jr., 2469
- Odan, N., 2541
- Ogilvie, J. F., 2688
 Okutsu, E., 2684
 Onda, S., 2501
 Ornellas, D. L., 2390
- Padnos, N., 2335
 Pan, C., 2548
 Peterson, R. M., 2395
 Pino, P., 2400
 Pool, M. J., 2535
 Porter, D. F., 2300
 Pritchard, H. O., 2693
 Probst, A., 2576
 Purdie, N., 2496
- Quickenden, M. J., 2668
- Ramamurthy, P., 2371
 Ramasubramanian, N., 2371
 Ravenhill, J. R., 2668
 Redington, R. L., 2456
 Redington, T. E., 2456
 Retcofsky, H. L., 2619
 Rowsell, D. G., 2666
 Rubalcava, H. E., 2688
 Rusakowicz, R., 2680
- Sadek, H., 2358
 Salomon, M., 2431
 Schieler, L., 2628
 Schotte, W., 2422
 Schulte-Frohlinde, D., 2686
 Secoy, C. H., 2293
 Shaw, D. H., 2693
 Shaw, H., 2337
 Sherman, W. V., 2635
 Shida, T., 2597
 Sioda, R. E., 2322
 Smith, H. T., 2668
 Snider, W., 2469
 Solomon, W. C., 2307, 2311
 Spencer, H. E., 2384
 Steelhammer, J. C., 2671
- Stevens, B., 2582
 Strauss, U. P., 2507
 Subramanian, S., 2525, 2694
 Sudmeier, J. L., 2344
 Suito, E., 2446
 Sullivan, J. C., 2675
 Synnott, J. C., 2474
- Tanaka, I., 2684
 Tarpley, A. R., 2552
 Testa, A. C., 2680
 Thirsk, H. R., 2300
 Thompson, R. C., 2642
 Thynne, J. C. J., 2677
 Toby, S., 2337
 Trumbore, C. N., 2395
- Uyeda, N., 2446
- Vacek, K., 2686
 Varoqui, R., 2507
 Vaslow, F., 2645
 Veeravagu, P., 2417
 Vitagliano, V., 2588
- Waldstein, P., 2614
 Ward, J. W., 2689
 Weisberg, J., 2460
 Weiss, V. W., 2669
 Wentworth, W. E., 2671
 Wiley, R. H., 2417
 Williamson, M. P., 2678
 Willard, J. E., 2623
 Wilson, D. J., 2489
 Witherspoon, P. A., 2532
 Witkin, J., 2631
 Wolfgang, R., 2631
 Wong, P. K., 2623
 Wood, J. L., 2438
 Wu, Y. C., 2663
- Young, R. P., 2694
- Zahorian, E., 2489
 Zsakó, J., 2406

Ion-Molecule Reactions in the Gas Phase

Equilibrium Concepts in Natural Water Systems

Advances in Chemistry Series No. 67

Natural waters are open, dynamic systems with variable inputs and outputs of mass and energy. Their chemistry is complex and involves many variables. Simplified, manageable models are used to overcome this complexity and to help understand and predict real systems.

Sixteen papers represent the collaboration of aquatic chemists, analytical chemists, geologists, limnologists, and sanitary engineers. Among the topics covered are:

Thermodynamics of water systems
Limitations of trace metal analysis
Gibbs phase rule and marine sediments
Water-solute interactions
Heterogeneous equilibria
Coordination chemistry of the oceans
Equilibrium models of the Great Lakes

344 pages with index cloth bound (1967) \$8.50

Set of L.C. cards free with library orders.

Other books in the ADVANCES IN CHEMISTRY SERIES in physical and colloid chemistry include:

No. 63 Ordered Fluids and Liquid Crystals. Twenty-two studies on characterization, properties, and occurrence of these phenomena in many substances such as tristearin, *p*-azoxyanisole, mono- and di-hydric alcohols, phospholipids, and polypeptides.
332 pages Cloth bound (1967) \$9.50

No. 58 Ion-Molecule Reactions in the Gas Phase. Eighteen papers survey spectrometric and other methods for producing and studying ion-molecule reactions, such as pulsed sources for studying thermal ions, reactions in flames and electrical discharges.
336 pages Cloth bound (1966) \$8.50

No. 54 Advanced Propellant Chemistry. Primarily directed to the search for new oxidizers; 26 papers survey oxygen-containing oxidizers, fuels and binders, fluorine systems including oxygen difluoride and difluoramines, and liquid systems.
290 pages, Cloth bound (1966) \$8.50

No. 47 Fuel Cell Systems Developments in theory, performance, construction, and new systems for the energy converter that is proving itself in military and space uses.
360 pages with index, Cloth bound (1965) \$8.00

No. 43 Contact Angle, Wettability, and Adhesion Twenty-six papers on theoretical and practical approaches to wettability and adhesion; with summary of the surface chemical studies of W. A. Zisman, the 1963 Kendall Award winner.
389 pages with index, Cloth bound (1964) \$8.00

No. 40 Mass Spectral Correlations. By Fred W. McLafferty. Over 4000 spectra listed by mass/charge ratios of fragment ions with the most probable original structures for each.
117 pages, Paper bound (1963) \$4.75

No. 35 Azeotropic Data—II By Lee H. Horsley and William S. Tamplin. Supplements ADVANCES No. 6 with 1674 binary and 265 ternary and quaternary systems, many not published elsewhere.
100 pages Paper bound (1962) \$4.50

No. 33 Solid Surfaces and the Gas-Solid Interface Thirty-seven papers from the Kendall Award Symposium honoring Stephen Brunauer. Theory and techniques for studying surface phenomena.
381 pages with index Cloth bound (1961) \$9.00

No. 31 Critical Solution Temperatures By Alfred W. Francis. CST answers the question, "Do two liquids mix?" and is widely used for screening solvents. Over 6000 systems are included, 70% with a hydrocarbon as one component; nearly 1100 nonhydrocarbon solvents are listed.
246 pages Cloth bound (1961) \$5.00

No. 29 Physical Properties of Chemical Compounds—III By Robert R. Dreisbach. Supplements earlier volumes with properties of 434 aliphatic compounds and 22 miscellaneous compounds and elements. Index to volumes I, II, and III.
489 pages Cloth bound (1961) \$6.50

No. 25 Physical Functions of Hydrocolloids Papers on natural gums, gelatin, pectins and related polysaccharides, and theoretical and functional aspects of hydrocolloids, emulsions, foams, and dispersions. Strong food industry emphasis.
103 pages Paper bound (1960) \$3.75

No. 22 Physical Properties of Chemical Compounds—II By Robert R. Dreisbach. Properties of 476 alkanes, haloalkanes, alkenes, haloalkenes, diolefins, and alkynes.
491 pages with index Cloth bound (1959) \$6.50

No. 18 Thermodynamic Properties of the Elements By D. R. Stull and G. C. Sinke. Tabulated values of heat capacity, heat content, entropy, and free energy function of solid, liquid, and gas states of first 92 elements in range of 298° to 3000°K. Some auxiliary data frequently included.
234 pages with index Cloth bound (1956) \$5.00

No. 15 Physical Properties of Chemical Compounds By Robert R. Dreisbach. Tables of parameters for calculating physical properties of 511 organic cyclic compounds
536 pages with index Cloth bound (1955) \$5.85

No. 11 Natural Plant Hydrocolloids Surveys substances used as protective colloids: calcium pectinate, agar, gum arabic, gum karaya, tragacanth, guar gum, locust bean gum, algin, and Irish moss and red seaweed extracts.
103 pages Paper bound (1954) \$2.50

No. 6 Azeotropic Data By Lee H. Horsley. Data on 14,501 binary and 407 ternary systems with a few charts on alcohol-ketone azeotropes vs. pressure and two chapters on predicting azeotropes.
328 pages Cloth bound (1952) \$5.00

Postpaid in U.S. and Canada, plus 20 cents in PUAS and elsewhere.

Order from: Dept. M
Special Issues Sales
American Chemical Society
1155 Sixteenth St., N.W.
Washington, D. C. 20036

THE JOURNAL OF PHYSICAL CHEMISTRY

Volume 72, Number 8 August 1968

Evidence for Molecular Dimers, $(I_2)_2$, in Iodine Vapor	A. A. Passchier and N. W. Gregory	2697
Methyl Radicals in Aqueous Solution as Studied by Electron Spin Resonance Spectroscopy	D. Mickewich and J. Turkevich	2703
Mass Spectrometry of the Vapors over $PbCl_2 + ACl$ Mixtures ($A = Na, K, Rb, \text{ or } Cs$). I. Thermodynamic Studies	H. Bloom and J. W. Hastie	2706
Properties of Amides in Aqueous Solution. I. A. Viscosity and Density Changes of Amide-Water Systems. B. An Analysis of Volume Deficiencies of Mixtures Based on Molecular Size Differences (Mixing of Hard Spheres)	P. Assarsson and F. R. Eirich	2710
Calorimetric Determination of $\log K_t^\circ$, ΔH_t° , and ΔS_t° Values for the Interaction at 25° of Thiourea with $Hg(CN)_2$ in Water-Ethanol Solvents	Reed M. Izatt, Delbert Eatough, and James J. Christensen	2720
The Thermodynamics of Bimolecular (Black) Lipid Membranes at the Water-Oil-Water Biface	H. Ti Tien	2723
Application of Significant Structure Theory to the Correlation of Thermodynamic Properties of CO_2 , COS , and CS_2 in Terms of the Respective Molecular Parameters	Melvin E. Zandler, James A. Watson, Jr., and Henry Eyring	2730
Temperature Dependence of the Solvent Stark Effect.	G. A. Gerhold and E. Miller	2737
Fluorescence Emission Band Shift with Wavelength of Excitation	Aaron N. Fletcher	2742
The Interactions between Trialkylsilanes and E-Glass or Aerosil Surfaces. Reactions of Trimethylsilanol, Trimethylchlorosilane, and Hexamethyldisilazane	F. O. Stark, O. K. Johannson, G. E. Vogel, R. G. Chaffee, and R. M. Laceyfield	2750
Kinetics of Adsorption from a Solution. Role of the Diffusion and of the Adsorption-Desorption Antagonism	J. F. Baret	2755
Excess Free Energies of Aqueous Mixtures of Some Alkali Metal Halide Salt Pairs	A. K. Covington, T. H. Lilley, and R. A. Robinson	2759
Interactions in Benzene. Investigation of Collision Complexes of Free and of Coordinated Monoethyl, Diethyl, and Cyanoethyl Esters and Benzene by Nuclear Magnetic Resonance Spectroscopy	Andrzej Kemula and Reynold T. Iwamoto	2764
The Dehydration of Alcohols over Alumina. VIII. The Ether Formation from the Deuterated Methanols CH_3OH , CD_3OH , CH_2OD , and CD_2OD	H. Knözinger, A. Scheglila, and A. M. Watson	2770
Low-Temperature Hydrogen Adsorption on Copper-Nickel Alloys	D. A. Cadenhead and N. J. Wagner	2775
The Voltammetric Behavior of the Aqueous System $I^- - I_2 - ICl - Cl^-$ on Smooth Platinum	Giovanni Piccardi and Rolando Guidelli	2782
The Thermodynamics of Cation Exchange. VI. Selectivity and Activity Coefficients in Moderately Concentrated Solutions	P. Meares and J. F. Thain	2789
The Photochemical Decomposition of Silver Perchlorate	V. R. Pai Verneker and J. N. Maycock	2798
Isotropic Rotational Relaxation of Photoselected Emitters and Systematic Errors in Emission Decay Times	A. H. Kalantar	2801
Nuclear Quadrupole Relaxation of ^{79}Br in Aqueous Solutions of Quaternary Ammonium Bromides	Björn Lindman, Sture Forsén, and Erik Forslind	2805
The Electronic Spectrum of the Cyclooctatetraenyl Radical Anion	Paul I. Kimmel and Herbert L. Strauss	2813
A Procedure for Determining the Absorption Spectra of Mixed Photochromic Isomers Not Requiring Their Separation	Joseph Blanc and Daniel L. Ross	2817
The Pressure Dependence of the Decomposition of the Isopropoxyl Radical	M. J. Yee Quee and J. C. J. Thynne	2824

The Extraction of Tetraheptylammonium Fluoride and the Solvation of the Fluoride Ion	D. J. Turner, A. Beck, and R. M. Diamond	2831
The Crystal Structure of 1,8-Diazacyclotetradecane-2,7-dione, a Cyclic Monomeric Model of Nylon 66	Maurits G. Northolt and Leroy E. Alexander	2838
Realization of Quantitative Differential Thermal Analysis. II. A Solid-Gas Reaction	D. M. Speros and R. L. Woodhouse	2846
Photolysis of Alcohols Adsorbed on Alumina as Studied by Electron Spin Resonance	Yoshio Ono and Tominaga Keii	2851
The Adsorption and Oxidation of Hydrocarbons on Noble Metal Electrodes. VII. Oxidative Adsorption of Methane on Platinum Electrodes	A. H. Taylor and S. B. Brummer	2856
Adsorption of DNA at the Air-Water Interface	M. A. Frommer and I. R. Miller	2862
Ion-Mobility Measurements of Inorganic and Organic Phosphorus Compounds	Morton R. Kagan and George G. Guilbault	2867
Studies of Membrane Phenomena. VII. Effective Charge Densities of Membrane	M. Yuasa, Y. Kobatake, and H. Fujita	2871
Electrical Potentials of Glass Electrodes in Molten Salts.	R. H. Doremus	2877
Thermal Isomerization of Hexafluorobicyclo[2.2.0]hexa-2,5-diene	Ivan Haller	2882
Ion Exchange in Molten Salts. I. The Ion-Exchange Properties of Sodium Zeolite A in Molten NaNO_3 ; Exchange Reactions with Alkali Metal, Thallium, and Silver Cations	M. Liquornik and Y. Marcus	2885
The Rate of Shear Dependence of the Intrinsic Viscosity of Monodisperse Polymer	Ichiro Noda, Yoshihiko Yamada, and Mitsuru Nagasawa	2890
Pendular-Ring Condensation on Teflon Powders	William H. Wade and James W. Whalen	2898
Electrode Potentials and Thermodynamic Data for Aqueous Ions. Copper, Zinc, Cadmium, Iron, Cobalt, and Nickel	J. W. Larson, P. Cerutti, H. K. Garber, and L. G. Hepler	2902
Infrared Studies of Amine Complexes with Some Organophosphorus Compounds	Sanji Nishimura and Norman C. Li	2908
Excitation of Violanthrone by Singlet Oxygen. A Chemiluminescence Mechanism	E. A. Ogryzlo and A. E. Pearson	2913
The Effect of Fluoride on Surface "Acid" Sites on γ -Alumina and Silica-Alumina	J. B. Peri	2917
The Surface Structure of Silica Gel	J. B. Peri and A. L. Hensley, Jr.	2926
Solvent Effects on Aromatic Chromophores and Their Relation to Ultraviolet Difference Spectra of Proteins	D. A. Chignell and W. B. Gratzer	2934
A Thermochemical Test of Interatomic Potential Functions for Hydrocarbons.	J. E. Mark	2941
Pulse Radiolysis Studies. XII. Kinetics and Spectra of the Cyclohexadienyl Radicals in Aqueous Benzoic Acid Solution	R. Wander, P. Neta, and Leon M. Dorfman	2946
Carbonium Ion Salts. XII. Thermodynamic and Infrared Spectral Studies on Hydroxytropylium Halide Hydrates	Kenneth M. Harmon and Thomas T. Coburn	2950
Dependence of sp^3 Geminal Coupling Constants in Acetal and Some Haloacetals on Solvent and Concentration	Lana S. Rattet, Ashley D. Williamson, and J. H. Goldstein	2954
Electric Conductance and pH Measurements of Isoionic Salt-Free Bovine Mercaptalbumin Solutions. An Evaluation of Root-Mean-Square Proton Fluctuations	Leonard S. Baskin	2958
An Electron Spin Resonance Study of the Dinitrogen Tetroxide-Nitrogen Dioxide System	David W. James and Robert C. Marshall	2963
Thermodynamic Properties of Nonaqueous Solutions. IV. Free Energies and Entropies of Solvation of Some Alkali Metal Halides in N,N -Dimethylformamide	Cecil M. Criss and Eugene Luksha	2966
Thermodynamic Properties of Nonaqueous Solutions. V. Ionic Entropies: Their Estimation and Relationship to the Structure of Electrolytic Solutions	Cecil M. Criss, Robert P. Held, and Eugene Luksha	2970
The Ion-Selective Properties of Sintered Porous Glass Membranes	I. Altug and M. L. Hair	2976
Pure Quadrupole Resonance of Nitrogen-14 in Some Metal Cyano Complexes	Ryuichi Ikeda, Daiyu Nakamura, and Masaji Kubo	2982
The Absorption of Iodine by Perylene	Carolus M. Cobb and Elbridge B. Wallis	2986
Polymer Studies by Gel Permeation Chromatography. III. Polymerization Initiated by Azobisisobutyronitrile	James A. May, Jr., and William B. Smith	2993
Solubility and Thermodynamics of Solution of Argon in the Water-Ethylene Glycol System	A. Ben-Naim	2998

Friction Constants for Fused Salts	Graham Morrison and John E. Lind, Jr.	3001
Chronopotentiometric Measurements of Chemical Reaction Rates. II. Kinetics and Mechanism of the Dehydration of <i>p</i> -Hydroxyphenylhydroxylamine	Henry N. Blount and Harvey B. Herman	3006
The Formation of Phenol and Nitrogen by a Negative Ion-Molecule Chain Reaction on Irradiation of Gaseous Benzene-Nitrous Oxide Mixtures	Stefan J. Rząd and John M. Warman	3013
Energy Transfer and Quenching of Triplet States by Chromium(III) Complexes	D. J. Binet, Edward L. Goldberg, and Leslie S. Forster	3017
The Effect of Structure-Making and -Breaking Solutes on the Temperature of Maximum Density of Water	A. J. Darnell and J. Greyson	3021
Kinetics of Chlorine Oxide Reactions. I. The Reaction of Oxygen Atoms with Cl ₂ O	C. G. Freeman and L. F. Phillips	3025
Kinetics of Chlorine Oxide Reactions. II. The Reaction of Nitrogen Atoms with Cl ₂ O	C. G. Freeman and L. F. Phillips	3028

NOTES

Kinetics of Chlorine Oxide Reactions. III. The Reaction of Hydrogen Atoms with Cl ₂ O	C. G. Freeman and L. F. Phillips	3031
The Temperature of Maximum Density of Heavy Water Solutions	A. J. Darnell and J. Greyson	3032
A Modified VWJ Equation for Calculating the Totality of States of a Collection of Harmonic Oscillators	James C. Tou and Austin L. Wahrhaftig	3034
Circular-Dichroism Pattern of Methylpyrrolidone Can Resemble That of the α Helix	Dan W. Urry	3035
Comments on the Planarity of Dinitrogen Tetroxide	Thomas F. Redmond and Bradford B. Wayland	3038
Ionization and Dissociation of the Alkali Halides by Electron Impact	H. Bloom, J. W. Hastie, and J. D. Morrison	3041
π Bonding by Germanium and the Ultraviolet Spectra of Some Phenylgermanes	James M. Meyer and A. L. Allred	3043
Reaction Rate and Dissociation of Sulfuric Acid	O. Redlich and W. E. Gargrave	3045
Gas-Phase Far-Ultraviolet Absorption Spectrum of Hydrogen Bromide and Hydrogen Iodide	B. J. Huebert and R. M. Martin	3046
Volume Changes on Mixing Solutions of Potassium Halides and Symmetrical Tetraalkylammonium Halides. Evidence for Cation-Cation Interaction. A Correction and Further Comments	Wen-Yang Wen, Kenichi Nara, and R. H. Wood	3048
The Substitution of Energetic Chlorine Atoms for Hydrogen Atoms in Butyl Chlorides	Chien M. Wai and F. S. Rowland	3049
Mercury-Photosensitized Decomposition of Acetaldehyde. Evidence for a Two-Quantum Process	A. S. Buchanan and J. A. McRae	3052
Thermodynamics of Aqueous Mixtures of Electrolytes and Nonelectrolytes. V. Enthalpies of Transfer in the Limiting Region at 25°	J. H. Stern, J. Lazartie, and D. Fost	3053
The Thermal Decomposition of Perfluoropropene	Richard A. Matula	3054
Nuclear Magnetic Resonance Study of Micelle Formation in Sodium Perfluorocaprylate and -propionate	Rizwanul Haque	3056
Contact Charge-Transfer Spectra of Iodine in Some Hydrocarbon Solvents	Larry M. Julien and Willis B. Person	3059
Tropylium Ion Formation in the Mass Spectra of Stereoisomeric Pentacyclo[8.2.1.1 ^{4,7} .0 ^{2,3} .0 ^{3,8}]tetradecanes	G. G. Meisels and D. R. Arnold	3061
Magnetic Resonance Studies of Outer-Sphere Ion-Pair Formation in <i>N,N</i> -Dimethylformamide Solutions of Aluminum(III) Halides	W. G. Movius and N. A. Matwiyoff	3063
Spectroscopic Evidence for Brønsted Acidity in Partially Dehydrated Group Ia Forms of Zeolites X and Y	Yoshihiro Watanabe and Henry W. Habgood	3066
Observation of a Minimum in the Kerr Constants of Light and Heavy Water Near 30°	Yeong-ji Chen and William H. Orttung	3069

COMMUNICATIONS TO THE EDITOR

Comment on the Electrochemiluminescence from Phenanthrene Solutions.	C. A. Parker and G. D. Short	3071
The Reaction of Hydrogen Zeolite Y with Ammonia at Elevated Temperatures	George T. Kerr and George F. Shipman	3071

AUTHOR INDEX

- Alexander, L. E., 2838
 Allred, A. L., 3043
 Altug, I., 2976
 Arnold, D. R., 3061
 Assarsson, P., 2710
- Baret, J. F., 2755
 Baskin, L. S., 2958
 Beck, A., 2831
 Ben-Naim, A., 2998
 Binet, D. J., 3017
 Blanc, J., 2817
 Bloom, H., 2706, 3041
 Blount, H. N., 3006
 Brummer, S. B., 2856
 Buchanan, A. S., 3052
- Cadenhead, D. A., 2775
 Cerutti, P., 2902
 Chaffee, R. G., 2750
 Chen, Y., 3069
 Chignell, D. A., 2934
 Christensen, J. J., 2720
 Cobb, C. M., 2986
 Coburn, T. T., 2950
 Covington, A. K., 2759
 Criss, C. M., 2966, 2970
- Darnell, A. J., 3021, 3032
 Diamond, R. M., 2831
 Doremus, R. H., 2877
 Dorfman, L. M., 2946
- Eatough, D., 2720
 Eirich, F. R., 2710
 Eyring, H., 2730
- Fletcher, A. N., 2742
- Forsén, S., 2805
 Forslind, E., 2805
 Forster, L. S., 3017
 Fost, D., 3053
 Freeman, C. G., 3025, 3028, 3031
 Frommer, M. A., 2862
 Fujita, H., 2871
- Garber, H. K., 2902
 Gargrave, W. E., 3045
 Gerhold, G. A., 2737
 Goldberg, E. L., 3017
 Goldstein, J. H., 2954
 Gratzer, W. B., 2934
 Gregory, N. W., 2697
 Greyson, J., 3021, 3032
 Guidelli, R., 2782
 Guilbault, G. G., 2867
- Habgood, H. W., 3066
 Hair, M. L., 2976
 Haller, I., 2882
 Haque, R., 3056
 Harmon, K. M., 2950
 Hastie, J. W., 2706, 3041
 Held, R. P., 2970
 Hensley, A. L., Jr., 2926
- Hepler, L. G., 2902
 Herman, H. B., 3006
 Huebert, B. J., 3046
- Ikeda, R., 2982
 Iwamoto, R. T., 2764
 Izatt, R. M., 2720
- James, D. W., 2963
- Johannson, O. K., 2750
 Julien, L. M., 3059
- Kagan, M. R., 2867
 Kalantar, A. H., 2801
 Keii, T., 2851
 Kemula, A., 2764
 Kerr, G. T., 3071
 Kimmel, P. I., 2813
 Knözinger, H., 2770
 Kobatake, Y., 2871
 Kubo, M., 2982
- Lacefield, R. M., 2750
 Larson, J. W., 2902
 Lazartic, J., 3053
 Li, N. C., 2908
 Lilley, T. H., 2759
 Lind, J. E., Jr., 3001
 Lindman, B., 2805
 Liquornik, M., 2885
 Luksha, E., 2966, 2970
- Marcus, Y., 2885
 Mark, J. E., 2941
 Marshall, R. C., 2963
 Martin, R. M., 3046
 Matula, R. A., 3054
 Matwiyoff, N. A., 3063
 May, J. A., Jr., 2993
 Maycock, J. N., 2798
 McRae, J. A., 3052
 Meares, P., 2789
 Meisels, G. G., 3061
 Meyer, J. M., 3043
 Mickewich, D., 2703
 Miller, E., 2737
 Miller, I. R., 2862
 Morris, E. R., 3063
- Morrison, G., 3001
 Morrison, J. D., 3041
 Movius, W. G., 3063
- Nagasawa, M., 2890
 Nakamura, D., 2982
 Nara, K., 3048
 Neta, P., 2946
 Nishimura, S., 2908
 Noda, I., 2890
 Northolt, M. G., 2838
- Ogryzlo, E. A., 2913
 Ono, Y., 2851
 Orttung, W. H., 3069
- Pai Verneker, V. R., 2798
 Parker, C. A., 3071
 Passchier, A. A., 2697
 Pearson, A. E., 2913
 Peri, J. B., 2917, 2926
 Person, W. B., 3059
 Phillips, L. F., 3025, 3028, 3031
 Piccardi, G., 2782
- Quee, M. J. Y., 2824
- Rattet, L. S., 2954
 Redlich, O., 3045
 Redmond, T. F., 3038
 Robinson, R. A., 2759
 Ross, D. L., 2817
 Rowland, F. S., 3049
 Rzad, S. J., 3013
- Scheglila, A., 2770
 Shipman, G. F., 3071
- Short, G. D., 3071
 Smith, W. B., 2993
 Speros, D. M., 2846
 Stark, F. O., 2750
 Stern, J. H., 3053
 Strauss, H. L., 2813
- Taylor, A. H., 2856
 Thain, J. F., 2789
 Thynne, J. C. J., 2824
 Tien, H. T., 2723
 Tou, J. C., 3034
 Turkevich, J., 2703
 Turner, D. J., 2831
- Urry, D. W., 3035
- Vogel, G. E., 2750
- Wade, W. H., 2898
 Wagner, N. J., 2775
 Wahrhaftig, A. L., 3034
 Wai, C. M., 3049
 Wallis, E. B., 2986
 Wander, R., 2946
 Warman, J. M., 3013
 Watanabe, Y., 3066
 Watson, A. M., 2770
 Watson, J. A., Jr., 2730
 Wayland, B. B., 3038
 Wen, W.-Y., 3048
 Whalen, J. W., 2898
 Williamson, A. D., 2954
 Wood, R. H., 3048
 Woodhouse, R. L., 2846
- Yamada, Y., 2890
 Yuasa, M., 2871
- Zandler, M. E., 2730

NOTICE TO AUTHORS

I. General Considerations

The Journal of Physical Chemistry is devoted to reporting both experimental and theoretical research dealing with fundamental aspects of physical chemistry. Space limitations necessitate giving preference to research articles dealing with previously unanswered basic questions in physical chemistry. Acceptable topics are those of general interest to physical chemists, especially work involving new concepts, techniques, and interpretations. Research that may lead to reexaminations of generally accepted views is, of course, welcome.

The Journal of Physical Chemistry publishes three types of manuscripts: *Articles*, *Notes*, and *Communications to the Editor*.

Authors reporting data should include, if possible, an interpretation of the data and its relevance to the theories of the properties of matter. However, the discussion should be concise and to the point and excessive speculation is to be discouraged. Papers reporting redeterminations of existing data will be acceptable only if there is reasonable justification for repetition: for example, if the more recent or more accurate data lead to new questions or to a reexamination of well known theories. Manuscripts that are essentially applications of chemical data or reviews of the literature are, in general, not suitable for publication in *The Journal of Physical Chemistry*. Detailed comparisons of methods of data analysis will be considered only if the paper also contains original data, or if such comparison leads to a genesis of new ideas.

Authors should include an introductory statement outlining the scientific rationale for the research. The statement should clearly specify the questions for which answers are sought and the connection of the present work with previous work in the field. All manuscripts are subject to critical review. It is to be understood that the final decision relating to a manuscript's suitability rests solely with the editorial staff.

Symposium papers are sometimes published as a group, but only after special arrangement with the editor.

Authors' attention is called to the "Handbook for Authors," available from the Special Issues Sales Department, American Chemical Society, 1155 Sixteenth St., N.W., Washington, D. C. 20036, in which pertinent material is to be found.

II. Types of Manuscripts

A. *Articles* should cover their subjects with thoroughness, clarity and completeness. However, authors should also strive to make their *Articles* as concise as possible, avoiding unnecessary historical background. Abstracts to *Articles* should be brief—300 words is a maximum—and should serve to summarize the significant data and conclusions. The abstract should convey the essence of the *Article* to the reader.

B. *Notes*. Papers submitted in the category of *Notes* should report work that represents a complete and self-contained study of limited nature. *Notes* are a luxury in the present scientific literature; authors should not use a *Note* to report work that is part of a continuing study. *Notes* are not to be used for reporting preliminary results; reports of such work should be postponed until the work is completed or should be submitted as *Communications* if the results are of immediate or unusual interest to physical chemists. The same criteria of suitability for publication apply to *Notes* as to *Articles* (see General Considerations). The length of a *Note*, including tables, figures, and text, must not exceed 1.5 journal pages (1500 words or the equivalent). A *Note* should not be accompanied by an abstract.

C. *Communications to the Editor* are of two types, *Letters* and *Comments*. Both types are restricted to three-quarters of a page (750 words or the equivalent) including tables, figures and text, and both types of *Communications* are subject to critical review, but special efforts will be made to expedite publication.

Letters should report preliminary results whose immediate availability to the scientific community is deemed important, and whose topic is timely enough to justify the double publication that usually results from the publication of a *Letter*.

Comments include significant remarks on the work of others. The editorial staff will generally permit the authors of the work being discussed to reply.

III. Introduction

All manuscripts submitted should contain brief introductory remarks describing the purpose of the work and giving sufficient background material to allow the reader to appreciate the state-of-knowledge at the time when the work was done. The introductory remarks in an *Article* should constitute the first section of the paper and should be labeled accordingly. In *Notes* and *Communications*, the introductory material should not be in such a separate section. To judge the appropriateness of the manuscript for *The Journal of Physical Chemistry*, the editorial staff will place considerable weight on the author's intentions as stated in the Introduction.

IV. Functions of Reviewers

The editorial staff requests the scientific advice of reviewers who are active in the area of research covered by the manuscript. The reviewers act only in an advisory capacity and the final decision concerning a manuscript is the responsibility of the editorial staff. The reviewers are asked to comment not only on the scientific content, but also on the manuscript's suitability for *The Journal of Physical Chemistry*. With respect to *Communications*, the reviewers are asked to comment specifically on the urgency of publication. All reviews are anonymous and the reviewing process is most effective

if reviewers do not reveal their identities to the authors. An exception arises in connection with a manuscript submitted for publication in the form of a comment on the work of another author. Under such circumstances the first author will, in general, be allowed to review the communication and to write a rebuttal, if he so chooses. The rebuttal and the original communication may be published together in the same issue of the journal. Revised manuscripts are generally sent back to the original reviewers, who are asked to comment on the revisions. If only minor revisions are involved, the editorial staff examines the revised manuscript in light of the recommendations of the reviewers and without seeking further opinions. For the convenience of reviewers, authors are advised to indicate clearly, either in the manuscript or in a covering letter, the specific revisions that have been made.

V. Submission of Manuscripts

All manuscripts must be submitted in duplicate, including an original typewritten double-spaced copy. All original data which the author deems pertinent must be submitted along with the manuscript. For example, a paper reporting a crystal structure should include structure factor tables for use by the reviewers. Manuscripts must be submitted on $8\frac{1}{2} \times 11$ in. paper; legal-sized paper is not acceptable. Authors submitting figures must include original drawings or photographs thereof. Xerographic copies of figures are acceptable for review purposes only. Graphs must be black ink on white or blue paper. Lettering at the sides of graphs may be penciled in and will be typeset. Figures and tables should be held to a minimum consistent with adequate presentation of information.

Footnotes and references to the literature should be numbered consecutively within the paper; the number should also be placed in parentheses in the left margin opposite the line in which the reference first appears. A complete list of references should appear at the end of the paper. Initials of the authors referred to in the citations should be included in the complete reference at the back of the paper. Nomenclature should conform to that used in *Chemical Abstracts* and mathematical characters should be underlined for italics, Greek letters should be annotated, and subscripts and superscripts clearly marked.

Papers should not depend for their usefulness on unpublished material, and excessive reference to material in press is discouraged. References not readily available (*e.g.*, private technical reports, preprints, or articles in press) that are necessary for a complete review of the paper must be included with the manuscript for use by the reviewers.

VI. Revised Manuscripts

A manuscript sent back to an author for revision should be returned to the editor within 6 months; otherwise it will be considered withdrawn and treated as a

new manuscript when and if it is returned. Revised manuscripts returned to the editor must be submitted in duplicate, and all changes must be made by typewriter, since handwritten additions or corrections are unacceptable. Unless the changes are very minor, all pages affected by revision must be retyped. If revisions are so extensive that a new typescript of the manuscript is necessary, it is requested that a copy of the original manuscript be submitted along with the revised one.

VII. Supplementary Material

By arrangement with the American Documentation Institute (ADI), supplementary material, such as extensive tables, graphs, spectra, and calculations, can be distributed in the form of microfilms or photoprints readable without optical aids. This material should accompany the manuscript for review by the editors and reviewers. Upon acceptance, it will be sent by the editor to the ADI where it is assigned a document number. A deposit fee of \$2 is required and should be included with the material sent to the editor. The check must be made out to *Chief, Photoduplication Service, Library of Congress*. Further details can be found in the ACS "Handbook for Authors" (1967).

VIII. Proofs and Reprints

Galley proofs, original manuscript, cut copy, and reprint order form are sent by the printer directly to the author who submitted the manuscript. The attention of the authors is directed to the instructions which accompany the proof, especially the requirement that all corrections, revisions, and additions be entered on the proof and not on the manuscript. Proofs should be checked against the manuscript (in particular all tables, equations, and formulas, since this is not done by the editor) and returned as soon as possible. No paper is released for printing until the author's proof has been received. Alterations in an article after it has been set in type are made at the author's expense, and it is understood that by entering such alterations on proofs the author agrees to defray the cost thereof. The filled-out reprint form must be returned with the proof, and if a price quotation is required by the author's organization a request for it should accompany the proof. Since reprinting is generally done from the journal press forms, all orders must be filed before press time. None can be accepted later, unless a previous request has been made to hold the type. Reprint shipments are made a month or more after publication, and bills are issued by the printer subsequent to shipment. Neither the editors nor the Washington office keeps any supply of reprints. Therefore, only the authors can be expected to meet requests for single copies of papers.

A page charge is assessed to cover in part the cost of publication. Although payment is expected, it is not a condition for publication. Articles are accepted or rejected only on the basis of merit, and the editor's decision to publish the paper is made before the charge is assessed. The charge per journal page is \$35.

THE JOURNAL OF PHYSICAL CHEMISTRY

Registered in U. S. Patent Office © Copyright, 1968, by the American Chemical Society

VOLUME 72, NUMBER 5 MAY 15, 1968

The Temperature Variation of the Dipole Moment of *o*-Dimethoxybenzene

by Louis M. DiBello, Helen M. McDevitt, and Dominic M. Roberti¹

Chemistry Department, Villanova University, Villanova, Pennsylvania 19085 (Received January 2, 1968)

The dipole moment of *o*-dimethoxybenzene has been measured over a temperature range of from 25 to 160° for liquid *o*-dimethoxybenzene and over a total range of from -20 to 165° for solutions of *o*-dimethoxybenzene in benzene, decalin, and paraffin oil. The dipole moment increases with temperature with nearly the same slope in all four series of measurements. The dipole moments calculated from measurements on decalin and paraffin oil solutions become constant above 90° at a value below that expected for free rotation. The exclusion of certain rotational positions because of steric factors may account for the difference. The dipole moments of *m*- and *p*-dimethoxybenzene, measured on solutions in decalin, were found to remain constant over the temperature range from 20 to 130°.

Previous studies of *o*-dimethoxybenzene show that, unlike *m*- and *p*-dimethoxybenzene, its electric dipole moment varies with temperature. Mizushima^{2a} reported values of from 1.19 to 1.33 D for solutions of *o*-dimethoxybenzene in an unspecified solvent from 10 to 40°, and Jatkar^{2b} found values from 1.15 to 1.31 D for the liquid from 25 to 85°. In addition, while all three isomers show shortened dielectric relaxation times, interpreted as indicating rotational orientation of the methoxy groups, only the *ortho* isomer showed two separable dispersion regions.³

By choosing solvents with a long liquid range, it has been possible to extend the study of the dipole moments of the dimethoxybenzenes to higher temperatures. This study reveals a change in behavior just beyond the range studied in previous works, *i.e.*, a levelling off of the dipole moment to a constant value at higher temperatures for *o*-dimethoxybenzene in both decalin and paraffin oil.

Additional measurements were made on liquid *o*-dimethoxybenzene, solutions of *o*-dimethoxybenzene in benzene, and solutions of *m*- and *p*-dimethoxybenzene in decalin, all over a range of temperatures.

Experimental Section

o-Dimethoxybenzene was distilled over calcium hydride, and the fraction boiling at 206–207° was taken, giving a refractive index of 1.5319 at 25°. *m*-

Dimethoxybenzene was distilled over calcium hydride, and the fraction boiling at 216–218° was taken, giving a refractive index of 1.5250 at 20°. *p*-Dimethoxybenzene was purified by distillation, giving a melting point of 56.5–57.0°. Paraffin oil, from Fisher Scientific Co., was used as a solvent without further purification. All measurements made use of oil from a single batch, giving a refractive index of 1.4793 at 25°. Benzene was purified by fractional distillation over calcium hydride. Decalin was fractionally distilled over calcium hydride. The fraction boiling from 188 to 189°, with a density of 0.88165 at 25° and a refractive index of 1.4763 at 20°, was analyzed by gas chromatography and found to consist of approximately 60% *cis*- and 40% *trans*-decalin.

Dielectric constants were measured at 1.0 MHz using a General Radio 716-CS1 capacitance bridge with a General Radio 1211-C unit oscillator as the signal source and an Allied Radio R-100A communications receiver, with an S meter, as the null detector. The dielectric cell, similar to that described by Smyth,⁴

(1) Address correspondence to this author at St. Joseph's College, Philadelphia, Pa. 19131.

(2) (a) S. Mizushima, Y. Morino, and H. Okazaki, *Sci. Papers Inst. Phys. Chem. Research (Tokyo)*, **34**, 1147 (1938); (b) S. K. K. Jatkar and C. M. Deshpande, *J. Indian Chem. Soc.*, **37**, 1 (1960).

(3) D. M. Roberti and C. P. Smyth, *J. Amer. Chem. Soc.*, **82**, 2106 (1960).

consists of concentric rhodium-plated brass cylinders enclosed in glass. It is estimated that the apparatus yields a precision of 0.1% in the dielectric constant. General Electric No. 10 insulation oil was used in the constant-temperature bath. Low temperatures were attained by immersing a bulb containing Dry Ice and acetone into the bath.

Measurements of density, using an Ostwald pycnometer, and refractive index, with an Abbe refractometer, were made for the liquid and for each solution over a range of temperatures from 25 to 50°. Extrapolated values were used in calculation of dipole moments at other temperatures.

The dipole moment of the liquid was calculated with the Onsager equation,⁵ using n_D^2 for ϵ_∞ . The dipole moments in nonpolar solvents were calculated by the method of Halverstadt and Kumler,⁶ using five solutions and calculating the slopes by a least-squares analysis. The solutions had the following ranges of weight fractions of *o*-dimethoxybenzene for each solvent: benzene, 0.01–0.16; paraffin oil, 0.003–0.05; decalin, 0.01–0.06. The ranges of weight fractions in decalin were from 0.024 to 0.118 for *m*-dimethoxybenzene and from 0.0057 to 0.069 for *p*-dimethoxybenzene.

Results and Discussion

Values of the dipole moment of *o*-dimethoxybenzene are plotted against temperatures in Figure 1. Measurements in benzene give values of 1.30 D at 20° and 1.32 D at 25°, identical with values reported by Klages⁷ and Weissberger,⁸ respectively. In all four series the dipole moment increases with temperature at approximately the same rate. The slopes for the range between 25 and 60° are 0.0039, 0.0038, 0.0043, and 0.0038 for the liquid, benzene, paraffin oil, and decalin, respectively. While there may be some error in the slopes for the solutions owing to variation of the solvent effect with temperature,⁹ the similarity of the slope for the solutions and for the liquid seems to eliminate a role for the solvent as an explanation of the temperature variation.

The dipole moment reaches a constant value above 90° at 1.58 D in paraffin oil and 1.64 D in decalin. The dipole moment of the liquid has not yet levelled off at the highest temperature measured, 160°, where its value is 1.63 D.

The dipole moments of *m*- and *p*-dimethoxybenzene in decalin were found to be constant over the range from 20 to 130°. Values from measurements made on solutions in decalin have not previously been reported, but the values of 1.48 D for the *meta* and 1.84 D for the *para* isomer compare reasonably well with values reported for the other solvents.^{2a,7,10,11}

The temperature variation of a dipole moment, for example, of 1,2-dichloroethane,¹² has been interpreted as resulting from the effect of temperature on the relative numbers of several conformers of different polarity.

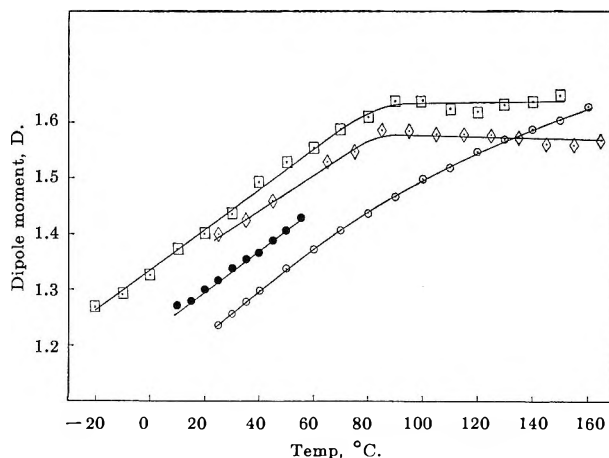


Figure 1. The dependence of the dipole moment of *o*-dimethoxybenzene on temperature for measurements of liquid *o*-dimethoxybenzene (open circles) and solutions of *o*-dimethoxybenzene in benzene (closed circles), paraffin oil (diamonds), and decalin (squares).

The observed dipole moment would be the statistical average of the dipole moments of the conformers. At sufficiently high temperatures, the potential energy barriers hindering interconversion of the conformers are surmounted, and a state of essentially free rotation results. The observed dipole moment will then remain constant with further increase in temperature.

The free-rotation value of the dipole moment may be calculated by the method of Eyring.¹³ For *o*-dimethoxybenzene, the calculated free-rotation value¹⁴ is 1.93 D, still above the maximum values observed in this study.

The results of the present study indicate that there are two separate phenomena to be considered for *o*-dimethoxybenzene. There is first a temperature-dependent restriction on rotation which reduces the contribution of the more polar conformers at lower temperatures. Since this temperature dependence is not observed with the *meta* and *para* isomers, it presumably involves relatively short-range interactions, possibly electrostatic interactions between the adjacent methoxy groups.

An additional restriction on rotation must be assumed to account for the observation that the maxi-

(4) C. P. Smyth and S. O. Morgan, *J. Amer. Chem. Soc.*, **50**, 1547 (1928).

(5) L. Onsager, *ibid.*, **58**, 1486 (1936).

(6) I. F. Halverstadt and W. K. Kumler, *ibid.*, **64**, 2988 (1942).

(7) G. Klages and E. Klopping, *Z. Elektrochem.*, **57**, 369 (1953).

(8) A. Weissberger and R. Sangewald, *Physik. Z.*, **30**, 792 (1929).

(9) H. O. Jenkins, *Trans. Faraday Soc.*, **30**, 739 (1934).

(10) G. Klages and A. Zentek, *Z. Naturforsch.*, **16a**, 1016 (1961).

(11) M. Aroney, R. J. W. Le Fevre, and S. Chang, *J. Chem. Soc.*, 3173 (1960).

(12) C. P. Smyth, *J. Amer. Chem. Soc.*, **46**, 2151 (1924).

(13) H. Eyring, *Phys. Rev.*, **39**, 746 (1932).

(14) C. P. Smyth, "Dielectric Behavior and Structure," McGraw-Hill Book Co., Inc., New York, N. Y., 1955, p 371.

imum value of the dipole moment observed for *o*-dimethoxybenzene in the two solutions which showed a levelling was still considerably smaller than the value calculated for free rotation. Examination of molecular scale models shows that certain rotational positions are restricted sterically. The *cis-cis* position in which both methoxy carbons are adjacent and coplanar with the benzene ring is most severely restricted. In addition, other positions in which the methoxy carbons

are coplanar with the ring are somewhat restricted by the ring hydrogens. Reduction of the contribution of these rotational positions may account for the difference between the observed maximum dipole moment and the calculated free rotation value.

Acknowledgment. The authors wish to acknowledge the contribution of Villanova University in providing financial support for carrying out this study.

The Calculation of Cohesive and Adhesive Energies from Intermolecular Forces at a Surface

by J. F. Padday and N. D. Uffindell

Research Laboratories, Kodak Ltd., Wealdstone, Harrow, Middlesex, England (Received November 15, 1967)

Surface tensions of the *n*-alkanes and interfacial tensions between the *n*-alkanes and water have been calculated. The calculations use a modified form of the Moelwyn-Hughes' equation for the dispersion interaction between two particles, the integration method of Hamaker to derive the total interaction across a plane surface, the geometric mean relationship of Good and Girifalco for the interaction of two dissimilar phases, and an assumption that the entropy of surface formation equals the difference between the interaction energy so calculated and the total internal energy of surface formation. The calculated surface tensions of the *n*-alkanes are compared with and agree well with experimentally determined values; also, some of their calculated interfacial-tension, contact-angle, and spreading-coefficient measurements with water all agree with the corresponding experimental values. For other systems, calculations are limited to the contribution of the dispersion forces to the total interaction of the system.

Introduction

The work of cohesion, W_c , and the work of adhesion, W_a , are defined by Young¹ and Dupré² by the equations

$$W_c = 2\gamma_L \quad (1)$$

$$W_a = \gamma_L + \gamma_s + \gamma_{SL} \quad (2)$$

W_c and W_a are both surface free energy terms of an idealized system and in practice their values have been obtained by substituting appropriate surface and interfacial tensions into eq 1 and 2.³ Such substitution is unjustified for almost all real solid-liquid systems because the surface tension is likely to vary from one part of the surface to another and because some elastic deformation of the bulk solid is inevitable. These calculations are confined to pure liquids and to low-energy hydrocarbon surfaces where such effects, although present, are unlikely to produce significant errors.

The interaction energy W_{12} arising from physical or van der Waals forces between two particles is given by

$$W_{12} = W_{12}^d + W_{12}^D + W_{12}^K \quad (3)$$

where W_{12}^d is the dispersion contribution and W_{12}^D and W_{12}^K the respective Debye and Keesom contributions to the total interaction energy. In this treatment, the calculations are restricted to nonpolar systems in which the Debye and Keesom forces are zero.

The dispersion interaction energy, W_{12}^d , between two particles is the decrease in their potential energy arising from only dispersion forces when bringing them from an infinite distance of separation to a distance r apart and is given by Moelwyn-Hughes⁴ as

(1) T. Young, "Collected Works," Vol. 1, G. Peacock, Ed., John Murray, London, 1855.

(2) A. Dupré, "Theorie Mecanique de la Chaleur," Gauthier-Villars, Paris, 1869, p 369.

(3) N. K. Adam, "The Physics and Chemistry of Surfaces," 3rd ed, Oxford University Press, London, 1941, p 2; F. O. Koenig, *Z. Elektrochem.*, **57**, 361 (1953); R. E. Johnson, *J. Phys. Chem.*, **63**, 1655 (1959).

(4) E. A. Moelwyn-Hughes, "Physical Chemistry," 2nd ed, Pergamon Press Ltd., London, 1961, p 392.

$$W_{12}^d = -\frac{3he\alpha_0^{1/2}(SZ)^{1/2}}{8\pi(m)^{1/2}r^6} \quad (4)$$

obtained by replacing the ν_0 of Slater and Kirkwood's⁵ expression with $\nu_0 S^{1/2}$ where ν_0 is given by

$$\frac{e}{2\pi(m\alpha_0)^{1/2}}$$

Moelwyn-Hughes found S , the effective number of dispersion electrons, to be smaller than Z . We have taken the value of S in these calculations to be the valency or valencies of the atom or atoms involved.

To obtain the total interaction arising from dispersion forces at the surface of a macroscopic system, we calculate the decrease in potential energy, W_m^d , of unit area of a system in which two semiinfinite and parallel surfaces of a liquid, separated by a large or infinite distance, are brought together to a distance at which the surface region is indistinguishable from the bulk liquid. W_m^d is thus obtained by summing the energy change of every pair interaction acting across the semiinfinite surfaces, using eq 4 to obtain the coefficient, β , of $1/r^6$ for the interaction of a single pair.

To obtain W_m^d , eq 4 was integrated according to the method of Hamaker⁶ (see Overbeek⁷) to give

$$W_m^d = \frac{\pi N_0^2 \beta_{11}}{12r_{11}^2} = -\frac{A_{11}}{12\pi r_{11}^2} \quad (5)$$

where β_{11} is the coefficient of $1/r^6$ of eq 4 and A is the Hamaker constant. This method of calculation is preferred to that of Fowkes,⁸ who integrated London's⁹ equation for surface volume elements only.

To obtain the total interaction energy of a system in which the semiinfinite surfaces of two different and mutually insoluble materials are brought together, the β_{11} coefficient of eq 5 is replaced by the coefficient β_{12} for the interaction between two liquids (or phases) using the geometric mean relationship of van Laar¹⁰ and Good and Girifalco¹¹

$$\beta_{12} = (\beta_{11}\beta_{22})^{1/2} \quad (6)$$

Relationship between the Total Interaction Potential and Surface Tension

The total interaction energy derived by eq 5 is the increase in potential energy of the system when two unit areas of liquid surface are formed from bulk liquid. It represents the work done on the system. During the process of separation no account has been taken of the equilibration of the surface region. It has been assumed that the bulk structure of the liquid phase is maintained right up to the surface and is retained at all stages of surface formation. The structure of the surface region is unlikely to be the same as the bulk due to the imbalance of attractive forces; therefore, further energy must enter or leave the system as the freshly formed surfaces approach equilibrium.

The algebraic sum of these two energies, W_m^d and Q (the quantity of heat entering the system to obtain equilibrium), divided by 2 gives the increase in internal energy, E^d , for surface formation

$$E^d = \frac{W_m^d + Q}{2} \quad (7)$$

where

$$E^d - TS = \gamma \quad (8)$$

Thus to obtain the surface tension, γ , from W_m^d it is necessary to know Q (a quantity almost impossible to measure) and S , the entropy of surface formation.

It is implicit in Fowkes's⁸ work that the quantities $Q/2$ and TS are numerically equal and cancel each other, but no clear reason for this has been given.

In this work we have found, like Fowkes, that the potential energy term, $W_m^d/2$, equals the surface tension for a surprising number of systems over relatively wide temperature ranges and we will, therefore, make the same assumption.

A second assumption to be made is that the calculated value of the surface free energy, *i.e.*, the surface tension, applies to solid as well as liquid surfaces. Using this assumption it is now possible to calculate such properties as contact angle, spreading coefficient, and work of adhesion according to the relationships given below. However, to avoid writing out all the components of the coefficient $1/r_{11}^2$ in the expression for W_m^d , the Hamaker constant, A_{LL} , will be used, as in eq 5, for the interaction between two like liquid particles and A_{LS} for that between two unlike particles of liquid and solid.

Relationships between the Hamaker Constant and Wetting Properties

The energy of interaction, W_m^d , arising from dispersion forces between two semiinfinite plane surfaces of a liquid, has been derived above in eq 5. The relationships between this interaction energy and wetting properties may be summarized as follows.

(i) *Surface Tension of a Pure Liquid*, γ_L . Within the assumption, eq 5, 7, and 8 may be written as

$$\frac{1}{2}W_m^d = \frac{A_{LL}}{24\pi r_{LL}^2} = \gamma_L \quad (9)$$

(5) J. C. Slater and J. G. Kirkwood, *Phys. Rev.*, **37**, 682 (1931).

(6) H. C. Hamaker, *Physica*, **4**, 1058 (1937).

(7) J. Th. G. Overbeek, "Colloid Science," Vol. I, H. R. Kruyt, Ed., Elsevier Publishing Co., The Netherlands, 1952, Chapter 6.

(8) F. M. Fowkes, *Ind. Eng. Chem.*, **56** (12), 40 (1964); *Advances in Chemistry Series*, No. 43, American Chemical Society, Washington, D. C., 1964, p 99.

(9) F. London, *Z. Phys.*, **63**, 245 (1930); *Trans. Faraday Soc.*, **33**, 8 (1937).

(10) J. J. van Laar, "Die Thermodynamik einheitlicher Stoffe und binärer Gemische," Noordhoff, Denmark, 1936.

(11) R. J. Good and L. A. Girifalco, *J. Phys. Chem.*, **64**, 561 (1960).

where

$$A_{LL} = \pi^2 N_{LL}^2 \beta_{LL} = \frac{3\pi N_{LL}^2 h e \alpha_0^{1/2} (SZ)^{1/2}}{8(m)^{1/2}} \quad (10)$$

In practice both N_{LL} and r_{LL} are obtained from the density, ρ_L , of the liquid for the temperature at which A_{LL} is required. The symbols on the right-hand side of eq 10 are all identified in the Glossary.

(ii) *Interfacial Tension between Two Liquids or a Solid and a Liquid*, γ_I . If mutual insolubility is assumed, the interfacial tension may be expressed using eq 6 and 9 to give

$$\gamma_I = \frac{A_{SS}}{24\pi r_{SS}^2} + \frac{A_{LL}}{24\pi r_{LL}^2} - 2 \left[\frac{A_{SS}A_{LL}}{(24\pi)^2 \left(\frac{r_{SS} + r_{LL}}{2}\right)^4} \right]^{1/2} \quad (11)$$

This equation has also been used for water in contact with a nonpolar surface⁸ in which case

$$\gamma_I = \frac{A_{SS}}{24\pi r_{SS}^2} + \gamma_L - 2 \left[\frac{A_{SS}A_{LL}^d}{(24\pi)^2 \left(\frac{r_{SS} + r_{LL}}{2}\right)^4} \right]^{1/2} \quad (12)$$

where A_{LL}^d is the dispersion contribution to the total energy of water and γ_L is the true experimental surface tension. The terms A_{SS} and r_{SS} although designated to describe the properties of a solid surface may, of course, be those of a second pure liquid.

Because r_{SS} and r_{LL} are often not very different, an approximation is sometimes used⁸

$$\gamma_I = \gamma_S + \gamma_L - 2(\gamma_S^d \gamma_L^d)^{1/2} \quad (13)$$

where γ_S^d and γ_L^d are the hypothetical surface tensions the solid and liquid would possess if only dispersion forces acted at their respective surfaces.

(iii) *Contact Angle*, θ . Combining the Young equation

$$\gamma_S - \gamma_I = \gamma_L \cos \theta \quad (14)$$

with eq 10 and 11 gives

$$\cos \theta = -1 + 2 \left[\frac{A_{SS}A_{LL}}{(24\pi)^2 \left(\frac{r_{SS} + r_{LL}}{2}\right)^4} \right]^{1/2} \gamma_L \quad (15)$$

When this equation is used for a system including a polar liquid or water, A_{LL} refers to the dispersion contribution A_{LL}^d and γ_L is the total surface tension of the liquid.

(iv) *Spreading Coefficient*, S_c . The spreading coefficient is defined by

$$S_c = \gamma_S - \gamma_I - \gamma_L \quad (16)$$

Therefore, from eq 10, 11, and 16

$$S_c = -2\gamma_L + 2 \left[\frac{A_{SS}A_{LL}}{(24\pi)^2 \left(\frac{r_{SS} + r_{LL}}{2}\right)^4} \right]^{1/2} \quad (17)$$

(v) *Wetting Energy or Adhesion Tension*, W_e . The wetting energy is defined by the equation

$$W_e = \gamma_L \cos \theta \quad (18)$$

Therefore

$$W_e = -\gamma_L + 2 \left[\frac{A_{SS}A_{LL}}{(24\pi)^2 \left(\frac{r_{SS} + r_{LL}}{2}\right)^4} \right]^{1/2} \quad (19)$$

(vi) *Work of Adhesion*, W_a . The work of adhesion is defined by

$$W_a = \gamma_L (\cos \theta + 1) \quad (20)$$

Therefore

$$W_a = 2 \left[\frac{A_{SS}A_{LL}}{(24\pi)^2 \left(\frac{r_{SS} + r_{LL}}{2}\right)^4} \right]^{1/2} \quad (21)$$

Equations 15, 17, and 19 all contain the work of adhesion. In order to simplify calculations the expression for the work of adhesion may be replaced by the geometric mean of the dispersion contribution to the surface tension without serious error, as in the derivation of eq 13.

These relationships have been used to calculate the surface properties of systems which rely on dispersion forces alone. These relationships may also be used to calculate the surface properties of systems in which one component is polar by estimating the contribution due to dispersion forces to obtain the work of adhesion and using the experimental value of the surface tension for the total of all contributions.

To use the above equations it is necessary to calculate first the Hamaker constants from values of α_0 , S , Z , and N_{11} . The value of N_{11} equals $(1/r_{11}^3)$ and is obtained from ρ , the density, according to

$$N_{11} = \frac{\rho N_A}{M} \quad (22)$$

For large molecules the interparticle distance r_{11} will vary for each part of the molecule; therefore, in the subsequent calculations with the n -alkanes we have calculated the Hamaker constants on the basis that CH_2 or CH_3 groups are the basic volume elements or particles.

Calculation of the Surface Tension of n -Alkanes

The surface tensions of the n -alkanes at 20° calculated using eq 9 are given in Table I. To illustrate the difference between taking the CH_2 unit and the whole molecule as the volume element, n -hexane is taken as an example. The values of the various terms in eq 9

Table I: Surface Tensions of the *n*-Alkanes, C_nH_{2n+2}

<i>n</i>	ρ (20°), ^a g/ml	$10^{-21}N_{LL}$	r_{LL} , Å	$-(a = 0.35, b = 1.83)^b$			$-(a = 0.425, b = 1.77)^c$			γ_L , ergs/cm ²		γ_L with water, ergs/cm ²		
				$10^{24}\alpha_0$, cm ³	α_0/n , cm ³	γ_L (calcd), ergs/cm ²	$10^{24}\alpha_0$, cm ³	α_0/n , cm ³	γ_L (calcd), ergs/cm ²	Measd	Ref	Calcd	Measd	Ref
1	0.144 ^d	5.4	5.70	2.53	2.53	0.34	2.62	2.62	0.38					68.0
2	0.286 ^d	11.4	4.44	4.36	2.18	2.12	4.39	2.20	2.15					62.1
3	0.430 ^d	17.6	3.84	6.19	2.06	6.16	6.16	2.08	6.25					57.2
4	0.567 ^d	23.5	3.49	8.02	2.01	12.7	7.93	1.98	12.4					54.3
5	0.626	26.1	3.37	9.85	1.97	16.4	9.70	1.94	16.1	16.0	<i>h</i>			53.7
6	0.660	27.7	3.30	11.70	1.95	19.0	11.45	1.91	18.4	18.4-19.24	<i>i-k</i>	53.6	50.2-51.1	<i>l, o, p</i>
7	0.684	28.8	3.26	13.50	1.93	20.6	13.25	1.895	20.1	20.4	<i>l, h</i>	53.6	50.2-52.6	<i>l, o, p</i>
8	0.704	29.8	3.22	15.35	1.92	22.5	15.00	1.875	21.7	21.5-21.8	<i>h, j, k</i>	53.7	50.8-51.68	<i>l, o-q</i>
9	0.718	30.3	3.21	17.20	1.91	23.2	16.75	1.86	22.3	22.9	<i>h, j</i>	53.7		
10	0.730	30.8	3.19	19.00	1.90	24.1	18.55	1.855	23.3	23.9	<i>h, l</i>	53.8	51.2-52.3	<i>l, q</i>
11	0.741	31.4	3.17	20.85	1.895	25.3	20.30	1.845	24.4	24.7	<i>h, l</i>	54.0		
12	0.751	31.8	3.15	22.70	1.89	26.2	22.05	1.84	25.2	25.4	<i>h</i>	54.1	52.78	<i>q</i>
13	0.757	32.2	3.14	24.50	1.885	26.9	23.85	1.835	25.8	25.9	<i>m</i>	54.2		
14	0.765	32.5	3.13	26.30	1.88	27.5	25.65	1.83	26.2	25.6-26.7	<i>i, l, n</i>	54.3	52.2-54.2	<i>l, n, p</i>
15	0.769	32.7	3.13	28.15	1.875	27.6	27.40	1.825	26.6			54.3		
16	0.775	32.9	3.12	30.00	1.875	28.2	29.15	1.82	27.0	27.6	<i>i, j</i>	54.4	53.77	<i>q</i>
17	0.778	33.1	3.11	31.80	1.87	28.6	30.95	1.82	27.5			54.5		
18	0.777 ^e	33.1	3.11	33.65	1.87	28.6	32.70	1.815	27.4			54.5		
19	0.777 ^f	33.1	3.11	35.50	1.87	28.6	34.45	1.815	27.4			54.5		
20	0.778 ^g	33.2	3.11	37.30	1.865	28.7	36.25	1.81	27.4			54.5		
30	0.765	33.4	3.11	55.60	1.865	29.0	53.95	1.80	27.5			54.5		

^a "Handbook of Chemistry and Physics," 37th ed, Chemical Rubber Publishing Co., Cleveland, Ohio, 1955-1956. ^b H. H. Landolt and R. Börnstein, "Zahlenwerte und Funktionen," Vol. 1, Springer-Verlag, Heidelberg, Germany, 1950-1951. ^c Th. G. Scholte and F. C. deVos, *Rec. Trav. Chim.*, **72**, 625 (1953). ^d Liquid density at 20°. ^e Liquid density at 28°. ^f Liquid density at 32°. ^g Liquid density at 37°. ^h O. R. Quayle, *et al.*, *J. Amer. Chem. Soc.*, **66**, 938 (1944). ⁱ A. I. Vogel, *J. Chem. Soc.*, 133 (1946); 616 (1948). ^j F. M. Fowkes, *J. Phys. Chem.*, **67**, 2538 (1963). ^k W. D. Harkins and E. H. Grafton, *J. Amer. Chem. Soc.*, **42**, 2534 (1920). ^l See ref 11. ^m E. G. Shafrin and W. A. Zisman, *J. Phys. Chem.*, **66**, 740 (1962). ⁿ A. Weissberger, "Techniques of Organic Chemistry," Vol. 1, 3rd ed, Interscience Publishers, Inc., New York, N. Y., 1959, p 763. ^o W. D. Harkins, *et al.*, *J. Amer. Chem. Soc.*, **42**, 700 (1920). ^p J. A. Krynitsky and W. D. Garrett, *J. Colloid Sci.*, **18**, 893 (1963). ^q R. Aveyard and D. A. Haydon, *Trans. Faraday Soc.*, **61**, 2255 (1965).

Table II: The Constants Involved in the Calculation of the Contributions of Dispersion Forces to the Surface Tensions of *n*-Hexane and Water

Term	Relationship	Volume element		
		C ₆ H ₁₂ in <i>n</i> -hexane	CH ₂ in <i>n</i> -hexane	H ₂ O in water
N_{LL}	N_{Ap} /mol wt	4.62×10^{21}	27.7×10^{21}	3.34×10^{21}
Z	Outer electrons	38	6	8
S	Valency electrons	38	6	4
α_0	Ref 9, 13, 14	11.80×10^{-24} cm ³	1.97×10^{-24} cm ³	1.48×10^{-24} cm ³
r_{LL}	$(N_0)^{-1/3}$	6.01×10^{-8} cm	3.3×10^{-8} cm	3.114×10^{-8} cm
γ_L^d (20°)	Eq 8	14.9 ergs/cm ²	18.7 ergs/cm ²	19.2 ergs/cm ²

and 10 are set out in Table II for *n*-hexane and CH₂ taken as the volume element. The calculated values of γ_L of 14.9 and 18.7 ergs/cm² compare with experimental values between 18.4 and 19.24 ergs/cm² given in the literature cited in Table I.

This method of calculation is suitable for all the alkanes for which the polarizabilities are known. Since γ_L is dependent on $\alpha_0^{2/3}$, it is important to have good experimental values of the polarizability. In order to obtain unknown values by interpolation, known values

of molecular polarizability of the *n*-alkanes were plotted as a function of the number, *n*, of carbon atoms in the alkane chain, and a straight line was obtained. The equation $\alpha_0 = nb + 2a$, where *b* is the polarizability of the CH₂ group and *a* + *b* that of the CH₃ group, fitted these data. Hence the polarizability of any alkane was calculated by inserting the requisite value of *n*.

Two literature sources^{12,13} have been used for values of polarizability of the alkanes and these are shown plotted in Figure 1. These two sets of data have been

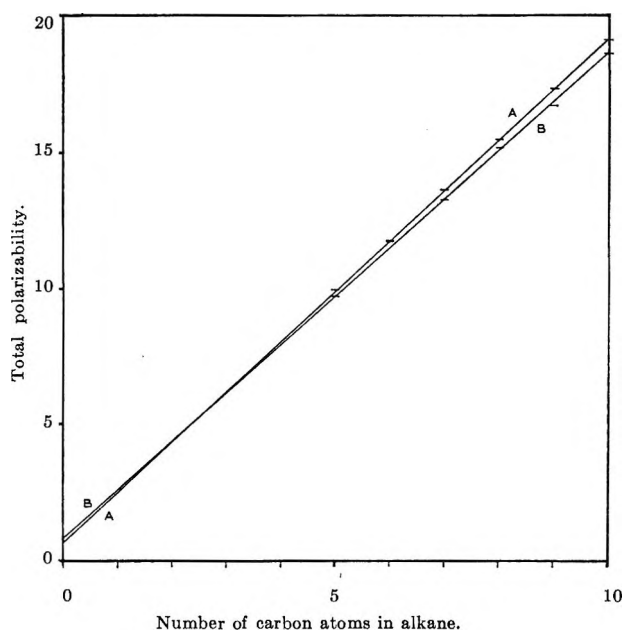


Figure 1. The total molecular polarizabilities of *n*-alkanes as a function of the number of carbon atoms: (A) $2a = 0.70$, $b = 1.83$ (see ref 12); (B) $2a = 0.85$, $b = 1.77$ (see ref 13).

used independently to calculate, by means of eq 9, two sets of surface-tension data. These are shown in Table I and plotted in Figure 2 together with the experimental values taken from the literature. The surface tension of the gases methane, ethane, propane, and butane are those calculated for liquids under some 40–50 atm of pressure at 20°. The liquid densities of these four alkanes were obtained by plotting the densities of the higher alkanes at 20° against the number, n , of carbon atoms in the alkane molecule and extrapolation to the lower values of n .

Calculation of the Dispersion-Force Contribution to the Surface Tension of Water

Substituting the values given in the last column of Table II into eq 9 and 10, taking the water molecule as the volume element, one obtains a value of 19.2 ergs/cm² for the dispersion contribution to the total surface tension. Thus dispersion forces contribute 26% of the true surface tension of water. We shall use γ_L^d to distinguish this value from the total surface tension γ_L of the liquid.

From the value of γ_L^d of water and on the basis that polar liquids interact principally through dispersion forces with nonpolar substances, the wetting properties between nonpolar compounds and water were calculated.

Calculation of the Interfacial Tension between *n*-Hexane and Water

Using eq 11 or 13 the interfacial tension between *n*-hexane and water has been calculated. Using the latter equation

$$\gamma_I = 18.7 + 72.8 -$$

$$2(18.7 \times 19.2)^{1/2} = 53.6 \text{ ergs/cm}^2$$

Similar calculations have been performed for other alkanes with water, as shown in Table I. Use of eq 13 instead of the more accurate eq 11 introduces no appreciable error because, as seen in Table II, the interparticle distances for water and CH₂ in *n*-hexane are very similar. The calculated value of 53.6 ergs/cm² is compared with the experimental value of 51.1 ergs/cm².

Calculation of the Interfacial Tension between *n*-Hexane and Mercury

Fowkes⁸ gives the experimental value of γ_L^d for mercury as 200 ergs/cm². Calculation of this value was not attempted because α_0 , the polarizability, is unknown. The interfacial tension is calculated as before using eq 13.

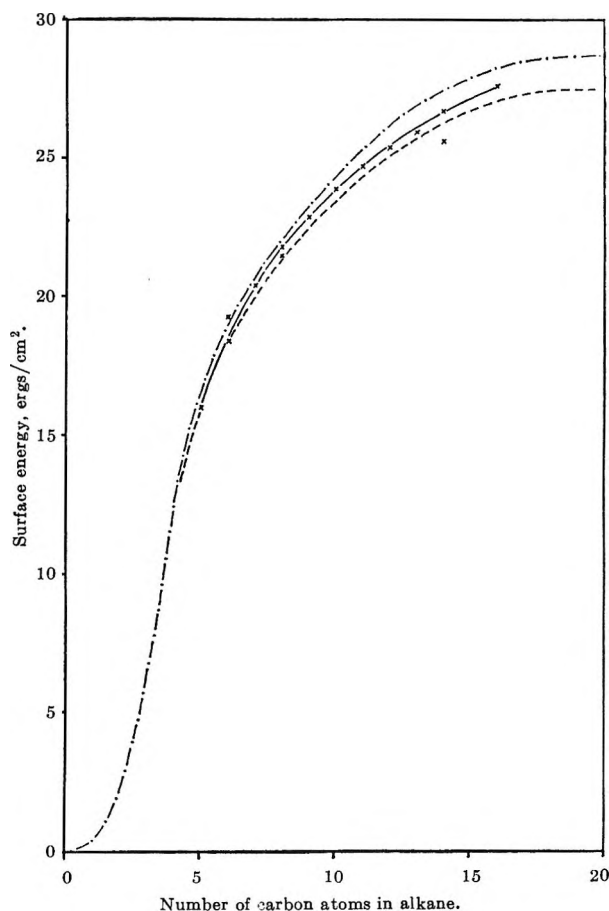


Figure 2. The calculated and measured surface energies of *n*-alkanes at 20° as a function of the number of carbon atoms: —, experimental values; ---, calculated values from α_0 values of ref 13; - · - · - calculated values from α_0 values of ref 12.

(12) "Handbook of Chemistry and Physics," 37th ed, Chemical Rubber Publishing Co., Cleveland, Ohio, 1955–1956.

(13) H. H. Landolt and R. Bärnstein "Zahlenwerte und Funktionen," Vol. 1, Springer-Verlag, Heidelberg, Germany, 1950–1951.

$$\gamma_I = 18.7 + 484 - 2(18.7 \times 200)^{1/2} = 380 \text{ ergs/cm}^2$$

This compares well with the observed value¹⁴ of 378 ergs/cm²

Calculation of the Spreading Coefficient of Water on Triacontane

According to eq 16 and the simplified eq 13

$$S_c = -2(72.8) + 2(19.2\gamma_{ss})^{1/2}$$

γ_{ss} is the calculated surface tension of triacontane shown in Table I. Two values are given, the mean of which is 28.2 ergs/cm². Inserting this value in the above calculations gives $S_c = -99$ ergs/cm². The measured S_c on paraffin wax is -99 ergs/cm².

Calculation of the Angle of Contact of Water on Triacontane

$$\begin{aligned} \cos \theta &= -1 + 2 \frac{(28.2 \times 19.2)^{1/2}}{72.8} \\ &= -0.36 \\ \theta &= 110^\circ \end{aligned}$$

This compares with the measured contact angle of water on paraffin wax, 110–115°.¹⁵

Calculation of the Work of Adhesion of Water on Triacontane

$$W_a = 2(28.2 \times 19.2)^{1/2} = 46.6 \text{ ergs/cm}^2$$

Using the more precise eq 21 gives 45.9 ergs/cm².

The Effect of the Presence of the Vapor Phase

In the derivation of eq 9 it was supposed that the bulk liquid surface was ruptured to produce two unit areas of semiinfinite liquid surface. In practice such a process involves the replacement of each semiinfinite surface of liquid with a corresponding semiinfinite surface of vapor. The effective surface tension of the vapor has been calculated using eq 9 and 10, wherein all quantities except N_{LL} are the same as for the liquid.

Using eq 11 with the substitution of A_{ss} by A_{vv} , the Hamaker constant of the vapor phase, and r_{ss} by r_{LL} , it being assumed that the distance of closest approach in the vapor is equal to that in the liquid, then

$$\begin{aligned} \gamma_{LV} &= \frac{[A_{VV} + A_{LL} - 2A_{LL}A_{VV}]^{1/2}}{24\pi r_{LL}^2} \\ &= \frac{[A_{LL}^{1/2} - A_{VV}^{1/2}]^2}{24\pi r_{LL}^2} \end{aligned} \quad (23)$$

Substituting values for A_{LL} and A_{VV} from eq 10 in terms of the common value β_{11} (*i.e.*, β_{LL}), eq 23 becomes

$$\gamma_{LV} = \frac{\beta_{LL}}{24r_{LL}^2}(N_L - N_V)^2 \quad (24)$$

At temperatures well below the critical point, N_V is so small compared with N_L that it may be neglected

and the simpler expression of eq 9 used without serious error. At 20° the liquid and vapor densities of *n*-hexane are 0.6595 and 0.0006 g/ml; thus the difference between N_L^2 and $(N_L - N_V)^2$ is only 0.2%. As the critical temperature is approached, N_V approaches N_L and γ_{LV} tends toward zero.

Discussion

The London,⁹ the Slater–Kirkwood,⁵ the Neugebauer,¹⁶ the Moelwyn-Hughes,⁴ and the Lifshitz^{17,18} formulas have all been used to calculate the β coefficient for dispersion interaction between two particles.^{18,19}

The Lifshitz formula used by Gregory was for fully retarded forces applied at large distances (r , 2000 Å) and is not applicable to the wetting system here because the unretarded forces acting over molecular dimensions are thought to predominate. Of the formulas applicable to these surface systems, the London expression gives the lowest value, Neugebauer's the next, then Slater–Kirkwood's, and finally Moelwyn-Hughes', giving the largest value for β_{11} .

Strictly, London's equation should be applied to interaction of hydrogen-like atoms having one orbital electron. The equation of Moelwyn-Hughes used in these calculations takes account of all outer shell electrons and also, unlike the other equations, the difference between their average frequency of oscillation and the frequency of each electron in isolation.

The integration of the pair potential by the method of Hamaker assumes that the radial distribution function of volume elements is a discontinuous stepped function as shown in Figure 3, curve a for water at 20°. This is compared with the radial distribution function given by Narten, Danford, and Levy²⁰ (curve b) ob-

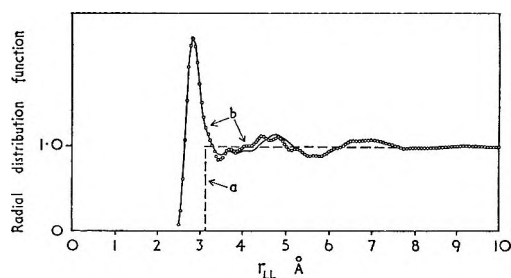


Figure 3. Radial distribution function of water at room temperature: (a) assumed from Hamaker summation, 20°; (b) from X-ray diffraction of water²⁰ at 25°.

(14) W. D. Harkins, "The Physical Chemistry of Surface Films," Reinold Publishing Corp., New York, N. Y., 1952.

(15) R. B. Ray and F. E. Bartell, *J. Colloid Sci.*, **8**, 214 (1953).

(16) T. Neugebauer, *Z. Phys.*, **107**, 785 (1937).

(17) I. E. Dzyaloshinskii, E. M. Lifshitz, and L. P. Pitaevskii, *Soviet Phys. JETP*, **37**, 229 (1959).

(18) J. Gregory, *Discussions Faraday Soc.*, **42**, 168 (1966).

(19) R. H. Ottewill and J. N. Shaw, *ibid.*, **42**, 154 (1966).

(20) A. H. Narten, M. D. Danford, and H. A. Levy, *ibid.*, **43**, 97 (1967).

tained from X-ray diffraction data. The latter curve refers to 25° but the authors show that the temperature coefficient is sufficiently small to allow comparison of the radial distribution at 25° with that at 20°. The step of the Hamaker curve lies to the right-hand side of the peak of the X-ray diffraction curve and this would have the effect of producing a low value for the calculated dispersion contribution to the surface tension. If the value for r_{LL} is taken as 2.76 Å, the length of the hydrogen bond, then the dispersion contribution to the surface tension of water is increased from 19.2 to 24.4 ergs/cm². A similar comparison of radial distribution functions of the *n*-alkanes is not possible because of lack of data.

In calculating the wetting properties of water at the surface of a *n*-alkane we have assumed that the Debye contribution to the work of adhesion is negligible. The calculated interfacial tensions of Table I are all greater than the measured values and this could be explained either by our calculated value of the dispersion contribution to the surface tension of water being too low or by the Debye forces being significant. The extent of the Debye interaction of water dipoles with CH₂ groups of a *n*-alkane is proportional to $\alpha_0\mu^2$, where α_0 refers to the polarizability of CH₂ groups and μ refers to the dipole moment of water. The constant obtained is 5% of the dispersion value given by Moelwyn-Hughes' formula and represents about 2.3 ergs/cm².

Moelwyn-Hughes²¹ derived an expression for W_M^d that took into account Born repulsion and equated it to the internal energy of surface formation. His expression for W_M^d is proportional to the inverse square of the interparticle distance but is not suitable for calculating surface tension at other temperatures than 0°K. Powkes¹⁸ expression for surface tension was a different function of interparticle distance obtained (erroneously we believe) by summing the potential energy of surface molecules only and ignoring bulk-bulk attraction. The expression for W_M^d used here thus seemed to be more adequate.

The assumption that the work or potential energy term W_M^d of eq 5 equals the surface free energy (and hence surface tension of a pure liquid) involves the arbitrary assumption that $Q/2$ of eq 7 equals TS of eq 8, where S is the surface entropy. The main justification in this assumption lies in the ability of eq 9 to predict, in the same way as Moelwyn-Hughes,²¹ the surface tension the liquid would possess if it were at 0°K.

Using eq 9, the surface tension of *n*-decane at 0°K is calculated to be 44 ± 4 ergs/cm², using the density data of Timmermans,²² which is somewhat lower than the extrapolated experimental value of 50 ± 2 ergs/cm². At 0°K, TS must be zero and $Q/2$ is likely to be small or zero, hence some agreement is expected. The agreement, although not good, suggests that the large value

of TS at room temperature (-26 ergs/cm²) is, in fact, compensated for in the method of calculation we have used.

To summarize, it was found that the contribution of dispersion forces to the total interaction between two particles could be calculated. Difficulties in finding a suitable value for the ionization potential have been avoided by using the equation of Moelwyn-Hughes. Only polarizabilities and densities are then required and these are known with certainty. The integration of pair potentials for a bulk system followed Hamaker's method and the total energy of surface formation was equated to the surface tension on the basis that the entropy term cancels with the energy required to bring a freshly formed surface to equilibrium. The surface tensions of the *n*-alkanes so calculated agree within a few per cent of the measured values. The surface free energy of a *n*-alkane that is solid at 20° was calculated and agreed well with values derived from experiment either directly or indirectly, *mutatis mutandis*, from the angle of contact, the work of adhesion, or other wetting properties. We have also attempted to clarify the assumptions made in the calculation of surface tension implicit in the work of Good and Girifalco, Powkes, and the present authors.

Glossary

A	Hamaker constant ($=\pi^2 N_0^2 \beta$); area
e	Electronic charge ($=4.80 \times 10^{-10}$ esu)
h	Planck's constant ($=6.62 \times 10^{-27}$ erg/sec)
m	Electronic mass ($=9.11 \times 10^{-28}$ g)
N_A	Avogadro's number ($=6.02 \times 10^{23}$ mol ⁻¹)
N_{LL}	Number of molecules or volume elements per cubic centimeter
P	Pressure
r_{LL}	Intermolecular distance or distance between volume elements
S	Entropy; effective number of dispersion electrons, taken as valency
S_0	Spreading coefficient
T	Temperature (°K)
V	Volume
W_a	Work of adhesion
W_c	Work of cohesion
W_e	Wetting energy; adhesion tension
W_{12}	Interaction energy between isolated pairs of molecules
W_M	Interaction energy between macroscopic surfaces
Z	Number of outer-shell electrons
α_0	Static polarizability
β	Dispersion constant (coefficient of r^{-6})
γ	Surface tension; force required to stretch unit surface
E	Surface energy; energy required to create unit new surface
ρ	Density
θ	Angle of contact between two phases
ν_0	Proper frequency of an isolated electron

(21) E. A. Moelwyn-Hughes, *J. Colloid Sci.*, **11**, 501 (1956).

(22) J. Timmermans, "Physico-chemical Constants of Pure Organic Compounds," Vol. 2, Elsevier Publishing Co., London, 1965, p 41.

μ	Dipole moment	S or SS	Solid phase (subscript)
d	Dispersion contribution (superscript)	I	Interface (subscript)
L or LL	Liquid phase (subscript)	m	For a macroscopic system (subscript)

The Semiempirical Method for the Calculation of Some Parameters for High-Resolution Nuclear Magnetic Resonance Spectra

by P. G. Maslov

A. I. Gerzen State Pedagogical Institute, Leningrad, U. S. S. R. (Received October 28, 1966)

In the present paper, a useful semiempirical method for calculating magnetic shielding constants, σ , chemical shifts, δ , the polarizabilities, α , the Langevin magnetism, χ_d , Van Vleck paramagnetism, χ_p , and other molecular parameters is offered. In the work, it is shown that at least part of the known difficulties, connected with the calculations of the above mentioned parameters, can be removed by means of using an equation of weighted averages. Comparative data leave no doubt as to the effectiveness and rather high precision of the proposed method, of the order of 0.1–1.0%.

The study of nmr spectra at the present time has acquired great scientific and practical significance.^{1–20} However, one entire category of questions on the theory of nmr spectra still awaits resolution.^{1–4} For example, there is still no development of the theory of nmr spectra for nuclei with spin $I \geq 1$ available. In the case of nuclei with spin $I = 1/2$, the calculation of nmr spectra is often difficult because of the lack of the necessary parameters: the magnetic shielding constant, σ , of nuclei in molecules, the chemical shifts, and others.^{1–4} Approximate quantum-mechanical methods,^{1–4, 21, 22} unfortunately, are not available at a level sufficient to permit theoreticians to calculate, in important cases, the nmr parameters with sufficient precision to have practical importance.

In such situations, the development of new methods, even if they are approximate or semiempirical, but which are not constrained with the deficiencies of the quantum-mechanical methods, becomes urgent.

In the present paper, a useful semiempirical method for calculating magnetic shielding constants, σ , chemical shifts, δ , the polarizabilities, α , the Langevin magnetism, χ_d , Van Vleck paramagnetism, χ_p , and other molecular parameters is offered. The susceptibility is given by eq 1

$$\chi = \frac{1}{3}(\chi_{xx} + \chi_{yy} + \chi_{zz}) = \frac{1}{3}(\chi_1 + \chi_2 + \chi_3) = \frac{\chi_v M}{d} \quad (1)$$

where χ_i ($i = 1, 2, 3$) are the components of the molecu-

lar magnetic susceptibility, χ , averaged along all directions, M is the molecular weight, d is the density of the substance, and χ_v is the volume magnetic susceptibility.

- (1) J. W. Emsley, J. Feeney, and L. H. Sutcliffe, "High Resolution Nuclear Magnetic Resonance Spectroscopy," Pergamon Press, Oxford, 1965.
- (2) A. Lösche, "Kerninduktion," Veb Deutscher Verlag der Wissenschaften, Berlin, 1957.
- (3) J. A. Pople, W. G. Schneider, and H. J. Bernstein, "High-Resolution Nuclear Magnetic Resonance," McGraw-Hill Book Co., Inc., New York, N. Y., 1959.
- (4) E. R. Andrew, "Nuclear Magnetic Resonance," Cambridge University Press, London, 1955.
- (5) R. E. Richards, *Advan. Spectr.*, **2**, 101 (1961).
- (6) G. H. Townes and A. L. Schawlow, "Microwave Spectroscopy," McGraw-Hill Book Co., Inc., New York, N. Y., 1955.
- (7) R. H. Bible, "Interpretation of NMR Spectra, An Empirical Approach," Plenum Press, New York, N. Y., 1965.
- (8) M. A. Eliashevich, "Atomic and Molecular Spectroscopy," State Physical and Mathematical Publishing, Moscow, 1962.
- (9) P. Pascal, A. Pacault, and J. Hoarau, *Compt. Rend.*, **233**, 1078 (1951).
- (10) P. Pacault, *Experientia*, **X**, 41 (1954).
- (11) P. G. Maslov, Dissertation, V. I. Lenin State Pedagogical Institute, Moscow, 1953.
- (12) I. Mizoguchi and M. Inoue, "Nuclear Magnetic Relaxation in Magnetite," Tokyo, 1966.
- (13) J. M. Anderson and J. D. Baldeschwieler, *J. Chem. Phys.*, **40**, 3241 (1964).
- (14) J. M. Anderson, *J. Chem. Educ.*, **42**, 363 (1965).
- (15) R. H. Herber, *Ann. Rev. Phys. Chem.*, **17**, 261 (1966).
- (16) M. T. Jones and W. D. Phillips, *ibid.*, **17**, 323 (1966).
- (17) J. S. Waugh, Ed., "Advances in Magnetic Resonances," Academic Press, New York, N. Y., 1965.

Table I: Molar Magnetic Susceptibilities and Other Constants for Given Molecules, j , Representative of Particular Families

Compound j	Physical constants B_j					
	$10^{24}\alpha$	$-10^6\chi_d$	$-10^6\chi$	$10^6\chi_p$	$10^{22}\Phi$	$10^{16}\sum r_l^2/l$
CH ₄	2.61	16.00	16.9	-0.9	-0.9	5.6497
CCl ₄	~11	85.5	66.8	18.7	3.98	30.1906
CBr ₄	...	137.0	93.7	43.3	9.21	48.3557
CJ ₄	...	187.5	124.3	64.2	13.66	62.6765
C(OH) ₄	5.12	47.40	37.4	10.0	2.13	16.7373
C(C ₆ H ₅) ₄	41.86	263	214.10	48.9	13.86	92.9024
C[(CH ₂) _n NH ₂] ₄	1.89 + 1.84 × 4z	10.4 + 12 × 4z	-5.1 + 11.4 × 4z	15.5 + 0.6 × 4z
C(CHO) ₄	10.42	81.8	42.0	39.8
C(CH ₂ OH) ₄	12.56	95.6	83.9	11.7
C(CH ₃) ₄	10.26	64.4	63.1	1.3	0.28	22.7401
C(C ₂ H ₅) ₄	17.62	102.4	108.7	3.7	0.79	39.6892
C(C _n H _{2n+1}) ₄	3.21 + 1.84 × 4z	16 + 12 × 4z	17.14 + 11.4 × 4z	-1.14 + 0.6 × 4z	-0.24 + 0.12765 × 4z	5.6497 + 4.23728 × 4z
C(COOH) ₄	13.37	112	79.9	32.9	7.0	39.5480
C(CH ₂ COOH) ₄	20.73	160	125	35.3	7.51	56.4971
C[(CH ₂) _n COOH] ₄	28.09	208	171	37.7	8.02	73.4463
C[(CH ₂) _n COOH] ₄	13.37 + 1.84 × 4z	112 + 12 × 4z	79.9 + 11.4 × 4z	32.1 + 0.6 × 4z	6.83 + 0.12765 × 4z	39.5480 + 4.23728 × 4z
C(NO ₂) ₄	11.33	107.6	37	71	15.1057	37.9943
C(CN) ₄	...	72.3	59.6	12.7	2.7020	25.5296
C[(CH ₂) _n OH] ₄	5.37 + 1.84 × 4z	48 + 12 × 4z	38.1 + 0.6 × 4z	9.9 + 0.6 × 4z	2.1063 + 0.1276 × 4z	16.9491 + 4.23728 × 4z

According to Van Vleck,^{2,3,21-23} the average magnetic susceptibility, $10^6\chi$, of diamagnetic molecules is composed of two terms: the Langevin molecular magnetic susceptibility ($-10^6\chi_d$) and the Van Vleck molecular paramagnetic susceptibility ($10^6\chi_p$), namely

$$\chi = -\chi_d + \chi_p = -\frac{e^2N}{6mc^2} \sum_l \langle k | \bar{r}_l^2 | k \rangle + \frac{2}{3}N \sum_{l \neq k} \frac{| \langle k | M_z | l \rangle |^2}{E_l^0 - E_k^0} = -h_1 \sum_l \bar{r}_l^2 + h_2 \Phi \quad (2)$$

Here

$$\Phi = \sum_{l \neq k} \frac{| \langle k | M_z | l \rangle |^2}{E_l^0 - E_k^0} \quad (3)$$

is the so-called Φ function,²¹ which enters not only into the expression for the Van Vleck paramagnetism

$$\chi_p = \frac{2}{3}N\Phi \quad (4)$$

but into the spin-rotation interaction of the molecule. In the preceding formulas, $\langle k | M_z | l \rangle$ is the off-diagonal matrix element of the operator for the magnetic moment in the direction of H , parallel to Z , connecting the ground state k with the l th excited state; N is Avogadro's number; c is the speed of light *in vacuo*; m and e are the mass and charge of the electron.

The calculation of magnetic susceptibility and its

components $-\chi_d$ and χ_p by means of eq 2 is practically impossible, since it is impossible to find wave functions and energies of all excited states of the molecule.^{1-4,21} In this connection, the literature suggests^{9,10,21,24,25} versions of an empirical, semiempirical, and approximate quantum-mechanical character.

In the present work, it is shown that at least part of the above mentioned difficulties, it seems, can be removed for the calculation of the nmr quantities to which we have referred by using an "equation of weighted averages"²⁶⁻³⁴

$$B_i = \frac{1}{s} \sum_j \delta_j B_j \quad (5)$$

Here $s = \sum_j \delta_j$ is the valency of the coordinating group,

(18) B. D. Nageswara Rao, J. D. Baldeschwieler and J. M. Anderson, *J. Phys. Rev.*, **137**, 1477 (1955).

(19) B. Dischler, *Angew. Chem.*, **78**, 653 (1966).

(20) R. C. Hirst, D. M. Grant, and E. G. Paul, *J. Chem. Phys.*, **44**, 4305 (1966).

(21) Jak. G. Dorfman, "Diamagnetism and Chemical Bond," State Physical and Mathematical Publishing, Moscow, 1961.

(22) N. F. Ramsey, *Phys. Rev.*, **77**, 567 (1950); **78**, 221, 695, 699 (1950); **86**, 243 (1952).

(23) J. H. Van-Vleck, "The Theory of Electric and Magnetic Susceptibilities," Oxford University Press, London, 1932.

(24) P. Pascal, *Ann. Chim. Phys.*, **XIX**, 5 (1910).

(25) M. G. Veselov, N. N. Adamov, and G. K. Rebane, *News Acad. Sci. USSR, Phys.*, **22**, 1015 (1958).

Table II: Molar Magnetic Susceptibilities and Other Constants for Given Molecules, j , Representative of Particular Families

Compound j	Physical constants B_j					
	$10^{24}\alpha$	$-10^6\chi_d$	$-10^6\chi$	$10^6\chi_p$	$10^{18}\Phi$	$10^{18}\frac{\sum r^2}{l}$
Ethylene Family						
C_2H_4	4.27	25.5	20.5	5.2	1.1063	9.0042
$C_2(CH_3)_4$	11.83	74.2	65.9	8.3	1.7659	26.2005
$C_2(C_2H_5)_4$	19.75	123	111.7	11.3	2.4041	23.4322
$C_2[(CH_3)(CH_2)_3]_4$	34.47	218.3	201.3	17	3.6168	77.0833
$C_2(C_nH_{2n+1})_4$ ($n = z \geq 2$)	$5.3 +$ 1.84 $\times 4z$	$27.5 +$ $12 \times$ $4z$	$20.5 +$ 11.4 $\times 4z$	$7 +$ $0.6 \times$ $4z$	$1.4893 +$ 0.1276 $\times 4z$	$9.7104 +$ 4.23728 $\times 4z$
C_2Cl_4	12	98	81.6	16.4	3.4892	34.6045
C_2F_4	...	38.4
C_2Br_4	...	114.0
C_2J_4 (liq)	...	81.6
$C_2(C_6H_5)_4$	45.33	278.5	212.85	64.55	13.7334	98.3403
Amine Family						
NH_3	2.29	14.9	10.6	4.3	0.9148	5.2613
$N(C_2H_5)_3$	13.75	87.0	81.4	5.6	1.1914	30.7203
$N(CH_3)_3$	8.23	51.0	47.2	3.8	0.8085	18.0085
$N(C_nH_{2n+1})_3$ ($n = z \geq 1$)	$2.71 +$ 1.84 $\times 3z$	$14 +$ $12 \times$ $3z$	$13.0 +$ 11.4 $\times 3z$	$1.0 +$ $0.6 \times$ $3z$	$0.4468 +$ 0.1276 $\times 3z$	$4.9435 +$ 4.23728 $\times 3z$
Thiophene Family						
H_2S	3.78	25.7	25.5	0.2	0.0426	9.0748
$(CH_3)_2S$	7.46	50.0	45.2	4.8	1.0212	17.6554
$(C_2H_5)_2S$	11.14	74.5	68	6.5	1.3829	26.3065
$[C_nH_{2n+1}]_2S$	$3.78 +$ 1.84 $\times 2z$	$25.7 +$ $12 \times$ $2z$	$25.5 +$ 11.4 $\times 2z$	$0.2 +$ $0.6 \times$ $2z$	$0.0426 +$ 0.1276 $\times 2z$	$9.0748 +$ 4.23728 $\times 2z$
Metal n -Alkyl Family						
$HgCl_2$	9.1	98.5	82.0	16.5	3.5104	34.7810
$Hg(C_nH_{2n+1})_2$	$5.8 +$ 1.84 $\times 2z$	$73 +$ $12 \times$ $2z$	$45.8 +$ 11.4 $\times 2z$	$27.2 +$ $0.6 \times$ $2z$	$5.7870 +$ 0.1276 $\times 2z$	$25.7768 +$ 4.23728 $\times 2z$

common for all representatives of the chosen family of molecules which are related in structure; B_j and B_i are the values of a particular property for molecules j which are given, and molecule i which is unknown.²⁶⁻³⁴

It is important to say at once that eq 5 rests upon more general principles than the idea of additivity, and, so it would seem, presents unstudied possibilities of applying the periodic law of D. I. Mendeleev in conformity with the molecular systems. As is well known, additivity means that every structural group in the molecule (atom, bond, or group of atoms) introduces into the total magnitude of a sought-after property some characteristic, but unique, contribution. Meanwhile, eq 5 turns out to be correct for numerous physicochemical parameters of all kinds of compounds, for which the idea of additivity is in general meaningless.²⁶⁻⁴⁰

However, the idea of additivity is a special case of eq 5. The application of eq 5 to the extremely accurate calculation of a large group of physicochemical (in particular, thermodynamic, thermochemical, electrical, etc.) characteristics of complex substances in all their

phases, either directly by eq 5, or on the basis of methods based on eq 5, is now rather well known.²⁶⁻⁴⁰

(26) P. G. Maslov and Y. P. Maslov, *J. Phys. Chem. Acad. Sci. USSR*, **32**, 1715 (1958).

(27) P. G. Maslov, Y. P. Maslov and *Report Acad. Sci. USSR*, **132**, N5 (1960).

(28) P. G. Maslov, "Advances in Molecular Spectroscopy," Pergamon Press Ltd., London, 1962, p 266.

(29) P. G. Maslov, *Successes Chem.*, **25**, 1069 (1956).

(30) P. G. Maslov, *J. Phys. Chem. Sci. USSR*, **38**, 2, 304 (1964).

(31) P. G. Maslov and A. A. Antonov, *ibid.*, **38**, 600 (1964).

(32) P. G. Maslov, *Acta Chim. Acad. Sci. Hung.*, **40**, 197 (1964).

(33) Y. P. Maslov and P. G. Maslov, *Opt. i Spektroskopiya*, **3**, 38 (1957).

(34) P. G. Maslov, *J. Phys. Chem. Acad. Sci. USSR*, **35**, 1553 (1961).

(35) P. G. Maslov, *J. Phys. Chem. Sci. USSR*, **29**, 1413 (1959).

(36) P. G. Maslov, *ibid.*, **35**, 974 (1961).

(37) P. G. Maslov, *ibid.*, **33**, 1461 (1959).

(38) A. A. Vedensky, "The Thermodynamic Calculations of the Oil-Chemical Processes," State Printing, Leningrad, 1960.

(39) S. S. Bhatnagar and N. G. Mitra, *J. Indian Chem. Soc.*, **13**, 329 (1936).

(40) P. Mazerolles and D. Voigt, *Compt. Rend.*, **240**, 2144 (1950).

Table III: Molar Magnetic Susceptibilities and Other Constants for Given Molecules, *j*, Representative of Particular Families

Compound <i>j</i>	Physical constants B_j					
	$10^{24}\alpha$	$-10^6\chi_d$	$-10^6\chi$	$10^{16}\chi_p$	$10^{19}\Phi$	$10^{16}\sum r_i^2$
Water Family						
H ₂ O	1.48	12.0	12.96	-0.96	-0.2042	4.2373
(CH ₃) ₂ O	5.2	36.0	26.3	9.7	2.0637	12.7118
(C ₂ H ₅) ₂ O	8.84	60	55.1	4.9	1.0425	21.1864
(<i>n</i> -C _{<i>n</i>} H _{2<i>n</i>+1}) ₂ O	1.44 + 1.84 × 2 <i>z</i>	11.6 + 12 × 2 <i>z</i>	8.64 + 11.4 × 2 <i>z</i>	2.96 + 0.6 × 2 <i>z</i>	0.6298 + 0.1276 × 2 <i>z</i>	4.0961 + 4.23728 × 2 <i>z</i>
(NO ₂) ₂ O	6.62	58.8	26.84	29.74	6.3274	20.7627
[(CH ₃) ₂ CH ₂] ₂ O	12.9	84.5	79.4	5.1	1.0851	29.8375
[(CH ₃) ₂ CH(CH ₂) ₂] ₂ O	...	133	128.6	4.4	0.9361	46.9632
Symmetric Ketone Family						
H ₂ CO	2.9	20.5	12.3	8.2	1.7446	7.2387
(OH) ₂ CO	...	35.6	29.6	6.0	1.2765	12.5706
Cl ₂ CO	...	57.5	44.0	13.5	2.8084	20.3036
(CH ₃) ₂ CO	6.3	44.5	33.8	10.7	2.2765	15.7133
(HOOC) ₂ CO	...	65.3	40.6	24.7	5.2551	23.0579
[HOOC(CH ₂) ₂] ₂ CO	...	89.3	63.4	25.9	5.5104	31.5325
(C ₂ H ₅) ₂ CO	...	68.5	57.4	11.1	2.3616	24.1878
[HOOC(CH ₂) ₂] ₂ CO	...	113.3	86.2	27.1	5.7657	40.0070
(C ₆ H ₅) ₂ CO	22.5	144	109.6	~34.4	~7.3188	...
(C _{<i>n</i>} H _{2<i>n</i>+1}) ₂ CO	...	20.5 + 12 × 2 <i>z</i>	12.3 + 11.4 × 2 <i>z</i>	8.2 + 0.6 × 2 <i>z</i>	1.3829 + 0.1276 × 2 <i>z</i>	7.2387 + 4.23728 × 2 <i>z</i>
[HOOC(CH ₂) _{<i>n</i>}] ₂ CO	...	65.3 + 12 × 2 <i>z</i>	40.6 + 11.4 × 2 <i>z</i>	24.7 + 0.6 × 2 <i>z</i>	5.25507 + 0.1276 × 2 <i>z</i>	23.0579 + 4.23728 × 2 <i>z</i>

In this work, eq 5 applies to the calculation of the characteristics σ and δ , which are necessary for the theoretical calculation of nmr spectra. However, for this it is necessary to demonstrate the applicability of eq 5 to the calculation of magnetic susceptibilities, χ , and their constituents, $-\chi_d$ and χ_p .

Thorough analysis of the experimental and theoretical material available in the literature^{2-4,21,22} shows us that eq 5 is directly suitable for the calculation of magnetic susceptibilities and their components, $-\chi_d$, χ_p , and χ_i ($i = 1, 2, 3$), with the rather good precision of the order of 0.1-1.0%. Relation 5 turns out to be effective, in addition, for the calculation of the corresponding susceptibilities of para- and ferromagnetic materials (see Tables I-V). More than that, from the execution of eq 5 for the determination of Langevin magnetism ($-\chi_d$) and Van Vleck paramagnetism (eq 4), it follows directly (eq 2-4) that eq 5 is correct as well for the determination of the Φ function eq 3, and the mean size of the electronic orbits of molecules, $\sum r_i^2$. This fact is noteworthy for its own sake. The fact that eq 5 can be used for the determination of the polarizability, α , and its components, α_i ($i = 1, 2, 3$), was known earlier.²⁶

In Tables I-V are given values of χ , $-\chi_d$, χ_p , χ_i , Φ , and $\sum r_i^2$ for the given molecules, *j*, either as found by us, or as borrowed in prepared form from ref 2-4 and

21; therein is cited data for entire series of families of related compounds: (1) derivatives of methane, CX₄, for X = H, Cl, Br, I, OH, C₆H₅, CH₃, C₂H₅, C_{*n*}H_{2*n*+1} ($n \geq 3$), COOH, CH₂COOH, (CH₂)₂COOH, (CH₂)_{*n*}-COOH ($n \geq 2$), COOC_{*n*}H_{2*n*+1} ($n \geq 2$), NO₂, CH₃O, (CH₂)_{*n*}OH, CHO, CH₂OH, (CH₂)_{*n*}NH₂; (2) derivatives of ethylene, C₂X₄, for X = H, CH₃, C₂H₅, C₄H₉, C_{*n*}H_{2*n*+1} ($n \geq 3$), Cl, C₆H₅, F, Br, I; (3) derivatives of ammonia, NX₃, X = H, CH₃, C₂H₅, C_{*n*}H_{2*n*+1} ($n \geq 3$); (4) the family of derivatives of hydrogen sulfide, X₂S, for X = H, CH₃, C₂H₅, C_{*n*}H_{2*n*+1} ($n \geq 0$); (5) the family of derivatives of HgX₂, X = Cl, C_{*n*}H_{2*n*+1} ($n \geq 2$); (6) the family of derivatives of benzene of the type C₆X₆, X = H, Cl, NO₂, CH₃; (7) the family of derivatives of water, X₂O, for X = H, CH₃, C₂H₅, C_{*n*}H_{2*n*+1}, NO₂, (CH₃)₂CH, (CH₃)₂CH(CH₂)₂; (8) the family of derivatives of formaldehyde of the type X₂CO, for X = H, Cl, OH, CH₃, C₂H₅, C_{*n*}H_{2*n*+1} ($n \geq 3$), HOOC, HOO(CH₂), HOOC(CH₂)₂, HOOC(CH₂)_{*n*} ($n \geq 0$), C₆H₅; (9) the families of derivatives of crystalline hydrates of the type MSO₄·*m*H₂O and MCO₃·*m*H₂O (M is Mg, Ca, Ba, Sr, Na₂, K₂, Rb₂, Cs₂ and several others).

The magnetic characteristics of the molecules desired should be calculable from the equation of weighted averages, eq 5, in that form. For example, (1) for derivatives of AX₄, where A = C, C₂, Sn, Ge, and

Table IV: Molar Magnetic Susceptibilities and Other Constants for Given Molecules, *j*, Representative of Particular Families

Compound <i>j</i>	Physical constants B_j					
	$10^{11}\alpha$	$-10^6\chi_d$	$-10^6\chi$	$10^6\chi_p$	$10^{11}\Phi$	$10^{16}\Sigma\tau_j^2/l$
C ₆ H ₆	10.3	65.0	54.85	10.15	2.1595	22.9520
C ₆ Cl ₆	22.5	176	147	21.5	4.5742	50.8474
C ₆ (NO ₂) ₆	25.2	206.5	95.2	111.5	23.7223	72.9166
C ₆ (CH ₃) ₆	23.5	144 (?)	122.5	21.5	4.5742	...
Ge(C _n H _{2n+1}) ₄	5.4 +	42 +	35.6 +	6.4 +	1.3616 +	14.8305 +
(<i>z</i> = <i>n</i> ≥ 1)	1.84	12 ×	11.4	0.6 ×	0.12728	4.23728
	× 4 <i>z</i>	4 <i>z</i>	× 4 <i>z</i>	4 <i>z</i>	× 4 <i>z</i>	× 4 <i>z</i>
Sn(C _n H _{2n+1}) ₄	6.98 +	60 +	51.7 +	8.3 +	1.7659 +	...
(<i>z</i> = <i>n</i> ≥ 1)	1.84	12 ×	11.4	0.6 ×	0.12765	...
	× 4 <i>z</i>	4 <i>z</i>	× 4 <i>z</i>	4 <i>z</i>	× 4 <i>z</i>	...
MgSO ₄ · <i>m</i> H ₂ O	4.849 +	55.39 +	43.83 +	11.558 +	2.4590 +	...
	1.593 <i>m</i>	12.73 <i>m</i>	13.124 <i>m</i>	-0.394 <i>m</i>	0.08383 <i>m</i>	...
MgCO ₃ · <i>m</i> H ₂ O	3.9 +	39.81 +	33.328 +	6.482 -	1.3791 +	...
	1.593 <i>m</i>	12.73 <i>m</i>	13.124 <i>m</i>	0.394 <i>m</i>	-0.08383 <i>m</i>	...
CaCO ₃ · <i>m</i> H ₂ O	4.85 +	48.4 +	38.2 +	10.2 -	2.1701 -	...
	1.593 <i>m</i>	12.73 <i>m</i>	13.124 <i>m</i>	0.394 <i>m</i>	0.08383 <i>m</i>	...
SrCO ₃ · <i>m</i> H ₂ O	5.65 +	61 +	47 +	14 -
	1.593 <i>m</i>	12.73 <i>m</i>	13.124 <i>m</i>	0.394 <i>m</i>
BaCO ₃ · <i>m</i> H ₂ O	6.3 +	72 +	58.9 +	28.7 -
	1.593 <i>m</i>	12.73 <i>m</i>	13.124 <i>m</i>	0.394 <i>m</i>
CaSO ₄ · <i>m</i> H ₂ O	6.15 +	63.5 +	49.7 +	13.8 -
	1.593 <i>m</i>	12.73 <i>m</i>	13.124 <i>m</i>	0.394 <i>m</i>
SrSO ₄ · <i>m</i> H ₂ O	6.55 +	73.5 +	58 +	15.5 -
	1.593 <i>m</i>	12.73 <i>m</i>	13.124 <i>m</i>	0.394 <i>m</i>
BaSO ₄ · <i>m</i> H ₂ O	7.5 +	86 +	65.8 +	10.2 -
	1.593 <i>m</i>	12.73 <i>m</i>	13.124 <i>m</i>	0.394 <i>m</i>
Na ₂ SO ₄ · <i>m</i> H ₂ O	5.88 +	63 +	52 +	11 -
	1.593 <i>m</i>	12.73 <i>m</i>	13.124 <i>m</i>	0.394 <i>m</i>
K ₂ SO ₄ · <i>m</i> H ₂ O	7.7 +	79.5 +	67 +	12.5 -
	1.593 <i>m</i>	12.73 <i>m</i>	13.124 <i>m</i>	0.394 <i>m</i>

others, and $s = 4$

$$B_{AX_a^I X_b^{II} X_c^{III} X_d^{IV}} =$$

$$1/4(aB_{AX_a^I} + bB_{AX_b^{II}} + cB_{AX_c^{III}} + dB_{AX_d^{IV}}) \quad (5^I)$$

(2) for the family of mixed derivatives of the type AX₃ for which $s = 3$

$$B_{AX_a^I X_b^{II} X_c^{III}} = 1/3(aB_{AX_a^I} + bB_{AX_b^{II}} + cB_{AX_c^{III}}) \quad (5^{II})$$

(3) and for derivatives of the type AX₂ (A = S, Hg, O, CO), for which $s = 2$

$$B_{AX_a^I X_b^{II}} = 1/2(aB_{AX_a^I} + bB_{AX_b^{II}}) \quad (5^{III})$$

and so on. Since $s = \Sigma_j \delta_j$, it may happen that some of the δ_j (a, b, c, d above) may be zero.

It is now advisable to turn our attention to the fact that eq 5 apparently permits one to check data obtained by different methods or from experiment. For example, it was revealed in our analysis that the experimental quantities $-10^6\chi$ (ppm), cited in ref 21, 39, and 40 for the molecules Sn(C₄H₉)₄ and Sn(C₇H₁₅)₄, would seem doubtful. This follows from the fact of additivity of the indicated characteristics for the

methylene group CH₂, of the linear carbon chain. Actually, in ref 22, 39, and 40 $-10^6\chi$ (ppm) should have the following values: for Sn(CH₃)₄, 97.3 instead of 98.7; for Sn(C₂H₅)₄, 142.9 instead of 139.9; for Sn(*n*-C₃H₇)₄, 188.5 as given in the references; for Sn(*n*-C₅H₁₁)₄, 279.7 as given in the references; for Sn(*n*-C₇H₁₅)₄, and 370.9 instead of 376.3. Meanwhile, other quantities, for example α , fit well into the additivity scheme. For this reason, the magnitudes of the molecular magnetic susceptibilities, $-10^6\chi$ (ppm) for Sn(*n*-C₄H₉)₄ and Sn(*n*-C₇H₁₅)₄, cited in ref 21, 39, and 40 provoke doubt. Our values seem to be somewhat better. For the same reason, the values of $-10^6\chi$ (ppm), found in the same source for *n*-C₇H₁₅OH and *n*-C₁₆H₃₃OH and various others, respectively, 91.7 and 184.6, are scarcely believable. Actually, they should be 90.6 and 193.2. The doubt expressed in ref 21 concerning the number 184.6 is correct. Doubtful data for other compounds in Tables I-V are indicated by question marks. The results of the author in the present work seem more likely.

One of the advantages of the proposed method is that it offers the possibility of deriving general calculational formulas for the determination of the physical quantities mentioned above for whole classes and families

Table V: Comparison of Molar Magnetic Susceptibilities Calculated by Our Method with Experimental Data and Various Quantum-Mechanical Methods^{21, a, b}

Substance	10 ⁶ χ, ppm						
	Experi- mental data ²¹	Author's method ^c	Difference	Quantum mechanical methods			
				a	Difference	b	Difference
<i>n</i> -Hexane	74	73.9	+0.10	72.68	+1.32	78.91	-4.91
2,2-Dimethylbutane	76.24	74.5	+1.71	72.68	+3.53	78.91	-2.70
<i>n</i> -Heptane	85.21 } 85.5 }	85.3	-0.20	83.97	+1.53	91.27	-5.77
2-Methylhexane	86.24	85.66	+0.58	83.97	+2.27	91.27	-5.03
Cycloheptane	66.0 (?)	62.50	+3.50	67.74	-1.41	74.16	-8.07
<i>trans</i> -Butene	43.3	43.2	+0.10	43.90	-0.60	47.03	-3.73
Heptene-1	75.9 } 77.6 }	75.9	0.00 } +1.70 }	75.27	+0.63 } +2.33 }	83.03	-1.13 } -5.43 }
<i>n</i> -Butylamine	58.9	56.83	+2.07	59.24	-0.34
<i>n</i> -Heptylamine	93.1	91.23	+1.87	93.26	-0.16
Di- <i>n</i> -butylamine	103.7	103.4	+0.30	105.07	-1.37
Ethyl alcohol	34.2	33.6	+0.60	33.34	+0.86
<i>n</i> -Propyl alcohol	45.0	45.0	0.00	44.68	+0.32
<i>n</i> -Nonyl alcohol	101.6 (?)	113.4	-11.8 (?)	101.37 (?)	+0.23
<i>n</i> -Octyl alcohol	102.7	102.0	+0.7
Triethylamine	81.4	81.4	0.0	82.86	-1.46
(CH ₃) ₂ C=CH ₂ (<i>cis</i>)	44.4 } 42.6 }	43.3	+1.1 } +0.70 }	43.9	+0.50 } -1.30 }	47.03	-2.66 } -4.43 }
2-Methylpentane	75.26	74.4	+0.86	72.68	+2.60	78.91	-3.65
2,2,3-Trimethylbutane	88.36	83.97	+4.39	91.27	-2.93

^a J. Tillieu, *Ann. Phys.*, **2**, 471, 631 (1957). ^b J. Bandet, J. Tillieu, and J. Grey, *Compt. Rend.*, **244**, 920 (1957). ^c P. G. Maslov, The Sixth Ukrainian Conference on Physical Chemistry at Kiev, 1964, p 93.

of related compounds. We shall illustrate this statement with examples.

Example 1. Knowing $-10^6\chi$ (ppm) for NH₃ and N(C_{*n*}H_{2*n*+1})₃ to be 10.6 and 13.0 + 11.4(3*z*) from Table II, calculate the corresponding formula for $-10^6\chi$ (ppm) for primary and secondary amines. Solution: let us use eq 5 and take X^I to be H, X^{II} = X^{III} = C_{*n*}H_{2*n*+1}.

(a) For primary amines ($a = b = 2$, and $c = 1$), we obtain

$$B_i = \frac{1}{3}[2B_{\text{NH}_3} + B_{\text{N}(\text{C}_n\text{H}_{2n+1})_3}] = \frac{1}{3}[2 \times 10.6 + (13 + 11.4 \times 3z)]$$

or, finally

$$-10^6\chi = [11.4 + 11.4z] \text{ ppm} \quad (5^{\text{IV}})$$

($z \geq 3$)

(b) For secondary amines

$$B_i = \frac{1}{3}[B_{\text{NH}_3} + 2B_{\text{N}(\text{C}_n\text{H}_{2n+1})_2}] = \frac{1}{3}[10.6 + 2(13 + 11.4 \times 3z)]$$

or, finally

$$-10^6\chi = [12.2 + 11.4(2z)] \text{ ppm} \quad (5^{\text{V}})$$

($z \geq 3$)

One easily can convince oneself of the satisfactory precision of the derived formulas (5^{IV}, 5^V) from Tables V and VI.

Example 2. Given $-10^6\chi$ (ppm) for H₂O (12.0) and for *n*-alcohols (11.8 + 12*z* (see Table III), derive the corresponding expressions for the family of symmetrical ethers (*n*-C_{*n*}H_{2*n*+1})₂O. Solution: taking X^I = H and X^{II} = *n*-C_{*n*}H_{2*n*+1}, from the equation of weighted averages eq, 5^{III}, we obtain

$$B_{\text{AX}_2\text{II}} = 2B_{\text{AX}^{\text{I}}\text{X}^{\text{II}}} - B_{\text{AX}^{\text{I}}}$$

$2B_{\text{n-C}_n\text{H}_{2n+1}\text{OH}} - B_{\text{H}_2\text{O}} = 2(11.8 + 12z) - 12$
or, finally

$$-10^6\chi = [11.6 + 12(2z)] \text{ ppm} \quad (5^{\text{VI}})$$

($z \geq 0$). In the degree of precision of the correlations obtained, one can be convinced of the validity of eq 5 by means of such concrete calculations. For example, for H₂O we obtain 11.6 instead of 12.0;^{3,21} for CH₃OH, 23.6 instead of 23.8;^{3,21} for C₂H₅OH, 35.6 instead of 36.0,^{3,21} and for *n*-C₃H₇OH, 47.6 instead of 48.0;^{3,21} for more complicated representatives, complete coincidence with the data of ref 3 and 21 is obtained.

Example 3. To calculate $-10^6\chi$ (ppm) for tartaric acid HOOCCHOHCOOH, using the data of Table I. Solution: one can consider the molecule as a derivative of CH₄, *i.e.*, as CH(OH)(COOH)₂. Then, by the data referred to in Table I, and the equation of weighted averages, we find

$$B_i = \frac{1}{4}[B_{\text{CH}_4} + B_{\text{C}(\text{OH})_4} + 2B_{\text{C}(\text{COOH})_4}] = \frac{1}{4}(16.9 + 47.4 + 2 \times 112)$$

Table VI: Comparison of Molar Magnetic Susceptibilities Calculated by Our Method with Experimental Data and Various Quantum-Mechanical Methods^{21, a, b}

Substance	$-10^6\chi_d$			$-10^6\chi$			$10^6\chi_p$		
	Author's method ^c	Data from ref 21	Difference	Author's method ^c	Data from ref 21	Difference	Author's method ^c	Data from ref 21	Difference
Dimethyl ketone	44.5	44.7	-0.20	35.1	33.8	+1.3	10.7	10.9	-0.20
Methylethyl ketone	56.5	56.5	0.00	45.6	45.6	0.00	10.9	10.9	0.00
Methylpropyl ketone	68.5	68.5	0.00	57.29	57.4	+0.11	11.25	11.1	+0.15
Methylbutyl ketone	80.5	79.5 (?)	1.00	68.65	69.1	-0.45	11.85	10.4	+1.45
Methylhexyl ketone	104.5	104.5	0.00	92.1	92.1	0.00	13.05	12.4	+0.65
Diisobutyl ketone	116.5	117.0	-0.50	103.5	104.3	-0.80	13	12.7	+0.30
Diphenyl	127	127	0.00	104.6	102.5	+2.10	22.4	~25.2	-2.8
Dibenzyl	151	151	0.00	127.4	127.4	0.00	23.6	24	-0.4
Formic acid	28.05	28.0	+0.05	20.95	18.9	+1.05	7.10
Acetic acid	40.05	40.20	-0.15	31.7	31.8	-0.10	8.25
Methanedicarboxylic acid	62.45	63.0	-0.55	46.5	46.3	+0.20	15.95	16.7	-0.75
1,2-Ethanedicarboxylic acid	74.45	74.5	-0.05	57.9	57.9	0.00	16.55	16.60	-0.05
Stilbene	152	154	-2.00	116.68	116.25	0.43	35.32	37.75	-2.43
<i>n</i> -Butylamine	62.6	62	+0.60	57.0	58.90 } 56.8 } 61.0 }	1.90 } 1.00 } -3.20 }	5.0	3.1	+2.00
Diethylamine	62.97	63	-0.03	57.8	63.5 } 61.0 }	-5.70 } -3.20 }	5.17	6.20	-1.03
Di- <i>n</i> -heptylamine	182.3	~182	+0.30	171.8	171.5	-0.30	10.2	10.0	+0.20
Methyl chloride	33.38	33.6	-0.22	29.38	31.7	-2.32	4	2.0	+2.0
Nitroethane	51.0	51.1	-0.10	33.47	33.6	-0.13	17.52	17.5	+0.02
Dimethylnitromethane	63.1	63.1	0.00	45.02	45.7	-0.68	18.08	17.5	+0.58
Acetonitrile	30.08	30.2	-0.12	27.57	27.6	-0.03	2.5	2.6	-0.10
Propionitrile	42.18	42.2	-0.02	39.12	38.8	+0.32	3.05	3.4	-0.35
Toluene	77.75	77	+0.75	66.12	66.1	+0.02	11.65	10.9	+0.65
<i>p</i> -Xylene	91.33	90	+0.33	77.40	76.82	0.58	13.93	13.13	+0.80

^a See footnote a, Table V. ^b See footnote b, Table V. ^c See footnote c, Table V.

Answer: $-10^6\chi = 72.08$ ppm.

Example 4. To find $-10^6\chi$ and $-10^6\chi_p$ of propionaldehyde. Solution: (a) First we take the molecule as a derivative of methane; then, by the data given in Table I and formula 5^I we obtain

$$-10^6\chi = \frac{1}{4}[2\chi_{\text{CH}_4} + \chi_{\text{C}(\text{CH}_3)_4} + \chi_{\text{C}(\text{CHO})_4}] = \frac{1}{4}(2 \times 16.9 + 63.1 + 42) = 34.72 \text{ ppm}$$

(b) We shall now consider our molecule as an unsymmetrical ketone of the type $(\text{C}_2\text{H}_5)_2\text{HCO}$; then, by the data of Table III and formula 5^{III} we have

$$-10^6\chi = \frac{1}{2}(\chi_{(\text{C}_2\text{H}_5)_2\text{CO}} + \chi_{\text{H}_2\text{CO}}) = \frac{1}{2}(57.4 + 12.3) = 34.85 \text{ ppm}$$

Both results, for practical purposes, coincide; the average of them is taken for the one result, $-10^6\chi = 34.78$ ppm.

By an analogous method, we find for $-10^6\chi_p$ by the first variation 9.65, and by the second, 9.8; the mean value will be 9.74; the additive method in ref 21 gives 10.6 ppm. Answer: $-10^6\chi = 34.78$; $-10^6\chi_p = 10$ ppm.

Comparative data, found in Tables V and VI, leave

no doubt as to the effectiveness and rather high precision of the proposed method, of the order of 0.1-1.0%.

The given values, found in Tables I-V for the known molecules, *j*, offer the possibility of simple and extremely precise calculation of the most important characteristics of molecules: magnetic susceptibilities; $-10^6\chi$, their components $-10^6\chi_d$, $10^6\chi_p$, $10^6\chi_i$ ($i = 1, 2, 3$); the polarizabilities $10^{24}\alpha$; Φ function; and $\sum_{i,r} \frac{1}{r^2}$ for a large quantity of more complicated representatives of the families of molecules indicated in the tables, amounting to tens of thousands of molecules.

We show now that we may adapt the equation of weighted averages, eq 5, for the calculation of the magnetic shielding constant of nuclei in molecules, σ , and the components σ_i ($i = 1, 2, 3$), their chemical shifts, δ , without knowledge of which it is impossible to calculate nmr spectra.

As is well known

$$\sigma = \frac{1}{3}[\sigma_{11} + \sigma_{22} + \sigma_{33}] = \frac{1}{3}[\sigma_1 + \sigma_2 + \sigma_3] \quad (6)$$

and the chemical shifts

$$\delta = \sigma - \sigma_{\text{std}} = \frac{H - H_{\text{std}}}{H_{\text{std}}} \quad (7)$$

Table VIII: Comparison of Chemical Shifts, δ (ppm), of Some Nuclei Calculated by Our Method with Data of Other References^{a, b}

Molecule	$10^6\delta_{CH_2}$		$10^6\delta_{CH_3}$		Molecule	$10^6\delta_M$	
	Data from ref 3	Author's data	Data from ref 3	Author's data		Data from ref 3	Author's data
CH ₃ CH ₂ J	4.34*	4.33	5.73*	5.73	RbJ	-149*	-169
CH ₃ CH ₂ Br	4.08*	4.06	5.83*	5.83	RbBr	-129*	-119
CH ₃ CH ₂ Cl	3.80*	3.83	5.93*	5.93	RbCl	-89*	-94
CH ₃ CH ₂ F	2.87*	3.52	6.07*	6.03	RbF	-60*	-50
CH ₃ J	2.00*	1.94	CsJ	-252*	-253
CH ₃ Br	2.02*	2.05	CsBr	-208*	-208
CH ₃ Cl	2.10*	2.04	CsCl	-163*	-164
CH ₃ F	2.10*	2.18	CsF	-90*	-118

Molecule	$10^6\delta_{P^{31}}$		Molecule	$10^6\delta_{Si^{28}}$		Molecule	$10^6\delta_{Si^{29}}$	
	Data from ref 3	Author's data		Data from ref 3	Author's data		Data from ref 3	Author's data
POF ₃	15.8*	...	Si(CH ₃) ₄	-21*	...	Si(C ₂ H ₅ O)F ₃	-82	
POFCl ₂	-69.0*	...	Si(C ₂ H ₅ O) ₄	+59*	...	Si(CH ₃) ₂ (C ₂ H ₅ O)F	-28	
POClF ₂	-30.4	-27	Si(CH ₃)(C ₂ H ₅ O) ₃	+19	+39	Si(C ₂ H ₅ O) ₂ (CH ₃)F	-8	
...	SiF ₄	-129*	...	SiF ₂ (CH ₃)(C ₂ H ₅ O)	-55	
...	Si(CH ₃) ₃ F	...	-48			
...	Si(CH ₃) ₃ (C ₂ H ₅ O)	...	-2			
...	Si(CH ₃) ₂ F ₂	...	-75			
...	Si(CH ₃) ₂ (C ₂ H ₅ O) ₂	...	+19			
...	Si(CH ₃)F ₃	...	-102			
...	Si(C ₂ H ₅ O) ₃ F	...	+12			
...	Si(C ₂ H ₅ O) ₂ F ₂	...	-35			

^a Methyl and methylene group chemical shifts are measured relative to benzene; the phosphorous halides from CF₃COOH at 6365 G. the silicon compounds relative to the silicone DC-200 with viscosity 100 Cp; and the metals relative to the saturated solution of their chlorides. ^b M = Rb, Cs.

Table IX: The Chemical Shifts of Nuclei P³¹ in Different Molecules Calculated by Using the Equation of Weighted Averages, Eq 5^a

Molecule	$10^6\delta_{P^{31}}$, ppm		Molecule	$10^6\delta_{P^{31}}$, ppm		Molecule	$10^6\delta_{P^{31}}$, ppm	
	Data from ref 3	Author's data		Data from ref 3	Author's data		Data from ref 3	Author's data
PH ₃	238*	...	PH(C ₆ H ₅) ₂	...	+83.2	P(CH ₃) ₂ (C ₆ H ₅)	...	+42.3
P(CH ₃) ₃	61*	...	PH ₂ (C ₂ H ₅ S)	...	+120.1	P(CH ₃)(C ₆ H ₅) ₂	...	+24.3
P(C ₂ H ₅) ₃	20.4*	...	PH(C ₂ H ₅ S) ₂	...	+2.2	P(CH ₃) ₂ (C ₂ H ₅ S)	...	+2.1
P(C ₆ H ₅) ₃	5.9*	...	PH ₂ [(CH ₃) ₂ N]	...	+118	P(CH ₃)(C ₂ H ₅ S) ₂	...	-56.7
P(C ₂ H ₅ S) ₃	-115.6*	...	PH[(CH ₃) ₂ N] ₂	...	-2	P(CH ₃) ₂ [(CH ₃) ₂ N]	...	0.00
P[(CH ₃) ₂ N] ₃	-122*	...	PH ₂ (CH ₃ O)	...	+111.7	P(CH ₃)[(CH ₃) ₂ N] ₂	...	-40.7
P(CH ₃ O) ₃	-141*	...	PH(CH ₃ O) ₂	...	-14.7	P(CH ₃) ₂ (CH ₃ O)	...	-6.3
P(C ₂ H ₅ O) ₃	-138*	...	PH ₂ (C ₂ H ₅ O)	...	+112.7	P(CH ₃)(CH ₃ O) ₂	...	-73.7
PCl ₃	-215*	...	PH(C ₂ H ₅ O) ₂	...	-12.7	P(CH ₃) ₂ (C ₂ H ₅ O)	...	-5.3
PBr ₃	-222*	...	PH ₂ Cl	...	+87	P(CH ₃)(C ₂ H ₅ O) ₂	...	-71.7
PJ ₃	-178*	-230*	PHCl ₂	...	-64	P(CH ₃) ₂ Cl	...	-31
PF ₃	-97*	...	PH ₂ Br	...	+84.7	P(CH ₃)Cl ₂	...	-123
PH ₂ (CH ₃)	163.5	179	PHBr ₂	...	-68.7	P(CH ₃) ₂ Br	...	-33
PH(CH ₃) ₂	98.5	120	PH ₂ J	...	+82	P(CH ₃)Br ₂	...	-124.3
PH(CH ₃ O) ₂	-181(?)	-15	PHJ ₂	...	-74	P(CH ₃) ₂ J	...	-36
PH ₂ (CH ₃ O)	...	+112	PH ₂ F	...	+126	P(CH ₃)J ₂	...	-133
PH ₂ (C ₂ H ₅)	...	+166	PHF ₂	...	+14.7	P(CH ₃) ₂ F	...	+8.3
PH(C ₂ H ₅) ₂	...	+93	P(CH ₃) ₂ C ₂ H ₅	...	+47.5	P(CH ₃)F ₂	...	-44.3
PH ₂ (C ₆ H ₅)	...	+161	P(CH ₃)(C ₂ H ₅) ₂	...	+34	P(C ₂ H ₅) ₂ (C ₆ H ₅)	...	+15.6

^a The chemical shifts $\delta_{P^{31}}$ are measured relative to 85% aqueous H₃PO₄.

Table X: The Chemical Shifts, $\delta_{P^{31}}$, of Nuclei P^{31} in Different Molecules Calculated by Using the Equation of Weighted Averages, Eq 5

Molecule	$10^6\delta_{P^{31}}$, ppm	Molecule	$10^6\delta_{P^{31}}$, ppm	Molecule	$10^6\delta_{P^{31}}$, ppm
$P(C_2H_5O)F_2$	-110.7	$PH(CH_3)Br$	+25.7	$PH(C_2H_5S)[(CH_3)_2N]$	+0.1
PCl_2Br	-214	$PH(CH_3)J$	+23.0	$PH(C_2H_5S)(CH_3O)$	-6.2
$PClBr_2$	-216.3	$PH(CH_3)F$	+67.3	$PH(C_2H_5S)(C_2H_5O)$	-5.2
PCl_2J	-220	$PH(C_2H_5)(C_6H_6)$	+88.1	$PH(C_2H_5S)Cl$	-30.9
PCl_2	-225	$PH(C_2H_5)(C_2H_5S)$	+47.6	$PH(C_2H_5S)Br$	-33.2
PCl_2F	-142.3	$PH(C_2H_5)[(CH_3)_2N]$	+45.5	$PH(C_2H_5S)J$	-35.9
$PClF_2$	-136.3	$PH(C_2H_5)(CH_3O)$	+35.8	$PH(C_2H_5S)F$	+8.5
PBr_2J	-224.7	$PH(C_2H_5)(C_2H_5O)$	+40.1	$PH[(CH_3)_2N](CH_3O)$	-8.3
PBr_2	-227.3	$PH(C_2H_5)Cl$	+14.5	$PH[(CH_3)_2N](C_2H_5O)$	-7.3
PBr_2F	-180.3	$PH(C_2H_5)Br$	+12.1	$PH[(CH_3)_2N]Cl$	-33.0
$PBrF_2$	-138.7	$PH(C_2H_5)J$	+9.5	$PH[(CH_3)_2N]Br$	-35.3
PJ_2F	-185.7	$PH(C_2H_5)F$	+53.8	$PH[(CH_3)_2N]J$	-34.7
PJF_2	-141.3	$PH(C_6H_5)(C_2H_5S)$	+42.8	$PH[(CH_3)_2N]F$	+6.3
$PH(CH_3)(C_2H_5)$	-106.5	$PH(C_6H_5)[(CH_3)_2N]$	+40.6	$PH(CH_3O)(C_2H_5O)$	-13.7
$PH(CH_3)(C_6H_5)$	+101.6	$PH(C_6H_5)(CH_3O)$	+34.3	$PH(CH_3O)Cl$	-39.3
$PH(CH_3)(C_2H_5S)$	+61.1	$PH(C_6H_5)(C_2H_5O)$	+35.3	$PH(CH_3O)Br$	-41.7
$PH(CH_3)[(CH_3)_2N]$	+59.0	$PH(C_6H_5)Cl$	+9.6	$PH(CH_3O)J$	-44.3
$PH(CH_3)(CH_3O)$	+52.7	$PH(C_6H_5)Br$	+7.3	$PH(CH_3O)F$	0.0
$PH(CH_3)(C_2H_5O)$	+53.7	$PH(C_6H_5)J$	+4.6	$PH(C_2H_5O)Cl$	-38.3
$PH(CH_3)Cl$	+28.0	$PH(C_6H_5)F$	+48.9	$PH(C_2H_5O)Br$	-40.7

It is known that, by experimental measurements of chemical shifts, δ , with the use of an external standard substance, a correction for the difference between the volume diamagnetic susceptibilities of the standard substance, $\chi_{v, std}$, and the unknown sample, χ_v , should be introduced.³ This is connected with the fact that the field actually at the site of a given nucleus of a molecule in a cylindrical sample depends on the magnitude of the net applied magnetic field.

If the length of the sample is much larger than the radius of a sphere centered on the nucleus, then, as is known,³ the magnetic field intensity inside such a sphere is

$$H_{sph} = H_0 \left[1 - \frac{2\pi}{3} \chi_v \right] \quad (10)$$

where H_0 is the magnitude of the external magnetic field. From this, the influence of the magnetization of an ampoule of the substance in a cylindrical sample is equivalent to the addition to σ of $(2\pi/3)\chi_v$.³

Consequently, the chemical shift of the unknown nuclei in molecules of substances enclosed in long cylindrical ampoules must be calculated, not by eq 7, but by a relation of the form

$$\delta_{sph} = \sigma - \sigma_{std} + \frac{2\pi}{3} [\chi_{v, std} - \chi_v] = \delta + \frac{2\pi}{3} [\chi_{v, std} - \chi_v] \quad (11)$$

In the preceding expression, one may take into consideration the fact that the volume diamagnetic sus-

ceptibility, χ_v , is connected with the molecular magnetic susceptibility by an equation of the type

$$\chi = \frac{M\chi_v}{d} \quad (12)$$

We shall rewrite eq 11, namely in the form

$$\chi = \chi_{std} + \frac{3M}{2\pi d} [\delta - \delta_{sph}] = 3V_0[2\pi]^{-1} [\delta - \delta_{sph}] + \chi_{std} \quad (13)$$

or

$$\chi = 3V_0[2\pi]^{-1} [(\sigma - \sigma_{std}) - (\sigma - \sigma_{std})_{sph}] + \chi_{std} \quad (13^I)$$

In the preceding relations, M is the molecular weight, d is the density, and V_0 is the molar volume.

In eq 13 and 13^I, the left side, *i.e.*, χ is determined by the law of weighted averages; the quantities V_0 , σ_{std} , and χ_{std} which appear in the right side remain identical for all members of the chosen families of substances, or for them, eq 5 is automatically implemented. For this reason, putting eq 13 or 13^I into eq 5, in place of B_i and B_j , for the unknown molecule, i , and the given molecule, j , and comparing the corresponding terms of the left and right sides of the equations obtained, it is not difficult to see that, at least in conformity with the families of related compounds, the law of weighted averages remains in force both for the magnetic shielding constant and the chemical shifts, δ ; that is to say

$$\sigma_i = \frac{1}{s} \sum_j m_j \sigma_j \quad (14)$$

Table XI: The Chemical Shifts, $\delta_{P^{31}}$, of Nuclei P^{31} in Different Molecules Calculated by Using the Equation of Weighted Averages, Eq 5

Molecule	$10^6\delta_{P^{31}}$, ppm	Molecule	$10^6\delta_{P^{31}}$, ppm	Molecule	$10^6\delta_{P^{31}}$, ppm	Molecule	$10^6\delta_{P^{31}}$, ppm
$P(C_2H_5)(C_6H_5)_2$	+10.7	$P(C_6H_5)_2[(CH_3)_2N]$	-36.7	$P(C_2H_5S)(C_2H_5O)_2$	-180.5	$P[(CH_3)_2N]_2F$	-113.7
$P(C_2H_5)_2(C_2H_5S)$	-25.0	$P(C_6H_5)[(CH_3)_2N]_2$	-79.4	$P(C_2H_5S)_2Cl$	-148.7	$P[(CH_3)_2N]_2F_2$	-105.3
$P(C_2H_5)(C_2H_5S)_2$	-70.2	$P(C_6H_5)_2(CH_3O)$	-43.1	$P(C_2H_5S)Cl_2$	-181.9	$P(CH_3O)_2(C_2H_5O)$	-140.0
$P(C_2H_5)_2[(CH_3)_2N]$	-27.1	$P(C_6H_5)(CH_3O)_2$	-92.0	$P(C_2H_5S)_2Br$	-151.1	$P(CH_3O)(C_2H_5O)_2$	-139.0
$P(C_2H_5)[(CH_3)_2N]_2$	-74.5	$P(C_6H_5)_2C_2H_5O$	-42.1	$P(C_2H_5S)_2Br_2$	-186.5	$P(CH_3O)_2Cl$	-165.7
$P(C_2H_5)_2(CH_3O)$	-33.4	$P(C_6H_5)(C_2H_5O)_2$	-90.0	$P(C_2H_5S)_2J$	-153.7	$P(CH_3O)Cl_2$	-193.7
$P(C_2H_5)(CH_3O)_2$	-87.2	$P(C_6H_5)_2Cl$	-64.4	$P(C_2H_5S)J_2$	-191.9	$P(CH_3O)_2Br$	-168.0
$P(C_2H_5)_2(C_2H_5O)$	-32.4	$P(C_6H_5)Cl_2$	-141.3	$P(C_2H_5S)_2F$	-109.4	$P(CH_3O)Br_2$	-195.0
$P(C_2H_5)(C_2H_5O)_2$	-85.2	$P(C_6H_5)_2Br$	-70.1	$P(C_2H_5S)_2F_2$	-103.2	$P(CH_3O)_2J$	-170.7
$P(C_2H_5)_2Cl$	-58.1	$P(C_6H_5)Br_2$	-146.0	$P[(CH_3)_2N]_2(CH_3O)$	-128.3	$P(CH_3O)J_2$	-200.3
$P(C_2H_5)Cl_2$	-136.5	$P(C_6H_5)_2J$	-72.4	$P[(CH_3)_2N](CH_3O)_2$	-134.7	$P(CH_3O)_2F$	-126.3
$P(C_2H_5)_2Br$	-60.4	$P(C_6H_5)J_2$	-151.4	$P[(CH_3)_2N]_2(C_2H_5O)$	-127.3	$P(CH_3O)F_2$	-111.7
$P(C_2H_5)Br_2$	-141.2	$P(C_6H_5)_2F$	-28.4	$P[(CH_3)_2N](C_2H_5O)_2$	-132.7	$P(C_2H_5P)_2Cl$	-163.7
$P(C_2H_5)_2J$	-63.1	$P(C_6H_5)F_2$	-62.7	$P[(CH_3)_2N]_2Cl$	-153.0	$P(C_2H_5O)Cl_2$	-189.3
$P(C_2H_5)J_2$	-146.5	$P(C_2H_5S)_2[(CH_3)_2N]$	-117.7	$P[(CH_3)_2N]Cl_2$	-184.0	$P(C_2H_5O)_2Br$	-166.0
$P(C_2H_5)_2F$	-18.7	$P(C_2H_5S)[(CH_3)_2N]_2$	-119.9	$P[(CH_3)_2N]_2Br$	-155.3	$P(C_2H_5O)Br_2$	-194.0
$P(C_2H_5)F_2$	-58.0	$P(C_2H_5S)_2(CH_3O)$	-124.1	$P[(CH_3)_2N]Br_2$	-188.7	$P(C_2H_5O)_2J$	-168.7
$P(C_6H_5)_2(C_2H_5S)$	-34.6	$P(C_2H_5S)(CH_3O)_2$	-132.5	$P[(CH_3)_2N]_2J$	-158.0	$P(C_2H_5O)J_2$	-199.3
$P(C_6H_5)(C_2H_5S)_2$	-75.1	$P(C_2H_5S)_2(C_2H_5O)$	-123.1	$P[(CH_3)_2N]J_2$	-194.0	$P(C_2H_5O)_2F$	-124.3

$$\delta_i = \frac{1}{s} \sum_j m_j \delta_j \quad (15)$$

Here $s = \sum_j m_j = \sum_j \delta_j$ (do not confuse δ with δ_j in $s = \sum_j \delta_j$).

In Tables VII–XI are found chemical shifts, δ , of a series of given molecules, j , and unknown molecules, i , with the nuclei H^1 , F^{19} , and P^{31} . The corresponding material of Tables VIII and IX testifies to the satisfactory agreement of our results with data of other sources.^{2,3} The given materials were borrowed from ref 2 and 3 or found by us by the use of the eq 5. They are indicated in the tables by an asterisk. In Tables

IX–XI are found chemical shifts for a large group of compounds and their molecules, chemical shifts for which, it seems, are not known. Of course, the precision of the quantities found is not great, which is connected in significant measure with the low precision of the given data. With the availability of more reliable values for given molecules, the proposed method will allow the calculations of the indicated characteristics more precisely. One may hope that a new possibility of semiempirical calculation of chemical shifts and magnetic shielding constants, in turn, will be useful for calculation of nmr spectra.

Sorption and Magnetic Susceptibility Studies on Metal-Free-Radical Systems: Nitric Oxide on Palladium

by Richard W. Zuehlke, Maurice Skibba, and Carl Gottlieb

Department of Chemistry, Lawrence University, Appleton, Wisconsin 54911 (Received January 24, 1967)

Sorption and simultaneous magnetic-susceptibility measurements were made on a nitric oxide-palladium black system from -196 to 42° . The results suggest that NO is adsorbed in one (possibly two) chemisorption form, a low-energy state reached through physisorbed NO as a precursor state. In addition, a transition temperature of -120° is observed for equilibrium between mobile and immobile forms of chemisorbed NO. Pertinent energetics for the system are summarized in an energy profile, thereby justifying an observed case of high-temperature physisorption.

Introduction

The investigation described below was undertaken to shed some light on the nature of the interaction between an "odd molecule" and a free-metal surface unperturbed even by a support matrix.

Adsorption studies involving nitric oxide are limited in number but are rather varied in adsorbent and technique. Included are a series of oxide gels by straight isotherms,¹ potassium chloride by straight isotherms,² iron and nickel by infrared,³ transition metals and oxides by infrared,⁴ and several refractory oxides and palladium by magnetic methods referred to below. Several catalytic-decomposition studies have been made at elevated temperatures,⁵ but they will not be considered here.

The picture that emerges from these studies is that NO, by virtue of its free-radical character, can adsorb in a variety of different ways, depending upon the nature of the adsorbent and, for a given adsorbent, upon the exact position of adsorption on the surface and upon the temperature of adsorption. This paper does not alter that picture at all and further supplies some details of the energetics of adsorption of nitric oxide on an unsupported palladium surface.

Experimental Section

Palladium samples used were all supplied in one lot by Engelhard Industries, Inc. Typical analyses have been presented,⁶ and all samples have been shown to be purely paramagnetic through a susceptibility-field strength investigation.

Nitric oxide came from Matheson cylinders and was fractionally distilled through a tetratrap at -139° until the frozen product was snow-white in color (usually five distillations). Tank hydrogen (99.9%) was purified by passage through a Deoxo purifier, through hot magnesium perchlorate, and finally through activated charcoal at -196° . Tank oxygen (99.5%) was passed through ascarite, over hot CuO,

and finally through a Dry Ice-ether trap for purification.

The experimental system used was a classical gravimetric-sorption system employing a Cahn RG electrobalance, a vacuum system capable of regular production of 10^{-6} torr, and a needle valve for dosing. The null-seeking electrobalance was also used for simultaneous magnetic-sorption determinations through the use of the Faraday susceptibility technique; the pole-tip configuration used with the 4.5-in. magnet has been described.⁶

Sorption-rate studies were made at constant pressure using a Pirani gauge as a monitor and the needle valve as a regulator. During a series of magnetic-sorption determinations, the maximum nitric oxide pressure used was about 1 torr.

Since the investigation was, in part, designed to study the influence of palladium surface states on the adsorption process, it was necessary to retain a fixed particle size throughout; consequently, only a mild cleaning process could be used in pretreating the samples. The pretreatment process finally selected (and referred to as CP-II) was: (1) hydrogen scrubbing (300 μ pressure, room temperature), (2) evacuation and pump off at 80° , (3) oxygen (40 μ , 80°), (4) evacuation at 80° , (5) hydrogen (300 μ , room temperature), (6) evacuation at 80° , (7) nitric oxide (300 μ , room temperature), (8) evacuation at 80° , and (9) repeat steps 1-6.

After a sample had been exposed to nitric oxide during a run, the nitric oxide was pumped off at room

(1) L. I. Kuznetsov-Fetisov and E. S. Krasnyi, *Tr. Kazan. Khim.-Tekhnol. Inst.*, 106 (1958); *Chem. Abstr.*, 53, 21029e (1959).

(2) A. Granville and P. G. Hall, *J. Phys. Chem.*, 70, 937 (1966).

(3) G. Blyholder and M. C. Allen, *ibid.*, 69, 3998 (1965).

(4) A. Terenin and L. Røev, *Spectrochim. Acta*, 946 (1959).

(5) J. T. Yates, Jr., and T. E. Maday, *J. Chem. Phys.*, 45, 1623 (1966), and references therein.

(6) R. W. Zuehlke, Ph.D. Thesis, University of Minnesota, Minneapolis, Minn., 1960.

temperature, and the sample was subjected to step 9.

Starting weights for a given sample (usual weight, 150 mg) agreed within 50 μg . When discrepancies greater than this occurred, the sample was discarded. While this procedure admittedly does not yield a "clean" surface, the data obtained suggest that there are substantial areas of bare metal formed, and, at the very least, they are formed reproducibly. Return of the magnetic susceptibility to the precleaning value after cleaning indicated that neither appreciable particle-size change nor hydrogen uptake occurred as a result of the cleaning.

Occasionally, reference will be made to samples cleaned with procedure CP-I. This consisted of several consecutive exposures of the sample to hydrogen at low pressures and room temperature, with evacuation and pump off at room temperature occurring between each exposure.

Data. The adsorption of NO on palladium is generally irreversible, except near monolayer coverage (monolayer coverage for NO is defined with respect to nitrogen BET areas); *i.e.*, at this coverage an added increment of gas can be readily removed by pumping at constant temperature. Therefore, isosteric heats of adsorption obtained by a Clausius-Clapeyron analysis are generally invalid except in the region of monolayer coverage. Figure 1 shows such an analysis in the 0–28° temperature range for the NO-Pd system cleaned with procedure CP-I, where the minimum in the curve occurs at monolayer coverage. In this case, the observed heat of adsorption of 3.56 kcal/mol corresponds very closely to the heat of liquefaction of nitric oxide, 3.29 kcal/mol.⁷ For the samples used in this study (cleaned by procedure CP-II), however, the adsorption at monolayer coverage is not entirely reversible, and the Clausius-Clapeyron heats (of questionable validity) at roughly the same temperatures range from 4.5 to 6.0 kcal/mol. These observations suggest that extensive physical adsorption occurs at monolayer coverage, either exclusively or concurrently with a more energetic chemisorption, depending upon the exact nature of the substrate surface.

Studies of the desorption kinetics of the nitric oxide indicate that two types of nitric oxide binding are involved. Thus in the temperature range 25–50°, nitric oxide, preadsorbed at 25°, desorbs with an energy of 4.07 kcal/mol. After removal of the weakly bound NO, which typically amounts to about 50%, desorption in the temperature range 69–162° occurred with an energy of 10.5 kcal/mol. These observations are in good agreement with the postulates presented in the preceding paragraph.

In Figure 2, redrawn recorder traces show the rate of adsorption of nitric oxide on a freshly cleaned surface under a constant pressure of 75 μ in the temperature range from –22.5 to –77.6°. It will be noted that at

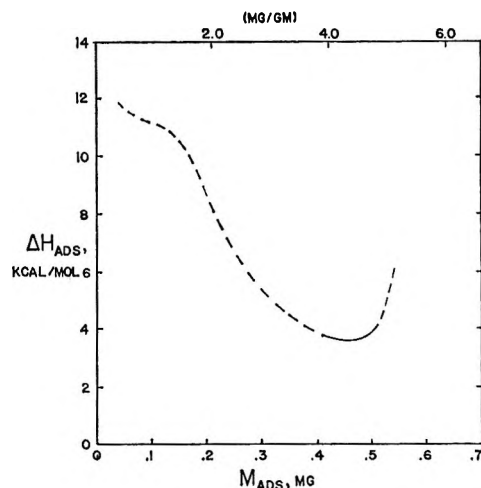


Figure 1. Isosteric heats of adsorption (after Clausius-Clapeyron) of nitric oxide on palladium black (sample weight, 150 mg).

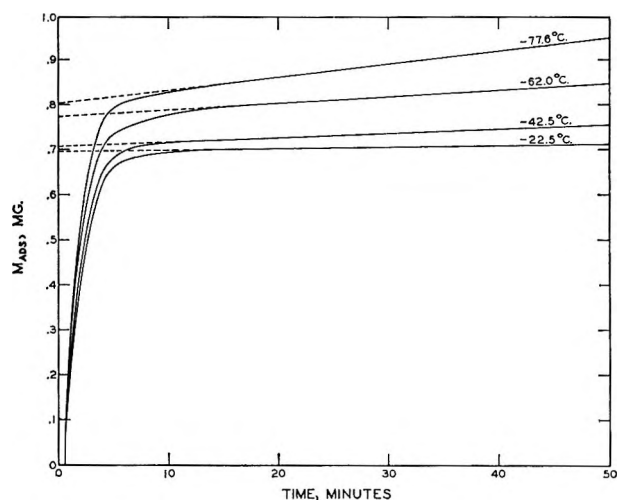


Figure 2. Time dependence of nitric oxide adsorption on palladium black (sample weight, 150 mg). Initially clean surfaces exposed to a constant pressure.

these temperatures an initial rapid adsorption occurs, followed by a much slower sorption, the rate of which increases with decreasing temperature. It seems reasonable to assume that the slow and linear increase (with time) of adsorption represents a chemisorption process. Should this be true, an extrapolation back to zero time would give the amount of physisorbed NO.

An Arrhenius plot for the chemisorption rates leads to an apparent negative activation energy of –3.39 kcal/mol. Since this situation is identical with that found in the nitric oxide-alumina system (*vide infra*), it is taken as further support for the postulate of coexisting chemisorption and physisorption, even at temperatures exceeding the critical temperature of nitric oxide.

Figure 3 shows two sets of isobars obtained at 75 μ

(7) D. M. Yost and H. Russell, "Systematic Inorganic Chemistry," Prentice-Hall, Inc., Englewood Cliffs, N. J., 1944, p 25.

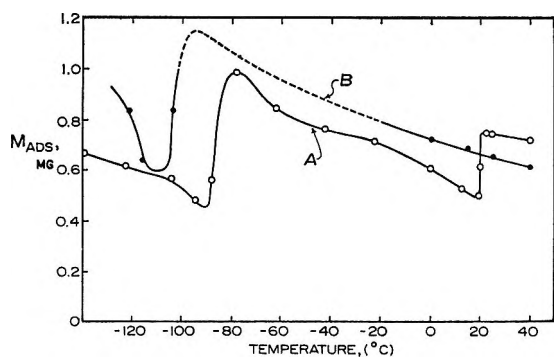


Figure 3. Isobars (at 75μ pressure) for nitric oxide on palladium black (sample weight, 150 mg): curve A, single exposures of initially clean surface; curve B, points selected from isotherms.

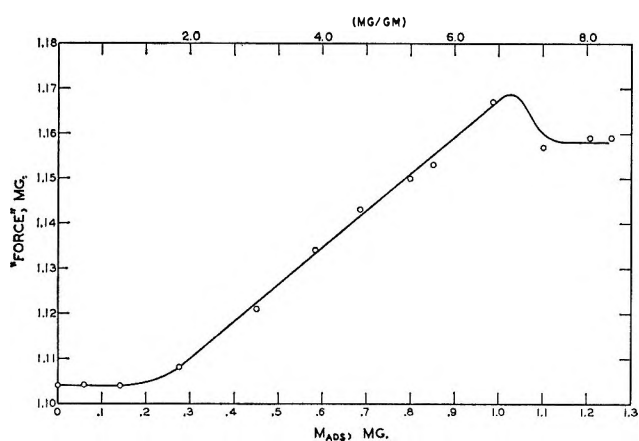


Figure 4. Magnetotherm (-196°) for nitric oxide on palladium black (sample weight, 150 mg). Cleaning procedure II used.

pressure for the nitric oxide-palladium system. Data for isobar A were obtained by following the extent of sorption when an initially clean sample was exposed to a constant NO pressure of 75μ . The temperature sequence was more or less random, and a given point could be reproduced within approximately $\pm 20 \mu\text{g}$. The points shown represent the amount of gas adsorbed after an exposure of 1 hr; at temperatures below -85° and above $+21^\circ$, this is an apparent equilibrium amount, while in the temperature range -85 to $+21^\circ$, a slow adsorption is still taking place after this time (see Figure 2).

Isobar B is formed from points taken from isotherm data. The disagreement between the two isobars is striking and will be shown below to be intimately related to the observed irreversibility of adsorption. Isobars having the shape of curve A have been observed⁸ and are taken to be an indication of several different forms of sorption which can take place on the surface.

Magnetic Studies. The magnetic data obtained are summarized in the form of "magnetotherms" (plots of amount adsorbed against the ratio of observed sus-

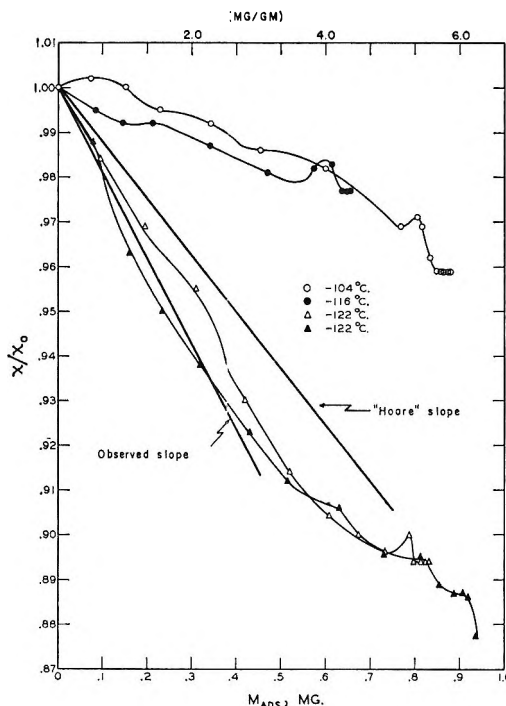


Figure 5. Magnetotherms (-104 to -122°) for nitric oxide on palladium black (sample weight, 150 mg). The inclusion of two curves at -122° shows the reproducibility of a typical magnetotherm. Cleaning procedure II used.

ceptibility, χ , to the susceptibility of the clean sample, χ_0).

At -196° (Figure 4), a positive slope suggesting physisorption⁹ is observed. It should be noted that the maximum NO pressure used at this temperature was 31μ , well below the expected equilibrium liquid-vapor value of about 75μ . While this evidence for physisorption is reassuring, the nature of the adsorption as deduced from the details of the magnetotherms (see below) is not as simple as one might expect.

For temperatures above -120° , the magnetotherms (Figures 5 and 6) are seen to be essentially independent of temperature. Below -120° , a new slope is observed, one which has a slightly steeper slope than that of an equivalent palladium-silver alloy curve (the "Hoare¹⁰ slope"). The Hoare slope represents the decline in susceptibility observed when palladium is alloyed with silver; the slope shown in Figure 5 is drawn for corresponding electron concentrations in a palladium-silver and a palladium-nitric oxide system. Needless to say, the parallels between the two systems are striking and form a basis for discussing the mechanism of chemisorption of NO at these temperatures.

With several exceptions, all the magnetotherms are

(8) P. H. Emmett and R. W. Harkness, *J. Amer. Chem. Soc.*, **57**, 1631 (1935).

(9) A. Solbakken and L. H. Reyerson, *J. Phys. Chem.*, **63**, 1622 (1959).

(10) F. E. Hoare, J. C. Matthews, and J. C. Walling, *Proc. Roy. Soc. (London)*, **A216**, 502 (1953).

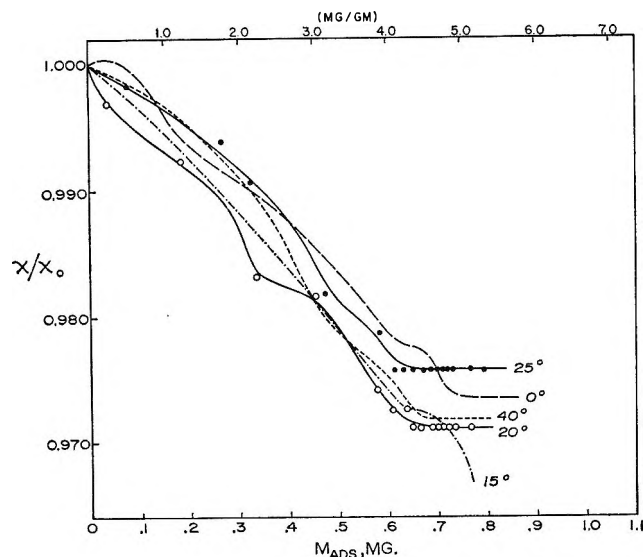


Figure 6. Magnetotherms (0–40°) for nitric oxide on palladium black (sample weight, 150 mg). Cleaning procedure II used.

seen to consist of a steep, initial negative slope, followed by a declining slope at higher coverages, and a final “bottoming out” at monolayer coverages. The continuing decline beyond monolayer coverage at -122 and $+25^\circ$ is taken to be an indication of the nonreproducibility of the surfaces. In approximately 30 runs taken during this series, only three were observed to exhibit this behavior.

Discussion

Physisorption. The physisorption state is typified by the -196° magnetotherm of Figure 4. While the initial 0.2 mg of sorbed NO causes no change in the magnetic properties (a presently unexplainable fact), the following positive slope is indicative of sorption in a paramagnetic state similar to that found on both silica and alumina.^{9,11} In this investigation, the slope of Figure 4 indicates that the magnetic moment of sorbed NO is 1.23 BM. This may be compared with a predicted value¹² of 1.34 BM at the same temperature; it is thus apparent that a palladium surface apparently physisorbs NO in a state electronically comparable with that of the gas at the same temperature.

It will also be noted that in Figure 4 a slight decline at the end of the magnetotherm is followed by a “bottoming out.” It appears that after a significant amount of physisorption has occurred, a cooperative rearrangement follows which involves either dimerization or freezing into a diamagnetic layer.

It was mentioned earlier and will be further discussed below that the initial rapid adsorption shown in Figure 2 is attributable to physisorption. Although it is extremely unusual to observe physisorption at such high temperatures, the evidence for this is unmistakable. The enthalpy of adsorption, the energy of desorption at such high temperatures, the evidence for

this is unmistakable. The enthalpy of adsorption, the energy of desorption, and the observed isobars are strong evidence in favor of this concept. In addition, it can be shown that the temperature dependence of the amount of physisorbed NO at constant pressure (see Figure 2) is in accord with the BET adsorption model. (A plot of $\ln m_{\text{adsorp}}$ against $1/T$ at “high” temperatures and low pressure is linear.) Thus the initially physically adsorbed NO apparently loads up portions of the surface “piggy-back” style, leaving appreciable sections of bare surface open for subsequent chemisorption.

The observation of the existence of infrared bands around 1876 cm^{-1} (the gas-phase stretching frequency) for NO adsorbed on a number of transition elements (including palladium) at room temperature^{4,13} and their disappearance upon evacuation also constitute evidence for this “anomalous” physisorption. It is to be noted that similar observations have not been recorded for sorption systems involving molecules with singlet ground states (*i.e.*, carbon monoxide). This suggests that such physisorption is unique to free-radical adsorbates, and this is discussed at length in a later section.

Chemisorption. For temperatures below -120° , the similarities between the magnetotherm slopes and the Hoare slope suggests that chemisorption follows roughly the same mechanism observed in the process of alloying silver with palladium. Thus it seems apparent that a net of approximately 1.5 electrons/NO molecule is transferred to the *bulk* palladium d band. A detailed analysis of this electron transfer is treated in a forthcoming publication.¹⁴

The temperature-independent slopes of magnetotherms obtained above -120° suggest that extensive chemisorption also occurs at these temperatures; however, if it involves electron transfer, it involves less than 1 electron/NO. Comparison of these magnetotherm slopes with the Hoare slope suggests several possible mechanisms regarding the effect of nitric oxide on the magnetic susceptibility of palladium.

The following conclusions are possible, all of which are designed to account for the transfer of less than one electron per NO molecule.

- (a) The “alloy mechanism” is followed in the case of nitric oxide; however, a polymer of NO is formed and donates 1 electron/polymer to the palladium bulk band.
- (b) Alternatively, each nitric oxide molecule gives up one-half an electron to the palladium bulk band (*i.e.*, a covalent bond is formed with, perhaps, *the* odd electron).

(11) A. Solbakken and L. H. Reyerson, *J. Phys. Chem.*, **64**, 1903 (1960).

(12) J. H. Van Vleck, “The Theory of Electric and Magnetic Susceptibilities,” Oxford University Press, London, 1932, p 269.

(13) K. H. Rhee, private communication.

(14) R. W. Zuehlke, to be published.

2. Nitric oxide is adsorbed in several different states, one of which involves the donation of 1 or more electrons/NO molecule in that state to the bulk band of palladium.

3. Nitric oxide is adsorbed as in 1 or 2, but electron transfer involves surface states of palladium rather than bulk electronic states.¹⁵

The third conclusion is significant but is probably not applicable in this particular study. All palladium samples used had average particle sizes (normal to the $\langle 111 \rangle$ plane) ranging from 150 to 250 Å; according to a surface-state analysis,¹⁴ surface states in these particles are empty and only bulk states would be involved in determining magnetic susceptibility. Indeed, if surface states were involved (as they should be for much smaller particles), the nature of nitric oxide adsorption should be changed considerably.

Conclusion 1a is of questionable value because the only reasonable polymer to be expected is N_2O_2 , a molecule which has only been observed at very low temperatures. On the other hand, conclusions 1a and 1b, which involve one electron covalence, have some credibility, since both mechanisms predict temperature independence of the magnetotherms. This follows because a ratio of two susceptibilities is involved, each of which would be expected to have essentially the same temperature dependence.

The second conclusion, which is hinted at by the shapes of the isobars and the low-temperature magnetotherms, is probably the most reasonable one. With this mechanism, any effect of temperature on the magnetotherms is simply explained through its influence on the distribution of nitric oxide among the several postulated sorption states.

The chemisorption state following from these arguments is assumed to be exactly equivalent to that observed below -120° . However, if the magnetotherm slopes are plotted against temperature as in Figure 7, it is apparent that a marked discontinuity appears at -120° . This is indicative of a first-order phase transition and, in the case of adsorption, is commonly attributed to a transition from mobile to immobile adsorption. If this is indeed the case, -120° is the equilibrium temperature for the transition at 75 μ pressure. If the two states differ only by the gain or loss of one degree of translational freedom, the two-dimensional Sackur-Tetrode equation may be applied.¹⁶ With the assumption that the area available per molecule is 1.07×10^{-15} cm² (*i.e.*, calculation made at half-coverage), the entropy change is found to be approximately 13 kcal/mol deg, from which an energy difference (ΔH) of approximately 2.0 kcal/mol follows.

It is assumed that when transition to the mobile chemisorbed phase occurs, extensive physisorption can also occur. This results in a decreased slope of the magnetotherms above -120° , and this decreased slope

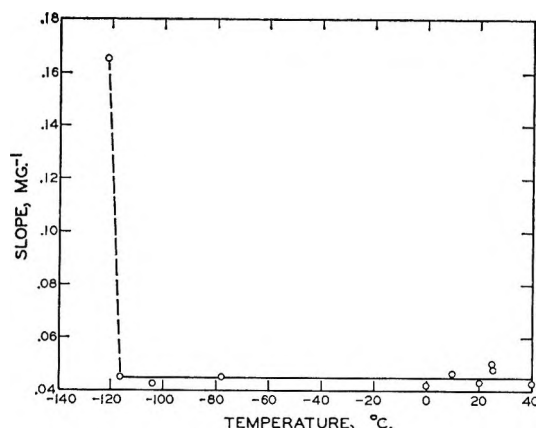


Figure 7. Temperature dependence of magnetotherm slopes (cleaning procedure II).

will be discussed more extensively when the detailed model is presented below.

Activated Complex. The negative activation energy of -3.39 kcal/mol for adsorption into the mobile chemisorbed state has already been presented. The existence of such a negative activation energy frequently implies a two-step reaction mechanism, with the rate-determining second step involving a species in temperature-dependent equilibrium with the original reactants. The apparent mechanism in this case is



Following the classical argument of Solbakken and Reyerson¹¹ developed for NO on alumina, one sees that the apparent negative activation energy, E_{app}^\ddagger , is composed for the energy of physisorption, ΔH_{pa} , and the true activation energy for transition from physisorption to chemisorption, E^\ddagger

$$E_{app}^\ddagger = E^\ddagger + \Delta H_{pa}$$

Substituting the Clausius-Clapeyron heat of physisorption into the above expression gives a true activation energy of 170 cal/mol. (Existing experimental data force the use of low-temperature rate data with room-temperature equilibrium data; however, it is likely that the heat capacity of liquid NO is slightly greater than that of gaseous NO. This being the case, the heat of physisorption at low temperatures would be slightly more negative, thus making the true energy of activation slightly higher than the calculated 170 cal/mol.)

It is most interesting to note that the observed negative activation energy is exactly equal to that found for NO on alumina. It therefore seems apparent that the activated complexes on the two surfaces are essentially identical. This fact, along with a discussion of the bonding mechanisms in the chemisorption and

(15) R. W. Zuehlke, *J. Chem. Phys.*, **45**, 411 (1966).

(16) C. Kamball, *Proc. Roy. Soc. (London)*, **A187**, 73 (1946).

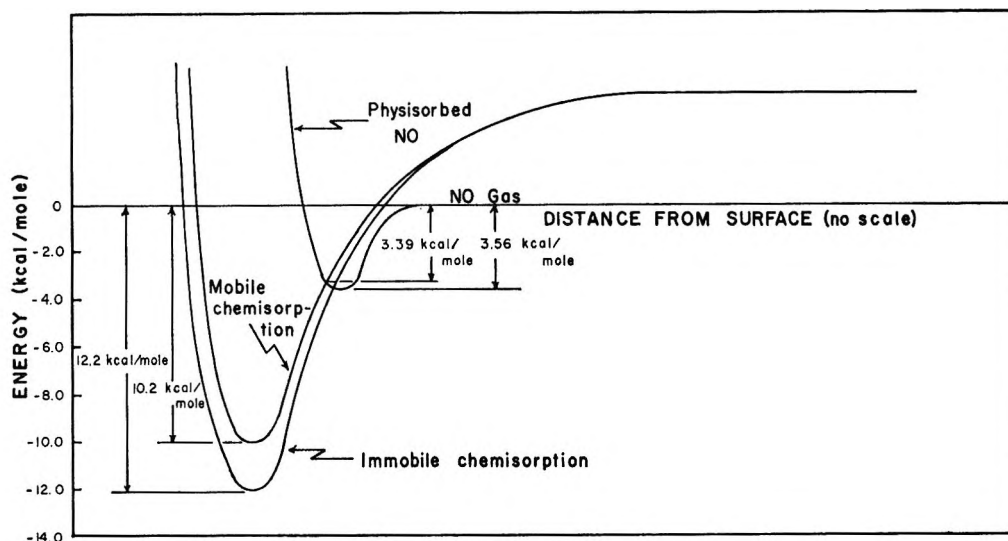


Figure 8. Energy profile for nitric oxide adsorption on palladium black.

physisorption states, are dealt with in another publication.¹⁴

Model. The energy profile for the adsorption of nitric oxide on palladium as deduced from the study above is shown in Figure 8 (the ordinate is drawn to scale; the abscissa is not). The curve representing physisorption is shown to have a minimum at 3.6 kcal/mol; this is in accord with the Clausius-Clapeyron heats observed on samples cleaned with CP-I. The minima in the mobile and immobile chemisorption curves have already been discussed. The points at which these curves cross the physisorption curve are of interest, however.

The negative activation energy discussed above was found in connection with the mobile chemisorption and the physisorption states. According to classical kinetic analyses, the crossing of these two curves occurs at the point which represents the energy of the activated complex (*i.e.*, -3.39 kcal/mol). Reyerson and Solbakken have shown¹¹ that the transmission coefficient for the corresponding process on alumina gel is of the order of 10^{-8} . A simple analysis shows that an equally small coefficient is observed in this case. This situation is related^{17,18} to the nature of the crossing of these two curves and suggests that the resonance energy of the activated complex (which is related to the physisorption and chemisorption states) is very small. In effect, this means that the two curves actually do cross and are not rounded off into two separate, noncrossing curves with a small energy gap between them. This is not at all surprising, because the magnetic data show a spin multiplicity change between the two states. Hence the resonance energy at the curve intersection is essentially zero and the two curves effectively cross at the activated complex and give rise to a very small transmission coefficient. Thus even at relatively high temperatures, extensive physisorption of NO (in a

paramagnetic state) may take place, and a very large fraction of the molecules may have sufficient kinetic energy to surmount the activation energy barrier. However, since the physisorption and chemisorption curves cross, the probability of a molecule bound in the physisorption well changing its position to be trapped in a chemisorption well is very small. Therefore, one observes an anomalously high percentage of physisorption.

The crossing of the immobile chemisorption and physisorption curves is somewhat more difficult to portray. The fact that physisorption alone is observed at very low temperatures suggests that an activation-energy barrier exists between the two states, although it is very small. Therefore, the crossing must occur to the left of the physisorption minimum. However, since a spin multiplicity change is involved here as well, the transmission coefficient might also be expected to be low. If two potential energy curves cross, the transmission coefficient might be expected, intuitively, to be related to the angle at which the curves cross (*i.e.*, the sharper the angle of crossing, the lower the transmission coefficient). The crossing shown in Figure 8 is a manifestation of these principles, with the crossing shown just beyond the minimum in the physisorption curve, where the small negative slope of the physisorption curve gives rise to both a small activation energy and a reasonable transmission coefficient.

With the aid of the model and the data presented, the shapes of the magnetotherms and isobars may be readily understood. Above -120° , the magnetotherm

(17) S. Glasstone, K. J. Laidler, and H. Eyring, "The Theory of Rate Processes," McGraw-Hill Book Co., Inc., New York, N. Y., 1941, Chapter III.

(18) K. J. Laidler, "Chemical Kinetics," McGraw-Hill Book Co., Inc., New York, N. Y., 1950, Chapter 13.

slopes suggest that both physisorption and chemisorption occur in the early stages of the process, and, when monolayer coverage is approached, an increasing percentage of physisorption occurs. The Clausius-Clapeyron data are useful here, for they suggest that, when a relatively high percentage of oxide coverage is present (*i.e.*, surface cleaned by CP-I), the heat of physisorption approaches very closely the heat of liquefaction of nitric oxide. On the other hand, when a larger percentage of the surface is clean (*i.e.*, CP-II is used), the adsorption process occurring near monolayer coverage is considerably more energetic. These observations suggest that something like an oxide substrate is necessary for true physisorption of NO to occur.

The kinetic data, however, indicate that above -120° only a small portion of the initially physisorbed NO is converted to the chemisorbed state during the time intervals of observation. The chemisorption layer then forms an ideal base for relatively pure physisorption and effectively blocks out additional chemisorption sites for future doses of gas. Therefore, as successive increments of gas are added, the observed percentage of chemisorption resulting from each dose will be observed to decrease. Ultimately, when nearly all chemisorption sites are blocked, pure physisorption results, and the magnetotherm slopes bend to the horizontal or become slightly positive. The bottoming out mentioned earlier apparently results from a co-

operative dimerization of the entire physisorbed layer. The adsorption process is seen to be "autocatalytic" with respect to the promotion of physisorption.

The difference in shapes of the two isobars of Figure 3 can also be explained by this model. The magnetotherms show only one discontinuity at -120° , and this agrees rather well with the break shown in isobar B. Curve A, on the other hand, is markedly different; however, it was obtained using single doses of NO, while curve B was obtained from isotherm data. Since the character of NO adsorption has been shown to be dependent on the sample's history of prior exposure to NO and since the samples used in the magnetotherms and isobar B have similar (essentially identical) histories, one might expect to see agreement between the magnetotherms and isobar B and substantial disparity between isobars A and B. It can perhaps be concluded that the shape of isobar A reflects the nature of the oxide contamination on the clean surface at the start of adsorption.

Acknowledgment. The authors are grateful to the Petroleum Research Fund, administered by the American Chemical Society, and to the Directorate of Chemical Sciences of the United States Air Force Office of Scientific Research (Grant No. AF-AFOSR-114-63) for their support of this work. This work was presented in part before the Division of Colloid and Surface Chemistry at the 150th National Meeting of the American Chemical Society, Atlantic City, N. J., Sept 1965.

The Hg(¹P₁)-Photosensitized Decomposition of Cyclobutane^{1a}

by E. G. Spittler^{1b} and G. W. Klein

Radiation Research Laboratories, Mellon Institute, Pittsburgh, Pennsylvania 15213 (Received February 28, 1967)

The Hg(¹P₁)-photosensitized decomposition of cyclobutane has been studied at room temperature in the pressure range 15–760 mm. Ethylene is always the major hydrocarbon product, accounting for 50% of the total product at 15 mm and over 90% above 300 mm. Other products, in order of decreasing importance, are H₂, cyclobutylcyclobutane, cyclobutene, butane, ethane, propane, and traces of acetylene, propylene, cyclopropane, and a C₅ product (probably methyl cyclobutane). Hydrogen decreases from 50% of the C₂H₄ at 15 mm to <5% of the C₂H₄ above 300 mm. With >5% added C₂D₄, NO, or O₂ at 15 mm, the H₂ yield decreases by 50%; above 300 mm, it decreases by 60–80%. These results can be reasonably interpreted in terms of the processes: (1) Hg(¹P₁) + *c*-C₄H₈ → Hg(¹S₀) + *c*-C₄H₈^{*}, (2) *c*-C₄H₈^{*} → 2C₂H₄, (3) *c*-C₄H₈^{*} → H₂ + *c*-C₄H₆, (4) *c*-C₄H₈^{*} → H + *c*-C₄H₇, (5) *c*-C₄H₈^{*} → CH₂ + C₃H₆. Reactions 2–4 account for most of the products at all pressures, with reaction 2 predominating at high pressures. Reaction 5 is suggested to account for the formation of small amounts of methyl cyclobutane, propylene, and cyclopropane at pressures > 400 mm. The marked pressure dependence of the amount and distribution of products indicates that complete quenching of the Hg(¹P₁) atoms does not occur below 400 mm. It also seems necessary to postulate at least two precursors for reactions 2–5, at least one of which may be a vibrationally excited ground state of cyclobutane. Using mixtures of *c*-C₄H₈ and *c*-C₄D₈, a significant over-all isotope effect was observed for the formation of ethylene.

Introduction

Two methods for isolating the 1849-Å output of a low-pressure Hg resonance lamp have become available in recent years.^{2,3} The first involves the use of a solution filter containing 9,10-dimethylantracene in deoxygenated cyclohexane, and the second, a γ -irradiated lithium fluoride crystal. The application of these methods opens up the possibility of comparing the Hg(¹P₁)-sensitized reactions of hydrocarbons at 1849 Å with the corresponding Hg(³P₁)-sensitized reactions at 2537 Å, which have been extensively investigated.⁴ Pertel and coworkers have reported some results recently for the Hg(¹P₁)-sensitized reactions of C₂H₄⁵ and CO₂.⁶ They found considerable difference in the isotopic hydrogen yields produced from the *cis* and *trans* dideuterioethylene isomers,⁵ while Hg(³P₁) sensitization produces the same isotopic hydrogen distribution from the two isomers.⁷ Holroyd and Pierce have employed the ¹⁴C₂H₄ scavenger technique⁸ to study the distribution of radicals formed in the Hg(¹P₁)-sensitized reactions of several hydrocarbons.⁹ They found the Hg(¹P₁) sensitization of propane produced about equal yields of *n*-propyl and isopropyl radicals.⁹ The Hg(³P₁) sensitization of propane yielded 90% isopropyl and 10% *n*-propyl radicals.¹⁰ Preliminary studies of the Hg(¹P₁)-sensitized reactions of cyclopropane and methylcyclopropane indicated that the processes occurring in these systems were more complicated than for the Hg(³P₁)-sensitized reaction. For example, in addition to C–H bond rupture, C–C bond rupture occurs to a significant extent, giving CH₂ radicals that lead to very complex reaction mixtures.¹¹ In view of these results, cyclobutane was chosen for a

more extensive study, since its decomposition appeared to be less complex than that of cyclopropane and methylcyclopropane. Also, it was deemed possible to compare these results with those already known for the Hg(³P₁) sensitization¹² and the direct photolysis in the vacuum ultraviolet.¹³

Experimental Section

Lamp and Filter. The source of 1849-Å radiation was a 4-cm flat spiral, Hanovia low-pressure Hg lamp, made of suprasil quartz which was operated at 40 mA from a Sola constant-voltage transformer. The output

- (1) (a) Supported, in part, by the U. S. Atomic Energy Commission; (b) John Carroll University, University Heights, Cleveland, Ohio 44118.
- (2) C. M. Wolff and R. Pertel, *J. Opt. Soc. Amer.*, **54**, 1168 (1964).
- (3) J. L. Weeks, S. Gordon, and G. M. A. C. Meaburn, *Nature*, **191**, 1186 (1961).
- (4) (a) W. A. Noyes, Jr., and P. A. Leighton, "The Photochemistry of Gases," Reinhold Publishing Corp., New York, N. Y., 1941, pp 211 ff; (b) E. W. R. Steacie, "Atomic and Free Radical Reactions," Vol. I, Reinhold Publishing Corp., New York, N. Y., 1954, pp 411 ff; (c) H. E. Gunning and O. P. Strausz, "Advances in Photochemistry," Vol. I, Interscience Publishers, Inc., New York, N. Y., 1963, pp 209 ff.
- (5) N. L. Ruland and R. Pertel, *J. Amer. Chem. Soc.*, **87**, 4213 (1965).
- (6) C. M. Wolff and R. Pertel, *J. Phys. Chem.*, **69**, 4047 (1965).
- (7) P. Ausloos and R. Gorden, *J. Chem. Phys.*, **36**, 5 (1962).
- (8) R. A. Holroyd and G. W. Klein, *J. Amer. Chem. Soc.*, **84**, 4000 (1962).
- (9) R. A. Holroyd and T. E. Pierce, *J. Phys. Chem.*, **68**, 1392 (1964).
- (10) R. A. Holroyd and G. W. Klein, *ibid.*, **67**, 2273 (1963).
- (11) E. G. Spittler and G. W. Klein, Southeastern Regional ACS Meeting, Louisville, Ky., Oct, 1966.
- (12) H. E. Gunning and D. L. Kantro, *J. Chem. Phys.*, **21**, 1797 (1953).
- (13) R. D. Doepker and P. Ausloos, *ibid.*, **43**, 3814 (1965).

was ~95% at 2537 Å and ~5% at 1849 Å. It was mounted at the center of a 4.0-cm hole at one end of an 8.0 cm in diameter by 10 cm hollow copper cylinder, which was flushed with N₂ to eliminate the absorption at 1849 Å by O₂ in the air and to keep the lamp cool. A second stream of N₂ was directed between the lamp and the cell during photolysis. The lamp was placed 1.6 cm from the bottom surface of the cell to allow for positioning the filter and shutter.

The unwanted 2537-Å radiation was removed with an LiF filter (2 × 50 × 50 mm), which had been irradiated with a ⁶⁰Co γ source so that the absorbance at 2537 Å was > 4. The absorbance was monitored against an irradiated LiF reference crystal on a Cary Model 14 recording spectrophotometer. The absorbance at 1849 Å was always < 1. With this type of filter and under the conditions of the experiment more than 98% of the light reaching the sample was of 1849-Å wavelength.

Cell and Circulating System. A solenoid-operated, all-glass circulating pump maintained a steady movement of reactants through the photolysis zone. Two photolysis cells with suprasil quartz windows were arranged in series so that either could be used. Both cells were 4.5 cm in diameter; one was 1 cm thick and the other was 1 mm thick. The total volume of the system was ~173 cm³, approximately ten times the volume of the larger cell.

The mercury concentration was kept at a constant value by circulating the reactant continuously through a spiral trap containing droplets of mercury and maintained at 0° with an ice bath.

Mercury vapor at room temperature absorbs 54% of the incident 2537-Å light in a 5-cm path.¹⁴ Assuming an absorption of 6.2×10^{-11} cc atom⁻¹ cm⁻¹,¹⁶ it is possible to calculate that Hg vapor at 0° will absorb ~99% of the incident 1849-Å radiation in a path length of 0.05 mm. However, if the emission spectrum is greatly broadened with respect to the absorption spectrum of the Hg in the reaction cell, it is possible that the unabsorbed portion may cause direct photolysis. To eliminate this possibility, reactions were carried out in both cells. Under comparable conditions of pressure, temperature, mercury concentration, and 1849-Å intensity, no significant difference in per cent decomposition or product distribution was observed.

Gas-Handling Procedure. Reactants were transferred from the metering system to the reaction system by condensing them at liquid N₂ temperature in a cold finger located in the reaction system. The lamp was turned on and allowed to warm up for 0.5 hr with the shutter in place. The reactants were warmed to room temperature and circulated for 0.5 hr through the mercury trap before the reaction was begun. Nitric oxide and oxygen were added by measuring in a known volume and then expanding into the reaction system.

Analysis. After the reaction was completed, the products were analyzed in a three-stage process. In

the first, the reaction mixture was frozen down in a cold finger within the reaction system. Products not condensable at liquid N₂ temperature were passed through a second trap maintained at solid N₂ temperature, were collected in a Toepler pump-gas buret, and were measured. They were then transferred to a sampling bulb for mass spectrometric analysis.

In the second stage of the analysis, the products that were condensable at liquid N₂ temperature were transferred into a U trap and then flushed directly into a gas chromatographic system.

In the third stage of the analysis, components, usually C₂, C₃, and C₄ compounds, could be trapped out after the first glpc separation and separated further on a different column or collected for mass spectrometric analysis. A proportional counter could be used with either glpc stage whenever radioactive products were expected from ¹⁴C₂H₄ tracer experiments.

It was found that the pressure of H₂ is 10² higher than the pressure of O₂ over silica gel at liquid N₂ temperature. Therefore, in runs with added O₂, H₂ was separated from O₂ by pumping off the H₂ through a silica gel trap at -196° with a small Hg diffusion pump.

In runs with added C₂D₄, the isotopic composition of the hydrogen was analyzed mass spectrometrically. The total hydrogen yield was corrected for D₂ and HD so that only the true H₂ yield from C₄H₈ is reported.

Materials. The impurities (butane, butene, and traces of C₂ and C₃ hydrocarbons) were eliminated from the cyclobutane (Merck) by glpc purification on a 12-m column of 25% by weight Dow-Corning silicone grease on 30-60 mesh firebrick. Cyclobutane-d₈ (Volk Radiochemical Co.) which contained similar impurities was purified in the same fashion. Mass spectrometric analysis indicated the presence of 6.9% C₄D₇H. C₂D₄ (Volk) was degassed and distilled from -160 to -196°. Mass spectrometric analysis indicated the presence of 3.5% C₂D₃H. ¹⁴C₂H₄ was purified by glpc using a modified silica gel column and diluted to an activity of ~0.1 mCi/mmol with normal C₂H₄.

Oxygen and nitric oxide were obtained from lecture bottles (Matheson). Oxygen was used without further purification. Nitric oxide was vacuum distilled at -160 to -196° to remove possible traces of N₂O.

Results and Discussion

The Hg(¹P₁)-photosensitized decomposition of cyclobutane was studied at room temperature as a function of time at 15 mm and the results are given in Table I. The pressure dependence of the major products in the range 15-760 mm is shown in Table II. Above 300 mm, C₂H₄ constitutes over 90% of the total products. Although the C₂H₄ fraction drops to ~50% of the

(14) K. Yang, *J. Amer. Chem. Soc.*, **86**, 3941 (1964).

(15) P. H. Garrett, *Phys. Rev.*, **40**, 779 (1932).

Table I: Time Dependence of Products^a

Time, min	μmol								
	C ₂ H ₄	H ₂	C ₂ H ₆	C ₃ H ₈	C ₄ H ₁₀	c-C ₄ H ₈	C ₅ H ₁₂	C ₆ H ₁₄	C/H
10	0.58	0.29	0.05	0.02	0.06	0.06	0.46
15	0.68	0.28	0.06	0.04	0.06	0.07	0.11	0.13	0.47
20	0.82	0.37	0.06	0.04	0.08	0.06	0.13	0.13	0.46
30	1.44	0.37	0.06	0.07	0.09	0.04	0.19	0.19	0.48
45	2.94	1.03	0.14	0.14	0.20	0.15	0.35	0.35	0.47
60	3.64	1.42	0.24	0.13	0.30	0.20	0.53	0.53	0.47
60	3.00	1.18	0.18	0.13	0.24	0.16	0.40	0.40	0.47

^a Pressure, 15 mm; constant intensity; circulating system.**Table II:** Pressure Dependence of Products^a

Pressure, mm	μmol										
	Measured C ₂ H ₄	H ₂	C ₂ H ₆	C ₃ H ₈	C ₄ H ₁₀	c-C ₄ H ₈	C ₅ H ₁₂	C ₆ H ₁₄	C ₇ H ₁₆	c-C ₇ H ₁₄	C/H
15	0.82	0.37	0.05	0.04	0.08	0.06	0.13	0.47
42.3	3.18	0.61	0.08	0.03	0.18	0.19	0.25	0.48
219	10.8	0.64	0.08	0.06	0.11	>0.06	0.20	0.11	0.04	0.04	0.49
445	15.6	0.71	0.10	0.09	0.12	Not measured	0.23	0.09	0.05	0.05	0.50
758	15.6	0.87	0.11	0.08	0.13	>0.34	0.23	0.09	0.03	0.03	0.49

^a Time, 20 min; constant intensity.**Table III:** Runs with Added C₂D₄^a

Run no.	C ₂ D ₄ , %	μmol										
		C ₂ D ₄ added	C ₂ H ₄	H ₂	HD	D ₂	C ₂ H ₆	C ₃ H ₈	C ₄ H ₁₀	c-C ₄ H ₈	C ₅ H ₁₂	C ₆ H ₁₄
25	0.35	0.42	...	0.41	0.0034	0.077	0.08	...	0.15	0.15	0.03	0.17
24	0.66	0.70	...	0.31	0.0044	0.104	0.06	0.05	0.14	0.12	0.11	...
22	1.90	2.82	...	0.20	0.0063	0.257	0.07	...	0.13	0.10	0.08	0.18
21	1.92	2.83	1.25	0.20	0.0049	0.284	0.07	0.03	0.13	0.10	0.14	0.15
27	2.82	5.23	1.40	0.20	0.0066	0.470	0.08	0.04	0.21	0.16	0.06	0.20
23	5.26	7.75	1.40	0.17	0.0076	0.617	0.07	0.05	0.17	0.12	0.12	0.13
26	10.5	14.1	1.30	0.15	0.0106	0.916	0.08	0.04	0.18	0.11	0.07	0.18
52 ^b	0.32	13.3	16.7	0.98	0.0079	0.012	0.15	...	0.20
54 ^b	1.14	46.7	14.7	0.37	0.0084	0.027	0.14	...	0.25
53 ^b	3.1	126.0	10.2	0.19	0.0100	0.052	0.13	...	0.12
60 ^b	12.2	560.0	...	0.31	0.028	0.31	...	0.12	0.36	0.20	...	0.13

^a Time, 20 mins; pressure, 15 mm; constant intensity. ^b Pressure, 440 mm.

total at 15 mm, it is always the major product of the reaction. In addition to the principal products indicated in Tables I and II, small amounts of methylcyclobutane, ethylcyclobutane, and methane (<2% of H₂) are observed.

A series of runs at 15 mm with added C₂D₄ was carried out to determine to what extent hydrogen is produced by a molecular process (Table III). The H₂ yield decreases to a constant value in the presence of >5% C₂D₄ and seems to be approaching the cyclobutene yield as a limiting value (Figure 1). The rate of C₂H₄ formation is not appreciably affected by the presence of up to 10% C₂D₄.

In the presence of added O₂ or NO, the only hydrocarbon product detected was ethylene (Table IV). Hydrogen was also found as a product in a yield slightly lower than the H₂ yield in the presence of >5% C₂D₄ (Figure 1). The difference is probably not significant since H₂ had to be separated from a large excess of O₂ or NO. c-C₄H₈ and C₃H₈ were not found.

For a few runs carried out with pure cyclobutane, a mass balance was calculated on the basis of the total C/H ratio in the products. The balance is reasonably good (Tables I and II). A consistently low value of C/H, however, could possibly be explained by the loss of a small amount of c-C₄H₈ product.

Table IV: Runs with Added NO and O₂^a

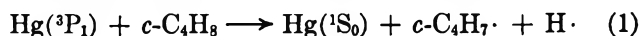
Added gas, %	μmol	
	H ₂	C ₂ H ₄
	NO	
1.99	0.15 ^b	1.77
2.15	0.24	1.69
4.13	0.23	1.56
12.2	0.12	1.82
		Av 1.71
	O ₂	
1.84	0.19	1.26
1.85	(0.09) ^c	1.30
4.95	0.12	1.51
5.09	(0.33) ^c	1.42
8.00	0.11 ^b	1.50
12.9	0.11	1.42
		Av 1.40

^a Time, 20 min; pressure, 15 mm; constant intensity. ^b Analyzed on a carbowax column. ^c Analyses are uncertain.

Two series of runs with mixtures of *c*-C₄H₈ and *c*-C₄D₈ revealed significant over-all isotope effects. In a 1:1 mixture, the ratio H₂/D₂ is ~12. For two runs in which the isotopic distribution of the ethylene products was determined, the average value of the ratio (C₂H₄/*c*-C₄H₈)/(C₂D₄/*c*-C₄D₈) is ~2.7, Table V, showing that the reaction producing C₂H₄ from C₄H₈ is favored over that producing C₂D₄ from C₄D₈.

A few runs, carried out in the presence of 0.5–4% ¹⁴C₂H₄, gave the following information. Cyclobutylcyclobutane, cyclobutene, methyl cyclobutane, and propylene show no radioactivity. Propane had a trace of radioactivity. Ethane, butane, and ethylcyclobutane were highly radioactive, indicating that they are formed from ¹⁴C₂H₅· precursors. The ratio of the specific activity of butane to that of ethylcyclobutane was ~2. The ratio [C₆H₁₂]²/([C₄H₁₀][C₈H₁₄]) ≈ 4 for the ¹⁴C₂H₄ runs indicates that the butane, ethylcyclobutane, and cyclobutylcyclobutane are formed from radical precursors. The significance of these results is discussed below.

I. The Quenching Reaction. The only significant products observed in the Hg(³P₁)-photosensitized study of cyclobutane¹² were H₂, cyclobutylcyclobutane, *n*-butylcyclobutane, and probably butenylcyclobutane. The product distribution can be reasonably explained in terms of the over-all quenching and decomposition reaction (1). This is followed by combination, dis-



proportionation, and rearrangement of *c*-C₄H₇ radicals and addition and abstraction by H atoms. Cyclobutane completely quenches the Hg(³P₁) atom at pressures > 35 mm.

The distribution of products observed in the Hg(¹P₁)-photosensitized reaction of cyclobutane indicates

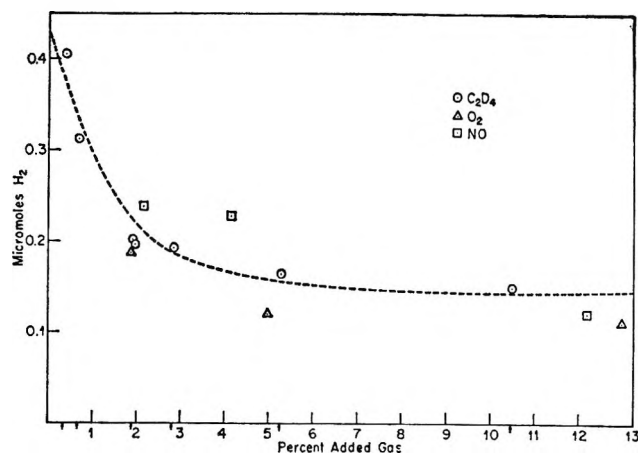
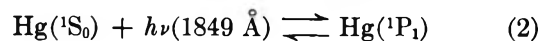
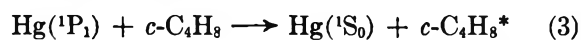


Figure 1. Dependence of the hydrogen yield on the added gas concentration. Total pressure ~15 torr and irradiation period 20 min.

that the reaction follows a course quite different from that observed in the Hg(³P₁)-sensitized reaction. The initiating process for the Hg(¹P₁)-sensitized reaction is presumed to be similar to that for the Hg(³P₁) reaction. Resonance radiation is absorbed by ground-state Hg atoms leading to an equilibrium between absorption and emission in the absence of foreign gases.



In the presence of a sufficiently high pressure of cyclobutane substrate, quenching by the cyclobutane competes with emission from the singlet excited state. It is accompanied by excitation of the substrate molecule, followed by decomposition



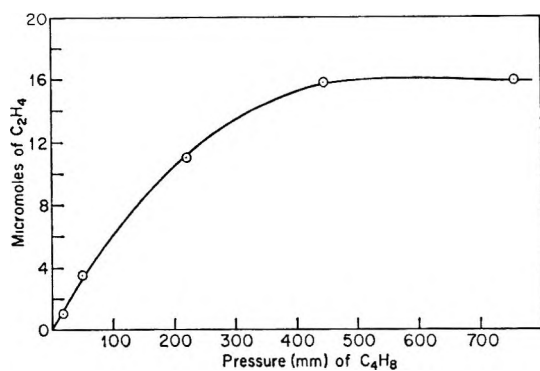
where *c*-C₄H₈* is an excited state of the cyclobutane molecule. The Hg(³P₁) atom is known to have a lifetime of ~10⁻⁷ sec, while that of the Hg(¹P₁) atom is ~10⁻⁹ sec.¹⁶ Hence, the Hg(¹P₁) atom should not be quenched as easily as the Hg(³P₁) atom. From the pressure dependence of ethylene formation (Figure 2), it can be seen that the quenching plateau for the Hg(¹P₁) atom does not occur below 400 mm, a factor of 10 higher than the pressure at which the Hg(³P₁) atom quenching plateau is reached.

II. The Primary Decomposition Modes of Cyclobutane. The excited state of cyclobutane formed in the quenching reaction (3) may undergo one of a number of possible processes. Only those processes which result in decomposition will be considered. In addition to reaction 6, analogous to eq 1 in the Hg(³P₁) system, at least three other primary processes (5, 7, and 8) are

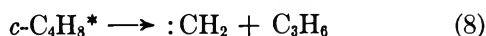
(16) (a) A. C. G. Mitchell and M. W. Zemansky, "Resonance Radiation and Excited Atoms," Cambridge University Press, London, 1961, p 147; (b) A. Lurio, *Phys. Rev.*, **140**, A1505 (1965).

Table V: Mass Spectrometer Analysis of Hydrogen and Ethylenes: C₄H₈-C₄D₈ Runs

C ₄ D ₈ / C ₄ H ₈	%			%				(H ₂ /C ₄ H ₈)/ (D ₂ /C ₄ D ₈)	(H ₂ /C ₂ H ₄)/ (D ₂ /C ₂ D ₄)
	H ₂	HD	D ₂	C ₂ H ₄	C ₂ H ₃ D	C ₂ D ₃ H	C ₂ D ₄		
∞ ^a	5.01	12.0	83.0	0.8	0.5	4.8	93.9
8.82	21.2	36.8	42.1	19.6	2.1	4.1	73.0	4.5	1.88
6.22	38.1	31.2	30.8	28.8	2.1	3.8	64.9	7.7	2.78
2.51	47.8	38.4	12.6	9.5	...
2.34	55.0	30.3	14.8	51.1	2.6	2.9	43.4	8.7	3.14
1.00	67.5	26.7	5.7	11.8	...

^a Contains 6.9% C₄D₇H.**Figure 2.** Ethylene production vs. pressure of C₄H₈. Irradiation period 20 min at constant light intensity.

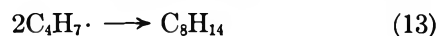
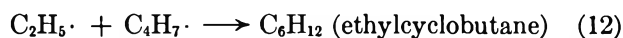
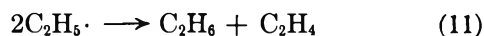
necessary to account for the products observed in the Hg(¹P₁) system. Formation of ethylene by a molecular



decomposition process (5) is confirmed by nearly all aspects of the present study. Under all conditions studied, over 50% of the cyclobutane decomposed yields ethylene. Ethylene formation is not suppressed or diminished by 10% NO or 10% O₂. It is not, therefore, produced from radical intermediates. Over 90% of the ethylenes formed in C₄D₈-C₄H₈ mixtures are C₂H₄ and C₂D₄. The amount of C₂H₄ found as a product in runs with added C₂D₄ corresponds, within experimental error, to the amount of C₂H₄ found in the absence of added C₂D₄. Thus, the principal primary process in the Hg(¹P₁)-sensitized reaction yields ethylene. Ethylene is the only product in the pyrolysis of cyclobutane¹⁷ and it is the major product in the direct photolysis in the vacuum ultraviolet.¹³

The evidence for the occurrence of eq 6 is extensive. In the runs with pure cyclobutane, ethane and butane products require an ethyl radical precursor. This is reasonably accounted for by the addition to ethylene (9) of H atoms formed in reaction 5, followed by combination, disproportionation, and addition reactions of

ethyl radicals (10-12). The presence of C₈H₁₄ (cyclo butylcyclobutane) (13) among the products also requires the occurrence of eq 6.

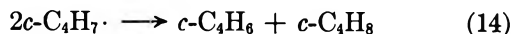


Reaction 6 is further supported by a consideration of the distribution of ¹⁴C radioactivity in the products of the runs carried out in the presence of ¹⁴C₂H₄. C₂H₆, C₄H₁₀, and C₆H₁₂ (ethyl cyclobutane) are the only products with high ¹⁴C content. They must, therefore, come from a ¹⁴C₂H₅· precursor, formed in eq 9 followed by eq 10-12 in which the ethyl radical is ¹⁴C₂H₅·. Finally, the presence of a small amount of C₂H₃D and C₂D₃H among the ethylene products of C₄H₈-C₄D₈ mixtures (Table V) is also most easily accounted for by disproportionation reactions of C₂D₄H and C₂H₄D, formed by H and D addition to C₂D₄ and C₂H₄, respectively.

The principal evidence for reaction 7 comes from a study of the isotopic distribution of hydrogens in the C₄H₈-C₄D₈ system (Table V), and from the presence of a significant amount of H₂ in the C₄H₈-10% C₂D₄ system (Figure 1 and Table III). Since H atoms formed in eq 6 are almost completely scavenged in the presence of >5% C₂D₄, the remaining H₂ must be formed molecularly. The fact that H₂ is found as a product in the presence of O₂ or NO also confirms the importance of eq 7 as a primary process. Furthermore, in the C₂D₄-C₄H₈ system the yield of c-C₄H₆ is 80% that of molecular H₂. The agreement is good, since some c-C₄H₆ could be lost by polymerization or H-atom addition. If 1,3-butadiene is formed in eq 7, it is below the level of detection of our analytical technique and is not more than 10% of the c-C₄H₈ yield. Finally,

(17) (a) C. T. Genaux and W. D. Walters, *J. Amer. Chem. Soc.*, **73**, 4497 (1951); (b) F. Kern and W. D. Walters, *ibid.*, **75**, 6196 (1953); (c) J. Langrish and H. O. Pritchard, *J. Phys. Chem.*, **62**, 761 (1958); (d) R. Srinivasan, *J. Amer. Chem. Soc.*, **81**, 5891 (1959).

in the presence of ¹⁴C₂H₄, the cyclobutene peak shows no radioactivity, again confirming that it must originate in a primary process. Although some of the cyclobutene may be formed by disproportionation of *c*-C₄H₇ radicals (14), this reaction seems to be of minor importance.



Reaction 8 is suggested by the presence of traces of C₅H₁₀ (probably methyl cyclobutane) among the products. A second piece of evidence for this reaction comes from a study of the ¹⁴C-containing products in the presence of ¹⁴C₂H₄. The C₃H₈ product contains a small amount of radioactivity. This could be traceable to the combination of CH₃· and ¹⁴C₂H₅·, where a plausible source of CH₃· radicals is abstraction of an H atom by CH₂ radicals formed in reaction 8. Methyl radicals may also be formed by CH₂ insertion into the substrate followed by decomposition of the excited intermediate to yield CH₃ plus other radicals.¹⁸ The abstraction reaction by CH₂ radicals has been postulated to explain the mechanism of the photolysis of ethylene oxide.¹⁹

Finally at high pressures, in addition to C₃H₆, *c*-C₄H₆ begins to appear as a product. This suggests that the precursor is a species capable of yielding either product, the distribution of which is pressure dependent. These results may constitute further indirect evidence for the occurrence of the elusive trimethylene diradical. It has often been proposed to account for the reactions of cyclopropane²⁰ and the pyrolysis of 1-pyrazoline.²¹ In all of these systems the ratio, C₃H₆/Δ is a decreasing function of pressure.

III. Relative Importance of the Primary Processes.

From the products of the reaction at various pressures (Table II), it is possible to determine an approximate pressure-dependent distribution of the primary processes (5–8). Ethylene (corrected for C₂H₆ and C₄H₁₀ formation) is a direct measure of eq 5; C₃H₈ gives an approximate measure of eq 8; atomic hydrogen formation from eq 6 can be estimated from twice the C₃H₁₄ yield; and finally, molecular hydrogen from eq 7 can be estimated from the difference between total hydrogen yield and twice the C₃H₁₄ yield. A lower limit for molecular hydrogen can also be obtained from the *c*-C₄H₆ yield. The results of these calculations are presented in Figure 3.

From the C₄H₈-C₄D₈ runs, it is also possible to estimate the relative importance of eq 6 and 7 by considering the hydrogen isotope distribution. If it is assumed that all the HD product is formed by processes involving atomic H and D, from the ratio (HD)²/((H₂)(D₂)) ≈ 4, the H₂ and D₂ yield can be corrected for atomic processes. Using the last line of data from Table V, this calculation indicates that 76% of the hydrogen is formed atomically and 24% is formed molecularly. From Table VI, the conclusion is that

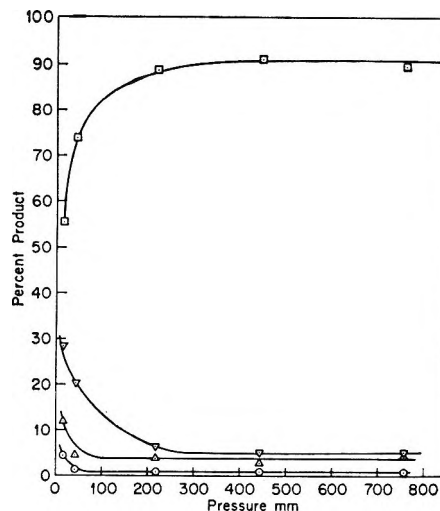


Figure 3. Distribution of primary processes as a function of pressure: □, $\frac{1}{2}$ C₂H₄(cor) [and $\frac{1}{2}$ C₂H₄(cor) = $\frac{1}{2}$ (C₂H₄(obsd) + 2C₄H₁₀ + C₂H₆)]; ▽, 2C₃H₁₄(obsd); Δ, H₂ - 2C₃H₁₄; ○, C₃H₈. Each compound measures the relative importance of one of the reactions (5–8).

~30% of the H₂ should be formed molecularly. The agreement is reasonably good, considering the nature of the approximations involved in making use of the empirical formula for the hydrogen isotope equilibrium ratio.

Table VI: Pressure Dependence of the Primary Processes

	% (15 mm)	% (758 mm)
<i>c</i> -C ₄ H ₈ * → 2C ₂ H ₄	55.5	89.4
<i>c</i> -C ₄ H ₈ * → H ₂ + <i>c</i> -C ₄ H ₆	12	4.6
<i>c</i> -C ₄ H ₈ * → H + <i>c</i> -C ₄ H ₇	28	5.1
<i>c</i> -C ₄ H ₈ * → CH ₂ + C ₃ H ₆	4.5	0.9

IV. *Excited States of Cyclobutane.* The most interesting feature of the Hg(¹P₁)-sensitized reaction is the striking pressure dependence of the distribution of primary processes. The importance of eq 5 compared to eq 6–8 is evident from Figure 3. If all of the products come from the same cyclobutane precursor, the distribution should be pressure independent, even below the quenching plateau. For as the quenching plateau is approached, all processes should increase

(18) J. A. Bell and G. B. Kistiakowsky, *J. Amer. Chem. Soc.*, **84**, 3417 (1962).

(19) B. C. Roquette, *J. Phys. Chem.*, **70**, 2699 (1966).

(20) (a) T. S. Chambers and G. B. Kistiakowsky, *J. Amer. Chem. Soc.*, **56**, 399 (1934); (b) H. E. Gunning and E. W. R. Steacie, *J. Chem. Phys.*, **17**, 351 (1959); (c) S. W. Benson and P. S. Nangia, *ibid.*, **38**, 18 (1963); (d) S. W. Benson, *ibid.*, **34**, 521 (1961); (e) D. W. Setser and B. S. Rabinovitch, *J. Amer. Chem. Soc.*, **86**, 565 (1964).

(21) R. J. Crawford, R. J. Dummel, and A. Mishra, *ibid.*, **87**, 3023 (1965).

in the same ratio. This is not the case. At high pressures, eq 5 increases relative to eq 6-8.

The question arises, what is the mechanism by which eq 5 becomes more important with increasing pressure? It seems necessary to invoke at least two precursors to account for the results shown in Figure 3, but how is the second precursor formed, and what is its nature? Two of several possible explanations will be considered.

The first precursor is presumed to be formed in the initial photosensitization reaction (3). Spin conservation²² would seem to suggest that a singlet state should result from interaction between $\text{Hg}(^1\text{P}_1)$ and ground-state cyclobutane. Furthermore, saturated hydrocarbons are not known to possess low-lying triplet states. Hence, the first precursor is likely to be either an excited singlet state of cyclobutane or a high vibrational level of the ground state. Cyclobutane has a very low, but measurable ($0.78 \text{ atm}^{-1} \text{ cm}^{-1}$)²³ continuous absorption in the $1849\text{-}\text{\AA}$ region, hence an accessible excited state. The second precursor could then be a vibrationally excited ground state obtained either by internal conversion from the excited singlet state or by collisionally induced transition from the high vibrational level of the ground state formed initially. Whatever the nature of the precursors may be, it is likely that ethylene is formed from a precursor of lower energy, since the ethylene-forming reaction is favored with increasing pressure. The activation energy for ethylene formation, determined from the pyrolysis of cyclobutane is known to be relatively low, 62.5 kcal/mol .²⁴ The experimental evidence does not permit us to characterize either precursor any further, or to define the processes by which they are formed.

V. Isotope Effects. From the results of the C_4H_8 - C_4D_8 runs, it is possible to estimate the magnitude of the isotope effects for reactions 5 and 7 in the $\text{Hg}(^1\text{P}_1)$ -sensitized decomposition of C_4H_8 and C_4D_8 . The ratio $R_1 = (\text{C}_2\text{H}_4/\text{C}_4\text{H}_8)/(\text{C}_2\text{D}_4/\text{C}_4\text{D}_8)$ is found to be ~ 2.7

(Table V). In order to form two molecules of ethylene from cyclobutane, two C-C bonds are broken, and two C=C bonds are formed. The effect of deuterium substitution does not appreciably affect the C-C and C=C bond strengths. Hence the ratio R_1 should measure the relative isotope effect for the over-all decomposition of C_4H_8 and C_4D_8 to ethylene. For the thermal decomposition, a value of 1.41 has been found for the isotope effect, $(k_{\text{H}}/k_{\text{D}})$, at 100 mm.²⁵ If this effect is allowed for, the value of $R_2 = R_1 k_{\text{D}}/k_{\text{H}}$ is ~ 1.9 and should be a reasonable estimate of the relative quenching efficiency of C_4H_8 to C_4D_8 in reaction 3.

The ratio of the measured quenching cross sections for *c*- C_3H_6 and *c*- C_3D_6 is 3.8 for $\text{Hg}(^3\text{P}_1)$ photosensitization.^{4c} Since there is more energy available with the $\text{Hg}(^1\text{P}_1)$ atom than with the $\text{Hg}(^3\text{P}_1)$ atom, it is not surprising that the $\text{Hg}(^1\text{P}_1)$ atom should be less selective and the isotope effect smaller.

If the ratio $R_3 = (\text{H}_2/\text{C}_4\text{H}_8)/(\text{D}_2/\text{C}_4\text{D}_8)$ is averaged from column 9 of Table V and corrected for the relative quenching efficiency of C_4H_8 to C_4D_8 , it is possible to estimate an isotope effect for reaction 7 of ~ 5.1 , favoring molecular detachment of H_2 from C_4H_8 over D_2 from C_4D_8 . The value seems a bit high, though it is consistent with the trend observed by Doepker and Ausloos¹³ for direct photolysis in the vacuum uv region of 1:1 C_4D_8 - C_4H_8 mixtures. H_2/D_2 has a value of 2.7 at 1470 \AA and 1.6 at 1236 \AA .

(22) (a) K. J. Laidler, *J. Chem. Phys.*, **10**, 43 (1942); (b) J. G. Calvert and J. N. Pitts, Jr., "Photochemistry," John Wiley and Sons, Inc., New York, N. Y., 1966, pp 88 ff.

(23) N. Moll, E. G. Spittler, and G. W. Klein, unpublished data.

(24) (a) C. T. Genaux, F. Kern, and W. D. Walters, *J. Amer. Chem. Soc.*, **75**, 6196 (1953); (b) C. T. Genaux and W. D. Walters, *ibid.*, **73**, 4497 (1951); (c) R. W. Carr and W. D. Walters, *J. Phys. Chem.*, **67**, 1370 (1963); (d) The activation energy for any of the other three processes is surely greater than this.

(25) R. W. Carr and W. D. Walters, *J. Amer. Chem. Soc.*, **88**, 884 (1966).

A Study of the Solubility of Metals in Liquid Sodium. II.

The System Sodium-Lead

by G. J. Lamprecht, L. Dicks, and P. Crowther

National Nuclear Research Centre, Pelindaba, Pretoria, South Africa

Accepted and Transmitted by The Faraday Society (May 11, 1967)

The solubility of lead in liquid sodium has been determined in the temperature range 100–260°. X-Ray data are given on a newly isolated intermetallic compound $n\text{Na}_5\text{Pb}$. From the solubility data the heat, $\Delta\bar{H}_{f(\text{sol})}$, entropy, $\Delta\bar{S}_{f(\text{sol})}$, and free energy, $\Delta\bar{F}_f$, of solution have been calculated.

Introduction

In an earlier article,¹ methods for the determination of the solubility of dilute tin alloys in sodium were described. The present paper is the second in a series of investigations into the solubilities of metals in liquid sodium.

Experimental Section

Reagents. Helium used as cover gas in all experiments was purified as previously described² and contained no detectable amounts of O_2 , N_2 , H_2O , CO_2 , and CH_4 . The lead was spectroscopically pure as supplied by Johnson Matthey and Co. The sodium used was commercial, dry packed as supplied by E. Merck and Co. It was purified with respect to oxygen by successive filtration through 5- μ sintered glass filters at 110°. This method¹ yielded sodium with an oxygen content of 11 ± 2 ppm.

Procedure. Solubility Determination. Because no suitable radioactive lead isotope is available, it was not possible to carry out the solubility determinations by the radioactive technique used previously.¹ The lead solubility determinations were therefore carried out with inactive lead in the apparatus shown in Figure 1.

An amount of lead chips, in excess of its solubility under the particular experimental conditions selected, was placed on the filter of flask C and approximately 100 g of sodium was introduced into flask A. The whole apparatus was then heated to 120° and evacuated to a pressure of 10^{-5} mm for 2 hr. The sodium was then successively filtered from A to B to C at 120°.

After the filtration the temperature of flask C was raised to the required value. The lead and the sodium were allowed to remain in contact with each other for 6 hr. Homogenization was assisted by bubbling small amounts of helium through the mixture from time to time. The sodium solution of lead was then filtered off into trap D and analyzed by direct acid-base titration for sodium and gravimetrically as chromate for

lead.³ The above procedure was repeated at a number of different temperatures.

Intermetallic Compounds. The solubility apparatus was also used for the preparation of the intermetallic compounds.

The initial intermetallic compound which formed between sodium and lead was prepared in vessel C by the reaction of 30 g of sodium and 10 g of lead at 120°. Owing to the exothermic nature of the reaction, the temperature rose (after 5 min) to 140°. This temperature was maintained for 10 min. The excess sodium was then drawn off into vessel D and the compound remaining on the filter C was analyzed. A stoichiometric ratio of Na_4Pb was obtained. (See Table I.)

Table I

	Na_4Pb	Na_5Pb
Melting point	374°	390°
Mole ratio ^a	1:4.02 \pm 0.06	1:5.01 \pm 0.09
X-Ray data	Cubic	Hexagonal
	$a = 13.02$	$a = 10.6$ $c = 11.5$

^a Average of six determinations.

The above procedure was repeated, with the exception that the sodium-lead mixture in vessel C was heated up to 160°, where it was kept constant for 70 hr, and the excess sodium then was filtered off. Analysis of the compound retained on filter C gave a stoichiometric ratio of Na_5Pb (see Table I), indicating the slow conversion of Na_4Pb to Na_5Pb in the presence of excess sodium.

(1) G. J. Lamprecht, P. Crowther, and D. M. Kemp, *J. Phys. Chem.*, **71**, 4209 (1967).

(2) J. Malgiolio, E. A. Limoncelli, and R. E. Cleary, "The Purification and Gas Chromatic Analysis of Helium," PWAC-352.

(3) A. I. Vogel, "Quantitative Inorganic Analysis," 2nd ed, Longmans, Green and Co., New York, N. Y., p 420.

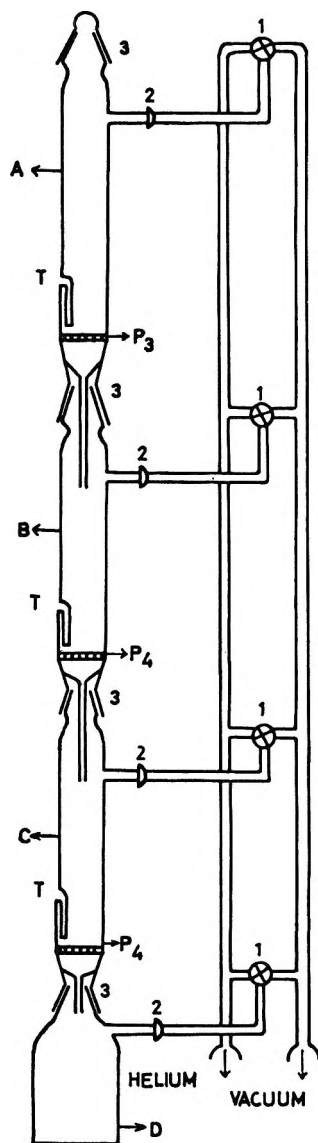


Figure 1. Solubility and intermetallic compound preparation apparatus: 1, stopcocks; 2, glass ball joints; 3, B 29/32 glass cones and sockets; T, thermocouple holes; P_3 , 10- μ filter; P_4 , 5- μ filters.

The compound Na_5Pb was also prepared as follows by crystallization. Sodium (30 g) at 110° was filtered from vessel A to vessel B where it reacted with 10 g of lead. The temperature was raised to 250° for 2 hr. The sodium plus dissolved lead was then filtered from vessel B to vessel C at 250° and the solution was cooled down to 110° , followed by filtering off the excess sodium to vessel D. Long needlelike crystals crystallized out of solution. Analysis gave a stoichiometric ratio of Na_5Pb . These crystals were used for crystallographic analysis.

Results and Discussion

In Figure 2, the plot of the mole fraction of lead dissolved in sodium *vs.* reciprocal absolute temperature is given. The plot resulted in a good straight line with

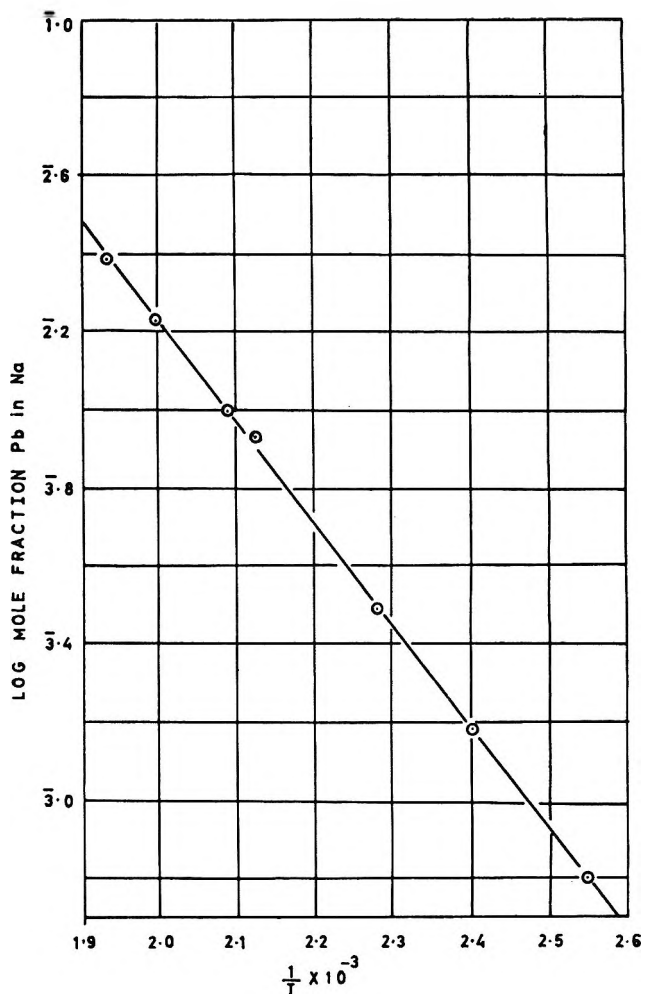


Figure 2. Lead solubility in sodium; log (mole fraction of Pb in Na) *vs.* reciprocal absolute temperature.

slope -2.64×10^3 , and the equation for the solubility based on the least-squares fit to Figure 2 is

$$y = 3.515 - \frac{2.639 \times 10^3}{T} \quad (1)$$

with a standard deviation in the value of y of ± 0.019 , where $y = \log$ (mole fraction of Pb in Na) and T is the absolute temperature.

The heat $\Delta\bar{H}_{i(\text{sol})}$ and entropy $\Delta\bar{S}_{i(\text{sol})}$ of solution can be calculated from the solubility data by means of the relation

$$\ln X_i = \frac{-\Delta\bar{H}_{i(\text{sol})}}{RT} + \frac{\Delta\bar{S}_{i(\text{sol})}}{R} \quad (2)$$

where X_i is the mole fraction of component i , and R is the molar gas constant.

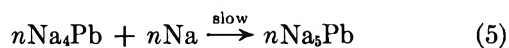
From the slope of the graph the heat of solution was calculated as $12.03 \text{ kcal mole}^{-1}$, and from the intercept on the $\log X$ axis at $1/T = 0$, the entropy of solution was calculated as $16.06 \text{ cal mole}^{-1} \text{ deg}^{-1}$. The partial molal free energy of solution $\Delta\bar{F}_i$, relative to the intermediate solid solute Na_5Pb , is given by the following expression for solutions not saturated in the solute as

$$\Delta \bar{F}_i = 12,030 - 16.06T + 1.987T \ln X \quad (3)$$

The intermetallic compound Na_4Pb has a melting point of 374° . This compound has previously been reported in the literature⁴ where a melting point of 373° is given, whereas a compound $\text{Na}_{15}\text{Pb}_4$ with a melting point of 386° is reported by Hansen.⁵

The newly isolated compound Na_5Pb which crystallized out of solution has a melting point of 390° .

From the results obtained in the experiments describing the preparation of the intermetallic compounds it may be concluded that in the temperature range studied, 120 – 245° , the compound Na_4Pb is initially formed but does not reach stable equilibrium, reacting further with the molten sodium to form Na_5Pb . At equilibrium, therefore, the reference solute is $n\text{Na}_5\text{Pb}$.



The stoichiometric integer n in eq 5 has been included since the crystallographic data given below preclude the simple formulation Na_5Pb .

Crystallographic Data

Single crystals of the compound Na_5Pb were prepared as described above. Inside a glove box filled with purified helium, a single crystal was sealed into a thin-

walled Lindemann glass capillary for rotation and Weissenberg photographs. Exposures were taken of the zero and first layer lines along the C axis. The cell dimensions were: hexagonal, $a = 10.6 \text{ \AA}$; $c = 11.5 \text{ \AA}$.

Considering the compound Na_4Pb , Zintl and Harder⁶ have reported single-crystal work on a compound $\text{Na}_{15}\text{Pb}_4$ and showed the compound to have a body-centered cubic structure with parameter $a = 13.32 \text{ \AA}$. Shoemaker, Weston, and Rathlev⁷ have confirmed the conclusion of Zintl and Harder⁶ that this compound is body-centered cubic based on the composition $\text{Na}_{15}\text{Pb}_4$ and find no support for the conclusion of Stillwell and Robinson,⁸ who claim on the basis of X-ray powder photographs that a phase to which they assigned a composition $\text{Na}_{31}\text{Pb}_8$ has a face-centered cubic lattice with $a = 13.30 \text{ \AA}$.

The relevant chemical and physical data for the two compounds Na_4Pb and Na_5Pb are summarized in Table I.

(4) C. J. Smithells, "Metals Reference Book," Butterworth and Co. Ltd., London, 1955.

(5) M. Hansen and K. Aderko, "Constitution of Binary Alloys," 2nd ed, McGraw-Hill Book Co. Inc., New York, N. Y., 1958.

(6) E. Zintl and A. Harder, *Z. Physik. Chem.*, **B34**, 238 (1936).

(7) D. P. Shoemaker, N. E. Weston, and J. Rathlev, *J. Am. Chem. Soc.*, **77**, 4226 (1955).

(8) C. W. Stillwell and W. R. Robinson, *ibid.*, **55**, 217 (1933).

Kinetics of Electrode Processes in Molten Salts. II. The Influence of Solvent Anions and Cations on the Molybdenum-Molybdenum(III) Electrode

by Sidney M. Selis

Research Laboratories, General Motors Corporation, Warren, Michigan 48090 (Received May 12, 1967)

The kinetics of the electrode Mo-Mo^{3+} have been studied in various molten alkali metal chloride and bromide electrolytes. Kinetic parameters have been determined and are found to be subject to strong solvent effects. The comparisons are made at corresponding-states melting points. The electrode process is slower in bromide melts than in chloride melts and is slower in LiBr than in LiBr-KBr , whereas in chloride melts, the fastest, medium, and slowest electrode reactions occur in LiCl , LiCl-KCl , and NaCl-KCl , respectively. These observations are interpreted in terms of different degrees of covalent bonding and in terms of electrostatic and steric considerations.

When molybdenum(III) ion is dissolved in a molten alkali metal chloride, the ion is apparently stabilized by solvation, the degree of stabilization of Mo^{3+} depending upon the solvent cation.¹ This has been shown by Smirnov and Ryzhik² and by Selis,³ who determined the emf's of cells of the type Mo(c)-MoCl_3 in $\text{MCl(l)-Cl}_2(\text{g})$, C, where M represents Li, Li-K, K, or Cs. The solvent cation effect is a large one, and it seems reasonable that solvation might also affect the kinetics of electrode processes involving molybdenum ion. Moreover, it is reasonable that there would be a solvent anion effect. Accordingly, a study of electrode kinetics was undertaken.

A galvanostatic technique was used. Measurements were made at electrode potentials within a few millivolts of the equilibrium potentials. It has not yet been determined where these potentials are situated on the double-layer capacitance-potential curves and whether there will be repulsion of electroactive and solvent cations and attraction of anions, or whether the reverse will occur at the electrode. It may be pointed out that results with other electrodes in molten alkali metal chlorides all show that the thermodynamic equilibrium potential is positive with respect to the zero-charge potential. This is the case for a number of monovalent, divalent, and trivalent metal-metal ion electrodes.⁴ The electrode metals so investigated were liquid, for the most part, or else easily polished. In the present work there was some difficulty in making reproducible capacity measurements at different potentials. This seemed to be due to an inability to prepare the molybdenum electrode appropriately (although there was no problem in making the differential capacity measurements that are referred to below). It will be presumed that for all determinations reported here, the equilibrium potentials bear the same qualitative relationship to the zero-charge potential and that the variations in kinetic behavior are not due to

major differences in the electrostatic effects on reactive species within the double layer.

The results of the work will be discussed below in terms of solvent effects and stabilization of the molybdenum(III) ion. Inferences will be drawn with regard to the electrode reaction mechanism.

Experimental Section

Materials and Cell Construction. Table I includes a list of the alkali metal halide solvents (single components and mixtures). They were purified by the procedure of melting under HCl or HBr and filtering through a glass frit, as has been already described.³ Magnesium turnings were mixed with the salts and preelectrolysis was thus obviated. The criterion of purity was the polarographic residual reduction current value.

A Vycor compartment with a fritted bottom was lowered into the cell container with the aid of a stainless steel hook. Two electrodes were used within the compartment. These were a piece of sheet molybdenum with an area of about 10 cm^2 which served as a reference electrode and a microelectrode made by sealing molybdenum wire into an aluminosilicate glass free of heavy metals (Corning 1720). The glass was ground to expose the end of the wire which was polished to a mirror finish. The area of exposed metal was about 10^{-2} cm^2 , known precisely.

(1) Spectroscopic data on the molybdenum ion in molten alkali metal halides are not available, and reference to stabilization of Mo^{3+} implies no specific knowledge of complex ions or even of groupings with less definite configurations.

(2) M. V. Smirnov and O. A. Ryzhik, *Tr. Inst. Elektrokhim., Akad. Nauk SSSR, Ural'sk. Filial*, No. 7, 27 (1965); No. 8, 43 (1966).

(3) S. M. Selis, *J. Electrochem. Soc.*, **113**, 37 (1966).

(4) A. D. Graves, G. J. Hills, and D. Inman, "Advances in Electrochemistry and Electrochemical Engineering," Vol. 4, P. Delahay, Ed., Interscience Publishers, Inc., New York, N. Y., 1966, pp 152, 153.

Table I: Kinetic Parameters for the Electrode Mo-Mo(III) in Molten Alkali Metal Halides

Solvent ^a	T_M , °K	α	i_o , ^b A cm ⁻²
LiCl	876	0.54	0.58
LiCl-KCl (60:40)	940	0.43	0.50
NaCl-KCl (50:50)	1042	0.49	0.34
LiBr	820	0.21	0.040
LiBr-KBr (60:40)	889	0.32	0.19

^a Mole percent ratios are given for the mixtures. ^b These are the values at the corresponding-states melting temperatures (T_M). They are for a molybdenum(III) concentration of 10.0×10^{-6} mol cm⁻².

Current was passed through a graphite electrode outside the compartment and through the large molybdenum electrode inside the compartment in order to generate molybdenum(III) ion coulometrically within the compartment. The molybdenum(III) ion was generated with unit efficiency in every case as was verified by analysis using the photometric thiocyanate method.⁵ The total amount of electrolyte in the compartment was determined by using ordinary chemical methods, and the volume was calculated using the density values for the molten salts.^{6,7}

Measurement of Polarization Characteristics. Constant current was passed through the test (polarizable) electrode; this passage was immediately preceded by a very brief charging pulse during which the current was relatively large. This prepulse was applied in order to charge the double layer immediately so that the intrinsic kinetics of the electrode could be measured without undue complication by mass-transport effects. In other words, by using the preliminary charging pulse, the useful portion of the plot of overpotential vs. $t^{1/2}$ is lengthened at the beginning of the constant-current passage.

Use was made of the apparatus designed by Birke and Roe,⁸ although a timer arrangement was not needed and the present equipment did not include it. Potentials of the electrode were measured against the large molybdenum sheet in the compartment with fritted bottom. The oscilloscope sweep rate was 5 μ sec cm⁻¹, and overpotentials were no higher than 4 or 5 mV. Current was passed in both the anodic and cathodic directions.

For a given molybdenum ion concentration at a particular temperature, overpotential measurements were made with several different applied currents so that the determinations of exchange-current densities would be verified. The molybdenum ion concentration was then increased by further anodization of the large molybdenum electrode, and additional constant-current measurements were made. After the cell was measured with the highest molybdenum ion concentrations, 8.0 – 8.9×10^{-6} mol cm⁻³, the temperature was raised

and current-potential data were taken at various temperatures.

Measurement of the Differential Capacity of the Double Layer. The differential capacity was measured with the technique and apparatus used previously.⁹ A relatively large constant current was passed through the test electrode. Potential (or overpotential) was linear with time for the first few tenths of a microsecond, giving the value of dE/dt , which was used to calculate the differential capacity $i(dt/dE)$. The latter was used in the determination of exchange-current density. The validity of the circuitry for determining differential capacity was verified by measuring appropriate capacitors put in the circuit in place of the cell.

Calculation of Kinetic Parameters. Birke and Roe¹⁰ wrote an expression for overpotential as a function of time, applicable to the constant-current method. It includes two terms in $t^{-1/2}$. If they are excluded, there remains the relationship presented by Berzins and Delahay after making certain simplifications.¹¹ The latter relationship is satisfactory for describing the variation of overpotential with time for larger values of t (between 50 μ sec and 100 msec), provided the quantity $(C_O/C_O^0) + (C_R/C_R^0)$ is approximately 2 during the current passage and if the overpotentials are no greater than a few millivolts. (Here C_O and C_R refer to the concentrations of oxidized and reduced electroactive species at the reaction site, and C_O^0 and C_R^0 are the concentrations in the bulk of the melt.) If the reduced phase is the pure metal, so that $(C_O/C_O^0) + (C_R/C_R^0)$ is not 2, and if the electrode reaction is fast, the use of the Birke-Roe equation as such is suggested. Moreover, the short times involved would necessitate a precharging pulse, as discussed above. The duration of the charging pulse was 0.1 μ sec or less (small compared with the length of the oscillographic sweep), and it was of a form as if it were apparently superimposed on the galvanostatic curve. Beyond that first instant the potential-time curve displayed characteristics typical for the technique, as have already been considered in detail in the literature.¹⁰⁻¹²

In the work reported here, overpotential was plotted as a function of $t^{1/2}$ for times of 5–50 μ sec ($t^{1/2}$ of 2–7 μ sec^{1/2}), and this linear segment was extrapolated to

(5) M. Kapron and P. L. Hehman, *Ind. Eng. Chem., Anal. Ed.*, **17**, 573 (1945).

(6) E. R. Van Artsdalen and I. S. Yaffe, *J. Phys. Chem.*, **59**, 118 (1955).

(7) A. Klemm, *Molten Salt Chem.*, **564**, 565, 567 (1964).

(8) R. L. Birke and D. K. Roe, *Anal. Chem.*, **37**, 455 (1965).

(9) S. M. Selis, *J. Phys. Chem.*, **68**, 2538 (1964).

(10) R. L. Birke and D. K. Roe, *Anal. Chem.*, **37**, 450 (1965).

(11) T. Berzins and P. Delahay, *J. Amer. Chem. Soc.*, **77**, 6448 (1955).

(12) D. Inman, J. O'M. Bockris, and E. Blomgren, *J. Electroanal. Chem.*, **2**, 506 (1961).

zero time. This was done for current passages in both the anodic and cathodic directions. The relationship without the terms in $t^{-1/2}$ was first used, and the overpotential was found for the critical times defined as^{11,12}

$$t_c^{1/2} = \frac{\pi^{1/2}}{2} \frac{RTC_{d1}}{n^2 F^2 C_O^0 D_O^{1/2}} \quad (1a)$$

$$t_c^{1/2} = -\frac{\pi C_{d1} d(E - E_e)}{4i_a dt^{1/2}} \quad (1b)$$

where C_{d1} is the differential capacity of the double layer as defined above, D_O is the diffusion coefficient of the oxidized species, E_e is the potential of the electrode at equilibrium, and i_a is the constant-current density passed through the electrode. Values of C_{d1} were from 50 to 80 $\mu\text{F cm}^{-2}$ for the various electrodes, and D_O was taken as $10^{-6} \text{ cm}^2 \text{ sec}^{-1}$. Actually, the critical times in the work reported here could be taken as zero, with potentials being read from the extrapolated plots. In doing so, variations larger than inherent experimental variations were not incurred.

The overpotential at the critical times is related to the exchange-current density (i_o) in a simple manner (eq 2). The approximate value of i_o obtained with this equation was inserted in the Birke-Roe relationship to obtain the coefficient of the $t^{-1/2}$ term so that a more precise value of i_o would be determined. It was

$$(E - E_e)_{t_c^{1/2}} = -\frac{RT}{nF} \frac{i_a}{i_o} \quad (2)$$

found, however, that the inclusion of the two terms in $t^{-1/2}$ did not significantly affect the determined values of i_o , and the relationship *without* those two terms could be successfully used in the present study with $t^{1/2}$ in the region of 2-7 $\mu\text{sec}^{1/2}$. In this manner the overpotential-time traces at various current densities were the experimental basis for finding i_o . Values of the transfer coefficient (α) were then obtained on the basis of relationship 3, which is actually a definition of exchange current in terms of α and the heterogeneous

$$i_o = nFk_b C_O^{0(1-\alpha)} \quad (3)$$

rate constant (k_b). It is seen here that a plot of $\log i_o$ against $\log C_O^0$ will have a slope of $1 - \alpha$.

Results

Figure 1 contains plots of $\log i_o$ vs. $\log C_O^0$ for the electrode Mo-Mo³⁺ in five alkali metal halide solvents. The results shown were verified by replicate experiments, and the lines were established by the method of least squares. Molybdenum ion concentrations were in the same range for all five solvents. The particular results in Figure 1 are for the lowest temperature used with each electrolyte, consistent with rapid solubility of the molybdenum additions. Values of i_o were also found for different concentrations at other fixed temperatures, and α values were thereby established as a

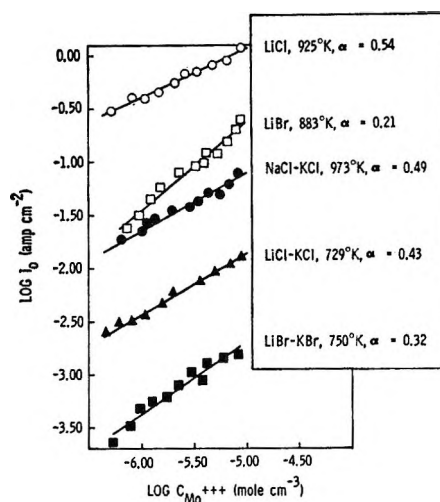


Figure 1. Typical plots of $\log i_o$ as a function of $\log C_{\text{Mo}^{3+}}$ for different solvents.

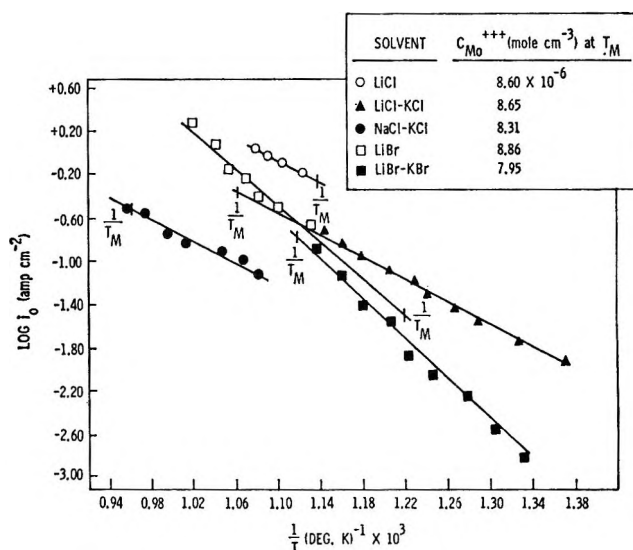


Figure 2. Plots of $\log i_o$ as a function of $1/T$ for different solvents.

function of temperature. The transfer coefficient, α , does increase slowly with temperature; however, in the temperature ranges used, α changed by no more than 0.05 for the bromide melts and by only 0.01-0.02 for the chlorides. Considering the precision of i_o determinations (see Figures 1 and 2), transfer coefficient values are here considered as constant with respect to temperature.

As shown in Figure 2, $\log i_o$ is a linear function of $1/T$. The lines in this figure were established by the method of least squares. Extrapolations of these lines were made to appropriate temperature points at which the behavior of one system might be validly compared with the behavior of the others. Values of "melting points" (T_M) were calculated by means of the corresponding-states treatment developed by Reiss, Mayer, and Katz,¹³ which makes use of the relationship

$$T_M \approx \tau_M Z^2 / \lambda_0 \quad (4)$$

where τ_M is a corresponding-states parameter and λ_0 is the interatomic distance for the solvent. Z , the charge on solvent anion or cation, is 1 in all cases. Weighted average values of τ_M and λ_0 were used to calculate respective melting points of LiCl-KCl, NaCl-KCl, and LiBr-KBr, and data extrapolated to these temperatures were used in the comparison. It should be noted that these melting points are not the experimentally observed physicochemical liquidus temperatures. In the case of the single components (LiCl and LiBr), the melting points calculated by the corresponding-states treatment do coincide with the physicochemical melting points.

Table I lists the five alkali metal halide solvents, their melting points (T_M), and kinetic parameters for the systems. The latter include the transfer coefficients (α) and the exchange-current densities (i_0) at stated concentrations (C_0^0) at the melting points.

Discussion

Some of the steps in the Mo-Mo³⁺ electrode process may involve extensively solvated molybdenum ions, and some probably do not. One of those in the first category is the movement of the solvated ion, toward or away from the electrode, under the influence of a concentration gradient or an electric field, the rate being determined in part by the magnitude of the electric field. Based on their chronopotentiometric data on the Mo-Mo³⁺ electrode in LiCl-KCl, Senderoff and Mellors concluded that another step, the dissociation of Mo₂Cl₉³⁻ to form MoCl₆³⁻, limits the rate in the electrodeposition of molybdenum at 600° and that this step becomes considerably faster at 700 and 800°.¹⁴ Still others in the first category are the solvation or desolvation of the Mo³⁺ particle which may partially occur while the latter is adsorbed on the metal surface and adsorption and desorption of the ion on the metal surface, differences being determined mainly by steric effects if the equilibrium potential has approximately the same relationship to the zero-charge potential in the case of each electrolyte.

Steps which do not generally involve solvated ions are charge transfer and movement of a metal atom between a site of adsorption and a position in the lattice. (Senderoff and Mellors believe that when molybdenum is deposited in coherent form, the three-electron charge transfer occurs irreversibly and rapidly in one stage.¹⁴)

The rate-determining part of the process is probably in the first category involving solvated species, because solvent effects are certainly evident from the experimental results. Table I shows that the exchange currents of the Mo-Mo³⁺ electrode are lower in the bromide melts than in the chloride melts. It is not unlikely that the attachment of the molybdenum ion to

the bromide ligands is much stronger than the attachment of Mo³⁺ to chloride ions. Studies have been made of silver ion with chloride, bromide, and iodide ions in nitrate melts and of cadmium ion with bromide and iodide ions in nitrate melts. Association constants have been compiled, and it is seen from the latter that the degree of stabilization of both the monovalent and divalent cations increases as the larger bromide ions are used.¹⁶ The bonds between the metal ions and bromide or iodide ion are stronger because of an increasingly covalent character of the bonds involving the larger anions.

There is also the cation effect. The mean cation-to-anion distances for the three chloride solvents (LiCl, LiCl-KCl, and NaCl-KCl) listed in Table I are 2.02, 2.28, and 2.51 Å, respectively; the values for single components are from the table prepared by Bauer and Porter.¹⁶ It is seen from the table that i_0 decreases with increasing solvent cation-to-anion distance. Again this can be associated with the strength of the bonds between the molybdenum ion and the anion ligands. If the solvent cation is small, it can hold the chloride ion more firmly, and, consequently, the Mo-Cl bond will be less firm. That the strength of the molybdenum-anion bond does indeed increase with increasing solvent cation-to-anion distance is supported by the determinations of the free energy of formation of MoCl₃ in alkali metal chloride melts. It was found that the free energy of formation of MoCl₃ becomes increasingly more negative as the radius of the solvent cation becomes larger.^{2,3}

There is a reversal of this order in the comparison of i_0 values in LiBr and LiBr-KBr, for the exchange current is higher in the latter solvent. Two interpretations of this are possible. It is seen in Figure 2 that all exchange currents measured with the LiBr solvent were larger than any exchange current measured with LiBr-KBr (cation-to-anion distances being 2.17 and 2.43 Å, respectively). However, when the LiBr plot was extrapolated to a lower temperature and the LiBr-KBr plot was extrapolated to a higher temperature, the exchange-current density in LiBr at its melting point was less than the corresponding value for LiBr-KBr. A question could then be raised as to the complete validity of comparing rates at corresponding-states melting points.

The second interpretation is that the Mo-Br bond might not be disrupted or stretched very much by next nearest neighbor solvent cations. At the same time, the field around the lithium ion is stronger than the

(13) H. Reiss, S. W. Mayer, and J. L. Katz, *J. Chem. Phys.*, **35**, 820 (1961).

(14) S. Senderoff and G. W. Mellors, *J. Electrochem. Soc.*, **114**, 556 (1967).

(15) M. Blander, *Molten Salt Chem.*, **226**, 227 (1964).

(16) S. H. Bauer and R. F. Porter, *ibid.*, **642** (1964).

average field around the lithium and potassium ions, and the solvent cation attachment may be firmer in pure lithium bromide. This would result in larger steric effects and retard the electrochemical processes involving Mo^{3+} ion.

Table I shows that the transfer coefficients (α) are larger for the chloride solvents than for the bromides. It is, of course, not unusual that transfer coefficients for a particular reaction do vary in different solvents. As suggested above, they remain essentially constant with changing temperature in the temperature region used in this work.

Table I is a quantitative statement of what has been offered above: that there is a marked solvent effect on the exchange-current densities of the molybdenum electrode, the comparison being made at corresponding-states melting temperatures. The values of i_0 in

Table I are for a molybdenum(III) concentration of $10 \mu\text{mol cm}^{-3}$. Because the transfer coefficients are not the same for the different solvents, it is not valid to compare heterogeneous rate constants (k_h) which really express electrode reaction rates at *unit concentration* (1 mol cm^{-3}), as has been emphasized by Laitinen, Tischer, and Roe.¹⁷ To make such comparisons would require extrapolations across five orders of magnitude of concentration.

Acknowledgment. The author expresses his appreciation to Mr. Richard B. Loranger of the Research Laboratories, General Motors Corp., for the photometric analyses for molybdenum ion.

(17) H. A. Laitinen, R. P. Tischer, and D. K. Roe, *J. Electrochem. Soc.*, **107**, 546 (1960).

Mean Amplitudes of Vibration of Comparatively Large

Molecules. I. Isotopic Naphthalenes

by G. Hagen and S. J. Cyvin

Institute of Physical Chemistry, Technical University of Norway, Trondheim, Norway

Accepted and Transmitted by The Faraday Society (May 25, 1967)

A complete harmonic-vibration analysis for naphthalene was performed. The derived force constants were used to compute mean amplitudes of vibration in naphthalene, naphthalene- d_8 , and five selected partially deuterated naphthalenes. It was found possible to present the results as characteristic values for the various types of distances, applicable to any deuterated naphthalene compound. Good agreement with similar data for benzene was also found.

Many comparatively large molecules have been investigated by modern gas electron diffraction. Some examples are: naphthalene, anthracene, coronene,¹ n -alkanes through heptane,^{2,3} triphenylamine,⁴ triphenylmethane,⁵ cyclooctane, and cyclotetradecadiyne.⁶ For many of these and similar compounds reasonably reliable values of mean amplitudes of vibration are available from the electron-diffraction measurements. It would be desirable to pursue such investigations by spectroscopic calculations of mean amplitudes of vibration. So far, some hexacarbonyls⁷ (thirteen-atomic) are the largest molecules for which the mean amplitudes have been calculated rigorously, *i.e.*, from a complete harmonic force field. Still this analysis of hexacarbonyls was not too complicated because of the high degree of separation of normal coordinates into

symmetry species by virtue of the high molecular symmetry; the maximum species dimensionality was only four. The spectroscopic analysis increases rapidly in complexity with an increasing number of atoms. Nevertheless it is now feasible to perform this kind of calculations for comparatively large molecules by

(1) A. Almendingen, O. Bastiansen, and F. Dyvik, *Acta Cryst.*, **14**, 1056 (1961).

(2) R. A. Bonham, L. S. Bartell, and D. A. Kohl, *J. Am. Chem. Soc.*, **81**, 4765 (1959).

(3) L. S. Bartell and D. A. Kohl, *J. Chem. Phys.*, **39**, 3097 (1963).

(4) Y. Sasaki, K. Kimura, and M. Kubo, *ibid.*, **31**, 477 (1959).

(5) P. Andersen, *Acta Chem. Scand.*, **19**, 622 (1965).

(6) A. Almendingen, O. Bastiansen, and H. Jensen, *ibid.*, **20**, 2689 (1966).

(7) J. Brunvoll, *J. Mol. Spectry.*, **15**, 386 (1965).

extensive use of modern high-speed computers. Some few examples of molecules for which the normal-coordinate analysis has been accomplished are: *n*-alkanes,^{8,9} tetramethylmethane,¹⁰ naphthalene (see below), and anthracene (in-plane).¹¹ None of these computations includes the mean amplitudes of vibration. Our first computer program series including computations of mean amplitudes of vibration was designed for the Gier machine,¹² which has a limited capacity. Already molecules like benzene were not easily manageable. These programs have now been extended and rewritten for the Univac 1107 machine and are intended to be used for comparatively large molecules. We have a special personal interest in performing this work, namely, to see at which point the program series breaks down, as inevitably must happen when the number of atoms is steadily increased. At the same time the results of these calculations are expected to be of appreciable interest in future electron-diffraction investigations.

In this first communication we report some results on naphthalene and some of its deuterated compounds.

Force Constants

The assignment of fundamental frequencies for naphthalene and some deuterated naphthalenes has been studied by many workers. Condensed summaries and suggestions of complete assignments for naphthalene are found in two recent works by Krainov¹³ and Hollas.¹⁴ The in-plane vibrations of naphthalene (and anthracene) have very recently been studied by Neto, *et al.*¹¹ Two of the here mentioned works^{11,13} (among several others) contain calculated vibrational frequencies as a result of tentative harmonic force fields for naphthalene, but no workers give a detailed specification of the complete set of symmetrized force constants. This is quite understandable because such data, besides being rather voluminous, will depend on a complicated system of symmetry coordinates, which may be defined in various ambiguous ways. We have succeeded to construct a complete set of valence coordinates with no redundants involved.¹⁵ However, the presently communicated results of calculation of course do not depend on the specific choice of symmetry coordinates.

We constructed an initial harmonic force field by transferring *compliant*s¹⁶ rather than force constants from benzene and ethylene (for the central part of the molecule) and neglecting numerous interaction terms. The possible transferability of compliant ("inverse" force constants) was proposed by Cyvin and Slater¹⁷ some time ago, but never fully explored. Table I includes the calculated frequencies for naphthalene and naphthalene-*d*₈ from the initial force field. The general agreement with observed fundamentals, incidentally taken from Krainov,¹³ seems quite remarkable and tends to support the hypothesis of transferability of compli-

ants. However, the naphthalene molecule seems too large to be well suited as a test molecule in this respect. The existing uncertainties in the assignment of fundamentals is only one reason. Thus it is at present impossible to decide about the superiority or inferiority of transferring compliant as compared to other approaches. Neto, *et al.*,¹¹ applied a Urey-Bradley force field with notable success.

The assignment of frequencies is established with best confidence^{11,13,14} for the planar vibrations $a_g + b_{3g} + b_{1u} + b_{2u}$. For the out-of-plane vibrations varieties of controversial assignments have been published. Our calculated frequencies (from the initial constants) of b_{1g} in naphthalene and naphthalene-*d*₈ and b_{2g} in naphthalene show remarkably close agreement with the assignment of Mitra and Bernstein,¹⁸ thus giving support to this particular set; *cf.* column *c* of Table I. The conclusion is not at all decisive, however. It seems also that one should take into account some possible modifications of the assignment of planar frequencies. In particular, one should allow for the possibility of a lowest frequency $<300\text{ cm}^{-1}$ in species a_g and b_{2u} .

We produced the final set of force constants by adjusting to the observed frequencies of naphthalene and naphthalene-*d*₈ and taking averages of the independently derived results. Throughout these refinements the fundamentals from Krainov¹³ were applied. The resulting force field was applied to naphthalene and naphthalene-*d*₈ (same force constants for both isotopic compounds); Table I includes the calculated frequencies, which may be compared with the observed values. There is seen to be a generally good correspondence. Still better agreement could no doubt be obtained by further refinements. They seem however not worthwhile performing at present because of the existing uncertainties in the assignment of observed fundamentals. We also used the final force constants to calculate the frequencies of α -naphthalene-*d*₄ and β -naphthalene-*d*₄. The results, which we do not report here for the sake of brevity, showed an altogether satisfactory agreement with observed fundamentals.¹³

(8) J. H. Schachtschneider and R. G. Snyder, *Spectrochim. Acta*, **19**, 117 (1963).

(9) J. N. Gayles, Jr., W. T. King, and J. H. Schachtschneider, *ibid.*, **23A**, 703 (1967).

(10) K. Shimizu and H. Murata, *Bull. Chem. Soc. Japan*, **30**, 487 (1957).

(11) N. Neto, M. Serocco, and S. Califano, *Spectrochim. Acta*, **22**, 1981 (1966).

(12) J. Brunvoll and S. J. Cyvin, *Acta Polytech. Scand.*, **Matl**, **1** (1964).

(13) E. P. Krainov, *Opt. i Spektroskopiya*, **16**, 763 (1964); *Opt. Spectry*, **16**, 415 (1964).

(14) J. M. Hollas, *J. Mol. Spectry*, **9**, 138 (1962).

(15) G. Hagen and S. J. Cyvin, *J. Phys. Chem.*, **72**, 1451 (1968).

(16) J. C. Decius, *J. Chem. Phys.*, **38**, 241 (1963).

(17) S. J. Cyvin and N. B. Slater, *Nature*, **188**, 485 (1960).

(18) S. S. Mitra and H. J. Bernstein, *Can. J. Chem.*, **37**, 553 (1959).

Table I: Calculated and Observed Vibrational Frequencies (cm^{-1}) in Naphthalene and Naphthalene- d_8

Species		Naphthalene				Naphthalene- d_8			
		Calcd		Obsd		Calcd		Obsd	
		Initial ^a	Final	b	c	Initial ^a	Final	b	c
a_g	1	3072	3057	3060		2349	2279	2293	
	2	3065	2976	3031		2273	2261	2263	
	3	2088	1644	1577		1967	1550	1550	
	4	1409	1507	1460		1242	1358	1383	
	5	1270	1388	1376		1170	1260	1290	
	6	1111	1151	1145		842	881	864	
	7	917	995	1025		796	850	833	
	8	614	745	758		579	701	693	
	9	213	520	512		495	485	495	
b_{1g}	1	1250	905	943	1239	1135	821	777	1006
	2	715	717	717	717	539	540	540	541
	3	235	411	386	195	182	319	339	180
b_{2g}	1	1751	950	980	1099	1688	914	875	875
	2	988	869	876	874	940	805	760	752
	3	719	817	846	770	572	666	671	671
	4	283	502	461	285	212	377	408	270
b_{3g}	1	3073	3092	3092		2289	2311	2302	
	2	3066	3062	3060		2275	2271	2275	
	3	1834	1675	1624		1829	1659	1604	
	4	1489	1443	1438		1368	1315	1330	
	5	1338	1241	1239		1120	1048	1030	
	6	1223	1130	1158		992	923	927	
	7	871	981	936		721	807	833	
	8	524	467	506		493	441	(490)	
a_u	1	1014	919	970		952	860	797	
	2	782	831	841		628	666	655	
	3	414	617	581		315	474	...	
	4	219	202	195		190	175	180	
b_{1u}	1	3073	3063	3065		2292	2285	2284	
	2	3066	3057	3058		2275	2268	2266	
	3	1544	1601	1595		1459	1515	1545	
	4	1429	1392	1389		1321	1285	1260	
	5	1334	1300	1265		1041	1016	1040	
	6	1052	1089	1125		896	917	885	
	7	739	777	747		644	686	715	
	8	301	358	359		276	329	328	
b_{2u}	1	3072	3070	3090		2301	2294	2284	
	2	3063	3032	3027		2268	2250	2248	
	3	1542	1533	1509		1451	1444	1466	
	4	1494	1377	1361		1432	1317	1318	
	5	1276	1251	1209		1035	1051	1087	
	6	1099	1122	1138		920	878	830	
	7	981	980	1008		793	820	825	
	8	224	623	618		210	585	593	
b_{3u}	1	1329	912	958		1233	843	791	
	2	740	796	782		572	616	626	
	3	364	481	476		301	397	404	
	4	131	181	176		114	158	(163)	

^a Compliance constants transferred from benzene and ethylene. ^b Quoted by Krainov.¹² ^c Mitra and Bernstein.¹³

We feel that our force field is good enough for calculations of mean amplitudes of vibration for naphthalene and any of its isotopic substitutions. It should be noted that only the planar vibrations are involved in these calculations.

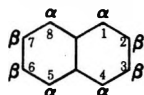
Mean Amplitudes of Vibration

Naphthalene and Naphthalene- d_8 . The calculated mean amplitudes of vibration (u) for naphthalene and naphthalene- d_8 are shown in Table II. The numbering of atoms follows common usage in organic chemistry.

Table II: Mean Amplitudes of Vibration (\AA) for Naphthalene and Naphthalene- d_8 . Values for Benzene (at 0°K) Are Included for Comparison

Dist ^a	(Equil dist)	Benzene, ^b 0°K	Naphthalene		Benzene- d_8 , ^b 0°K	Naphthalene- d_8	
			0°K	298°K		0°K	298°K
C ₂ -H	(1.084)	0.077	{ 0.077	0.077	0.066	{ 0.066	0.066
C ₁ -H	(1.084)		{ 0.077	0.077		{ 0.066	0.066
C ₂ -C ₃	(1.415)	0.046	{ 0.058	0.061	0.046	{ 0.058	0.061
C ₁ -C ₂	(1.364)		{ 0.046	0.046		{ 0.046	0.046
C ₁ -C ₉	(1.421)	(ortho)	{ 0.046	0.047	(ortho)	{ 0.046	0.047
C ₉ -C ₁₀	(1.420)		{ 0.046	0.046		{ 0.046	0.046
C ₁ ...C ₃	(2.414)	0.054	{ 0.059	0.062	0.054	{ 0.059	0.062
C ₂ ...C ₉	(2.415)		{ 0.051	0.052		{ 0.051	0.052
C ₁ ...C ₁₀	(2.450)	(meta)	{ 0.052	0.054	(meta)	{ 0.052	0.054
C ₁ ...C ₈	(2.483)		{ 0.056	0.060		{ 0.055	0.060
C ₂ ...C ₁₀	(2.801)	0.057	{ 0.054	0.057	0.057	{ 0.054	0.057
C ₁ ...C ₄	(2.804)	(para)	{ 0.054	0.056	(para)	{ 0.053	0.056
C ₁ ...C ₇	(3.722)		{ 0.057	0.060		{ 0.057	0.060
C ₁ ...C ₆	(3.745)		{ 0.056	0.058		{ 0.055	0.058
C ₂ ...C ₇	(4.831)		{ 0.055	0.057		{ 0.055	0.057
C ₁ ...C ₆	(4.221)		{ 0.059	0.063		{ 0.059	0.063
C ₂ ...C ₈	(5.034)		{ 0.058	0.061		{ 0.058	0.061
C ₁ ...C ₄	(2.171)	0.099	{ 0.106	0.108	0.086	{ 0.093	0.096
C ₂ ...H ₁	(2.122)		{ 0.100	0.101		{ 0.087	0.088
C ₁ ...H ₂	(2.118)		{ 0.098	0.098		{ 0.085	0.085
C ₁₀ ...H ₁	(2.176)		{ 0.098	0.099		{ 0.085	0.086
C ₂ ...H ₄	(3.397)	0.096	{ 0.100	0.102	0.084	{ 0.089	0.092
C ₁ ...H ₃	(3.390)		{ 0.100	0.102		{ 0.088	0.091
C ₉ ...H ₂	(3.397)		{ 0.092	0.093		{ 0.081	0.081
C ₉ ...H ₅	(3.435)		{ 0.094	0.094		{ 0.082	0.083
C ₁ ...H ₈	(2.724)	0.092	{ 0.124	0.128	0.081	{ 0.107	0.113
C ₁ ...H ₄	(3.888)		{ 0.090	0.091		{ 0.079	0.081
C ₉ ...H ₃	(3.885)		{ 0.090	0.092		{ 0.079	0.081
C ₂ ...H ₈	(4.081)		{ 0.124	0.128		{ 0.107	0.113
C ₁ ...H ₇	(4.598)		{ 0.103	0.105		{ 0.090	0.094
C ₁ ...H ₅	(4.622)		{ 0.102	0.104		{ 0.089	0.092
C ₂ ...H ₇	(5.795)		{ 0.098	0.099		{ 0.086	0.088
C ₂ ...H ₅	(4.867)		{ 0.115	0.119		{ 0.100	0.105
C ₁ ...H ₆	(5.305)		{ 0.093	0.095		{ 0.083	0.086
C ₂ ...H ₆	(6.092)		{ 0.094	0.095		{ 0.083	0.085
H ₂ ...H ₃	(2.499)	0.157	{ 0.161	0.163	0.133	{ 0.136	0.141
H ₁ ...H ₂	(2.434)	(ortho)	{ 0.158	0.159	(ortho)	{ 0.133	0.136
H ₁ ...H ₃	(4.283)	0.132	{ 0.136	0.139	0.112	{ 0.117	0.121
		(meta)			(meta)		
H ₁ ...H ₈	(2.516)		{ 0.174	0.180		{ 0.148	0.157
H ₁ ...H ₄	(4.971)	0.117	{ 0.116	0.117	0.100	{ 0.099	0.100
		(para)			(para)		
H ₁ ...H ₇	(4.775)		{ 0.160	0.164		{ 0.136	0.143
H ₁ ...H ₆	(5.572)		{ 0.128	0.130		{ 0.109	0.111
H ₂ ...H ₇	(6.708)		{ 0.131	0.133		{ 0.111	0.115
H ₁ ...H ₆	(5.935)		{ 0.138	0.141		{ 0.118	0.123
H ₂ ...H ₆	(7.159)		{ 0.118	0.120		{ 0.101	0.103

^a The numbering of atoms follows usual conventions in organic chemistry



H stands here for both ^1H and $^2\text{H} = \text{D}$. ^b From Cyvin.²⁰

For further identification of the atom pairs the values used as equilibrium interatomic distances¹⁹ are given in parentheses. The skeleton structural parameters are

adopted from Cruickshank¹⁹ while some CCH angles are assumed to be 120° , and all C-H distances, 1.084 \AA . Mean amplitudes of vibration for benzene from earlier

computations²⁰ are included in Table II for the sake of comparison.

The magnitudes of the calculated mean amplitudes all seem to be reasonable. As a general conclusion it is found that the mean amplitudes for the largest distances are not at all abnormally large. For instance the skeleton mean amplitudes at absolute zero never exceed 0.06 Å. The altogether largest mean amplitude is found for H···H in the *peri* position (H₁···H₈), viz., 0.174 Å at absolute zero. Still this value is not substantially larger than the mean amplitude for the *ortho* H···H distance in benzene (0.157 Å). The *u* value for H···H in the *amphi* position (H₂···H₆) in naphthalene (0.118 Å) is seen to be markedly smaller than the *ortho* H···H *u* value for benzene but corresponds rather to the *para* H···H *u* value (0.117 Å). The mean amplitude values in naphthalene and benzene show, in general, satisfactory agreement. Only one detail may perhaps be surprising. The *u* value for the bonded C₂-C₃ (*i.e.*, ββ) distance in naphthalene is significantly larger than the bonded C-C value of *u* in benzene. The C₁-C₂ and C₁-C₉ *u* values in naphthalene correspond as expected to the latter value (in benzene), as also does the C₉-C₁₀ (middle bond) value of *u*. The influence of isotopic substitution on the skeleton mean amplitudes is negligible, as in benzenes.²⁰

Partially Deuterated Naphthalenes. It is not the intention here to give a detailed report of complete sets of mean amplitudes of vibration in all kinds of partially deuterated naphthalenes. Such voluminous material would be quite incomprehensible and of rather limited interest. One would have to include too many decimals, for which no physical significance could be claimed, in order to detect the influence of isotopic substitutions on mean amplitudes for atom pairs which are not directly involved in the substitution. It seems therefore better to discuss the results of the present calculations in more general terms.

Deuterated naphthalenes may belong to the symmetry groups of D_{2h}, C_{2h}, C_{2v}, and C_s. The normal vibrations are distributed among the various symmetry species according to

$$\Gamma(D_{2h}) = 9a_g + 3b_{1g} + 4b_{2g} + 8b_{3g} + 4a_u + 8b_{1u} + 8b_{2u} + 4b_{3u}$$

$$\Gamma(C_{2h}) = 17a_g + 7b_g + 8a_u + 16b_u$$

$$\Gamma(C_{2v}) = 17a_1 + 7a_2 + 8b_1 + 16b_2$$

$$\Gamma(C_{2v}^*) = 17a_1 + 8a_2 + 7b_1 + 16b_2$$

$$\Gamma(C_s) = 33a' + 15a''$$

The distinction between the two C_{2v} symmetry structures (C_{2v} and C_{2v}^{*}) is rather formal, depending on conventions about the species designations. Here we have to make this distinction because we adhere strictly to the recommendations of Mulliken's report.²¹

In planar C_{2v} molecules the twofold symmetry axis is taken as the *z* axis, while the *x* axis is perpendicular to the molecular plane. In the above notation the C_{2v} and C_{2v}^{*} structures pertain to the *z* axis along and perpendicular to the middle bond, respectively.

The most symmetrical tetradeuterio substitutions, viz., α-naphthalene-*d*₄ and β-naphthalene-*d*₄ possess the full symmetry of naphthalene itself, and the same is of course the case with the totally substituted compound, naphthalene-*d*₈. All of the lower symmetry models are represented among the ten dideuterio compounds. We have selected the following compounds, besides naphthalene and naphthalene-*d*₈ (see Table II), for computations of mean amplitudes of vibration: α-naphthalene-1,4,5,8-*d*₄ and β-naphthalene-2,3,6,7-*d*₄, both belonging to D_{2h}; *amphi*-naphthalene-2,6-*d*₂ with C_{2h} symmetry; *peri*-naphthalene-1,8-*d*₂ and naphthalene-1,2,3,4-*d*₄, both belonging to C_{2v}, but should in the present notation be assigned to C_{2v} and C_{2v}^{*}, respectively.

We were not able to perform the computations for a deuterated naphthalene of the C_s symmetry. The memory capacity of the computer was namely exceeded when using our current programs with the 33-dimensional symmetry species block. We had however no difficulties carrying through the computations when a 17-dimensional species was involved.

We are convinced that the computational results for

Table III: Mean Amplitudes of Vibration (Å) for HD Distances in Selected Partially Deuterated Naphthalenes at 298°K. For All Other Types of Distances the Values Given in Table II May Be Transferred

(H···D equil dist) ^a	α- C ₁₀ H ₄ D ₄	β- C ₁₀ H ₄ D ₄	<i>amphi</i> - C ₁₀ H ₆ D ₂	<i>peri</i> - C ₁₀ H ₆ D ₂	1,2,3,4- C ₁₀ H ₄ D ₄
(2.499)			0.152		
(2.434)	0.148	0.148	0.148	0.148	
(4.283)	0.130	0.130	0.130	0.130	
(2.516)					0.169
(4.971)				0.109	
(4.775)	0.153	0.156	0.156	0.153	0.153
(5.572)				0.121	0.121
(6.708)			0.125		0.125
(5.935)	0.130	0.135	0.135	0.130	0.130
(7.159)					0.135
					0.112

^a The distances are given in the same sequence as the corresponding distances at the end of Table II.

(19) D. W. J. Cruickshank, *Proc. Roy. Soc. (London)*, **A258**, 270 (1960).

(20) S. J. Cyvin, "Molecular Vibrations and Mean Square Amplitudes," Universitetsforlaget, Oslo, 1968.

(21) R. S. Mulliken, *J. Chem. Phys.*, **23**, 1997 (1955).

the presently selected compounds give material sufficient for the general conclusions about deuterated naphthalenes as stated below.

All of the mean amplitudes of vibration for the CC (bonded and nonbonded) distances were shown to be entirely unaffected by the isotopic substitutions of hydrogen within the reported number of decimals (at 298°K). The values listed in Table II may therefore be applied to all deuterated naphthalenes. Also the CH, CD, HH, and DD mean amplitudes were shown to have characteristic magnitudes for every type of the distance; consequently their values may again be depicted from Table II. Strictly speaking, there is one (hardly significant) exception, as the mean amplitude of the C···H (4.867 Å) type showed a slight variation between 0.118 and 0.119 Å at 298°K. Otherwise all of the figures in Table II were reproduced exactly within the reported decimals at 298°K.

There remains for us to give an account of the mean

amplitudes for the HD distances, which are not found in naphthalene and naphthalene-*d*₈. The resulting values of the present computations are shown in Table III. Again one finds a constancy of the mean amplitudes for corresponding distances in the various compounds. In this connection some explanations should be made as to the atom pairs identified by the equilibrium distances (4.775 and 5.935 Å). They refer to pairs of α, β positions in the different rings, *viz.*, 1,7 and 1,6, respectively. To take the former case of 4.775 Å as an example, the two mean amplitudes, *viz.*, 0.153 and 0.156 Å (see Table III), are actually not of the same type. The two quoted values refer to D in the α position and H in the β position (in α -C₁₀H₄D₄ and *peri*-C₁₀H₆D₂) and *vice versa* (in β -C₁₀H₄D₄ and *amphi*-C₁₀H₆D₂). Both types occur in 1,2,3,4-C₁₀H₄D₄. In general all of the mean amplitudes for HD distances are found (as expected) between the values for the corresponding HH and DD distances.

Tentatively Standardized Symmetry Coordinates for Vibrations of Polyatomic Molecules. VI. Naphthalene and Biphenyl Models

by G. Hagen and S. J. Cyvin

Institute of Physical Chemistry, Technical University of Norway, Trondheim, Norway

Accepted and Transmitted by The Faraday Society (May 25, 1967)

Symmetry coordinates are given for molecular vibrations of the naphthalene and biphenyl molecule models. Also included are the correlation diagrams for symmetry species of isotopically substituted naphthalenes and rotational isomers of biphenyl. One has succeeded to construct complete sets of coordinates without involving any redundants.

In this part of the series on tentatively standardized symmetry coordinates, we are treating some models of aromatics, including the naphthalene and biphenyl molecular model. We are specifying suitable sets of symmetry coordinates, but do not include the expressions of G and C^α matrix elements, as was done in previous parts of this series.^{1,2} The complete evaluation of the expressions would be rather tedious, although not particularly difficult. The main reason why they are not included here is that they are not believed to be of much interest in practical calculations. The normal-coordinate analysis of comparatively large molecules like naphthalene and biphenyl can hardly be performed without the use of modern computers. In such computations it is expedient to apply numerical G and C^α

matrix elements obtained from general programs without explicit use of the algebraic expressions for the specific molecule models in question.

The harmonic-vibration analysis of naphthalene has attracted many investigators, reference is here made to some of the more recent works.³⁻²¹ Also a valuable

(1) S. J. Cyvin, J. Brunvoll, B. N. Cyvin, I. Elvebredd, and G. Hagen, submitted for publication.

(2) S. J. Cyvin, B. N. Cyvin, I. Elvebredd, G. Hagen, and J. Brunvoll, submitted for publication.

(3) W. B. Person, G. C. Pimentel, and O. Schnepf, *J. Chem. Phys.*, **23**, 230 (1955).

(4) G. C. Pimentel, A. L. McClellan, W. B. Person, and O. Schnepf, *ibid.*, **23**, 234 (1955).

(5) E. R. Lippincott and E. J. O'Reilly, Jr., *ibid.*, **23**, 238 (1955).

(6) A. L. McClellan and G. C. Pimentel, *ibid.*, **23**, 245 (1955).

amount of work has been done on biphenyl²²⁻²⁴ and decafluorobiphenyl.²⁵ As far as we can see, none of the workers has devised a set of symmetry coordinates without unnecessary redundants²⁶ for the pertinent molecular models. It is therefore believed to be of particular interest here to give a specification of our symmetry coordinates. Both for the naphthalene and biphenyl models they do not include redundants whatsoever, without any loss of completeness.

Planar Bicyclic Naphthalene-Type Model

Symmetry Coordinates. The naphthalene-type $W_2[(XU)_2(YV)_2]_2$ molecular model (Figure 1) has the symmetry of D_{2h} . The notation used for structure

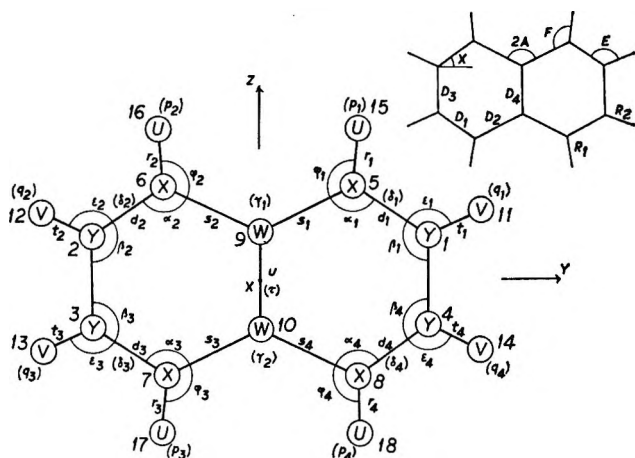


Figure 1. Planar bicyclic (naphthalene-type) $W_2[(XU)_2(YV)_2]_2$ model; symmetry D_{2h} . The equilibrium structure of the skeleton ($W_2X_4Y_4$) of the model is in general determined by five parameters, say, $D_1 = X-Y$, $D_2 = W-X$, $D_3 = Y-Y$, $D_4 = W-W$, and the XWX angle, $2A$; cf. the auxiliary figure. Then the angle X as given on the auxiliary figure (upper right), may be found from $2D_1 \sin X = 2D_2 \cos A - D_2 + D_4$. To determine the equilibrium structure of the whole model, one needs four additional parameters, say, $R_1 = X-U$, $R_2 = Y-V$, $F = WXU$, $E = XYV$.

The main figure tends to explain the notation used for valence coordinates. The out-of-plane coordinate symbols are parenthesized and are specified below. The torsions of the $X-Y$ bonds are identified by the symbol δ . The γ and τ coordinates are similar to corresponding coordinates in the ethylene-type model: the γ 's refer to out-of-plane bendings involving the $W-W$ bond, and τ represents a twisting of the same bond. The latter coordinate may be specified more rigorously (in analogy with tentatively standardized coordinates for ethylene) as $-\tau = \tau_{5,9,10,7} + \tau_{6,9,10,8}$. Finally, the symbols p and q are used to denote the out-of-plane bendings involving the $X-U$ and $Y-V$ bonds, respectively.

parameters and the valence coordinates is explained by Figure 1. The symmetry coordinates are specified in the following.

$$S_1(A_g) = 1/2(d_1 + d_2 + d_3 + d_4)^*$$

$$S_2(A_g) = 1/2(s_1 + s_2 + s_3 + s_4)^*$$

$$S_3(A_g) = u^*$$

$$S_4(A_g) = 1/2(D_1 D_2)^{1/2}(\alpha_1 + \alpha_2 + \alpha_3 + \alpha_4)^*$$

$$S_5(A_g) = 1/2(D_1 D_3)^{1/2}(\beta_1 + \beta_2 + \beta_3 + \beta_4)^*$$

$$S_6(A_g) = 1/2(\tau_1 + \tau_2 + \tau_3 + \tau_4)$$

$$S_7(A_g) = 1/2(t_1 + t_2 + t_3 + t_4)$$

$$S_8(A_g) = 1/2(R_1 D_2)^{1/2}(\varphi_1 + \varphi_2 + \varphi_3 + \varphi_4)$$

$$S_9(A_g) = 1/2(R_2 D_1)^{1/2}(\epsilon_1 + \epsilon_2 + \epsilon_3 + \epsilon_4)$$

$$S_1(B_{1g}) = 1/2(D_2 D_3)^{1/2}(\delta_1 + \delta_2 - \delta_3 - \delta_4)^*$$

$$S_2(B_{1g}) = 1/2[R_1(D_1 D_2)^{1/2}]^{1/2}(p_1 - p_2 - p_3 + p_4)$$

$$S_3(B_{1g}) = 1/2[R_2(D_1 D_3)^{1/2}]^{1/2}(q_1 - q_2 - q_3 + q_4)$$

$$S_1(B_{2g}) = 1/2(D_2 D_3)^{1/2}(\delta_1 - \delta_2 - \delta_3 + \delta_4)^*$$

$$S_2(B_{2g}) = 1/2[R_1(D_1 D_2)^{1/2}]^{1/2}(-p_1 - p_2 + p_3 + p_4)$$

$$S_3(B_{2g}) = 1/2[R_2(D_1 D_3)^{1/2}]^{1/2}(-q_1 - q_2 + q_3 + q_4)$$

$$S_4(B_{2g}) = 2^{-1/2}(D_2 D_4)^{1/2}(-\gamma_1 + \gamma_2)^*$$

$$S_1(B_{3g}) = 1/2(d_1 - d_2 + d_3 - d_4)^*$$

$$S_2(B_{3g}) = 1/2(s_1 - s_2 + s_3 - s_4)^*$$

$$S_3(B_{3g}) = 1/2(D_1 D_2)^{1/2}(\alpha_1 - \alpha_2 + \alpha_3 - \alpha_4)^*$$

$$S_4(B_{3g}) = 1/2(D_1 D_3)^{1/2}(\beta_1 - \beta_2 + \beta_3 - \beta_4)^*$$

$$S_5(B_{3g}) = 1/2(r_1 - r_2 + r_3 - r_4)$$

$$S_6(B_{3g}) = 1/2(t_1 - t_2 + t_3 - t_4)$$

$$S_7(B_{3g}) = 1/2(R_1 D_2)^{1/2}(\varphi_1 - \varphi_2 + \varphi_3 - \varphi_4)$$

$$S_8(B_{3g}) = 1/2(R_2 D_1)^{1/2}(\epsilon_1 - \epsilon_2 + \epsilon_3 - \epsilon_4)$$

$$S_1(A_u) = 1/2(D_2 D_3)^{1/2}(\delta_1 + \delta_2 + \delta_3 + \delta_4)^*$$

$$S_2(A_u) = D_2 \tau^*$$

- (7) H. Sponer and C. D. Cooper, *J. Chem. Phys.*, **24**, 646 (1955).
- (8) H. Luther, K. Feldmann, and B. Hampel, *Z. Elektrochem.*, **59**, 1008 (1955).
- (9) H. Luther, G. Brandes, H. Günzler, and B. Hampel, *ibid.*, **59**, 1012 (1955).
- (10) J. Brandmüller and E. Schmid, *Z. Physik*, **144**, 428 (1956).
- (11) D. B. Scully and D. H. Whiffen, *J. Mol. Spectry.*, **1**, 257 (1957).
- (12) R. W. Bayer and E. J. O'Reilly, *J. Phys. Chem.*, **62**, 504 (1958).
- (13) W. Bruhn and R. Mecke, *Z. Elektrochem.*, **62**, 441 (1958).
- (14) E. W. Schmid, *ibid.*, **62**, 1005 (1958).
- (15) S. S. Mitra and H. J. Bernstein, *Can. J. Chem.*, **37**, 553 (1959).
- (16) D. P. Craig, J. M. Hollas, M. F. Redies, and S. S. Wait, *Proc. Chem. Soc.*, 361 (1959).
- (17) D. E. Freeman and I. G. Ross, *Spectrochim. Acta*, **16**, 1393 (1960).
- (18) D. B. Scully and D. H. Whiffen, *ibid.*, **16**, 1409 (1960).
- (19) J. M. Hollas, *J. Mol. Spectry.*, **9**, 138 (1962).
- (20) E. P. Krainov, *Opt. Spektrosk.*, **16**, 763 (1964).
- (21) N. Neto, M. Scrocco, and S. Califano, *Spectrochim. Acta*, **22**, 1981 (1966).
- (22) J. E. Katon and E. R. Lippincott, *ibid.*, **15**, 627 (1959).
- (23) G. V. Peregudov, *Opt. Spectry.*, **9**, 155 (1960).
- (24) D. Steele and E. R. Lippincott, *J. Mol. Spectry.*, **6**, 238 (1961).
- (25) D. Steele, T. R. Nanney, and E. R. Lippincott, *Spectrochim. Acta*, **22**, 849 (1966).
- (26) S. J. Cyvin, *Acta Chem. Scand.*, **20**, 2616 (1966).

$$S_3(A_u) = 1/2[R_1(D_1D_2)^{1/2}]^{1/2}(p_1 - p_2 + p_3 - p_4)$$

$$S_4(A_u) = 1/2[R_2(D_1D_3)^{1/2}]^{1/2}(q_1 - q_2 + q_3 - q_4)$$

$$S_1(B_{1u}) = 1/2(d_1 + d_2 - d_3 - d_4)^*$$

$$S_2(B_{1u}) = 1/2(s_1 + s_2 - s_3 - s_4)^*$$

$$S_3(B_{1u}) = 1/2(D_1D_2)^{1/2}(\alpha_1 + \alpha_2 - \alpha_3 - \alpha_4)^*$$

$$S_4(B_{1u}) = 1/2(D_1D_3)^{1/2}(\beta_1 + \beta_2 - \beta_3 - \beta_4)^*$$

$$S_5(B_{1u}) = 1/2(r_1 + r_2 - r_3 - r_4)$$

$$S_6(B_{1u}) = 1/2(t_1 + t_2 - t_3 - t_4)$$

$$S_7(B_{1u}) = 1/2(R_1D_2)^{1/2}(\varphi_1 + \varphi_2 - \varphi_3 - \varphi_4)$$

$$S_8(B_{1u}) = 1/2(R_2D_1)^{1/2}(\epsilon_1 + \epsilon_2 - \epsilon_3 - \epsilon_4)$$

$$S_1(B_{2u}) = 1/2(d_1 - d_2 - d_3 + d_4)^*$$

$$S_2(B_{2u}) = 1/2(s_1 - s_2 - s_3 + s_4)^*$$

$$S_3(B_{2u}) = 1/2(D_1D_2)^{1/2}(\alpha_1 - \alpha_2 - \alpha_3 + \alpha_4)^*$$

$$S_4(B_{2u}) = 1/2(D_1D_3)^{1/2}(\beta_1 - \beta_2 - \beta_3 + \beta_4)^*$$

$$S_5(B_{2u}) = 1/2(r_1 - r_2 - r_3 + r_4)$$

$$S_6(B_{2u}) = 1/2(t_1 - t_2 - t_3 + t_4)$$

$$S_7(B_{2u}) = 1/2(R_1D_2)^{1/2}(\varphi_1 - \varphi_2 - \varphi_3 + \varphi_4)$$

$$S_8(B_{2u}) = 1/2(R_2D_1)^{1/2}(\epsilon_1 - \epsilon_2 - \epsilon_3 - \epsilon_4)$$

$$S_1(B_{3u}) = 1/2(D_2D_3)^{1/2}(-\delta_1 + \delta_2 - \delta_3 + \delta_4)^*$$

$$S_2(B_{3u}) = 1/2[R_1(D_1D_2)^{1/2}]^{1/2}(p_1 + p_2 + p_3 + p_4)$$

$$S_3(B_{3u}) = 1/2[R_2(D_1D_3)^{1/2}]^{1/2}(q_1 + q_2 + q_3 + q_4)$$

$$S_4(B_{3u}) = 2^{-1/2}(D_2D_4)^{1/2}(\gamma_1 + \gamma_2)^*$$

The same expressions are also applicable to the simpler model of the naphthalene skeleton. Then one only has to depict the coordinates which only involve the $(WX_2Y_2)_2$ atoms. They are each marked with an asterisk in the above specification. The coordinate set is complete. It is seen to involve no redundants, if one accepts the middle-bond twisting (τ) as one single coordinate, although it may be expressed as a combination of torsions; cf. the legend of Figure 1. Otherwise all of the valence coordinates belong to the four standard types: stretchings, bendings, torsions, and out-of-plane bendings.

Isotopically Substituted Molecule Models. The symmetry coordinates for naphthalene (see above) are applicable, according to a general rule, to all substituted naphthalenes, including those of lower symmetries. In those cases one must allow the mixing of valence coordinates from different symmetrically equivalent sets, but the approach is practically convenient when treating the isotopically substituted compounds. The substituted naphthalene-type molecules of lower symmetries may belong to the symmetry groups of C_{2h} , C_{2v} , or C_s . One finds correlations between the symmetry species of the appropriate groups as shown in Figures 2

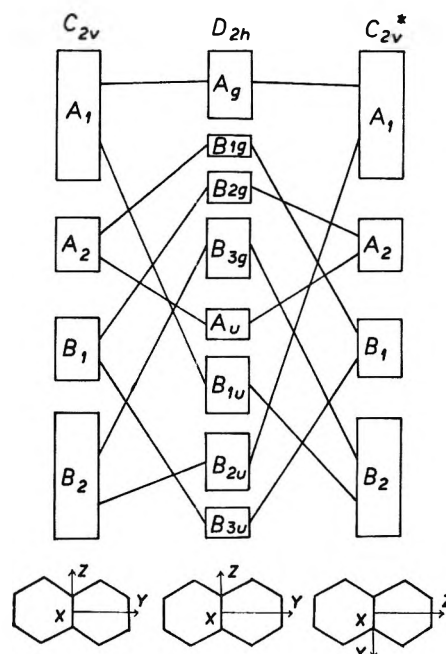


Figure 2. Correlations between the symmetry species of D_{2h} and C_{2v} , pertaining to isotopically substituted naphthalenes.

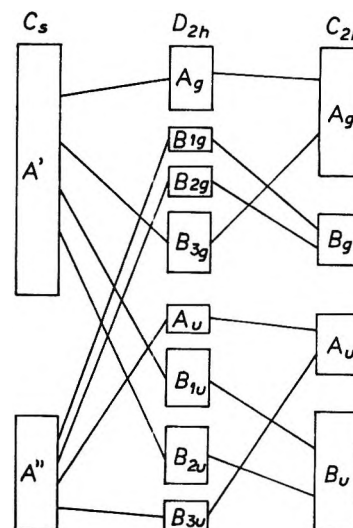


Figure 3. Correlations between the symmetry species of D_{2h} , C_{2h} , and C_s , pertaining to isotopically substituted naphthalenes.

and 3. When evaluating these correlations we have throughout followed the recommendations of Mulliken's report²⁷ as to the species notation. Hence we have to distinguish between two types of C_{2v} models, here designated C_{2v} and C_{2v}^* . In these models the z axis, which conventionally is taken along the twofold symmetry axis, lies along and perpendicular to the middle bond, respectively; cf. the auxiliary drawings in Figure 2. In both models (as in naphthalene itself) the x axis is taken perpendicular to the molecular plane.

(27) R. S. Mulliken, *J. Chem. Phys.*, **23**, 1997 (1955).

This latter convention should also be applied in planar molecules of C_8 symmetry. In the present C_{2h} model, on the other hand, the z axis (taken along the twofold symmetry axis) should be oriented perpendicular to the molecule plane.

Below we give an account on the deuterionaphthalenes and their symmetries.

The most symmetrical tetradeuterionaphthalenes, *viz.*, naphthalene- α - d_4 and naphthalene- β - d_4 , possess the full symmetry (D_{2h}) of naphthalene itself and naphthalene- d_8 .

All the lower symmetries are represented among the ten dideuterio compounds: naphthalene-1,5- d_2 and (*amphi*-)naphthalene-2,6- d_2 belong to C_{2h} , while the 1,8-, 2,7-, 1,4-, and 2,3- d_2 compounds possess the C_{2v}

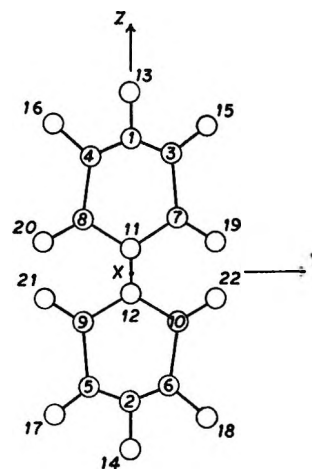


Figure 5. Planar bicyclic model; symmetry D_{2h} , showing the cartesian coordinate axes and numbering of atoms. This model is the special case for $T = 0$ of the $W_2[(XT)_2(YU)_2ZV]_2$ model in Figure 4, which should be consulted for equilibrium parameters and valence coordinates.

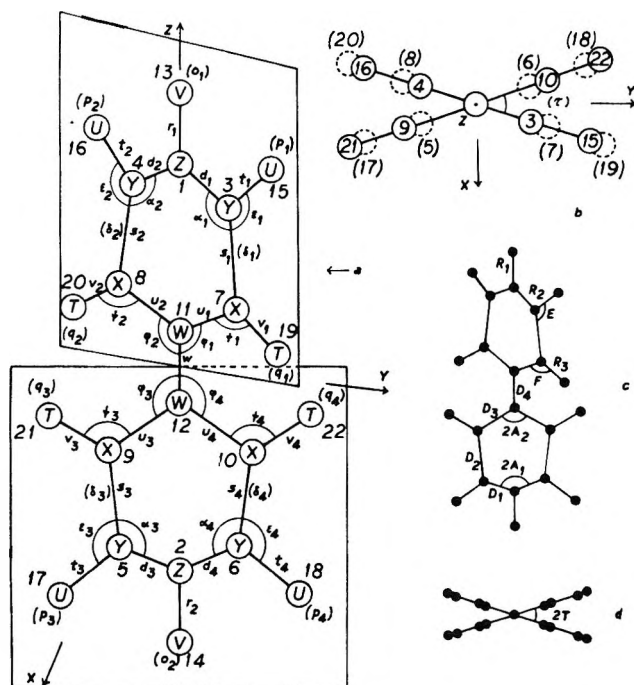


Figure 4. Bicyclic (biphenyl-type) $W_2[(XT)_2(YU)_2ZV]_2$ model; symmetry D_2 . The equilibrium structure of the skeleton ($W_2X_4Y_4Z_2$) of the model is determined by seven parameters, say $D_1 = Y-Z$, $D_2 = X-Y$, $D_3 = W-X$, $D_4 = W-W$, and the YZY ($2A_1$) and XWX ($2A_2$) angles (*cf.* part c); in addition to the angle of rotation ($2T$) between the planes of the two halves of the model (*cf.* part d). To determine the structure of the whole model, one needs five additional parameters, say, $R_1 = Z-V$, $R_2 = Y-U$, $R_3 = X-T$, and the angles $E = XYU$, $F = WXT$; *cf.* part c.

The main figure (a) tends to explain the notation used for valence coordinates. In-plane coordinates not included on the figure, are the two "waggings," $\omega_1 = 1/2(\eta_1 - \eta_2)$, $\omega_2 = 1/2(\eta_3 - \eta_4)$, where η_i represents the YZV angle bendings, and $i = 1, 2, 3$, and 4 refers to the atoms 3-1-13, 4-1-13, 9-2-14, and 10-2-14, respectively. The out-of-plane coordinate symbols are given in parentheses. Some of them are not found on the figure, namely, γ_1 and γ_2 , denoting the out-of-plane bendings involving the middle bond; and the two σ 's defined by $\sigma_1 = 2^{-1/2}(\tau_{4,1,3,7} - \tau_{3,1,4,8})$ and $\sigma_2 = 2^{-1/2}(\tau_{8,2,5,9} - \tau_{6,2,6,10})$. Middle-bond twisting (τ) may be defined as in ethylene (and naphthalene; *cf.* Figure 1).

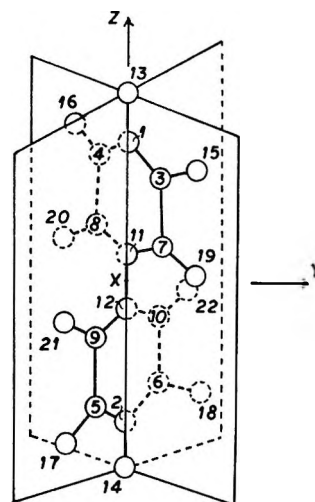


Figure 6. Twisted (right-angled) bicyclic model; symmetry D_{2d} , showing the cartesian coordinate axes and numbering of atoms. This model is the special case for $2T = \pi/2$ of the $W_2[(XT)_2(YU)_2ZV]_2$ model in Figure 4, which should be consulted for equilibrium parameters and valence coordinates.

symmetry. The two former ones of these compounds, *viz.*, (*peri*-)naphthalene-1,8- d_2 and naphthalene-2,7- d_2 should be assigned to C_{2v} , while the two latter ones, the 1,4- and 2,3- d_2 compounds, should be assigned to C_{2v}^* in the present notation. There remain four dideuteriona-

phthalenes, all belonging to C_s . The ten hexadeuterio compounds may be treated as negative images of the corresponding dideuterio compounds.

Among the tetradeuterionaphthalenes of lower symmetries, one has naphthalene-1,2,5,6- d_4 and naphthalene-1,3,5,7- d_4 , both belonging to C_{2h} ; naphthalene-1,2,7,8- d_4 and naphthalene-1,3,6,8- d_4 of C_{2v} ; and naphthalene-1,2,3,4- d_4 and naphthalene-1,4,6,7- d_4 to be assigned to C_{2v}^* . In addition, there exist, if we are not mistaken, 14 tetradeuterionaphthalenes of C_s symmetry.

All 14 trideuterio- (and 14 pentadeuterio-) naphthalenes also belong to C_s . The same is the case with the two monodeuterio compounds, *viz.*, naphthalene- α - d and naphthalene- β - d (and the two heptadeuterio compounds).

Bicyclic Biphenyl-Type Models

Rotation Isomers. Here we are treating three bicyclic $[W(XT)_2(YU)_2ZT]_2$ models, to which the biphenyl molecule tentatively may be assigned: the planar D_{2h} model (Figure 5), the twisted (right-angled) D_{2d} model

(Figure 6), and the intermediate, general case of the symmetric model of D_2 symmetry (Figure 4). The dihedral angle of rotation ($2T$) is defined so that the D_{2h} and D_{2d} models correspond to $T = 0$ and $2T = \pi/2$, respectively. The constructed set of symmetry coordinates (see below) is applicable to all three of the models according to the correlation scheme given in Figure 7.

In this case of biphenyl molecule models it seems more important to consider the rotational isomers than the isotopic substitutions. The latter considerations, which were done for the naphthalene model treated above, are left out here for the sake of brevity.

Symmetry Coordinates. The constructed set of symmetry coordinates is given below, using mainly the notation which pertains to the planar D_{2h} model. Formally, the same expressions are applicable to the symmetry coordinates in the two other models in question, as is indicated in the left-hand column. In the D_{2d} model the degenerate coordinate pairs, say, (S_{1a} , S_{1b}), transform like the rigid translations, (T_x , T_y).

$$\begin{array}{l}
 \left. \begin{array}{l}
 S_1(A_g) - S_{11}(A_1) \\
 \text{in } D_{2d}; \\
 S_1(A) - S_{11}(A) \\
 \text{in } D_2
 \end{array} \right\} \begin{array}{l}
 S_1(A_g) = 1/2(d_1 + d_2 + d_3 + d_4)^* \\
 S_2(A_g) = 1/2(s_1 + s_2 + s_3 + s_4)^* \\
 S_3(A_g) = 1/2(u_1 + u_2 + u_3 + u_4)^* \\
 S_4(A_g) = w^* \\
 S_5(A_g) = 1/2(D_1D_2)^{1/2}(\alpha_1 + \alpha_2 + \alpha_3 + \alpha_4)^* \\
 S_6(A_g) = 1/2(D_3D_4)^{1/2}(\varphi_1 + \varphi_2 + \varphi_3 + \varphi_4)^* \\
 S_7(A_g) = 2^{-1/2}(r_1 + r_2) \\
 S_8(A_g) = 1/2(t_1 + t_2 + t_3 + t_4) \\
 S_9(A_g) = 1/2(v_1 + v_2 + v_3 + v_4) \\
 S_{10}(A_g) = 1/2(R_2D_2)^{1/2}(\epsilon_1 + \epsilon_2 + \epsilon_3 + \epsilon_4) \\
 S_{11}(A_g) = 1/2(R_3D_2)^{1/2}(\psi_1 + \psi_2 + \psi_3 + \psi_4)
 \end{array} \\
 \\
 \left. \begin{array}{l}
 S_1(A_2) - S_5(A_2) \\
 \text{in } D_{2d}; \\
 S_1(B_1) - S_5(B_1) \\
 \text{in } D_2
 \end{array} \right\} \begin{array}{l}
 S_1(B_{1g}) = 1/2(D_1D_3)^{1/2}(\delta_1 + \delta_2 - \delta_3 - \delta_4)^* \\
 S_2(B_{1g}) = 1/2[R_2(D_1D_2)^{1/2}]^{1/2}(p_1 - p_2 - p_3 + p_4) \\
 S_3(B_{1g}) = 1/2[R_3(D_2D_3)^{1/2}]^{1/2}(q_1 - q_2 - q_3 + q_4)
 \end{array} \\
 \\
 \left. \begin{array}{l}
 S_{11b}(E) - S_{16b}(E) \\
 \text{in } D_{2d}; \\
 S_{11}(B_2) - S_{16}(B_2) \\
 \text{in } D_2
 \end{array} \right\} \begin{array}{l}
 S_1(B_{2g}) = 1/2(D_1D_3)^{1/2}(\delta_1 - \delta_2 - \delta_3 + \delta_4)^* \\
 S_2(B_{2g}) = 2^{-1/2}(D_1D_2)^{1/2}(-\sigma_1 + \sigma_2)^* \\
 S_3(B_{2g}) = 2^{-1/2}(D_3D_4)^{1/2}(-\gamma_1 + \gamma_2) \\
 S_4(B_{2g}) = 2^{-1/2}(R_1D_1)^{1/2}(-o_1 + o_2) \\
 S_5(B_{2g}) = 1/2[R_2(D_1D_2)^{1/2}]^{1/2}(-p_1 - p_2 + p_3 + p_4) \\
 S_6(B_{2g}) = 1/2[R_3(D_2D_3)^{1/2}]^{1/2}(-q_1 - q_2 + q_3 + q_4)
 \end{array} \\
 \\
 \left. \begin{array}{l}
 S_{1a}(E) - S_{10a}(E) \\
 \text{in } D_{2d}; \\
 S_1(B_3) - S_{10}(B_3) \\
 \text{in } D_2
 \end{array} \right\} \begin{array}{l}
 S_1(B_{3g}) = 1/2(d_1 - d_2 + d_3 - d_4)^* \\
 S_2(B_{3g}) = 1/2(s_1 - s_2 + s_3 - s_4)^* \\
 S_3(B_{3g}) = 1/2(u_1 - u_2 + u_3 - u_4)^* \\
 S_4(B_{3g}) = 1/2(D_1D_2)^{1/2}(\alpha_1 - \alpha_2 + \alpha_3 - \alpha_4)^* \\
 S_5(B_{3g}) = 1/2(D_3D_4)^{1/2}(\varphi_1 - \varphi_2 + \varphi_3 - \varphi_4)^* \\
 S_6(B_{3g}) = 1/2(t_1 - t_2 + t_3 - t_4) \\
 S_7(B_{3g}) = 1/2(v_1 - v_2 + v_3 - v_4) \\
 S_8(B_{3g}) = 2^{-1/2}(R_1D_1)^{1/2}(\omega_1 + \omega_2) \\
 S_9(B_{3g}) = 1/2(R_2D_2)^{1/2}(\epsilon_1 - \epsilon_2 + \epsilon_3 - \epsilon_4) \\
 S_{10}(B_{3g}) = 1/2R_3D_2)^{1/2}(\psi_1 - \psi_2 + \psi_3 - \psi_4)
 \end{array}
 \end{array}$$

$$\begin{array}{l}
 S_1(B_1) - S_4(B_1) \\
 \text{in } D_{2d}; \\
 S_{12}(A) - S_{15}(A) \\
 \text{in } D_2
 \end{array}
 \left\{
 \begin{array}{l}
 S_1(A_u) = 1/2(D_1D_3)^{1/2}(\delta_1 + \delta_2 + \delta_3 + \delta_4)^* \\
 S_2(A_u) = D_3\tau^* \\
 S_3(A_u) = 1/2[R_2(D_1D_2)^{1/2}]^{1/2}(p_1 - p_2 + p_3 - p_4) \\
 S_4(A_u) = 1/2[R_3(D_2D_3)^{1/2}]^{1/2}(q_1 - q_2 + q_3 - q_4)
 \end{array}
 \right.$$

$$\begin{array}{l}
 S_1(B_2) - S_{10}(B_2) \\
 \text{in } D_{2d}; \\
 S_6(B_1) - S_{14}(B_1) \\
 \text{in } D_2
 \end{array}
 \left\{
 \begin{array}{l}
 S_1(B_{1u}) = 1/2(d_1 + d_2 - d_3 - d_4)^* \\
 S_2(B_{1u}) = 1/2(s_1 + s_2 - s_3 - s_4)^* \\
 S_3(B_{1u}) = 1/2(u_1 + u_2 - u_3 - u_4)^* \\
 S_4(B_{1u}) = 1/2(D_1D_2)^{1/2}(\alpha_1 + \alpha_2 - \alpha_3 - \alpha_4)^* \\
 S_5(B_{1u}) = 1/2(D_3D_4)^{1/2}(\varphi_1 + \varphi_2 - \varphi_3 - \varphi_4)^* \\
 S_6(B_{1u}) = 2^{-1/2}(r_1 - r_2) \\
 S_7(B_{1u}) = 1/2(t_1 + t_2 - t_3 - t_4) \\
 S_8(B_{1u}) = 1/2(v_1 + v_2 - v_3 - v_4) \\
 S_9(B_{1u}) = 1/2(R_2D_2)^{1/2}(\epsilon_1 + \epsilon_2 - \epsilon_3 - \epsilon_4) \\
 S_{10}(B_{1u}) = 1/2(R_3D_2)^{1/2}(\psi_1 + \psi_2 - \psi_3 - \psi_4)
 \end{array}
 \right.$$

$$\begin{array}{l}
 S_{11a}(E) - S_{10b}(E) \\
 \text{in } D_{2d}; \\
 S_1(B_2) - S_{10}(B_2) \\
 \text{in } D_2
 \end{array}
 \left\{
 \begin{array}{l}
 S_1(B_{2u}) = 1/2(d_1 - d_2 - d_3 + d_4)^* \\
 S_2(B_{2u}) = 1/2(s_1 - s_2 - s_3 + s_4)^* \\
 S_3(B_{2u}) = 1/2(u_1 - u_2 - u_3 + u_4)^* \\
 S_4(B_{2u}) = 1/2(D_1D_2)^{1/2}(\alpha_1 - \alpha_2 - \alpha_3 + \alpha_4)^* \\
 S_5(B_{2u}) = 1/2(D_3D_4)^{1/2}(\varphi_1 - \varphi_2 - \varphi_3 + \varphi_4)^* \\
 S_6(B_{2u}) = 1/2(t_1 - t_2 - t_3 + t_4) \\
 S_7(B_{2u}) = 1/2(v_1 - v_2 - v_3 + v_4) \\
 S_8(B_{2u}) = 2^{-1/2}(R_1D_1)^{1/2}(\omega_1 - \omega_2) \\
 S_9(B_{2u}) = 1/2(R_2D_2)^{1/2}(\epsilon_1 - \epsilon_2 - \epsilon_3 + \epsilon_4) \\
 S_{10}(B_{2u}) = 1/2(R_3D_2)^{1/2}(\psi_1 - \psi_2 - \psi_3 + \psi_4)
 \end{array}
 \right.$$

$$\begin{array}{l}
 S_{11a}(E) - S_{16a}(E) \\
 \text{in } D_{2d}; \\
 S_{11}(B_3) - S_{16}(B_3) \\
 \text{in } D_2
 \end{array}
 \left\{
 \begin{array}{l}
 S_1(B_{3u}) = 1/2(D_1D_3)^{1/2}(-\delta_1 + \delta_2 - \delta_3 + \delta_4)^* \\
 S_2(B_{3u}) = 2^{-1/2}(D_1D_2)^{1/2}(\sigma_1 + \sigma_2)^* \\
 S_3(B_{3u}) = 2^{-1/2}(D_3D_4)^{1/2}(\gamma_1 + \gamma_2)^* \\
 S_4(B_{3u}) = 2^{-1/2}(R_1D_1)^{1/2}(o_1 + o_2) \\
 S_5(B_{3u}) = 1/2[R_2(D_1D_2)^{1/2}]^{1/2}(p_1 + p_2 + p_3 + p_4) \\
 S_6(B_{3u}) = 1/2[R_3(D_2D_3)^{1/2}]^{1/2}(q_1 + q_2 + q_3 + q_4)
 \end{array}
 \right.$$

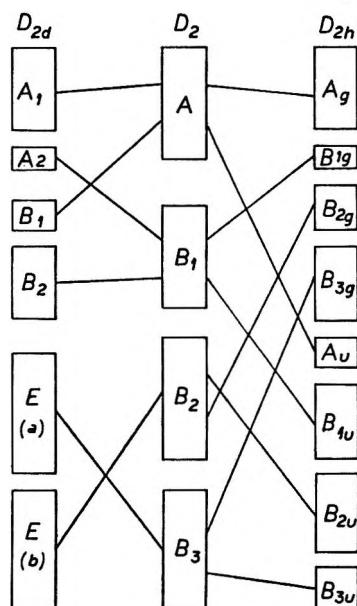


Figure 7. Correlations between the symmetry species of D_{2h} , D_{2d} , and D_2 , pertaining to rotational isomers of biphenyl.

Again, the same expressions are also applicable to the skeleton models, *viz.*, $(WX_2Y_2Z)_2$. The coordinates to

be used in those cases are each marked with an asterisk.

Numerous redundants were avoided by leaving out whole sets of symmetrically equivalent valence coordinates. Here we want to emphasize that one cannot drop out such coordinate sets arbitrarily without possible loss of completeness. For instance, among the α 's, φ 's, and WXY angle bendings we found that the last set could be left out without damage, but it could be substituted for one of the others without introducing redundants. We also want to point out some formal objections against our statement about complete absence of redundants. In order to accept this statement to be true, we must allow a twisting about the middle bond (as in naphthalene) to be considered as one single valence coordinate. Moreover, we must accept the two symmetrically equivalent ω coordinates as valence coordinates. This type of coordinate is sometimes referred to as "wagging" and is known from benzene and many other molecules. Finally, we have (apart from the four conventional types) a set of two σ coordinates. They are some sorts of out-of-plane distortions and are derived as combinations of four torsional coordinates; *cf.* the legend of Figure 4.

γ -Radiation-Induced *cis-trans* Isomerization of Stilbenes in Liquid Naphthalene

by O. G. Malan, H. Güsten, and D. Schulte-Frohlinde

Institut für Strahlenschervie, Kernforschungszentrum Karlsruhe, Karlsruhe, West Germany

Accepted and Transmitted by The Faraday Society (Received June 5, 1967)

The Co^{60} γ -radiation-induced *cis-trans* isomerization of 4-nitro-4'-methoxystilbene in molten naphthalene as solvent has been measured and the dependence on dose, concentration, and additives has been studied. The $G(\text{trans} \rightarrow \text{cis})$ is lowered by naphthacene and 4,4'-dimethoxystilbene and enhanced by pyrene as additives. The results could be explained using kinetic equations derived from a proposed reaction scheme involving excitation transfer. Naphthalene is much more efficient in energy transfer than benzene.

Introduction

Several papers have recently been published on the solvent-sensitized radiolytic *cis-trans* isomerization of olefins and stilbenes.¹⁻⁷ Most of this work has been done using benzene as solvent. In this paper we extend the measurements of Fischer, *et al.*,⁵ using liquid naphthalene as solvent. We show that liquid naphthalene is more efficient in energy transfer than benzene. Furthermore we are able to describe the effect of dose, concentration, and the influence of additives on the radiolytic *cis-trans* isomerization with kinetic equations derived from a proposed reaction scheme.

Experimental Section

A. Materials. Naphthalene (Hopkin and Williams Ltd., microanalytical standard) was either zone-refined by passing *ca.* 30 zones or used without further purification. *trans*- and *cis*-4-nitro-4'-methoxystilbene were prepared as described before⁸ and the former was zone-refined, mp 132–133°. Pyrene and naphthacene were obtained from Ges. f. Teerverwertung, Duisburg-Meiderich, West Germany. The former was zone-refined and the latter resublimed in the dark. 4,4'-Dimethoxystilbene (Aldrich) was recrystallized from methanol, mp 210–212°.

B. Procedure. Dilute mixtures (0.1–1.0%) of the substances were made in naphthalene by quenching melts in sealed containers. 1-, 2-, or 10-mm cells were filled with powdered mixtures, cooled in liquid nitrogen, evacuated to below 10^{-4} mm, and sealed off.

Irradiation took place in a "Gammacell 220" Co^{60} γ source (dose rate *ca.* 1.5×10^{17} eV mol⁻¹ min⁻¹) in a specially constructed container thermostated at $90 \pm 1^\circ$.

Spectrophotometry was carried out with the cells at 90° . The extinction at 380 m μ was corrected for absorption losses at cell windows by subtraction of the (usually negligible) absorbance at 500 m μ . At both wavelengths a cell with pure molten naphthalene served

as reference. The extinction coefficients of the *trans* and *cis* forms were, respectively, 2.26×10^4 and 7.2×10^3 at 380 m μ .

The triplet energy level of *trans*-4-nitro-4'-methoxystilbene was determined by the oxygen perturbation method⁹ at an oxygen pressure of 180 atm.

C. Dosimetry. Fricke dosimetry [$G(\text{Fe}^{3+}) = 15.5$; $\epsilon(\text{Fe}^{3+}, 304 \text{ m}\mu, 23.7^\circ) = 2174$] was carried out in the heated container and the dose rate for naphthalene was corrected for its electron density.

Results

In $(0.5\text{--}15) \times 10^{-5}$ M *trans*-4-nitro-4'-methoxystilbene in molten naphthalene at 90° the absorbance change at 380 m μ was found to be first order with respect to dose to over 95% conversion (Figure 1).

The radiostationary composition was 60% *cis*:40% *trans* at all concentrations. The results are represented graphically in Figure 2, where $D_{1/2}$, the dose which causes half the maximum absorbance change, is plotted against concentration. The upper and lower curves represent, respectively, results obtained with zone-refined and unrefined naphthalene.

Figure 3 describes the change of isomerization with concentration of 4-nitro-4'-methoxystilbene for (0.5–

(1) R. B. Cundall and P. A. Griffiths, *Trans. Faraday Soc.*, **61**, 1968 (1965).

(2) M. A. Golub and C. L. Stephens, *J. Phys. Chem.*, **70**, 3576 (1966).

(3) R. Hentz, D. B. Peterson, S. B. Srivastava, H. F. Barzynski, and M. Burton, *ibid.*, **70**, 2362 (1966).

(4) H. P. Lehmann, G. Stein, and E. Fischer, *Chem. Commun.*, 583 (1965).

(5) E. Fischer, H. P. Lehmann, and G. Stein, *J. Chem. Phys.*, **45**, 3905 (1966).

(6) D. Schulte-Frohlinde and H. Güsten, *Z. Physik. Chem. (Frankfurt)*, **29**, 281 (1961).

(7) H. Güsten, Report No. KFK-244, AEC Accession No. 13402, Gesellschaft für Kernforschung, Karlsruhe, West Germany, 1964.

(8) D. Schulte-Frohlinde, H. Blume, and H. Güsten, *J. Phys. Chem.*, **66**, 2486 (1962).

(9) D. F. Evans, *J. Chem. Soc.*, 1351 (1957).

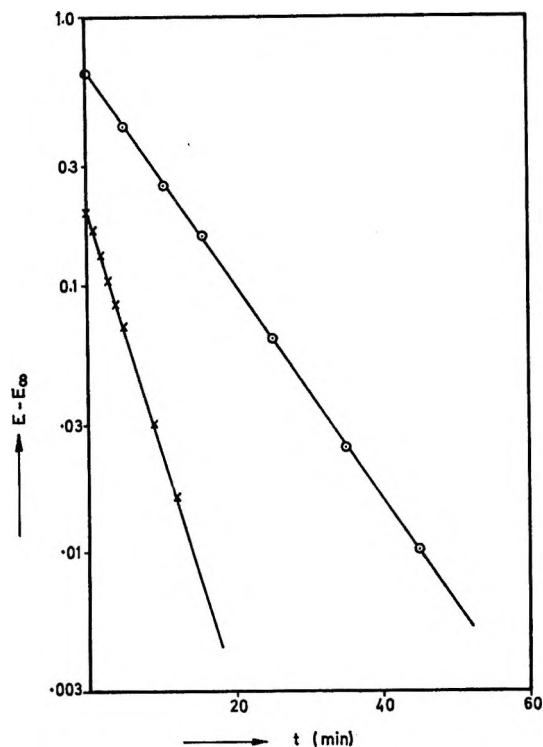


Figure 1. Dose dependence of the radiation-induced *trans* \rightarrow *cis* isomerization of 4-nitro-4'-methoxystilbene in molten naphthalene at 90°: \times , $c = 1.95 \times 10^{-5} M$; \circ , $c = 7.6 \times 10^{-5} M$.

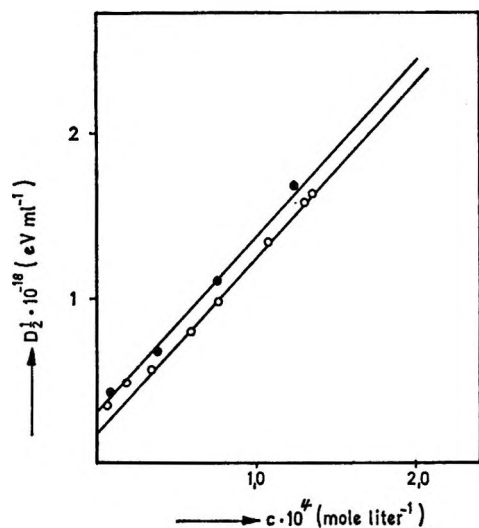


Figure 2. Radiation-induced *trans* \rightarrow *cis* isomerization of 4-nitro-4'-methoxystilbene in molten naphthalene in absence of air at 90°. Ordinate: $D_{1/2}$. Abscissa: concentration of *trans*-4-nitro-4'-methoxystilbene; upper curve, naphthalene (zone refined); lower curve, naphthalene (Hopkin and Williams Ltd).

$15) \times 10^{-5} M$. Figure 3 indicates that $G(\text{trans} \rightarrow \text{cis})$ reaches a limiting value.

The effect of the additives pyrene, naphthacene, and 4,4'-dimethoxystilbene in the concentration range of $(0-4) \times 10^{-5} M$ on the absorbance change during

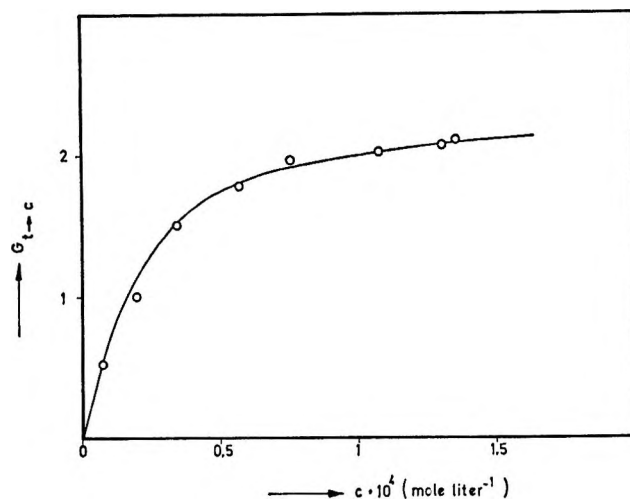


Figure 3. Change of $G(\text{trans} \rightarrow \text{cis})$ with concentration of *trans*-4-nitro-4'-methoxystilbene in zone-refined molten naphthalene in absence of air at 90°.

irradiation of $8 \times 10^{-5} M$ *trans*-4-nitro-4'-methoxystilbene in unrefined naphthalene was also studied. A similar first-order change with dose was found. The results are represented graphically in Figure 4.

In Figure 5 the stationary value of the absorbance is presented as a function of additive concentration.

In the case of pyrene the change in the stationary value of the absorbance corresponds to change in *cis*:*trans* ratio of 60:40 without additive to a limiting *cis*:*trans* ratio of 72:28 in the radiostationary state.

Discussion

The stilbene and the additives are present at very low concentrations. This excludes direct excitation of the stilbene. Catalytic *cis* \rightarrow *trans* isomerization caused by free radicals or other transients existing during irradiation can be excluded. Catalysis shifts the *cis*:*trans* ratio to thermal equilibrium which is completely in favor of the *trans* form in the case of 4-nitro-4'-methoxystilbene. However, the observed radiolytic stationary state in liquid naphthalene is found at 60% *cis* form. This indicates that the *cis*-*trans* isomerization is caused by energy transfer from the solvent to the solute. The energy transfer may include ionic processes and singlet-singlet or triplet-triplet energy transfer. Ionic processes have been observed in benzene solution at higher stilbene concentrations ($>10^{-2} M$).³ At concentrations lower than $10^{-2} M$ the addition of electron scavengers, e.g., N_2O , have no effect on the rate of isomerization.^{1,5} At lower stilbene concentrations than $10^{-2} M$ as used in this work, ionic processes are not very probable.

A contribution by singlet-singlet energy transfer cannot definitely be excluded. However, the experimental results in this work can be described by kinetic equations assuming only one excited species. Since the lifetime of this species is in the range of micro-

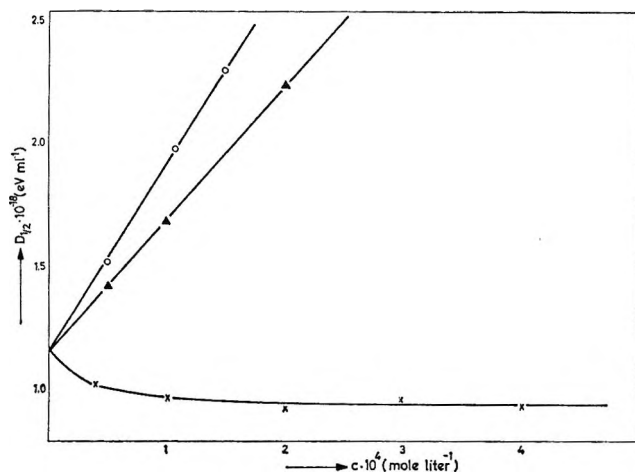


Figure 4. Effect of additives on the radiation-induced *trans* → *cis* isomerization of $8 \times 10^{-6} M$ *trans*-4-nitro-4'-methoxystilbene in molten naphthalene in absence of air at 90°: O, naphthacene; ▲, 4,4'-dimethoxystilbene; ×, pyrene.

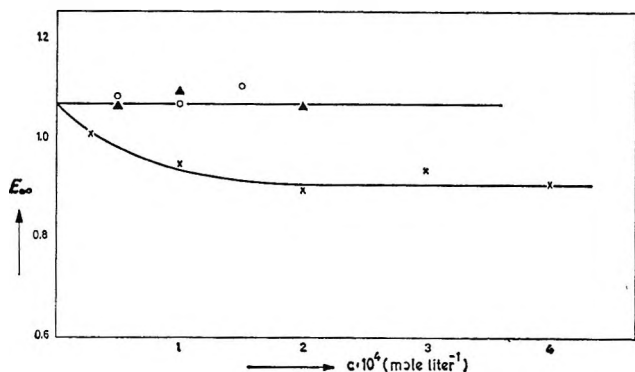
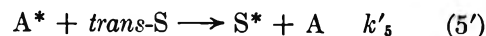
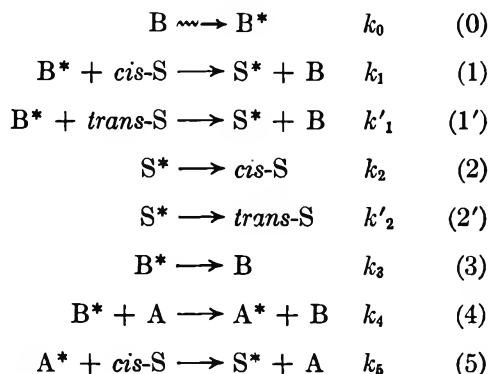


Figure 5. Effect of additives on the radiostationary extinction of $8 \times 10^{-6} M$ *trans*-4-nitro-4'-methoxystilbene in molten naphthalene in absence of air at 90°: O, naphthacene; ▲, 4,4'-dimethoxystilbene; ×, pyrene.

seconds, we assume that this species is the triplet state of naphthalene rather than the singlet state. We therefore discuss our results in terms of triplet-triplet energy transfer.

The proposed reaction scheme involves the following equations where B represents solvent, S the stilbene, A the additive, and the asterisk the lowest triplet state.



An extension of this scheme referring to the eq 2 and 2' is discussed in the following section.

Isomerization without Additives. (a) *Kinetic Equations.* In a system containing solvent and stilbene only, reactions 0-3 are applicable. Since

$$k_0 = G_T \frac{dD}{dt}$$

where G_T is the G value for triplet formation in the solvent and dD/dt the dose rate, the application of steady-state conditions gives

$$\begin{aligned}
 &\frac{k_1 k'_1 S (k_2 + k'_2) + k_3 (k_2 k'_2 + k'_1 k_2)}{(k_1 k'_2 + k'_1 k_2)^2} \times \\
 &\ln \frac{(x - k_1 k'_2 S) / (k_1 k'_2 + k'_1 k_2)}{(S - k_1 k'_2 S) / (k_1 k'_2 + k'_1 k_2)} + \\
 &\frac{(k'_1 - k_1)(x - S)}{k_1 k'_2 + k'_1 k_2} = - \frac{G_T D}{k_2 + k'_2} \quad (7)
 \end{aligned}$$

where x represents the *trans*-stilbene concentrations, S the total (*trans* + *cis*) stilbene concentration, and D the radiation dose. The radiostationary *trans*:*cis* ratio, r , is given by

$$r = \frac{k_1 k'_2}{k'_1 k_2}$$

Since it was found experimentally that the change in absorbance A is first order with dose within experimental error (see Figure 1), it was concluded that the second term in eq 7 is negligible and hence $k_1 \approx k'_1$.

Equation 7 may then be simplified to

$$\ln \frac{x - \frac{rS}{r+1}}{S - \frac{rS}{r+1}} = - \frac{G_T D k_1}{k_1 S + k_3}$$

and this may be written as

$$\ln \frac{(A - A_{\infty})}{(A_0 - A_{\infty})} = - \frac{G_T D k_1}{k_1 S + k_3}$$

where A_0 , A , and A_{∞} are, respectively, the initial absorbance, the absorbance at dose D , and the absorbance in the radiostationary state. This equation expresses the experimentally found first-order change of absorbance with dose, Figure 1.

$D_{1/2}$ is given by

$$D_{1/2} = \frac{0.693}{G_T} (S + (k_3/k_1)) \quad (8)$$

The proposed reaction scheme is only valid when k_2'/k_2 has the same value for both the excited *cis* and the *trans* forms. Only under these conditions will the G value

measured from the slope of $D_{1/2}$ vs. S give the true G value for the triplet states produced in the solvent. Equation 8 is analogous to the expression of G^{-1} in terms of (concentration) $^{-1}$ derived by Cundall and Griffiths¹ except for the fact that it has the advantage of being independent of the radiostationary *trans*:*cis* ratio, r . It may be shown that the initial G values for isomerization are given by

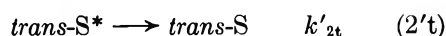
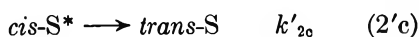
$$G_{c \rightarrow t} = \frac{0.693S}{D_{1/2}} \frac{r}{r+1} \quad (9)$$

$$G_{t \rightarrow c} = \frac{0.693S}{D_{1/2}} \frac{1}{r+1} \quad (10)$$

where $G_{t \rightarrow c}$ and $G_{c \rightarrow t}$ are, respectively, the G values for the *trans* \rightarrow *cis* and *cis* \rightarrow *trans* isomerizations, and thus

$$\frac{G_{c \rightarrow t}}{G_{t \rightarrow c}} = r \quad (11)$$

If k'_2/k_2 is not identical for the excited *cis* and *trans* forms, reactions 2 and 2' must be replaced by



and the equation corresponding to (8) may be derived, based on the same arguments as above.

$$D_{1/2} = \frac{0.693}{G_T \left(\frac{k'_{2c}}{k_{2c} + k'_{2c}} + \frac{k_{2t}}{k_{2t} + k'_{2t}} \right)} ((S + (k_3/k_1)) \quad (12)$$

The experimental G value, G' , measured from the slope of $D_{1/2}$ against concentration is given by

$$G' = G_T \left(\frac{k'_{2c}}{k_{2c} + k'_{2c}} + \frac{k_{2t}}{k_{2t} + k'_{2t}} \right)$$

Equations 9 and 10 may then be written as

$$G_{c \rightarrow t} = G_T \left(\frac{k_1 S}{k_1 S + k_3 k_{2c}} \frac{k'_{2c}}{k_{2c} + k'_{2c}} \right)$$

$$G_{t \rightarrow c} = G_T \left(\frac{k_1 S}{k_1 S + k_3 k_{2t}} \frac{k_{2t}}{k_{2t} + k'_{2t}} \right)$$

$$\frac{G_{c \rightarrow t}}{G_{t \rightarrow c}} = \frac{k'_{2c}(k_{2t} + k'_{2t})}{k_{2t}(k_{2c} + k'_{2c})} = r \quad (13)$$

Thus it is clear that the identity of eq 11 and 13 does not exclude the possibility of a barrier to free rotation in the triplet state. The sum of the limiting G values at high stilbene concentration is given by

$$G(\text{isom}) = G_{c \rightarrow t} + G_{t \rightarrow c} = \left(\frac{k'_{2c}}{k_{2c} + k'_{2c}} + \frac{k_{2t}}{k_{2t} + k'_{2t}} \right) G_T \quad (14)$$

From eq 14 it follows that $G(\text{isom}) = G'$ will only give the true triplet G value in the special case when

$$\frac{k'_{2c}}{k_{2c}} = \frac{k'_{2t}}{k_{2t}}$$

(b) *Comparison with Experiment.* Our experimental data in Figure 2 can be represented by the expressions

$$D_{1/2} = 1.05 \times 10^{22}(S + (3.05 \times 10^5)) \text{ eV ml}^{-1} \quad (12a)$$

$$D_{1/2} = 1.05 \times 10^{22}(S + (1.85 \times 10^5)) \text{ eV ml}^{-1} \quad (12b)$$

respectively, for unrefined and zone-refined naphthalene. Because the values of k_{2c}'/k_{2c} and k_{2t}'/k_{2t} are not known for our system, the value of G_T cannot be obtained. By comparison of eq 12a and 12b with eq 12, the following values are obtained.

$$G' = 4.0 \text{ molecules/100 eV}$$

$$k_3/k_1 = 3.05 \times 10^{-5} M \quad (\text{from (12a)})$$

$$k_3/k_1 = 1.85 \times 10^{-5} M \quad (\text{from (12b)})$$

As expected, a lower value is obtained with zone-refined naphthalene. A comparison of the values of k_3/k_1 with the corresponding value obtained in benzene solution at 20° ($k_3/k_1 \sim 10^{-2} M$)¹⁻³ shows that in naphthalene as solvent a much lower concentration of stilbene is necessary to scavenge all of the radiogenic triplets (see also Figure 3).

Influence of Additives. In systems containing an additive as well as solvent and stilbene, reactions 4-6 must also be taken into consideration. Since also in these systems a first-order variation of extinction with dose was found experimentally, the assumption $k_1 \approx k_1'$ is also valid here and the analogous assumption $k_5 \approx k_5'$ may also be made, although experimental evidence is available to indicate that the second assumption may not always be justified (see remarks about shift in radiostationary *cis*:*trans* ratio). Applying the same reasoning as above, the expression corresponding to (8) is

$$D_{1/2} = \frac{0.693 S + (k_3/k_1) + (Ak_4/k_1)}{G' \left(1 + \frac{Ak_4/k_1}{S + (k_6/k_5)} \right)} \quad (15)$$

where A is the additive concentration. Depending on the properties of the additives, three special cases may be distinguished.

(a) $k_5 = 0$: *No Energy Transfer from the Additives to the Stilbene.* In this case eq 15 simplifies to

$$D_{1/2} = \frac{0.693}{G'} (S + (k_3/k_1) + (Ak_4/k_1)) \quad (16)$$

A prerequisite for triplet-triplet energy transfer is that the triplet energy level of the donor should not be appreciably below that of the acceptor. This condition is not fulfilled in the case of energy transfer from

naphthalene, $E_T = 29$ kcal mole⁻¹,¹⁰ to *trans*- or *cis*-4-nitro-4'-methoxystilbene, $E_T = 46.5$ kcal mole⁻¹ (exptl) and ~ 53 kcal mole⁻¹ (estimated).

Consequently the triplet energy which is transferred from naphthalene to naphthalene cannot be transferred to 4-nitro-4'-methoxystilbene and is lost for isomerization.

The linear relationship found between $D_{1/2}$ for a constant 4-nitro-4'-methoxystilbene concentration and increasing naphthalene concentration (see Figure 4) is in accord with eq 16 as expected. From the slope of this curve a value of $k_4/k_1 = 0.71$ is found for naphthalene as additive. From Figure 5 it is clear that the radiostationary *cis:trans* ratio is not affected as expected.

(b) k_5 Very Large; the Triplet Lifetime of the Additive Is Short. In this case eq 15 will also simplify to eq 16. Hammond¹¹ has found that the stilbene triplet in benzene solution has a decay rate constant of at least 1.3×10^7 sec⁻¹. If it is assumed that the triplet decay constant of 4,4'-dimethoxystilbene has approximately the same value, it follows that triplet energy cannot be transferred from this additive to 4-nitro-4'-methoxystilbene because the triplet decays before it can be transferred. From the expected linear relationship between $D_{1/2}$ for a constant 4-nitro-4'-methoxystilbene concentration and increasing 4,4'-dimethoxystilbene concentration (see Figure 4) a value of $k_4/k_1 = 0.50$ is found for 4,4'-dimethoxystilbene as additive. The radiostationary ratio is not affected in agreement with experiment (see Figure 5).

(c) $k_5 \neq 0$, $k_6 < k_3$: Energy Transfer Takes Place from the Additive Which Has a Longer Triplet Lifetime Than the Solvent. Our experimental data for the three-component system naphthalene, *trans*-4-nitro-4'-methoxystilbene (8×10^{-5} M), and pyrene in Figure 4 may be expressed as

$$D_{1/2} = 1.05 \times 10^{22} \frac{1.1 \times 10^{-4} + 2.9A}{1.0 + 3.3 \times 10^4 A} \text{ eV ml}^{-1} \quad (15a)$$

which gives an experimentally determined relation between $D_{1/2}$ at constant 4-nitro-4'-methoxystilbene concentration and additive concentration, which is a special case of eq 15 with

$$\begin{aligned} k_4/k_1 &= 2.9 \\ k_6/k_5 &= 8 \times 10^{-6} \end{aligned}$$

In this case, as can be seen from Figure 5, increasing pyrene concentration shifts the stationary value of the absorbance until a limiting value corresponding to a *cis:trans* radiostationary ratio of 72% *cis*:28% *trans* is reached, compared to a *cis:trans* ratio of 60:40 without additive. Variations in the photostationary *cis:trans* ratio in the photosensitized isomerization of stilbene and 1,2-diphenylpropene with various sensitizers have been reported by Herkstroeter and Hammond.¹² This was explained as being due to different rates of energy transfer from the sensitizer to the *cis* and *trans* forms, caused by differences in the triplet energy level of the two forms. In our case this would mean that $k_5 \neq k_5'$, because triplet energy transfer from pyrene ($E_T = 48$ kcal mole⁻¹)⁹ to the lower lying triplet of *trans*-4-nitro-4'-methoxystilbene ($E_T = 46.5$ kcal mole⁻¹) is faster than from pyrene to the triplet of *cis*-4-nitro-4'-methoxystilbene ($E_T \approx 53$ kcal mole⁻¹) which lies higher than that of pyrene. The difference between k_5 and k_5' nevertheless does not seem large enough to cause a measurable deviation in the observed first-order dependence of the absorbance change with radiation dose.

The result that $k_5/k_6 > k_1/k_3$ implies that the addition of pyrene enhances the isomerization of stilbene because the probability of triplet energy transfer to 4-nitro-4'-methoxystilbene is increased. Assuming $k_1 \approx k_6$ since both should be diffusion controlled, the observed effect is mainly due to the increased lifetime of the triplet state of pyrene relative to that of naphthalene. If $k_1 \cong k_5 \cong 10^{10}$ mole⁻¹ sec⁻¹, the triplet lifetime for naphthalene in naphthalene at 90° is 5.4×10^{-6} sec and for pyrene in naphthalene is 1.3×10^{-5} sec.

The agreement between the experimental results and the theoretical equations in three different special cases supports the proposed reaction scheme.

Acknowledgment. O. G. M. wishes to thank the Alexander von Humboldt Stiftung, Bad Godesberg, West Germany, for a stipend during the tenure of which this investigation was undertaken.

(10) S. P. McGlynn, M. R. Padhye, and M. Kasha, *J. Chem. Phys.*, **23**, 593 (1955).

(11) G. S. Hammond, J. Saltiel, A. A. Lamola, N. J. Turro, J. S. Bradshaw, D. O. Cowan, R. C. Counsell, V. Vogt, and C. Dalton, *J. Amer. Chem. Soc.*, **86**, 3197 (1964).

(12) W. G. Herkstroeter and G. S. Hammond, *ibid.*, **88**, 4769 (1966).

Relationships between the Two Types of Frequency-Temperature

Representation of Dielectric Relaxation Data

by M. E. Baird

Department of Applied Physics, Institute of Science and Technology, University of Wales, Cardiff, Wales

Accepted and Transmitted by The Faraday Society (June 5, 1967)

Relationships are derived between the plots of \log (frequency of maximum dielectric loss) at a given temperature $T^\circ\text{K}$ against $1/T$ and of \log (frequency) against the reciprocal of absolute temperature (T_m) of maximum loss for materials conforming to a Fuoss-Kirkwood distribution of relaxation times. The theory is applied to experimental data for polyoxymethylene where the width of the distribution of relaxation times changed comparatively rapidly as the temperature was varied and a considerable discrepancy between the loci occurred. Good agreement between calculated and observed differences in the loci was obtained. The activation energy should be obtained from the slope of the plot of \log (frequency of maximum loss) against $1/T$ since the slope of the other plot may be considerably in error.

When a material conforms with the Arrhenius relation $\tau = K_1 \exp(Q/RT)$, where K_1 is a constant, R is the gas constant per mole, T is the temperature on the absolute Kelvin scale, and τ is the most probable relaxation time, the activation energy Q is usually obtained from the slope of the curve of \log (frequency of maximum dielectric loss), $\log f_m$, at a given temperature T , against $1/T$. However, measurements are often made as a function of temperature at constant frequency, f , and it is of interest to derive relationships between the loci of $\log f_m$ against $1/T$ and $\log f$ against $1/T_m$, where T_m is the temperature of maximum loss at a given frequency. Many materials conform approximately to a Cole-Cole¹ or Fuoss-Kirkwood² distribution of relaxation times. These distributions are reasonably similar³ and so relationships derived for a Fuoss-Kirkwood distribution should hold for a wide variety of materials. Relationships are derived in this paper, and although an understanding of their physical significance is limited by the empirical nature of the Fuoss-Kirkwood distribution, the results of the analysis are considered to have some use and show that considerable discrepancies may occur between the loci.

Theory

For a Fuoss-Kirkwood² distribution, the loss factor ϵ'' (imaginary part of complex dielectric constant) is given by

$$\epsilon''(\omega\tau) = \frac{\beta(\epsilon_0 - \epsilon_\infty)(\omega\tau)^\beta}{1 + (\omega\tau)^{2\beta}} \quad (1)$$

where ω is the angular frequency, $\epsilon_0 - \epsilon_\infty$ is the dielectric constant increment, and β is the parameter determining the width of the distribution ($0 < \beta \leq 1$ and as β increases the distribution becomes narrower). When ω is varied at constant temperature, the maximum

value of ϵ'' occurs at an angular frequency ω_m ⁴ given by $\omega_m\tau$ equal to unity. When the temperature is varied at constant ω , the maximum value of ϵ'' would occur for a relaxation time τ_m given by $\omega\tau_m$ equal to unity if $\epsilon_0 - \epsilon_\infty$ and β were independent of temperature. In either case the maximum value of ϵ'' is given by $\epsilon''_m = \beta(\epsilon_0 - \epsilon_\infty)/2$. However, both $\epsilon_0 - \epsilon_\infty$ and β may vary with temperature. For dipolar relaxation, $\epsilon_0 - \epsilon_\infty$ will show anomalous behavior near a transition, but otherwise for a liquid or disordered solid⁵ $\epsilon_0 - \epsilon_\infty$ is approximately equal to K_2/T , where K_2 is another constant.

Materials Conforming to the Arrhenius Relation with Both β and $\epsilon_0 - \epsilon_\infty$ Being Functions of Temperature. Differentiating with respect to temperature gives the condition for maximum ϵ'' as

$$(\omega\tau_m)^{2\beta\tau_m} = \frac{\frac{\beta\tau_m Q}{RT_m} + \left(\frac{A}{T_m}\right) - T_m \left(\frac{d\beta}{dT}\right)_{T_m} \left(\frac{1}{\beta\tau_m} + \ln \omega\tau_m\right)}{\frac{\beta\tau_m Q}{RT_m} - \left(\frac{A}{T_m}\right) + T_m \left(\frac{d\beta}{dT}\right)_{T_m} \left(\frac{1}{\beta\tau_m} - \ln \omega\tau_m\right)} \quad (2)$$

where

$$A = \left[\frac{d \ln (\epsilon_0 - \epsilon_\infty)}{d \left(\frac{1}{T}\right)} \right]_{T_m}$$

- (1) K. S. Cole and R. H. Cole, *J. Chem. Phys.*, **9**, 341, (1941).
- (2) R. M. Fuoss and J. G. Kirkwood, *J. Amer. Chem. Soc.*, **63**, 385, (1941).
- (3) W. Kauzmann, *Rev. Mod. Phys.*, **14**, 12, (1942).
- (4) C. J. F. Böttcher, "The Theory of Electric Polarization," Elsevier Publishing Co., Amsterdam, The Netherlands, 1952, Chapter 10.
- (5) H. Fröhlich, "Theory of Dielectrics," Clarendon Press, Oxford, England, 1958, Chapter 2.

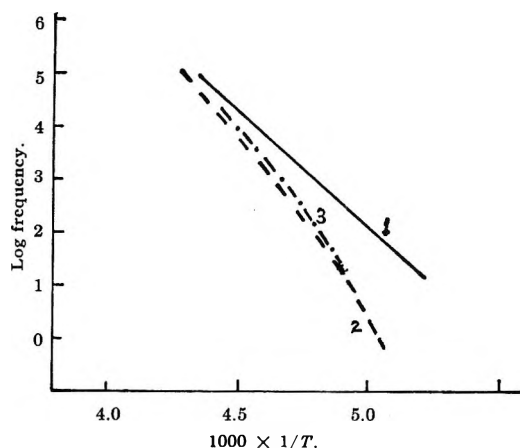


Figure 1. Comparison of loci for dielectric relaxation of polyoxymethylene: curve 1, observed $\log f_m$ against $1/T$ plot; curve 2, observed $\log f$ against $1/T_m$ plot; curve 3, calculated $\log f$ against $1/T_m$ plot.

Distributions usually become narrower as the temperature is raised and $d\beta/dT$ is then positive.

If ω_m is found at a particular temperature, T_0 (and relaxation time τ_0) and ω is held at this value while T is varied, the value of the relaxation time, τ_m , giving maximum ϵ'' is now different from τ_0 , so that T_m and T_0 are also different. Simple mathematical manipulation gives

$$\frac{1}{T_m} - \frac{1}{T_0} = \frac{2.303R \log [(\omega\tau_m)^{2\beta} T_m]}{2\beta T_m Q} \quad (3)$$

When β is independent of temperature (fixed distribution of relaxation times) and $\epsilon_0 - \epsilon_\infty = K_2/T$, $A = T_m$ and eq 2 reduces to

$$(\omega\tau_m)^{2\beta} = \left(\frac{\beta Q}{RT_m} + 1 \right) / \left(\frac{\beta Q}{RT_m} - 1 \right) \simeq 1 + \frac{2RT_m}{\beta Q}$$

when $RT_m/\beta Q \ll 1$.

The locus $\log f$ against $1/T_m$ will lie above the $\log f_m$ against $1/T$ plot. With measurements in the audio-radio frequency range and a medium-width distribution of relaxation times (e.g., $\tau_m = 10^{-6}$ sec, $\beta = 0.5$, $K_1 = 10^{-13}$ sec and $T_m = 300^\circ\text{K}$, corresponding to $Q \simeq 10$ kcal/mol), then $(1/T_m) - (1/T_0) \simeq 0.047 \times 10^{-3}$, $T_0 - T_m \simeq 4.2^\circ\text{K}$. The separation of the plots

will be less for higher activation energies or narrower distributions and will often be small.

Reverting to the more general case of both β and $\epsilon_0 - \epsilon_\infty$ being functions of temperature, eq 2 and 3 were applied to the interesting experimental data for polyoxymethylene (Read and Williams⁶), where a considerable discrepancy between the loci occurs.

At temperatures above about 300°K $d\beta/dT$ is very small ($\simeq 1.5 \times 10^{-3} \text{ }^\circ\text{K}^{-1}$) and the loci are close together with the \log (frequency) against $1/T_m$ plot lying slightly below that for $\log f_m$ against $1/T$, because in this region $\epsilon_0 - \epsilon_\infty$ is increasing, not decreasing, as the temperature is raised. However, as the temperature is lowered $d\beta/dT$ increases significantly, being about $9 \times 10^{-3} \text{ }^\circ\text{K}^{-1}$ around 200°K and this causes the $\log f$ against $1/T_m$ locus to deviate increasingly downward from the $\log f_m$ against $1/T$ plot at higher $1/T$ values. In this region, an approximate locus \log (frequency) against $1/T_m$ was calculated. From the observed plots and other data given, eq 2 and 3 were used to calculate $(1/T_m) - (1/T_0)$ at five different frequencies, employing successive approximations.

The calculated plot was then drawn using the observed $\log f_m$ against $1/T$ plot as a reference. The loci obtained experimentally in this region are shown redrawn in Figure 1 together with the calculated locus, and it is seen that the (approximate) calculated $\log f$ against $1/T_m$ plot agrees fairly well with the observed one, particularly at lower temperatures when the effect of variation of β with temperature is dominant. Discrepancies may be attributed to difficulties in obtaining accurate β and $d\beta/dT$ values and, possibly, to experimental and other errors. This type of behavior emphasizes that in such cases the activation energy should be obtained from the plot of $\log f_m$ against $1/T$, since the slope of the other plot is considerably in error at lower temperatures. This applies also to the corresponding dynamic mechanical case when the distribution of relaxation times changes rapidly with temperature. Further applications of the analysis are not readily made because much information is needed for any particular example, but the above type of behavior will certainly occur with other polymers and with other materials.

(6) B. E. Read and G. Williams, *Polymer*, 2, 239, (1961).

Pulse Radiolysis of Solutions of Amines of Low Ionization Potential

by T. J. Kemp,¹ J. P. Roberts,

School of Molecular Sciences, University of Warwick, Coventry, Great Britain

G. A. Salmon, and G. F. Thompson

University of Leeds, Cookridge High Energy Research Center, Cookridge Hospital, Leeds, Great Britain

Accepted and Transmitted by The Faraday Society (June 22, 1967)

Pulse radiolysis of dilute ($\sim 10^{-2}$ M) solutions of triphenylamine (TPA), N,N,N',N'-tetramethyl-*p*-phenylenediamine (TMPD), and N,N-dimethyl-*p*-phenylenediamine (DMPD) in solvents including aromatic and aliphatic hydrocarbons, certain ethers, benzyl alcohol, and dimethyl sulfoxide (DMSO) produced transient, intense absorptions closely resembling those of the corresponding amine radical cations. In most of the solvents, however, the effects of added second solutes, including electron and positive-ion scavengers, energy acceptors, and paramagnetic materials, indicate that the absorbing species are not positive ions but are triplet states of the amines. In DMSO, however, the converse appears to be the case.

Introduction

In a preliminary article² we reported an attempt to use amines of low ionization potential as scavengers for solvent positive ions produced in the pulse radiolysis of benzene, following the determination of $G(\text{C}_6\text{H}_{12}^+)$ from the pulse radiolysis³ of solutions of aniline, N,N-dimethylaniline, and diaminodurene in cyclohexane. Although strong absorptions closely resembling those of the corresponding radical cations were produced in benzene, the decays of these were unexpectedly of the first order kinetically, and addition of several second solutes, such as naphthalene, nitrous oxide, sulfur hexafluoride, air, oxygen, and methanol, produced effects suggesting that the absorptions are not those of cations but rather of triplet states. The unexpected similarity between the absorptions of the amine radical cation and the triplet excited amine, which has been reported by two other groups,^{4,5} has obvious implications for those engaged in flash-photolysis or pulse-radiolysis studies of these amines. We report here more fully on the work with benzene solutions and on extensions to other solvents and a third amine, N,N-dimethyl-*p*-phenylenediamine (DMPD).

Experimental Section

Chemicals. BDH Analar grade benzene was shaken with concentrated sulfuric acid for 24 hr and, following separation, neutralization, washing, and preliminary drying, was fractionally distilled from P_2O_5 . Spectroscopic grade cyclohexane was fractionally distilled. Toluene was of scintillation grade and paraffin was of refractive index grade. Analar grade dioxane was refluxed with (molten) sodium under a stream of oxygen-free nitrogen for 15 hr prior to fractional distillation from sodium under nitrogen. Reagent grade 1,2-dimethoxyethane (DME) was dried with CaH_2 and further with Na-K alloy (stirred

magnetically). It was refluxed for 3 hr over the alloy (under N_2) before fractional distillation. Tetrahydrofuran (THF) was purified likewise. BDH micro-analytical grade diethyl ether was fractionally distilled under N_2 . Reagent grade benzyl alcohol was fractionally distilled at low pressure, bp 107° at 24 mm. Dimethyl sulfoxide (DMSO) was from two sources: (i) Matheson Coleman and Bell spectroquality reagent was used without further purification; and (ii) Hopkin and Williams reagent grade was fractionally distilled from CaH_2 at low pressure, bp 88° at 27 mm. Spectroscopic grade methanol was employed.

*N,N,N',N'-Tetramethyl-*p*-phenylenediamine (TMPD).* The hydrochloride was dissolved in a minimum of water and the free base was precipitated by the addition of concentrated aqueous KOH. The crude material was dried thoroughly and vacuum sublimed twice, mp 51° .

*N,N-Dimethyl-*p*-phenylenediamine (DMPD).* The BDH reagent grade material was recrystallized from 80–100° ligroin at -78° . The white crystals became pink rapidly even at -10° .

Triphenylamine (TPA). BDH reagent grade material was recrystallized twice from 80% ethyl acetate–20% ethanol, mp 126.5° .

Naphthalene was of scintillation grade. Recrystallized ferric acetylacetonate was used. Argon (of 99.995% purity) and nitrous oxide were supplied by the British Oxygen Co. Sulfur hexafluoride was purchased from the Matheson Co., Inc.

(1) To whom all correspondence should be addressed.

(2) T. J. Kemp, J. P. Roberts, G. A. Salmon, and G. F. Thompson, *J. Phys. Chem.*, **71**, 3052 (1967).

(3) J. P. Keene, E. J. Land, and A. J. Swallow, *J. Amer. Chem. Soc.*, **87**, 5284 (1965).

(4) K. D. Cadogan and A. C. Albrecht, *J. Chem. Phys.*, **43**, 2550 (1965).

(5) N. Yamamoto, Y. Nakato, and H. Tsubomura, *Bull. Chem. Soc. Jap.*, **39**, 2603 (1966).

Pulse Radiolysis. Irradiations were performed with short pulses (0.2, 0.6, 1.2, and 2.3 μsec) of 3-MeV electrons obtained from a Van de Graaff machine constructed by High Voltage Engineering N.V. (Amersfoort, Holland). The vertical electron beam delivered from the accelerator was deflected through 90° by an electromagnet and focussed by means of two quadrupole magnets on to a silica cell of dimensions $1.0 \times 1.0 \times 0.7$ cm containing the sample under investigation. An estimate of the dose delivered by each pulse was afforded by passing the beam through a secondary emission chamber (SEC). The positive charge resulting from loss of electrons from the emission foil due to the passage of a pulse was accumulated on a capacitor and the voltage developed measured by an electrometer system. Day-to-day calibration of the SEC was performed by examination of a sample of oxygenated aqueous potassium ferrocyanide ($5 \times 10^{-3} M$) for which $G(\text{ferricyanide})$ is known⁶ to be 3.2 molecules/100 eV. $\epsilon_{4200 \text{ \AA}}$ for ferricyanide was taken⁷ to be 10^3 . Doses for all other media were computed using the approximation that the stopping power of 3-MeV electrons is proportional to the electron density of the medium.

Solutions were degassed by flushing with argon in an apparatus from which they could be transferred by application of slight pressure of argon into syringes which were used for filling the irradiation cell. These syringes were connected to the cell *via* a remotely operated three-way tap which controlled the filling and emptying of the cell. A second inlet to the cell was connected to a supply of argon (or other suitable gas) at a pressure a little in excess of atmospheric. This gas supply served to fill the cell with an inert atmosphere when the cell was drained. Filling the cell was achieved by allowing the plunger of the syringe, which was loaded with a small brass weight, to fall under gravity.

Radiation-induced chemical changes were detected optically. Light from a compact-source xenon lamp (Philips CSX 150) was passed through appropriate optical filters to the sample cell which had two optical windows of highest purity silica. The emergent light beam was then conducted from the irradiation area by a system of mirrors through further optical filters to a Bausch and Lomb high-intensity grating monochromator set at a preselected wavelength. The monochromatic light then passed to a photomultiplier-tube type (EMI 9558 BQ) and the resulting signal, suitably differentiated or integrated, was fed to a cathode-ray oscilloscope (Tetronix, Type 545A, Series B plug-in unit). Changes in optical absorption occurring on the firing of a pulse were recorded either by visual estimation or photographically as a function of time, thereby facilitating a kinetic analysis of any decay or buildup of a transient absorption. Spectra were obtained by a point-to-point procedure.

Further details of the pulse-radiolysis apparatus are to be published separately.⁸

Results

Spectra. Figures 1–3 present spectra obtained at the end of the pulse for the amines in various solvents. For a given amine, the spectrum is almost independent of the medium, although there is a small shift to the red for both TMPD and TPA in DMSO as compared with the other solvents. The spectrum obtained with DMPD in benzene is poor (the value of the product, $G\epsilon$, was markedly affected by changes in the size of individual pulses), but the agreement with that of

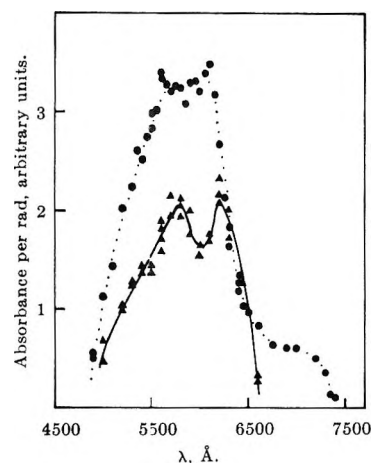


Figure 1. Spectra produced on pulse radiolysis of solutions of TMPD in benzene ($1.05 \times 10^{-2} M$) and DMSO ($8.40 \times 10^{-3} M$): ●, benzene; ▲, DMSO.

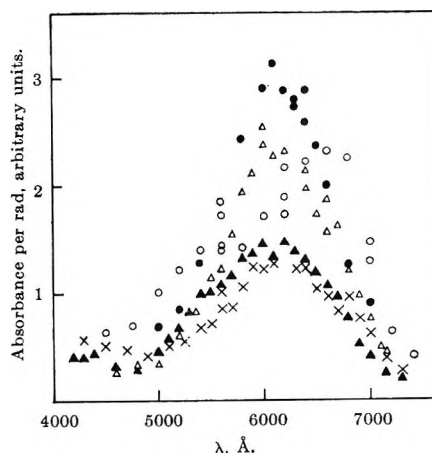


Figure 2. Spectra produced on pulse radiolysis of solutions of TPA in cyclohexane ($9.88 \times 10^{-3} M$), dioxane ($1.5 \times 10^{-2} M$), DMSO ($1.01 \times 10^{-2} M$), DME ($9.95 \times 10^{-3} M$), and benzyl alcohol ($1.02 \times 10^{-2} M$): ●, cyclohexane; △, dioxane; ○, DMSO; ▲, DME; ×, benzyl alcohol.

(6) G. E. Adams, J. W. Boag, and B. D. Michael, *Trans. Faraday Soc.*, **61**, 492 (1965).

(7) G. Hughes and C. Willis, *Discussion Faraday Soc.*, **36**, 223 (1963).

(8) F. Wilkinson, *et al.*, unpublished data.

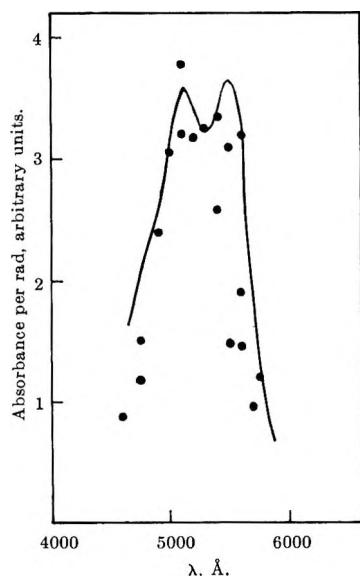


Figure 3. Comparison of spectrum produced on pulse radiolysis of DMPD in benzene ($1.07 \times 10^{-2} M$) with chemically⁸ prepared $\text{DMPD}^{\cdot+}$: ●, pulse-radiolysis spectrum; continuous line, $\text{DMPD}^{\cdot+}$.

chemically⁹ prepared $\text{DMPD}^{\cdot+}$ (Figure 3) is sufficient to corroborate the point made in our preliminary publication² that the spectra obtained on pulse radiolysis closely resemble those of the radical cations. A solution of DMPD in dioxane gave an absorption in the same region, with similar intensity and half-width, but with even greater scatter. A spectrum of TMPD in DMSO saturated with N_2O was measured very carefully at the same concentration of TMPD as in the TMPD-DMSO-argon system; the two systems gave identical spectra and very similar optical densities per unit dose. Aeration of TMPD and TPA in DMSO caused no changes in the spectra and only small reductions in the optical densities. Spectra were recorded using a variety of pulse sizes, and relative intensities apparent from the figures should be regarded as only a rough indication of relative yields.

Yields. Pulse radiolysis affords values only of the product $G\epsilon$ at the wavelength of investigation. This product can be resolved only by utilizing values of ϵ (usually) or G determined by some independent method. There is often some doubt surrounding literature values for ϵ or G , and, accordingly, our results are presented as the composite $G\epsilon$. Assessment of G values is deferred to the Discussion.

Yields of transient species produced by pulse radiolysis are often dose dependent.¹⁰ Figure 4 shows the remarkable insensitivity of the yield of the TPA transient to the dose delivered in the pulse. Strict linearity between the optical density (OD) of the transient and the dose was also found for $10^{-2} M$ TPA in cyclohexane (up to 6 krad), in benzyl alcohol (up to 2.5 krad), and in DMSO (up to 8 krad), and for $10^{-2} M$ TMPD in benzene (up to 2 krad) and DMSO (up to 3.5 krad).

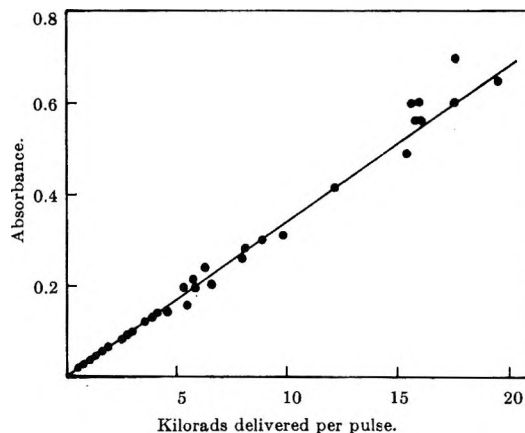


Figure 4. Dose dependence of optical absorption at $6400 \pm 50 \text{ \AA}$ for TPA in benzene ($1.02 \times 10^{-2} M$).

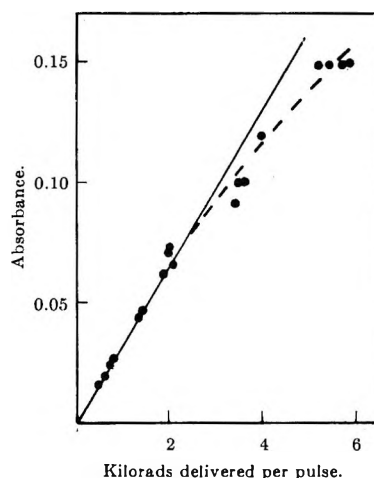


Figure 5. Dose dependence of optical absorption at $5650 \pm 50 \text{ \AA}$ for TMPD in benzene ($1.05 \times 10^{-2} M$).

Figure 5 illustrates the sensitivity to pulse magnitude of the TMPD absorption in benzene, and Table I lists that for DMPD in benzene.

Table I: Effect of Dose in Pulse upon $G\epsilon$ for $1.07 \times 10^{-2} M$ DMPD in Benzene ($\lambda 5300 \text{ \AA}$)

	Dose, krad					
	3.9	6.3	7.0	15.6	18.3	19.2
$10^{-4}G\epsilon$	1.53	1.36	1.24	1.17	0.81	0.83

Values of $G\epsilon$ at the wavelength of maximum absorption for the systems we have studied, usually at a solute concentration of about $10^{-2} M$, are recorded in Table II. A concentration dependence of $G\epsilon$ was determined

(9) L. Michaelis, M. P. Schubert, and S. Granick, *J. Amer. Chem. Soc.*, **61**, 1981 (1939).

(10) T. J. Kemp, J. P. Roberts, G. A. Salmon, and G. F. Thompson, "Proceedings of the Second Tihany Symposium on Radiation Chemistry," Akadémiai Kiadó, Budapest, 1967, p 333.

Table II: Values of G_e and Rate Constants for Solute Concentrations of Approximately $10^{-2} M$

Solvent	Concentration, mol l. ⁻¹	Dose, krads	$10^{-4}G_e$	$10^{-4}k_1$, sec ⁻¹
(i) Solutions of TMPD				
Benzene	9.36×10^{-3}	2.40	3.5 ± 0.3^a	<i>b</i>
Cyclohexane	9.54×10^{-3}	15.2	0.46	24
Paraffin	7.15×10^{-3}	14.3	0.35	5.6
Dioxane	1.11×10^{-2}	{ 15.6 4.7	{ 0.40 0.59	{ ... 15
DMSO	8.40×10^{-3}	1.90	2.05	<i>c</i>
(ii) Solutions of TPA				
Benzene	1.03×10^{-2}	0.92-18.9	4.4 ± 0.6^a	0.24 ± 0.03^d
Toluene	1.00×10^{-2}	2.35	2.81	0.54
Benzyl alcohol	{ 1.05×10^{-2} 1.02×10^{-2}	2.20	0.795	1.5
		21.0	0.64	...
Cyclohexane	9.88×10^{-3}	3.52	1.36	2.9
Dioxane	1.15×10^{-2}	{ 1.99 5.30 16.3	{ 1.46 1.26 0.90	{ 0.67 1.6 2.4
		4.1	0.73	...
		2.14	0.15	...
DME	9.95×10^{-3}	7.7	0.09	...
Diethyl ether	1.12×10^{-2}	8.7	1.42	...
THF	9.95×10^{-3}			...
DMSO	1.00×10^{-2}			<i>e</i>
(iii) Solutions of DMPD				
Benzene	1.07×10^{-2}	3.9	1.53	28.3
Dioxane	1.21×10^{-2}	{ 6.7 18.0	{ 0.50 0.35	{ <i>f</i> <i>f</i>

^a Mean values obtained from results measured over a period of 18 months; other values noted in tables or on figures are *not* averaged. ^b See Table III. ^c $k_2 = 4.3 \times 10^6 \epsilon_{5600} \text{ } \ddot{A} M^{-1} \text{ sec}^{-1}$. ^d Mean of 14 runs taken at intervals over entire range of dose. ^e $k_2 = 1.7 \times 10^6 \epsilon_{5400} \text{ } \ddot{A} M^{-1} \text{ sec}^{-1}$. ^f Unresolvable kinetics.

Table III: Effects of Dose in Pulse upon Decay Constant of ³TMPD in Benzene, [TMPD] $\sim 10^{-2} M$

$10^{-4}k_1$, sec ⁻¹	Dose, krads								
	0.59	1.86	3.1	5.4	5.7	7.1	8.7	15.5	26.4
	6.3	6.7	8.1	12.0	14.4	19.5	17.3	36	44

for only two systems, *i.e.*, TPA in benzene and in cyclohexane solutions, and the results are presented graphically in Figure 6.

Kinetics. Analyses of the decays of the transients were made for all the systems examined. Strict first-order behavior was found for TPA-benzene at all pulse sizes and no dose dependence of the decay rate was found between 700 and 20,000 rads. TMPD-benzene, however, gave good first-order kinetics only at fairly low doses (<7 krads) and, furthermore, the rate constant itself was dependent on dose (Table III). Solutions of TPA and TMPD in DMSO gave good and mediocre second-order kinetics, respectively. The contrast between decays of the TPA transient in benzene and DMSO is evident from Figure 7. Other systems gave decays varying from reasonably good first order to an unresolvable mixture of first- and second-order behavior. Results obtained from individual systems are summarized in Table II.

Effects of Added Second Solutes. Second solutes included: (i) electron scavengers, *e.g.*, N₂O and SF₆; (ii) a positive ion scavenger (methanol); (iii) an energy acceptor (naphthalene); and (iv) paramagnetic species such as molecular oxygen (or air) and Fe(III) acetylacetonate. The effects of their introduction depended markedly upon the system concerned, both yields and decay rates being subject to change of an order of magnitude (Table IV). The most pronounced differences can be seen to be between solutions of TMPD in benzene and DMSO, the former being extremely sensitive to the presence of several scavengers and the latter being barely affected by any. The effects of air and oxygen upon both yield and rate constant for the decay of the transient were partly reversible, in the sense that repeated pulsing of a given O₂-containing sample restored the absorption and lengthened its decay time.

Second solutes were chosen because of the low prob-

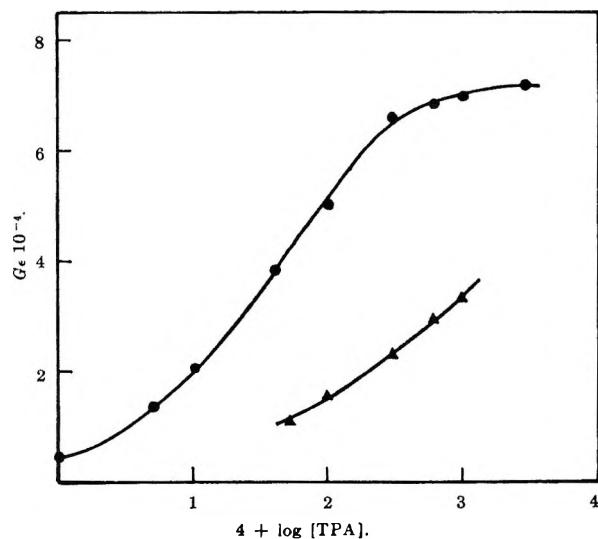


Figure 6. Concentration dependence of $G\epsilon$ for TPA in benzene (●) and cyclohexane (▲) at $6300 \pm 50 \text{ \AA}$.

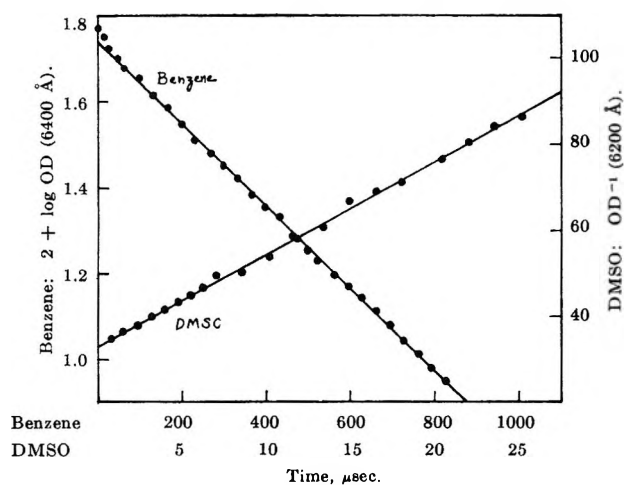


Figure 7. Kinetics of decay of transient for TPA in benzene ($1.02 \times 10^{-2} M$) and DMSO ($1.05 \times 10^{-2} M$). Other conditions: benzene, $\lambda 6400 \text{ \AA}$ (pulse size = 19,650 rads); DMSO, $\lambda 6200 \text{ \AA}$ (pulse size = 2040 rads).

ability of their producing intermediates or stable products likely to mask the spectra originating from the amines. In general, no interference was found and only naphthalene produced any quantity of an absorbing species, namely triplet naphthalene with its characteristic narrow absorption at $4000\text{--}4200 \text{ \AA}$. The value of $G\epsilon_{\text{max}}$ for triplet naphthalene in the presence of TMPD ($9.13 \times 10^{-3} M$) in benzene solution with a naphthalene concentration of $9.75 \times 10^{-3} M$ was 2.63×10^4 , which compares with a figure of 2.8×10^4 obtained from the published¹¹ graph of $G(\text{triplet naphthalene})$ vs. naphthalene concentration.

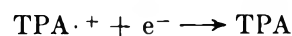
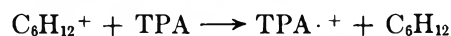
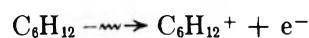
Discussion

In our preliminary report² we assigned the absorption obtained from TPA and TMPD in benzene to amine triplet states rather than to the spectrally similar radical

cations. This assignment was made in view of the first-order decay kinetics of the species, the effects of added energy acceptors and molecular oxygen, and the lack of effects of adding electron scavengers and a positive-ion scavenger (methanol to $1 M$). No subsequent work has caused us to modify this view and, indeed, the similarity of the spectra of $\text{TMPD}^{\cdot+}$ and triplet TMPD (${}^3\text{TMPD}$) has been the subject of further comment.⁵

It is clear, however, that our initial results form part of a larger pattern. Figures 1–3 show that transient spectra almost identical with those of chemically prepared radical cations are produced from all three amines on irradiation in solvents covering a range of polarity and chemical characteristics. However, a number of differences exist between TMPD and TPA for a given solvent and between solvents for a given amine, with regard to yields, kinetics, and effects of second solutes.

Differences between TMPD and TPA. The greatest difference between the intermediates produced from these amines is that of longevity. This is most apparent when benzene is employed as the solvent, the half-lives for a dose of ca. 20 krad being 1.57 and 316 μsec , respectively. The latter result is remarkable for what we believe to be a triplet state under pulse-radiolysis conditions; for example, triplet naphthalene has a half-life of 2.7 μsec for a pulse of similar size in benzene solution.¹⁰ Although ${}^3\text{TPA}$ is peculiarly long lived in benzene, it has half-lives of 128, 103, and 24 μsec in toluene, dioxane, and cyclohexane, respectively, for small (2–4 krad) pulses. The first-order decays and the half-lives again² preclude the possibility of the production of $\text{TPA}^{\cdot+}$ by a route³ such as



The longevity of ${}^3\text{TPA}$ implies that this excited molecule is relatively unperturbed by the presence of solvent radicals generated during radiolysis. This is further reflected in the lack of dependence of $G({}^3\text{TPA})$ upon dose (Figure 4) and in the comparatively mild effects of air and oxygen upon the yield and lifetime of ${}^3\text{TPA}$ (Table IV). Aeration of TMPD in benzene almost eradicates ${}^3\text{TMPD}$, which is also much more sensitive to the presence of naphthalene than is ${}^3\text{TPA}$. Presumably naphthalene can accept energy from ${}^3\text{TMPD}$; singlet-state transfer is probably not involved as TMPD fluoresces⁵ at a longer wavelength than does naphthalene. The presence of approximately $10^{-3} M$ ferric acetylacetonate, an excellent quencher¹² of triplet

(11) T. J. Kemp, G. A. Salmon, and F. Wilkinson, *Chem. Commun.*, 73 (1966).

(12) A. J. Fry, R. S. H. Liu, and G. S. Hammond, *J. Amer. Chem. Soc.*, **88**, 4781 (1966).

Table IV: Effect of Addition of Second Solutes

Amine	[Amine], <i>M</i>	Second solute	[Second solute], <i>M</i>	Dose, krads	$10^{-4}G_{\text{max}}$	$10^{-4}k_1$, sec ⁻¹
(i) Solutions in Benzene						
TMPD	8.07×10^{-3}	9.0	3.72	...
TMPD	8.07×10^{-3}	N ₂ O	Satn	5.0	0.10	...
TMPD	8.07×10^{-3}	Naphthalene	1.00×10^{-2}	7.8	0	...
TMPD	9.29×10^{-3}	Air	Satn	6.4	0.075	<0.2
TMPD	9.29×10^{-3}	Fe(Acac) ₃	9.51×10^{-4}	5.9	0.07	...
TPA	1.04×10^{-2}	19.7	3.91	0.24 ± 0.03^b
TPA	1.03×10^{-2}	N ₂ O	Satn ^a	20.0	2.85	0.17
TPA	1.03×10^{-2}	SF ₆	Satn	18.0	2.69	0.23
TPA	1.03×10^{-2}	Naphthalene	$\begin{cases} 1.01 \times 10^{-2} \\ 8.21 \times 10^{-3} \end{cases}$	$\begin{cases} 19.0 \\ 5.0 \end{cases}$	$\begin{cases} 0.66 \\ 0.87 \end{cases}$	$\begin{cases} \dots \\ 0.25 \pm 0.02^c \end{cases}$
TPA	1.72×10^{-2}	2.5	4.22	...
TPA	1.72×10^{-2}	Oxygen	Satn	3.8	0.44	5.8
TPA	1.72×10^{-2}	O ₂ followed by multiple pulsing	Satn	4.0	1.50	0.76
DMPD	1.07×10^{-2}	6.3	1.36	26.3
DMPD	1.07×10^{-2}	N ₂ O	Satn ^a	6.5	0.92	...
(ii) Solutions in Cyclohexane						
TMPD	9.54×10^{-3}	15.0	0.46	24
TMPD	9.54×10^{-3}	N ₂ O	Satn ^d	16.0	0.08	...
TMPD	9.80×10^{-3}	Naphthalene	4.42×10^{-3}	15.0	0	...
TPA	9.88×10^{-3}	6.0	1.36	3.3
TPA	9.88×10^{-3}	N ₂ O	Satn ^d	5.6	0.24	4.8
(iii) Solutions in Benzyl Alcohol						
TPA	1.02×10^{-2}	21.0	0.64	...
TPA	9.87×10^{-3}	Naphthalene	9.55×10^{-3}	18.0	0.485	...
(iv) Solutions in DMSO						
TMPD	9.59×10^{-3}	2.06	1.62 ^e	2.4
TMPD	9.59×10^{-3}	N ₂ O	Satn	3.28	1.69	2.1
TMPD	9.59×10^{-3}	Naphthalene	1.05×10^{-2}	4.75	1.79	6.0
TMPD	9.59×10^{-3}	Air	Satn	3.90	1.55	3.3 ^f
TPA	1.004×10^{-2}	8.7	1.42	<i>g</i>
TPA	1.004×10^{-2}	Air	Satn	9.4	1.34	<i>h</i>
TPA	1.004×10^{-2}	O ₂	Satn	7.9	1.37	<i>h</i>

^a The solubility of N₂O in benzene at 22.9° has been shown to be 0.142 *M*: S. Sato, R. Yugeta, K. Shinsaka, and T. Terao, *Bull. Chem. Soc. Jap.*, **39**, 156 (1966). ^b Mean of 14 determinations. ^c Mean of 12 determinations. ^d The solubility of N₂O in cyclohexane at 22.9° has been shown to be 0.108 *M* (reference the same as in footnote a). ^e Second-order kinetics were obtained with TMPD in DMSO. They were, however, frequently very poor at the start of the decay and because all these solutions gave an approximately equal initial absorption, we have presented decay rates in terms of pseudo-first-order rate constants. ^f This figure was obtained for a solution given a prior dose of 120 krads. A fresh solution gave an absorption unchanged after 500 μsec and a half-life beyond the measuring capacity of the apparatus. Examination of the recovery of the transmitted light on a meter indicated $t_{1/2} \sim$ several seconds. ^g $k_2 = 1.7 \times 10^6_{6400 \text{ Å}} \text{ M sec}^{-1}$. ^h Aeration and oxygenation changed the decay kinetics from smooth second order on a 25-μsec time scale (Figure 7) to a two-stage process comprising a "fast" decay (about one-half the rate of the decay in argon-flushed solution) and a "slow" decay persisting over several hundred microseconds. Multiple pulsing of the solution, however, caused the decay to become single stage and similar to the argon-flushed solution decay.

states, removes the absorption of ³TMPD. A striking difference between the amines is in their behavior toward saturation of their solutions in benzene with N₂O. Both ³TPA and ³DMPD are subject to a 30% reduction in yield by this treatment, but ³TMPD is completely removed. Normally N₂O only marginally affects solute triplet yields for solutions in benzene, e.g., naphthalene and 2,5-diphenyloxazole,¹⁰ and it is clear that N₂O does not interact appreciably with any

precursor of the solute triplet such as triplet or singlet benzene. Evidently ³TMPD, or a precursor such as singlet excited TMPD, must be reactive toward N₂O, which is not expected to display powers of physical quenching. Such an interaction of N₂O with excited molecules possessing only 3.3 eV of energy, (i.e., that of singlet excited TMPD) has implications which we propose to pursue further.

Differences between Solvents. It is clear that for

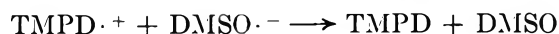
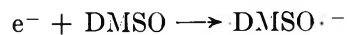
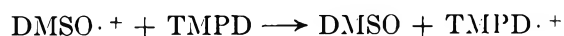
solutions of amine concentration of $10^{-2} M$, benzene gives the highest yields of triplet amine and, in the case of TPA, the longest lifetime and the lowest dose dependence. The lifetime suggests a special stabilization of ^3TPA by benzene, for the lifetimes of triplet naphthalene produced by pulse radiolysis are very similar in benzene and cyclohexane.¹⁰ ^3TPA is produced more efficiently in benzene than in cyclohexane over a wide concentration range (Figure 6), although the yield in benzene almost achieves a plateau.

The quenching effect of N_2O in the case of TPA-cyclohexane is not particularly significant, as N_2O reduces $G(^3\text{naphthalene})$ in the case of cyclohexane-naphthalene.¹⁰

More significant, however, is the comparison between the significant yields of the TPA transient in dioxane and DME on the one hand and the negligible yields in diethyl ether and THF on the other. This difference does not accord with the production of amine positive ions, which would be expected to occur with equal facility in DME and THF which have almost the same dielectric constant,¹³ but does parallel the situation observed with solutions of naphthalene in these ethers: namely, large yields of triplet naphthalene are found in dioxane and DME but very low yields are observed for diethyl ether and THF.¹⁴ This parallelism augments the evidence that, in general, the absorptions from amines of this type are due to excited states rather than ions.

Comparison of sections i and iv of Table IV indicates a clear difference in behavior between the transients produced from the amines in benzene and DMSO. Although the spectra are not dissimilar (Figures 1 and 2), the kinetic orders and durations of the decays (Figure 7) are quite different. $^3\text{TMPD}$ in benzene is reduced by at least 97% by an electron scavenger (N_2O), an energy acceptor (naphthalene), and paramagnetic oxygen and ferric acetylacetonate, while the absorption in DMSO is almost unaffected by all of these, apart from the increase in the lifetime produced on introduction of O_2 .

All the arguments which compel an assignment of the TMPD transient in benzene to $^3\text{TMPD}$ are completely reversed for the case of TMPD in DMSO, and, accordingly, we assign this transient to $\text{TMPD}\cdot^+$. This would be formed in a reaction sequence



The final step would be second order, as observed, for both species should be formed in equal concentration at the end of the pulse.

The effect of air on both TPA- and TMPD-DMSO may be due to a chain reaction, leading to the continued reoxidation of amine to radical cation by some intermediate constantly regenerated from the oxygen present, or to almost complete removal of strongly reducing species, such as $\text{DMSO}\cdot^-$, by O_2 , which prevents charge neutralization of the radical cation on a short time scale. Flash photolysis of TMPD in ethanol and acetonitrile⁵ produces $\text{TMPD}\cdot^+$, which disappears in a second-order fashion with a first half-life of about 4 sec.

Quantitative Assessment of Yields. This depends on the availability of accurate values of ϵ for the radical cations. No value for $\text{TPA}\cdot^+$ appears to have been recorded, but the values for $\text{TMPD}\cdot^+$ and $\text{DMPD}\cdot^+$ of Michaelis, *et al.*,⁹ of 1.19×10^4 and 6.5×10^3 , respectively, afford a G value for $\text{TMPD}\cdot^+$ in DMSO of 1.7 and, if the same value can be used for the triplet states,⁴ G values of $^3\text{TMPD}$ and $^3\text{DMPD}$ in benzene of 2.9 and 2.35, respectively for $10^{-2} M$ solutions. These compare with a G value¹¹ of 2.15 for triplet naphthalene in benzene at the same solute concentration.

Acknowledgment. We thank the Science Research Council for a grant to purchase the Van de Graaff machine and ancillary equipment and for maintenance grants to J. P. R. and G. F. T. We also thank Dr. F. Wilkinson and Mr. D. Ellison of Cookridge High Energy Radiation Research Center, Leeds University, who were responsible for design, construction and maintenance of much of the apparatus. Dr. F. S. Dainton, FRS, took great interest in this work throughout its progress and Professor V. M. Clark offered encouragement and support to T. J. K. and J. P. R.

(13) C. Carvajal, K. J. Tölle, J. Smid, and M. Szwarc, *J. Amer. Chem. Soc.*, **87**, 5548 (1965).

(14) T. J. Kemp, *et al.*, unpublished data.

Infrared Study of Benzene Adsorption on Aerosil

by Adriano Zecchina, Carlo Versino, Anna Appiano, and Giancarlo Occhiena

Istituto di Chimica Fisica dell'Università di Torino, Torino, Italy

Accepted and Transmitted by The Faraday Society (June 25, 1967)

Adsorption of benzene on highly dehydroxylated Aerosil, having surface concentrations of hydroxyls included between 1 and 2 OH/100 Å², is studied by infrared spectroscopy. At low coverages, adsorption occurs mainly on hydroxyl sites, by a 1:1 interaction, involving the π -electron system of the ring. When the number of perturbed hydroxyls is a significant fraction of the whole, adsorption on completely dehydroxylated areas becomes important.

The adsorption of benzene on silica has been studied both from the calorimetric¹ and spectroscopic^{2,3} point of view. The first kind of work pointed out that the isosteric adsorption heat is strongly affected by the degree of hydroxylation of the surface, and spectroscopic measurements showed that benzene interacts by its π -electron system with the surface hydroxyls. As a consequence,^{2,3} a broad band appears at about 3630 cm⁻¹, and a decrease in intensity of the stretching band of the unperturbed hydroxyls at 3750 cm⁻¹ occurs.

The aim of this research is to study if a correlation exists between the number of adsorbed molecules and that of perturbed hydroxyls, in order to define exactly the type of interaction arising between the OH groups and benzene.

Experimental Section

A Degussa Aerosil, having a specific surface of 310 m²/g, was employed.

The Aerosil was compressed by hand into plates about 0.5 mm thick, 24 mm in diameter, and weighing about 50 mg. The slight pressure used gave samples of good infrared transparency, with a fairly high mechanical resistance.

Benzene was dried on metallic sodium and purified by distillation.

A relative pressure of 5×10^{-3} represents the lowest limit in order to obtain a satisfactory spectrum of physisorbed benzene, without employing thicker samples and exceedingly wide slits.

The infrared cell had a very small optical path (about 1 mm), which allowed us to study the spectrum of physisorbed gases, even under high equilibrium pressures, without appreciable trouble due to the vapor phase.

Spectra were run at a constant temperature of $24 \pm 1^\circ$, and the heating effect of the beam was reduced by flowing dry and thermostated air around the cell walls in contact with the sample.⁴

In the measurement of the intensities, account was taken of the scattering effect produced by the adsorption, which causes a uniform loss of transparency along

the whole spectrum. Modalities of correction are described in previous papers,^{5,6} to which the reader is also addressed for the other experimental details.

Thermal dehydration went on, in each experiment, at temperatures $\geq 700^\circ$, in such a way as to have on the surface a large preponderance of isolated hydroxyls.^{6,7} In these conditions, in fact, the infrared spectrum (Figure 1) shows either a nearly symmetric band at 3750 cm⁻¹ or a completely symmetric one, in the most dehydrated samples. The slight asymmetry indicates the presence of a very small fraction of nonisolated hydroxyls, *i.e.*, reciprocally interacting hydroxyls.⁸ Their quantity cannot be exactly determined. In fact,

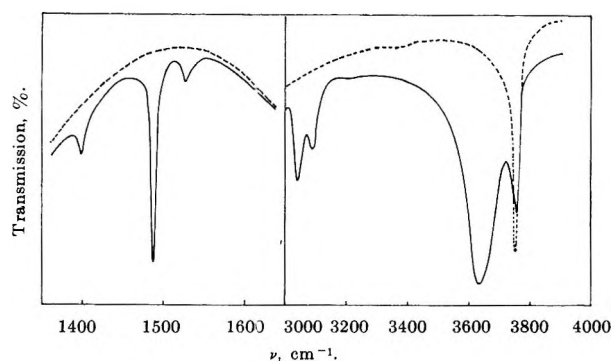


Figure 1. Infrared spectrum of benzene adsorbed on highly dehydroxylated Aerosil; broken line is the background.

- (1) A. V. Kiselev, "Tenth Symposium of the Colston Research Society," Butterworth and Co. Ltd., London, 1958, p 195.
- (2) M. R. Basila, *J. Chem. Phys.*, **35**, 1151 (1961).
- (3) G. A. Galkin, A. V. Kiselev, and V. I. Lygin, *Trans. Faraday Soc.*, **60**, 431 (1964).
- (4) In this paper we always use optical densities on the maximum instead of integrated intensities. In fact, owing to the difficulties inherent to the graphic separation of the bands at 3750 and 3630 cm⁻¹, such errors are made in the evaluation of the wings, that the obtained data do not represent a real improvement.
- (5) E. Borello, A. Zecchina, and C. Morterra, *J. Phys. Chem.*, **71**, 2938 (1967).
- (6) E. Borello, A. Zecchina, C. Morterra, and G. Ghiotti, *ibid.*, **71**, 2945 (1967).
- (7) J. J. Fripiat and J. Uytterhoeven, *ibid.*, **66**, 800 (1962).
- (8) J. A. Hockey and B. A. Pethica, *Trans. Faraday Soc.*, **57**, 2247 (1961).

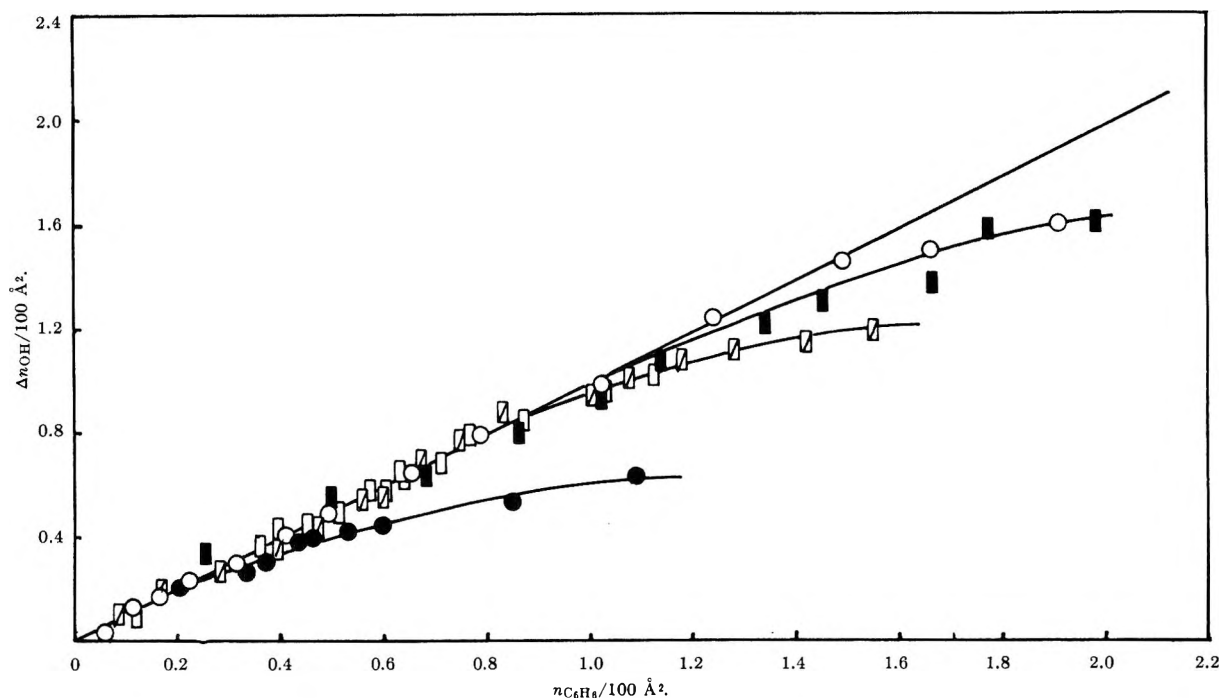


Figure 2. Decrease in concentration of the free surface hydroxyls vs. the concentration of adsorbed benzene ($\Delta n_{\text{OH}}/100 \text{ \AA}^2$ vs. $n_{\text{C}_6\text{H}_6}/100 \text{ \AA}^2$). Initial numbers of free hydroxyls for every 100 \AA^2 are: ●, 1.39; ◻, 1.73; ◻, 1.92; ■, 1.96; ○, 2.04.

as previously shown,⁵ for samples dehydrated at temperatures higher than 700° , there is a direct proportionality between weight loss and lowering of the optical density on the 3750-cm^{-1} maximum. The proportionality coefficient, taking into account the experimental errors, is the same for all of the outgassing temperatures between 700 and 900° . Thus, even if present, the hydroxyls giving rise to the above-mentioned asymmetry are so few in percentage that their influence is negligible compared with the experimental errors.

The intensity of the 3750-cm^{-1} band can be varied using activation temperatures between 750 and 850° and different outgassing times. So it is possible to obtain samples with different concentrations of hydroxyls, generally included between 1 and $2 \text{ OH}/100 \text{ \AA}^2$.

The concentration of the surface hydroxyls is measured from the intensity of the 3750-cm^{-1} band, using as extinction coefficient on the maximum the value of $35 \pm 1 \text{ l. cm}^{-1} \text{ mole}^{-1}$.

Sintering, and hence a decrease (from 310 to $280 \text{ m}^2/\text{g}$) of the surface area, occurs only at temperatures higher than 950° . This has been checked by determining the BET area of samples thermally treated in the same way as for spectroscopic measurements.

Discussion

The low concentrations of surface hydroxyls used in this work are necessary, when a quantitative investigation on the dependence of the concentration of free hydroxyls from the coverage is undertaken.

In fact, for higher values of the concentration of OH

groups, the number of mutually interacting hydroxyls is no more negligible. Such hydroxyls do not represent a well-defined surface species, because they give rise to an absorption that is strongly affected by thermal treatments. As previously pointed out,⁵ this can be ascribed to the fact that, on increasing the surface concentration of hydroxyls, the interactions arising among the various groups are of different intensity; in fact, on the heterogeneous surface of the silica, different distances among the OH groups are possible.

For all of these reasons, we limited our investigation to samples largely dehydroxylated, and this is the main difference between our work and that of Galkin, *et al.*,³ who studied the adsorption on Aerosil thermally treated at lower temperatures.

The stretching band of the hydroxyls perturbed by benzene adsorption at 3630 cm^{-1} appears rather symmetric with a constant half-intensity band width of $95\text{--}100 \text{ cm}^{-1}$ in the range of relative pressures investigated ($5 \times 10^{-3}\text{--}0.6$) and does not shift with coverage.

Some other features of the spectrum of physisorbed benzene (Figure 1) are worthy of interest. The CH stretching bands at about 3000 cm^{-1} have practically the same frequency and half band width as in the liquid phase and in CCl_4 solution; their intensity increases with coverage. The nuclear stretching band at 1483 cm^{-1} shows also the same constancy in frequency and half band width compared with the liquid phase and CCl_4 solution and appears shifted of only 2 cm^{-1} with respect to the liquid phase. This remark agrees with what has been spectroscopically observed by Galkin,

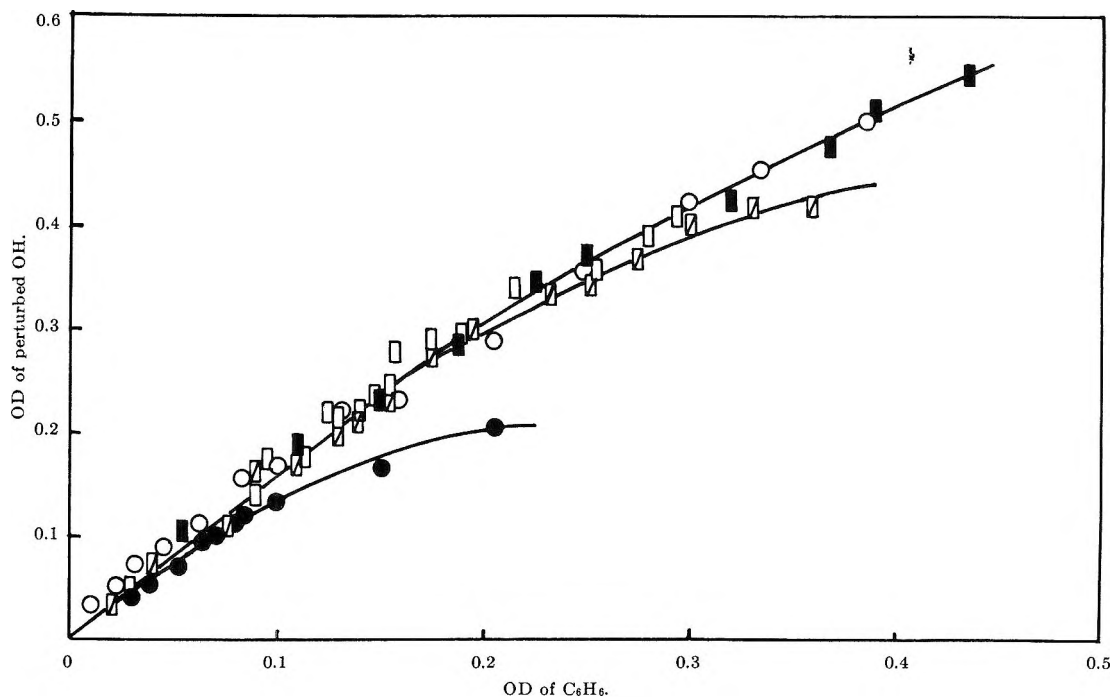


Figure 3. Optical density of perturbed hydroxyls at 3630 cm^{-1} as a function of the optical density of adsorbed benzene at 1483 cm^{-1} . Initial numbers of free hydroxyls for every 100 \AA^2 are: ●, 1.39; ◻, 1.73; ◻, 1.92; ■, 1.96; ○, 2.04.

et al.,³ who found that only the out-of-plane bending at 685 cm^{-1} is clearly perturbed by the adsorption.

Such observations allow us to assume, with good reliability, that physisorption does not substantially alter, with respect to the CCl_4 solution, the extinction coefficient measured at 1483 cm^{-1} on the maximum of the most intense absorption in the spectral range investigated. So surface concentrations of benzene have been calculated using an extinction coefficient of $62 \pm 1\text{ l. cm}^{-1}\text{ mole}^{-1}$.

In Figure 2 the decrease in concentration of the free OH groups is plotted *vs.* the surface concentration of benzene for samples with starting surface hydroxyl concentrations: 2.04 ± 0.06 , 1.96 ± 0.06 , 1.92 ± 0.06 , 1.73 ± 0.06 , and $1.39 \pm 0.06\text{ OH}/100\text{ \AA}^2$. The straight line drawn in Figure 2 represents the theoretical one that the data ought to follow if the interaction were 1:1 for every coverage.

A quite similar behavior is shown, obviously, by the relationship between the optical density at 3630 cm^{-1} and the optical density at 1483 cm^{-1} (Figure 3).

As we can easily observe from Figure 2, in spite of the considerable scattering of the data, interaction is really of the 1:1 type at low coverages. The three samples with starting hydroxyl concentrations equal to 2.04, 1.96, and 1.92 give rise to a single curve, since the differences are probably of the same order of the scattering of the data.

At higher coverages, a deviation from the proposed interaction scheme can clearly be observed, and the number of perturbed hydroxyls is less than the number

of benzene molecules adsorbed. More exactly, the greater the starting surface hydroxyl concentration is, the longer appears the rectilinear stretch of the 1:1 interaction.

Moreover, when the intensity of the band at 3630 cm^{-1} is plotted *vs.* the decrease of the band at 3750 cm^{-1} , a series of points, individualizing rather well a straight line, are obtained (Figure 4), even for those coverages that in the preceding figures deviated from the straight line. The independence of these data from the coverage indicates that the band at 3630 cm^{-1} does not shift, and its extinction coefficient on the maximum does not change, in agreement with the observed constancy of the band width. As a consequence, the interaction $\text{OH}-\text{C}_6\text{H}_6$ involves a practically constant energy.

The shift $\Delta\nu = 120\text{ cm}^{-1}$ of the OH stretching band has, over all of the range of relative pressures investigated, the maximum value observed at the higher coverages by Galkin, *et al.*,³ on more hydroxylated silicas, indicating also the maximum possible interaction energy. Thus, effects such as closer interaction or reorientation of the molecules with growing coverage are of little importance to our samples.

The deviation from linearity in the plot of Figure 2 could then be explained considering a competitive adsorption on completely dehydrated areas. In fact, the adsorption energies for the two types of sites are not very different, owing to the slight spectral shift of the perturbed hydroxyls ($\Delta\nu = 120\text{ cm}^{-1}$), from which we can roughly deduce an interaction energy of the order of a few kilocalories per mole. Since, following Galkin,

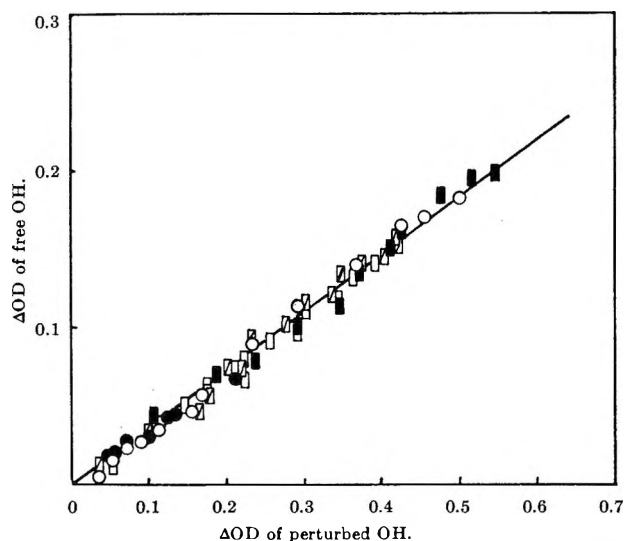


Figure 4. Decrease of the optical density of the free hydroxyls at 3750 cm^{-1} as a function of the optical density of the perturbed hydroxyls at 3630 cm^{-1} . Initial numbers of free hydroxyls for every 100 \AA^2 are: ●, 1.39; ◻, 1.73; □, 1.92; ■, 1.96; ○, 2.04.

et al.,³ $\Delta\nu$ gives a measure of the specific interaction between aromatic ring and hydroxyl, the total amount of energy involved in the adsorption is greater than it is possible to deduce from the spectral shift, because we must take into account the nonspecific contribu-

tion of the interaction between the benzene molecules adsorbed on the hydroxyls and the surface as a whole. This quantity is not exactly valuable by means of spectroscopic measures, but following the data reported by Galkin, *et al.*,³ we can think that the gas-solid interaction energy of the molecules adsorbed on the OH groups is about 2 kcal/mole greater than that of the molecules adsorbed on a dehydrated zone. The slight difference justifies the fact that, when a part of the hydroxyls is bonded, the adsorption on dehydroxylated areas becomes important.

The scheme of the 1:1 interaction can be valid only for silica having concentrations of surface hydroxyls lower than $2\text{ OH}/100\text{ \AA}^2$. In fact, for higher concentrations the probability of finding hydroxyls at sufficiently short distance to interact at the same time with a single benzene molecule becomes higher. Therefore, for scarcely dehydroxylated silica, one must expect the stretching band of the perturbed hydroxyls to vary in frequency with the coverage, as a consequence of the formation of hydrogen bonds of variable intensity.

Furthermore, we cannot exclude that, at relative pressures lower than 5×10^{-3} , the most hydroxylated samples can give rise to more complex interactions. Unfortunately, this fact cannot be revealed by infrared spectroscopy, owing to the low values of the extinction coefficient.

Low-Conversion Radiolysis of Methane Containing

Traces of Oxygen and Olefins

by D. C. Myers¹ and F. Schmidt-Bleek²

Department of Chemistry, Purdue University, Lafayette, Indiana 47907 (Received July 11, 1967)

Mixtures of CH₄ with 0.1–1 vol % of oxygen and mixtures of methane with 0.1 vol % of oxygen and 0.1 vol % of either ethylene-¹⁴C, acetylene-¹⁴C, or propyne-3-¹⁴C were exposed to ⁶⁰Co γ radiation. The applied doses varied from 10⁻³ to 30 \times 10⁻³ eV/molecule. With oxygen present, $G(\text{C}_2\text{H}_6) = 0.276$, irrespective of olefinic additives. Hydrogen atoms do not take part in the ethane formation whether oxygen is present or not. With either oxygen or olefins or both present, $G(\text{H}_2) = 3.14$. $G(\text{H})$ in methane was tentatively assigned the value of 4 ± 0.3 . The minimum dose (eV/molecule) required to remove oxygen radiolytically from methane is $D = [\text{O}_2](1.3 \times 10^{-5})$, where $[\text{O}_2]$ is in parts per million. The radiolytic oxidation of methane leads to CO₂, while acetylene and ethylene are the principal precursors of CO.

Introduction

The effects of ionizing radiation on pure hydrocarbons and on hydrocarbon mixtures have been the object of many studies in the past.^{3–6} Particular attention has been given to methane in the gas phase.^{7–12} It is known that the presence of oxygen greatly affects the distribution and yields of radiolytic products.¹⁰ Oxygen has frequently been used as a free-radical scavenger in concentrations of 1–10 vol %^{13,14} and the reactions of oxygen in this concentration range have been studied.^{10,15} There are also data available on the influence of olefinic additives in the radiolysis of methane and other hydrocarbons.^{10–12,16,17} In recent years, a number of researchers have begun to investigate the radiolysis of methane at low conversion (less than 0.4%).^{7,9,16,18} In spite of a large number of experimental studies in methane, however, the effect of traces of oxygen on low-conversion experiments was not completely understood.

The present study was, therefore, undertaken to investigate the influence of traces of oxygen on the radiolysis of methane at low conversion. Carbon-14-labeled olefins were added in order to elucidate details of hydrogen atom and other radical reactions in the presence and absence of oxygen. The concentration of additives was chosen to be about 0.1 vol %, so that in the applied-dose range substantial fractions of both oxygen and olefin and in some cases all of the oxygen would be consumed. This concentration assures that essentially all of the energy is deposited in the methane, while the radicals formed react almost exclusively with the additives. Control experiments were performed with methane-¹⁴C and also with hydrogen replacing the methane as the major component.

Experimental Section

Nonradioactive methane, ethylene, oxygen, and acetylene were purchased from Matheson Co. Me-

thane (ultrahigh purity) was further purified by freeze trapping all impurities with the exception of oxygen and nitrogen (to less than 1 ppm) on a vacuum line. Acetylene was purified by bulb-to-bulb distillation and thoroughly degassed before use. The ethylene (CP) was subjected to gas chromatographic purification. Oxygen (extra dry, 99.6% minimum purity) was used without further purification. Both acetylene and ethylene were used to dilute the carbon-14-labeled olefins. Hydrogen was purchased from the Linde Division of Union Carbide and purified by cooling one of two hydrogen-containing connected flasks on the vacuum line for several hours to -196° . The hydro-

(1) Work performed in partial fulfillment of the requirement for the Ph.D. degree at Purdue University, Lafayette, Ind.

(2) To whom all correspondence should be addressed.

(3) A. V. Topchiev and R. A. Holroyd, Ed., "Radiolysis of Hydrocarbons," Elsevier Publishing Co., Amsterdam, The Netherlands, 1964.

(4) A. J. Swallow, "Radiation Chemistry of Organic Compounds," Pergamon Press Ltd., London, 1960.

(5) J. W. T. Spinks and R. J. Woods, "An Introduction to Radiation Chemistry," John Wiley and Sons, Inc., New York, N. Y., 1964.

(6) S. C. Lind, C. J. Hohanadel, and J. A. Ghormley, "Radiation Chemistry of Gases," ACS Monograph No. 151, Reinhold Publishing Corp., New York, N. Y., 1961.

(7) F. W. Lampe, *J. Amer. Chem. Soc.*, **79**, 1055 (1957).

(8) P. J. Ausloos and S. G. Lias, *J. Chem. Phys.*, **38**, 2207 (1963).

(9) L. W. Sieck and R. H. Johnsen, *J. Phys. Chem.*, **67**, 2281 (1963).

(10) R. W. Hummel, *Discussions Faraday Soc.*, **36**, 75 (1963).

(11) W. P. Hauser, *J. Phys. Chem.*, **68**, 1576 (1964).

(12) R. Gorden, Jr., and P. Ausloos, *J. Chem. Phys.*, **46**, 12, 4823 (1967).

(13) J. A. Bell and G. B. Kistiakowsky, *J. Amer. Chem. Soc.*, **78**, 5699 (1956).

(14) J. A. Bell and G. B. Kistiakowsky, *ibid.*, **84**, 3417 (1962).

(15) G. R. A. Johnson and G. A. Salmon, *J. Phys. Chem.*, **65**, 177 (1961).

(16) R. A. Back, *ibid.*, **64**, 124 (1960).

(17) P. J. Lucchesi and W. Bartok, *J. Amer. Chem. Soc.*, **82**, 4108 (1960).

(18) R. H. Johnsen, *J. Phys. Chem.*, **69**, 3218 (1965).

gen in the flask at ambient temperature showed no impurities larger than 1 ppm after this treatment. Propyne was prepared from methyl iodide, Columbia Organic Chemicals Co., and a lithium acetylide-ethylenediamine complex,¹⁹ Foote Mineral Co. Subsequently it was purified by gas chromatography.²⁰

Radioactive ethylene-1,2-¹⁴C with a specific activity of 3 mCi/mmol was obtained from New England Nuclear Co. Acetylene-1,2-¹⁴C with a specific activity of 4 mCi/mmol was purchased from Volk Radiochemical Co. Both compounds were purified by gas chromatography. The radiopurity checks for all compounds as well as the radioactivity analyses of irradiated samples were carried out with internal proportional quartz counters in conjunction with memory scalers with digital data output.^{21,22} Methane-¹⁴C with a specific activity of 2 mCi/mmol was obtained from New England Nuclear Co. Because of its vapor pressure of 10 mm at -195.5°, any freeze trapping of methane from the effluent stream of a gpc apparatus is ineffective. Therefore, CH₄ was purified by placing a 100 × 10 mm glass tube packed with 5A molecular sieve between the shipping vial and the storage vessel (large relative volume) on the vacuum line. After diffusion, the only detectable impurities were oxygen, nitrogen, and traces of carbon monoxide-¹⁴C. Propyne-3-¹⁴C was produced from methyl iodide-¹⁴C (New England Nuclear Co., specific activity 1.2 mCi/mmol) and lithium acetylide-ethylenediamine.²⁰ Purification was achieved with gas chromatography. All radioactive olefins were then diluted with purified "cold" analogs to approximately 0.01 mCi/mmol. In each case the purification and dilution was done only immediately prior to the sample preparation in order to exclude buildup of self-radiation products.

The gas mixing and sample filling were performed on a conventional vacuum line. The samples were sealed in Pyrex glass tubes, 14 mm i.d. and 180 mm in length, equipped with break-off tips. Irradiations were carried out in a fixed position in a GR-12 ⁶⁰Co γ source (U. S. Nuclear Co.), calibrated upon installation (March 15, 1966) to have a dose rate, in air, of 6.1×10^5 rads/hr.

The data presented here have all been converted to dose in electronvolts per molecule and corrections have been made for the decay of the ⁶⁰Co in the source. The conversion factors used for the dose D (rads) in methane and hydrogen are $1.096D_{\text{air}}$ (roentgens) and $1.754D_{\text{air}}$ (roentgens), respectively. The validity of these factors were checked by determining $G(\text{C}_2\text{H}_6)$ in pure methane. A value of 2.0 was found (lit. 2.0–2.27,^{9,10,23}).

Radio gas chromatography was used as the only analytical tool. Since the upper limit of any product formed is only about 1 μg/aliquot in our samples, no special attempts were made to determine strongly polar compounds, such as H₂O, H₂O₂, and CH₃O₂H, by means other than glpc. The irradiated samples were opened

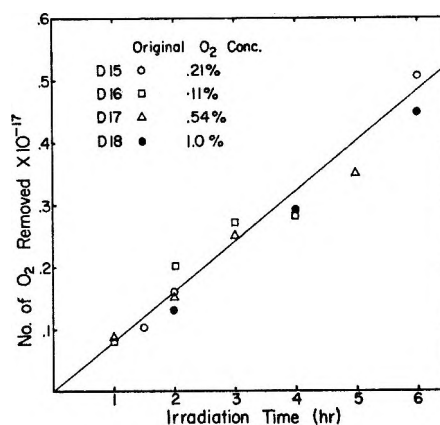


Figure 1. The radiolytic consumption of oxygen at different oxygen concentrations in methane (0.5 vol % acetylene present in all mixtures).

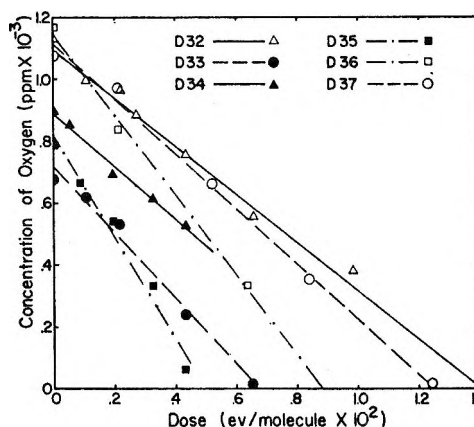


Figure 2. The disappearance of oxygen vs. applied dose in various mixtures. For compositions see Table I.

on a vacuum line. Known aliquots were equilibrated into loops and then injected onto columns by turning multiple-path stopcocks. The following separation

Table I

Designation	Major component	Added olefin	Oxygen, ppm × 10 ⁻²	Olefin, ppm × 10 ⁻²
D32	CH ₄		11.0	
D33	CH ₄	C ₂ H ₂ - ¹⁴ C	7.0	9.1
D34	H ₂		8.9	
D35	H ₂	C ₂ H ₂ - ¹⁴ C	8.1	9.7
D36	CH ₄	C ₃ H ₄ - ¹⁴ C	11.4	7.7
D37	CH ₄	C ₂ H ₄ - ¹⁴ C	11.1	15.0
D38	CH ₄ - ¹⁴ C	C ₂ H ₂	10.0	7.0

(19) O. F. Beumel and R. F. Harris, *J. Org. Chem.*, **28**, 2775 (1963).

(20) D. C. Myers and F. Schmidt-Bleek, *J. Label Compounds*, **3**, 62 (1967).

(21) R. M. Statnick, F. Schmidt-Bleek, *Z. Anal. Chem.*, **217**, 321 (1966).

(22) J. K. Lee, F. Schmidt-Bleek, *Adv. Anal. Chem. Instr.*, in press.

(23) K. Yang and P. J. Manno, *J. Amer. Chem. Soc.*, **81**, 3507 (1959).

Table II

	Sample					
	D32	D33	D34	D35	D36	D37
$-G(O_2)$	7.77 ± 0.41	10.69 ± 0.52	8.53 ± 0.51	16.36 ± 1.3	12.89 ± 0.86	8.93 ± 0.65

Table III

	Sample			
	D35	D36	D33	D37
Olefin	C_2H_2	C_3H_4	C_2H_2	C_2H_4
Major compound	H_2	CH_4	CH_4	CH_4
$-G(\text{olefin})$	9.67 ± 0.64^a	5.16 ± 0.61^a	4.83 ± 0.05^a 3.18 ± 0.4^b	7.02 ± 0.2^a 4.5 ± 0.3^b

^a Oxygen present. ^b Oxygen absent.

columns were used: molecular sieve (0.25-in. copper), Safrole (0.25-in. stainless steel), and Porapak Q (0.25-in. stainless steel). Helium served as carrier gas and propane was added as counting gas before the effluent stream reached the counter. Where "specific activities" are mentioned in the text, they refer to the activity observed per number of molecules, compared to the activity per number of molecules of the added labeled compound (1.0). All irradiations were performed at 700 mm and ambient temperature.

Results

Oxygen. Figure 1 shows the oxygen disappearance in methane containing 0.5 vol % of acetylene. The original oxygen concentrations varied from 0.1 to 1 vol %. The number of oxygen molecules consumed is plotted *vs.* irradiation time. It is obvious that, within experimental error, $-d[O_2]/dt$ is a linear function of the absorbed dose, irrespective of the original oxygen concentration.

Figure 2 shows the oxygen disappearance in various systems in parts per million of O_2 observed *vs.* applied dose. In further discussion we shall use the short descriptions, found in Table I, for various original mixtures. As was found for various oxygen concentrations in methane containing small amounts of acetylene, Figure 2 shows that the oxygen consumption is a linear function of dose. The curves in Figure 2 were obtained by linear least-square analysis of the data, and the values for $-G(O_2)$, shown in Table II, were calculated from the slopes. The minimum dose required for the complete removal of oxygen in methane can, therefore, be given as $D_{\min} \cong [O_2](1.3 \times 10^{-5})$, where D = dose in electronvolts per molecule and $[O_2]$ = original oxygen concentration in parts per million.

Olefins. Figure 3 shows the disappearance rate of the olefins with respect to dose. In the mixtures D35 and D36, the applied dose was not sufficient to remove

all of the oxygen and $-d(\text{olefin})/dt$ remains constant over the dose range studied, whereas a slight change in the consumption rate was observed at doses where all oxygen was consumed in D33 and D37. The lines in Figure 3 were obtained by least-square analysis of the data, and the values for $-G(\text{olefin})$, shown in Table III, were calculated from the slopes.

Hydrogen. Figure 4 shows all data points obtained for hydrogen formation in the various systems where methane is the major component. The curve in this figure was obtained from a least-square fit of all points from all mixtures.

It is important to note that the rate of hydrogen production in all these mixtures is the same, as long as oxygen or any of the added olefins are present. The average $G(H_2)$ value, as calculated from the slope of the curve in Figure 4, is 3.14 ± 0.07 and may be compared to $G(H_2) = 5.6-5.7^{7,9,10,24}$ in pure methane. (The value of 3.14 ± 0.07 is based on a thermal response ratio of $H_2/CH_4 = 28.75 \pm 1.47$, as determined in our laboratory.)

Ethane. Figure 5 contains all data points collected for the formation of ethane in the various mixtures under investigation. As long as oxygen is present, the rate of ethane formation is constant and independent of the type of olefin added. The average $G(C_2H_6)$, as calculated by least-square analysis, is 0.276 ± 0.02 and may be compared with literature values of 0.1¹⁰ and 0.155²⁴ both of which were obtained in methane containing radical scavengers. In our series D33, D37, and D38, some irradiations were carried out with doses sufficient for the complete oxygen removal, and sharp increases of ethane productions were observed. There are not enough data available to determine $G(C_2H_6)$ for the oxygen-free mixtures, but an estimate shows $G(C_2H_6)$ to be about 1.7-2.0. This value is in reasonable agreement with published values of $G(C_2H_6) = 2.0-$

(24) K. Yang, *J. Phys. Chem.*, **65**, 42 (1961).

Table IV

	Sample				
	D32	D33	D35	D36	D37
Olefin		$C_2H_2-^{14}C$	$C_2H_2-^{14}C$	$C_2H_4-^{14}C$	$C_2H_4-^{14}C$
Major compounds	CH_4	CH_4	H_2	CH_4	CH_4
$G(CO_2)^a$	0.46 ± 0.082^b	0.985 ± 0.1^b	0.936 ± 0.1^b	1.29 ± 0.29^b	1.036 ± 0.45^b

^a Oxygen present. ^b $G(CO_2)$ average 1.172 ± 0.07 .

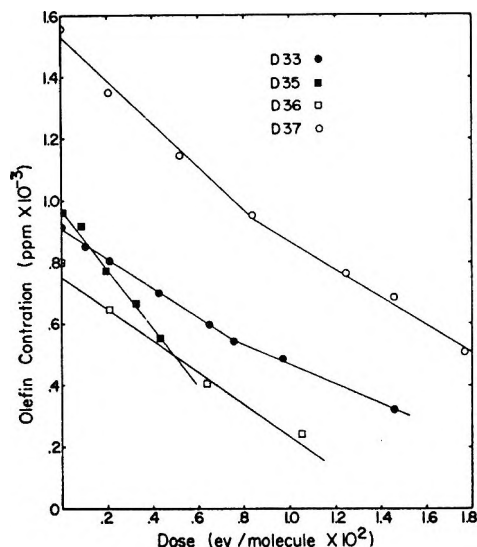


Figure 3. The radiolytic consumption of ethylene (O), acetylene (●), and propyne (□) in methane and acetylene in hydrogen (■). The slope changes for D37 and D33 occur at doses where molecular oxygen disappears from the mixtures.

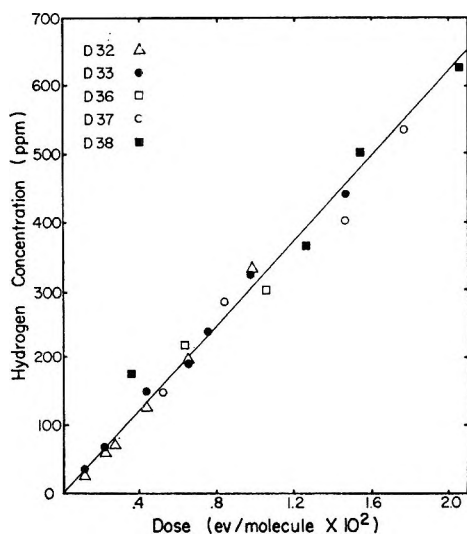


Figure 4. The production of H_2 with respect to dose.

2.2,^{7,9,10,23} The radioactivity observed in ethane is of particular interest. In D38, where CH_4 was labeled, the specific activity of the ethane is 1.9 ± 0.2 times the specific activity of methane. When C_3 -labeled propyne was added, the amount of radioactive ethane repre-

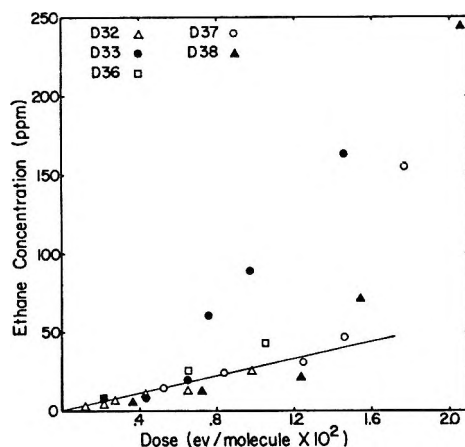


Figure 5. The production of C_2H_6 with respect to dose. Points above the line are values obtained at doses where molecular oxygen is no longer present.

sented about 5% of the total ethane produced. In both, D33 ($C_2H_2-^{14}C$) and D37 ($C_2H_4-^{14}C$) the upper limit of radioactive ethane is 3%. It can, therefore, be stated that ethane is formed almost exclusively from methane.

Carbon Dioxide. Carbon dioxide was observed as a radiolysis product in all mixtures containing a source of carbon, either methane or olefin or both. The data obtained are summarized in Figure 6. The G values for all mixtures are given in Table IV, along with an average $G(CO_2)$ value for all mixtures except D32. Only those values were considered where oxygen had not yet been completely consumed. The rate of CO_2 production of D32 is close to one half of that found in samples where olefins are present. This suggests that approximately one half of the carbon dioxide produced in our mixtures comes from methane and one half is produced from the added olefins. This is also borne out by the finding that the specific activity of CO_2 in D33 and D37 is 0.25 ± 0.03 . It is also of interest that $G(CO_2)$ in the hydrogen samples (D35) is the same as $G(CO_2)$ in the systems where methane is the major component.

Carbon Monoxide. No carbon monoxide was observed in D32 (CH_4 , no added olefin). Under our experimental conditions a value of $G(CO) > 0.04$ would have been detected. The data from series D33, D35, and D37 are summarized in Figures 7 and 8. The

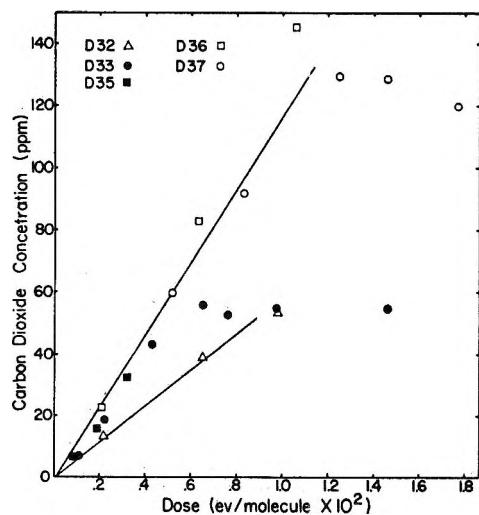


Figure 6. The production of CO_2 . Note that D32 (Δ) does not contain added olefin.

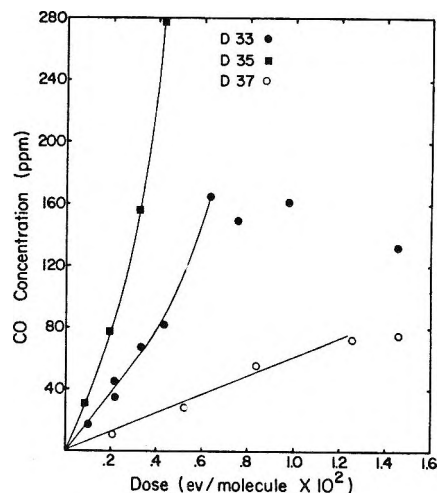


Figure 7. The production of CO. In samples containing acetylene (\bullet, \blacksquare) the formation is nonlinear with increasing dose.

Table V

	Sample		
	D33	D35	D37
Olefin	$\text{C}_2\text{H}_2\text{-}^{14}\text{C}$	$\text{C}_2\text{H}_2\text{-}^{14}\text{C}$	$\text{C}_2\text{H}_4\text{-}^{14}\text{C}$
Major compound	CH_4	H_2	CH_4
$G(\text{CO})$	2.08 ± 0.16^a	1.86 ± 0.11^a	0.56 ± 0.04^a

^a Oxygen present.

$G(\text{CO})$ values as tabulated in Table V were calculated from the linear parts of the curves in Figure 7.

As shown in Figure 7, the carbon monoxide production in D37 ($\text{C}_2\text{H}_4\text{-}^{14}\text{C}$ added) has a linear relationship to the absorbed dose as long as oxygen is present (up to 1.25×10^{-2} eV/molecule). In D35 (H_2 with $\text{C}_2\text{H}_2\text{-}^{14}\text{C}$ added), the production of CO is linear only to a dose of about 0.2×10^{-2} eV/molecule. At larger doses, up to the maximum applied, the formation of CO is linear with respect to the square of the dose with $[\text{CO}] = 15 \times 10^6$ ppm/eV² molecule², as shown in Figure 8. Similarly, in D33 ($\text{C}_2\text{H}_2\text{-}^{14}\text{C}$ in CH_4 , the CO formation is linear with respect to dose first (up to 0.3×10^{-2} eV/molecule) and then, based on a single measurement (highest dose at which O_2 is still present), also seems to follow the square of the dose with $[\text{CO}] = 4.08 \times 10^6$ ppm/eV² molecule². In D33 the oxygen is completely removed at about 0.65×10^{-2} eV/molecule and in D35 at 0.5×10^{-2} eV/molecule. In these systems the specific activity observed in CO clearly indicates that it is primarily formed from acetylene-¹⁴C.

Ethylene. Ethylene formation is observed in all cases where methane is the major component and as long as oxygen is present. In D37, with added ethylene-¹⁴C, the analysis had to be based on a very small change in the specific activity of ethylene and these data are omitted. Figure 9 summarizes the findings.

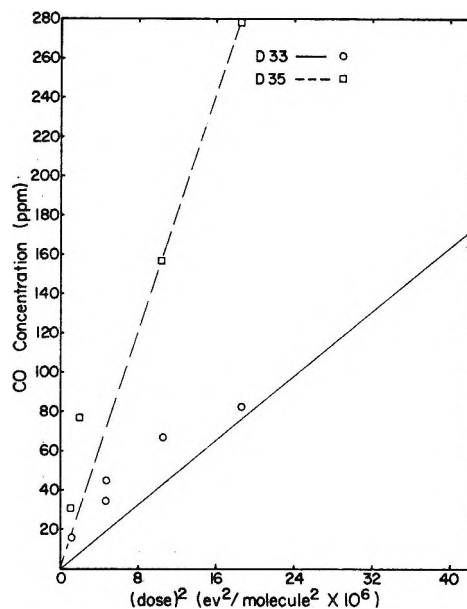


Figure 8. The formation of CO in acetylene containing samples with respect to dose.⁴

The line drawn was calculated by least-square analysis for the data of D32 (methane plus oxygen), and from the slopes of this line, we obtain $G(\text{C}_2\text{H}_4) = 0.624 \pm 0.021$. This value may be compared with $G(\text{C}_2\text{H}_4) = 0.65$, obtained by Hummel¹⁰ in the radiolysis of methane containing 1% of oxygen, and also with $G(\text{C}_2\text{H}_4) = 0.66$, a value which Hauser¹¹ found in the radiolysis of methane-¹⁴C when 0.17% of "cold" ethylene was added. Gordon and Ausloos¹² have very recently performed a detailed study and suggested that ethylene is largely produced by the insertion of CH into CH_4 during the radiolysis of pure methane. They arrived at a G value of 0.45–0.6 as the "original" ethylene production in pure methane. With methane as the major component, there is no evidence in our results that any ap-

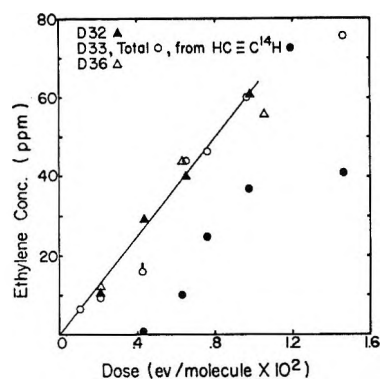
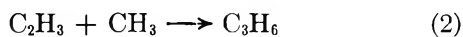
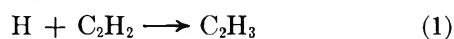


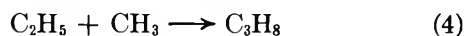
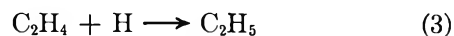
Figure 9. The formation of ethylene. The black dots represent the ethylene formation from the reaction of acetylene after oxygen removal.

preciable amount of ethylene is formed from olefins as long as oxygen is present (only very little radioactivity is observed in D33 and D36.). As is shown in Figure 9, however, acetylene-¹⁴C can effectively be reduced to ethylene-¹⁴C after total oxygen consumption (black dots). In D35 (H₂ plus C₂H₂-¹⁴C) only traces of ethylene-¹⁴C were observed. The production levels off at about 0.3×10^{-2} eV/molecule, with a maximum of 7.5 ppm at 0.4 eV-molecule.

Minor Products. With the exception of ethane and ethylene, the yields of all hydrocarbon products were very small at doses below the dose required to remove the oxygen. Since most irradiations were carried out below this limit, the following discussion is restricted to the relatively few samples which were irradiated beyond this limit. Propylene was found in small amounts in both D36 and D33. The specific activities observed clearly show that in D36 propylene is a reduction product of the added propyne and in D33 propylene originates from acetylene *via* the sequence



A significant amount of propane was found in D37. In the sample with the highest dose, about 80 ppm was obtained and the specific activity was 0.91. Its formation can, therefore, be primarily ascribed to the sequence



Smaller amounts of propane were found in D33 and D36. In D33 the observed specific activity was 0.5. The data from D36 do not allow a reliable estimate, but the specific activity is certainly less than 0.5.

Normal butane was observed in D37 and its specific activity was 1.9, suggesting that reaction 3, followed by ethyl radical combination, is the only important source for its formation. These conclusions are concurrent with those reached by several authors.^{9,10,25}

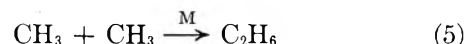
Acetylene was found in D36, D37, and D38. The value for $G(\text{C}_2\text{H}_2)$, using all data points, is estimated to be 0.045–0.06. There is one low measurement of C₂H₂ in the D38 series, which indicates that acetylene begins to disappear as soon as it is no longer "protected." At this particular dose (1.55×10^{-2} eV/molecule), the originally added cold acetylene was depleted to about 200 ppm. The data from series D32, where acetylene was undoubtedly formed, do not lend themselves to an accurate evaluation of acetylene. Of the oxygen containing products, other than CO₂ and CO, formaldehyde is probably the most important one. It was, however, only found in two instances where special measures were taken to detect it. Using these values, $G(\text{CH}_2\text{O}) = 0.33$ in D33 and $G(\text{CH}_2\text{O}) = 0.082$ in D35 were computed. The error in these values may be as high as 50%.

Methanol was observed in both D33 and D32. The D32, $G(\text{CH}_3\text{OH})$ was found to be 0.68 ± 0.06 . The largest amount of CH₃OH found in D33 corresponds to $G(\text{CH}_3\text{OH}) = 0.8$. This value may, however, be low because all oxygen had been consumed for the dose at which it was taken. Hummel finds $G(\text{CH}_3\text{OH}) = 1.6$ in methane²⁶ containing 10% oxygen.

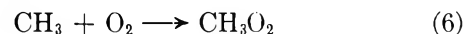
Estimated G values for acetaldehyde formation are: D32, 0.27; D33, 0.8; D37, 0.23.

Discussion

Ethane and Hydrogen. Reaction 5 has been suggested as the major source of ethane formed in the radiolysis of methane^{7,9} since methyl radicals are among the most



prominent radicals formed.^{27,28} If we assume a rate constant of 2.2×10^{10} l./mol sec^{29,30} for reaction 5, with methane as the third body, a steady-state concentration of 3.7×10^{-11} mol/l. is necessary for our observed $G(\text{C}_2\text{H}_6) = 0.276$. If the rate constant for reaction 6



is taken as 1.4×10^9 l./mol sec,^{31,32} $-G(\text{O}_2)$ would have to be about 2×10^4 for oxygen concentrations of 1000 ppm, whereas the G values observed ranged from 7.7 to 10 in our methane mixtures. With oxygen present, reaction 5 can, therefore, be excluded as source of ethane.

(25) P. Ausloos, R. Gorden, Jr., and S. G. Lias, *J. Chem. Phys.*, **40**, 1854 (1964).

(26) J. A. Hearne and R. W. Hummel, AERE-R 4871, 1964.

(27) J. H. Gevantman and R. W. Russell, Jr., *J. Phys. Chem.*, **56**, 569 (1952).

(28) G. G. Meisels, W. H. Hamill, and R. R. Williams, Jr., *ibid.*, **61**, 1456 (1957).

(29) A. Shepp, *J. Chem. Phys.*, **24**, 939 (1956).

(30) C. A. Heller, *ibid.*, **28**, 1255 (1958).

(31) W. C. Sleppy and J. C. Calvert, *J. Amer. Chem. Soc.*, **81**, 769 (1958).

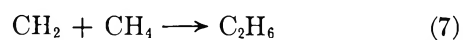
(32) G. S. Pearson, *J. Phys. Chem.*, **67**, 1686 (1963).

Sieck and Johnsen⁹ have suggested that part of the observed ethane is formed by successive addition of hydrogen atoms to the ethylene which is formed as a primary product in methane radiolysis. Hauser¹¹ too has tried to explain some of his findings on the basis of this mechanism. Underlying Sieck and Johnsen's argument is their finding that $G(\text{C}_2\text{H}_6)$ in methane is dose dependent, rising sharply from a value of about 1.1 at a dose of 2×10^{-3} eV/molecule to a value of 2.2 at 2×10^{-2} eV/molecule. Above this dose, $G(\text{C}_2\text{H}_6)$ remains constant up to about 6×10^{-2} eV/molecule. Similarly, they observed a sharp decrease for $G(\text{H}_2)$ from an extrapolated value of 6.47 at zero dose to a constant value of 5.74 beyond 0.02 eV/molecule energy input. Both $G(\text{C}_2\text{H}_6) = 2.2$ and $G(\text{H}_2) = 5.74$ are well accepted values for methane radiolysis.^{7,10}

As pointed out before, there is no evidence in our systems, be it with oxygen present or after complete oxygen consumption, that ethane is formed by successive reduction of either acetylene or ethylene. Indeed, we failed to find any evidence for the possibility of hydrogen addition to any $\text{C}_n\text{H}_{2n+1}$ radical in any of our experiments. This finding is in itself rather interesting and warrants further investigations. Furthermore, a careful study of ethane formation in oxygen-free methane, performed in our laboratory at doses from 0.1×10^{-2} to 10^{-2} eV/molecule, revealed a completely linear dependence of the ethane production upon the dose with $G(\text{C}_2\text{H}_6) = 2.0$.³³

Sieck and Johnsen's data, however, can readily be explained with our findings. Figure 10 contains their ethane data, recalculated and plotted with the same coordinates as we use to present our data. It seems evident that the curve does not pass through the origin of the coordinates. Assuming that no olefin impurities were present in their original methane, we can explain their ethane-production pattern by the presence of 75–90 ppm of oxygen in the parent material. This oxygen was then consumed in the early stages of the radiolysis with $-G(\text{O}_2) = 7.7$, as indicated in the insert in Figure 10. The required dose for complete oxygen removal is below their lowest dose measurement. When plotting the hydrogen data from Sieck and Johnsen in the same fashion, one obtains, based upon the apparent precision of their measurements, a straight line intercepting the y coordinate at *ca.* 10 ppm original hydrogen impurity. It seems, however, reasonable to suggest that the experimental error, involved in measuring the hydrogen production at very low doses, may have been large enough to justify plotting a straight line through the origin. In this case the dose dependency of $G(\text{H}_2)$ is no longer a valid conclusion either.

Several authors^{10,12,25,34} have suggested that, independent of the presence of oxygen, methylene can react with methane according to reaction 7 to form ethane. We have no direct evidence that ethane is formed by this



mechanism. However, it is consistent with all observations. (A close check of our data did not reveal the presence of cyclopropane-¹⁴C in D37 which contained ethylene-¹⁴C. The failure to find cyclopropane as a reaction product, however, does not exclude reaction 9 as the source of ethane, since under prevailing conditions the probability of a π -bond insertion would have to be approximately 50 times higher than the probability to undergo reaction 7 before cyclopropane could have been detected.)

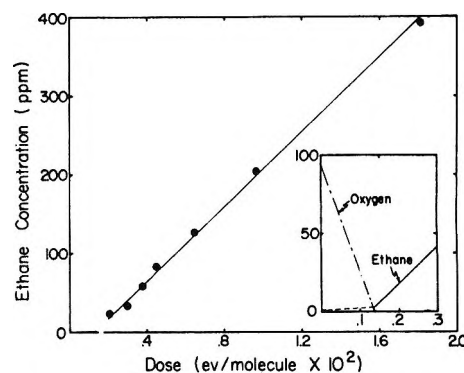
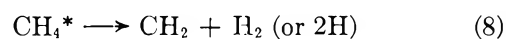


Figure 10. Replotted data for ethane formation from Sieck and Johnsen's work.⁹ The insert shows that the initially low G values found can be explained by fast removal of oxygen at very low doses.

If methylene is indeed the precursor of ethane, then $G(\text{CH}_2)$ (singlet) should be equal or larger than the observed $G(\text{C}_2\text{H}_6) = 0.276$. A likely source of methylene is provided by reaction 8, the decomposition of excited methane.^{12,34,35} The sharp increase in the ethane formation after all oxygen has been consumed can be



largely explained by reaction 5, which then is no longer in competition with reaction 6.

The rate of molecular hydrogen formation is, within experimental error, constant for all systems we report on here. In addition we observed the same $G(\text{H}_2)$ in oxygen-free methane containing 0.1 vol % acetylene.³³ It may, therefore, be surmised that while all added olefins as well as oxygen remove hydrogen atoms quantitatively they do not interfere with the formation of molecular hydrogen when present in concentrations up to 0.2 vol %. Of the major ions formed in radiolyzed methane, CH_5^+ and C_2H_5^+ have low reaction cross sections with methane; they are known, however, to react very efficiently with added olefins and also oxygen.^{36,37} It can, therefore, be assumed that the

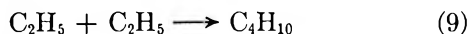
(33) P. R. Reed, personal communication.

(34) E. M. Magee, *J. Chem. Phys.*, **39**, 855 (1963).

(35) V. Aquilanti, *J. Phys. Chem.*, **69**, 3434 (1965).

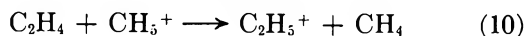
reactions of these ions have little effect upon the formation of molecular hydrogen.

Other Hydrocarbons. Based on the preceding discussion, it can be stated that oxygen completely scavenges both atomic hydrogen and methyl radicals. It also seems apparent that none of the added olefins constitutes an effective scavenger for methyl radicals since immediately after the consumption of oxygen C_2H_6 begins to increase sharply. The stable products to be expected from reactions 3, 4, and 9 were ob-



served in D37 (added ethylene- ^{14}C) as major products after oxygen removal, and the specific activities of *n*-butane and propane were found to be 1.98 and 0.91, respectively. There can obviously be little doubt that these products originate from labeled ethyl radicals. It is generally accepted³⁸ that reactions 4 and 9 are accompanied by disproportionation to an extent of 6 and 14%, respectively. Reaction 4 would, therefore, barring abstraction, have to yield 1.5–3% carbon-14-labeled methane relative to propane. The uncertainty in the calculated yield arises from the fact that no commercially available ethylene-1,2- ^{14}C is entirely double labeled. We observed methane- ^{14}C , corresponding to 1.7% of the activity found in methane. As was mentioned already, in D37 we observed traces of ethane- ^{14}C and the amount can easily be accounted for by the disproportionation accompanying reaction 9.

We have pointed out that the formation of ethane in our systems by the addition of a hydrogen atom to an ethyl radical can be excluded. We can, furthermore, surmise that added olefins, even at concentrations as low as 300 ppm, scavenge hydrogen atoms quantitatively. The corrected disappearance of ethylene in the methane-ethylene mixtures (after oxygen removal) could, therefore, be taken as a convenient measure for the production of hydrogen atoms—were it not for the fact that olefins also constitute effective ion scavengers. CH_5^+ and $C_2H_5^+$ react at least three orders of magnitude faster with ethylene than with methane.³⁶ Hydride-transfer reactions to these ions can be excluded since the proton-transfer reactions



certainly occur¹² and produce ^{14}C -labeled ethyl ions, which in turn would yield labeled ethane by hydride transfer.

Ausloos and coworker¹² have very recently suggested that the lower limit of $G(D)$ in CD_4 is 4.3 by using H_2S as a D atom interceptor. They pointed out that this value may be in error owing to the interception of $C_2D_5^+$ (and other ions) by H_2S causing a suppression of D atom formation which would occur in pure methane by neutralization. In our system CH_5^+ is effectively transferred into a (labeled) ethyl ion by reaction 10 and this ion will react in turn *via* reaction 11. Eventual neutralization of ethyl ions will yield ethylene and hydrogen atoms with no net loss in either ethylene through proton transfer nor hydrogen atoms through neutralization. However, since our present data do not allow the assessment of the extent of condensation reactions and the subsequent reactions of the product ions, the quantitative interpretation of our $-G(C_2H_4)$ value has to await further information.

Carbon Monoxide. In D33 and D35 it was observed that the CO production is linear with respect to low doses, whereas at higher doses the rate of formation follows the square of the dose (see Figures 7 and 8). The radioactivity in carbon monoxide shows that all comes from acetylene. Mikhailov, *et al.*, have suggested³⁹ that CO is a decomposition product of formaldehyde which we did observe in D33 and D35 with a specific activity indication that it comes primarily from the acetylene- ^{14}C . These findings can be explained then by an HO_2 attack on acetylene forming both CO and formaldehyde (zero order) and a subsequent decomposition (first order) of CH_2O to form CO.

Acknowledgments. The financial support received from the Advanced Research Project Agency is gladly acknowledged. We are grateful for the permission to use the facilities of the Radiation Laboratory at Notre Dame University for some preliminary studies. We also have to thank a referee for drawing our attention to ref 12 which had not yet appeared when the first manuscript was written.

(36) S. Wexler, *et al.*, in "Ion Molecule Reactions in the Gas Phase," R. F. Gould, Ed., *Advances in Chemistry Series*, No. 58, American Chemical Society, Washington, D. C., p 193.

(37) P. Ausloos, S. G. Lias, and R. Gorden, *J. Chem. Phys.*, **39**, 3341 (1963).

(38) J. A. Kerr and A. F. Trotman-Dickenson, "Progress in Reaction Kinetics," Vol. 1, G. Porter, Ed., Pergamon Press, Ltd., 1961, Chapter 3.

(39) B. M. Mikhailov, M. E. Kuimova, and V. S. Bogdanov, *Proc. 1st All-Union Conf. Radiat. Chem., Moscow*, **5**, 223 (1957).

Vicinal Effects on the Optical Activity of Some Adenine Nucleosides

by Daniel W. Miles, S. J. Hahn, Roland K. Robins, Morris J. Robins, and Henry Eyring

Department of Chemistry and Institute for the Study of Rate Processes, University of Utah, Salt Lake City, Utah 84112
(Received July 20, 1967)

The optical rotatory dispersion, absorption, and, in some cases, the circular dichroism of some adenine nucleosides having diverse substituents in the carbohydrate ring have been examined. Solvent and temperature studies have also been performed when possible. Explanations for the changes in rotation with substituent are sought through theoretical means in correlation with available structural information. The changes in the 260-m μ Cotton effect produced by the introduction of new π -electron systems can be accounted for quantitatively.

I. Introduction

Concurrently with the study of chromophoric substituent effects^{1,2} we have examined the optical rotatory dispersion (ORD), absorption spectra, and, in some cases, the circular dichroism (CD) of purine nucleosides having diverse substituents on the carbohydrate ring. Previous work in this area has shown that the replacement of the 2'-OH group by hydrogen or chlorine does not alter the sign of the characteristic 260-m μ Cotton effect,³ while, in contrast, a sulfur substituent at the 5' position does reverse the sign,⁴ and the optical activity of 5'-mononucleotides and the corresponding nucleoside are not significantly different.^{5,6} Thus it appears that the phosphate group, despite its polar nature and π electrons, does not contribute significantly to the rotation. Recent interpretations⁷⁻⁹ of ORD and CD studies on dinucleoside phosphates and other model systems of RNA and DNA have used this fact to justify omitting all phosphate-base interactions. Meanwhile, several conflicting proposals, based mainly on ORD studies, have been made regarding the conformation of ribonucleosides^{3,4} in solution.

In this paper we describe the optical activity of some adenine nucleosides having, for the most part, polar and moderate to weakly polarizable substituents. The optical rotatory dispersion of these derivatives are found to differ only slightly from one another. In addition we have measured the optical rotatory dispersion and circular dichroism of several derivatives having nonpolar and moderately polarizable groups, such as the carbon-carbon double bond and the thioether group. These substituents generally induce dramatic changes in the optical activity, with almost no effect on the absorption spectra down to 220 m μ . Temperature studies demonstrate the presence of preferred conformations in the adenine nucleosides. A quantitative analysis based on the Kirkwood-Tinoco polarizability expression is carried out on representative compounds. All possible sugar-base conformations and several puckered conformations of the ribose moiety have been considered with the aid of a computer.

These results, intended to be but a first step toward the use of optical-rotation theory on the purine and pyrimidine nucleosides, demonstrate the dependence of optical rotation on the nature of the substituents, the sugar-base torsion angle,¹⁰ and changes in the puckered conformations of the ribose residue. While an analysis of these preliminary results in concert with other physicochemical evidence tend to suggest that an *anti* range of the torsion angle is preferred in adenine nucleosides, conclusive evidence awaits a more systematic study on suitable model adenine nucleosides.

II. Experimental Procedures

Absorption and optical rotatory dispersion curves were determined on the Cary Model 14 spectrophotometer and the Cary Model 60 spectropolarimeter, respectively. The circular dichroism curves were measured on the Cary Model 6001 CD attachment for the Model 60. The CD unit was calibrated using the Cary Model 1401 circular dichroism attachment for the Model 14. The standard used was an aqueous solution of *d*-10-camphorsulfonic acid (J. T. Baker, Lot No. 9-361) with an $\epsilon_L - \epsilon_R$ of 2.2 at 290 m μ . The Cary thermostatable sample cell of path length 1 cm was used

- (1) D. W. Miles, R. K. Robins, and H. Eyring, *Proc. Nat. Acad. Sci. U. S.*, **57**, 1137 (1967).
- (2) D. W. Miles, R. K. Robins, and H. Eyring, *J. Phys. Chem.*, **71**, 3931 (1967).
- (3) T. R. Emerson, R. Swan, and T. L. V. Ulbricht, *Biochem. Biophys. Res. Commun.*, **22**, 505 (1966).
- (4) W. A. Klee and S. H. Mudd, *Biochemistry*, **6**, 988 (1967).
- (5) C. Y. Lin, D. W. Urry, and H. Eyring, *Biochem. Biophys. Res. Commun.*, **17**, 642 (1964).
- (6) J. T. Yang, T. Samejima, and P. K. Sarkar, *Biopolymers*, **4**, 623 (1966).
- (7) M. M. Warshaw, C. A. Bush, and I. Tinoco, *Biochem. Biophys. Res. Commun.*, **18**, 633 (1965).
- (8) C. A. Bush and J. Brahms, *J. Chem. Phys.*, **46**, 79 (1967).
- (9) C. A. Bush and I. Tinoco, *J. Mol. Biol.*, **23**, 601 (1967).
- (10) J. Donohue and K. N. Trueblood, *J. Mol. Biol.*, **2**, 363 (1960). The torsion angle, ϕ_{CN} , is defined as the angle formed by the trace of the plane with the projection of the C_{1'}-O bond when the projection is taken along the glycosidic bond. The angle is taken as zero when the carbohydrate ring oxygen is antiplanar to C₂ of the purine or pyrimidine ring, and positive angles are taken as those measured in a clockwise direction when viewing the C_{1'} to the ring nitrogen.

Table I: The ORD Measurements of Adenosine and Related Derivatives

Compound	Structure ^a	Posn. ^b m μ	[M'] ^c	Amplitude	λ_{\max} . m μ	ϵ_{\max}																																																																																																							
2',3',5'-Trideoxyadenosine	I	276	-1,400	-2,200	260	14,600																																																																																																							
		245	+800				2',3',5'-Trideoxy-2',3'-dideoxyadenosine	II	270	+5,400	+13,000	259.5	14,800	240	-7,600	Adenosine	III	276	-2,700	-4,000	260.5	14,900	245	+1,300	2',3'-Dideoxy-2',3'-dideoxyadenosine	IV	270	+5,000	+12,000	259.5	15,200	240	-7,000	6-Amino-9-(5'-S-ethyl-5'-thio-2',3',5'-trideoxy-2',3'-dideoxyhydro- β -D-glycero-pentofuranosyl)purine	V	272	+13,000	+37,000	259.5	14,900	239	-24,000	Adenosine 5'-monophosphate	VI	272	-2,800	-4,200	260	15,000	246	+1,400	2',3'-Dideoxyadenosine	VII	273	-1,600	-2,600	259.5	14,600	246	+1,000	Adenosine 5'-monoacetate	VIII	274	-2,500	-4,000	260	14,800	246	+1,500	Adenosine 5'-monopropionate	IX	274	-2,600	-4,100	260	14,900	246	+1,500	2'-Deoxyadenosine	X	272	-1,400	-3,200	259.5	14,900	245	+1,800	2'-Deoxyadenylic acid	XI	270	-2,200	-3,400	260	15,000	250	+1,200	5'-Deoxyadenosine	XII	274	-2,000	-3,900	260	14,800	246	+1,900	2',3'-O-Isopropylideneadenosine	XIII	276	-2,600
2',3',5'-Trideoxy-2',3'-dideoxyadenosine	II	270	+5,400	+13,000	259.5	14,800																																																																																																							
		240	-7,600				Adenosine	III	276	-2,700	-4,000	260.5	14,900	245	+1,300	2',3'-Dideoxy-2',3'-dideoxyadenosine	IV	270	+5,000	+12,000	259.5	15,200	240	-7,000	6-Amino-9-(5'-S-ethyl-5'-thio-2',3',5'-trideoxy-2',3'-dideoxyhydro- β -D-glycero-pentofuranosyl)purine	V	272	+13,000	+37,000	259.5	14,900	239	-24,000	Adenosine 5'-monophosphate	VI	272	-2,800	-4,200	260	15,000	246	+1,400	2',3'-Dideoxyadenosine	VII	273	-1,600	-2,600	259.5	14,600	246	+1,000	Adenosine 5'-monoacetate	VIII	274	-2,500	-4,000	260	14,800	246	+1,500	Adenosine 5'-monopropionate	IX	274	-2,600	-4,100	260	14,900	246	+1,500	2'-Deoxyadenosine	X	272	-1,400	-3,200	259.5	14,900	245	+1,800	2'-Deoxyadenylic acid	XI	270	-2,200	-3,400	260	15,000	250	+1,200	5'-Deoxyadenosine	XII	274	-2,000	-3,900	260	14,800	246	+1,900	2',3'-O-Isopropylideneadenosine	XIII	276	-2,600	-3,800	260	14,900	246	+1,200				
Adenosine	III	276	-2,700	-4,000	260.5	14,900																																																																																																							
		245	+1,300				2',3'-Dideoxy-2',3'-dideoxyadenosine	IV	270	+5,000	+12,000	259.5	15,200	240	-7,000	6-Amino-9-(5'-S-ethyl-5'-thio-2',3',5'-trideoxy-2',3'-dideoxyhydro- β -D-glycero-pentofuranosyl)purine	V	272	+13,000	+37,000	259.5	14,900	239	-24,000	Adenosine 5'-monophosphate	VI	272	-2,800	-4,200	260	15,000	246	+1,400	2',3'-Dideoxyadenosine	VII	273	-1,600	-2,600	259.5	14,600	246	+1,000	Adenosine 5'-monoacetate	VIII	274	-2,500	-4,000	260	14,800	246	+1,500	Adenosine 5'-monopropionate	IX	274	-2,600	-4,100	260	14,900	246	+1,500	2'-Deoxyadenosine	X	272	-1,400	-3,200	259.5	14,900	245	+1,800	2'-Deoxyadenylic acid	XI	270	-2,200	-3,400	260	15,000	250	+1,200	5'-Deoxyadenosine	XII	274	-2,000	-3,900	260	14,800	246	+1,900	2',3'-O-Isopropylideneadenosine	XIII	276	-2,600	-3,800	260	14,900	246	+1,200													
2',3'-Dideoxy-2',3'-dideoxyadenosine	IV	270	+5,000	+12,000	259.5	15,200																																																																																																							
		240	-7,000				6-Amino-9-(5'-S-ethyl-5'-thio-2',3',5'-trideoxy-2',3'-dideoxyhydro- β -D-glycero-pentofuranosyl)purine	V	272	+13,000	+37,000	259.5	14,900	239	-24,000	Adenosine 5'-monophosphate	VI	272	-2,800	-4,200	260	15,000	246	+1,400	2',3'-Dideoxyadenosine	VII	273	-1,600	-2,600	259.5	14,600	246	+1,000	Adenosine 5'-monoacetate	VIII	274	-2,500	-4,000	260	14,800	246	+1,500	Adenosine 5'-monopropionate	IX	274	-2,600	-4,100	260	14,900	246	+1,500	2'-Deoxyadenosine	X	272	-1,400	-3,200	259.5	14,900	245	+1,800	2'-Deoxyadenylic acid	XI	270	-2,200	-3,400	260	15,000	250	+1,200	5'-Deoxyadenosine	XII	274	-2,000	-3,900	260	14,800	246	+1,900	2',3'-O-Isopropylideneadenosine	XIII	276	-2,600	-3,800	260	14,900	246	+1,200																						
6-Amino-9-(5'-S-ethyl-5'-thio-2',3',5'-trideoxy-2',3'-dideoxyhydro- β -D-glycero-pentofuranosyl)purine	V	272	+13,000	+37,000	259.5	14,900																																																																																																							
		239	-24,000				Adenosine 5'-monophosphate	VI	272	-2,800	-4,200	260	15,000	246	+1,400	2',3'-Dideoxyadenosine	VII	273	-1,600	-2,600	259.5	14,600	246	+1,000	Adenosine 5'-monoacetate	VIII	274	-2,500	-4,000	260	14,800	246	+1,500	Adenosine 5'-monopropionate	IX	274	-2,600	-4,100	260	14,900	246	+1,500	2'-Deoxyadenosine	X	272	-1,400	-3,200	259.5	14,900	245	+1,800	2'-Deoxyadenylic acid	XI	270	-2,200	-3,400	260	15,000	250	+1,200	5'-Deoxyadenosine	XII	274	-2,000	-3,900	260	14,800	246	+1,900	2',3'-O-Isopropylideneadenosine	XIII	276	-2,600	-3,800	260	14,900	246	+1,200																															
Adenosine 5'-monophosphate	VI	272	-2,800	-4,200	260	15,000																																																																																																							
		246	+1,400				2',3'-Dideoxyadenosine	VII	273	-1,600	-2,600	259.5	14,600	246	+1,000	Adenosine 5'-monoacetate	VIII	274	-2,500	-4,000	260	14,800	246	+1,500	Adenosine 5'-monopropionate	IX	274	-2,600	-4,100	260	14,900	246	+1,500	2'-Deoxyadenosine	X	272	-1,400	-3,200	259.5	14,900	245	+1,800	2'-Deoxyadenylic acid	XI	270	-2,200	-3,400	260	15,000	250	+1,200	5'-Deoxyadenosine	XII	274	-2,000	-3,900	260	14,800	246	+1,900	2',3'-O-Isopropylideneadenosine	XIII	276	-2,600	-3,800	260	14,900	246	+1,200																																								
2',3'-Dideoxyadenosine	VII	273	-1,600	-2,600	259.5	14,600																																																																																																							
		246	+1,000				Adenosine 5'-monoacetate	VIII	274	-2,500	-4,000	260	14,800	246	+1,500	Adenosine 5'-monopropionate	IX	274	-2,600	-4,100	260	14,900	246	+1,500	2'-Deoxyadenosine	X	272	-1,400	-3,200	259.5	14,900	245	+1,800	2'-Deoxyadenylic acid	XI	270	-2,200	-3,400	260	15,000	250	+1,200	5'-Deoxyadenosine	XII	274	-2,000	-3,900	260	14,800	246	+1,900	2',3'-O-Isopropylideneadenosine	XIII	276	-2,600	-3,800	260	14,900	246	+1,200																																																	
Adenosine 5'-monoacetate	VIII	274	-2,500	-4,000	260	14,800																																																																																																							
		246	+1,500				Adenosine 5'-monopropionate	IX	274	-2,600	-4,100	260	14,900	246	+1,500	2'-Deoxyadenosine	X	272	-1,400	-3,200	259.5	14,900	245	+1,800	2'-Deoxyadenylic acid	XI	270	-2,200	-3,400	260	15,000	250	+1,200	5'-Deoxyadenosine	XII	274	-2,000	-3,900	260	14,800	246	+1,900	2',3'-O-Isopropylideneadenosine	XIII	276	-2,600	-3,800	260	14,900	246	+1,200																																																										
Adenosine 5'-monopropionate	IX	274	-2,600	-4,100	260	14,900																																																																																																							
		246	+1,500				2'-Deoxyadenosine	X	272	-1,400	-3,200	259.5	14,900	245	+1,800	2'-Deoxyadenylic acid	XI	270	-2,200	-3,400	260	15,000	250	+1,200	5'-Deoxyadenosine	XII	274	-2,000	-3,900	260	14,800	246	+1,900	2',3'-O-Isopropylideneadenosine	XIII	276	-2,600	-3,800	260	14,900	246	+1,200																																																																			
2'-Deoxyadenosine	X	272	-1,400	-3,200	259.5	14,900																																																																																																							
		245	+1,800				2'-Deoxyadenylic acid	XI	270	-2,200	-3,400	260	15,000	250	+1,200	5'-Deoxyadenosine	XII	274	-2,000	-3,900	260	14,800	246	+1,900	2',3'-O-Isopropylideneadenosine	XIII	276	-2,600	-3,800	260	14,900	246	+1,200																																																																												
2'-Deoxyadenylic acid	XI	270	-2,200	-3,400	260	15,000																																																																																																							
		250	+1,200				5'-Deoxyadenosine	XII	274	-2,000	-3,900	260	14,800	246	+1,900	2',3'-O-Isopropylideneadenosine	XIII	276	-2,600	-3,800	260	14,900	246	+1,200																																																																																					
5'-Deoxyadenosine	XII	274	-2,000	-3,900	260	14,800																																																																																																							
		246	+1,900				2',3'-O-Isopropylideneadenosine	XIII	276	-2,600	-3,800	260	14,900	246	+1,200																																																																																														
2',3'-O-Isopropylideneadenosine	XIII	276	-2,600	-3,800	260	14,900																																																																																																							
		246	+1,200																																																																																																										

^a Structural formulas are given in Figure 1. ^b Extremum positions of the ORD curves. ^c The Lorenz correction has been applied to all data reported in this paper using Na D line values for n .

for all optical rotatory dispersion measurements so as to virtually eliminate the problem of base-line shifting (provided suitable care was exercised in manipulating the sample compartment). All measurements were triplicated and gave average values within $\pm 0.0004^\circ$. The temperature of the cell compartment was controlled by the P. M. Tamson circulation thermostat Model T-3, with the cooling spiral accessory for low-temperature studies. In the temperature study, it was necessary to guard against heat-induced decomposition. All measurements were performed first at the minimum temperature and then at the maximum temperature. The intervals between were measured as the sample was returned stepwise to the minimum temperature. In all reported data the two minimum curves were superimposable. Cell temperature was monitored by thermocouple techniques.

All solvents were of spectral grade. All compounds were made and purified in the laboratory of Professor Robins or were commercial samples of high purity. Details of the preparation and characterization of these nucleosides are given elsewhere.¹¹

The optical rotatory dispersion data are reported in terms of the reduced molecular rotation, $[M']$, defined as $[M'] = 100\alpha/cL(3/n^2 + 2)$, where α is the observed

rotation in degrees, c is the concentration in moles per liter of the solute, L is the path length in centimeters, and n should be the index of refraction of the solution at the wavelength that α is measured. However, we have used only the Na D line value in the Lorenz correction factor for the internal electric field. Values of $[M']$ were corrected for volume expansion upon heating.

III. Results

The results of the ORD and absorption measurements on the adenine ribonucleosides derivatives are summarized in Table I. The ORD curves of the adenine nucleosides display but a single Cotton effect above 230 m μ centered at approximately 260 m μ . The structural formulas of the compounds studied are contained in Figure 1.

Figure 2 shows the optical rotatory dispersion mea-

(11) J. R. McCarthy, Jr., M. J. Robins, L. B. Townsend, and R. K. Robins, *J. Amer. Chem. Soc.*, **88**, 1549 (1966); M. J. Robins, J. R. McCarthy, Jr., and R. K. Robins, *Biochemistry*, **5**, 224 (1966); M. J. Robins and R. K. Robins, *J. Amer. Chem. Soc.*, **86**, 3585 (1964); R. J. Rousseau, L. B. Townsend, and R. K. Robins, *Biochemistry*, **5**, 224 (1966); J. R. McCarthy, Jr., M. J. Robins, and R. K. Robins, *Chem. Commun.*, 536 (1967). The authors wish to thank G. B. Whitfield, Jr., of the Upjohn Co. for an authentic sample of decoyinine (Angustmycin A) used in this study.

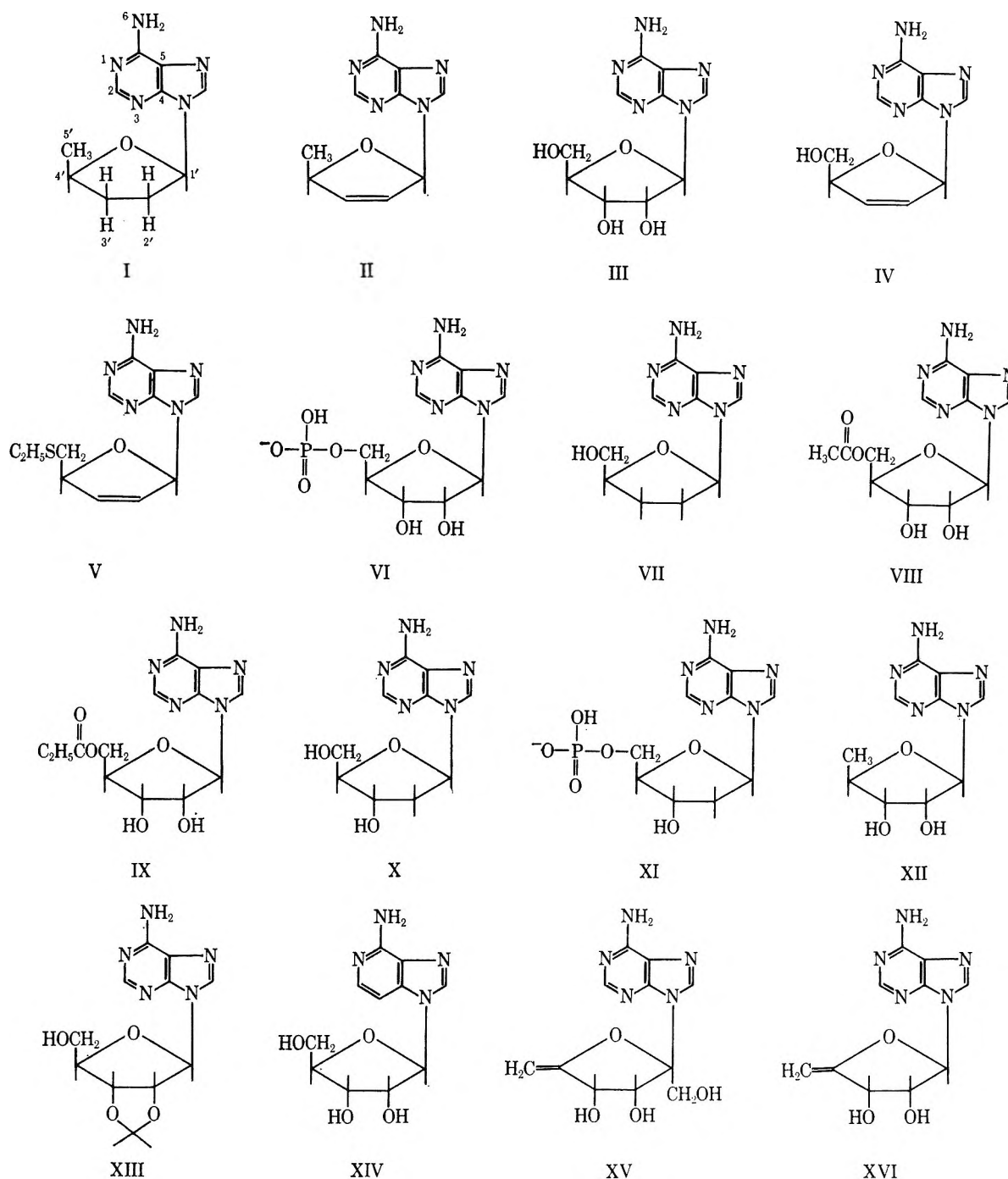


Figure 1. The structural formulas of the compounds discussed in this paper.

sured in the uv region for 2',3',5'-trideoxyadenosine (I), 2',3',5'-trideoxy-2',3'-didehydroadenosine (II), adenosine (III), 2',3'-dideoxy-2',3'-didehydroadenosine (IV), 6-amino-9-(5'-S-ethyl-5'-thio-2',3',5'-trideoxy-2',3'-didehydro- β -D-glycero-pentofuranosyl)purine (V), and adenosine 5'-monophosphate (VI), which are typical of the compounds studied and which will be emphasized in the Theory and Discussion sections. Among these compounds are three unsaturated furano-

syladenine nucleosides. The sign is negative for all saturated furanosyladenine nucleosides and positive for the unsaturated derivatives with the π -electron system α , β , to $C_{1'}$. The effect of a carbon-carbon double bond in this position is best demonstrated by comparing the ORD curves of structure II and its reduced form, structure I. The substitution of a π bond for 2'-H and 3'-H changes the amplitude from -2200 to 13,000. The theoretical treatment of the

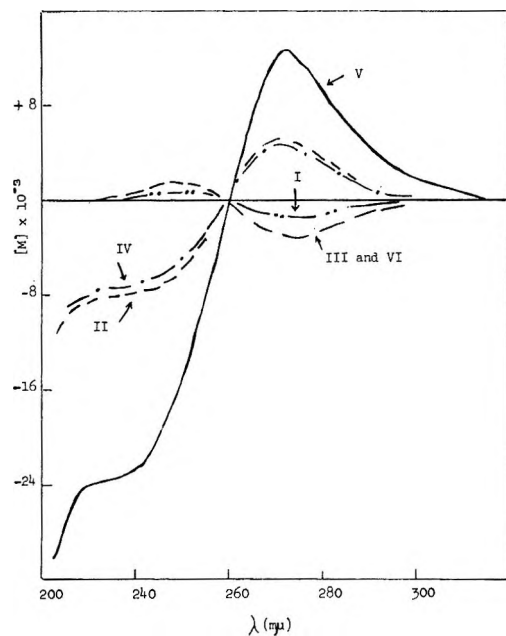


Figure 2. The optical rotatory dispersion (in aqueous solution at pH 7) of some adenosine ribonucleoside derivatives. The curves for compounds I and II demonstrate the effect of the carbon-carbon double bond on the 260-m μ Cotton effect. Curves for compounds III and VI (which appear to be identical owing to choice of coordinates) show the effect of the 5'-phosphate group. Curves for compounds IV and V show the effect of the 5'-thioether group.

next section predicts that the base-double bond interactions will contribute approximately four times as much to the rotation as the base-single bond interactions for the same spatial relationship.

Hydroxyl groups at C₂', C₃', and C₅' apparently make negative contributions to the rotation, since the amplitude of the 260-m μ Cotton effect decreases with successive removal of the hydroxyl function. Thus the amplitude of structure III is greater than the amplitude of structure XII and the amplitude of structure III > X > VII > I. The 5'-OH in the unsaturated derivatives seems to make a negative contribution also (compare the amplitude of structure II with that of IV). Polar substituents with π -electrons systems, such as the phosphate or acetyl groups when attached to the 5'-carbon, are found to be just slightly more effective negative contributors to the rotation than the hydroxyl function. For example, compare the amplitude of adenosine, III (-4000) with the amplitude of adenosine 5'-monophosphate, VI (-4200). On the other hand, a remarkable enhancement in the rotation is observed when a nonpolar substituent replaces a polar substituent at the 5'-carbon. For example, compare the amplitude of structure II (13,000) with that of structure V (37,000). These effects are even more dramatically revealed in the circular dichroism spectra of these compounds. Figure 3 shows that adenosine (III) and adenosine 5'-monophosphate (VI) give maxi-

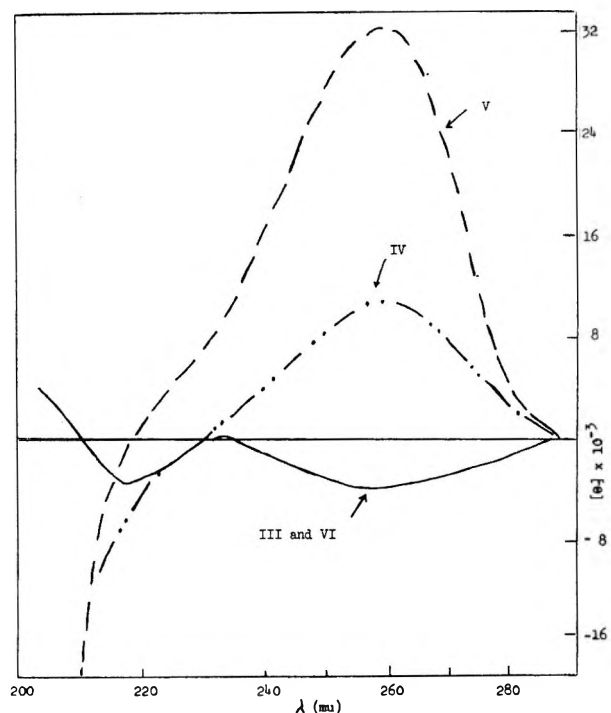


Figure 3. The circular dichroism curves of some adenosine ribonucleoside derivatives in aqueous solution at pH 7. These curves were used to obtain the rotational strengths of the 260-m μ Cotton effects.

imum ellipticities of -2100 and -2200, respectively,¹² at 260 m μ , whereas compounds II (with the C₂'-C₃' double bond) and compound V (with both the C₂'-C₃' double bond and the 5'-thioether group) give large positive ellipticities at 260 m μ of 11,000 and 30,000, respectively. Figure 4 shows the circular dichroic spectra of angustmycin A (XV) and 4'-exocyclic methylene adenosine (XVI). Both these compounds have a C₄'-C₅' double bond. These compounds, in contrast to compounds II, IV, and V, give a small negative 260-m μ CD band. Adequate interpretation of the ORD and CD data of adenine nucleosides should include explanations of the low amplitudes exhibited by adenosine 5'-monophosphate, angustmycin A, and 4'-exocyclic methylene adenosine, and the remarkable effect of the 5'-thioether group and the C₂'-C₃' double bond. A more detailed discussion of these effects will follow the development of the theory.

Figure 5 contains the results of temperature and solvent studies on the nucleosides containing the C₂'-C₃' double bond. The measured amplitudes of the 260-m μ Cotton effect are given as a function of temperature in water, methanol, acetonitrile, and dioxane. Decreases in amplitude of 30-35% are observed over a temperature range of 80°. The unsaturated nucleoside with the thioether function (V) is found to undergo a 50% loss of amplitude by the combination of temperature

(12) The CD curves of structure III and VI in Figure 3 appear to be superimposable because of choice of coordinates.

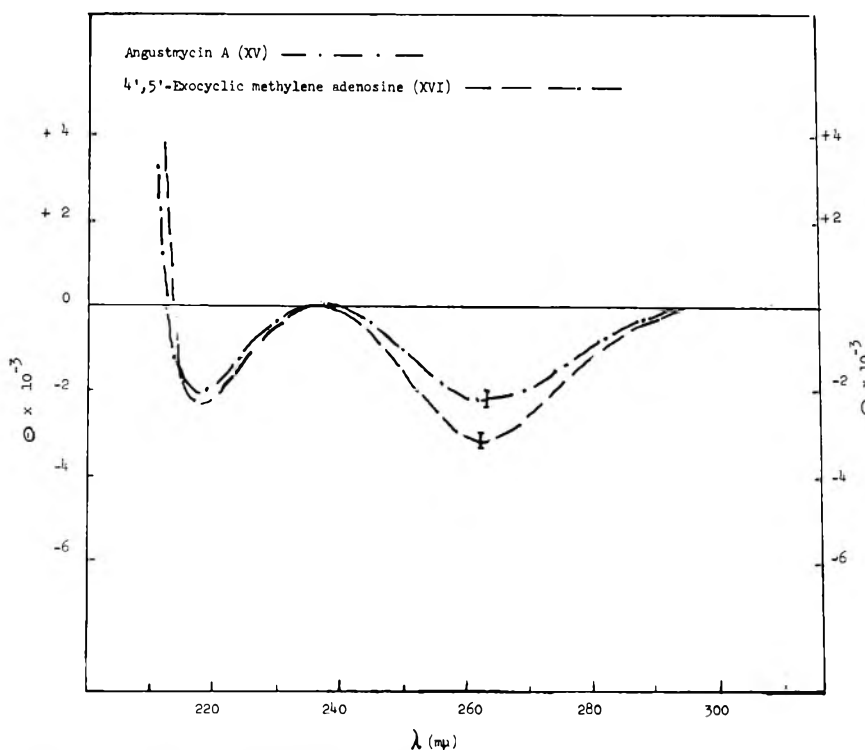


Figure 4. The circular dichroism curves of angustmycin A (XV) and 4'-exocyclic methyleneadenosine (XVI) in aqueous solution at pH 7.

and solvent effects. The temperature effects on compound II and IV (see Figure 5), which cannot be ascribed to changes in solvent perturbation with temperature since the circular dichroism curves of the rigid cyclonucleosides are invariant to temperature changes over this temperature range,¹³ definitely support the idea of a preferred range of torsion angle.¹⁴ For example, the amplitude of the 260-m μ Cotton effect of II decreases from 14,000 to 9000 over the temperature range 0–80°.

In Figure 6 we show the ORD of 3-deazaadenosine (XIV) at neutral and acidic pH values. The complexity in the 220–250-m μ region for the pH 7 curve has been attributed to the $n \rightarrow \pi^*$ transition in this region, which is blue shifted upon protonation.¹⁵ The 260-m μ Cotton effect is negative and slightly smaller than the 260-m μ Cotton effect of adenosine (the Lorentz correction factor has not been applied to Figure 6). This compound is included in this study because the absence of the nitrogen at position 3 eliminates the electrostatic repulsion between the oxygen in the carbohydrate ring and the nitrogen. This interaction has been considered as one of the factors³ that stabilize the adenosine derivatives in the *anti* conformation. However, the implications of Figure 6 are complicated by the fact that removal of the N-3 nitrogen is predicted to shift the B_{2u} -transition moment by approximately 30° (see Figure 13 and discussion of ref 2).

IV. Theory

Several recent papers^{2,8,9,16,17} have utilized the general

treatment of optical rotation devised in 1962 by Tinoco.¹⁸ Tinoco's derivation retains the formalism of the one-electron model as originated by Condon, Altar, and Eyring¹⁹ and Gorin, Walter, Kauzmann, and Eyring^{20,21} which focused attention on the contribution of individual electronic transitions. The Kirkwood model is revised by the Tinoco treatment so that it too emphasizes the individual rotational strengths. For Cotton effects of strong absorption bands interacting with vicinal groups containing nonpolar but fairly polarizable substituents, the coupled oscillator model of Kirkwood should account for most of the rotational strength. The rotational strength of the 260-m μ adenine transition arising from each base-sugar

(13) D. W. Miles, R. K. Robins, and H. Eyring, unpublished data.

(14) That changes in rotation with temperature does not ensue from changes in the conformational equilibrium involving 3'-*endo*, 3'-*exo*, or 2'-*endo* puckered conformations of the ribose ring is indicated by our calculations (see next sections). The extreme situation involving 100% depopulation of one puckered state in favor of another generally affects the calculations by only 10–20%. There is no evidence that more drastic changes in ribose conformation can be induced by temperature.

(15) D. W. Miles, Ph.D. Thesis, University of Utah, Salt Lake City, Utah, 1967.

(16) R. W. Woody and I. Tinoco, *J. Chem. Phys.*, **46**, 4927 (1967).

(17) E. S. Pysh, *J. Mol. Biol.*, **23**, 587 (1967).

(18) I. Tinoco, *Advan. Chem. Phys.*, **4**, 113 (1962).

(19) E. U. Condon, W. Altar and H. Eyring, *J. Chem. Phys.*, **5**, 753 (1937).

(20) E. Gorin, J. Walter, and H. Eyring, *ibid.*, **6**, 824 (1938).

(21) W. J. Kauzmann, J. Walter, and H. Eyring, *Chem. Rev.*, **26**, 339 (1940).

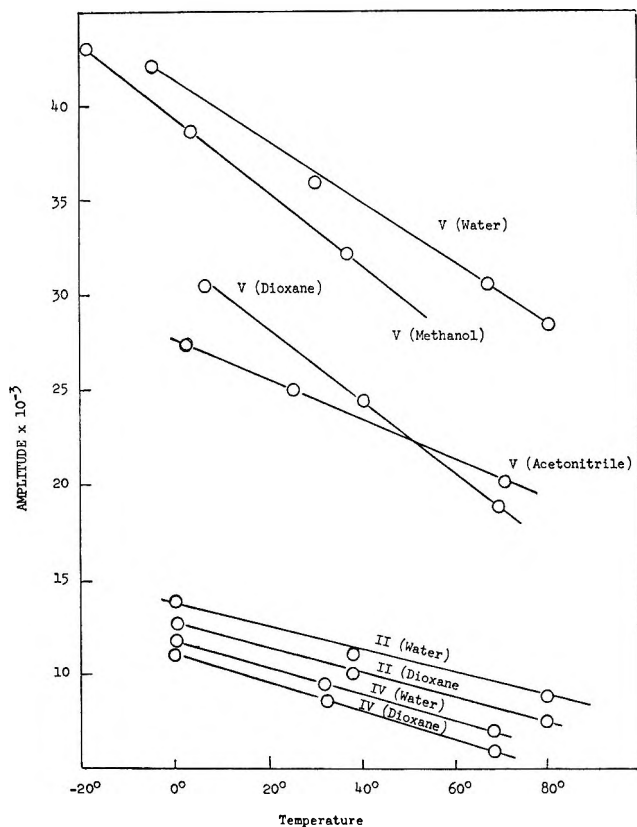


Figure 5. The amplitude of the 260-m μ Cotton effect as a function of temperature and solvent of the unsaturated adenine nucleosides. Roman numerals refer to the structures of Figure 1.

bond interaction is given by the Kirkwood-Tinoco¹⁸ expression

$$R_j = \frac{\pi \nu_a \nu_0^2 \mu_{i0a}^2 (\alpha_{33} - \alpha_{11})_j (GF)_j}{c(\nu_0^2 - \nu_a^2)}$$

$$(GF)_j = \frac{1}{r_{ij}^3} \left[\hat{e}_i \cdot \hat{e}_j - \frac{3 (\hat{e}_i \cdot r_{ij})(\hat{e}_j \cdot r_{ij})}{r_{ij}^2} \right] \hat{e}_i \times \hat{e}_j \cdot r_{ij} \quad (1)$$

where the symbols and the center of the adenine ring used in the calculation of r_{ij} are as defined in ref 2. Equation 1 has been used in several recent calculations to account for the rotational strength arising from the interaction of strong electric dipole transitions with the far-uv transitions of the vicinal groups.^{2,8,17,18} The emphasis on bond polarizabilities rather than group polarizabilities eliminates the arbitrary division of the molecule into groups. For a given i, j pair, the rotational strength is seen to be a function of the distance r_{ij} , their mutual orientation, and the anisotropy ($\alpha_{33} - \alpha_{11}$) of the j th bond. The polarizability ellipsoid for each bond is localized at the midpoint of each bond. The anisotropy of bond polarizabilities (taken from the work of Lefevre²²) and ν_0 (see ref 2) to be used in eq 1 are given in Table II. These values when substituted into eq 1 (along with $\nu_a = 1.15 \times 10^{15} \text{ sec}^{-1}$, $\mu_{i0a} = 4D^9$, $\gamma = 45^\circ$ (transition-moment direction²³))

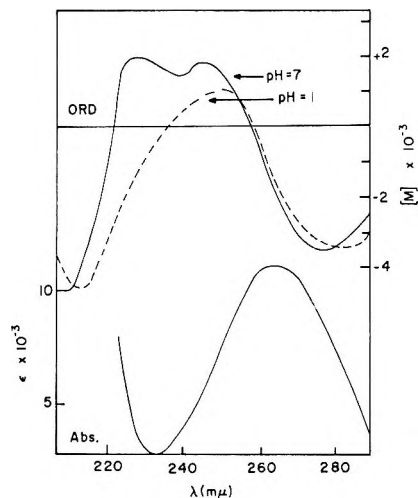


Figure 6. The optical rotatory dispersion and absorption spectra of 3-deazaadenosine at neutral and acidic pH values.

Table II

Bond	$10^{24}(\alpha_{33} - \alpha_{11})$, cc	$10^{-16}\nu_0$, sec ⁻¹
C—C	0.75	2.3
C—O	0.43	2.0
O—H	0.30	2.0
C=C	2.14	1.8
C—H	0.00	2.3

which are parameters characteristic of the 260-m μ transition of adenine) give for the specific case where the subscript j refers to a C—C, C=C, C—O, or O—H bond (in biots²⁴)

$$R_{C=C} = 670(GF)_{C=C}$$

$$R_{C-C} = 190(GF)_{C-C}$$

$$R_{C-O} = 130(GF)_{C-O}$$

$$R_{O-H} = 90(GF)_{O-H}$$

In the above expressions the geometrical factor, GF, must be expressed in ångström units. The geometrical factor can be evaluated once the atomic coordinates of

(22) R. J. W. LeFevre and C. G. LeFevre, *J. Chem. Soc.*, 3549 (1956); R. J. W. LeFevre, A. Sundaram, and R. K. Pierens, *ibid.*, 479 (1963); M. Aroney and R. J. W. LeFevre, *ibid.*, 3002 (1958); R. Bramley, C. G. LeFevre, R. J. W. LeFevre, and B. P. Rao, *ibid.*, 1183 (1959).

(23) Stewart and Jensen (R. F. Stewart and L. H. Jensen, *J. Chem. Phys.*, 40, 2071 (1964)) have found two orientations ($\gamma = 45^\circ$ or -3° relative to an axis from C₄-C₅ and measured positive toward C₆) for the B_{2u} transition of the adenine chromophore which are consistent with the crystal symmetry and dichroic ratio. We have chosen the former value because it is more consistent with theoretical means of estimating polarization directions and because this orientation gave such good agreement in a recent theoretical treatment of cycloadenosine.²

(24) This unit has a value of 10^{-40} cgs (L. Velluz, M. Legrand, and M. Grosjean, "Optical Circular Dichroism," Academic Press Inc., New York, N. Y., 1965, p 75.

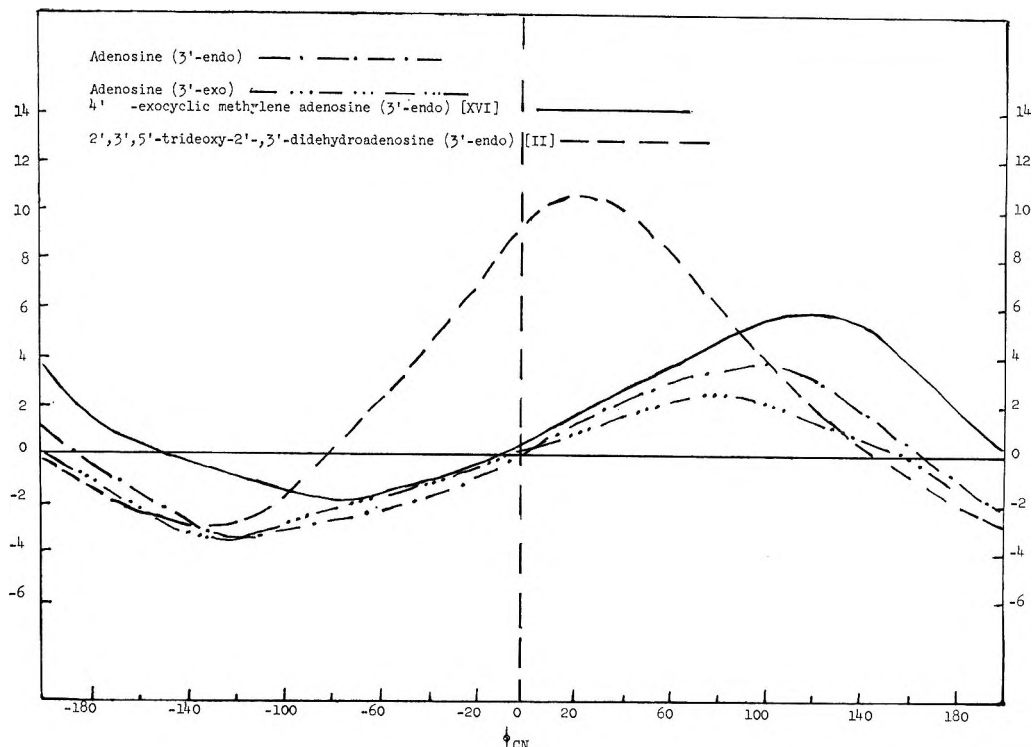


Figure 7. The calculated rotational strengths of adenosine (3'-endo), adenosine (3'-exo), 4'-exocyclic methyleneadenosine (3'-endo), and 2',3',5'-trideoxy-2',3'-didehydroadenosine (3'-endo) as a function of the torsion angle. The calculations were based on eq 1 of the text summed over all i, j pairs.

the system are known. In this study, the coordinates for adenosine in the 3'-endo conformation are taken from the X-ray data.²⁵ Drieding and Fiesers' molecular models were used to estimate the coordinates of the other molecules. Using eq 1 we have calculated *via* computer the rotational strengths of the 260-m μ adenine band for all values of the sugar-base torsion angle. The calculations were made with the ribose moiety in the 3'-endo conformation, *i.e.*, C'-3 is out of the plane defined by C'-1, the furanose ring oxygen, and C'-4 and is lying on the same side of the sugar plane as C'-5 and the ring of the base. Calculations were also made with the ribose moiety in the 3'-exo and 2'-endo conformations. The results for the calculations performed on adenosine (3'-endo), adenosine (3'-exo), and 4'-exocyclic methyleneadenosine (3'-endo) are displayed graphically in Figure 7. In comparing experiment with theory, we shall be concerned more with explaining relative changes in the rotation as a function of substituents and changes in the orientation of sugar and base rather than attaining actual numerical agreement.

We proceed with the initial assumption that the same preferred range of torsion angle is favored by all adenine nucleosides at room temperature in neutral aqueous solution. This range will be taken from 10 to -60° or from 25 to -85°, in correlation with the structural information available in Table III. The information summarized in Table III is taken from the

Table III: Summary of Structural Information for Adenine Nucleosides and Nucleotides^a

Adenine structure	Out-of-plane atom	Allowed ϕ_{CN} range, ^b deg	Torsion angle, deg
Deoxyadenosine	C'-3 <i>exo</i>	25 to -85	-6
Adenosine 5'-phosphate	C'-3 <i>endo</i>	10 to -60 -85 to -140	-20
Adenosine 3'-phosphate	C'-3 <i>endo</i>	-10 to -60 -85 to -140	-4
Adenosine in 5-bromouridine-adenosine complex	C'-3 <i>endo</i>	-10 to -60 -85 to -140	-11
Adenosine in the coenzyme of vitamin B ₁₂	C'-3 <i>endo</i>	-10 to -60 -85 to -140	-69

^a Taken from Table I of ref 26. ^b Allowed ϕ_{CN} range is taken from Table III of ref 26.

recent analysis of steric interactions present in nucleoside systems by Haschemeyer and Rich.²⁶

In Figure 7 it is seen that the rotational strength of each derivative changes slowly and in a regular manner as the torsion angle is varied. This is found to be true

(25) J. Kraut and L. H. Jensen, *Acta Crystallogr.*, **16**, 79 (1963).

(26) A. E. A. Haschemeyer and A. Rich, *J. Mol. Biol.*, **27**, 369 (1967).

also of the individual contributions of each ribose bond. Our procedure is to compare the calculated rotational strengths of a specific derivative averaged over its "allowed" range of torsion angle with other derivatives and with experiment. The results are summarized in Table IV.

Table IV: Comparison of the Experimental (R_{exptl}) and Theoretical (R_{theor}) Rotational Strengths

Structure	R_{exptl} , biots ^a	R_{theor} , biots
2',3'-5'-Trideoxy-2',3'-dideoxyadenosine (II)	8.5 ^a	7
2',3'-Dideoxy-2',3'-dideoxyadenosine (IV)	8.0 ^a	6.6
Angustmycin A (XV)	-1.5 ^a	-0.5
4'-Exocyclic methylene adenosine (XVI)	-2.3 ^a	-1.3
Adenosine (III)	-1.6 ^a	-1.4
2'-Deoxyadenosine (X)	-1.3 ^b	-0.6
2',3'-Dideoxyadenosine (VII)	-1.0 ^b	-0.4
2',3',5'-Trideoxyadenosine (I)	-0.8 ^b	-0.2
6-Amino-9-(5'-S-ethyl-5'-thio-2',3',5'-trideoxy-2',3'-dideoxy- β -D-glycero-pentofuranosyl) purine (V)	30.0	27.0 ^c
2'-O-Methyladenosine	-1.7	-2.1

^a The rotational strengths of these compounds have been estimated from the circular dichroism curves from the expression (see ref 2) $R_K = 1.23 \times 10^{-2} [\theta_0] \Delta / \lambda_0$, where $[\theta_0]$ is the molecular ellipticity at the wavelength of transition, λ_0 , and Δ is the half-width of the band (the difference between the wavelength at the peak of the band and the wavelength at which θ falls to θ_0/e). R_K has the unit of biots. The other rotational strengths were determined by the simple ratio (amp)₁/(amp)₂ = $R_K(1)/R_K(2)$, where the reference compound is II. ^b The 3'-*exo* conformation has been used for these compounds. ^c Calculation based on a sandwich arrangement of the sulfur atom directly below C-8 of the adenine ring. The anisotropy of the C-S bond was taken equal to that of the carbon-carbon double bond.

V. Discussion

This article attempts to decipher the experimental information attained by theoretical rather than by purely empirical means. This procedure reflects our belief that approximate calculations of the rotational strengths should give an excellent "steer" and a better idea of how things go and, ultimately, permit a better systematization and understanding of the data than the purely empirical approach. Moreover, the theoretical approach is unquestionably more fruitful in suggesting suitable model compounds for future systematic studies.

On the basis of the several simplifying assumptions, some initial success toward correlating theory with experiment has been achieved. The most remarkable success of the theory is the prediction of a small, nega-

tive rotational strength for the 260-m μ Cotton effect of the 4',5' unsaturated derivatives (see Figure 4) and a large positive rotational strength for the 2',3' unsaturated derivatives (see Figure 3). The orientation of the C_{4'}-C_{5'} double bond relative to the 260-m μ transition moment of the adenine chromophore is generally found to be less favorable for producing large rotational strengths than the C_{2'}-C_{3'} double bond. Another noteworthy success is the prediction by theory that the reduction of the C_{2'}-C_{3'} double bond will change the rotational strength from a large positive value to a very small negative value, as is found experimentally (compare the rotational strength given in Table IV, of compound II with compound I). In contrast, the theory predicts that the reduction of the 4',5' site of unsaturation will only slightly affect the rotational strength, as is observed to be the case by comparing the experimental rotational strengths of adenosine and 4'-exocyclic methyleneadenosine. Of lesser significance is the fact that the theory qualitatively accounts for the successive removal of the 2',3'-, and 5'-OH groups and the alkylation of the carbohydrate ring (2'-O-methyladenosine), and the presence or absence of the 1'-CH₂OH group in the 4',5' unsaturated compounds. Several factors combine to make the theory less reliable for these compounds. The per cent error in the experimental data increases from less than 5% for compound II to 20% for compound I as the signal-to-noise ratio decreases with decreasing optical activity. In addition, the rotations and the bond anisotropies of the C-H, O-H, and C-O bonds are relatively small such that the one-electron effects could be relatively more significant. These initial results serve to point out that a more systematic study involving the positioning of polarizable substituents such as Cl, Br, I, SH, CN, C-S-C, and C=C in or on the carbohydrate ring could conceivably pinpoint the sugar-base conformation and determine whether or not substituents greatly alter the conformation in a more conclusive manner.

Finally, utilizing the hydrophobic and hydrophilic natures of the thioether and phosphate groups, respectively, the remarkable effect of the 5'-thioether function on the rotation, as compared to the minimal effect of the 5'-phosphate function, can be rationalized without postulating any large changes in the sugar-base torsion angle. Assuming a base-stacking arrangement for the thioether function and a moderate C-S bond anisotropy, we can account for the very large rotational strength exhibited by compound V (see Table IV). In view of the hydrophilic nature of the phosphate group, one would expect the 2',3', or 5'-phosphate group to be extended away from the base into the solvent system. The combination of numerous possible conformations and large r_{ij} values would greatly limit the contribution of this group to the rotational strength.

In conclusion, the theory has successfully described many of the interesting features of the optical activity

of the adenine nucleosides. In view of the several assumptions and the stratagem of using one allowed range of the torsion angle (10 to -60°) and ignoring the other allowed range (-80 to -140°),²⁷ the results to date cannot be cited as conclusive evidence that the preferred conformation for the sugar ring is *anti*. The results are offered as an indication in favor of this conformation and have additional value in that they provide insight into the factors which contribute to the rotational strength and they suggest future experiments that may give more definitive information.

Acknowledgment. The authors wish to acknowledge the National Institutes of Health Research Grant

GM-12862-02 and the National Cancer Institute of the National Institutes of Health Research Grant CA-08109-02 for financial support relative to the present study. We also wish to thank Dr. Dan Urry and the Institute for Biomedical Research for the use of the Cary 6001 circular dichroism attachment to the Cary 60 and for the use of their computer facilities. This paper was taken in part from the Ph.D. Thesis of D. W. Miles, University of Utah, 1967.

(27) However, from σ -bond moments and π -bond moments and bond lengths, a charge of -0.87×10^{-19} and -0.7×10^{-19} C is found to be on the N-3 of the adenine ring and the furanose ring oxygen, respectively. This interaction is expected to stabilize the adenosine derivatives in the 10 to -60° range.

Kinetics and Mechanism of the Reaction between Bromine Trifluoride Vapor and Uranium Tetrafluoride

by Tsutomu Sakurai and Matae Iwasaki

*Division of Research, Japan Atomic Energy Research Institute, Tokai-mura, Ibaraki-ken, Japan
(Received July 24, 1967)*

The reaction between BrF_3 vapor and UF_4 was investigated in the temperature range from room temperature to 300° and a range of BrF_3 partial pressure from 6 to 45 mm. Argon saturated with BrF_3 vapor was introduced into a reactor at a fixed flow rate, and the BrF_3 was treated with the UF_4 , the weight change of which was measured by a thermobalance. The reaction mechanism was also studied and UF_6 and UF_{4+z} ($0 < x < 1$) were captured as the intermediates of the reaction. From these experiments it was found that (1) the reaction proceeded even at room temperature; (2) the rate of reaction was proportional to the BrF_3 partial pressure and changed little with increasing temperature; (3) at temperatures below 100° , UF_4 was converted to UF_6 through the reaction $\text{UF}_4 \rightarrow \text{UF}_{4+z}$ ($0 < x < 1$) $\rightarrow \text{UF}_5 \rightarrow \text{UF}_6$, at temperatures of 100 – 200° ; however, the reaction mechanism was complicated, probably due to the occurrence of an interaction between the produced UF_6 and the remaining UF_4 ; and (4) owing to this temperature dependence of the reaction mechanism, the rate constant, calculated from the slope of the weight loss vs. time curve, rose to a peak at 185° and then fell to a minimum at 220° . The activation energy, calculated from the Arrhenius equation, has a low value of 1.0 kcal/mol.

Introduction

Interhalogen compounds such as chlorine trifluoride, bromine trifluoride, and bromine pentafluoride convert many uranium compounds to uranium hexafluoride.^{1–4} As compared with the reactions between uranium compounds and elemental fluorine,^{5,6} these reactions proceed even at considerably lower temperatures, and the resulting activation energies, calculated from each Arrhenius plot, generally show smaller values.

In addition, in some of these reactions, an unusual behavior of the reaction rate has been reported: for the reaction between UF_4 and ClF_3 , Labaton has reported that the reaction rate passed through a

maximum at 105° , fell to a minimum at 148° , and then rose again.¹ For this he has explained that the reduced rate between 105 and 148° was due to a lower rate of the reaction of ClF_3 with a UF_{4+z} surface, produced as an intermediate, rather than with a UF_4 surface.¹ A

(1) V. Y. Labaton, *J. Inorg. Nucl. Chem.*, **10**, 86 (1959).

(2) N. S. Nikolaev and Yu. D. Shishkov, *Proc. Acad. Sci. USSR, Chem. Sec. (English Transl.)*, **143**, 168 (1962).

(3) M. Iwasaki and T. Sakurai, *J. Nucl. Sci. Technol.*, **2**, 225 (1965).

(4) R. L. Jarry and M. J. Steindler, *J. Inorg. Nucl. Chem.*, **29**, 1591 (1967).

(5) V. Y. Labaton and K. D. B. Johnson, *ibid.*, **10**, 74 (1959).

(6) M. Iwasaki, *ibid.*, **26**, 1853 (1964).

similar phenomenon has been reported by Nikolaev and Shishkov for the $\text{UF}_4\text{-ClF}_3$ reaction.² On the other hand, for the reaction between U_3O_8 and BrF_3 , previously reported by the authors, the reaction rate rose to a peak at 200° and then fell to a minimum at 225° , for which no cause has yet been clarified.³

The present work was carried out to ascertain whether such an anomaly of the rate constant as in the $\text{UF}_4\text{-ClF}_3$ reaction also appears in the reaction between UF_4 and gaseous BrF_3 and to obtain further information about these anomalies. Experiments were mostly concerned with the kinetic study of the reaction by use of a thermobalance, and its mechanism was also studied.

Experimental Materials and Procedure

1. *Materials. Bromine Trifluoride.* Commercial grade bromine trifluoride, from the Harshaw Chemical Co., was purified by distillation, as reported previously.⁷

Uranium Tetrafluoride. Fine powder of UF_4 , was provided by Mitsubishi Kinzoku Kogyo Co., Ltd., of 98% purity, the remaining 2% being uranium dioxide and uranyl fluoride. The purity is almost the same as that of uranium tetrafluoride generally used for kinetic studies of fluorination by other investigators.^{1,4,5} The small amount of these impurities does not affect the validity of the experiments, as possible weight changes of these impurities would be very small and within the experimental accuracy.

Sedimentograph analysis showed that the particle sizes were distributed in the range below $10\ \mu$. The surface area, determined by krypton adsorption, was $1.0\ \text{m}^2/\text{g}$. The water content, determined by infrared spectrophotometry, was negligibly small, *viz.* 0.25%. The sample was used without further purification.

2. *Procedure.* The apparatus and procedure were similar to those used previously.³ However, improvements were made on the apparatus in order to prevent corrosion by bromine trifluoride. In the thermobalance previously used, the spring column was made of a glass tube and the argon stream was brought into the reaction tube from the top of the spring column to protect the spring column from attack by BrF_3 from the convection currents set up in the reaction tube. However, at reaction temperatures above 200° , the spring column was considerably corroded by the BrF_3 in the hot convection currents.

In the thermobalance used in the present work, the spring column was made of a Kel-F or Teflon tube, and the sensing element was a nickel-plated phosphor-bronze spring, the extension of which was measured by a differential transformer and recorded automatically.⁸ Therefore, all of the surfaces in contact with the reactant gas in the thermobalance were made of materials not affected by BrF_3 . The detailed diagram of the thermobalance is shown in Figure 1. The spring column was maintained at a temperature a little above

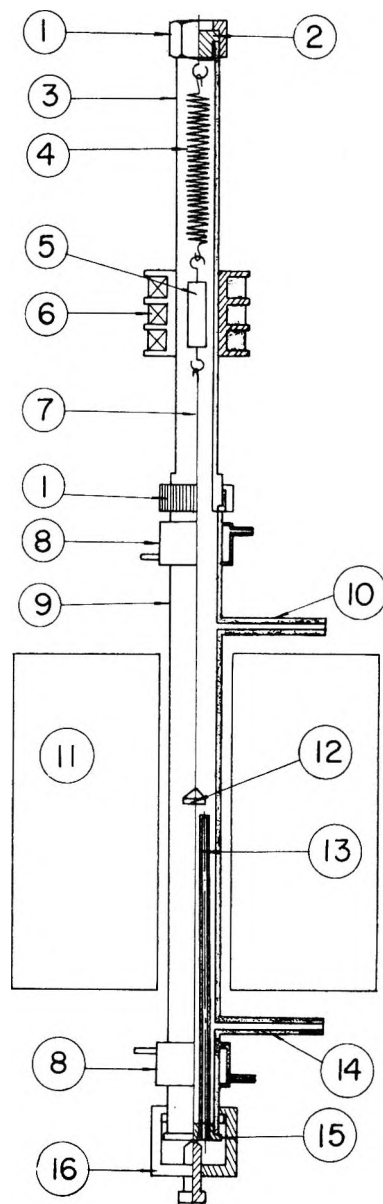


Figure 1. Diagram of the thermobalance: 1, nut; 2, Kel-F block provided with a hook; 3, Kel-F tube; 4, nickel-plated phosphor-bronze spring; 5, ferrite core of differential transformer (sealed by Teflon-100X tube); 6, differential transformer; 7, nickel wire; 8, cooling water jacket; 9, monel reactor tube; 10, reactant-gas inlet; 11, electric furnace; 12, sample pan; 13, monel thermocouple well; 14, gas outlet; 15, cover of reactor tube; 16, device to close the cover.

the temperature of the thermostat (to be described below) by means of a thermostated air bath in order to keep the column temperature from affecting the spring sensitivity and to prevent condensation of the BrF_3 vapor. The accuracy of the thermobalance was 1 mg for weight changes up to 100 mg.

(7) T. Sakurai, Y. Kobayashi, and M. Iwasaki, *J. Nucl. Sci. Technol.*, **3**, 10 (1966).

(8) S. Tsujimura, G. Fujisawa, and A. Takahashi, Japan Atomic Energy Research Institute Report No. 1070, Tokyo, 1964.

From the desired spring movement, the amount of uranium tetrafluoride used in a run was fixed between 76 and 78 mg; the bed was about 0.7 mm deep. However, in order to see the effect of the amount of the sample on the reaction rate, various weights of sample between 30 and 180 mg were used in various runs by replacing this spring with another.

Bromine trifluoride vapor was supplied to the reaction tube in the following manner, using argon as the carrier gas. Liquid bromine trifluoride, 70–80 mm deep in a bubbling vessel, was bubbled by the argon stream with a fixed flow rate and was vaporized into that stream. The argon, containing the BrF_3 vapor, was then introduced into a thermostat; during the passage through the thermostat, the argon was saturated with the BrF_3 vapor because the thermostat was of a lower temperature than the liquid BrF_3 in the bubbling vessel. The argon saturated with BrF_3 vapor was introduced into the reaction tube at a constant flow rate, and the uranium tetrafluoride sample was fluorinated to UF_6 by the BrF_3 . All the paths taken by the BrF_3 vapor were heated to prevent condensation of the BrF_3 vapor.

Prior to the kinetic studies, the partial pressure of BrF_3 in the carrier gas from the thermostat was checked, using He as the carrier gas. Keeping the temperature of the thermostat at $50 \pm 0.5^\circ$ and that of the liquid BrF_3 at $65 \pm 1^\circ$, He gas was passed through the system at constant flow rates between 10 and 15 l./hr, and the BrF_3 , contained in the gas exiting from the thermostat, was collected in a liquid nitrogen cold trap every 10 min. Consequently, 0.42–0.64 g of bromine trifluoride was collected in the cold trap, depending upon the flow rates of He gas. From the amounts of the collected bromine trifluoride, the vapor pressure of BrF_3 in the He gas was calculated to be 34 ± 2 mm; the ± 2 mm corresponds to a deviation of $\pm 5.9\%$. The value is very close to that of the corresponding saturation vapor pressure of BrF_3 (33 mm) calculated from the empirical formula obtained by Oliver and Grisard.⁹

Hence, it is considered that the vapor pressure of BrF_3 in the carrier gas is kept constant, with deviations of less than $\pm 6\%$, in the range of the flow rates described above. This small deviation does not affect the validity of the experiments, as will be discussed later, and the following kinetic studies were carried out with the assumption that the carrier gas was saturated with BrF_3 vapor.

Results and Discussion

1. *Kinetics of the Reaction.* In most of the literature on the kinetics of fluorination reactions of uranium compounds, in which the products are entirely gaseous, the results are treated using the diminishing sphere model.¹⁰ In this kinetic model, the reaction rate is expressed by

$$-\frac{dM}{dt} = k(4\pi r^2) \quad (1)$$

where M and r are the mass and radius of the reacting particle at time t , and k is the rate constant for a given temperature and partial pressure of the reactant gas. The final equation derived is

$$(1 - F)^{1/3} = 1 - k't \quad (2)$$

where F is the fraction of reacted solid; k' is a reaction rate constant, related to the rate constant in eq 1 by the expression $k' = k/r_0\mu$ (r_0 = initial radius and μ = the bulk density of the particle). Therefore, the rate constant k' is obtained from the slope of straight line in a graph of the value $(1 - F)^{1/3}$ vs. time.

However, in the present experiments, a plot of $(1 - F)^{1/3}$ vs. time did not give a straight line in the part of curve, which excludes the beginning of the reaction where the plot of $(1 - F)^{1/3}$ vs. time deviated from the straight line for the time required for the reactant gas to replace the inert gas in the reaction tube.^{1,5,10} This seemed to be due to the bed depth of the sample uranium tetrafluoride in the pan, since a bed depth of 0.7 mm was considerably thick compared with the particle sizes of the uranium tetrafluoride. In such a case, it has been indicated by other authors that a plot of $(1 - F)$ vs. time gives a straight line, except the portion at the end of the reaction where $(1 - F)^{1/3}$ gives a better fit.¹⁰

In Figure 2, the values of $(1 - F)$ and $(1 - F)^{1/3}$ for a typical run are plotted against time. Also, in the present experiments, a plot of $(1 - F)$ vs. time gave a straight line, except the portions at the beginning and end of the reaction. This means that the rate of reaction is expressed as

$$-\frac{dW}{dt} = K \quad (3)$$

where W is the weight of the solid reactant at time t , and K is a constant. The reason is that eq 3 takes the following form, when integrated

$$(1 - F) = 1 - (K/W_0)t \quad (4)$$

where W_0 is the initial weight of the solid reactant.

On the other hand, when the reaction was stopped before completion, it was found that the remaining material in the pan, the color of which was dark brown, had caked considerably.

From these facts, it is considered that, owing to the thickness of the bed of the solid reactant and its caking during the process of the reaction, the diminishing-sphere model is not applicable in the present experiments and a plot of $(1 - F)$ vs. time shows a better fit. In other words, in the present experiments, it seems that UF_6 is produced in a relatively thin layer at the surface

(9) G. D. Oliver and J. W. Grisard, *J. Amer. Chem. Soc.*, **74**, 2705 (1952).

(10) C. E. Johnson and J. Fischer, *J. Phys. Chem.*, **65**, 1849 (1961).

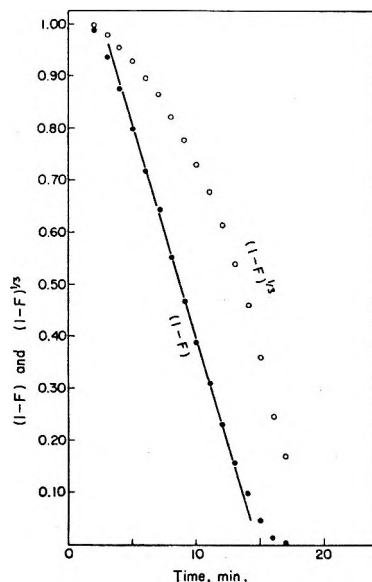


Figure 2. Plots of $(1 - F)$ and $(1 - F)^{1/2}$ vs. time: initial weight of $\text{UF}_4 = 77$ mg, partial pressure of $\text{BrF}_3 = 15$ mm, gas velocity = 55.4 cm/min, temp = 110° .

of the bed and, for this, the thickness of the bed decreases with time at the rate determined by the reaction temperature and the BrF_3 partial pressure.

In a plot of $(1 - F)$ vs. time, the deviation at the beginning of a run is explained by the experimental conditions used. The reaction tube is initially filled with argon, and it takes 3–4 min for the argon– BrF_3 mixture in the reaction tube to become the value fixed for the run. Consequently, the reaction rate at the beginning of the reaction is considerably low.

The causes of deviation at the end of the reaction were not clarified thoroughly, however, one of the causes may be that, owing to the small amount of the sample remaining, the rate of reaction reverts to a diminishing-sphere model.¹⁰

Therefore, in the following experiments, the constant K in eq 3 and 4 was used as the rate constant in the treatment of the kinetics of the reaction.

2. Influence of Gas Velocity. The effect of gas velocity on the reaction rate was checked at a given reaction temperature, with the partial pressure of bromine trifluoride kept constant. The velocity of argon in the reaction tube varied from 17.7 to 55.4 cm/min, keeping the BrF_3 partial pressure at 15 mm.

The results are shown in Table I. It is evident that the diffusion rate of bromine trifluoride in the gaseous phase has no effect on the reaction rate, as long as the gas velocity exceeds 45 cm/min. Therefore, in the following experiments, the velocity of argon was fixed at 55 cm/min, that is, an argon flow rate of 15 l./hr.

3. Influence of the Partial Pressure of BrF_3 . In several runs, the BrF_3 partial pressure was varied from 7 to 45 mm by changing the temperature of the thermostat and of the liquid BrF_3 in the bubbling vessel, in accordance with the required partial pressures.⁹

Table I: Effect of Gas Velocity on the Rate Constant^a

Gas velocity, cm/min	Gas flow rate, l./hr	Rate constant (10^3K), ^b g/min
17.7	4.8	4.9
28.0	7.6	5.4
36.9	10.0	5.6 ± 0.1
45.8	12.4	6.2 ± 0.1
55.4	15.0	6.2 ± 0.4

^a Initial weight of UF_4 , 77 ± 1 mg; temperature, 110° ; partial pressure of BrF_3 , 15 mm. ^b Each value averaged.

Table II shows the effect of the partial pressure of BrF_3 on the reaction rate at a temperature of 110° . This effect can be expressed approximately in the form

$$K \text{ (g/min)} = (6.96 \times 10^{-4})P^{0.8} \text{ (mm)} \quad (5)$$

4. Influence of Temperature. In the present work, effort was mostly devoted to the clarification of the temperature dependence of the reaction rate.

The 76–78 mg of the uranium tetrafluoride was allowed to react in the temperature range 50 – 300° , keeping constant the partial pressure of bromine trifluoride (15 mm).

Table II: Effect of Partial Pressure of BrF_3 on the Rate Constant at 110° ^a

Partial pressure of BrF_3 , mm	Rate constant ^b (10^3K), g/min	Reaction period ^b min
7	2.2 ± 0.3	44
10	4.6 ± 0.2	24 ± 1
15	6.2 ± 0.5	17
22	8.0 ± 0.3	14
31	11.4 ± 0.4	12 ± 1
45	14.5 ± 0.3	7

^a Initial weight of UF_4 , 77 ± 1 mg; gas velocity, 55.4 cm/min. ^b Each value averaged.

Typical examples of the weight loss vs. time curves at different temperatures are shown in Figure 3. At temperatures below 80° , the rate of reaction was small and the reaction stopped halfway, as shown by the curve of 55° . However, the reaction proceeded rapidly at temperatures above 90° , and the weight loss vs. time curves changed in shape with increasing temperature. Thus at temperatures near 185° , the curve, as shown in Figure 3, had a characteristic, in that an induction period appeared in the initial stage of the reaction, *i.e.*, for the initial 7 min, and then the weight loss increased rapidly. At temperatures above 220° , the induction period disappeared again, and the weight loss increased steadily with time, as shown by the curve of 240° in

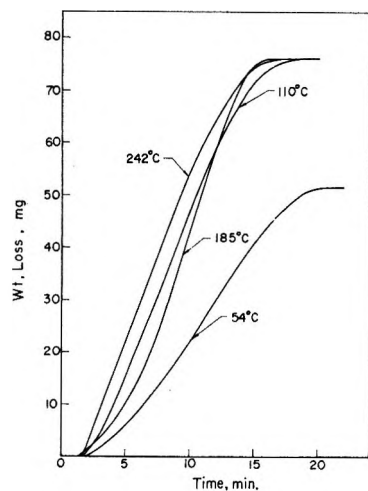


Figure 3. Weight loss vs. time curves at different temperatures: initial weight of $\text{UF}_4 = 77 \pm 1$ mg, partial pressure of $\text{BrF}_3 = 15$ mm, gas velocity = 55.4 cm/min.

Figure 3. On the other hand, the reaction period was almost constant in the temperature range described already, that is, for each 75 mg of the sample, 17 ± 1 min at 110° and 16 ± 1 min in the range of 185 – 240° .

In several runs, the amount of uranium tetrafluoride was varied in the range of 30–180 mg, but the shape of the weight loss vs. time curve at each temperature did not change remarkably, although the reaction period changed in proportion to the amount of the sample used.

These facts indicate that the mechanism of the reaction changes with temperature, the details of which will be discussed later.

In Figure 4, the rate constant K is plotted against the temperature; the constant K was calculated from the graph of the plot of $(1 - F)$ vs. time, using eq 4. The rate constant increased with increasing temperature up to 185° , fell to a minimum at 220° , and then remained almost the same thereafter; the relation is similar to that of the reaction of ClF_3 with UF_4 and of BrF_3 with U_3O_8 .¹⁻³

This relation between the rate constant and temperature is not influenced significantly by the previously described deviation of the partial pressure of BrF_3 in the carrier gas, since the resulting deviation of rate constant K , calculated from eq 5, is 5%, which is within the observed deviation of the K in Figure 4.

In Figure 5, the Arrhenius plot for the reaction is shown in the range 90 – 190° , from which the activation energy was calculated to be 1.0 kcal/mol. The value is much lower than that for the UF_4 – F_2 reaction, which is 15.5–19.9 kcal/mole,⁵ and it is close to that of 3.4–5.6 kcal/mol for the UF_4 – ClF_3 reaction.¹

From the value of the activation energy and eq 5, the following equation was derived to represent the temperature and BrF_3 partial pressure dependence of the present reaction, in the temperature range 90 – 190° and in the BrF_3 partial pressure range of 7–45 mm.

$$\ln K = 0.8 \ln P - (0.49 \times 10^3)(1/T) - 5.98 \quad (6)$$

5. *Intermediates of the Reaction.* To observe the processes of the reaction, the uranium tetrafluoride was treated in a horizontal reaction tube made of a translucent Kel-F tube (o.d. 10 mm and i.d. 7 mm).

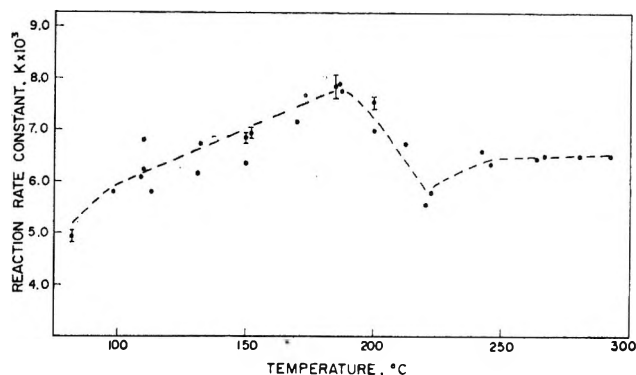


Figure 4. Temperature dependence of the rate constant K : initial weight of $\text{UF}_4 = 77 \pm 1$ mg, partial pressure of $\text{BrF}_3 = 15$ mm, gas velocity = 55.4 cm/min.

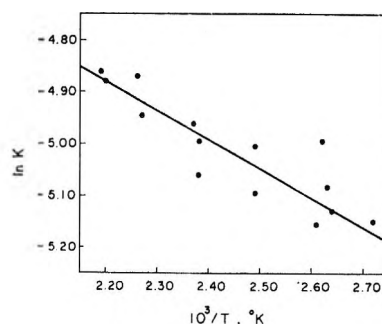


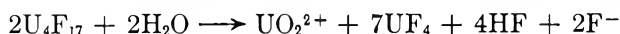
Figure 5. Arrhenius plot for the region 90 – 190° .

After 100–200 mg of the sample was placed in the reaction tube, argon containing 10 mm of the BrF_3 partial pressure was passed through the reaction tube. Consequently, when the argon– BrF_3 mixture was brought into the reaction tube, the color of the sample changed to dark brown within 3 min and then changed to whitish yellow from dark brown within 30 min, during which the amount of the material decreased very slowly owing to the conversion to UF_6 .

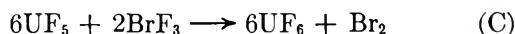
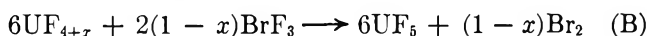
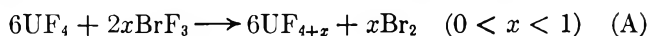
Both the dark brown and whitish yellow materials were unstable in air, and their colors turned green upon exposure to air. Identification by X-ray diffraction was done on both the materials, after sealing in thin-walled glass capillaries in a glove box filled with argon. X-Ray diffraction patterns of the whitish yellow material were in agreement with that of β - UF_6 , reported by Zachariassen,¹¹ whereas the patterns of the dark brown one agree with that of UF_4 . However, when added to water, the dark brown material was found through chemical analysis to be hydrolyzed and to produce

(11) W. H. Zachariassen, *Acta Crystallogr.*, 2, 296 (1949).

UO_2F_2 and UF_4 . Therefore, the dark-brown material should be also an intermediate of the reaction, *i.e.*, UF_{4+x} ($0 < x < 1$), since it has been known that intermediate uranium fluorides (U_4F_{17} , U_2F_9 , and UF_5) react with water producing UO_2F_2 , UF_4 , and HF , *e.g.*¹²



Hence, at near room temperatures, the reaction seems to proceed through the following three steps



In these steps, as seen by direct observation, step A proceeds much more rapidly than the other steps.

6. *Mechanism of the Reaction.* From the results obtained in the above experiments, the following conclusions concerning the mechanism of the reaction can be drawn.

In the temperature range from room temperature to near 100° , the reaction proceeds by the three steps already described, in which step A proceeds much more rapidly than the others.

However, at temperatures above 100° , the mechanism of the reaction becomes considerably complicated. The cause cannot be explained by assuming that the reaction also proceeds by the three steps at temperatures above 100° .

To obtain an insight into the temperature dependence of the mechanism, it is advantageous to utilize a differential curve of the weight loss *vs.* time curve, *i.e.*, the rate of weight loss *vs.* time curve. In Figure 6, typical examples of the differential curves at different temperatures are shown, which were calculated from each weight loss *vs.* time curve. Comparing the curves in Figure 6, the following facts are found.

(i) The differential curves at temperatures above 220° are similar in shape to those at 98 and 110° .

(ii) The differential curve at 185° is remarkable in that an induction period appears in the initial stage of the run and then the rate of weight loss increases abruptly up to a maximum which is the largest in all the curves.

From the results, it seems that, in the reaction near 185° , the UF_6 produced in the initial stage tends to be retained in the remaining sample for some length of time, without immediate evaporation, and then evaporates together with the UF_6 produced in the next stage; that is, an interaction occurs between the produced UF_6 and the remaining material.

As to the reaction between UF_6 and UF_4 , the following facts have been reported.¹²

(i) The reaction occurs at temperatures above 100° , producing such intermediate fluorides as UF_5 , U_2F_9 , and U_4F_{17} .

(ii) At a fixed vapor pressure of UF_6 , the resulting

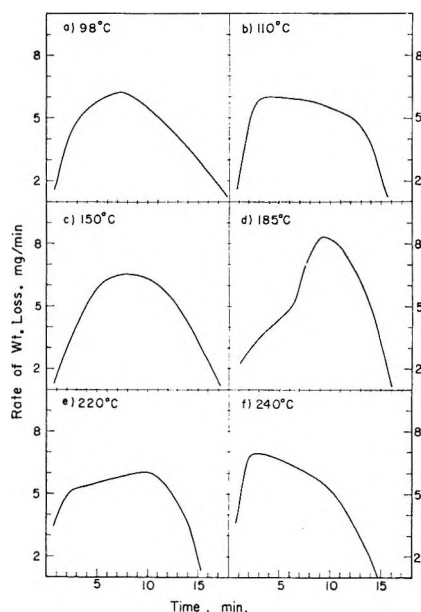


Figure 6. Differential curves of the weight loss *vs.* time curves at different temperatures: initial weight of $\text{UF}_4 = 77 \pm 1$ mg, partial pressure of $\text{BrF}_3 = 15$ mm, gas velocity = 55.4 cm/min.

product is UF_5 at relatively low temperatures, while at elevated temperatures above 200° , it is U_2F_9 or U_4F_{17} ; that is, the amount of UF_6 reacting with a unit mass of UF_4 decreases with increasing temperature at temperatures above near 200° .

From these facts and from the shapes of the curves in Figure 6, it is concluded that the UF_6 produced in the initial stage of the reaction reacts with the remaining UF_4 at temperatures above 100° , and its reaction rate rises to a peak at 185° .

Hence, in the weight loss *vs.* time curve at 185° , the initial induction period indicates that, during the time, the reaction



proceeds simultaneously with steps A–C, and the rapid increase of weight loss in the next portion indicates that the over-all reaction proceeds through steps B and C, owing to the disappearance of UF_4 .

On the other hand, at temperatures above 200° , since the amount of UF_6 consumed by the remaining UF_4 decreases with increasing temperature, the weight loss *vs.* time curves and their differential curves approach those near 100° in shape.

Thus because of this temperature dependence of the mechanism of reaction, the rate constant K , calculated from each weight loss *vs.* time curve, passes through a maximum at 185° and then falls to a minimum at 220° , as shown in Figure 4. The minimum point at 220° corresponds to the transition point of the mecha-

(12) J. J. Katz and E. Rabinowitch, "The Chemistry of Uranium, The Element, Its Binary and Related Compounds," Dover Publications, Inc., New York, N. Y., 1961, pp 382–392.

nism of reaction from the UF_6 - UF_4 interaction to non-interaction.

Acknowledgment. Thanks are due to Mr. S. Tsujimura, Mr. A. Takahashi, and Mr. G. Fujisawa for their

aid in the construction of the thermobalance, and to Dr. S. Suzuki and other members of the Analytical Section, Japan Atomic Fuel Corp., for their analysis of the water content in the sample of uranium tetrafluoride.

Oxidation of Thiourea and Thioacetamide by Alkaline

Hexacyanoferrate(III)

by M. C. Agrawal and S. P. Mushran

Chemical Laboratories, University of Allahabad, Allahabad, India (Received July 28, 1967)

Kinetics of the oxidation of thiourea and thioacetamide with alkaline hexacyanoferrate(III) has been studied in aqueous solution. The reaction with thiourea has been found to be first order with respect to thiourea, hexacyanoferrate(III), and hydroxyl ion, while that with thioacetamide shows zero-order dependence on $Fe(CN)_6^{3-}$ and first-order dependence on both thioacetamide and OH^- ion. Potassium chloride concentrations showed accelerating effect on the reaction rate, while the effect of ferrocyanide ion concentration was negligible. Increase in dielectric constant (D) enhanced the reaction rate and the plot of $\log k$ against $1/D$ showed a linear relation. A suitable mechanism for the oxidation processes has been proposed.

Introduction

Hexacyanoferrate(III) is well known for its oxidative power in alkaline media and can be described as one of the efficient electron-abstracting reagents. Though uncatalyzed oxidations by hexacyanoferrate(III) ion are, in general, fairly fast, osmium(VIII) ion has been observed to exert a positive catalytic influence, and several inorganic and organic substances may directly be titrated against hexacyanoferrate(III) in its presence.¹

The kinetics of the oxidation of 3-mercaptopropionic acid has been studied by Bohning and Weiss,² while Kolthoff and coworkers³ have investigated the mechanism of oxidation of 2-mercaptoethanol by hexacyanoferrate(III) in acid medium. In another publication, Kolthoff and coworkers⁴ have studied the oxidation of *n*-octyl mercaptan by alkaline hexacyanoferrate(III) in acetone-water medium. Recently, Gorin and Godwin⁵ have suggested that the oxidation of some mercaptans is catalyzed by metal ions. In spite of the above work, the literature on the kinetics of oxidation reactions of organic sulfur compounds by hexacyanoferrate(III) appears to be scanty.

In the present communication, the kinetics of the oxidation of thiourea and thioacetamide by alkaline hexacyanoferrate(III) has been investigated in some detail, in order to shed some further light on oxidation mechanisms involving hexacyanoferrate(III) ion. The

reactions have been studied in presence of sodium carbonate-bicarbonate buffer, to avoid the effects of any possible pH variations during the progress of the reactions. Influence of several variable factors such as dielectric constant and the concentrations of potassium chloride, potassium hexacyanoferrate(II), and hydroxyl ion has been investigated to ascertain the exact nature of the oxidation processes.

Experimental Section

Materials. (i) Aqueous potassium hexacyanoferrate(III) was prepared from an AnalaR BDH sample and the concentration was checked by iodometry.⁶ (ii) Aqueous thiourea was prepared from a *pro analysi* E. Merck reagent. (iii) Aqueous thioacetamide was also prepared from a *pro analysi* E. Merck sample. (iv) All other reagents were of analytical grade. (v) Doubly distilled water was employed for preparing solutions and for diluting where necessary, and in every case glass vessels of Jena Geratglas were

(1) F. Solymosi, *Magy. Kem. Folyoirat*, **63**, 294 (1957).

(2) J. J. Bohning and K. Weiss, *J. Am. Chem. Soc.*, **82**, 4724 (1960).

(3) E. J. Meehan, I. M. Kolthoff, and H. Kakiuchi, *J. Phys. Chem.*, **66**, 1238 (1962).

(4) I. M. Kolthoff, E. J. Meehan, M. S. Tsao, and Q. W. Choi, *ibid.*, **66**, 1233 (1962).

(5) G. Gorin and W. E. Godwin, *J. Catalysis*, **5**, 279 (1966).

(6) A. Berka, J. Vulterin, and J. Zýka, "Newer Redox Titrants," Pergamon Press Inc., New York, N. Y., 1965.

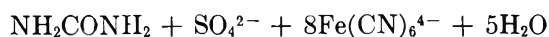
used. The reaction vessel was coated from outside with black Japan to exclude photochemical effects.

Procedure. The reactions were carried out at constant pH 11.0 using standard carbonate-bicarbonate buffer. The kinetics of the oxidation of thiourea and thioacetamide were followed by estimating hexacyanoferrate(III) with the progress of time. Samples (10 ml) of the reaction mixture were withdrawn at definite intervals and the amount of unconsumed hexacyanoferrate(III) was estimated colorimetrically using a Klett-Summerson photoelectric colorimeter with blue filter no. 42 (transmission 400–450 m μ). It was ascertained that hexacyanoferrate(II) did not absorb in this region and also that Beer's law was valid with aqueous hexacyanoferrate(III). The absorption cell was chilled before adding an aliquot portion of the reaction mixture in order to quench the reaction at lower temperatures.

In general, the procedure gave satisfactory results but in a few cases the reaction mixture turned turbid. This probably was due to the precipitation of sulfur at higher concentrations of the reducing substrate. Hence, concentrations of thiourea and thioacetamide were chosen where the reaction mixtures did not develop any turbidity.

Results

Stoichiometry. Reaction mixtures with slight excess of potassium hexacyanoferrate(III) were maintained at 50°, pH 11.0, for 24 hr, when the reaction was complete. The hexacyanoferrate(II) formed equivalent to thiourea and thioacetamide was determined titrimetrically using ceric sulfate. The amounts of reducing substrates consumed and of hexacyanoferrate(II) formed showed that the over-all reactions are



Kinetics. Effect of Hexacyanoferrate(III) Concentration. To evaluate the order of the reactions with respect to the oxidant, the reactions were carried out at different concentrations of hexacyanoferrate(III). The kinetic analysis was mainly applied to the initial stages of the reaction, approximately up to the half-life of the reaction. For a particular concentration of the oxidant, the reaction with thiourea followed first-order disappearance to hexacyanoferrate(III) at all concentrations of thiourea (Figure 1). The reaction with thioacetamide showed zero-order dependence to hexacyanoferrate(III) which in later stages tended to become first order in hexacyanoferrate(III) (Figure 2). Since in this case the concentrations of the sulfur compound are low, the apparent decrease in zero-order

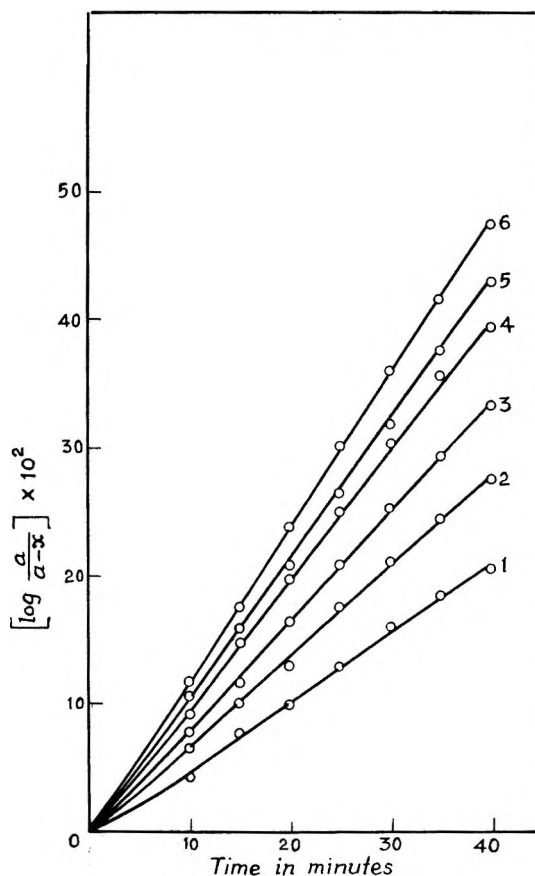


Figure 1. Reaction of hexacyanoferrate(III), $[\text{Fe}(\text{CN})_6^{3-}] = 4 \times 10^{-4} \text{ M}$, pH 11.0, temperature 40°. Concentration of NH_2CSNH_2 : (1) $3.5 \times 10^{-3} \text{ M}$, (2) $4.0 \times 10^{-3} \text{ M}$, (3) $4.5 \times 10^{-3} \text{ M}$, (4) $5.0 \times 10^{-3} \text{ M}$, (5) $5.5 \times 10^{-3} \text{ M}$, (6) $6.0 \times 10^{-3} \text{ M}$.

rate constant may in part be ascribed to the change in the concentration of thioacetamide during the reaction. Further, change in concentration of hexacyanoferrate(III) showed no effect on the first-order and zero-order rate constants with respect to the oxidant for reactions with thiourea and thioacetamide, respectively (Table I). This confirms that the oxidation of thiourea has first-order dependence to hexacyanoferrate(III), while that of thioacetamide is independent of the hexacyanoferrate(III) concentration.

Table I: Hexacyanoferrate(III) Dependence

$10^4[\text{Fe}(\text{CN})_6^{3-}]$, ^a M	Thiourea $10^3 k_{\text{exptl.}}$, ^b min ⁻¹	Thioacetamide $10^3 k_{\text{exptl.}}$, ^c mole l. ⁻¹ min ⁻¹
3.0	14.9	3.64
3.5	16.0	3.87
4.0	16.0	3.73
4.5	16.3	3.82

^a pH 11.0 and temperature 35°. ^b $[\text{Thiourea}] = 4 \times 10^{-3} \text{ M}$.
^c $[\text{Thioacetamide}] = 2 \times 10^{-4} \text{ M}$.

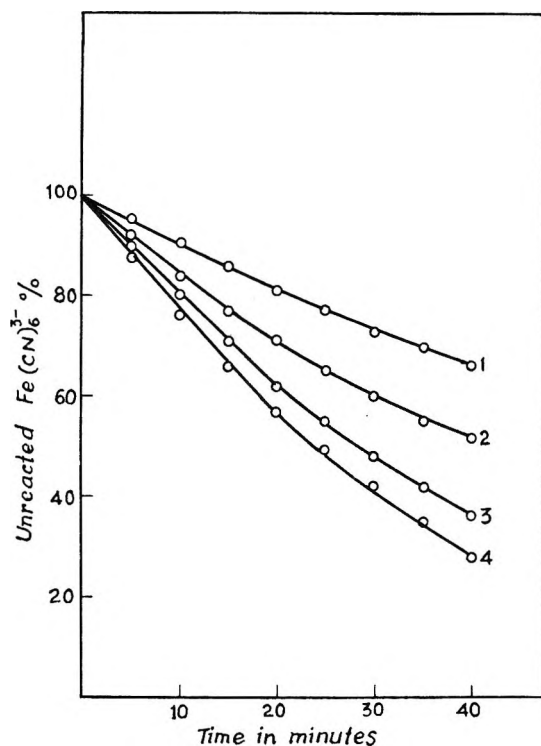


Figure 2. Reaction of hexacyanoferrate(III), $[\text{Fe}(\text{CN})_6^{3-}] = 4 \times 10^{-4} \text{ M}$, pH 11.0, temperature 40° . Concentration of CH_3CSNH_2 : (1) $1.5 \times 10^{-4} \text{ M}$, (2) $2.0 \times 10^{-4} \text{ M}$, (3) $2.5 \times 10^{-4} \text{ M}$, (4) $3.0 \times 10^{-4} \text{ M}$.

Effect of Changing the Reductant Concentration. In order to determine the order of the reaction with respect to the reducing substrate, the reactions were studied at different concentrations of thiourea and thioacetamide. The first-order and zero-order constants with respect to hexacyanoferrate(III) are observed to be directly proportional to the concentrations of thiourea and thioacetamide, respectively. Thus, both the reactions are first order in the reducing substrate (Table II). The over-all bimolecular and unimolecular rate constants for the oxidation of thiourea and thioacetamide, respectively, show fairly concordant values at all concentrations of the reactants. Average values of $k_{\text{exptl}}/[\text{thiourea}]$ and $k_{\text{exptl}}/[\text{thioacetamide}]$ have been

Table II: Thiourea and Thioacetamide Dependence

$10^3[\text{thiourea}]$, M	$10^3 k_{\text{exptl}}$, min^{-1}	$k_{\text{exptl}}/$ [thiourea], l. mole^{-1} min^{-1}	$10^4[\text{thioacetamide}]$, M	$10^6 k_{\text{exptl}}$, mole l.^{-1} min^{-1}	$10^3 k_{\text{exptl}}/$ [thioacetamide], min^{-1}
4.0	16.0	4.0	1.50	2.80	18.7
4.5	18.9	4.2	2.00	3.73	18.7
5.0	22.8	4.5	2.50	4.92	19.7
5.5	24.5	4.4	3.00	5.61	18.7
6.0	27.0	4.5

^a $[\text{Fe}(\text{CN})_6^{3-}] = 4 \times 10^{-4} \text{ M}$, temperature 35° , pH 11.0.
^b First-order rate constants. ^c Zero-order rate constants.

obtained as $4.30 \text{ l. mole}^{-1} \text{ min}^{-1}$ and $18.9 \times 10^{-3} \text{ min}^{-1}$, respectively, at 35° and pH 11.0.

Effect of Alkali Concentration. The oxidation of thiourea and thioacetamide is very susceptible to changes in the alkali concentrations. The oxidations are directly proportional to the concentration of alkali, and the average values $k_{\text{exptl}}/[\text{OH}^-]$ for the oxidations of thiourea and thioacetamide were calculated as $16.9 \text{ l. mole}^{-1} \text{ min}^{-1}$ and $6.94 \times 10^{-3} \text{ min}^{-1}$, respectively (Table III).

Table III: Alkali Dependence

$10^4[\text{NaOH}]$, M	$10^3 k_{\text{exptl}}$, min^{-1}	$k_{\text{exptl}}/$ [OH ⁻], l. mole^{-1} min^{-1}	$10^6 k_{\text{exptl}}$, mole l.^{-1} min^{-1}	$10^3 k_{\text{exptl}}/$ [OH ⁻], min^{-1}
4.0	6.90	17.2	2.76	6.90
6.0	9.85	16.4	4.20	7.00
8.0	13.4	16.7	5.50	6.87
10.0	17.2	17.2	6.97	6.97

^a $[\text{Fe}(\text{CN})_6^{3-}] = 4 \times 10^{-4} \text{ M}$, temperature 35° . ^b [Thiourea] = $4 \times 10^{-3} \text{ M}$. ^c [Thioacetamide] = $4 \times 10^{-4} \text{ M}$.

On increasing the concentration of alkali twofold, the rate constants are almost doubled showing first-order dependence to alkali.

Influence of Dielectric Constant of the Medium. The oxidations of thiourea and thioacetamide by alkaline hexacyanoferrate(III) were studied in different methanol-water mixtures. The results are represented in Table IV.

Table IV: Influence of Dielectric Constant

% methanol ^a	D^b	k_2^c , l. mole^{-1} min^{-1}	$10^3 k_1^d$, min^{-1}
0	74.83	4.56	23.7
5	72.76	3.50	18.4
10	70.68	2.67	14.3
15	68.62	1.91	9.49
20	66.52	1.13	7.08
25	64.38	0.61	...

^a $[\text{Fe}(\text{CN})_6^{3-}] = 4 \times 10^{-4} \text{ M}$, pH 11.0, temperature 35° .
^b Dielectric constant. ^c [Thiourea] = $4 \times 10^{-3} \text{ M}$. ^d [Thioacetamide] = $4 \times 10^{-4} \text{ M}$.

It is evident that the decrease in the dielectric constant of the medium results in a decrease in rate constants. The plots of the reciprocal of dielectric constant against $\log k$ gave straight lines having negative slopes (Figures 3 and 4). The data, however, could not be correlated with the theoretical expressions for ion-ion and ion-molecule reactions.

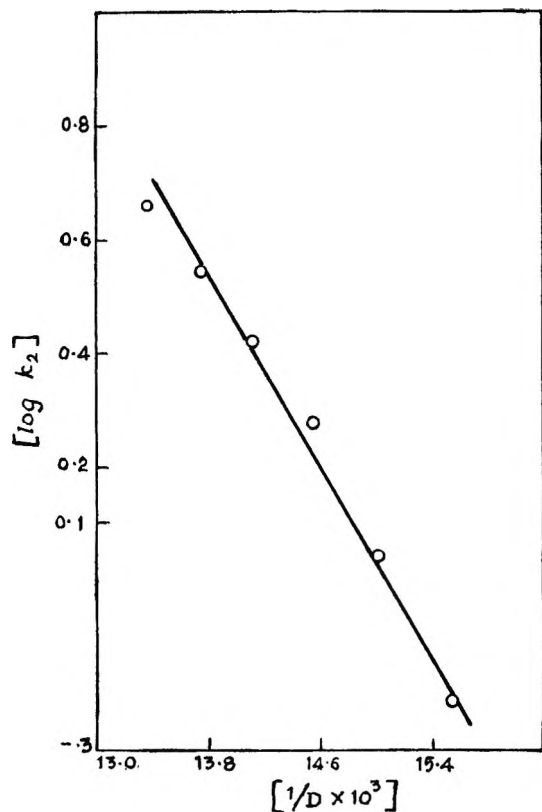


Figure 3. Effect of dielectric constant, $[\text{Fe}(\text{CN})_6^{3-}] = 4 \times 10^{-4} M$, $[\text{NH}_2\text{CSNH}_2] = 4 \times 10^{-3} M$, temperature 35° .

The influence of several other factors on the reaction rates has also been investigated. Addition of potassium chloride showed a marked accelerating effect on the oxidation of thiourea. Effect of temperature was also studied and the energies and the entropies of activation are 11.65 kcal and -27.28 eu (thiourea) and 16.70 kcal and -21.36 eu (thioacetamide). Platinum(IV) appears to be inactive as a catalyst but the osmium(VIII) ion has strong catalytic influence on both of these reactions.

Discussion

The alkali dependence of the oxidation processes involved clearly indicates that the oxidation of thiourea and thioacetamide takes place through an intermediate enolic anion of the reducing substrate formed with hydroxyl ions. In accordance with this view, it has been shown by Waters, *et al.*,⁷ that substances like benzaldehyde, which cannot enolize or do not form an intermediate anion, are not oxidized by alkaline hexacyanoferrate(III), whereas substances like acetone and propanal, which exist in the enolic form, are easily oxidizable. Thus, taking into consideration the kinetic data obtained, the following scheme for the oxidation of thiourea and thioacetamide is proposed on the basis of the mechanism proposed by Speakman and Waters⁷ for the oxidation of carbonyl compounds by alkaline hexacyanoferrate(III).

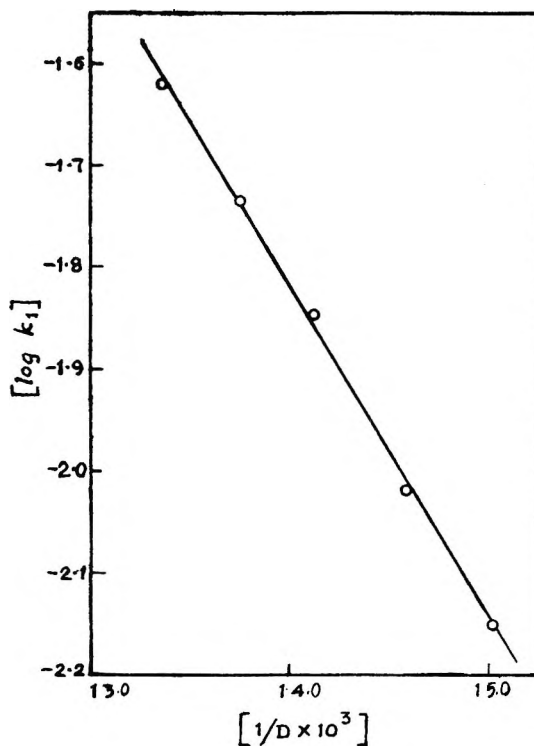
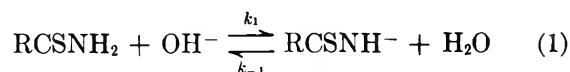
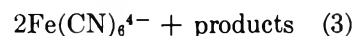
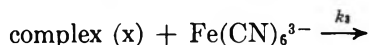
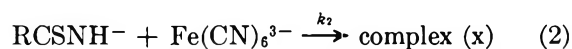


Figure 4. Effect of dielectric constant, $[\text{Fe}(\text{CN})_6^{3-}] = 4 \times 10^{-4} M$, $[\text{CH}_3\text{CSNH}_2] = 4 \times 10^{-4} M$, temperature 35° .

The first step (1) involves the formation of the enolic intermediate anion of the substrate which is essentially reversible in nature and may be fast or slow depending upon the nature of the reductant



This is followed by



In step 2 the intermediate anion forms a complex with the oxidant which is subsequently followed by a fast step 3 which gives the products of the reaction. Step 2 may be fast or slow depending upon the stability of the intermediate enolic anion obtained in step 1. Step 3 is a relatively fast step and gives the products of the reaction. In view of the stoichiometry step 3 cannot form the products of the reaction, and it seems likely that step 3 generates intermediate products which react further in a sequence of reactions which are very rapid relative to steps 1-3.

Now under the steady-state conditions, the rates of formation and destruction of the intermediate anion must be equal. Hence

(7) P. T. Speakman and W. A. Waters, *J. Chem. Soc.*, 40 (1955).

$$\frac{d}{dt}[\text{RCSNH}^-] = k_1[\text{RCSNH}_2][\text{OH}^-] -$$

$$k_{-1}[\text{RCSNH}^-] - k_2[\text{RCSNH}^-][\text{Fe}(\text{CN})_6^{3-}] = 0$$

or

$$[\text{RCSNH}^-] = \frac{k_1[\text{RCSNH}_2][\text{OH}^-]}{k_{-1} + k_2[\text{Fe}(\text{CN})_6^{3-}]} \quad (4)$$

Also the loss of hexacyanoferrate(III) may be represented as

$$-\frac{d}{dt}[\text{Fe}(\text{CN})_6^{3-}] = k_2[\text{RCSNH}^-][\text{Fe}(\text{CN})_6^{3-}] + k_3[\text{complex (x)}][\text{Fe}(\text{CN})_6^{3-}] \quad (5)$$

or

$$-\frac{d}{dt}[\text{Fe}(\text{CN})_6^{3-}] = \frac{2k_1k_2[\text{RCSNH}_2][\text{OH}^-][\text{Fe}(\text{CN})_6^{3-}]}{k_{-1} + k_2[\text{Fe}(\text{CN})_6^{3-}]} \quad (6)$$

According to the above-derived rate law, if the rate-determining step is (2) as we propose for the oxidation of thiourea, then k_{-1} will become much larger than k_2 and the rate law will approximate to

$$-\frac{d}{dt}[\text{Fe}(\text{CN})_6^{3-}] = \frac{2k_1k_2}{k_{-1}}[\text{NH}_2\text{CSNH}_2][\text{OH}^-][\text{Fe}(\text{CN})_6^{3-}] \quad (7)$$

and if the rate-determining step is (1), as we propose for the oxidation of thioacetamide, then rate law 6 will reduce to

$$-\frac{d}{dt}[\text{Fe}(\text{CN})_6^{3-}] = 2k_1[\text{CH}_3\text{CSNH}_2][\text{OH}^-] \quad (8)$$

The derived rate laws (7) and (8) reveal that the oxidation of thiourea by alkaline hexacyanoferrate(III) would have first-order dependence on thiourea, hexacyanoferrate(III), and hydroxyl ions, while the oxidation of thioacetamide would be independent of the concentration of the oxidant. The kinetic data obtained agree well with derived rate law equations and the mechanism proposed. For the oxidation of thioacetamide by hexacyanoferrate(III), however, at lower concentration of the oxidant step 2 will become slow and rate determining. The rate law equation in that case will correspond to (7) as for thiourea and the reaction will have first-order dependence to hexacyanoferrate(III). Figure 2 also represents similar results.

According to above rate laws, the rate-determining step involves interaction between two negatively charged ions or between a negatively charged ion and a polar molecule and thus should correspond to a negative entropy change. This has been found to be true from the experimental data recorded earlier.

For the reactions involving the interaction between similarly charged ions or between a negatively charged ion and dipole, the plots of $\log k$ against the reciprocal of dielectric constant would be straight lines having negative slopes. In the present investigations also similar results have been obtained (Figures 3 and 4), which further show that the experimental observations agree well with the mechanism proposed for the oxidation of these sulfur compounds by hexacyanoferrate(III) in an alkaline medium.

Acknowledgment. The authors thank the Council of Scientific and Industrial Research, New Delhi, India, for a Senior Research Fellowship to M. C. A.

Binding of Divalent Metal Ions by Cross-Linked Polyacrylic Acid

by Richard L. Gustafson and Joseph A. Lirio

Rohm and Haas Company, Research Division, Philadelphia, Pennsylvania 19137 (Received July 31, 1967)

The degrees of complexation of Ca^{2+} , Ni^{2+} , Cu^{2+} , and Zn^{2+} ions by a polyacrylic acid (PAA)-divinylbenzene (DVB) copolymer have been measured potentiometrically at 4.4, 25.0, and 49.4° in 1.0 *M* NaNO_3 . The equilibrium binding constants increased in the order $\text{Ca}^{2+} < \text{Ni}^{2+} < \text{Zn}^{2+} < \text{Cu}^{2+}$, demonstrating the unusual specificity of PAA for Zn^{2+} over Ni^{2+} that was observed previously in the case of polymethacrylic acid (PMA) complexes. The enthalpies of complex formation are positive and become less favorable as the extent of metal ion binding increases. The entropy changes upon complexation increase in the order $\text{Ni}^{2+} < \text{Ca}^{2+} < \text{Cu}^{2+} < \text{Zn}^{2+}$. The reaction $\text{Zn}^{2+} + \text{H}_2\text{A}_2 \rightleftharpoons \text{ZnA}_2 + 2\text{H}^+$ is favored by 15–18 cal/deg mol over the similar reaction involving Ni^{2+} ions.

Introduction

In a recent study¹ of the binding of Ca^{2+} , Ni^{2+} , Cu^{2+} , and Zn^{2+} ions by a polymethacrylic acid (PMA)-divinylbenzene (DVB) gel, it was shown that there was an unusual specificity for Zn over Ni. An examination of the literature has shown that the free energy of chelation of Ni^{2+} by monomeric, polydentate ligands is greater than that of zinc in nearly all cases. In the case of complexation by the PMA gel, the entropy change upon binding of Zn^{2+} is approximately 20 cal/mol deg greater than that observed in the case of Ni^{2+} . This more than compensates for a 4–5 kcal/mol difference in ΔH° which favors the binding of nickel. This evidence suggests that the tetrahedral stereochemical configuration of the Zn^{2+} ion permits binding by the PMA gel with less steric strain than is encountered in the case of the Ni^{2+} ion. In the case of the more flexible linear PMA polymer, the formation of the Zn^{2+} complex is still favored over that of Ni^{2+} , although the difference is much less than that found in the case of the cross-linked PMA.

It was considered desirable to compare the degrees of complexation of Ni^{2+} and Zn^{2+} ions by a more flexible polycarboxylate structure in order to see if the order of binding followed the usual trend. Accordingly, the interaction of these ions, as well as Ca^{2+} and Cu^{2+} , with a polyacrylic acid (PAA) resin containing 7.5% divinylbenzene as a cross linker has been measured at 4.4, 25.0, and 49.4° in 1.0 *M* NaNO_3 . Free energies, enthalpies, and entropies of complex formation have been calculated.

A number of workers^{2–7} have investigated the interaction of Cu^{2+} ions with linear or cross-linked polyacrylic acid. It has been shown^{2,4} that a maximum of two carboxylate groups of PAA are bound per cupric ion, although data⁵ concerning the binding of Cu^{2+} by linear polymethacrylic acid are consistent with the assumption that four carboxylate groups are bound per metal ion. All available evidence suggests that, in the case of cross-linked PAA and PMA, the cupric ion is bound by a maximum of two carboxylate groups. Such a condition

has been assumed to be valid in the calculations described in this paper.

Experimental Section

Resin. A sample of a polyacrylic acid resin which contained 7.5% divinylbenzene was placed in a glass column and conditioned by treatment with three alternate washings each with 1 *M* NaOH and 1 *M* HCl. The acidified resin was washed with water until chloride free and oven dried at 110°. The capacity of the resin was found to be 11.40 ± 0.02 mequiv/g.

Equilibrations. The methods of equilibration of the resins with equivalent amounts of Ca^{2+} , Ni^{2+} , Cu^{2+} , and Zn^{2+} nitrates in a 1.0 *M* NaNO_3 medium which contained varying amounts of standard NaOH were the same as those described previously.¹ Measurements of the pH's of the solution phases in contact with the resin were made after equilibrium was attained at 4.4, 25.0, and 49.4°. In addition, after the resin had been separated from the solution at 25°, the bound metal ions were eluted from the resins with dilute HCl. The concentrations of the divalent ions were determined by complexometric titrations with EDTA.⁸ These measurements permitted a comparison between the actual amount of metal bound and that calculated on the basis of potentiometric measurements of the hydrogen ion concentration in solution.

(1) R. L. Gustafson and J. A. Lirio, *J. Phys. Chem.*, **69**, 2849 (1965).

(2) F. T. Wall and S. J. Gill, *ibid.*, **58**, 1128 (1954).

(3) H. P. Gregor, L. B. Luttinger, and E. M. Loebl, *ibid.*, **59**, 34 (1955).

(4) H. P. Gregor, L. B. Luttinger, and E. M. Loebl, *ibid.*, **59**, 366 (1955).

(5) E. M. Loebl, L. B. Luttinger, and H. P. Gregor, *ibid.*, **59**, 559 (1955).

(6) A. M. Kotliar and H. Morawetz, *J. Amer. Chem. Soc.*, **77**, 3692 (1955).

(7) H. Morawetz, *J. Polym. Sci.*, **17**, 442 (1955).

(8) G. Schwarzenbach, "Complexometric Titrations," Interscience Publishers, Inc., New York, N. Y., 1957.

Mathematical Treatment of Data

Values of the binding constant, K_3 , for the reaction



between metal ions and dicarboxylic acid chain segments were calculated by the use of the equations

$$K_3 = \frac{[MA_2][H^+]^2}{[M^{2+}][H_2A_2]} = \frac{\bar{n}}{1 - \bar{n}} \frac{[H^+]^2}{[H_2A_2]} \quad (2)$$

$$\bar{n} = \frac{T_A - 2[H_2A_2] - 2[A^{2-}]}{2T_M} \quad (3)$$

$$2[H_2A_2] = T_A(1 - \alpha) - [H^+] \quad (4)$$

$$K_a = \frac{[H^+][A^{2-}]}{[H_2A_2]} \left(\frac{2[A^{2-}]}{T_A - 2[A^{2-}]} \right)^{\alpha-1} \quad (5)$$

Here, T_A and T_M are the total molar concentrations of carboxylic groups and metal ions, respectively; \bar{n} is the average number of dicarboxylate groups bound per metal ion; α is the number of moles of hydroxide ion added per equivalent of metal ion; and K_a is the dissociation constant of the polyacid.

Values of ΔH° were calculated algebraically from K_3 values obtained at the three temperatures employed. The entropies of reaction were calculated by the expression $\Delta S^\circ = (\Delta H^\circ - \Delta F^\circ)/T$, where $\Delta F^\circ = -2.303RT \log K_3$.

Results and Discussion

Dissociation Constant of PAA Gel. Plots of $-\log [H^+]$ vs. $\log \alpha/(1 - \alpha)$ were linear in the range $\alpha = 0.3$ – 0.7 in accordance with the empirical equation

$$-\log [H^+] = pK_a + n \log \frac{\alpha}{1 - \alpha}$$

The values of pK_a and n obtained in $1 M NaNO_3$ at various temperatures are shown in Table I. As is the case for most carboxylic acids, including cross-linked polymethacrylic acid, the values of pK_a and n are essentially constant in the temperature range of interest. The average values obtained for the PAA and PMA resins are

	pK_a	n
PAA	5.31 ± 0.02	1.89 ± 0.02
PMA	5.91 ± 0.01	1.60 ± 0.00

The polyacrylic acid resin is more acidic than PMA by $0.6 pK$ unit. The higher value of the slope n in the former case indicates that the Coulombic interactions between neighboring functional groups are greater in the case of the polyacrylate resin.

Binding of Divalent Metal Ions. The titration data obtained upon the interaction of partially neutralized PAA resin and metal ions are presented in the form of Henderson-Hasselbach plots in Figure 1. Values of $-\log [H^+]$ at the half-neutralization point ($\alpha = 0.5$) and n are presented in Table II. Similar values ob-

Table I: Values of Slope n and $-\log [H^+]$ at Half-Neutralization Points (pK_a) of PAA-DVB Gel at Various Temperatures in $1.0 M NaNO_3$

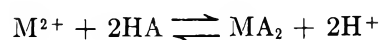
Temp. °C	pK_a	n
4.4	5.29	1.89
25.0	5.29	1.87
49.4	5.34	1.92

tained previously upon the interaction of the same metal ions with a PMA gel are listed for comparison. In each case the difference between the $-\log [H^+]$ value obtained at $\alpha = 0.5$ in the presence of an equivalent amount of divalent metal ion and pK_a for the resin is greater upon binding by PAA than by PMA; *i.e.*, a greater pH drop is observed upon the addition of the metal ion in the former case. This indicates a greater binding tendency of PAA, which might be produced by the lower degree of steric strain which is encountered in this case in conforming to the geometrical requirements of the metal ion. The difference between the pH drop observed in the formation of the PAA complex and that of PMA is least in the case of zinc.

Table II: Values of Slope n and $-\log [H^+]$ at $\alpha = 0.5$ for Interactions of Metal Ions with PAA and PMA Gels at 25° in $1.0 M NaNO_3$

Metal ion	Polyacrylate resin		Polymethacrylate resin	
	$-\log [H^+]$ ($\alpha = 0.5$)	n	$-\log [H^+]$ ($\alpha = 0.5$)	n
Na^+	5.29	1.87	5.91	1.60
Ca^{2+}	4.79	1.50	5.54	1.41
Ni^{2+}	4.42	1.31	5.26	1.26
Zn^{2+}	4.08	1.12	4.78	1.18
Cu^{2+}	3.28	1.30	4.06	1.02

The order of selectivity ($Ca^{2+} < Ni^{2+} < Zn^{2+} < Cu^{2+}$) is similar to that found by Gregor, *et al.*,⁹ in the case of a linear polyacrylic acid. These workers found that values of $-\log B_{av}$ for the reaction



where

$$B_{av} = B_2^{1/2} = \left(\frac{[MA_2][H^+]^2}{[M^{2+}][HA]^2} \right)^{1/2} \quad (6)$$

decreased in the order Mg^{2+} (3.8) > Ca^{2+} (3.7) > Co^{2+} (3.4) > Mn^{2+} (3.0) = Zn^{2+} (3.0) > Cu^{2+} (1.8) in $1 M KCl$. The $-\log B_{av}$ values in the present case at 25° are as follows: Ca^{2+} , 4.78; Ni^{2+} , 3.50; Zn^{2+} , 3.06;

(9) H. P. Gregor, L. B. Luttinger, and E. M. Loebl, *J. Phys. Chem.*, **59**, 990 (1955).

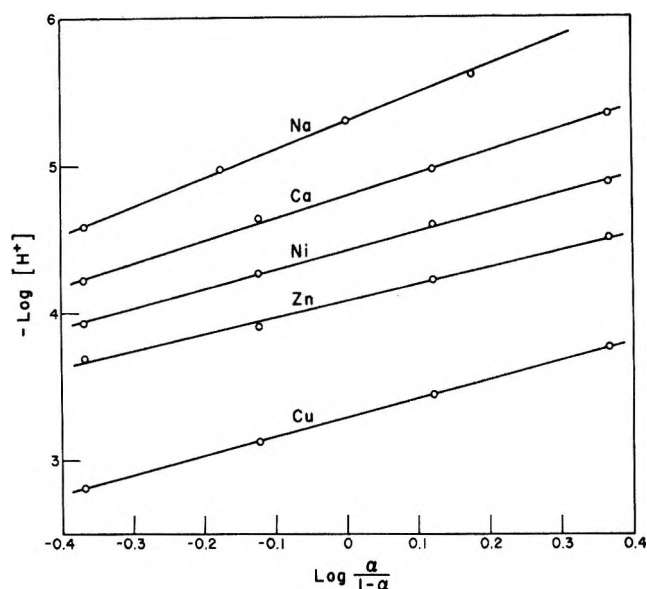
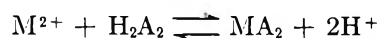


Figure 1. Henderson-Hasselbalch plots obtained upon the interaction of metal ions with cross-linked polyacrylic acid.

Cu^{2+} , 2.08. Gregor, *et al.*,⁴ previously obtained $-\log B_{av}$ values of 1.67 and 1.70 in 0.2 and 2.0 M NaNO_3 solutions, respectively, upon the binding of cupric ions by Amberlite XE-89, a cross-linked polyacrylic acid. Thus the polyacrylic acid resin used in the present study has a somewhat lower affinity for Cu^{2+} than does XE-89. The PAA-7.5% DVB resin binds Ca^{2+} and Cu^{2+} less efficiently than did the linear PAA studied by Gregor, *et al.* This is expected because of the lower flexibility of the cross-linked resin. It is interesting to note that both the cross-linked and linear PAA have nearly identical affinities for Zn^{2+} , however.

Calculation of Thermodynamic Quantities. Values of $\log K_3$ as well as ΔF° , ΔH° , and ΔS° for reaction 1 are shown in Table III. As in the case of binding of divalent metal ions by a PMA gel,¹ the free energies and enthalpies of binding become more positive with an increasing degree of complexation, whereas the entropy of binding becomes more favorable as \bar{n} increases. Similar results have been observed in cases of physical adsorption on activated carbon and synthetic polymeric adsorbents. It has been assumed in these studies that the adsorbent surfaces are heterogeneous and that the energetically preferred sites are occupied first. It is reasonable to assume that a similar effect takes place in the present case because of the supposed heterogeneity (which is the result of the different reactivity ratios of the acrylate and divinylbenzene) of the PAA gel. The free energies of the reaction



are more favorable for the binding by PAA than by PMA in every case as is illustrated in Table IV. The

same is true for ΔH° , although complexation by PMA is favored on an entropy basis. Although the unusual selectivity of Zn^{2+} over Ni^{2+} is observed in the case of

Table III: Thermodynamic Functions for the Reaction of Divalent Metal Ions with a PAA-DVB Gel according to the Reaction $\text{M}^{2+} + \text{H}_2\text{A}_2 \rightleftharpoons \text{MA}_2 + 2\text{H}^+$

\bar{n}	Ca^{2+}	Ni^{2+}	Zn^{2+}	Cu^{2+}
$-\log K_{25}$				
0.1	8.03
0.2	8.71	7.37	6.65	...
0.3	9.39	7.71	6.78	4.60
0.4	...	8.05	6.98	4.90
0.5	7.22	5.19
0.6	5.49
ΔF°_{25} , kcal/mol				
0.1	10.96
0.2	11.89	10.06	9.08	...
0.3	12.82	10.52	9.25	6.27
0.4	...	10.99	9.52	6.68
0.5	9.85	7.08
0.6	7.49
ΔH° , kcal/mol				
0.1	6.6 ^a
0.2	9.5 ^a	4.5 ± 0.6	7.9 ± 1.0	...
0.3	...	5.1 ± 0.9	8.9 ± 0.7	5.0 ± 0.2
0.4	...	6.5 ± 0.5	10.4 ± 0.4	5.0 ± 0.5
0.5	11.7 ± 0.4	5.4 ± 0.4
0.6	6.0 ± 0.3
ΔS° , cal/mol deg				
0.1	-14 ^a
0.2	-8 ^a	-19 ± 2	-4 ± 3	...
0.3	...	-18 ± 3	-1 ± 2	-4 ± 1
0.4	...	-15 ± 2	+3 ± 1	-6 ± 2
0.5	+6 ± 1	-6 ± 1
0.6	-5 ± 1

^a Calculated from 4.4 and 49.4° data only.

Table IV: Comparison of Thermodynamic Quantities Calculated at $\bar{n} = 0.4$ for Binding of Ni, Cu, and Zn Ions by PMA and PAA Gels at 25°

M^{2+}	ΔF° , kcal/mol	ΔH° , kcal/mol	ΔS° , eu
PAA			
Ni	10.99	6.5	-15
Cu	6.68	5.0	-6
Zn	9.52	10.4	+3
PMA			
Ni	13.42	10.6	-9
Cu	8.85	8.9	0
Zn	11.19	14.2	+10
	$\Delta F^\circ_{\text{PMA}} - \Delta F^\circ_{\text{PAA}}$	$\Delta H^\circ_{\text{PMA}} - \Delta H^\circ_{\text{PAA}}$	$\Delta S^\circ_{\text{PMA}} - \Delta S^\circ_{\text{PAA}}$
Ni	2.4	4.1	6
Cu	2.2	3.9	6
Zn	1.7	3.8	7

PAA, the data of Table IV show that there is a somewhat smaller difference $\Delta F^\circ_{\text{PMA}} - \Delta F^\circ_{\text{PAA}}$ in the case of Zn^{2+} than in the case of Ni^{2+} . In general, the differences in ΔF° , ΔH° , and ΔS° of metal ion binding by the two polymers are remarkably similar.

Selectivities of PAA and PMA Gels for Divalent Ions. The quantities of metal ions bound by the various resin samples were determined by direct measurement. As was found previously in the PMA gel binding studies, more metal ion is bound than is calculated on the basis of the pH determinations. The ratios of calculated to actual amounts of metal ions complexed by PAA and PMA gels at $\alpha = 0.5$ are shown in Table V. Here it may be seen that the discrepancy decreases as the binding affinity increases and that the agreement between the actual and calculated values is better upon binding by PAA, except in the case of Ca^{2+} . Although the previously described calculations of K_3 do not permit accurate determinations of the species distributions in the resin phases, the K_3 values give a relative measure of binding affinities. The enthalpy calculations, which demonstrate an increase in binding with increasing temperature, are independent of the inaccuracies produced by the fact that the presence of the metal ions apparently affects the dissociation relation (eq 5) of the polyacid.

Table V: Ratios of Calculated to Actual Amounts of Metal Ions Bound by Polyacrylate and Polymethacrylate Gels at $\alpha = 0.5$

M^{2+}	PAA	PMA
Ca	0.565	0.587
Ni	0.810	0.761
Zn	0.915	0.904
Cu	0.978	0.938

In Figure 2, the fraction of carboxylate groups bound to metal ions, α'/α (where α' = milliequivalents of M^{2+} bound per milliequivalent of resin), has been plotted as a function of the degree of neutralization, α . Whereas the α'/α values tend to level off at α values in excess of 0.5 in the case of the PMA complexes, the plots for the PAA complexes continue to rise. Thus while the selectivity coefficients, $K_{\text{Na}^+ \text{M}^{2+}}$ (equal to $m^r_{\text{M}^{2+}}(m^s_{\text{Na}^+})^2 / m^s_{\text{M}^{2+}}(m^r_{\text{Na}^+})^2$, where m is the molality and r and s refer to resin and solution phases, respectively), of PMA are greater than those of PAA at low degrees of neutralization, the selectivities of PAA for Ca^{2+} , Ni^{2+} , and Zn^{2+} ions exceed those of PMA for the same metal ions above α values of 0.34, 0.56, and 0.8, respectively.

The over-all superiority of binding by the PAA gel is illustrated in Figure 3, in which the quantities of metal

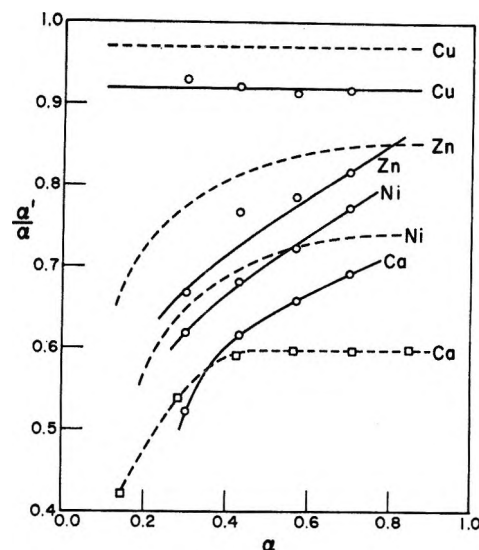


Figure 2. Plots of the fraction of bound carboxylate groups, α'/α , vs. the degree of neutralization for M^{2+} -PAA and M^{2+} -PMA gels in 1.0 M NaNO_3 at 25°: solid lines, PAA; dashed lines, PMA.

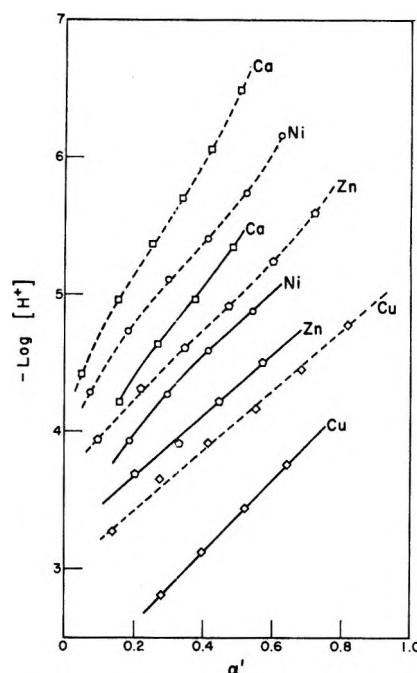


Figure 3. Plots of $-\log [\text{H}^+]$ vs. milliequivalent of divalent metal ion bound per milliequivalent of PAA or PMA gel: solid lines, PAA; dashed lines, PMA.

ion bound per milliequivalent of resin have been presented as a function of pH. At pH 5, over twice as much Ca^{2+} is bound by PAA as by PMA. Similar relationships will be noted for the other systems studied. Naturally, as the pH of the solution phase increases, the percentage difference in the amount of metal ion bound by each resin will decrease.

The Radiolysis of Aqueous Solutions of Cobalt Complexes

by Nicholas Zevos¹

*Sloan Kettering Institute for Cancer Research, Division of Biophysics, New York, New York 10021
(Received August 1, 1967)*

The radiolysis of acidic and neutral solutions containing hexaamminecobalt(III) perchlorate and tris(ethylenediamine)cobalt(III) perchlorate by Co^{60} γ rays has been investigated. In air-saturated acidic solutions, $G(\text{Co}^{2+})$ is 2.3 and 0.31 ions/100 eV for $\text{Co}(\text{en})_3(\text{ClO}_4)_3$ and $\text{Co}(\text{NH}_3)_6(\text{ClO}_4)_3$, respectively. The radiolysis of $\text{Co}(\text{NH}_3)_6(\text{ClO}_4)_3$ is characterized by an induction period at low doses which is removed by the presence of Co^{2+} . $\text{Co}(\text{en})_3(\text{ClO}_4)_3$ does not display an induction period under similar conditions. It appears that the ligand of $\text{Co}(\text{en})_3^{3+}$ undergoes reaction with the hydroxyl radical directly. In neutral solutions, the central metal atom is reduced to Co^{2+} by hydrated electrons. For air-free solutions, there is a nonlinear increase of the cobaltous ion concentration with absorbed dose; while in air-saturated solutions, there is a linear response with $G(\text{Co}^{2+}) = 3.3$ ions/100 eV for $\text{Co}(\text{NH}_3)_6(\text{ClO}_4)_3$ and $G(\text{Co}^{2+}) = 2.4$ ions/100 eV for $\text{Co}(\text{en})_3(\text{ClO}_4)_3$.

Introduction

There has been very little work reported on the radiolysis of aqueous solutions of coordination complexes of cobalt. Katakis and Allen² have investigated the radiolysis of hexaamminecobalt(III) perchlorate and aquopentaamminecobalt(III) perchlorate in 0.1 *N* HClO_4 . We have studied the radiolysis of two cobalt complexes, tris(ethylenediamine)cobalt(III) and hexaamminecobalt(III) perchlorate in 0.1 *N* HClO_4 . Our investigation also describes the behavior of the radiolysis of these cobalt complexes in neutral solution. A comparison is made of the reduction of Co^{3+} complexes in acidic and neutral solutions.

Experimental Section

Preparation and Purification of Compounds. Cobalt(II) perchlorate was prepared by acidification of cobalt(II) carbonate with perchloric acid. The crude cobalt(II) perchlorate was then recrystallized from triply distilled water.

Hexaamminecobalt(III) perchlorate was prepared by addition of perchloric acid to a solution of the bromide salt obtained from the K & K Chemical Co. The crude precipitate was recrystallized three times from 0.5 *N* HClO_4 . *Anal.* Calcd for $\text{Co}(\text{NH}_3)_6(\text{ClO}_4)_3$: N, 18.20. Found: N, 18.28.

Tris(ethylenediamine)cobalt(III) perchlorate was prepared by a method described by Brubaker³ which involves a metathesis reaction between tris(ethylenediamine)cobalt(III) chloride and silver perchlorate. A slight excess of the silver salt was added, the solution was concentrated, and the crude salt was precipitated by the addition of ethanol. *Anal.* Calcd for $\text{Co}(\text{en})_3(\text{ClO}_4)_3$: C, 13.39. Found: C, 13.44.

Analysis of Co^{2+} in the Presence of the Various Complexes. Analytical work in this radiation chemical study requires a determination of Co^{2+} in the presence of the complex. The method used was the one described by Katakis and Allen² in which 5 ml of the Co^{2+}

solution, 5 ml of a NH_4SCN (566 g/l.) solution, and 5 ml of methyl isobutyl ketone were mixed and shaken for 1 min. The optical density of the organic layer was determined at 620 $\text{m}\mu$ in a Beckman DU spectrophotometer. All spectrophotometric measurements were carried out at 25°.

For the hexaamminecobalt(III), the calibration may be divided into two parts: the linear portion at optical densities greater than 0.2, and a nonlinear portion at optical densities less than 0.2. In the first region the concentration of Co^{2+} in the presence of the complex is given by the empirical equation determined by Katakis and Allen.² At concentrations less than 100 μM , the amount of Co^{2+} was estimated by reference to a calibration curve.

A similar equation was developed for the determination of Co^{2+} in the presence of $\text{Co}(\text{en})_3(\text{ClO}_4)_3$. The concentration of Co^{2+} is given by $[\text{Co}^{2+}] = 5.24 \times 10^2 \Delta\text{OD}$, where $[\text{Co}^{2+}]$ is the concentration of Co^{2+} in micromoles per liter. $\Delta\text{OD} = \text{OD}_S - \text{OD}_B$, OD_S and OD_B being the optical density of the sample and blank, respectively.

The Determination of Hydrogen Peroxide. The titanium sulfate method was used for the determination of hydrogen peroxide. Co^{2+} and other known products did not interfere with the determination. Calibration curves were constructed using known quantities of hydrogen peroxide in solutions containing the complexes.

Dosimetry. The absorbed dose was determined by using the Fricke dosimeter with $G(\text{Fe}^{2+}) = 15.5$ ions/100 eV. All irradiations were carried out with a Co^{60} γ cell (Atomic Energy of Canada Ltd.) with a dose rate of 2500 rads/min.

(1) Present address: Department of Chemistry, Cornell University, Ithaca, N. Y. 14850.

(2) D. Katakis and A. O. Allen, *J. Phys. Chem.*, **68**, 1359 (1964).

(3) C. H. Brubaker and T. E. Haas, *ibid.*, **65**, 866 (1961).

Preparation of Solutions. All solutions were prepared with triply distilled water produced in all-glass stills. Air-free solutions were prepared on a vacuum line by subjecting the mixture to a cycle of freezing, pumping, melting, and shaking. Other air-free samples were prepared by saturating the solution with pre-purified nitrogen which was passed through a trap containing activated charcoal maintained at -90° .

Analyses. The presence of ammonium ion was determined by Nessler's reagent⁴ (Fisher Scientific Co.). Chloroplatinic acid (10%) (Fisher Scientific Co.) was used to prepare the chloroplatinates of the amine derivatives formed by radiolysis. To form the chloroplatinates, the irradiated solutions were concentrated by a factor of 3 by slow evaporation on a hot plate. The solutions were allowed to cool and 1 ml of 10% chloroplatinic acid was added for every 25 ml of concentrated solution.

Spectra. All ultraviolet and visible spectra reported in this work were obtained with a Cary Model 15B and a Beckman DU spectrophotometer. A Perkin-Elmer Model 21 ir spectrophotometer was used to obtain infrared spectra of the chloroplatinate compounds. Solid solutions containing 1% of the chloroplatinate in KBr were pressed into disks 1 mm in thickness.

Calculation of $G(-Complex)$. The radiation chemical yields for the disappearance of the complex ions were determined by the decrease in optical density of the solutions as a function of dose. Peaks in the visible region of the spectrum were used for both complexes. The molar extinction coefficients calculated from the optical density of solutions of known concentrations agreed with values given in the literature.^{5,6}

Results

Product Analysis. Irradiation of all the complexes resulted in reduction of Co^{3+} to Co^{2+} . This reaction is balanced in the case of $Co(NH_3)_6(ClO_4)_3$ with the formation of nitrogen gas.² The products formed in the radiolysis of $Co(en)_3(ClO_4)_3$ are more complex. In both neutral and acidic solutions, nitrate and nitrite could not be detected. We tested the possibility that NH_4^+ and an amine aldehyde formed in the photochemical reaction might also be formed in the radiolysis. The experiments confirmed the presence of NH_4^+ and the absence of any compound containing the aldehyde functional group. The ir spectrum of the precipitates formed by the addition of a 10% chloroplatinic acid solution to a concentrated portion of an irradiated air-free solution was compared to the ir spectrum of $(NH_4)_2PtCl_6$. The infrared spectra of the precipitates obtained from acidic and neutral radiolysis contain the peaks at 3.08 and 7.13 μ found in the $(NH_4)_2PtCl_6$ spectrum, but they also contain other groups of peaks, indicating a mixture of amine-type compounds.

The ir spectra of the precipitates obtained from irradiated acid and neutral solutions are similar.

The Yield of Co^{2+} in 0.1 N $HClO_4$ Solutions. Radiolysis of $10^{-3} M Co(NH_3)_6(ClO_4)_3$ in 0.1 N $HClO_4$ resulted in $G(Co^{2+}) = 2.3$ ions/100 eV; the value reported by Katakis and Allen is 2.5 ions/100 eV. The presence of $10^{-2} M NaCl$ caused a decrease similar to the one reported by the above authors. In air-saturated solutions, $G(Co^{2+}) = 0.34$ ion/100 eV. An induction period similar to the one observed by Katakis and Allen was obtained.²

The formation of Co^{2+} in irradiated solutions of $10^{-3} M Co(en)_3(ClO_4)_3$ in 0.1 N $HClO_4$ is shown in Figure 1. After an initial nonlinear portion, the radiolysis of the air-free solutions results in $G(Co^{2+}) = 2.9$ ions/100 eV. The presence of air in the solution lowers the yield to 2.3 ions/100 eV, while the addition of $10^{-4} M Co(ClO_4)_2$ to the air-saturated solutions does not affect $G(Co^{2+})$. Addition of $10^{-2} M NaCl$ lowers the yield to 0.64 ion/100 eV.

The Yield of Co^{2+} in Neutral Solutions. The relationship between the absorbed dose and Co^{2+} concentration for irradiated neutral solutions of the complexes is shown graphically in Figures 2 and 3. The formation of Co^{2+} in neutral air-saturated solutions is a linear function of the absorbed dose with $G(Co^{2+}) = 3.3$ ions/100 eV for $Co(NH_3)_6(ClO_4)_3$ and $G(Co^{2+}) = 2.4$ ions/100 eV for $Co(en)_3(ClO_4)_3$. In air-free solutions, there is a nonlinear relationship between cobaltous ion formation and the absorbed dose, which is given by

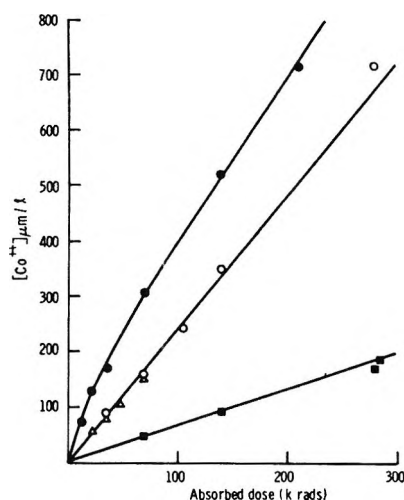


Figure 1. Formation of Co^{2+} in irradiated solutions of $Co(en)_3(ClO_4)_3$ in 0.1 N $HClO_4$: ●, $10^{-3} M$ complex (air free); ○, $10^{-3} M$ complex (air saturated); △, $10^{-3} M$ complex, $10^{-4} M Co^{2+}$ (air saturated); ■, $10^{-3} M$ complex, $10^{-2} M NaCl$ (air saturated).

(4) F. Feigl, "Spot Tests in Inorganic Analysis," Elsevier Publishing Co., New York, N. Y., 1958, p 238.

(5) A. W. Adamson and A. H. Sporer, *J. Amer. Chem. Soc.*, **80**, 3865 (1958).

(6) C. W. Moeller, *ibid.*, **80**, 265 (1958).

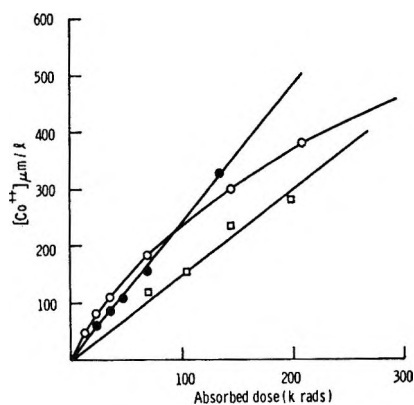


Figure 2. Formation of Co^{2+} in irradiated neutral solutions of $10^{-3} M \text{Co}(\text{en})_3(\text{ClO}_4)_3$: \circ , $10^{-3} M$ complex (air free); \bullet , $10^{-3} M$ complex (air saturated); \square , $10^{-3} M$ complex, $10^{-2} M$ acetone.

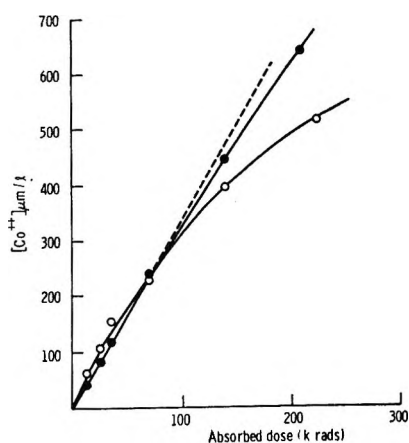


Figure 3. Formation of Co^{2+} in irradiated neutral solutions of $10^{-3} M \text{Co}(\text{NH}_3)_6(\text{ClO}_4)_3$: \bullet , $10^{-3} M$ complex (air saturated); \circ , $10^{-3} M$ complex (air free).

the general equation $\log [\text{Co}^{2+}] = m \log D + b$, where $[\text{Co}^{2+}]$ is in $\mu\text{mol/l}$ and the absorbed dose, D , in krads. The slope (m) and the y intercept are $m = 0.74$ and $b = 1.01$ for $\text{Co}(\text{NH}_3)_6(\text{ClO}_4)_3$ and $m = 0.71$ and $b = 0.93$ for $\text{Co}(\text{en})_3(\text{ClO}_4)_3$. The addition of $10^{-2} M$ acetone to the $\text{Co}(\text{en})_3(\text{ClO}_4)_3$ solution lowers the yield to $G(\text{Co}^{2+}) = 1.6$, the points being somewhat scattered. The presence of $10^{-2} M$ methanol increases the yield of Co^{2+} to $G(\text{Co}^{2+}) = 4.9$ ions/100 eV.

The Hydrogen Peroxide Yield and the Yields for the Disappearance of the Complex Ions. The values for the disappearance of the complex ions under various conditions are given in Table I. All values are normal and are about equal to the corresponding values for the production of Co^{2+} . In neutral solution the yields for the disappearance of the ions could not be determined, owing to an increase in the absorbance at the wavelengths which were used to determine the yields in acidic solutions. The table also includes values for the hydrogen peroxide formation in irradiated $0.1 N \text{HClO}_4$ solutions containing the complexes.

Table I: Radiation Chemical Yields (ions/eV) in Irradiated Solutions of Cobalt Coordination Compounds

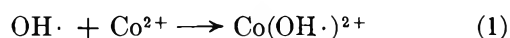
Complex	Medium	G (-com- plex) (air free)	G (-com- plex) (air satu- rated)	$G(\text{H}_2\text{O}_2)$ (air satu- rated)
$\text{Co}(\text{NH}_3)_6(\text{ClO}_4)_3$	$0.1 N \text{HClO}_4$	1.9	0.31	2.11
$\text{Co}(\text{en})_3(\text{ClO}_4)_3$	$0.1 N \text{HClO}_4$	3.0	2.3	2.70

Discussion

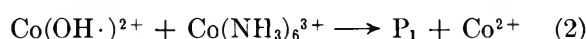
Katakis and Allen² have described the behavior of complex ions in irradiated acid solutions. They reported two essential features which are required to decompose the ion and cause reduction of metal atoms present.

(1) The yield $G(\text{Co}^{2+})$ depends on the presence of an oxidizing radical as well as a reducing radical. The assumption is that the oxidizing radical initially attacks the ligand of the complex. This reaction is followed by the reduction of the central atom by the hydrogen atoms present.

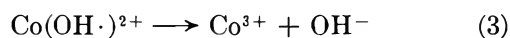
(2) The presence of Co^{2+} appears to be necessary to reduce the induction period found at low doses. This presence of Co^{2+} necessitates the postulation of an intermediate, since Co^{2+} is oxidized by hydroxyl radicals,⁷ so that the reaction sequence may be pictured as



now $\text{Co}(\text{OH}\cdot)^{2+}$ may react by two different modes



where P_1 is a free-radical intermediate which may subsequently be attacked by $\text{H}\cdot$, the end products being Co^{2+} and an oxidized product of the ligand. Secondly, the reaction



must also take place to some extent.

We were able to obtain similar results for $\text{Co}(\text{NH}_3)_6^{3+}$ in acidic solution, which indicated an induction period and a decrease in $G(\text{Co}^{2+})$ by the presence of chloride ion. In air-saturated solutions of the ethylenediamine complex, the presence of chloride ion lowers $G(\text{Co}^{2+})$ from 2.3 to 0.64 ions/100 eV, indicating that the hydroxyl radical is required in the over-all reduction reaction. In the radiolysis of the air-free ethylenediamine complex, we were unable to observe an induction period similar to the one observed by Katakis and Allen² for irradiated air-free solutions of $\text{Co}(\text{NH}_3)_5\text{H}_2\text{O}^{3+}$ and $\text{Co}(\text{NH}_3)_6^{3+}$. Secondly, the presence of Co^{2+} does not change the Co^{2+} yield. In the air-free

(7) M. J. Lefort, *J. Chim. Phys.*, **54**, 782 (1957).

solutions, $G(\text{Co}^{2+}) = 2.95$ ions/100 eV. This value represents the limit in the yield, since $G_{\text{OH}} = 2.95$.⁸ The absence of an induction period and the independence of the yield on (Co^{2+}) suggests that the radiation chemistry of acidic solutions of $\text{Co}(\text{en})_3^{3+}$ is different from $\text{Co}(\text{NH}_3)_6^{3+}$ and $\text{Co}(\text{NH}_3)_5(\text{H}_2\text{O})^{3+}$. It appears that $\text{Co}(\text{en})_3^{3+}$ reacts directly with the hydroxyl radical. This difference could arise from the reactivity of the ligands with the hydroxyl radical. Comparison of the radiation chemistry of the ligands indicates that ammonia cannot be oxidized by ionizing radiation in air-free acidic solution,⁹ while under similar conditions the oxidation of ethylenediamine solutions occurs readily.¹⁰ This ligand reactivity might contribute to the high yield in the case of $\text{Co}(\text{en})_3(\text{ClO}_4)_3$.

The Hydrogen Peroxide Yield. The results of Katakis and Allen² indicate that $G(\text{H}_2\text{O}_2) = G_{\text{H}_2\text{O}_2} + 1/2(G_{\text{H}} - G_{\text{OH}})$ or 1.20 molecules/100 eV for the aquopentaammine complex. We have found that $G(\text{H}_2\text{O}_2)$ is nearly twice this value for the hexaammine and ethylenediamine complexes.

Hydrogen peroxide arises from two sources in air-saturated irradiated solutions: there is a contribution from the molecular yield and a contribution from the reaction of hydrogen atoms with the dissolved oxygen and subsequent disproportionation of the hydroperoxyl radicals to form H_2O_2 . If all H atoms reacted with the oxygen present rather than the dissolved solute, then the hydrogen peroxide yield would be given by

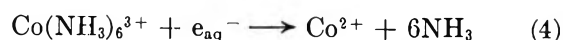
$$G(\text{H}_2\text{O}_2) = G_{\text{H}_2\text{O}_2} + \frac{G_{\text{H}}}{2} = 2.55$$

Our value of 2.70 for $\text{Co}(\text{en})_3^{3+}$ is very close to this. For the hexaammine complex, the value is 2.11, indicating that some of the hydrogen atoms react by the above scheme to form H_2O_2 and some are used to reduce the complex. Actually the number which react with the complex is small since $G(\text{Co}^{2+}) = 0.31$ ion/100 eV. For the ethylenediamine complex, it appears that all the H atoms form H_2O_2 *via* reaction with the dissolved oxygen. Then one must account for the reduction of the complex since $G(\text{Co}^{2+}) = 2.3$ ions/100 eV. Since in this case the initial attack by the hydroxyl radical is on the ligand as proposed above, this must convert the ethylenediamine into a reducing radical which subsequently attacks the central atom in some manner to bring about the reduction to Co^{2+} .

Neutral Solutions. In neutral solutions the predominant reducing species is the hydrated electron, but there also appears to be a small yield of hydrogen atoms. The values given by Allen¹¹ for each of the species is $G_{e_{\text{aq}}^-} = 2.85$ and $G_{\text{H}} = 0.55$; therefore, the predominant reduction will involve the hydrated electrons.

It has been shown by observing the disappearance of

the absorption maximum of the hydrated electron that the reaction



proceeds with a rate constant equal to $9.0 \times 10^{10} M^{-1} \text{sec}^{-1}$,¹² so that under initial conditions $G(\text{Co}^{2+}) = G(e_{\text{aq}}^-) = 2.85$. As the reaction proceeds, the Co^{2+} which has been formed (eq 4) may react with e_{aq}^- ¹³



The reaction with cobaltous ion is known to proceed with a rate constant of $1.22 \times 10^{10} M^{-1} \text{sec}^{-1}$. The hydrated electrons will be used up by reactions 4-6, but only reaction 4 produces Co^{2+} ; therefore, one would expect a decrease in Co^{2+} production in the latter stages of the reaction. The $\text{Co}(\text{NH}_3)_6^{3+}$ and $\text{Co}(\text{en})_3^{3+}$ both appear to exhibit this type of behavior.

The hydroxyl radical does not appear to be involved in the mechanism for the conversion of Co^{3+} complexes to Co^{2+} in neutral solutions. If the hydroxyl radical was involved, then $G(\text{Co}^{2+})$ would be equal to $G_{e_{\text{aq}}^-} + G_{\text{OH}}$. Experimentally, $G(\text{Co}^{2+}) = G_{e_{\text{aq}}^-}$. The hydroxyl radicals generated by the ionizing radiation must react with another component present in the system, probably one of the products.

$G(\text{Co}^{2+})$ in the Presence of Radical Scavengers (Neutral Solutions). In the presence of oxygen the plots of Co^{2+} vs. absorbed dose have a linear response (Figures 2 and 3). $G(\text{Co}^{2+})$ for the irradiated solutions containing $\text{Co}(\text{NH}_3)_6^{3+}$ is 3.3 ions/100 eV. If we take $G_{e_{\text{aq}}^-} = 2.85$ and $G_{\text{H}} = 0.55$, the sum of these two quantities would represent the total possible reduction yield of 3.4. This agrees well with our value, indicating that the bulk of the reaction of the complex in neutral solution is carried out by the hydrated electrons. There is no indication of what role the hydrogen atoms play in the reduction under these conditions. The presence of oxygen appears to decrease the effectiveness of reactions 5 and 6. For irradiated air-saturated solutions of $\text{Co}(\text{en})_3(\text{ClO}_4)_3$ in neutral solutions, $G(\text{Co}^{2+})$ is 2.4 ions/100 eV. The rate constant for the reaction between $\text{Co}(\text{en})_3(\text{ClO}_4)_3$ and the hydrated electron is $8.2 \times 10^{10} M^{-1} \text{sec}^{-1}$, which is comparable to the rate constant for the reaction between e_{aq}^- and $\text{Co}(\text{NH}_3)_6^{3+}$. Both rate constants were determined under similar conditions in neutral water.¹³ Thus the large decrease

(8) A. O. Allen, "The Radiation Chemistry of Water and Aqueous Solutions," D. Van Nostrand Co., Inc., Princeton, N. J., 1961, p 41.

(9) T. Rigg, G. Scholes, and J. Weiss, *J. Chem. Soc.*, 3034 (1952).

(10) M. Anbar, R. A. Munoz, and P. Rona, *J. Phys. Chem.*, **67**, 2708 (1963).

(11) A. O. Allen, *Radiat. Res. Suppl.*, **4**, 54 (1964).

(12) M. Anbar and E. J. Harz, *J. Phys. Chem.*, **69**, 973 (1965).

(13) J. H. Baxendale, E. M. Felden, C. Capellos, J. M. Francis, J. V. Davies, M. Ebert, C. W. Gilbert, J. D. Keene, E. J. Land, A. J. Swallow, and J. M. Nosworthy, *Nature*, **201**, 468 (1964).

in $G(\text{Co}^{2+})$ for solutions containing $\text{Co}(\text{en})_3(\text{ClO}_4)_3$ under similar initial conditions cannot readily be explained.

The radiolysis of air-free $\text{Co}(\text{en})_3^{3+}$ containing $10^{-2} M$ methanol resulted in $G(\text{Co}^{2+}) = 4.8$ ions/100 eV. This value is much too high to be accounted for by the action of the reducing radicals only. The addition of alcohol must convert the oxidizing radical ($\text{OH}\cdot + \text{CH}_3\text{OH} \rightarrow \cdot\text{CH}_2\text{OH} + \text{H}_2\text{O}$) into a reducing species. Thus $G(\text{Co}^{2+})$ should equal $G_{\text{e}_{\text{aq}}^-} + G_{\text{OH}}$ or 5.60 ions/100 eV. The agreement between the observed

and calculated value is fairly good. It would be interesting to see if a higher alcohol concentration would bring the values closer together.

Acknowledgments. The author wishes to thank Dr. Alexander Amell and Mr. Steve Stepenack of the University of New Hampshire Chemistry Department for their constructive suggestions in the preparation of the manuscript. He is also indebted to Mrs. Denise Martin Zevos, his wife, for proofreading the manuscript.

A Semiempirical Model for Simple Liquids

by F. Ciani, G. Cicogna,¹ and M. Maestro

Istituto di Chimica Fisica dell'Università Pisa, Pisa, Italy

Accepted and Transmitted by The Faraday Society (August 3, 1967)

A model for simple liquids is given, based on a semiempirical partition function, which is the sum of a "solid-like" term and a "gas-like" one. The model is applied to liquid argon; the results are compared with the experimental data and with the results of cell theory and of significant structure theory.

In this article, a brief sketch of a possible model for simple liquids is given. This approach is based on the usual canonical partition function technique, in analogy with other liquid-state theories such as the cell theory^{2a} and the significant structure theory.^{2b} In the present work, we shall apply our model, in its most simple form, to liquid argon; the first results we shall give seem to encourage this approach.

We can conveniently introduce our argument, using just the cell theory as a starting point. A quantistic version of this theory has been proposed:³ the energy eigenvalues of the Schrödinger equation with the Lennard-Jones and Devonshire potential have been found, requiring the wave function to be zero at the cell boundaries; the partition function has then to be written as an infinite sum over all of these eigenvalues.

On pure physical grounds, it does not appear to be completely satisfying to consider each molecule of a liquid as confined into a little region by an infinitely deep potential and to treat all its energy levels as discrete vibrational "solid-like" ones. In fact, the molecules surely possess some translational degrees of freedom. We know, in addition, that an important physical quantity can be defined and experimentally measured: the activation energy for viscous flow.⁴ This quantity may be viewed as a sort of critical

parameter; roughly, when a molecule of the given fluid has an energy larger than this value (which we shall indicate with ϵ), it can escape from its equilibrium position and move into the "sea" of the other molecules.

It would be not impossible to imagine some expression of the intermolecular potential accounting for this situation; starting from this, we could calculate the molecular energy levels and then obtain the partition function for the liquid. We do not follow this approach here; we prefer to write down directly the simplest form of the partition function which can be easily justified on the grounds of pure phenomenology.

We shall imagine that a molecule having an amount of energy lower than the critical value ϵ is bound by the intermolecular potential; in this situation, we suppose that it vibrates as a simple three-dimensional quantistic oscillator, with a fundamental frequency ω .

(1) Istituto Matematico dell'Università Pisa.

(2) (a) See, e.g., J. A. Barker, "Lattice Theories of the Liquid State," Oxford University Press, Oxford, 1963 (see also ref 7); (b) J. Walter and H. Eyring, *J. Chem. Phys.*, **9**, 393 (1941); H. Eyring and P. Marchi, *J. Chem. Educ.*, **40**, 562 (1963).

(3) J. M. H. Levelt and R. P. Hurst, *J. Chem. Phys.*, **32**, 96 (1950).

(4) J. O. Hirschfelder, C. F. Curtiss, and R. B. Bird, "Molecular Theory of Gases and Liquids," John Wiley and Sons, Inc., New York, N. Y., 1954.

The contribution f_1 of the corresponding energy levels to the one-particle partition function is then readily written

$$f_1 = \sum_{n=0}^s g_n e^{-(n+1/2)(h\omega/kT)} \quad (1)$$

The highest energy level E_s appearing in the summation is fixed by the condition $E_s \leq \epsilon \leq E_{s+1}$, and the degeneracy factor g_n is taken to be

$$g_n = N(n+1)(n+2)/2 \quad (2)$$

In (2), the factor N takes into account the degeneracy arising from the N potential wells. Actually, the interaction between them will split this degeneracy and will give rise to energy bands larger and larger when approaching the top of the wall; we completely neglect this effect. The other factor in g_n is the usual geometrical degeneracy factor for the three-dimensional oscillator.

For molecular energies larger than ϵ , we suppose that the molecule behaves as a nearly free particle, and that in this case its energy levels belong to a continuous band, whose bottom is fixed to be ϵ . Then, the corresponding contribution f_2 to the partition function is assumed to be a modified form of the usual free-particle term

$$f_2 = V' e^{-\epsilon/kT} (2\pi mkT/h^2)^{3/2} \quad (3)$$

where V' is the total volume which can be spanned by the molecule, *i.e.*, the total volume of the liquid, diminished by the volume V_s , that the molecules would occupy if they were in the solid state.

Summarizing, we are led to write the following form of the total partition function.

$$Z_N = \frac{1}{N!} \left\{ \sum_{n=0}^s g_n e^{-(n+1/2)(h\omega/kT)} + (V - V_s) e^{-\epsilon/kT} \left(\frac{2\pi mkT}{h^2} \right)^{3/2} \right\}^N \quad (4)$$

There is no doubt that (4) represents a very schematic picture of the liquid state. At very low energies, the levels will be of vibrational type, and they will show a continuous structure at the highest energies; however, it is clear that no discontinuity will appear in their structure such as we have supposed, at the value ϵ . Several aspects of this partition function could be improved; we believe that the form we now considered could represent a first rough approximation of the physical situation.

In order to obtain explicitly the partition function and then the thermodynamic properties at definite T and V , we have to fix the parameters entering in (4). In the following, we shall refer to the case of liquid argon.

The most important parameter is the energy ϵ . For lack of experimental data, we suppose⁴ that this

quantity is proportional to the vaporization energy ΔU

$$\epsilon \simeq \Delta U/2.5 \quad (5)$$

Relation 5, which is well satisfied for many liquids, gives for argon^{5,6} $\epsilon \simeq 4 \times 10^{-14}$ erg/molecule. Actually, ϵ is not independent of V and T , but it is well approximated by a constant for large intervals (except in the region very near to the critical point). In practice, we performed our calculations for three different values of ϵ , *i.e.*, 4, 4.5, and 5×10^{-14} erg/molecule; the corresponding results will be labeled, respectively, I, II, III.

The fundamental frequency ω may be deduced in various ways, with results that are very insensitive to different hypotheses. One could, for instance, consider a sinusoidal potential of height about ϵ and period determined by the volume, and directly calculate the fundamental frequency of small oscillations around the equilibrium positions; thus one obtains for ω a value 3.8×10^{12} sec⁻¹, which is influenced very little by variations of volume in the liquid region. The choice of Lennard-Jones and Devonshire potential would give a value $\omega = 3.66 \times 10^{12}$ sec⁻¹. Finally, we assume for V_s a value equal to 24.98 cm³ (solid molar volume at the triple point).

Figure 1 gives our results (curves marked I, II, III) for the entropy S

$$S = k \ln Z_N + kT \left(\frac{\partial \ln Z_N}{\partial T} \right)_V \quad (6)$$

along the saturation curve, obtained using the three values we have chosen for ϵ . The results are compared with those given by Din⁶ from experiments. In the same figure, a vertical bar marked c.e. shows the quantity Nk , that is the maximum value of the so-called "communal entropy,"⁴ roughly representing the typical contribution of translational degrees of freedom. Our curves exhibit a correct behavior with respect to Din's data and exceed these by a quantity smaller than this term, thus showing that our main error amounts to a partial overestimation of the gas-like contributions. Note, of course, that detailed calculations based on the hypothesis of multiply occupied cells into the liquid give an actual value for the c.e. term largely smaller than Nk , as pointed out by Pople.⁷ The situation occurring in our model can be usefully compared with the one in the cell theory, where, instead, gas-like contributions are somewhat disregarded. We refer to Figure 2, where a comparison is shown with the results obtained by means of this theory^{2a,8} ("N.L. ∞

(5) H. Landolt and R. Börnstein, "Physikalische-Chemische Tabellen," 5th ed, Springer-Verlag, Berlin, 1935.

(6) F. Din, "Thermodynamic Functions of Gases," Vol. II, Butterworth and Co., Ltd., London, 1956.

(7) J. A. Pople, *Phil. Mag.*, **42**, 459 (1951).

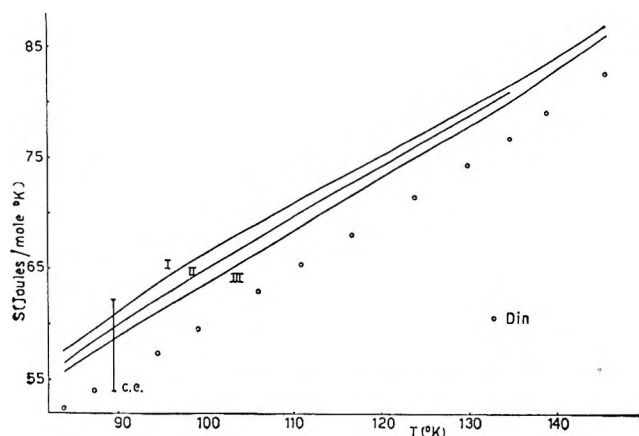


Figure 1.

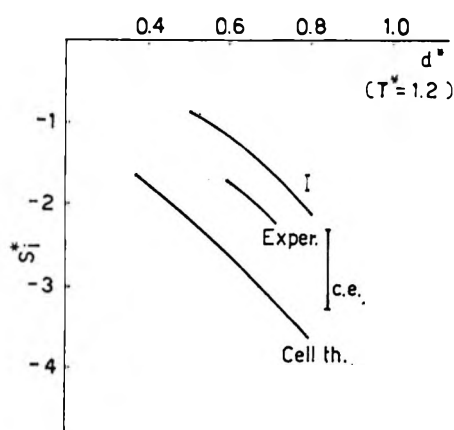


Figure 2.

–3” method) for the internal entropy S_i . These results are given, together with experimental data, by Levelt and Cohen⁸ (“reduced” quantities are used: $d^* = 1/V^* = N\sigma^3/V$; $T^* = T/\eta$; $S^* = S/Nk$; $\sigma = 3.405 \text{ \AA}$; $\eta = 119.8^\circ\text{K}$). As a further example, we can similarly compare the result $S_i^* = -5.51$ at $T^* = 0.7$ (near the triple point), given by Barker^{2a} using the cell theory, with the experimental value -3.64 ,^{2a} and with our -3.06 (case I) or -3.27 (case III).

Also, the change of entropy ΔS_v for the vaporization can be easily calculated, supposing, *e.g.*, that we treat the vapor as a perfect gas. At the normal boiling point, we obtain (choice I) $\Delta S_v = 16.6 \text{ cal/mole } ^\circ\text{K}$, to be compared to the experimental value 17.85 and to the result 19.04 obtained by means of the significant structure theory.^{2b}

Figure 3 gives an important test for our model; it compares with the experimental values^{6,9} our results for the molar specific heat at constant volume C_v

$$C_v = \frac{\partial}{\partial T} \left(kT^2 \frac{\partial \ln Z_N}{\partial T} \right)_v \quad (7)$$

Figure 3 indicates that the “best” value of ϵ is

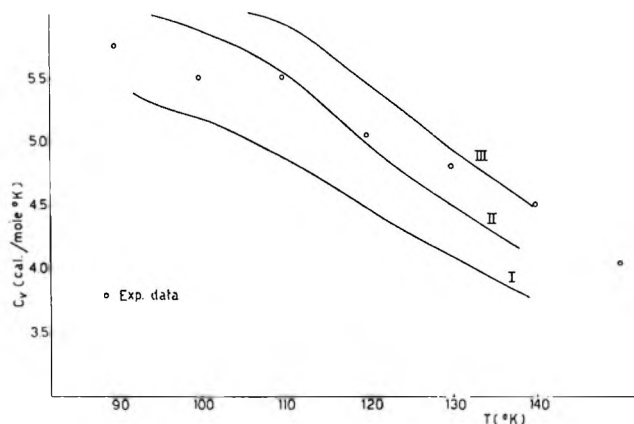


Figure 3.

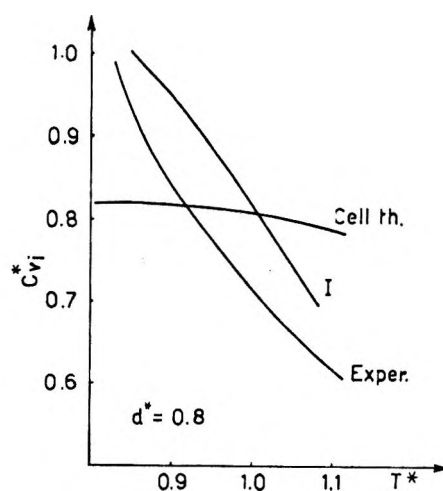


Figure 4.

$4.5 \times 10^{-14} \text{ erg/molecule}$, very close to the empirical datum suggested by (5). This fact may indicate that the parameter ϵ is not to be considered a simple “unphysical” adjustable parameter, thus confirming the intrinsic correctness of the original idea.

As before, we can compare (Figure 4) our results with the values obtained by means of cell theory for the “internal reduced” specific heat⁸ $C_{v_i}^*$ ($C_{v_i}^* = C_v/Nk$).

The present exposition is clearly far from complete. For instance, the introduction of a “zero point” lattice energy term could allow one to obtain free energy curves, etc.¹⁰ In this paper, we have confined our attention to showing the physical grounds of the model and its first applications; the conclusion seems to be that the model is not inconsistent and that it appears not completely useless, even in its most simple version.

(8) J. M. H. Levelt and E. G. D. Cohen in “Studies in Statistical Mechanics,” Vol. II, Part B, J. de Boer and G. E. Uhlenbeck, Ed., North-Holland Publishing Company, Amsterdam, 1964.

(9) A. Eucken and F. Hauck, *Z. Physik. Chem.*, **134**, 161 (1928).

(10) For further details on the whole subject, the reader can be referred to F. Ciani, Thesis, University of Pisa, 1967.

Acknowledgment. The authors are very grateful to Professor E. Scrocco, who suggested the model, and to

Professor S. Franchetti for his kind interest in the subject.

Thermal Decomposition of Some Polynitroalkanes¹

H. P. Marshall, F. G. Borgardt, and P. Noble, Jr.

Lockheed Palo Alto Research Laboratory, Palo Alto, California 94304 (Received August 3, 1967)

The rates of thermal decomposition of tetranitromethane, bromotrinitromethane, chlorotrinitromethane, and 1,2-dichlorotetranitroethane were determined in a number of solvents. The decomposition of the methane series of compounds in CCl₄ proceeds by a first-order reaction; their specific rate constants are best represented by $k = 10^{16.3} \exp((-38,400 \pm 1400)/RT)$. The products of reaction from the thermal decomposition of tetranitromethane are best represented by the equation $C(NO_2)_4 = CO_2 + 0.25N_2O + 2.25NO_2 + 1.25NO$. Based on the kinetic data, the rate-determining step for the decomposition of the polynitromethanes is the rupture of the C-N bond. The decomposition of 1,2-dichlorotetranitroethane in solution proceeds at a rate 1.8×10^5 times faster than that of tetranitromethane at 85°. The decomposition proceeds by a first-order reaction with $k = 10^{16.6} \exp(-31,000/RT)$, the increased rate of decomposition relative to tetranitromethane being due to a much smaller energy of activation.

Introduction

As part of the general study of the chemistry of polynitro compounds, the rates of thermal decomposition of tetranitromethane (TNM), chlorotrinitromethane (Cl-TNM), bromotrinitromethane (BrTNM), and 1,2-dichlorotetranitroethane (DCITNE) were determined in selected solvents at various temperatures. The results of this study are discussed and a mechanism for the decomposition is proposed.

Experimental Section and Results

The solvents Freon 113 and Freon 114B2 (purchased from Du Pont) were distilled prior to use. CCl₄, reagent grade, was used as received, and the cyclohexane was purified by the method of Wiberg.² TNM (Hummel Chemical Co., Newark, N. J.) was purified by distillation at reduced pressure. The BrTNM and Cl-TNM were prepared by halogenation of potassium trinitromethane as described by MacBeth³ for the preparation of the bromo compounds. Final purification of the compounds was achieved by distillation at reduced pressure. DCITNE was prepared by chlorination of symmetrical dipotassium tetranitroethane, as outlined by Borgardt, *et al.*⁴ The polynitro compounds gave characteristic infrared spectra and the elemental analyses were compatible for this class of compounds.

The rate of decomposition of TNM was determined by three techniques previously described for hexanitroethane (HNE).⁵ The rates of the halonitromethanes were determined by only the infrared technique.

The rates of decomposition of DCITNE were deter-

mined by following the rate of formation of 1,2-dichloro-1,2-dinitroethylene, a product of decomposition. The molar extinction coefficient of the 1,2-dichloro-1,2-dinitroethylene in Freon 113 and in cyclohexane at 265 m μ is about 5400, whereas for DCITNE it is only about 146. The rates were determined by analysis of the solution at this wavelength. Corrections were made for the absorption due to the presence of DCITNE in calculating the rates. The dichlorodinitroethylene undergoes further reaction to other products, but the reaction in these dilute solutions is extremely slow and does not present any problems in obtaining good rate data.

The specific rate constants listed in Table I were computed by the use of the first-order rate expression. The rate constants are the average of four runs, each run comprising a minimum of eight points. The decomposition reaction in each case was followed to about 70% completion. Typical results in terms of specific first-order rate constants are given in Tables II-V for the decomposition of TNM, Cl-TNM, BrTNM, and DCITNE, respectively.

The 1,2-dichloro-1,2-dinitroethylene, a liquid, was

(1) Portions of this work have been carried out as part of the Lockheed Independent Research Program.

(2) A. K. Wiberg, "Laboratory Techniques in Organic Chemistry," McGraw-Hill Book Co., Inc., New York, N. Y., 1960.

(3) K. MacBeth and D. D. Pratt, *J. Chem. Soc.*, 354 (1921).

(4) F. G. Borgardt, A. K. Seeler, and P. Noble, Jr., *J. Org. Chem.*, 31, 2806 (1966).

(5) H. P. Marshall, F. G. Borgardt, and P. Noble, Jr., *J. Phys. Chem.*, 69, 25 (1965).

Table I: Kinetic Data and Activation Parameters for the Decomposition of Some Polynitro Compounds

Compound ^a	Solvent	Temp, °C	k , sec ⁻¹ ^b	$\Delta E \pm$	$\Delta S \pm_{\text{ass}}$	Log A	Relative rate at 85°
C(NO ₂) ₄ ^c	CCl ₄	85	2.6×10^{-8} ^d				1.0
		100	$3.08 \pm 0.14 \times 10^{-7}$	39.7	15.7	16.7	
		120	$4.56 \pm 0.19 \times 10^{-6}$				
		135	$3.24 \pm 0.22 \times 10^{-6}$				
		150	$1.65 \pm 0.09 \times 10^{-4}$				
	Freon 114B-2	120	$4.71 \pm 0.22 \times 10^{-7}$	41.3	20.0	17.7	
		135	$3.42 \pm 0.13 \times 10^{-6}$				
	Freon 113	100	$3.30 \pm 0.16 \times 10^{-7}$	39.8	16.1	16.8	
120		$4.58 \pm 0.21 \times 10^{-6}$					
135		$3.32 \pm 0.15 \times 10^{-6}$					
ClC(NO ₂) ₃	CCl ₄	85	2.2×10^{-7} ^d				8.5
		120	$2.56 \times 0.05 \times 10^{-5}$	38.0	14.7	16.5	
		135	$1.46 \pm 0.06 \times 10^{-4}$				
		146.1	$5.34 \times 0.09 \times 10^{-4}$				
BrC(NO ₂) ₃	CCl ₄	85	4.3×10^{-7} ^d				17
		100	$3.46 \pm 0.13 \times 10^{-6}$	37.6	15.3	16.6	
		120	$4.68 \pm 0.12 \times 10^{-6}$				
		134.4	$2.53 \pm 0.11 \times 10^{-4}$				
ClC(NO ₂) ₂ C(NO ₂) ₂ Cl	Freon 113	45	$1.96 \pm 0.06 \times 10^{-5}$	31.0	15.0	16.6	
		55	$8.21 \pm 0.15 \times 10^{-6}$				
		70	$6.82 \pm 0.19 \times 10^{-4}$				
		85	4.6 ± 10^{-3} ^d				1.8 × 10 ⁶
	Cyclohexane	45	$1.84 \pm 0.03 \times 10^{-6}$	30.7	13.8	16.3	
		55	$7.49 \pm 0.17 \times 10^{-5}$				
		70	$6.26 \pm 0.24 \times 10^{-4}$				
C(NO ₂) ₃ C(NO ₂) ₃	CCl ₄	85	2.2×10^{-5} ^e				860

^a Concentration of polynitro compounds was $\sim 6 \times 10^{-2}$ mol/l. for TNM, ClTNM, and BrTNM; for DCITNE, the concentration was $\sim 2 \times 10^{-3}$ mol/l. ^b k 's are average of four runs, average deviation given for each k . ^c J. M. Sullivan and A. E. Axworthy, *J. Phys. Chem.*, **70**, 3366 (1966), give $k = 10^{17.43} \exp(-40875/RT)$ sec⁻¹ for gas-phase pyrolysis. ^d Extrapolated from data at other temperatures. ^e Taken from ref 5, $k = 10^{18.5} \exp(-37,800/RT)$.

Table II: Decomposition of TNM at 135° in CCl₄^a

t , min	$X/a =$ $1 - e^{-kt}$ ^b	$10^4 k$, min ⁻¹
120	0.244	2.33
180	0.313	2.09
243	0.368	1.88
300	0.468	2.10
375	0.542	2.08
465	0.602	1.98
555	0.642	1.85
675	0.726	1.92
735	0.769	1.99

Av 2.02 ± 0.11

^a Analysis of TNM by the infrared method. ^b Fraction decomposed.

Table III: Decomposition of ClTNM at 135° in CCl₄^a

t , min	$X/a =$ $1 - e^{-kt}$ ^b	$10^4 k$, min ⁻¹
16	0.149	10.08
45	0.320	8.57
60	0.415	8.94
77	0.496	8.89
90	0.563	9.20
110	0.633	8.87
130	0.698	9.21
150	0.756	9.40

Av 9.15 ± 0.33

^a Analysis of ClTNM by the infrared method. ^b Fraction decomposed.

prepared in large quantities from the decomposition of DCITNE for ten half-lives in Freon 113 at 47°. During the preparation a stream of argon was passed through the solution to sweep out the NO₂. The solution was concentrated by removal of solvent at reduced pressure, followed by distillation of the 1,2-dichloro-1,2-dinitroethylene product: bp 34–35° at 0.03 mm, $n_D^{25} = 1.5172$. *Anal.* Calcd for C₂Cl₂N₂O₄: C, 12.85; Cl,

37.93; N, 14.35. Found: C, 12.67; Cl, 36.98; N, 14.25. Attempted chlorination of 1,2-dichloro-1,2-dinitroethylene by standard techniques was unsuccessful; the starting material was recovered unchanged in essentially quantitative yield.

The stoichiometry of the decomposition reaction of DCITNE was determined as follows. DCITNE (0.5 g) was decomposed *in vacuo* in a modified U tube, with the center part of the tube plugged with glass wool. One

Table IV: Decomposition of BrTNM at 135° in CCl₄^a

<i>t</i> , min	$X/a =$ $1 - e^{-kt}$ ^b	10 ³ <i>k</i> , min ⁻¹
10	0.114	1.19
20	0.248	1.42
30	0.331	1.34
40	0.450	1.49
50	0.544	1.57
60	0.591	1.49
70	0.658	1.53
80	0.695	1.48
95	0.732	1.38

Av 1.43 ± 0.09

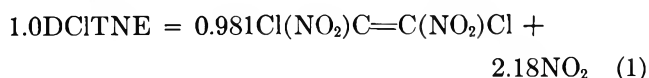
^a Analysis of BrTNM by the infrared method. ^b Fraction decomposed.**Table V:** Decomposition of DCITNE at 55° in Freon 113^a

<i>t</i> , min	$X/a =$ $1 - e^{-kt}$ ^b	10 ³ <i>k</i> , min ⁻¹
20	0.0842	4.39
30	0.130	4.62
40	0.170	4.66
50	0.200	4.46
70	0.271	4.52
100	0.366	4.56
130	0.449	4.58
225	0.645	4.60
300	0.752	4.62

Av 4.56 ± 0.06

^a Analysis by the ultraviolet method. ^b Fraction decomposed.

arm of the tube contained the sample which was placed in a bath at about 70° and the other arm was cooled in liquid nitrogen. The center part of the U tube containing the glass wool was heated with an air gun. First, one arm was placed in the heated temperature bath and then the other, but at all times keeping the nonheated arm at liquid-nitrogen temperature. This procedure was used because the DCITNE sublimes readily and may be transported into the cold arm of the U tube. Also, cooling with liquid nitrogen was employed to maintain an extremely low partial pressure of NO₂ in the system. From the weights and analysis of the reaction products in each arm of the U tube, the over-all reaction can be represented by



In the arm of the U tube containing the NO₂, a small amount of "chloride" was shown to be present, equivalent to 0.049 mol as AgCl. The mass balance for the reaction was determined as 102%.

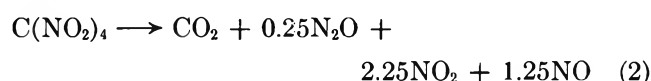
Other attempts were made to determine the number of moles of NO₂ formed per mole of DCITNE. Samples of

DCITNE in glass ampoules, which were sealed *in vacuo*, were heated at 78° for various times. The NO₂ was determined tritrimetrically after separating it from the 1,2-dichloro-1,2-dinitroethylene. The NO₂ determined was 2.28 and 2.44 ± 0.10 mol for heating times of 2.8 and 4.0 hr, respectively. These experiments show the continued formation of NO₂ upon prolonged heating of DCITNE. Pressure-measurement techniques⁵ indicated the formation of 3.58 ± 0.12 mol of gaseous products for a sample of DCITNE heated overnight (~16 hr) at 85°.

Attempts to obtain the rates of decomposition of solid DCITNE were unsuccessful. The decomposition of solid DCITNE is complicated by other reactions taking place. They probably are: (a) reaction of the dichlorodinitroethylene with the NO₂ formed and/or with the starting material, DCITNE; and (b) the change of phase of DCITNE due to the dichlorodinitroethylene formed during the reaction, resulting in a change in the decomposition rates as described by Garner.⁶

Freon 114B2 appears to react with either TNM or its decomposition products. The formation of Br₂ in small amounts was observed. However, this side reaction did not appear to have a significant effect on the measured rates of reaction.

The only reaction products detected from the thermal decomposition of TNM were NO, NO₂, N₂O, and CO₂, as also reported by Sullivan.⁷ Using procedures previously described by us,⁵ 3.52 (±1%) mol of NO and NO₂ and 4.75 (±1%) mol of total gaseous products were formed per mole of decomposed TNM. Thus the over-all reaction for the decomposition of TNM is best represented by



Discussion

The rate-determining step for the decomposition of the polynitromethanes is the rupture of the C-N bond

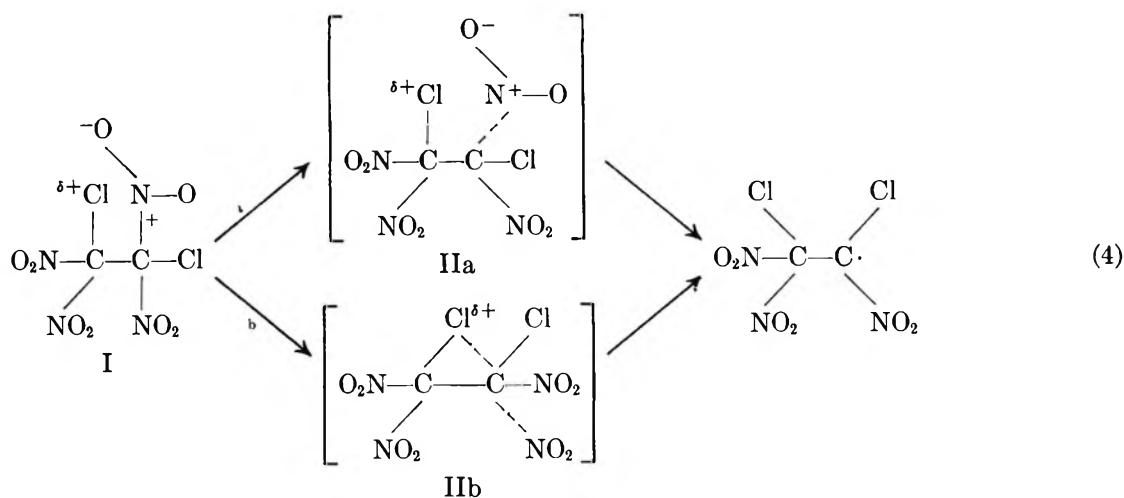


(where X = Cl, Br, or NO₂) as proposed by Sullivan⁷ from gas-phase pyrolysis studies and by Bielski⁸ from photolysis studies of the decomposition of TNM. The observed activation energies (38–39 kcal/mol) and the preexponential factors (~10¹⁷) are essentially the same for the three polynitromethanes in the present studies, indicating that the initial step (rate-controlling step) is probably the same. Within experimental error, our observed values of the activation parameters for TNM solution are the same as reported by Sullivan⁷ from gas-phase pyrolysis studies.

(6) W. E. Garner, Ed., "The Chemistry of the Solid State," Butterworth and Co., Ltd., London, 1955, Chapter 10.

(7) J. M. Sullivan and A. E. Axworthy, *J. Phys. Chem.*, **70**, 3366 (1966).

(8) B. H. J. Bielski and R. B. Timmons, *ibid.*, **68**, 347 (1964).



It is interesting to note that the thermal decomposition of chloropicrin⁹ (Cl_3CNO_2) is associated with (k (400–450°K) = $10^{15.7} \exp(-37,700/RT) \text{ sec}^{-1}$) activation parameters very similar to that of the polynitromethanes, indicating that the decomposition process is again associated with cleavage of the C–N bond. Thus the suggestion of Benson¹⁰ that bond rupture within a molecule is associated with a high preexponential factor appears to hold for the present series of compounds.

The case for the DCITNE decomposition with a lower activation energy, about 9 kcal/mol, and a "high" preexponential factor, *i.e.*, 10^{16} , as compared to the polynitromethanes and hexanitroethane is somewhat surprising. A reasonable mechanism involving a loose "cyclic" transition state can be devised to accommodate the observed activation parameters, yet is consistent with the proposed mechanism for decomposition of the polynitromethanes and hexanitroethane. Thus a decomposition path as given in eq 4 is proposed. In DCITNE, the ground state can be described by resonance hybrids of I. The loose "cyclic" transition state is represented by II. Looking at the reaction path 4a, which we presently favor, a comparison of structure I and IIa should be made. In I, the ground state, there is Coulombic interaction between the positive chlorine¹¹ and the nitro group, but the forces are not sufficient to cause "freezing" of the system into a rigid cyclic struc-

ture.¹² This interaction exists also in the transition state, IIa, but with the NO_2 group somewhat removed from carbon. Thus the decomposition of DCITNE is simply the rupture of the C–N bond yielding two polyatomic radicals with the expected "high" preexponential factor.¹⁰ The lower activation energy for the decomposition of DCITNE is the same as that proposed for the polynitromethanes and hexanitroethane. Reaction path 4b would also be compatible with the data and can be justified by arguments along similar lines as given above.

The behavior of DCITNE in Freon 113 and in cyclohexane was found to be the same as indicated by the similarity of their activation parameters. Therefore, it does not appear that the DCITNE forms a complex that is effective in changing reaction parameters with hydrocarbon solvents, as observed for TNM¹² and inferred for hexanitroethane⁵ from rate studies.

(9) E. W. R. Steacie and W. McF. Smith, *Can. J. Res.*, **16B**, 222 (1939).

(10) S. W. Benson, *Ind. Eng. Chem.*, **56**, 18 (1964); S. W. Benson and W. B. DeMore, *Ann. Rev. Phys. Chem.*, **16**, 397 (1955).

(11) Note: The reactions of 1-halo-1,1-dinitroethanes with various bases apparently involve reductive attack by the base on the positive halogen; see L. Zeldin and H. Schechter, *J. Amer. Chem. Soc.*, **79**, 4708 (1957). Also, these compounds do not form silver halide precipitates upon treatment of the halo-nitro compounds with AgNO_3 in aqueous ethanol.

(12) D. Evans, *J. Chem. Soc.*, 4229 (1957).

An Investigation of the Electrical Polarizations of Several Molecules Which Have Been Assigned Anomalous Dipole Moments¹

by Ernest N. DiCarlo, Thomas P. Logan,² and Robert E. Stronski³

Department of Chemistry, Saint Joseph's College, Philadelphia, Pennsylvania 19131 (Received September 1, 1967)

Static dielectric constants and specific volumes have been measured for benzene solutions of chromium(III), iron(III), and aluminum acetylacetonates at 25, 35, 45, and 55°, cobalt(III) acetylacetonate at 20, 25, and 55°, *p*-dinitrobenzene at 30, 35, 40, and 55°, and tetramethyl-1,3-cyclobutanecione at 25, 40, and 55°. These data were used to calculate total molar polarizations by the method of Halverstadt and Kumler. The total polarizations of the above molecules were found to be invariant with temperature well within the experimental error of the measurements. In all cases, with the exception of cobalt(III) acetylacetonate for which vapor-phase data are not available, the solution total polarizations are shown to be in good agreement with previously determined vapor-phase values. The present results, however, are in marked disagreement with those of other solution studies which showed a pronounced variation of polarization, over a small temperature range, for *p*-dinitrobenzene and ferric acetylacetonate. The agreement between the present solution polarizations and earlier vapor-phase values lead to the conclusion that none of these substances, with the possible exception of the cobalt complex, possesses a component of orientation polarization resulting from the existence of a permanent dipole moment in the molecule.

The objective of this study was to obtain accurate values of total polarization for the above molecules in solution in an effort to establish their possible polarity⁴ or nonpolarity by demonstrating disagreement or agreement between the polarizations of these substances as determined in solution and in the vapor phase. This work was undertaken for two reasons. First, it will serve as a basis for other studies which will be concerned with whether or not the total polarizations of a "select group of nonpolar molecules" differ in the pure liquid (or in solution) and the solid phase.⁵ Secondly, since several metal acetylacetonates in benzene solution have been found by the present investigators to exhibit microwave absorption,⁶ the question of whether or not these particular molecules possess orientation polarization is an important one.

Experimental Section

Apparatus. Static dielectric constants, ϵ , were measured with a General Radio GR 716-CS1 capacitance bridge at 1 MHz. Figure 1 shows a block diagram of the apparatus. A GR 1214-M oscillator supplies about 300 mW power to the bridge. A RF heterodyne receiver consisting of a GR 1203-B power supply, a GR 1211-C variable oscillator, a GR 1232-P1 RF mixer, and a GR 1232-A tuned amplifier was employed as the detector. The local oscillator is tuned to 1.1 MHz in order to match the intermediate frequency to the tuned 100 kHz amplifier. With this heterodyne receiver, the apparatus is very sensitive and capable of detecting changes in the capacitance to be measured of *ca.* 0.002 pF.

Parallel to the dielectric cell, a GR 1422-ME pre-

cision capacitor is connected to the bridge. Provided that the air capacitance of the dielectric cell does not change significantly after it is cleaned and dried, the precision capacitor can be used in dilute-solution measurements to compensate for the small capacitance change, ΔC , from the solvent-filled cell to the solution-filled cell. In this case, the corresponding change in the dielectric constant, $\Delta\epsilon$, is calculated from ΔC by

$$\Delta\epsilon = \frac{\Delta C}{C_0} \quad (1)$$

where C_0 is the cell constant. This method takes advantage of the high absolute accuracy of the external precision capacitor, which has one range from 0 to

(1) Research supported by the National Science Foundation under Grant GP-5361.

(2) This paper represents part of the work submitted by T. P. Logan to the Chemistry Department of Saint Joseph's College in partial fulfillment of the requirements for the degree of Master of Science.

(3) Participant in the undergraduate research program, Saint Joseph's College, Philadelphia, Pa., 1965-1966.

(4) Disagreement between the total polarization of a molecule as determined in vapor and solution measurements cannot be taken as conclusive evidence for the existence of a permanent dipole moment, since the solution polarization value may reflect a solvent effect. See H. O. Jenkins, *J. Chem. Soc.*, 862 (1936); 910 (1936); F. C. Frank and L. E. Sutton, *Trans. Faraday Soc.*, **33**, 1307 (1937).

(5) This study has been initiated on several nonpolar molecules which have two common characteristics; *i.e.*, very flexible structures and many highly polar bonds. Examples of the latter type of molecule are iron pentacarbonyl and symmetrical metal acetylacetonates.

(6) Aluminum, iron(III), chromium(III), and thorium(IV) acetylacetonates in benzene solution exhibit considerable microwave absorption and have very short mean relaxation time values. A detailed account of a microwave investigation covering several nonpolar metal acetylacetonates will be discussed in another paper.

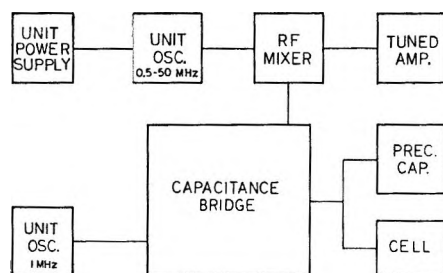


Figure 1. Block diagram of the dielectric constant apparatus.

10.5 pF and another from 0 to 105 pF. Using this approach, the bridge capacitor, having a range from 100 to 1150 pF, is only employed when balancing the solvent-filled (benzene) dielectric cell (over-all capacity, including cables, of *ca.* 680 pF). The air-filled cell has an over-all capacity, including cables, of *ca.* 410 pF.

The measurements on aluminum, iron(III), and chromium(III) acetylacetonates in benzene solution were made with a dielectric cell (C_0 of *ca.* 200 pF) similar to the type used by Smyth and Morgan.⁷ Since the air capacitance of this cell was found to change significantly after it was cleaned and dried, it was necessary to employ the bridge capacitor to measure the air capacitance (empty cell) after each cleaning and drying. $\Delta\epsilon$ was then calculated as the difference between the dielectric constant of any given solution, ϵ_2 , and that of the solvent, ϵ_1 , as given by

$$\epsilon_1 = \frac{C_1 - C_{\text{air}}}{C_0} + 1 \quad (2)$$

$$\epsilon_2 = \frac{C_2 - C_{\text{air}}}{C_0} + 1 \quad (3)$$

where C_1 and C_2 are the capacitances of the solvent- and solution-filled dielectric cells, respectively. In this case, the dielectric cell limits the accuracy of the measurement owing to the inherently larger error (*ca.* ± 0.2 pF) introduced by the necessity of employing the bridge capacitor to determine the capacitance rather than the more accurate precision capacitor. However, by using at least seven solutions, the slope α , $d\Delta\epsilon/dw$, where w is the weight fraction, could be determined to *ca.* $\pm 2\%$ for the aluminum, iron(III), and chromium(III) acetylacetonates. For the latter measurements, the temperature was maintained constant to within 0.01° of the desired temperature. Table I lists a typical set of data obtained for aluminum acetylacetonate in benzene solution at 25° . The deviations of $\Delta\epsilon$ from the least-squares fit ($\Delta\epsilon$ vs. w) for the aluminum complex in benzene at 25° were calculated as the differences between the observed and calculated values of $\Delta\epsilon$. The latter values were determined from the least-squares slope and intercept, 0.8759 and 0.0004, respectively.

Table I: Weight Fractions, w , Observed Differences in Dielectric Constant, $\Delta\epsilon$, between the Given Solution and the Solvent (Benzene), and Deviations, D , of $\Delta\epsilon$ from the Least-Squares Fit for Aluminum Acetylacetonate in Benzene Solution at 25° ^a

$10^6 w$	$10^4 \Delta\epsilon$	$10^4 D$
4922.5	41	-6.4
8116.4	76	0.6
12067	112	2.0
15198	144	6.6
19055	171	-0.2
22484	204	2.8
28576	249	-5.5

^a Reference 7 describes the cell employed.

In an effort to improve the accuracy of the measurement, a different dielectric cell⁸ was employed for the $\Delta\epsilon$ determinations made on the benzene solutions of cobalt(III) acetylacetonate, *p*-dinitrobenzene, and tetramethylcyclobutanedione. A cross section of the cell is shown in Figure 2. This cell consists of two concentric cylinders, the inner supported by a Teflon ring. The spacing between the two cylinders is 1 mm, giving an effective volume of *ca.* 30 cm³,⁹ compared to a volume of *ca.* 1 cm³ for the cell which was employed for the other measurements reported in this work. All parts in contact with the dielectric liquid were made from stainless steel. Water from a constant-temperature bath is circulated through the jacket surrounding the outer cylinder to keep the temperature constant to within 0.01° of the desired temperature. The inner cylinder is connected to the plug at the center of the dielectric cell by a wire. A very thin wire was used for this purpose in order to minimize heat losses to the cable at higher temperatures. This cell was found to be much more stable, both electrically and mechanically,¹⁰ than the one previously described⁷ and the accuracy of the $\Delta\epsilon$ measurement improved considerably. The air capac-

(7) C. P. Smyth and S. O. Morgan, *J. Amer. Chem. Soc.*, **50**, 1547 (1928).

(8) This cell was designed by Horst Kilp of Johannes Gutenberg Universität, Mainz, Germany.

(9) This large effective volume makes solution-concentration uncertainty resulting from retention of traces of solute or wash liquid (usually the solvent) after the cleaning and drying of the cell essentially zero. For a cell with an effective volume of only 1 cm³, significant solution-concentration uncertainty may result from inadequate cleaning or insufficient drying time. To minimize the latter possibility, a cell of small effective volume should be rinsed several times with the given solution prior to the capacitance measurement. This procedure was followed in the present work for all determinations made with the type of cell described previously.

(10) The cell described by Smyth and Morgan consists of three concentric platinum cylinders which are enclosed in glass and held apart by means of glass beads. Slight shaking of this type of cell was found to cause a displacement of the cylinders relative to one another. Also, the problem of entrapped air in the solution to be measured, which is frequently encountered with a cell of this construction, is virtually nonexistent with a cell of the type depicted in Figure 2.

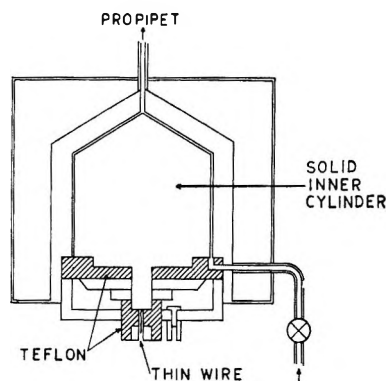


Figure 2. Dielectric cell.

itance of this cell was not found to vary as a result of cleaning and drying. The bridge capacitor was only used when balancing the solvent-filled cell and kept at this capacitance setting during the measurements made on the dilute solutions. Therefore, the capacity changes due to the dilute solutions were compensated only by the external precision capacitor. The difference in dielectric constant between any given solution and the solvent is given by eq 1. The accuracy of the $\Delta\epsilon$ measurements in this case depends mainly on the accuracy of the precision capacitor, since the cell constant C_0 can be determined to within *ca.* 0.1%. The precision capacitor employed in the present work is accurate to ± 0.02 pF in its 0–10.5-pF range and ± 0.05 pF in its 0–105-pF range. Since the value of C_0 for the cell described above is *ca.* 200 pF, it follows that $\Delta\epsilon$ values between 0 and 0.05 can be measured to an accuracy of ± 0.0001 (using the 0–10.5-pF range of the precision capacitor), and values between 0 and 0.5 can be determined to an accuracy of ± 0.0003 (employing the 0–105-pF range). It was found that the $\Delta\epsilon$ value of a 0.0005 mol fraction solution of chlorobenzene in benzene (30°) could be measured to an accuracy of *ca.* $\pm 0.5\%$. Employing four solutions of chlorobenzene in the range 0–0.008 mol fraction, the slope $d\Delta\epsilon/dN$, where N is the mole fraction, could be determined to *ca.* $\pm 0.5\%$ (30°). Table II lists a typical set of data obtained for *p*-dinitrobenzene in benzene solution at 30°. The deviations were calculated as described previously. The least-squares slope and intercept were found to be 0.3574 and 0.00002, respectively, for this determination.

Employing seven solutions and the cell depicted in Figure 2, α could be determined to better than ± 1 , ± 0.5 , and $\pm 3\%$ for benzene solutions of *p*-dinitrobenzene, cobalt(III) acetylacetonate, and tetramethylcyclobutanedione, respectively.

Refractive index measurements were carried out using a Bausch and Lomb precision refractometer equipped with a sodium-vapor lamp. A Lipkin bicapillary pycnometer¹¹ was employed to measure densities.

Table II: Weight-Fractions, w , Observed Differences in Dielectric Constant, $\Delta\epsilon$, between the Given Solution and the Solvent (Benzene), and Deviations, D , of $\Delta\epsilon$ from the Least-Squares Fit for *p*-Dinitrobenzene in Benzene Solution at 30°^a

$10^4 w$	$10^4 \Delta\epsilon$	$10^4 D$
2673.6	11.1	1.37
4740.6	15.7	-1.41
6973.1	24.1	-0.99
8663.5	31.3	0.16
10661	39.2	0.92
13512	48.7	0.23
15616	55.7	-0.29

^a Figure 2 depicts the cell employed.

For all density measurements, the temperature was kept constant to within 0.01° of the desired temperature. Duplicate density results differed by not more than 0.0001 g/ml. Reproducibility of the density measurements was better than 0.0002 g/ml. From two independent determinations made on chromium(III) acetylacetonate in benzene solution at 35°, the reproducibility of slope β , dv/dw , where v is the specific volume and w is the weight fraction, was found to be of the order of 0.2%. In a similar study made on tetramethylcyclobutanedione in benzene at 25°, two independently determined values of β agreed to within *ca.* 0.1%. In the above reproducibility studies, seven solutions were employed for each determination. For all of the specific volume measurements, with the exception of those made on tetramethylcyclobutanedione in benzene solution, the largest deviation of v from the least-squares fit (v vs. w) was found to be *ca.* 0.01%. For tetramethylcyclobutanedione in benzene solution, which has a β value *ca.* five times smaller than the corresponding value of the other substances investigated, the largest deviation of v from the least-squares fit was of the order of 0.03%.

Materials. The substances investigated were obtained from (A) the Aceto Chemical Co., (B) the J. T. Baker Chemical Co., (C) the Eastman Kodak Co., and (D) the Fisher Scientific Co. The source of each compound, the method of purification, and the melting point or the index of refraction are listed in Table III. Following purification, a carbon-hydrogen analysis was performed on each of the acetylacetonates investigated. *Anal.* Calcd for Cr(C₅H₇O₂)₃: C, 51.57; H, 6.06. Found: C, 51.85; H, 6.03. Calcd for Fe(C₅H₇O₂)₃: C, 51.01; H, 5.99. Found: C, 51.01; H, 6.10. Calcd for Al(C₅H₇O₂)₃: C, 55.55; H, 6.53. Found: C, 55.68; H, 6.56. Calcd for Co(C₅H₇O₂)₃: C, 50.57; H, 5.94. Found: C, 51.04; H, 6.08.

(11) M. R. Lipkin, J. A. Davison, W. T. Harvey, and S. S. Kurtz, Jr., *Ind. Eng. Chem.*, 16, 55 (1944).

Table III: Sources, Methods of Purification, Melting Points or Refractive Index

Compound	Source	Mp, °C
Chromium(III) acetylacetonate ^a	A	214.0–215.0
Iron(III) acetylacetonate ^a	A	182.5–184.0
Aluminum acetylacetonate ^a	A	193.5–195.0
Cobalt(III) acetylacetonate ^a	B	213.0–214.0
Tetramethylcyclobutanedione ^b	C	114.0–114.5 (sealed tube)
<i>p</i> -Dinitrobenzene ^c	C	175.0–175.8
Benzene ^d	D	n_D^{20} 1.50111

^a Repeated crystallization from benzene–petroleum ether (bp 68–70°) and drying under vacuum over phosphorus pentoxide.

^b Crystallization from benzene–petroleum ether (bp 68–70°) followed by sublimation at 110° and drying under vacuum over phosphorus pentoxide. ^c Repeated crystallization from benzene and drying under vacuum over phosphorus pentoxide. ^d Reagent grade, thiophene-free benzene was fractionally distilled over lithium hydride and stored over Drierite.

Results and Discussion

Table IV contains polarization data as a function of temperature for the substances investigated. Together with the total molar polarizations, $P_{2\infty}$, the derivatives and intercepts of dielectric constant and specific volume with respect to weight fraction (α , β , ϵ_1 , and v_1 , respectively) are listed. The measured or assumed values of the dielectric constant, ϵ , of pure benzene are also tabulated. The assumed values are given to four significant figures, while the measured dielectric constants of pure benzene are given to five significant figures. The concentration range in weight fraction is given in parentheses for each set of solutions in Table IV. The total polarizations were calculated by the method of Halverstadt and Kumler.¹² For each substance investigated, seven benzene solutions were employed for the determination of the slopes, α and β , and intercepts, ϵ_1 and v_1 . The latter quantities were calculated by the method of least squares. The values of the dielectric constant and specific volume obtained by extrapolation to zero weight fraction were used in all polarization calculations. The values of $P_{2\infty}$ deduced from the parameters listed in Table IV were checked by comparison with the values of the polarization calculated from the dielectric constant and density data for each concentration. No systematic variation of polarization with concentration was observed. For all polarization determinations made on a given substance (with two exceptions noted in Table IV), the same set of solutions was employed at the different temperatures. As seen from Table IV, the agreement between the dielectric constants of pure benzene and the values obtained by extrapolation is good. This fact, together with the good least-squares linear fits of v and $\Delta\epsilon$ vs. w (see Tables I and II) over the concen-

tration range investigated for each of the compounds, indicates normal behavior on the part of the solutions studied.

The present total-polarization results are in marked disagreement with earlier studies^{13,14} made in benzene solution which showed a pronounced variation of polarization, over a small temperature interval, for *p*-dinitrobenzene and several metal acetylacetonates. A detailed error analysis of the present results is, therefore, imperative before any comparisons are made or conclusions drawn. (A complete analysis of the errors of the dielectric constant–density method has been described elsewhere.¹⁵) An examination of the scattering of the experimental points ($\Delta\epsilon$ vs. w and v vs. w) indicates reliability in the present data with regard to normal random error. The magnitude of errors due to absorption is probably insignificant at the concentrations employed. Constant errors, such as those due to introduction of moisture in the handling of solutions, evaporation losses from the solutions, purity of the chemicals used, inductance corrections, and nonlinearity of the capacitor with dielectric constant, have been carefully minimized. The absolute errors in the Halverstadt–Kumler $P_{2\infty}$ values of Table IV were estimated to be ± 1 and ± 2 cm³ for *p*-dinitrobenzene and tetramethylcyclobutanedione, respectively, ± 3 cm³ for cobalt(III) and aluminum acetylacetonates, ± 4 cm³ for chromium(III) and iron(III) acetylacetonates. The relative errors in the $P_{2\infty}$ values determined at the different temperatures were estimated to be ± 0.7 cm³ for *p*-dinitrobenzene and tetramethylcyclobutanedione and ± 2 cm³ for the acetylacetonates.

p-Dinitrobenzene and Tetramethyl-1,3-cyclobutanedione. *p*-Dinitrobenzene has been studied in the vapor phase,¹⁶ in benzene solution,^{14,17} and in the solid state.¹⁴ Coop and Sutton¹⁶ found that the vapor total polarization, P , was constant from ca. 200 to 255° and differed by not more than 1 cm³ from the value of 46 cm³ in benzene solution¹⁷ at 25°. Therefore, an assignment of 8.2 cm³ was made to the atomic polarization¹⁶ P_A , $P - P_E$, where P_E is the electronic polarization. Wright, *et al.*,¹⁴ however, from dielectric-constant determinations of pellets of this substance concluded that the distortion polarization, $P_E + P_A$, was only about 2 cm³ higher than P_E . In order to confirm this result, they determined the polarization of *p*-dinitrobenzene in benzene solution at 20, 30, and 40° and obtained values of 53.0, 51.1,

(12) I. F. Halverstadt and W. D. Kumler, *J. Amer. Chem. Soc.*, **64**, 2988 (1942).

(13) C. C. Meredith, L. Westland, and G. F. Wright, *ibid.*, **79**, 2385 (1957).

(14) P. Podleschka, L. Westland, and G. F. Wright, *Can. J. Chem.*, **36**, 574 (1958).

(15) H. A. Pohl, M. E. Hobbs, and P. M. Gross, *Ann. N. Y. Acad. Sci.*, **40**, 389 (1940).

(16) I. E. Coop and L. E. Sutton, *J. Chem. Soc.*, 1269 (1938).

(17) C. G. LeFèvre and R. J. W. LeFèvre, *ibid.*, 957 (1935).

Table IV: Polarization Data

Temp, °C	ϵ	ϵ_1	$10^4\alpha$	$-10^4\beta$	ν_1	$P_{2\infty}$, cm ³
<i>p</i> -Dinitrobenzene (0-0.016)						
30	2.264	2.2640	3574	4655	1.1514	45.6
35	2.254	2.2552	3565	4658	1.1588	45.9
40	2.244	2.2452	3532	4276	1.1664	45.7
55	2.214	2.2133	3816	5023	1.1882	46.1
Tetramethyl-1,3-cyclobutanedione (0-0.129)						
25	2.274	2.2740	1194	661	1.1446	48.2
40	2.244	2.2454	1307	663	1.1657	48.8 ^a
55	2.214	2.2141	1099	873	1.1886	47.6
Iron(III) Acetylacetonate (0-0.025)						
25	2.274	2.2738	10837	3836	1.1446	152.1
35	2.2551	2.2543	10620	3909	1.1586	152.0
45	2.2332	2.2329	10936	4283	1.1734	152.5
55	2.2130	2.2120	11161	4526	1.1885	154.0
Chromium(III) Acetylacetonate (0-0.026)						
25	2.274	2.2735	9987	4354	1.1452	139.5
35	2.2549	2.2534	9807	4560	1.1591	138.2
45	2.2337	2.2335	9571	4348	1.1732	140.8
55	2.2122	2.2116	9532	4604	1.1884	140.1
Cobalt(III) Acetylacetonate (0-0.112)						
20	2.284	2.2840	7904	3996	1.1378	131.2 ^b
25	2.274	2.2730	8215	4044	1.1444	133.6
55	2.214	2.2136	8037	4466	1.1882	133.6
Aluminum Acetylacetonate (0-0.029)						
25	2.274	2.2744	8759	3349	1.1451	131.7
35	2.2553	2.2545	8590	3342	1.1588	132.4
45	2.2327	2.2340	8201	3352	1.1730	131.4
55	2.2138	2.2125	7956	3503	1.1883	130.0

^a Determination made employing a different sample of tetramethylcyclobutanedione (purified by repeated crystallization from benzene and drying under vacuum over phosphorus pentoxide) and a weight fraction range of 0-0.123. ^b Determination made employing a different sample of cobalt(III) acetylacetonate (purified as described in Table III) and a weight fraction range of 0-0.042.

and 49.7 cm³, respectively. Since their measured solution polarizations varied appreciably with temperature, they concluded that *p*-dinitrobenzene had a dipole moment which varied from about 0.8 to 0.7 D over their 20° temperature range. Since *p*-dinitrobenzene is usually postulated to be a centrosymmetrical molecule, which should have zero moment, a further investigation of this anomaly was undertaken. As seen from Table IV, the findings of the present investigation do not agree with those of Wright, *et al.* Considering the relative error (± 0.7 cm³) in the polarization values obtained for *p*-dinitrobenzene at the different temperatures, the variation of *ca.* 3 cm³ observed previously¹⁴ over a 20° temperature interval would have been experimentally detectable. Furthermore, all of the $P_{2\infty}$ values found for *p*-dinitrobenzene (Table IV) are, within the estimated absolute experimental error (± 1 cm³), in good agreement with the value of 46 cm³ reported by LeFèvre and LeFèvre from measurements in benzene solution (25°) and with 46.5 cm³ obtained by Coop and Sutton, from a vapor-phase determination (255°). The temperature-independent

polarization results obtained in the present work taken in conjunction with the earlier vapor-phase data lead to the conclusion that *p*-dinitrobenzene does not possess a component of orientation polarization. This conclusion is in agreement with fairly recent microwave absorption studies,¹⁸ made in benzene solution, which have shown that *p*-dinitrobenzene cannot have a permanent moment greater than 0.20 D.¹⁹

Tetramethyl-1,3-cyclobutanedione has been studied by several investigators.^{14,16,18,20} Coop and Sutton¹⁶ found that in the vapor phase the polarization is constant over a 60° range of temperature. It was concluded from these measurements that this molecule is nonpolar, possessing an exceptionally large atomic polarization of *ca.* 10 cm³. However, from solid meas-

(18) E. N. DiCarlo and C. P. Smyth, *J. Amer. Chem. Soc.*, **84**, 1128 (1962).

(19) This upper limit to the moment corresponds to the maximum possible experimental error in the microwave absorption measurements.

(20) D. L. Hammick, G. C. Hampson, and G. I. Jenkins, *J. Chem. Soc.*, 1263 (1938).

urements¹⁴ the atomic polarization was determined to be only 0.9 cm³. The residual polarization, *ca.* 9 cm³, was assigned as orientation polarization.¹⁴ This amounts to a dipole moment of *ca.* 0.8 D at 25°. The present results do not agree with this assignment. The polarization value 48.2 cm³ at 25° in benzene solution (Table IV) differs by only 1.3 cm³ from that of the vapor¹⁶ (46.9 cm³) at 225°, indicating the absence of significant orientation polarization. Furthermore, microwave absorption measurements¹⁸ made on this substance in benzene solution place an upper limit of 0.10 D¹⁹ for the dipole moment, hardly indicative of orientation polarization. The observed decrease in polarization of 0.6 cm³ from 25 to 55° (Table IV) is not to be regarded as establishing the existence of such a variation, since it is within the estimated relative error (± 0.7 cm³) in the $P_{2\infty}$ values for this compound. In fact, an independent polarization determination at 40° using a different sample of tetramethylcyclobutanedione yielded a value of 48.8 cm³, 0.6 cm³ higher than that at 25°. Finally, all of the $P_{2\infty}$ values found for this substance (Table IV) agree, within the estimated absolute experimental error (± 2 cm³), with the vapor total-polarization value 46.9 cm³ (225°).

Metal Acetylacetonates. Ferric acetylacetonate has been investigated in the vapor phase,¹⁶ in benzene solution,^{13,21,22} and in the solid state.¹³ Based on the assumption that this molecule has a symmetric octahedral structure (zero dipole moment), an assignment of 57 cm³ was made to the atomic polarization, $P - P_E$, from measurements at 25° in benzene solution.²¹ It was later shown that the vapor total polarization¹⁶ 146.6 cm³ measured at *ca.* 230° agreed, within experimental error, with the solution value²¹ 148.6 cm³ at 25°, confirming an exceptionally large atomic polarization. Wright, *et al.*,¹³ however, from dielectric-constant determinations of pellets of this substance concluded that the atomic polarization was only 21.2 cm³. In the latter study, the total polarization of benzene solutions of ferric acetylacetonate was also determined and found to decrease by *ca.* 25 cm³ from 20 to 40°. This variation was interpreted in terms of permanent moments of 1.48, 1.35, 1.25, and 1.05 D at 20, 25, 30 and 40°, respectively. These moments correspond to total polarizations of 158.8, 150.6, 144.5, and 133.6 cm³. The findings of the present work do not agree with those of this earlier investigation. Considering the relative error (± 2 cm³) in the $P_{2\infty}$ values obtained for ferric acetylacetonate at the different temperatures (Table IV), the variation of *ca.* 25 cm³ which had been detected over a 20° temperature interval¹³ should have been easily confirmed. Failure to observe the previously reported temperature variation of the solution polarization of ferric acetylacetonate and the relatively good agreement between the vapor polarization and the present solution values lead to the conclusion that this molecule has negligible orientation

polarization. Finally, the $P_{2\infty}$ values determined for this substance (Table IV) are, within the estimated absolute experimental error (± 4 cm³), in agreement with the values, 148.6²³ and 151.4 cm³,²² determined from earlier measurements in benzene solution at 25°.

As seen from Table IV, no variation, within experimental error, of the solution total polarization of chromic, cobaltic, and aluminum acetylacetonates was observed over the temperature range investigated. This is in marked contrast to earlier studies^{13,14} in which several metal acetylacetonates²⁴ which have long been considered to be symmetrical were shown to exhibit large temperature coefficients in benzene solution.

A total polarization of 137.5 cm³ has been reported²¹ for chromic acetylacetonate from measurements in benzene solution at 25° by treatment of the data according to the Debye-Clausius-Mosotti method. The Halverstadt-Kumler method, when applied to these data, yields a value of 138.9 cm³, in excellent agreement with 139.5 cm³ (Table IV). The vapor-phase value,¹⁶ 136 cm³ (*ca.* 250°), also agrees, within the estimated absolute error (± 4 cm³), with the presently determined solution values.

The three $P_{2\infty}$ values found for cobaltic acetylacetonate compare favorably, within the absolute error (± 3 cm³), with the polarization of 131.5 cm³²⁵ (25°) as determined from measurements in benzene solution.²¹ Since vapor-phase data are not available for the cobalt complex and the temperature range investigated in the present work is small, the question of whether or not this molecule possesses orientation polarization cannot be resolved.

The measurements confirm that aluminum acetylacetonate is nonpolar. The change of polarization over a 200° temperature range is found not to be more than 1 cm³ when the present results are combined with the vapor-phase value,¹⁶ 130.8 cm³ at *ca.* 240°.

The fact that aluminum, iron(III), and chromium(III) acetylacetonates lack orientation polarization is quite significant, since they have been found to exhibit considerable absorption in benzene solution at microwave frequencies⁶ of 24,560 and 9133 MHz. Also, their relaxation times are very short.²⁶ Since the above molecules are nonpolar, their dielectric losses in the

(21) A. E. Finn, G. C. Hampson, and L. E. Sutton, *J. Chem. Soc.*, 1254 (1938).

(22) J. Macqueen and J. W. Smith, *ibid.*, 1821 (1956).

(23) The value of 148.6 cm³ was calculated using the Debye-Clausius-Mosotti method, which involves extrapolation of the polarization data to infinite dilution. Treatment of the data by the Halverstadt-Kumler (H-K) method yielded essentially the same value, 148.7 cm³.

(24) Besides the solution total polarization of ferric acetylacetonate, those of thorium and zirconium acetylacetonate have also been reported to vary greatly (by *ca.* 50 and 30 cm³, respectively) over a 20° temperature range. These substances will be discussed in another paper.

(25) The original value cited, 129.5 cm³, was determined by extrapolating the polarization data to infinite dilution. Treatment of the data according to the H-K method yielded a value of 131.5 cm³.

microwave region cannot be explained as the relaxation losses of rotating permanent dipoles. Possible relaxation mechanisms, not depending on molecular dipole rotation, that might be associated with the short relaxation times of the nonpolar acetylacetonates will be discussed in another paper.

The reasons for the differences between the present solution results and those of Wright and his co-workers^{13,14} are unknown. The disagreement between the two sets of data is greater than can be accounted for by the absolute errors in the polarization values reported in this work. Two differences between the studies are the concentration ranges used for the solution measurements and the number of solutions examined at each temperature. The concentration range employed in the present investigation for *p*-dinitrobenzene and ferric acetylacetonate was two and four times greater, respectively, than that used for the same sub-

stance in the earlier work. The number of solutions measured previously was either four or five, as compared to seven examined in all cases in this work. In addition to these experimental differences, another point deserves consideration; *i.e.*, the assumption employed by Wright, *et al.*, that the distortion polarization of a molecule is independent of the conditions under which it is measured. To our knowledge there is no conclusive experimental evidence to justify the assumption that the distortion polarization in the solid state does not differ significantly from that in the liquid,¹⁸ particularly for molecules with very flexible structures and many polar bonds. A study dealing with the above question has been started.⁵

(26) The relaxation time observed for aluminum acetylacetonate in benzene solution at 45° (*ca.* 3×10^{-12} sec) is much smaller than would be expected for simple rotational orientation of a rigid polar molecule of the same size and shape.

Complex Refractive Index of Colloidal Silver Bromide

in the Near-Ultraviolet¹

by E. J. Meehan and Jerry K. Miller

School of Chemistry, University of Minnesota, Minneapolis, Minnesota 55455 (Received September 5, 1967)

The complex refractive index of silver bromide in the form of colloidal particles in aqueous suspension has been measured by a combination of light scattering and absorption methods, at the wavelengths 366, 405, and 436 m μ . The radius of the smallest particles investigated was about 4 m μ . The real part of the refractive index appears to be the same for colloidal material and for bulk. However, the imaginary part, proportional to the absorption coefficient, for colloidal particles is definitely different from that of bulk, that of the particles being *ca.* 50% smaller, 10% larger, and 60% larger at wavelengths 436, 405, and 366 m μ , respectively.

This paper describes the use of light-scattering measurements to obtain the complex refractive index of silver bromide in the form of colloidal particles in aqueous suspension. The results show that the absorption by small colloidal particles is different from that by material in bulk form. The complex refractive index, \hat{n}_B , of an absorbing substance in bulk is given by

$$\hat{n}_B = n_B - i\gamma_B' \quad (1)$$

in which n_B is the real part and γ_B' is related to the bulk absorption coefficient, γ_B , by

$$\frac{I}{I_0} = \exp(-\gamma_B z) = \exp\left(-\frac{4\pi n_B' z}{\lambda_V}\right) \quad (2)$$

In eq 2, I_0 and I are intensities incident upon and trans-

mitted (corrected for reflections) by thickness z , and λ_V is the vacuum wavelength. Equations identical in form to eq 1 and 2 connect the corresponding values of \hat{n}_P , n_P , n_P' , and γ_P of material in the form of colloidal particles. Obviously, it is necessary to consider whether the latter set of values depends upon particle size.

The scattering and absorption by a spherical particle of radius r , suspended in a nonabsorbing medium of refractive index n_M , can be calculated from exact Mie theory, given the values of \hat{m} and α

$$\hat{m} = \frac{n_P}{n_M} - i\frac{\gamma_P'}{n_M} = m - im' = m(1 - ik) \quad (3)$$

(1) Taken from the Ph.D. thesis of J. K. Miller, University of Minnesota, Minneapolis, Minn., 1966.

$$\alpha = \frac{2\pi r}{\lambda_M} = \frac{2\pi n_M r}{\lambda_V} \quad (4)$$

\hat{m} is the complex refractive-index ratio,² and λ_V and λ_M are wavelengths *in vacuo* and in the medium, respectively. Conversely, \hat{m} can be calculated from suitable scattering and transmission measurements if α is known. This procedure is used in the present paper. Additionally, as is described in the section on Calculations, m may be derived in some cases by measurement of the refractive-index increment. Values of n_B' for silver bromide have been determined by several workers down to λ_V 254 m μ , but n_B has been measured only over the range 436–671 m μ .^{3,4} Direct measurements at shorter λ are complicated not only by the relatively strong absorption but also by the photosensitivity. No data exist in the literature on absorption by colloidal silver bromide.

Silver bromide is transparent, or practically so, above 436 m μ , and it has been shown already by comparison of results of scattering and electron microscopy that $n_P = n_B$, at least for r greater than about 100 m μ .⁵ The question of a possible dependence of n_P on r has been considered critically. All the data presented in this paper can be accounted for satisfactorily on the assumption that $n_P = n_B$ down to the smallest sizes investigated.

Experimental Section

Transmission measurements were made using either a Beckman DU or Cary 15 spectrophotometer. Ten-millimeter cell compartments were used with 4-mm apertures to limit the angle of view. The geometry of the light beam is different in the two instruments, but the values of $\log I_0/I$ always agreed within 0.003. The turbidity τ is calculated from

$$\tau = \frac{1}{l} \ln \frac{I_0}{I} \quad (5)$$

where l is the path length in centimeters. The specific turbidity, τ/c , for monodisperse spherical particles is related to the total extinction coefficient, K_T ,⁶ by

$$\frac{\tau}{c} = \frac{3\pi}{2\lambda_M D} \frac{K_T}{\alpha} \quad (6)$$

where c is the concentration of the suspension (g ml⁻¹) and D is the density of the particle. The values of τ/c were extrapolated to $c = 0$. Angular scattering measurements were made with a Brice-Phoenix instrument. The relative intensity $G(\theta)$ of the vertically polarized scattered component of unpolarized incident light was measured for various mercury wavelengths over the angular range 30–90° and extrapolated to $\theta = 0$ to obtain $G(0)$. In order to obtain absolute scattering intensities from $G(0)$, the instrument was calibrated with "small-particle" Ludox. As recommended by Deželić and Krahtovil⁷ the Ludox was centrifuged at

12,000 rpm for 90 min. The suspension was poured off and 1-, 2-, 3-, and 10-ml portions were diluted to 100 ml with 0.05 *M* sodium chloride⁸ and were filtered through a 0.45- μ Millipore filter. The value of i_{45}/i_{135} was 1.07 and the wavelength exponent was 3.9, in good agreement with the closest approach to small-particle scattering previously observed.⁷ The turbidities of the Ludox suspensions were measured spectrophotometrically. The ratio $G(0)/\tau$ was plotted *vs.* τ and extrapolated to $\tau = 0$. This procedure eliminates the effect of secondary scattering. For small particles, the relation between τ and the Rayleigh ratio, R_θ , for the vertically polarized scattered component of unpolarized incident light, is given by⁹

$$\tau = \frac{16\pi}{3} R_\theta = \frac{16\pi}{3} R_0 \quad (7)$$

In this way the forward-scattered intensity per unit solid angle, per unit volume of suspension, and per unit illumination is found. Calling this quantity $V(0)$, and using the notation of Gumprecht and Sliepcevič,¹⁰ one obtains

$$V(0) = \frac{N\lambda_M^2}{8\pi^2} i_1(0) \quad (8)$$

for a suspension containing N particles per milliliter. The specific forward scattering, $V(0)/c$ (compare eq 6), is given by

$$\frac{V(0)}{c} = \frac{3}{4\lambda_M D} \frac{i_1(0)}{\alpha^3} \quad (9)$$

The difference in the refractive index of the colloidal suspension and the medium (*i.e.*, water containing the same concentrations of dissolved electrolytes), $\Delta\mu$, was measured with a Brice-Phoenix differential refractometer. For work at 366 m μ a plate of uranium glass was placed at the focal plane of the projection lens, and the displacement of the fluorescent slit image was measured. The instrument was calibrated by visual measurements as usual with sucrose solutions

(2) H. C. van de Hulst, "Light Scattering by Spherical Particles," John Wiley and Sons, Inc., New York, N. Y., 1957, pp 130, 269; see also P. Latimer and F. D. Bryant, *J. Opt. Soc. Amer.*, **55**, 1554 (1965).

(3) T. F. W. Barth, *Amer. J. Sci.*, **19**, 135 (1930).

(4) H. Schröter, *Z. Physik.*, **67**, 24 (1931).

(5) E. J. Meehan and W. H. Beattie, *J. Phys. Chem.*, **64**, 1006 (1960).

(6) Definitions of K_T and related quantities are given in ref 2, p 127f. The quantity K_T is called Q_{ext} by van de Hulst. Also see D. Sinclair, *J. Opt. Soc. Amer.*, **37**, 475 (1947).

(7) Gj. Deželić and J. P. Krahtovil, *Kolloid Z.*, **173**, 38 (1960).

(8) D. A. I. Goring, M. Senez, B. Melanson, and M. M. Huque, *J. Colloid Sci.*, **12**, 412 (1957).

(9) W. F. H. M. Mommaerts, *ibid.*, **7**, 71 (1952).

(10) R. O. Gumprecht and C. M. Sliepcevič, "Tables of Light-Scattering Functions for Spherical Particles," Engineering Research Institute, University of Michigan, Ann Arbor, Mich., 1951.

at 546 $m\mu$, the displacement of slit image, Δd , is proportional to $\Delta\mu$: at 546 $m\mu$

$$\Delta\mu_{546} = k_{546}\Delta d_{546}$$

and at any wavelength

$$k_\lambda = k_{546} \frac{M_{546}}{M_\lambda}$$

where M is the magnification. Values of M are supplied by the manufacturer at 589, 546, and 436 $m\mu$. Since M varies very little with λ , a short extrapolation to shorter λ seems entirely reliable. The values used were

λ_V	546.1	435.8	404.7	366.1
M	9.686	9.705	9.712	9.72

Chemicals were as described before.¹¹ Measurements were made on a variety of sols. Small-particle sols having a radius of $\leq 10 m\mu$ were made in a rapid-mixing apparatus, described elsewhere,¹² in which mixing was complete in 0.006 sec or less. Measurements on sols with radius *ca.* 7 $m\mu$ were made in the rapid-mixing apparatus either during flow or with stopped flow. Sols with radii 7–10 $m\mu$ were prepared in the same apparatus; the effluent was collected and stabilized at a given radius by addition of a solution of polyvinylpyrrolidone (PVP),¹¹ which either prevented particle growth entirely or made growth so slow that any change in radius could be corrected for easily. Sols of radius 10–30 $m\mu$ were prepared using a mechanical stirrer and stabilized with PVP. Radius was determined by scattering and transmission measurements over the range λ_V 436–800 $m\mu$, assuming that $n_P = n_B$.¹³ The validity of this assumption is confirmed by the fact that the values of r thus found were the same within a few per cent over the entire range of wavelength. Equation 6 was used to obtain α from measurements of transmission, which yielded τ/c , combined with Mie theory values of K_T . Radius was found from α by eq 4. Equation 9 was used to obtain α from scattering measurements extrapolated to 0° , which yielded $V(0)/c$, combined with Mie theory values of $i(0)$. All the small-particle sols were relatively homogeneous, as shown by the fact that even *ca.* 30 min after mixing, at which time the radius in the absence of stabilizer was much larger than Rayleigh size, measurements over this range of wavelength gave the same radius within a few per cent. In addition, some heterogeneous sols containing larger particles (modal radius, 48 $m\mu$; see Figure 1) were prepared by ordinary mixing, as described earlier.¹¹

Calculations

Values of the scattering coefficient, K_S , the total extinction coefficient, K_T , and forward scattering were calculated from exact Mie theory for many values of m and k (see eq 3), at intervals of 0.05 in α . The value

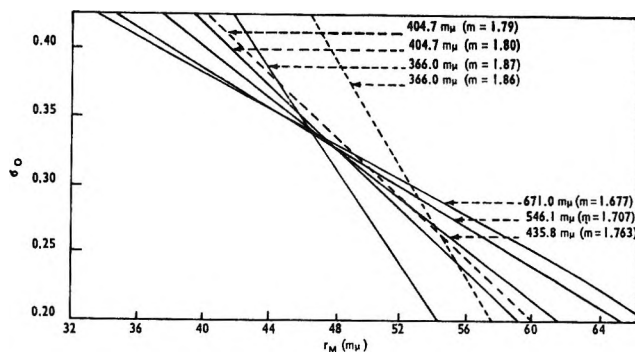


Figure 1. Determination of m from transmission measurements on a heterogeneous suspension.

of γ_B at 366 $m\mu$ is $6.0 \times 10^3 \text{ cm}^{-1}$.¹⁴ This corresponds (using the value of n_P derived in this paper) to $m_B' = 1.3 \times 10^{-2}$ and $k_B = 7.0 \times 10^{-3}$. Mie calculations were made for values of k_P smaller than, equal to, and larger than k_B , up to 0.1, which proved to be larger than the actual value. Similar calculations were made (with appropriately smaller k) for 405 and 436 $m\mu$.

Tables I–III contain a few examples, selected from the very extensive calculations for homogeneous suspensions, which illustrate the principles used in obtaining \hat{m} .

Scattering measurements are considered first. K_S determines the total scattering and $i_1(0)$ is proportional to forward-scattered intensity, eq 8. Table I shows that for small particles, $\alpha \leq 0.5$,¹⁵ the scattering is practically independent of k up to $k = 0.01$. Even for $k = 0.1$, which corresponds to very strong absorption,¹⁶ the scattering differs by only a few per cent from that of a nonabsorbing substance. Of course the scattering for small α is sensitive to m , as is shown in Table II. Therefore, measurements of *forward scattering* in homogeneous sols of *small radius* serve to determine m , no matter what the value of k is (up to the above-stated limit at least).

The quantity $\text{Re } i_1^*(0)$ given in Table I is the real part of the complex forward-scattering function which determines $i_1(0)$

$$i_1(0) = |\text{Re } i_1^*(0) + i\text{Im } i_1^*(0)|^2 \quad (10)$$

There is no general uniformity of notation among

(11) E. J. Meehan and G. Chiu, *J. Phys. Chem.*, **70**, 1389 (1966).

(12) E. J. Meehan and J. K. Miller, *ibid.*, in press.

(13) The experimental values of n_B extend only up to 671 $m\mu$, but a short extrapolation to 800 $m\mu$ should be reliable. The value of n_P used for 800 $m\mu$ was 2.210, corresponding to $m_P = 1.664$.

(14) Y. Okamoto, *Nachr. Akad. Wiss. Goll.*, IIA, 275 (1956); F. Moser and F. Urbach, *Phys. Rev.*, **102**, 1519 (1956); F. Moser, Eastman Kodak Co., Rochester, N. Y., personal communication, 1964.

(15) At λ_V 366 $m\mu$, $n_M = 1.346$, and $\alpha = 0.5$ corresponds to $r = 21.7 m\mu$.

(16) A layer 0.1-mm thick of a substance having $k = 0.1$ and $n_B = 1.87 \times 1.346$ (compare eq 2 and 3) would transmit only 0.02% at λ_V 366 $m\mu$.

Table I: Values of K_T , K_S , $i_1(0)$, and $\text{Re } i_1^*(0)$ for $m = 1.85$ and Various Values of k

k	K_T	K_S	$i_1(0)$	$\text{Re } i_1^*(0)$
$\alpha = 0.25$				
0	0.002119	0.002119	5.1363×10^{-5}	7.1667×10^{-3}
0.001	0.002858	0.002119	5.1362×10^{-5}	7.1666×10^{-3}
0.005	0.005815	0.002119	5.1365×10^{-5}	7.1664×10^{-3}
0.01	0.009510	0.002120	5.1380×10^{-5}	7.1665×10^{-3}
0.1	0.07582	0.002219	5.3782×10^{-5}	7.2373×10^{-3}
$\alpha = 0.5$				
0	0.03568	0.03568	3.8024×10^{-3}	6.1623×10^{-2}
0.001	0.03740	0.03567	3.8020×10^{-3}	6.1616×10^{-2}
0.005	0.04430	0.03566	3.8006×10^{-3}	6.1587×10^{-2}
0.01	0.05292	0.03564	3.7997×10^{-3}	6.1553×10^{-2}
0.1	0.20761	0.03698	3.9426×10^{-3}	6.1435×10^{-2}
$\alpha = 1$				
0	0.5916	0.5916	0.3587	0.5804
0.001	0.5965	0.5909	0.3584	0.5798
0.005	0.6160	0.5882	0.3571	0.5774
0.01	0.6402	0.5849	0.3556	0.5745
0.1	1.0570	0.5523	0.3413	0.5210
$\alpha = 2$				
0	3.5872	3.5872	17.891	2.2412
0.001	3.5876	3.5672	17.855	2.2325
0.005	3.5887	3.4887	17.707	2.1973
0.01	3.5884	3.3938	17.512	2.1530
0.1	3.4003	2.2094	13.568	1.4162
$\alpha = 3$				
0	4.6413	4.6413	113.78	-2.1740
0.001	4.6194	4.5735	112.52	-2.1297
0.005	4.5302	4.3207	107.75	-1.9620
0.01	4.4273	4.0411	102.39	-1.7782
0.1	3.4119	1.9693	59.09	-0.3948
$\alpha = 6$				
0	2.7847	2.7847	630.31	1.4798
0.001	2.8018	2.7305	637.93	1.4398
0.005	2.8528	2.5331	660.73	1.2323
0.01	2.8820	2.3251	673.63	0.9249
0.1	2.6153	1.3025	556.18	-1.4713

Table II: Values of K_S for Various m ; $k = 0$

m	K_S	
	$\alpha = 0.5$	$\alpha = 0.6$
1.80	0.03242	0.06860
1.831	0.03443	0.07302
1.85	0.03568	0.07575
1.87 ^a	0.03697	0.07854

^a These values are exact for $k = 0.00694$ and are practically identical with those for $k = 0$.

workers in this field. Note that i_1 as used in this paper corresponds to i_1 of ref 10; i_1^* as used in this paper corresponds to i_1^* of Zimm and Dandliker¹⁷ and to i_1' of Lowan.¹⁸ The relevance of $\text{Re } i_1^*(0)$ in the present problem is its relation to the refractive-index increment as shown in eq 11, due to Zimm and Dandliker¹⁷

$$\frac{d\mu}{dc} = \frac{3\mu'}{2\alpha^3 D} \text{Re } i_1^*(0) \quad (11)$$

where μ' is the refractive index of the suspension.

The values of $\text{Re } i_1^*(0)$ given in Table I for $\alpha \leq 0.5$ are practically independent of k up to $k = 0.01$. Thus measurements of the refractive-index increment in homogeneous sols of small radius can serve to determine m in the same way as scattering measurements. (At larger values of α , both the scattering and the refractive-index increment depend significantly upon k ; compare the values for $k = 0$ and $k = 0.001$ at $\alpha = 6$.)

(17) B. H. Zimm and W. B. Dandliker, *J. Phys. Chem.*, **58**, 644 (1954).

(18) A. N. Lowan, "Tables of Scattering Functions for Spherical Particles," National Bureau of Standards Circular AMS-4, U. S. Government Printing Office, Washington, D. C., 1948, p 6.

Table III: Sensitivity of Specific Turbidity to k ; Illustrative Examples for λ_V 366.0 $m\mu$

r , $m\mu$	α	K_T/α^a						R^b
		$k =$ 0.006470	$k =$ 0.008364	$k =$ 0.009758	$k =$ 0.011152	$k =$ 0.012546	$k =$ 0.013940	
4.2	0.097	0.02004	0.02395	0.02786	0.03177	0.03568	0.03959	1.976
9.4	0.217	0.02593	0.02997	0.03402	0.03807	0.04211	0.04616	1.780
12.5	0.289	0.03451	0.03869	0.04287	0.04705	0.05123	0.05542	1.606
19.3	0.446	0.07471	0.07932	0.08394	0.08855	0.09317	0.09778	1.309
24.3	0.561	0.13094	0.13598	0.14102	0.14607	0.15111	0.15614	1.192
27.8	0.643	0.1893	0.1947	0.2001	0.2055	0.2109	0.2163	1.143

^a Directly proportional to specific turbidity, eq 6. ^b R is the ratio of K_T/α for $k = 0.01394$ to K_T/α for $k = 0.00697$.

In practice, the best procedure to obtain m from measurements on sols of small α is to calculate exact values of $i_1(0)/\alpha^3$ and $\text{Re } i_1^*(0)/\alpha^3$ as a function of m for each value of α , the latter being determined as stated above from the scattering and the transmission measurements at longer λ , assuming $n_P = n_B$. A plot of each quantity vs. m is made for each α , from which the exact value of m is found easily.

Next consider transmission measurements. The value of K_T , which determines the specific turbidity, eq 6, is practically proportional to k for small α . Therefore transmission measurements on homogeneous sols of small radius can serve to determine k if m is known independently, e.g., by the measurements of the scattering and the refractive-index increment explained above. The following procedure is used. Exact values of K_T are calculated for each m and α for a range of values of k . The experimental quantity τ/c gives K_T/α (eq 6), and a plot of K_T/α vs. α , which is practically linear for the values involved, gives k .

Obviously the precision in determining k is the greater, the smaller the value of α . Table III illustrates the situation at 366 $m\mu$. (The values of r given in Table III correspond to various experimental suspensions described later.) A 100% variation in k corresponds to 98 and 14% variation in τ/c for r equal to 4.2 and 27.8 $m\mu$, respectively.

It is evident from Table I that transmission measurements on suspensions of moderate α , e.g., 2, are useless to determine k , but can serve to determine m . This principle was used to obtain m from measurements on heterogeneous sols. Values of τ/c were calculated for heterogeneous suspensions. The distribution of particle size was assumed to follow the "zero-order logarithmic distribution."¹⁹ This has two parameters, r_M (corresponding to the modal radius) and σ_0 (corresponding to the width of the distribution). τ/c was obtained for a range of values of r_M and σ_0 by numerical integration over 500 equally spaced values of r , up to 1 μ (much larger than any particle present in any appreciable amount in any of the suspensions studied). The use of these calculations to obtain m is explained in the next section.

Results and Discussion

A. Determination of m_P . (a) Homogeneous Suspensions of Small Radius. As mentioned under the Experimental Section, the values of α were derived from scattering and transmission measurements, 436–800 $m\mu$, assuming $n_B = n_P$. The assumption is confirmed directly by the result that r is independent of λ . Additional confirmation is provided by the results for $d\mu/dc$, given in Table IV. Within experimental error the values of n_P at $\lambda_V \geq 436$ are the same as of n_B .

Table V gives the results derived from forward scattering. The value found at 405 $m\mu$ is in excellent agreement with the given in Table IV. The average value of m_B at 366 $m\mu$ agrees reasonably well with that in Table IV, but the deviation of the individual results is greater. There is no indication of a trend in m_P with r , and hence these results together with the earlier ones indicate that the real part of the refractive index is the same for colloidal particles having $r \geq 8.9$ $m\mu$ as for bulk material.

(b) Heterogeneous Suspensions. The result of measurements of τ/c (extrapolated to $c = 0$) for heterogeneous suspensions is given in Figure 1, which is a plot of σ_0 vs. r_M .¹⁹ An experimental measurement at a single λ yields a single σ_0 - r_M curve. Measurements at several yield a family of curves which ideally intersect at a point if the assumed distribution is of the correct form. Figure 1 shows such curves based upon transmission measurements over the range λ_V 366–671 $m\mu$. The curves for 436, 546, and 671 $m\mu$, which are calculated for $m_P = m_B$, come very close to intersection at a point. Curves for the two shorter wavelengths were calculated for various values of m_P . (The bulk value of k was used, since for the values of α involved the exact value is of minor consequence.) Two such curves are shown for each of the wavelengths in question. The results indicate values of m_P of 1.868 and 1.800 at 366.0 and 404.7 $m\mu$, respectively.

Taking into account the various assumptions and

(19) W. F. Espenscheid, M. Kerker, and E. Matijević, *J. Phys. Chem.*, **68**, 3093 (1964); also see ref 5.

Table IV: Values of m_P Derived from Refractive-Index Increment (Small Particle Size, Homogeneous Suspension)

λ_V , $m\mu$	n_M	m_B	r , $m\mu^a$	α	$\Delta\mu/\Delta c^b$	m_P
546.1	1.334	1.707	18.6	0.285	0.123	1.702
			19.1	0.294	0.124	1.709
435.8	1.340	1.763	18.5	0.357	0.135	1.769
			19.0	0.366	0.132	1.745
404.7	1.342	...	18.5	0.386	0.139	1.784
			17.1	0.356	0.137	1.781
366.0	1.346	...	18.5	0.428	0.148 ^c	1.834
			18.7	0.433	0.160 ^d	1.920

^a Radius based upon transmission measurements at 546.1 $m\mu$. ^b The uncertainty in $\Delta\mu/\Delta c$ is about ± 0.002 , except at 366 $m\mu$. ^c ± 0.006 . ^d ± 0.011 . ^e Double weight is given to the first value.

Table V: Values of m_B Derived from Forward Scattering

λ_V , $m\mu$	r , $m\mu^a$	α	$V(0)/c^b$	$10^3 i_1(0)/\alpha^3$	m_B
404.7	8.9	0.185	4.34	1.13	1.773
	15.0	0.313	22.3	5.82	1.78
	17.6	0.366	36.2	9.43	1.773
366.0	8.9	0.206	7.2	1.69	1.812
	15.0	0.346	42.4	9.95	1.899
	17.6	0.406	61.0	14.3	1.814

^a Average of values measured at 546 and 436 $m\mu$, which agreed within 1%. ^b Specific forward scattering, extrapolated to infinite dilution; see eq 8 and 9.

experimental precision, the following values are adopted.

$\lambda_V, m\mu$	435.8	404.7	366.0
m_P	1.763	1.800	1.868
n_P	2.362	2.416	2.514

It is possible that the exact value of m_P at 404.7 is as low as 1.79.

B. Determination of k_P . The experimental values of K_T/α , calculated from specific turbidity and an assumed particle density of 6.473 g ml⁻¹, together with the derived values of k_P , are summarized in Table VI. For the reasons given previously, the precision in k is greatest for the smallest r . Figure 2 is a plot of the ratio k_P/k_B as a function of r . Equations 1-3 yield

$$\frac{k_P}{k_B} = \frac{\gamma_P m_B}{\gamma_B m_P} = \frac{\gamma_P}{\gamma_B} \quad (12)$$

The latter relation is based upon the assumption that $n_P = n_B$ at all the wavelengths; the data in this paper show this is true at 436 $m\mu$ and above.

The results show definitely that the absorption coefficient of colloidal silver bromide is different from that of bulk, and that the ratio depends upon the wavelength. There is no clear indication of a trend of

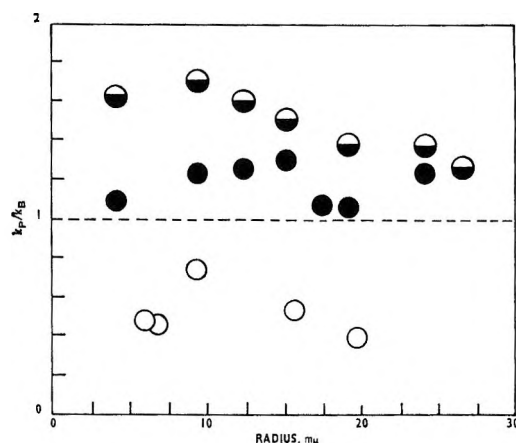


Figure 2. Ratio of absorption coefficient of colloidal particle to that of bulk: \circ , 436 $m\mu$; \bullet , 405 $m\mu$; \ominus , 366 $m\mu$.

γ_P/γ_B with increasing r , and because of the nature of the measurements (*cf.* Discussion and Table III), it is unlikely that such a trend could be established. The values of k at the smallest values of r should be reliable within a few per cent, whence it can be concluded that the particle absorption coefficient is about 50% smaller, 10% larger, and 60% larger than the bulk coefficient at wavelengths 436, 405, and 366 $m\mu$, respectively.

Doremus²⁰ has measured the optical properties of small particles of gold both in glass and in aqueous suspension. He found that the real part of the refractive index is the same for particles as for bulk, for particles above *ca.* 4 $m\mu$ in radius. This is in agreement with the result found in this work for silver bromide. In regard to the absorption coefficient, Doremus concluded that this was somewhat different for particles in aqueous suspension and for bulk; particles in glass (down to the above given radius) had an absorption coefficient similar to that of bulk. He attributed the difference between the two types of particles to imper-

(20) R. H. Doremus, *J. Chem. Phys.*, **40**, 2389 (1964).

Table VI: Values of k_P

r , $m\mu$	435.8		404.7		366.0	
	K_T/α	k_P	K_T/α	k_P	K_T/α	k_P
	0.000692		0.00213		0.00697	
4.2			0.00697	0.00234	0.0325	0.0114
6.0	0.0017	0.00034				
6.75	0.00194	0.00032				
9.4	0.0043	0.00053	0.0114	0.00264	0.0402	0.0119
12.5			0.0168	0.00268	0.0479	0.0114
15.2	0.0143 (?)	0.00076 (?)	0.0244	0.00277	0.0574	0.0106
15.8	0.0143	0.00037	0.0244	0.00211		
17.5			0.0318	0.00228		
19.3			0.0403	0.00225	0.0835	0.0096
19.8	0.0274	0.00037				
23.4					0.119	0.0069
24.3			0.0764	0.00263	0.1402	0.0095
27.8			0.1082	0.0016 (?)	0.196	0.0088
28.3					0.1952	0.0062

^a Using the value $n_B = n_P$.

fections in the aqueous particles and particularly to contamination at their surfaces. It is questionable if either of these explanations would be applicable to our results with silver bromide because there is no evidence

of a trend in the values of k_P with radius. The importance both of imperfection and of surface contamination would be expected to decrease markedly with increasing r , in the range studied.

Thermodynamics of Binary Liquid Mixtures by Rayleigh Light Scattering^{1,2}

by Raymond L. Schmidt and H. Lawrence Clever

Department of Chemistry, Emory University, Atlanta, Georgia 30322 (Received September 14, 1967)

The density, total Rayleigh scattering, and depolarization were determined over the full composition range at 303.15°K and incident wavelengths of 436 and 546 $m\mu$ for binary mixtures of dichloromethane with dibromomethane, diiodomethane, chloroform, and bromoform. Excess volumes of mixing have been calculated from the density data. The scattering resulting from concentration fluctuations has been used to calculate the activity coefficients and free energy of mixing for dichloromethane with dibromomethane, diiodomethane, and bromoform.

The activities of the components in binary solution have fundamental thermodynamic importance. Methods suitable for the determination of nonelectrolyte activities can be divided into two classes, methods in which the activity of one component is experimentally obtained and the activity of the other component is calculated using the Gibbs-Duhem relation (osmotic pressure, freezing point depression, solubility) and

methods in which the activity of each component is directly determined and the results confirmed by consistency with the Gibbs-Duhem equation (partial pres-

(1) This paper is taken from the work submitted by R. L. Schmidt to the Graduate School of Emory University in partial fulfillment of the requirement for the degree of Doctor of Philosophy.

(2) Work supported by National Science Foundation Grant GP5937 and presented at the Southeastern Regional Meeting of the American Chemical Society, Atlanta, Ga., Nov 1967.

sure measurements). Recently, another method of the first class has been described by Coumou and Mackor,³ who have shown how Rayleigh light scattering and depolarization data from binary solution can be used to get the activities of the components of the solution. This paper discusses the light scattering method and gives results of its application to the binary solutions of dichloromethane with dibromomethane, diiodomethane, chloroform, and bromoform.

The total Rayleigh scattering of a pure liquid is the result of two additive contributions, isotropic scattering, R_{is} , caused by density fluctuations, R_d , and anisotropic scattering, R_{an} , caused by orientation fluctuations of anisotropic molecules. For binary solutions there are additional contributions to the isotropic scattering due to fluctuations in concentration, R_c . It has been assumed in most molecular weight determinations by light scattering that the density and concentration fluctuations are statistically independent, but several authors⁴⁻⁶ have shown this assumption to be false, and a cross term, $R^\#$, is appreciable in some cases and should be calculated for each solution studied. The total isotropic scattering of a binary solution is given by $R_{is} = R_d + R_c + R^\#$, where

$$R_d = (\pi^2/2\lambda_0^4)kT\kappa_T[N(\partial\epsilon/\partial N)_T]^2 \quad (1)$$

$$R_c = (2\pi^2/\lambda_0^4)kTVX_1(n\partial n/\partial X_2)^2/(\partial\mu_2/\partial X_2) \quad (2)$$

$$R^\# = (\pi^2/\lambda_0^4)kT\kappa_T[N(\partial\epsilon/\partial N)][C(\partial\epsilon/\partial C)] \quad (3)$$

and λ_0 is the wavelength of incident radiation in a vacuum, κ_T is the mixture isothermal compressibility, N is the number density of the liquid, ϵ is the optical dielectric constant ($\epsilon = n^2$, n is the refractive index), C is the concentration of the solute in g ml⁻¹, V is the molar volume, X_2 is the mole fraction of the solute, and μ_2 is the solute chemical potential.

For an ideal solution, $\partial\mu_2/\partial X_2 = RT/X_2$ and R_c becomes R_{id} and can be calculated from a knowledge of the density, concentration, and refractive index increment $\partial n/\partial X_2$ from

$$R_{id} = (2\pi^2/\lambda_0^4)VX_1X_2(n\partial n/\partial X_2)^2/N_a \quad (4)$$

where N_a is Avogadro's number.

For a real solution, $\partial\mu_2/\partial X_2 = RT/X_2 + \partial\mu_2^e/\partial X_2$, where μ_2^e is the excess chemical potential of component 2 due to the nonideality of the solution, and can be calculated from the function

$$[1 - (R_{id}/R_c)] = -X_2(\partial\mu_2^e/\partial X_2)/RT = X_1X_2(\partial^2g^e/\partial X_1\partial X_2)/RT \quad (5)$$

where g^e is the molar excess Gibbs free energy. Using the Gibbs-Duhem equation, $X_1d\mu_1 + X_2d\mu_2 = 0$, and activity coefficients, f_i , defined as $\mu_i^e = RT \ln f_i$, one can write

$$[1 - (R_{id}/R_c)] = \frac{-d \ln f_1}{d \ln X_1} = -X_1 d \ln f_1/dX_1 = -X_2 d \ln f_2/dX_2 \quad (6)$$

from which the activity coefficients can be obtained by numerical integration of

$$\ln f_1 = \int_0^X \frac{1}{X_1} [1 - (R_{id}/R_c)] dX_2 \quad (7)$$

The excess Gibbs free energy is calculated from

$$g^e = RT(X_1 \ln f_1 + X_2 \ln f_2)$$

In the special case of a regular solution

$$g_{reg}^e = AX_1X_2$$

$$(\partial\mu_2^e/\partial X_2)_{reg} = -2AX_1$$

and

$$[1 - (R_{id}/R_c)]_{reg} = 2AX_1X_2/RT = 2g_{reg}^e/RT \quad (8)$$

The determination of the activity coefficients and the excess Gibbs free energy of mixing of a binary solution by the light scattering technique involves the following steps. The total Rayleigh scattering and depolarization of the two pure liquids and of five to eight solutions is measured. The total Rayleigh scattering, R_{90} , is separated into its component parts R_{is} and R_{an} . Theoretical values of R_d and $R^\#$ are computed and R_c is obtained by the difference, $R_{is} - R_d - R^\#$. The ideal concentration scattering, R_{id} , and the function $[1 - (R_{id}/R_c)]$ is computed, and the activity coefficients and excess free energy are obtained by the numerical integration of $[1 - (R_{id}/R_c)]/X$.

Notes on the Calculations

Separation of R_{is} from R_{90} . The isotropic and anisotropic contributions to the total Rayleigh scattering (Table I) can be separated by the Cabannes relation

$$R_{is} = R_{90}(6 - 7\rho_\mu)/(6 + 6\rho_\mu)$$

$$R_{an} = R_{90} - R_{is} = R_{90}13\rho_\mu/(6 + 6\rho_\mu) \quad (9)$$

where R_{90} and ρ_μ are the total Rayleigh scattering and depolarization at 90° to the unpolarized incident beam, respectively. These relations have been derived rigorously for vapors^{7,8} and have been experimentally verified for liquids.⁹

(3) D. J. Coumou and E. L. Mackor, *Trans. Faraday Soc.*, **60**, 1726 (1964).

(4) R. K. Bullough, *J. Polymer Sci.*, **46**, 517 (1960); *Proc. Roy. Soc. (London)*, **A275**, 271 (1963).

(5) Y. Sicotte and M. Rinfret, *Trans. Faraday Soc.*, **58**, 1090 (1962).

(6) Y. Sicotte, *J. Chim. Phys.*, **61**, 1086 (1964).

(7) J. Cabannes, "La Diffusion Moleculaire de la Lumiere," Les Presses Universitaires de France, Paris, 1929, Chapter X.

(8) J. A. Prins and W. Prins, *Physica*, **22**, 576 (1956); **23**, 253 (1957).

(9) D. J. Coumou, E. L. Mackor, and J. Hijmans, *Trans. Faraday Soc.*, **60**, 1539 (1964).

Table I: Rayleigh Scattering and Depolarization, 303.15°K

X_2	Density, g/ml	436 m μ		546 m μ	
		$R_{90} \times 10^6$, cm $^{-1}$	ρ_{μ}	$R_{90} \times 10^6$, cm $^{-1}$	ρ_{μ}
Dichloromethane (1)–Dibromomethane (2)					
0.0000	1.3072	18.45	0.275	6.70	0.280
0.1231	1.4686	22.85	0.280	8.00	0.255
0.1746	1.5306	24.95	0.280	8.90	0.250
0.2772	1.6553	28.50	0.285	9.70	0.250
0.5201	1.9469	35.90	0.310	11.65	0.265
0.6966	2.1459	39.55	0.340	12.50	0.325
0.7254	2.1758	40.25	0.360	12.70	0.305
0.8461	2.3083	42.15	0.400	13.10	0.360
0.8540	2.3178	41.75	0.405	13.20	0.355
1.0000	2.4704	43.80	0.450	13.45	0.415
Dichloromethane (1)–Diiodomethane (2)					
0.0000	1.3072	18.5	0.255	6.65	0.280
0.1486	1.6722	66.5	0.125	21.70	0.105
0.2043	1.8022	88.5	0.115	28.35	0.095
0.2613	1.9293	110.0	0.110	35.35	0.075
0.3731	2.1792	164.0	0.095	49.55	0.070
0.5084	2.4592	178.0	0.145	57.35	0.120
0.6195	2.6621	173.5	0.155	56.10	0.130
0.6545	2.7272	178.0	0.175	55.65	0.155
0.8100	2.9992	148.0	0.270	47.50	0.255
0.9253	3.1840	133.0	0.390	42.95	0.385
1.0000	3.2670	127.0	0.510	41.30	0.490
Dichloromethane (1)–Bromoform (2)					
0.0000	1.3072	17.15	0.275	6.75	0.275
0.0584	1.4322	21.25	0.210	8.30	0.230
0.1355	1.5889	27.15	0.195	10.35	0.210
0.2859	1.8695	36.10	0.145	13.55	0.145
0.3805	2.0340	40.00	0.165	14.35	0.145
0.5322	2.2683	42.75	0.180	15.10	0.180
0.6831	2.4859	44.45	0.250	15.80	0.270
1.0000	2.8683	42.00	0.370	14.15	0.375

Calculation of Solution Refractive Index. Solution refractive indices are required at the incident wavelengths in the calculations of R_{90} , R_c , and $R^{\#}$. The pure component refractive indexes at the incident wavelength were obtained by fitting refractive index dispersion data taken from Timmermans¹⁰ to the Cauchy dispersion formula, $n_{\lambda} = A + B/\lambda^2$. The calculated n_{λ} was corrected to the temperature of the scattering measurements.

The mixture refractive indices were calculated by the Lorentz–Lorenz equation

$$n_{12} = [(2A' + 1)/(1 - A')]^{1/2} \quad (10)$$

where

$$A' = \left[\left(\frac{n_1^2 - 1}{n_1^2 + 2} \right) \frac{1}{d_1} - \left(\frac{n_1^2 - 1}{n_1^2 + 2} \right) \frac{p_2}{d_1} + \left(\frac{n_2^2 - 1}{n_2^2 + 2} \right) \frac{p_2}{d_2} \right] d_{12}$$

where n_i , d_i , and p_i are the refractive index, density, and weight fraction of component i and d_{12} is the mixture

density. Heller¹¹ has shown that for an extensive concentration range the Lorentz–Lorenz equation appears to be the most reliable of the refractive index mixture rules.

Calculation of R_d . To evaluate R_d , calculations of $N(\partial\epsilon/\partial N)_T$ and κ_T must be made. The dielectric constant term was calculated using the Clausius–Mosotti equation, with a correction for dense media

$$N(\partial\epsilon/\partial N)_T = \frac{(n^2 - 1)(n^2 + 2)}{3}(1 - 0.07345) \quad (11)$$

The refractive indices are the solution refractive indices calculated from the Lorentz–Lorenz equation. The empirical correction factor, 0.07345, is the average value of the deviation between the experimental $N(\partial\epsilon/\partial N)_T$ and that calculated by the simple Clausius–Mosotti equation for liquids over a wide range of refractive indices.⁹ The mixture compressibility was assumed to be represented by

$$(\kappa_T)_{12} = \left(-\frac{1}{V_{12}} \right)_T \left[X_1 \left(\frac{\partial V}{\partial P} \right)_1 + X_2 \left(\frac{\partial V}{\partial P} \right)_2 \right] \quad (12)$$

where $(\partial V/\partial P)_i$ is calculated from the density scattering of the pure components. The calculation includes the effect of the volume change upon mixing in the estimation of R_d for the mixture.

The $[1 - (R_{id}/R_c)]$ Function. The experimental values of $[1 - (R_{id}/R_c)]$ at the two wavelengths were combined and smoothed (Table II) using the general equation for excess thermodynamic properties described by Myers and Scott.¹² The activity coefficient rela-

Table II: Least-Squares Coefficients¹² for $[1 - (R_{id}/R_c)]$ Data

	CH ₂ Cl ₂ / CH ₂ I ₂	CH ₂ Cl ₂ / CH ₂ Br ₂ ^a
Y_1	2.102 ± 0.05	0.658 ± 0.03
Y_2	0.475 ± 0.20	0.090 ± 0.07
Y_3	0.636 ± 0.24	...
Y_4	-1.313 ± 0.55	...
B	0.000	0.000

^a Coefficients used to smooth $R_c \times 10^6$ cm $^{-1}$ data before calculating $[1 - (R_{id}/R_c)]$.

tions, $\ln f_i$, were obtained by numerical integration of the smoothed values of $[1 - (R_{id}/R_c)]/X$ on an analog computer with two X–Y recorders and an electronic line follower.

(10) J. Timmermans, "Physicochemical Constants of Pure Organic Compounds," Vol. 1 and 2, Elsevier Publishing Co., New York, N. Y., 1950, 1965.

(11) W. Heller, *J. Phys. Chem.*, **69**, 1123 (1965).

(12) D. B. Myers and R. L. Scott, *Ind. Eng. Chem.*, **55**, 43 (1963).

Experimental Section

Chemicals. Benzene, Mallinckrodt Nanograde, was used as received as a primary standard; methyl alcohol, Baker Analyzed, Reagent grade, was used as received; dichloromethane, Matheson Coleman and Bell, was used as received. Bromoform (Spectrograde), dibromomethane, and diiodomethane, all Eastman organic chemicals, were used as received except the iodo compound which was fractionally crystallized just prior to use. Chloroform (certified ACS Spectrograde, 0.75% EtOH preservative), Fisher Scientific, was used as received. Tests with the optical filters supplied with the light-scattering photometer showed all the pure liquids were free of fluorescing impurities.

Sample Preparation. Mixture samples were prepared by weight in 25- or 50-ml volumetric flasks shortly before the filtration and scattering measurements. Some of the $\text{CH}_2\text{Cl}_2 + \text{CH}_2\text{I}_2$ samples were prepared by dilution because only a limited amount of pure CH_2I_2 was available. Never more than two successive dilutions were made before a new sample was prepared from the pure components.

The sample cell was cleaned with potassium dichromate cleaning solution and rinsed with distilled water. The interior of the cell was splashed with condensing methanol vapors to remove water and clinging dust particles. The samples were filtered into the cell through an ultrafine porosity glass disk (Owens-Illinois, Kimax, No. 28400) Büchner funnel using oil-pumped N_2 as a pressure head. Samples were rejected as being insufficiently dust-free if dust could be seen visually using a light source and magnifying lens or if the 45:135° dissymmetry ratio was greater than 1.00 ± 0.02 .

Density. The pure liquid and solution densities were measured in 15-ml density bottles made with a constant-bore, calibrated capillary neck ($0.00073 \text{ cm}^3/\text{mm}$). The bottles were calibrated with freshly boiled deionized-distilled water at 30°. The densities were measured at 30.0° in a large capacity water bath with the temperature controlled to $\pm 0.005^\circ$.

Equipment. All light-scattering measurements were made with a Brice-Phoenix Series 2000 Universal light-scattering photometer at incident wavelengths of 435.8 and 546.0 μm . The photometer output was measured on a Honeywell Series 3400 dc spotlight galvanometer of $5.4 \times 10^{-4} \mu\text{A}/\text{mm}$ scale division sensitivity. Measurements were made on samples contained in a small cylindrical cell (Brice-Phoenix No. C-105) requiring 15 ml of sample. The cell exterior surface was painted with Kodak No. 4 dull black brushing lacquer and the beam diaphragms and detector nose piece were coated with carbon black from burning benzene to reduce stray light effects. The temperature of the sample in the photometer was controlled by circulating constant-temperature distilled water through

the cored sample table and cell jacket. The temperature was measured on a 0.1° graduated thermometer placed in the circulating tube just after the thermostatting liquid left the scattering chamber. The temperature is considered to be reliable to $\pm 0.1^\circ$.

Instrument Calibration. Benzene was used as a primary standard to calibrate the instrument. The Rayleigh ratio values of $46.5 \times 10^{-6} \text{ cm}^{-1}$ at 436 μm and $16.1 \times 10^{-6} \text{ cm}^{-1}$ at 546 μm obtained by Dezelic and Vavra¹³ at 25° were used. The values are consistent with the values calculated from other physical constants¹⁴ and compare well with values recommended for benzene.¹⁵

The absolute scattering ratios of other samples were calculated relative to benzene from the equation

$$R_{90} = R_{90, \text{std}} \frac{F(G_{90}/G_0)an^2(Rw/Rc)(r/r')}{F_{\text{std}}(G_{90}/G_0)_{\text{std}}a_{\text{std}}n_{\text{std}}^2(Rw/Rc)_{\text{std}}(r/r')_{\text{std}}} \quad (13)$$

where G_{90}/G_0 is the ratio of galvanometer deflections when viewing the scattered radiation at 90° to that for the transmitted radiation at 0°. F is the transmittance of the combination of neutral filters used to determine the scattering ratio, a is a constant relating the working standard to the opal glass reference standard, n is the refractive index of the sample, Rw/Rc is a correction factor reported by the instrument manufacturer for the incomplete compensation for the refraction effects at the cell glass-liquid interface, and r/r' is an experimentally determined calibration factor relating the narrow beam geometry to the standard beam geometry. The label "std" identifies values for the benzene standard. The Rw/Rc ratio was calculated for each liquid by interpolation of the data reported by the instrument manufacturer. The r/r' ratio was assumed to vary linearly between the two experimentally determined values for the two pure liquids.

Depolarization. In the cylindrical cell, the depolarization of the sample was measured from the angular dependence of the scattering using the equation¹³

$$(G_\theta/G_{90}) \sin \theta = 1 + (1 - \rho_\mu) \cos^2 \theta / (1 + \rho_\mu) \quad (14)$$

where ρ_μ is the depolarization and G_θ and G_{90} are the galvanometer readings at the scattering angles of θ ($45 \leq \theta \leq 135$) and 90°, respectively. The left side of the above equation was multiplied by an empirical factor, $f(\theta)$, to correct for any optical defects in the sample cell and for residual stray light which could not be eliminated by painting the exterior cell surface and blackening the beam diaphragms with carbon black. The $f(\theta)$ factor was determined for benzene using the known depolarization values of Coumou¹⁶ of 0.42 at

(13) G. Dezelic and J. Vavra, *Croat. Chem. Acta*, **38**, 35 (1966).

(14) G. Dezelic, *J. Chem. Phys.*, **45**, 185 (1966).

(15) J. P. Kratochvil, G. Dezelic, M. Kerker, and E. Matijevic, *J. Polymer Sci.*, **57**, 59 (1962).

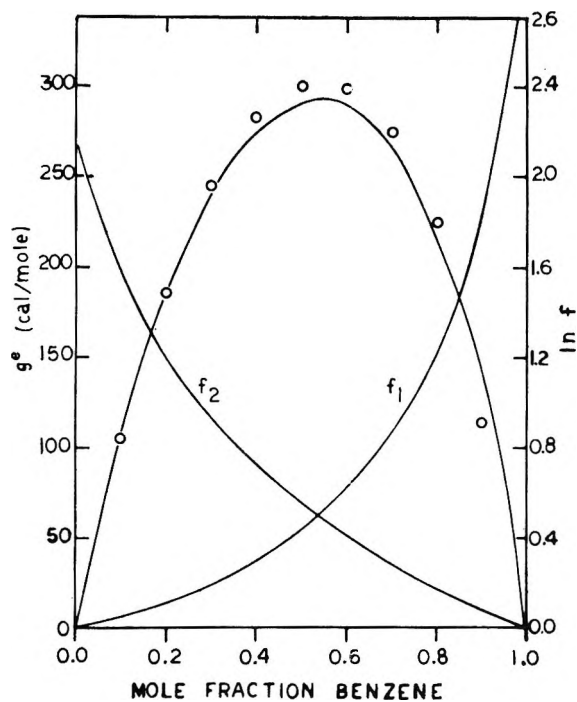


Figure 1. Activity coefficients and excess free energy of mixing for the methanol-benzene system at 25°: —, light scattering; O, vapor pressure.

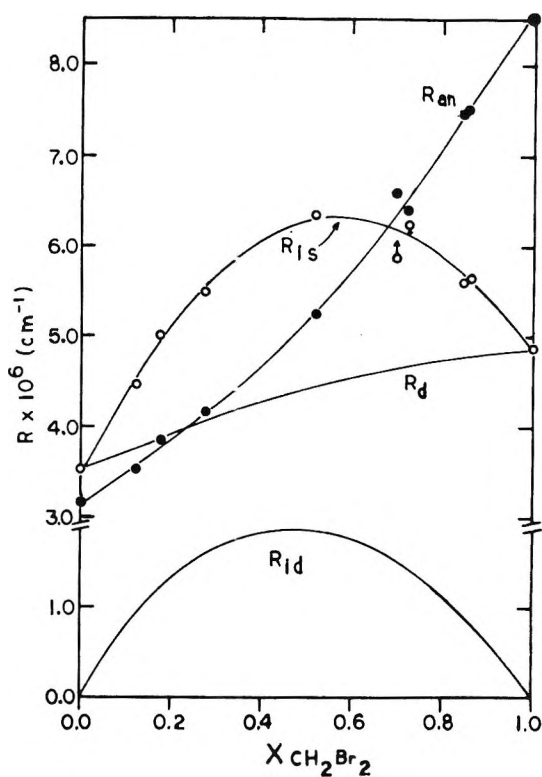


Figure 3. Contributions to the total Rayleigh scattering ratio: dichloromethane-dibromomethane systems, 546 $m\mu$, 30°.

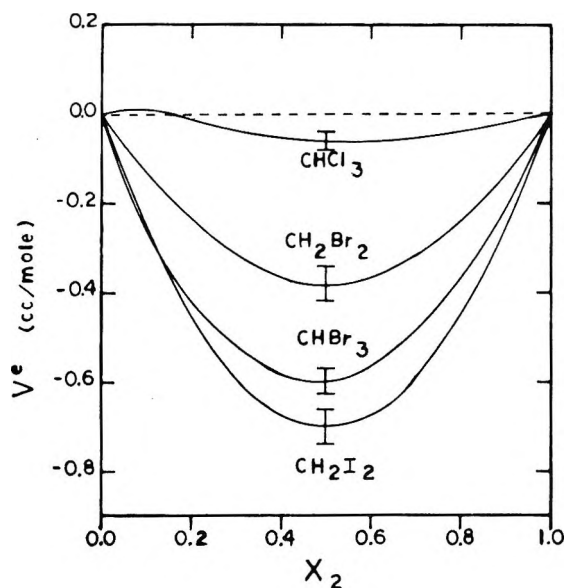


Figure 2. Excess volume vs. mole fraction solute; dichloromethane mixtures, 30°; I, error in smooth curve.

436 $m\mu$ and 0.41 at 546 $m\mu$, and for carbon tetrachloride using the values reported by Kratochvil, Kerker, and Oppenheimer¹⁷ of 0.051 at 436 $m\mu$ and 0.057 at 546 $m\mu$.

Results and Discussion

The light-scattering technique was applied to the benzene-methanol system at 25°. Activity coefficients and excess free energies of mixing have been reported for the system by the light-scattering technique and by vapor pressure measurements. Our results for the

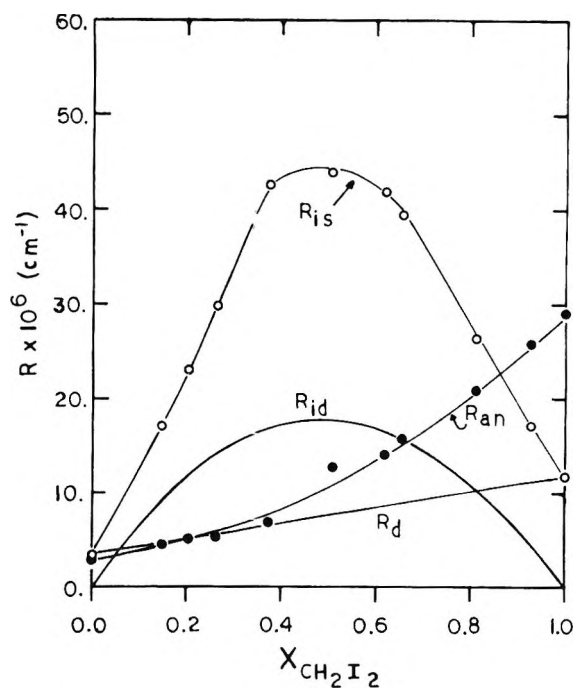


Figure 4. Contributions to the total Rayleigh scattering ratio; dichloromethane-diiodomethane systems, 546 $m\mu$, 30°.

activity coefficients and excess free energy of mixing are shown in Figure 1 and Table III. The results are

(16) D. J. Coumou, *J. Colloid Sci.*, **15**, 408 (1960).

(17) J. P. Kratochvil, M. Kerker, and L. E. Oppenheimer, *J. Chem. Phys.*, **43**, 914 (1965).

Table III: Activity Coefficients and Free Energy of Mixing

—MeOH + C ₆ H ₆ (298.15°K)—				—CH ₂ Cl ₂ + CH ₂ Br ₂ (303.15°K)—			—CH ₂ Cl ₂ + CH ₂ I ₂ (303.15°K)—			
X_2	$\ln f_1$	$\ln f_2$	g^e , cal/ mole	$\ln f_1$	$\ln f_2$	g^e , cal/ mole	$\ln f_1$	$\ln f_2$	g^e , cal/ mole	
0.0	0.00	2.10	0	0.00	-0.55	0	0.00	1.11	0	
0.1	0.03	1.52	106	-0.01	-0.36	-25	0.01	0.92	61	
0.2	0.10	1.16	197	-0.02	-0.25	-40	0.05	0.72	109	
0.3	0.18	0.92	238	-0.04	-0.18	-50	0.10	0.55	141	
0.4	0.29	0.72	274	-0.07	-0.13	-55	0.18	0.40	160	
0.5	0.43	0.56	293	-0.09	-0.10	-57	0.27	0.28	165	
0.6	0.62	0.40	289	-0.12	-0.07	-55	0.38	0.18	159	
0.7	0.87	0.27	267	-0.16	-0.05	-48	0.52	0.11	140	
0.8	1.22	0.16	220	-0.22	-0.02	-38	0.68	0.06	108	
0.9	1.83	0.06	140	-0.31	-0.01	-24	0.90	0.02	63	
1.0	3.20	0.00	0	...	0.0	0	1.19	0.00	0	

virtually identical with those of Coumou and Mackor.³ Also shown are excess free energies of mixing calculated from the five-parameter equation reported by Scatchard and Ticknor¹⁸ from vapor pressure measurements. The agreement is about 1%.

The experimental values of the densities, the total Rayleigh scattering, and depolarization at 436 and 546 μ for the binary mixtures of dichloromethane with dibromomethane, diiodomethane, and bromoform at 30° are given in Table I. The excess volumes of mixing for the four systems were calculated from the densities. The excess volumes were smoothed by the general equation for excess thermodynamic properties.¹² Excepting the dichloromethane-chloroform system which shows a change in sign, all excess volumes are negative (Figure 2). Figures 3, 4, and 5 show the various terms contributing to the total scattering for these systems. The $R^{\#}$ term is not shown in the figures since it is only slightly larger than the experimental error in the light-scattering measurements. However, the term is included in our calculations and should be considered when determining thermodynamic data by the light-scattering method.

For the dichloromethane-dibromomethane system, the ideal scattering is symmetrical at *ca.* 0.5 mole fraction as a result of the excess volume. The concentration scattering is less than the ideal scattering indicating a negative free energy. In the regions of dilute solutions, calculations are difficult since the difference between the concentration and ideal scattering approaches experimental error and $[1 - (R_{id}/R_c)]$ approaches zero. The data at 546 μ gave the best behavior in these regions and R_c was smoothed¹² prior to the calculation of $[1 - (R_{id}/R_c)]$. The activity coefficients and excess free energy are tabulated in Table III. The excess free energy is negative and reaches a minimum value of -57 cal/mole at 0.5 mole fraction. The activity coefficient relations are very nearly regular.

In a study of the thermodynamic properties of the

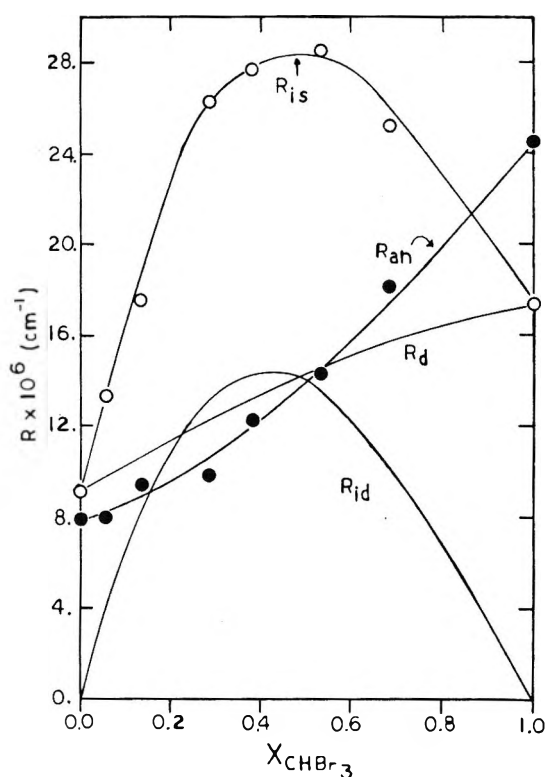


Figure 5. Contributions to the total Rayleigh scattering ratio; dichloromethane-bromoform system, 436 μ , 30°.

series of di-, tri-, and tetrachloromethane with methyl iodide, Moelwyn-Hughes and Missen¹⁹ found evidence for specific attractive forces between chloroform and methyl iodide where g^e , h^e , and V^e are all negative. For the dichloromethane-dibromomethane system, g^e and V^e are both negative.

For the dichloromethane-diiodomethane system the isotropic scattering is chiefly the result of concentration

(18) G. Scatchard and L. B. Ticknor, *J. Amer. Chem. Soc.*, **74**, 3724 (1952).

(19) E. A. Moelwyn-Hughes and R. W. Missen, *Trans. Faraday Soc.*, **53**, 607 (1957).

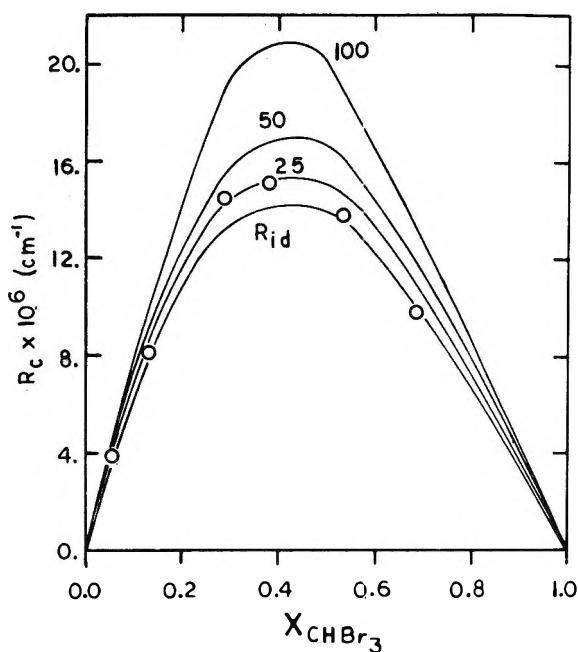


Figure 6. Dichloromethane-bromoform system, 436 $m\mu$, 30°: O, experimental R_c values; upper three curves, calculated R_c values assuming a regular solution and excess free energies of mixing of 25, 50, and 100 cal/mole.

fluctuations and reaches a maximum value of $136 \times 10^{-6} \text{ cm}^{-1}$ for 436 $m\mu$ and $44.5 \times 10^{-6} \text{ cm}^{-1}$ for 546 $m\mu$ at about 0.45 mole fraction diiodomethane. The free energy and activity coefficient relations are shown in Table III. The excess free energy and excess volume are surprisingly large for this system and of opposite sign.

Analysis of the light-scattering and depolarization results from the dichloromethane-chloroform solutions showed isotropic scattering to be a linear function of concentration and to be identical within experimental error with the density scattering. The refractive index difference in the two pure components is only 0.02, and fluctuations in the optical dielectric constant resulting from concentration fluctuations are too small to measure with any degree of accuracy. No estimate of the activity coefficient and excess free energy can be made by the light-scattering technique.

The terms contributing to the total scattering for the dichloromethane-bromoform system (Figure 5) indicate that the concentration scattering is only slightly larger than the ideal scattering. Owing to this small difference in R_{id} and R_c , only a crude estimation of the excess free energy could be made. In Figure 6 are shown various curves for the concentration scattering by back calculating from the regular solution model and assumed values of the free energy of mixing. This calculation indicates that the system is nearly ideal with an excess free energy of mixing less than 25 cal/mole.

The depolarization of the excess radiation scattered by an anisotropic solute in the presence of a more iso-

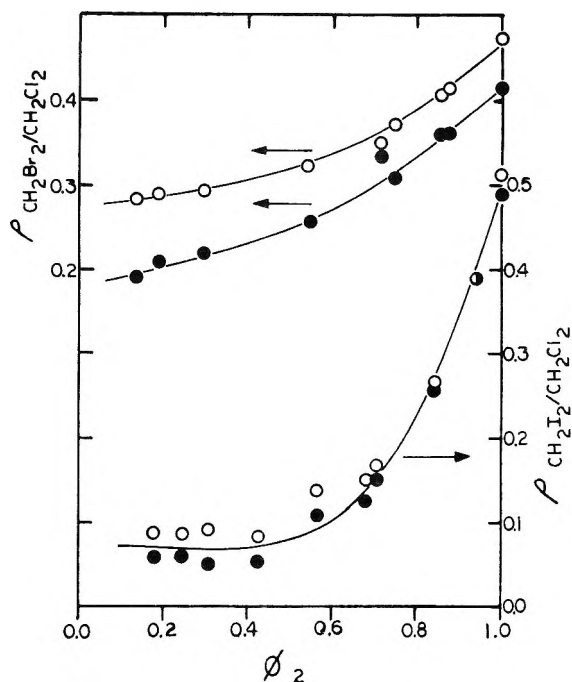


Figure 7. Excess depolarization vs. volume fraction, 30°; upper curves, dichloromethane-dibromomethane; lower curve, dichloromethane-diiodomethane system; O, 436 $m\mu$; ●, 546 $m\mu$.

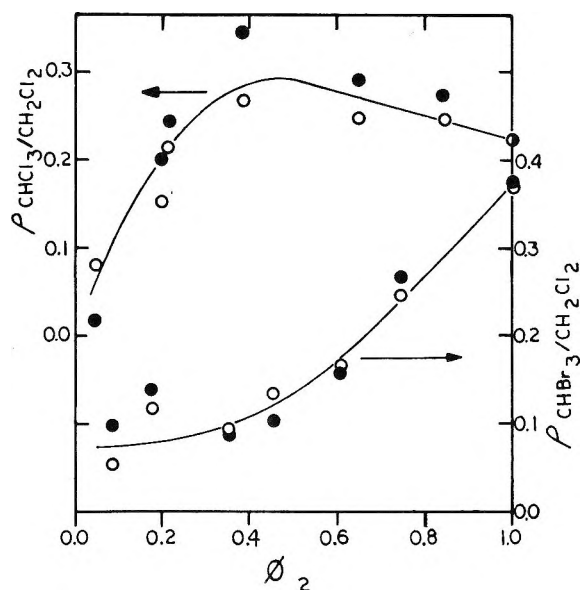


Figure 8. Excess depolarization vs. volume fraction, 30°; upper curve, dichloromethane-chloroform; lower curve, dichloromethane-bromoform system; O, 436 $m\mu$; ●, 546 $m\mu$.

tropic solvent gives information about the optical anisotropy of the solute molecules in the solution. This excess depolarization, $\rho_{2/1}$, is calculated according to a modification given by Sicotte⁵ of an equation proposed by Lotmar²⁰ and Powers and Stein²¹

(20) W. Lotmar, *Helv. Chim. Acta*, **21**, 792 (1938).

(21) J. Powers and R. S. Stein, *J. Chem. Phys.*, **21**, 1613 (1953).

$$\rho_{2/1} = \frac{\frac{R_{12}^0}{R_1^0} \left(\frac{\rho_{12}}{1 + \rho_{12}} \right) - \left(\frac{\rho_1}{1 + \rho_1} \right) \phi_1}{\frac{R_{12}^0}{R_1^0} \left(\frac{\rho_1}{1 + \rho_{12}} \right) - \left(\frac{\rho_1}{1 + \rho_1} \right) \phi_1} \quad (15)$$

where ρ_{12} and ρ_1 are the depolarizations for the mixture and solvent, respectively, ϕ_1 is the volume fraction of the solvent, and R_{12}^0 and R_1^0 are the total Rayleigh ratios of the mixture and pure solvent, respectively.

The results are shown in Figures 7 and 8. Definite breaks are indicated in the data for dichloromethane with diiodomethane and with chloroform. Sicotte has suggested that such breaks are indicative of a change in the liquid state structuring in the solution.

Acknowledgment. We thank the Emory Biomedical Data Processing and Analysis Center for use of the computer.

The Independence of Isothermal Equilibria in Electrolyte Solutions on Changes in Dielectric Constant¹

by Arvin S. Quist and William L. Marshall

Reactor Chemistry Division, Oak Ridge National Laboratory, Oak Ridge, Tennessee 37830 (Received September 18, 1967)

The importance of including the molar concentration of the solvent as a variable in the equilibrium constant (K^0) is discussed. When the solvent is considered to participate actively in the equilibrium, isothermal values of K^0 are found to be independent of changes in dielectric constant of the solvent mixtures. Extensive examples are given in support of this general principle. The new principle contrasts with existing theory that considers $\log K$ (the conventional constant not containing solvent species as concentration variables) to be a linear function of $1/D$. It is shown to apply to electrolyte behavior in water, water-organic, and organic-organic solvent systems over a wide range of temperature and pressure. For example, in water-dioxane solvent mixtures where electrolytes (ions and polar molecules) are preferentially solvated by water molecules, a plot of $\log K$ (dissociation) vs. $\log C_{H_2O}$ in moles per liter yields a straight line of intercept K^0 and slope representing the net change in waters of solvation between equilibrium reactants and products. From the slope and an estimate of the hydration number of the ion pair, the "ion size" parameter can be calculated. Many examples in support of this new principle are presented both for homogeneous and heterogeneous equilibria.

Introduction

In an earlier communication, we have proposed a general principle that the inclusion of solvent species of variable concentration directly into the conventional equilibrium constant (K) for ion-ion-pair-solvent equilibria provides a complete constant (K^0) that is independent of changes in dielectric constant at constant temperature.² It is the purpose of this paper to present substantial evidence to support this principle, to show that it provides an independent method for calculating hydration numbers and ion size parameters, and to present a clearer description of solution equilibria in general.

Previously, changes in conventional, isothermal equilibrium constants involving electrolytes in aqueous-organic and organic-organic solvents have been almost universally correlated with changes in the measurable dielectric constant (D) of the solvent mixtures. The decrease in a conventional dissociation

constant [expressed herein always as dissociation constants for direct comparisons and consistency] with decreasing concentration of the more polar component of a binary solvent mixture has usually been related to the simultaneous decrease in the measurable dielectric constant of the solvent mixture. Thus the Bjerrum equation,³ relating ion-pair formation to the dielectric constant of the solvent and to ionic size, was used by Fuoss and Kraus⁴ to relate $\log K$ for the ionization of tetraisoamylammonium nitrate in water-dioxane mixtures to $\log D$. The currently accepted Denison-Ramsey-Fuoss theory^{5,6} of ion-pair formation predicts

(1) Work sponsored by the U. S. Atomic Energy Commission under contract with Union Carbide Corporation.

(2) W. L. Marshall and A. S. Quist, *Proc. Natl. Acad. Sci. U. S.*, **58**, 901 (1976).

(3) N. J. Bjerrum, *Kgl. Danske Vidensk. Selskab.*, **7**, No. 9 (1926).

(4) R. M. Fuoss and C. A. Kraus, *J. Am. Chem. Soc.*, **55**, 1019 (1933).

that $\log K$ should be a linear function of $1/D$, with a slope that is proportional to the ion size. The latter relationship holds moderately well for most ionization constants when the concentration of added organic solvent is not great, but the correlation (although observed over limited ranges of very low dielectric constant) is not observed over wide ranges of solvent composition.

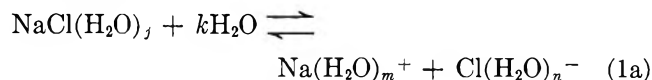
The Denison-Ramsey-Fuoss theory of ion-pair formation is based on a sphere-in-a-continuum model and considers that the measurable dielectric constant is the controlling factor in association. However, in recent years evidence has been accumulating⁷⁻⁹ to indicate that ion-solvent interaction must be considered and that the dielectric constant of the solvent mixture may not be the only significant factor in ion association. If the important factors in short-range electrostatic attractions between oppositely charged ions, ion pairs, and solvent molecules in solution are the charges on the ions and the dipole moments (assumed constant at constant temperature) of the reacting species, and if ions and ion pairs in mixed solvents are selectively solvated, then a complete, isothermal constant K^0 involving also solvent species as variables would be expected to remain constant over a large range of solvent compositions.¹⁰ Therefore, it would appear that the Denison-Ramsey-Fuoss theory as presently derived, using the measurable dielectric constant and considering the incomplete constant K , is probably incorrect. This theory considers also that only contact ion pairs are formed in the association process.⁹ Eigen¹¹ and Atkinson,¹² however, have demonstrated the existence of a three-step ion-association process for 2-2 electrolytes, involving stepwise removal of solvent molecules from between ions.

We propose that the activity (or concentration) of solvent molecules indeed be included, in molar concentration units,¹³ as very important *variables* in the complete equilibrium constant, K^0 . When this is done, it is found that the isothermal K^0 for a particular equilibrium is independent of changes in dielectric constant, whether these changes are made by varying the density of the solution system by pressurization or by adding an "inert" solvent (*i.e.*, one that does not significantly solvate the ions or polar molecules of the electrolyte), such as dioxane, to water. Tests of this general principle have shown remarkable agreement over a wide range of conditions for a variety of aqueous-organic and some organic-organic solvents at room temperature and atmospheric pressure, and also for equilibrium behavior in water alone. The agreement far surpasses that shown by existing theories that correlate the change in the incomplete equilibrium constant (not K^0) with changes in the measurable dielectric constant.

Aqueous Electrolyte Behavior at Supercritical Temperatures

Sodium chloride is generally considered to be completely ionized in aqueous solutions at room temperature

and atmospheric pressure. However, it becomes progressively a weaker electrolyte as the temperature increases. From electrical conductance measurements on dilute NaCl solutions at temperatures to 800° and at pressures to 4000 bars,¹³ conventional equilibrium constants (K) have been calculated which are related to the complete equilibrium constants as



$$K^0 = \frac{a_{\text{Na}(\text{H}_2\text{O})_m^+} a_{\text{Cl}(\text{H}_2\text{O})_n^-}}{a_{\text{NaCl}(\text{H}_2\text{O})_j} a_{\text{H}_2\text{O}}^k} = K/a_{\text{H}_2\text{O}}^k \quad (1b)$$

$$\log K = \log K^0 + k \log a_{\text{H}_2\text{O}} \quad (1c)$$

where K^0 is the complete constant assumed to be independent of $a_{\text{H}_2\text{O}}$, K is the conventional constant that varies with $a_{\text{H}_2\text{O}}$, and the a 's are activities based on molar concentration units. In his studies on KCl solutions at supercritical temperatures and pressures, Franck¹⁴ some 11 years ago showed that a plot of $\log K$ (at constant temperature) against $\log C_{\text{H}_2\text{O}}$ (moles per liter) gave nearly a straight line. Our own recent and extensive values of $\log K$ for NaCl show a linear relationship for similar plots.

The values of K (at a particular temperature and density) as obtained from the conductance measurements represent the values of this parameter at infinite dilution of the electrolyte. Under these conditions, the solvent has the same properties as the pure solvent and its activity can be set equal to its molar concentration. Consequently, eq 1c can be written as

$$\log K = \log K^0 + k \log C_{\text{H}_2\text{O}} \quad (2)$$

where $C_{\text{H}_2\text{O}}$ refers to the molar concentration of water. Thus, if water is considered a reactant of variable concentration in the equilibrium, the linear relationship between $\log K$ and $\log C_{\text{H}_2\text{O}}$ is explained. Ordinarily, in studies of equilibria in aqueous solutions under the usual conditions of 25° and atmospheric pressure, the activity of water is effectively constant and is arbitrarily assigned a value of unity, whereby the equilibrium is expressed by the conventional K . However, as seen in the above example, in studies of equilibria in solutions at supercritical temperatures and pressures where wide ranges of water concentrations are encoun-

(5) J. T. Denison and J. B. Ramsay, *J. Am. Chem. Soc.*, **77**, 2615 (1955).

(6) R. M. Fuoss, *ibid.*, **80**, 5059 (1958).

(7) A. D'Aprano and R. M. Fuoss, *J. Phys. Chem.*, **67**, 1704, 1722 (1963).

(8) G. Atkinson and S. Petrucci, *J. Am. Chem. Soc.*, **86**, 7 (1964).

(9) G. Atkinson and S. Petrucci, *J. Phys. Chem.*, **70**, 3122 (1966).

(10) Note that the measurable dielectric constant still remains important for long-range electrostatic interactions.

(11) M. Eigen and K. Tamm, *Z. Elektrochem.*, **66**, 93, 107 (1962).

(12) G. Atkinson and S. K. Kor, *J. Phys. Chem.*, **69**, 128 (1965).

(13) A. S. Quist and W. L. Marshall, *ibid.*, **72**, 684 (1968).

(14) E. U. Franck, *Z. Physik. Chem. (Frankfurt)*, **8**, 107 (1956).

tered, it is necessary to include the activity of water as a variable in calculating the complete equilibrium constant.

For the NaCl solutions, this linear relationship was observed at temperatures from 400 to 800° and at densities from 0.30 to 0.75 g cm⁻³. Furthermore, the values of k were essentially constant throughout this temperature range, indicating that j , m , and n may be primary hydration numbers. A value of K^0 can therefore be calculated with eq 2 at each temperature. This K^0 is independent of density (pressure) at constant temperature, and therefore meets one of the requirements of a "true" thermodynamic equilibrium constant.¹⁵

This concept of a true, isothermal equilibrium constant has been experimentally verified for several different ionization equilibria over a wide range of solution densities and over wide temperature regions. The evaluations for most of the published data for aqueous solutions at high temperatures and pressures are summarized in Table I. Since the isothermal equilibrium constants K^0 for the equilibria summarized in Table I are independent of solvent density, it became evident to us that these constants were also independent of changes in dielectric constant of the solvent. Although at 400° the dielectric constant of water decreases from 19.5 at a density of 0.8 g cm⁻³ to 4.9 at a density of 0.3 g cm⁻³,¹⁶ the value of K^0 is constant. This observation is highly significant in demonstrating that the measurable dielectric constant of the solvent is not the determining factor in predicting the true equilibrium constant, in contrast to present theory on the variation of the conventional K .⁷ In the following sections this principle is extended to include ionic equilibria in water-organic and organic-organic solvents.

Equilibrium Behavior in Water-Organic Solvents at Room Temperature

The above expectations and observations indicated that for ionic equilibria in mixed solvents the inclusion

of the solvent species as reactants of variable concentration might provide equilibrium constants that were truly independent of changes in solvent composition. In the examples described above, the concentration of water was varied by changing the pressure on the solutions. The molarity of water can also be changed by adding an "inert" solvent, such as dioxane. The addition of this inert solvent does not appear to affect significantly the hydration of ions since the water molecule is much more polar than the dioxane molecule and consequently water molecules selectively solvate the ions.^{17,18} Therefore, the relative hydration of ions should be nearly independent of total water concentration, and the hydration numbers in an equation like eq 1a should remain constant over a wide range of water-dioxane compositions. Kunze and Fuoss¹⁹ have calculated conventional ionization constants for NaCl for the equilibrium represented by K in eq 1c from conductance measurements in several water-dioxane mixtures at 25°. When the ionization constants reported

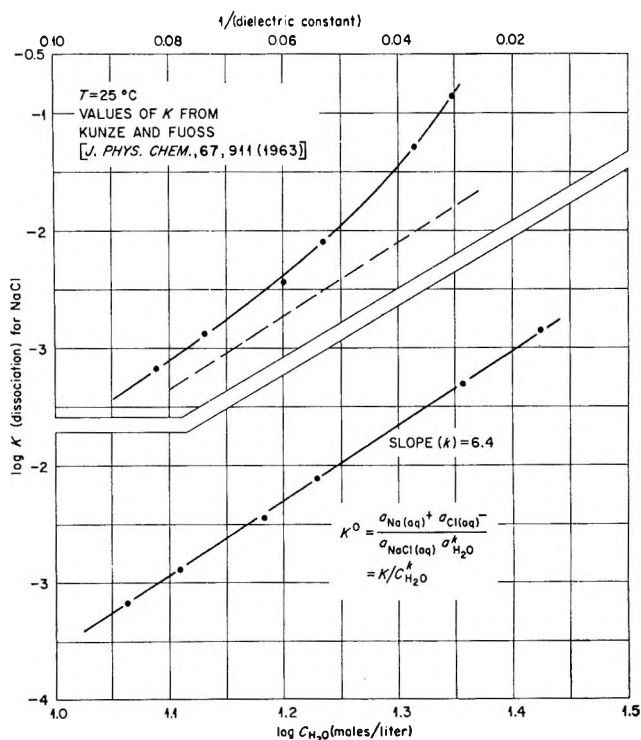


Figure 1. Log K (dissociation) of sodium chloride vs. log C_{H_2O} (moles per liter) in dioxane-water mixtures; also compared vs. $1/(\text{dielectric constant}, D)$; K values of Kunze and Fuoss (1963).

Table I

Electrolyte	Solvent system	Temp. °C	Net change in waters of hydration on ionization	Lit. ref
HSO_4^-	H_2O to 4000 bars	100–300	20	<i>a</i>
H_2SO_4	H_2O to 4000 bars	400–800	11	<i>b</i>
KHSO_4	H_2O to 4000 bars	400–800	8.5	<i>a</i>
NaCl	H_2O to 4000 bars	400–800	10	<i>c</i>
KCl	H_2O to 2700 bars	400–750	9	<i>d</i>
HCl	H_2O to 2700 bars	400–700	9	<i>e</i>
KOH	H_2O to 2700 bars	400–700	8	<i>e</i>

^a A. S. Quist and W. L. Marshall, *J. Phys. Chem.*, **70**, 3714 (1966). ^b A. S. Quist, *et al.*, *ibid.*, **69**, 2726 (1965). ^c Reference 13. ^d Reference 14. ^e E. U. Franck, *Z. Physik. Chem. (Frankfurt)*, **8**, 192 (1956).

(15) W. J. Moore, "Physical Chemistry," 3rd ed, Prentice-Hall, Inc., Englewood Cliffs, N. J., 1962, p 174.

(16) A. S. Quist and W. L. Marshall, *J. Phys. Chem.*, **69**, 3165 (1965).

(17) T. W. Davis, J. E. Ricci, and C. G. Sauter, *J. Am. Chem. Soc.*, **61**, 3274 (1939).

(18) A. Fratiello and D. C. Douglass, *J. Chem. Phys.*, **39**, 2017 (1963).

(19) R. W. Kunze and R. M. Fuoss, *J. Phys. Chem.*, **67**, 911 (1963).

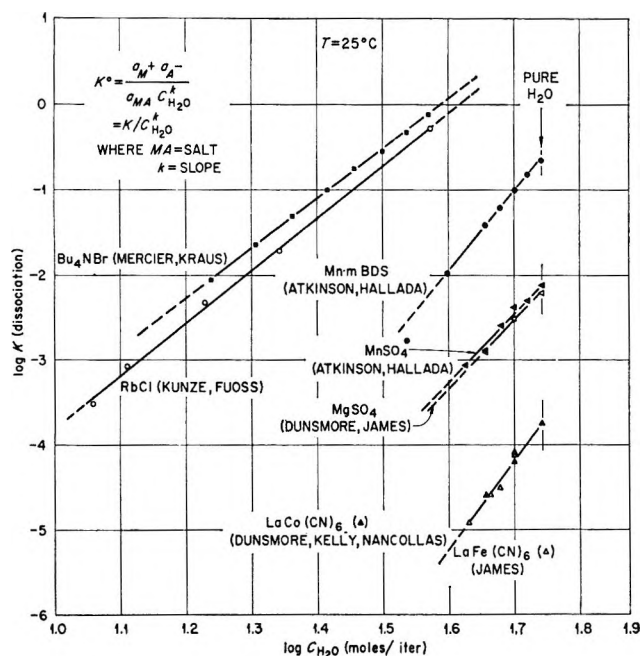


Figure 2. Logarithm of the conventional equilibrium constant K for several salts vs. $\log C_{H_2O}$ (moles per liter) in dioxane-water mixtures at 25° .

by Kunze and Fuoss (K in eq 1c) are plotted against $\log C_{H_2O}$, a straight line is obtained as shown in Figure 1 with a random deviation of ± 0.005 pK unit ($\pm 1\%$ in K). This linear relationship indicates that the complete equilibrium is represented by an equation like eq 1a, as was the case with the NaCl data at supercritical temperatures and pressures. It also indicates the constancy of the hydration numbers with varying water concentration. Figure 1 also includes a plot of $\log K$ for NaCl in water-dioxane mixtures as a function of $1/D$ and shows a maximum deviation of 0.25 pK unit (a factor of 1.8 in K), which is typical of the behavior of most alkali metal halides in these mixtures.

Equilibrium constants for many ionization processes have been measured in water-dioxane mixtures at 25° . We have plotted $\log K$ (for the ionization process that does not consider hydration) as a function of $\log C_{H_2O}$ over as much as 0.5 log unit for many types of equilibria in water-dioxane mixtures, and in nearly all of these cases we have obtained straight lines, yielding constant values for K^0 according to eq 2. Several examples of these plots are shown in Figure 2, and Table II summarizes our evaluations of some of the literature data according to our proposal for the equilibrium including hydration. Of the examples shown in Table II, only those involving RbI and LiCl showed significant deviations from linearity.

Table II also contains the results of our evaluations of literature data for some acetone-water and methanol-water systems. Of the examples cited, appreciable deviations from linearity were observed for the equilibria involving $MnSO_4$, Mn *m*-benzenedisulfonate,

Table II

Electrolyte	Solvent system	Net change in waters of hydration on ionization	Lit. ref
LiCl	Water-dioxane	3.6-7.2	a
NaCl	Water-dioxane	6.4	b
KCl	Water-dioxane	6.5	c
RbCl	Water-dioxane	6.3	d
CsCl	Water-dioxane	6.2	e
RbBr	Water-dioxane	6.3	f
RbI	Water-dioxane	3-8	g
LiI	Water-dioxane	5.1	h
MgSO ₄	Water-dioxane	8.2	i
MgSO ₄	Water to 2000 bars	8.4	j
MnSO ₄	Water-dioxane	9	k
MnSO ₄	Water-acetone	6.6	l
MnSO ₄	Water-methanol	4.6	m
MnSO ₄	Water to 2000 bars	9	n
Mn <i>m</i> BDS ^{aa}	Water-dioxane	9	k
Mn <i>m</i> BDS	Water-acetone	6	l
Mn <i>m</i> BDS	Water-methanol	4.5	m
Ca <i>m</i> BDS	Water-acetone	4.4	o
Ca <i>m</i> BDS	Water-methanol	2.6	o
LaFe(CN) ₆	Water-dioxane	10.8	p
LaFe(CN) ₆	Water to 2000 bars	8.4	q
(Bu) ₄ NBr	Water-dioxane	5.8	r
(CH ₃) ₄ N picrate	Water-dioxane	8.4	r
(C ₅ H ₁₁) ₄ NNO ₃	Water-dioxane	10 (ion pairs)	s
(C ₅ H ₁₁) ₄ NNO ₃	Water-dioxane	2.4 (triple ions)	t
Acetic acid	Water-dioxane	7.6	u
Acetic acid	Water to 2000 bars	12	v
Acetic acid	Water-methanol	2.2-2.8	w
H ₂ O(Kw)	Water-dioxane	6.2-6.6	x
H ₂ O(Kw)	Water to 2000 bars	20	y
NH ₄ OH	Water to 2000 bars	28	z
CH ₃ NH ₂ OH	Water to 2000 bars	25	z

^a T. L. Fabry and R. M. Fuoss, *J. Phys. Chem.*, **68**, 971 (1964). ^b Reference 19. ^c J. E. Lind, Jr., and R. M. Fuoss, *J. Phys. Chem.*, **65**, 999 (1961). ^d R. W. Kunze and R. M. Fuoss, *ibid.*, **67**, 914 (1963). ^e J. C. Justice and R. M. Fuoss, *ibid.*, **67**, 1707 (1963). ^f J. E. Lind, Jr., and R. M. Fuoss, *ibid.*, **66**, 1722 (1962). ^g T. L. Fabry and R. M. Fuoss, *ibid.*, **68**, 974 (1964). ^h G. Atkinson and Y. Mori, *J. Chem. Phys.*, **45**, 4716 (1966). ⁱ H. S. Dunsmore and J. C. James, *J. Chem. Soc.*, 2925 (1951). ^j F. H. Fisher, *J. Phys. Chem.*, **66**, 1607 (1962). ^k G. Atkinson and C. J. Hallada, *J. Am. Chem. Soc.*, **84**, 721 (1962). ^l Reference 8. ^m C. J. Hallada and G. Atkinson, *J. Am. Chem. Soc.*, **83**, 3759 (1961). ⁿ F. H. Fisher and D. F. Davis, *J. Phys. Chem.*, **69**, 2595 (1965). ^o H. Tsubota and G. Atkinson, *J. Am. Chem. Soc.*, **87**, 164 (1965). ^p J. C. James, *J. Chem. Soc.*, 1094 (1950). ^q S. D. Hamann, P. J. Pearce, and W. Strauss, *J. Phys. Chem.*, **68**, 375 (1964). ^r P. L. Mercier and C. A. Kraus, *Proc. Natl. Acad. Sci.*, **41**, 1033 (1955). ^s Reference 4. ^t R. M. Fuoss and C. A. Kraus, *J. Am. Chem. Soc.*, **55**, 2387 (1933). ^u H. S. Harned, *et al.*, *ibid.*, **58**, 1912 (1936); ref 33. ^v A. J. Ellis and D. W. Anderson, *J. Chem. Soc.*, 1765 (1961). ^w T. Shedlovsky and R. L. Kay, *J. Phys. Chem.*, **60**, 151 (1956). ^x H. S. Harned and L. D. Fallon, *J. Am. Chem. Soc.*, **61**, 2374 (1939). ^y S. D. Hamann, *J. Phys. Chem.*, **67**, 2233 (1963). ^z S. D. Hamann and W. Strauss, *Trans. Faraday Soc.*, **51**, 1684 (1955). ^{aa} *m*-Benzenedisulfonate.

(20) S. Luz and S. Meiboom, *J. Chem. Phys.*, **40**, 1058 (1964).

and acetic acid in methanol-water solutions. Also, the values of the slopes of the lines ($\log K$ vs. $\log C_{H_2O}$) were generally lower in acetone-water and methanol-water mixtures as compared to the values obtained from the dioxane-water mixtures, which indicates that fewer waters of hydration were involved in the change. These comparisons indicate that there is some solvation by acetone and methanol, which might be expected after considering that these two molecules are more polar than the dioxane molecule. Mixed methanol-water complexes of cobalt have previously been reported in methanol-water mixtures at low temperatures.²⁰

The literature also contains the results of several investigations on the change in a conventional equilibrium constant with pressure at 25°. We have evaluated these results, considering hydration as part of the equilibria and using literature values for the density (concentration) of water at the various pressures, and again we observe the linear relationship between $\log K$ and $\log C_{H_2O}$. The values obtained for the net changes in waters of hydration are included in Table II.

Several features of the hydration changes as reported in Table II should be mentioned. For the alkali metal halides (with the exception of the lithium salts) the net change in waters of hydration for the ionization of the neutral molecule (or ion pair) is usually near 6. Hydration changes near 9 are observed with $MgSO_4$ and $MnSO_4$ in both water-dioxane mixtures and in aqueous solutions under pressure. However, the net change in hydration for the dissociation of weak acids in aqueous solutions under pressure at room temperature is large compared to the value obtained in water-dioxane mixtures. Similarly large changes are observed for the dissociation constants of weak bases under pressure at room temperature. These large hydration changes may possibly be related to the "extra" mobility of the hydrogen and hydroxide ions, the structure of water at room temperature, and their changes when solvent concentrations are varied by pressure alone.

From the above results, it is clear that the use of the molar concentration of water in the complete equilibrium constant expression provides an explanation of the change in the conventional equilibrium "constant" with water concentration over wide ranges of water-organic solvent compositions. By comparison, the deviation from linearity of plots of $\log K$ against $1/D$ is usually quite large, and therefore in disagreement with presently accepted theory.

Selective Solvation in Nonaqueous Solvent Mixtures

Selective solvation of electrolytes might also be expected to occur in nonaqueous solvent mixtures. The logarithms of the conventional ionization constants of electrolytes in these systems would therefore be expected to show the same linear dependence on the

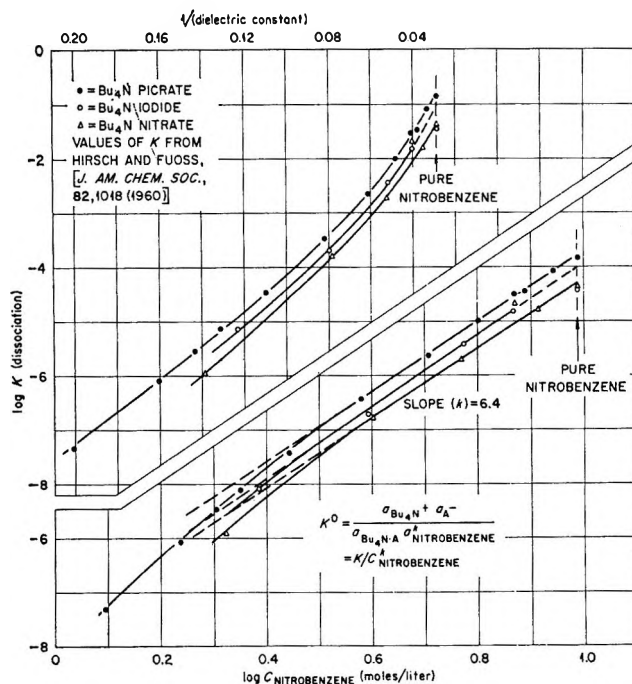
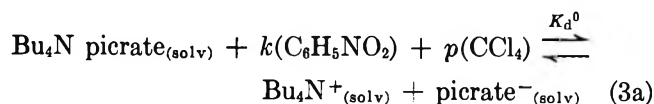


Figure 3. $\log K$ (dissociation) of several tetrabutylammonium salts vs. \log nitrobenzene molarity in carbon tetrachloride-nitrobenzene mixtures; also compared vs. $1/D$ (dielectric constant, D); K values of Hirsch and Fuoss (1960); $T = 25^\circ$.

logarithm of the molarity of the polar component where the other component is essentially nonpolar as was observed for aqueous systems. Fuoss and Hirsch²¹ have reported ionization constants for several quaternary ammonium salts in nitrobenzene-carbon tetrachloride mixtures. Since nitrobenzene is much more polar (dipole moment of 4.3 D) than carbon tetrachloride (dipole moment of 0), selective solvation by nitrobenzene would be expected. Figure 3 shows a linear relationship from pure nitrobenzene to moderately low concentrations when the logarithm of these ionization constants is plotted against the logarithm of the nitrobenzene molarity. Included also in Figure 3 are the comparative plots of $\log K$ against $1/D$. The initial slopes of the $\log K$ vs. $\log C_{\text{nitrobenzene}}$ lines appear to have nearly the same value (6.4) for all the quaternary ammonium salts given in Figure 3.

Although it seems surprising that a deviation from linearity at low concentrations of nitrobenzene occurs in carbon tetrachloride-nitrobenzene solutions (Figure 3, lower segment) and not in corresponding dioxane-water solutions (Figure 1), this behavior might be explained by considering the smaller polarity characteristic of nitrobenzene ($D = 35$) as compared to water ($D = 78$). Thus, the comparative energy of solvation with nitrobenzene could be less than that with water and might allow a small but detectable solvation by CCl_4 . If minor solvation by CCl_4 does occur, then an expression as follows might apply

(21) R. M. Fuoss and E. Hirsch, *J. Am. Chem. Soc.*, **82**, 1013, 1018 (1960).



$$K_d^0 = \frac{a_{\text{Bu}_4\text{N}^+_{(\text{solv})}} a_{\text{picrate}^-_{(\text{solv})}}}{a_{\text{Bu}_4\text{N picrate}_{(\text{solv})}} C^k_{\text{C}_6\text{H}_5\text{NO}_2} C^p_{\text{CCl}_4}} \quad (3b)$$

$$= K / (C^k_{\text{C}_6\text{H}_5\text{NO}_2} C^p_{\text{CCl}_4}) \quad (3c)$$

where K_d^0 is now the complete constant and k and p represent the net (selective) changes in solvation in the reaction equilibrium of solvents $\text{C}_6\text{H}_5\text{NO}_2$ and CCl_4 , respectively. By a method of least squares, values of k of 7.7 and p of 0.61, respectively, were obtained that provided a fit to the conventional K 's of $\pm 15\%$, within the experimental precision of the K 's, over the entire range of compositions (but not including pure nitrobenzene, where eq 3 cannot apply).

Solubility Equilibria in Aqueous Solution

In accordance with the concept of water as a necessary concentration variable, a complete solubility product equilibrium for the dissolution of an anhydrous salt may be written as



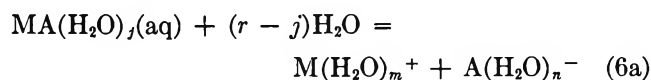
$$K_{sp}^0 = \frac{a_{\text{M}(\text{H}_2\text{O})_m^+} a_{\text{A}(\text{H}_2\text{O})_n^-}}{a_{\text{MA}(\text{s})} a_{\text{H}_2\text{O}}^r} \quad (4b)$$

where the activity of the solid phase is a constant and may be set equal to unity at all temperatures and pressures, and where the solute is completely ionized in solution. When the solute remains undissociated in solution, the solubility equilibrium may be written as



$$K_s^0 = \frac{a_{\text{MA}(\text{H}_2\text{O})_j(\text{aq})}}{a_{\text{MA}(\text{s})} a_{\text{H}_2\text{O}}^j} \quad (5b)$$

Equations 4 and 5 are related by the complete equilibrium constant for the dissociation of the neutral species in solution



$$K_d^0 = \frac{a_{\text{M}(\text{H}_2\text{O})_m^+} a_{\text{A}(\text{H}_2\text{O})_n^-}}{a_{\text{MA}(\text{H}_2\text{O})_j} a_{\text{H}_2\text{O}}^{(r-j)}} \quad (6b)$$

Dickson, Blount, and Tunell²² have measured the solubility of anhydrous CaSO_4 in water from 100 to 275° and at pressures to 1000 bars. When the logarithm of the molar solubility of CaSO_4 is plotted against $\log C_{\text{H}_2\text{O}}$, at 250°, a straight line is obtained. If it is considered that CaSO_4 is nearly completely ionized under these conditions²³ a hydration change of 28 is calculated according to the equilibrium of eq 4b. Since the solid phase is anhydrous, this number, although large, corresponds to the sum of the hydration numbers of the calcium and sulfate ions and not to the net change of

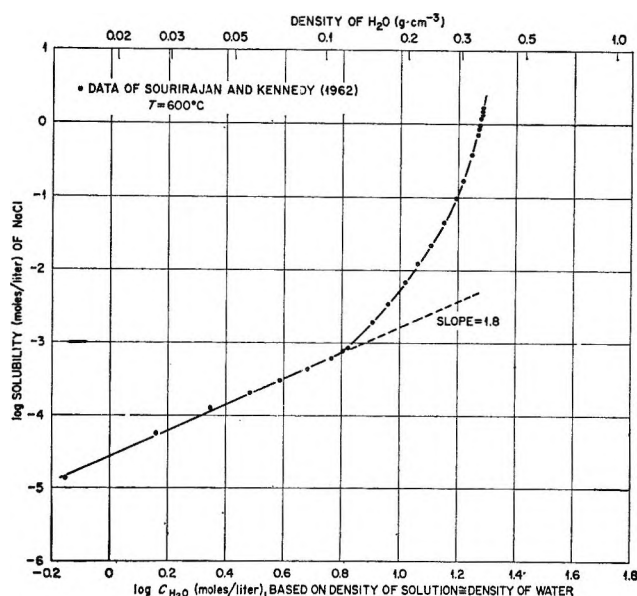


Figure 4. Logarithm of the molar solubility of NaCl vs. log molar concentration of water at 600°.

hydration numbers between the solvated ion pair and the ions as listed in Tables I and II. When the solubility data for NaCl at 600°²⁴ are treated in a similar manner, the graph shown in Figure 4 is obtained. At low solution densities where NaCl exists nearly completely in the form of neutral species¹³ and eq 5b would be expected to apply predominantly, the slope of the line gives a hydration number of approximately 2 for this neutral species. At higher solution densities, NaCl has been observed to ionize appreciably, and so the slope of the line approaches that number equal to $1/2$ the sum of the hydration numbers of the sodium and chloride ions. In Figure 4 the densities of the solutions have been assumed to be those of pure water, a reasonable assumption at low solubilities but invalid for the concentrated solutions. This causes the graph to become nonlinear at high concentrations of water where the solubility of NaCl is quite large. If at high solubilities the mean activity coefficient of NaCl would change markedly with changing water concentration, nonlinearity could occur also from this effect. However, at solution saturation, this coefficient would be expected to remain constant as discussed in the next section.

The solubilities of inorganic salts in water-organic solvent mixtures also exhibit the two types of behavior shown by eq 4a and 5a. Ricci and coworkers have measured the solubilities of several salts in water-dioxane mixtures; among these are AgAc ,¹⁷ Ag_2SO_4 ,¹⁷ Ba-

(22) F. W. Dickson, C. W. Blount, and G. Tunell, *Am. J. Sci.*, **261**, 61 (1963).

(23) W. L. Marshall and R. Slusher, *J. Phys. Chem.*, **70**, 4015 (1966).

(24) S. Sourirajan and G. C. Kennedy, *Am. J. Sci.*, **260**, 115 (1962).

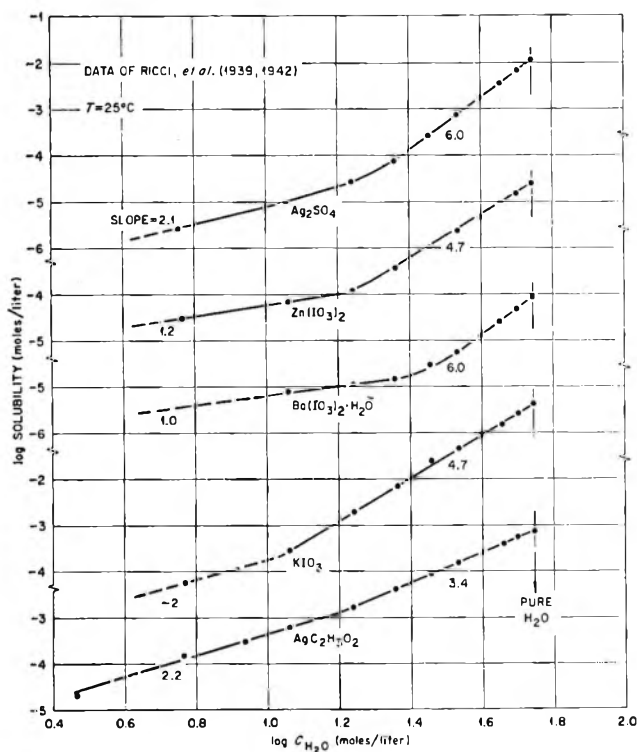


Figure 5. Log solubility (moles per liter) for several salts vs. $\log C_{H_2O}$ in dioxane-water mixtures at 25°; data of Ricci, *et al.* (1939, 1942). (Added in proof: add +0.4 and -0.2 to log solubilities for Ag_2SO_4 and $Zn(IO_3)_2$, respectively; corrected upper slopes = 5.7 for both Ag_2SO_4 and $Ba(IO_3)_2 \cdot H_2O$, and 3.2 for $AgC_2H_3O_2$.)

$(IO_3)_2 \cdot H_2O$,¹⁷ KIO_3 ,²⁵ and $Zn(IO_3)_2$.²⁵ For most of these salts, when the logarithm of molar solubility is plotted against the logarithm of water molarity, the straight line that is observed at high water concentrations in all cases undergoes a change in slope at moderately low water concentrations, as shown in Figure 5. In this figure, the slope at very low concentrations of water approaches that corresponding to the hydration number of the neutral molecules (eq 5b). At high water molarities the slope approaches a value related to the sum of the hydration numbers of the ions. For silver sulfate, this sum is equal to three times the slope since the product of the ion concentrations is proportional to the cube of the solubility of silver sulfate. Table III summarizes the results of our interpretation of some of the solubility measurements contained in the literature, where H_2O in $Ba(IO_3)_2 \cdot H_2O$ is included in the total.

Constancy of Electrolyte Activity Coefficients in Saturated Water-Organic Mixtures

Ricci and Davis²⁶ have mentioned several systems in which the activity coefficients of an electrolyte in its saturated solution, based on the use of the Debye-Hückel limiting law with the measured dielectric constants of the solvent mixtures, are nearly constant and independent of the nature of the water-organic solvents. For example, the mean ionic activity coefficient of

Table III

From solubilities		Temp. °C	Total waters of hydration of ions in solution	Lit. ref
$CaSO_4$	Water to 1000 bars	250	28	a
KIO_3	Water-dioxane	25	9.4	b
$Zn(IO_3)_2$	Water-dioxane	25	14.1	b
$AgAc$	Water-dioxane	25	6.4	c
Ag_2SO_4	Water-dioxane	25	17.1	c
$NaNO_3$	Water-dioxane	25	3.2	d
$Ba(IO_3)_2 \cdot H_2O$	Water-dioxane	25	18.1	c

^a Reference 22. ^b Reference 25. ^c Reference 17. ^d B. Selikson and J. E. Ricci, *J. Am. Chem. Soc.*, **64**, 2474 (1942).

silver acetate in saturated solution at 25° was found to remain essentially constant in water and in several compositions of ethanol-water, acetone-water, and dioxane-water. Since all of these solutions contain water, on the basis of the concepts in this paper we may write for the complete solubility product equilibrium



$$K_{sp}^0 = \frac{a_{Ag(H_2O)_m^+} a_{Ac(H_2O)_n^-}}{a_{AgAc(s)} a_{H_2O}^r} = \frac{K_{sp}}{a_{H_2O}^r} \quad (7b)$$

If the activity of solid silver acetate (a constant) by convention is taken to be unity, if the activity of water is set equal to its molar concentration (a reasonable assumption for these solutions of low concentrations), and if the conventional K_{sp} is expressed by

$$K_{sp} = a_{Ag(H_2O)_m^+} a_{Ac(H_2O)_n^-} = Q_{sp} f_{\pm}^2 \quad (8a)$$

then eq 7b may be written as

$$\log Q_{sp} = \log K_{sp}^0 + r \log C_{H_2O} - 2 \log f_{\pm} \quad (9)$$

For saturated solutions of silver acetate in acetone-water, ethanol-water, and dioxane-water at relatively high water concentrations we have obtained the following relationships from the experimental data

$$\frac{\partial \log Q_{sp}}{\partial \log C_{H_2O}} = r = 6.0, 5.4, 6.4 \text{ (respectively)} \quad (10)$$

Since

$$\frac{\partial \log K_{sp}^0}{\partial \log C_{H_2O}} = 0 \quad (11)$$

(the true, isothermal equilibrium constant is invariant), then

$$\frac{\partial \log f_{\pm}}{\partial \log C_{H_2O}} = 0 \quad (12)$$

for these systems, which is what Ricci and others have

(25) J. E. Ricci and G. J. Nesse, *J. Am. Chem. Soc.*, **64**, 2305 (1942).

(26) J. E. Ricci and T. W. Davis, *ibid.*, **62**, 407 (1940).

observed using the Debye-Hückel limiting law to calculate f_{\pm} for these systems. If the extended Debye-Hückel equation involving the ion-size parameter is used instead of the limiting law, the calculated activity coefficient should still remain constant with change in water concentration since it appears that the hydration number (and therefore ionic size)²⁷ does not change with water concentration. Consequently, the constancy of the mean ionic activity coefficients for saturated silver acetate solutions in several solvent mixtures appears to be related to the apparent selective hydration of ions over a wide range of solvent composition and the related constancy of the complete equilibrium constant.

On the basis of their observed constancies of activity coefficients for electrolytes in various solvents, and with the use of the Debye-Hückel theory, Ricci and Davis²⁸ proposed that a plot of \log solubility *vs.* $\log D$ would give a straight line of slope 3. They showed an order of magnitude agreement for many solvent systems, but considerably better agreement with dioxane-water mixtures. With this latter solvent system where we consider dioxane to be an "inert" diluent, $\log C_{\text{H}_2\text{O}}$ is nearly a linear function of $\log D$ over a very wide range of $C_{\text{H}_2\text{O}}$, and therefore if linearity is observed for \log solubility (or $\log K$) plotted against $\log C_{\text{H}_2\text{O}}$, it will also be approximately observed for \log solubility (or $\log K$) *vs.* $\log D$. The dielectric constant is, therefore, a function chiefly of the molar concentrations of *polar* species in the solvent system.

Liquid-Liquid Equilibria in Aqueous Inorganic Systems

Uranyl sulfate-water systems are unique in that they are among the very few examples of electrolyte-water systems (that do not contain organic solvents) that exhibit liquid-liquid immiscibility. Secoy²⁸ was the first to report this characteristic behavior exhibited by uranyl sulfate solutions at high temperatures and pressures. In later studies at this laboratory,²⁹ the effect of pressure on the temperature at which the second liquid phase appears in these solutions was determined. This system was studied to 400° and 1700 bars, and it was found that temperature of liquid-liquid immiscibility was strongly dependent on *solvent* density. Since the molar concentration of water varies directly with its density, another direct link between a phenomenon that probably involves ion-solvent interactions³⁰ and the molar concentration of water is shown.

The Ion-Size Parameter and Related Comments on Debye-Hückel Theory and Structure of Water

The principle can be used to calculate values for \bar{a} , the ion-size parameter of the extended Debye-Hückel theory. For example, from plots such as Figure 1, the value of k can be estimated. For NaCl, this value was 6.4. From the available solubility information on NaCl and related salts (Figures 4 and 5), we have estimated a

value of 2 molecules of H₂O for the number involved in the hydration of the neutral NaCl ion pair. The average ion volume then can be expressed as

$$\bar{V}_{\text{av}} = [V_{\text{Na}^+} + V_{\text{Cl}^-} + (k + 2)(2V_{\text{H}^+} + V_{\text{O}_2^-})]/2 \quad (13)$$

where V_{Na^+} , V_{Cl^-} , V_{H^+} , and $V_{\text{O}_2^-}$ are ionic volumes obtained from a tabulation of crystallographic radii³¹ ($r_{\text{Na}^+} = 0.95 \text{ \AA}$, $r_{\text{Cl}^-} = 1.81 \text{ \AA}$, $r_{\text{O}_2^-} = 1.40 \text{ \AA}$), and $2V_{\text{H}^+}$ is considered negligible compared with $V_{\text{O}_2^-}$. Since $\bar{V}_{\text{av}} = \pi(\bar{a})^3/6$, it follows that \bar{a} for sodium chloride solutions is 4.9 \AA . This value is in very good agreement with that of 5.2 \AA given by Robinson and Stokes and obtained from the evaluation of transport numbers by extended Debye-Hückel theory.³² The constancy of the slope, n , of Figure 1 produces an ion size parameter that is *independent* of the added "inert" solvent. This constancy of n and of K^0 also implies that any isothermal changes in the structure of water may be unimportant to the electrolyte-solvent equilibrium.

Although for the example given above, a value of 2 was roughly estimated for the hydration number of NaCl⁰, the solubility data in mixed solvents were not available for a more exacting estimate. When a value of 4 was used for the hydration number of the neutral NaCl species, an ion size of 5.2 was obtained. The attainment of rather exact ion-size parameters for a variety of electrolytes by this method may have to await additional solubility measurements of electrolytes in dioxane-water mixtures, or the availability of reliable hydration numbers of neutral species by other methods.

The use of a complete K^0 does not contradict Debye-Hückel theory and its use of the dielectric constant of the solvent or solvent mixture in calculating mean ionic activity coefficients. Long-range interionic effects on ions are certainly still dependent on the solvent dielectrics. The concept indeed appears to support the extended Debye-Hückel theory by providing comparable hydrated ion-size parameters. The actual value of K^0 will depend upon the dipole moments (and ionic charges) or the various reactants and products in the equilibrium. These values will change with temperature. Knowledge of these quantities might provide a means for an *a priori* calculation of K^0 .

Previous Proposals

A relationship between an ionization constant in a mixed solvent system and the amount of one of the

(27) See ref 4.

(28) C. H. Secoy, *J. Am. Chem. Soc.*, **72**, 3343 (1950).

(29) W. L. Marshall and J. S. Gill, *J. Inorg. Nucl. Chem.*, **25**, 1033 (1963).

(30) H. L. Friedman, *J. Phys. Chem.*, **66**, 1595 (1962).

(31) L. Pauling, "The Nature of the Chemical Bond," Cornell University Press, Ithaca, N. Y., 1945.

(32) R. A. Robinson and R. H. Stokes, "Electrolyte Solutions," 2nd ed revised, Butterworth and Co. Ltd., London, 1965, p 158.

solvents present has been reported previously. Harned and Fallon³³ used an empirical equation

$$\log K = -C - C'N \quad (14)$$

for the interpolation of ionization constants of acetic acid in several water-dioxane mixtures (to 82% dioxane). In this equation, K is the ionization constant (not considering hydration) and N is the mole fraction of water (or dioxane). Feakins and French³⁴ used an approach to the problem of ion solvation in water-organic solvent mixtures as developed by Hudson and Saville³⁵ to show that a plot of the standard potential (E_c^0 , molar scale) of the cell $H_2(Pt)|HCl|AgCl-Ag$ in these mixtures was linearly related to the logarithm of the volume fraction of water in the solvent medium. Aksnes³⁶ considered electrostatic effects in the ionization of weak acids in water-dioxane mixtures and concluded that the main reason for the decrease in the ionization constant of the weak acid with increasing dioxane concentration was due to a statistical effect; that is, water must be regarded as a reactant because it hydrates the proton. He concluded that the dielectric constant to be used in the Born equation (for calculating the attraction between oppositely charged ions in solution) should be the dielectric constant of the water only in the solvent mixture.

The relationship between the solubility of substances in supercritical water and the density of the water has been recognized for some time. Kennedy³⁷ mentioned the linearity between the solubility of quartz and the logarithm of the specific volume of supercritical water. Morey³⁸ also commented on the relation between solubility and solvent density in connection with his measurements on the solubility of quartz in steam. Jasmund³⁹ showed that the concentration of KCl in steam could be represented by the equation

$$C_{KCl} = Ad^n \quad (15)$$

where A and n are constants. This equation can also be written as

$$\log C_{KCl} = \log A + n \log d \quad (16)$$

Styrikovich⁴⁰ has used equations similar to eq 15 to obtain hydration numbers for several inorganic substances in high temperature water. Franck⁴¹ derived by statistical methods a relationship between the logarithm of the mole fraction of solid in a gas phase and the logarithm of the density of the gas phase. More recently, Tur'yan⁴² has calculated hydration numbers

from the solubilities of several slightly soluble salts in isodielectric ethanol-water and methanol-water mixtures of high water content.

Conclusions

It has been apparent for some times that theories of ion-pair formation based on the Born equation are not adequate to describe completely the experimentally observed behavior. By considering solvent species as reactants of variable concentration in the equilibrium process, the isothermal equilibrium constant is found to be invariant with changes in molar solvent concentrations (changed by means of pressure or composition changes) which, when molar activity units are used, is one of the requirements of a true equilibrium constant. Although linear relationships between conventional equilibrium constants (not including waters of hydration) and some function of the concentration of water have been reported in the literature (usually for equilibria involving the ionization of weak acids), this is believed to be the first time that such a relationship has been applied to the appropriate concentration unit (molarity)¹³ for complete equilibrium constants, and it is the first time that it has been shown to apply over a wide range of temperature, pressure, and solvent composition. This exacting linear relationship over wide ranges of solvent composition is not observed when conventional ionization constants are related to the reciprocal of the dielectric constant, which is the relationship predicted by the usual electrostatic theories of ionic association. We expect the present approach to lead to a better understanding of the details of ion association and ion-solvent interaction and to furnish a powerful tool for extrapolations into regions where data do not exist.

(33) H. S. Harned and L. D. Fallon, *J. Am. Chem. Soc.*, **61**, 2377 (1939).

(34) D. Feakins and C. M. French, *J. Chem. Soc.*, 2581 (1957).

(35) R. F. Hudson and B. Saville, *ibid.*, 4114 (1955).

(36) G. Aksnes, *Acta Chem. Scand.*, **16**, 1967 (1962).

(37) G. C. Kennedy, *Econ. Geol.*, **45**, 629 (1950).

(38) G. W. Morey and J. M. Hesselgesser, *Trans. ASME*, **73**, 865 (1951).

(39) K. Jasmund, *Heidelberger Beitr. Mineral. Petrogr.*, **3**, 380 (1953); *Chem. Abstr.*, **47**, 11899 (1953).

(40) M. A. Styrikovich, I. Kh. Khaibullin, and D. G. Tskhviraashvili, *Dokl. Akad. Nauk SSSR*, **100**, 1123 (1955); *Chem. Abstr.*, **49**, 1707c (1955).

(41) E. U. Franck, *Z. Physik. Chem. (Frankfurt)*, **6**, 345 (1956).

(42) Ya. I. Tur'yan, *Russ. J. Inorg. Chem.*, **10**, 369 (1965).

Electrical Conductances of Aqueous Hydrogen Bromide Solutions

from 0 to 800° and at Pressures to 4000 Bars¹

by Arvin S. Quist and William L. Marshall

Reactor Chemistry Division, Oak Ridge National Laboratory, Oak Ridge, Tennessee 37830 (Received September 25, 1967)

The electrical conductances of dilute (0.002 to 0.015 *m*) aqueous hydrogen bromide solutions have been measured at temperatures to 800° and at pressures to 4000 bars. Limiting equivalent conductances for HBr were calculated at integral temperatures and densities under conditions where it behaved as a strong or moderately strong electrolyte. Hydrobromic acid becomes progressively a weaker electrolyte as the temperature increases and the solution density decreases. Equilibrium constants for the ionization of HBr were calculated from the conductance measurements at temperatures of 400° and above, and at densities below 0.85 g cm⁻³. By considering hydration to be an essential part of the ionization process, values of the isothermal equilibrium constant were obtained that were independent of density.

Introduction

The properties of aqueous electrolyte solutions at high temperatures and pressures have been the subject of several researches in recent years. The information that has been obtained thus far indicates that these solutions exhibit simpler behavior than corresponding ones at room temperature and atmospheric pressure. These results have also led to a new approach for the interpretation of equilibrium constants for ionic reactions occurring in polar solvents.^{2,3} Measurements of the electrical conductances of aqueous electrolyte solutions provide a simple and direct method for obtaining information about the existence and behavior of ions in these solutions. Such studies at high temperatures and pressures have been performed at several laboratories during the past few years. More recently, an extensive study of NaCl solutions has been carried out in this laboratory.⁴ The present paper contains the results of measurements on dilute (0.002 to 0.015 *m*) aqueous hydrogen bromide solutions at temperatures from 0 to 800° and at pressures to 4000 bars. To our knowledge, these are the first conductance measurements on this electrolyte at elevated temperatures and pressures.

Experimental Section

A complete description of the equipment and procedures used for these measurements has been given previously.⁴ The latest model of the conductance cell (no pressure seals in the high-temperature region) was used exclusively. A stock solution of HBr (approximately 1.0 *m*) was prepared from reagent grade HBr (J. T. Baker Chemical Co., 47–49% HBr). This stock solution was standardized, using weight buret techniques, by titration with standard NaOH solution and also by comparison against sodium carbonate (anhydrous). An additional verification of the concentrations of the solutions prepared from this stock solution

was made by measuring their conductances at 25.00 ± 0.01°, 1 atm, in a glass conductance cell and calculating their concentrations from the known conductance of HBr as a function of concentration as obtained from the literature. Four concentrations of HBr were studied; these were 0.001957, 0.004937, 0.01000, and 0.01471 *m*. Conductivity water obtained from a quartz still was used to prepare all solutions.

Three different inner electrodes were used with the conductance cell. Their cell constants were 1.98, 0.510, and 0.489 cm⁻¹ as determined from 0.01 and 0.1 demal KCl solutions at 25.00 ± 0.01°.

Results and Discussion

Results. Specific conductances and equivalent conductances were calculated from the experimental data in the manner described previously.⁴ Figures 1–4 show the experimentally determined specific conductances of HBr solutions (corrected for solvent conductance) as a function of pressure at the temperatures of the measurements. The curves for which individual points are not shown represent averages of two or more separate runs at approximately the same temperature. These separate runs near the same temperature were usually made with different inner electrodes. From graphs such as those in Figures 1–4, specific conductances at integral pressures were obtained by interpolation. Isobaric specific conductances as a function of temperature are shown in Figure 5 for a 0.01000 *m* HBr solution. The graphs for the other concentrations are very similar in shape to those in Figure 5. Figure 6 shows a comparison of the isobaric specific conductances of 0.01 *m*

(1) Research sponsored by the U. S. Atomic Energy Commission under contract with Union Carbide Corporation.

(2) W. L. Marshall and A. S. Quist, *Proc. Natl. Acad. Sci.*, **58**, 901 (1967).

(3) A. S. Quist and W. L. Marshall, *J. Phys. Chem.*, **72**, 1536 (1968).

(4) A. S. Quist and W. L. Marshall, *ibid.*, **72**, 684 (1968).

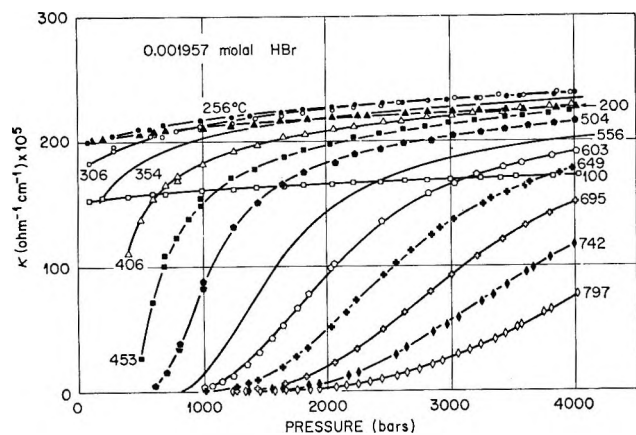


Figure 1. Specific conductances of 0.001957 *m* HBr solutions as a function of pressure at several temperatures.

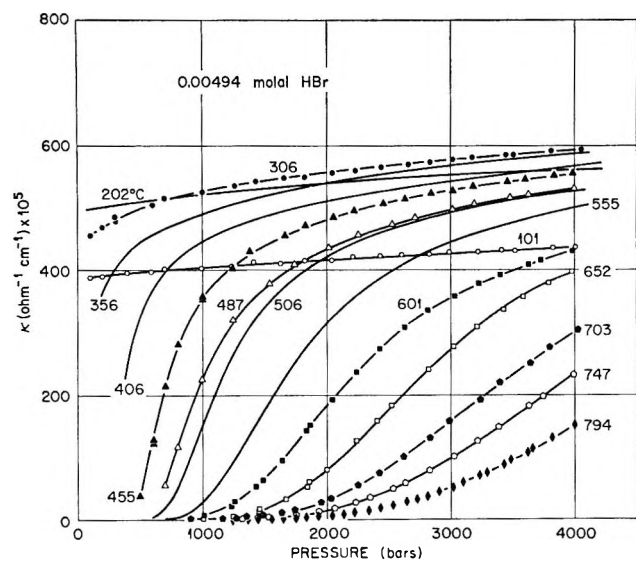


Figure 2. Specific conductances of 0.00494 *m* HBr solutions as a function of pressure at several temperatures.

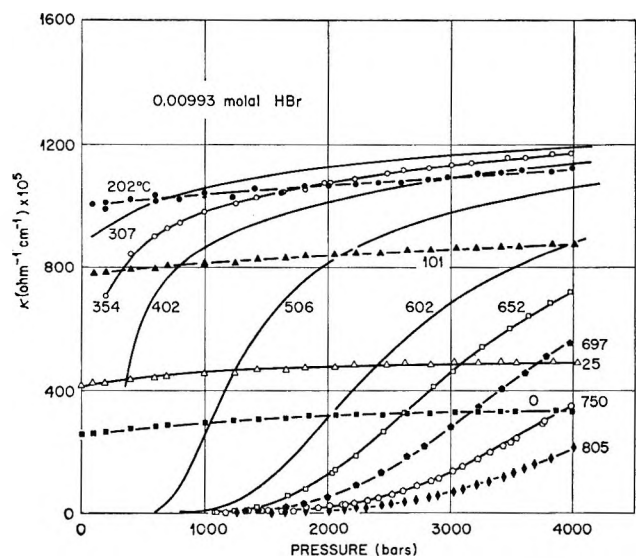


Figure 3. Specific conductances of 0.00993 *m* HBr solutions as a function of pressure at several temperatures.

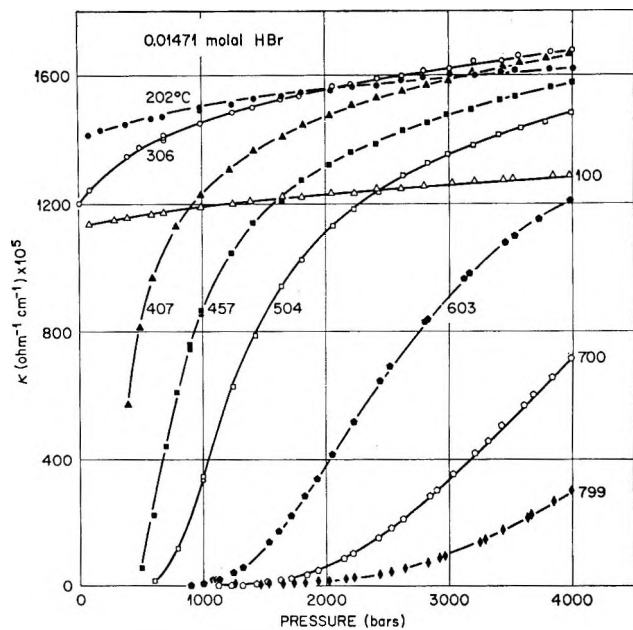


Figure 4. Specific conductances of 0.01471 *m* HBr solutions as a function of pressure at several temperatures.

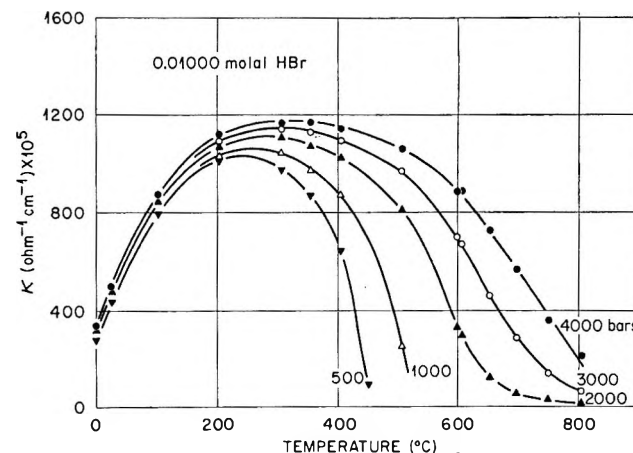


Figure 5. Isobaric variation of specific conductances of 0.01000 *m* HBr solutions as a function of temperature; pressures from 500 to 4000 bars.

HBr with those of 0.01 *m* NaBr⁵ as a function of temperature at pressures of 500 and 4000 bars. At 4000 bars the very sharp drop in the conductance of HBr at high temperatures, compared to the lesser decrease in NaBr conductance, indicates that HBr is a much weaker electrolyte than NaBr at elevated temperatures. [NaBr is quite similar in its behavior to that of NaCl⁴.] Values of ionization constants for HBr are given in a later section of this paper. Other differences in the behavior of NaBr and HBr are also apparent in Figure 6. For example, below 300° the conductance of NaBr is greater at 500 bars than at 4000 bars, whereas for HBr the opposite is true. The behavior of NaBr below

(5) From recent experimental measurements at this laboratory.

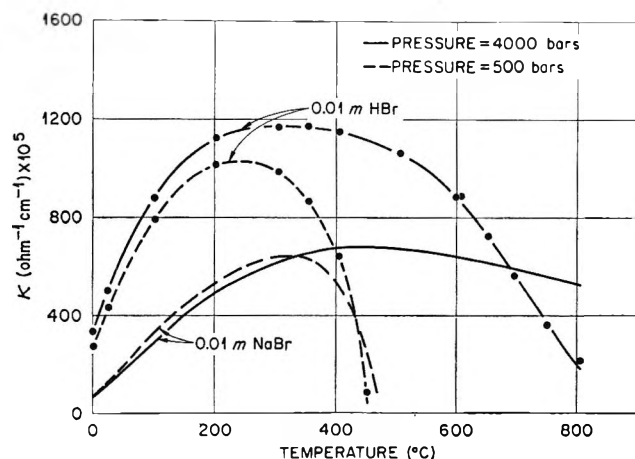


Figure 6. Comparison of isobaric specific conductances of equimolar HBr and NaBr solutions as a function of temperature.

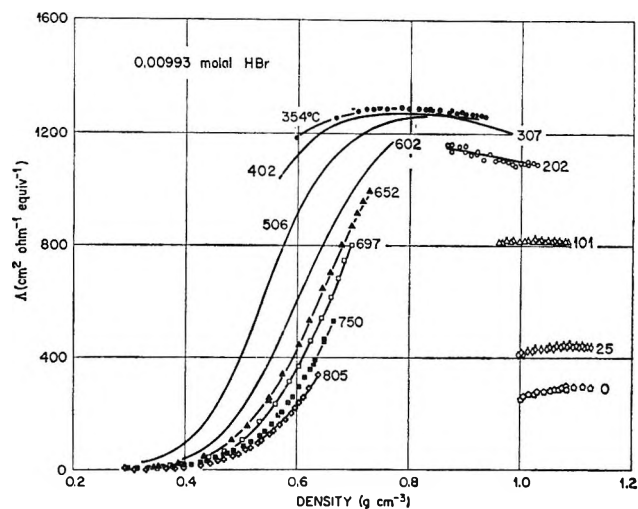


Figure 9. Equivalent conductances of 0.00993 *m* HBr solutions as a function of density at several temperatures.

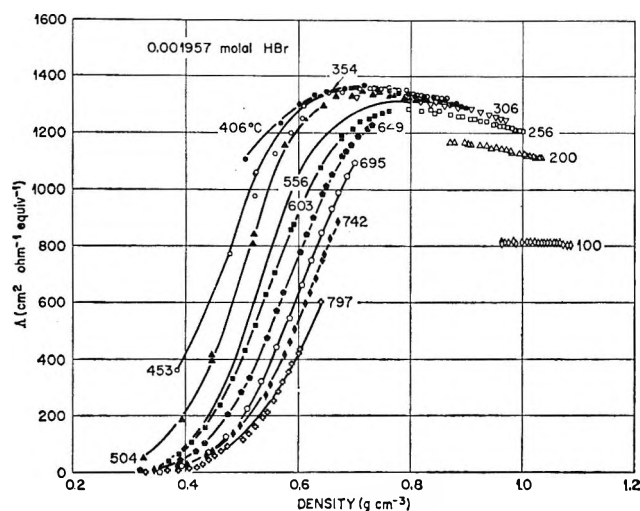


Figure 7. Equivalent conductances of 0.001957 *m* HBr solutions as a function of density at several temperatures.

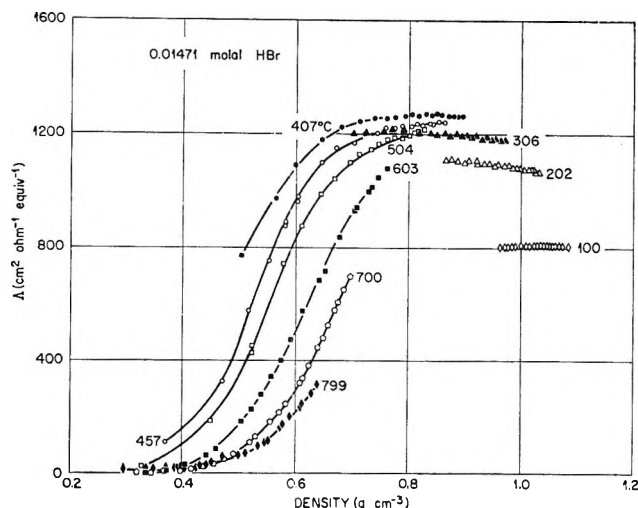


Figure 10. Equivalent conductances of 0.01471 *m* HBr solutions as a function of density at several temperatures.

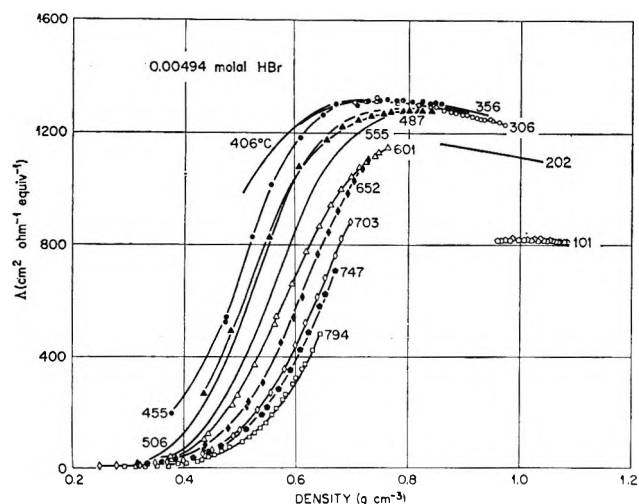


Figure 8. Equivalent conductances of 0.00494 *m* HBr solutions as a function of density at several temperatures.

300° is consistent with a viscosity effect on a strong electrolyte; increasing the pressure increases the viscosity of the solution and therefore decreases the ionic mobility. The behavior of HBr is similar to the effect of pressure on a weak electrolyte; increasing the pressure increases the degree of ionization and hence gives a greater specific conductance.

Isotherms of equivalent conductances of the HBr solutions as a function of the density are shown in Figures 7–10. These curves resemble somewhat those obtained previously for NaCl⁴ except that at the highest temperatures the corresponding equivalent conductances of HBr are much lower than for NaCl. This again indicates that HBr is a much weaker electrolyte than NaCl under these conditions. Tables I–IV contain equivalent conductances for the HBr solutions at integral temperatures and densities obtained by interpolation and extrapolation of the experimental data.

Table I: The Equivalent Conductances ($\text{cm}^2 \text{ohm}^{-1} \text{equiv}^{-1}$) of 0.001957 *m* HBr Solutions at Integral Temperatures and Densities

Temp, °C	Density, g cm^{-3}													
	0.35	0.40	0.45	0.50	0.55	0.60	0.65	0.70	0.75	0.80	0.85	0.90	0.95	1.00
100													(818)	824
150														1000
200											(1175)	1170	1150	1130
250												1235	1225	1200
300								(1360)	1350	1330	1305	1280	1265	1240
350								1310	1340	1370	1360	1345	1320	1300
400				1160	1250	1320	1350	1360	1360	1360	1345	1325	1305	
450		400	660	900	1120	1280	1340	1360	1350	1340	1320			
500		210	410	680	980	1220	1310	1340	1340	1340	1335	1310		
550		110	260	500	800	1100	1240	1310	1310	1320				
600		80	180	370	650	940	1130	1240	1280	1300				
650		60	130	270	530	760	1020	1170	1250					
700		40	90	200	420	610	890	1090	1200					
750		30	70	160	320	500	780							
800		20	50	120	230	410	650							

Table II: The Equivalent Conductances ($\text{cm}^2 \text{ohm}^{-1} \text{equiv}^{-1}$) of 0.004937 *m* HBr Solutions at Integral Temperatures and Densities

Temp, °C	Density, g cm^{-3}													
	0.35	0.40	0.45	0.50	0.55	0.60	0.65	0.70	0.75	0.80	0.85	0.90	0.95	1.00
100													(814)	818
150														986
200											(1160)	1150	1135	1114
250												1210	1200	1180
300								(1310)	1300	1305	1290	1260	1240	1220
350							1260	1300	1320	1320	1310	1300	1285	1265
400				1000	1140	1240	1300	1320	1320	1310	1300	1285	1265	
450	110	260	420	710	980	1180	1260	1300	1310	1305	1295	1285		
500	65	140	280	520	780	1060	1180	1260	1290	1290	1290			
550	35	85	190	370	600	900	1080	1200	1260	1265				
600	24	60	130	270	460	700	940	1120	1210	1230				
650	16	40	100	200	350	560	820	1020	1150					
700	14	30	70	140	260	440	700	930	1080					
750	12	25	50	110	220	380	600							
800	10	16	40	90	180	320	490							

Table III: The Equivalent Conductances ($\text{cm}^2 \text{ohm}^{-1} \text{equiv}^{-1}$) of 0.01000 *m* HBr Solutions at Integral Temperatures and Densities

Temp, °C	Density, g cm^{-3}													
	0.35	0.40	0.45	0.50	0.55	0.60	0.65	0.70	0.75	0.80	0.85	0.90	0.95	1.00
0														256
25													(412)	416
100													(808)	814
150														974
200											(1142)	1135	1115	1095
250												1190	1180	1160
300								(1270)	1270	1275	1260	1235	1220	1200
350						1180	1240	1280	1280	1285	1275	1260	1240	
400				860	1020	1140	1230	1260	1280	1280	1280	1280	1265	1250
450	100	205	340	600	850	1080	1180	1230	1260	1270	1270			
500	50	110	220	420	670	940	1080	1180	1230	1250	1260			
550	26	60	140	300	500	770	940	1100	1190	1210				
600	15	40	100	200	370	600	810	1010	1140	1165				
650	10	30	70	140	270	460	680	910	1080					
700	8	20	50	100	200	360	560	820	1020					
750	6	15	40	80	160	280	460							
800		12	30	60	130	240	400							

Table IV: The Equivalent Conductances ($\text{cm}^2 \text{ohm}^{-1} \text{equiv}^{-1}$) of 0.01471 *m* HBr Solutions at Integral Temperatures and Densities

Temp., °C	Density, g cm^{-3}													
	0.35	0.40	0.45	0.50	0.55	0.60	0.65	0.70	0.75	0.80	0.85	0.90	0.95	1.00
100														
150													(802)	808
200														966
250											(1108)	1105	1090	1080
300								(1220)	1230	1230	1220	1200	1190	1175
350								1230	1240	1245	1240	1230	1210	
400				740	940	1100	1180	1220	1240	1250	1250	1245		
450	85	180	280	490	760	1000	1120	1190	1220	1235	1245	1255		
500	45	90	190	340	590	860	1010	1110	1170	1205	1220			
550	20	50	120	240	440	680	880	1020	1130	1170				
600	10	30	80	160	320	520	740	930	1070	1125				
650		15	50	110	230	400	620	820	1000					
700		10	40	70	160	300	490	720						
750		10	30	60	130	240	410							
800		10	20	50	110	210	340							

Table V: Limiting Equivalent Conductances ($\text{cm}^2 \text{ohm}^{-1} \text{equiv}^{-1}$) of HBr at Integral Temperatures and Densities

Temp., °C	Density, g cm^{-3}										
	0.55	0.60	0.65	0.70	0.75	0.80	0.85	0.90	0.95	1.00	
100										(835)	838
150											1022
200							(1220)	1210	1185	1158	1158
250								1280	1260	1232	1232
300				(1440)	1415	1390	1360	1325	1305	1275	1275
350		1420	1425	1445	1430	1400	1375	1350	1340		
400	1470	1450	1450	1445	1430	1400	1375	1350			
450	1420	1450	1460	1450	1425	1400	1370				
500	1350	1455	1470	1455	1430	1400	1370				
550	1230	1465	1430	1460	1410	1400					
600			1430	1410	1390	1395					
650			1350	1380	1370						

The values in parentheses represent conductances at saturation vapor pressure at that temperature.

Calculation of Limiting Equivalent Conductances. Limiting equivalent conductances were calculated from the conductances given in Tables I–IV by the several methods described previously.⁴ At temperatures of 400° and below, at densities of 0.65 g cm^{-3} and above, the Robinson–Stokes equation,⁶ the Fuoss–Onsager equation,⁷ and the Shedlovsky equation (including an ionization constant)⁸ gave essentially identical results. At lower densities and at higher temperatures, where HBr behaved as a progressively weaker electrolyte, the Shedlovsky equation, which includes the effect of incomplete dissociation, gave a better fit to the data than the first-named equations. The limiting equivalent conductances as obtained from the experimental data are given in Table V. Since the Shedlovsky equation gave the best fit over the widest range of temperature and density, the values in Table V are those obtained using this equation (except under the conditions noted above, when all three equations gave the same results).

Table V does not include limiting equivalent conductances for all the temperatures and densities at which equivalent conductances were obtained for the several concentrations. Because at the lowest densities and the highest temperatures HBr is a very weak electrolyte, sufficiently accurate conductance measurements could not be made in the low concentration range to permit reliable extrapolation in obtaining limiting equivalent conductances. Thus the $\Lambda_0(\text{HBr})$ values obtained under these conditions were lower than one would expect. Some of these low values have been included in Table V to indicate the rate of decline of the extrapolated limiting equivalent conductances. A line of demarcation is given in Table V to indicate that only the limiting equivalent conductances given in this table for the highest densities and lowest temperatures are considered

(6) R. A. Robinson and R. H. Stokes, *J. Am. Chem. Soc.*, **76**, 1991 (1954).

(7) R. M. Fuoss, L. Onsager, and J. F. Skinner, *J. Phys. Chem.*, **69**, 2581 (1965).

(8) T. Shedlovsky, *J. Franklin Inst.*, **225**, 739 (1938).

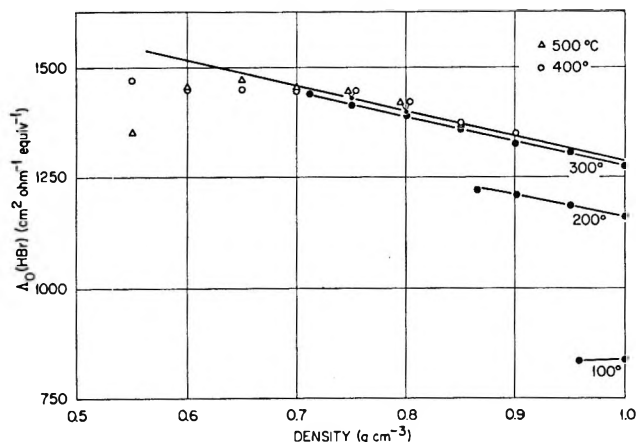


Figure 11. Limiting equivalent conductances of HBr as a function of density.

reliable (above and to the right of the line). The standard errors associated with the values in Table V are less than 1% at densities of 0.70 g cm^{-3} and above (at temperatures of 550° and below). At higher temperatures and lower densities the uncertainty in the extrapolated limiting equivalent conductances becomes progressively greater as HBr becomes a weaker electrolyte.

Isothermal plots of the limiting equivalent conductance of HBr against density are given in Figure 11. A linear relationship is observed, but it does not extend to as high a temperature or as low a density as was previously observed with NaCl⁴ and KHSO₄.⁹ Since the deviation from linearity is believed to be due only to the limitations of our experiments, it seems reasonable to assume that the general features of the behavior of HBr are the same as for NaCl and KHSO₄. Thus, above 400° the limiting equivalent conductance of HBr can be described by an equation that is a function only of the density of the solvent, as was previously observed with NaCl⁴ and KHSO₄.⁹ This equation, obtained from Figure 11, follows

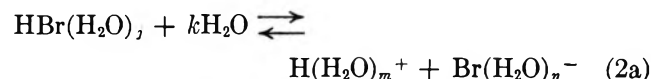
$$\Lambda_0(\text{HBr}) = 1840 - 560d \quad (1)$$

where d is the density of water. Although the density dependence (slope) from eq 1 is less for HBr than for NaCl (1160) or KHSO₄ (1100) and may be related to the extra mobility of the hydrogen ion and its decrease with decreasing solvent density, the intercepts for the three electrolytes are reasonably close together (1876 for NaCl, 1740 for KHSO₄), indicating that perhaps all uni-univalent electrolytes may have limiting equivalent conductances near 1800 $\text{cm}^2 \text{ohm}^{-1} \text{equiv}^{-1}$ at zero density. This value appears to be the maximum value for 1-1 electrolytes since the data indicate that the limiting equivalent conductance (at constant density) does not increase for temperatures above 400°. This result also indicates that at zero solvent density there is no "extra" mobility of the proton. No simple relationship between the Walden product ($\Lambda_0\eta_0$) and density was

observed. The deviation from a linear relationship was even greater than that previously observed with NaCl.⁴

The limiting equivalent conductances of HBr given in Table V for saturation vapor pressures at 100, 200, and 300° (values in parentheses) may be compared with the corresponding values for HCl summarized previously.¹⁰ At 100, 200, and 300° the limiting equivalent conductances for HCl are 845.4, 1214 and 1455, respectively. The corresponding values for HBr are (except for 200°) somewhat lower, 835, 1220, and 1440, which indicates that the mobility of the bromide ion is less than that of the chloride ion under these conditions. Since at 100 and 300° $\Lambda_0(\text{HBr})$ is less than $\Lambda_0(\text{HCl})$ whereas at 200° $\Lambda_0(\text{HBr})$ is greater than $\Lambda_0(\text{HCl})$, this may indicate that the values for HBr at 200° are probably about 1-2% too large.

Calculation of the Dissociation Constant of HBr. The ionization of HBr in aqueous solutions can be represented by the following equations.^{2,3}



$$K^0 = \frac{a_{\text{H}(\text{H}_2\text{O})_m} a_{\text{Br}(\text{H}_2\text{O})_n}}{a_{\text{HBr}(\text{H}_2\text{O})_j} a_{\text{H}_2\text{O}}^k} \quad (2b)$$

$$K^0 = K/a_{\text{H}_2\text{O}}^k \quad (2c)$$

$$\log K = \log K^0 + k \log a_{\text{H}_2\text{O}} \quad (2d)$$

where K^0 is the complete ionization constant including hydration and K is the conventional ionization constant. The integers j , m , and n represent hydration numbers of HBr, H^+ , and Br^- , respectively; k is the net change in hydration number when one molecule of HBr ionizes. By using the Shedlovsky method,⁸ values of the conventional ionization constant for HBr were obtained from the experimental data simultaneously with $\Lambda_0(\text{HBr})$. This method was satisfactory as long as the K 's were greater than about 10^{-5} (this value corresponds to the approximate limits below which reliable $\Lambda_0(\text{HBr})$'s were not obtained). At lower densities and higher temperatures, the conventional ionization constants calculated by the Shedlovsky method were greater than would be expected for the same reasons given earlier in explaining the low values of $\Lambda_0(\text{HBr})$ obtained simultaneously by the same method. However, by using eq 1 to calculate $\Lambda_0(\text{HBr})$ at all densities at temperatures of 400° and above, K 's could be calculated from the experimental data by Shedlovsky's equations.⁸ Table VI contains negative logarithms of these conventional ionization constants calculated in this manner. These constants are based on the hypothetical 1 M standard state. The mean ionic activity coefficients used in Shedlovsky's equations were calculated with the Debye-Hückel equation in the manner described previously.⁴ The activity

(9) A. S. Quist and W. L. Marshall, *J. Phys. Chem.*, **70**, 3714 (1966).

(10) A. S. Quist and W. L. Marshall, *ibid.*, **69**, 2984 (1965).

Table VI: Negative Logarithm of the Conventional Equilibrium Constant, K , for the Dissociation of HBr into H^+ and Br^- ; Standard State Is the Hypothetical 1 M Solution

Temp. °C	Density, $g\ cm^{-3}$									
	0.35	0.40	0.45	0.50	0.55	0.60	0.65	0.70	0.75	0.80
400				2.67	2.24	1.79	1.35	0.95	0.38	
450	5.04	4.30	3.78	3.15	2.58	2.01	1.59	1.17	0.73	0.06
500	5.56	4.86	4.15	3.51	2.90	2.31	1.90	1.50	1.11	0.63
550	6.16	5.34	4.54	3.83	3.22	2.63	2.20	1.77	1.34	1.01
600	6.65	5.71	4.86	4.17	3.52	2.95	2.46	2.00	1.56	1.28
650	6.89	6.09	5.19	4.48	3.81	3.23	2.69	2.22	1.76	
700	7.05	6.41	5.44	4.81	4.10	3.49	2.94	2.41	1.94	
750	7.24	6.56	5.67	4.98	4.28	3.70	3.13			
800		6.71	5.94	5.18	4.46	3.84	3.31			

coefficient of the HBr molecule was taken to be unity at all concentrations, temperatures, and densities. The average standard error associated with the values in Table VI is 0.03 pK unit. As might be expected, the largest standard errors were at the highest temperatures and lowest densities (the largest standard error was 0.14 pK unit at 750° and 0.35 $g\ cm^{-3}$). On comparing the ionization constants of HBr with those previously reported for the first ionization constant of H_2SO_4 in the same temperature and pressure range,¹¹ it appears that HBr is a stronger acid than H_2SO_4 at high densities but a weaker acid at low densities.

If the activity of water in eq 2d is taken to be equal to its molar concentration,^{2,3} then isothermal plots of $\log K$ vs. $\log C_{H_2O}$ (the molar concentration of water) should give straight lines with slope k . By using the values of $\log K$ given in Table VI, the lines shown in Figure 12 were obtained for temperatures from 400 to 800°. Although the lines in Figure 12 are essentially straight at each temperature, there is an increase with increasing temperature in the value of k . The values of k determined at 400, 500, 600, 700, and 800° are 12.2, 13.7, 15.0, 15.7, and 16.2, respectively.

The reliability of the increasing values of k was considered as follows. The values of K as calculated from the experimental data depend upon the value assigned to $\Lambda_0(HBr)$. The K 's given in Table VI were calculated by using the limiting equivalent conductances calculated by eq 1. If the true $\Lambda_0(HBr)$ values at low densities are less than those given by eq 1, and if these lower values of Λ_0 are used in the calculations, then larger values of K will be obtained at these low densities. This might possibly result in smaller values of k at the high temperatures. Conventional equilibrium constants were calculated using limiting equivalent conductances given by the equation $\Lambda_0(HBr) = 1500 - 100d$, with constants selected to give lower values of Λ_0 . With this approach, larger values of K were calculated at the higher temperatures and lower densities; however, the difference was not appreciable and the k values were nearly the same as before. Therefore, it appears that the increase in k with increasing temperature is real.

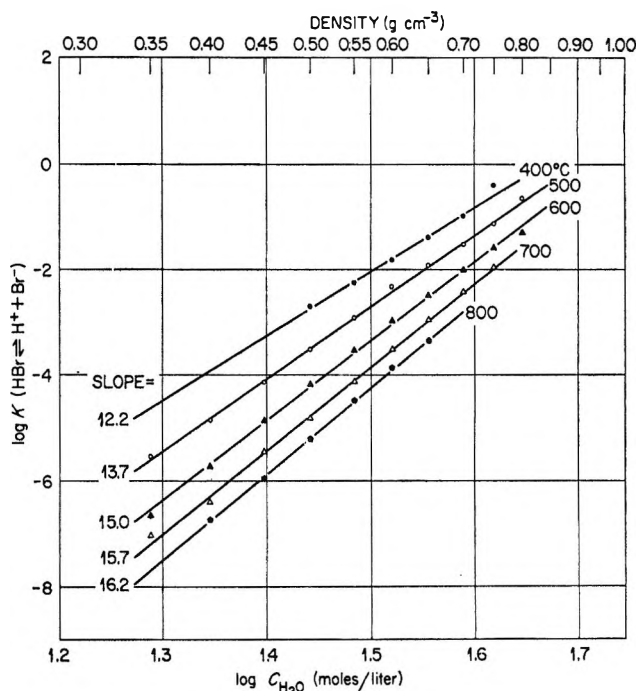


Figure 12. $\log K$ (molar units) for the equilibrium $HBr \rightleftharpoons H^+ + Br^-$ as a function of the logarithm of the molar concentration of water at temperatures from 400 to 800°.

This behavior can result from a decrease in the value of j , an increase in the value of m and/or n , or from both changes.

With the values of k obtained from the data in Table VI and Figure 12, values of $\log K^0$ were calculated by eq 2d (where the activity of water has been replaced by its molar concentration). At 400, 500, 600, 700, and 800°, these calculated values of $\log K^0$ were -20.4 , -23.3 , -25.8 , -27.4 , and -28.6 , respectively. These complete equilibrium constants, which include the concentration of the solvent water as a variable, are independent of changes in dielectric constant, or any other property related to density, at constant temperature.^{2,3}

(11) A. S. Quist, W. L. Marshall, and H. R. Jolley, *J. Phys. Chem.*, **69**, 2726 (1965).

Since k changes with temperature, the equilibrium expressed by eq 2a cannot represent the same chemical reaction over the entire range of temperature. Therefore, when $\log K^0$ is plotted against $T(^{\circ}\text{K})^{-1}$, the slope will not be ΔE_v^0 but will also contain a term involving

dk/dT^{-1} . It is of interest to note that from the data, $d \log K^0/dT^{-1} = -2(dk/dT^{-1})$.

Acknowledgment. The authors wish to thank Wiley Jennings for his technical assistance in making the conductance measurements.

Free Radicals by Mass Spectrometry. XXXVII. The Ionization

Potential and Heat of Formation of Dichlorocarbene¹

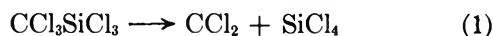
by J. S. Shapiro² and F. P. Lossing

Division of Pure Chemistry, National Research Council of Canada, Ottawa, Ontario, Canada (Received September 25, 1967)

Electron impact measurements of CCl_2 , generated by the pyrolysis of $\text{CCl}_3\text{SiCl}_3$, give $\text{IP}_{\text{vert}}(\text{CCl}_2) = 9.76$ V. Appearance potentials for dissociative ionization of CHCl_3 and C_2Cl_4 give $\Delta H_f(\text{CCl}_2^+) = 279$ kcal/mole and $\Delta H_f(\text{CCl}_2) = 57$ kcal/mole. A comparison of C=C bond dissociation energies in halo-substituted ethylenes $\text{CX}_2=\text{CY}_2$ with that in ethylene itself show that the stabilization of CCl_2 with respect to CH_2 is large, being about half that of CF_2 .

Introduction

The presence of dichlorocarbene, CCl_2 , as an intermediate in the gas-phase pyrolysis of chloroform and carbon tetrachloride has been postulated by several workers.^{3,4} The use of cyclohexene or other compounds as trapping agents, leading to adducts which have been isolated and identified, has confirmed the existence of CCl_2 as a free carbene in gas-phase reactions.⁵⁻⁸ Some years ago the production of CCl_2 radicals from the pyrolysis of CCl_4 on tungsten filaments at 1100–1600° was observed by means of a mass spectrometer. In two independent studies Blanchard and LeGoff⁹ and Reed and Snedden¹⁰ measured the ionization potential of CCl_2 by electron impact, obtaining concordant results of 13.2 and 13.1 V, respectively. By comparison, however, with the ionization potentials of CH_2 (10.396 V¹¹) and CF_2 (11.7 V^{12,13}), a value of ~ 13 V for $\text{IP}(\text{CCl}_2)$ seems to be unreasonably high. It was thought that a redetermination of $\text{IP}(\text{CCl}_2)$ would be worthwhile, using a much more convenient source of CCl_2 now available⁸ through pyrolysis of $\text{CCl}_3\text{SiCl}_3$



Experimental Section

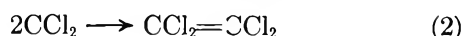
Trichloromethyltrichlorosilane was prepared¹⁴ by the chlorination of trichloromethylsilane (Matheson Coleman and Bell, pure grade) under reflux, aided in the initial stages by radiation from a mercury lamp. Chlorination was continued until the vapor temperature

rose above 110°. The $\text{CCl}_3\text{SiCl}_3$ was distilled and a middle fraction, shown by nmr and mass spectral analysis to be free from partially chlorinated impurities, was used.

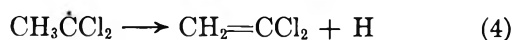
Dichlorocarbene was generated from this sample by pyrolysis, at 10^{-3} torr and millisecond contact times, in a fused-silica capillary furnace leading to the ionization chamber of a mass spectrometer.¹² The thermal decomposition of $\text{CCl}_3\text{SiCl}_3$ required a furnace tem-

- (1) Issued as NRC Contribution No. 10073.
- (2) National Research Council of Canada Postdoctorate Fellow, 1965–1967.
- (3) G. P. Semeluk and R. B. Bernstein, *J. Am. Chem. Soc.*, **79**, 46 (1957).
- (4) A. E. Shilov and R. D. Sabirova, *Dokl. Akad. Nauk SSSR*, **114**, 1058 (1957); *Proc. Acad. Sci. USSR, Phys. Chem. Sect.*, **114**, 411 (1957).
- (5) A. E. Shilov and R. D. Sabirova, *Zh. Fiz. Khim.*, **33**, 1365 (1959).
- (6) F. E. Kung and W. E. Bissinger, *J. Org. Chem.*, **29**, 2739 (1964).
- (7) L. D. Westcott and P. S. Skell, *J. Am. Chem. Soc.*, **87**, 1721 (1965).
- (8) W. I. Bevan, R. N. Haszeldine, and J. C. Young, *Chem. Ind. (London)*, 789 (1961).
- (9) L. P. Blanchard and P. LeGoff, *Can. J. Chem.*, **35**, 89 (1957).
- (10) R. I. Reed and W. Snedden, *Trans. Faraday Soc.*, **54**, 301 (1958).
- (11) G. Herzberg, *Can. J. Phys.*, **39**, 1511 (1961).
- (12) I. P. Fisher, J. B. Homer, and F. P. Lossing, *J. Am. Chem. Soc.*, **87**, 957 (1965).
- (13) R. F. Pottier, *J. Chem. Phys.*, **42**, 2607 (1965).
- (14) C. Tamborski and H. W. Post, *J. Org. Chem.*, **17**, 1400 (1952).

perature of 650° and above. Above this temperature the major products were found to be CCl₂ and SiCl₄, as shown by the use of 50-V and low-energy ionizing electrons. The principal mode of decomposition of CCl₃SiCl₃ under these conditions is evidently reaction 1 as reported by Haszeldine, *et al.*⁸ A significant fraction of CCl₂ radicals were found to dimerize



Further confirmation of the presence of free CCl₂ was provided by a "titration" of the reaction at 700° with CH₃ radicals formed concurrently in the reactor by the thermal decomposition of ethyl nitrite. The major product of this addition was CH₂=CCl₂, most probably through the sequence



The double addition product (CH₃)₂CCl₂ was not detected, and it seems likely that reaction 4 is very fast at this temperature.

The ionization and appearance potentials were evaluated by a curve-matching procedure described earlier.¹⁵ To avoid peak interference in some cases three standard gases were employed: xenon, benzene, and carbon disulfide. The ionization efficiency curves for the latter two were matched to that of xenon in separate calibration experiments.

Results and Discussion

The ionization potential measurements for CCl₂ are summarized in Table I. Each of the values obtained by calibration against the three standard gases is the average of several determinations. Although the internal agreement is quite satisfactory, it should be

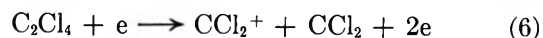
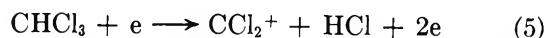
Table I: Ionization and Appearance Potential Measurements for CCl₂

Calibrating gas	IP(CCl ₂), V
Xenon	9.78
Benzene	9.72
Carbon disulfide	...
	Av 9.76
Parent compound	AP(CCl ₂ ⁺), V
CHCl ₃	12.2
C ₂ Cl ₄	14.7
CCl ₄	15.4

noted that, owing to the low-energy resolution and relatively low sensitivity of these measurements, the result presumably corresponds to the vertical IP rather than the adiabatic IP.

The ionization potential of CCl₂ can also be evaluated

independently by the indirect method from the appearance potentials for the processes



The gas-phase enthalpies of these reactions are, respectively

$$\Delta H_5 = \Delta H_f(\text{CCl}_2^+) + \Delta H_f(\text{HCl}) - \Delta H_f(\text{CHCl}_3) \quad (7)$$

$$\Delta H_6 = \Delta H_f(\text{CCl}_2^+) + \Delta H_f(\text{CCl}_2) - \Delta H_f(\text{C}_2\text{Cl}_4) \quad (8)$$

From these can be derived the relationship

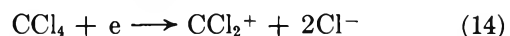
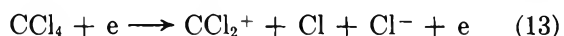
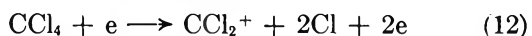
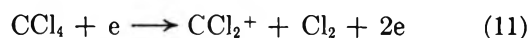
$$\begin{aligned} \text{IP}(\text{CCl}_2) = \Delta H_f(\text{CCl}_2^+) - \Delta H_f(\text{CCl}_2) = \\ 2\Delta H_5 - \Delta H_6 - 2\Delta H_f(\text{HCl}) + \\ 2\Delta H_f(\text{CHCl}_3) - \Delta H_f(\text{C}_2\text{Cl}_4) \quad (9) \end{aligned}$$

If it is assumed that the enthalpies are given by the appearance potentials for CCl₂⁺ from CHCl₃ and C₂Cl₄ according to dissociation reactions 5 and 6, then

$$\begin{aligned} \text{IP}(\text{CCl}_2) = 2\text{AP}_5 - \text{AP}_6 - 2\Delta H_f(\text{HCl}) + \\ 2\Delta H_f(\text{CHCl}_3) - \Delta H_f(\text{C}_2\text{Cl}_4) \quad (10) \end{aligned}$$

Taking the AP values from Table I and using $\Delta H_f(\text{HCl}) = -22.06$,¹⁶ $\Delta H_f(\text{CHCl}_3) = -25.0$,¹⁶ and $\Delta H_f(\text{C}_2\text{Cl}_4)$ ¹⁷ = -3.6 kcal/mole, one obtains $\text{IP}(\text{CCl}_2) = 9.64$ V, in good agreement with the direct measurement. From eq 7 and 8 can be derived also $\Delta H_f(\text{CCl}_2^+) = 279$ kcal/mole and $\Delta H_f(\text{CCl}_2) = 56.5$ kcal/mole.

The appearance potential for CCl₂⁺ from CCl₄ measured in this work (Table I) is 0.7–1.1 V lower than earlier values.^{9,10} There are four possible dissociative processes



Using $\Delta H_f(\text{CCl}_2^+) = 279$ kcal/mole as derived above, $\Delta H_f(\text{CCl}_4) = -26$ ¹⁶ and $\Delta H_f(\text{Cl}) = 28.9$ kcal/mole,¹⁶ and the electron affinity of Cl atom (3.70 V¹⁸), the calculated enthalpies for these four processes are $\Delta H_{11} = 13.22$ V, $\Delta H_{12} = 15.73$ V, $\Delta H_{13} = 12.03$ V, and $\Delta H_{14} = 8.33$ V. The appearance potential found in the present work is just significantly lower than required by reaction 12, suggesting possibly some minor participation of one or more of the lower energy processes for CCl₂⁺ formation.

(15) R. Taubert and F. P. Lossing, *J. Am. Chem. Soc.*, **84**, 1523 (1962).

(16) "JANAF Thermochemical Tables," Dow Chemical Co., Midland, Mich., 1961, and supplements to date.

(17) Evaluated from $\Delta H_f[\text{C}_2\text{Cl}_4(l)]$ (L. Smith, L. Bjellerup, S. Krook, and H. Westermarck, *Acta Chem. Scand.*, **7**, 65 (1953)) and ΔH_{vap} (D. R. Stull, *Ind. Eng. Chem.*, **39**, 517 (1947)).

(18) T. L. Bailey, *J. Chem. Phys.*, **28**, 797 (1958).

Bond Dissociation Energies Derived from $\Delta H_f(\text{CCl}_2)$

Owing to the nature of the errors in electron impact measurements, a reliable limit of error cannot be assigned to the present value for $\Delta H_f(\text{CCl}_2)$. The good agreement between the direct and indirect methods for $\text{IP}(\text{CCl}_2)$ suggests, however, that $\Delta H_f(\text{CCl}_2) = 56.5$ kcal/mole is probably not in error by more than ± 5 kcal/mole. It is of interest to see what degree of stabilization with respect to CH_2 this heat of formation represents. The stability of CF_2 has been the subject of considerable comment,¹⁹ and a recent value of $\Delta H_f(\text{CF}_2) = -39$ kcal/mole²⁰ confirms earlier predictions as to the unusual stability of this radical. The heat of formation of CH_2 is not established with precision, but a value of $\Delta H_f(\text{CH}_2) = 86$ kcal/mole²¹ is probably not in error by more than ± 6 kcal/mole. The dissociation energies for the $\text{X}_2\text{C}=\text{CY}_2$ bond in substituted ethylenes containing CF_2 and CCl_2 groups, calculated from $\Delta H_f(\text{CH}_2) = 86$, $\Delta H_f(\text{CF}_2) = -39$, and $\Delta H_f(\text{CCl}_2) = 57$ kcal/mole, are given in Table II along with the $\Delta H_f(\text{X}_2\text{C}=\text{CY}_2)$ values employed.

Some interesting relationships are observed in these bond dissociation energies. For example in the series $\text{CH}_2=\text{CH}_2$, $\text{CH}_2=\text{CCl}_2$, $\text{CH}_2=\text{CF}_2$, replacement of CH_2 by CCl_2 decreases the bond dissociation energy by 18 kcal/mole, while replacement of CH_2 by CF_2 decreases it by 35 kcal/mole. Evidently the stabilization of dichlorocarbene relative to methylene is quite considerable, being about half that of difluorocarbene. This illustrates the point that the weak double bond in tetrafluoroethylene is not an exception but part of a more general pattern. A second observation is that in a sequence of substitution $\text{CH}_2=\text{CH}_2$, $\text{CH}_2=\text{CX}_2$, $\text{CX}_2=\text{CX}_2$, the decrease in bond dissociation energy in the second step is greater than that in the first. For

Table II: Bond Dissociation Energies (kcal/mole)

Compound	$\Delta H_f(\text{g})$	Calcd $D(\text{X}_2\text{C}=\text{CY}_2)$
$\text{CH}_2=\text{CH}_2$	12.5 ^a	160
$\text{CH}_2=\text{CCl}_2$	0.9 ^b	142
$\text{CH}_2=\text{CF}_2$	-77.5 ^c	125
$\text{CCl}_2=\text{CCl}_2$	-3.6 ^d	118
$\text{CCl}_2=\text{CF}_2$	-83 ^e	101
$\text{CF}_2=\text{CF}_2$	-152 ^{e,f}	74

^a F. D. Rossini, *et al.*, "Selected Values of Physical and Thermodynamic Properties of Hydrocarbons and Related Compounds," Carnegie Press, Pittsburgh, Pa., 1953. ^b Estimated from $\Delta H_f[\text{CH}_2\text{CCl}_2(l)]$ (G. C. Sinke and D. R. Stull, *J. Phys. Chem.*, **62**, 397 (1958)) and ΔH_{vap} (D. R. Stull, *Ind. Eng. Chem.*, **39**, 517 (1947)). ^c C. A. Neugebauer and J. L. Margrave, *J. Phys. Chem.*, **60**, 1318 (1956). ^d Reference 17. ^e A. S. Rodgers, *J. Phys. Chem.*, **71**, 1996 (1967). ^f V. P. Kolesov, I. D. Zenkov, and S. M. Skuratov, *Zh. Fiz. Khim.*, **36**, 89 (1962).

example, in the series $\text{CH}_2=\text{CH}_2$, $\text{CH}_2=\text{CCl}_2$, $\text{CCl}_2=\text{CCl}_2$, the dissociation energy decreases by 18 kcal/mole in the first step and 24 in the second. For the series $\text{CCl}_2=\text{CCl}_2$, $\text{CCl}_2=\text{CF}_2$, $\text{CF}_2=\text{CF}_2$, the steps are 17 and 23 kcal/mole. Corresponding decreases in the series $\text{CH}_2=\text{CH}_2$, $\text{CH}_2=\text{CF}_2$, and $\text{CF}_2=\text{CF}_2$ are 35 and 51 kcal/mole. Since this effect appears in all three series, it seems probable that it is real and that it arises from the effect of H-X and X-X interactions on the ground-state energies of the molecules.

(19) A brief summary of proposed values has been given recently in ref 12.

(20) J. L. Margrave, *J. Am. Chem. Soc.*, in press.

(21) J. A. Kerr, *Chem. Rev.*, **66**, 465 (1966). Table XXX of this reference gives 90 kcal/mole by error, but the correct derivation from $D(\text{CH}_2-\text{H}) = 104$ kcal/mole is given in the text.

Adsorption from Solution on a Free Liquid Surface and on an Inert Solid

by S. K. Suri and V. Ramakrishna¹

Chemistry Department, Indian Institute of Technology, New Delhi, India (Received October 2, 1967)

The surface tension of solutions of benzene and cyclohexane has been redetermined at 20 and 30°. The concentration and thermodynamic activities of the components in the free liquid surface have been calculated. Using the data of Lu and Lama for the adsorption from these liquid mixtures on silica gel, the properties of the interfacial layer in equilibrium with the solid surface have also been calculated. A comparison has been made of the various thermodynamic models used, and it has been shown that the surface occupancy of the molecules (A_s) is a significant parameter in such analysis.

Several models have been proposed for the estimation of the surface concentration and activity coefficients of components at the free liquid surface of a binary solution.²⁻⁹ Attempts have also been made by Schay and Nagy¹⁰ and Kipling¹¹ to compare the thermodynamic properties of the surface layer of liquid mixtures with the interface in equilibrium with an inert solid. Everett^{12,13} has recently developed a rigorous theory for such comparisons. However, even in the simplest systems, *viz.*, binary liquid mixtures of nonpolar solvents and an inert solid surface, these comparisons are fraught with uncertainties. Lu and Lama¹⁴ have published reliable data for the adsorption from binary mixtures of benzene and cyclohexane on known silica surfaces. They have compared the activity coefficients of the components in the bulk liquid with those in the adsorbed phase. For the binary liquid mixture itself, without the solid, the available data on surface tensions were found to be inconsistent. We have, therefore, undertaken a thorough investigation of this binary liquid system and have provided means for reliable comparison of the free liquid surface with that in equilibrium with the solid absorbent.

Experimental Section

The liquids were purified by standard procedures.¹⁵ After the recommended chemical treatment, benzene was crystallized and separated a number of times, and cyclohexane was fractionally distilled. The final distillation of the solvents before use was carried out in the presence of metallic sodium. Some of the physical properties measured for the liquids are compared with the literature values in Table I.

Surface tension measurements were made by a modified maximum bubble pressure method as described by Quayle.¹⁶ The entire apparatus was mounted in a thermostatic cabin, whose temperature could be maintained to within 0.1° of the desired temperature. Reproducibility checks were made with pure liquids at all stages of measurement. The accuracy of surface tension (γ) data given in Table II is expected to be ± 0.1 dyn/cm. These data are plotted in Figure 1,

together with some literature values and the $\gamma^E = 0$ line at 20°, in order to indicate the curvature of the lines. It is clear that the data of Wolf for 20° are inconsistent with those of Hammick and Andrews for 25° and with our own values in the figure for 20 and 30°. The surface tensions of pure benzene and cyclohexane quoted by Wolf for 20° are also inconsistent.

Thermodynamic Treatment of Results

(a) *Free Liquid Surface of the Binary Mixture.* From the surface tension data, we have calculated the adsorption or "surface excess" by using the Gibbs equation. Thus

$$-d\gamma = \Gamma_1 d\mu_1 + \Gamma_2 d\mu_2 \quad (1)$$

where Γ_i is the actual concentration of the species in

- (1) To whom all correspondence may be addressed.
- (2) E. A. Guggenheim, "Mixtures," Clarendon Press, Oxford, 1952.
- (3) R. Defay, I. Prigogine, A. Bellemans, and D. H. Everett, "Surface Tension and Adsorption," Longmans, Green and Co., London, 1966.
- (4) J. W. Belton and M. G. Evans, *Trans. Faraday Soc.*, **41**, 1 (1945).
- (5) J. H. Hildebrand and R. L. Scott, "The Solubility of Non-Electrolytes," 3rd ed, Dover Publications, Inc., New York, N. Y., 1964.
- (6) T. P. Hoar and D. A. Melford, *ibid.*, **53**, 315 (1957).
- (7) (a) F. B. Sprow and J. M. Prausnitz, *Can. J. Chem.*, **45**, 25 (1967); (b) F. B. Sprow and J. M. Prausnitz, *Trans. Faraday Soc.*, **62**, 1105 (1966); (c) C. A. Eckert and J. M. Prausnitz, *A.I.Ch.E. J.*, **10**, 677 (1964).
- (8) J. C. Eriksson, "Advances in Chemical Physics," Vol. VI, Interscience Publishers, Inc., New York, N. Y., 1964.
- (9) J. G. Eberhart, *J. Phys. Chem.*, **70**, 1183 (1966).
- (10) (a) G. Schay, L. Gy. Nagy, and T. Szekrenyesy, *Periodica Polytech.*, **6**, 91 (1962); (b) L. Gy. Nagy, *ibid.*, **7**, 75 (1963).
- (11) J. J. Kipling, "Adsorption from Solutions of Non-Electrolytes," Academic Press Inc., New York, N. Y., 1965.
- (12) D. H. Everett, *Trans. Faraday Soc.*, **60**, 1803 (1964).
- (13) D. H. Everett, *ibid.*, **61**, 2478 (1965).
- (14) B. C. Y. Lu and R. F. Lama, *ibid.*, **63**, 727 (1967).
- (15) A. Weissberger, "Techniques of Organic Chemistry, Organic Solvents," Vol. VII, 2nd ed, Interscience Publishers, Inc., New York, N. Y., 1960.
- (16) O. R. Quayle, *Chem. Rev.*, **53**, 439 (1953).

Table I: Some Physical Properties of Benzene and Cyclohexane Used

Physical property	Our value	Lit. value ^c
Benzene		
Melting point, °C	5.50	5.53
Density, g/ml (20°)	0.8790	0.8790
Density, g/ml (30°)	0.8685	0.8685
Surface tension, ^a dyn/cm (20°)	28.85	28.88
Surface tension, ^a dyn/cm (30°)	27.55	27.57
Cross sectional area ^b (A_1), cm ² /mol (30°)	1.695×10^9	
Cyclohexane		
Melting point, °C	6.60	6.68
Density, g/ml (20°)	0.77865	0.7785
Density, g/ml (30°)	0.7694	0.7690
Surface tension, dyn/cm (20°)	25.00	25.20
Surface tension, dyn/cm (30°)	23.85	23.82
Cross sectional area ^b (A_2), cm ² /mol (30°)	1.932×10^9	

^a Schmidt, *et al.* (*J. Phys. Chem.*, **70**, 3912 (1966)) have found γ for benzene at 25° = 28.15 dyn/cm with $d\gamma/dT = -0.134$ dyn/cm deg, which agrees closely with our values. ^b Calculated from $A_i = (v_i^{2/3})(N^{1/2})$. ^c J. Timmermans, "Physico-chemical Constants of Pure Organic Compounds," Elsevier Publishing Co., Amsterdam, The Netherlands, 1950.

the surface layer ($\mu\text{mol}/\text{m}^2$) and μ_i is the chemical potential. Equation 1 when combined with

$$X_1^1 d\mu_1 + X_2^1 d\mu_2 = 0 \quad (2)$$

yields

$$X_1^1 \frac{d\gamma}{d\mu_2} = \Gamma_1 X_2^1 - \Gamma_2 X_1^1 = -X_2^1 \frac{d\gamma}{d\mu_1} \quad (3)$$

X_i^1 being the mole fraction in the bulk liquid. For the comparison of the free liquid surface with the interface in equilibrium with the solid, we have used the following convention for defining the surface excess^{11,12}

$$\Gamma_1^{(N)} = \Gamma_1 - X_1^1(\Gamma_2 + \Gamma_1) \quad (4)$$

or

$$\Gamma_1^{(N)} = \Gamma_1 X_2^1 - \Gamma_2 X_1^1 = X_1^1 \frac{d\gamma}{d\mu_2} \quad (5)$$

where $\Gamma_i^{(N)}$ gives the adsorption or the surface excess ($\mu\text{mol}/\text{m}^2$). In terms of the activity in the bulk liquid, the excess concentrations are obtained as

$$\Gamma_1^{(N)} = (X_1^1/RT) d\gamma/d \ln a_2^1 \quad (6)$$

The activities of benzene and cyclohexane in the bulk liquid at various concentrations have been calculated from the expressions given by Lu and Lama¹⁴ and are tabulated in Table III, with $\Gamma_1^{(N)}$ values obtained from eq 6.

The surface concentration, X_i^σ , can be calculated by

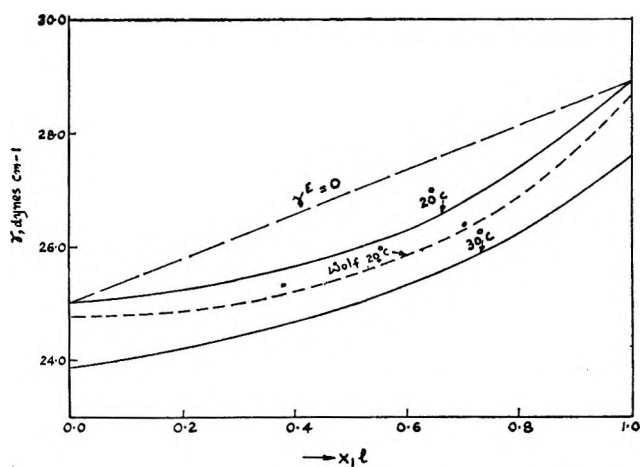


Figure 1. Surface tension vs. composition for the system benzene (1) and cyclohexane (2): ---, Wolf (J. Timmermans, "Physico-chemical Constants of Binary Systems," Interscience Publishing Co., New York, N.Y., 1959), 20°; ···, Hammick and Andrews (J. Timmermans, "Physico-chemical Constants of Binary Systems," Interscience Publishing Co., New York, N.Y., 1959), 25°.

postulating a model for the surface phase. Since the mixture of benzene and cyclohexane was found to be nonideal, as shown by excess volumes calculated from Table II, it was considered worthwhile to apply the regular-solution model for the surface phase. Two such models have been used recently with some degree of success. Hoar and Melford⁶ have shown that the surface tension of the mixture, γ , is related to the surface tensions of the pure components, γ_1 and γ_2

$$\begin{aligned} \gamma &= \gamma_1 + (RT/A_1) \ln (X_1^\sigma f_1^\sigma / X_1^1 f_1^1) \\ &= \gamma_2 + (RT/A_2) \ln (X_2^\sigma f_2^\sigma / X_2^1 f_2^1) \end{aligned} \quad (7)$$

where, A_i is the surface occupancy of the molecules (cm^2/mol) and

$$\ln f_i^1 = \ln (a_i^1/X_i^1) = (\omega^1/RT)(1 - X_i^1)^2$$

and

$$\ln f_i^\sigma = \ln (a_i^\sigma/X_i^\sigma) = (\omega^\sigma/RT)(1 - X_i^\sigma)^2 \quad (8)$$

$\omega^1 = \Delta H^M/X_1^1 X_2^1$ is a constant for an isothermal solution and $\omega^\sigma = l'\omega^1$, l' being a fraction. Hoar and Melford have suggested the values of $l' = 0.75$ or 0.50 . We have calculated ω^1 to be 90 cal from the solubility parameters of the solvents given by Hildebrand and Scott⁵ using equimolar composition. From the expressions given by Lu and Lama¹⁴ for $\log f_i^1$, however, ω^1 works out to be about 300 cal. Taking $\omega^\sigma = 0.5\omega^1$ in eq 8, the $\log f_i^\sigma$ and X_i^σ values obtained from eq 7 are tabulated in Table III. The test of the model is shown in Figure 2 by plotting γ^E vs. composition. The X_i^σ values obtained from eq 7 are shown in Figure 3.

The other approach to regular solution model for the surface phase is that of Sprow and Prausnitz.⁷ The activity coefficients in the surface phase are given

Table II: Surface Tension and Molar Volume of Binary Mixtures of Benzene and Cyclohexane at 20 and 30°

Mole fraction of cyclohexane	Surface tension, dyn cm ⁻¹ (20°)	Mole fraction of cyclohexane	Surface tension, dyn cm ⁻¹ (30°)	Mole fraction of cyclohexane	Mole volume, cm ³ mol ⁻¹	
					20°	30°
0.0000	28.85	0.0000	27.55	0.0000	88.860	89.941
0.1526	27.47	0.0864	27.05	0.0897	90.763	91.876
0.2564	26.86	0.1723	26.56	0.1751	92.578	93.553
0.3399	26.52	0.2509	26.13	0.2564	94.277	95.409
0.4490	25.97	0.3627	25.65	0.3521	96.196	97.374
0.5505	25.70	0.4379	25.32	0.4490	98.105	99.306
0.7764	25.25	0.5574	24.80	0.5515	100.084	101.302
1.0000	25.00	0.6620	24.50	0.6485	101.920	103.162
		0.7595	24.36	0.7733	104.166	105.447
		0.8668	24.10	0.8602	105.719	106.997
		1.0000	23.85	1.0000	108.079	109.415

Table III: Surface Equilibrium Data for the System Benzene (1) and Cyclohexane (2) at 30°

X ₁	Log f ₁ ^l	Log f ₂ ^l	Surface tension, dyn cm ⁻¹	Γ ₂ (N), μmol/m ²
0.0	23.85	0.00
0.2	0.1334	0.0056	24.22	0.21
0.4	0.0798	0.0291	24.72	0.36
0.6	0.0378	0.0742	25.48	0.43
0.8	0.0079	0.1368	26.40	0.40
1.0	27.55	0.00

Hoar and Melford's model				Prausnitz's model		
X ₁ ^l	X ₁ ^σ	Log f ₁ ^σ	Log f ₂ ^σ	X ₁ ^σ	Log f ₁ ^σ	Log f ₂ ^σ
0.2	0.166	0.0520	0.0021	0.247	0.0130	0.0012
0.4	0.337	0.0328	0.0085	0.423	0.0080	0.0038
0.6	0.529	0.0166	0.0209	0.575	0.0045	0.0072
0.8	0.744	0.0049	0.0414	0.745	0.0017	0.0127

in terms of "surface solubility parameters" (δ_i^σ), which are square roots of surface cohesive energy density (C_i^σ). Thus

$$RT \ln f_i^\sigma = A_i(1 - \theta_i)^2(\delta_i^\sigma - \delta_j^\sigma)^2 \quad (9)$$

where

$$\theta_i = X_i^\sigma A_i / \sum X_i^\sigma A_i \quad (10)$$

$$(\delta_i^\sigma)^2 = C_i^\sigma =$$

$$\frac{\Delta h_i^{vap} + (h_i^{ideal} - h_i^{sat}) - (RT - p^{sat}V_i)}{A_i} \quad \gamma_i + Td\gamma_i/dT \quad (11)$$

These equations combined with eq 7 can be solved for X_i^σ and f_i^σ. The difference between the surface cohesive energy density of benzene and cyclohexane from eq 12 was found to be extremely small. We have, therefore, considered

$$\eta = C_1^\sigma + C_2^\sigma - 2\sqrt{C_1^\sigma C_2^\sigma} \cong 0 \quad (12)$$

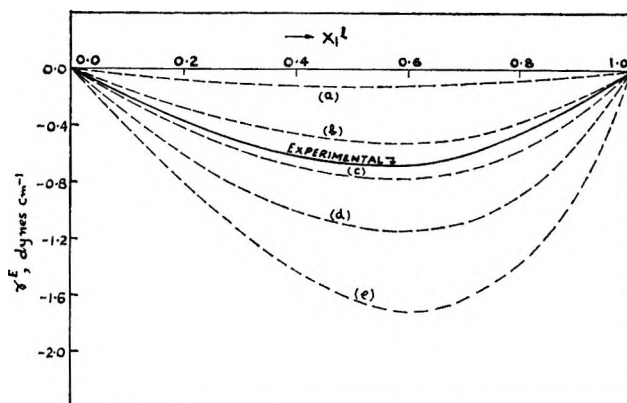


Figure 2. γ^E (30°) as a function of X₁^l: (a) ideal solution model; (b) HM model (ω^l = 90 cal, ω^σ = 0.5 ω^l); (c) HM model (ω^l = 90 cal, ω^σ = 0); (d) HM model (ω^l = 300 cal, ω^σ = 0.5 ω^l); (e) SP model.

and used the following simplified equation of Eckert and Prausnitz^{7c} for the calculation of X_i^σ

$$X_1^\sigma = [1 + (X_2^l f_2^l / X_1^l f_1^l) \exp(A_1 \gamma_1 - A_2 \gamma_2) / RT]^{-1} \quad (13)$$

The X₁^σ values were then introduced into the combined expression of eq 7 and 9 given below to obtain the γ of the solution

$$\gamma = \theta_1 \gamma_1 + \theta_2 \gamma_2 + \theta_1 \theta_2 \eta + [RT / (A_1 X_1^\sigma + A_2 X_2^\sigma)] [X_1^\sigma \ln (X_1^\sigma / X_1^l f_1^l) + X_2^\sigma \ln (X_2^\sigma / X_2^l f_2^l)] \quad (14)$$

The plots of γ^E and X₁^σ vs. X₁^l are shown in Figures 2 and 3, respectively.

(b) *Interfacial Layer in Equilibrium with a Solid Surface.* The surface concentrations of benzene and cyclohexane in contact with a silica gel of surface area 666 m²/g have been calculated by Lu and Lama.¹⁴ The following equations derived by Everett¹² for ideal solutions were applied to the adsorption data

$$X_1^1 X_2^1 / (n_0 \Delta X_1^1 / m) = (m/n^s) [X_1^1 - (1/1 - K_1)] \quad (15)$$

and

$$X_1^s = (n_0 \Delta X_1^1 / n^s) + X_1 \quad (16)$$

for calculating n^s (number of moles in adsorbed phase), $K_1 (= X_1^s X_2^1 / X_2^s X_1^1)$, and X_1^s . In the above equations m is the mass of adsorbent used, n_0 is the total number of moles of liquid mixture initially, and ΔX_1^1 is the change in mole fraction of component 1 in the bulk liquid due to adsorption. Everett¹² derived eq 15 for a "perfect adsorbed monolayer" with the assumptions:

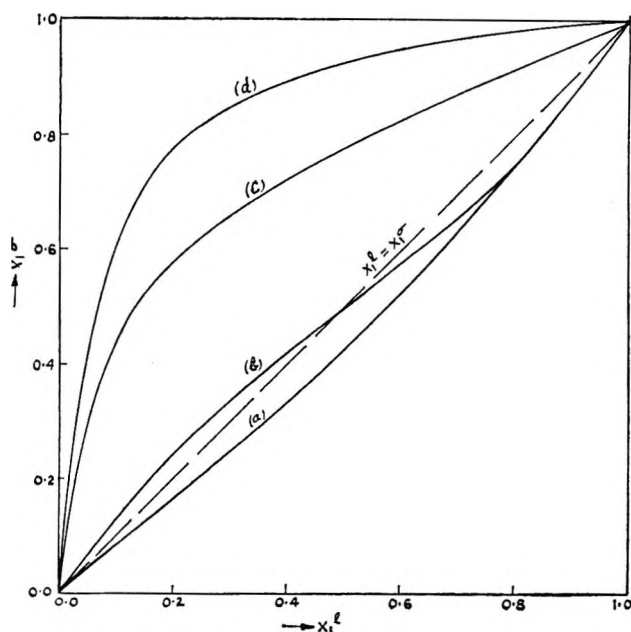


Figure 3. Equilibrium $X_1^s - X_1^1$ diagram at 30°: (a) free liquid surface (HM model); (b) free liquid surface (SP model); (c) interface in equilibrium with silica (eq 18-20); (d) interface in equilibrium with silica (Lu and Lama data), 25°.¹⁴

(i) each component follows a Langmuir-type adsorption isotherm; (ii) preferential adsorption of one component takes place, with K_1 a constant, at all concentrations. The values of X_1^s obtained from eq 15 and 16 were introduced into eq 17 derived by Everett for nonideal solutions¹² for calculating the activity coefficient of

$$\ln f_2^s = X_1^s \ln [(X_1^s / X_2^s)(X_2^1 f_2^1 / X_1^1 f_1^1)] - \int_0^{X_1^s} \ln [(X_1^s / X_2^s)(X_2^1 f_2^1 / X_1^1 f_1^1)] dX_1^s \quad (17)$$

the components in the adsorbed phase. We have calculated the surface concentration X_i^s as well as the surface activity coefficients by an alternative approach, in order to compare the results with those of Lu and Lama¹³ based on Everett's equations. From a material balance, using monolayer adsorption on an inert solid of specific surface area S (m^2/g), Schay and Nagy⁹ obtained

$$X_1^s = (SX_1^1 + A_2 \chi_1) / [S + (A_2 - A_1) \chi_1] \quad (18)$$

where χ_1 is the amount of specific adsorption ($\mu\text{mol}/\text{g}$) of component 1. Further

$$\log f_i^s = \log (X_i^1 f_i^1 / X_i^s) - (\gamma_i - \gamma) A_i / 2.303 RT \quad (19)$$

and

$$(\gamma_i - \gamma) A_i / 2.303 RT = (A_i / S) \int_{A_i=1}^{A_i} \chi_i / (1 - X_i^1) d \log (X_i^1 f_i^1) \quad (20)$$

similarly for the other component. The γ 's refer to the interfacial tension between the solid and the liquids or liquid mixture. Equation 19 is another form of eq 7; it assumes that the thermodynamic relationships applicable to a free liquid surface of a mixture of liquids are valid for the adsorbed phase on an inert solid. Equation 20 is an integral form of the Gibbs equation (6) with $\Gamma_1^{(N)}$ (on the solid surface) = $n_0 \Delta X_1^1 / Sm$. The integration shown in eq 20 was performed graphically. The values of X_i^s and f_i^s obtained from eq 18 and 19 are recorded in Table IV. In Figures 3 and 4, these values are compared with the results of Lu and Lama.¹⁴

Discussion

The ideal-solution line in Figure 2, obtained from eq 7 by writing the activity coefficients equal to 1, shows no agreement with the experimental curve. Also, the curvature of the latter cannot be reproduced. Both the regular-solution models used, on the other hand, reproduce the curvature of the experimental line more faithfully. However, the choice of $\omega^1 = 300$ cal based on calorimetric and vapor-liquid equilibrium measurements¹⁴ does not give as good a fit as the value of $\omega^1 = 90$ cal which was calculated from solubility parameters of the solvents. This is rather surprising; ω^1 may, therefore, be considered only as an adjustable parameter in the HM model. The agreement between the two regular-solution models, HM and SP models, is rather good, as shown in Figure 2. However, the X_1^s line in Figure 3 from the SP model crosses the $X_1^1 = X_1^s$ line. According to the Gibbs adsorption equation (6), this is possible only if the surface tension of the binary solution passes through a minimum, which is not the case (Figure 1). Even if the approximation $\eta \cong 0$, which we have introduced in the calculation of X_1^s by this model, eq 13, is removed, we find that the X_1^s values are still across the $X_1^1 = X_1^s$ line at the cyclohexane end. We have reason to believe, as will follow later, that this may be due to another assumption made in eq 7 and 13 regarding the surface occupancy of the molecules; namely, $\bar{A}_i \cong A_i = (V_i^{2/3}) (N^{1/3})$. Unlike the observation of Schmidt and coworkers,¹⁷ who found the

(17) R. L. Schmidt, J. C. Randall, and H. L. Clever, *J. Phys. Chem.*, **70**, 3912 (1966).

Table IV: Adsorption Equilibrium Data for the System Benzene (1) and Cyclohexane (2) on Silica Gel^a

X_1^1	$\text{Log } f_1^1$	$\text{Log } f_2^1$	$10^{27}n_0X_1^1/m$	X_1^σ	$(\gamma_1 - \gamma)A_1 / 2.303RT$	$(\gamma_2 - \gamma)A_2 / 2.303RT$	$\text{Log } f_1^\sigma$	$\text{Log } f_2^\sigma$
0.0100	0.1768	0.00001	1.346	0.0488	0.5468	0.0098	+0.0351	+0.0075
0.0500	0.1693	0.00025	7.126	0.2503	0.4789	0.0812	-0.0514	+0.0219
0.0953	0.1595	0.00102	12.56	0.4398	0.4042	0.1525	-0.1005	+0.0566
0.2331	0.1246	0.0081	14.02	0.6091	0.2531	0.3273	-0.0394	-0.0266
0.5901	0.0367	0.0804	8.732	0.8183	0.0985	0.5040	-0.0067	-0.0703
0.7372	0.0143	0.1158	5.972	0.8915	0.0579	0.5540	-0.0103	-0.0540
0.8659	0.0034	0.1635	2.941	0.9414	0.0229	0.5928	-0.0100	-0.0698

^a Experimental data of ref 14.

Prausnitz model quite satisfactory in the case of benzene-*n*-hexane mixtures, our results for benzene-cyclohexane (Figures 2 and 3) indicate a large discrepancy. This difficulty, however, does not arise to the same extent in the application of the HM model.

It is interesting to note in Figure 2 the γ^E line drawn for the condition $\omega^\sigma = 0$, *i.e.*, assuming an ideal surface phase. The agreement with the experimental values is reasonably good, indicating that the bulk activity coefficients of the components are much more significant than the corresponding surface values in determining the surface behavior. Similar observations have been made by Hildebrand and Scott⁶ and Schay and Nagy.¹⁰

The preferential adsorption of benzene on the silica surface shown in Figure 3, according to eq 18, is somewhat different compared to the results of Lu and Lama,¹⁴ although the nature of the curves is the same. The X_1^σ values of these authors depend on the evaluation of n^σ (eq 16), the total number of moles in the adsorbed phase per grams of solid, which is obtained graphically from the data using Everett's expression (eq 15). Our values, on the other hand, obtained from eq 18, depend on the surface occupancy of the molecules, A_1 and A_2 , and also on the assumption that the entire surface of the solid is occupied by one or the other molecule. Following Schay and Nagy,¹⁰ A_i has been calculated from $(V_i^{2/3})(N^{1/3})$, assuming spherical molecules, as shown in Table I. The justification for this assumption, particularly for flat molecules like benzene in contact with a solid surface, needs to be examined. In fact, it is of interest to calculate A_1 and A_2 from eq 18, using the adsorption and X_i^σ data of Lu and Lama.¹⁴ These calculated values are compared in Table V.

The agreement in the values recorded in columns b-d of Table V is striking. This suggests that the assumption of spherical molecules for calculating A_i in contact with a solid is far from satisfactory, particularly for molecules like benzene. The $\text{log } f_i^\sigma$ curves shown in Figure 4 are of interest, although some uncertainty is involved in the graphical integration of eq 20, particularly at the low X_i^σ values. The general nature of the curves for both components, at higher X_i^1 values, is

Table V: Comparison of Surface Occupancy (cm²/mol) of Benzene and Cyclohexane Molecules

	a	b	c	d
Benzene ($A_1 \times 10^{-9}$)	1.695 ^a	2.71 ^b	2.54 ^c	2.98 ^d 2.31 ^d
Cyclohexane ($A_2 \times 10^{-9}$)	1.932 ^a	2.65 ^b	2.36 ^c	...

^a From $A_i = (v_i^{2/3})(N^{1/3})$. ^b Using Lu and Lama data with eq 18 (averaged out values). ^c Generally accepted literature values for molecules flat on solid surface: L. H. Boulton, B. R. Clark, M. T. Coleman, and J. M. Thorp, *Trans. Faraday Soc.*, **62**, 2928 (1966). ^d The value 2.98, calculated from available absorption data; 2.31, theoretical value for flat benzene molecules. Both calculated from E. H. M. Wright, *Trans. Faraday Soc.*, **62**, 1275 (1966).

comparable to those obtained by Lu and Lama;¹⁴ however, the actual values of $\text{log } f_i^\sigma$ are different. If the surface occupancy given in column c of Table V are used in the calculations rather than the values in column a, the nature of the $\text{log } f_i^\sigma$ curves for the components changes, especially at low X_i^1 values. It will be observed in Figure 4 that under these conditions the curve for cyclohexane agrees very well with that obtained by the earlier workers;¹⁴ the curve for benzene, however, does not. The reason for this significantly large difference becomes clearer by examining the $(\gamma_i - \gamma) A_i / 2.303 RT$ plots in Figure 5. The values for cyclohexane obtained from eq 20, using the surface-occupancy values given in column a and c of Table V, as well as those from Lu and Lama's data, using eq 19, all agree very closely, even at low X_2^1 values. For benzene, the agreement is far from satisfactory, although the surface-occupancy values in column c of Table V improve it considerably. It is possible that in the case of benzene, which is the preferentially adsorbed component, the assumptions of eq 15 and 16 for calculating X_i^σ , as also the constancy of surface occupancy assumed in the application of eq 18, do not hold good, especially at lower concentrations. Eriksson⁸ has earlier pointed out that A_i , in some binary solutions, may have to be used as an adjustable parameter.

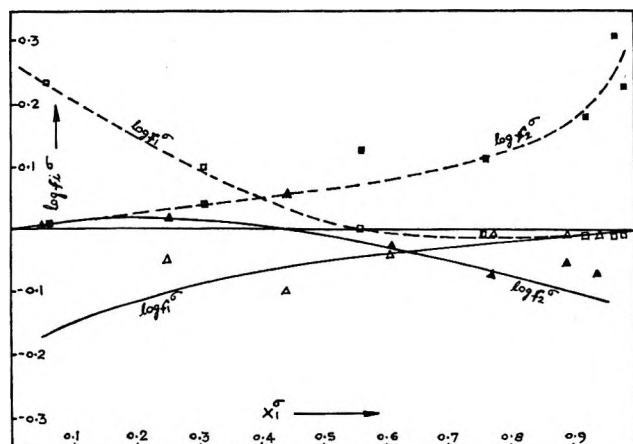


Figure 4. $\log f_i^\sigma$ values as a function of X_i^σ : Δ , benzene (A_i from spherical molecules); \blacktriangle , cyclohexane (A_i from spherical molecules); \square , benzene (A_i from flat molecules); \blacksquare , cyclohexane (A_i from flat molecules).

Conclusions

The free liquid surface of a binary solution of benzene and cyclohexane can be adequately described by eq 7 and 8 or 13 and 14. However, the use of ω^l values based on calorimetric and vapor-liquid equilibrium data in eq 7 and 8 does not give a completely satisfactory fit for the surface tension data. This is to be attributed to the constant A_i values used in the calculations based on spherical molecules.

The analysis of the interfacial layer of these solutions in equilibrium with silica gel by two alternative procedures, eq 15-17 and eq 18-20, lends strong support to the consideration that the surface occupancy is better

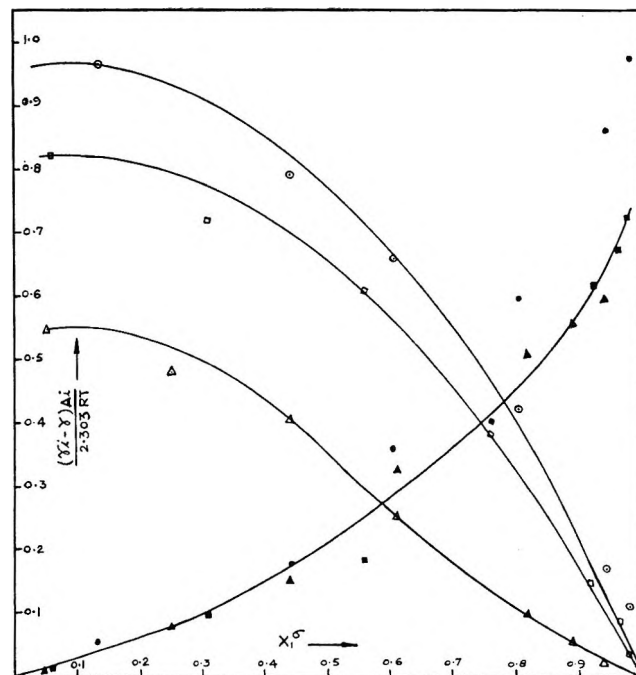


Figure 5. $(\gamma_i - \gamma)A_i/2.303 RT$ values as a function of X_i^σ : \circ , benzene; \bullet , cyclohexane (from Lu and Lama data¹⁴); Δ , benzene; \blacktriangle , cyclohexane; (A_i from spherical molecules); \square , benzene; \blacksquare , cyclohexane; (A_i from flat molecules).

calculated assuming flat-lying molecules on the solid surface. It is also possible that the surface occupancy at low concentrations of the component is a function of the composition. Everett's expression (eq 15 and 16, which do not require a knowledge of A_i for calculating X_i^σ) is more advantageous when applicable.

The Crystal Structure of the Triphenylphosphine Sulfide-Iodine Addition Complex

by W. W. Schweikert¹ and Edward A. Meyers

Department of Chemistry, Texas A & M University, College Station, Texas 77843 (Received October 9, 1967)

The crystal structure of the triphenylphosphine sulfide-iodine addition complex, $2(\text{C}_6\text{H}_5)_3\text{PS}\cdot 3\text{I}_2$ has been determined from the intensities of 843 independent X-ray reflections. The crystal is triclinic, $\text{P}\bar{1}$, with $a = 9.70 \pm 0.02 \text{ \AA}$, $b = 13.28 \pm 0.03 \text{ \AA}$, $c = 8.94 \pm 0.02 \text{ \AA}$, $\alpha = 65.2 \pm 0.5^\circ$, $\beta = 81.5 \pm 0.5^\circ$, $\gamma = 90.6 \pm 0.5^\circ$. The positions of all atoms except hydrogen were located by Fourier techniques and refined by least squares ($R = 0.11$, photographic data). One iodine atom of the iodine molecule, $\text{I}(2)-\text{I}(3)$, forms a strong bond to the sulfur atom of $(\text{C}_6\text{H}_5)_3\text{PS}$, with distances $\text{P}-\text{S} = 2.01 \pm 0.03 \text{ \AA}$, $\text{S}-\text{I}(3) = 2.69 \pm 0.02 \text{ \AA}$, $\text{I}(3)-\text{I}(2) = 2.86 \pm 0.01 \text{ \AA}$, and angles $\text{P}-\text{S}-\text{I}(3) = 107 \pm 1^\circ$, $\text{S}-\text{I}(3)-\text{I}(2) = 175 \pm 1^\circ$. The lengths of the S-I and I-I bonds are consistent with those observed in other addition compounds, while the P-S bond appears to be long. Carbon atom parameters have large standard deviations. The above I_2 molecule and the one centrosymmetrically related to it are coupled by a third, normal I_2 molecule, ($\text{I}(1)-\text{I}(1) = 2.73 \pm 0.02 \text{ \AA}$) with a short contact distance $\text{I}(2)-\text{I}(1) = 3.57 \pm 0.02 \text{ \AA}$. The entire group of six iodine atoms in $2(\text{C}_6\text{H}_5)_3\text{PS}\cdot 3\text{I}_2$ lie in one plane ($\pm 0.01 \text{ \AA}$), and there are no short I to C or C to C contact distances.

Introduction

The existence of crystalline addition complexes between phosphine sulfides or selenides and iodine or interhalogens was reported by Zingaro and Meyers.² Crystals of the triphenylphosphine sulfide complex with iodine were found to have the stoichiometric formula $2(\text{C}_6\text{H}_5)_3\text{PS}\cdot 3\text{I}_2$ ($2\text{TPPS}\cdot 3\text{I}_2$). This was considered to be unusual since only 1:1 complexes were found for all of the other compounds studied, including triphenylphosphine sulfide-iodine monobromide.

In earlier structural work^{3,4} halogen complexes with sulfur-containing organic molecules were shown to possess definite halogen to sulfur bonds. In other structural work⁵ on solid halogen-benzene adducts, evidence was presented for short halogen to ring contacts. Hence at the outset of this structure determination, it was thought that the origin of the unusual stoichiometry of $2\text{TPPS}\cdot 3\text{I}_2$ would lie in the presence of several donor sites in the TPPS molecule. This turned out not to be the case. Rather, the expected sulfur-halogen bond was observed, as well as a definite link between crystallographically and structurally distinct I_2 molecules.

Experimental Section

Crystals of $2\text{TPPS}\cdot 3\text{I}_2$ were supplied by Zingaro. An approximately cylindrical specimen of the material was sealed in a thin-walled glass capillary, 0.3 mm in diameter. Precession photographs (Mo $K\alpha$ radiation) were taken about the needle axis. The crystal was found to be triclinic, P1 or $\text{P}\bar{1}$, with $a = 9.70 \pm 0.02 \text{ \AA}$, $b = 13.28 \pm 0.03 \text{ \AA}$, $c = 8.94 \pm 0.02 \text{ \AA}$, $\alpha = 65.2 \pm 0.5^\circ$, $\beta = 81.5 \pm 0.5^\circ$, and $\gamma = 90.6 \pm 0.5^\circ$. The needle axis coincided with the a axis. For one group,

$2\text{TPPS}\cdot 3\text{I}_2$, per unit cell, $\rho(\text{calcd}) = 2.19 \text{ g/cc}$ and $\rho(\text{measd}) = 2.13 \text{ g/cc}$.²

Timed exposures were taken of the $(hk0)$ and $(h0l)$ zones by means of the Buerger precession camera with Zr-filtered Mo $K\alpha$ radiation. Multiple-film exposures were made of $(0kl)-(4kl)$ zones with an integrating Weissenberg camera⁶ and Ni-filtered Cu $K\alpha$ radiation. The crystal decomposed under exposure to X-rays and a powder pattern was apparent in the upper-level Weissenberg photographs. An attempt was made to collect data from $(5kl)$, but only a powder pattern was obtained. Since, initially, the linear absorption coefficient was $\mu = 382 \text{ cm}^{-1}$ for Cu $K\alpha$ radiation,⁷ and the crystal diameter was 0.3 mm, the value of $\mu R = 5.7$ was calculated and used to correct the Weissenberg data in the early stages of the structure analysis. It was realized that, as a result of the decomposition, this value of μR was highly uncertain. For Mo $K\alpha$ radiation, $\mu R = 0.72$,⁷ and this absorption correction was ignored.

An effort was next made to decide between the possible space groups, P1 and $\text{P}\bar{1}$. Wilson's ratio⁸ $(\overline{F_o})^2/(\overline{F_o^2}) = 0.785$ for a noncentrosymmetric crystal

(1) Submitted in partial fulfillment of the requirements for the M.S. degree in Chemistry, Texas A & M University, 1966.

(2) R. A. Zingaro and E. A. Meyers, *Inorg. Chem.*, **1**, 771 (1962).

(3) C. Romming, *Acta Chem. Scand.*, **14**, 2145 (1960).

(4) G. Y. Chao and J. D. McCullough, *Acta Crystallogr.*, **13**, 727 (1960).

(5) O. Hassel and K. O. Stromme, *Acta Chem. Scand.*, **12**, 1146 (1958); **13**, 1781 (1959).

(6) C. E. Nordman and A. L. Patterson, *Rev. Sci. Instrum.*, **28**, 384 (1957).

(7) "International Tables for X-Ray Diffraction," Vol. III, The Kynoch Press, Birmingham, England, 1962.

(8) A. J. C. Wilson, *Acta Crystallogr.*, **2**, 318 (1949).

(P1) and 0.637 for a centrosymmetric crystal ($P\bar{1}$). For the ($hk0$) zone, the ratio was calculated to be 0.614. The distribution curves⁹ for the two symmetries were compared with a composite of the statistics for the ($hk0$) and ($h0l$) zones and the result clearly favored the centrosymmetric structure. Finally, the crystals were treated by the procedure described by Wheatley,¹⁰ and no pyroelectric or piezoelectric behavior was detected. These results all supported the selection of the space group as $P\bar{1}$.

Structure Determination and Refinement

The coordinates of the iodine atoms were obtained from examination of two-dimensional Patterson functions calculated¹¹ for projections along the a , b , and c axes. By means of Fourier projections¹¹ and a least-squares refinement,¹² coordinates of all of the heavy atoms (iodine, sulfur, and phosphorus) were obtained. A three-dimensional Fourier function with the heavy atoms removed was calculated in which the 843 independent reflections from the five zones of Weissenberg data and two zones of precession data were employed. (Whenever both Weissenberg and precession intensity values were available for a given reflection, the precession value was selected because it had been recorded before extensive decomposition of the crystal occurred.) Tentative positions for all 18 carbon atoms were obtained from the difference Fourier map, and the least-squares refinement of all atomic positions with individual atom isotropic temperature factors was carried out. The value of $R_2 = [\Sigma(F_o - F_c)^2 / \Sigma F_o^2]^{1/2}$ was 0.264 for the heavy atoms only and became 0.156 after the inclusion of carbon atoms. When the carbon atom temperature factors were fixed at their best isotropic values and the heavy-atom temperature factors were varied anisotropically, $R_2 = 0.135$.

The reflections were now examined for a systematic variation in $(\sin \theta) / \lambda$. As expected, at low $(\sin \theta) / \lambda$, $|F_o| > |F_c|$ for the Weissenberg data, since the original choice of $\mu R = 5.7$ was too large as a result of decomposition of the crystal. Least-squares refinement of the 843 independent data were carried out with $\mu R = 5.0, 4.0, 3.0$, and 2.0 , for the Weissenberg data, and the best value of $R_2 = 0.123$ was obtained for $\mu R = 3.0$. We did not wish to discard the Weissenberg data for low $(\sin \theta) / \lambda$, so the value $\mu R = 3.0$ was used in the calculation of the final atomic parameters given in Table I and in the calculation of the bond distances and angles¹³ presented in Table II. The value of $\mu R = 3.0$ may be considered simply as another parameter in a least-squares analysis, though not of a customary type. In the final refinement, the coordinates of all atoms were permitted to vary, as well as the anisotropic temperature factors for iodine, sulfur, and phosphorus, the isotropic temperature factors for carbon, and the scale factors for the different zones. The final value of $R_1 = \Sigma |F_o - F_c| / \Sigma |F_o| = 0.11$. The function mini-

mized in the full-matrix least-squares refinement was $\Sigma w(|F_o| - |F_c|)^2$, where $W = 1$. From an examination of $|\Delta F|$, this weighting scheme appears to be self-consistent, except for large $|F_o|$. In the last of ten cycles of refinement, the shift in positions of P and S was 1.4×10^{-4} Å; the rms shift for the I atoms was 2.6×10^{-5} Å, with a maximum shift of 3.2×10^{-5} Å for I(3); the rms shift for the C atoms was 5.9×10^{-4} Å, with a maximum shift of 15.1×10^{-4} Å for C(18). The shifts in temperature factors, $|\Delta \beta_{ij}|$, in the last cycle of refinement in no case exceeded 0.01 of the estimated standard deviation in the corresponding β_{ij} . To prevent oscillation and slow convergence of light-atom parameters, a damping factor was used in the final refinement, and the final shifts given above have corrected for this. (A table of observed and calculated structure factors may be obtained from the authors upon request.)

Discussion of the Structure

With the possible exception of the P-S bond, the bond distances and angles found for the TPPS moiety in the complex $2TPPS \cdot 3I_2$ were those expected for a normal TPPS molecule. The S-P bond distance was 2.01 ± 0.03 Å, compared to 1.95 and 1.96 Å for similar bond distances in P_4S_7 and P_4S_{10} .¹⁴ However, a bond distance of close to 1.86 Å has been found for $(C_2H_5)_3PS$,¹⁵ F_3PS ,¹⁶ Cl_3PS ,¹⁶ Br_3PS ,¹⁷ FBr_2PS ,¹⁷ and F_2BrPS .¹⁷ The weight of evidence would seem to indicate that the S-P bond in $2TPPS \cdot 3I_2$ has been lengthened from the value expected for TPPS. The three P-C bonds had an average length of 1.82 Å. The greatest variation from this value was found for P-C(7) = 1.72 ± 0.07 Å and cannot be considered significant (difference $< 3\sigma$). The mean value of the P-C bond length was 1.828 Å in triphenylphosphorus (TPP).¹⁸ In $2TPPS \cdot 3I_2$, the average C-C bond distance in the phenyl rings was 1.44 Å, compared to the value 1.400 Å found in TPP and 1.397 Å found in

(9) E. R. Howells, D. C. Phillips, and D. Rogers, *Acta Crystallogr.*, **3**, 210 (1950).

(10) P. J. Wheatley, *J. Chem. Soc.*, 615 (1965).

(11) W. G. Sly, D. P. Shoemaker, and J. H. Van den Hende, "Two- and Three-Dimensional Crystallographic Fourier Summation Program for the IBM 7090 Computer," CBRL-22M-62, Massachusetts Institute of Technology, Esso Research and Engineering Co., 1962.

(12) W. R. Busing, K. O. Martin, and H. A. Levy, "ORFLS, a Fortran Crystallographic Least-Squares Program," ORNL-TM-305, Oak Ridge National Laboratory, Oak Ridge, Tenn., 1962.

(13) W. R. Busing, K. O. Martin, and H. A. Levy, "ORFFE, a Fortran Crystallographic Function and Error Program," ORNL-TM-306, Oak Ridge National Laboratory, Oak Ridge, Tenn., 1964.

(14) A. Vos and E. H. Wiebenga, *Acta Crystallogr.*, **8**, 217 (1955).

(15) M. van Meerssche and A. Leonard, *Bull. Soc. Chim. Belges*, **68**, 683 (1959).

(16) Q. Williams, J. Sheridan, and W. Gordy, *J. Chem. Phys.*, **20**, 164 (1952).

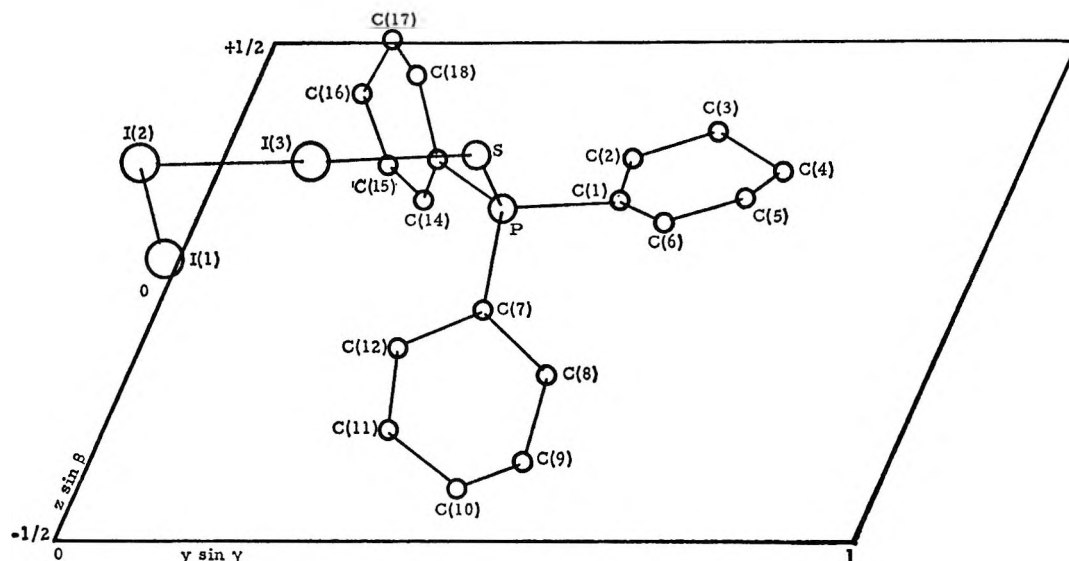
(17) J. H. Secrist and L. O. Brockway, *J. Amer. Chem. Soc.*, **66**, 1941 (1944).

(18) J. J. Daly, *J. Chem. Soc.*, 3799 (1964).

Table I: Atomic Coordinates of $2\text{TPPS} \cdot 3\text{I}_2^{a,b}$

Atom	x	y	z	β_{11}	β_{22}	β_{33}	β_{12}	β_{13}	β_{23}
I(1)	-0.1385 (8)	-0.0274 (5)	0.0653 (9)	0.0786 (16)	0.0090 (5)	0.0364 (19)	-0.0010 (7)	-0.0160 (15)	-0.0055 (8)
I(2)	-0.4974 (7)	-0.0990 (4)	0.2581 (8)	0.0172 (16)	0.0081 (5)	0.0284 (17)	0.0043 (6)	-0.0056 (12)	-0.0079 (8)
I(3)	-0.5549 (6)	0.1116 (4)	0.2588 (7)	0.0076 (9)	0.0065 (4)	0.0159 (12)	0.0008 (4)	-0.0043 (8)	-0.0031 (6)
S	-0.5874 (27)	0.3086 (16)	0.2724 (27)	0.0180 (46)	0.0093 (19)	0.0149 (48)	0.0051 (23)	-0.0054 (42)	-0.0037 (25)
P	-0.7549 (21)	0.3709 (13)	0.1658 (22)	0.0070 (27)	0.0050 (12)	0.0131 (35)	0.0015 (15)	-0.0081 (31)	-0.0044 (18)
C(1)	-0.790 (7)	0.502 (4)	0.184 (7)	[0.0050]	[0.0032]	0.0071 (83)	[0.0003]	[-0.0010]	[-0.0020]
C(2)	-0.924 (8)	0.508 (5)	0.270 (9)	[0.0091]	[0.0058]	0.0130 (103)	[0.0006]	[-0.0018]	[-0.0037]
C(3)	-0.937 (8)	0.609 (5)	0.289 (9)	[0.0112]	[0.0071]	0.0159 (107)	[0.0007]	[-0.0022]	[-0.0045]
C(4)	-0.832 (7)	0.694 (4)	0.237 (7)	[0.0053]	[0.0034]	0.0076 (83)	[0.0003]	[-0.0011]	[-0.0021]
C(5)	-0.695 (8)	0.677 (5)	0.178 (8)	[0.0091]	[0.0058]	0.0130 (100)	[0.0006]	[-0.0018]	[-0.0037]
C(6)	-0.667 (7)	0.581 (5)	0.152 (8)	[0.0095]	[0.0060]	0.0136 (104)	[0.0006]	[-0.0019]	[-0.0039]
C(7)	-0.737 (8)	0.404 (5)	-0.044 (8)	[0.0100]	[0.0063]	0.0142 (104)	[0.0006]	[-0.0020]	[-0.0040]
C(8)	-0.716 (7)	0.520 (4)	-0.168 (8)	[0.0080]	[0.0051]	0.0114 (98)	[0.0005]	[-0.0016]	[-0.0032]
C(9)	-0.692 (6)	0.540 (4)	-0.346 (7)	[0.0049]	[0.0031]	0.0070 (78)	[0.0003]	[-0.0010]	[-0.0020]
C(10)	-0.663 (9)	0.459 (6)	-0.404 (10)	[0.0152]	[0.0096]	0.0217 (131)	[0.0010]	[-0.0031]	[-0.0062]
C(11)	-0.687 (6)	0.359 (4)	-0.288 (6)	[0.0025]	[0.0016]	0.0035 (67)	[0.0002]	[-0.0005]	[-0.0010]
C(12)	-0.707 (7)	0.328 (5)	-0.113 (8)	[0.0083]	[0.0053]	0.0118 (101)	[0.0005]	[-0.0017]	[-0.0034]
C(13)	-0.914 (8)	0.268 (5)	0.252 (8)	[0.0081]	[0.0051]	0.0116 (97)	[0.0005]	[-0.0016]	[-0.0033]
C(14)	-1.016 (11)	0.284 (8)	0.168 (13)	[0.0231]	[0.0147]	0.0331 (195)	[0.0015]	[-0.0047]	[-0.0094]
C(15)	-1.144 (6)	0.207 (4)	0.247 (7)	[0.0062]	[0.0040]	0.0089 (81)	[0.0004]	[-0.0013]	[-0.0025]
C(16)	-1.152 (9)	0.136 (7)	0.403 (11)	[0.0175]	[0.0111]	0.0251 (151)	[0.0011]	[-0.0035]	[-0.0071]
C(17)	-1.055 (7)	0.138 (4)	0.516 (7)	[0.0070]	[0.0044]	0.0099 (89)	[0.0005]	[-0.0014]	[-0.0028]
C(18)	-0.902 (22)	0.210 (16)	0.459 (27)	[0.063?]	[0.0401]	0.0002 (581)	[0.0011]	[-0.0127]	[-0.0236]

^a Standard deviation is placed in parentheses and applied to the last digit of a number.^b Values in brackets are calculated from β_{33} isotropic temperature factors.

Figure 1. The asymmetric unit in *a*-axis projection.Table II: Bond Distances and Bond Angles^a

Bond distances, Å		Bond angles, deg	
I(1)-I(1)	2.72 (2)	I(2)-I(3)-S	174.6 (6)
I(2)-I(3)	2.86 (1)	I(3)-S-P	107 (1)
I(3)-S	2.69 (2)	S-P-C(1)	109 (2)
S-P	2.02 (3)	S-P-C(7)	115 (2)
P-C(1)	1.84 (6)	S-P-C(13)	113 (2)
P-C(7)	1.72 (7)	C(1)-P-C(7)	105 (5)
P-C(13)	1.88 (7)	C(7)-P-C(13)	102 (3)
C(1)-C(2)	1.44 (9)	C(13)-P-C(1)	112 (3)
C(2)-C(3)	1.42 (9)	C(1)-C(2)-C(3)	114 (6)
C(3)-C(4)	1.39 (8)	C(2)-C(3)-C(4)	126 (8)
C(4)-C(5)	1.42 (8)	C(3)-C(4)-C(5)	119 (6)
C(5)-C(6)	1.42 (9)	C(4)-C(5)-C(6)	121 (6)
C(6)-C(1)	1.49 (8)	C(5)-C(6)-C(1)	116 (7)
C(7)-C(8)	1.46 (8)	C(6)-C(1)-C(2)	123 (6)
C(8)-C(9)	1.47 (8)	C(7)-C(8)-C(9)	117 (5)
C(9)-C(10)	1.39 (9)	C(8)-C(9)-C(10)	125 (5)
C(10)-C(11)	1.29 (8)	C(9)-C(10)-C(11)	114 (7)
C(11)-C(12)	1.42 (8)	C(10)-C(11)-C(12)	125 (6)
C(12)-C(7)	1.40 (9)	C(11)-C(12)-C(7)	123 (5)
C(13)-C(14)	1.30 (10)	C(12)-C(7)-C(8)	113 (6)
C(14)-C(15)	1.48 (10)	C(13)-C(14)-C(15)	118 (8)
C(15)-C(16)	1.30 (9)	C(14)-C(15)-C(16)	117 (7)
C(16)-C(17)	1.48 (9)	C(15)-C(16)-C(17)	126 (7)
C(17)-C(18)	1.65 (20)	C(16)-C(17)-C(18)	126 (9)
C(18)-C(13)	1.70 (21)	C(17)-C(18)-C(13)	94 (11)
I(1)-I(2)	3.57 (2)	C(18)-C(13)-C(14)	135 (10)
		I(1)-I(1)-I(2)	176.7 (4)
		I(1)-I(2)-I(3)	97.1 (5)

^a Standard deviation is placed in parentheses and applies to the last digit of a number.

benzene. The greatest deviation from this value was found for C(17)-C(18) = 1.70 ± 0.21 Å and was not considered significant.

The mean S-P-C bond angle was 113° and the maximum, but not significant, deviation was found for S-P-C(1) = 109 ± 2°. The mean C-P-C bond angle

was 106°. The average ring C-C-C bond angle was 119.5°, compared to 120° which was expected for planar phenyl rings. The maximum deviation occurred for C(17)-C(18)-C(13) = 94 ± 11°. The mean value for the C-C-C angle in TPP was 120.0°.

In 2TPPS·3I₂, the phenyl rings were arranged in a propeller-like manner, similar to that found in TPP. The angles between the ring planes [C(1)-C(6), C(7)-C(12), C(13)-C(18)] and the plane normal to the S-P bond were 60, 50, and 23°, respectively. A labeled drawing of the asymmetric unit, TPPS·³/₂I₂, present in the crystal is given in Figure 1. In Figure 2, the TPPS·³/₂I₂ unit and the moiety related to it by the center of symmetry at (0, 0, 0) are drawn.

The values of the I-I bond distance in solid I₂^{19,20} have been reported as 2.68 and 2.715 Å. The distance I(1)-I(1) was 2.73 ± 0.02 Å and if an uncertainty of ±0.01 to ±0.02 Å was assumed in the value of 2.68 obtained from the earlier study of solid I₂, there was probably no evidence for significant lengthening of the I(1)-I(1) bond distance. This was not true for I(2)-I(3) = 2.86 ± 0.01 Å, where there appeared to be a significant increase in the I-I bond distance. This kind of behavior has been observed before. For example, in such structures as C₄H₈S₂·2I₂³ and (C₆H₅-CH₂)₂S·I₂⁴ I-I bond lengths of 2.79 and 2.82 Å, respectively, have been obtained for I₂ molecules that were closely bonded to sulfur, at I-S distances of 2.87 and 2.78 Å, respectively. In 2TPPS·3I₂, the distance I(3)-S = 2.69 ± 0.02 Å, and this appeared to be significantly shorter than the corresponding I-S distances in C₄H₈S₂·2I₂ and (C₆H₅CH₂)₂S·I₂. A plot of I-I vs. I-S bond distances was made and found to be

(19) A. I. Kitajgorodskij, T. L. Khocjanova, and Ju. T. Struckov, *Zh. Fiz. Khim.*, **27**, 780 (1953).

(20) F. van Bolhuis, P. B. Koster, and T. Migchelson, *Acta Crystallogr.*, **23**, 90 (1967).

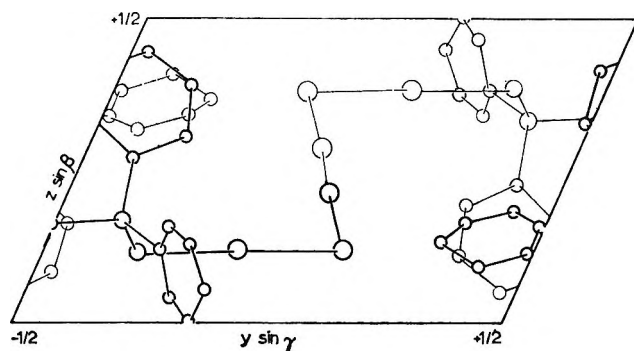


Figure 2. Projection of the contents of one unit cell down the a axis. The asymmetric unit (light lines) and the moiety related by a center of symmetry (heavy lines) are shown.

close to linear. The angle $I(2)-I(3)-S = 175 \pm 1^\circ$ was in fair agreement with corresponding angles of 177.9 ± 0.4 and 179° found for $C_4H_9S_2 \cdot 2I_2$ and $(C_6H_5-CH_2)_2S \cdot I_2$.

The outstanding feature of the present structure was the very strong complex formed between the $I(2)-I(3)$ molecule and the sulfur atom of TPPS. This had been expected and still left unexplained the unusual stoichiometry of the complex, $2TPPS \cdot 3I_2$, compared to the 1:1 complexes obtained with other phosphine sulfides and halogens.

The contact distances between various carbon atoms and the closest iodine atoms were calculated, and in no case was the $I-C$ distance below 3.85 \AA , the normal van der Waals contact sum for I (2.15 \AA) and a benzene ring (1.7 \AA). All of the $C-C$ contacts were normal. However, one short $I-I$ contact was found, $I(1)-I(2) = 3.57 \pm 0.02 \text{ \AA}$. Similar contacts have been reported in the structure of solid I_2 , and, in fact, the configuration of atoms along the diagonal in the ac plane of solid I_2 was very similar to that found in the present structure. The ac plane of solid I_2 is shown in Figure 3, with the I atoms labeled to correspond to the configuration of I atoms in the structure of the complex, $2TPPS \cdot 3I_2$.

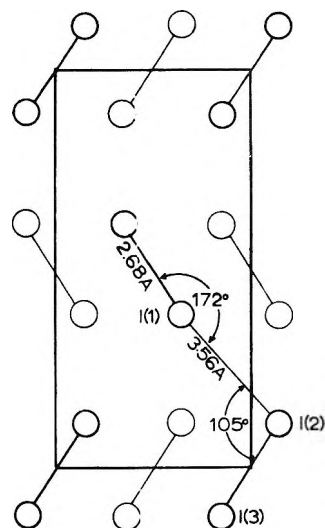


Figure 3. Projection of the structure of solid iodine on the ac plane: heavy lines represent atoms at $x = 0$; light lines represent atoms at $x = 1/2$.

To sum up the results, the phenyl rings appeared to play no direct role in the complex formed between $2TPPS$ and $3I_2$ molecules. Rather, one very strong $I-S$ link has been formed, $I(3)-S = \bar{I}(3)-\bar{S} = 2.69 \text{ \AA}$, with the $I(2)-I(3) = \bar{I}(2)-\bar{I}(3) = 2.86 \text{ \AA}$ distance appreciably lengthened from the normal $I-I$ distance of 2.71 \AA . The $TPPS \cdot I_2$ complexes have been linked into dimers by $I-I$ bonds, $\bar{I}(1)-\bar{I}(2) = 3.57 \text{ \AA}$, and the six iodine atoms of the complex lie in one plane ($\pm 0.01 \text{ \AA}$). A line formula for the complex would be $(TPPS \cdot I-I) \cdot (I-I) \cdot (I-I \cdot TPPS)$.

Acknowledgments. The financial support of The Robert A. Welch Foundation is gratefully acknowledged. The facilities of the Data Processing Center of the Texas A & M University system have been used extensively in this work. Dr. R. A. Zingaro supplied us with beautiful crystals and considerable encouragement.

Phenomenological Coefficients for Volume Flow across an Ion-Exchange Membrane¹

by A. S. Tombalakian

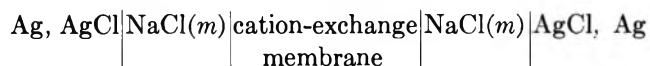
Department of Chemistry and Engineering, Laurentian University, Sudbury, Ontario, Canada (Received October 9, 1967)

Volume flow across a polystyrenesulfonic acid ion-exchange membrane has been measured at several different values of chemical and electrical potential differences. The experimental results have been interpreted in terms of linear phenomenological equations. These relationships have been used to estimate the magnitudes of the phenomenological coefficients for volume flow across the ion-exchange membrane. The dependence of the phenomenological coefficients on membrane properties and the ion species has been determined. The validity of the phenomenological equation in volume flow across the ion-exchange membrane has been tested by direct measurements.

Introduction

Water transport across ion-exchange membranes has been the subject of numerous investigations.²⁻⁸ A complete listing of these studies is given by Helfferich⁹ in his comprehensive treatise on ion exchange. Several theoretical descriptions of water-transport phenomena across ion-exchange membranes also have been presented.⁹⁻¹⁴ This report supplements the preceding studies and, more specifically, introduces experimental details for the measurements of phenomenological coefficients for volume flow across an ion-exchange membrane when two forces (chemical and electrical potentials) are involved.

When a certain electrical potential difference is maintained across the cell



transfer of fluid (cations and solvent molecules) occurs in the direction of positive electricity from one cell compartment to the other. At the same time an osmotic potential difference between the solutions sets up across the ion-exchange membrane, which induces osmotic flow of water in the direction of the convection produced by the applied electrical potential difference. The volume change (ΔV , cc) observed in each cell compartment resulting from the electrochemical process is given by

$$\Delta V = t_w \bar{V}_w + t_{Na} \bar{V}_{NaCl} - V_{AgCl} - V_{Ag} \quad (1)$$

where t_w and t_{Na} are the moles of water and sodium ion transferred per faraday (F) of charge passed; and \bar{V} signifies partial molal volume. The quantity $\Delta V/18$ has been shown³ to be a good approximation to the moles of water transferred per faraday by sodium ions across a polystyrenesulfonic acid ion-exchange membrane separating sodium chloride solutions in the concentration range 0.05–4.0 M .

If the resultant flow of volume across the ion-exchange membrane is considered as a single fluid, the production of entropy (S) at temperature T ($^{\circ}K$) due to volume flow and transfer of charges may be written¹⁵ as

$$TS = J\Delta P + I\Delta E \quad (2)$$

where the fluxes are the total volume flow (J) and the total electric current (I); the forces are the osmotic pressure difference (ΔP) and the electrical potential difference (ΔE). The linear phenomenological expressions may consequently be written as

$$J = L_{11} \frac{\Delta P}{T} + L_{12} \frac{\Delta E}{T} \quad (3)$$

$$I = L_{21} \frac{\Delta P}{T} + L_{22} \frac{\Delta E}{T} \quad (4)$$

(1) Presented at the 17th Canadian Chemical Engineering Conference, Niagara Falls, Ont., Canada, Oct 16–18, 1967.

(2) A. G. Winger, R. Ferguson, and R. Kunin, *J. Phys. Chem.*, **60**, 556 (1956).

(3) R. J. Stewart and W. F. Graydon, *ibid.*, **61**, 164 (1957).

(4) N. W. Rosenberg, J. H. B. George, and W. D. Potter, *J. Electrochem. Soc.*, **104**, 111 (1957).

(5) A. S. Tombalakian, H. J. Barton, and W. F. Graydon, *J. Phys. Chem.*, **66**, 1006 (1962).

(6) N. Lakshminarajaniah, *Proc. Indian Acad. Sci.*, **A55**, 200 (1962).

(7) A. S. Tombalakian, M. Worsley, and W. F. Graydon, *J. Am. Chem. Soc.*, **88**, 661 (1966).

(8) J. H. B. George and R. A. Courant, *J. Phys. Chem.*, **71**, 246 (1967).

(9) F. Helfferich, "Ion-Exchange," McGraw-Hill Book Co., Inc., Toronto, 1962.

(10) A. J. Staverman, *Trans. Faraday Soc.*, **48**, 176 (1952).

(11) P. B. Lorenz, *J. Phys. Chem.*, **56**, 775 (1952).

(12) G. Schmid, *Z. Elektrochem.*, **56**, 181 (1952).

(13) R. Schlögl, *Discussions Faraday Soc.*, **21**, 46 (1956).

(14) K. S. Spiegler, *Trans. Faraday Soc.*, **54**, 1409 (1958).

(15) S. R. deGroot and P. Mazur, "Non-equilibrium Thermodynamics," North-Holland Publishing Co., Amsterdam, 1962.

in which the Onsager symmetry relation $L_{12} = L_{21}$ may be assumed.^{15,16} It is evident from these relations that the phenomenological coefficients L_{11} and L_{22} are related to the hydrodynamic and electrical resistances of the ion-exchange membrane, respectively, while the cross-phenomenological coefficients L_{1z} and L_{z1} describe the "interference" of the volume flow and the transport of electrical current.

From eq 3 it follows that when $\Delta E = 0$

$$J = L_{11} \frac{\Delta P}{T} \quad (5)$$

where L_{11} describes the osmotic permeability of the membrane in a given ionic form. It is evident that measurements of volume flow for various values of osmotic pressure differences at a constant temperature can directly yield the value of L_{11} .

It follows from eq 4 that when $\Delta P = 0$

$$I = L_{22} \frac{\Delta E}{T} \quad (6)$$

On comparing eq 6 with the expression for the specific conductivity (\bar{k}) of the membrane in a given ionic form, one finds that

$$\frac{L_{22}}{T} = \frac{\bar{k}A}{d} \quad (7)$$

where A is the membrane cross section and d is the distance between the electrodes. Since the specific conductivity of a membrane in a given ionic form is approximately independent of ΔE , the quantity L_{22} is expected to be largely independent of ΔE at constant temperature.

From eq 3 it follows that when $\Delta P = 0$

$$J_{\Delta P=0} = L_{12} \frac{\Delta E}{T} \quad (8)$$

It is evident that measurements of electroosmotic flow for various values of ΔE at constant temperature can directly yield the value of L_{12} .

A comparison of eq 8 with eq 6 yields

$$(J/I)_{\Delta P=0} = \frac{L_{12}}{L_{22}} \quad (9)$$

It will be noted that the product of $(J/I)_{\Delta P=0}$ and $(F/18)$ represents the water transference number (W_T) of the membrane in a given ionic form. It has been shown previously⁵ that the ratio of the water transference number to membrane equivalent moisture content (W_D) is a constant for a series of polystyrenesulfonic acid ion-exchange membranes, having the same nominal exchange capacity but various degrees of cross-linking, in a given ionic form over a wide range of external solution concentration. This ratio W_T/W_D is a function of the membrane-exchange capacity.⁵ An empirical representation of the dependence of the ratio L_{12}/L_{22} on mem-

brane exchange capacity and moisture content for the sodium form of the membrane may consequently be written as

$$\frac{L_{12}}{L_{22}} = 0.38W_D(\text{exchange capacity})^{0.42}(18/F) \quad (10)$$

The results of phenomenological coefficients for volume flow across a polystyrenesulfonic acid ion-exchange membrane for various ionic forms are presented in this report. Similar results for the flow of conductivity water through sintered Pyrex glass induced by pressure and electrical potential differences have been recently reported.¹⁷

Experimental Section

(1) *Membrane.* The polystyrenesulfonic acid ion-exchange membrane used in this study was prepared by the bulk copolymerization of the *n*-propyl ester of *p*-styrenesulfonic acid with styrene, divinylbenzene, and benzoyl peroxide as catalysts and subsequent hydrolysis in 5% caustic soda solution following the procedure described previously.^{5,18} The membrane had a nominal cross-linking of 6 mol % DVB, an exchange capacity of 2.80 mequiv/g of dry resin (Na form), a moisture content of 15.2 mol of H₂O/equiv in the leached Na form at 100% relative humidity at 25°, and a thickness of 0.0602 ± 0.0002 cm.

(2) *Measurements of Volume Flow.* A two-compartment Lucite cell fitted with capillary tubes and silver-silver chloride electrodes (10.5 cm apart) was used to measure osmotic and electroosmotic water transport across a membrane (1 cm in diameter) separating solutions of HCl, NH₄Cl, KCl, and NaCl by the methods described previously.^{3,5,7} The electrodes were silver rods (1 cm in diameter) coated with silver chloride. Heathkit Models IP-20 and PS-3 regulated variable-voltage power supplies were used as a source of emf for voltages varying from 2 to 50 V and 50 to 130 V, respectively. Fluctuations in voltage were of the order 2–5%. A Philips Type PM2411 multimeter was used to measure the strength of the current drawn. All measurements were made at $25 \pm 0.1^\circ$.

In order to determine the extent to which the osmotic and electroosmotic water flux values are simply additive, volume flow across a membrane separating different solutions of sodium chloride was measured in three series of experiments (A, B, and C). In experiments A, a steady current of 3 mA was passed from the dilute to the concentrated side for 20 min and the changes in the heights of solutions in the capillary tubes were determined. In experiments B, the above procedure was repeated passing the same quantity of electricity from the concentrated to the dilute side. In

(16) K. G. Denbigh, "The Thermodynamics of the Steady State," Methuen and Co., Ltd., London, 1965.

(17) R. P. Rastogi and K. M. Jha, *J. Phys. Chem.*, **70**, 1017 (1966).

(18) W. F. Graydon and R. J. Stewart, *ibid.*, **59**, 86 (1955).

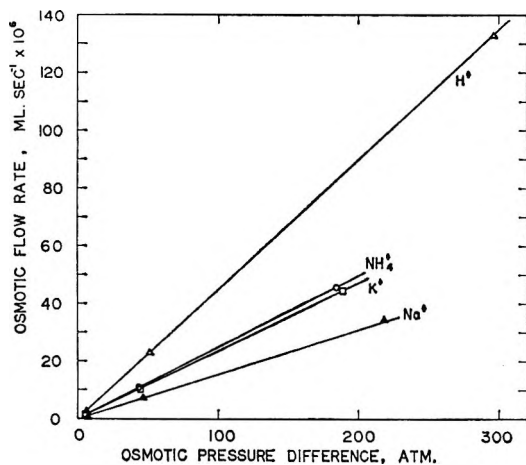


Figure 1. The variation of osmotic flow rate with calculated osmotic pressure differences at 25° for various ionic forms of the ion-exchange membrane. The solutions of chloride salts and hydrochloric acid used were in the concentration range 0.1–4.0 *M*.

experiments C, the transfer of water induced by chemical potential difference between the two solutions for the same time interval was determined. These measurements were made with solutions of sodium chloride in the concentration range 0.05–4.0 *M*.

Results and Discussion

A verification of the linear relation between isothermal volume flow and osmotic pressure difference is shown in Figure 1 for various membrane ionic forms. The plots are based on results of measurements using various solutions of hydrochloric acid, ammonium chloride, potassium chloride, and sodium chloride in the concentration range 0.1–4.0 *M*. The linear plots of Figure 1 seem to converge at the origin. However, osmotic flow across an ion-exchange membrane is not expected to conform to Poiseuille's law for liquid flow through an ordinary capillary tube, since the kinetic energy of the flowing liquid is unaccounted for in Poiseuille's equation. The slopes of the straight lines correspond to phenomenological coefficients L_{11}/T for osmotic flow across the ion-exchange membrane. For the various membrane ionic forms, these values of the phenomenological coefficients L_{11}/T (expressed in $\text{ml sec}^{-1} \text{atm}^{-1} \times 10^7$) are observed for: H^+ , 4.5; NH_4^+ , 2.5; K^+ , 2.4; Na^+ , 1.6. It may be noted that the phenomenological coefficients L_{11}/T of the membrane in the various ionic forms decrease in the order hydrogen, ammonium, potassium, and sodium. This effect is consistent with the variation in the effective radii¹⁹ of these ions in their hydrated forms in aqueous solution.

The effect of variation of the electrical potential difference on conductance of electric current and electro-osmotic flow across the ion-exchange membrane was investigated. Examples of the strength of the electric current drawn through the cell at different electrical

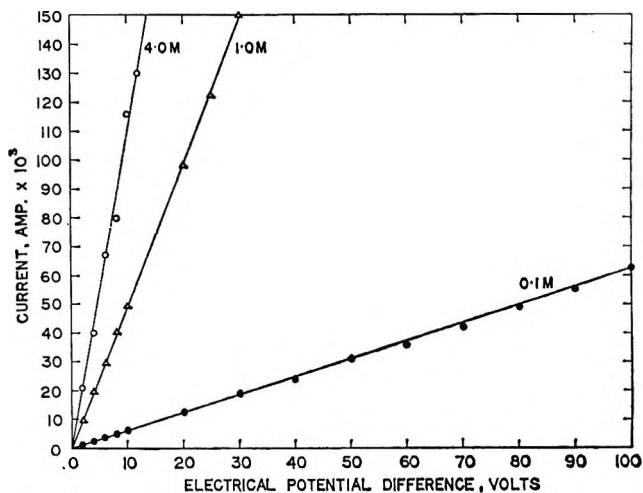


Figure 2. Electric conductance of the membrane cell as a function of electrical potential difference at 25°. The solutions of sodium chloride used were 0.1, 1.0, and 4.0 *M*.

potential differences using various solutions of sodium chloride are presented in Figure 2. It can be seen that for a given solution concentration the current increases in direct ratio to electrical potential difference. The slopes of the straight lines correspond to phenomenological coefficients L_{22}/T for the conductance of electricity through the membrane cell. Samples of such values of membrane phenomenological coefficients L_{22}/T for the various solutions of sodium chloride, potassium chloride, ammonium chloride, and hydrochloric acid are given in Table I. It may be noted from the data that the phenomenological coefficient L_{22}/T tends to decrease with decreasing external solution concentration and also in the order hydrogen, ammonium, potassium, and sodium. These results may be compared with values of L_{22}/T estimated at infinite dilution from membrane specific resistances, as determined previously²⁰ in membrane electrical resistance measurements, using eq 7, which are listed in the last column in Table I. Although some difference may be noted between the values of L_{22}/T calculated at infinite dilution and similar values obtained by extrapolation of the experimental data, the relative differences are quite similar.

The data obtained for isothermal volume flow induced by electrical potential difference for the various univalent cations are presented in Figures 3–6. These measurements were made using various solutions of sodium chloride, potassium chloride, ammonium chloride, and hydrochloric acid in the concentration range 0.1–4.0 *M*. It may be seen that the increase of the rate of volume flow with increasing electrical potential difference gave smooth curves passing through the origin. The slopes of the plots correspond to phenomenological

(19) R. A. Robinson and R. H. Stokes, "Electrolyte Solutions," Butterworth and Co. Ltd., London, 1959.

(20) J. Ciric and W. F. Graydon, *J. Phys. Chem.*, **66**, 1549 (1962).

Table I: Phenomenological Coefficients for Conductance of Electric Current through Membrane Cell

System	$L_{22}/T, \text{ ohm}^{-1} \times 10^4$			
	4.0 M	1.0 M	0.1 M	0 M
HCl	48.0	21.9	2.1	10.1 ^a
NH ₄ Cl	17.7	7.4	0.82	2.7 ^a
KCl	17.0	7.0	0.75	2.4 ^a
NaCl	11.1	5.0	0.63	1.5 ^a

^a Calculated from experimental values of membrane electrical resistances²⁰ using eq 7.

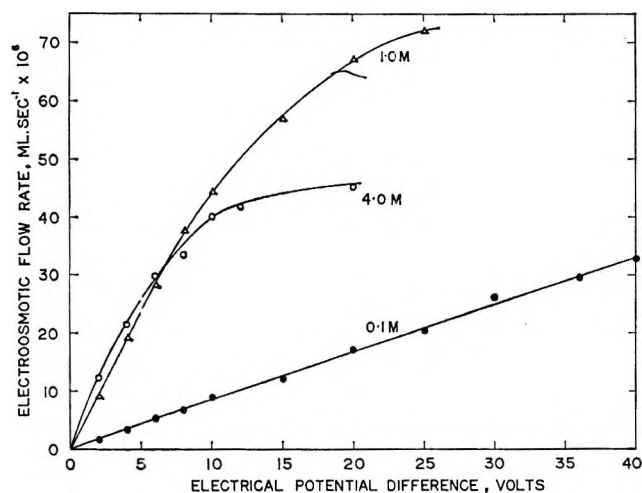


Figure 3. The variation of electroosmotic flow rate with electrical potential difference at 25°. The solutions of sodium chloride used were 0.1, 1.0, and 4.0 M.

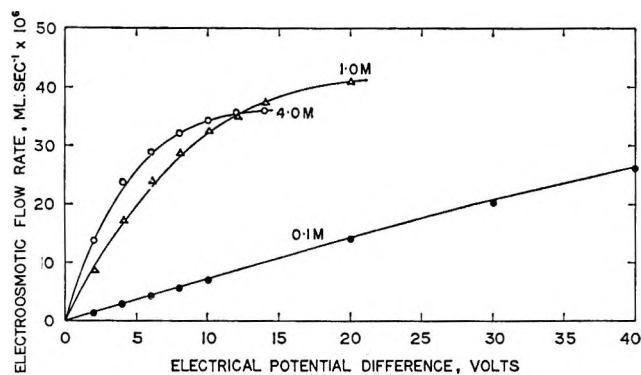


Figure 4. The variation of electroosmotic flow rate with electrical potential difference at 25°. The solutions of potassium chloride used were 0.1, 1.0, and 4.0 M.

coefficients L_{12}/T for electroosmotic flow across the ion-exchange membrane, which show a decreasing tendency with increasing electrical potential difference. A self-consistent set of phenomenological coefficients L_{12}/T for electroosmotic flow may be estimated from the graphs by taking the limiting slopes of the plots. These limiting phenomenological coefficients L_{12}/T serve to correlate the electroosmotic flow behavior of the membrane for the various univalent cations.

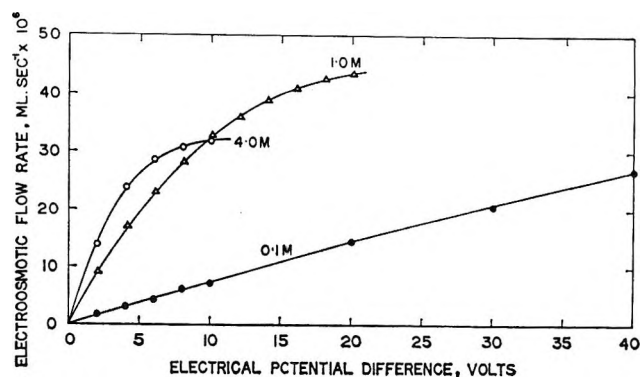


Figure 5. The variation of electroosmotic flow rate with electrical potential difference at 25°. The solutions of ammonium chloride used were 0.1, 1.0, and 4.0 M.

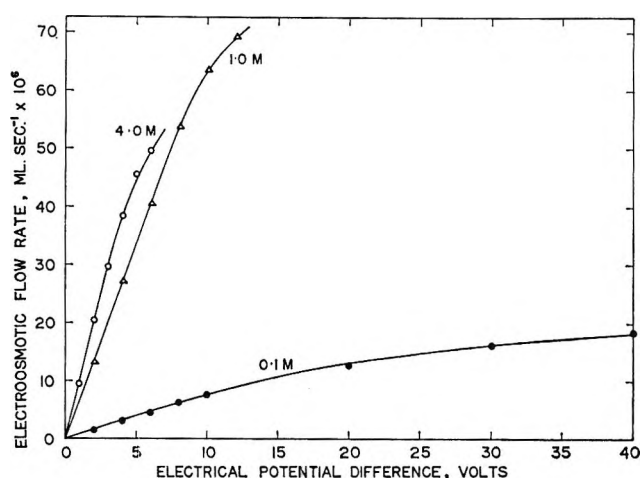


Figure 6. The variation of electroosmotic flow rate with electrical potential difference at 25°. The solutions of hydrochloric acid used were 0.1, 1.0, and 4.0 M.

Samples of such values of phenomenological coefficients L_{12}/T (limiting slopes of plots of electroosmotic flow against electrical potential difference) for various solutions of ammonium chloride, potassium chloride, sodium chloride, and hydrochloric acid are given in Table II. It may be seen that the phenomenological coefficient L_{12}/T of the membrane for electroosmotic flow tends to increase with increasing external solution concentration and also in the order ammonium, potassium, sodium, and hydrogen.

The combined effects of electrical and chemical

Table II: Phenomenological Coefficients for Electroosmotic Flow

System	$L_{12}/T, \text{ ml sec}^{-1} \text{ V}^{-1} \times 10^4$		
	0.1 M	1.0 M	4.0 M
NH ₄ Cl	0.80	4.4	6.4
KCl	0.80	4.7	6.6
NaCl	0.85	5.0	7.5
HCl	0.80	6.8	10.0

potential differences on volume flow were determined using unsymmetrical external solution concentrations of sodium chloride. Examples of the results of volume flow, which have been obtained in three series of experiments (A, B, and C), are given in Table III. In experiments A, where the chemical potential difference caused the flow of solvent in the direction of the convection produced by the electrical potential difference, the values of solvent transport are large. For experiments B, in which the chemical potential difference moved the solvent in opposite direction to the convection produced by the electrical potential difference, the values of solvent transport are low. In experiments C, where no electrical potential difference was applied between the unsymmetrical solutions of sodium chloride, the chemical potential difference caused the flow of solvent. The close agreement obtained between the sum of volume flows for experiments A and B and twice the value found in experiments C substantiates the validity of the linear phenomenological eq 3 in the range of study.

A comparison may be made between the experimental values of water transference numbers (W_T) and

$(L_{12}/L_{22})(F/18)$. The results obtained by direct measurements are given in Table IV. These results may be compared with values of $(L_{12}/L_{22})(F/18)$ calculated from membrane-exchange capacity and moisture content, using eq 10, which are also shown in Table IV. It

Table IV: Membrane Transference Numbers for Water

System	Soln concn, M	W_T , exptl, direct meast	$(L_{12}/L_{22})(F/18)$	
			Exptl	Calcd eq 10
NaCl	0.1	7.9	7.2	8.0
	1.0	5.6	5.4	6.3
	4.0	3.3	3.7	4.4
KCl	0.1	5.1	5.5	
	1.0	3.9	3.6	
	4.0	2.8	2.1	
NH ₄ Cl	0.1	4.9	5.2	
	1.0	3.6	3.2	
	4.0	2.6	1.9	
HCl	0.1	2.0	2.0	
	1.0	1.7	1.7	
	4.0	1.2	1.1	

Table III: Volume Flow under Combined Electrical and Chemical Potential Differences

—NaCl soln concn, M —		Net vol flow ^a into half-cell 2, ml sec ⁻¹ × 10 ⁶		
Half-cell 1	Half-cell 2	Expt A	Expt B	Expt C
0.05	0.1	5.32	-3.99	0.66
0.1	0.2	5.20	-3.07	1.09
0.2	0.4	5.49	-2.34	1.55
0.5	1.0	7.02	0.55	3.73
1.0	2.0	12.88	6.82	9.95
2.0	4.0	19.01	15.03	17.12

^a Volume flow from half-cell 2 into half-cell 1 is considered negative.

may be seen that, within the limits of experimental error and the uncertainty in the values of L_{12}/T , fair agreement is found between the values of W_T and the quantity $(L_{12}/L_{22})(F/18)$ obtained by direct measurements with values of this quantity estimated from membrane properties. This analysis indicates that useful information on volume flow across an ion-exchange membrane during cation migration may be obtained from simple measurements of the exchange capacity and moisture content of the membrane.

Acknowledgment. The author is indebted to the National Research Council, Ottawa, Ont., Canada, for financial support.

Composition of Electrosorbed Methanol

by T. Biegler

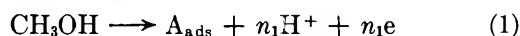
Division of Mineral Chemistry, CSIRO, Port Melbourne, Victoria, Australia (Received October 12, 1967)

The composition of the dehydrogenated species formed when methanol adsorbs from acid solution onto a smooth Pt electrode is examined by electrochemical techniques. Use is made of the fact that adsorption of methanol and oxidation of the adsorbed species can be studied separately. This allows determination of the charges involved in adsorbing (Q_{ads}) and stripping off (Q_{ox}) a given quantity of adsorbed intermediate. Q_{ads} is measured by integration of current-time curves for methanol adsorption and Q_{ox} by linear-sweep voltammetry after washing the electrode. The ratio $Q_{\text{ads}}/Q_{\text{ox}}$ is potential dependent, a result for which several explanations are suggested. $Q_{\text{ox}}^{\text{max}}$ is found to be $278 \mu\text{C}/\text{cm}^2$. The most probable composition of the adsorbed species is one for which two electrons are released when each particle is oxidized to CO_2 . At potentials below 0.4 V part of the adsorbed layer may be in a more reduced form. Comparison of current-voltage curves for adsorbed methanol, carbon monoxide, and "reduced CO_2 " indicates some similarities among the three species and suggests that part of the surface layers formed on adsorption of methanol and "reduced CO_2 " is the same as adsorbed carbon monoxide.

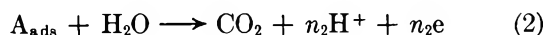
Introduction

Electrocatalytic oxidations of many organic compounds, including methanol, involve adsorbed intermediates which have more than a transitory existence at the electrode surface. Naturally enough, attention has been concentrated on establishing the nature of these stable species although it should always be remembered that such multistep electrode reactions undoubtedly proceed by way of numerous more elusive intermediates.

In the case of the electrooxidation of methanol on platinum in sulfuric acid solution, it has recently been shown¹⁻⁵ that the stability of the adsorbed species follows from the fact that at low potentials (0.2-0.5 V) the dehydrogenation reaction



which gives rise to the intermediate A_{ads} is much faster than the further oxidation of A_{ads} to CO_2 , which can be written as



A reasonable quantitative picture for the low-potential region can be obtained by considering the over-all reaction to proceed by way of these two successive irreversible steps, both obeying Elovich kinetics. According to this scheme, the steady-state coverage by intermediate is reached when the rates of reactions 1 and 2 are equal. In earlier work⁶ it was not recognized that the species present on the electrode surface at low potentials was not methanol itself.

In view of the large difference in rates of the two steps at low potentials, it should be possible to determine the oxidation state of the intermediate by comparing the charges released during adsorption (reaction 1) and oxidation (reaction 2) of a given quantity of A_{ads} . In the following these charges will be referred

to as Q_{ads} and Q_{ox} , respectively, and their ratio as R . From (1) and (2) it follows that

$$\frac{Q_{\text{ads}}}{Q_{\text{ox}}} = R = \frac{n_1}{n_2} \quad (3)$$

Bagotskii and coworkers^{4,7} measured Q_{ads} by integrating the current-time curve for methanol adsorption after a cathodic potential step from 1.2 V to the potential of interest or after adding methanol to a cell containing supporting electrolyte in which the electrode was being held at this potential. Rapid anodic potential sweeps (80-160 V/sec) were used to obtain Q_{ox} , contributions from bulk methanol being eliminated by the high sweep rate. These authors found Q_{ads} and Q_{ox} to be equal and concluded that $n_1 = n_2 = 3$, since $n_1 + n_2 = 6$. With this evidence they assigned the composition C-OH to the adsorbed intermediate.

A potential-step technique for examining methanol adsorption onto a clean platinum surface was developed independently by Biegler and Koch,⁵ who used it to estimate $Q_{\text{ads}}^{\text{max}}$, the maximum value of Q_{ads} ; the value found was about $440 \mu\text{C}/\text{cm}^2$. The corresponding oxidation charge was taken to be around $190 \mu\text{C}/\text{cm}^2$,^{2,6} giving $R = 2.3$ for the case of maximum coverage. It was concluded⁵ that $n_1 = 4$, $n_2 = 2$, and the oxidation state of A_{ads} corresponded to that of CO.

(1) V. S. Bagotskii and Yu. B. Vasil'ev, *Electrochim. Acta*, **9**, 869 (1964).

(2) K. Lal, O. A. Petrii, and B. I. Podlovchenko, *Elektrokhimiya*, **1**, 316 (1965).

(3) O. A. Petrii, B. I. Podlovchenko, A. N. Frumkin, and K. Lal, *J. Electroanal. Chem.*, **10**, 253 (1965).

(4) V. S. Bagotskii and Yu. B. Vasil'ev, *Electrochim. Acta*, **11**, 1439 (1966).

(5) T. Biegler and D. F. A. Koch, *J. Electrochem. Soc.*, **114**, 904 (1967).

(6) M. W. Breiter and S. Gilman, *ibid.*, **109**, 622 (1962).

(7) S. S. Beskorovainaya, Yu. B. Vasil'ev, and V. S. Bagotskii, *Elektrokhimiya*, **2**, 167 (1966).

In a radiotracer study of methanol adsorption⁸ it was suggested that at low potentials on prerduced electrodes the surface species consisted of methyl radicals while at higher potentials formation and polymerization of CH₂ radicals occurred.

Recently, Breiter⁹ studied the intermediates formed during oxidation of methanol, formic acid, and formaldehyde on platinized platinum. The use of charging curves combined with gas chromatography led to the conclusion that two electrons were released during the formation of a CO₂ molecule from each adsorbed radical; *i.e.*, in the present notation for methanol, $n_2 = 2$.

In this communication, previous work⁵ on establishing the nature of the adsorbed species through eq 3 is extended. Current-time curves for adsorption of methanol onto smooth platinum are used, as before,⁵ to determine the charge (Q_{ads}) passed in forming a chemisorbed layer. After washing the electrode, the charge associated with oxidation of this layer is determined by means of anodic linear-sweep voltammetry.

Experimental Section

Apparatus. The all-glass cell was designed to allow use of a fairly small quantity (~40 ml) of solution. The main compartment contained the working electrode (30- or 34-gauge platinum wire sealed into soft glass) and a platinum-foil counterelectrode. Into the side of this compartment was sealed a Luggin capillary which connected with a small reference electrode compartment. This was designed so that it was completely filled with electrolyte and sealed when the reference electrode was inserted, thus avoiding entrance of nitrogen bubbles into the Luggin capillary during the pressure changes accompanying the washing procedure described below.

Supporting electrolyte and methanol solutions were held in two reservoirs provided with facilities for degassing with purified nitrogen. A three-way tap allowed addition of either solution to the cell *via* a side arm. Cell contents could be blown out with nitrogen through an outlet tube. In this way, replacement of solutions and washing of the cell with supporting electrolyte could be carried out in the absence of air.

A mercury-mercurous sulfate, 1 *M* sulfuric acid electrode was used as reference. Its potential was 0.68 V with respect to a reversible hydrogen electrode (rhe) in 1 *M* H₂SO₄ to which all potentials in this work are referred. Experiments were carried out at room temperature (22 ± 2°).

The electrode potential was controlled by a Wenking fast-rise potentiostat and programmed with a sawtooth-function generator, constructed in this laboratory, together with a bias unit of potential dividers and switches for potential steps and pulses. Current-voltage curves were recorded on a Moseley 7035A X-Y recorder and fast-current transients on a Tektronix Type 533 oscilloscope. External time-base Type 17108A

(Moseley) was used in conjunction with the X-Y recorder for displaying longer term current-time traces.

Area Determinations. Electrode areas were determined by measuring the amount of hydrogen adsorbed from 1 *M* H₂SO₄ during a cathodic potential sweep. The surface was first cleaned by a series of potential steps between 0.58 and 1.55 V; then it was held at 0.58 V for 10 sec, and the cathodic sweep was started. A sweep rate of 37 mV/sec, although slower than recommended by some workers,^{10,11} was found convenient and gave results in good agreement with sweep rates up to 4 V/sec. Gilman's procedure¹¹ was used for integrating these curves to obtain the saturation hydrogen coverage Q_{H}^{S} . This quantity was determined before and after each run because of area changes which were observed during these experiments. These changes are discussed in a separate communication.¹² "Real" electrode areas were calculated on the basis that $Q_{\text{H}}^{\text{S}} = 210 \mu\text{C}/\text{real cm}^2$.

Procedure. Current-time (I_1-t) curves for adsorption of methanol were measured, as before,⁵ by applying a short (15–50 msec) rectangular potential pulse between the potential of interest, ϕ_{ads} , and 1.55 V, causing formation and removal of an oxide layer on the electrode with subsequent chemisorption of methanol onto a bare surface. The solution was left unstirred during the adsorption process. After the appropriate adsorption time, the methanol solution was blown out and supporting electrolyte was added. This was again blown out, a further batch of acid added, and an anodic potential sweep, generally 37 mV/sec, was run, starting from ϕ_{ads} . In the presence of adsorbed methanol, a current peak appeared at about 0.78 V (Figure 1). With repetitive sawtooth scanning this peak was absent from the second and subsequent curves, as observed in previous work² with washed electrodes bearing adsorbed methanol. The washing procedure was adequate to ensure that dissolved methanol remaining in the cell did not contribute significantly to the current during a potential sweep so long as the initial methanol concentration was less than about 1 *M*.

There exists with this technique the possibility of errors due to adsorption from a film of solution adhering to the electrode while at open circuit for about 15 sec between removal of the methanol solution and addition of the first batch of supporting electrolyte. Such errors were minimized by allowing adsorption under controlled-potential conditions to proceed until the rate was small enough to ensure that further adsorption for 15 sec would make a negligible contribution to the

(8) R. E. Smith, H. B. Urbach, J. H. Harrison, and N. L. Hatfield, *J. Phys. Chem.*, **71**, 1250 (1967).

(9) M. W. Breiter, *J. Electroanal. Chem.*, **14**, 407 (1967).

(10) F. G. Will and C. A. Knorr, *Z. Elektrochem.*, **64**, 258 (1960).

(11) S. Gilman, *J. Phys. Chem.*, **67**, 78 (1963).

(12) T. Biegler, *J. Electrochem. Soc.*, **114**, 1261 (1967).

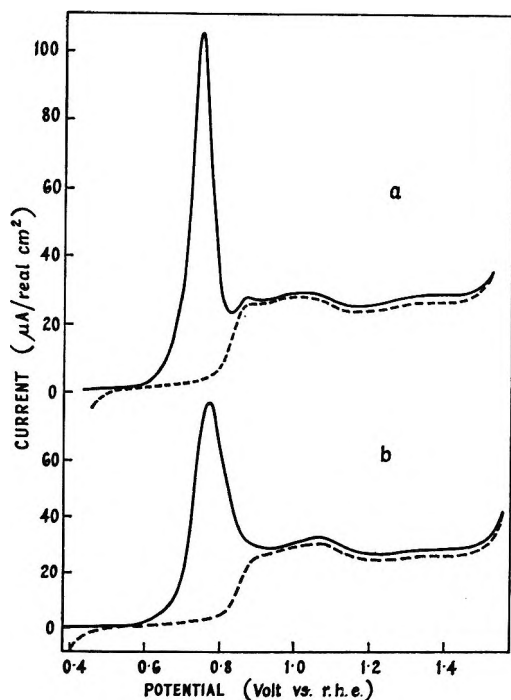


Figure 1. Anodic sawtooth sweeps for a washed electrode after 2-min adsorption of methanol from (a) 0.02 *M* methanol in 0.1 *M* sulfuric acid at 0.43 V and (b) 0.10 *M* methanol in 1 *M* sulfuric acid at 0.38 V. Broken curves show the second sawtooth sweeps. Sweep rate 37 mV/sec.

total amount of methanol adsorbed. An adsorption time of 2 min generally fulfilled this condition. The total time between the end of the adsorption period and the start of the stripping sweep was 60–70 sec.

Solution purity was found to be an important factor, mainly because of the vigorous agitation of the solution during emptying and refilling of the cell. In methanol adsorption experiments and also in blank runs with 1 *M* H₂SO₄ made up from AnalaR reagent, a broad peak in the region 1.0–1.5 V was observed and several sweeps were needed before it disappeared. On the other hand, in unstirred 1 *M* H₂SO₄, the absence of significant changes in current-voltage curves indicated that electrodes remained clean for at least 5 min. Further evidence for an impurity was given by the fact that the second peak was lowered by using 0.1 *M* H₂SO₄ or by purifying the acid by distillation under reduced pressure (boiling point around 160°). Even so, traces of impurities remained, as indicated by small differences in current in the oxide region (0.9–1.5 V) for the first and second sweeps of Figures 1 and 2. All results reported here were obtained with purified acid.

Evaluation of Q_{ads} and Q_{ox} . Q_{ads} was determined as before⁵ by integration of I_1-t curves, starting from the time of application of the cathodic potential step (i.e., 1.55 V \rightarrow ϕ_{ads}). Currents for short times, where the cathodic current for oxide reduction predominated, were taken from extrapolated I_1^{-1} vs. t plots; linear plots of approximately constant slope, indicating that

the reaction obeys Elovich kinetics, were found at all but the highest potentials studied.⁵ In general, the lower the potential the longer was the fit to Elovich kinetics. Below 0.35 V, I_1^{-1} vs. t plots often fitted Elovich kinetics for the whole of the adsorption period (2 min). Analytical integration of current-time curves was used where the I_1^{-1} vs. t plot was linear; otherwise curves were integrated graphically.

Q_{ox} was obtained by graphical integration of the peak in the anodic stripping curve. The second sweep, or a blank curve in sulfuric acid alone, was used as the base line for this integration. This assumes that oxidation of the platinum surface and the adsorbed organic occur independently, an assumption which requires that the first and second curves coincide at potentials anodic to the methanol peak. Although this never occurs in practice because of residual impurity adsorption, the fact that at high methanol coverages in purified solutions the curves are very close together (Figure 1) indicates that the procedure is justified.

Results and Discussion

Irreversibility of Methanol Adsorption. Several procedures were tried to determine any losses of adsorbate during and after replacement of the methanol solution with supporting electrolyte. The time of contact with supporting electrolyte was purposely extended, either by holding for 2 min at the initial potential before starting the anodic stripping scan or by increasing to 4 the number of times the supporting electrolyte was changed. In neither case was there a significant decrease in Q_{ox} . Similarly, the stripping peak did not alter when the period during which the electrode was at open circuit (out of the solution) was extended. These experiments do not rule out the possibility that loss of a weakly adsorbed fraction occurs rapidly upon contact with supporting electrolyte. However, any further loss of adsorbate is shown to be very slow.

In one experiment, methanol was adsorbed at 0.48 V for 60 sec from 0.1 *M* methanol in 1 *M* H₂SO₄, and the solution was replaced with 1 *M* H₂SO₄ alone. The potential was then lowered to 0.08 V and held there for 60 sec after which the anodic sweep was started. Q_{ox} was the same as when the period at 0.08 V was omitted, indicating that the adsorbed layer remained unaltered at the lower potential.

These experiments emphasize the irreversible nature of methanol chemisorption and support the earlier interpretation⁵ of methanol adsorption in terms of successive irreversible reactions leading to a steady-state coverage by the adsorbed intermediate.

Results for Q_{ads} and Q_{ox} . Values of Q_{ads} and Q_{ox} , expressed as ratios of the saturation hydrogen coverage Q_{H}^{S} , are shown in Table I and may be converted to charges by multiplying by 210 $\mu\text{C}/\text{cm}^2$. It can be seen that there is a marked potential dependence of the ratio $Q_{\text{ads}}/Q_{\text{ox}}$, in contrast to the work of Beskorovainaya,

et al.,⁷ who found that $Q_{ox} = Q_{ads}$ in the potential range 0.2–0.4 V. These authors⁷ gave insufficient data to allow full comparison of the two sets of results but it appears that both Q_{ads} and Q_{ox} are much higher here than in their work. For example, after 2-min adsorption at 0.4 V from 0.1 M methanol and 0.5 M H₂SO₄, Beskorovainaya, *et al.*,⁷ found Q_{ads} and Q_{ox} to be 150 and 154 $\mu\text{C}/\text{cm}^2$, respectively. The corresponding figures from the present work (in 1 M H₂SO₄) are 386 and 256 $\mu\text{C}/\text{cm}^2$.

Table I: Charges Involved in Adsorbing (2 min) and Stripping Methanol Layers Formed under Various Conditions

Solution	Potential,	Q_{ads}/Q_H^S	Q_{ox}/Q_H^S	Q_{ads}/Q_{ox}
	V vs. r.h.e.			
0.05 M methanol, 1 M H ₂ SO ₄	0.28	0.88	0.64	1.37
	0.33	1.21	0.74	1.64
	0.38	1.43	0.87	1.65
	0.43	1.96	0.95	2.06
	0.48	3.06	0.98	3.1
0.1 M methanol, 1 M H ₂ SO ₄	0.28	1.18	0.85	1.39
	0.33	1.46	1.01	1.44
	0.38	1.73	1.17	1.48
0.5 M methanol, 1 M H ₂ SO ₄	0.18	0.89	1.19	0.75
	0.28	1.35	1.19	1.13
	0.33	1.56	1.22	1.28
	0.38	2.24	1.24	1.81
	0.43	3.09	1.31	2.36
0.02 M methanol, 0.1 M H ₂ SO ₄	0.48	5.20	1.20	4.3
	0.28	0.95	0.66	1.43
	0.33	1.20	0.74	1.62
	0.38	1.51	0.92	1.64
	0.43	1.99	1.01	1.98
	0.48	3.02	1.06	2.84

Part of the discrepancy in Q_{ads} can be attributed to the fact that Beskorovainaya, *et al.*,⁷ made no correction for the oxide reduction current which passes after the cathodic potential step. This was done in the present work by the extrapolation procedure outlined earlier. In this example, neglect of the correction would have reduced Q_{ads} by only 35 $\mu\text{C}/\text{cm}^2$ for the short anodic pulses used here. Beskorovainaya, *et al.*,⁷ held their electrode at 1.2 V for 5–20 sec before applying the cathodic potential step and it is known⁵ that the greater amount of oxide formed under these conditions leads to suppression of the early part of the current–time curve for methanol adsorption. Even so, it is difficult to believe that all of the discrepancy can be accounted for by this factor.

The fast anodic sweep used by Beskorovainaya, *et al.*,⁷ to determine Q_{ox} gives lower values than the present method which can be expected to give results erring only on the low side owing to losses of adsorbate on washing. The low values of Q_{ox} ⁷ are difficult to reconcile with the fact that Breiter and Gilman⁶ were able

show that Q_{ox} remained independent of sweep rate over the range 100–1000 V/sec. Breiter and Gilman⁶ found the maximum value of Q_{ox}/Q_H^S to be 0.88. Beskorovainaya, *et al.*,⁷ did not give a value for Q_{ox}^{max} but, according to earlier work,⁴ fractional coverage is 0.8 in the experiment for which they find $Q_{ox} = 154 \mu\text{C}/\text{cm}^2$. This leads to $Q_{ox}^{max}/Q_H^S = 0.92$. Both of these results are appreciably less than the value of 1.32 found here (see below). It appears that the fast-sweep method may cause some underestimation of the charge required to oxidize adsorbed methanol.

Maximum Coverage Conditions. Maximum coverage is known to be attained at high methanol concentrations (1 M and above) in the region 0.4–0.5 V.⁴ Determinations of Q_{ox}^{max} were made after adsorption for 2 min from 1 M methanol at 0.48 and 0.53 V. The ratio Q_{ox}^{max}/Q_H^S was found to be 1.32 ± 0.05 , yielding $Q_{ox}^{max} = 278 \pm 11 \mu\text{C}/\text{cm}^2$.

The area remaining available to hydrogen adsorption was also measured under these conditions by running a cathodic sweep after allowing maximum adsorption of methanol. The amount of hydrogen adsorbed was 40 $\mu\text{C}/\text{cm}^2$ (fractional coverage of 0.19), in good agreement with Khazova, *et al.*,¹³ who found that 15–20% of the surface was still available for hydrogen adsorption at maximum methanol coverage.

Interpretation of R Values. It can be seen from Table I that Q_{ox} values rise with increasing potential and tend to approach a limiting value, except in the case of 0.5 M methanol where Q_{ox} is fairly constant over the whole potential range examined. Q_{ads} , on the other hand, shows no signs of reaching a limiting value and in fact rises steeply at the positive end of the potential range. The variations in R result from the fact that Q_{ads} increases faster with potential than does Q_{ox} ; the sharp increase in R at potentials positive to 0.43 V is a reflection of a similar increase in Q_{ads} .

The simple reaction scheme for methanol adsorption and oxidation outlined previously⁵ requires that $R = 1, 2, \text{ or } 5$ or their reciprocals. The potential-dependent, nonintegral values of R found here indicate the possibility of a more complex mechanism. Several factors which could explain these results are discussed below.

(a) Variation of R could result from a potential dependence of adsorbate composition.⁸ For example, if C–OH were the preponderant form at low potentials and CO at higher potentials, R would increase from 1 to 2. Some indication of the existence of two adsorbed species is given by the presence of a shoulder or double peak (Figure 2) on curves obtained with low coverages at potentials below about 0.3 V. On the other hand, such an explanation cannot account for a large variation in R accompanied by an almost constant Q_{ox} , as found with 0.5 M methanol.

(13) O. A. Khazova, Yu. B. Vasil'ev, and V. S. Bagotskii, *Elektrokhimiya*, 1, 84 (1965).

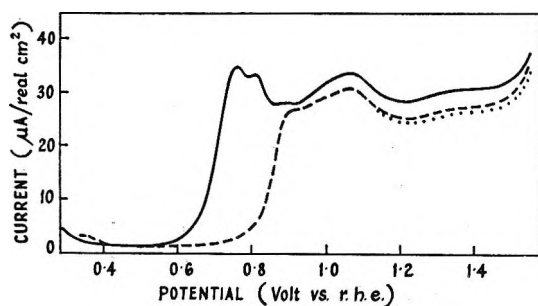
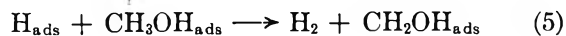


Figure 2. Anodic sawtooth sweeps for a washed electrode after 2-min adsorption at 0.28 V from 0.05 *M* methanol in 1 *M* sulfuric acid: —, first sweep; ---, second sweep;, third and subsequent sweeps. Sweep rate 37 mV/sec.

(b) The current which flows during methanol adsorption results from dehydrogenation with the release of protons and electrons. As the potential is lowered, the formation of adsorbed H atoms is favored over the formation of a separate proton and electron. At the same time one can expect an increased tendency for reaction 1 to become



Any formation of A_{ads} by this pathway will cause R to be less than n_1/n_2 . Such an explanation would require that some hydrogen leave the surface, presumably as H_2 , during the adsorption process since this commences on a surface already partly covered with hydrogen (kinetics of H adsorption is much faster than that of methanol). The mechanism of such hydrogen loss without charge transfer can be envisaged as a pairing between an adsorbed H atom and an H atom from an adjacent adsorbed methanol molecule, *e.g.*



In this process, Pt-C bonds form, Pt-H and C-H bonds weaken, and consequently H-H bonds can form. H_2 desorbs with the end result that the methanol molecule loses an H atom without passage of current through the external circuit.

(c) Values of R exceeding 2 at potentials anodic to about 0.43 V (depending on methanol concentration) could be explained by one or more of the following postulates.

(i) The adlayer at these potentials contains a proportion of an intermediate for which $n_2 = 1$. This is considered unlikely in view of the fact that Q_{ox} remains constant (in 0.5 *M* methanol) or increases only slightly over the potential range 0.38–0.48 V, a result which requires that two particles of the adsorbed species for which $n_2 = 1$ occupy the same site as one particle having $n_2 = 2$.

(ii) Higher potentials favor reaction pathways leading to formation of stable, soluble intermediates (*e.g.*, formic acid, formaldehyde^{14–16}) which can diffuse away from the electrode. Since the oxidation of

methanol to these intermediates would contribute to Q_{ads} without a corresponding contribution to Q_{ox} , this mechanism would tend to give higher apparent values of R than are characteristic of the adsorbed species.

(iii) The condition that reaction 2 can be ignored is no longer fulfilled when $\phi_{\text{ads}} > 0.43$ V. The finding that it is just at those potentials for which $R > 2$ that major deviations from Elovich kinetics occur lends support to this explanation. Currents are higher than expected from the kinetics of reaction 1 and do not decay to zero even after several minutes of adsorption. Both facts suggest that further oxidation of intermediate to CO_2 occurs at these potentials and gives rise to spuriously high values of Q_{ads} .

Composition of Adsorbed Intermediate. Deduction of the nature of the adsorbed species from the observed R values is not as straightforward as supposed earlier.⁵ Although the above discussion provides reasonable explanations for the potential dependence of R , complete interpretation would require further evidence on the quantitative significance of each factor. The species corresponding to $n_1 = n_2 = 3^{4.7}$ is undoubtedly not the only one formed since R is almost always greater than unity. Furthermore, assumption of three-site adsorption of such a species^{4,7} with 80% of Pt sites occupied at maximum coverage would lead to $Q_{\text{ox}}^{\text{max}} = 170 \mu\text{C}/\text{cm}^2$, well below that observed.

The most likely interpretation is that $n_2 = 2$ for the predominant species present at potentials higher than about 0.4 V. At lower potentials, where $R < 2$, an unspecified proportion of the adsorbate may be in a more reduced form, *i.e.*, $n_2 > 2$. It is not possible to separate the effect of such a component on R from the effects outlined under (b) above. Further support for a species with $n_2 = 2$ comes from the work of Breiter⁹ cited earlier.

The possible compositions of species having $n_2 = 2$ have been tabulated by Breiter.⁹ Species with more than two carbon atoms are regarded as unlikely, leaving CO , H_2CO_2 , C_2O_2 , and $\text{H}_2\text{C}_2\text{O}_3$. Breiter⁹ has pointed out differences and similarities between charging curves for adsorbed CO and the intermediates formed from methanol, formic acid, and formaldehyde. Further comparisons will be made in the following section.

Given that $Q_{\text{ox}}^{\text{max}}$ is $278 \mu\text{C}/\text{cm}^2$ and $n_2 = 2$, it can be concluded that at least some of the intermediate particles are adsorbed on a single Pt site. If this were true for all of the adsorbate, then, on a surface with maximum coverage, 66% of the sites are covered, 19% are still capable of adsorbing hydrogen, and the remaining 15% are not. The data can also be satisfied

(14) T. O. Pavela, *Ann. Acad. Sci. Fennicae*, A59 (1954).

(15) R. P. Buck, L. R. Griffith, R. T. MacDonald, and M. J. Schlatter, *Proc. 15th Annual Power Sources Conf.*, 16 (1961).

(16) S. Gilman and M. W. Breiter, *J. Electrochem. Soc.*, 109, 1099 (1962).

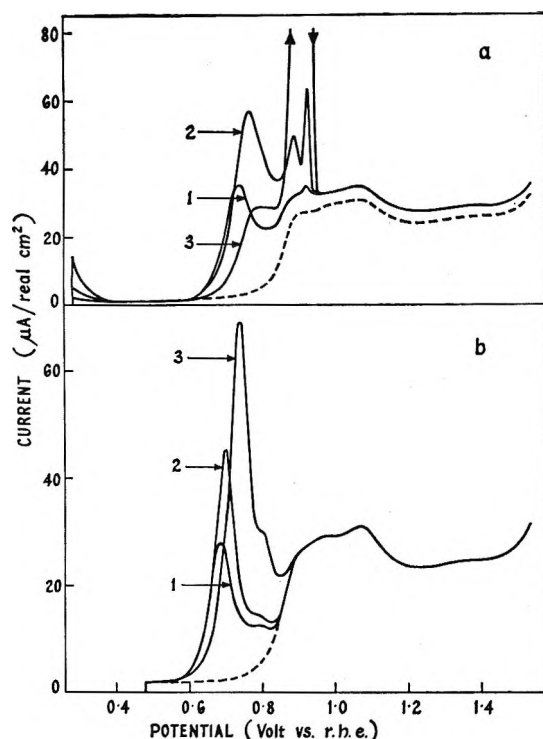


Figure 3. Anodic current-voltage curves for (a) CO adsorbed at 0.28 V from dilute solution ($\sim 2 \times 10^{-6} M$) in 1 M sulfuric acid, where adsorption time was (1) 10 sec, (2) 40 sec, and (3) 80 sec; (b) reduced CO_2 formed at 0.08 V in 1 M sulfuric acid saturated with CO_2 , where the electrode was held at 0.08 V for (1) 10 sec, (2) 20 sec, and (3) 120 sec. Broken curves are for 1 M sulfuric acid alone. All sweep rates 37 mV/sec.

by considering that all of the sites (81%) not available to hydrogen are in fact attached to an adsorbed methanol fragment. This requires that 51% of the sites each hold one particle and 30% share an adsorbate molecule between two Pt atoms (bridged form). There is no real evidence to distinguish between these two arrangements or something between them. However, as one would hardly expect all sites not directly involved in bonding with adsorbate to show the same activity for H adsorption as does a bare platinum surface, the second extreme case described above is considered unlikely.

Comparison with Other Adsorbed Species. Anodic current-voltage curves for adsorbed CO and the species known as "reduced CO_2 "¹⁷ are shown in Figure 3. The experiments with CO were designed to obtain results for small coverages at the sweep rate used with methanol. This was achieved by saturating 1 M H_2SO_4 with CO and then purging with N_2 until the CO concentration was sufficiently small to allow effective control of the amount adsorbed by the rate of diffusion. The solution was left unstirred, the surface cleaned with a few pulses between 0.28 and 1.55 V, adsorption allowed to occur at 0.28 V for a period, and the anodic sweep commenced. Calculations from the initial rate of adsorption indicated that the CO concentration was

around $2 \times 10^{-5} M$. The small diffusion current in the oxide region (Figure 3a) was of the magnitude expected for such a concentration.

Reduced CO_2 was formed by holding the electrode at 0.08 V in 1 M H_2SO_4 saturated with CO_2 . The adsorption period was preceded by a few anodic cleaning pulses between 0.08 and 1.55 V. After the final cleaning pulse adsorption was left to proceed for a time, the potential was then switched to 0.48 V where adsorption ceased¹⁷ and the anodic scan started. Maximum coverage under these conditions was $190 \mu\text{C}/\text{cm}^2$. From Figure 3b there seems to be no question that a distinct surface species is formed, in contrast to the view of Piersma, *et al.*¹⁸

It is notable that such slow sweeps show more detailed structure than charging curves^{9,19} and fast sweeps¹¹ used to study adsorbed layers. Interpretation is correspondingly more difficult and no attempt will be made here to account in detail for the shapes of these curves.

Adsorbed methanol, CO, and reduced CO_2 all show a peak in the region 0.70–0.78 V. This low-potential peak for CO does not appear to have been reported previously; Gilman¹¹ examined low CO coverages using only fast sweeps (360 V/sec) and was therefore unable to observe it. With increasing coverage the peak reaches a maximum and then decreases at the expense of the characteristic sharp and high peak at 0.94 V. Such an effect is expected from what is known about inhibition of CO oxidation at high coverages.^{20,21} However, Figure 3a shows that the peak at 0.94 V develops even at low coverages and, moreover, a third peak can be seen at intermediate potentials. These peaks are absent for adsorbed methanol and reduced CO_2 . Another difference is that inhibition of the first CO peak commences when the coverage exceeds about $190 \mu\text{C}/\text{cm}^2$. This effect was not found for methanol up to the maximum coverage ($278 \mu\text{C}/\text{cm}^2$). Coverages higher than $190 \mu\text{C}/\text{cm}^2$ were not obtained with reduced CO_2 so in this case the comparison cannot properly be made.

It can be concluded from the above description that there are several differences between the properties of these three adsorbed species. On the basis of shapes of charging curves, Breiter⁹ considered that intermediates from methanol, formic acid, and formaldehyde were very similar but found that adsorbed CO gave a slightly different behavior. However, he suggested²² that adsorbed CO and reduced CO_2 were identical. In the present study there are enough similarities to sug-

(17) J. Giner, *Electrochim. Acta*, **8**, 857 (1963).

(18) B. J. Piersma, T. B. Warner, and S. Schuldiner, *J. Electrochem. Soc.*, **113**, 841 (1966).

(19) S. B. Brummer and J. I. Ford, *J. Phys. Chem.*, **69**, 1355 (1965).

(20) S. Gilman, *ibid.*, **66**, 2657 (1962).

(21) S. Gilman, *ibid.*, **68**, 70 (1964).

(22) M. W. Breiter, *Electrochim. Acta*, **12**, 1213 (1967).

gest that at least part of the surface layers formed upon adsorption of methanol and reduced CO_2 is the same as adsorbed CO. Unfortunately, there is insufficient evidence to allow a more definite conclusion.

A final comment on the comparison of adsorbed species of different origins seems appropriate at this point. An obvious and commonly used²³ criterion for such a comparison is the amount of adsorbate present at maximum coverage. We feel that this is not a reliable diagnostic property for the following reasons. Maximum coverage is reached when the rate of adsorption of the bulk species, present at high concentration, becomes equal to the rate of desorption of the surface species. In the examples of interest, adsorption is catalyzed by the electrode surface and the rate of

adsorption generally decreases as coverage increases. The adsorption rate is, of course, a function of the nature of both the initial reactant and the adsorbed intermediate. Hence, even if a group of compounds gives rise to identical adsorbed species, the steady-state coverage will depend on the initial species. Maximum coverage alone is therefore an inadequate criterion of the nature of the surface species.

Acknowledgment. The author wishes to thank Dr. D. F. A. Koch with whom he had many helpful discussions and Dr. K. J. Cathro who designed and constructed the sawtooth-function generator.

(23) S. B. Brummer, *J. Phys. Chem.*, **69**, 1363 (1965).

Radiation-Induced Solid-State Polymerization of Derivatives of Methacrylic Acid. IV. Electron Spin Resonance Spectra of Barium Methacrylate Dihydrate

by M. J. Bowden and J. H. O'Donnell

Chemistry Department, University of Queensland, Brisbane, Australia (Received October 12, 1967)

The esr spectrum of γ -irradiated barium methacrylate dihydrate at -196° , attributed to the radical $(\text{CH}_3)_2\dot{\text{C}}\text{-COO}^-$, was observed to change to the spectrum characteristic of the propagating radical $\text{RCH}_2\dot{\text{C}}(\text{CH}_3)\text{COO}^-$ on warming above -100° . This transformation was temperature and time dependent. The spectrum of the propagating radical after several days at -80° consisted of 9 lines with hfs of 11.5 G and an increasing intensity distribution. Immediately on warming to 50° the spectrum was similar, but on cooling back to -80° an alternating intensity distribution was observed, and further cooling to -154° resulted in splitting of the intermediate lines; this effect was reversible. When maintained at 50° , the intensities of the intermediate lines decreased continuously so that the increasing intensity distribution changed to an alternating intensity distribution and finally to a 5-line spectrum. These different spectra are all attributed to the methacrylate propagating radical and are considered to result from different conformations of the β -methylene carbon-hydrogen bonds. The conformation of the radical, and hence the esr spectrum, is believed to depend on (1) the length of the radical chain, (2) the temperature, and (3) the environment. Various models are considered to explain the changes in conformation.

Introduction

The interpretation of the electron spin resonance (esr) spectrum obtained from methacrylate monomers and polymers by a variety of methods has been the subject of considerable controversy over many years. The well-known 9-line (5- + 4-line) spectrum with an alternating intensity distribution and hyperfine splitting (hfs) of 11.5 G was first reported by Schneider, from the X irradiation of poly(methyl

methacrylate).¹ Later, it was shown that the same spectrum resulted from γ irradiation² or mechanical degradation.³ A similar spectrum was also obtained

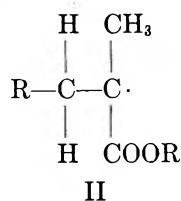
(1) E. E. Schneider, M. J. Day, and G. Stein, *Nature*, **168**, 645 (1951).

(2) R. J. Abraham, H. W. Melville, D. W. Ovenall, and D. H. Whiffen, *Trans. Faraday Soc.*, **54**, 1133 (1955).

(3) S. E. Bresler, E. N. Kazbekov, and E. M. Saminskii, *Polymer Sci. (U.S.S.R.)*, **1**, 55 (1960).

from occluded radicals in gelled, polymerizing methacrylate monomers.^{4,5}

The controversy has been mainly whether the observed 9-line spectrum is due to one or two radical species. The interpretation in terms of a single radical species, *viz.*, the propagating radical



has gained persuasive weight over the past few years. Symons⁶ first postulated that the alternating intensity distribution of the 9 lines could be explained by an asymmetrical arrangement of the two β -methylene carbon-hydrogen bonds relative to the p orbital of the unpaired electron. O'Donnell, McGarvey, and Morawetz⁷ showed that in γ -irradiated barium methacrylate dihydrate at 20° this corresponded to a twist of about 4°. Fischer⁸ found that the spectrum obtained from methacrylic acid, methyl methacrylate, and ethyl methacrylate in a titanous chloride-hydrogen peroxide aqueous redox flow system contained 16 lines, but that these are in groups which would coalesce at greater line widths to give the 9-line spectrum of alternating intensity. Kourim and Vacek⁹ have investigated the spectra from deuterated poly(methyl methacrylates) irradiated in air at ambient temperature and their results are consistent with a single radical (II).

A fundamental difficulty in studying the esr spectra of irradiated solids is that more than one type of radical may be present. This is particularly true for polymers which undergo main-chain scission, *e.g.*, poly(methacrylates).¹⁰ Reaction of the second radical with residual monomer has frequently been postulated¹¹ to account for the apparent appearance of only one radical species, and anomalous spectra (tending toward 5 lines) have been observed in vigorously purified polymer.¹²

When barium methacrylate dihydrate is irradiated at -196° and then warmed to 50°, appreciable polymerization occurs and apparently the only radical species present is the propagating radical (II). However, anomalous intensity distributions of the 9-line spectra, varying from an increasing intensity distribution to an alternation approaching a 5-line spectrum have been observed. This paper describes a careful examination of the temperature dependence of the spectrum and provides an explanation of these apparently anomalous results.

Experimental Section

Barium methacrylate dihydrate was prepared and recrystallized as previously described.⁷ Single crystals and finely ground powder were sealed in Spectrosil

ultrahigh-purity silica tubes under vacuum. They were irradiated at -196° with ⁶⁰Co γ rays and stored in liquid nitrogen until measurement.

The esr spectra were obtained with a Varian V4502 instrument, which was fitted with a dual sample cavity. A liquid-nitrogen dewar was inserted in the cavity for measurements at -196° and a Varian variable-temperature accessory was used for measurements between -170 and 50°. The actual temperature of the sample was obtained by calibration of the temperature controller with a standardized thermocouple. The spectra saturated readily; therefore, a low microwave power level (0.52 mW = 25 db) was used for all measurements. Relative radical concentrations were obtained by double integration of the recorded first-differential spectra using a computer.

Theoretical spectra were calculated for various values of (1) line positions, (2) line widths, (3) relative line intensities, and (4) line shapes, using the C.S.I.R.O. CDC 3600 computer and drawn by a Calcomp plotter. The expression used for the first derivative of a resonance line with a Gaussian shape was

$$I = (4I_0/\Delta H^2)(H_0 - H) \exp\{-2[(H - H_0)/\Delta H]^2\}$$

and for a Lorentzian line shape was

$$I = (8I_0/3\Delta H^2)(H_0 - H) \times \{1/(1 + 4/3[(H - H_0)/\Delta H]^2)\}$$

where I is the amplitude of the resonance; I_0 is the value of I at resonance position, *i.e.*, maximum amplitude; ΔH is the line width measured between positions of maximum and minimum slope of the resonance line; H is the magnetic field, and H_0 is the value of H at the resonance position.

Results and Discussion

Spectrum at -196°. The esr spectrum of barium methacrylate dihydrate at -196° after γ irradiation (Figure 1a) consisted predominantly of 7 equally spaced lines with a binomial intensity distribution and hfs of 23 G. This spectrum is similar to that reported by O'Donnell, McGarvey, and Morawetz⁷ and has been attributed to the initiating radical (I) formed by addition of a hydrogen atom to a monomer molecule.

(4) D. J. E. Ingram, M. C. R. Symons, and M. G. Townsend, *Trans. Faraday Soc.*, **54**, 409 (1958).

(5) N. Nishimura, *J. Makromol. Sci.*, **A-1**, 257 (1966).

(6) M. C. R. Symons, *J. Chem. Soc.*, 277 (1963).

(7) J. H. O'Donnell, B. McGarvey, and H. Morawetz, *J. Am. Chem. Soc.*, **86**, 2322 (1964).

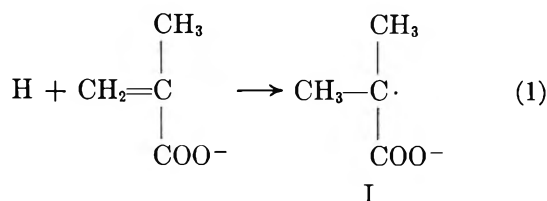
(8) H. Fischer, *J. Polymer Sci.*, **B-2**, 529 (1964).

(9) P. Kourim and K. Vacek, *Trans. Faraday Soc.*, **61**, 415 (1965).

(10) P. Alexander, A. Charlesby, and M. Ross, *Proc. Roy. Soc. (London)*, **A223**, 392 (1954).

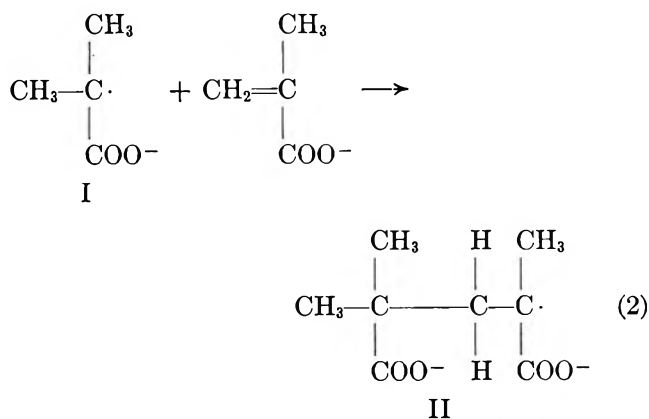
(11) W. B. Gager, F. A. Sliemers, J. F. Kircher, and R. I. Leininger, *Polymer Preprints*, **3**, 67 (1962).

(12) I. S. Ungar, W. B. Gager, and R. I. Leininger, *J. Polymer Sci.*, **44**, 295 (1960).



The spectrum also shows the presence of 4 intermediate lines, which can be attributed to a proportion of propagating radicals (II). We have synthesized the spectra for combinations of I and II in various proportions by computer from the spectra of pure I and II and hence have estimated the proportion of propagating radical to be 8%. This probably results from a "hot" radical reaction during irradiation since no change in the spectrum was observed when the sample was kept at -196° .

Transformation above -100° . When the sample was warmed above -100° the 2 outer lines disappeared and the 4 intermediate lines increased in intensity. This change was temperature and time dependent. After the sample had been kept at -80° for several days, no further change occurred and the spectrum consisted of 9 lines with an increasing intensity distribution (Figure 1b). This spectrum is considered to be due to the propagating radical (II) formed by the reaction of the initiating radical (I) with a monomer molecule.



On warming to 50° , the spectrum was similar, but when cooled again it changed markedly. At 0° the intensity distribution changed to an alternating pattern (Figure 1c). Further cooling caused the intensity alternation to become more pronounced (Figure 1d), and some splitting of the intermediate lines occurred (Figure 1e). This temperature effect was completely reversible. Similar changes were reported by Piette¹³ on high-temperature studies of irradiated poly(methyl methacrylate), but he interpreted this as evidence for two radical species. We have confirmed the anisotropy of the propagating radical.⁷ With the magnetic field parallel to the *a* or *b* axis of a single crystal, the spectrum at 50° consisted of 9 lines and is similar to the powder spectra (Figure 2b). With the field parallel

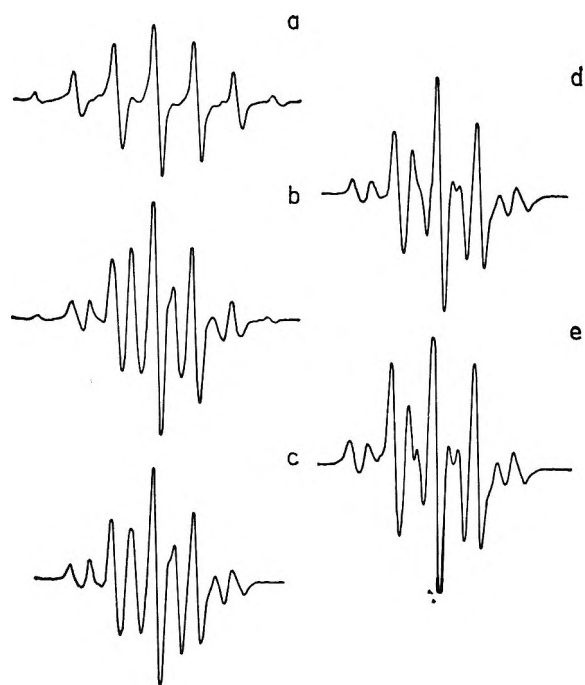


Figure 1. ESR spectra of polycrystalline barium methacrylate dihydrate after 0.2 Mrad of γ irradiation: (a) -196° ; (b) after 24 hr at -80° ; (c) warmed to 50° (5 min) and then cooled to 0° ; (d) cooled to -80° ; (e) cooled to -154° .

to the *c* axis, the spectrum consisted of 13 lines, the intermediate broad lines of the spectrum having split into two narrow components.

Polymerization at 50° . When the sample was maintained at 50° , the intensities of the intermediate lines decreased continuously. The intensity distribution became progressively more alternating as shown in Figure 2 until after 100 hr, when about 20% of the monomer should be converted to polymer, it approached a 5-line spectrum, with an increased line width. We believe that this spectrum is due to the long-chain methacrylate polymer radical in a largely polymer environment in barium methacrylate. This is supported by the observation of a similar spectrum after 38-hr γ irradiation of the dihydrate at 25° , corresponding to 40% conversion to polymer.

Further, a sample of barium methacrylate dihydrate was subjected to an electric discharge in an atmosphere of 1 mm of hydrogen at 25° . The spectrum at 25° consisted of 9 lines of alternating intensity, evidently due to propagating radicals on the surface, resulting from reactions 1 and 2. On warming to 50° the spectrum rapidly changed to the 5-line spectrum. The attainment of a comparable number of spins on the surface of the solid to the number formed throughout the bulk of the solid indicates that the actual radical concentration must be higher. The rate of conversion to long-chain polymer at 50° varies with radi-

(13) L. H. Piette in "N.M.R. and E.P.R. Spectroscopy," Pergamon Press Ltd., Oxford, 1960.

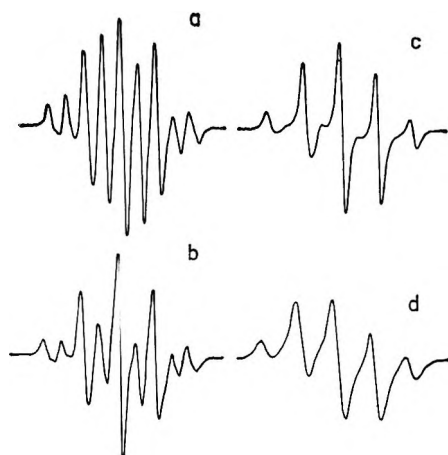


Figure 2. Time dependence of the spectrum of the propagating radical at 50° : (a) 0 hr; (b) 10 hr; (c) 100 hr; (d) after 38-hr in-source γ irradiation at 25° and a dose rate of 335,000 rads/hr.

cal concentration and therefore the polymer concentration in the surface layer after a given time would be much higher than for the bulk reaction.

Conformation of the Radical. We have interpreted our results in terms of the model proposed by Symons.⁶ The unpaired electron is considered to occupy a p_z orbital on the trigonally hybridized α -carbon atom. According to Heller and McConnell,¹⁴ the splitting constant of each β -hydrogen atom is given by

$$a_{\beta H} = B \cos^2 \theta \quad (3)$$

where B is a constant (46 G) and θ is the angle between the carbon-hydrogen bond and the symmetry axis of the p_z orbital, both projected onto a plane perpendicular to the C_α - C_β bond. The methyl group is considered to rotate rapidly so that these three hydrogen atoms interact equally ($\theta_{av} = 45^\circ$). The polymeric chain of the radical will occupy an intermediate spatial position between the methyl and carboxyl groups as shown in Figure 3; hence the β -methylene C-H bonds will be at an approximate angle of $\theta = 60^\circ$. Steric and polarity differences between the methyl and carbonyl groups result in slight nonequivalence of the angles θ_1 and θ_2 and hence of the splittings.

We have investigated the effect of varying the amount of twist of the β -methylene group from the symmetrical (60 - 60°) position and of different line widths by computer calculation of theoretical spectra. These computed spectra have been compared with the spectra observed experimentally under different conditions and the conformations of the radical deduced. Gaussian line shapes gave a better match than Lorentzian; for rigid systems in which the relative orientations and positions of randomly distributed and interacting species do not change with time this is usually the case.¹⁵ The appropriate computed spectra are shown in Figure 4.

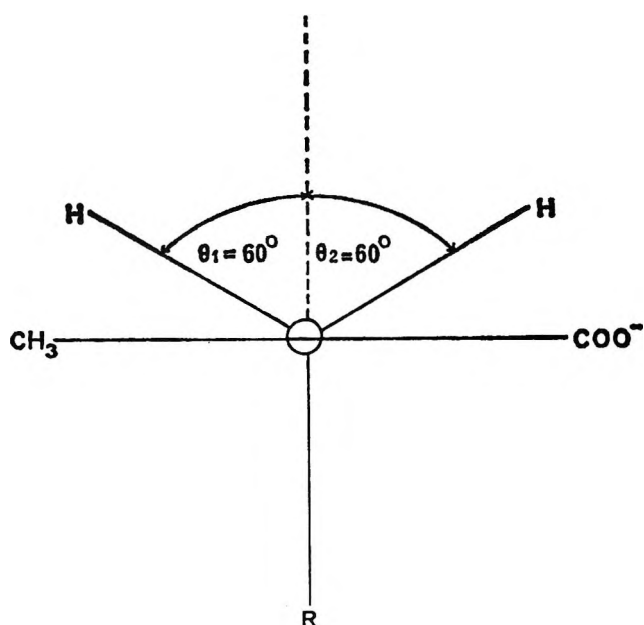


Figure 3. Conformation of the propagating radical with equivalent methylene hydrogens.

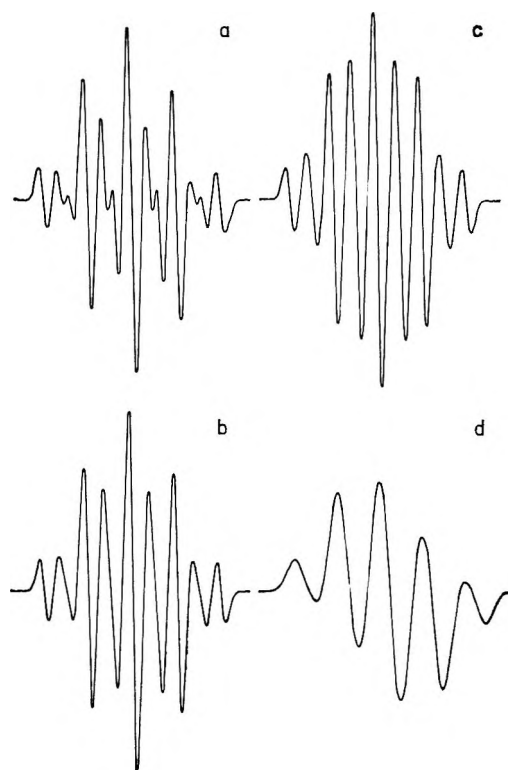


Figure 4. Theoretical spectra showing the effect of changing the conformational angle: (a) 56 - 64° ; (b) 57 - 63° ; (c) 58 - 62° ; (d) 53 - 67° . Line width of a, b, and c, 5 G; line width of d, 8 G.

Our computed spectra are calculated from splitting constants due to the isotropic component of hyperfine

(14) C. Heller and H. M. McConnell, *J. Chem. Phys.*, **32**, 1538 (1960).

(15) A. Abragam, "The Principles of Nuclear Magnetism," Clarendon Press, Oxford, 1961.

splitting and are similar to spectra obtained when the a or b axis of the crystal is parallel to the magnetic field. The anisotropy of the spectrum of the propagating radical is such that (a) there is no significant change in g value and (b) the position of the alternate major peaks is unchanged. Usually if the single-crystal spectrum is anisotropic, the powder spectrum ought to have complicated line shapes.¹⁶ However, since anisotropy in the present system is confined to a splitting of intermediate broad peaks into two narrow components, then broadening in the powder sample would be expected to give a spectrum similar to that calculated from isotropic coupling constants and can be approximated by Gaussian line shapes. Anisotropy in single crystals is generally due to interaction with α protons although small anisotropies due to interaction with β -methylene hydrogens have been reported.¹⁷

Thus the propagating radical formed on warming the γ -irradiated monomer to -80° and keeping it at this temperature for several days has the 58 – 62° conformation. On further warming to 50° , the radical still has the same conformation, but this is due to cancellation of the opposing effects of an increase in radical chain length, producing an increase in twist and an increase in temperature, which causes a decrease in twist. This is confirmed by the temperature dependence; the spectrum now shows an alternating intensity distribution on cooling back to -80° (57 – 63°), which is reversible. Further cooling to -154° produced splitting of the intermediate lines (56 – 64°).

The increasing alternation in intensity when the sample was kept at 50° can be explained by a progressive increase in twist with an accompanying increase in line width. The near 5-line spectrum, which is eventually obtained, would be explained by a 53 – 67° conformation. The change with time cannot be accounted for merely by an increase in line width since the computed spectra show that this would produce a marked reduction in the size of the center line relative to the other peaks. We suggest that the increasing polymer content of the environment is responsible for the increasing twist of the β -methylene conformation. This is confirmed by the observation that the change in the spectrum occurs more rapidly after higher doses of γ irradiation, corresponding to greater yields of polymer after the same time at 50° , but not longer chains.

Interpretation of Conformation Change. The variation in the conformation of the propagating radical can be interpreted in several ways. First, there may be a change in the actual angle of the β -methylene group, relative to the radical plane. Second, there may be an exchange between two equilibrium positions, similar to the well-known phenomenon in nmr spectra. Such an exchange mechanism would cause two separate resonance lines to move together with increasing temperature and ultimately to coalesce when the ex-

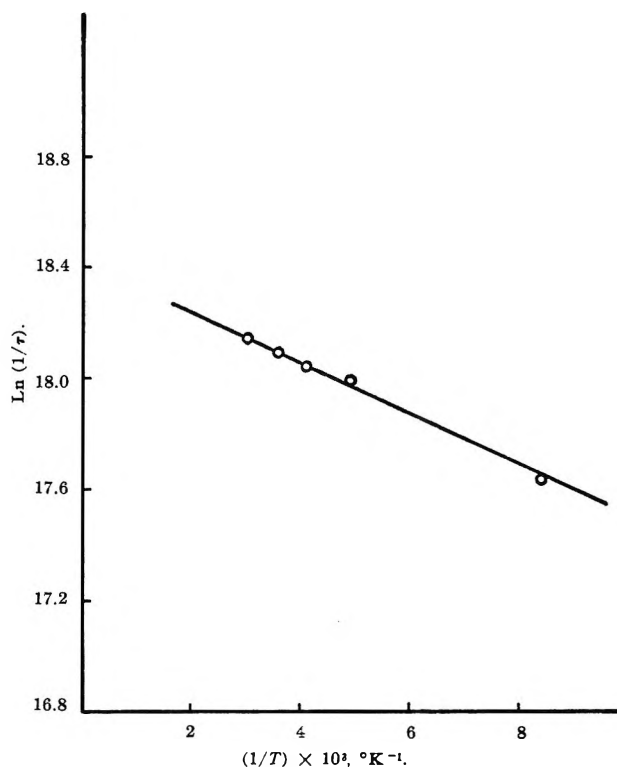


Figure 5. Arrhenius plot of $\ln(1/\tau)$ vs. $1/T$. Points correspond to values calculated from experimentally observed hfs; line is best fit to points.

change frequency exceeds the difference between the two resonance frequencies. We have considered our spectra in terms of the model proposed by Ohnishi, *et al.*,¹⁸ and have calculated values of τ , where τ is the relaxation time for the exchange, from the coupling constant at different temperatures. The coupling constants for zero exchange rate were taken as those corresponding to θ equal to 55.2 and 64.8° . A plot of $\log(1/\tau)$ vs. reciprocal temperature was linear (Figure 5) and gave a value of $180 \text{ cal mole}^{-1}$ for E_a , the activation energy for the exchange. This value is low compared to that obtained for other systems.^{18,19} The line width would be expected to increase appreciably at low temperatures, whereas only a small change was observed.

Third, the β -methylene group can be considered to undergo torsional oscillation, which is temperature dependent. If a quantum mechanical oscillator is used as a model and Boltzmann statistics are assumed, the average value of the coupling constant is given by

$$a_{\beta\text{H}} = \frac{\sum_n \langle \psi_n | B \cos^2 \theta | \psi_n \rangle \exp(-E_n/kT)}{\sum_n \exp(-E_n/kT)} \quad (4)$$

(16) H. Sternlicht, *J. Chem. Phys.*, **33**, 1128 (1960).

(17) J. R. Morton and A. Horsfield, *Mol. Phys.*, **4**, 219 (1961).

(18) S. Ohnishi, S. Sugimoto, and I. Nitta, *J. Chem. Phys.*, **37**, 1283 (1962).

(19) C. Corvaja, *ibid.*, **44**, 1958 (1966).

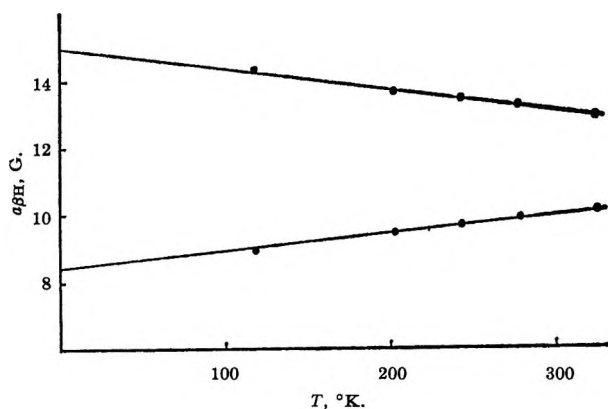


Figure 6. Temperature dependence of β -methylene hydrogen splitting constants. Points are experimental hfs; line is computed from anharmonic oscillator model.

where ψ_n represents the n th eigenstate of the oscillator. The variation of the coupling constants with temperature is then governed by the wave function and the eigenvalues of the torsional vibrator. Kashiwagi and Kurita²⁰ solved this equation for the case of an anharmonic oscillator in which the potential energy function was of the form

$$V = V_0/2[(\theta - \theta_1)^2 - \delta(\theta - \theta_1)^3] \quad (5)$$

where θ_1 is the value of θ at the potential minimum. We have performed calculations for the methacrylate propagating radical using the equation in ref 20. When $B = 46$ G, $\theta_1 = 55.2^\circ$, $\theta_2 = 64.8^\circ$, $I = 50 \times 10^{-40}$ erg sec², $V_0 = 3$ kcal mole⁻¹, and $\delta = 0.40$ rad, a satisfactory explanation of our experimental observations of the temperature dependence of the long-chain propagating radical in a monomer environment is obtained (Figure 6).

Conclusions

The esr spectrum of the methacrylate propagating radical in barium methacrylate dihydrate varies from 9 lines with an increasing intensity distribution to 5 lines

with an approximately binominal intensity distribution. This results from a variation in the conformational angles of the two β -methylene carbon-hydrogen bonds which depends on (1) the degree of polymerization, (2) the temperature, and (3) the environment of the radical end. In particular, three distinct conditions have been distinguished in γ -irradiated barium methacrylate dihydrate: A, short-chain polymer radicals (believed to be dimer) in a monomer environment; B, long-chain polymer radicals in a monomer environment; and C, long-chain polymer radicals in a polymer environment. The temperature dependence of the conformation for each case is shown in Table I.

Table I: Variation of the Conformation of the Propagating Radical with Environment and Temperature

Temp, °C	A Dimer radical in monomer matrix	B Polymer radical in monomer matrix	C Polymer radical in polymer matrix
-154	58-62°	56-64°	53-67° ^a
-80	58-62°	57-63°	
0		57.5-62.5°	
50		58-62°	53-67°

^a Asymmetry of conformation greater than 53-67° will produce similar spectra.

Acknowledgments. We wish to thank (1) the Australian Institute of Nuclear Science and Engineering for supporting this project; (2) the Australian Atomic Energy Commission for use of their irradiation facilities; (3) Mr. B. M. O'Leary for organization of the irradiations; (4) Professor L. E. Lyons for making the esr spectrometer available to us; (5) Professor H. Morawetz for his initial stimulus in this field; and (6) C.S.I.R.O. for providing a studentship for M. J. B.

(20) M. Kashiwagi and Y. Kurita, *J. Chem. Phys.*, **39**, 3165 (1963).

Flash Photolysis and Time-Resolved Mass Spectrometry. II. Decomposition of Methyl Iodide and Reactivity of $I(^2P_{1/2})$ Atoms^{1,2}

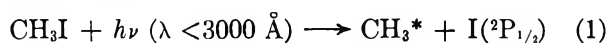
by Richard T. Meyer

Sandia Laboratory, Albuquerque, New Mexico 87116 (Received October 12, 1967)

The flash photolysis of methyl iodide has been studied by time-resolved mass spectrometry. Mixtures of CH_3I vapor with Ar, O_2 , Kr, and N_2 at total pressures of 5–12 torr have been photolyzed with flash durations as short as 18 μsec . The ultraviolet light flux was about 3×10^{18} quanta/ cm^2 . A time-of-flight mass spectrometer provided 1.4- μsec sampling intervals every 50 μsec . Over-all decomposition of CH_3I was 20–75%, with the larger decompositions occurring in the absence of the added gases. I_2 , CH_4 , C_2H_6 , C_2H_4 , and some C_2H_2 were formed as final products. All systems showed I_2 formation by two processes, one fast and one slow. The fast process occurred within 75 μsec after the flash peak and accounted for about 50% of the total I_2 production. This rapid formation of I_2 is not consistent with the termolecular recombination of atomic iodine, an elevated temperature reaction between ground-state I atoms and CH_3I , or a pyrolysis of CH_3I to C_2H_6 and I_2 . It is concluded that excited, metastable $I(^2P_{1/2})$ atoms are produced in the primary decomposition and that these excited atoms have sufficient energy (21.7 kcal/mol) to undergo the reaction $I(^2P_{1/2}) + \text{CH}_3\text{I} \rightarrow \text{CH}_3 + \text{I}_2 + 3 \text{ kcal}$. This bimolecular reaction is proposed for the rapid formation of molecular iodine. The slow process accounting for the remainder of the I_2 production is attributed to termolecular atom recombination, although it has not been studied in detail. The relative yields of the several final products are analyzed in terms of known atom and radical reactions. It is shown further that the chemical reactivity of $I(^2P_{1/2})$ atoms is strongly affected by collisional deactivation.

Introduction

Previous studies^{3–7} on the steady-state photolysis of methyl iodide established that the primary step is dissociation of the C–I bond



Reactions of the hot methyl radicals, CH_3^* , have been extensively explored^{8,9} and reviewed.¹⁰ Methane is a principal product and is accounted for by reaction 2.



Methyl radicals were also detected in the flash photolysis of methyl iodide by Herzberg¹¹ and by McGarvey and McGrath.¹² In addition, Harris and Willard⁷ found no difference in the photolysis products at 1849 and 2537 \AA . Thus the evidence indicates that reaction 1 applies to both low-intensity photolysis and flash photolysis of methyl iodide.

Porret and Goodeve¹³ deduced from the ultraviolet absorption spectrum of CH_3I that the iodine atoms are produced in the excited, metastable $^2P_{1/2}$ state. Recently, Kasper and Pimentel¹⁴ and Kasper, *et al.*,¹⁵ proved this decomposition mechanism. They reported detection of laser action during the flash photolysis of gaseous CH_3I and several other alkyl iodides. They attributed the stimulated emission to the $^2P_{1/2} \rightarrow ^2P_{3/2}$ transition of atomic iodine. Their experiments also suggest the occurrence of excited iodine atom abstraction reactions with the alkyl iodides.

The chemical reactivity of excited $I(^2P_{1/2})$ atoms has

been considered in other studies.^{16,17} However, the experimental evidence does not appear conclusive. It is known that ground-state $I(^2P_{1/2})$ atoms react with CH_3I at high temperatures to form molecular iodine according to reaction 3.^{18–20} Since the $I(^2P_{1/2})$ atoms

(1) This work was supported by the United States Atomic Energy Commission.

(2) The principal results of this paper were reported at the 149th National Meeting of the American Chemical Society, Detroit, Mich., April 1965, Abstract S17.

(3) W. West and L. Schlessinger, *J. Amer. Chem. Soc.*, **60**, 961 (1938).

(4) R. R. Williams and R. A. Ogg, Jr., *J. Chem. Phys.*, **15**, 696 (1947).

(5) R. D. Schultz and H. A. Taylor, *ibid.*, **18**, 194 (1950).

(6) W. H. Hamill and R. H. Schuler, *J. Amer. Chem. Soc.*, **73**, 3466 (1951).

(7) G. M. Harris and J. E. Willard, *ibid.*, **76**, 4678 (1954).

(8) F. P. Hudson, R. R. Williams, and W. H. Hamill, *J. Chem. Phys.*, **21**, 1894 (1953).

(9) R. D. Souffie, R. R. Williams, Jr., and W. H. Hamill, *J. Amer. Chem. Soc.*, **78**, 917 (1956).

(10) J. R. Majer and J. P. Simons, *Advan. Photochem.*, **2**, 137 (1964).

(11) G. Herzberg, *Proc. Chem. Soc.*, 116 (1959).

(12) J. J. McGarvey and W. D. McGrath, *Trans. Faraday Soc.*, **60**, 2196 (1964).

(13) D. Porret and C. F. Goodeve, *Proc. Roy. Soc.*, **A165**, 31 (1938).

(14) J. V. V. Kasper and G. C. Pimentel, *Appl. Phys. Letters*, **5**, 231 (1964).

(15) J. V. V. Kasper, J. H. Parker, and G. C. Pimentel, *J. Chem. Phys.*, **43**, 1827 (1965).

(16) R. A. Durie and D. A. Ramsay, *Can. J. Phys.*, **36**, 35 (1958).

(17) J. F. McKellar and R. G. W. Norrish, *Proc. Roy. Soc.*, **A263**, 51 (1961).

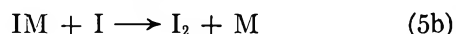
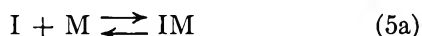
(18) S. W. Benson and E. O'Neal, *J. Chem. Phys.*, **34**, 514 (1961).



produced in the photolysis of methyl iodide possess electronic energy of 21.7 kcal/mol, it is conceivable that the exothermic reaction 4 may occur directly. Molec-



ular iodine has been observed as a major final product of methyl iodide photolysis.^{9,17,21} However, its formation has been ascribed generally to the termolecular recombination reaction



We recently reported preliminary experiments on the flash photolysis of methyl iodide, as studied by time-resolved mass spectrometry.²² The experiments consisted of time-resolved measurements of the formation of molecular iodine as a function of total pressure and of the ratio of an inert gas (helium) to CH_3I . From a first-order kinetic analysis and from the temperature dependence of the rate data, it was concluded that the excited iodine atom reaction 4 did indeed occur. We report here the analysis of earlier flash-photolysis studies which provided the foundation for the previous publication²² and which provided some of the first evidence for the occurrence of reaction 4. In a subsequent paper, we shall report extended quantitative studies of the reaction rate and temperature dependence of the excited iodine atom reaction with methyl iodide.

Experimental Techniques

Description of Apparatus. Detailed descriptions of the apparatus and technique have been published.²³⁻²⁶ A Bendix 14-101 time-of-flight mass spectrometer is coupled with a flash lamp and Pyrex-quartz reaction vessel (see Figure 1). The spectrometer provides a complete mass spectral analysis of the reacting gaseous mixture every 50 μsec . The successive mass spectral patterns are displayed on a Tektronix 517A oscilloscope and time is resolved with a Beckman and Whitley 364-2 oscillographic drum camera. The spectrometer electron gun operates with a pulse width of 1.4 μsec and produces a trap current of 25 μA at 70 eV. The sensitivity of the spectrometer, as previously reported, is 5×10^{-8} mol/l.²⁴

The capacitor-discharge flash lamps are operated at electrical-input energies of 1470 J at 7 kV (lamp B, ref 22) and 908 J at 11 kV (lamps C and D, ref 24). Flash durations are 90 and 18 μsec , respectively. The ultraviolet light flux to the reaction vessel ranges from 10^{18} to 3×10^{18} quanta/cm² per flash. The reacting gaseous mixture is sampled by the spectrometer through a Pyrex orifice $65 \pm 15 \mu$ in diameter.

Sample Preparation. Eastman Kodak Co. methyl iodide (liquid) was dried over anhydrous sodium sulfate and fractionally distilled *in vacuo*. The middle fraction

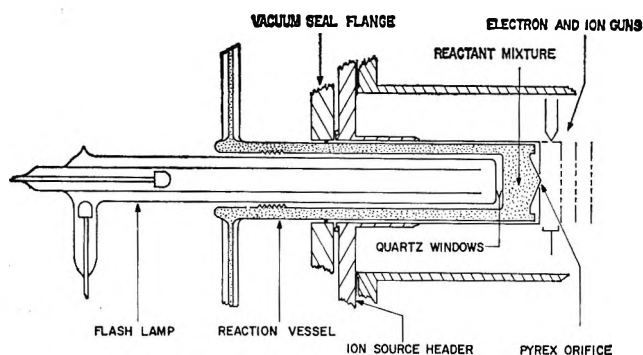


Figure 1. Geometry of the coaxial flash lamp and reaction vessel adapted to the ion source of the Bendix TOF mass spectrometer.

was stored at liquid-nitrogen temperature in the presence of a copper wire. Vapor samples were withdrawn and mixed in a 12-l. darkened bulb with oxygen, argon, nitrogen, or krypton for 30-60 min or longer. Linde high-purity gases were used without further purification. Pressures were recorded with a dibutyl phthalate manometer.

Calibration and Correction Procedures. Nutt, *et al.*,²⁶ and Barber, *et al.*,²⁷ have considered various aspects of mass spectrometric sampling in the adiabatic flow region, and calibration with known gas mixtures appears to be best. Partial calibrations were performed in the present work and their applicability is discussed under Results. However, most of the data reported are ion intensities.

Argon is used as a standard internal substance in all reactant mixtures. All ion intensities are referenced to the argon ion intensity for each point in the time-resolved record. The principal systematic disturbance to the spectrometer analysis arises from the heating and expansion of the reactant mixture. In the absence of methyl iodide, no heating of the argon is observed. In cases of excessive heating, the argon ion intensity fails as a quantitative indicator of systematic fluctuations. The degree of heating is greater in the absence of added nitrogen. The gases remain heated for 10 msec or longer before any significant cooling and signal increase is observed.

Figure 2 shows typical time-resolved records of argon in the presence of methyl iodide, with and without

(19) R. K. Boyd, G. W. Downs, J. S. Gow, and C. Horrex, *J. Phys. Chem.*, **67**, 719 (1963).

(20) M. C. Flowers and S. W. Benson, *J. Chem. Phys.*, **38**, 882 (1963).

(21) N. Davidson and T. Carrington, *J. Amer. Chem. Soc.*, **74**, 6277 (1952).

(22) R. T. Meyer, *J. Chem. Phys.*, **46**, 4146 (1967).

(23) R. T. Meyer, *Rev. Sci. Instrum.*, **35**, 1064 (1964).

(24) R. T. Meyer, *J. Sci. Instrum.*, **44**, 422 (1967).

(25) R. T. Meyer, *J. Chem. Phys.*, **46**, 967 (1967).

(26) C. W. Nutt, G. W. Penmore, and A. J. Biddlestone, *Trans. Faraday Soc.*, **55**, 1516 (1959).

(27) M. Barber, J. Farren, and J. W. Linnett, *Proc. Roy. Soc.*, **A274**, 293 (1963).

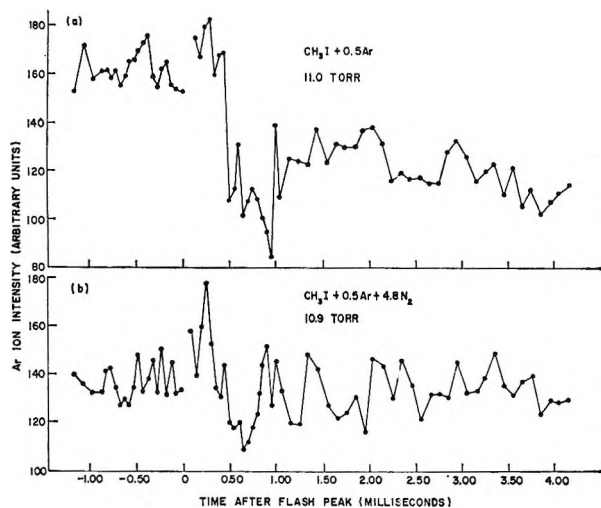


Figure 2. Time-resolved records of argon ion intensity in typical methyl iodide flash photolysis experiments: (a) without N₂; (b) with N₂ added. Negative time represents time prior to the flash; flash-lamp C.²⁴ The decreasing argon amplitude corresponds to a constant-pressure expansion of the flash-heated gas mixture. The degree of heating is greater in the absence of added N₂.

added nitrogen. The argon ion intensity increases for a few cycles after the flash because of electromagnetic interference from the flash discharge. Then it decreases to a level lower than the preflash intensity and finally recovers to a nearly constant value which remains less than the preflash value for several milliseconds. This longer duration of lower intensity is caused by flash heating of the gas sample and can be explained by the mass flow into and out of the ionization zone of the spectrometer. Barber, *et al.*,²⁷ have given the equation for the total mass flow through an orifice where the mean free path is small compared with the dimensions of the orifice. From this it can be derived that the ion intensity is inversely proportional to the gas temperature on the high-pressure side of the orifice.

The important question of density effects on reaction rates must be considered. The density decrease arising from the gas expansion would lead to reaction deceleration. An increase of density at the orifice due to wall cooling could also occur, which would accelerate the chemical reactions. However, at gas pressures for which the mean free path is much smaller than the dimensions of the reaction vessel, only a small percentage of molecules will strike the walls and be sampled through the orifice, and wall cooling will have only a minor effect on reaction rates.

The production of molecular iodine in the flash photolysis of methyl iodide leads to contamination of the metal walls of the ion source reactor housing. Subsequent flashes desorb this iodine producing a background I₂⁺ ion intensity. Only liquid chemical cleanup of the metal walls is effective. Since this cannot be performed after each experiment, blank

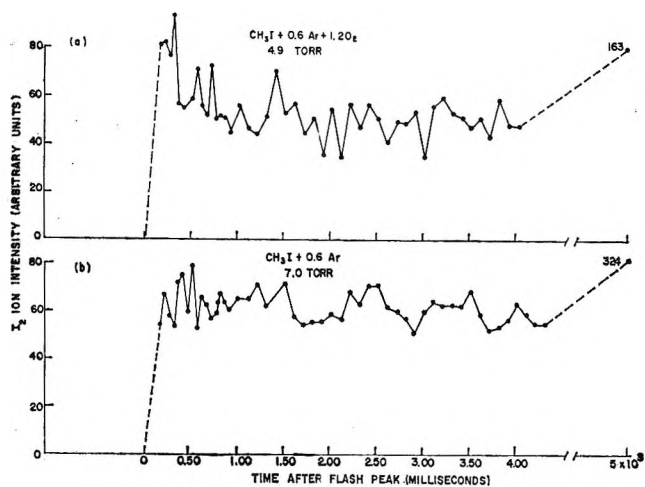


Figure 3. Time-resolved records of molecular iodine formation: (a) with O₂ added; (b) without O₂. First data points after flash are at 170 μ sec; flash-lamp B.²⁴ I₂ ion intensities are plotted every 50 μ sec for 1 msec after the flash and every 100 μ sec for the succeeding 3 msec. The data point at 5×10^{-3} msec represents the average final ion intensity. Different total pressures apply to a and b as shown.

experiments with gas mixtures excluding the methyl iodide at the same total pressures were run to obtain corrective data. It has been definitely established that the rapid formation of I₂ in the flash photolysis of CH₃I is not influenced by this effect.²²

Experimental Results

Mixtures of CH₃I vapor with Ar, O₂, Kr, and N₂ at total pressures of 5–12 torr were flashed. Quantitative gas sampling was achieved as early as 75 μ sec after the flash peak. Several time-resolved experiments are shown in Figures 3–5. Molecular iodine positive ion intensities are plotted every 50 μ sec for the first millisecond and every 100 μ sec for the succeeding 3 msec. A final data point at 5000 msec represents the average of 400 cycles of spectrometer output at that time. Different flash-lamp parameters apply to each of the three pairs of experiments. Data variations for the three experiments with CH₃I + Ar mixtures reflect differences in the flash intensity. Corrections have been made for systematic instrumental variations, including temperature effects, and for contributions from residual iodine desorption.²⁸ Excessive flash heating in the Figure 5b experiment prevented complete correction for the sample density decrease due to expansion.

Table I is a summary of initial (defined as 75–250 μ sec after the flash) and final ion intensity ratios for the specific individual experiments of Figures 3–5. One additional pair of experiments is included. The data of Table II pertain to final product ion intensities for a

(28) For details of the corrective procedures, see R. T. Meyer, C. E. Olson, and R. R. Berlant, Abstracts, 14th Annual Conference on Mass Spectrometry and Allied Topics, Dallas, Texas, 1966.

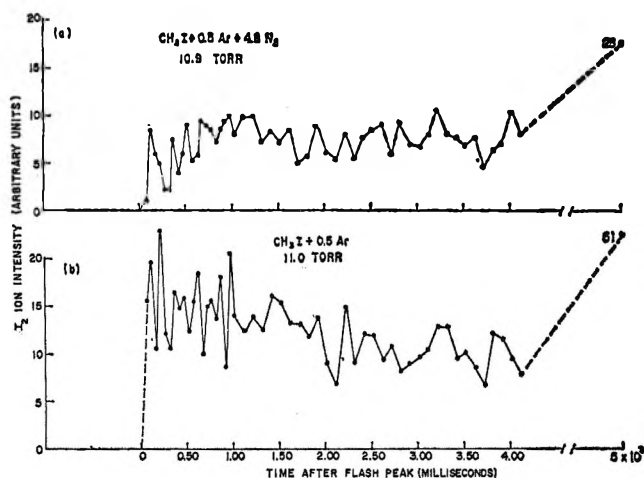


Figure 4. Time-resolved records of molecular iodine formation: (a) with N_2 added; (b) without N_2 . First data points after flash peak are at $75 \mu\text{sec}$; flash-lamp C.²⁴ Final data points at 5×10^3 msec are off scale; numerical values are shown.

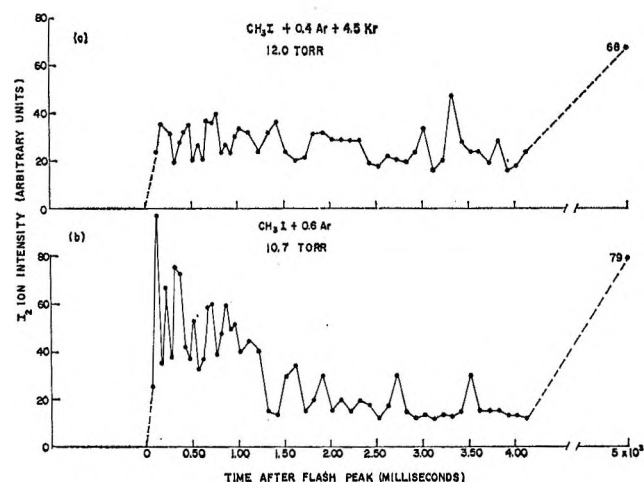


Figure 5. Time-resolved records of molecular iodine formation: (a) with Kr added; (b) without Kr. First data points after flash peak are at 125 and $75 \mu\text{sec}$ for a and b, respectively; flash-lamp D.²⁴ Final data points at 5×10^3 msec are off scale; numerical values are shown.

larger number of experiments. It is readily estimated from the data that both the initial and final vapor pressures of iodine correspond to pressures in the range of 0.2–1.5 torr. The later value is equivalent to a few degrees above room temperature, which is not inconsistent with the experimental conditions.

These are the important experimental observations. The I_2 buildup is very rapid after the flash. Amounts of I_2 equal to 20–70% of the total final concentration of I_2 are observed at the first sampling time of $75 \mu\text{sec}$ or within the first $250 \mu\text{sec}$. After the initial rapid rise in I_2 , the concentration remains fairly constant for 4 msec. The experiments represented by Figures 3a, 4b, 5a, and 5b show gradual decreases in the I_2 concentration after the initial rise. A further increase in the I_2 concentration

occurs in all cases between 4 and 5000 msec. The reaction is considered complete at 5000 msec. The large statistical fluctuations in the data and the temperature variations of the reacting sample obscure the true behavior of the I_2 concentration during the interval from 0.25 to 4 msec. The actual response during this period is slow compared to the initial rise in I_2 concentration.

Where $F = \text{Ar}, N_2, \text{Kr}, O_2$, or the sum of them, the ion intensity ratio of initial I_2 to original CH_3I increases with an increasing $\text{CH}_3\text{I}:F$ ratio. This increase is also observed in the final I_2 ratio. For the experiments with N_2 or Kr at total pressures of 11 ± 1 torr, the ratios of the final products I_2, CH_4 , and C_2H_6 to original CH_3I all differ from the comparable experiments without added gases. In decreasing the $\text{CH}_3\text{I}:F$ ratio from 2.0 to as little as 0.2, the relative I_2 intensity decreases from 1.0 to approximately 0.7, while the CH_4 decreases from 1.0 to 0.3. The decrease in CH_4 is accompanied by an increase in C_2H_6 . Also observed are decreases in the final product ion intensities for C_2H_4 and C_2H_2 ; their presence is based upon an analysis of the mass spectral patterns for masses 24–30. The oxygen experiments are in qualitative agreement but do differ quantitatively.

The per cent of CH_3I decomposition is always less for experiments with higher partial pressures of added gases. Thus there is a qualitative consistency between the amount of I_2 and CH_4 formed and the amount of CH_3I decomposed. In fact, a plot of per cent of I_2 formation vs. per cent of decomposition, both based on ion intensities, yields a straight line with a positive slope of 0.84 and a zero intercept. The per cent of I_2 formation is herein defined as the ratio of final ion intensity of I_2 to original ion intensity of CH_3I . It is obvious from Table II that the data on the per cent of CH_3I decompo-

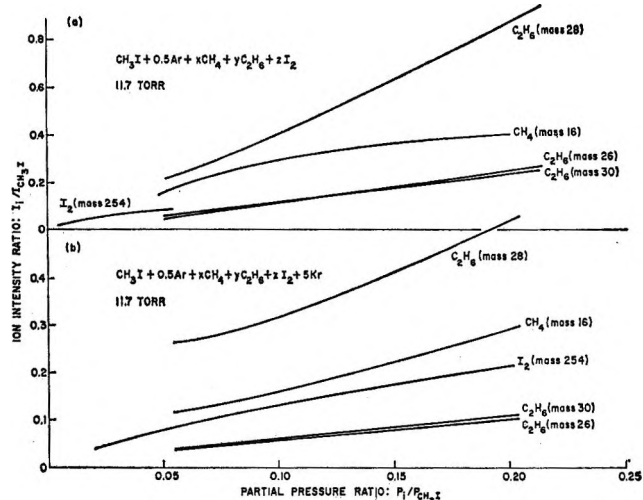


Figure 6. Calibration curves of ion intensity ratios vs. partial pressure ratios for several final product constituents, i , using prepared gas mixtures: (a) without Kr, (b) with Kr added. Ion intensity ratios are based upon the mass-142 peak of CH_3I .

Table I: Summary of Initial and Final Ion Intensity Ratios from Figures 3-5

Figure ref	Reactant mixture	Initial fraction of total I ₂ formation ^a (I ₂) _i /(I ₂) _f	Ion intensity of I ₂ relative to original CH ₃ I	
			Initial ^a (I ₂) _i /(CH ₃ I) ₀	Final ^b (I ₂) _f /(CH ₃ I) ₀
3b	CH ₃ I + 0.6Ar	0.19	0.066	0.34
3a	CH ₃ I + 0.6Ar + 1.2O ₂	0.50	0.065	0.13
None	CH ₃ I + 0.5Ar	0.39	0.050	0.13
None	CH ₃ I + 0.5Ar + 1.0N ₂	0.59	0.047	0.08
4b	CH ₃ I + 0.5Ar	0.31	0.035	0.14
4a	CH ₃ I + 0.5Ar + 4.8N ₂	0.24	0.019	0.08
5b	CH ₃ I + 0.6Ar	0.70	0.23	0.33
5a	CH ₃ I + 0.4Ar + 4.5Kr	0.40	0.092	0.23

^aInitial refers to the time interval of 75-250 μsec after the flash peak. ^bFinal refers to 5 sec after the flash peak.

Table II: Effect of Added Gases on Relative Amounts of Final Products Formed in the Flash Photolysis of Methyl Iodide (Data Are Based on Ion Intensities Except Where Otherwise Noted)

Reactant mixture	Total pressure, torr	Partial pressure of CH ₃ I, torr	No. of expts averaged	Flash parameters	Final % CH ₃ I decomposition per flash		Ion intensity ratio of final products to original CH ₃ I ^a				
					Meas ^d	Calcd	I ₂	CH ₄ ^b	C ₂ H ₆ ^c	C ₂ H ₄ ^d	C ₂ H ₂ ^e
CH ₃ I + 0.6Ar	7.1	4.5	4	B	19 ± 1	76	0.32	0.06	0.02	0.09	~0
CH ₃ I + 0.6Ar + 1.2O ₂	5.1	1.8	4	B	15 ± 3	31	0.13	0.04	0.04	0.06	~0
CH ₃ I + 0.5Ar	10.7	7.2	3	C	15 ± 1	36	0.15	0.18	0.04	0.17	~0
CH ₃ I + 0.5Ar + 1.0N ₂	10.2	4.1	1	C	11	19	0.08	0.06	0.06	f	f
CH ₃ I + 0.5Ar	10.9	7.2	2	C	11 ± 1	33	0.14	0.06	0.04	0.08	~0
CH ₃ I + 0.5Ar + 4.8N ₂	11.2	1.8	3	C	9 ± 1	21	0.09	0.02	0.03	f	f
CH ₃ I + 0.6Ar	11.0	7.0	5	D	34 ± 3	67	0.28	0.32	0.07	0.10	0.11
					(76 ± 1) ^g			(0.10)	(0.07)		
CH ₃ I + 0.6Ar + 4.5Kr	12.0	2.0	4	D	28 ± 1	52	0.22	0.11	0.09	0.02	0.06
							(0.20)	(0.05)	(0.16)		

^a Numbers in parentheses are absolute partial pressure ratios obtained from the calibration curves of Figure 6. ^b Analyzed from mass 16. ^c Analyzed from mass 30. ^d Analyzed from mass 28 by subtracting contributions from C₂H₆. ^e Analyzed from mass 26 by subtracting contributions from C₂H₄ and C₂H₂. ^f Not measurable in presence of excess N₂. ^g This value was obtained from a separate ion intensity vs. partial pressure calibration.

sition and on the per cent of I₂ formation are inconsistent, since the first should be at least twice the second for a material balance. This can be explained by differences in calibration factors.

Calibration experiments indicate that the final product ion intensity ratios are representative of the absolute molecular concentration ratios. Figure 6 shows the calibration curves of ion intensity ratios vs. partial pressure ratios for prepared gas mixtures. Mixtures were used containing methyl iodide, argon, methane, ethane, iodine, and krypton in amounts similar to the final state of the photolysis experiments. The a and b curves for the corresponding masses have similar shapes but have average slopes which differ by a factor of about 2. This illustrates the dependence of mass flow through an orifice upon the composition of the gas mixture. Even less similarity is observed for nonratio plots of ion intensity vs. partial pressure. The absolute partial pressure ratios of iodine, methane, and

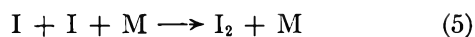
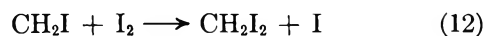
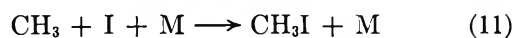
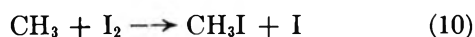
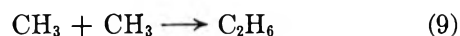
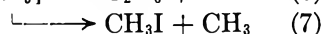
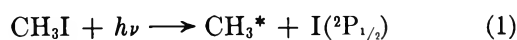
ethane to methyl iodide for the flash-photolysis experiments are shown in parentheses in Table II. The relative decreases in I₂ and CH₄ production by adding krypton remain approximately the same as measured by the ion intensity ratios. However, the increase in C₂H₆ production becomes more pronounced.

A separate calibration of ion intensity vs. partial pressure of CH₃I for a mixture of CH₃I and Ar at a total pressure of 11 torr was performed to obtain an absolute measure of the per cent of decomposition. This calibration is considered applicable only to the group of experiments consisting of CH₃I + 0.6Ar at 11.0 torr. A value of 76% was obtained. This compares favorably with the calculated minimum value of 67%. The latter was calculated from 2 times 28%, the ion intensity measure of the per cent of I₂ formation, divided by 0.84, the slope of the empirical ion intensity relationship between per cent of I₂ formation and per cent of CH₃I decomposition. Thus it is concluded that

the values of per cent decomposition based on changes in the ion intensity of CH_3I are low. Better estimates are calculated from the final I_2 to original CH_3I ion intensity ratios. Values of 20–75% are obtained and are tabulated in Table II.

Discussion

The composite chemical mechanism found in the literature for the photochemical decomposition of methyl iodide is



Specific discussion of the fate of the $\text{I}(^2\text{P}_{1/2})$ atoms is meager. It is assumed generally that the atoms are collisionally deactivated and then removed by reaction 5. The present work represents the second time-resolved study of molecular iodine formation in the photolysis of methyl iodide. Preliminary results have been reported by McKellar and Norrish¹⁷ from a study principally concerned with the combustion of methyl iodide. Their experiments provide evidence for the occurrence of $\text{I}(^2\text{P}_{1/2})$ atom reactions with O_2 but do not show any rapid formation of I_2 .

It is proposed that the present time-resolved experiments demonstrate the presence of excited, metastable $\text{I}(^2\text{P}_{1/2})$ atoms and the formation of I_2 by a rapid, bimolecular reaction involving the excited atoms, namely, reaction 4. This proposal will now be examined in terms of the experimental results and of facts already established in the literature. It will be shown that no other reaction can account for the observed rapid formation of I_2 and that reaction 4 is reasonable on the bases of energetics and excited-atom reactivity.

The proposed reactivity of $\text{I}(^2\text{P}_{1/2})$ is in agreement with evidence obtained by Kasper, Pimentel, and Parker in laser studies on CF_3I , CH_3I , and other alkyl iodides.^{14,15,29,30} The laser action is accorded to the stimulated emission of $\text{I}(^2\text{P}_{1/2})$ atoms produced in the primary flash-photolysis act. Furthermore, laser quenching is observed in all cases. In the case of CF_3I , it is found that this quenching is related to a temperature rise. With high-energy flashes, laser quenching is very pronounced and is accompanied by over 75% decomposition of the CF_3I . These authors suggest an explanation in terms of an accelerated

reaction of $\text{I}(^2\text{P}_{1/2})$ atoms with CF_3I , analogous to reaction 4.

Termolecular Recombination. Porter's data³¹ on the termolecular recombination rates of atomic iodine in the presence of various foreign gases are used to calculate reaction half-times for the present conditions. For the fractional decomposition of methyl iodide in the primary act, values equal to about half the corrected final decomposition are assumed. Thus for the $\text{CH}_3\text{I} + 0.5\text{Ar}$ and the $\text{CH}_3\text{I} + 0.5\text{Ar} + 4.8\text{N}_2$ mixtures at 11 torr, the initial fractional decompositions are taken as 15 and 10%, respectively. The corresponding termolecular recombination half-times are calculated as 0.31 and 6.8 msec. For another example, the pair of experiments with and without added oxygen are considered. A half-time of 0.58 msec is obtained for the $\text{CH}_3\text{I} + 0.6\text{Ar}$ mixture if the initial decomposition is 30%; if the primary dissociation is 15% for the oxygen experiments, a reaction half-time of 6.0 msec is expected. The reaction time data of Figures 3–5 do not show either the same absolute magnitudes or the order-of-magnitude variation with total pressure, as calculated. Thus it is concluded that termolecular recombination, reaction 5, cannot account for the rapid initial formation of I_2 , but it probably does account for the unrecorded slow increase in I_2 which occurs after 4 msec; that is, iodine atoms which are deactivated before undergoing reaction 4 are subsequently removed by reaction 5.

Thermochemical Considerations. The excitation energy of $\text{I}(^2\text{P}_{1/2})$ is 21.7 kcal/mol.³² The iodine atom also carries kinetic energy from the flash decomposition. The dissociation energy of the $\text{CH}_3\text{—I}$ bond is not well-defined in the literature, but it may be estimated at 55 ± 2 kcal/mol.^{19,20,33,34} The absorption maximum for CH_3I occurs at 2580 Å (111 kcal/mol).¹³ Therefore, 34 kcal/mol is available as kinetic energy for CH_3 and I , with the I atom taking about 4 kcal/mol. The total energy, electronic and kinetic, associated with each iodine atom is approximately 26 kcal. Earlier thermochemical data indicate that the reaction of ground-state iodine atoms with methyl iodide is endothermic by 16.5 kcal/mol.³⁵ Recent kinetic data obtained by Flowers and Benson²⁰ and Golden, *et al.*,³⁴ indicate that the total activation energy for reaction 3

(29) J. H. Parker and G. C. Pimentel, 152nd National Meeting of the American Chemical Society, New York, N. Y., Sept 1966, Abstract V74.

(30) J. V. V. Kasper, ref 29, Abstract V75.

(31) G. Porter, *Discussions Faraday Soc.*, **33**, 198 (1962).

(32) "JANAF Thermochemical Tables," D. R. Stull, Ed., The Dow Chemical Co., Midland, Mich., 1965.

(33) C. Horrex and R. Lapage, *Discussions Faraday Soc.*, **10**, 233 (1951).

(34) D. M. Golden, R. Walsh, and S. W. Benson, *J. Amer. Chem. Soc.*, **87**, 4053 (1965).

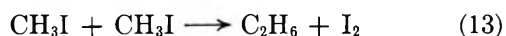
(35) "Selected Values of Chemical Thermodynamic Properties," National Bureau of Standards Circular 500, U. S. Government Printing Office, Washington, D. C., 1961.

is closer to 20.5 ± 0.5 kcal/mol. From this evidence it seems reasonable to conclude that the excited iodine atom has sufficient energy to make reaction 4 exothermic. The flash-lamp output extends down to 2000 Å and below, as does the absorption by methyl iodide. Therefore, some of the $I(^2P_{1/2})$ atoms carry 7.5 kcal/mol of excess kinetic energy.

Since adiabatic heating of the reacting gases occurs, various temperature-sensitive reactions are examined. A negative temperature coefficient is reported for the termolecular recombination of iodine atoms.³⁶ Therefore, the rapid formation of I_2 is again not explicable in terms of this process.

There does exist the possibility of ground-state $I(^2P_{1/2})$ atoms reacting with CH_3I at elevated temperatures. A reaction half-time less than 100 μsec must be satisfied. Assuming a maximum Arrhenius frequency factor of 10^{11} l. mol⁻¹ sec⁻¹ and a minimum total activation energy of 17 kcal/mol, reaction temperatures are calculated for the concentration parameters of the present experiments. This minimum value of the activation energy is the sum of the heat of reaction, obtained from the NBS tables,³⁵ and the activation energy of the reverse reaction, estimated by Benson and O'Neal¹⁸ to be equal to or less than 0.6 kcal/mol. Consider as the extreme low-temperature condition the system $CH_3I + 0.5Ar + 4.8N_2$, with the original concentration $[CH_3I]_0 = 1.8$ torr and the degree of primary dissociation $\alpha = 0.1$. Then a temperature exceeding 1300°K must apply to correspond to a reaction half-time equal to or less than 100 μsec. The system $CH_3I + 0.6Ar$, with $[CH_3I]_0 = 7$ torr and $\alpha = 0.3$, is considered to be the extreme high-temperature condition. A reaction temperature in excess of 1100°K is calculated. These temperatures are absolute minima, since smaller frequency factors and larger activation energies than the assumed values have been reported for reaction 3.¹⁸⁻²⁰

Pyrolysis of methyl iodide, leading directly to ethane and molecular iodine, is considered.



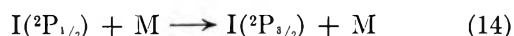
Horrex and Lapage³³ obtained a value of k (sec⁻¹) = $2.6 \times 10^{13} \exp(-54700/RT)$ for the first-order thermal decomposition. This means that a temperature of 1300°K must prevail to account for the rapid formation of I_2 . In fact, Lossing, *et al.*,³⁷ found that a reactor temperature of 1500°K was necessary to detect CH_3 radicals from the thermal decomposition of methyl iodide. By using the methods for estimating temperature rise which have been demonstrated in other studies^{24,25} to be fairly reliable, the expected absolute temperatures are no higher than 400-600°K. Such temperature increases are insufficient to account for 50% of the iodine by reaction 3 or 13 in times less than 100 μsec. However, pyrolysis may make a minor contribution to the total methyl iodide decomposition

in the high-temperature experiments of Figures 3b and 5b.

The possibility that the constancy or gradual decrease of the iodine concentration out to 4 msec may be due to a high-temperature equilibrium between I_2 and I has not been overlooked. For our experimental conditions it is calculated from the JANAF tables³² that absolute temperatures of 600-900°K can give rise to equilibria corresponding to the ratio of initial to final I_2 intensity (Table I); in fact, pyrolysis of half the I_2 could occur within 100 μsec at 860°K. At 600°K this dissociation would require 400 msec.

There is further evidence for the absence of temperature-sensitive reactions as principal processes in the system. An increase in the foreign gas:methyl iodide ratio at constant total pressure would decrease the translational temperature of the reacting mixture, and an activation energy of 8-13 kcal/mol has been suggested for the methane-producing reaction 2.^{5,38} Since the total activation energy of I_2 formation is at least 17 kcal/mol, cooling the reaction should affect the production of I_2 more than CH_4 ; the experiments show the opposite trend. Thus the principal forming reaction for I_2 has a weaker temperature dependence than that for CH_4 , consistent with expectations for reaction 4.

Secondary Reactions and Quantum Yields. The fact that the final concentration ratio $I_2:CH_4$ changes upon the addition of foreign gases suggests that different elementary reactions are responsible for their formation. In addition, both the per cent decomposition of methyl iodide and the per cent formation of iodine depend upon the pressures of foreign gases in the constant-pressure systems. For a simple photodecomposition with no secondary reactions or for a photodecomposition in which the dissociation fragments react only with the parent compound, the per cent decomposition would be independent of the partial pressure of CH_3I . It appears, therefore, that a competing secondary reaction involving the collisional deactivation of $I(^2P_{1/2})$ is occurring as shown in



The formation of C_2H_6 is evidence for the deactivation of CH_3^* radicals, as shown in reaction 8. No conclusions can be drawn, however, on the relative specific rates of reactions 8 and 14. Since the rapid bimolecular reactive processes including C_2H_6 formation are observed to be nearly complete in 100 μsec, the deactivation processes must involve less than a few thousand collisions. This conclusion is in general agreement with

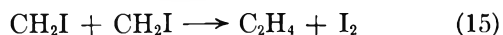
(36) G. Porter and J. A. Smith, *Proc. Roy. Soc.*, **A261**, 28 (1961).

(37) F. P. Lossing, K. U. Ingold, and I. H. S. Henderson, "Applied Mass Spectrometry," The Institute of Petroleum, London, 1954, p 102.

(38) C. E. H. Bawn and C. F. H. Tipper, *Discussions Faraday Soc.*, **2**, 104 (1947).

the results of Donovan and Husain^{39,40} on $I(^2P_{1/2})$ deactivation.

The occurrence of reaction 15 between two CH_2I radi-



cals formed in reaction 2 is a possible source of ethylene.⁴¹ Although ethylene and acetylene are produced in measurable quantities in the present experiments, the absolute molar concentration of iodine significantly exceeds that of all other detected products. Therefore, it is unlikely that reaction 15 is a major source of I_2 . An alternative reaction of the CH_2I radicals is with I_2 to form CH_2I_2 by reaction 12; however, CH_2I_2 is not detected mass spectrometrically. This is reasonable, since the concentration of I_2 is initially zero.

The over-all quantum yield for CH_3I decomposition is estimated²⁴ as 0.6. This figure is based upon observed values of 20–75% decomposition and incident ultraviolet light fluxes of 10^{18} to 3×10^{18} quanta/cm², respectively. The corresponding quantum yields for I_2 and CH_4 formation, excluding the experiments with added O_2 , are about 0.2 and 0.07, respectively. The ethane yield is at least 0.05. These yields are by no means limiting values.

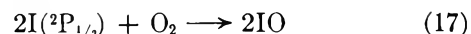
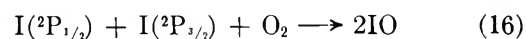
The I_2 quantum yield is in agreement with the value of 0.2 reported by Davidson and Carrington²¹ for flash-photolysis experiments with no accumulated iodine. The high quantum yields for CH_3I decomposition and for I_2 formation are attributed to the insignificant occurrence of reactions 10 and 11. In single flash-photolysis experiments, C_2H_6 formation by reaction 9 predominates over the regeneration of CH_3I by reaction 10. Although the specific rates of these processes are nearly equal ($k_9 \sim k_{10} \sim 10^{10} - 2 \times 10^{10}$ l. mol⁻¹ sec⁻¹),^{16,42} the high initial concentration of CH_3 radicals and the essentially zero initial concentration of I_2 favor the occurrence of reaction 9. Reaction 11 is essentially noncompeting with other CH_3 radical reactions. A third body is probably required because of the excess energy carried by either or both CH_3 and I .

The high absolute CH_4 yield is an order of magnitude greater than that previously reported.^{5,7} Harris and Willard found that the quantum yield for CH_3I decomposition was 12 times higher at 1849 Å than at 2537 Å. This was accompanied by a smaller increase in the CH_4 yield. They suggested that the additional energy carried by the hot CH_3^* radicals was vibrational energy, which would be more effective in reactive collisions. Similarly, the broad spectral absorption in the present studies may account for the large CH_4 yield.

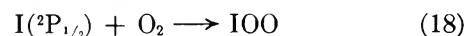
Implications of Scavenger Experiments. The proposal on the reactivity of metastable iodine ($^2P_{1/2}$) atoms is in agreement with quantum yields reported for radical-scavenger experiments. Several investigators observed iodine quantum yields $\Phi_{I_2} = 1/2$ when NO or O_2

were employed to scavenge the CH_3 radicals and to prevent the occurrence of reaction 10.^{43–45} Since the limiting value was obtained only when the ratio of NO or O_2 to CH_3I was equal to or greater than unity, it is concluded that the $I(^2P_{1/2})$ atoms were scavenged or deactivated. If not, the occurrence of reaction 4 would have led to an iodine quantum yield approaching $\Phi_{I_2} = 1$. Donovan and Husain have reported that NO is the most effective quencher of $I(^2P_{1/2})$.⁴⁰

In the flash photolysis of iodine and oxygen, Durie and Ramsay¹⁶ observed the formation of IO. They attributed its formation to the $I(^2P_{1/2})$ atom reaction 16 or 17. McKellar and Norrish¹⁷ also have detected IO



in the slow flash combustion of methyl iodide. The absence of IO during the high-temperature explosive combustion of CH_3I , however, is explained by reaction



18. Since the final products are I_2 and O_2 , the quantum yield for I_2 production in the oxygen-scavenger experiments would be unaffected.

Excited atoms are produced in the photolysis of molecular iodine at wavelengths less than 4995 Å. However, Kasper, *et al.*,¹⁵ have not detected laser action. They attribute this to the rapid deactivation of $I(^2P_{1/2})$ atoms by I_2 , which is consistent with the data obtained by Donovan and Husain.³⁹ It may also explain the unimportance of reaction 4 in those steady-state photolysis experiments in which I_2 was added or allowed to accumulate as a product. For example, Davidson and Carrington²¹ measured a differential iodine quantum yield of only 0.005 when I_2 was present initially in the flash photolysis of CH_3I .

Comparison with Radioiodine-Exchange Experiments. Harris and Willard⁷ reported a quantum yield of unity for the 2537 Å photochemical exchange reaction between CH_3I and $^{131}I_2$. Their $CH_3I:I_2$ ratio was 30, which may have been sufficient to guarantee a competition between reactive collisions of $I(^2P_{1/2})$ with CH_3I and deactivating collisions with I_2 . A quantum yield greater than unity should result, however, if the atoms

(39) R. J. Donovan and D. Husain, *Nature*, **206**, 171 (1965); **209**, 609 (1966).

(40) R. J. Donovan and D. Husain, *Trans. Faraday Soc.*, **62**, 11, 1050, 2023 (1966).

(41) D. Lewis and G. J. Mains, 149th National Meeting of the American Chemical Society, Detroit, Mich., April 1965, Abstract S18.

(42) G. B. Kistiakowsky and E. K. Roberts, *J. Chem. Phys.*, **21**, 1637 (1953).

(43) W. J. Blaedel, R. A. Ogg, Jr., and P. A. Leighton, *J. Amer. Chem. Soc.*, **64**, 2500 (1942).

(44) T. Iredale and E. R. McCartney, *ibid.*, **68**, 144 (1946).

(45) M. I. Christie, *Proc. Roy. Soc.*, **A244**, 411 (1958); **A249**, 248 (1959).

react with CH_3I producing additional CH_3 radicals. An increase in exchange rate did occur when 1849-Å radiation was not filtered out. More recent work by Aditya and Willard⁴⁶ also gives negative results. A mixture of $^{131}\text{I}_2$ and CH_3I was photolyzed at 4500, 4600, and 4900 Å. $\text{CH}_3\text{I}:\text{I}_2$ ratios of 130 and 650 were used. No $\text{CH}_3^{131}\text{I}$ was detected in excess of that produced by the dark reaction. Thus a significant discrepancy exists between the results reported herein, which are consistent with the observations of Pimentel and coworkers^{14,15,29,30} and the radioiodine-exchange experiments.

The explanation may involve differences in kinetic energies. For similar partial and total pressures of reactants, the broad absorption occurring in flash photolysis generates higher temperatures than are produced in monochromatic, steady-state photolyses. If a small activation energy, in addition to the heat of reaction, applies to the abstraction reaction 4, the average temperature of the system or the excess kinetic energy of the iodine atoms may weakly control the reaction rate; that is, the excited atoms must have a large kinetic energy in order to accelerate the reaction appreciably. Iodine ($^2\text{P}_{1/2}$) atoms generated from I_2 at 4900 and 4500 Å possess about 0.2 and 2.8 kcal/mol of excess kinetic energy, respectively. As previously noted, the $\text{I}(^2\text{P}_{1/2})$ atoms produced by flash photolysis of CH_3I have 4–7.5 kcal/mol.

Conclusion

Time-resolved studies of molecular iodine formation in the flash photolysis of methyl iodide indicate a rate of I_2 production too fast to be explained by termolecular recombination. Consideration of the electronic and kinetic energy available to the primary iodine atom shows that the excited-atom abstraction reaction 4 is energetically possible. Heat capacity calculations of

effective temperatures and reaction half-time estimates support the absence of pyrolysis and other high-temperature processes. The dependence of the relative yields of I_2 and CH_4 on added inert gases suggests that the I_2 -forming reaction has a weak positive temperature dependence, which probably explains the different conclusions from the radioiodine-exchange experiments by Aditya and Willard.⁴⁶ Existing knowledge of iodine atom reactions with nitric oxide, oxygen, and molecular iodine allows an explanation of earlier methyl iodide studies in which $\text{I}(^2\text{P}_{1/2})$ atoms surely were present. The data and interpretation are consistent with the laser studies of Pimentel and coworkers,^{14,15,29,30} which definitely establish the presence of $\text{I}(^2\text{P}_{1/2})$ atoms and suggest the chemical reactivity of them with the parent alkyl iodide.

The chemical reactivity of $\text{I}(^2\text{P}_{1/2})$ atoms has been indicated in other recent studies. For example, Callear and Wilson⁴⁷ attributed the high yield of isopropyl iodide in the photolysis of I_2 and C_3H_8 to a hydrogen abstraction from C_3H_8 by $\text{I}(^2\text{P}_{1/2})$ atoms. In addition, Donovan and Husain³⁹ have allowed the possibility that the deactivation of $\text{I}(^2\text{P}_{1/2})$ by $\text{C}_2\text{H}_5\text{I}$ may be due to a chemical reaction with $\text{C}_2\text{H}_5\text{I}$ or one of its decomposition products. It is concluded, therefore, that the rapid formation of I_2 observed in the present studies demonstrates the reaction between excited iodine atoms and methyl iodide.

Acknowledgments. The author acknowledges the valuable assistance of J. M. Freese in performing the experiments. Appreciation is also expressed to Drs. J. Yguerabide and L. S. Nelson for many helpful discussions.

(46) S. Aditya and J. E. Willard, *J. Chem. Phys.*, **44**, 418 (1966).

(47) A. B. Callear and J. F. Wilson, *Nature*, **211**, 517 (1966).

Pulse Radiolysis of Ammonia Gas—Rate of Disappearance

of the $\text{NH } ^3\Sigma$ Radical¹

by G. M. Meaburn

Centre D'Etudes Nucleaires de Saclay, Saclay, France

and Sheffield Gordon

Chemistry Division, Argonne National Laboratory, Argonne, Illinois 60439 (Received October 16, 1967)

The radiolysis of ammonia gas at pressures ranging from 300 to 1000 torr has been studied using pulse techniques. The absorption spectrum of the NH radical due to the $A^3\pi \rightarrow X^3\Sigma$ transition at 3360 Å has been obtained and the disappearance of this radical under various experimental conditions has been studied by following the decay of this band. The NH radical forms with a G value of ~ 0.4 and decays by a second-order process in pure ammonia. An upper limit of $7 \times 10^{11} M^{-1} \text{sec}^{-1}$ for the second-order rate constant for the reaction of two NH radicals has been calculated from the data. Scavengers such as O_2 , propylene, and ethylene react with NH , their relative rate constants being $k_{\text{NH}+\text{O}_2}:k_{\text{NH}+\text{Pr}}:k_{\text{NH}+\text{Eth}} = 40:2:1$. Ammonia vapor and water vapor (up to 6%) do not react with NH in the triplet ground state.

Introduction

The radiolysis of ammonia gas has been studied by several investigators²⁻⁸ using γ irradiation and fast electron bombardment. Recently, Sorokin and Pshezhetskii^{6,7} determined the yields of hydrogen, nitrogen, and hydrazine produced by irradiating ammonia at pressures ranging from 200 to 600 torr with both γ rays and fast electrons. On the basis of their kinetic data, they proposed a reaction mechanism involving the NH_2 radical and the H atom as the only reactive primary species. Like the earlier investigators, they did not consider the NH radical to be an important primary entity.

We have studied the radiolysis of pure ammonia at pressures ranging from 300 to 1000 torr and of ammonia containing a number of additives using short single pulses of 300-kV electrons. Under these conditions we were able to observe the absorption band assigned to the $X^3\Sigma \rightarrow A^3\pi$ transition of the NH radical. From the present results it appears that the NH radical has to be considered in any mechanism proposed to account for the radiation-induced decomposition of ammonia.

Experimental Section

The source of pulsed electrons used in this work consisted of a 300-kV Field Emission Corp. pulse generator connected through external transmission lines to a cathode adapted from a klystron manufactured by the Compagnie Sans Fil (France). The emitted electrons were collimated magnetically through a 27- μ titanium window of 25-mm diameter. Single pulses of approximately 250-kV electrons were delivered to the irradiation cell. The rise time of the pulse was about 15 nsec, and the width at half-height was approximately

130 nsec. The apparatus will be described in detail in another publication.

A schematic drawing of the stainless steel irradiation cell used in this work is shown in Figure 1. The electron beam enters the cell vertically through a stainless steel window (A) which is 10 μ thick and 50 mm in diameter. The analyzing light beam traverses the cell at right angles to the electron beam axis. The windows (B and C) of the cell are made of Supersil quartz. The cell is used with an external multiple pass mirror system (D and E) based on the White design.⁹ Throughout this work 12 passes were used. The total optical path length in the cell is about 96 cm, the electron beam width at this point being about 8 cm. Because of the narrow band widths of the transient absorptions observed, a photomultiplier detection system was not easily adapted. The spectra were recorded with the aid of a Hilger medium quartz spectrograph using Ilford HP3 plates. The decay of the transient absorption was determined from microdensitometer readings of the optical density changes,

(1) Work performed at Saclay. S. G. gratefully acknowledges the support of the Commissariat à l'Énergie Atomique of France and the U. S. Atomic Energy Commission for support during his stay at Saclay.

(2) (a) E. Wourtsel, *Compt. Rend.*, **158**, 571 (1914); (b) G. R. Gedye and T. E. Allibone, *Proc. Roy. Soc. (London)*, **A130**, 346 (1931).

(3) G. M. Schwab, *Z. Anorg. Allgem. Chem.*, **236**, 296 (1938).

(4) H. Essex, *J. Phys. Chem.*, **58**, 42 (1954).

(5) B. P. Burt and T. Baumer, *J. Chem. Phys.*, **23**, 466 (1955).

(6) B. P. Burt and A. B. Zahlen, *ibid.*, **26**, 846 (1957).

(7) Yu. A. Sorokin and S. Ya Pshezhetskii, *Zh. Fiz. Khim.*, **38**, 798 (1964); *Russ. J. Phys. Chem.*, 434 (1964).

(8) Yu. A. Sorokin and S. Ya Pshezhetskii, *Zh. Fiz. Khim.*, **39**, 1955 (1965); *Russ. J. Phys. Chem.*, 1037 (1965).

(9) J. V. White, *J. Opt. Soc. Am.*, **32**, 285 (1942).

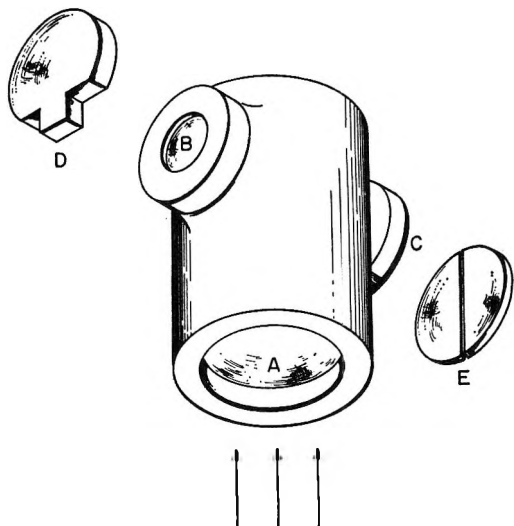


Figure 1. Schematic of irradiation cell: A, 10- μ stainless steel window; B, C, Supersil window; D, E, front surface aluminized Supersil.

recorded on the photographic plates. A small argon-filled spectroflash lamp provided the source of analyzing light. It was operated with an electrical input of about 70 J. A representative continuum is shown in Figure 2. A single flash produced an optical density of about 0.8 on the photographic plates and this value was determined to lie on the linear portion of the Γ curve for these plates where $\Gamma_{3360} = 1$. The pulse shape of the analytical flash is shown in Figure 3. The width at half-height of the light pulse is about 2 μ sec.

Dose rates were determined using the nitrous oxide dosimeter, assuming a $G(\text{N}_2)$ of 9.68.¹⁰⁻¹²

Ammonia was purified by freezing out the ammonia from a cylinder of dry ammonia. It was further purified by a process of repeated freezing, pumping, and melting and trap-to-trap distillation. The cell was pumped to a pressure lower than 10^{-5} torr and flushed with ammonia several times before the final filling. A similar technique was used to purify the additive gases.

The product gases, nitrogen and hydrogen, were pumped from the irradiated ammonia and analyzed by gas-solid chromatography. Hydrazine was determined colorimetrically by converting to HNO_2 and coupling with *p*-dimethylaminobenzaldehyde.¹³

Results

1. *Pure Ammonia.* The radiolysis of pure ammonia was studied at pressures ranging from 300 to 1000 torr. With a single pulse of electrons it was possible to observe the absorption band assigned to the $X^3\Sigma \rightarrow A^3\pi$ transition of the NH radical.¹⁴ All optical density measurements were carried out at 3360 Å on the partially resolved Q branch of the (0, 0) band. The (1, 1) band of the same electronic transition appears weakly at 3370 Å indicating that a small proportion of the NH radicals are produced in the first vibration

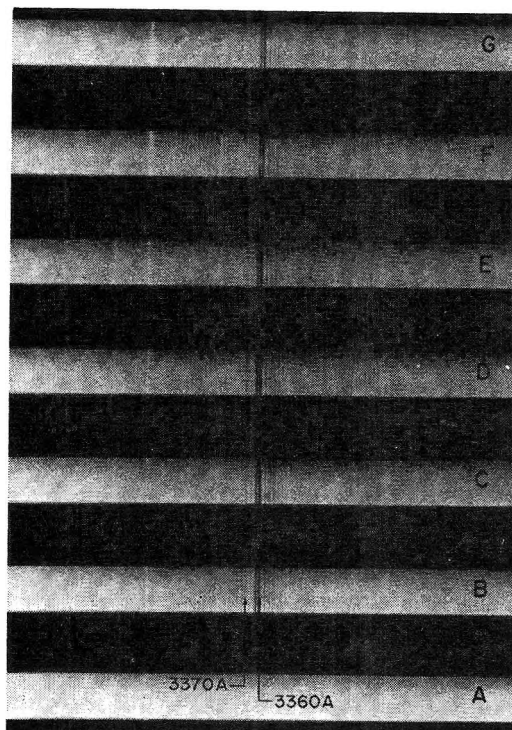


Figure 2. Spectra of the $A^3\pi \rightarrow X^3\Sigma$ transition of the NH radical produced in electron-pulsed NH_3 (740 mm); produced with a 40-nsec pulse from a Febetron Model 701 pulser: A, spectral flash; B, 1 μ sec after A; C, 3 μ sec after A; D, 6 μ sec after A; E, 10 μ sec after A; F, 20 μ sec after A; G, 40 μ sec after A.

level and have not relaxed after sustaining many collisions (10^3 after 1 μ sec after the pulse). The spectrum is shown in Figure 2. This was the only transient absorption observed in the spectral region between 2300 and 6500 Å. The detection system was not adapted to the observation of the NH_2 radical absorption. Lambert's law was verified by measuring the optical density of the NH radical absorption for different numbers of passes through the absorption cell. This, together with the fact that the NH concentration is very low, makes our assumption of the Lambert-Beers law a reasonable one.

The NH radical absorption appears to decay according to second-order kinetics. The data for different ammonia pressures are plotted in Figure 4. The half-lives ($t_{1/2}$) and initial optical densities (D_0) determined from these plots are given in Table I. Using the ordinary kinetic treatment, a plot of $\log t_{1/2}$ vs. $\log D_0$ should give a straight line whose slope is equal to $-(n - 1)$, where n is the order of the reaction. The data are plotted in this manner in Figure 5 together

(10) P. Harteck and S. Dondes, *Nucleonics*, **14**, 66 (1956).

(11) B. P. Burt and I. E. Kircher, *Radiation Res.*, **9**, 1 (1958).

(12) G. R. A. Johnson, *J. Inorg. Nucl. Chem.*, **24**, 461 (1962).

(13) F. Feigl, "Spot Tests," Elsevier Publishing Co., Amsterdam, 1939, p 320.

(14) R. N. Dixon, *Can. J. Phys.*, **37**, 1171 (1959).

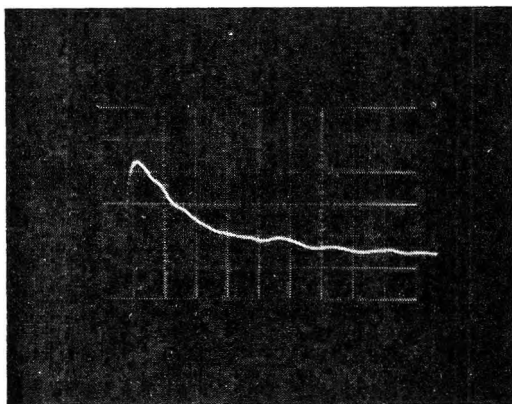


Figure 3. Photomultiplier output signal from spectral flash lamp; 1 μ sec/division.

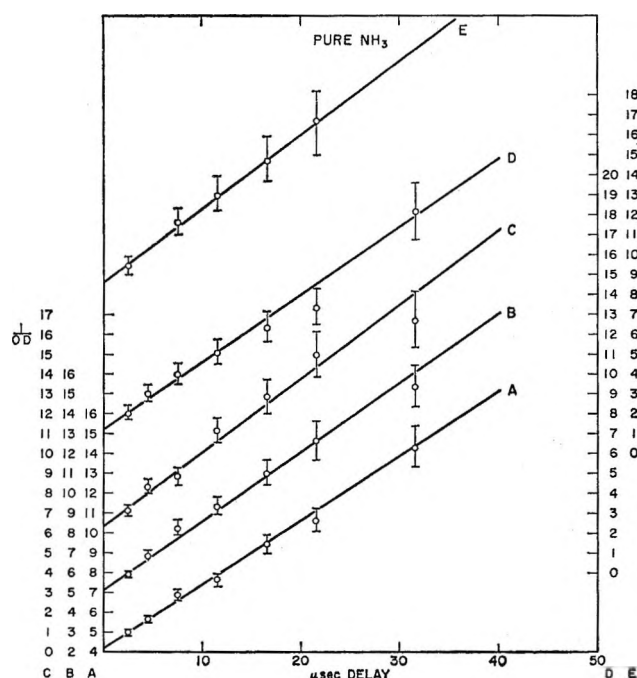


Figure 4. Second-order plots of NH decay in pure NH_3 : A, 300 mm of NH_3 ; B, 400 mm of NH_3 ; C, 500 mm of NH_3 ; D, 750 mm of NH_3 ; E, 1000 mm of NH_3 .

with a straight line corresponding to $n = 2$. In Figure 6, the dependence of D_0 on dose is shown.

It should be noted that although this figure illustrates the linear dependence of initial optical density with dose over the range of pressure studied, the straight line does not extrapolate to zero OD and zero dose (zero pressure). One possible explanation is that at the pressures at which measurements were made, the divergence of the beam due to electron scattering results in NH radicals forming in the complete volume element of the cell traversed by the analyzing light beam. Since the dose is determined from N_2 production at equivalent N_2O pressures, the NH radical concentration would be proportional to the pressure of NH_3 . At lower pressures of NH_3 , the beam divergence

Table I: Dependence of $(\text{OD})_0$ on Dose

P_{NH_3} , mm	$t_{1/2}$, μ sec	$(\text{OD})_0$	Dose absorbed/pulse
300	23.2	0.116	1.62×10^{18}
400	21.2	0.138	2.16×10^{18}
500	17.2	0.157	2.69×10^{18}
725	14.2	0.175	3.92×10^{18}
1000	13.0	0.238	5.12×10^{18}

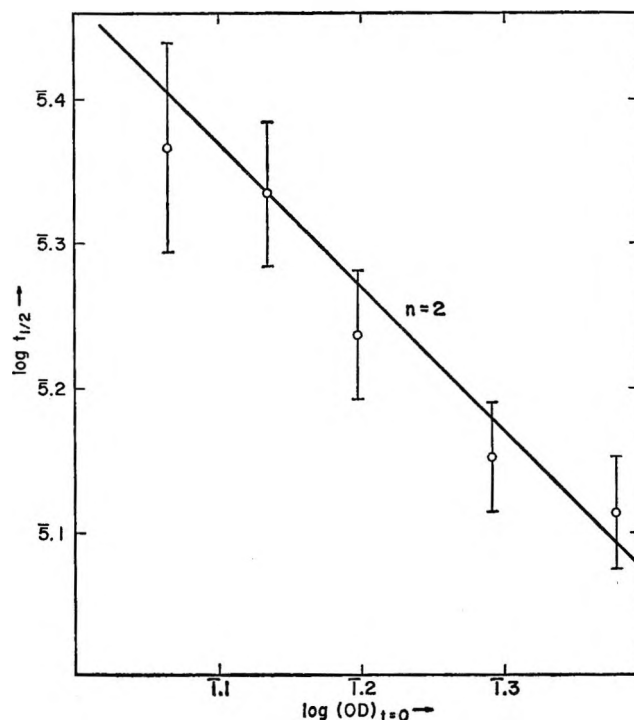


Figure 5. Second-order test of NH decay.

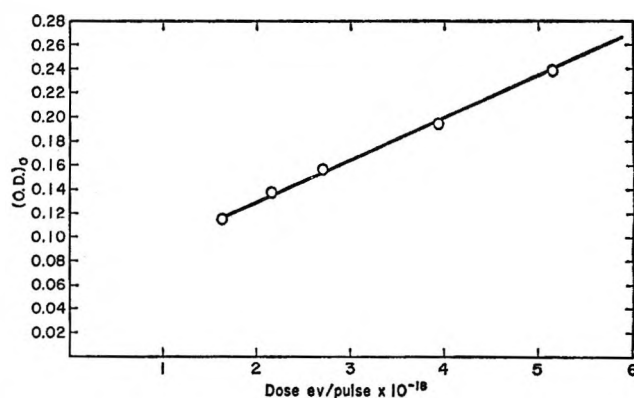


Figure 6. Dose vs. initial optical density of the NH radical absorption at 3360 \AA .

is less and the volume element traversed by the analyzing light may not be filled. In this case, the NH radical concentration would not be proportional to pressure.

2. *Ammonia-Additive*. An attempt has been made

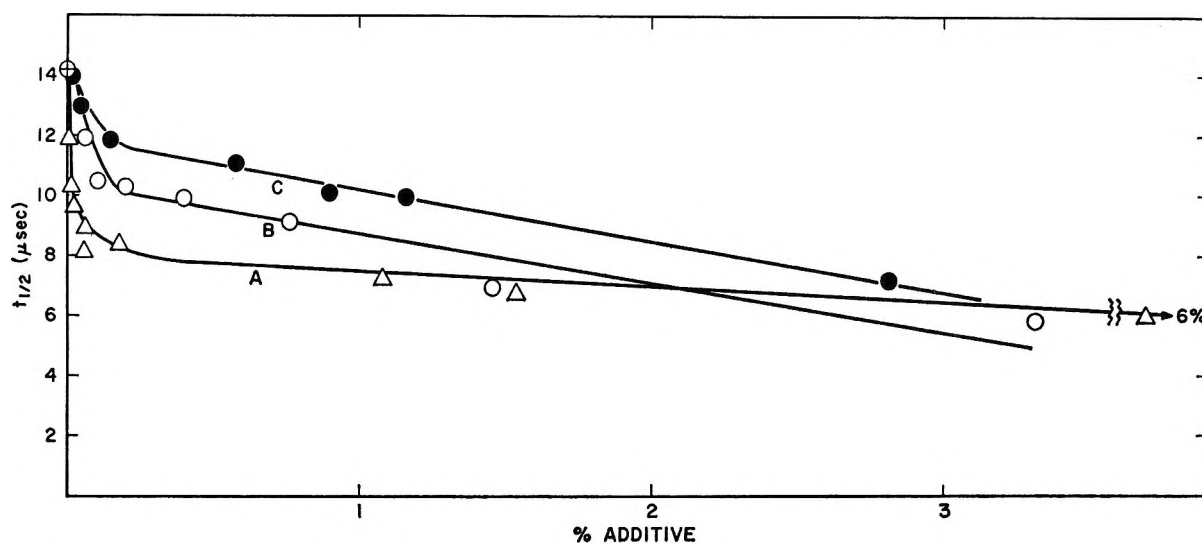


Figure 7. Effect of additives on $t_{1/2}$ for NH absorption decay: Δ , O₂; O, propylene; ●, ethylene.

to determine the effect of potential NH radical scavengers on the rate of disappearance of the NH absorption. The effect of adding small amounts of ethylene, propylene, or oxygen to ammonia is to change the order of the reaction with respect to NH from second to pseudo-first order. Because of a lack of resolution in time, it was not possible to follow the change of order in a precise manner; hence it was not possible to obtain good estimates of the pseudo-first-order rate constants for the reactions between NH and additives. The first-order plots for the NH radical decay curves at different concentrations of additive which reduce its half-life to below 10 μsec seem to follow first-order kinetics better than the curves representing concentrations of additive which result in an NH half-life longer than 10 μsec .

A plot of $t_{1/2}(\text{NH})$ against additive concentration is shown in Figure 7. The possible reasons for the slow decrease of $t_{1/2}$ after the initial fast decrease will be discussed later.

In the case of ammonia containing oxygen, two new absorption spectra were observed at the highest oxygen concentration used in this work (6%): a very weak transient at 3100 \AA and a broad permanent absorption growing in below 3000 \AA . No new absorptions were seen in ammonia containing either propylene or ethylene.

Ammonia containing 1% water vapor was also irradiated. No effect was observed on the half-life of the NH radical and the NH decay reaction remained second order. No new absorption spectra were seen in this case.

The effect of propylene on the yield of hydrogen, nitrogen, and hydrazine was determined. The results are shown in Table II and plotted in Figure 8.

Discussion

1. Formation of Primary Species. In a study of

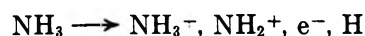
Table II: Effect of Propylene upon H₂, N₂, and N₂H₄ Yields from Irradiated NH₃

% C ₃ H ₆	$G(\text{H}_2)$	$G(\text{N}_2)$	$G(\text{N}_2\text{H}_4)$	No. of shots ^a
0	2.3 ± 0.2^b	0.68 ± 0.03^b	...	5
0.10	1.30	0.65	...	5
0.20	1.24	0.58	...	5
0.40	1.06	0.55	...	5
0.76	0.99	0.50	...	5
1.46	0.75	0.38	...	5
3.32	0.84	0.47	...	5
0	0.07	5
3.3	0.18	5

^a Dose per pulse = 4.0×10^{18} eV (NH₃ pressure = 740 torr).

^b $G(\text{H}_2)$ and $G(\text{N}_2)$ for pure NH₃ are mean values of four runs.

the radiolysis of liquid ammonia, Cleaver and co-workers¹⁵ extrapolated the data available from the mass spectral studies of ammonia¹⁶⁻¹⁸ and concluded that the following ionic reactions were important in their system



Recently, Harrison and Thynne¹⁸ have shown that reaction 2 becomes increasingly important at higher pressures of NH₃ and with increasing electron bombard-

(15) D. Cleaver, E. Collinson, and F. S. Dainton, *Trans. Faraday Soc.*, **56**, 1040 (1960).

(16) M. M. Mann, A. Hustralid, and J. T. Tate, *Phys. Rev.*, **58**, 346 (1940).

(17) L. Dorfman and P. C. Noble, *J. Phys. Chem.*, **63**, 980 (1959).

(18) A. G. Harrison and J. C. J. Thynne, *Trans. Faraday Soc.*, **62**, 2804 (1966).

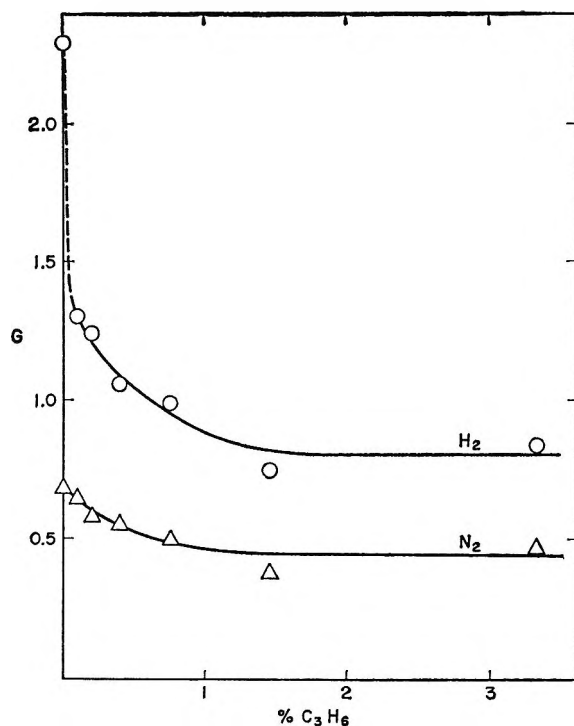
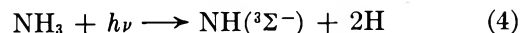


Figure 8. Effect of propylene concentration on yields of nitrogen and hydrogen.

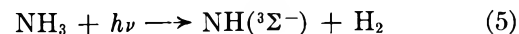
ment energy, due to the fact that the energy required to produce NH_2^+ from NH_3 is higher than that required to produce NH_3^+ from NH_3 by approximately 4 eV.

We can do no better than make the same assumptions for the primary production of these species (NH , NH_2 , and H) in the gas-phase radiolysis of ammonia. We can now safely assume that reactions 1, 2, and 3 will be completed within 10^{-9} sec for our systems.

In addition, a proportion of the primary radical yield will arise from direct excitation processes. Both NH_2 and NH radicals have been produced in ammonia by continuous and flash photolysis methods.¹⁹⁻²³ Bayes, Becker, and Welge¹⁹ and Stuhl and Welge²⁰ observed the $^3\Sigma \rightarrow ^3\pi$ transition in absorption by flashing ammonia at pressures ranging from 0.1 to 8 torr with a vacuum uv flash source. At wavelengths $>2000 \text{ \AA}$ they detected NH_2 and no NH ; between 1600 and 2000 \AA both NH_2 and NH were observed, whereas below 1600 \AA NH was obtained very strongly and little or no NH_2 was indicated. The lack of NH_2 detection was attributed, as we do, to insensitivity of the experimental arrangement. The photographic plates used were insensitive in the region of maximum NH_2 absorption and the mirror coating absorbed somewhat in this region. Stuhl and Welge found that the NH appears less than $1 \mu\text{sec}$ (their time resolution) after the flash and concluded from their experimental conditions that it is formed as a primary species. The following primary process is postulated

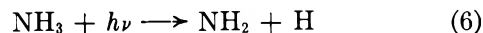


They excluded the formation of the molecular hydrogen directly from the reaction



because it would violate the Wigner spin conservation rule.

McNesby²⁴ showed that at 1236 \AA under steady light illumination 14% of the primary decomposition proceeds by reaction 5 and 86% by reaction 4 and the reaction



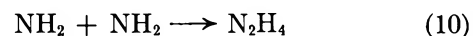
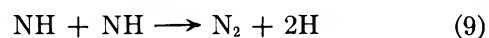
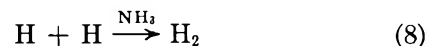
One other possibility stems from the work of Becker and Welge,²¹ who studied the luminescence produced on flashing ammonia with light at 1165, 1236, and 1295 \AA . They find that practically all the luminescence observed can be attributed to the $'\pi \rightarrow '\Delta$ transition of the NH radical. The possibility then remains in our studies, as was also discussed by Stuhl and Welge,²⁰ that a transition without emission through exchange of spin and orbit momentum results from collision between $\text{NH} (' \Delta)$ with NH_3 , (approximately 10^3 collisions in $2 \mu\text{sec}$ at 1000 torr of ammonia) according to the reaction



in which NH_3^* is formed in a singlet state.²⁵ The fact that the $'\Delta \rightarrow '\pi$ transition at 3240 \AA was not seen does not alter the possibility that reaction 7 occurs since the $'\Delta \rightarrow '\pi$ transition can escape observation because of too low concentration of NH and too low resolving power of the spectrograph since the lines of this absorption are widely spaced and weak.

2. Reactions Leading to Final Products. The only products resulting from ammonia radiolysis are considered to be hydrogen, nitrogen, and hydrazine. From the measured yields shown in Table II, it can be seen that a material balance has been achieved for pure ammonia with a N:H ratio close to 1:3.

The following reactions involving the primary atoms and radicals are expected to occur after the ionization and excitation events are complete.



(19) K. D. Bayes, K. H. Becker, and K. H. Welge, *Z. Naturforsch.* **17a**, 676 (1962).

(20) F. Stuhl and K. H. Welge, *ibid.*, **18a**, 900 (1963).

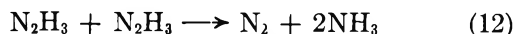
(21) K. H. Becker and K. H. Welge, *ibid.*, **19a**, 1006 (1964).

(22) W. Groth, *Angew. Chem.*, **75**, 734 (1963).

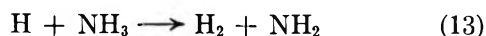
(23) W. Groth and H. J. Rommel, *Z. Physik. Chem. (Frankfurt)*, **45**, 96 (1965).

(24) J. R. McNesby, T. Tanaka, and H. Okaba, *J. Chem. Phys.*, **36**, 605 (1962).

(25) R. J. Johnson and A. B. F. Duncan, *ibid.*, **14**, 573 (1946).

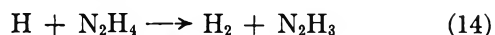


Under our conditions the following reaction will not be important



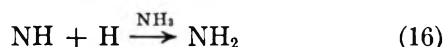
since the rate constant for this reaction has been determined to be $k_{13} \simeq 5 \text{ mol}^{-1} \text{ sec}^{-1}$,^{26,27} whereas the rate constant for reaction 8 has been determined²⁸ to be $k_8 \simeq 8 \times 10^9 \text{ l.}^2 \text{ mol}^{-2} \text{ sec}^{-1}$. Production of NH by secondary radical-radical reactions or radical-molecule reactions in pure ammonia cannot be important since we have shown that NH disappears by a second-order process immediately after the pulse (10^{-6} sec).

Reactions involving secondary attack of hydrazine will be insignificant during or after a single electron pulse. Hence reactions such as



will be omitted from the postulated mechanism. Hydrazine is certainly susceptible to attack by H alone as is shown by the results in Table II where the protective effect of propylene is demonstrated. On the basis that $G(\text{N}_2\text{H}_4) = 0.18$ is a true measure of the hydrazine resulting from reaction 10 when sufficient propylene is present to scavenge NH and eliminate reaction 11, it is concluded that the NH_2 radical is mainly consumed by reaction 11.

3. *Disappearance of NH from the System.* By following the decay of the NH absorption at 3360 \AA , we are in a position to observe the consequences of reactions 9, 11, and possibly



but we are not able to isolate the individual reactions. It is not surprising that, given our analytical technique with a time resolution which is low as a result of the short lifetimes involved, an apparently single second-order kinetic expression can be used to fit the experimental data. We can make a rough estimate of the concentration of NH radicals (and to a lesser extent the NH_2 radical) in the system immediately after the pulse by assuming the extinction coefficient for the NH radical obtained by Schnepf and Dressler²⁹ produced from NH_3 in a solid argon matrix. They estimate a molar extinction coefficient ϵ of 40,000 for this radical. Since

$$\text{OD} = \epsilon c$$

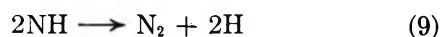
at 1000 torr and with an optical path l of approximately 100 cm we obtain an $(\text{OD})_0$ of 0.2. This means that with one pulse we have an NH concentration c of $5 \times 10^{-8} M$. Our dosage at this pressure is $5 \times 10^{18} \text{ eV/pulse}$ and our cell volume is 680 ml, which leads to a

$G(\text{NH})$ of 0.41. It is interesting to note that $G(\text{N}_2)$ which would result from reactions 9, 11, and 12 is 0.21. This is further borne out by the fact that $G(\text{N}_2)$ is decreased by approximately this amount (Figure 8) when 1% of propylene is added to the ammonia. This indicates that half of the N_2 observed in pure ammonia arises from reactions 9, 11, and 12. The nonscavengable N_2 could arise from further reactions involving NH_2 radical.

Using this value of $5 \times 10^{-8} M$ for the NH concentration and the $t_{1/2}(\text{NH})$ of $14 \times 10^{-6} \text{ sec}$, one can calculate a specific rate constant for NH disappearance from the relationship

$$t_{1/2} = \frac{1}{k_1(\text{NH})_0}$$

This turns out to be $1.4 \times 10^{12} M^{-1} \text{ sec}^{-1}$, and therefore for the reaction of two NH radicals



$$k = 7 \times 10^{11} M^{-1} \text{ sec}^{-1}.$$

In this calculation we have ignored reaction 11 since we were unable to detect the NH_2 radical and follow its decay using the experimental technique described. Therefore, this rate constant is an upper limit for reaction 9.

Although this is too high for a bimolecular reaction, one can say that the reaction of 2 NH radicals goes on every collision. The high rate constant for this reaction may be due to the fact that the NH radical is in a triplet state and could have a somewhat higher effective collision diameter for a bimolecular reaction.

The assumption of the value for ϵ_{NH} obtained by Schnepf and Dressler is subject to some criticism as one would expect the NH band in a solid matrix to be broadened somewhat compared to that obtained in the gas phase at 1000 torr, but the consistency of $G(\text{NH})$ calculated from their value and the reduction in $G(\text{N}_2)$ when propylene is added leads us to believe that that assumption is a reasonable one.

The dependence of the NH half-life on additive concentration (Figure 7) shows some interesting features. The $t_{1/2}$ for NH disappearance drops precipitously when O_2 is added up to a composition of approximately 0.05% O_2 . This is followed by a marked flattening off of the $t_{1/2}(\text{NH})$ vs. O_2 plot. We have mentioned earlier that after 6% O_2 has been added we observe two new bands appearing: a transient band at 3100 \AA and a permanent absorption growing in below 3000 \AA . The transient absorption corresponds closely to that attributed to the OH radical and the permanent band

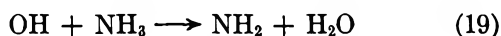
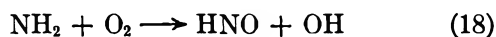
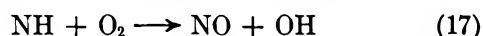
(26) M. Schiavello and G. G. Volpi, *J. Chem. Phys.*, **37**, 1510 (1962).

(27) K. T. Aganesyan and A. B. Nalbandyan, *Dokl. Akad. Nauk SSSR*, **160** (1), 162 (1965).

(28) C. B. Kretschmer and H. L. Peterson, *J. Chem. Phys.*, **39**, 1772 (1963).

(29) O. Schnepf and K. Dressler, *ibid.*, **32**, 1682 (1960).

appears where NO absorbs. The appearance of these bands may be accounted for by the following reactions.



In this reaction scheme, reactions 18 and 19 are propagated by the chain carrier NH_2 , the chain eventually being terminated by reaction 20 regenerating NH . Thus, we continue to see NH up to the highest concentration of O_2 used and this would lead to a flattening of the curve (Figure 7). Reactions 17-20 have also been postulated by Husain and Norrish³⁰ in their study of the explosive oxidation of ammonia initiated by flash photolysis.

In the case of ethylene and propylene, the initial drop is also rather sharp (Figure 7), that for propylene being more pronounced than that for ethylene. After the initial fast decrease, both curves show a slow decrease in $t_{1/2}(\text{NH})$ with further addition of gas. In view of the fact that in this region of added gas concentration the NH decay appears to follow pseudo-first order kinetics, we are at a loss to explain this behavior on kinetic grounds. One likely explanation is that the small values of $t_{1/2}(\text{NH})$ in this region of additive

concentration are due to an artifact introduced by the effect of the small tail on the pulse shape of our analyzing flash lamp (Figure 3) which limits our time resolution leading to excessively large values of the half-life for the NH radical in this region of additive concentration.

Another contributing factor to this slow decrease of $t_{1/2}(\text{NH})$ with further addition of gas may be the reformation of NH due to reaction 20.

An estimate of the relative effectiveness in removing NH from the system can be made by comparing the concentrations of different additives necessary to reduce the half-life of NH to, say 10 μsec . It is seen that, on this basis

$$k_{\text{NH}+\text{O}_2} : k_{\text{NH}+\text{Pr}} : k_{\text{NH}+\text{Eth}} = 40 : 2 : 1$$

Acknowledgment. The authors wish to express their appreciation to Dr. H. Hering for his support in this investigation and for his aid in bringing the pulser used in this work into operation. It was his original conception of this apparatus and material aid in the design work that made this investigation possible. We also wish to express our thanks to Mr. A. Reifsteck, Dr. D. Perner, and Dr. J. Sutton for their cooperation in this work.

(30) D. Husain and R. G. W. Norrish, *Proc. Roy. Soc. (London)*, **A273**, 145 (1963).

Pulse Radiolytic Studies of the Competition $H + H$ and $H +$ Ferricyanide. The Absolute Rate Constants¹

by J. Rabani

Department of Physical Chemistry, The Hebrew University, Jerusalem, Israel

and D. Meyerstein²

Chemistry Division, Argonne National Laboratory, Argonne, Illinois 60439 (Received October 16, 1967)

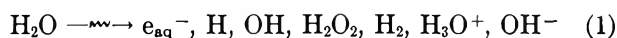
The bimolecular rate constant of the reaction of hydrogen atoms with ferricyanide ions has been measured in aqueous solutions. We get $k(H + Fe(CN)_6^{3-}) = (6.5 \pm 0.5) \times 10^9 M^{-1} sec^{-1}$ in the region pH 2-3. Competition between $H + Fe(CN)_6^{3-}$ and $H + H$ yielded $2k(H + H) = (2.5 \pm 0.4) \times 10^{10} M^{-1} sec^{-1}$.

Introduction

Recently, measurements of several absolute rate constants for hydroxyl radical reactions have been reported.³ Using these absolute rate constants together with previous competition results⁴ made it possible to obtain many other OH reaction rate constants. As to hydrogen atoms, previous direct measurements gave: $k(H + H_2O_2) = 9 \times 10^7 M^{-1} sec^{-1}$,⁵ $k(H + O_2) = 2.1 \times 10^{10} M^{-1} sec^{-1}$,^{6a} $k(H + \text{tetranitromethane}) = 5.5 \times 10^8 M^{-1} sec^{-1}$,^{6b} $k(H + MnO_4^-) = 2.4 \times 10^{10} M^{-1} sec^{-1}$,^{6c} and $k(H + Ag^+) = 1.1 \times 10^{10} M^{-1} sec^{-1}$.^{6d}

The purpose of this work was to obtain additional information on the reactivity of hydrogen atoms in aqueous solutions. We measured $k(H + \text{ferricyanide})$ and used it for cross checking previous data. Also we determined $k(H + H)$ and compared the result with previously reported values.

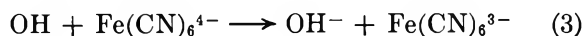
When water is irradiated, a variety of products is formed according to



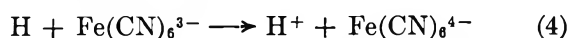
In the presence of 10^{-2} - $10^{-3} M$ perchloric acid, the hydrated electrons are converted into H atoms according to reaction 2. Except for OH^- the other species on the right-hand side of eq 1 are inert toward perchloric acid.⁷ When ferrocyanide ions are also



present, OH radicals react with them^{3a} ($k_3 = 1.07 \times 10^{10} M^{-1} sec^{-1}$)



Appropriate ferrocyanide ion concentrations can be chosen so that after $\sim 1 \mu sec$ all of the OH radicals have decayed away by reaction 3. Hydrogen atoms formed by process 1 and by reaction 2 are scavenged by the ferricyanide ions according to



Masri and Haissinsky⁸ reported small yields of ferroaquopentacyanide, $Fe(CN)_5H_2O^{3-}$, formed by the reduction of ferricyanide ions exposed to irradiation. They concluded that HO_2 radicals formed in the presence of O_2 lead to the formation of ferroaquopentacyanide in acid or neutral solutions. As will be discussed later, our results justify the neglect of ferroaquopentacyanide formation under our conditions.

If an appropriate concentration of ferricyanide is added initially so that all of the H atoms react with it, k_4 can be obtained from the decay curves of the ferricyanide optical absorption. By this method the measurement of k_4 is direct from the pseudo-first-order decay of ferricyanide. Reaction 5 is the only reaction which may contribute significantly to the decay of H

(1) Based on work performed under the auspices of the U. S. Atomic Energy Commission. The experimental work was carried out at Argonne National Laboratory and the computer calculations at The Hebrew University.

(2) On leave of absence from the Israel Atomic Energy Commission.

(3) (a) J. Rabani and M. S. Matheson, *J. Phys. Chem.*, **70**, 761 (1966); (b) M. S. Matheson, W. A. Mulac, J. L. Weeks, and J. Rabani, *ibid.*, **70**, 2092 (1966); (c) G. E. Adams, J. W. Boag, and B. D. Michael, *Trans. Faraday Soc.*, **61**, 1417 (1965); (d) J. K. Thomas, *ibid.*, **61**, 702 (1965).

(4) (a) J. Rabani and G. Stein, *ibid.*, **58**, 2150 (1962); (b) R. W. Matthews and D. F. Sangster, *J. Phys. Chem.*, **69**, 1938 (1965); (c) I. Kraljic and C. N. Trumbore, *J. Am. Chem. Soc.*, **87**, 2547 (1965); (d) M. Anbar, D. Meyerstein, and P. Neta, *J. Chem. Soc., B*, 742 (1966); (e) M. Anbar, D. Meyerstein, and P. Neta, *J. Phys. Chem.*, **70**, 2660 (1966).

(5) L. M. Dorfman and M. S. Matheson, *Progr. Reaction Kinetics*, **3**, 239 (1965).

(6) (a) S. Gordon, E. J. Hart, and J. K. Thomas, *J. Phys. Chem.*, **68**, 1262 (1964); (b) J. Rabani, W. A. Mulac, and M. S. Matheson, *ibid.*, **69**, 53 (1965); (c) J. H. Baxendale, J. P. Keene, and D. A. Stott in "Pulse Radiolysis," M. Ebert, Ed., Academic Press Inc., New York, N. Y., 1965, p 107; (d) J. H. Baxendale and P. L. T. Bevan in "The Chemistry of Ionization and Excitation," G. R. A. Johnson and G. Scholes, Ed., Taylor and Francis Ltd., London, 1967, p 254.

(7) (a) D. Katakis and A. O. Allen, *J. Phys. Chem.*, **68**, 3107 (1964); (b) C. J. Hochanadel, *Radiation Res.*, **17**, 286 (1962).

(8) (a) E. Masri and M. Haissinsky, *J. Chim. Phys.*, **60**, 397 (1963); (b) M. Haissinsky, A. M. Koulekès, and E. Masri, *ibid.*, **63**, 1129 (1966).

atoms and introduce an error in k_4 . Under our conditions the corrections made in k_4 due to reaction 5 were not more than 10%.



Experimental Section

The experimental procedure has been described before.⁹ We used a 4-cm cell with 8-cm light path in all the experiments. Materials were of Analar grade, and the water was triply distilled. Syringes have been baked at 500° before use. A 450-W Osram xenon lamp produced the analyzing light. A shutter between the lamp and the cell was opened only shortly (about 1 sec) before the electron pulse. A Corning 3-74 glass filter helped to minimize the photolysis of ferrocyanide and ferricyanide by the analyzing light.

The formation and decay of ferricyanide was followed at 4200 Å (ϵ 1000 M^{-1} cm^{-1}). A Tektronix 555 oscilloscope was employed so that two sweep rates could be used simultaneously.

Ferri- and ferrocyanide air-free solutions were prepared and kept in syringes for not more than 30 hr in a refrigerator and 12 hr at room temperature before use. In order to prevent the oxidation of ferrocyanide by air, O_2 was first removed from the water by bubbling argon, and only then was the ferrocyanide dissolved. Since ferri- and ferrocyanide solutions are less stable in acid pH,⁸ the solutions were made acid 10–15 min before use, by injecting the necessary amount of HClO_4 from a deaerated stock solution with the aid of a microsyringe.^{9e} The duration of the electron pulse was 1 μsec , but in some cases a 0.4- μsec pulse has been used. The temperature was 24°.

Results and Discussion

k_4 . A typical oscillogram showing the formation and decay of ferricyanide is shown in Figure 1. It has been projected and plotted on paper which has a scale of optical density. The final optical density is negative, since more ferricyanide is destroyed than formed in agreement with $G_{(\text{H})} > G_{\text{OH}}$.¹⁰ ($G_{(\text{H})}$ is the sum of yields of H atoms formed by process 1 and reaction 2. G_{OH} is the radical yield of OH.)

When $\log(D_t - D_\infty)$ was plotted *vs.* time (D_t is the optical density at 4200 Å at time t), a straight line was obtained from the slope of which we calculated k_4 .

Table I summarizes the experiments used for the evaluation of k_4 . There seems to be no effect of pH in the region between pH 2 and 3. We obtain an average $k_4 = (6.5 \pm 0.5) \times 10^9 M^{-1} \text{sec}^{-1}$ ($0.5 \times 10^9 M^{-1} \text{sec}^{-1}$ is the standard deviation).

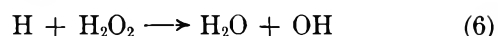
$2k_5$. The competition between reactions 4 and 5 at relatively low ferricyanide concentrations can be used to evaluate $2k_5$. The experimental D *vs.* t curves were fitted with the aid of an IBM 7040 computer, using a program written by Schmidt.¹¹ The only important

Table I: k_4 at Various Ferricyanide Concentrations^a

10^3 [ferricyanide], M	pH ^b	$10^{-9}k_4$, ^c $M^{-1} \text{sec}^{-1}$
5.1	2.00	5.9 (2)
1.3	2.50	6.2 (2)
2.4	2.50	6.1 (4)
4.8	2.50	6.9 (7)
9.7	2.50	5.8 (2)
4.8 ^d	2.50	7.2 (2)
9.3 ^d	2.50	6.3 (2)
5.3	3.00	7.5 (2)

^a In $4.0 \times 10^{-4} M$ potassium ferrocyanide. ^b HClO_4 . ^c Corrections have been made for the small contribution of reaction 5 and for the depletion of ferricyanide. The number in parentheses represents the number of individual experiments from which an average value for k_4 was calculated. ^d Pulse intensity 1.3×10^{20} eV l.⁻¹. In other experiments the pulse intensity was 5.5×10^{19} eV l.⁻¹.

reactions responsible for the decay of hydrogen atoms are (4) and (5). Reaction 6 ($k_6 = 9 \times 10^7 M^{-1}$



sec^{-1})⁵ can be neglected since the computer results show that it never accounted for the decay of more than 0.2% of the hydrogen atoms.

Figure 2 demonstrates the competition between reactions 4 and 5. Computation no. 1 in Table II gives good agreement with the experimental results and is also included in Figure 2.

Five different sets of parameters have been used in

Table II: Effect of Changing Parameters on Computed D *vs.* t Curves^a

No.	$G_{(\text{H})}$	k_4^b	$2k_5^c$	Final optical density $\times 10^2$
1	3.2	6.5	2.20	2.02
2	3.2	7.8	2.64	2.02
3	3.2	6.5	2.64	2.20
4	2.6	6.5	2.20	2.25
5	2.6	6.5	1.70	2.02

^a For $2.27 \times 10^{-6} M$ ferricyanide initially present, $4.0 \times 10^{-4} M$ ferrocyanide, $3 \times 10^{-3} M$ HClO_4 , 1.25×10^{20} eV l.⁻¹ per pulse, 1- μsec pulse duration, G_{OH} assumed 2.6. ^b In units of $10^9 M^{-1} \text{sec}^{-1}$. ^c In units of $10^{10} M^{-1} \text{sec}^{-1}$.

(9) For radiolysis apparatus see: (a) M. S. Matheson and L. M. Dorfman, *J. Chem. Phys.*, **32**, 1870 (1960); (b) L. M. Dorfman, I. A. Taub, and R. E. Buhler, *ibid.*, **36**, 3051 (1962); for syringe technique and cell filling see: (c) S. Gordon, E. J. Hart, M. S. Matheson, J. Rabani, and J. K. Thomas, *Discussions Faraday Soc.*, **36**, 193 (1963); (d) C. Senvar and E. J. Hart, *Proc. Intern. Conf. Peaceful Uses At. Energy, 2nd Geneva, 1955*, **29**, 19 (1958); (e) E. J. Hart, S. Gordon, and J. K. Thomas, *J. Phys. Chem.*, **68**, 1271 (1964).

(10) A. O. Allen, "The Radiation Chemistry of Water and Aqueous Solutions," D. Van Nostrand Co., Inc., Princeton, N. J., 1961.

(11) K. H. Schmidt, ANL-Report 7199, Argonne National Laboratory, Argonne, Ill., 1966.

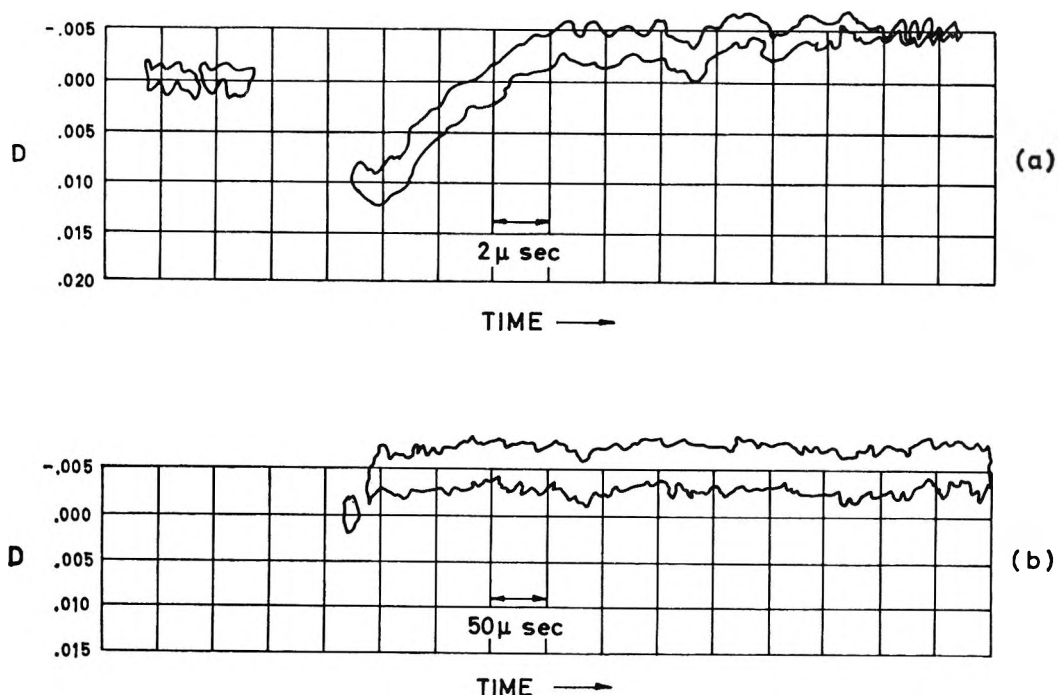


Figure 1. Decay curve of ferricyanide in $4.4 \times 10^{-4} M$ ferrocyanide, $9.29 \times 10^{-6} M$ ferricyanide initially present, $3 \times 10^{-3} M$ HClO₄, 1-μsec pulse of 1.3×10^{20} eV l.⁻¹.

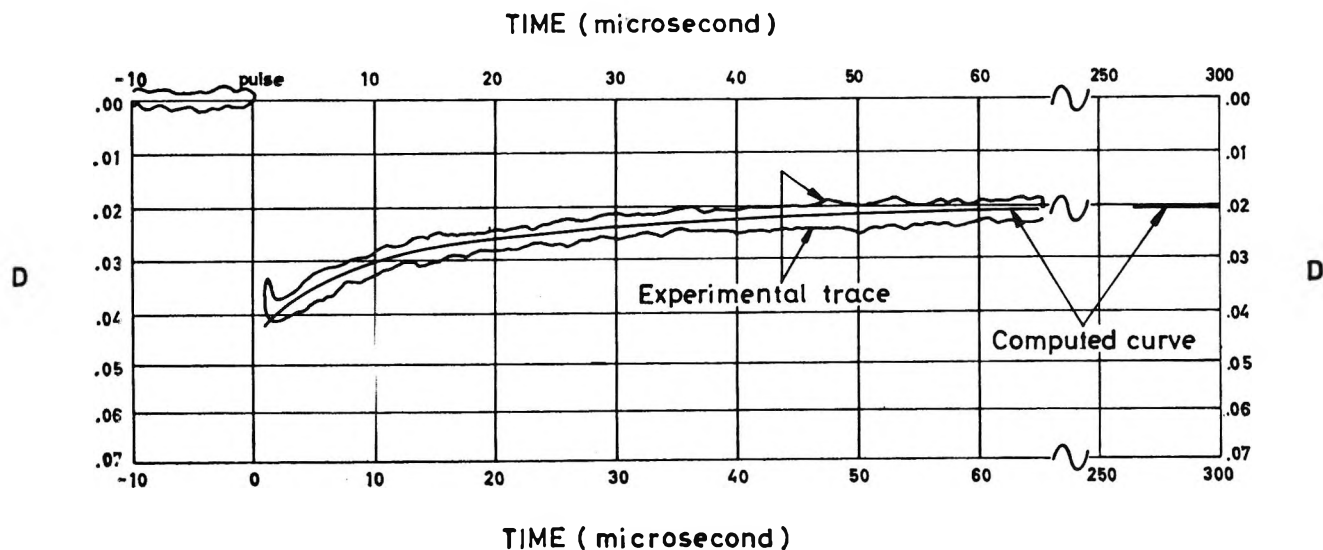


Figure 2. Comparison of experimentally observed and computer-calculated optical density vs. time, during the competition H + H and H + ferricyanide; $4.4 \times 10^{-4} M$ ferrocyanide, $2.27 \times 10^{-6} M$ ferricyanide initially present, $3 \times 10^{-3} M$ HClO₄. The computed curve was obtained with $G_{(H)} = 3.2$, $G_{(OH)} = 2.6$, 1.25×10^{20} eV l.⁻¹, 1-μsec pulse, $k_4 = 6.5 \times 10^9$, $k_5 = 1.1 \times 10^{10} M^{-1} sec^{-1}$. An extinction coefficient of $1000 M^{-1} cm^{-1}$ was used for ferricyanide.

order to investigate the effect on the D vs. t curves. Comparison of the computed curves obtained with different parameters is given in Table II.

From the computations summarized in Table II, it can be concluded: (a) When both k_4 and k_5 are changed but their ratio remains constant, only the rate of change in the optical density is affected, but not the final optical density, D_∞ . (This means that the distribution of H between reactions 4 and 5 is unaffected.) (b) Under the conditions of Table II and Figure 2 an

increase of 20% in k_5 increases the computed D_∞ by 9%.

Computations 4 and 5 demonstrate the sensitivity to $G_{(H)}/G_{(OH)}$. The intensity of the electron pulse was calculated from the initial optical absorption using $G_{(OH)} = G(\text{ferricyanide}) = 2.6$. Therefore, the computation does not depend on the specific $G_{(OH)}$ value which was chosen, but on the ratio $G_{(H)}/G_{(OH)}$. Although in different systems somewhat different $G_{(H)}$ and $G_{(OH)}$ have been measured,¹² the ratio $G_{(H)}/G_{(OH)}$ is about the same.

Computations 4 and 5 show that changing $G_{(H)}/G_{OH}$ from 1.23 to 1.00, while other parameters were kept constant, caused a deviation of 11% in the computed D_{∞} . In order to obtain the same D_{∞} , $2k_5$ had in addition to be changed to $1.7 \times 10^{10} M^{-1} sec^{-1}$. However, the error in $G_{(H)}/G_{OH}$ is not more than 5% under our conditions. Therefore, it can be concluded that in experiments such as described in Table II and Figure 2 the reasonable error in $G_{(H)}/G_{OH}$ has only little effect on the computed value of $2k_5$. This is not the case at higher ferricyanide concentrations where most of the hydrogen atoms react with ferricyanide. The greater the fraction of H reacting *via* (4), the greater is the effect of deviations in $G_{(H)}/G_{OH}$ on the computed curve. Thus, for $1.39 \times 10^{-5} M$ ferrocyanide and $2k_5 = 2.5 \times 10^{10} M^{-1} sec^{-1}$ (other conditions as in Table II), $D_{\infty} = 9.83 \times 10^{-3}$ is computed, taking $G_{(H)}/G_{OH} = 1.23$. In order to get the same D_{∞} with $G_{(H)}/G_{OH} = 1.00$, $2k_5 = 1.43 \times 10^{10} M^{-1} sec^{-1}$ should be chosen. In Table III we summarize the results obtained from figures such as Figure 2. For most of the results presented in Table III the uncertainty in $G_{(H)}/G_{OH}$ introduces only a small error in $2k_5$.

Table III: Evaluation of $2k_5$

Ferricyanide ^a	Dose rate ^b	$10^{-9}k_4, M^{-1} sec^{-1}$	$10^{-10}2k_5, M^{-1} sec^{-1}$	% recombination ^c
<i>d</i>	0.560	6.5	2.5	67
<i>d</i>	0.595	6.5	2.9	69
<i>d</i>	0.150	6.5	1.8	61
<i>d</i>	1.370	6.6	2.8	68
<i>d</i>	2.150	6.6	2.2	64
2.27	0.540	6.5	2.4	51
2.27	1.200	6.5	2.1	56
3.15	0.567	6.5	3.4	54
4.59	0.600	6.0	2.3	44
4.59	1.300	6.5	1.9	48
4.59	1.340	6.5	2.4	53
6.50	0.540	6.0	2.8	40
6.82	0.582	6.5	2.4	36
6.82	1.310	6.5	2.1	45
9.02	0.550	6.0	3.0	36
9.02	1.300	6.5	2.4	43
11.1	1.740	6.5	2.2	43
13.9	0.580	6.5	2.6	25.7
13.9	1.43	6.5	2.0	35.0

^a Concentration before pulse, in units of $10^{-6} M$. All experiments in $5 \times 10^{-4} M$ ferrocyanide. ^b In units of $10^{26} eV l^{-1} sec^{-1}$. ^c The per cent H atoms reacted *via* reaction 5. ^d No ferricyanide initially present.

We conclude $2k_5 = (2.4 \pm 0.4) \times 10^{10} M^{-1} sec^{-1}$. (The error limit here is the standard deviation. It does not include systematic errors due to k_4 and $G_{(H)}/G_{OH}$.)

If $2k_5$ is normalized to $k_4 = 6.5 \times 10^9 M^{-1} sec^{-1}$, $2k_5 = (2.5 \pm 0.4) \times 10^{10} M^{-1} sec^{-1}$ results.

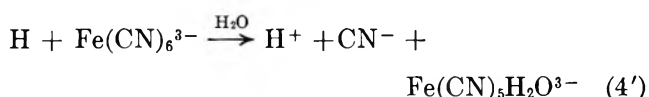
Comparison with Previous Work

$2k_5$. Our value of $2k_5 = 2.5 \times 10^{10} M^{-1} sec^{-1}$ is in agreement with $3.0 \times 10^{10} M^{-1} sec^{-1}$ measured by Schwarz¹³ and $2.0 \times 10^{10} M^{-1} sec^{-1}$ by Sweet and Thomas.¹⁴

k_4 . The value of $k_4 = 6.5 \times 10^9 M^{-1} sec^{-1}$ is higher by a factor of 4.3 than the one reported by Navon and Stein in neutral solutions at 4°. ¹⁵

Other Rates. Using $k_4 = 6.5 \times 10^9 M^{-1} sec^{-1}$, it is possible to calculate several rate constants for hydrogen atoms. Ferricyanide has been used to compete with ethanol for H atoms, and, from the reported rate constant ratio of 240,¹⁶ we get $k(H + ethanol) = 2.7 \times 10^7 M^{-1} sec^{-1}$ as compared with $k = 1.32 \times 10^7$ obtained by Baxendale and Bevan.^{6d} Using other rate constant ratios¹⁷ we get: $k_{H+OH^-} = 1.8 \times 10^7 M^{-1} sec^{-1}$, in good agreement with previously reported values.¹⁸ On the basis of the competitions between ferricyanide and ethanol, and of O₂ and ethanol,¹⁷ we find $k_{H+O_2} = 1.4 \times 10^{10} M^{-1} sec^{-1}$. This value is in satisfactory agreement with the previously reported values of 2.1×10^{10} ,^{6a} 2.4×10^{10} ,¹³ and 1.0×10^{10} ,^{16c} and in very good agreement with the value of $1.3 \times 10^{10} M^{-1} sec^{-1}$ reported by Fricke and Thomas.¹⁹

Ferroaquopentacyanide. Our computations were based on the assumption that reactions 4 and 5 were the only reactions in which H atoms were involved. We have neglected the possible formation of ferroaquopentacyanide⁸ by



This is justified by the results obtained under conditions of total H atom scavenging by ferricyanide (see Figure 1). D_{∞} of Figure 1 corresponds to the known¹⁰ difference of $G_{(H)} - G_{OH}$ at pH 2-3. Thus, any optical absorption at 4200 Å due to reaction 4' can be neglected.

In conclusion, ferroaquopentacyanide has not been formed in our experiments in any significant amount or at least it could not have any effect on the evaluation of $2k_5$.

As to k_4 , we calculated it assuming that under our conditions reaction 4 was the only reaction between

(12) A. O. Allen, *Radiation Res. Suppl.*, **4**, 54 (1964).

(13) H. A. Schwarz, *J. Phys. Chem.*, **67**, 2827 (1963).

(14) J. P. Sweet and J. K. Thomas, *ibid.*, **68**, 1363 (1964).

(15) G. Navon and G. Stein, *ibid.*, **69**, 1384 (1965).

(16) J. Rabani, *ibid.*, **66**, 361 (1962).

(17) See references in J. Rabani, *Advances in Chemistry Series*, No. 50, American Chemical Society, Washington, D. C., 1965, p 242.

(18) (a) M. S. Matheson and J. Rabani, *J. Phys. Chem.*, **69**, 1324 (1965); (b) E. J. Hart, S. Gordon, and E. M. Fielden, *ibid.*, **70**, 150 (1966).

(19) H. Fricke and J. K. Thomas, *Radiation Res. Suppl.*, **4**, 35 (1964).

ferricyanide and H atoms. If (4') is included, our value $k_4 = 6.5 \times 10^9 M^{-1} \text{sec}^{-1}$ should be replaced by $k_4 + k_4' = 6.5 \times 10^9 M^{-1} \text{sec}^{-1}$.

Acknowledgment. We are indebted to Dr. M. S. Matheson for helpful discussions. We wish to thank

Mr. U. Shainok of The Hebrew University for his help with the computer calculations. We wish also to thank the Linac group for their careful operation and Mr. S. Petrek of ANL for maintaining the electronic equipment.

The Photolysis of 1,3-Difluoro- and 1,1,3,3-Tetrafluoroacetone

at Low Pressure¹

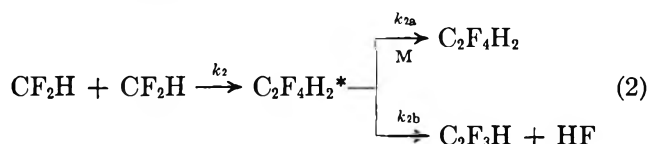
by G. O. Pritchard and J. T. Bryant

Department of Chemistry, University of California, Santa Barbara, California 93106 (Received October 17, 1967)

1,3-Difluoroacetone and 1,1,3,3-tetrafluoroacetone, and their mixtures, were photolyzed at low pressures (about 0.1 torr). The disproportionation:combination ratio between two CF_2H radicals is redetermined to be 0.19-0.20, and that for $\text{CFH}_2 + \text{CF}_2\text{H} \rightarrow \text{CFH}_3 + \text{CF}_2$ is determined to be about 0.06; the alternative reaction to yield $\text{CF}_2\text{H}_2 + \text{CFH}$ does not occur, nor is there any disproportionation between two CFH_2 radicals. The elimination of HF from the vibrationally excited molecule $\text{CF}_2\text{HCF}_2\text{H}^*$ is discussed in terms of the RRK theory of unimolecular reactions, and an estimation of the activation energy of the process $\text{C}_2\text{F}_4\text{H}_2 \rightarrow \text{C}_2\text{F}_3\text{H} + \text{HF}$ of 56 kcal mol⁻¹ is obtained. The elimination of HF from "hot" $\text{CF}_2\text{HCFH}_2^*$ leads to the formation of 1,1- and *cis*- and *trans*-difluoroethylenes. An effect of added nitrogen on the relative rates of formation of the three fluoroethylenes is observed, which is discussed in terms of the critical energies involved in the eliminations.

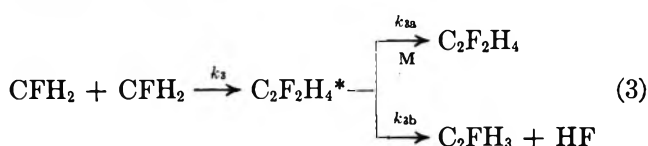
Introduction

In our previous investigation² of the photolysis of 1,1,3,3-tetrafluoroacetone (TFA), we observed the radical-radical interactions 1 and 2a but at the pres-



ures used we were unable to observe the elimination of HF from the vibrationally excited molecule, reaction 2b. Part of this report constitutes an investigation under conditions of lower pressure, in order that reaction 2b may effectively compete with the collisional quenching process, 2a.

In a prior investigation³ with 1,3-difluoroacetone (DFA) we observed the reaction sequences

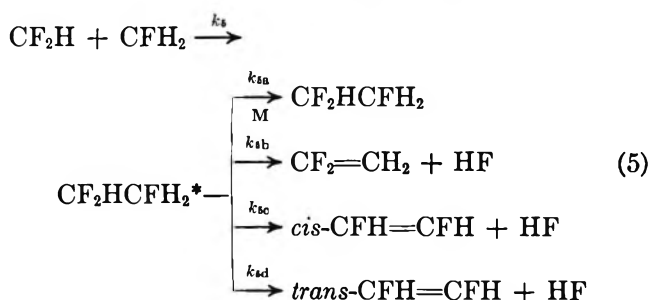


but the importance of the disproportionation



was not determined. The possible occurrence of this reaction is investigated.

In a preliminary communication⁴ we have reported on the photolysis of mixtures of DFA and TFA at low pressures, where the reactions of interest are



Herein we give more extensive data and describe the effect of added nitrogen on the various sequences de-

(1) This work was supported by a grant from the National Science Foundation, GP-4090.

(2) G. O. Pritchard and J. T. Bryant, *J. Phys. Chem.*, **70**, 1441 (1966).

(3) G. O. Pritchard, M. Venugopalan, and T. F. Graham, *ibid.*, **68**, 1786 (1964).

(4) J. T. Bryant, B. Kirtman, and G. O. Pritchard, *ibid.*, **71**, 1960 (1967).

picted in reaction 5. The possible disproportionation reactions and the cross-combination ratio between the two radicals are also discussed.

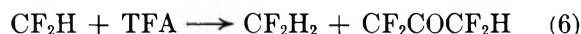
Experimental Section

The procedures have, in the main, been described elsewhere.^{2,3,5} Chromatographically pure samples of DFA and TFA were used, and analysis was carried out by means of low-temperature fractionation and vpc. All compounds were identified by comparative retention times with known samples and by their mass spectra.⁵ The *cis*- and *trans*-1,2-difluoroethylenes were distinguished by their infrared spectra.⁶

The low-pressure vacuum apparatus was mercury and grease free. Westef⁷ Teflon stopcocks with Viton A O rings were used in place of conventional stopcocks. The cylindrical quartz reaction cell was 50 cm long by 5.8 cm in diameter, with a volume of 1321 cm³, and it was fully illuminated by a collimated light beam in the 3130-Å region. Sufficient products for accurate analysis were thereby obtained at low total pressures and small percentage conversions. Reactant pressures were measured on a thermocouple gauge calibrated for TFA with a McLeod gauge in the range 0–0.36 torr. Higher pressures, and pressures of added N₂, were measured on a Wallace and Tiernan Bourdon-type gauge, which was calibrated in the range 0–110 torr. In the experiments with added N₂, the products were pumped into a large trap filled with glass beads at –195°. This prevented any loss of the 1,1-difluoroethylene, some of which was swept through an unpacked trap by the excess N₂.

Results and Discussion

TFA and DFA at Low Pressures. i. Disproportionation. The results of a number of runs with TFA are given in Table I. The disproportionation:combination ratio for CF₂H radicals, k_1/k_2 , at pressures where reaction 2b is negligible (note that $k_{-2} \ll k_{2b}$ ⁸) is well established at about 0.19.^{2,9,10} The data in Table I, where k_1/k_2 is now $R_{CF_2H_2}/(R_{C_2F_3H} + R_{C_2F_4H_2})$ and R is rate of formation, gives an average value of 0.20 for the 20 experiments between 303 and 516°K. From this and the variation in TFA pressure, *e.g.*, tenfold at ~515°K, it is evident that reaction 6, abstraction



from the ketone, is unimportant, under the experimental conditions. The activation energy for this reaction is also considerably higher¹⁰ than we have given previously.² At 551°K and above the ratio is >0.2, which may indicate the onset of reaction 6. Alternatively, the consumption of C₂F₃H by CF₂H radicals may occur¹¹ (CF₂H + C₂F₃H + CF₂H) and this will become of increasing importance at elevated temperature. This is borne out somewhat by the decrease in the mass-balance ratios with temperature, shown in Table I, since the ratio

Table I: Data on CF₂HCOCF₂H Photolysis

Temp, °K	Pressure, torr	Time, sec	Products, 10 ⁶ mol				Mb ^a
			C ₂ F ₃ H	CF ₂ H ₂	C ₂ F ₄ H ₂	CO	
303	0.273	20	0.642	0.940	4.078		
362	0.273	20	1.164	0.842	3.868		
399	0.360	10	0.993	0.750	3.417		
401	0.051	20	0.452	0.156	0.337		
402	0.098	20	0.941	0.341	0.974		
402	0.178	20	1.032	0.448	1.540		
402	0.273	20	1.416	0.814	3.272		
441	0.247	20	1.484	0.730	1.960		
482	0.260	20	1.685	0.860	2.236		
513	0.221	20	1.407	0.572	1.232		
513	0.273	20	1.837	0.724	1.965		
514	0.034	20	0.542	0.120	0.110		
514	0.070	20	0.865	0.244	0.335		
514	0.095	20	0.958	0.360	0.498		
514	0.140	20	0.812	0.290	0.454		
515	0.302	20	1.826	0.948	2.471		
516	0.181	20	1.772	0.586	1.265		
516	0.347	20	2.050	1.180	3.264		
551	0.273	20	1.539	0.772	1.368		
590	0.277	20	1.443	0.896	1.221		
478	0.143	20	0.790	0.280	0.616		
477	0.153	20	1.390	0.470	1.111	3.31	0.90
573	0.169	20	1.172	0.424	0.724	3.46	0.67
579	0.160	20	1.070	0.450	0.674	3.51	0.62
577	0.150	20	0.951	0.425	0.505	2.88	0.65

$$^a \text{Mass balance} = (R_{CF_2H_2} + R_{C_2F_3H} + R_{C_2F_4H_2})/R_{CO}$$

would not be affected if the acetyl radical produced in reaction 6 combined with a CF₂H radical. Radicals will also be consumed by the CF₂ species produced in reaction 1; however, no temperature dependence would be assumed in this case.¹² An attempt was made to identify any C₃ and C₄ fluorohydrocarbon products in the reaction mixture at 306°, but it was inconclusive. Products may also be formed and radicals lost by addition to the >C=O in the ketone.

Benson¹³ has effectively summarized the evidence against the "common transition state" assumption for disproportionation and recombination reactions of

(5) J. T. Bryant, Ph.D. Thesis, University of California, Santa Barbara, Calif., 1967.

(6) H. G. Viehe, *Chem. Ber.*, **93**, 1697 (1960).

(7) West-glass Corp., South El Monte, Calif.

(8) S. W. Benson and G. Haugen, *J. Phys. Chem.*, **69**, 3898 (1965).

(9) M. G. Bellas, O. P. Strausz, and H. E. Gunning, *Can. J. Chem.*, **43**, 1022 (1965).

(10) M. J. Perona, J. T. Bryant, and G. O. Pritchard, unpublished data.

(11) See R. D. Giles and E. Whittle, *Trans. Faraday Soc.*, **61**, 1425 (1965), for a discussion of the possible loss of CF₂=CH₂ in the CF₃ + CH₃ system.

(12) C₃F₂H₂ has been identified in the Hg-sensitized decomposition of CF₂HCl formed by CF₂H + CF₂ + CF₂H,⁹ and C₃F₃ and C₃F₄H formed *via* CF₃ + CF₂ + CF₃ and CF₃ + CF₂ + CF₂H, respectively, in the photolysis of pentafluoroacetone: J. B. Hynes, R. C. Price, W. S. Brey, Jr., M. J. Perona, and G. O. Pritchard, *Can. J. Chem.*, **45**, 2278 (1967).

(13) S. W. Benson, *Advan. Photochem.*, **2**, 1 (1964).

alkyl radicals. It is evident from the present work that the reaction channel that leads to disproportionation is an alternative one to that which leads to the "hot" ethane intermediate.

Data on DFA are presented in Table II. The only observed products were CO and vinyl fluoride. The complete absence of CFH_3 rules out the occurrence of reaction 4 and abstraction from the ketone, under the reaction conditions. The absence of $\text{C}_2\text{F}_2\text{H}_4$ indicates that $k_{3b} \gg k_{3a}[\text{M}]$; at higher ketone concentrations, *i.e.*, at higher $[\text{M}]$, it is readily observable.³ The decreasing mass-balance ratios with temperature may be attributed to the addition of CFH_2 radicals to C_2FH_3 . A search for the fluorobutane was again inconclusive.

Table II: Data on $\text{CFH}_2\text{COCFH}_2$ Photolysis^a

Temp., °K	Pressure, torr	Products, 10 ⁶ mol		Mb ^b
		CO	C ₂ FH ₃	
395	0.169	1.210	1.098	0.91
396	0.130	1.015	0.850	0.84
476	0.157	1.152	0.976	0.85
572	0.160	1.182	0.830	0.70
576	0.164	1.733	1.200	0.69

^a Time of all runs was 20 min. ^b Mass balance = $R_{\text{C}_2\text{FH}_3}/R_{\text{CO}}$.

ii. HF Elimination. From reaction scheme 2 we may write

$$\frac{R_{\text{C}_2\text{F}_4\text{H}_2}}{R_{\text{C}_2\text{F}_3\text{H}}} \frac{1}{[\text{M}]} = \frac{k_{2a}}{k_{2b}} \text{mm}^{-1} \quad (7)$$

where $[\text{M}]$ is the pressure of ketone, P_{TFA} , in mm. A plot of the data at two temperatures is given in Figure 1, in accord with eq 7,¹⁴ and a plot of k_{2a}/k_{2b} vs. temperature is given in Figure 2. The temperature dependence for $k_{\text{stab}}/k_{\text{elim}}$ has been treated by the simple-collision theory and the Rice-Ramsperger-Kassel theory of unimolecular decompositions for the "hot" molecules $\text{CFH}_2\text{CFH}_2^*$,⁸ C_2FH_5^* ,¹⁵ and $\text{CF}_2\text{HCH}_3^*$,¹⁶ and we may treat $\text{CF}_2\text{HCF}_2\text{H}^*$ in a similar manner. Details of the method and definition of the parameters can be found elsewhere.^{8,15,16} The upward curvature seen at low temperatures in Figure 2 was not observed in the previous systems^{8,15,16} over the same temperature range, but would presumably occur if experiments could be extended to lower temperatures. The region in which curvature occurs will be determined by the characteristics of the "hot" molecule and the nature of the moderating environment, as given by the theoretical equation^{8,15,16}

$$\frac{k_{2a}}{k_{2b}} = \frac{QZ}{A} \left(\frac{E}{E - E^*} \right)^{n-1} \quad (8)$$

For $\text{CF}_2\text{HCF}_2\text{H}^*$ we take E (internal energy) to vary between 85.4 kcal mol⁻¹ at 298°K and 93.9 kcal mol⁻¹

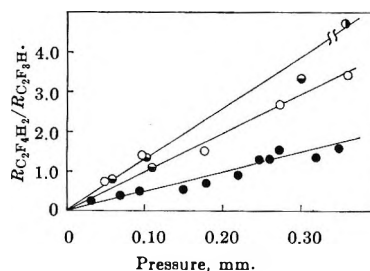


Figure 1. $R_{\text{C}_2\text{F}_4\text{H}_2}/R_{\text{C}_2\text{F}_3\text{H}}$ vs. ketone pressure, in mm: ○, TFA (399–402°K); ●, TFA (513–516°K); ◐, approximately 1:1 mixture of TFA + DFA (370–372°K); ○, same conditions but ratio is 9.56 at a total ketone pressure of 0.72 mm.

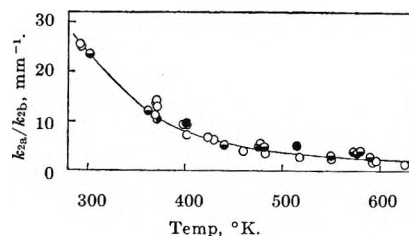


Figure 2. k_{2a}/k_{2b} , in min^{-1} , vs. absolute temperature: ●, TFA; ●, derived from slopes in Figure 1; ○, approximately 1:1 mixture of TFA + DFA; ○, derived from slope in Figure 1.

at 560°K.⁶ Taking n (number of effective oscillators) = 15,⁸ the theoretical and experimental curves are fitted in Figure 3.¹⁷ Some representative curves for values of the critical energy, E^* , of 50, 56, and 62 kcal mol⁻¹ are given. The best over-all fit appears to be with $E^* \cong 56$ kcal mol⁻¹. A similar result is obtained by taking a value of $n = 14$, and from a consideration of the number of effective (lower frequency) C–F oscillators in $\text{CF}_2\text{HCF}_2\text{H}^*$, a value of $n = 14$ –15 is certainly very reasonable.^{8,15,16} Assuming $n = 15$ and $E^* = 56$ kcal mol⁻¹, and taking the preexponential factor for the unimolecular decomposition, A , as $10^{13.5}$ sec⁻¹, and the collision frequency, Z , as 1.35×10^7 collisions mm⁻¹ sec⁻¹, we may calculate a collisional quenching efficiency factor, Q , of 18, which is meaningless. (Previously,^{8,15,16} values of Q in the range 0.1–1 were obtained, based on similar assumptions.) Smaller values of Q may be obtained⁸ by either raising E^* or n . If $n = 15$ is retained and $E^* = 62$ kcal mol⁻¹ is adopted, $Q \cong 1.0$, but from Figure 3 it is seen that these parameters do not give a good fit. If $E^* = 56$ kcal mol⁻¹ is retained, n must be raised to 18 before Q decreases below unity. If the low-temperature points in Figure

(14) At pressures below 0.10 torr, where mean free paths approach 1 mm, some wall stabilization may occur.

(15) G. O. Pritchard and R. L. Thommarson, *J. Phys. Chem.*, **71**, 1674 (1967).

(16) J. T. Bryant and G. O. Pritchard, *ibid.*, **71**, 3439 (1967).

(17) The quantity $1/2(1 - \text{Mb})R_{\text{CO}}$ has been added to $R_{\text{C}_2\text{F}_3\text{H}}$ to allow for the loss of $\text{C}_2\text{F}_3\text{H}$ by radical addition. Mb at each temperature was estimated from the data in Table I, and it was assumed to be unity at 298°K.

Table III: Data on $\text{CF}_2\text{HCOCF}_2\text{H}$ and $\text{CFH}_2\text{COCFH}_2$ Photolysis

Temp, °K	Reactant pressure, torr		Products, 10 ⁶ mol								
	TFA	DFA	CF_2CH_2	CFHCH_2^a	CF_2CFH	<i>trans</i> - CFHCFH	CF_2H_2	<i>cis</i> - CFHCFH	$\text{C}_2\text{F}_4\text{H}_2$	CO	Mb ^b
395	0.155	0.159	12.04	28.89	43.21	43.15	27.30	67.71	93.84	405.6	0.78
475	0.150	0.160	14.79	43.70	55.42	46.22	26.80	72.64	63.81	421.8	0.77
574	0.151	0.160	19.63	54.00	72.77	41.61	47.00	65.69	62.75	467.6	0.78
573	0.150	0.153	15.84	33.67	79.19	36.76	42.60	54.78	67.56	437.1	0.76
471	0.160	0.150	8.48	9.38	88.05	27.07	42.60	40.16	124.3	423.3	0.80
371	0.146	0.164	13.17	24.66	41.76	44.28	33.30	68.76	152.2	433.4	0.87

^a The vinyl fluoride also contains small amounts of CFH_3 . In the mass-balance calculation, they are assumed to have equal sensitivities on the vpc. ^b Mass balance = $(\Sigma R_{\text{C}_2\text{F}_2\text{H}_2} + R_{\text{CFH}_3} + R_{\text{C}_2\text{FH}_3} + R_{\text{C}_2\text{F}_3\text{H}} + R_{\text{CF}_2\text{H}_2} + R_{\text{C}_2\text{F}_4\text{H}_2})/R_{\text{CO}}$.

Table IV: Data on $\text{CF}_2\text{HCOCF}_2\text{H}$ and $\text{CFH}_2\text{COCFH}_2$ Photolysis

Temp, °K	Reactant pressure, torr		Products, 10 ⁶ mol					
	TFA	DFA	CF_2CH_2	CF_2CFH	<i>trans</i> - CFHCFH	CF_2H_2	<i>cis</i> - CFHCFH	$\text{CF}_2\text{HCF}_2\text{H}$
399	0.178	0.169	20.28	64.00	64.96	47.00	103.8	202.0
401	0.160	0.160	19.07	60.75	63.27	41.80	96.80	179.5
402	0.155	0.157	18.83	49.54	56.32	35.00	93.16	130.9
424	0.160	0.143	18.58	78.65	57.37	42.80	89.04	166.5
431	0.160	0.160	21.65	71.69	63.91	38.00	111.8	139.3
461	0.273	0.287	30.06	99.44	85.65	65.80	137.8	222.3
518	0.160	0.160	18.75	78.11	45.25	37.40	71.59	72.13
593	0.049	0.051	4.484	26.22	10.87	12.75	16.40	4.774
595	0.273	0.287	25.21	88.41	48.32	88.40	76.60	89.51
594	0.160	0.178	21.01		42.66		64.64	
595	0.094	0.103	14.46		27.31		42.99	
591	0.052	0.051	5.818		12.40		18.46	
371	0.360	0.360	17.78	30.01	57.37	52.80	86.94	286.8
372	0.051	0.052	7.151	25.67	18.26	11.75	28.08	33.17
370	0.150	0.150	13.57	37.97	43.47	31.60	70.54	127.1
371	0.030	0.033	3.434	15.23	11.57	6.15	15.82	13.63
371	0.053	0.057	4.646	20.34	16.64	9.85	23.67	22.44
482	0.151	0.188	15.03	60.57	42.82	32.50	66.34	73.11
550	0.143	0.169	14.54	54.69	35.15	37.60	54.22	43.98
625	0.198	0.198	16.32	55.60	30.78	54.10	48.16	29.87
295	0.198	0.198	8.807	22.42	32.89	45.20	51.71	220.9
294	0.159	0.157	7.110	22.37	27.35	39.00	43.35	181.3

Table V: Data on $\text{CF}_2\text{HCOCF}_2\text{H}$ and $\text{CFH}_2\text{COCFH}_2$ Photolysis

Temp, °K	Reactant pressure, torr		Products, 10 ⁶ mol				
	TFA	DFA	CF_2CH_2	CFH_3	<i>trans</i> - CFHCFH	<i>cis</i> - CFHCFH	$\text{CFH}_3/\Sigma\text{C}_2\text{F}_3\text{H}_2^a$
393	0.160	0.152	14.87	8.29	45.65	68.44	0.064
389	0.054	0.053	4.85	2.31	16.67	19.90	0.056
387	0.302	0.302	19.98	9.83	66.90	110.8	0.050
402	0.155	0.157	18.83	11.89 ^b	56.32	93.15	0.071

^a No $\text{C}_2\text{F}_3\text{H}_3$ was observed until the pressure was increased to 0.72 torr. ^b In this experiment CFH_3 and C_2FH_3 were collected together and analyzed mass spectrometrically.

3 are omitted, a very good fit is obtained with $E^* = 50 \text{ kcal mol}^{-1}$ and $n = 15$; however, Q is in excess of 150.

Recently we have pointed out⁴ the possibility of an alternative reaction path that leads to HF elimination.

The simultaneous occurrence of both reactions would render the RRK equation used here invalid, as the two eliminations would have different A factors and critical energies. The measured Arrhenius parameters would then represent some weighted average values. This

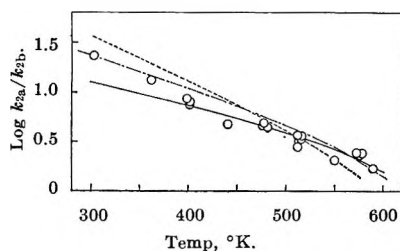


Figure 3. Comparison of the theoretical and observed temperature dependence of k_{2a}/k_{2b} for $n = 15$: O, experimental points (corrected, see ref 17); —, $E^* = 50$ kcal mole $^{-1}$ ($\log(QZ/A) = -4.15$); — · —, $E^* = 56$ kcal mole $^{-1}$ ($\log(QZ/A) = -5.12$); - - - -, $E^* = 62$ kcal mole $^{-1}$ ($\log(QZ/A) = -6.29$).

may well be the case with $\text{CF}_2\text{HCF}_2\text{H}^*$; note that if $A = 10^{12}$ sec $^{-1}$ is adopted, $Q = 0.56$ for $E^* = 56$ kcal mole $^{-1}$ and $n = 15$.

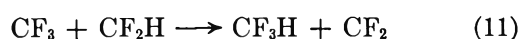
DFA and TFA Mixtures at Low Pressures. *i. Disproportionation.* Data on the DFA and TFA mixtures are collected in Tables III–V. No CF_2HCFH_2 or CFH_2CFH_2 was observed in the systems below a total pressure of 0.7 torr, indicating the unimportance of collisional quenching in reaction sequences 3 and 5 at these pressures. CO was measured in a number of experiments and the mass-balance ratios are given in Table III. The constancy of these with temperature indicates that radicals are being lost in the system by a predominantly temperature-independent reaction, presumably involving the CF_2 species.¹² Some further data are given in Table IV. The value of the disproportionation:combination ratio for CF_2H radicals, $R_{\text{CF}_2\text{H}_2}/(R_{\text{C}_2\text{F}_4\text{H}_2} + R_{\text{C}_2\text{F}_3\text{H}})$, calculated for 13 experiments between 294 and 461°K is 0.19 ± 0.02 , indicating no extraneous source of CF_2H_2 . (At higher temperatures, the ratio is >0.2 , for reasons already discussed.) This rules out the possible disproportionation



and also abstraction by CF_2H from DFA under the reaction conditions. The further disproportionation



must also be considered. By adjusting the chromatographic conditions,⁵ it was possible to resolve the CFH_3 and $\text{C}_2\text{F}_3\text{H}_3$ peaks, and the data are given in Table V. The ratio $R_{\text{CFH}_3}/\Sigma R_{\text{C}_2\text{F}_2\text{H}_2} = 0.06 \pm 0.01$ independent of pressure (attack by CFH_2 on TFA would not, in any case, be expected, considering the previous results) which may be taken as k_{10}/k_5 . It is seen that only the disproportionation reactions 1 and 10, in which CF_2 is produced, occur, while those which lead to the formation of CFH do not occur. These observations may be correlated with the considerable stabilization of CF_2 which has been noted.¹⁸ We¹⁰ have also observed the reaction



but data on



were inconclusive.¹⁶ The series of reactions 1, 10, 11, and 12 will be discussed more fully.¹⁰

ii. Cross Combination. In the absence of H-atom abstraction from the ketones and the collisional stabilization of $\text{C}_2\text{F}_2\text{H}_2^*$ and $\text{C}_2\text{F}_3\text{H}_3^*$ the cross-combination ratio, Ψ , for the two radicals is given by

$$\Psi = \frac{\Sigma R_{\text{C}_2\text{F}_2\text{H}_2} + R_{\text{CFH}_3}}{R_{\text{C}_2\text{F}_2\text{H}_2}^{1/2}(R_{\text{CF}_2\text{H}_2} + R_{\text{C}_2\text{F}_3\text{H}} + R_{\text{C}_2\text{F}_4\text{H}_2})^{1/2}} \quad (13)$$

Since $k_{10}/k_5 = 0.06$, we may use the data in Table III to redefine Ψ in eq 14

$$\Psi = \frac{1.06 \Sigma R_{\text{C}_2\text{F}_2\text{H}_2}}{(R_{\text{C}_2\text{F}_2\text{H}_2} - 0.06 \Sigma R_{\text{C}_2\text{F}_2\text{H}_2})^{1/2}(R_{\text{CF}_2\text{H}_2} + R_{\text{C}_2\text{F}_3\text{H}} + R_{\text{C}_2\text{F}_4\text{H}_2})^{1/2}} \quad (14)$$

Again considering only the experiments below 500°K, eq 14 leads to a value of $\Psi = 2.15 \pm 0.16$, which is the collision-theory prediction.¹⁹

iii. HF Elimination. The "hot" molecules of interest are $\text{C}_2\text{F}_4\text{H}_2^*$ and $\text{C}_2\text{F}_3\text{H}_3^*$. Data taken from Table IV on $R_{\text{C}_2\text{F}_4\text{H}_2}/R_{\text{C}_2\text{F}_3\text{H}}$ at 371°K are plotted in Figure 1 as a function of total pressure in the system $P_{\text{DFA}} + P_{\text{TFA}}$. The temperature variation of the function given in eq 7 is shown in Figure 2, where $[M] = P_{\text{TFA}} + P_{\text{DFA}}$, in mm. It is evident that the quenching efficiencies of the two ketones with respect to $\text{C}_2\text{F}_4\text{H}_2^*$ must be very similar. This is further shown for $\text{C}_2\text{F}_3\text{H}_3^*$ by the data presented in Table VI and Figure 4, where for the "hot" molecule in reaction sequence 5, we have

$$\frac{R_{\text{C}_2\text{F}_3\text{H}_3}}{\Sigma R_{\text{C}_2\text{F}_2\text{H}_2}} = \frac{k_{5a}[M]}{k_{5b} + k_{5c} + k_{5d}} \quad (15)$$

and $[M]$ is $P_{\text{TFA}} + P_{\text{DFA}}$. The data are well described by eq 15, even though there are large variations in the relative ketone pressures, indicating that the deactivating efficiencies are not very different.¹⁶

Data on the predicted⁸ and experimental $k_{\text{stab}}/k_{\text{elim}}$ for the vibrationally excited fluoroethanes at 298°K together with the critical energies obtained by the RRK method are given in Table VII. The agreement is satisfactory, except for $\text{CF}_2\text{HCF}_2\text{H}^*$, where the predicted ratio is not approached until a temperature of 600°K; see Figure 2. However, as we have already noted, the frequency factor for this particular elimination could be a factor of 30 less than that assumed by Benson and Haugen.⁸

(18) I. P. Fisher, J. B. Homer, and F. P. Lossing, *J. Amer. Chem. Soc.*, **87**, 957 (1965); J. P. Simons, *Nature*, **205**, 1308 (1965).

(19) J. A. Kerr and A. F. Trotman-Dickenson, *Progr. Reaction Kinetics*, **1**, 105 (1961).

Table VI: Data on $\text{CF}_2\text{HCOCF}_2\text{H}$ and $\text{CFH}_2\text{COCFH}_2$ Photolysis

Temp, °K	Ketone pressure, torr		Products, 10^6mol			
	TFA	DFA	CF_2CH_2	<i>trans</i> - CFHCFH	<i>cis</i> - CFHCFH	CF_2HCFH_2
391	0.9	1.2	79.51	215.3	384.0	490.6
390	2.3	2.7	59.47	136.1	258.6	698.7
391	3.7	1.2	33.13	73.69	131.9	338.0
391	0.2	4.8	34.34	75.95	120.7	383.0
391	0.2	2.4	32.24	91.14	148.6	209.8

Table VII: Comparison of Predicted and Experimental $k_{\text{stab}}/k_{\text{elim}}$ Ratios^a

"Hot" molecule	$k_{\text{stab}}/k_{\text{elim}}$ (298°K), mm^{-1}		Quencher [M]	E^* , kcal mol ⁻¹	Ref
	Predicted ^b	Exptl			
CFH_2CH_3	5.9×10^{-3}	5×10^{-3}	$\text{CFH}_2\text{COCH}_3$	59	15
		10^{-2}	?	51	c
CFH_2CFH_2	4.1×10^{-2}	2×10^{-2}	$\text{CFH}_2\text{COCH}_3$	59	15
		4.1×10^{-2}	DFA	62	3, 8
CF_2HCH_3	4.1×10^{-2}	1.4×10^{-2}	TFA + CH_3COCH_3	53	16
		$\sim 10^{-2}$	$\text{CH}_2\text{CO} + \text{CF}_2\text{H}_2$...	d
CF_3CH_3	2.9×10^{-1}	3.4×10^{-2} (423°K)	CF_3COCF_3	...	
		1.5×10^{-2} (423°K)	CH_3COCH_3	...	
CF_2HCFH_2	2.9×10^{-1}	3.1×10^{-1} (390°K)	DFA + TFA	...	This work
$\text{CF}_2\text{HCF}_2\text{H}$	1.8	24.2	TFA	56 (?)	This work

^a Since the completion of the manuscript, a further report has been given on the kinetics of decomposition of "hot" alkyl fluorides by the authors in ref *b* at the Faraday Society Meeting, Toronto, Sept 1967. We shall reserve further comment until the results are made generally available. ^b Reference 8. ^c J. A. Kerr, A. W. Kirk, B. V. O'Grady, and A. F. Trotman-Dickenson, *Chem. Commun.*, 365 (1967). ^d G. O. Pritchard, J. T. Bryant, and R. L. Thommarson, *J. Phys. Chem.*, **69**, 2804 (1965).

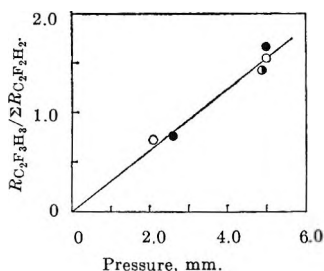


Figure 4. $R_{\text{C}_2\text{F}_3\text{H}_3} / \sum R_{\text{C}_2\text{F}_2\text{H}_2}$ vs. ketone (DFA + TFA) pressure, in mm, at 390–391°K: ○, 1:1 mixture; ●, 0.2 mm of TFA + DFA (see Table VI); ●, 3.7 mm of TFA + 1.2 mm of DFA.

Discussion of runs, based on the data in Table IV, on the molecule $\text{CF}_2\text{HCFH}_2^*$ has already been presented by us.⁴ Although these dehydrohalogenations are generally accepted as proceeding *via* a four-center transition state,²⁰ α,β elimination, from our observation^{4,10} of the formation of d_3 - as well as d_2 -vinyl fluoride in the interaction of CF_2H with CD_3 radicals, we have suggested that the "hot" molecule $\text{CF}_2\text{HCD}_3^*$ may decompose by elimination of HF from the same carbon atom in a three-center process, α,α elimination. No evidence has previously been presented for an α,α process in the dehydrohalogenation of haloethanes in either thermal or chemical activation systems,²¹ and it should be noted that in chemical activation systems involving

CHCl_2 with CH_3 or CH_2Cl radicals²² chloroethylenes can be formed by pathways not involving "hot" chloroethane intermediates. If the α,α elimination is established, detailed quantitative conclusions will depend upon an analysis of the isotope effects. These experiments are currently being undertaken by us.¹⁰ An α,α elimination does occur²³ in the photolysis of CH_3CD_3 at 1470 Å where



is the major molecular hydrogen elimination process.

iv. Experiments with Added N_2 . Data on runs conducted in the presence of varying pressures of N_2 are given in Table VIII. The total pressure of ketones is such that no collisional stabilization of $\text{C}_2\text{F}_3\text{H}_3^*$ occurs in the absence of added N_2 , so that we may apply eq 15 to the data, where [M] is now P_{N_2} . This is shown in Figure 5. The slope of the line at 391°K is 0.074 mm^{-1} , which may be compared to the slope of the line in Figure 4 which is 0.31 mm^{-1} . Assuming an average molecular weight and collision diameters of 6.0 \AA for the ketones,

(20) S. W. Benson and A. N. Bose, *J. Chem. Phys.*, **39**, 3463 (1963); S. W. Benson and G. R. Haugen, *J. Amer. Chem. Soc.*, **87**, 4036 (1965); J. C. Hassler and D. W. Setser, *J. Chem. Phys.*, **45**, 3246 (1966).

(21) D. W. Setser, private communication, 1967.

(22) J. C. Hassler and D. W. Setser, *J. Chem. Phys.*, **45**, 3237 (1966).

(23) H. Okabe and J. R. McNesby, *ibid.*, **34**, 668 (1961).

Table VIII: Data on $\text{CF}_2\text{HCOCF}_2\text{H}$ and $\text{CFH}_2\text{COCFH}_2$ Photolysis with Added N_2

Temp, °K	Reactant pressure, torr			Products, 10 ⁶ mol			
	TFA	DFA	N ₂	CF ₂ CH ₂	trans-CFHCFH	cis-CFHCFH	CF ₂ HCFH ₂
390	0.148	0.198	46.0	4.20	6.87	14.58	87.07
392	0.155	0.198	61.4	3.27	4.04	8.08	62.74
392	0.156	0.198	11.5	9.70	22.62	42.90	80.24
391	0.117	0.198	20.8	6.59	13.21	25.65	68.17
391	0.136	0.198	32.1	5.01	8.57	17.13	76.13
392	0.169	0.210	4.9	13.90	39.59	69.73	57.04
579	0.146	0.210	69.7	3.68	5.45	10.26	37.25
577	0.160	0.198	29.9	7.51	15.84	27.63	42.52
577	0.160	0.274	16.1	12.48	25.73	48.28	33.72
576	0.155	0.198	4.9	13.74	32.52	56.03	8.73
575	0.150	0.198	2.5	13.94	32.40	52.76	6.60
622	0.136	0.210	5.0	14.50	30.22	47.95	
620	0.130	0.210	10.4	11.11	24.32	41.53	
619	0.143	0.210	15.05	9.70	20.32	35.19	19.75
621	0.140	0.198	20.0	7.47	14.02	22.14	18.74
620	0.151	0.198	30.9	9.41	15.11	26.91	33.45
621	0.143	0.210	50.5	5.13	9.25	16.73	33.87
622	0.143	0.210	2.4	16.93	35.31	57.49	
621	0.136	0.198	7.8	12.44	22.87	39.59	

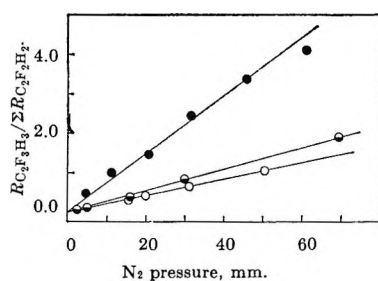


Figure 5. $R_{\text{CF}_2\text{F}_3\text{H}_3} / \sum R_{\text{CF}_2\text{F}_3\text{H}_2}$ vs. N_2 pressure, in mm: ●, 390–392°K; ■, 575–579°K; ○, 619–621°K.

3.7 Å for N_2 , and 5.5 Å for $\text{CF}_2\text{HCFH}_2^*$, we obtain a relative quenching efficiency of N_2 to ketone of 0.36 on a collision-for-collision basis. Similarly Giles and Whittle¹¹ find relative efficiencies of N_2 with CH_3COCH_3 and CF_3COCF_3 of 0.19 and 0.10, respectively, for the quenching of CF_3CH_3^* . These results demonstrate the “stronger” collision assumption for polyatomic and the “weaker” collision assumption for atoms and diatomic molecules.²⁴ Although the two fluoroethanes are formed with roughly the same energy of excitation, the two systems are not directly comparable. It should be noted that there will be a lower critical energy for HF elimination from the CF_3CH_3^* , as opposed to the $\text{CF}_2\text{HCFH}_2^*$ “hot” molecule.²⁵ Setser and Hassler²⁶ have also suggested that the relative N_2 quenching efficiency given by Giles and Whittle¹¹ is too low. In collisional quenching experiments on chemically activated $\text{CH}_2\text{ClCH}_2\text{Cl}^*$ with added N_2 , they find that about 6 kcal mol⁻¹ of energy is transferred per collision, whereas about 2.5 kcal mol⁻¹ would more normally be expected.²⁴ Our data in Figure 5 support “stronger” deactivating collisions, since some curvature

would be expected¹⁵ in the plots at low pressures if “weaker” collisions were taking place.

From the data in Table VIII it can be shown that the *cis:trans* 1,2-difluoroethylene ratio rises gradually from the average value of 1.55 (obtained from Table IV, quoted in ref 4) with increasing N_2 pressure. The data above 50 torr are not very accurate, owing to the small amount of elimination products formed, but the experiments at 575–579°K and 619–622°K generally tend toward a *cis:trans* ratio of about 1.8 with increasing pressure. The effect is greater at lower temperatures and the data are presented in Figure 6, together with additional data from Table IX, for a temperature of about 391°K. It is seen that values in excess of 2.0 are obtained for the *cis:trans* ratio with increasing pressure.²⁷ With increasing ketone pressure, Table VI, the ratio also increases, the five runs giving an average value of 1.74 ± 0.15 .

Our previous report on the low-pressure data (given in Table IV) showed the *cis:trans* ratio to be 1.55 ± 0.1 independent of temperature, indicating that $E_{cis}^* = E_{trans}^*$. (The experimental scatter could conceal a difference in the activation energies⁴ of about 1 kcal mol⁻¹.) A possible explanation of the variation of the *cis:trans* ratio with added N_2 may be due to the fact that

(24) F. J. Fletcher, B. S. Rabinovitch, K. W. Watkins, and D. J. Locker, *J. Phys. Chem.*, **70**, 2823 (1966).

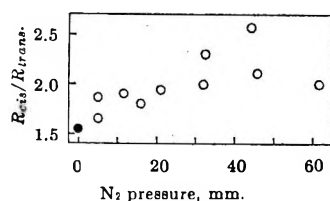
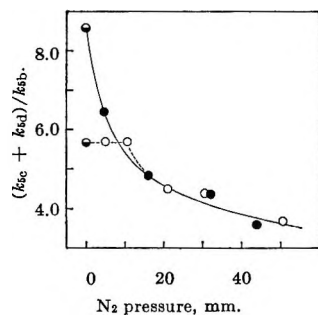
(25) α - and β -halogenation effects have been fully discussed by A. Maccoll, *Advan. Phys. Org. Chem.*, **3**, 91 (1965); “Studies on Chemical Structure and Reactivity,” Methuen, London, 1966, pp 53–72. Note also the experimental values of k_{stab}/k_{elim} for the two molecules in Table VII.

(26) D. W. Setser and J. C. Hassler, *J. Phys. Chem.*, **71**, 1364 (1967).

(27) If $E_{cis}^* = E_{trans}^*$, the *cis:trans* ratio would not be expected to be a function of pressure.

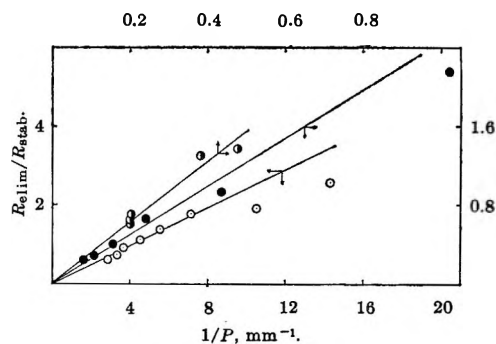
Table IX: Data on $\text{CF}_2\text{HCOCF}_2\text{H}$ and $\text{CFH}_2\text{COCFH}_2$ Photolysis with Added N_2

Temp, °K	Reactant pressure, torr			Products, 10 ⁷ mol		
	TFA	DFA	N_2	$\text{CF}_2=\text{CH}_2$	<i>trans</i> - $\text{CFH}=\text{CFH}$	<i>cis</i> - $\text{CFH}=\text{CFH}$
572	0.160	0.188	11.2	1.05	2.36	3.66
570	0.160	0.199	4.9	1.34	2.74	4.91
571	0.199	0.199	20.8	1.07	1.75	3.07
571	0.199	0.199	30.8	0.88	1.26	2.59
576	0.178	0.199	50.6	0.48	0.66	1.11
393	0.178	0.199	15.8	0.99	1.69	3.07
391	0.199	0.199	4.9	1.45	3.56	5.89
392	0.199	0.199	32.3	0.53	0.70	1.61
391	0.199	0.199	44.1	0.57	0.58	1.45

**Figure 6.** R_{cis}/R_{trans} for 1,2-difluoroethylenes vs. N_2 pressure, in mm: \circ , 390–393°K; \bullet , average value from ref 4 (Table IV) with no N_2 .**Figure 7.** $(R_{cis} + R_{trans})/R_{1,1-}$ for difluoroethylenes, $(k_{sc} + k_{sd})/k_{sb}$, vs. N_2 pressure, in mm: \bullet , 391–393°K; \circ , 570–576°K; \ominus , from published data (ref 4) with no N_2 .

the initially formed 1,2-difluoroethylene is sufficiently energized that it undergoes isomerization. This process is quenched more rapidly by the addition of excess N_2 , so that the *cis:trans* ratio approaches that value which may be expected from reaction path degeneracy considerations.²⁸ Alternatively, Rabinovitch and his coworkers²⁹ have studied the effect of pressure on the competitive unimolecular decomposition of vibrationally excited 3-hexyl radicals into 1-pentene and 1-butene. Application of these considerations²⁷ to the *cis:trans* ratios does not seem warranted until we can establish the possible extent of any *cis* \rightleftharpoons *trans* isomerization in this complex nonequilibrium system.

The ratio (*cis* + *trans*):1,1- for the difluoroethylenes, $(k_{sc} + k_{sd})/k_{sb}$, is shown as a function of N_2 pressure at two temperatures in Figure 7. The data are obtained from Table IX. The data in Table VIII show a similar

**Figure 8.** R_{elim}/R_{stab} vs. reciprocal pressure, mm^{-1} : \bullet , $\Sigma R_{\text{C}_2\text{F}_2\text{H}_2}/R_{\text{C}_2\text{F}_2\text{H}_2}$ vs. $1/(P_{\text{TFA}} + P_{\text{DFA}})$ (390–391°K); \bullet , $\Sigma R_{\text{C}_2\text{F}_2\text{H}_2}/R_{\text{C}_2\text{F}_2\text{H}_2}$ vs. $10^2/P_{\text{N}_2}$ (390–392°K); \circ , $R_{\text{C}_2\text{F}_2\text{H}_2}/R_{\text{C}_2\text{F}_2\text{H}_2}$ vs. $1/P_{\text{TFA}}$ (513–516°K).

dependence, but are scattered due to the loss of small amounts of $\text{CF}_2=\text{CH}_2$ in some of the experiments, see the Experimental Section. The ratio behaves similarly with increasing total ketone pressure, Table VI. Under conditions of no collisional stabilization the function $(k_{sc} + k_{sd})/k_{sb}$ shows a strong temperature dependence (shown as Figure 1 in ref 4), indicating a higher critical energy for $E_{1,1-}^*$ than for E_{cis}^* and E_{trans}^* .

Equations 7 and 15 are tested in the form of R_{stab}/R_{elim} vs. pressure in Figures 1, 4, and 5 which demonstrates that R_{stab} approaches zero with decreasing pressure, in accord with reaction sequences 2 and 5. However a plot of R_{elim}/R_{stab} vs. reciprocal pressure is required²² to demonstrate that R_{elim} approaches zero at infinite pressure, as predicted by our mechanism. Some of the data presented in Figures 1, 4, and 5 are shown in this manner in Figure 8, and the lines are arbitrarily drawn to intersect at zero. The test of reaction 2 for $\text{C}_2\text{F}_4\text{H}_2^*$ is good³⁰ and to within the

(28) The small temperature effect, if real, may reflect a temperature dependence of the deactivation efficiency of the added N_2 .

(29) D. C. Tardy, B. S. Rabinovitch, and C. W. Larson, *J. Chem. Phys.*, **45**, 1163 (1966).

(30) The scatter at high $1/P$ may be due to the relatively small values of $R_{\text{C}_2\text{F}_2\text{H}_2}$ obtained at low pressures.

experimental scatter it would also appear that the test for reaction 5 for $C_2F_3H_3^*$ is valid.³¹ A more critical test would be to examine $R_{1,1-}/R_{C_2F_3H_3}$ and $(R_{cis} + R_{trans})/R_{C_2F_3H_3}$ as functions of $1/P$, but such plots of our data (corresponding to those given in Figure 8 and Table VIII at 575–579°K and 619–621°K) lead to intercepts which are very close to zero in all cases.³² It is, therefore, evident that the data depicted in Figure 7 cannot be rationalized on the basis that any appreciable amount of $CF_2=CH_2$ is formed in a process which does not involve elimination from a "hot" intermediate, and the "hot" molecule mechanism for the formation of all three isomers is satisfactorily established.

Our data on the total 1,2 elimination *vs.* 1,1 elimination are satisfactorily explained in terms of Rabinovitch's treatment,²⁹ since $E_{1,1-}^* > E_{1,2-}^*$ and the average energy of the reacting species increases with increasing pressure.³³

An additional complicating consideration is provided by the fact that our data¹⁰ on the dehydrohalogenation

of the "hot" molecule $CD_3CF_2H^*$ in the presence of added quenchers indicate that the d_3 -vinyl fluoride arises *only via* a "hot" molecule mechanism. The possibility, therefore, of the formation of any, or all, of the difluoroethylene isomers *via* a competing α, α elimination process from $CF_2HCFH_2^*$ cannot be ruled out at this juncture.

Acknowledgments. We thank Dr. Bernard Kirtman, Dr. R. M. Martin, and M. J. Perona for several helpful discussions.

(31) The data on $\Sigma R_{C_2F_3H_3}/R_{C_2F_3H_3}$ with added N_2 at 391°K may well be better represented by a small positive intercept at ~ 0.05 , but it is apparent that a large number of runs would have to be performed (see for instance ref. 22) to permit a clear-cut determination as to the existence of an intercept, or not.

(32) Similarly, so did plots of $R_{cis}/R_{C_2F_3H_3}$ and $R_{trans}/R_{C_2F_3H_3}$, although any difference in behavior of these two functions would certainly not be anticipated.

(33) The data in Figure 7 only show the ratio of the products, but the absolute amount of elimination products is, of course, reduced with increasing pressure.

Dissociation Energy of PN and Other Thermodynamic

Properties for the Vaporization of P_3N_5 ^{1a,b}

by O. Manuel Uy, Fred J. Kohl,^{1c} and K. Douglas Carlson

Department of Chemistry, Case Western Reserve University, Cleveland, Ohio 44106 (Received October 18, 1967)

The chemistry of the phosphorus–nitrogen system has been the subject of a number of studies in past years., Nevertheless, some of the published data on this system are contradictory or questionable. In particular the dissociation energy of the PN molecule is uncertain and the available thermodynamic properties of the solid phases are very questionable. This article describes a mass spectrometric study of the solid–vapor equilibria in the vaporization of solid P_3N_5 to clarify some of these questions. The equilibrium vapor of P_3N_5 was found to consist of PN and N_2 with relatively minor concentrations of P_2 . The D_0° of PN was determined to be 7.57 ± 0.03 eV, and the heat of formation of solid P_3N_5 was found to be -230 ± 20 kcal mole⁻¹.

Introduction

Elements of the group Va nitrogen family combine among themselves to form a number of condensed phases and a wide variety of gaseous polyatomic molecules.^{2,3} As a class of chemically related substances, however, these have been studied incompletely. The P–N system has been the most extensively studied of the mixed pnictides,^{4–7} but the data are questionable and incomplete. This article describes a study of the solid–vapor equilibria in this system by molecular beam sampling of the vapor above solid P_3N_5 to establish a

reliable value for the dissociation energy of the PN molecule and to clarify certain questionable thermodynamic data for the solid phase.

The known molecules of nitrogen and phosphorus are

(1) (a) Research sponsored by the U. S. Army Research Office (Durham), Department of the Army, Contract No. DA-31-124-ARO-D-304. (b) Based in part on the Ph.D. Thesis submitted by O. M. Uy to Case Institute of Technology, Cleveland, Ohio, 1967. (c) National Aeronautics and Space Administration Predoctoral Fellow.

(2) K. D. Carlson, F. J. Kohl, and O. M. Uy in "Applications of Mass Spectrometry in Inorganic Chemistry," *Advances in Chemistry Series*, American Chemical Society, Washington, D. C., in press.

N_2 , P_2 , P_4 , and PN . The dissociation energies of the first three are reasonably well established. The dissociation energy of PN , however, is uncertain. Herzberg and co-workers⁸ in 1933 determined a value of 7.8 eV for its dissociation energy D_0 by a linear Birge-Sponer extrapolation of the electronic ground state vibrational levels. Because a similar procedure yields too large a D_0 for N_2 , however, they subsequently revised their initial estimate to 6.3 eV on the basis of a linear extrapolation for the excited $A^1\Pi$ state, with corrections to ground state species.⁹ Most recently, Huffman and associates¹⁰ derived a value of 7.1 ± 0.05 eV from equilibrium constants determined by static total pressure measurements of the gaseous equilibrium of PN , P_2 , and N_2 . Our recalculation of their data shows a severe temperature-dependent error in their measurements, so that the quoted precision of their value is an unrealistic estimate of its reliability.

The solid P_3N_5 of nearly stoichiometric composition is the only crystalline binary phase of the P-N system thermodynamically stable under conditions of the experiments reported here.² Both heat capacities and the heat of formation of P_3N_5 have been published, but it is almost certain that these are unreliable. Heat capacities in the range of 0–305° for a solid phase purporting to be P_3N_5 were published by Satoh⁶ in 1938. The sample employed, however, was described as being very unstable to vaporization somewhat below 500°. This characteristic is contrary to the observations of others⁴ that P_3N_5 is stable to vaporization under vacuum at least up to 700°. Therefore, Satoh's sample either was badly contaminated with a volatile impurity or was an impure P-N phase. A standard heat of formation of -70.4 kcal mole⁻¹ reported in 1907 by Stock and Wrede⁷ may be unreliable for similar or other reasons. This heat was obtained from oxygen bomb calorimetry. Thus, it depends on a reliable value for the heat of formation of P_2O_5 , and this may be uncertain because of the problem of the formation of suboxides and different forms of the pentoxide on combustion of phosphorus.¹¹ No studies have been carried out on the vaporization equilibria of P_3N_5 .

Experimental Methods

Commercial samples of crystalline P_3N_5 (A. D. Mackay, New York, N. Y.), purified by vaporizing off a P_2O_{10} impurity, were used in this research. The stoichiometry, phase composition, and purity of the treated samples were confirmed by chemical, infrared, and X-ray analyses and by comparison of these data with the most reliable published information. Repeated and detailed preliminary vaporization measurements unquestionably demonstrated that P_3N_5 vaporizes congruently in the absence of surface depletion effects and without reaction with high-density graphite, which was used as a container material in all vaporization experiments reported here. The stability of P_3N_5 to vaporization

below 700° under conditions similar to those described by Satoh⁶ was examined also in preliminary studies. No evidence supporting his conclusions on the instability of the solid was obtained. This confirms at least that the sample employed by Satoh was not pure P_3N_5 .

Experiments were carried out over a temperature range of about 690–950°, with temperatures measured by calibrated chromel-alumel thermocouples. Relative partial pressures of molecular species in the vapor of P_3N_5 were measured with a Bendix time-of-flight mass spectrometer having a Knudsen cell inlet system. Ion currents for the thermodynamic measurements were produced with 35-eV electrons bombarding a collimated molecular beam effusing from an orifice of 1.1-mm diameter in a graphite Knudsen cell identical with that used for Bi in an earlier study.^{3a} The equipment, procedures, and techniques involved in the measurements of appearance potentials and ion currents and employed in the heating and temperature control of the Knudsen cell were basically identical with those used earlier.

Total apparent pressures to scale the relative values to absolute quantities were measured by the Knudsen effusion method using a vacuum balance apparatus constructed from a modified Ainsworth semimicro vacuum balance, Type RV-AU-1. The basic design of the subsidiary equipment, vacuum system, thermocouple leads, and other relevant features of construction and operation were based on an apparatus described elsewhere.¹² The effusion cells were similar in design to those used in the mass spectrometric measurements, except that the orifice was located in the side to keep the corrosive phosphorus vapors out of the balance chamber and away from the thermocouple leads.

Molecular Vapor Species. The molecular composition of the equilibrium vapor of $P_3N_5(s)$ was determined by careful identification of the ion species formed from electron impact processes, from considerations of their ionization efficiency curves, and from analyses of the

(3) (a) F. J. Kohl, O. M. Uy, and K. D. Carlson, *J. Chem. Phys.*, **47**, 2667 (1967); (b) F. J. Kohl, J. E. Prusaczyk, and K. D. Carlson, *J. Am. Chem. Soc.*, **89**, 5501 (1967).

(4) A. Stock and B. Hoffmann, *Ber.*, **36**, 314 (1903); H. Moureu and P. Rocquet, *Compt. Rend.*, **198**, 1691 (1934); H. Moureu and G. Wettruff, *ibid.*, **204**, 436 (1937); E. Huffman, G. Tarbutton, G. Elmore, A. Smith, and M. Roundtree, *J. Am. Chem. Soc.*, **79**, 1765 (1957).

(5) J. R. Van Wazer, "Phosphorus and Its Compounds," Vol. 1, Interscience Publishers Inc., New York, N. Y., 1964, p 331.

(6) S. Satoh, *Sci. Papers, Inst. Phys. Chem. Res. (Tokyo)*, **34**, 888 (1938); **35**, 385 (1939).

(7) A. Stock and F. Wrede, *Ber.*, **40**, 2923 (1907).

(8) J. Curry, L. Herzberg, and G. Herzberg, *J. Chem. Phys.*, **1**, 749 (1933).

(9) J. Curry, L. Herzberg, and G. Herzberg, *Z. Physik*, **86**, 348 (1933).

(10) E. Huffman, G. Tarbutton, K. Elmore, W. Cate, H. Walters, Jr., and G. Elmore, *J. Am. Chem. Soc.*, **76**, 6239 (1954).

(11) "JANAF Thermochemical Tables," Dow Chemical Company, Midland, Mich., Aug 1965.

(12) K. D. Carlson, P. W. Gilles, and R. J. Thorn, *J. Chem. Phys.*, **38**, 2725 (1963).

relative intensities of the species. The ions formed by impact of 6–60-eV electrons with the vapor species of the molecular beam issuing from the Knudsen cell were found to be P^+ , P_2^+ , P_3^+ , P_4^+ , N^+ , N_2^+ , PN^+ , and PN^{2+} . Aside from a $P_4O_{10}^+$ impurity which was eliminated with continued heating, no other ions were observed up to mass-to-charge ratios of 1800 at the highest temperatures employed in this investigation. Ionization efficiency curves and appearance potentials were obtained at 850° by both the linear extrapolation and the R.P.D. methods, and it was demonstrated from these that the neutral parent molecules in the vapor were N_2 , PN , P_2 and P_4 . All other ion species were found to be fragmentation products. Details and results of these measurements have been adequately described elsewhere.²

It was necessary to study the relative intensities and shutter effects of the parent molecule ions in some detail because of a problem with severe scattering of the uncollimated portion of the molecular beam from the surfaces of the heat shields surrounding the Knudsen cell. The P_3N_5 vapors led to unusual difficulties in this regard because N_2 was totally noncondensable and the phosphorus species were only partially condensable under the conditions of these experiments.¹³ As a consequence, the ion intensities of N_2^+ were found to be abnormally large and the shutter effects to be relatively small for N_2^+ , PN^+ , and P_2^+ and entirely absent for P_4^+ , suggesting that P_4 was a spurious product. Several experiments were carried out to examine these effects in detail for different arrangements of the heat shields, and the results confirmed that P_4 was not an important molecule in the P_3N_5 vapor but, instead, was a reaction product formed from the phosphorus species on the shields and surfaces of the inlet system. The shutter-corrected intensities of N_2^+ , PN^+ , and P_2^+ at 750° were found to be 6.0, 6.6, and 0.7, respectively. Therefore, N_2 and PN are the major molecules, P_2 is a relatively minor species, and P_4 is entirely negligible in the equilibrium vapor of P_3N_5 .

The shutter-corrected intensity of 6 for N_2^+ is a value of considerable uncertainty because it is the difference between the large shuttered and unshuttered intensities of about 800 due to excessive scattering of N_2 into the ionization chamber. To avoid such uncertainties, we chose to neglect the shutter intensity readings of N_2^+ and to determine temperature trends of nitrogen from the total intensity readings, corrected, however, for the small residual background pressure in the mass spectrometer when an isolation valve separating the ionization chamber from the inlet system was closed. The validity of this procedure was confirmed in several preliminary experiments which showed that there was no buildup in the N_2 pressure with time and that both the unshuttered and shutter-corrected ion intensities followed identical temperature trends within the precision of the measurements.

Temperature Dependence and Total Effusion Rates

Two series of measurements of ion intensities of N_2^+ , PN^+ , and P_2^+ at various temperatures over the range 697–899° were carried out to determine heats of the reactions involved in the vaporization equilibria. Within the precision of the measurements, the quantities $\log(IT)$, where I is the ion current and T is the absolute temperature of the cell, were linear functions of the reciprocal temperature $1/T$. The ion intensity data, consequently, were adjusted to linear equations by the method of least squares.

Total rates of molecular effusion of solid P_3N_5 were measured as a function of temperature in the range 722–946° both to provide a basis for obtaining absolute partial pressures of the molecular species and to examine the question of a vaporization coefficient. This question is especially pertinent here because substantially small vaporization coefficients are known for a number of group Va elements and compounds, for example $P(\text{red})$ ¹⁴ and Mg_3N_2 .¹⁵ Under-saturation effects arising from an influential nonunit vaporization or condensation coefficient would show some kind of dependence of the measured rate of effusion on the size of the orifice area and other geometric factors. An examination of this for the P_3N_5 system was carried out by measuring the total rates of effusion at three temperatures with five orifices of different areas a ranging from 2.9×10^{-4} to 139×10^{-4} cm². The measured total mass rates of effusion dw/dt were used to obtain apparent total pressures p_s based on the formula weight M_s of the P_3N_5 solid, according to the Knudsen formula

$$p_s = \frac{(dw/dt)}{a} (2\pi RT/M_s)^{1/2} \quad (1)$$

It was found that the apparent pressures measured with the different orifices agreed within a factor of 2 or 3 at each temperature. In view of the normal experimental uncertainties in these values and a leakage problem with Knudsen cells having very small orifices, we concluded that this agreement was reasonable under the circumstances and that measurements with orifices comparable in size to that used for the mass spectrometric experiments would be satisfactory. If P_3N_5 has a nonunit vaporization coefficient, it is apparently not appreciably influential. Brewer and Kane¹⁶ have proposed that low vaporization coefficients might be expected for systems in which the major vaporizing gaseous species are not present as such in the condensed phase or in which the atoms of the molecular gaseous

(13) Phosphorus has a vapor pressure of 1 atm at about 431°, which is considerably below the temperatures of 690° and higher for the present studies.

(14) H. W. Melville and S. C. Gray, *Trans. Faraday Soc.*, **32**, 1026 (1936).

(15) J. R. Soulen, P. Sthapitaponda, and J. L. Margrave, *J. Phys. Chem.*, **59**, 132 (1955).

(16) L. Brewer and J. S. Kane, *ibid.*, **59**, 105 (1955).

species are too widely separated in the solid. Neither of these circumstances appears to hold for P_3N_5 , whose major vapor species are N_2 and PN with atoms in close proximity in the disordered polymeric structure proposed by Steger.¹⁷

Apparent equilibrium pressures p_s , defined by eq 2, were then determined as a function of temperature with a cell having an orifice of effective cross-sectional area $29.4 \times 10^{-4} \text{ cm}^2$, which is comparable with that of the cell used in the mass spectrometric measurements. A conventional logarithmic plot of the apparent pressure as a function of the reciprocal absolute temperature defined a linear curve. A least-squares adjustment of the data gave the equation

$$\log p_s(\text{atm}) = (-15,780 \pm 280)/T + (9.936 \pm 0.256) \quad (2)$$

where the errors are standard deviations in the slope and intercept for unit weighted data.

Absolute Partial Pressures

The apparent partial pressures determined from the total effusion measurements were used to scale the relative ion intensities of N_2 , PN , and P_2 to absolute partial pressures.¹⁸ The pressure p_i of each molecular species is related to the experimental ion intensity I_i at each temperature T according to the well-known expression

$$p_i = k_i I_i T \quad (3)$$

Partial pressures also are related to the total rate of effusion expressed by the apparent pressure p_s of eq 1 through equations that maintain a mole balance of the atomic constituents of P_3N_5 . Thus, for a nitrogen mole balance

$$5p_s/\sqrt{M_s} = p_{PN}/\sqrt{M_{PN}} + 2p_{N_2}/\sqrt{M_{N_2}} \quad (4)$$

and for a phosphorus mole balance

$$3p_s/\sqrt{M_s} = p_{PN}/\sqrt{M_{PN}} + 2p_{P_2}/\sqrt{M_{P_2}} \quad (5)$$

Equations 3-5 may be used to obtain the scaling factors k_i , subject to the one reasonable assumption that $k_{PN}/k_{P_2} = 1$, so that

$$p_{PN}/p_{P_2} = I_{PN}/I_{P_2} \quad (6)$$

Values of the pressure ratio (6) at 1100 and 1000°K were calculated first from the least-squares equations for the ion currents of PN^+ and P_2^+ from the second series, which we consider to be the most reliable. Then values of p_s were obtained from the least-squares eq 2 for the same two temperatures. The two values of p_s and the pressure ratio (6) were used to obtain from eq 4 and 5 the reference partial pressures listed in Table I. The uncertainties listed here are based on propagated errors in p_s and the pressure ratio (6) with an *a priori* estimate of $\pm 100\%$ as the uncertainty in the value $k_{PN}/k_{P_2} = 1$.

Finally, scaling factors k_i for each series of experi-

Table I

	1100°K	1000°K
p_{N_2}	$1.70 (\pm 0.05) \times 10^{-6} \text{ atm}$	$6.17 (\pm 0.13) \times 10^{-7} \text{ atm}$
p_{PN}	$5.94 (\pm 0.12) \times 10^{-6} \text{ atm}$	$2.20 (\pm 0.03) \times 10^{-6} \text{ atm}$
p_{P_2}	$1.21 (\pm 0.71) \times 10^{-6} \text{ atm}$	$3.32 (\pm 1.99) \times 10^{-8} \text{ atm}$

mental ion intensities were obtained from eq 3 with the use of the least-squares values of $(I_i T)$ at 1100 and 1000°K and the above reference partial pressures. The scaling factors showed no appreciable temperature dependence, but they were averaged to obtain constants applicable to the entire temperature range of the measurements. The scaling factors appropriate to the second series are listed in Table II. The value for N_2 is small because it applies to an unshuttered intensity. Each experimental value of I_i was multiplied by $k_i T$ to obtain the related partial pressure of the species. Least-squares equations for the temperature dependence of each molecular species were then derived by combining data from both series of measurements. Parameters of these equations are given in Table II, and the temperature dependence of the partial pressures is illustrated in Figure 1.

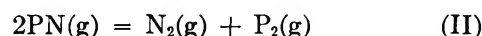
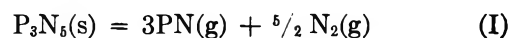
Table II: Intensity-Pressure Scaling Constants k_i^a and Least-Squares Parameters A and B^b for the Partial Pressures of PN , N_2 , and P_2

Molecular species	k_i , atm amp ⁻¹ deg ⁻¹	A	B
PN	80.0	-15694 ± 182	10.046 ± 0.185
N_2	0.278	-14396 ± 181	8.267 ± 0.184
P_2	80.0	-18167 ± 806	10.649 ± 0.787

$$^a p(\text{atm}) = k_i I_i T. \quad ^b \text{Log } p(\text{atm}) = A/T + B.$$

Thermodynamic Properties

The congruent vaporization of P_3N_5 may be characterized by the two equilibrium processes



We consider first the thermodynamics of reaction I. The equilibrium constant for this reaction was calculated at each temperature for each set of scaled partial pressures. A least-squares adjustment of the values gave the equation

$$\log K_I = (-61478 \pm 626)/T + (38.364 \pm 0.602) \quad (7)$$

(17) E. Steger, *Chem. Ber.*, **94**, 266 (1961).

(18) E. D. Cater and R. J. Thorn, *J. Chem. Phys.*, **44**, 1342 (1966).

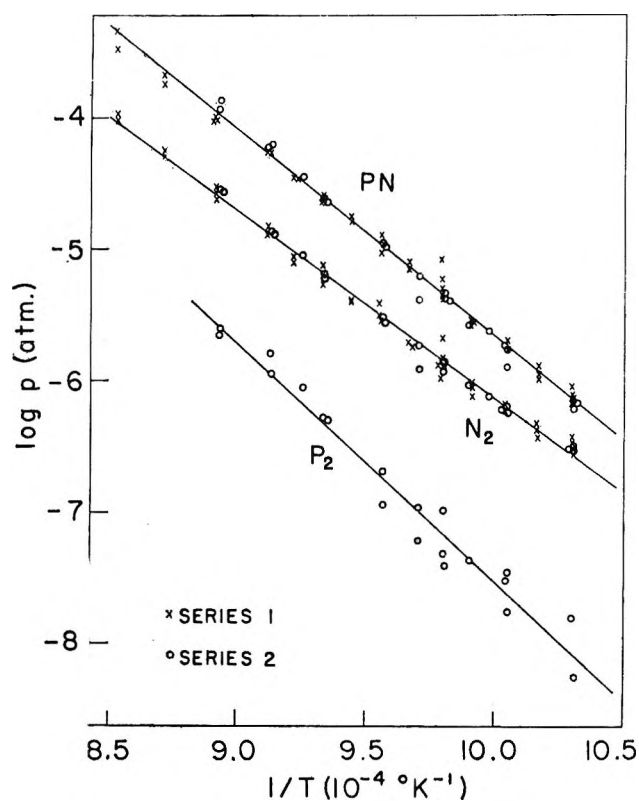


Figure 1. Temperature dependence of the partial pressures of PN, N₂, and P₂ in the vapor of P₃N₅(s).

This yields the following second-law heat and entropy of reaction I

$$\Delta H^{\circ}_{1041} = 281 \pm 3 \text{ kcal mole}^{-1};$$

$$\Delta S^{\circ}_{1041} = 176 \pm 3 \text{ eu}$$

The second-law entropy for reaction I is substantially larger than the third-law value of 138 eu based on the tenuous heat capacity measurements of Satoh.⁶ A more reasonable third-law estimate of 174 eu based on the entropy of Si₃N₄¹¹ compares favorably, however. The heat and entropy of reaction I at 298°K based on the thermodynamic properties of Si₃N₄,¹¹ the enthalpy and entropy functions reported for PN⁻¹ and N₂,¹⁹ and the second-law values obtained from the mass spectrometric measurements are

$$\Delta H^{\circ}_{298} = 282 \pm 20 \text{ kcal mole}^{-1};$$

$$\Delta S^{\circ}_{298} = 176 \pm 20 \text{ eu}$$

The uncertainties include liberal estimates for the unknown thermodynamic properties of the solid. Because of the lack of reliable entropy data for the P₃N₅ solid, however, no third-law determination of the heat of reaction I was carried out.

We now consider the gas-phase equilibrium of reaction II, for which the entropies and enthalpies of the species involved are well established. A third-law calculation gave $\Delta H^{\circ}_{298} = 8.02 \pm 0.61$ kcal. This heat represents a very small slope for the temperature de-

pendence of K_{II} , and this leads to large uncertainties in a second-law determination. A pseudo-second-law value can be estimated by combining the least-squares parameters for the individual partial pressures given in Table II. These yield 10.0 ± 4.1 kcal for the heat and -2.4 ± 4.0 eu for the entropy, both corrected to 298°K. The third-law entropy is -2.99 eu. This agreement is reasonable confirmation of the reliability of the measurements.

The standard heat of formation of crystalline P₃N₅ at 298°K was obtained by combining the heats of reactions I and II and the reported heat of formation of P₂(g) from triclinic red phosphorus.¹⁹ This value was found to be -230 ± 20 kcal mole⁻¹. This heat is about a factor of 3 more negative than that reported by Stock and Wrede,⁷ but it is more consistent with the apparent stability of P₃N₅ implied by others⁴ from cursory volatility experiments.

Finally, the dissociation energy of PN may be derived from the heat of reaction II, corrected to 0°K, and the well-established dissociation energies of N₂ ($D_0^{\circ} = 9.756$ eV)²⁰ and P₂ ($D_0^{\circ} = 5.031$ eV).²¹ This gives $D_0^{\circ}(\text{PN}) = 7.57 \pm 0.03$ eV, which is comparable with the larger of the two spectroscopic estimates. The heat of reaction II would have to be 60 kcal smaller than that measured here to give a dissociation energy of 6.3 eV. A summary tabulation of the dissociation energy of PN, heat of formation of P₃N₅, and other quantities determined in this research, including estimates of the first and second ionization potentials of PN from the appearance potential measurements, is given in Table III.

Discussion

It is of interest to consider how the present dissociation energy of PN fits into the general trends in dissociation energies of its neighboring molecules. Recent approximate Hartree-Fock calculations²² for PN(¹Σ⁺) show that the bonding electrons occupy the orbitals 7σ and 2π, in order of increasing orbital energies, for a configuration 7σ²2π⁴ above closed subshells 1σ² to 6σ² and 1π⁴. Furthermore, the molecule is isoelectronic with PO⁺. The final electron of neutral PO, therefore, should go into the antibonding 3π orbital to give a ²Π_r ground state, as observed. Hence, the dissociation energy of PO should be less than that of PN. There is considerable uncertainty in the D_0 of PO, but it lies between 6.2 and 7.1 eV.²¹ The value 7.57 for PN, then, is consistent with this qualitative comparison.

In Tables IV and V are summarized the experimental

(19) D. R. Stull and G. C. Sinke, *Advances in Chemistry Series*, No. 18, American Chemical Society, Washington, D. C., 1956.

(20) A. E. Douglas, *Can. J. Phys.*, **30**, 302 (1952).

(21) G. Herzberg, "Spectra of Diatomic Molecules," D. Van Nostrand and Co., Inc., New York, N. Y., 1950.

(22) A. D. McLean and M. Yoshimine, "Tables of Linear Molecule Wave Functions," a supplement to a paper to be published in *IBM J. Res. Develop.*

Table III: Measured Quantities Associated with the P_3N_6 Equilibrium System

Reaction	This research	Lit.
$P_3N_6(s) = 3PN(g) + \frac{5}{2}N_2(g)$	$\Delta H^\circ_{298} = 282 \pm 20 \text{ kcal mole}^{-1}$	
$3P(c, V) + \frac{5}{2}N_2(g) = P_3N_6(s)$	$\Delta H^\circ_{298} = -230 \pm 20 \text{ kcal mole}^{-1}$	$-71.5 \text{ kcal mole}^{-1}{}^a$
$2PN(g) = N_2(g) + P_2(g)$	$\Delta H^\circ_{298} = 8.02 \pm 0.61 \text{ kcal}$	$7.8 (6.3) \text{ eV}{}^b$
$PN(g) = P(g) + N(g)$	$D_0^\circ = 7.57 \pm 0.03 \text{ eV}$	$7.1 \pm 0.05 \text{ eV}{}^c$
$PN \rightarrow PN^+ + e$	A.P. = $11.8 \pm 0.1 \text{ eV} \simeq \text{I.P. (I)}$	
$PN \rightarrow PN^{2+} + 2e$	A.P. = $40 \pm 1 \text{ eV}$	
$PN^+ \rightarrow PN^{2+} + e$	I.P. (II) $\simeq 28 \pm 1 \text{ eV}$	

^a Reference 11. ^b References 8, 9. ^c Reference 10.

Table IV: Dissociation Energies of N_2 , PN , and P_2 by Linear Extrapolations Compared with Experimental Values

Mole- cule	D_0° , eV, from ground states ^a	D_0° , eV, from excited states ^a	D_0° , eV, exptl
N_2	11.79 ($X^1\Sigma_g^+$)	10.61 ($A^1\Pi_g$)	9.756 ^b
PN	7.85 ($X^1\Sigma^+$)	6.28 ($A^1\Pi$)	7.57 ^c
P_2	6.68 ($X^1\Sigma_g^+$)	5.61 ($A^1\Pi_g$)	5.031 ^a

^a Reference 21. ^b Reference 20. ^c This study.

dissociation energies of the family of molecules N_2 , PN , and P_2 and the family O_2 , SO , and S_2 , respectively. These are compared with values obtained by linear Birge-Sponer extrapolations for both the electronic ground states and excited states. In both sequences, the homonuclear molecules have energies in closer agreement with the excited-state extrapolations while the heteronuclear species have energies more in agreement with the ground-state extrapolations. In this regard, the value 7.57 eV for PN is not out of line with general trends. Because PN is a fairly polar molecule,²²

Table V: Dissociation Energies of O_2 , SO , and S_2 by Linear Extrapolations Compared with Experimental Values

Mole- cule	D_0° , eV, from ground states	D_0° , eV, from excited states	D_0° , eV, exptl
O_2	6.30 ($X^3\Sigma_g^-$)	6.01 ($B^3\Sigma_u^-$)	5.115 ^a
SO	6.33 ($X^3\Sigma^-$)	6.98 ($B^3\Sigma^-$)	5.357 ^b
S_2	5.68 ($X^3\Sigma_g^-$)	4.88 ($B^3\Sigma_u^-$)	4.4 ^c

^a Reference 21. ^b D. G. H. Marsden, *J. Chem. Phys.*, **31**, 1144 (1959). ^c R. Colin, P. Goldfinger, and M. Jeunehomme, *Trans. Faraday Soc.*, **60**, 306 (1964).

it would be expected to dissociate along a potential energy curve considerably different from those of the nonpolar homonuclear species. It is not possible to predict *a priori* in what way the curves should differ, however. Unfortunately, the comparisons presented in Tables IV and V cannot be extended to other neighboring molecules to study this further because of uncertainties in other experimental dissociation energies.

Solvation of Extracted Complex Metal Acids. IV.

The HAuCl_4 -Nitrobenzene System¹

by Stephen L. Law and R. L. McDonald²

Department of Chemistry, University of Hawaii, Honolulu, Hawaii 96822 (Received October 23, 1967)

The effects of nitrobenzene, metal, and acid concentrations on the distribution of Au(III) between aqueous HCl and benzene solutions of nitrobenzene have been studied. The nitrobenzene solvation number of the extracted, dissociated HAuCl_4 is 11; the results also indicate that 6 molecules of nitrobenzene are involved in the dissociation of extracted HCl ion pairs. Results obtained to date support the view that the large solvation numbers observed for nitrobenzene result, in part, from additional solvation that occurs during the ion-pair dissociation process.

Previous reports from this laboratory³⁻⁵ have discussed the need for studies of hydration and solvation of HMX_4 species which have been extracted by very weakly basic organic substances. Although there is little doubt that only cation solvation is observable (in distribution studies) with the more strongly basic organophosphorus compounds,⁶⁻⁹ no such simple model appears to explain our data for nitrobenzene^{3,4} and diethyl ether.⁵

In the present work, we have extended our nitrobenzene solvation studies to an acid possessing a square-planar anion. (The ones studied earlier were tetrahedral.) In addition, we have been able to examine the "trace" metal concentration region discussed (but not studied) previously.³

Experimental Section

Reagents. Eastman White Label nitrobenzene was purified by vacuum distillation under a nitrogen, reduced pressure atmosphere in a Podbielniak still. The middle fraction was collected and diluted with reagent grade benzene to the desired concentrations. Reagent grade HCl was extracted at least twice with nitrobenzene before being diluted with deionized water. Reagent grade $\text{HAuCl}_4 \cdot 3\text{H}_2\text{O}$ was dissolved in HCl solutions prepared as described above, and the gold concentration was determined gravimetrically using hydroquinone.¹⁰ Series of solutions of desired gold concentrations were prepared from these stock solutions by dilution with purified HCl of the same concentration. One milliliter of ca. 14 *N* ultrapure HNO_3 (Brinkman Instruments, Westbury, N. Y.) was added to each 250 ml of gold(III) solution to minimize reduction of the gold (see results). Carrier-free gold-195 chloride solution in aqueous HCl was used as purchased from Nuclear Science and Engineering Co.

Procedure. All experiments were done at least in duplicate, but more often in higher multiplicates. For each measurement, 5 ml of each phase containing the

desired concentrations of nitrobenzene, HCl, gold(III), and gold-195 tracer were placed in a glass culture tube fitted with a screw cap containing a Teflon liner. The tubes were shaken for at least 2 hr at $25 \pm 0.2^\circ$ on a water bath platform shaker. (Earlier studies, verified here, have shown that these systems reach equilibrium in about 15 min.³) After shaking, phase separation was facilitated by centrifugation, and 2-ml aliquots were pipetted from each phase for radioassay. The γ activity of each sample was determined by counting with a well-type NaI(Tl) scintillation crystal and a single-channel analyzer. The distribution ratio, *E* (ratio of total metal concentration in the organic phase to that in the aqueous phase), was taken as the ratio of the counts per minute in the organic phase to those in the aqueous phase after correction for background radiation. The reproducibility among multiplicates was almost always better than 10%.

Results and Discussion

It has been shown in systems where ion-pair dissociation is extensive, such as nitrobenzene, that metal

(1) Research sponsored by the Air Force Office of Scientific Research, Office of Aerospace Research, U. S. Air Force, under Grant No. AF-AFOSR-983-65.

(2) To whom correspondence should be addressed.

(3) R. L. Erickson and R. L. McDonald, *J. Am. Chem. Soc.*, **88**, 2099 (1966).

(4) C. V. Kopp and R. L. McDonald, "Solvent Extraction Chemistry," D. Dyrssen, *et al.*, Ed., North-Holland Publishing Co., Amsterdam, 1967, pp 447-453.

(5) D. A. Meyers and R. L. McDonald, *J. Am. Chem. Soc.*, **89**, 486 (1967).

(6) D. C. Whitney and R. M. Diamond, *J. Phys. Chem.*, **67**, 209 (1963).

(7) D. C. Whitney and R. M. Diamond, *ibid.*, **67**, 2583 (1963).

(8) M. I. Tocher, D. C. Whitney, and R. M. Diamond, *ibid.*, **68**, 368 (1964).

(9) T. J. Conocchioni, M. I. Tocher, and R. M. Diamond, *ibid.*, **69**, 1106 (1965).

(10) A. I. Vogel, "Quantitative Inorganic Analysis," Longmans, Green and Co., New York, N. Y., 1939, p 532.

concentrations must be accurately known if meaningful solvation numbers are to be obtained.³ Since gold(III) in HCl apparently undergoes reduction, particularly at low concentrations,¹¹ it was necessary to examine methods for minimizing this reduction. Addition of Cl₂ gas to the aqueous stock solutions had been tried by others,¹¹ but this appeared to attack the organic phase in our work. Hydrogen peroxide also proved unsatisfactory because of the difficulty encountered in attempting to pipet accurately the effervescing solutions. Finally, the addition of 1 ml of *ca.* 14 *N* ultrapure HNO₃ per 250 ml of stock HCl–AuCl₃ solution was chosen as the most desirable means of minimizing reduction of the gold(III). Figure 1 compares the results obtained for trace gold extraction with HNO₃ or H₂O₂ added to those with nothing added. The slope of the plot of log *E* vs. log nitrobenzene activity¹² is the same for either HNO₃ or H₂O₂ and is approached at high nitrobenzene concentrations when nothing is added. Although the extraction is much greater when HNO₃ is added, this increase is not a function of HNO₃ concentration. This was verified by varying the HNO₃ concentration from 0.15 ml to 2.5 ml of *ca.* 14 *N* HNO₃ per 250 ml of stock solution; no change in gold(III) extraction was observed.

Figure 2 shows typical plots of log *E* vs. log *C_M* (*C_M* = equilibrium aqueous phase gold(III) concentration) for gold(III) extraction from aqueous HCl of fixed concentration (with HNO₃ added) by mixtures of nitrobenzene

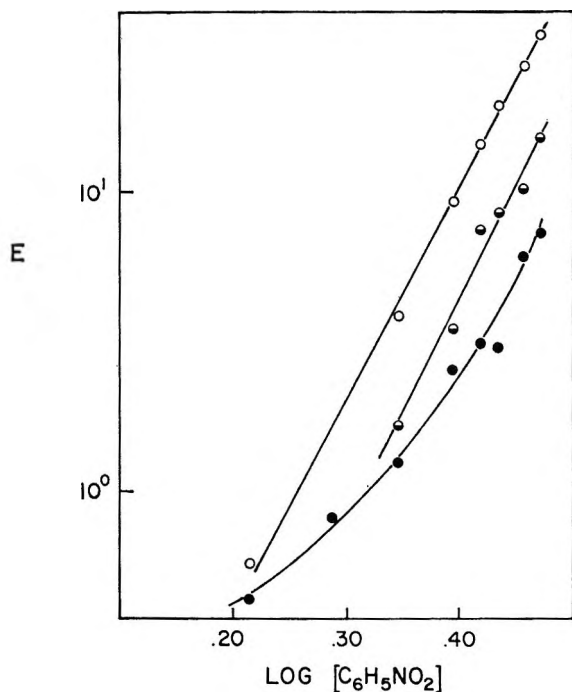


Figure 1. Log-log plot of distribution coefficient vs. vapor pressure of nitrobenzene for trace Au(III) extraction from 6.02 *M* HCl with: ○, 1 ml of HNO₃/250 ml of aqueous solution; ◐, 4 ml of H₂O₂/250 ml of aqueous solution; ●, nothing added.

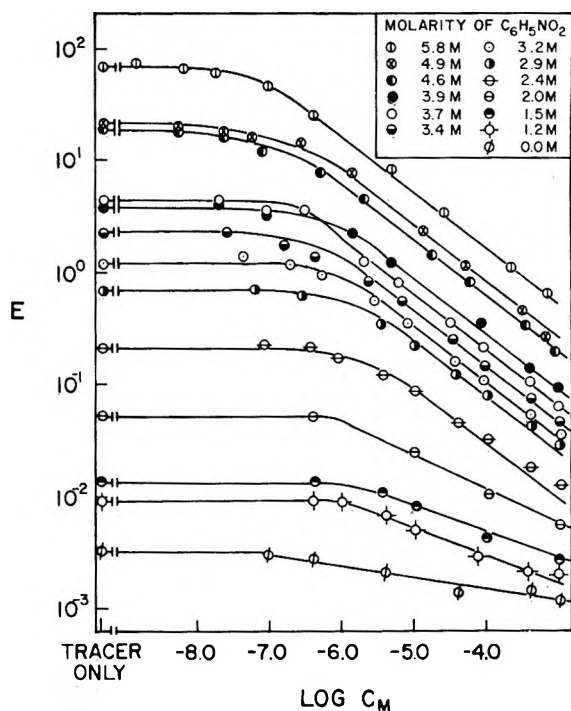


Figure 2. Log-log plot of distribution coefficient vs. equilibrium aqueous phase metal concentration for Au(III) extraction from 7.42 *M* HCl by nitrobenzene-benzene mixtures.

in benzene. At nitrobenzene concentrations above about 2.5 *M*, the data show the *C_M* dependence predicted for solvents of sufficiently high dielectric constant to permit acidic dissociation of the complex metal acid.³ At the lower nitrobenzene concentrations, the increase in slope of the metal concentration dependent region is probably due to both benzene extraction and a decrease in acidic dissociation. As is pointed out elsewhere,³ it is not possible to correct realistically for benzene extraction in the metal concentration dependent region. Thus no attempts will be made here to analyze these data at low nitrobenzene concentrations.

The relationship between *E*, nitrobenzene activity, and solvation number is given by

$$E = \frac{K[C_6H_5NO_2]^n}{(K_M)_0} + \frac{K[C_6H_5NO_2]^n}{g_{\pm}[KC_M[C_6H_5NO_2]^n + (K_{HX})_0(HX)_0]^{1/2}} \quad (1)$$

where all of the symbols have been defined previously.³ It was shown that, so long as one operates in the region where $\partial \log E / \partial \log C_M = -0.5$, the solvation number, *n*, can be obtained from the relationship³

(11) A. M. Poskanzer, *et al.*, "Radioisotopes in Scientific Research," Vol. II, Pergamon Press, New York, N. Y., 1958, pp 518–527.

(12) Nitrobenzene activities in this work were taken as before,³ *i.e.*, they are the vapor pressures of nitrobenzene above benzene solutions at 70° (A. R. Martin and C. M. George, *J. Chem. Soc.*, 1413 (1933)).

$$\frac{\partial \log E}{\partial \log [C_6H_5NO_2]} = \frac{n}{2} \quad (2)$$

Figure 3 shows a plot of $\log E$ vs. $\log [C_6H_5NO_2]$ at constant C_M ($3 \times 10^{-5} M$). The least-squares slope of the line is 5.41; Table I gives the slopes of similar plots at other HCl concentrations. Using the average slope of 5.45, one concludes that $n = 11$. This is satisfyingly close to the value of 12 reported by us for $HFeCl_4$, $HFeBr_4$, and $HInBr_4$.³

Table I: Least-Squares Slopes of $\log E$ vs. $\log [C_6H_5NO_2]$ Plots

(HCl), <i>M</i>	C_M , <i>M</i>	Slope ($C_6H_5NO_2$) > 1.5 <i>M</i>	Slope ($C_6H_5NO_2$) < 1.5 <i>M</i>
6.02	3×10^{-5}	5.41 ^a	...
7.42	2×10^{-6}	5.29 ^a	...
8.76	3×10^{-5}	5.65 ^a	...
6.02	Trace	7.95	3.98 ^b
6.02	Trace	7.50	...
7.42	Trace	7.90	3.39 ^b
7.42	Trace	7.94	3.56 ^b
8.76	Trace	7.87	3.51 ^b
8.76	Trace	8.37	...

^a These slopes obtain only at ($C_6H_5NO_2$) > 2.5 *M*. ^b After correction for benzene extraction.

At sufficiently low metal concentrations (hereafter referred to as trace metal concentration), the term $K C_M [C_6H_5NO_2]^n$ should become negligible with respect to $(K_{HX})_0 (HX)_0$. Thus eq 1 reduces to (g_{\pm} is assumed to be unity³)

$$E = \frac{K [C_6H_5NO_2]^n}{[(K_{HX})_0 (HX)_0]^{1/2}} \quad (3)$$

On the basis of this result, it was suggested earlier³ that a plot of $\log E$ vs. $\log [C_6H_5NO_2]$ should yield a slope of n if trace metal concentration could be attained experimentally.

Figure 4 shows a typical plot of $\log E$ vs. $\log [C_6H_5NO_2]$ for experiments in which the only gold present was a sufficient quantity of carrier-free gold-195 to provide a measurable amount of radioactivity in each phase. Since all reagents had been carefully purified, it is reasonably certain that the extractable metals were at trace concentrations in these experiments. This view is supported by the data presented in Figure 2 where no significant increase in E is seen below about $10^{-7} M$ gold. This is certainly much greater than the metal concentration (including Fe(III) impurity) present in the trace metal experiments. However, the slope of the straight portion of the line in Figure 4 is about 8 rather than 11 as predicted. Table I lists the least-squares slopes of all of our trace metal studies. Two values

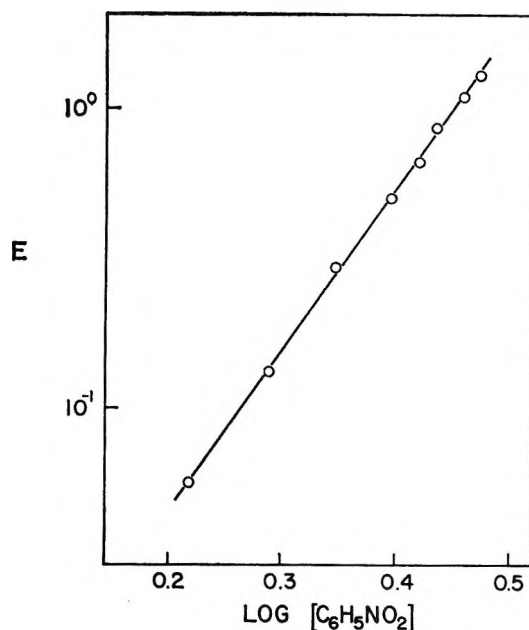


Figure 3. Log-log plot of distribution coefficient vs. vapor pressure of nitrobenzene over benzene for Au(III) extraction from 6.02 *M* HCl at constant $C_M = 3 \times 10^{-5} M$.

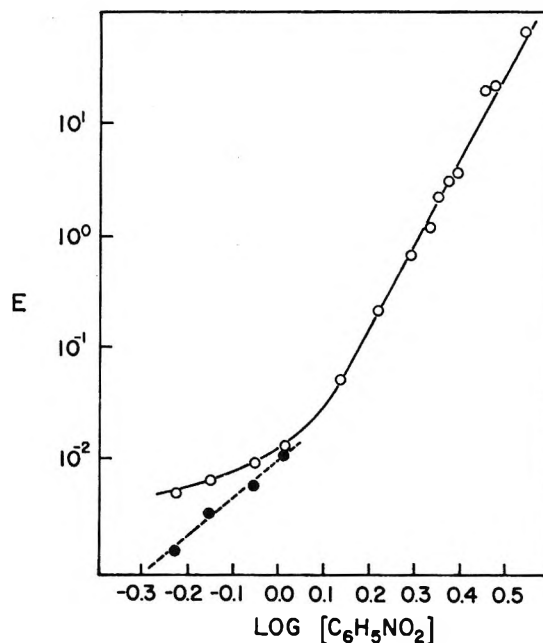


Figure 4. Log-log plot of distribution coefficient vs. vapor pressure of nitrobenzene over benzene for trace Au(III) extraction from 7.42 *M* HCl. The dashed line results after correction for benzene extraction.

are listed for each HCl concentration since two separate determinations were made at different times.

The discrepancy in the two apparent solvation numbers almost certainly originates in our original assumption that the denominator of eq 3 is independent of nitrobenzene concentration. Glover¹³ has shown that the ionization constant of a weak acid can be written

(13) D. J. Glover, *J. Am. Chem. Soc.*, **87**, 5279 (1965).

$$K' = \frac{(H^+)(A^-)}{(S)^m(HA)} \quad (4)$$

where it is understood that the ions are solvated by m moles of solvent S ; K' is a true constant; *i.e.*, it is independent of solvent. If we assume that HX (*i.e.*, HCl in this paper) can be treated in a similar manner,¹⁴ we can write

$$(K'_{HX})_0 = \frac{(H^+)_0(X^-)_0}{[C_6H_5NO_2]^m(HX)_0} = (K_{HX})_0 [C_6H_5NO_2]^{-m} \quad (5)$$

where it is assumed that nitrobenzene is the only solvating solvent. Substitution of this into eq 3 yields upon differentiation

$$\frac{\partial \log E}{\partial \log [C_6H_5NO_2]} = n - \frac{m}{2} - \frac{1}{2} \frac{\partial \log (HX)_0}{\partial \log [C_6H_5NO_2]} \quad (6)$$

The last term in eq 6 is negligible as can be seen from the following argument. In view of the very poor extraction of HCl by both benzene and nitrobenzene, coupled with the fact that only a very small amount of the HCl actually undergoes ion-pair dissociation in the organic phase, it may be assumed that extracted HCl is essentially unsolvated. So long as the mixtures do not deviate greatly from ideal-solution behavior, the following equation should apply¹⁵ for a fixed aqueous phase HX concentration

$$\log (HX)_0 = \log (HX)_{C_6H_6} + N[\log (HX)_{C_6H_5NO_2} - \log (HX)_{C_6H_6}] \quad (7)$$

Here N is the mole fraction of nitrobenzene in the benzene-nitrobenzene mixture and $(HX)_0$, $(HX)_{C_6H_6}$, and $(HX)_{C_6H_5NO_2}$ are the concentrations of HX in the mixture, pure benzene, and pure nitrobenzene, respectively, in equilibrium with aqueous HX solutions of equal concentrations. Now

$$\frac{\partial \log (HX)_0}{\partial \log [C_6H_5NO_2]} \approx \frac{\partial \log (HX)_0}{\partial \log N} = N[\log (HX)_{C_6H_5NO_2} - \log (HX)_{C_6H_6}] \quad (8)$$

For HCl, the quantity in the brackets can be estimated from data in the literature.^{14,16} It is independent of aqueous HCl concentration and *ca.* 0.3. Since N was never greater than 0.56 in this work, the last term in eq 6 is within experimental error.

A value of m can now be estimated. Assuming $n = 11$, then $m = 6$; in other words, 6 molecules of nitro-

benzene appear to be involved in the dissociation of an HCl ion pair. This is within the range of values found by Glover.¹³

The change in slope from 8 to *ca.* 3.5 at low nitrobenzene concentrations, $< ca.$ 1.5 M , remains to be discussed. (See Table I.) The extraction due to benzene is significant in this region, but the straight (dashed) lines were obtained after subtracting the metal distribution coefficient in pure benzene. The objection to this procedure raised for metal concentration-dependent data³ no longer applies here. Thus we feel that this decrease in apparent solvation number is real. A probable reason for it is a significant decrease in the dissociation of the $HAuCl_4$ ion pairs at low nitrobenzene concentrations accompanied by a loss of solvation. This, of course, assumes that the large solvation numbers seen in our work with nitrobenzene result in part from involvement of nitrobenzene in the ionization process. This view gains additional support from current studies in our laboratory which indicate that the solvation of dissociated $HFeCl_4$ by bis(2-chloroethyl) ether involves at least three times as many ether molecules than does the solvation of $HFeCl_4$ ion pairs by diethyl ether.^{5,17}

Finally, let us examine briefly the role of anion solvation in the solvent extraction process. Although there is good evidence that it contributes negligibly to the free-energy change when fairly strong basic extractants are used,⁶⁻⁹ there is no evidence to support this conclusion for weakly basic extractants, such as nitrobenzene. Since nitrobenzene possesses very little proton attracting ability,¹⁸ it is unreasonable *a priori* to assign all of the free energy of extraction to interactions involving only the hydrated proton. If, as appears likely, solvation numbers (obtained from distribution studies) for polar solvents include the number of solvent molecules involved in the ion-pair dissociation process, then electrostatic solvation can play a far more important part in extraction than has heretofore been noted. There is no obvious reason for limiting this electrostatic solvation to cations only.

(14) J. C. Mendez, Ph.D. Thesis, MIT, Cambridge, Mass., 1959, estimated the dissociation constant for HCl in nitrobenzene, $(K_{HCl})_0$, to be of the order of 10^{-7} ; it is probably much less in benzene solutions of nitrobenzene.

(15) H. Irving and F. J. C. Rossotti, *J. Chem. Soc.*, 2475 (1956).

(16) J. E. Such and R. H. Tomlinson, *J. Soc. Chem. Ind.*, 67, 110 (1948).

(17) T. H. Hufen and R. L. McDonald, work in progress.

(18) W. Gordy, *J. Chem. Phys.*, 7, 93 (1939).

The Photolysis of Cyclobutanone

by T. Howard McGee

Department of Chemistry, The University of Texas, Austin, Texas 78712 (Received October 23, 1967)

The photolysis of cyclobutanone has been investigated between 40 and 250° and in the pressure range 5.0–40.0 torr of cyclobutanone. Quantum yields for CO, C₂H₄, C₃H₆, and *c*-C₃H₆ have been determined as a function of temperature, pressure, and inert gas. The yield of C₃H₆ was found to increase with decreasing cyclobutanone pressure and with shorter wavelengths, while the yield of *c*-C₃H₆ was unaffected. Added gas lowered the C₃H₆ yield. No effect was noted on the *c*-C₃H₆ yield. Isomerization of *cis*- to *trans*-butene-2 was observed. A mechanism involving formation of C₃H₆ from an excited triplet cyclobutanone, possibly involving a diradical intermediate, has been proposed.

Introduction

The mechanism of the photochemical decomposition of cyclobutanone has been recently investigated and discussed.¹ The present work was undertaken to extend this investigation primarily through the determination of the quantum yields of the reaction products: carbon monoxide, ethylene, propylene, and cyclopropane. These quantum yields have been measured as a function of pressure, temperature, and inert gas.

Benson and Kistiakowsky² first reported the formation of CO, C₂H₄, C₃H₆, and ketene in a photochemical flow system. Quantum yields were obtained for CO, C₃H₆, and *c*-C₃H₆³ at 3130 and 2654 Å and found to be independent of temperature in the range 100–300° at pressures of cyclobutanone between 100 and 150 torr. A mechanism postulating the formation of diradicals was proposed. Later work with ethylene as a scavenger⁴ seemed to support this mechanism, as five-carbon olefins were formed. However, a recent study¹ has not been able to reproduce this effect.

The results of Klemm, *et al.*,¹ cast doubt on the quantum yields reported by Blacet and Miller.³ The former found the ratio $N_{\text{CO}}/(N_{\text{C}_3\text{H}_6} + N_{\text{c-C}_3\text{H}_6})$ to be 1.1 ± 0.1 and the ratio $N_{\text{C}_2\text{H}_4}/N_{\text{CO}}$ to be 1.7 ± 0.1 at 100°, in the pressure range 10–200 torr of cyclobutanone at incident wavelengths of 3130 and 2537 Å. They also found that the *c*-C₃H₆ to C₃H₆ ratio decreases sharply with a decrease in cyclobutanone pressure or with shorter wavelengths. In contrast, Blacet and Miller reported a $N_{\text{CO}}/(N_{\text{C}_3\text{H}_6} + N_{\text{c-C}_3\text{H}_6})$ ratio greater than unity at 3130 and 2654 Å and a marked wavelength effect on the C₂H₄/CO ratio. In other work on cyclobutanone photolysis, Srinivasan⁵ has reported the formation of 3-butenal to an almost negligible extent.

The thermal decomposition of cyclobutanone in contrast to the photolysis yields only ethylene and ketene as major products.⁶ A review of the photolysis of cyclic ketones is given by Srinivasan.⁷

Experimental Section

Apparatus. A usual high-vacuum system was employed. The reaction vessel consisted of a T-shaped cell with quartz windows and had a volume of 42 ml. It was enclosed in a brass case, which was wrapped with nichrome wire and asbestos tape. The voltage across the nichrome heating element was regulated with a Variac; this enabled rather close control of temperature to $\pm 1^\circ$. No run was conducted unless the system pressure was 10^{-5} torr or less, as measured on a calibrated McLeod gauge.

The light source was an Osram HBO-500 high-pressure mercury arc. When operated at 500 W, it was found to be very steady. Monochromatic light was obtained by a Bausch and Lomb grating monochromator with a dispersion of 16 Å/mm, with entrance and exit slits set at 2 mm. The beam was rendered parallel by quartz lenses and made to pass through and completely fill the cell. Transmitted radiation was then focused on an RCA 935 phototube, the output of which was read on a Keithley Model 410 microammeter. An RCA 1P28 photomultiplier tube measured emission, if any.

In experiments with inert gas, the cyclobutanone was put in the cell and the desired amount of inert gas added. The two gases were then allowed to mix for several hours.

In separate experiments on the fluorescence and phosphorescence of cyclobutanone an Aminco-Bowman spectrophotofluorimeter was used. The light

(1) R. F. Klemm, D. N. Morrison, P. Gilderson, and A. T. Blades, *Can. J. Chem.*, **43**, 1934 (1965).

(2) S. W. Benson and G. B. Kistiakowsky, *J. Amer. Chem. Soc.*, **64**, 80 (1942).

(3) F. E. Blacet and A. Miller, *ibid.*, **79**, 4327 (1957).

(4) M. C. Flowers and H. M. Frey, *J. Chem. Soc.*, 2758 (1960).

(5) R. Srinivasan, *J. Amer. Chem. Soc.*, **81**, 5541 (1959).

(6) M. N. Das, F. Kern, T. D. Coyle, and W. D. Walters, *ibid.*, **76**, 6271 (1954).

(7) R. Srinivasan, "Advances in Photochemistry," Vol. I, John Wiley and Sons, Inc., New York, N. Y., 1963, p 84.

source was a xenon lamp. Emission was read either on a photomultiplier microphotometer, or on an Analab 1100 oscilloscope.

Analysis

The products of the photolysis experiments were analyzed in the following manner. First, the products and remaining cyclobutanone were trapped in a cold finger immersed in solid nitrogen. Carbon monoxide was removed with a Toepler pump, was collected in a known volume, and was measured with a McLeod gauge. The condensables—ethylene, propylene, cyclopropane, ketene, and cyclobutanone—were solidified in a small melting-point tube attached to the vacuum system. The tube was sealed, was removed from the vacuum system, and was broken inside the injector block of a gas chromatograph by use of a solid sample injector.

A Varian-Aerograph Model 600 gas chromatograph with a hydrogen-flame detector was used for all determinations. The products were identified by comparison of retention times with those of known samples. A 1.83-m, 0.32-cm column packed with 120–150 mesh Porapak Type Q was used for C_2H_4 , C_3H_6 , and $c-C_3H_6$. A peak for ketene was observed, but it could not be reproduced for quantitative analysis. A 107-m, 0.32-cm column of 20% 2,4-dimethylsulfolane was used for analysis of *cis*- and *trans*-butene-2.

Actinometry. 3-Pentanone was employed as an internal actinometer. The quantum yield of carbon monoxide is near unity for the wavelengths studied at 130° .⁸ Condensables were trapped in a cold finger at liquid-nitrogen temperature and the CO was pumped into a known volume with a Toepler pump and measured on a McLeod gauge.

As a check on the 3-pentanone actinometry, acetone was photolyzed. The noncondensable fraction contained CH_4 as well as CO. A sample was withdrawn from the vacuum system in a 500-ml bulb and analyzed on a CEC mass spectrometer. The mass spectrometer was calibrated for CH_4 and CO, the CH_4/CO ratio was determined, and from that the amount of CO in the noncondensable fraction was calculated. In this manner, the quantum yields of CO formation from the acetone photolysis, with 3-pentanone as the internal actinometer, were found to be 0.98 ± 0.02 at 2654 Å, 0.97 ± 0.02 at 2804 Å, 0.96 ± 0.02 at 2967 Å, and 0.98 ± 0.02 at 3130 Å.

Materials. Cyclobutanone was obtained from Aldrich Chemical Co., Inc. A small lower boiling impurity was present and this was removed by preparative gas chromatography on a Varian-Aerograph Model 90-P gas chromatograph. The ketone was dried with calcium sulfate and stored under vacuum in a blackened vessel. The sample was degassed by pumping on it at liquid nitrogen temperature before each run.

The acetone and 3-pentanone were Spectroquality

grade (Matheson Coleman and Bell). They were stored in black vessels and degassed before each experiment. *cis*-Butene-2, 1,3-butadiene, 1,3-pentadiene, and *n*-hexane, research grade, were obtained from Phillips Petroleum Co.; CO, C_2H_4 , C_3H_6 , $c-C_3H_6$, CF_4 , and SF_6 were obtained from the Matheson Co., Inc. Each was used directly after degassing. The *cis*-butene-2 had an impurity of 0.04% *trans*-butene-2.

Results

Table I lists the quantum yields of formation of CO and of C_3H_6 at 40° and at several wavelengths. Ketene was not determined. Quantum yields of $c-C_3H_6$ and of C_2H_4 were constant throughout the pressure range reported, at each wavelength. The quantum yields for C_2H_4 were: 0.57 at 2654 Å, 0.63 at 2804 Å, 0.65 at 2967 Å, and 0.70 at 3130 Å; those for $c-C_3H_6$ were: 0.26 at 2654 Å, 0.30 at 2804 Å, 0.25 at 2967 Å, and 0.26 at 3130 Å.

The ratio of cyclopropane to propene decreases with decreasing pressure at each wavelength and also decreases with shorter wavelengths in agreement with previous work.¹ The data indicate that these changes with pressure are due entirely to an increase in the quantum yield of C_3H_6 at lower pressures. The quantum yield of $c-C_3H_6$ is constant, within experimental error, at all pressures at each wavelength. If C_3H_6 and $c-C_3H_6$ are both formed from a common precursor, as suggested by Klemm, *et al.*,¹ an increase in the quantum yield of C_3H_6 should be accompanied by a corresponding decrease in the $c-C_3H_6$ quantum yield. Although such changes would be difficult to identify at longer wavelengths (the change in the C_3H_6 yield is of the same magnitude as the experimental error in the $c-C_3H_6$ yield), at 2654 Å any such effect should be evident. The C_3H_6 quantum yield increases at 2654 Å from 0.13 at 41.0 torr to 0.26 at 5.0 torr, but the yield of $c-C_3H_6$ is constant within experimental error. The quantum yield of carbon monoxide is also seen to increase with decreasing pressure at each wavelength and, furthermore, the changes in the CO yield are equal, within experimental error, to the corresponding changes in the C_3H_6 yield. The ratio $N_{CO}/(N_{C_3H_6} + N_{c-C_3H_6})$ equals 1.00 ± 0.05 at all pressures and wavelengths at 40° .

The effect of temperature on the quantum yields at 2654 Å is shown in Table II. The yields for $c-C_3H_6$ were: 0.25 at 100° , 0.24 at 130° , 0.24 at 170° , 0.24 at 200° , and 0.25 at 250° ; those for C_2H_4 were: 0.56 at 100° , 0.54 at 130° , 0.48 at 170° , and 0.42 at 200° . Both yields were unaffected by changes in pressure. At 250° a thermal reaction leads to the formation of an appreciable amount of C_2H_4 and a small amount of cyclopropane. The reported yields of CO and of $c-C_3H_6$ are thus slightly high at this temperature.

(8) V. R. Eells and W. A. Noyes, Jr., *J. Amer. Chem. Soc.*, **61**, 2492 (1939).

Table I: Variation of Product Quantum Yields with Pressure and Wavelength at 40°

$10^{-12}I_a$, quanta/ ml sec	Time of irradia- tion, sec	$P_{C_4H_8O}$, torr	Φ_{CO}	$\Phi_{C_2H_4}$
λ 3130 Å				
3.92	2400	42.0	0.25	0.008
3.46	2400	37.0	0.26	0.010
2.80	2400	30.0	0.24	0.011
2.24	2400	24.0	0.26	0.011
1.78	2700	19.0	0.27	0.014
1.31	3000	14.0	0.27	0.014
0.937	3600	10.0	0.27	0.015
0.644	4200	7.0	...	0.022
0.418	4200	4.5	0.28	0.026
$\Phi_{C_2H_4} = 0.70, \Phi_{c-C_3H_6} = 0.26$				
λ 2967 Å				
3.38	3600	44.5	0.26	0.014
2.78	3600	36.5	0.27	0.017
2.32	3600	30.5	0.26	0.021
1.90	3600	25.0	0.28	0.028
1.38	3600	18.0	0.26	0.024
1.10	3600	14.5	0.30	0.030
0.637	4200	8.5	0.32	0.039
0.382	4800	5.0	0.31	0.054
$\Phi_{C_2H_4} = 0.65, \Phi_{c-C_3H_6} = 0.25$				
λ 2804 Å				
2.76	3000	41.5	0.36	0.059
2.32	3000	35.0	0.37	0.065
1.99	3000	30.0	0.37	0.068
1.53	3000	23.0	0.39	0.079
1.26	3000	19.0	0.41	0.084
0.932	3000	14.0	0.42	0.105
0.621	5400	9.5	0.42	0.128
0.294	5400	4.5	0.47	0.153
$\Phi_{C_2H_4} = 0.63, \Phi_{c-C_3H_6} = 0.30$				
λ 2654 Å				
3.08	2700	41.0	0.39	0.13
2.63	2700	35.0	0.40	0.14
2.18	2700	29.0	0.42	0.13
1.84	2700	24.5	0.43	0.15
1.43	2700	19.0	0.42	0.17
1.04	2700	14.0	0.46	0.18
0.668	5400	9.0	0.48	0.21
0.576	5400	5.0	0.50	0.26
$\Phi_{C_2H_4} = 0.57, \Phi_{c-C_3H_6} = 0.26$				

The effect of pressure on the yields of C_3H_6 and of $c-C_3H_6$ was studied with added gases (Table III). Experiments without gas are included for comparison. The C_3H_6 yield is lowered significantly by n -hexane with little change evident either in the CO or in the $c-C_3H_6$ yield. Propane was also formed, the yield of which increased with increasing n -hexane pressures. No propane impurity was detectable in the n -hexane used. With added CO_2 , CF_4 , and SF_6 , propane was not formed, but effects on the yields of C_3H_6 , CO, and $c-C_3H_6$ were comparable to the n -hexane results.

Table II: Effect of Temperature on the Quantum Yields at 2654 Å

$10^{-12}I_a$, quanta/ ml sec	Time of irradia- tion, sec	$10^4 C_{C_4H_8O}$, mol/l.	Φ_{CO}	$\Phi_{C_2H_4}$	$\Phi_{CO}/$ $(\Phi_{C_2H_4} +$ $\Phi_{c-C_3H_6})$
Temp, 100°					
2.09	2700	13.3	0.43	0.12	1.16
1.38	2700	8.8	0.46	0.17	1.10
0.741	2700	4.7	0.49	0.21	1.19
$\Phi_{c-C_3H_6} = 0.25, \Phi_{C_2H_4} = 0.56$					
Temp, 130°					
1.93	2700	12.5	0.46	0.14	1.21
1.22	2700	8.0	0.47	0.17	1.15
0.603	2700	4.0	0.55	0.22	1.19
$\Phi_{c-C_3H_6} = 0.24, \Phi_{C_2H_4} = 0.54$					
Temp, 170°					
1.62	2700	10.5	0.56	0.14	1.44
0.950	2700	6.2	0.57	0.18	1.39
0.555	2700	3.6	0.56	0.22	1.30
$\Phi_{c-C_3H_6} = 0.24, \Phi_{C_2H_4} = 0.48$					
Temp, 200°					
1.97	2700	12.8	0.61	0.12	1.70
1.58	2700	10.2	0.60	0.14	1.58
1.13	2700	7.3	0.63	0.14	1.66
0.412	2700	2.7	0.63	0.21	1.40
$\Phi_{c-C_3H_6} = 0.24, \Phi_{C_2H_4} = 0.42$					
Temp, 250°					
1.24	2700	8.0	0.76	0.16	1.85
0.920	2700	6.0	0.72	0.18	1.68
0.585	2700	3.8	0.77	0.23	1.60
$\Phi_{c-C_3H_6} = 0.25$					

Tests were made for an excited triplet at 2654 Å by use of 1,3-butadiene, 1,3-pentadiene, and *cis*-butene-2. The results were similar to those produced by n -hexane. With *cis*-butene-2, however, isomerization to *trans*-butene-2 was observed, indicating the possibility of a triplet state of cyclobutanone. The sensitized isomerization of *cis*- to *trans*-butene-2 has been previously used to determine triplet yields.⁹ From the per cent of *trans*-butene-2 formed in an experiment with 15.5 torr of cyclobutanone and 34.5 torr of *cis*-butene-2, the triplet-state quantum yield was calculated to be 0.074. In this calculation, a value of 1.02 was used for the branching ratio.¹⁰ This can be compared to the quenching of the C_3H_6 yield by 0.09 with 36.0 torr of *cis*-butene-2 (Table III). No fluorescence or phosphorescence was detected from cyclobutanone in the gas phase.

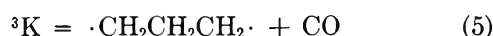
(9) R. B. Cundall, F. J. Fletcher, and D. G. Metne, *Trans. Faraday Soc.*, **60**, 1146 (1964).

(10) C. A. Haninger, Jr., and E. K. C. Lee, *J. Phys. Chem.*, **71**, 3104 (1967).

Table III: Effect of Added Gases on the Quantum Yields of C_3H_6 and $c-C_3H_6$ at 2654 Å and 40°

$10^{-12}I_a$, quanta/ ml sec	Time of irradiation, sec	$P_{C_3H_6O}$, torr	P_x , torr	x	Φ_{CO}	$\Phi_{C_3H_6}$	$\Phi_{c-C_3H_6}$	$\Phi_{C_3H_8}$
0.340	5400	4.5	0.50	0.27	0.26	0.00
0.340	5400	4.5	33.5	<i>n</i> -Hexane	0.50	0.15	0.27	...
1.31	2700	17.5	0.43	0.18	0.27	...
1.24	2700	16.5	13.0	<i>n</i> -Hexane	0.43	0.12	0.26	0.01
1.09	2700	14.5	22.5	<i>n</i> -Hexane	0.46	0.12	0.27	0.02
1.20	2700	16.0	30.0	<i>n</i> -Hexane	0.46	0.10	0.27	0.02
1.16	2700	15.5	45.0	<i>n</i> -Hexane	0.44	0.08	0.27	0.04
2.22	2700	29.5	0.42	0.13	0.26	0.00
2.22	2700	29.5	36.0	<i>n</i> -Hexane	0.41	0.08	0.26	...
1.16	2700	15.5	26.0	CO ₂	0.46	0.14	0.26	0.00
1.16	2700	15.5	8.5	CF ₄	...	0.16	0.27	0.00
1.16	2700	15.5	28.0	CF ₄	...	0.13	0.27	0.00
1.20	2700	16.0	30.5	SF ₆	0.44	0.11	0.27	0.00
1.12	2700	15.0	36.0	1,3-Butadiene	0.45	0.12	0.29	0.02
1.12	2700	15.0	31.0	1,3-Pentadiene	0.43	0.09	0.27	0.02
1.16	2700	15.5	36.0	<i>cis</i> -Butene-2	0.43	0.09	0.28	0.02

The photolysis of cyclobutanone may be explained best in terms of the simple mechanism



where K, 1K , and 3K represent ground, excited-singlet, and triplet states of cyclobutanone, respectively.

As written, the mechanism states that cyclopropane and ethylene are formed from the excited singlet state. Carbon monoxide is formed by eq 2 and 5. Thus one may write

$$N_{CO} - N_{C_3H_6} = N_{c-C_3H_6} \quad (8)$$

Reference to Table I indicates that this relationship is reasonably well obeyed. At each wavelength, quantum yields of $c-C_3H_6$ and of C_2H_4 were quite independent of pressure. Yields of C_2H_4 increase somewhat with decrease in wavelength. This may indicate either that eq 3 occurs to some extent before vibrational relaxation, or that 3K formed with considerable vibrational energy may undergo a small amount of reaction similar to eq 3. There may be an anomalous effect at 2804 Å, since the yield of $c-C_3H_6$ is high, but the difference is probably not more than experimental error and no attempt is made to offer an explanation of it.

The ratio $N_{c-C_3H_6}/N_{C_3H_6}$ decreases with decreasing pressure and also decreases at short wavelengths, in

agreement with earlier work.¹ However, the quantum yield of $c-C_3H_6$ is independent of pressure at each wavelength.

The data indicate, therefore, that C_3H_6 and $c-C_3H_6$ are not formed in single steps from the same precursor. Earlier work¹ would strongly suggest that an increase in C_3H_6 yield should be accompanied by a decrease in $c-C_3H_6$ yield. This effect would be hard to verify at the longer wavelengths, where the change in the C_3H_6 yield is about the same as the error in the $c-C_3H_6$ yield.

The constancy of the $c-C_3H_6$ yields indicates that eq 2 is a rapid reaction whose rate seems to be independent of the vibrational energy of the initially formed excited molecule. It would be interesting to speculate as to how eq 2 could take place in such a way, but such speculations would have little meaning at the present state of the art.

Some such reaction as eq 7 is necessary, since the sum of the quantum yields of eq 2, 3, and 5 is not unity under all experimental conditions. This sum should be given by $\Phi_{CO} + \Phi_{C_2H_4}$ if the mechanism contains all necessary steps. The ranges of the sums are as follows: 0.94–0.98 (3130 Å), 0.91–0.97 (2967 Å), 0.99–1.10 (2804 Å), and 0.96–1.07 (2654 Å). Since these data from Table I show some trends in carbon monoxide yields with time, particularly at the shorter wavelengths, it is probable that some secondary reactions which involve ketene occur. Sums of quantum yields for the various primary processes appear to be not far from unity and hence the importance of eq 7 is hard to estimate. The plot in Figure 1 tends to support the necessity for including it, however.

Certain rate constants can be evaluated from the data if steady-state concentrations are assumed. Thus

$$\Phi_{c-C_3H_6} = k_1/(k_1 + k_2 + k_3) \quad (9)$$

$$\Phi_{C_2H_4} = k_2 / (k_1 + k_2 + k_3) \quad (10)$$

$$1/\Phi_{C_2H_4} = (k_1 + k_2 + k_3)/k_2 + (k_1 + k_2 + k_3)k_4(M)/k_2k_5 \quad (11)$$

A plot of eq 11 for data at 40° is shown in Figure 1.

By use of the slopes and intercepts, one can obtain the following ratios from the data: $k_1/k_2 = 1.04$, $k_2/k_3 = 2.28$, $k_4/k_5 = 4.88 \times 10^{-2} \text{ l. mol}^{-1}$, all at 2654 Å at 40°.

One may conclude either that eq 7 has a very small effective cross section, or that eq 4 is an extremely fast reaction with a rate constant around 10^{10} sec^{-1} . No attempt has been made to obtain activation energy differences because they would be subject to quite large errors.

Some propane is formed when added gases contain hydrogen atoms. Very small amounts of C₃ compounds were formed when 30 torr of ethylene was added to 15 torr of cyclobutanone either at 200 or at 40° at 2654 Å. The isomerization of *cis*-butene-2 to *trans*-butene-2 may not be a certain way to determine triplet-state yields in this case because reactions of the trimethylene diradical might cause complications.

The yield of CO increases while that of C₂H₄ decreases with increase in temperature. $N_{CO}/(N_{C_2H_4} + N_{C-C_2H_4})$ is very close to unity at room temperature but rises well above unity at higher temperatures (Table II). Some polymeric material is formed and possibly

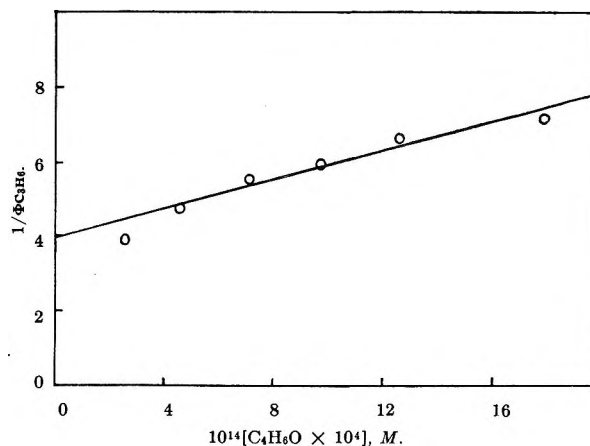


Figure 1. Plot of $1/\Phi_{C_2H_4}$ vs. concentration of cyclobutanone at 40° (λ 2654 Å).

this could account for the observed trend. At elevated temperatures, some thermal reactions of ketene may occur.

It may be concluded that the mechanism presented accounts for the main observed facts.

Acknowledgment. The author wishes to thank Professor W. A. Noyes, Jr., and Dr. H. D. Mettee for reviewing the manuscript and for making helpful suggestions. Support from Grant No. 26-0273-6950 from the Office of Aerospace Research, Air Force Office of Scientific Research, is gratefully acknowledged

Dimerization of Nitrogen Dioxide in Solution: a Comparison of Solution Thermodynamics with the Gas Phase¹

by Thomas F. Redmond and Bradford B. Wayland

John Harrison Laboratory of Chemistry and Laboratory for Research on the Structure of Matter, University of Pennsylvania, Philadelphia, Pennsylvania 19104 (Received October 23, 1967)

The equilibrium of N_2O_4 with NO_2 has been determined in cyclohexane, carbon tetrachloride, and acetonitrile. The equilibrium constants and enthalpies for N_2O_4 dissociation at 298°K have been determined and are respectively, 1.77×10^{-4} and 14.6 kcal in cyclohexane and carbon tetrachloride and 0.30×10^{-4} and 16 kcal in acetonitrile. These data are compared with the gas-phase values of 1.51×10^{-1} and 13.64 kcal for N_2O_4 dissociation. The differences in gas and solution thermodynamics are discussed.

Introduction

There has recently been increased interest in the relationship of gas-phase equilibrium to the corresponding process in solution.²⁻⁵ There remains a need for further investigations which permit comparison of simple equilibria in the gas phase with that in solution. Because of the extensive gas-phase equilibrium data for the dissociation of N_2O_4 ,^{6,7} and the capability of studying this reaction in solution, this equilibrium offers an unusual opportunity for investigating the difference between the gas and solution processes.

Since the early work of Cundall⁸ as interpreted by later authors,^{9,10} very little work has appeared pertaining to solvent effects on the thermodynamics for N_2O_4 dissociation. This paper reports the measurement of equilibrium constants and enthalpies for the dissociation in the noncoordinating solvents, cyclohexane and carbon tetrachloride, and in the coordinating solvent, acetonitrile. The resulting data are discussed with reference to the corresponding gas-phase values.

The equilibrium constants were determined by taking advantage of the paramagnetism of NO_2 . The nmr technique has been applied to the measurement of solution susceptibility and these data have been utilized to determine the concentrations of NO_2 and N_2O_4 present in solution. The magnetic technique is a convenient direct method for studying this equilibrium, in contrast with electronic spectral measurements which can yield only relative equilibrium constants, owing to the uncertainty of medium effects on extinction coefficients.³

Experimental Section

Materials and Sample Preparation. Fisher Spectro-analyzed cyclohexane and carbon tetrachloride were used without further purification. Fisher reagent grade acetonitrile was shaken with barium oxide, allowed to stand for several days, and then redistilled, bp 81.7° (uncor). Nitrogen dioxide was obtained 99%

pure from Matheson Scientific Co. On freezing samples of the dioxide to liquid nitrogen temperatures, blue and green colors were often detected, indicating the presence of other oxides of nitrogen. Samples were fractionally distilled until a pure white solid melting at approximately -11° was obtained.

Cyclohexane and carbon tetrachloride were selected as representative noncoordinating solvents on the basis of positive deviations from ideality in vapor pressure¹¹ and additivity of volumes¹² for solutions of N_2O_4 in these solvents. Acetonitrile solutions of N_2O_4 show negative deviations in vapor pressure, which is taken to imply complex formation.

Magnetic resonance samples were prepared by vacuum distillation of purified oxide and solvent into nmr tubes from reservoir bulbs which were weighed before and after transfer. Bulbs with Teflon stopcocks were used to eliminate the need for grease. The bulbs were tested and proved capable of holding vacuum and constant weight for considerably longer periods of time than required for weighing, transfer, and reweighing.

Since N_2O_4 is a powerful oxidizing agent, samples were stored at liquid nitrogen temperature until immediately before use. The equilibrium measurements

(1) Abstracted in part from the Ph.D. Thesis of Thomas F. Redmond, University of Pennsylvania, Philadelphia, Pa., 1968. Inquiries should be addressed to B. B. Wayland.

(2) J. Prochorow and A. Tramer, *J. Chem. Phys.*, **44**, 4545 (1966).

(3) P. Trotter, *J. Amer. Chem. Soc.*, **88**, 5721 (1966).

(4) J. M. Goodenow and M. Tamres, *J. Chem. Phys.*, **43**, 3393 (1965).

(5) F. T. Lang and R. L. Strong, *J. Amer. Chem. Soc.*, **87**, 2345 (1965).

(6) W. F. Giauque and J. D. Kemp, *J. Chem. Phys.*, **6**, 40 (1938).

(7) I. C. Hisatsune, *J. Phys. Chem.*, **65**, 2249 (1961).

(8) J. T. Cundall, *J. Chem. Soc.*, **67**, 794 (1895).

(9) P. Gray and H. Joffe, *Chem. Rev.*, **55**, 1077 (1955).

(10) P. Gray and P. Rathbone, *J. Chem. Soc.*, 3550 (1958).

(11) C. C. Addison and J. C. Sheldon, *ibid.*, 1937 (1957).

(12) C. C. Addison and B. C. Smith, *ibid.*, 3664 (1958).

were found to be reversible with changing temperatures, which precludes significant irreversible reactions during the time required for the magnetic measurements.

Procedure. By analogy with the theory of atomic dipoles, the shift of the nmr position of a sample due to a change in volume magnetic susceptibility can be expressed in terms of a ratio of geometric factors,¹³ such that for a capillary tube containing pure solvent inside an nmr tube containing solution

$$\Delta\chi_V = \frac{3\delta}{2\pi} \quad (1)$$

where $\Delta\chi_V$ is the total change in susceptibility from capillary to nmr tube and δ is the shift in ppm. $\Delta\chi_V$ can also be expressed in the NO_2 case as

$$\Delta\chi_V = \chi_{V\text{NO}_2} + \chi_{V\text{N}_2\text{O}_4} + \chi_{V_s} - \chi_{V_0} \quad (2)$$

where χ_{V_0} is the volume susceptibility of pure solvent and χ_{V_s} is the volume susceptibility of the solvent in the solution equal to $(V_0/V_s)\chi_{V_0}$, where V_s represents the total volume of the solution and V_0 represents the volume contribution of the pure solvent. Combining eq 1 and 2 and rearranging we have

$$\chi_{V\text{NO}_2} + \chi_{V\text{N}_2\text{O}_4} = \frac{3\delta}{2\pi} - \chi_{V_0}(V_0/V_s - 1) \quad (3)$$

This can be readily converted into gram susceptibilities

$$\chi_g(\text{NO}_2 + \text{N}_2\text{O}_4) = \frac{3\delta}{2\pi m} - \frac{\chi_{V_0}}{m}(V_0/V_s - 1) \quad (4)$$

where m is the total grams of NO_2 and N_2O_4 per milliliter of solution. From a knowledge of the magnetic susceptibilities for NO_2 and N_2O_4 the concentrations of these species can be calculated. This is essentially the method of Evans, and eq 4 can be readily converted into his original expression.¹⁴

For the cyclohexane measurements, the shift of the solvent peak itself was measured. In the case of carbon tetrachloride and acetonitrile, the solvent both in the tube and capillary contained approximately 5% cyclohexane as a standard.

Most measurements were carried out on a Varian A60A spectrometer with a few made on an HR-60. Temperature was controlled by a Varian temperature-control accessory using nitrogen gas and was measured by peak separation in ethylene glycol and methanol samples. Samples were scanned an average of six times on a 100-cycle scale. Shifts were on the order of 2–10 sec^{-1} and were reproducible within at least $\pm 0.03 \text{ sec}^{-1}$. Spinning problems were encountered occasionally due to the capillary tube. Attempts to overcome this problem by use of separate tubes for samples and standard led to nonreproducible results due to field drift and small differences in tube characteristics.

The diamagnetic susceptibilities of cyclohexane and

carbon tetrachloride were taken from the International Critical Tables while a value calculated from the data of Wickenden and Krause¹⁵ was used for acetonitrile. The diamagnetic susceptibility of N_2O_4 was taken as the commonly accepted value of 0.276×10^{-6} , as determined by Sone,¹⁶ and the diamagnetic susceptibility of NO_2 was assumed to be one half that of the dimer. Deviation of the diamagnetic susceptibility of NO_2 from this value would have little effect on the calculation, owing to the small contribution this term makes to the susceptibility of paramagnetic NO_2 .

The paramagnetic susceptibility of NO_2 was calculated from the g value, as determined by esr in CCl_4 solution.¹⁷ An experimental value of the susceptibility was determined directly by Havens¹⁸ in 1933 which would lower the equilibrium constants by 15% while leaving the enthalpies unchanged. The esr value is very close to the free-electron value and undoubtedly is the more accurate measurement of the susceptibility.

The solution composition was corrected for the presence of vapor above the solution. Deviations of the vapor pressure from ideality as expressed by Raoult's law were corrected for by extrapolation of data reported by Addison.¹¹ The corrections increased the equilibrium constant by as much as 5% in the case of cyclohexane but were unimportant with the other solvents. Several runs were made with nmr tubes sealed close to the surface of the solvents and the results supported the accuracy of the correction. The solutions were also corrected for deviations from ideality in terms of volume additivity by extrapolation of Addison's data.¹² The method is particularly sensitive to volume corrections, since the magnitude of the diamagnetic correction term in the susceptibility is large when compared to the susceptibility of the dissociated NO_2 species. The densities of the solvents were taken from Lange's Handbook of Chemistry, as were the coefficients of volume expansion for CCl_4 and CH_3CN . The volume expansion of cyclohexane over the temperature range employed was determined previously in this laboratory. The density of N_2O_4 as a function of temperature was taken from the work of Mittasch *et al.*¹⁹

Results

Representative data for the determination of equilibrium constants by the nmr method are shown in Table I for several temperatures and concentrations. The

(13) G. Dickinson, *Phys. Rev.*, **81**, 717 (1951).

(14) D. F. Evans, *J. Chem. Soc.*, 2003 (1959).

(15) A. E. Wickenden and R. A. Krause, *Inorg. Chem.*, **4**, 404 (1965).

(16) T. Sone, *Science Repts. Tohoku Imp. Univ.*, **11**, 139 (1922).

(17) M. Bersohn and J. C. Baird, *J. Chem. Phys.*, **28**, 738 (1958).

(18) G. G. Havens, *Phys. Rev.*, **41**, 337 (1932).

(19) Mittasch, Kuss, and Schlueter, *Z. Anorg. Chem.*, **159**, 1 (1927).

Table I: Representative Data for N₂O₄ Dissociation

Temp, °C	Wt of N ₂ O ₄ + NO ₂ , g	V ₀ , ml	V _{N₂O₄ + NO} , ml	V _s , ^a ml	δ _{ppm}	10 ⁶ χ _{N₂O₄ + N₂O₄} , ml g ⁻¹	10 ⁶ χ _{g NO₂ + N₂O₄} , ml g ⁻¹	Wt of 10 ⁴ NO ₂ , g	10 ⁴ K _c , mol l. ⁻¹
Cyclohexane									
26.7	0.06196	0.7577	0.0433	0.8068	0.0663	-0.00635	-0.08268	4.442	1.74
26.7	0.04768	0.4408	0.0333	0.4784	0.0823	-0.00982	-0.09850	3.134	1.90
34.3	0.06196	0.7661	0.0439	0.8161	0.0765	-0.00133	-0.01752	6.091	3.25
34.3	0.04768	0.4457	0.0338	0.4841	0.0937	-0.00428	-0.04345	4.217	3.40
42.0	0.06196	0.7748	0.0445	0.8257	0.0926	0.00655	-0.08733	8.772	6.73
42.0	0.04768	0.4507	0.0343	0.4898	0.1104	0.00393	0.04039	5.881	6.60
50.0	0.06196	0.7840	0.0452	0.8359	0.1067	0.01345	0.1815	11.331	11.19
50.0	0.04768	0.4561	0.0348	0.4960	0.1290	0.01300	0.1353	7.838	11.63
Carbon Tetrachloride									
26.5	0.05553	0.4707	0.0388	0.5116	0.0913	-0.01085	-0.10000	3.620	2.03
35.0	0.04120	0.6130	0.0292	0.6439	0.0720	0.00199	0.03109	4.821	3.90
35.3	0.05553	0.4756	0.0394	0.5171	0.1067	-0.00322	-0.02998	5.210	4.19
50.0	0.05553	0.4841	0.0405	0.5268	0.1364	0.01245	0.1181	8.749	11.74
53.0	0.04120	0.6264	0.0302	0.6583	0.1092	0.02016	0.3220	9.939	16.65
Acetonitrile									
35.0	0.06189	0.6123	0.0439	0.6562	0.0275	-0.01533	-0.1647	0.571	0.75
44.8	0.06189	0.6201	0.0447	0.6648	0.0368	-0.01074	-0.1136	0.859	1.67
53.0	0.06189	0.6268	0.0454	0.6722	0.0477	-0.00538	-0.05841	1.181	3.14

^a Cyclohexane and carbon tetrachloride solutions corrected for deviation from additivity of volumes by assumption of linear dependence of density on temperature and of validity of Biron relationship.¹²

Table II: Thermodynamic Values for N₂O₄ Dissociation

	K _c ²⁹⁸ , mol l. ⁻¹	ΔF ²⁹⁸ _{dissn.} , kcal mol ⁻¹	ΔH ²⁹⁸ _{dissn.} , kcal mol ⁻¹	ΔS ²⁹⁸ _{dissn.} , eu
Cyclohexane	1.77 ± 0.1 × 10 ⁻⁴	5.1	14.6 ± 0.5 ^a	31.8 ± 1.0
Carbon tetrachloride	1.78 ± 0.1 × 10 ⁻⁴	5.1	14.6 ± 1.0 ^b	31.8 ± 1.5
Acetonitrile	0.30 ± 0.1 × 10 ⁻⁴	6.1	16 ± 1.5	33.0 ± 2.5
Gas phase ^c	1.51 × 10 ⁻¹	1.12	13.64 ^d	42.8

^a Least-squares analysis of thirteen points with 80% confidence limits. ^b Least-squares analysis of eight points with 80% confidence limits. ^c Reference 7. ^d ΔH₀^o = 12.69 kcal mol⁻¹, ΔH₀²⁹⁸ - ΔPV = 13.0.

thermodynamic values calculated from these data are shown in Table II.

Discussion

Noncoordinating Solvent Effects. The N₂O₄ dissociation constant in CCl₄ and C₆H₁₂ determined in this study (K_c^{20°} = 1.1 ± 0.1 × 10⁻⁴ mol l.⁻¹) compares reasonably well with the value calculated from the data of Cundall (K_c^{20°} = 0.8 × 10⁻⁴ mol l.⁻¹)¹⁰ in CCl₄. The temperature dependence of K_c (ΔH = -14.6 kcal mol⁻¹) is, however, found to be significantly smaller than the value calculated from Cundall's data (ΔH = -18.8 kcal mol⁻¹) and the value for liquid N₂O₄ (ΔH = -17.8 kcal mol⁻¹).¹⁰ The enthalpy value reported here is fairly close to the gas-phase enthalpy and thus consistent with many other experimental observations on related systems, such as N₂F₄²⁰ and various molecular addition compounds.^{21,22} Since the enthalpy

of dissociation is increased only slightly in going from the vapor phase to a noncoordinating solvent environment, the drastic decrease in N₂O₄ dissociation in a solvent is primarily the result of a decreased entropy change (32 eu in solution vs. 43 eu in gas phase). This is in direct contrast to analysis of Cundall's data which predict an increase in the entropy of dissociation on going from the gas to the solution phase.

A decrease in dissociation entropy in solution compared to the gas phase is to be expected in terms of several simple models for noncoordinating solvent systems. Consideration of the solute molecules as

(20) (a) F. A. Johnson and C. B. Colburn, *J. Amer. Chem. Soc.*, **83**, 3043 (1961); (b) H. E. Doorenbos and B. R. Loy, *J. Chem. Phys.*, **39**, 2393 (1964).

(21) F. G. A. Stone, *Chem. Rev.*, **58**, 101 (1958).

(22) C. H. Henrickson and D. P. Eyman, *Inorg. Chem.*, **6**, 1461 (1967).

being subjected to a sharply decreased free volume when passing from the gas to the solution phase leads to a significant decrease in entropy for all solute species to approximately the same extent. A similar result would be expected for solute molecules in terms of very large internal or mechanical pressures exerted by the solvent on the solute. Thus in general, when the entropy change in going from the gas to the solution phase is dominated by the solvent structure and not by chemical interaction, a dissociative process will be less entropy favored in the solution compared to the vapor phase. This is shown to be true in many systems, such as the molecular addition compounds of boron and aluminum acceptors.^{21,22} Similar results are predicted from application of a crystalline model of solution in which the translational motions of the solute molecules are converted into low-frequency vibrations in the solvent lattice.

This general statement does not, however, account for some recently reported charge-transfer equilibria^{2,4,5} involving highly complex molecules such as tetracyanoethylene-xylene adducts.²³ In these cases, dissociation occurs more extensively in solution than in the vapor phase. These data are difficult to understand within the framework of current knowledge of the properties of liquids. The translational entropies of the solute molecules must be considerably smaller in the solution than the gas phase. This effect should favor higher association in solution. Deviations from ideality in the gas phase, solvation effects, and restriction of rotational motions for the large, unsymmetrical adducts may be responsible for the observed behavior.

Coordinating Solvent Effects. The dissociation of N_2O_4 in the coordinating solvent acetonitrile is even smaller than in noncoordinating solvents (Table II). The increase in the association of N_2O_4 results from the increase in the apparent enthalpy of N_2O_4 dissociation to 16 ± 1.5 kcal. This suggests that N_2O_4 is a better Lewis acid than NO_2 and thus is more highly associated with acetonitrile. These data may be compared with values ($K_c^{298} = 1.0 \times 10^{-4}$ mol l.⁻¹, $\Delta H = 17.8$ kcal)¹⁰ for dissociation in the coordinating solvent liquid N_2O_4 . The apparent entropy of dissociation is approximately the same as in the noncoordinating solvents suggesting that even when a weak specific interaction is involved in the system, the solvent structure may be the dominant factor in entropy reduction.

It is difficult to rigorously assess the significance of equilibrium data in coordinating solvents due to the probability of competitive equilibria involving species of varying degrees of complexation and solvation. It is most likely that the dominant equilibrium involves a simple process such as $2NO_2 \cdot B \rightleftharpoons N_2O_4 \cdot 2B$. The temperature dependence of the apparent equilibrium constant is consistent with a simple equilibrium but cannot be used to rule out the possibility of other competing equilibria such as $N_2O_4 + B \rightleftharpoons N_2O_4 \cdot B$, $N_2O_4 \cdot B + B \rightleftharpoons N_2O_4 \cdot 2B$, and $NO_2 + B \rightleftharpoons NO_2 \cdot B$.

Acknowledgment. We wish to thank the Advanced Research Projects Agency for its support of this research through Contract No. SD-69.

(23) M. Kroll and M. L. Ginter, *J. Phys. Chem.*, **69**, 3671 (1965).

Base Strengths of Amine–Amine Hydrochloride Systems in Toluene¹

by Robert R. Grinstead and James C. Davis

The Dow Chemical Company, Western Division Laboratories, Walnut Creek, California 94568 (Received October 26, 1967)

The apparent base strengths of a number of primary, secondary, and tertiary aliphatic amines have been determined in toluene–aqueous systems, using HCl as a reference acid. At very low concentrations of amine hydrochlorides in toluene, where aggregation effects are absent, the apparent pK_a values (pH at half-titration) for all types are similar, being mainly between 3.3 and 3.7. At higher concentrations, aggregation of the salts occurs, raising the apparent pK_a values. In the range of 0.05 *M* amine hydrochloride, the tertiaries are partly associated to form dimers and behave as the weakest bases ($pK_a = 4-5$). The primary amines exhibit aggregate formation to the extent of tetramers or pentamers and behave as the strongest bases ($pK_a = 7-8$). Secondary amines exhibit intermediate behavior. Within each type the more sterically hindered amines behave as the weaker bases and aggregate to a lesser extent. Extraction of water is greatest by the tertiary amine hydrochlorides, less for the secondaries, and almost negligible for the primaries. The large spread in apparent basicity at the higher concentrations is ascribed to the variation in the ease with which amine hydrochlorides can form stable aggregates. Primary amines, being relatively unhindered about the nitrogen atom, can form relatively stable aggregates. The increasing steric hindrance in proceeding through secondaries to tertiaries reduces the stability of the aggregate and hence the tendency to react with HCl.

In recent years considerable interest has arisen in high molecular weight amines and their salts as extractants for anionic species from aqueous solutions. This interest has centered around the recovery of anionic metal complexes,² but some work has been reported in which the basic properties of the amine itself have been of interest. In particular, the recovery of mineral acids^{3,4} and the transfer of acidity between two aqueous systems⁵ both involve the question of the base strength of the amine, that is, the tendency to react with an acid to form the salt in the organic phase of an extraction system.

Numerous studies have been made of the physical chemistry of tertiary amines and their mineral acid salts in various solvent systems.⁶⁻¹⁰ Hardly any, however, have involved secondary or primary amines,^{11,12} and none of these has utilized purified compounds. Yet, as will be shown, a considerable difference exists in the behavior of the three classes of amines as bases in liquid–liquid systems. Even in amine salt systems used to extract metal complexes, considerable differences exist in the behaviors of the amine types,¹³ and a deeper understanding of amine and amine salt systems appears highly desirable.

It has been fairly well established that the tertiary amine hydrohalides tend to form aggregates in many organic solvents in response to the need to solvate the ion pairs of the salt.⁷⁻⁹ In solvents which can interact strongly with the dipole (*e.g.*, chloroform) or which have high dielectric constants, this aggregation is minimized, but even in toluene, which is a relatively poor solvent by these standards, these salts deaggregate to monomers at concentrations below about 10^{-3} *M*. Some initial work with various primary and secondary amines showed that aggregation of these

types of amine salts in toluene was considerably more extensive than for tertiaries and, furthermore, appeared to be related to steric hindrance about the nitrogen atom.¹⁴ With the aid of tracer Cl³⁶, these studies have now been extended to sufficiently low concentrations of the hydrohalide salt in toluene to observe the monomeric species and to determine their formation constants. With these data, estimates of the extent of aggregation at higher concentrations have been made and correlated with the structure of the compound. The systems have been further characterized by determining water extraction up to 0.3 *M* hydrochloride concentration.

Because of the unavailability of suitable compounds for these studies, most of them were either synthesized

(1) This research was supported by the Office of Saline Water, U. S. Department of Interior, under Contract No. 14-01-0001-1134.

(2) M. J. Zakarias and M. J. Cahalan, *Trans. Inst. Mining Metall.*, **75C**, 245 (1966).

(3) W. H. Hardwick and P. F. Wace, *Chem. Process Eng.*, **46**, 283 (1965).

(4) D. J. Crouse, Jr., U. S. Patent 3,211,526 (1965).

(5) R. Kunin, *Ind. Eng. Chem.*, **56**, 35 (1964).

(6) A. S. Wilson and N. A. Wogman, *J. Phys. Chem.*, **66**, 1552 (1962).

(7) E. Högfeldt, *et al.*, *Trans. Roy. Inst. Technol.* (Stockholm), **224** (1964).

(8) W. Müller and R. M. Diamond, *J. Phys. Chem.*, **70**, 3469 (1966).

(9) G. Scibona, S. Basol, P. R. Danesi, and F. Orlandini, *J. Inorg. Nucl. Chem.*, **28**, 1441 (1966).

(10) W. E. Keder and A. S. Wilson, *Nucl. Sci. Eng.*, **17**, 287 (1963).

(11) C. F. Coleman, *et al.*, *Ind. Eng. Chem.*, **50**, 1755 (1958).

(12) G. Scibona, F. Orlandini, and P. R. Danesi, *J. Inorg. Nucl. Chem.*, **28**, 1701 (1966).

(13) C. F. Coleman, *Nucl. Sci. Eng.*, **17**, 274 (1963).

(14) R. R. Grinstead, Proceedings of International Conference on Solvent Extraction Chemistry, Göteborg, Sweden, 1966.

during this study by various standard procedures, or were purified from available commercial mixtures.

Experimental Methods

Materials. Amines. Trioctylamine was purchased as the hydrochloride and used directly in some cases. A supply of the free amine was obtained from Alamine 336, a commercial product obtained from the General Mills Corp. This material is a mixture of trialkylamines, primarily trioctyl,¹⁵ and was fractionally distilled to give a good cut of trioctylamine.

N-Methyldioctylamine and di-(2-ethylhexyl)amine were obtained from supply houses and either used directly or fractionated through an 8-in. Vigreux column to further purify them. Primene JM-T, which was used in a few experiments, was obtained from Rohm & Haas Co. It is a mixture of primary amines, wherein the amino group is attached to a tertiary carbon. The equivalent weight corresponds to about 21 carbon atoms.

Secondary amines were synthesized by reductive alkylation of a suitable amine with the appropriate aldehyde or ketone.¹⁶ The two starting materials were usually refluxed in toluene until all of the water of condensation was removed. Reduction of the Schiff base adduct was usually accomplished with methanolic sodium borohydride.¹⁷ A slightly modified procedure was required to dehydrate the intermediate in the preparation of N-(3,7-dimethyloctyl)-decylamine, owing to its tendency toward self-condensation.¹⁸ Since the starting aldehyde in this case was citronellal, containing a carbon-carbon double bond, it was reduced with hydrogen over a palladium-charcoal catalyst.

Two methods were used to synthesize the primary amines. The 7-amino-7-hexyltridecane was obtained by first preparing the corresponding alcohol through a Grignard reaction of bromohexane on diethylcarbonate.¹⁹ The alcohol was converted to the amine by the Ritter reaction,²⁰ using sodium cyanide in sulfuric acid, followed by hydrolysis of the substituted formamide to the amine. The 1-amino-2,2-dihexyloctane was prepared by alkylation of octonitrile by bromooctane in the presence of sodium amide,²¹ followed by reduction of the resultant nitrile with lithium aluminum hydride.²²

All of the products were fractionally distilled through an 8-in. Vigreux column under vacuum to purify them and were characterized in a variety of ways, including elemental analysis and titration with an acid to determine the equivalent weight. In early work using the pH method of equilibrium-constant determination, the amines were converted to the hydrochlorides by gassing a solution in pentane with hydrogen chloride and either filtering the precipitate or evaporating the pentane to a residue, followed by drying at 30–40° *in vacuo*. The hydrochlorides were characterized by elemental analysis, and also by examination of the pmr spectra. The

data for these compounds are shown in Table I. These were used in most of the work on determination of pK_a values in the concentration range above about 10^{-3} M, using method A.

For the work at lower concentrations and for water-extraction work, the amines were used directly, and purity was ascertained mainly by vapor-phase chromatography. In Table II are shown the glpc data, which in some cases apply to the preparations which were converted to hydrochlorides but, in most cases, refer to subsequent preparations by the same methods.

Chlorine-36 Tracer. The Cl^{36} tracer, a β^- emitter, was obtained from New England Nuclear Corp. as an aqueous HCl solution. The presence of a radioactive impurity in the Cl^{36} -tracer solution interfered with low-level counting, owing to the distribution of the impurity into the organic phase. The impurity was removed from the aqueous tracer by seven extractions of the stock hydrochloric acid solution with distilled reagent toluene in a 3:1 organic:aqueous phase ratio. Beyond this point, further extractions gave a constant activity in the toluene, which was assumed to represent the distribution of hydrogen chloride into toluene at that aqueous hydrochloric acid concentration. With aqueous hydrochloric acid concentrations of 0.0515 and 0.0125 M, the corresponding concentrations in toluene were 1.3×10^{-7} and 3.3×10^{-8} M, respectively.

Other Materials. Reagent grade toluene was used for most work. In one or two instances, acidic impurities were detected in this material, and all toluene used in tracer-chlorine experiments was distilled from potassium hydroxide prior to use.

Instrumentation. All pH measurements and titrations were made using an L & N Model 7401 or 7664 pH meter, utilizing a glass-calomel electrode system. The meter was standardized with a pH buffer at pH 4.00.

The analyses for Cl^{35} extractions were carried out in a Packard Model 4322 Tricarb liquid scintillation spectrometer using a toluene solution of 2,5-bis[2,5-*t*-butylbenzoxazolyl]thiophene (BBOT) as a scintillator. Counting times were adjusted to produce a maximum standard deviation of $\pm 2\%$ in the net count for amine hydrochloride concentrations down to 10^{-6} M. Higher deviations were accepted below this level, reaching

(15) G. Grossi and R. Vece, *J. Gas Chromatogr.*, **3**, 170 (1965).

(16) M. L. Moore, "Organic Reactions," Vol. 5, R. Adams, Ed. John Wiley and Sons, Inc., New York, N. Y., 1949, p 301.

(17) J. H. Billman and A. C. Diesing, *J. Org. Chem.*, **22**, 1068 (1957).

(18) K. H. Campbell, A. H. Sommers, and B. K. Campbell, *J. Amer. Chem. Soc.*, **66**, 82 (1944).

(19) W. W. Moyer and C. S. Marvel, "Organic Syntheses," Coll. Vol. II, John Wiley and Sons, Inc., New York, N. Y., 1943, p 602.

(20) J. J. Ritter and J. Kalish, *J. Amer. Chem. Soc.*, **70**, 4048 (1948).

(21) N. Sperber, D. Papa, and E. Schwenk, *ibid.*, **70**, 3091 (1948).

(22) L. H. Amundson and L. S. Nelson, *ibid.*, **73**, 242 (1951).

Table I: Data on Amine Hydrochloride Preparations

	Equiv wt			Elemental analysis				
	Theoretical	Acid titration		C	H	N	Cl	Total
N-Dodecyl-2-ethylhexylamine	334	344	Theor	72.0	13.2	4.2	10.6	100
			Actual	71.7	13.2	4.4	10.4	99.7
N-Dodecylisooctylamine	334	352 ^a	Theor	72.0	13.2	4.2	10.6	100
			Actual	71.6	12.2	4.2	10.4	98.4
N-(2,6,8-Trimethylnonyl-4)-2-ethylhexylamine	334	334	Theor	72.0	13.2	4.2	10.6	100
			Actual	71.4	13.0	4.2	10.9	99.5
Di-(2-ethylhexyl)amine	278	281	Theor	69.1	12.9	5.1	12.9	100
			Actual	67.2	12.9	4.9	11.8	96.8
N-Methyldioctylamine	292	298	Theor	70.0	13.0	4.9	12.1	100
			Actual	69.7	13.1	4.6	11.2	98.6
Trioctylamine	390	398	Not analyzed					
1-Amino-2,2-dihexyloctane	334	341	Theor	72.0	13.2	4.2	10.6	100
			Actual	71.9	13.0	4.4	10.9	100.3
7-Amino-7-hexyltridecane	320	321	Theor	71.3	13.2	4.4	11.1	100
			Actual	71.0	12.9	4.7	10.8	99.4

^a Titration indicates 5% of a stronger base, probably the primary amine starting material.

Table II: Purity of Amines by Vapor Phase Chromatographic Analysis^a

Compound	Estimated purity, %	Distillation range, °C (pressure, mm)
7-Amino-7-hexyltridecane ^b	>99	150–153 (1.8)
1-Amino-2,2-dihexyloctane	97	157–158 (1)
N-Dodecyl-2-ethylhexylamine	98	157–158 (1)
N-(3,7-Dimethyloctyl)decylamine	>99	144–146 (0.5)
N-(2,6,8-Trimethylnonyl-4)-2-ethylhexylamine	97	137–139 (2.5)
Di-(2-ethylhexyl)amine	99	90.5–92 (0.2)
N-Methyl dioctylamine	>99	102–104 (0.2)
Tri- <i>n</i> -octylamine	99	178° (0.1)

^a Column: length, 5 ft; silicone gum rubber SE 30, 5% on 100–120 mesh Chromosorb W, 30°; initial temperature, 100° (rising 6 deg/min). ^b Distilled twice, since first distillation gave only ~90% purity.

± 25% at the lowest concentrations. This corresponds to an uncertainty in the pK_a value of about 0.1 unit.

Procedures. Three methods were used to determine the apparent base strengths of the amines studied. Each method applied to a specific range of amine salt concentration. High concentrations of amine salt (down to 10^{-3} M) were studied through the use of the method previously described.¹⁴ This involved the determination of the pH of aqueous 1.00 M NaCl, which was in equilibrium with toluene containing equal concentrations of amine and amine salt (method A).

In method B, also used at amine salt concentrations

of 5×10^{-2} to 10^{-3} M, toluene solutions were shaken for 1 hr with a known volume and concentration of aqueous hydrochloric acid. The separated phases were titrated with standardized sodium hydroxide, using a pH meter, to determine the distribution of hydrochloric acid. For systems of amines of less than about 19 carbon atoms, significant concentrations of the alkylammonium ions (>5% of the total) were found in the aqueous phases and were detected and estimated by the presence of a second break in the titration curve at a somewhat higher pH. The aqueous chloride concentration was taken as the sum of any alkylammonium ion plus hydrogen ions. The free amine concentration in the organic phase was determined by difference.

Chlorine³⁶ tracer as aqueous hydrochloric acid was used to determine the apparent base strengths of amines in method C. Tracer solutions of known activity and hydrochloric acid concentration were contacted with known concentrations of free amine in toluene. The samples were shaken about 2 hr and then centrifuged a minimum of 15 min to eliminate entrainment. A 1-cc sample of each organic phase was then analyzed for amine salt by counting the extracted Cl³⁶. The chloride concentration was then obtained by use of a factor determined by both counting and titrating with base aliquots of a single organic phase. The amount of hydrochloric acid remaining in the aqueous phase was determined by difference and, in most cases, was essentially unchanged due to the large excess of acid over amine. All equilibrations were done at $23 \pm 2^\circ$.

The extent of distribution of amine hydrochloride into the aqueous phase was determined through the use

of a back extraction of the aqueous phase with a fresh portion of uncontacted amine solution or with toluene alone. A significant loss of BHCl into the aqueous layer in the original contact results in a different value of (ΣBHCl) in the second contact. In all cases, the losses were determined at the lowest possible total amine concentration, assuming that a high percentage of monomer (BHCl) would result in the highest percentage distribution into the aqueous phase.

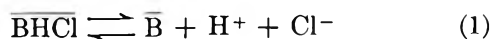
Determination of Water. Most water determinations in the organic phases were carried out by Karl Fischer titration in methanol. While amines are said to interfere in this titration, determinations of water in the free amine systems were carried out in the presence and absence of acetic acid (to convert amines to ammonium ions) with no significant differences in results.

In some systems, tritiated water was added to the aqueous phase in order to minimize the quantity of amine required, and the activity of the toluene solutions was determined by the same procedures as used for the chlorine tracer. A correction was required for the number of hydrogens on the amine or amine salt, since these are readily exchangeable with the water.

Osmometer Data. The data were obtained with a Mechrolab osmometer Model 30¹ in order to conform as closely as possible to the conditions of the equilibrium studies. Solutions of amine hydrochlorides were prepared in toluene and shaken with dilute aqueous hydrochloric acid (0.02–0.1 *M*) to prevent hydrolysis of the amine salts. Water-saturated toluene was used as the reference and solutions of benzil in water-saturated toluene were used as standards.

Experimental Data

Acid-Base Equilibria. The base strength of any species B can be defined by its tendency to react with an acid, in this case aqueous HCl. The reaction



where bars denote species in the organic phase, can be used to derive the associated equilibrium

$$K_a' = \frac{(\overline{\text{B}})(\text{H}^+)(\text{Cl}^-)\gamma_{\pm}^2}{(\overline{\text{BHCl}})} \quad (2)$$

where K_a' is the acid dissociation constant and is a measure of the base strength of B.¹⁴ The quantity γ_{\pm} is the mean activity coefficient of aqueous hydrochloric acid. Little is known about activity coefficients in the organic phase, and we are assuming in the following discussion that the concentration ratio $(\overline{\text{B}}):(\overline{\text{BHCl}})$ is equal to the ratio of activities of these species in the organic phase. Failure of this assumption may occur due to either or both of two reasons: departure of the behavior of these species from ideality, or the aggregation of the amine hydrohalide. The latter is a well known phenomenon, although the free amine is not

known to aggregate.⁷ For this reason we define an *apparent* acid dissociation constant, K_a , which is a measure of the *apparent* base strength

$$K_a = \frac{(\overline{\text{B}})(\text{H}^+)(\text{Cl}^-)\gamma_{\pm}^2}{(\Sigma\text{BHCl})} \quad (3)$$

The quantity (ΣBHCl) represents the total of amine hydrochloride in all species in the organic phase, and is defined by the relation

$$(\Sigma\text{BHCl}) = (\overline{\text{BHCl}}) + 2(\overline{\text{BHCl}})_2 + \dots \quad (4)$$

In eq 3, as in eq 2, we assume that the concentration ratio $(\overline{\text{B}}):(\Sigma\text{BHCl})$ is equal to the ratio of the activities in the organic phase. In other words, we assign all deviations from ideality in the organic phase to aggregation effects. As we shall show, it is possible to fit the data to fairly simple models of aggregate behavior, which provides strong support to the assumptions stated above.

By taking logarithms of eq 2 and 3 and subtracting, one gets

$$\text{p}K_a - \text{p}K_a' = \log (\Sigma\text{BHCl}) - \log (\overline{\text{BHCl}}) \quad (5)$$

Where aggregation occurs, the right side of eq 5 will not be zero and will depend on concentration, so that $\text{p}K_a$ will not be a constant. At sufficiently high dilution where aggregation does not occur

$$\begin{aligned} (\Sigma\text{BHCl}) &= (\overline{\text{BHCl}}) \\ \text{p}K_a &= \text{p}K_a' \end{aligned}$$

Values of $\text{p}K_a$ can be obtained from two-phase systems in which equal concentrations of the amine and amine hydrochloride are present in the organic phase (half-titration point). If the aqueous phase contains 1.00 *M* sodium chloride, eq 3 becomes, in its logarithm form

$$\text{p}K_a = -\log (\text{H}^+)_{1/2} - \log (\gamma_{\pm}^2)$$

where the first term on the right side refers to the hydrogen ion concentration at the half-titration point. The γ_{\pm} denotes the mean activity coefficient of hydrochloric acid in 1.00 *M* sodium chloride.

Provided the pH meter is calibrated with HCl solutions in 1.00 *M* NaCl

$$\text{pH}_{\text{meter}} = -\log (\text{H}^+)_{1/2}$$

and

$$\text{p}K_a = \text{pH}_{\text{exptl}} - \log (\gamma_{\pm}^2) \quad (6)$$

In practice, it was found convenient to calibrate the pH meter with a conventional buffer and to obtain a series of readings in 1.00 *M* NaCl solutions. Fortunately, in this medium, the relation

$$\text{pH}_{\text{meter}} = -\log (\text{H}^+)$$

is obeyed over at least the range of hydrogen ion con-

centration from 10^{-2} to $5 \times 10^{-5} M$. Thus no correction is required and eq 6 can be used directly. The value of $-\log(\gamma_{\pm}^2)$ is given by Robinson and Stokes²³ as $+0.24$. A further correction was necessary in cases where significant amounts of \overline{BHCl} dissociated to establish the aqueous hydrogen ion concentration. This correction was made from the organic phase:aqueous phase ratio and the measured pH of the aqueous phase.

In methods B and C the quantities in eq 3 were determined as described earlier and using, in addition, appropriate values of the mean activity coefficient for hydrochloric acid solutions.²⁴

In the case of N-methyldioctylamine, the lowest molecular weight amine used, aqueous distribution of amine hydrochloride was observed to be sufficiently high to affect the pK_a calculations. The use of one back extraction with pure toluene, although not recovering 100% of the aqueous amine hydrochloride made it possible to estimate the original $(\Sigma BHCl)$ and (\overline{B}) . The use of eq 2 and the necessary activity coefficients were then used to calculate values of pK_a .²⁴ For all other amines used, such corrections were negligible.

The pK_a data obtained are presented in Figures 1-3. It should be noted that the agreement among data from methods A-C was very good in all cases. As predicted from eq 5, it can be seen that at low $\Sigma BHCl$ concentrations the pK_a does become constant for most of the amines, indicating a region where only monomer $BHCl$ exists. The pK_a values at that level are also the pK_a' values and thus are a measure of the actual base strengths of the amines free of aggregation effects. Values of pK_a' for the amines studied are presented in Table III.

Table III

Tri- <i>n</i> -octylamine	3.68
N-Methyldioctylamine	3.68
(2,6,8-Trimethylnonyl-4)-2-ethylhexylamine	2.60
N-Dodecyl-2-ethylhexylamine	2.95
N-Decyl-3,7-dimethyloctylamine	3.60
1-Amino-2,2-dihexyloctane	3.30
7-Amino-7-hexyltridecane	<2.70

It is apparent from Table III that it is difficult to assign an order of basicity in the monomer region by type of amine, although it can be said that generally the tertiaries appear most basic and the primaries least. A relatively narrow range of pK_a' is observed, and it is interesting to note that for the least-hindered compound of each group, the values range only from 3.68 for the tertiary amine N-methyldioctylamine to 3.30 for the primary amine 1-amino-2,2-dihexyloctane.

Aggregation of High Molecular Weight Amine Hydro-

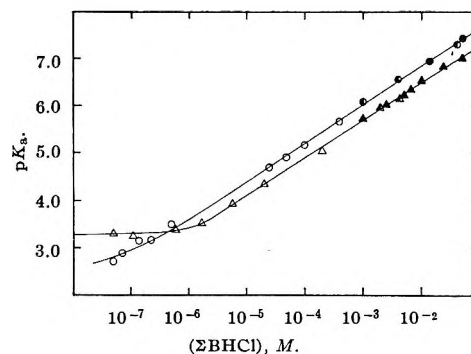


Figure 1. pK_a values as a function of amine hydrochloride concentration (primary amines): Δ , 1-amino-2,2-dihexyloctane; \circ , 7-amino-7-hexyltridecane; filled points, method A; half-filled points, method B; open points, method C.

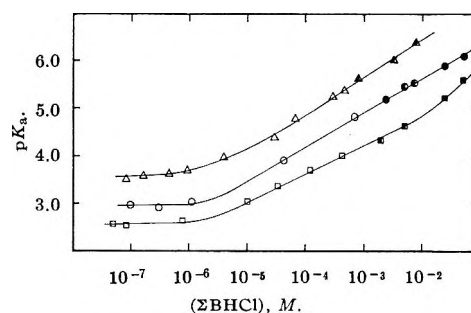


Figure 2. pK_a values as a function of amine hydrochloride concentration (secondary amines): Δ , N-decyl-3,7-dimethyloctylamine; \circ , N-dodecyl-2-ethylhexylamine; \square , N-(2,6,8-trimethylnonyl-4)-2-ethylhexylamine; filled points, method A; half-filled points, method B; open points, method C.

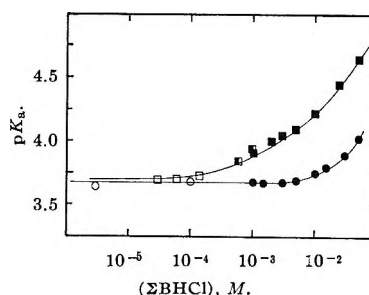
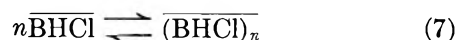


Figure 3. pK_a values as a function of amine hydrochloride concentration (tertiary amines): \square , N-methyldioctylamine; \circ , tri-*n*-octylamine; filled points, method A; half-filled points, method B; open points, method C.

chlorides. Information about aggregation of the amine hydrochlorides can be obtained from a consideration of the equilibrium in the organic phase



(23) R. A. Robinson and R. H. Stokes, "Electrolyte Solutions," 2nd ed, Academic Press, Inc., London, 1959, p 433.

(24) G. N. Lewis and M. Randall, "Thermodynamics," 1st ed, McGraw-Hill Book Co., Inc., New York, N. Y., 1923, p 336.

Table IV: Aggregation of Hydrochlorides^a

Amine	$\overline{(\text{BHCl})}$ range, <i>M</i>	Slope	Calculated <i>n</i>	<i>n</i> from vapor pressure data at 37° at BHCl concentration		
				0.040 <i>M</i>	0.10 <i>M</i>	0.20 <i>M</i>
(2,6,8-Trimethylnonyl-4)-2-ethylhexylamine	1×10^{-2} to 1×10^{-5}	0.60	2.5 ± 0.3	1.8	2.0	1.9
N-Dodecyl-2-ethylhexylamine	5×10^{-2} to 1×10^{-5}	0.70	3.3 ± 0.2	2.3	2.4	2.5
N-Decyl-3,7-dimethyloctylamine	1×10^{-2} to 1×10^{-5}	0.80	5.0 ± 0.2			
1-Amino-2,2-dihexyloctane	5×10^{-2} to 1×10^{-5}	0.78	4.5 ± 0.3	3.0	3.0	3.0
7-Amino-7-hexyltridecane	5×10^{-2} to 1×10^{-7}	0.78	4.5 ± 0.3	3.3	4.0	3.4

^a Temperature, 37°.

which defines

$$P_n = \frac{[\overline{(\text{BHCl})}_n]}{(\overline{\text{BHCl}})^n} \quad (8)$$

Combining eq 4 and 8, one gets

$$\overline{(\Sigma \text{BHCl})} = \overline{(\text{BHCl})} + 2P_2(\overline{\text{BHCl}})^2 + 3P_3(\overline{\text{BHCl}})^3 + \dots \quad (9)$$

Substituting eq 9 into eq 5 gives

$$\begin{aligned} \text{p}K_a - \text{p}K_a' &= \log \left[1 + 2P_2(\overline{\text{BHCl}}) + 3P_3(\overline{\text{BHCl}})^2 + \dots \right] \\ &= \log \left[\sum_{n=1}^{\infty} nP_n(\overline{\text{BHCl}})^{n-1} \right] \end{aligned} \quad (10)$$

Combining eq 2 and 3, one obtains the expression

$$\overline{(\text{BHCl})} = \frac{K_a}{K_a'}(\Sigma \text{BHCl}) \quad (11)$$

and by substitution of eq 11 into eq 10, one obtains

$$\text{p}K_a - \text{p}K_a' = \log \left[\sum_{n=1}^{\infty} nP_n(\Sigma \text{BHCl})^{n-1} \left(\frac{K_a}{K_a'} \right)^{n-1} \right] \quad (12)$$

If in a particular region of concentration one polymeric species predominates, the sum on the right side of eq 12 reduces to a single term

$$\text{p}K_a - \text{p}K_a' = \log \left[nP_n(\Sigma \text{BHCl})^{n-1} \left(\frac{K_a}{K_a'} \right)^{n-1} \right] \quad (13)$$

which can be rearranged to

$$\text{p}K_a - \text{p}K_a' = \frac{1}{n} \log nP_n + \frac{n-1}{n} \log \overline{(\Sigma \text{BHCl})} \quad (14)$$

Given the assumption of a single hydrochloride species, eq 14 predicts that a plot of $\text{p}K_a$ vs. $\log(\Sigma \text{BHCl})$ will give a straight line of slope $(n-1)/n$. Substantial portions of the curves in Figures 1 and 2 are indeed straight lines, from which are obtained the values of n shown in Table IV. In Table IV are also presented the average aggregation numbers obtained from vapor pressure measurements. These data were obtained in a higher concentration range than the $\text{p}K_a$ data, but the

Table V

$\overline{(\text{BHCl})}$, <i>M</i>	P_2	P_3
Tri- <i>n</i> -octylamine		
5.0×10^{-2}	32	980
2.3×10^{-2}	43	250
1.51×10^{-2}	31	215
1.13×10^{-2}	31	270
9.5×10^{-3}	37	380
9.0×10^{-3}	26	260
7.3×10^{-3}	17	183
4.6×10^{-3}	30	530
N-Methyldioctylamine		
5.0×10^{-2}	806	1.0×9810^5
1.0×10^{-2}	480	1.14×10^5
5.0×10^{-3}	520	1.93×10^5
3.0×10^{-3}	500	2.6×10^5
2.0×10^{-3}	570	3.9×10^5
1.1×10^{-3}	530	1.5×10^5
1.0×10^{-3}	330	2.9×10^5
6.0×10^{-4}	450	6.8×10^5
1.4×10^{-4}	480	24×10^5
6.0×10^{-5}	670	95×10^5

regions overlap slightly. The vapor pressure data give n values somewhat lower than those obtained from $\text{p}K_a$ values, but this may be due to the higher temperature of the former experiments. Aggregation data for the two tertiary amine hydrochlorides in Figure 3, which have no straight-line portion on their curves, were obtained from eq 12. Assuming the existence of monomer and only one polymeric species, values for P_n are calculable for each data point in Figure 3 where $\text{p}K_a \neq \text{p}K_a'$. The values of P_2 and P_3 for the tertiary amines are given in Table V. In both cases the assumption of a dimer gives a somewhat more constant value of the aggregation constants. The average values for the dimerization constants so obtained are, respectively, for trioctylamine, and for N-methyldioctylamine, 31 and 530.

Extraction of Water. In Figure 4 are shown the data for extraction of water by amine hydrochlorides up to 0.3 *M* in toluene. The data include both the water extracted by the toluene and that associated with the

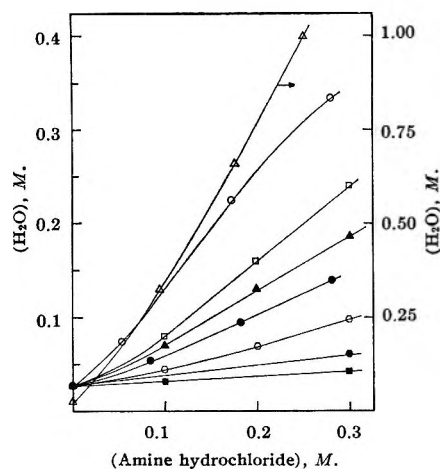


Figure 4. Extraction of water by amine hydrochlorides in toluene: Δ , N-methyldioctylamine; \circ , tri-*n*-octylamine; \square , N-dodecylisooctylamine; \blacktriangle , N-dodecyl-2-ethylhexylamine; \bullet , di-(2-ethylhexyl)amine; \circ , N-(2,6,8-trimethylnonyl-4)-2-ethylhexylamine; \bullet , 1-amino-2,2-dihexyloctane; \blacksquare , 7-amino-7-hexyltridecane; N-methyldioctylamine, right-hand scale; all others, left-hand scale.

amine hydrochloride. While the curves are not quite linear, they are similar in shape and demonstrate a wide variation in the extent to which they extract water. The two tertiary amine salts extract by far the greatest amount of water, while the primary amine salts extract very little. The secondary amine salts exhibit considerable variation, but are intermediate in their behavior. Water extraction by the free amines was

Table VI: Extraction of Water by Amines and Amine Hydrochlorides in Toluene^a

	Water absorption, —mol/mol of compound—	
	Amine	Amine hydro- chloride
7-Hexyl-7-aminotridecane	0.18	0.05
Primene JM-T	0.10	0.07
2-Amino-2,2-dihexyloctane	0.10	0.11
Octadecylamine	0.12 ^b	
N-(2,6,8-Trimethylnonyl-4)- 2-ethylhexylamine	0.025	0.23
Di-(2-ethylhexyl)amine	0.03	0.41
N-Dodecyl-2-ethylhexylamine	0.03	0.53
N-Dodecylisooctylamine	0.08	0.7
N-(3,7-Dimethyloctyl)decyl- amine	0.1	
Trioctylamine	0.01	1.1
N-Methyldioctamine	0.1	4.0 ^c

^a Data refer to water uptake at 0.3 M amine or salt concentration. ^b At 0.2 M. ^c At 0.25 M.

also determined, and the data for 0.3 M amines are given in Table VI, together with the corresponding values for the salts. Water extraction by the free amines is considerably less than for the salts in the case of tertiary

and secondary amines, but for some primary amines, the free base extracted more water than the salt. Within each amine type, water extraction increased with decreasing steric hindrance about the nitrogen atom.

Discussion

The relative base strengths of aliphatic amines have been found to vary greatly, depending upon the solvent in which they were measured. Two general effects have been recognized which contribute to these variations.²⁵⁻²⁸ In one direction, the increasing substitution of the nitrogen atom by carbon in going from primary to tertiary results in an increase in base strength, owing to the electron-donating property of the alkyl group. In the other direction, the increasing steric hindrance due to the bulk of the alkyl groups renders solvation of the ammonium cation or the ion pair more difficult and reduces the stability of the salt relative to the free amine. This tends to reduce the basicity of the more highly alkylated amines.

In the systems described here at very low concentrations, where aggregation effects do not exist, the data in Table III show there is no clear-cut order of basicity into which the three classes of amines can be placed. The two tertiary amines exhibit the greatest basicities, giving, in fact, identical values. A considerable spread of values occurs for secondary amines, the strongest one, N-(3,7-dimethyloctyl)decylamine, being almost as basic as the tertiaries. Except for the two tertiary amines, where the difference in structure has no effect, there is an obvious correlation of pK_a' with steric hindrance about the nitrogen, the more highly hindered being the weaker bases. The two primary amines are comparable to the secondaries in base strength, although the monomer region of the compound 7-amino-7-hexyltridecane was not accessible to this study. Again, however, the more sterically hindered compound was the weaker base. Since all of the pK_a' values which were determined are within about a power of 10, it can be concluded that, generally, the opposing electronic and steric effects are comparable. Within a particular amine type, however, where electronic effects are quite similar, the variations must be attributed to steric factors. This will take the form of either variations in the extent of solvation or in the firmness with which the chloride ion is bonded to the ammonium protons.

The amine hydrochlorides can be considered as ion pairs in nonpolar organic solvents; that is, the proton of the hydrohalide is bonded primarily to the nitrogen atom, while the bond of the proton to the halide is

(25) A. F. Trotman-Dickenson, *J. Chem. Soc.*, 1293 (1949).

(26) R. G. Pearson and D. C. Vogelsong, *J. Amer. Chem. Soc.*, **80**, 1038 (1958).

(27) H. K. Hall, Jr., *ibid.*, **79**, 5441 (1957).

(28) J. W. Bayles and A. F. Taylor, *J. Chem. Soc.*, 2328 (1958); 417 (1961).

more properly considered as a hydrogen bond.²⁹ In addition, no appreciable dissociation of the ion pair can be expected in a solvent such as toluene. As discussed previously,¹⁴ an examination of molecular models indicates the existence of some steric hindrance to the approach of a large chloride ion in the more hindered amines, but the effect resides more in restriction of free rotation of the alkyl groups than in an inability to form a hydrogen bond to the ammonium ion. On the other hand, the rather large tendency of the salts to aggregate at higher concentrations clearly indicates the need for solvation of the ion pair. While toluene no doubt has some tendency to act as a solvating agent, the important component of the solvent may well be the water. At the amine hydrochloride concentrations under consideration here, less than 10^{-6} *M*, the water content of saturated toluene (0.027 *M*) is many times greater than that of the amine salt.

It seems likely, therefore, that the steric effects which are apparent within a given amine class are due to differences in the ability of the dissolved water to solvate the ion pairs, rather than differences in chloride ion approach. It should be possible to decide this point by further studies of anhydrous systems.

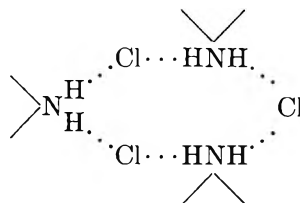
In contrast to the situation in the low-concentration region, steric factors appear to dominate at higher concentrations of the amine hydrochlorides. There is a considerable similarity again in the behavior of the primary and secondary amines, while the tertiaries stand out as distinctly different, in at least two respects. First of all, the tertiaries do not form aggregates to any significant degree below concentrations of 10^{-3} *M*. In contrast, aggregation of the other amines is noticeable starting at about 10^{-6} *M*. Second, the tertiary amine data are fairly compatible with the formation of only a dimer species in the concentration range studied. The primaries and secondaries, on the other hand, tend toward the formation of higher aggregates. On this point the vapor pressure data are roughly compatible with the equilibrium data.

The major feature of the pK_a values at high concentration, however, is the rather large spread of values (about three powers of 10) and the rather clear correlation with steric hindrance around the nitrogen atom. Additional data demonstrating this point with some additional compounds were reported earlier.¹⁴ The steric hindrance correlation is valid generally not only within the amine class, but also with respect to the differences between adjacent amine classes. That is, tertiaries would be expected to be more highly hindered than secondaries, and the latter more hindered than primaries. The exceptions to this correlation are the two primary amines, which will be discussed presently.

The basis for the variation in the apparent base strength at high concentrations seems to be the relative ease by which the respective amine hydrochlorides

can form aggregates. For primary and secondary salts, practically no monomer exists in the upper end of the concentration range studied, and even for the tertiary amine *N*-methyldioctylamine, it may be calculated that only about 10% of the hydrochloride is monomer at the highest concentration studied (0.05 *M*). The order of apparent base strength, therefore, is almost entirely a reflection of the characteristics of the aggregates. The stability of the aggregate would be expected to be greater for those hydrochlorides which can fit their dipolar portions together most compactly, and this, in turn, should be most readily accomplished by those which have the least sterically hindered nitrogen atoms.

It appears, however, that there is a fundamental difference between the aggregation process of the tertiaries, on the one hand, and the primaries and secondaries, on the other. The most obvious suggestion is that the latter two classes aggregate by forming some sort of hydrogen-bonded structure of special stability, utilizing the excess protons on the nitrogen atom. Such a species might be the following, which is a trimer derived from a secondary amine hydrochloride.



The structure would probably not be planar, and, in fact, might just as readily be constructed as a tetramer. The nitrogen and chloride atoms would form a six- or an eight-membered ring in these two cases, which is a reasonable structural hypothesis. For primary amines, an additional hydrogen is available and a three-dimensional structure can be envisioned, which would accommodate a higher aggregate. This is qualitatively compatible with the fact that the primary amines exhibited slightly higher aggregation numbers than the secondaries.

Tertiary amine hydrochlorides, on the other hand, have but one proton, which is presumably bonded to the chloride and is unavailable for participation in aggregate formation. This delays the aggregation process until relatively high concentrations of amine hydrochlorides are reached. The aggregates of tertiary amine salts, however, may not be simple electrostatic interactions because, in this case, considerable water is taken up by these compounds. Trioctylamine extracts one molecule of water and *N*-methyldioctylamine extracts four molecules of water per molecule of amine salt, so that the possibility exists of including water

(29) L. L. Burger, W. E. Keder, and A. S. Wilson, "Symposium on Processing of Irradiated Fuels," European Nuclear Energy Agency, Brussels, 1963.

in the aggregate structures on a stoichiometric basis.

On the other hand, the primary amine salts form aggregates which are almost devoid of water and, in fact, contain less water than the same concentration of free amine. This is explained by their ability to form well-fitting aggregates with sufficient hydrogen bonding to eliminate the need of water. The secondary amine salts provide an intermediate case, extracting widely variable amounts of water. Within the amine types, the water extraction increases with decreasing steric hindrance, which is to say, those amine salts which aggregate most readily within a class also incorporate the most water into the structure. The water thus appears to act as a kind of "mortar," which helps to form a stable aggregate.

The major exception to the correlation developed here is the pair of primary amines. The pK_a of the compound 1-amino-6-hexyldodecene-5 was reported to be about 8.4 at 0.05 M amine hydrochloride concentration.^{14,30} This is the highest pK_a value obtained in this study, and since steric hindrance should be at a minimum, this is in accord with the proposed model. Thus the anomaly seems to reside in the compound 7-amino-7-hexyltridecane. While the hydrochloride appears to exhibit a weaker interaction with water in the monomer region than its companion 1-amino-2,2-dihexyloctane, it apparently forms a relatively more stable aggregate, as evidenced by a higher pK_a in the higher concentration region. It is not apparent why this should be so, since the interaction of the hydrochloride with water, in one case, and another chloride, in the other case should involve hydrogen bonding with the ammonium protons in either case. Two possible suggestions can be offered. One is that the aggregation process involves fundamentally different structures from the hydration process in the monomer region and possesses less severe steric requirements. A second possibility arises from the fact that a significant difference in the electronic contributions to base strength exists in the two com-

pounds. The introduction of two alkyl groups at the α carbon should have the electronic effect of strengthening the basicity of the nitrogen in the tertiary alkyl amine. This may in some way exert a greater stabilizing effect on the aggregate structure than on the hydrated monomeric structure, though it is again not clear how this might be done.

A final comment should be offered on the suggestion of Scibona, Orlandini, and Danesi that the differences in pK_a among the three classes of amines are attributable to the *molecular size*.⁹ In their work the sizes of the three representative compounds were by coincidence in the increasing order primary < secondary < tertiary, and molecular size was used to estimate the interionic distance of the halide and alkylammonium ions. In the preceding paper, it was shown that variations in the alkyl chain length had little effect on the observed pK_a of the amines.¹⁴ The concept of size as represented by molecular volume or chain lengths is apparently not a determining factor. Therefore, what is important is the size as represented by the hindrance to approach by the halide ion. The suggestion of these authors that the H-Cl distance is important in determining pK_a values, is, therefore, probably true. It appears, however, that more direct measurements such as infrared spectra may be required to obtain this data.

Acknowledgments. The authors gratefully acknowledge the assistance of Mrs. Sigrid Snider in much of the experimental work. We particularly welcomed her enthusiasm for synthesis of the various compounds required, an attitude not commonly encountered among physical and inorganic chemists. We are also grateful to Dr. R. M. Diamond for many fruitful discussions and suggestions.

(30) The data in ref 14 were not corrected for activity of hydrochloric acid in the aqueous phase and should be increased by 0.24 to give comparable pK values.

The Reaction of Hydrogen Atoms with Hydrogen Iodide^{1a}

by Ralf D. Penzhorn^{1b} and B. deB. Darwent

*The Martin Maloney Chemistry Laboratory, The Catholic University of America, Washington, D. C. 20017
(Received October 26, 1967)*

The photolysis of HI has been investigated in the gas phase, between 303 and 533°K, in the presence of varying concentrations of I₂ and CO₂. The results show: (a) the efficiency of CO₂ in deactivating the photochemical "hot" H is given, with reasonable accuracy, by the simple "billiard ball" calculation; (b) the ratio of *k*'s for the reactions of thermal H with I₂ and HI is 4.95 exp(640/*RT*); (c) the ratio of the *k*'s for the reactions of "hot" H with I₂ and HI is approximately the same as that of the preexponential factors for the thermal H reactions.

Introduction

The mechanism proposed by Bodenstein and Lieneweg^{2a} and Bonhoeffer and Farkas^{2b} for the photolysis of HI has been widely accepted. Ogg and Williams³ showed that H atoms produced by the photolysis of HI reacted 3.8 ± 0.4 times as rapidly with I₂ as with HI and that, in the absence of an inert gas (cyclohexane), the activation energies of the two reactions were identical. In the presence of cyclohexane the ratio of the rate constants increased from 3.8 to 7.0 at 155°. Ogg and Williams suggested that the photochemically produced H atoms were hot and therefore did not require any activation energy to react with I₂ or HI and that the ratio 3.8 was that of the preexponential factors. The addition of cyclohexane served to deactivate the hot H atoms.

Schwarz, *et al.*,⁴ confirmed the presence of hot H and found the ratio of *A* factors to be 4 × 10⁻² and the differences in *E*'s to be 4.5 kcal mole⁻¹ for the reactions of thermal H with I₂ and HI.

Sullivan's data^{5,6} on the thermal reaction of H₂ and I₂ suggested Δ*E* ≈ 0.5 kcal mole⁻¹, in marked contrast to Schwarz, *et al.*⁴ However, Sullivan's result was obtained in a rather indirect manner, and it seemed desirable to reinvestigate the reactions more directly.

Experimental Section

Reagents. Pure anhydrous HI was prepared by dropping previously boiled 85% orthophosphoric acid (J. T. Baker) onto potassium iodide (Fisher Certified) under vacuum. The gas was passed through a trap of solid carbon dioxide, to remove moisture and iodine, and then frozen in liquid nitrogen. After outgassing, two more distillations were made from a -123° bath, the middle fraction being retained in each distillation. The HI, which appeared as a white solid when frozen, was then stored in a black painted storage bulb. The use of an alternate method of preparing hydrogen iodide, suggested by Martin and Willard,⁷ did not cause any detectable change in the experimental results.

Mass spectrometric analysis showed the HI to be 99.1% pure, the main impurity being HCl.

Carbon dioxide (Matheson Coleman grade) was further purified and outgassed. At least two distillations, where only the middle fraction was retained, were made from a solid CO₂ bath. The purity of the gas was then tested by photolyzing HI alone and in the presence of large quantities of CO₂. It was found that there was no detectable change in the rate of formation of hydrogen due to the presence of CO₂, even if the ratio of CO₂ to HI was as high as 110:1.

Apparatus. The high-vacuum apparatus used in this investigation, which was of the conventional all-Pyrex glass type, was kept in the dark during each run to prevent decomposition of HI by light.

The HI was measured in small volumes (23.7 or 69 cm³) and then transferred to the reaction system. A Kern glass spiral manometer, sensitive to ±0.01 torr, backed by a mercury manometer, was used to measure the pressure and to isolate the gas from mercury. A cathetometer was used for small pressures and the precision of the measurement was better than ±0.02 torr. The pressure of CO₂ was measured, with a Wallace and Tiernan (400 ± 0.5 torr) gauge, in a calibrated volume, and the gas was then transferred to the reaction system.

The reaction system had a total volume of 7000 ± 50 cm³ and was provided with a unidirectional circulating pump. Greaseless Viton A rubber diaphragm stop-

(1) (a) Acknowledgment is made to the donors of the Petroleum Research Fund, administered by the American Chemical Society, for partial support of this research (Grant No. PRF 1612-85). (b) Abstracted in part from a dissertation submitted in partial fulfillment of the requirements for the degree of Doctor of Philosophy of the Catholic University of America.

(2) (a) M. Bodenstein and F. Lieneweg, *Z. Physik. Chem.*, **119**, 123 (1926); (b) K. F. Bonhoeffer and L. Farkas, *ibid.*, **132**, 235 (1928).

(3) R. A. Ogg, Jr., and R. R. Williams, *J. Chem. Phys.*, **13**, 586 (1945).

(4) H. A. Schwarz, R. R. Williams, Jr., and W. H. Hamill, *J. Am. Chem. Soc.*, **74**, 6007 (1952).

(5) J. H. Sullivan, *J. Chem. Phys.*, **30**, 1293 (1959).

(6) J. H. Sullivan, *ibid.*, **36**, 1925 (1962).

(7) R. M. Martin and J. E. Willard, *ibid.*, **40**, 2995 (1964).

cocks were used in the gas-measuring and reaction sections.

The photolysis took place in a 180-cm³ reaction cell provided with a 0.35 mm thick Vycor window.

The light source was a Hanovia Type SH medium-pressure quartz mercury vapor lamp which was operated with a Sola constant-voltage transformer. The most important lines were at 2400, 2482, 2537, 2652, and 2804 Å.

Procedure. Iodine was prepared by photolyzing HI (3–6 torr) for various times depending upon the amount of iodine desired. Prior to each experiment HI was condensed from the storage bulb into a trap, evacuated, and distilled into the gas-measuring section from a –123° bath. The pressure was then measured and the gas condensed into the reaction system, expanded, photolyzed, and again condensed at liquid nitrogen temperature. The hydrogen was transferred to a Toepler pump and measured in a gas buret. The assumption was made that H₂ and I₂ were produced in equal amounts. The HI remaining from the photolysis was distilled into the measuring section from a –123° bath, the desired pressure was measured, and the HI was recondensed into the reaction system. A clean separation between iodine and HI could be accomplished by this technique because of the large differences in vapor pressures. The effectiveness of this technique was demonstrated as follows. (1) The HI recovered from the preliminary photolysis was condensed as a white powder. (2) A 0.5-hr. photolysis of the residual iodine did not produce any measurable amount of uncondensables, indicating essentially complete removal of the HI. (3) The intensity was checked frequently, by photolyzing a standard sample of HI, and the rates were corrected as necessary.

The mixture of I₂, HI, and CO₂ was expanded, mixed with the circulating pump for at least 0.5 hr, and photolyzed. The amount of hydrogen produced was usually about 50 and never less than 30 μmol.

The temperature was varied in a region (303–533°K) where there was no detectable thermal decomposition of hydrogen iodide.

Results

The rate of photolysis of HI, as measured by the rate of formation of H₂, was shown to be independent of time, up to a conversion of 0.28%, and to be unaffected by the addition of CO₂ even when the ratio CO₂/HI was as high as 110:1. Thus the photolysis was unaffected by the small amounts of I₂ produced in the photolysis and the CO₂ was adequately free of reactive impurities. In addition, the rates of photolysis of HI were independent of temperature, between 303 and 533°K, when the concentration of HI was kept constant. The quantum yield of H₂ (ϕ) was assumed to be unity in the photolysis of HI.

The effects of the addition of I₂ and CO₂ on ϕ are

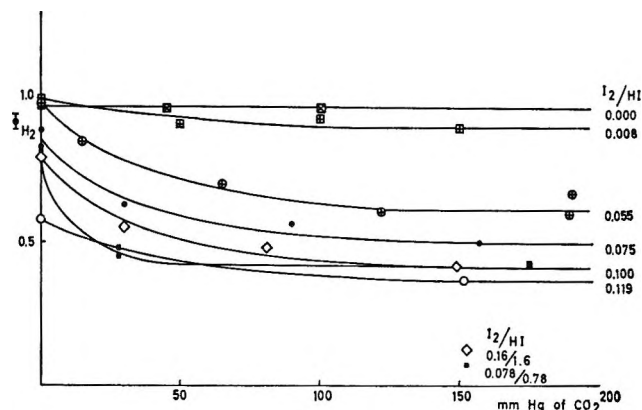


Figure 1. The effect of inert diluent on the quantum yield at various I₂/HI ratios at room temperature.

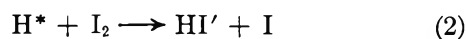
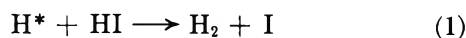
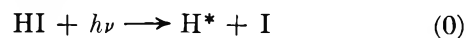
shown in Figure 1. For constant I₂/HI, ϕ decreases with increasing CO₂ and becomes constant and independent of CO₂ at the higher concentrations of CO₂. The effect of CO₂ on ϕ was shown to be directly related to the concentrations of HI at constant I₂/HI; thus, by halving [HI] and keeping I₂/HI constant, ϕ became independent of CO₂ at approximately half the value required formerly.

Accordingly, conditions can be and were attained such that ϕ is independent of the concentration of CO₂. We assume that, under those conditions, essentially all of the hot H were deactivated and the reaction of thermal H could be investigated.

The quantum yield was studied as a function of I₂/HI and temperature in the presence of a large excess of CO₂, and the results are presented in Table I.

Discussion

There is ample evidence that hot H atoms are produced in the photolysis of HI. Those atoms may possess translational energies of 41 kcal mole⁻¹, if I (²P_{1/2}) are produced, or 19 kcal mole⁻¹ if I (²P_{1/2}) are formed. The reactions



certainly occur. Whenever the energy of H^{*} is greater than 35.5 kcal mole⁻¹ (D_{I_2}), the HI' formed in (2) will have enough energy to decompose to H + I and may do so on every vibration



The H' atoms may have translational energies of between zero and 5.5 kcal mole⁻¹ and so may also react as hot atoms. Accordingly, in the absence of CO₂, we should consider at least three types of hot atoms, possessing 41, 19, or 0–5.5 kcal mole⁻¹, and the actual situation may well be very much more complex. We shall not attempt further analysis of this problem.

Table I^a

Expt no.	P_{HI} , mm	P_{I_2} , mm	P_{CO_2} , mm	I_2/HI	R_{H_2}	R_{H_2}	$1/\phi(H_2)$	k_3/k_4
303°K								
68c	1.131	0.147	150	0.13	11.0	31.5	2.88	14.46
70b	1.483	0.177	151.5	0.119	14.4	39.8	2.76	14.80
71d	2.018	0.187	196.5	0.093	21.7	50.0	2.30	13.99
65b	2.165	0.166	150	0.077	25.4	53.0	2.08	14.11
72a	3.126	0.188	196.5	0.060	37.5	69.0	1.84	13.97
59b	2.916	0.136	150	0.046	40.8	65.0	1.60	12.95
11a	18.65	0.15	150	0.008	199.0	224.0	1.12	15.0
415°K								
70e	1.478	0.18	196.5	0.123	13.5	31	2.3	10.56
71c	2.021	0.186	196.5	0.093	19.5	40	2.05	11.25
72c	3.118	0.192	196.5	0.062	33.0	55	1.67	10.88
59a	2.921	0.133	150	0.0455	35.9	53	1.48	10.55
478°K								
68a	1.133	0.146	150	0.129	10.2	22.7	2.23	9.61
70f	1.473	0.182	196.5	0.124	12.5	28	2.23	9.77
71a	2.028	0.182	196.5	0.090	18.8	36	1.92	10.25
533°K								
68d	1.133	0.146	151.5	0.129	10.2	22.6	2.22	9.46
70d	1.481	0.178	196.4	0.12	12.5	25	2.00	8.33
70c	1.481	0.178	151.5	0.12	12.5	25	2.00	8.33
64a	1.497	0.165	150	0.11	13.0	26	2.00	9.09
71b	2.03	0.185	196.5	0.091	19.0	32.5	1.71	7.81
65a	2.167	0.165	150	0.076	19.4	33.5	1.725	9.55
72b	3.12	0.191	196.5	0.061	28.0	44	1.57	9.3

^a The pressures were those observed at ambient temperature, and thus have not been corrected for the temperature of the reaction cell.

In the presence of CO_2 , the hot H may be deactivated



and we do not attempt to differentiate between the various types of hot H. In reaction 3 the H^* may require several collisions with CO_2 to be effectively deactivated and we define k_3 to allow for that possibility. Now the fraction of the photochemical H which will be deactivated is approximately $k_3m/(k_1x + k_2y + k_3m)$, where x , y , and m are concentrations of HI, I_2 , and CO_2 , respectively. Obviously, m can always be made large enough, relative to x and y , for that fraction to be close to unity.

The results of these experiments show clearly that essentially all of the H react as thermal species when m is, typically, 100 torr for $x = 3$ and $y = 0.2$ torr. Reference to Figure 1 shows that CO_2 had attained 50% of its effectiveness at about 10 torr when $x = 0.78$ and $y = 0.078$ torr and at about 20 torr when x and y are 1.6 and 0.16 torr, respectively. Let us assume that 50% of the hot H were deactivated at the 50% effective pressures. For a rough order of magnitude calculation we assume $k_2 = 5k_1$ and the results then suggest $k_1 \cong 10k_3$. The assumption $k_2 = k_1$ leads to $k_1 \cong 5k_3$. Accordingly, if reaction 2 occurs on every collision, as seems likely, CO_2 requires between 5 and 50 collisions to deactivate

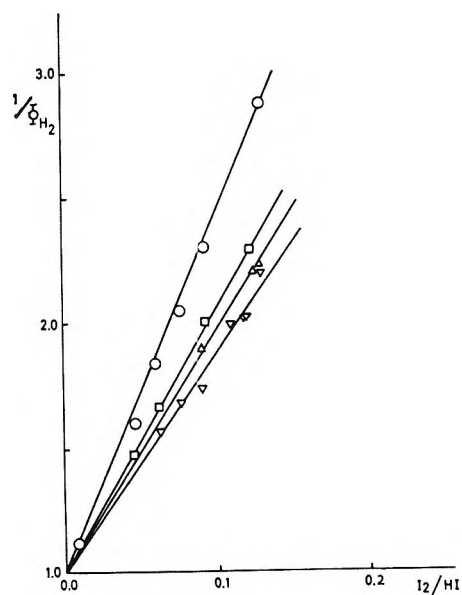
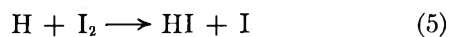


Figure 2. Effect of temperature on the quantum yield for various I_2/HI ratios: \circ , 303°K; \square , 415°K; \triangle , 478°K; ∇ , 533°K. (Data are in Table I.)

H^* . This agrees reasonably well with a simple billiard ball calculation to deactivate either 19- or 41-kcal mole⁻¹ H atoms by collision with CO_2 .

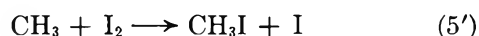
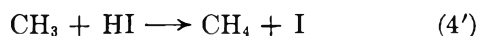
In the presence of an adequately large excess of CO₂ we need consider only reactions of the thermal H



which lead to the relationship

$$1/\phi = 1 + (k_5y/k_4x)$$

The values obtained for k_5/k_4 are given in Table I. Although the effect of temperature on k_5/k_4 is small, it is nevertheless significant (Figure 2) and leads to $k_5/k_4 = 4.95 \exp(640/RT)$. Since E_5 is generally regarded as being zero, $E_4 = 640 \text{ cal mole}^{-1}$ is in general agreement with Sullivan's^{5,6} value of $480 \pm 350 \text{ cal mole}^{-1}$ but not with that of Schwarz, Williams, and Hamill⁴ of $4500 \text{ cal mole}^{-1}$. Flowers and Benson,⁸ who competed the reactions



found $k_5/k_4 = 3.16 \exp(800/RT)$ with an uncertainty of $\pm 1000 \text{ cal mole}^{-1}$ in $E_5 - E_4$.

The ratio of preexponential factors A_5/A_4 was found to be 4.95. It is interesting to note that both the simple collision theory and the transition-state theory lead to values of about unity for that ratio. Schwarz, *et al.*, found, by transition-state theory, that the ratio of preexponential factors (A_5/A_4) was 4×10^{-2} . However they omitted the moment of inertia of the transition state in their calculation. The inclusion of that moment of inertia leads to a value of about unity for A_5/A_4 . A possible explanation for the high value found by Schwarz, *et al.*, for k_5/k_4 is that the presence of mercury in their reaction system, which reacts with I₂ to form HgI, may have affected their results.

The ratio of the rate constants for the hot reactions (k_2/k_1) was found to be 4.2 ± 0.2 by Schwarz, *et al.*,⁴ and 3.8 ± 0.3 by Williams and Ogg.³ Since the hot atoms require no energy of activation in reactions 1 and 2, it seems that the preexponential factors are essentially the same for both thermal and hot atoms.

(8) M. C. Flowers and S. W. Benson, *J. Chem. Phys.*, **38**, 882 (1962.)

Proton Nuclear Magnetic Resonance of Di- and Trisubstituted

Pyrazines and Their Cations

by R. H. Cox and A. A. Bothner-By

Mellon Institute, Carnegie-Mellon University, Pittsburgh, Pennsylvania 15213 (Received October 27, 1967)

The proton nmr spectra of eight substituted pyrazines in neutral and acidic solvents have been analyzed. Long-range couplings over five and seven bonds were found. Protonation effects on coupling constants are discussed. Results obtained from the analysis of compounds bearing a hydroxy substituent suggest they exist in the keto form.

Introduction

The factors affecting the nmr parameters of a variety of aromatic compounds are rapidly being elucidated. Considerable effort has been devoted to substituted benzenes¹⁻⁵ and pyridines,⁶⁻⁸ focusing on the nature of substituent effects. In an earlier paper⁹ we have shown that substituent effects in monosubstituted pyrazines parallel, roughly, the effects in monosubstituted benzenes and pyridines. Also, the magnitude of the vicinal coupling constant (J_{56}) and the chemical shifts were shown to reflect tautomeric structures in monosubstituted pyrazines.

By determining the effects of protonation on nmr parameters often, information regarding the site of

- (1) S. Castellano and C. Sun, *J. Am. Chem. Soc.*, **88**, 4741 (1966).
- (2) S. Castellano, R. Kostelnik, and C. Sun, *Tetrahedron Letters*, in press.
- (3) S. Castellano, private communication.
- (4) J. M. Read, Jr., R. E. Mayo, and J. H. Goldstein, *J. Mol. Spectry.*, **21**, 235 (1966).
- (5) J. M. Read, Jr., and J. H. Goldstein, *ibid.*, **23**, 179 (1967).
- (6) J. B. Merry and J. H. Goldstein, *J. Am. Chem. Soc.*, **88**, 5560 (1966).
- (7) S. Castellano, C. Sun, and R. Kostelnik, *J. Chem. Phys.*, **46**, 327 (1967), and references therein.

protonation and electronic redistribution within the molecule may be obtained. Several papers have appeared in the past few years on this subject.¹⁰⁻¹⁶ However, the main emphasis has been on chemical shift changes, and only recently have protonation effects on coupling constants been considered.^{6,8,12,17,18}

The relative simplicity of the nmr spectra of 2,3-disubstituted pyrazines makes this system ideally suited to a study of protonation effects on coupling constants. In this paper, we wish to report the analysis of the proton nmr spectra of four di- and three trisubstituted pyrazines. Parameters were obtained from both neutral and acidic solutions. Protonation effects and the structure of compounds containing the potentially tautomeric hydroxyl and amino substituents are discussed.

Experimental Section

Materials. 2-Methoxy-3-methylpyrazine (bp 70° (25 mm)) and 2-methoxy-3,6-dimethylpyrazine (bp 85° (27 mm)) were prepared from the chloro compounds by a modification of the procedure given for 2-methoxy-pyrazine.¹⁹ The remainder of the compounds were of commercial origin. Liquids were further purified by vacuum distillation. Crystalline solids were used as received. Solvents were reagent grade or better. No impurity peaks could be observed in any of the spectra obtained.

Samples were made up gravimetrically to 10 mole % of a solution containing 2% tetramethylsilane serving as internal reference and lock signal source. All samples were degassed and sealed under vacuum. To avoid the effects of decomposition with acidic solutions, all samples were run within 24 hr of preparation.

Spectra. Varian Associates A-60 and HA-100 spectrometers were used to obtain the proton nmr spectra. Frequency-sweep spin-decoupling experiments were performed using a Hewlett-Packard 201CR audio-oscillator monitored by a Varian V-4315 frequency counter. Calibration of spectra was by the side-band method. Line positions were obtained by averaging the results of two upfield and two downfield scans. Scan widths of 50 Hz were employed with sweep times of 500 and 1000 sec for the A-60 and HA-100, respectively.

Results

Analysis of the simple AB pattern presented by the aromatic protons of disubstituted pyrazines was carried out in the usual manner.²⁰ Long-range couplings to the protons of the methyl group were obtained from a first-order analysis of the methyl proton signals. Parameters obtained from the analysis are given in Table I. Although no coupling between the methyl protons and proton 6 could be resolved, a coupling was indicated since the signals from proton 6 became narrower when the methyl signals were irradiated.

The seven-bond long-range coupling between protons of the two methyl groups is unambiguously shown by spin-decoupling experiments and was observed in each trisubstituted pyrazine examined. Figure 1A shows the normal spectrum of the methyl protons of 2-chloro-3,6-dimethylpyrazine. When proton 5 was irradiated, each of the two multiplets collapsed into quartets with equal spacing between the lines (Figure 1B).

Discussion

Chemical Shifts. The use of a common solvent for all compounds was frustrated by limited solubilities. Comparison of chemical shifts is therefore less meaningful than in the ideal case. Nevertheless, trends are observable, particularly in those shifts resulting from transfer from a neutral to an acidic solvent.

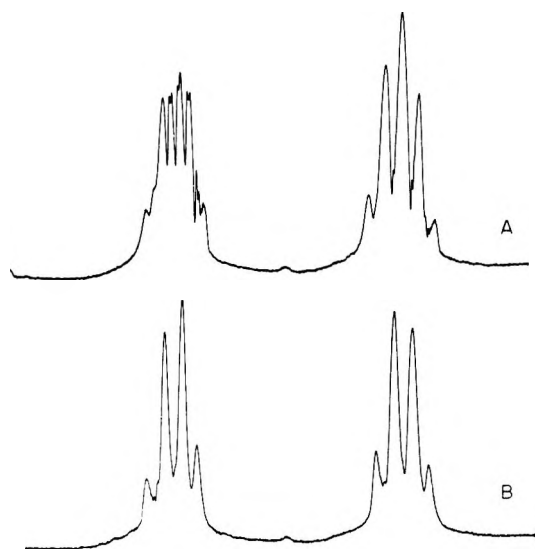
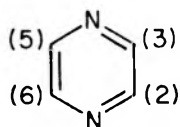


Figure 1. Proton nmr spectrum of the methyl protons of 2-chloro-3,6-dimethylpyrazine in chloroform-*d* solution at 100 MHz: (A) normal spectrum and (B) proton 5 irradiated spectrum.

- (8) S. Castellano and R. Kostelnik, *J. Am. Chem. Soc.*, in press.
- (9) R. H. Cox and A. A. Bothner-By, *J. Phys. Chem.*, in press.
- (10) J. M. Read, Jr., and J. H. Goldstein, *J. Am. Chem. Soc.*, **87**, 3440 (1965).
- (11) G. B. Barlin and W. V. Brown, *J. Chem. Soc., Sect. B*, 648 (1967).
- (12) S. Castellano, H. Günther, and S. Ebersole, *J. Phys. Chem.*, **69**, 4166 (1965).
- (13) G. B. Barlin and T. J. Batterham, *J. Chem. Soc., Sect. B*, 516 (1967).
- (14) H. Kamei, *J. Phys. Chem.*, **69**, 2791 (1965).
- (15) A. Mathias and V. M. S. Gil, *Tetrahedron Letters*, 3163 (1965).
- (16) R. L. Hinman and E. B. Whipple, *J. Am. Chem. Soc.*, **84**, 2534 (1962).
- (17) M. H. Palmer and B. Semple, *Chem. Ind. (London)*, 1766 (1965).
- (18) K. Tori, M. Ohtsuru, K. Aono, Y. Kawazoe, and M. Ohnishi, *J. Am. Chem. Soc.*, **89**, 2765 (1967).
- (19) A. Albert and J. N. Phillips, *J. Chem. Soc.*, 1294 (1956).
- (20) J. A. Pople, W. G. Schneider, and H. J. Bernstein, "High-Resolution Nuclear Magnetic Resonance," McGraw-Hill Book Co., Inc., New York, N. Y., 1959, p 119.

Table I: Nmr Parameters of Substituted Pyrazines



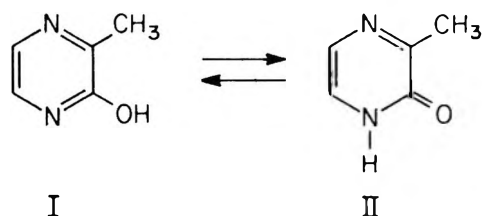
Substituents	Solvent ^a	δ_1^b	δ_2	δ_5	δ_6	J_{56}^c	J_{58}	J_{68}
2-CH ₃ , 5-CH ₃	CDCl ₃	2.507 ^d	8.330	2.507 ^d	8.330	0.15 ^d
	TFA	2.941 ^d	9.014	2.941 ^d	9.014	(<0.1) ^d
2-OH, 3-CH ₃	DMSO	...	2.285 ^d	7.250	7.166	0.64 ^d	(<0.2) ^d	4.20
	TFA	...	2.889 ^d	8.078	7.602	0.72 ^d	(<0.2) ^d	5.04
2-NH ₂ , 3-CH ₃	DMSO	6.117 ^d	2.328 ^d	7.786	7.641	0.66 ^d	(<0.2) ^d	2.96
	TFA	...	2.854 ^d	8.149	8.076	(<0.2) ^d	(<0.2) ^d	4.19
2-OCH ₃ , 3-CH ₃	DMSO	3.935 ^d	2.399 ^d	8.020	8.041	0.53 ^d	(<0.2) ^d	2.97
	TFA	4.266 ^d	2.799 ^d	8.716	8.093	0.64 ^d	(<0.2) ^d	3.56
2-Cl, 3-CH ₃	CDCl ₃	...	2.657 ^d	8.202	8.378	0.68 ^d	(<0.2) ^d	2.52
	TFA	...	3.011 ^d	8.711	9.045	0.68 ^d	(<0.2) ^d	3.23
2-OH, 3-CH ₃ , 6-CH ₃	CDCl ₃	...	2.296 ^d	7.154	2.414 ^d	0.77 ^d	0.71 ^d	(<0.2) ^d
	TFA	...	2.572 ^d	7.423	2.799 ^d	0.75 ^d	0.80 ^d	(<0.2) ^d
2-OCH ₃ , 3-CH ₃ , 6-CH ₃	CDCl ₃	3.939 ^d	2.385 ^d	7.826	2.403 ^d	0.65 ^d	0.65 ^d	(<0.2) ^d
	TFA	4.224 ^d	2.670 ^d	7.920	2.713 ^d	0.63 ^d	0.63 ^d	(<0.2) ^d
2-Cl, 3-CH ₃ , 6-CH ₃	CDCl ₃	...	2.500 ^d	8.240	2.599 ^d	0.71 ^d	0.72 ^d	0.36 ^d
	TFA	...	2.823 ^d	8.513	2.934 ^d	0.63 ^d	0.73 ^d	(<0.2) ^d

^a DMSO = dimethyl sulfoxide, TFA = trifluoroacetic acid. ^b In ppm downfield from TMS. ^c In hertz. ^d Shift or coupling constant of methyl or methoxyl protons at the given numbered position.

Chemical shifts of the ring protons in disubstituted pyrazines are very similar to the corresponding shifts in monosubstituted pyrazines. Introduction of a methyl group produces an upfield shift of ~ 0.2 ppm for the ring protons, compared to the corresponding shifts in the monosubstituted pyrazines.⁹ Furthermore, the 3-methyl group causes a reversal in the order of appearance of the ring protons from that found in monosubstituted pyrazines. For π -electron-donating groups, proton 6 appears at higher field, whereas for π -electron-withdrawing groups, proton 5 appears at higher field. At present, the factor(s) responsible for this reversal is (are) not apparent.

In trifluoroacetic acid, pyrazine at concentrations less than 0.2 M is completely protonated.¹⁴ Upon protonation of the disubstituted pyrazines, the ring protons are shifted to lower field by 0.45–0.75 ppm and the protons of the 3-methyl group are shifted to lower field by 0.35–0.60 ppm. For the trisubstituted pyrazines, the ring proton is shifted to lower field by 0.1–0.25 ppm and the protons of the methyl groups are shifted by 0.3 ppm. These protonation shifts are similar to those found in pyrazine,¹⁴ pyridine,⁵ and substituted pyridines.⁸ The downfield shifts are approximately identical for protons 5 and 6 of the disubstituted pyrazines suggesting equal protonation of both nitrogens. An exception to the shifts observed for disubstituted pyrazines is proton 6 of 2-methoxy-3-methylpyrazine which is shifted downfield by only 0.05 ppm. One possible explanation for this small shift is that a positive charge on nitrogen-1 could be stabilized by resonance with the 2-methoxy group.

The existence of possible tautomeric structures of the amino and hydroxy substituents is revealed in the chemical shifts. Protons 5 and 6 of 2-hydroxy-3-methylpyrazine appear to higher field by ~ 0.8 and 0.6 ppm compared to their shifts (Table I) in 2-methoxy-3-methylpyrazine and 2-amino-3-methylpyrazine, respectively. This upfield shift is similar to that found between protons 5 and 6 of 2-pyridone, N-methyl-2-pyridone, and 2-methoxypyridine²¹ and is consistent with 2-hydroxy-3-methylpyrazine existing in the keto form (II) in neutral solution. A similar conclusion was reached from the ir spectrum of this compound.²² A comparison of the chemical shifts in 2-amino-3-methyl-

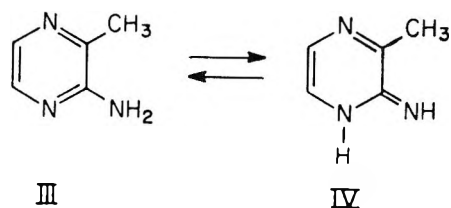


pyrazine suggests that it exists in the amino form (III). Integration of the amine protons *vs.* the methyl protons places a lower limit of 70% for this structure. Similar considerations applied to 2-hydroxy-3,6-dimethylpyrazine suggest that this compound exists in the keto form.

Vicinal Coupling Constants. Substituent effects on J_{56} of 2,3-disubstituted pyrazines parallel the effects found for 2-substituted pyrazines.⁹ The value of J_{56}

(21) R. H. Cox, unpublished results.

(22) H. Gainer, M. Kokorudz, and W. K. Langdon, *J. Org. Chem.*, 26, 2360 (1961).



decreases with increasing electronegativity of the 2-substituent. Introduction of a methyl group *ortho* to the substituent has little effect on J_{56} (*i.e.*, J_{56} varies by ~ 0.2 Hz from the value found in the corresponding monosubstituted pyrazine). Similar behavior for the effect of a methyl group can be found by comparing the corresponding coupling in benzene⁴ and toluene²³ and in pyridine^{6,7} and 2-methylpyridine.²⁴

Protonation produces an increase in J_{56} of 0.59–1.23 Hz for the disubstituted pyrazines. An increase of the same order of magnitude has been found for the similar coupling in pyridine,⁶ pyrazine,²¹ substituted pyridines,⁸ quinolines, isoquinolines, and cinnolines¹⁷ upon protonation. It is difficult to account for this increase solely on the basis of increasing electronegativity of the nitrogen atoms upon protonation. Recently, Castellano⁸ has reported that for a series of N-substituted pyridines, J_{56} increases with increasing electronegativity of the N substituent. These results were interpreted in terms of an alteration of charge along the σ framework and this satisfactorily accounts for the effect of substituents in the nmr spectra of monosubstituted benzenes, N-substituted pyridines, monosubstituted ethylenes, and 2-substituted butadienes. Using the interpretation of substituent effects given by Castellano,⁸ then, the increase in J_{56} upon protonation of disubstituted pyrazines found in this investigation can be rationalized as being similar to the pyridines.

Like the chemical shifts, J_{56} reflects the existence of tautomeric structures. For 2-hydroxy-3-methylpyrazine, J_{56} is 4.20 Hz, which is 1.23 Hz larger than J_{56} in the *O*-methyl derivative. Again these results are similar to those found for 2-pyridone, N-methyl-2-pyridone, and 2-methoxypyridine.²¹ Thus, this increase indicates some double-bond fixation and is consistent with 2-hydroxy-3-methylpyrazine existing in the keto form (II) in neutral solution. Comparison of J_{56} in 2-amino-3-methylpyrazine with J_{56} found in

other disubstituted pyrazines (Table I) suggests that it exists in the amino form (III).

Long-Range Couplings. In each of the di- and tri-substituted pyrazines examined,²⁵ a five-bond coupling of ~ 0.6 Hz (Table I) was observed between the protons of the methyl group and proton 5. A seven-bond coupling of ~ 0.7 Hz (Table I) between the protons of the two methyl groups was observed in the trisubstituted pyrazines. The similarity between the magnitude of this five-bond coupling in the disubstituted pyrazines and that found for 2-methylpyrazine⁹ suggests that substituents have very little effect on this coupling. Comparison of the seven-bond coupling in the trisubstituted pyrazines also suggests this independence of substituent. Four-bond couplings involving a methyl group in substituted toluenes²⁶ and thiophenes²⁷ are also insensitive to substituents.

Coupling constants over four or more bonds are usually thought of as being transmitted by a π -coupling mechanism.²⁸ In the pyrazines, the lone pair of electrons on the nitrogen atoms is in an orbital orthogonal to the π orbitals. Therefore, protonation of the lone pairs should affect what is commonly called the σ framework and have little effect on the π framework, except possibly to alter σ - π interactions slightly. The invariance of the long-range couplings (π mechanism) and the increase of J_{56} (σ mechanism) upon protonation are consistent with this interpretation.

Acknowledgment. This research was performed with support from the National Institutes of Health under Grant FR-00292. We wish to thank Dr. S. Castellano for making preprints available and Mr. R. H. Obenauf for technical assistance.

(23) S. Castellano, private communication.

(24) W. Brügel, *Z. Elektrochem.*, **66**, 159 (1961).

(25) This coupling in 2,5-dimethylpyrazine could not be resolved owing to the large line widths of the spectrum.

(26) W. C. Ripka and D. E. Applequist, *J. Am. Chem. Soc.*, **89**, 4035 (1967).

(27) R. A. Roffmann and S. Gronowitz, *Arkiv Kemi*, **16**, 471 (1961).

(28) Although one electron is indistinguishable from another, various authors have divided coupling constants into those which are transmitted predominantly by a σ mechanism and those which are transmitted predominantly by a π mechanism in an attempt to account theoretically for the transmission of this information from one proton to another. For references, see those listed in ref 26.

Proton Nuclear Magnetic Resonance Spectra of Monosubstituted Pyrazines

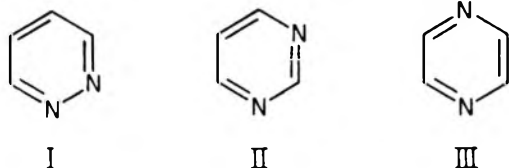
by R. H. Cox and A. A. Bothner-By

Melion Institute, Carnegie-Mellon University, Pittsburgh, Pennsylvania 15213 (Received October 27, 1967)

The proton spectra of eight monosubstituted pyrazines have been analyzed in terms of chemical shifts and coupling constants. Trends in the parameters obtained for the pyrazines parallel those of the monosubstituted benzenes and pyridines. Spin-tickling experiments show the sign of the *meta*-coupling constant across the nitrogen atom to be negative. Evidence for the existence of 2-hydroxypyrazine in the keto form is presented.

Introduction

Substituted benzenes, pyridines, and diazines [pyridazine (I), pyrimidine (II), and pyrazine (III)] form a related family of compounds of great current interest, providing abundant experimental test material for various concepts of electronic structure. Theories ranging from rule of thumb to sophisticated quantum mechanical analysis have been employed to predict such properties as basicity, ease of chemical attack, tautomeric behavior, and spectral characteristics including uv, ir, and nmr parameters.¹



Substituted benzenes have been the subject of a recent intensive investigation by Castellano,²⁻⁴ while pyridines have received attention from the Kowalewskis,⁵⁻⁷ Brügel,⁸ Castellano,⁹⁻¹¹ and Merry and Goldstein.¹² Among the diazines, pyridazines¹³⁻²¹ and pyrimidines²²⁻³³ have been examined in detail. However in the case of pyrazines, investigations have been much more limited in scope. Several workers have reported the C¹³-E coupling constants in pyrazines^{17,20} and in its methyl derivatives, as well as the proton shifts.^{15,16,18,34,35} An analysis of the proton spectrum of pyrazine, using the C¹³ satellite signals, has been given;¹⁵ and recently the spectra of a few carbonyl side-chain derivatives of pyrazine have been reported.³⁶

In this paper are reported the results of a complete analysis of the nmr spectra of eight monosubstituted pyrazines. Values obtained for the parameters are compared with results obtained from the analyses of substituted benzenes and pyridines.

Experimental Section

Materials. The chloro, amino, methyl, and amide derivatives were of commercial origin. Crystalline

solids were used as received; liquids were purified by vacuum distillation. Melting points and boiling points agreed with literature values. Known procedures were

- (1) A. R. Katritzky, Ed., "Physical Methods in Heterocyclic Chemistry," Vol. II, Academic Press Inc., New York, N. Y., 1963.
- (2) S. Castellano and C. Sun, *J. Am. Chem. Soc.*, **88**, 4741 (1966).
- (3) S. Castellano, R. Kostelnik, and C. Sun, *Tetrahedron Letters*, in press.
- (4) S. Castellano, private communication.
- (5) V. J. Kowalewski and D. G. de Kowalewski, *J. Chem. Phys.*, **36**, 266 (1962).
- (6) V. J. Kowalewski and D. G. de Kowalewski, *ibid.*, **37**, 2603 (1962).
- (7) V. J. Kowalewski, D. G. de Kowalewski, and E. C. Ferrà, *J. Mol. Spectry.*, **20**, 203 (1966).
- (8) W. Brügel, *Z. Elektrochem.*, **66**, 159 (1961).
- (9) S. Castellano and A. A. Bothner-By, *J. Chem. Phys.*, **41**, 3863 (1964).
- (10) S. Castellano, H. Günther, and S. E. Ebersole, *J. Phys. Chem.*, **69**, 4166 (1965).
- (11) S. Castellano, C. Sun, and R. Kostelnik, *J. Chem. Phys.*, **46**, 327 (1967).
- (12) J. B. Merry and J. H. Goldstein, *J. Am. Chem. Soc.*, **88**, 5560 (1966).
- (13) V. M. S. Gil, *Mol. Phys.*, **9**, 443 (1965).
- (14) K. Tori, M. Ogata, and H. Kano, *Chem. Pharm. Bull. (Tokyo)*, **11**, 235 (1963).
- (15) K. Tori and M. Ogata, *ibid.*, **12**, 272 (1964).
- (16) A. H. Gawer and B. P. Dailey, *J. Chem. Phys.*, **42**, 2658 (1965).
- (17) P. C. Lauterbur, *ibid.*, **43**, 360 (1965).
- (18) J. N. Murrell and V. M. S. Gil, *Trans. Faraday Soc.*, **61**, 402 (1965).
- (19) A. Mathias and V. M. S. Gil, *Tetrahedron Letters*, 3163 (1965).
- (20) K. Tori and T. Nakagawa, *J. Phys. Chem.*, **68**, 3163 (1964).
- (21) F. Declerck, R. Degroote, J. de Lannoy, R. Nasielski-Hinkens, and J. Nasielski, *Bull. Soc. Chim. Belges*, **74**, 119 (1965).
- (22) C. D. Jardetzky and O. Jardetzky, *J. Am. Chem. Soc.*, **82**, 222 (1960).
- (23) E. S. Gronowitz and R. A. Hoffman, *Arkiv Kemi*, **16**, 459 (1960).
- (24) E. S. Gronowitz, B. Norrman, B. Gestblom, B. Mathiasson, and R. A. Hoffman, *ibid.*, **22**, 65 (1964).
- (25) J. P. Kokko, J. H. Goldstein, and L. Mandell, *J. Am. Chem. Soc.*, **83**, 2909 (1961).
- (26) G. S. Reddy, R. T. Hobgood, Jr., and J. H. Goldstein, *ibid.*, **84**, 237 (1962).
- (27) R. U. Lemieux, R. K. Kullnig, H. J. Bernstein, and W. G. Schneider, *ibid.*, **79**, 1005 (1957); **80**, 6098 (1958).

Table I: Proton Nmr Parameters of Monosubstituted Pyrazines

Substituent	Solvent ^a	δ_2^b	δ_3	δ_5	δ_6	J_{35}^c	J_{36}	J_{56}	J_{23}	J_{25}	J_{26}
2-OH	DMSO	9.790 ^d	7.922	7.296	7.398	-0.047	1.338	3.914
2-NH ₂	DMSO	6.320 ^d	7.941 ^d	7.705	7.899	-0.277	1.541	2.771
2-OCH ₃	DMSO	3.958 ^d	8.309	8.219	8.224	-0.354	1.394	2.857
2-CH ₃	CDCl ₃	2.566 ^d	8.568	8.376	8.453	-0.199	1.479	2.555	$\pm 0.21^d$	$\pm 0.45^d$	$\pm 0.70^d$
2-Cl	DMSO	...	8.714	8.599	8.463	-0.395	1.432	2.606
2-F	DMSO	...	8.726	8.696	8.423	-0.462	1.331	2.667	-8.172	4.723	-1.433
2-CO ₂ CH ₃	DMSO	3.991 ^d	9.222	8.933	8.859	-0.296	1.487	2.426
2-CONH ₂	DMSO	7.900 ^d	9.253	8.896	8.756	-0.012	1.509	2.494
		8.280 ^d									

^a DMSO = dimethyl sulfoxide. ^b In ppm downfield from internal tetramethylsilane. ^c In hertz. ^d Shift or coupling constant of methyl protons at the given numbered position.

used to prepare the fluoro,³⁷ methoxy,³⁸ and methyl ester³⁹ derivatives. Hydroxypyrazine was prepared by acidifying the commercially available sodium salt of pyrazinol and working up the reaction mixture according to a procedure given by Erickson.⁴⁰ No impurity peaks could be observed in any of the recorded spectra.

Samples were made up gravimetrically to 10 mole % (except for the amide, which was 5 mole %) of a solution containing 2% tetramethylsilane as an internal reference and lock signal source. All samples were degassed and sealed under vacuum.

Spectra. Proton nmr spectra were obtained using a Varian Associates HA-100 spectrometer. Frequency-sweep spin-tickling and spin-decoupling experiments were performed using a Hewlett-Packard 201 CR audiooscillator monitored by a Varian V-4315 frequency counter. Calibration of the spectra was by the usual side-band method. Line positions were obtained by averaging the results of two upfield and two downfield scans. A scan width of 50 Hz was employed with sweep times of either 1000 or 2500 sec.

Results

Spectra were analyzed in terms of chemical shifts and coupling constants using the computer program LAOCN 3.⁴¹ Results obtained from the analyses are given in Table I. Data are reported to three decimal places as obtained from the output of the computer. Calculated probable errors for the parameters were less than 0.03 Hz. Although proton signals in the spectra of the monosubstituted pyrazines are broadened somewhat owing to residual coupling with the nitrogen atoms, resolution was sufficient to observe the expected lines. A typical spectrum is that of 2-chloropyrazine, shown in Figure 1.

Spin-tickling experiments⁴² were carried out on 2-chloro- and 2-fluoropyrazine in order to establish the

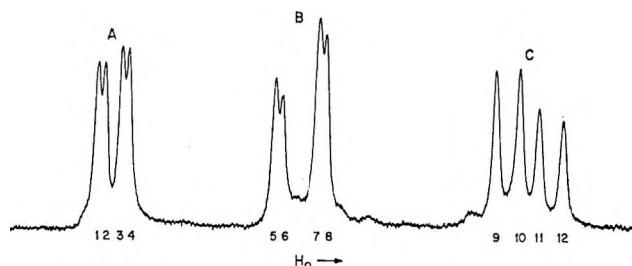


Figure 1. Proton nmr spectrum of 2-chloropyrazine in DMSO solution at 100 MHz.

relative signs of coupling constants. When line 12 (see Figure 1) of the C part of the spectrum of 2-chloropyrazine was irradiated with a weak radiofrequency

- (28) R. U. Lemieux, R. K. Kulinig, and R. Y. Moir, *J. Am. Chem. Soc.*, **80**, 2237 (1958).
 (29) J. B. Leane and R. E. Richards, *Trans. Faraday Soc.*, **55**, 518 (1959).
 (30) H. T. Miles, R. B. Bradley, and E. D. Becker, *Science*, **142**, 1569 (1963).
 (31) B. W. Roberts, J. B. Lambert, and J. D. Roberts, *J. Am. Chem. Soc.*, **87**, 5439 (1965).
 (32) L. Bauer, G. E. Wright, B. A. Mikrut, and C. L. Bell, *J. Heterocycl. Chem.*, **2**, 447 (1965).
 (33) D. Herbison-Evans and R. E. Richards, *Mol. Phys.*, **8**, 19 (1964).
 (34) H. Kamei, *J. Phys. Chem.*, **69**, 2791 (1965).
 (35) J. C. N. Ma and E. W. Warnhoff, *Can. J. Chem.*, **43**, 1849 (1965).
 (36) S. K. Chakrabarty and R. L. Levine, *J. Heterocycl. Chem.*, **4**, 109 (1967).
 (37) H. Rutner and P. E. Spoerri, *ibid.*, 492 (1965).
 (38) A. Albert and J. N. Phillips, *J. Chem. Soc.*, 1294 (1956).
 (39) S. A. Hall and P. E. Spoerri, *J. Am. Chem. Soc.*, **62**, 664 (1940).
 (40) A. E. Erickson and P. E. Spoerri, *ibid.*, **68**, 401 (1946).
 (41) A more efficient version of the program LAOCOON II, described by Castellano and Bothner-By.⁹
 (42) R. H. Cox and S. L. Smith, *J. Phys. Chem.*, **71**, 1809 (1967).

field, lines 5 and 7 of the B region and lines 1 and 3 in the A portion of the spectrum were affected. Similarly when line 9 was irradiated, lines 6 and 8 of the B region and lines 2 and 4 of the A portion of the spectrum were affected. These results demonstrate⁴³ that J_{35} must be opposite in sign from J_{36} and J_{56} . Making the usual assumption that vicinal H-H couplings are positive,^{44,45} the absolute sign of J_{35} in Table I is given as being negative. Spin-tickling experiments carried out on 2-fluoropyrazine establish the following in relation to signs of the various couplings: J_{35} opposite to J_{56} ; J_{35} opposite to J_{36} ; J_{26} opposite to J_{25} ; and J_{26} same as J_{24} . As before, J_{35} is deduced to be negative, and J_{36} and J_{56} are deduced to be positive. Relative signs of the H-F couplings cannot be related to the H-H couplings from these experiments. However, relative sign determinations of the H-F couplings in various 2-fluoropyridines⁴⁶ have shown J_{23} to be negative. Therefore, it seems reasonable to assume J_{23} to be negative in 2-fluoropyrazine, whence J_{26} is negative and J_{25} is positive.

Parameters were obtained for the ring protons of 2-methylpyrazine by recording the spectrum while irradiating the methyl signal, thereby reducing the spectrum to a three-spin case. Values given in Table I for couplings to the methyl protons were obtained from a first-order analysis of the methyl signals, and no signs were determined.

Discussion

Chemical Shifts. The effect of substituents on chemical shifts is roughly parallel to that in monosubstituted benzenes. Comparison of shifts in the 3, 5, and 6 positions of 2-substituted pyrazines, with *ortho*, *meta*, and *para* proton shifts in monosubstituted benzenes,²⁻⁴ shows similar behavior (Figure 2) with the protons of the pyrazines occurring ~ 1.4 ppm to low field of the corresponding protons in the benzenes. When the chemical shifts of 2-substituted pyrazines are compared with those of 2-substituted pyridines,^{6,8-10} the comparison is not as linear as that found between monosubstituted benzenes. Nevertheless, similar trends are observed.

As is the case with benzenes, there is a general, somewhat parallel movement of the chemical shifts of all three protons to lower field as conjugative electron donation (CH_3O , NH_2) gives way to conjugative electron withdrawal (CONH_2 , CO_2CH_3). For the 5 and 6 protons, the chemical shifts cross over each other at this point: $\delta_5 < \delta_6$ (CH_3O , NH_2 , CH_3) and $\delta_5 > \delta_6$ (Cl , F , CO_2CH_3 , CONH_2).

A deviation to the above parallelism of chemical shifts between benzenes and pyrazines is shown by 2-hydroxypyrazine. The signals for protons 5 and 6 (Table I) of 2-hydroxypyrazine are shifted upfield by 0.4 and 0.5 ppm, respectively, when compared to the same protons of 2-aminopyrazine and by 0.92 and 0.83

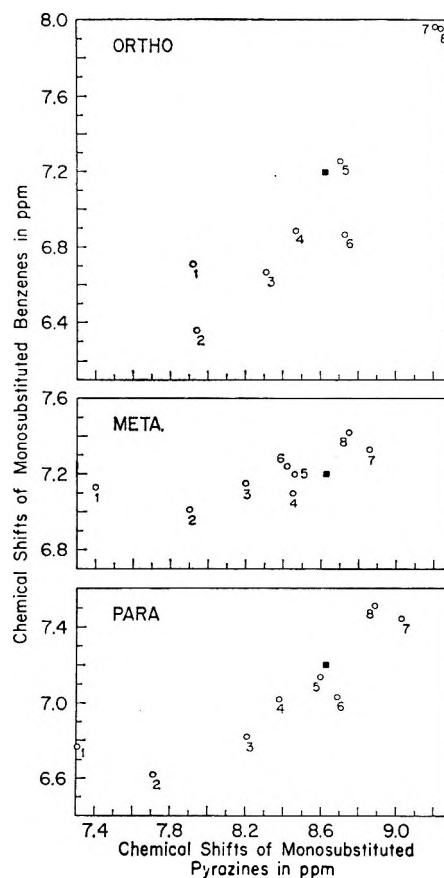


Figure 2. Plot of the proton chemical shifts of monosubstituted pyrazines vs. the corresponding proton chemical shifts of monosubstituted benzenes.

Substituents are (1) OH, (2) NH_2 , (3) OCH_3 , (4) CH_3 , (5) Cl , (6) F , (7) CO_2CH_3 , and (8) CONH_2 , and the dark squares are the parent compounds.

ppm, respectively, when compared to 2-methoxy-pyrazine. Extensive ir^{47,48} and uv^{49,50} studies on 2-hydroxy- and 2-aminopyrazine have been interpreted in terms of the tautomeric structure V for 2-hydroxypyrazine in neutral solution, while structure VI predominates for 2-aminopyrazine.

This upfield shift of protons 5 and 6 supports the conclusion that 2-hydroxypyrazine exists as V and that 2-aminopyrazine exists as VI. Since it is known that 2-hydroxypyridine exists in the keto form and 2-aminopyridine exists in the amino form,⁵¹ data supporting

(43) J. W. Emsley, J. Feeney, and L. H. Sutcliffe, "High-resolution Nuclear Magnetic Resonance Spectroscopy," Pergamon Press Inc., New York, N. Y., 1965, p 466.

(44) M. Karplus, *J. Am. Chem. Soc.*, **84**, 2458 (1962).

(45) P. C. Lauterbur and R. J. Kurland, *ibid.*, **84**, 3405 (1962).

(46) J. C. Deck, Ph.D. Thesis, University of Illinois, 1966.

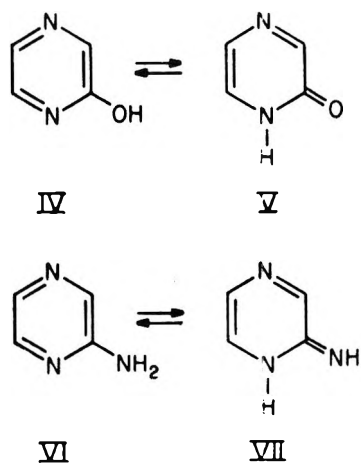
(47) S. F. Mason, *J. Chem. Soc.*, 4874 (1960).

(48) Y. N. Sheinker and Y. I. Pomerontsev, *Zh. Fiz. Khim.*, **30**, 79 (1956).

(49) S. F. Mason, *J. Chem. Soc.*, 5010 (1957).

(50) G. W. H. Cheeseman, *ibid.*, 242 (1960).

(51) A. R. Katritzky and J. M. Lagowski, *Advan. Heterocycl. Chem.*, **1**, 339 (1963).



structures V and VI are found in the chemical shifts of the hydroxyl and amine protons (9.79 and 6.32 ppm, respectively) when compared to the corresponding shifts of 2-hydroxy- and 2-aminopyridine protons (11.43 and 6.21 ppm, respectively).

Coupling Constants. The effect of substituents on coupling constants in 2-substituted pyrazines is likewise similar to that found for monosubstituted benzenes,²⁻⁴ pyridines,⁵⁻¹⁰ and pyrimidines.^{23,24} Neglecting the substituent which gives rise to a tautomeric structure (*i.e.*, hydroxy), the range of observed values of J_{35} is -0.012 to -0.462 Hz; that of J_{36} , $+1.331$ to $+1.541$ Hz; and that of J_{56} , $+2.426$ to $+2.857$. In identically substituted benzenes, the corresponding ranges are: J_o , 7.32–7.66 Hz; J_m , 1.10–1.62 Hz; and J_p , 0.40–0.77 Hz. The similarity between substituent effects on coupling constants in 2-substituted pyridines and 2-substituted pyrazines is shown in Figure 3.

For 2-hydroxypyridine, J_{56} is larger by ~ 1.4 Hz than J_{56} in other monosubstituted pyrazines. In 2-hydroxypyridine, J_{56} is ~ 7.0 Hz, an increase of ~ 2.0 Hz over J_{56} for other 2-substituted pyridines. Thus, this increase in J_{56} indicates some double-bond fixation, reflecting the existence of 2-hydroxypyridine as V. The small and normal value of J_{56} in 2-aminopyridine as compared with J_{56} in other monosubstituted pyrazines confirms that 2-aminopyridine exists in the amino form (VI).

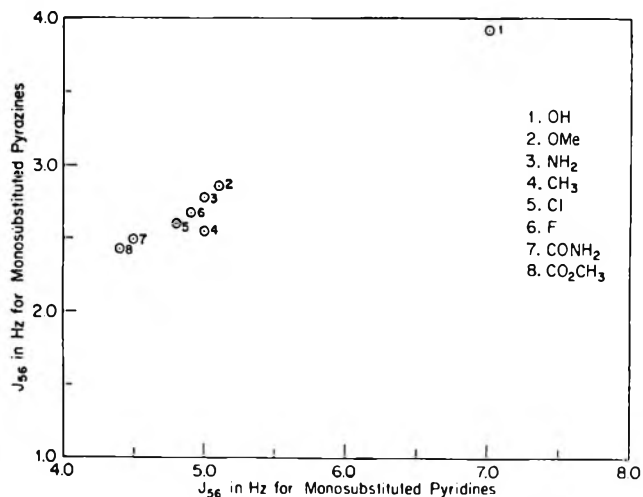


Figure 3. Plot of J_{56} in monosubstituted pyrazines vs. J_{56} in monosubstituted pyridines.

Introduction of two nitrogen atoms *para* into a six-membered ring (pyrazine) causes a lowering of the vicinal coupling constant about twice that found for the introduction of one nitrogen atom (pyridine). The vicinal coupling constant in benzene is 7.56 Hz,⁵² and in pyridine, the vicinal constant corresponding to J_{56} is 4.86 Hz,^{11,12} a difference of 2.70 Hz. In the monosubstituted pyrazines, J_{56} is ~ 2.5 Hz, a difference of ~ 2.4 Hz from J_{56} of pyridine.

The negative sign found for J_{35} is not surprising in view of recent reports. A negative sign for the H–H coupling across nitrogen has been reported for pyridine¹¹ and 3-acetylpyridine.⁷ Signs of the H–F couplings in 2-fluoropyridine are identical with those of similar couplings in various 2-fluoropyridines.⁴⁶

Acknowledgment. This research was performed with support from the National Institutes of Health under Grant FR-00292. We are grateful for technical assistance by Mr. R. H. Obenauf and wish to thank Dr. S. Castellano for many helpful discussions.

(52) J. M. Read, Jr., R. E. Mayo, and J. H. Goldstein, *J. Mol. Spectry.*, **22**, 419 (1967).

Influence of Double-Layer Charging in Chronopotentiometry

by Michael L. Olmstead and Richard S. Nicholson

Chemistry Department, Michigan State University, East Lansing, Michigan 48823 (Received October 27, 1967)

A rigorous theoretical treatment of chronopotentiometry is presented which includes double-layer charging. The treatment is based on a model that assumes reversible charge transfer and a potential-independent double-layer capacitance. The procedures for treating this model easily are extended to more complicated models. Results of theoretical calculations are presented as ratios of faradaic to total current and as theoretical potential-time curves. These potential-time curves are used to evaluate several methods of transition-time measurement, and it is concluded that the method of Laity and McIntyre is excellent for compensating effects of double-layer charging. In addition, several diagnostic methods often used to analyze chronopotentiometric data are discussed in relation to the theoretical calculations. Finally, the case of current reversal is treated, and the effect of double-layer charging on the ratio of forward to reverse transition times is determined.

Introduction

Chronopotentiometry is an experimental procedure which involves measuring the potential of a working electrode as a function of time during polarization by constant current. This technique has been used extensively in applications ranging from analysis to measurement of kinetics, adsorption, and transport properties. In all of these applications chronopotentiometry suffers the disadvantage that, although ideally 100% of the applied current is consumed by the faradaic process, in practice some of the current is used to charge the electrical double layer. The result is that rather than being constant, the faradaic current density actually is some unknown function of time. Although the theory of chronopotentiometry is relatively straightforward when double-layer effects are ignored, to account theoretically for these effects considerably complicates the problem. Thus previous attempts¹⁻⁷ to treat double-layer charging have been empirical or approximate. The purpose of this paper is to present a treatment of chronopotentiometry including double-layer charging which is rigorous within the framework of a reasonable model. Results of this theory permit evaluation of previous empirical treatments and serve as a general guide for determining the influence on chronopotentiograms of double-layer charging.

Theory

Model. The basis of our treatment is a simple model which describes the charge-transfer process in a conventional manner and includes the effect of double-layer charging. The model is based on the following points: (1) mass transport is by semiinfinite linear diffusion; (2) no adsorption or other accumulation occurs at the electrode surface; (3) electrochemical equilibrium is maintained at the electrode surface; (4) charging of the electrical double layer is as though the electrode were ideally polarized; and (5) the differential double-layer capacitance is independent of potential. Each of these

points can be restated mathematically. We show below that these statements lead to two possible integral equations which can be solved for potential-time relationships.

Although this model probably does not describe exactly any real experimental situation, results of calculations should serve as guide lines for evaluating the influence of double-layer charging for systems which the model approximates. Moreover, the procedures described below for treating the model should be applicable to cases in which some of the approximations are not made. For example, point 5 of the model could be modified by introducing any arbitrary dependence of double-layer capacitance on potential.

Derivation of Integral Equations. Fick law diffusion equations and points 1 and 2 of the model lead to the following expressions for surface concentrations of oxidized and reduced forms, respectively, of depolarizer.

$$C_{O^s}(t) = C_{O^*} - \frac{1}{nF\sqrt{\pi D_O}} \int_0^t \frac{i_f(\tau) d\tau}{\sqrt{t-\tau}} \quad (1)$$

$$C_{R^s}(t) = C_{R^*} + \frac{1}{nF\sqrt{\pi D_R}} \int_0^t \frac{i_f(\tau) d\tau}{\sqrt{t-\tau}} \quad (2)$$

There $i_f(t)$ is the faradaic current density, C_{O^*} and C_{R^*} are the bulk concentrations of depolarizer, and D_O and D_R are diffusion coefficients. Point 3 of the model is written as the Nernst equation

- (1) P. Delahay, "New Instrumental Methods in Electrochemistry," Interscience Publishers, Inc., New York, N. Y., 1954, p 207.
- (2) P. Delahay and T. Berzins, *J. Amer. Chem. Soc.*, **75**, 2486 (1953).
- (3) W. Lorenz, *Z. Elektrochem.*, **59**, 730 (1955).
- (4) W. H. Reinmuth, *Anal. Chem.*, **33**, 485 (1961).
- (5) A. J. Bard, *ibid.*, **33**, 11 (1961).
- (6) A. J. Bard, *ibid.*, **35**, 340 (1963).
- (7) R. W. Laity and J. D. E. McIntyre, *J. Amer. Chem. Soc.*, **87**, 3806 (1965).

$$\frac{C_{O^s}(t)}{C_{R^s}(t)} = \exp\left(\frac{nF}{RT}[E(t) - E^0]\right) \quad (3)$$

where $E(t)$ is the instantaneous electrode potential.

The total current density, i_T , in the chronopotentiometry experiment can be written as the algebraic sum of faradaic and double-layer charging current densities

$$i_T(t) = i_T = i_f(t) + i_c(t) \quad (4)$$

where $i_T(t)$ is written as time dependent to account for the possibility of current reversal. The double-layer current, $i_c(t)$ in eq 4, is given by

$$i_c(t) = -C_1 \frac{dE(t)}{dt} \quad (5)$$

where C_1 is the potential-independent differential double-layer capacitance referred to in point 5.

The initial condition, $E(0) = E_i$, and the definition

$$h(t) = i_c(t)/i_T(t) \quad (6)$$

permit statement of eq 5 in integral form

$$E(t) = E_i - \frac{i_T}{C_1} \int_0^t h(\tau) d\tau \quad (7)$$

Elimination of the instantaneous potential from eq 3 and 7 leads to

$$\frac{C_{O^s}(t)}{C_{R^s}(t)} = \frac{C_{O^*}}{C_{R^*}} \exp\left[\frac{nFi_T}{RTC_1} \int_0^t h(\tau) d\tau\right] \quad (8)$$

To retain generality in subsequent results, the following changes of variable are introduced which convert the time in eq 1, 2, 4, and 8 into dimensionless form

$$t = \frac{(nFC_{O^*}\sqrt{\pi D_O})^2 y}{4i_T^2} \quad (9)$$

$$\tau = \frac{[nFC_{O^*}\sqrt{\pi D_O})^2 x}{4i_T^2} \quad (10)$$

Combination of eq 1, 2, 4, and 8 results in the following nonlinear integral equation in the unknown function $h(y)$

$$\frac{1 - \exp\left[-\frac{1}{\psi} \int_0^y h(x) dx\right]}{1 + \exp\left[b - \frac{1}{\psi} \int_0^y h(x) dx\right]} = \sqrt{y} - \frac{1}{2} \int_0^y \frac{h(x) dx}{\sqrt{y-x}} \quad (11)$$

where

$$\exp(b) = \frac{C_{O^*}}{C_{R^*}} \sqrt{\frac{D_O}{D_R}} \quad (12)$$

$$\psi = \left(\frac{RT}{nF}\right) \frac{4i_T C_1}{(nFC_{O^*}\sqrt{\pi D_O})^2} \quad (13)$$

Potential variation of the electrode may be obtained with the aid of eq 11

$$n[E(y) - E_{1/2}] = \frac{RT}{F} \left[b - \frac{1}{\psi} \int_0^y h(x) dx \right] \quad (14)$$

There $E_{1/2}$ is the conventional polarographic half-wave potential. Equation 14 with $y = 0$ shows that the constant b determines the potential at which the redox couple is poised prior to initiation of electrolysis. A plot of the quantity $n[E(y) - E_{1/2}]$ obtained from eq 14 will be referred to subsequently as an E - y curve.

The model also may be reduced to a different integral equation in an unknown function which is directly related to potential. Thus by combining the definition

$$g(y) = \frac{nF}{RT}[E(y) - E_{1/2}] \quad (15)$$

with eq 1-5 and again using the changes of variable in eq 9 and 10, the following nonlinear integrodifferential equation is obtained

$$\frac{1 - \exp[g(y) - b]}{1 + \exp[g(y)]} = \sqrt{y} + \frac{\psi}{2} \int_0^y \frac{\left[\frac{dg(x)}{dx}\right] dx}{\sqrt{y-x}} \quad (16)$$

Equation 16 can be converted to an integral equation by Laplace transform techniques

$$(1 + e^{-b}) \int_0^y \frac{e^{g(x)} dx}{1 + e^{g(x)}} = y - \frac{2y^{3/2}}{3} - \frac{\psi}{2} \int_0^y \frac{[g(x) - b] dx}{\sqrt{y-x}} \quad (17)$$

Solution of eq 17 directly gives the E - y characteristic during electrolysis. Charging current can be obtained from $g(y)$ by the expression

$$h(y) = -\psi \frac{dg(y)}{dy} \quad (18)$$

Solution of Integral Equations. Except for the numerical approach discussed below, a general solution of eq 11 (or eq 17) cannot be obtained. Nevertheless, some limiting cases exist where explicit solutions can be found, and it is useful to consider these cases prior to discussion of the general results.

The limiting cases depend on the magnitude of the dimensionless double-layer parameter, ψ , which determines the contributions of charging current to total current. For example, as ψ approaches zero (small C_1 and/or i_T , or large C_{O^*}) one expects no effects of double-layer charging. For small ψ , eq 17 reduces to

$$(1 + e^{-b}) \int_0^y \frac{e^{g(x)} dx}{1 + e^{g(x)}} = y - \frac{2y^{3/2}}{3} \quad (19)$$

This integral equation is readily solved for $g(y)$ and the result is

$$g(y) = \ln \left[\frac{1 - \sqrt{y}}{e^{-b} + \sqrt{y}} \right] \quad (20)$$

Solution of eq 11 for small ψ also leads to eq 20.

As expected, eq 20 is independent of the double-layer parameter, ψ . Equation 20 is the well-known expression for chronopotentiograms when the electrode process is reversible and double-layer charging is not considered.

The second limiting case arises whenever ψ is large (or small y). In this case, for example, eq 11 can be linearized and the resulting integral equation can be solved for $h(y)$ and combined with eq 14 to give

$$n[E(y) - E_{1/2}] = \frac{RT}{F} \left[b - \frac{y}{\psi} \right] \quad (21)$$

For values of ψ intermediate between these limiting cases, the potential-time and current-density relationships can only be obtained by numerical solution of eq 11 or 17. We have solved both eq 11 and 17 using the step-functional method.⁸ In the present case application of this numerical method results in a system of nonlinear algebraic equations which can be solved successively for the unknown function. Solution of the nonlinear equations was performed by Newton-Raphson iteration which was continued until successive answers differed by a relative error of less than 10^{-7} . Initial guesses for solution of the first equation were obtained from the integral equations linearized for small values of the independent variable, y (e.g., eq 21). Subsequent calculations were performed with the most recently calculated numerical solution as an initial guess in the iteration procedure.

During preliminary calculations E - y curves obtained from eq 11 and 14 were compared with those from eq 17. These data showed that as the numerical integration interval was decreased, the E - y curves calculated from eq 14 converged more rapidly to the correct answer than those obtained from eq 17. Because of this fact, results reported in this paper were obtained from solutions of eq 11. The numerical values of $h(y)$ and $n(E(y) - E_{1/2})$ calculated from eq 11 and 14 were independent of b , except for small shifts along the y axis, provided that b was selected greater than about 6.5. This corresponds to the usual procedure of poisoning the system anodic of $E_{1/2}$ prior to the experiment. Results presented here are for the arbitrary value of $b = 7.0$. The integration interval used was 0.01, and solutions are accurate to approximately ± 0.5 mV.

For ψ about 0.1, more than 50% of total coulombs are involved in double-layer charging and, therefore, it is unlikely that values of ψ greater than 0.1 would be encountered experimentally. Thus discussions that follow are restricted to values of ψ in the range $0 < \psi < 0.1$.

Finally, to report solutions of integral equations in terms of potential, a temperature of 25° ($RT/F = 25.68857$ mV) has been assumed. To correct results to some other temperature simply involves multiplication by the appropriate factor.

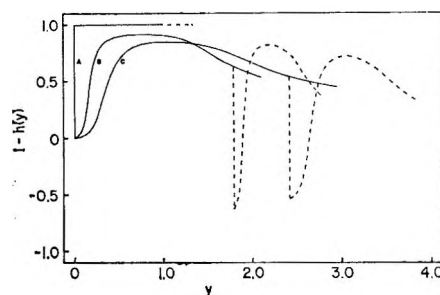


Figure 1. Variation of faradaic current density. Dashed lines are after current reversal. Values of ψ are: A, 0.0; B, 0.03; C, 0.06.

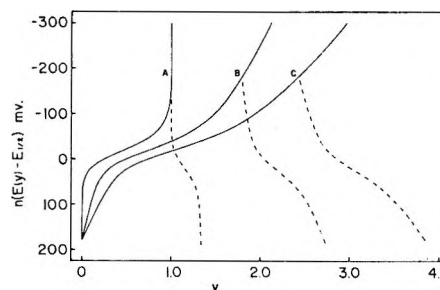


Figure 2. Theoretical chronopotentiograms. Dashed lines are after current reversal. Values of ψ are: A, 0.0; B, 0.03; C, 0.06.

Results and Discussion

Results of numerical solution of eq 11 for $h(y)$ are illustrated in Figure 1 (solid lines) where the ratio of faradaic to total current density [$i_f/i_T = 1 - h(y)$] is plotted for two values of ψ . For purposes of comparison, the case of ψ equal to zero also is included. In general the effect on i_f of increasing ψ is twofold. First, the faradaic current density is decreased, and second the faradaic current density becomes strongly time dependent. Both these effects markedly influence theoretical chronopotentiograms, as illustrated by Figure 2 (solid lines). For purposes of comparison with the case $\psi = 0$, Figure 2 also includes a plot of eq 20. Curves of Figure 2 show the expected distortion resulting from effects of the double-layer charging. For example, the time at which a transition of potential takes place becomes progressively greater because of the decrease of i_f with increasing ψ . An important application of curves like those of Figure 2 is evaluation of these transition times, which is discussed next.

The change of variable in eq 9 normalizes theoretical E - y curves to those obtained when the double-layer parameter is zero. The result is that measurements of transition times from theoretical chronopotentiograms will be *normalized transition times*, which are distances, y_t , on the y axis. These y_t values are related to experimental transition times, τ_t , by

(8) R. S. Nicholson, *Anal. Chem.*, **37**, 667 (1965).

$$\tau_t = \frac{(nFC_0^* \sqrt{\pi D_0})^2 y_t}{4i_t^2} \quad (22)$$

Because y_t is unity if τ_t in eq 22 is the transition time defined by the Sand equation, deviations of y_t from unity are a direct measure of deviations from the Sand equation caused by double-layer charging.

Ideally, a method of measuring transition times would be one that always gives a value of y_t equal to unity, regardless of the extent of double-layer charging. If this were possible then all experimental applications of chronopotentiometry based on transition-time measurements would be independent of the influence of double-layer charging. A number of different methods for measuring transition times have been proposed in the literature which have exactly this objective. By applying these methods to theoretical chronopotentiograms, it is possible to evaluate the extent to which these methods eliminate influences of double-layer charging. Of the various methods, we have used the theoretical chronopotentiograms to evaluate four of them: (1) measurement between two potentials, (2) the method of Delahay and Berzins,² (3) the method of Reinmuth,⁴ and (4) the method of Laity and McIntyre.⁷ The last three methods depend on graphical operations and will be discussed separately from the first method.

Transition Times from Potential Measurements. This method involves measurement between two potentials on the E - y curve. For example, in Figure 3 the selection of potentials E_A and E_B corresponding to points A and B produces a normalized transition time of $y_t = 1.65$, which is represented by segment A'B''. Although this method is extremely simple from a practical standpoint, normalized transition times which result are complicated by two factors. First, for a large double-layer parameter the transition times are much larger than those predicted by the Sand equation. Second, the normalized transition times are strongly dependent on the two potentials, E_A and E_B . To circumvent this latter difficulty, we have adopted an arbitrary procedure for selection of these two potentials. Thus, a value of $E_A = 120/n$ mV always was used, and the potential E_B was determined by defining a total

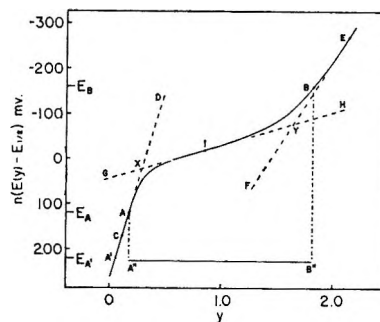


Figure 3. Theoretical chronopotentiogram for $\psi = 0.03$, illustrating constructions used for evaluating graphical methods.

potential excursion, ΔE_{AE} , from which E_B is determined by the relationship $E_B = E_A - \Delta E_{AB}$. For each E - y curve, normalized transition times were determined for several values of ΔE_{AB} , and these results are summarized in Table I.

Sometimes it may be convenient to select E_A anodic of $120/n$ mV. When this happens the data in Table I can be corrected to correspond to a new potential $E_{A'}$, at which the transition-time measurement is begun (see Figure 3). Clearly from Figure 3 the correction for the new transition time is the dimensionless time between points A and A'. This correction is easily obtained because the E - y curve in this region is described by eq 21. Thus the corrected normalized transition time, y_t' , is

$$y_t' = y_t + \frac{nF\psi}{RT} (E_{A'} - 120/n) \quad (23)$$

where y_t is taken from Table I. The new potential excursion, $\Delta E_{A'B}$ ($= E_{A'} - E_B$) is given by

$$\Delta E_{A'B} = \Delta E_{AB} + E_{A'} - 120/n \quad (24)$$

where ΔE_{AB} is the potential excursion in Table I.

An approximate equation for treating the effect of double-layer charging when transition times are measured by the two-potential method has been proposed by Bard.^{5,6} Bard's equation written in terms of the dimensionless parameters of this work takes the form

$$\sqrt{y_t} = 1 + \frac{nF\psi\Delta E_{AB}}{RT\sqrt{y_t}} \quad (25)$$

The extent of applicability of eq 25 can be determined by plotting the data of Table I according to eq 25 for each value of ΔE_{AB} . If eq 25 were rigorously applicable, all of these plots should have slopes and intercepts of 1. We find that this happens only for $\Delta E_{AB} = 240/n$ mV; for other values of ΔE_{AB} , eq 25 is only approximately obeyed.

Graphical Methods for Determination of Transition Times. The graphical methods to be discussed depend on construction of straight lines tangent to the E - y curve at selected points. To evaluate these graphical

Table I: Normalized Transition Times from Potential Measurements

ψ	$\Delta E_{AB}, \text{mV}$				
	240/n	280/n	320/n	360/n	400/n
0.005	1.089	1.144	1.184	1.218	1.249
0.01	1.181	1.260	1.321	1.374	1.423
0.02	1.348	1.464	1.560	1.645	1.724
0.03	1.504	1.652	1.777	1.890	1.995
0.04	1.652	1.830	1.982	2.120	2.250
0.06	1.936	2.167	2.370	2.556	2.733
0.08	2.208	2.490	2.739	2.971	3.191
0.10	2.472	2.801	3.095	3.370	3.633

methods, we have adopted arbitrary potentials at which two of these tangents are drawn. In addition, we have used a computer to construct tangents and to perform subsequent calculations of normalized transition times. Figure 3 illustrates the manner in which tangents were constructed: segment CD, tangent to the E - y curve at $E(y) - E_{1/2} = 170/n$ mV with slope, S_0 ; segment GH, tangent to the E - y curve at its inflection point, I, with slope S_1 ; and segment EF, tangent to the E - y curve at $E(y) - E_{1/2} = -270/n$ mV with slope S_2 .

A. *Method of Delahay and Berzins.*² Values of y_t measured according to the procedure of Delahay and Berzins are listed in Table II. These y_t values show that, contrary to the original claims of Delahay and Berzins, this method does not completely compensate the transition time for effects of double-layer charging. However, transition times by this method are compensated much better than those obtained by the two-potential method.

Table II: Normalized Transition Times Determined by (A) Method of Delahay and Berzins, (B) Method of Reinmuth, and (C) Method of Laity and McIntyre

ψ	$n(E'_{1/2} - E_{1/2})^a$ mV	A ^b	y_t B ^c	C ^d
0.005	0.17	1.017	1.056	0.989
0.01	0.04	1.042	1.100	0.979
0.02	0.06	1.088	1.175	0.974
0.03	0.18	1.128	1.240	0.972
0.04	0.35	1.165	1.298	0.970
0.06	0.74	1.231	1.401	0.968
0.08	1.14	1.289	1.493	0.967
0.10	1.52	1.342	1.576	0.966

^a $E_{1/2}$ is the true half-wave potential and $E'_{1/2}$ is the apparent half-wave potential measured by method of Delahay and Berzins. Values vary no more than 2 mV for tangents constructed on potential intervals from $130/n$ to $170/n$ mV and from $-260/n$ to $-290/n$ mV. ^b Values vary no more than 2% for tangents constructed on potential intervals from $130/n$ to $170/n$ mV and from $-260/n$ to $-280/n$ mV. ^c Values vary no more than 2% for tangents constructed on potential intervals from $130/n$ to $170/n$ mV and from $-260/n$ to $-290/n$ mV. ^d Values vary no more than 2% for tangents constructed on potential intervals from $150/n$ to $170/n$ mV and from $-240/n$ to $-290/n$ mV.

Delahay and Berzins also have described a procedure for measurement of $E_{1/2}$ from potential-time curves. We performed a similar measurement of $E_{1/2}$ on theoretical E - y curves and results are summarized in Table II. These data show that the method of Delahay and Berzins apparently is a very reliable means of measuring the half-wave potential from chronopotentiograms which are distorted by double-layer charging.

In a later paper Delahay and Mamantov⁹ proposed a variation of the above method for measurement of

transition times when slopes of tangents CD and EF in Figure 3 are markedly dissimilar. Our application of this method to theoretical E - y curves produced normalized transition times approximately 30% greater than those obtained by the method of Delahay and Berzins, and these results are not reported.

B. *Method of Reinmuth.*⁴ Reinmuth has discussed effects of double-layer charging on chronopotentiograms and has proposed a graphical method for measuring transition times. Normalized transition times obtained by application of Reinmuth's method to theoretical E - y curves also are included in Table II. From these data we conclude that Reinmuth's method is less satisfactory than the method of Delahay and Berzins for compensation of double-layer charging.

C. *Method of Laity and McIntyre.*⁷ Recently, Laity and McIntyre have considered effects of double-layer charging on chronopotentiograms and have proposed a new method for measuring transition times. Unlike the two methods just discussed, their method is not empirical but is based on fundamental properties of the potential-time curves. Their approach assumes that faradaic current can be approximated by a series of step functions and that the magnitude of these step functions can be obtained from slopes of tangents to the E - y curve. Their result in its simplest form is an equation for calculation of an effective transition time from the experimental potential-time curve. In terms of the dimensionless variables defined here this equation is

$$\sqrt{y_t} = \left(1 - \frac{S_1}{S_0}\right)\sqrt{y_1 + y_2} - \left(\frac{S_2 - S_1}{S_0}\right)\sqrt{y_2} \quad (26)$$

There S_0 , S_1 , and S_2 are the slopes defined in reference to Figure 3, y_1 is the abscissa distance between points X and Y, and y_2 is the abscissa distance between point Y and point E at $-270/n$ mV on the E - y curve. Table II includes results of normalized transition times calculated according to eq 26. These data show that eq 26 will reproduce the transition time predicted by the Sand equation within 3.5% for $\psi = 0.1$, and for smaller values of ψ the error is progressively less.

Because the method of Laity and McIntyre is as easy to apply as other methods and remarkably effective in minimizing interferences of double-layer charging, *this method should be adopted for all experimental transition-time measurements.*

Interpretation of Dimensionless Data. Chronopotentiometric experiments often are analyzed by various diagnostic plots designed to highlight some aspect of the electrode process. At high current densities these diagnostic methods of data treatment may display

(9) P. Delahay and G. Mamantov, *Anal. Chem.*, **27**, 478 (1955). A method attributed to Kuwana by C. D. Russell and J. M. Peterson, *J. Electroanal. Chem.*, **5**, 467 (1963), and by D. Hawley and R. N. Adams, *ibid.*, **10**, 376 (1965), apparently is identical with the method originally proposed by Delahay and Mamantov.

trends which are the result of double-layer charging but which are not readily identified as such. Thus for each transition time method it is important to rearrange the y_t vs. ψ data in Tables I and II in a way which allows prediction of these trends. An example of one rearrangement of the dimensionless data is implicit in the discussion of Bard's equation given above. Two other examples are cited below.

A commonly used diagnostic plot is the variation of $i_T\sqrt{\tau_t}/C_0^*$ vs. i_T . In terms of the dimensionless variables this is equivalent to variation of $\sqrt{y_t}$ with ψ . Thus deviations in $\sqrt{y_t}$ should reflect directly deviations in $i_T\sqrt{\tau_t}/C_0^*$ which are due to double-layer charging. These results will be quantitative if C_1 is known.

The Sand equation predicts that a plot of $i_T\tau_t$ vs. $1/i_T$ will have a slope of $(nFC_0^*\sqrt{\pi D_0}/2)^2$ and a zero intercept. In terms of the dimensionless variables, this is analogous to a plot of y_t/ψ vs. $1/\psi$. Because of double-layer charging these plots will have nonzero intercepts whose magnitudes depend on the method of transition-time measurement. If C_1 is known, the dimensionless plots will be useful in deciding if $i_T\tau_t$ at $1/i_T = 0$ is due completely to double-layer charging or adsorption, or both.

Current-Reversal Chronopotentiometry. Chronopotentiometry with current reversal is a useful technique for investigation of electrolysis mechanisms. For example, it has been used to study electrode kinetics, homogeneous chemical reactions coupled to charge transfer, and, in at least one instance, adsorption. The model considered here for treating effects of double-layer charging includes none of these possible complications. Nevertheless, it seemed instructive to calculate theoretical E - y curves for current reversal to evaluate the importance of double-layer charging in at least this simple case.

The characteristic parameter of reverse-current chronopotentiometry is the ratio of the forward to reverse transition times (τ_f/τ_r). The investigation undertaken here is aimed directly at evaluating effects of double-layer charging on this ratio.

For current reversal at the forward transition time, the total current density is defined as

$$i_T(t) = -i_r = i_f(t) + i_c(t) \quad (t > \tau_f) \quad (27)$$

Use of eq 27 in the same sequence of steps leading to eq 11 results in the integral equation

$$\frac{1 - \exp\left[-\frac{1}{\psi}\left(\int_0^{y_t} h(x) dx - \int_{y_t}^y h(x) dx\right)\right]}{1 + \exp\left[b - \frac{1}{\psi}\left(\int_0^{y_t} h(x) dx - \int_{y_t}^y h(x) dx\right)\right]} = y^{1/2} - 2(y - y_t)^{1/2} - \frac{1}{2}\left[\int_0^{y_t} \frac{h(x) dx}{\sqrt{y-x}} - \int_{y_t}^y \frac{h(x) dx}{\sqrt{y-x}}\right] \quad (28)$$

The potential after current reversal is given by

$$n[E(y) - E_{1/2}] = \frac{RT}{F}\left[b - \frac{1}{\psi}\left(\int_0^y h(x) dx - \int_{y_t}^y h(x) dx\right)\right] \quad (29)$$

Beyond the transition time ($y > y_t$), eq 28 was solved for $h(y)$ by the same procedure used to solve eq 11, and E - y curves were constructed from eq 29.

Figure 1 (dashed lines) shows typical results of the solution of eq 28. In the absence of double-layer charging, the ratio $i_f/i_r(t)$ [$= 1 - h(y)$] is always one during both forward and reverse current. For finite double-layer parameter the ratio becomes negative for a short duration immediately after current reversal. This happens because the potential (Figure 2, dashed lines) remains sufficiently cathodic of $E_{1/2}$ to continue reduction ($i_f > 0$), while at the same time $i_r(t)$ has changed sign. As the potential nears $E_{1/2}$, however, the faradaic current approaches zero and eventually becomes an anodic current, and the ratio again becomes positive. Figure 2 (dashed lines) illustrates how these effects influence E - y curves. Thus after current reversal the magnitude of the slope of the E - y curve is greater than its limiting slope given by eq 19, and charging current is greater than the total current until the magnitude of the slope becomes less than $RT/F\psi$.

Table III: Ratio of Forward to Reverse Transition Times

ψ	τ_f/τ_r^a
0.005	2.722
0.01	2.531
0.02	2.293
0.03	2.143
0.04	2.036
0.06	1.889
0.08	1.792
0.10	1.720

^a Switching potential is $-210/n$ mV. Forward transition time measured from $120/n$ mV to switching potential; reverse transition time measured from switching potential to $120/n$ mV.

The above effects cause disproportionately large increases in the reverse transition time, since the faradaic current after current reversal contains both cathodic and anodic components. These effects are illustrated by the data of Table III. These data show that the ratio, τ_f/τ_r , is decreased from the well-known value of 3 obtained in the absence of double-layer charging.¹⁰

(10) NOTE ADDED IN PROOF. After this manuscript had been accepted for publication, we became aware of two other papers dealing with double-layer charging in chronopotentiometry: R. S. Rodgers and L. Meites, *J. Electroanal. Chem. Interfacial Electrochem.*, 16, 1 (1968), and W. T. DeVries, *ibid.*, in press.

Acknowledgment. We thank Professor Stanley Bruckenstein and Mr. Peter Daum for helpful discussions. This work was supported by the National

Science Foundation (Grant No. GP-3830) and the United States Army Research Office, Durham, North Carolina (Contract No. DA-31-124-ARO-D-308).

On the Analysis of Dielectric Dispersion Data into Two Relaxation Regions

by E. A. S. Cavell and P. C. Knight

Department of Chemistry, The University, Southampton, England

Accepted and Transmitted by The Faraday Society (November 10, 1966)

A series of values of normalized permittivity (η') and loss (η'') have been calculated by means of the Cole-Cole equations with four different values of the distribution parameter (α). On the assumption that these values can also be represented as a sum of two superposed Debye dispersions, the appropriate relaxation times have been determined from them by the usual numerical method for a series of values of the Debye dispersion amplitudes, C_1 and $(1 - C_1)$. The sum of the squared deviations (S) between values of η' and η'' calculated by means of the Cole-Cole equations and those obtained for the "best" corresponding pair of Debye dispersions for each value of C_1 considered has been evaluated. It appears that as α increases, the minimum value of S also increases, although the sensitivity of S to changes in the value of C_1 decreases significantly as α approaches zero. A graphical method based on these calculations for obtaining preliminary estimates of the relaxation times of the Debye type dispersions has been outlined.

Introduction

The dielectric dispersion data of a surprisingly large number of pure liquids and of dilute solutions of simple polar molecules in nonpolar solvents can be represented within the limits of experimental error by means of the Debye relation.¹ In the majority of cases, however, the expressions of Cole and Cole,² and Davidson and Cole,³ which incorporate an empirical distribution parameter, have commonly been employed and various suggestions have been advanced to account for the need to employ these modified relations. Fröhlich,⁴ for example, considered that deviations from Debye behavior might arise from a distribution of orientational activation energies within a system, and Glarum⁵ has shown that a unidimensional defect diffusion model could quantitatively account for an apparent distribution of relaxation times.

Smyth and his collaborators,⁶⁻⁸ on the other hand, seem to prefer to analyze their own experimental data, where necessary, into two or more relaxation processes, associated with dipoles of varying sizes and characterized by single relaxation times. In certain cases, *e.g.*, benzyl chloride, rotation of a polar group, about the bond connecting the group to the remainder of the molecule, can make a characteristic contribution to the over-all dielectric dispersion in addition to that made by rotation of the molecule as a whole. In these circumstances the observed permittivity (ϵ') and loss (ϵ'')

can often be represented as the sum of the appropriately weighted terms for each relaxation process, *i.e.*

$$\epsilon' = \epsilon_{\infty} + \frac{C_1(\epsilon_0 - \epsilon_{\infty})}{1 + \omega^2\tau_1^2} + \frac{C_2(\epsilon_0 - \epsilon_{\infty})}{1 + \omega^2\tau_2^2} \quad (1)$$

$$\epsilon'' = \frac{C_1(\epsilon_0 - \epsilon_{\infty})}{1 + \omega^2\tau_1^2}\omega\tau_1 + \frac{C_2(\epsilon_0 - \epsilon_{\infty})}{1 + \omega^2\tau_2^2}\omega\tau_2 \quad (2)$$

In eq 1 and 2, ϵ_0 and ϵ_{∞} are the low and high frequency limiting values of ϵ' , ω is the angular frequency ($2\pi f$), C_1 and C_2 are the dispersion amplitudes such that $C_1 + C_2 = 1$, and τ_1 and τ_2 are the relaxation times characterizing the Debye type dispersions concerned.

In the most favorable case for which $C_1 = C_2$, separate absorption maxima are not observed⁹ unless $\tau_1/\tau_2 > (3 + 2\sqrt{2})$. For many practical cases, therefore, in

- (1) P. Debye, "Polar Molecules," Chemical Catalog Co., New York, N. Y., 1929, p 94.
- (2) K. S. Cole and R. H. Cole, *J. Chem. Phys.*, **9**, 341 (1941).
- (3) D. W. Davidson and R. H. Cole, *ibid.*, **19**, 1484 (1951).
- (4) H. Fröhlich, "Theory of Dielectrics," Oxford University Press, London, 2nd ed, 1958, p 92.
- (5) S. H. Glarum, *J. Chem. Phys.*, **33**, 639 (1960).
- (6) K. Higasi, K. Bergmann, and C. P. Smyth, *J. Phys. Chem.*, **64**, 880 (1960).
- (7) K. Bergmann, D. M. Roberti, and C. P. Smyth, *ibid.*, **64**, 665 (1960).
- (8) F. K. Fong and C. P. Smyth, *ibid.*, **67**, 226 (1963).
- (9) D. W. Davidson, *Can. J. Chem.*, **39**, 571 (1961).

which $1 < \tau_1/\tau_2 < 5$ and $C_1 \neq C_2$, a single broad dispersion results. The analysis of experimental data to yield the two discrete relaxation times may be carried out graphically,^{7,8} but generally the most convenient and reliable procedure is to regard C_1 , τ_1 , and τ_2 as adjustable parameters and then to calculate ϵ' and ϵ'' by means of eq 1 and 2 for an appropriate range of numerical values by means of an electronic computer. The set of values of C_1 , τ_1 , and τ_2 chosen is that set for which the sum of the squared deviations (S) is a minimum. S is commonly defined by means of an expression such as eq 3, sometimes refined by the insertion of weighting factors to allow for experimental uncertainties.

$$S = \Sigma(\epsilon'_{\text{calcd}} - \epsilon'_{\text{obsd}})^2 + \Sigma(\epsilon''_{\text{calcd}} - \epsilon''_{\text{obsd}})^2 \quad (3)$$

$$\epsilon' - j\epsilon'' = \epsilon_\infty + [\epsilon_0 - \epsilon_\infty]/[1 + (j\omega\tau_0)^{1-\alpha}] \quad (4)$$

Some authors seem to imply that the Cole-Cole relation (eq 4) on the one hand and two superposed Debye expressions (eq 1 and 2) on the other may be used as alternative representations of their experimental data,^{7,8,10} although the relations concerned are evidently not equivalent representations. In a recent review,¹¹ Smyth has stated explicitly that if two relaxation times are close together, it may be difficult to distinguish their effect from that of a distribution of relaxation times around a single, most probable value, *i.e.*, from dielectric behavior described by eq 4.

Experimental values of permittivity and loss are usually considered to be subject to uncertainties of least $\pm 1\%$ and $\pm 3\%$, respectively. It is conceivable, therefore, that within the limits of experimental error of this order, either formulation may be used in a purely *empirical* manner to represent the frequency dependence of ϵ' and ϵ'' . The object of the present paper was primarily to determine the magnitude of the numerical discrepancies which exist between values of permittivity and loss calculated by means of the Cole-Cole equation with selected values of τ_0 and α and those calculated from eq 1 and 2 employing the "best" values of the parameters, C_1 , τ_1 , and τ_2 , obtained by the computational procedure mentioned above. In this way, it should be possible with experimental data of sufficiently high precision to decide which of the two alternatives is the better representation. In those cases where the precision is such that this is not possible, the nature of the system investigated and the possible physical significance to be attached to the derived parameters concerned will probably determine the method of representation chosen.

Calculations

In order to calculate permittivity and loss for several different frequencies, the Cole-Cole relation shown in eq 4 may be transformed into eq 5 and 6 by separation of the appropriate real and imaginary terms. The parameter τ_0 is defined by the condition that $\omega_0\tau_0 = 1$, where ω_0 is the angular frequency at which ϵ'' has its

maximum value. Equations 5 and 6 have been employed in the present paper to calculate a series of values of normalized permittivity (η') and loss (η'') for $\omega\tau_0 = 1/3, 1$, and 3 and for four different values of α . These results constitute our "observed" data for the purposes of eq 3. The values of $\omega\tau_0$ employed were chosen so that the resulting values of loss would lie symmetrically on the corresponding Cole-Cole plot and hence would simulate typical experimental data.

$$\eta' = \frac{(\epsilon' - \epsilon_\infty)}{(\epsilon_0 - \epsilon_\infty)} = \frac{1}{2} \left\{ 1 - \frac{\sinh[(1-\alpha)\ln\omega\tau_0]}{\cosh[(1-\alpha)\ln\omega\tau_0] + \sin(\alpha\pi/2)} \right\} \quad (5)$$

$$\eta'' = \frac{\epsilon''}{(\epsilon_0 - \epsilon_\infty)} = \frac{1}{2} \left\{ \frac{\cos(\alpha\pi/2)}{\cosh[(1-\alpha)\ln\omega\tau_0] + \sin(\alpha\pi/2)} \right\} \quad (6)$$

An I.C.T. 1909 computer was then programmed to obtain optimum values of τ_1/τ_0 and τ_2/τ_0 for a range of fixed values of C_1 . This was achieved by varying τ_1/τ_0 and τ_2/τ_0 in steps of 0.025 between suitable limits determined by the magnitude of C_1 selected. The optimum values of τ_1/τ_0 and τ_2/τ_0 are those values which satisfy the condition of a minimum in S , expressed now in terms of normalized permittivities and losses. Values of η'_{calcd} and η''_{calcd} were obtained by means of appropriately modified versions of eq 1 and 2 for each of the three values of $\omega\tau_0$ quoted above. This procedure was repeated for a series of values of C_1 ranging from 0.15 to 0.85 in steps of 0.05. Figures 1 and 2 illustrate the manner in which the optimum values of τ_1/τ_0 and τ_2/τ_0 respectively, vary with the dispersion amplitude (C_1). Figure 3 shows the relationship between the magnitude of C_1 and the sum of the squared deviations (S) obtained when optimum values of τ_1/τ_0 and τ_2/τ_0 are employed in the calculation of normalized permittivity and loss by eq 1 and 2.

Discussion

The symmetrical character of a Cole-Cole plot requires the amplitudes of the two Debye dispersions derived from it to be equal, so that for all values of α examined here, S has its minimum value when $C_1 = 0.5$. The symmetry of the plots themselves about $C_1 = 0.5$, as shown in Figure 3, seems to be also a consequence of the symmetrical disposition on the Cole-Cole plot of the values of normalized permittivity and loss employed in the analysis. No great significance should therefore be attached to this symmetry. With actual experimental data, the symmetry would probably vanish while the minima in S would not necessarily

(10) W. F. Hassell and S. Walker, *Trans. Faraday Soc.*, **62**, 861, 2695 (1966).

(11) C. P. Smyth, *Ann. Rev. Phys. Chem.*, **17**, 442 (1966).

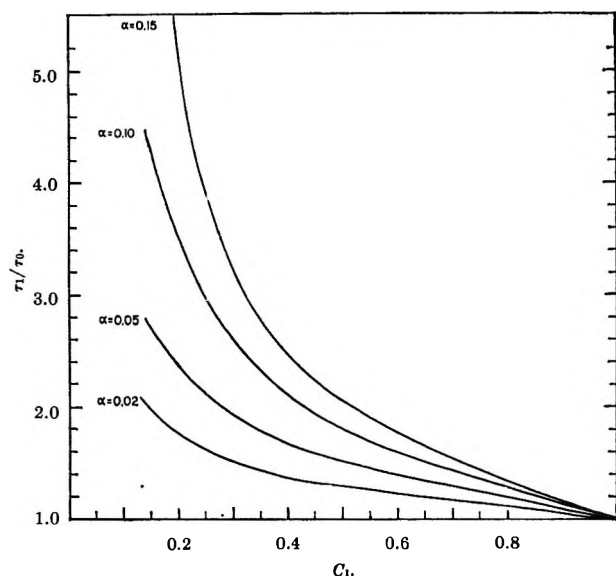


Figure 1. Variation of the optimum value of τ_1/τ_0 with dispersion amplitude C_1 for various values of α .

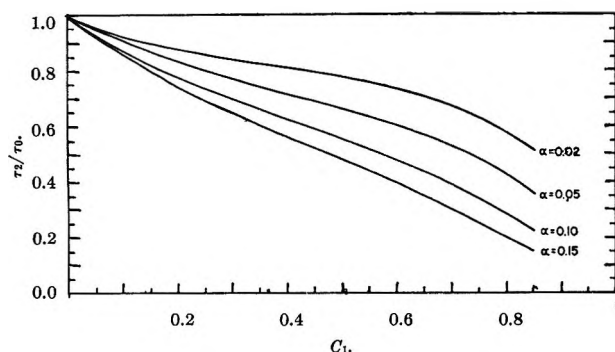


Figure 2. Variation of optimum value of τ_2/τ_0 with dispersion amplitude C_1 for various values of α .

occur at $C_1 = 0.5$. A decreasing sensitivity of S to changes in the value of C_1 as α becomes smaller is also to be expected since as α tends to zero, both τ_1/τ_0 and τ_2/τ_0 tend to unity as shown in Figures 1 and 2, and the Cole-Cole circular arc reduces to a single Debye semicircle.

The most significant feature of Figure 3 for present purposes is the increasing magnitude of the minimum value of S accompanying the increase in α . It appears that if a minimum in S is employed as the sole criterion, then for the Cole-Cole relation and two superposed Debye expressions to be regarded as alternative representations of the same experimental data, the value of α should be less than 0.15. However, some regard should also be paid to the frequency distribution of the individual experimental results involved. This point is best illustrated by reference to Figure 4, in which a Cole-Cole circular arc for $\alpha = 0.15$, obtained by plotting loss against permittivity, is compared with the corresponding curve resulting from the superposition of the appropriate "best" pair of Debye semicircles. The divergence between the two loci is most marked for

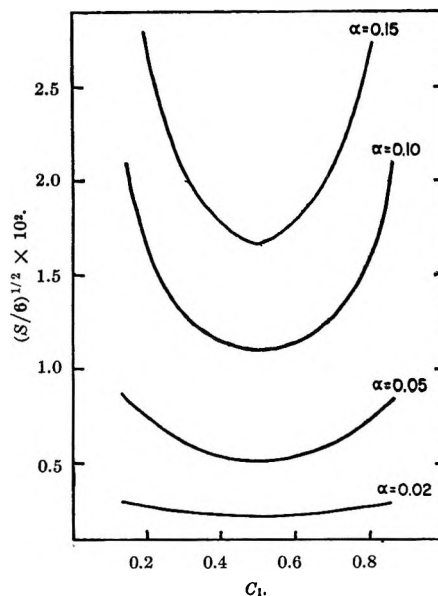


Figure 3. Dependence of the sum of the squared deviations (S) on the dispersion amplitude C_1 for various values of α .

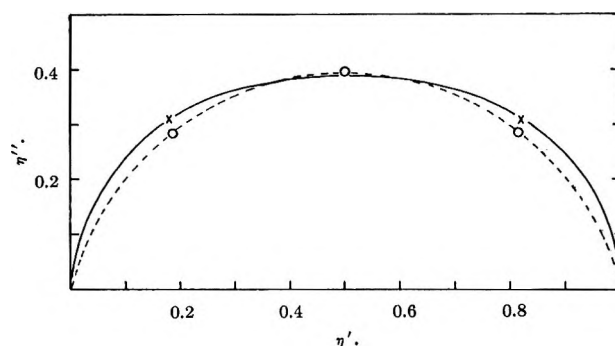


Figure 4. Comparison of values of normalized permittivity (η') and loss (η'') calculated by: (full line), eq 1 and 2 with $C_1 = 0.5$, $\tau_1/\tau_0 = 2.10$ and $\tau_2/\tau_0 = 0.475$; and (broken line), eq 5 and 6 with $\alpha = 0.15$ and $\omega\tau_0 = 1/3, 1, \text{ and } 3$.

values of $\omega\tau_0$ lying between $1/3$ and $1/6$ and between 3 and 6. It is important, therefore, to ensure that an adequate proportion of the experimental results analyzed refer to frequencies corresponding to these ranges of $\omega\tau_0$.

In order to illustrate the way in which the magnitude of the maximum divergence between the two representations depends on α , normalized permittivities and losses calculated with eq 5 and 6 for $\omega\tau_0 = 0.25$ are compared in Table I with those calculated by means of eq 1 and 2 with $C_1 = 0.5$ and the appropriate "best" values of τ_1/τ_0 and τ_2/τ_0 estimated from Figures 1 and 2. This comparison indicates that with experimental data having precision of the order quoted above, it will not be appropriate to regard the two formulations as alternative empirical representations of these data if α substantially exceeds 0.10.

When circumstances are such that alternative representations are possible, the less specific Cole-Cole

Table I: Comparison of Normalized Permittivity (η') and Loss (η'') Calculated with Eq 5 and 6 for $\omega\tau_0 = 0.25$ and Various Values of α with Those Calculated with Eq 1 and 2 with $C_1 = 0.5$ and Appropriate Values of τ_1/τ_0 and τ_2/τ_0 from Figures 1 and 2

α	0.02	0.05	0.10	0.15
τ_1' calcd by eq 1	0.934	0.923	0.907	0.885
τ_1' calcd by eq 5	0.932	0.920	0.891	0.866
$\Delta\eta'$	0.002	0.003	0.016	0.019
η'' calcd by eq 2	0.241	0.247	0.258	0.265
η'' calcd by eq 6	0.237	0.237	0.242	0.241
$\Delta\eta''$	0.004	0.005	0.016	0.024

addition, according to Grubb and Smyth,¹² the ratio of the amplitudes of the two dispersions involved, *i.e.*, $C_1/(1 - C_1)$ should be equal to (μ_1^2/μ_2^2) .

In order to calculate the relaxation times τ_1 and τ_2 from the appropriate experimental data, it may be more convenient in practice subject to the reservations noted above to evaluate the more readily obtainable Cole-Cole parameters τ_0 and α , before attempting computer analysis. If τ_0 and α are known and an estimate of C_1 can be made, then Figures 1 and 2 may be used to obtain preliminary estimates of τ_1 and τ_2 . It is obviously desirable to obtain initial estimates of

Table II: Comparison of Literature Values of τ_1/τ_0 and τ_2/τ_0 with Those Estimated from Figures 1 and 2

Compound	Temp, °C	α	Literature values			Estimated values	
			C_1	τ_1/τ_0	τ_2/τ_0	τ_1/τ_0	τ_2/τ_0
<i>p</i> -Dimethoxybenzene ^a	20	0.04	0.19	1.81	0.79	2.20	0.85
<i>p</i> -Phenylphenol ^b	40	0.07	0.80	1.23	0.25	1.25	0.35
1,4-Diacetobenzene ^b	60	0.08	0.82	1.11	0.30	1.23	0.32
1-Naphthol ^b	60	0.09	0.74	1.07	0.43	1.35	0.37
2-Naphthalene thiol ^c	60	0.10	0.82	1.24	0.17	1.25	0.25
1,4-Diacetobenzene ^b	20	0.11	0.85	1.10	0.31	1.20	0.22
1-Methoxynaphthalene ^a	20	0.12	0.61	1.44	0.50	1.65	0.45
Anisole ^a	20	0.15	0.38	1.97	0.72	2.58	0.58

^a Reference 12. ^b Reference 13. ^c Reference 8.

representation will probably be chosen unless there is independent experimental evidence for the existence of two independent relaxation mechanisms. If intramolecular orientation occurs in the system under consideration in addition to the normal molecular orientation process, then the existence of two relaxation times is obviously possible. Smyth¹¹ has reviewed the various types of intramolecular motion, which can in principle contribute to the total dielectric dispersion of a compound. Of the various possibilities considered, the commonest example of a second relaxation time seems to be that associated with the intramolecular rotation of a polar group about one of the principal axes of the molecule, when the direction of this axis does not coincide with the direction of the dipole moment of the group. In this case, the component (μ_1) of the molecular dipole lying along the axis about which the group rotates will be associated with the over-all molecular orientation, which in turn will be characterized by the larger relaxation time (τ_1). The component (μ_2) of the group moment perpendicular to the axis of rotation of the group will be associated with the intramolecular rotation of the group corresponding to the smaller relaxation time (τ_2). In

τ_1 and τ_2 as near as possible to the final values before computer analysis of the experimental data is attempted, and Figures 1 and 2 are suitable for this purpose.

The dielectric dispersion data of a variety of organic compounds have been analyzed to yield two relaxation times. A selection of these compounds is given in Table II,¹³ in which reported values of the relaxation times are compared with those obtained by interpolation from Figures 1 and 2. In some cases, literature values of τ_1 and τ_2 were calculated by different procedures from the one employed in the numerical computations undertaken for this paper. However, it is evident that in most cases the estimated values of τ_1/τ_0 and τ_2/τ_0 are within about 20% of those given in the literature, so that Figures 1 and 2 seem to provide a convenient method for obtaining initial estimates required for computational purposes.

Acknowledgment. We thank the Science Research Council for a research studentship to P. C. Knight.

(12) E. L. Grubb and C. P. Smyth, *J. Am. Chem. Soc.*, **83**, 4873 (1961).

(13) F. K. Fong and C. P. Smyth, *ibid.*, **85**, 1565 (1963).

Mass Spectrometric Studies at High Temperatures. XXVII. The Reactions of Aluminum Vapor with $S_2(g)$, $Se_2(g)$, and $Te_2(g)$

by P. J. Ficalora, J. W. Hastie, and J. L. Margrave

Department of Chemistry, Rice University, Houston, Texas 77001 (Received October 3, 1967)

High-temperature studies of the various species present when $Al(g)$ is equilibrated with $S_2(g)$, $Se_2(g)$, or $Te_2(g)$ have yielded thermodynamic data for the molecules $AlX(g)$, $Al_2X(g)$, and $Al_2X_2(g)$ when $X = S, Se, \text{ or } Te$. The species $AlTe_2(g)$ has also been observed. Bond energies have been evaluated and the trends correlated on the basis of the periodic table.

Introduction

Mass spectrometric studies^{1,2} have shown that $Al_2O_3(s)$ vaporizes to form $AlO(g)$, $Al_2O(g)$, and $Al_2O_2(g)$ molecules, and the heats of reaction involving the dissociation of the various species to the gaseous elements or lower molecular weight species were measured.

The present study of the reactions of $Al(g)$ with $S_2(g)$ and $Se_2(g)$ and $Te_2(g)$ provides sufficient data for correlating the energetics of the various reactions for the different chalcogens and obtaining a more fundamental understanding of the nature of the bonds involved.

Experimental Section

A Bendix time-of-flight mass spectrometer and Knudsen assembly similar to those previously described^{3,4} were used. Aluminum metal contained in a small tantalum crucible was placed in a larger tantalum Knudsen cell, having a knife-edge effusion hole of 0.5-mm diameter, which was loaded with either Cr_2S_3 , Cr_2Se_3 , or Cr_2Te_3 . The vaporization of aluminum produced $Al(g)$, and the decomposition of Cr_2X_3 produced $X_2(g)$ where $X = S, Se, \text{ or } Te$. Heating was accomplished by radiation and electron bombardment from tungsten filaments, and temperatures were measured with a Pt—Pt—10% Rh thermocouple located in a hole in the bottom of the cell. It was found necessary to protect the thermocouple from the $X_2(g)$ with a 0.5-mm tantalum foil cap.

Composition of the Vapor

Al(g) + S₂(g) Equilibria. The molecular ions observed in this system and their relative intensities at 15 eV are given in Table I. The ions were identified as species effusing from the Knudsen cell by their mass, their isotopic distribution, shutterability, and their appearance potentials. Ionization-efficiency curves showed that several molecular precursors existed for some of the ions; e.g., the AlS^+ ion intensity was due to $AlS(g)$ as well as fragments from Al_2S and $Al_2S_2(g)$. The ionization-efficiency curves for this system are

given in Figure 1, and breaks in the curves indicate the formation of an ion from several precursors. Appearance potentials (Table I) were measured by the vanishing-current method with water and argon⁵ as calibrants. Since the ionization potentials of Al and S_2 are known⁵ and could be reproduced to within ± 0.2 eV, they served as a set of secondary standards.

Table I: Appearance Potentials (AP)^a and Relative Intensities (*I*)^b

Ion	X						
	O	S		Se		Te	
	AP	AP	<i>I</i>	AP	<i>I</i>	AP	<i>I</i>
AlX^+	9.5	9.5	0.95	8.3	0.60	9.0	0.50
Al_2X^+	7.7	9.0	1.0	6.0	1.0	10.0	0.55
$Al_2X_2^+$	9.9	9.5	0.04	9.0	0.90	10.0	1.0
AlX_2^+	6.5	0.85

^a AP is given in electron volts (± 0.5). ^b Arbitrary units.

The shapes of the ionization-efficiency curves as well as the appearance potentials indicate that Al^+ , S_2^+ , AlS^+ , and $Al_2S_2^+$ are parent ions up to several electron volts above their appearance potentials. S^+ and Al_2^+ were observed as fragments. No higher polymers of sulfur molecules were observed. The ion-intensity-temperature data, shown in Figure 2, were collected at 10.5 eV, i.e., below the lowest break in any of the ionization efficiency curves, so that there were no significant contributions due to fragmentation.

Al(g) + Se₂(g) Equilibria. The appearance poten-

(1) J. Drowart, G. DeMaria, R. P. Burns, and M. G. Inghram, *J. Chem. Phys.*, **32**, 1366 (1960).

(2) R. F. Porter, P. Shissel, and M. G. Inghram, *ibid.*, **23**, 339 (1955).

(3) D. B. Harrington in "Encyclopedia of Spectroscopy," C. F. Clark, Ed., Reinhold Publishing Corp., New York, N. Y., 1960, p 628.

(4) A. Kant, *J. Chem. Phys.*, **41**, 1872 (1964).

(5) R. W. Kiser, "Introduction to Mass Spectrometry and Its Applications," Prentice-Hall, Inc., Englewood Cliffs, N. J., 1965.

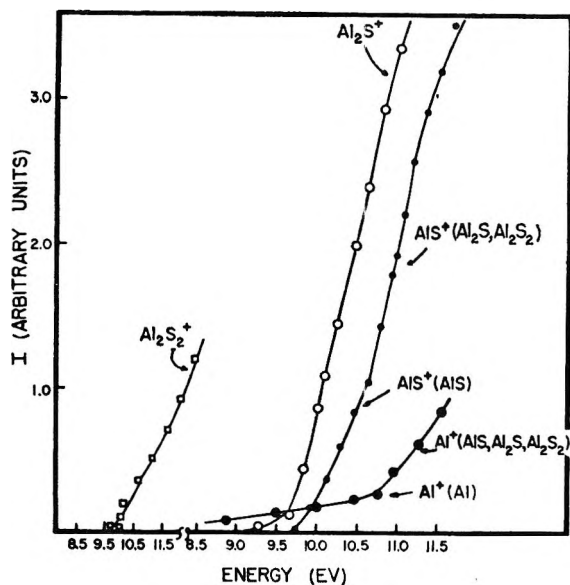


Figure 1. Ionization-efficiency curves for species in the Al(g)-S₂(g) system.

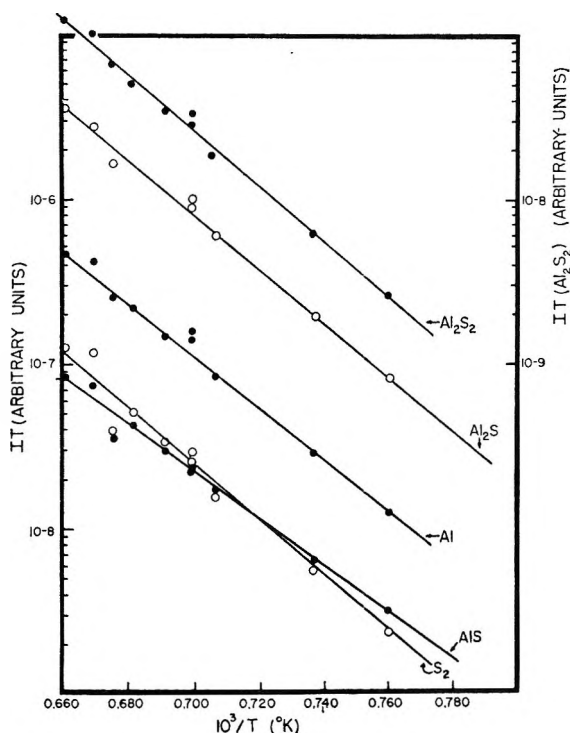


Figure 2. Ion-intensity data for the Al(g)-S₂(g) system as a function of temperature.

tials and the relative intensities of the species observed in this system are given in Table I. Again the appearance of the secondary standards, Al⁶ and Se₂,⁶ were reproduced to within ±0.2 eV.

The ions Al⁺, Se₂⁺, AlSe⁺, and Al₂Se₂⁺ were found to be parents, while Se⁺ and Al₂⁺ were fragments. No higher polymers of selenium were observed. All ion-intensity data were collected at 10.0 eV for the same reason mentioned previously and are shown in Figure 3.

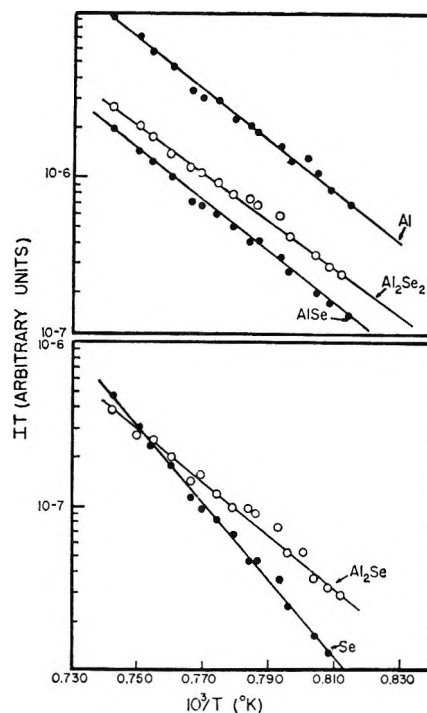


Figure 3. Ion-intensity data for the Al(g)-Se₂(g) system as a function of temperature.

Al(g) + Te₂(g) Equilibria. Appearance potentials and relative intensities of the species observed in this system are given in Table I. The appearance potentials of the secondary standards Al⁺ and Te₂⁺ were reproduced⁷ to within ±0.2 eV.

The ions Al⁺, Te₂⁺, AlTe⁺, Al₂Te⁺, and AlTe₂⁺ were found to be parents while Te⁺ and Al₂⁺ were fragments. The ion AlTe₂⁺ has no analog in the preceding systems and AlTe₂(g) is very stable. The absence of AlX₂ where X = O, S, or Se is consistent with the trends in the thermodynamic properties of these systems, as indicated in Table II, and a similar behavior occurs in the Sn(g)-S₂(g),⁸ -Se₂(g),⁹ and -Te₂(g)⁹ systems.

No higher polymers of tellurium were observed. All of the ion-intensity data shown in Figure 4 were taken at electron energies where fragmentation was negligible.

Calculations

The heat of vaporization of aluminum measured in this study ($\Delta H_{v, 298}^{\circ} = 75.0 \pm 2.0$ kcal/mol) is in excellent agreement with the accepted value^{10,11} sug-

(6) J. Berkowitz and W. A. Chupka, *J. Chem. Phys.*, **45**, 4289 (1966).

(7) R. Colin, *Ind. Chim. Belge*, **26**, 51 (1961).

(8) R. Colin and J. Drowart, *J. Chem. Phys.*, **37**, 1120 (1962).

(9) R. Colin and J. Drowart, *Trans. Faraday Soc.*, **60**, 673 (1964).

(10) L. Brewer and A. W. Searcy, *J. Amer. Chem. Soc.*, **73**, 5309 (1951).

(11) "JANAF Thermochemical Tables," D. R. Stull, Ed., The Dow Chemical Co., Midland, Mich., 1963; U. S. Government Document No. PB-168-370.

Table II: Second-Law Enthalpies and Entropies^a

Reaction ^b	$-\Delta H^\circ_T$ (temp ^c = 2300°K, X = O), kcal/mol	$-\Delta H^\circ_T$ (temp ^c = 1414°K, X = S), kcal/mol	$-\Delta S^\circ_T$ (temp ^c = 1414°K, X = S), eu	$-\Delta H^\circ_T$ (temp ^c = 1292°K, X = Se), kcal/mol	$-\Delta S^\circ_T$ (temp ^c = 1292°K, X = Se), eu	$-\Delta H^\circ_T$ (temp ^c = 1292°K, X = Te), kcal/mol	$-\Delta S^\circ_T$ (temp ^c = 1292°K, X = Te), eu
$\text{Al} + \frac{1}{2}\text{X}_2 = \text{AlX}$	57 ± 5	47.0	19.8	53.5	27.5	56.5	31.3
$2\text{Al} + \frac{1}{2}\text{X}_2 = \text{Al}_2\text{X}$	187 ± 7	107.0	36.1	122.4	54.8	129.7	59.5
$2\text{Al} + \text{X}_2 = \text{Al}_2\text{X}_2$	249	152.0	22.0	182.9	24.0	305.5	21.6
$\text{Al} + \text{AlX} = \text{Al}_2\text{X}$	131 ± 5	60.3	16.3	74.3	27.3	72.3	28.2
$2\text{AlX} = \text{Al}_2\text{X}_2$	135 ± 5	58.0	17.7	75.5	31.0	90.0	41.0
$\text{Al} + \text{X}_2 = \text{AlX}_2$	125.5	71.3
$\text{AlX} + \frac{1}{2}\text{X}_2 = \text{AlX}_2$	68.0	34.2
$\text{Al} + \text{AlX}_2 = \text{Al}_2\text{X}_2$	80.0	34.6

^a Uncertainties are $\approx 4\text{--}6\%$, unless indicated. ^b All species are gaseous. ^c Median temperature.

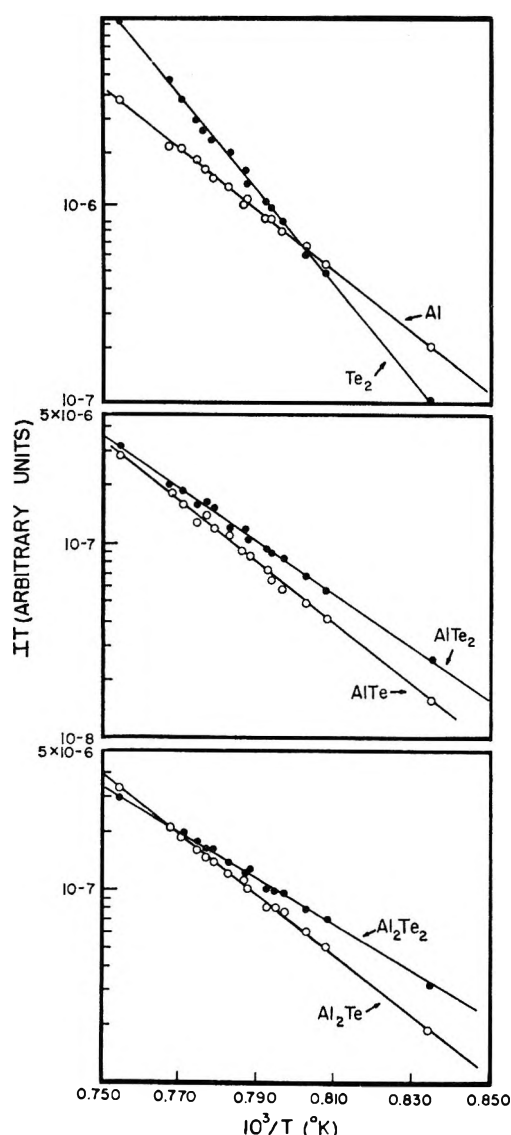


Figure 4. Ion-intensity data for the $\text{Al}(\text{g})\text{--Te}_2(\text{g})$ system as a function of temperature.

gesting that $\text{Al}(\text{l})$ was probably at unit activity. Further evidence for this fact is that elemental aluminum and not a solid sulfide, selenide, or telluride was

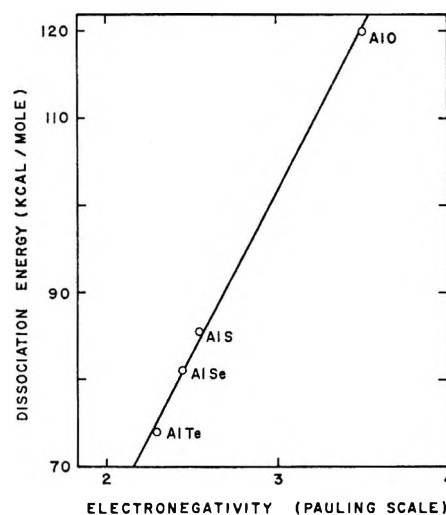


Figure 5. Dissociation energies of aluminum chalcogenides as a function of the chalcogen electronegativities.

recoverable after each experiment. An X-ray powder diffraction pattern, taken in the usual way, showed lines due to aluminum alone. Therefore, aluminum was used as an internal standard to convert ion intensities to pressures using the relation

$$P \approx \frac{IT}{\sigma\gamma} \left(\frac{A}{E - A} \right)$$

where P is the pressure,¹² I is the ion intensity, T is the temperature, σ is the ionization cross section, γ is the multiplier efficiency, A is the appearance potential, and E is the energy of the ionizing electrons. Cross sections were estimated by using the Otvos and Stevenson¹³ rule and the data of Mann.¹⁴ Efficiency terms relative to aluminum were then calculated from the relation¹⁵

(12) An. N. Nesmeyanov, "Vapour Pressure of the Elements," Academic Press Inc., New York, N. Y., 1963, p 234.

(13) J. W. Otvos and D. P. Stevenson, *J. Amer. Chem. Soc.*, **78**, 546 (1956).

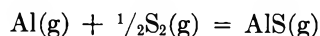
(14) J. B. Mann, *J. Chem. Phys.*, **46**, 1646 (1967).

(15) R. C. Schoonmaker and R. F. Porter, *ibid.*, **30**, 283 (1959).

$$\frac{\gamma_1}{\gamma_2} \approx \left(\frac{M_2}{M_1}\right)^{1/2}$$

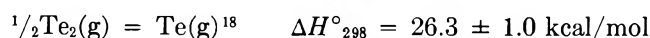
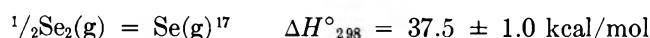
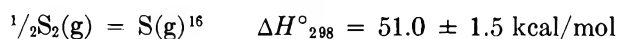
where M is the molecular weight. With these partial pressures, free energies for the various reactions were obtained, and a combination of these energies with the second-law enthalpies provided corresponding entropies, as given in Table II.

Since free-energy functions are available for Al(g), S₂(g), and AlS(g),¹¹ a third-law calculation for the reaction



yielded $\Delta H^\circ_{298} = -35.4 \pm 2.0$ kcal/mol, as compared to a second-law value of $\Delta H^\circ_{298} = -37.3 \pm 3.0$ kcal/mol. The agreement between second- and third-law values allows an uncertainty of $\leq \pm 3$ eu for the calculated entropies.

Finally, the dissociation energies of AlS(g), AlSe(g), and AlTe(g), and heats of formation of the various species were calculated as presented in Table III, based on the following heats of reaction.



The selenides and tellurides were assumed to have similar heat capacities to those of the sulfides.¹¹

Discussion

The dissociation energy of AlS is thus established as 86.0 ± 3.0 kcal/mol. By analogy with the AlO molecule and by adding 17% to the dissociation energy obtained from a linear extrapolation of the vibrational levels, the JANAF tables predicted $D^\circ_{298}(\text{AlS}) \approx 95$ kcal/mol, in fair agreement.

The AlX bond strengths can be used to elucidate the nature of the bonds. If one assumes that the bonds are covalent, then the dissociation energies should increase with the increasing polarizability from oxygen to tellurium. The values shown in Table III along with a value of 115.0 ± 5.0 kcal/mol for the heat of dissociation of AlO(g)¹¹ show that the above is not the

case; in fact, the dissociation energies decrease through the oxygen family.

If the relation given by Pauling,¹⁹ relating dissociation energy to electronegativity, is used to calculate the difference in electronegativities between the AlX species and this difference is used to deduce the per cent ionic character,²⁰ one finds that the AlO bond is 98% ionic, the AlS bond is 95%, the AlSe bond is 93%, and the AlTe bond is 90% ionic.

If the above calculations are meaningful, then the dissociation energies for the aluminum chalcogenides should follow the trend for the changes of electronegativities from oxygen to tellurium. Figure 5 shows the variation of dissociation energies with the electronegativities from oxygen to tellurium. The fact that the dissociation energies follow the changes in electronegativities indicates that the AlX bonds are largely ionic. Furthermore, this trend allows an estimation of D° (AlPo) equal to 70 ± 3 kcal/mol.

The trend in the heats of dimerization also proves valuable in understanding the bonding in these molecules. If one assumes that the structure of Al₂X₂(g), the dimer, is like that of the alkali halide dimers,²⁰ the relatively small increase in stability from Al₂S₂(g) to Al₂Te₂(g) can be explained. This assumption is considered consistent with the high per cent of ionic character of the AlX bond. The repulsive terms in the coulombic expression for the potential energy of the Al₂X₂(g) molecules should decrease in value from X = S to X = Te owing to the increasing size of the chalcogen ions. If the repulsive terms decrease faster than the attractive terms, one should find, and does in this case, that the stability of the molecules increases from X = S to X = Te.

The unusually high stability of the Al₂O₂(g) molecule ($D^\circ_0 = 365 \pm 7$ kcal/mol)¹ is the reverse of what one might expect to find from the above discussion and indicates a very different type of bonding in this case. This behavior has been noted for the Al₂X(g) molecules by Mal'tsev,²¹ who suggested that the subsulfide should have a bond type and configuration different from that of the suboxide.

Acknowledgment. This work was supported by the National Aeronautics and Space Administration and by the Robert A. Welch Foundation.

Table III: Dissociation Energies of AlX Molecules (X = O, S, Se, and Te)

Species	D°_{298} , kcal/mol
AlO	115 ± 5.0
AlS	86.0 ± 3.0
AlSe	81.0 ± 3.0
AlTe	74.0 ± 3.0

(16) J. Berkowitz and J. R. Marquart, *J. Chem. Phys.*, **30**, 283 (1963).

(17) M. Jeunehomme, Ph.D. Thesis, University of Brussels, Brussels, 1962.

(18) R. F. Porter, *J. Chem. Phys.*, **34**, 583 (1961).

(19) L. Pauling, "The Nature of the Chemical Bond," 3rd ed., Cornell University Press, Ithaca, N. Y., 1960.

(20) S. H. Bauer and R. F. Porter, "Molten Salt Chemistry," M. Blander, Ed., Interscience Publishing Corp., New York, N. Y., 1964, p 650.

(21) A. A. Mal'tsev and V. F. Shevel'kov, *Teplofiz. Vys. Temp.*, **2**, 650 (1964).

The Critical Temperature and Coexistence Curve for Aluminum Bromide¹

by J. W. Johnson, W. J. Silva, and Daniel Cubicciotti

Stanford Research Institute, Menlo Park, California 94025 (Received October 31, 1967)

The critical temperature of aluminum bromide has been determined to be $763 \pm 2^\circ\text{K}$, and the critical density has been found by extrapolation to be $0.8605 \pm 0.0023 \text{ g/cc}$. The experimental densities of the coexisting liquid and vapor phases were fitted to a modified Guggenheim relation

$$\rho(\text{g/cc}) = 0.8608 + 0.8968 \left(\frac{762.7 - T}{762.7} \right) \pm 1.6535 \left(\frac{762.7 - T}{762.7} \right)^{0.319}$$

over the temperature range 591 to 760°K . In the last term the upper sign refers to the liquid and the lower to the vapor. Unlike the bismuth halides and mercuric chloride, this salt does not follow the $T^{1/3}$ relation.

Introduction

Previous work in this laboratory has involved the determination of the critical temperatures and coexistence curves of bismuth chloride² and bromide³ and mercuric chloride.⁴ The Guggenheim relation⁵ has been used to describe the coexistence curves for these salts. Literature data on aluminum bromide⁶ indicated some modification of the exponents in the Guggenheim relation might be required. This is a report of the determination of the coexistence curve and critical temperature of aluminum bromide by methods employed for the other salts.

Experimental Section

Fisher certified reagent aluminum bromide was evacuated overnight at room temperature and then sublimed at 70° through a sintered glass filter into Pyrex ampoules. After approximately one-half of the aluminum bromide had been transferred, the sublimation was stopped and the residue was discarded. The ampoules, each containing about 5 g of the salt, were sealed off under vacuum and stored for future use. Bromine content of this preparation was found to average 89.95%, compared to a theoretical content of 89.88%.

The quartz tubes intended for critical temperature and liquid or vapor density measurements were attached to a manifold, one end of which was sealed to a vacuum line. To load these tubes an ampoule containing the salt was opened and inserted into the other end of the manifold; this end was then sealed off and the system was evacuated. The aluminum bromide was sublimed out of the storage ampoule, condensed in the upper portion of the manifold, and the end containing the empty ampoule was sealed off under vacuum. The manifold was then sealed off from the vacuum line and the desired amount of salt was distilled into the individual quartz tubes under its own vapor pressure. The quartz tubes containing the salt were sealed off

from the manifold and stored until the experimental measurements could be made.

The liquid phase densities were all determined by the quartz float method described previously,² as were some of the vapor densities near the critical temperature. The quartz floats of known density were placed in the tubes prior to attachment to the manifold. The filling was such as to ensure sufficient liquid or vapor volume to support the float entirely within the phase whose density was to be determined. All of these tubes were 5 cm long, but the bore varied depending on the diameter of the float used. Those tubes intended for the determination of the critical temperature were 5 cm long, 4 mm bore by 6 mm o.d., and were approximately one-third full of molten aluminum bromide at the melting point. In general the bore of the tube was 2 mm larger than the diameter of the float to provide sufficient clearance for vertical movement of the float.

Vapor density measurements below 0.3 g/cc (732°K) could not be made by the float method, since it was not possible to construct floats of reasonable size having densities lower than this value. Therefore, vapor density determinations over the range 540 to 745°K (0.017 to 0.370 g/cc) were made by a dilatometer method. In this method the change in the liquid phase volume is measured as the total volume of a system containing a fixed amount of aluminum bromide is reduced. First the liquid phase volume is measured,

(1) This work was made possible by the support of the Research Division of the U. S. Atomic Energy Commission under Contract No. AT(04-3)-106.

(2) J. W. Johnson and D. Cubicciotti, *J. Phys. Chem.*, **68**, 2235 (1964).

(3) J. W. Johnson, D. Cubicciotti, and W. J. Silva, *ibid.*, **69**, 1989 (1965).

(4) J. W. Johnson, W. J. Silva, and D. Cubicciotti, *ibid.*, **70**, 1169 (1966).

(5) E. A. Guggenheim, *J. Chem. Phys.*, **13**, 253 (1945).

(6) D. I. Zhuralev, *Zh. Fiz. Khim.*, **10**, 325 (1937).

over a range of temperature, in a given tube. Then all the salt is distilled to the bottom of the tube and a portion of the top is sealed off, reducing the total volume of the tube while the mass of aluminum bromide remains the same. The measurement of the liquid phase volume as a function of temperature was repeated for the new tube volume. For such a system the masses and volumes of each phase are related by the two equations

$$M = \rho_1 v_1' + \rho_2 v_2' \quad (1a)$$

$$M = \rho_1 v_1'' + \rho_2 v_2'' \quad (1b)$$

where M is the total mass of aluminum bromide, $\rho_1 v_1$ and $\rho_2 v_2$ denote the density and volume of the coexisting liquid and vapor phases, respectively, and the single and double primes refer to different total volumes of the system. The vapor phase volumes can be expressed as

$$v_2' = V' - v_1'; \quad v_2'' = V'' - v_1''$$

where V' and V'' represent the total volume of the system in the two cases. Substituting these relations into eq 1a and 1b and solving simultaneously gives

$$\rho_2 = \frac{\rho_1(v_1' - v_1'')}{(V' - V'') + (v_1' - v_1'')} \quad (2)$$

The reduction in total volume, $V' - V''$, is a constant at all temperatures; the other quantities in eq 2 are temperature dependent.

It is apparent that the larger the total volume reduction of the system the greater the difference in the liquid phase volumes at a given temperature. Thus, the larger the volume reductions the greater the accuracy of determination of the vapor densities. To cover the lower range of temperatures and densities, *i.e.*, 540 to 650°K or 0.017 to 0.100 g/cc, a dilatometer having an initial volume of 1.6105 cc and a final volume of 0.1429 cc or a volume reduction of 1.4676 cc was used. This dilatometer consisted of a 5-cm section of nominal 2-mm bore quartz tubing sealed to a 2-cm section nominal 8-mm bore quartz tubing. The 8-mm bore section was sealed off in the volume-reduction step, leaving approximately 4.5 cm of 2-mm bore tubing as the final tube. To cover the range from 660 to 745°K, or 0.100 to 0.370 g/cc, two nominal 5-mm bore tubes were used as dilatometers.

The total internal volume of the sealed dilatometer was determined as described in ref 4. That is, the volume of the dilatometer tube, sealed at one end, was determined as a function of height above the bottom by calibration with mercury. After the salt was distilled into the tube it was sealed just below the top of the calibrated range under vacuum. The volume of the liquid sample was determined from the height of the liquid level (bottom of the meniscus) above the bottom of the tube. The tube was then inverted in

the furnace and the volume of the gas phase was determined in the calibrated portion of the tube at the same temperature. The true liquid phase volume was larger than the measured liquid volume by the amount of meniscus error while the true gas phase volume was smaller than the measured gas volume by the same meniscus error. Addition of these two volumes eliminates the meniscus error. The initial volumes of the two dilatometers were 0.82768 and 0.88895 and their final volumes were 0.73411 and 0.74752 cc, respectively. The uncertainty in each of these volumes is estimated to be 5×10^{-5} cc.

The utility of the dilatometer method of determining vapor density depends on the accuracy and precision with which the liquid volumes can be determined. The section of 2-mm bore tubing was calibrated with mercury to determine the volume as a function of height of liquid, and an equation was developed to fit the data for each dilatometer. The difference in absolute volume of the aluminum bromide obtained from reading the bottom of the meniscus and the top of the mercury meniscus is eliminated, since only the differences in liquid phase volume are used in the calculation of vapor densities. The precision of measurements on the liquid phase volumes is illustrated in Figures 1a and b, which show the liquid phase volume differences for the largest and smallest dilatometer used in this work.

It is believed that the dilatometer method for determining the vapor phase densities is subject to less error than the technique of noting the temperature at which the last of the liquid phase disappears. In the latter method any less volatile impurities will tend to be concentrated in the liquid phase and lower the vapor pressure. This will result in raising the temperature of liquid phase disappearance above the true value. Thus while the vapor density calculated from the volume and mass of material will be correct, the temperature associated with this density will be too high. In the dilatometer method this error will be reduced, since an appreciable volume of liquid phase is always present, resulting in a lower concentration of impurities.

Results and Discussion

The liquid-vapor critical transition was observed in each of three tubes with increasing and decreasing temperatures. The volume of each tube and the mass of the salt were determined, and from these values the density of the critical fluid was calculated. The bromine content of the salt in each tube was also determined by precipitation as silver bromide. The results are given in Table I.

The temperature range over which the liquid-vapor interface disappears and reappears is not large, but the uncertainty in the temperature measurement generated by a finite heating and cooling rate make it

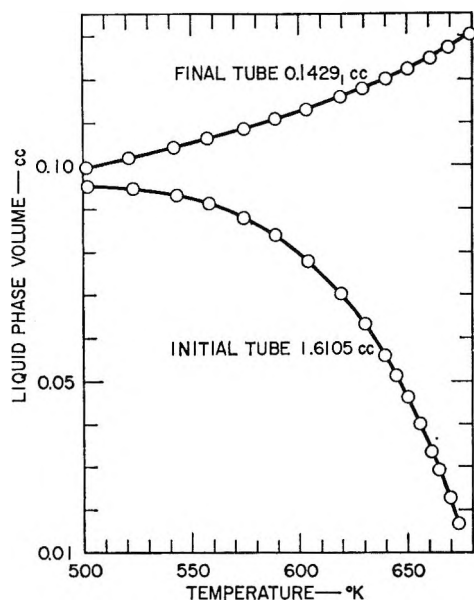


Figure 1a. Variation in liquid phase volume with temperature (large tube).

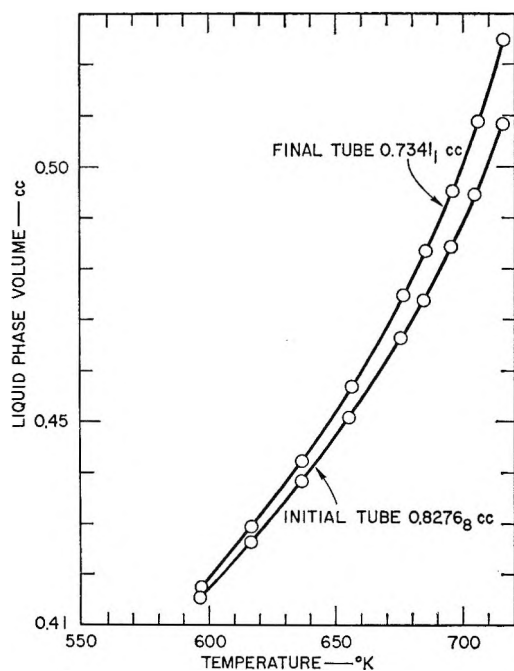


Figure 1b. Variation in liquid phase volume with temperature (small tube).

advisable to assign an error limit of $\pm 2^\circ$ to the critical temperature. The critical temperature of $763 \pm 2^\circ\text{K}$ found in this work is 5° below the 768°K reported by Zhuralev⁶ and 9° below the $772 \pm 1.5^\circ\text{K}$ given by Rotinjanz and Suchodski.⁷

The appearance of the aluminum bromide system as it undergoes the critical transition is very similar to that observed for mercuric chloride.⁴ On heating, the meniscus becomes a flat bright line which fades into a gray band that diffuses through the tube. On cool-

Table I: Observation of Meniscus in the Critical Region

Tube no.	Meniscus observation Disappearance, $T, ^\circ\text{K}$	Appearance, $T, ^\circ\text{K}$	Liquid height, cm	Density, g/cc	Bromine, %
1	763.8 763.5	763.3 763.4	1.850	0.7130	89.98
2	762.6 763.4	762.3 762.4	2.370	0.9311	89.90
3	763.2	763.5	0.708	0.6956	89.96
Av	763.3	763.0			89.95
Accepted value			$763 \pm 2^\circ\text{K}$	Theoretical	89.88

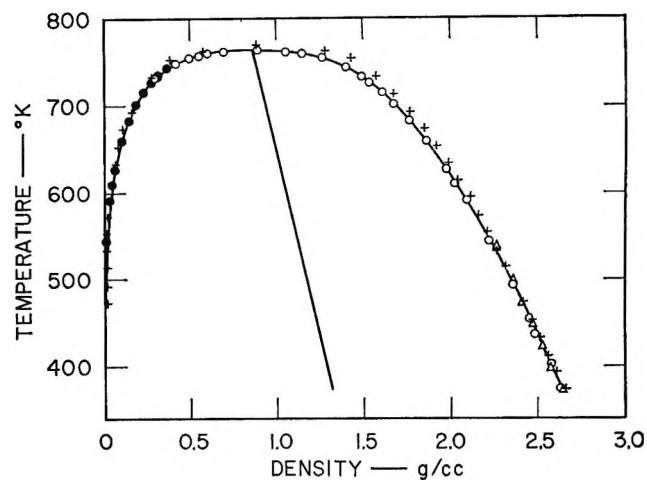


Figure 2. Coexistence curve for aluminum bromide: \circ , float data; \bullet , dilatometer data; $+$, Zhuralev; Δ , Biltz and Voigt.

ing from the supercritical region, a reddish brown cloud forms as a band across the tube; out of this a black line emerges, then droplets appear in the vapor space and bubbles, which are in violent motion in the liquid space.

The orthobaric density data for the liquid and vapor phases of aluminum bromide are presented in Table II and shown as a coexistence curve in Figure 2. The average density of the two phases from 401.2 to 742.6°K is related to the temperature by the expression

$$\frac{\rho_l + \rho_g}{2} = 1.7576 - 1.1758 \times 10^{-3} T^\circ\text{K} (\pm 0.0013 \text{ g/cc}) \quad (3)$$

Extrapolation of eq 3 to the critical temperature of $763 \pm 2^\circ\text{K}$ results in a critical density of $0.8605 \pm 0.0023 \text{ g/cc}$, where the uncertainty corresponds to the uncertainty of $\pm 2^\circ$ in the critical temperature.

(7) L. Rotinjanz and W. Suchodski, *Z. Physik. Chem.*, **87**, 635 (1914).

Table II: Experimental Densities of Aluminum Bromide

T, °K	Liquid-phase density, g/cc		Vapor-phase density, g/cc			Average density, g/cc	
	Obsd	Calcd	Obsd	Calcd	Ideal	Obsd	Calcd
374.3	2.6300	2.6320 ^a
401.2	2.5728	2.5711 ^a
436.9	2.4896	2.4885 ^a
454.5	2.4480	2.4467 ^a
492.8	2.3513	2.3528 ^a
543.5	2.2190	2.2210 ^a	0.0171	...	0.0165 ^b	1.1181	1.1185
591.0	2.0910	2.0902	0.0388	0.0351	0.0362 ^b	1.0649	1.0627
609.8	2.0220	2.0309	0.0519	0.0503	0.0472 ^b	1.0370	1.0406
626.3	1.9754	1.9760	0.0665	0.0664	0.0586 ^b	1.0210	1.0211
658.1	1.8612	1.8611	0.1047	0.1065	0.0867 ^b	0.9830	0.9838
683.0	1.7612	1.7589	0.1500	0.1501	...	0.9556	0.9545
700.8	1.6750	1.6757	0.1864	0.1915	...	0.9307	0.9336
714.1	1.6061	1.6049	0.2326	0.2309	...	0.9194	0.9179
726.2	1.5318	1.5307	0.2743	0.2767	...	0.9031	0.9037
732.1	0.3000	0.3041	0.8968
733.2	1.4883	1.4815	0.3046	0.3097	...	0.8964	0.8955
734.4	0.3173	0.3160	0.8941
742.6	1.4000	1.4026	0.3670	0.3662	...	0.8835	0.8844
748.9	0.4192	0.4199	0.8770
754.4	1.2607	1.2614	0.8706
754.9	0.4938	0.4869	0.8700
758.4	0.5504	0.5489	0.8659
759.8	1.1466	1.1438	0.8642
760.3	0.6015	0.6006	0.8636
761.5	0.6968	(0.6512)	0.8622
761.6	1.0051	(1.0673)	0.8621
762.3	0.8946	(1.0099)	0.8613
762.7	0.8852	(0.8608)	0.8608
	Av dev	±0.0021	Av dev	±0.0020		Av dev	±0.0013

^a Calculated by power series. ^b Calculated by ideal gas relation, assuming Al₂Br₃ as the only molecular species.

The coexistence curve, shown as a solid line in Figure 2, is calculated from a Guggenheim relation⁵

$$\rho = \rho_c + A \left(\frac{T_c - T}{T_c} \right) \pm B \left(\frac{T_c - T}{T_c} \right)^n \quad (4)$$

where ρ_c and T_c are identified with the critical density and critical temperature, n usually has the value of $1/3$, and A and B are empirical constants adjusted to fit the data. The positive sign is applied to the liquid phase and the negative sign is used for the vapor phase.

The data from Table II were fitted by the expression

$$\rho = 0.8608 + 0.8968 \left(\frac{T_c - T}{T_c} \right) \pm 1.6535 \left(\frac{T_c - T}{T_c} \right)^{0.319} \quad (5)$$

with average deviations of ± 0.0018 g/cc and ± 0.0023 g/cc for the liquid and vapor phase densities over the temperature range from 591.0 to 760.3°K. Below 591°K, the vapor phase densities calculated by eq 5 were too low, becoming zero at 524°K, and the calcu-

lated liquid densities were too high. The liquid phase densities in the range 374.3 to 543.5°K were fitted with a power series in temperature

$$\rho_l = 3.5590 - 3.1422 \times 10^{-3}T + 2.9431 \times 10^{-6}T^2 - 3.1121 \times 10^{-9}T^3 \quad (6)$$

The constants T_c , n , and B of eq 5 were evaluated by utilizing the difference in the liquid and vapor densities. From eq 4 this difference is

$$(\rho_l - \rho_v) = 2B \left(\frac{T_c - T}{T_c} \right)^n \quad (7)$$

or

$$\log (\rho_l - \rho_v) = \log 2B + n \log \left(\frac{T_c - T}{T_c} \right) \quad (7a)$$

The density differences were plotted against the quantity $(T_c - T)/T_c$ on a logarithmic scale using various values of T_c in the vicinity of 763°K. The value of T_c that gave a straight line over the largest temperature range (indicative of the constancy of n)

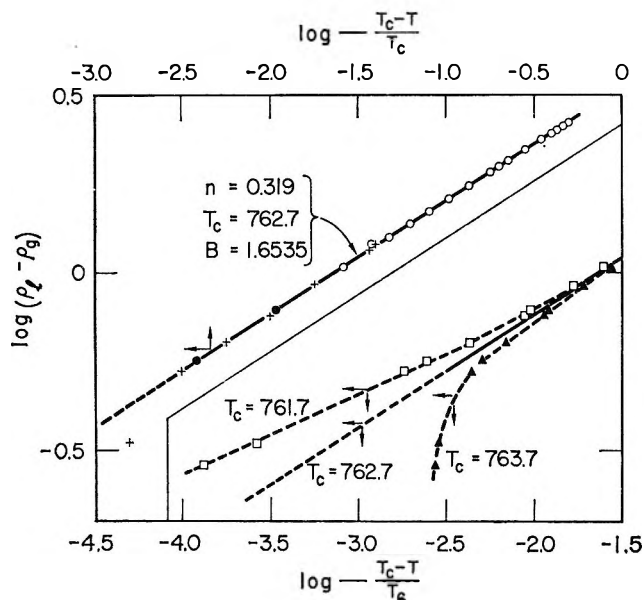


Figure 3. Density difference as a function of temperature: O, dilatometer and float data; +, vapor density only; ●, liquid density only.

was found to be 732.7°K as shown in Figure 3. The linearity of this plot is quite sensitive to the value of T_c . The inset in Figure 3 shows the effect of 1° variation in T_c on the linearity at the high temperatures. Above 742.6°K, where simultaneous values of the liquid and vapor densities are not available, the density difference was calculated using the average density value from eq 3 and the experimentally observed liquid or vapor density. The slope of the straight line in Figure 3 defines n as 0.319 using $T_c = 762.7^\circ\text{K}$, and B was calculated to be 1.6535. From eq 4 the

average density of coexisting liquid and vapor phases can be expressed as

$$\frac{\rho_l + \rho_g}{2} = \rho_c + A \left(\frac{T_c - T}{T_c} \right) \quad (8)$$

and converting eq 3 into this form, using $T_c = 762.7^\circ\text{K}$, ρ_c and A were found to be 0.8608 g/cc and 0.8968, respectively.

The value of $T_c = 762.7^\circ\text{K}$, derived in this manner, is very close to the value of $763 \pm 2^\circ\text{K}$ selected from the experimental observations, and it is tempting to call this the true critical temperature. However, eq 5 is an empirical relation and does not fit the experimental data above 760.3°K; indeed no reasonable assumption of a value for T_c could be found that does fit in this region. It is probable that the experimental data are at fault due to the turbulence in the system impeding the free movement of the floats.

The present work is compared with previous data on this compound in Figure 2 where the crosses represent the data of Zhuralev⁶ and the triangles are the data points reported by Biltz and Voight.⁸ Agreement is good at low temperatures, but the discrepancy from Zhuralev's data becomes large above 600°K.

For BiCl_3 , BiBr_3 , and HgCl_2 the value of n in the Guggenheim relation (eq 4 above) was $1/3$ —the same as for many organic fluids. The data for aluminum bromide are best fit by $n = 0.319$. Although n is sensitive to the nature of the fluid,⁹ it is not clear without further information on other similar systems whether the difference in the values of n is significant.

(8) W. Biltz and A. Voight, *Z. Anorg. Allgem. Chem.*, **126**, 39 (1923).

(9) L. P. Kadanoff, *et al.*, *Rev. Mod. Phys.*, **39**, 395 (1967).

The Vapor Pressure and Enthalpy of Vaporization of Molten

Aluminum Bromide to the Critical Point¹

by J. W. Johnson, W. J. Silva, and Daniel Cubicciotti

Stanford Research Institute, Menlo Park, California 94025 (Received October 31, 1967)

The vapor pressure of molten aluminum bromide has been measured by an inverted capillary technique from 536°K and 1.18 atm to 761°K and 28.3 atm. The data are represented by the relation $\log P(\text{atm}) = 4.6688 - 2451.9/T^\circ\text{K}$ from 639 to 761°K with an average deviation of 0.70% for the 14 experimental points. Extrapolation to the critical temperature ($763 \pm 2^\circ\text{K}$) gives a critical pressure of 28.5 ± 0.6 atm. From 536 to 639°K the Antoine vapor pressure relation, $\log P(\text{atm}) = 4.1893 - 1876.8/(T - 80)$ fits the data with an average deviation of 0.57% for the 15 experimental points. The enthalpy of vaporization has been calculated from 528°K (1 atm) to 761°K.

Introduction

The preceding paper² reported data for the co-existence and critical temperature of aluminum bromide. Fischer, Rahlfs, and Benze³ have determined the vapor pressure up to the normal boiling point (528°K), but experimental data above 1 atm are not available in the literature. This is a report of an investigation of the vapor pressure from the boiling point to temperatures just below the liquid-vapor critical point, and, together with our preceding paper, it characterizes the thermodynamics of vaporization to the critical point.

Experimental Section

The semimicro boiling point method employed for the vapor pressure measurements on bismuth chloride⁴ and mercuric chloride⁵ was used in this work. The apparatus has been described in detail elsewhere.⁶ The aluminum bromide used in this investigation was a part of the material prepared for the critical temperature and orthobaric density measurements.² The bromine content, determined by precipitation as silver bromide, was found to be 89.95% compared to a theoretical bromine content of 89.88%.

Results and Discussion

The vapor pressure of molten aluminum bromide was determined at 28 points over a temperature interval of 536–761°K and a pressure range of 1.18–28.3 atm. The experimental data are presented in Table I and Figure 1. The recorded temperatures are corrected for the temperature gradient between the position of the thermocouple and the liquid surface. These corrections varied from 2 to 3° depending on the temperature. Below 17 atm the observed pressures were corrected by the addition of 0.01 atm for the static head of aluminum bromide. Vapor pressure measurements above 17 atm are recorded to the nearest 0.1 atm, and the correction was negligible.

Two runs were made using different charges of aluminum bromide as indicated in Table I. There is no evidence of systematic deviation between the individual runs. It was found that the data could be fitted by the relation

$$\log P(\text{atm}) = 4.6688 - 2451.9/T^\circ\text{K} \quad (1)$$

from 760.8 to 639.5°K with an average deviation of 0.70% for the 14 experimental points. From 639.5 to 535.8°K the data are represented by the Antoine vapor pressure equation

$$\log P(\text{atm}) = 4.1893 - 1876.8/(T - 80) \quad (2)$$

with an average deviation of 0.57% for the 15 experimental points. As shown in Table I, the pressures calculated by eq 1 and 2 are identical at 639.5°K and the same is true for the calculated values of (dP/dT) at this temperature.

The critical pressure calculated by eq 1 is 28.5 ± 0.6 atm using the critical temperature of $763 \pm 2^\circ\text{K}$ reported previously² for aluminum bromide.

Figure 1 presents the experimental data on a $\log P$ vs. $1/T$ plot. The open circles represent the experimental data points obtained in this investigation and the solid circles are used for the experimental data of Fischer, Rahlfs, and Benze.³ The curve is calculated by eq 1 from 760.8 to 639.5°K and by eq 2 from

(1) This work was made possible by the support of the Research Division of the U. S. Atomic Energy Commission under Contract No. AT(04-3)-106.

(2) J. W. Johnson, W. J. Silva, and D. Cubicciotti, *J. Phys. Chem.*, **72**, 1664 (1968).

(3) W. Fischer, O. Rahlfs, and B. Benze, *Z. Anorg. Allgem. Chem.*, **205**, 1 (1932).

(4) J. W. Johnson, W. J. Silva, and D. Cubicciotti, *J. Phys. Chem.*, **69**, 3916 (1965).

(5) J. W. Johnson, W. J. Silva, and D. Cubicciotti, *ibid.*, **70**, 2985 (1966).

(6) W. J. Silva, J. W. Johnson, and D. Cubicciotti, *Rev. Sci. Instr.*, **36**, 1505 (1965).

Table I: Experimental Vapor Pressures of Aluminum Bromide

Run no.	T, °K	Pressure, atm		% dev	dP/dT × 10 ³
		Obsd	Calcd, eq 2		
2	535.8	1.18	1.18	0	24.54
2	542.4	1.35	1.35	0	27.29
2	550.7	1.59	1.59	0	31.01
1	552.0	1.63	1.63	0	31.62
1	553.1	1.66	1.67	0.60	32.24
2	566.3	2.12	2.14	0.94	39.11
1	566.9	2.13	2.16	1.41	39.37
1	576.4	2.54	2.56	0.79	44.90
1	584.3	2.94	2.93	-0.34	49.79
1	596.2	3.54	3.58	1.13	58.06
2	597.5	3.66	3.65	-0.27	58.90
2	606.6	4.17	4.22	1.20	65.76
1	615.4	4.88	4.83	-1.02	67.76
2	621.0	5.25	5.25	0	77.52
2	639.5	6.78	6.84	0.88	94.43
Av ±0.57%					
			Calcd, eq 1		
2	639.5	6.78	6.84	0.88	94.43
1	647.6	7.70	7.64	-0.78	102.85
2	652.7	8.12	8.17	0.62	108.27
2	664.2	9.41	9.49	0.85	121.41
2	672.2	10.53	10.51	-0.19	131.32
2	693.6	13.52	13.61	0.66	159.72
2	703.9	15.47	15.33	-0.90	174.68
1	709.5	16.29	16.34	0.30	183.26
2	726.5	20.0	19.7	-1.60	210.51
2	746.0	23.9	24.1	0.92	244.59
1	748.3	24.6	24.6	0	249.71
1	756.8	26.8	26.8	0	264.77
2	758.2	27.0	27.2	0.74	267.52
1	760.8	28.3	27.9	-1.31	272.52
C.P.	763.0	...	28.5	...	(276.77)
Av ±0.70%					

639.5 to 391.5°K. Fischer, *et al.*, reported the normal boiling point of aluminum bromide to be 528°K and our eq 2 also gives a value of 528°K. This is somewhat lower than the values 529.5°K selected by Kelley⁷ and 530°K given in the JANAF tables.⁸

Table II compares the experimental pressures of Fischer, Rahlfs, and Benze³ with those calculated by eq 2. Included in the table are the values of the pressures calculated by the free energy of vaporization relation developed by Kelley⁷ from the same data. While eq 2 is empirical, it reproduces the experimental points somewhat better than the theoretically based equation developed by Kelley. This is probably due to the choice of -25 cal/mole deg as the constant difference in the heat capacities of liquid and gaseous aluminum bromide. A value of -18, as derived from the enthalpies of vaporization given by ref 3 (13.9 and 12.1 kcal/mole at 410 and 510°K, respectively) would have given a better representation.

Table II: Comparison of Observed and Calculated Vapor Pressure of Aluminum Bromide below 1 Atm

Temp, °K	Pressure, atm			Calcd - obsd (atm)	
	Obsd, ref 3	Calcd, eq 2	Calcd, Kelley	Eq 2	Kelley
522.7	0.887	0.891	0.888	0.004	0.001
519.3	0.834	0.826	0.828	-0.008	-0.006
518.0	0.806	0.802	0.806	-0.004	0
500.0	0.526	0.526	0.540	0	0.014
495.2	0.468	0.467	0.482	-0.001	0.014
493.5	0.455	0.447	0.462	-0.008	0.007
493.5	0.453	0.447	0.462	-0.006	0.009
493.1	0.442	0.443	0.458	0.001	0.016
493.0	0.439	0.442	0.457	0.003	0.016
483.1	0.344	0.342	0.356	-0.002	0.012
465.5	0.212	0.209	0.219	-0.003	0.007
462.0	0.192	0.189	0.198	-0.003	0.006
461.8	0.191	0.188	0.196	-0.003	0.005
437.6	0.086	0.087	0.090	0.001	0.004
436.2	0.085	0.084	0.086	-0.001	0.001
430.2	0.067	0.067	0.069	0	0.002
422.0	0.049	0.050	0.051	0.001	0.002
414.4	0.038	0.038	0.038	0	0
413.7	0.036	0.037	0.037	0.001	0.001
Av dev				0.97%	2.42%
404.0	(0.026)	0.025	0.024	-0.001	-0.002
401.0	(0.022)	0.023	0.021	0.001	-0.001
400.5	(0.021)	0.021	0.021	0	0
391.5	(0.013)	0.015	0.014	0.002	0.001
Av dev				5.94%	4.98%
4 pts.					

The enthalpy of vaporization of aluminum bromide may be calculated from the present data using the Clapeyron relation

$$\Delta H_{\text{vap}} = \frac{T(V_g - V_l)(dP/dT)}{41,300} \quad (3)$$

where V_g and V_l represent the orthobaric molar volumes of vapor and liquid, (dP/dT) is the rate of change of vapor pressure with respect to temperature, and the numerical factor converts the value to kilocalories per mole. Fischer, *et al.*,³ reported that aluminum bromide vapor consisted almost entirely of Al_2Br_6 molecules; therefore, our calculations of $(V_g - V_l)$ and the enthalpy of vaporization refer to a mole of Al_2Br_6 .

Table III presents the results of these calculations. The enthalpy of vaporization, ΔH_{vap} , is very sensitive to the accuracy of the vapor density data, particularly at low vapor densities. Therefore, the experimental values of the density were used from ref 2 instead of the

(7) K. K. Kelley, U. S. Department of the Interior, Bureau of Mines, Bulletin No. 383, U. S. Government Printing Office, Washington, D. C., 1935.

(8) "JANAF Thermochemical Tables," The Dow Chemical Co., Midland, Mich.

Table III: Vaporization Data for Aluminum Bromide

T , $^{\circ}\text{K}^a$	Vapor, pressure, atm	$(V_g - V_l)$, cc/mole of Al_2Br_6	$T(dP/dT)$, atm	ΔH_{vap} , kcal/mole of Al_2Br_6	ΔH_{vap} , calcd eq 5	Dev, %
760.3	27.80	413	206.43	2.06	2.07	0.48
759.8	27.67	452	205.60	2.25	2.21	-1.78
758.4	27.29	518	203.15	2.55	2.55	0
754.9	26.36	652	197.14	3.11	3.19	2.57
754.4	26.23	687	196.30	3.26	3.26	0
748.9	24.83	873	187.19	3.96	3.97	0.25
742.6	23.29	1,072	177.04	4.60	4.59	-0.22
734.4	21.40	1,318	164.51	5.25	5.24	-0.19
733.2	21.13	1,393	162.70	5.49	5.32	-3.10
732.1	20.89	1,421	161.08	5.54	5.40	-2.53
726.2	19.62	1,596	152.53	5.89	5.78	-1.87
714.1	17.20	1,961	135.98	6.46	6.46	0
700.8	14.80	2,543	119.230	7.34	7.11	-3.13
683.0	12.00	3,253	99.193	7.81	7.84	0.38
658.1	8.78	4,808	75.322	8.77	8.73	-0.46
626.3	5.67	7,751	51.421	9.65	9.68	0.31
609.8	4.43	10,014	41.588	10.08	10.13	0.50
591.0	3.28	13,493	32.081	10.48	10.60	1.14
543.5	1.38	30,954	15.087	11.31	11.66	3.09
528.0	1.00	(42,100) ^c	11.370	(11.59)	11.98	3.36
410 ³	13.9	14.06	1.15
510 ³	12.1	12.33	1.90
528 ³	12.0	11.98	-0.17
529.5 ⁷	10.92	11.95	9.43 ^b
530 ⁸	12.00	11.94	-0.50

 Av dev % ± 1.21

^a Superscripts 3, 7, and 8 refer to literature sources. ^b Not included in average. ^c Calculated from extrapolated vapor density values.

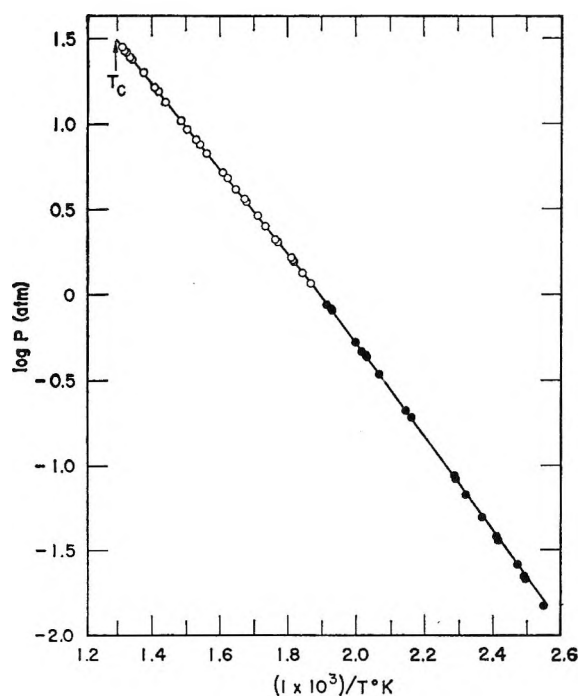


Figure 1. Vapor pressure of aluminum bromide: O, present work; ●, Fischer, Rahlfs, and Benze.

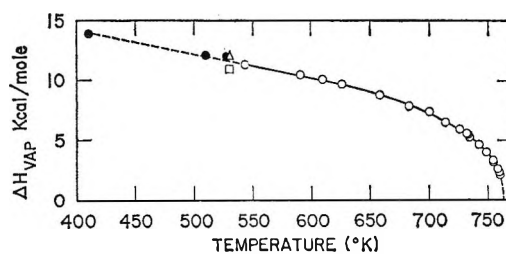


Figure 2. Enthalpy of vaporization of aluminum bromide: O, present work; ●, Fischer, Rahlfs, and Benze; △, JANAF tables; □, Kelley. Present data calculated per mole of Al_2Br_6 . Literature values are per mole of gas. See text.

values calculated from the Guggenheim equation so as to avoid introducing a trend in the values of $(V_g - V_l)$ at low vapor densities. The quantity $T(dP/dT)$ was calculated from eq 1 or 2 in the appropriate temperature range.

Figure 2 shows the variation of the enthalpy of vaporization with temperature. Included in this figure are the enthalpies of vaporization reported by Fischer, Rahlfs, and Benze,³ Kelley,⁷ and the JANAF tables.⁸ These literature values were calculated from the Clapeyron equation on the assumption that the

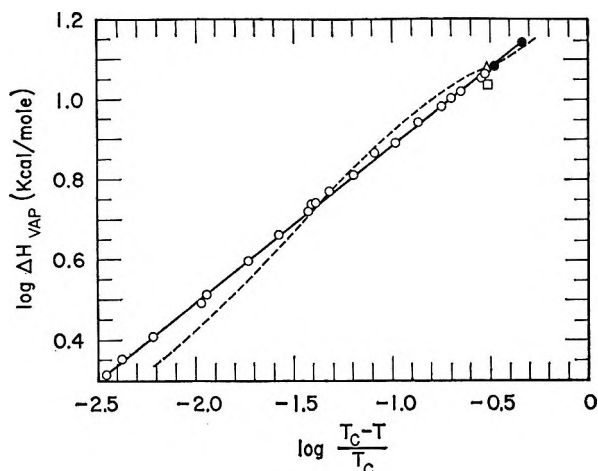


Figure 3. Log-log plot of enthalpy of vaporization vs. temperature: O, present work; ●, Fischer, Rahlfs, and Benze; Δ, JANAF tables; □, Kelley; - - -, Zhuralev and Kostrova.

vapor obeyed the ideal gas law. The enthalpy of vaporization derived in that way refers to a mole of the gaseous form of the substance. That is, if AlBr_3 were the only gaseous species, the ΔH would refer to 267 g of aluminum bromide; if Al_2Br_6 were the only gaseous species, the ΔH would refer to 534 g; and for mixtures of species in the gas phase, the molecular weight would be that of the proper average of the species. Therefore, the agreement of the literature values of ΔH near the boiling point (especially that of ref 3) with the values we obtained above, on the assumption that the molecular weight of the gas corresponded to Al_2Br_6 , is a verification that this assumption is valid.

The enthalpy of vaporization and its relation to temperature has been the subject of many empirical relations. Of these the relatively simple modification of Jones and Bowden⁹

$$\Delta H_{\text{vap}} = l_0 \frac{(T_c - T)^n}{T_c} \quad (4)$$

was applied to the present data on aluminum bromide. In this relation, l_0 and n are empirical constants. A log-log plot of the data is shown in Figure 3. The present data follow a straight line with the parameters $l_0 = 19.03$ and $n = 0.393$. These values can be compared with those given by Partington¹⁰ for several fluids. For n his values range from 0.3 to 0.45 and average about 0.39 for nonassociated liquids. For mercuric chloride,⁵ $l_0 = 18.50$ and $n = 0.394$. This relation also fits the enthalpy of vaporization reported by Fischer, Rahlfs, and Benze³ and the value selected for the normal boiling point in the JANAF tables;⁸ Kelley's value falls below this line. The dotted line in Figure 3 represents the tabular values of the enthalpy of vaporization listed by Zhuralev and Kostrova.¹¹ These authors extrapolated the vapor pressure curve of ref 3 up to their critical temperature of 768°K and combined these results with the orthobaric density data of Zhuralev.¹² Considering the vapor pressure curve was extrapolated over a temperature range of 240°, their results are surprisingly good.

The last column in Table III presents the enthalpy of vaporization of aluminum bromide according to eq 4. With the exception of the value selected by Kelley,⁷ all of the experimental data are fitted by eq 4 with an average deviation of $\pm 1.21\%$ and a maximum deviation of $+3.36\%$.

(9) W. J. Jones and S. T. Bowden, *Phil. Mag.*, **37**, 480 (1946).

(10) J. R. Partington, "An Advanced Treatise on Physical Chemistry," Vol. II, Longmans, Green and Co., London, 1951, pp 319-324.

(11) D. I. Zhuralev and N. W. Kostrova, *Zh. Tekh. Fiz.*, **7**, 1626 (1937).

(12) D. I. Zhuralev, *Zh. Fiz. Khim.*, **10**, 325 (1937).

The Kinetics of Hydrogen Isotope Exchange in Benzene Using a Homogeneous Platinum Catalyst

by R. J. Hodges and J. L. Garnett

*Department of Physical Chemistry, The University of New South Wales, Kensington, N.S.W., Australia
(Received November 2, 1967)*

The *homogeneous* exchange of benzene with isotopic hydrogen has been studied in solution in the presence of catalytic amounts of Pt^{II} and Pt^{IV} salts. Rate of exchange $k_{ex} \propto [\text{PtCl}_4^{2-}][\text{C}_6\text{H}_6]/[\text{Cl}^-]$. Both multiple and stepwise processes are observed in the reaction. The acidity of the solution is found to be important for stabilizing the *homogeneous* catalyst. An isotope effect for $k(\text{deuteration})/k(\text{dedeuteration})$ of 1.65 ± 0.05 has been observed. The data are shown to be consistent with a mechanism involving π -complex intermediates. The results of the present *homogeneous* exchange are shown to be relevant to the interpretation of analogous reactions in *heterogeneous* catalysis.

Introduction

Exchange between organic compounds, particularly aromatic hydrocarbons, and isotopic water has been extensively investigated with *heterogeneous* catalysts,¹ platinum generally being the most reactive. Mechanisms involving π -complex intermediates have been proposed to account for the observed reactivity.^{2,3} The type of bonding envisaged at the catalyst surface is thus analogous to the bonding observed in inorganic coordination complexes. In this respect the recently reported exchange under *homogeneous* conditions of aromatic compounds with isotopic water in the presence of platinum(II) catalysts⁴ is important for further clarification of the previous mechanisms proposed.

An amplification of our original communication⁴ in which the variables influencing *homogeneous* exchange were summarized will now be discussed. A detailed kinetic analysis of the deuteration of benzene has been performed using acetic acid as a common solvent for deuterium oxide and platinum salts of two different valences (Pt^{II} and Pt^{IV}). Platinum salts⁵⁻⁹ have been used as *homogeneous* catalysts for hydrogenation, isomerization, and oxidation; however, no previous work with the simplest of catalytic reactions, namely, *homogeneous* exchange, has been reported. Results of further studies involving substituted benzenes and polycyclic aromatics will be given in more detail in subsequent publications.

Experimental Section

Materials. Deuterioacetic acid (CH₃COOD) was prepared by refluxing equal moles of acetic anhydride (May and Baker) and heavy water (99.75% D₂O). Acetyl chloride (May and Baker) was used as a source of DCl. Matthey, Garrett and Co. Na₂PtCl₄, K₂PtCl₄ and H₂PtCl₆ were used as catalysts. C₆D₆ of 99.3%

isotopic purity was prepared by several exchanges with D₂O using *heterogeneous* platinum.

Exchange Procedure. Aliquots (2 ml) of acetic acid solution varying in concentration from 0 to 100 mol % containing catalyst (0.02 M) were added to a pre-constricted tube containing the organic compound in concentrations from 2 to 15 mol %. Acidity was varied by preparing DCl in the acetic acid master solution or (for concentrations of DCl higher than 0.05 M) by adding a small break-seal tube containing acetyl chloride. Samples were evacuated to 0.02 torr using two freeze-thaw cycles and were sealed at the prestriction. Reactions were carried out with shaking in a thermostated water bath at temperatures from 60 to 100°. Results at 130° were obtained using a thermostatically controlled oven. After reaction, the organic material was removed from the acetic acid solution by diluting with water. The organic phase was washed once, then dried over anhydrous sodium sulfate. In a study of the reduction of H₂PtCl₆, aliquots of the aqueous layer were diluted in 4 M HCl and the absorbance was measured at 262 m μ .¹⁰

(1) (a) Part XLIV of a series entitled "Catalytic Deuterium Exchange Reactions of Organics;" Part XLIII: J. L. Garnett and R. J. Hodges, *Chem. Comm.*, in press; (b) J. L. Garnett and W. A. Sollich-Baumgartner, *Advan. Catalysis*, 16, 95 (1966).

(2) R. R. Fraser and R. N. Renaud, *J. Am. Chem. Soc.*, 88, 4365 (1966).

(3) J. L. Garnett and W. A. Sollich-Baumgartner, *J. Phys. Chem.*, 68, 3177 (1964).

(4) J. L. Garnett and R. J. Hodges, *J. Am. Chem. Soc.*, 89, 4546 (1967).

(5) G. C. Bond, *Platinum Metals Rev.*, 8, 92 (1964).

(6) R. D. Cramer, E. L. Jenner, R. V. Lindsey, Jr., and U. G. Stoberg, *J. Am. Chem. Soc.*, 85, 1691 (1963).

(7) J. F. Harrod and A. J. Chalk, *ibid.*, 86, 1776 (1964).

(8) G. C. Bond and M. Hellier, *Chem. Ind. (London)*, 35 (1965).

(9) J. K. Nickolson and B. L. Shaw, *Tetrahedron Letters*, 3533 (1965).

(10) J. J. Kirkland and J. H. Yoe, *Anal. Chim. Acta*, 9, 441 (1953).

Apparatus. Deuterium analyses were performed on Metropolitan Vickers MS-2G and MS-9 mass spectrometers using a low ionization voltage technique.¹¹ Absorption measurements were performed on a Hitachi Perkin-Elmer 139 spectrophotometer. Gas chromatographic analysis was carried out on a Perkin-Elmer Model 800 instrument. Orientation of the deuterium in the aromatics^{12,13} was determined on a Varian Associates A-60 nmr spectrometer.

Results

Reduction of H_2PtCl_6 in Aqueous Media. Two types of platinum catalysts have been studied in the present series, *i.e.*, Pt^{II} and Pt^{IV} compounds. Initial results were obtained with H_2PtCl_6 in a two-phase liquid system with benzene. Severe precipitation of platinum occurred unless high concentrations (4 M) of hydrochloric acid were used. The kinetics (Figure 1) showed an induction period indicating that H_2PtCl_6 was not the catalyst; however, when K_2PtCl_4 was used, the rate of exchange was proportional to the concentrations of the Pt^{II} salt. From Figure 1, at 5.3 M HCl, a period of 150 hr is required at 130° for most of the H_2PtCl_6 to be reduced to H_2PtCl_4 . Uv spectrophotometry showed a progressive diminution of the H_2PtCl_6 absorption peak at 262 μ . Analysis of the benzene phases by gas chromatography and mass spectrometry indicated the presence of chlorobenzene as the major product with small amounts of biphenyl. These secondary products were all deuterated to a greater extent than the parent benzene (Table I). Thus the *homogeneous* reduction of the H_2PtCl_6 by benzene (eq 1, 2) is analogous to *heterogeneous* "self activation" or reduction of PtO_2 by benzene.¹⁴



If benzene in this reaction is replaced by chlorobenzene and biphenyl (Table I) then dichlorobenzene and chlorobiphenyl are the chlorinated by-products which correspond to chlorobenzene for benzene.

Table I: Deuteration of Aromatics Using H_2PtCl_6 , 0.05 M $H_2PtCl_6 \cdot 6H_2O$, 4 M HCl in D_2O , for 168 hr at 130°

Aromatic	% D		Products	% D in products
	Theoretical	Observed		
Benzene	52.0	40.8	Chlorobenzene	45.1
			Biphenyl	42.2
Chlorobenzene	50.4	3.5	Dichlorobenzene	27.1
Biphenyl	48.3	2.4	Chlorobiphenyl	33

Catalysis by K_2PtCl_4 in Aqueous Acetic Acid Solution. In order to allow a more complete investigation of the effects of temperature and concentration, a common solvent, aqueous acetic acid was necessary to overcome the problem of a two-phase system. Preliminary tests

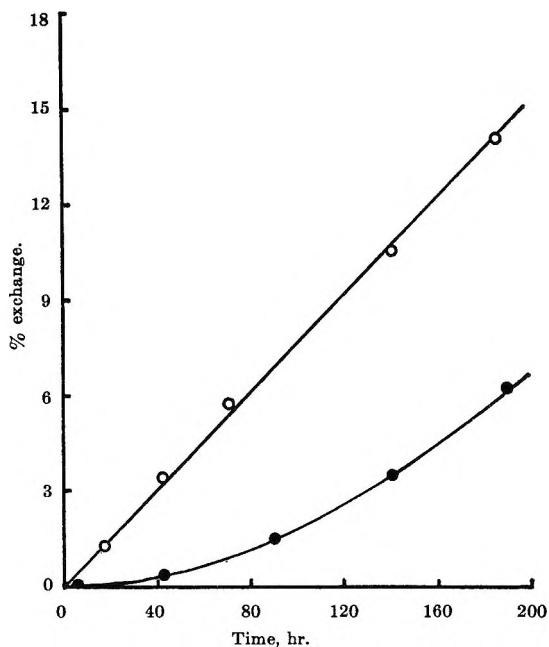


Figure 1. Deuteration of benzene using a two-phase liquid system: ●, 0.02 M H_2PtCl_6 in aqueous phase; O, 0.02 M K_2PtCl_4 , 130° (5.3 M HCl in D_2O).

indicated that K_2PtCl_4 was rapidly reduced to platinum in aqueous acetic acid if hydrochloric acid was absent; thus 4.6 M HCl was initially chosen to investigate the kinetics. At this acid concentration, considerable exchange was observed in the methyl group of the acetic acid during the reaction time. In order to avoid a correction for this deuterium effectively lost from the exchange system, C_6D_6 was used and exchange was carried out in the reverse direction. Relative rates *vs.* mole percentage of acetic acid are given in Figure 2. The maximum in this curve occurs at approximately 50 mol % acetic acid. In concentrated acetic acid solutions, K_2PtCl_4 has poor solubility, and below about 50 mol % acetic acid, two liquid phases are present.

Multiple Exchange Processes. The possibility that *homogeneous* exchange occurs by stepwise and multiple processes could be important mechanistically. In this respect the concept of the *M* value introduced by Anderson and Kemball¹⁵ for *heterogeneous* exchanges can be utilized. Briefly, the *M* value corresponds to the mean number of deuterium atoms entering each exchanged molecule under initial conditions. To measure *M* values in benzene one has to consider two rates. The first is the rate of deuterium entry into benzene. The amount of deuterium in benzene is given by

(11) J. L. Garnett and W. A. Sollich, *J. Catalysis*, **2**, 339 (1963).

(12) N. Jonathan, S. Gordon, and B. P. Dailey, *J. Chem. Phys.*, **36**, 2443 (1962).

(13) H. Spiesecke and W. G. Schneider, *ibid.*, **35**, 731 (1961).

(14) J. L. Garnett and W. A. Sollich, *Australian J. Chem.*, **18**, 993 (1965).

(15) J. R. Anderson and C. Kemball, *Advan. Catalysis*, **9**, 51 (1957).

$$\phi = u + 2v + 3w + 4x + 5y + 6z \quad (3)$$

where $u-z$ represent the percentages of benzene present as benzene- d_1 to $-d_6$. Kemball has shown on theoretical grounds that a simple first-order equation describes the variation of ϕ with time

$$\frac{d\phi}{dt} = \frac{k\phi}{\phi_\infty}(\phi_\infty - \phi) \quad (4)$$

where $k\phi$ is the initial rate of deuterium entry per 100 molecules of benzene- d_0 and ϕ_∞ is the equilibrium value.

The second rate to be considered is the disappearance of benzene- d_0 . A convenient method of obtaining this is to assume the equation

$$-\frac{db}{dt} = k_b \frac{(b - b_\infty)}{(100 - b_\infty)} \quad (5)$$

where k_b is the initial rate of disappearance of benzene- d_0 in percentage per unit time, b is the percentage of total benzene present as benzene- d_0 , and b_∞ is the equilibrium value calculated for complete randomization. M is then obtained by the ratio

$$M = \frac{k\phi}{k_b} \quad (6)$$

Thus the M value gives a direct indication of the relative emphasis of multiple to stepwise processes

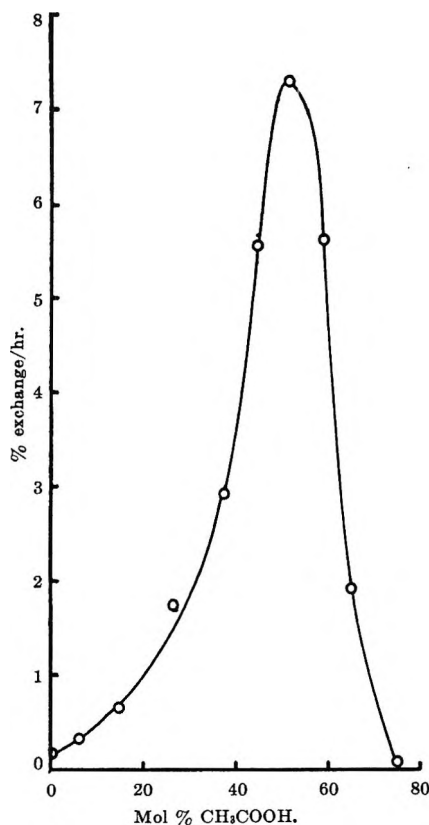


Figure 2. Effect of mole % CH_3COOH upon exchange rate of C_6D_6 at 130° , $4.6 M$ HCl , and $0.02 M$ K_2PtCl_4 .

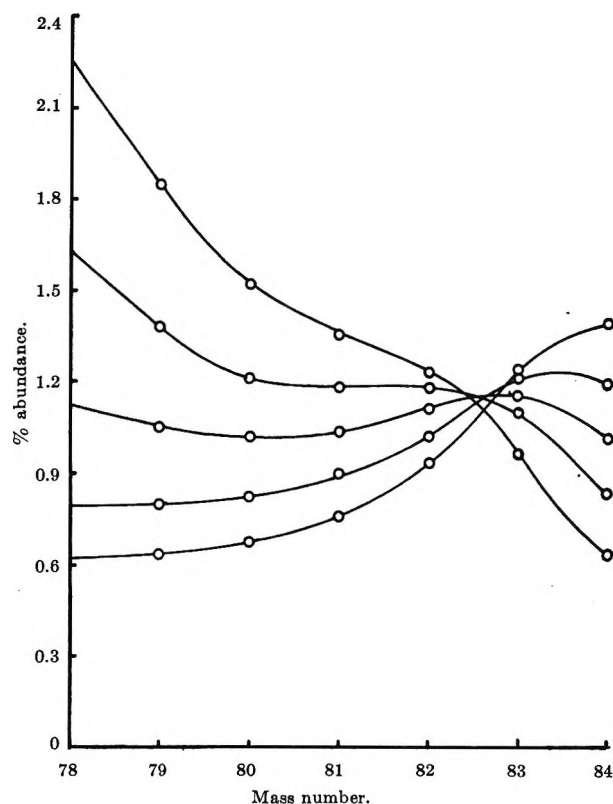


Figure 3. Variation in per cent abundance under initial conditions as a function of temperature. Solution consisted of $0.02 M$ Na_2PtCl_4 and $0.02 M$ DCl dissolved in a mixture of 1 mol of CH_3COOD , 1 mol of D_2O , and 0.167 mol of C_6H_6 . % D (theoret.) = 75. Distributions corrected to 5% approach to equilibrium. Curves from top to bottom at left: 100 , 88.7 , 79.6 , 70.0 , and 60.0° .

occurring during exchange. It has been found that in the initial stages of the present reaction with benzene exchange, the relative percentages of deuterated species d_1 to d_6 increase linearly with time; thus Kemball's treatment of *heterogeneous* data provides a useful comparison of M values under *homogeneous* conditions. The results of a temperature-dependence study (normalized to an arbitrary total exchange of 5% approach to equilibrium) are given in Figure 3. An increase in temperature reduces the multiple exchange even though the over-all exchange rate is increased. One limitation of the application of the M value concept to the present system is that the derivation does not include a consideration of the benzene molecules that are initially complexed but return to the parent benzene without deuteration. This aspect is important and the necessary correction will be considered in the Discussion section.

Catalysis by Na_2PtCl_4 . Sodium chloroplatinite is more soluble in acetic acid media than the corresponding potassium salt; however, Na_2PtCl_4 is hygroscopic, and absolute rates are more difficult to obtain. It does, however, provide useful comparisons of exchange rates and also permits exchange in solutions of higher acetic acid concentration, thus providing a satisfactory

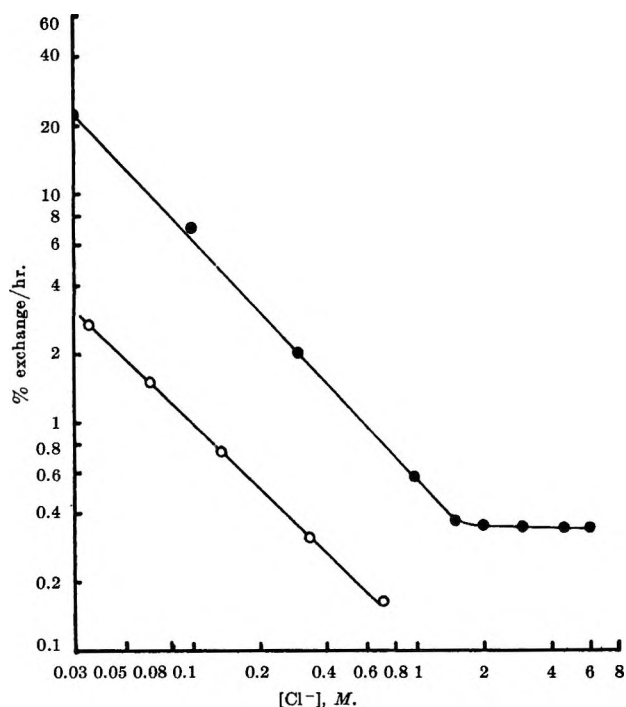


Figure 4. Logarithmic plot of per cent exchange per hour vs. concentration of chloride ion: ●, DCl curve at 100°; ○, NaCl curve at 82°.

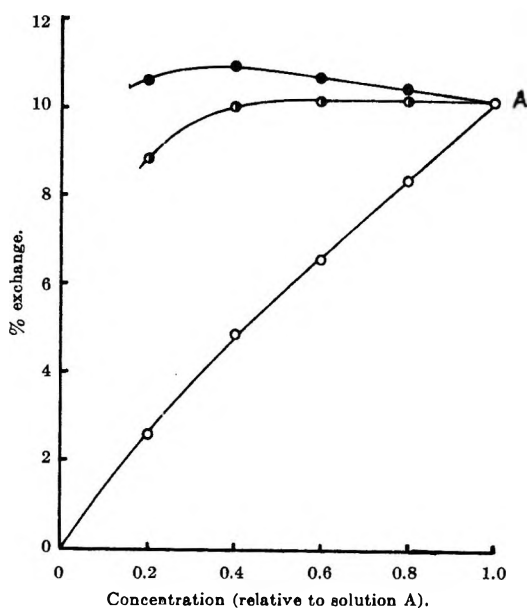


Figure 5. Comparative effect of Na_2PtCl_4 , DCl, and benzene concentrations upon exchange rate, at 75° for 8 hr. A 1:1 mole ratio of CH_3COOD to D_2O was utilized; solution A consisted of 0.02 M Na_2PtCl_4 , 0.04 M DCl, and 10% v/v benzene: ○, $[\text{Na}_2\text{PtCl}_4]$ varied, $[\text{C}_6\text{H}_6]$ and $[\text{Cl}^-]$ constant; ◐, $[\text{Na}_2\text{PtCl}_4]$ and $[\text{Cl}^-]$ varied, $[\text{C}_6\text{H}_6]$ constant; ●, $[\text{Na}_2\text{PtCl}_4]$, $[\text{Cl}^-]$, and $[\text{C}_6\text{H}_6]$ varied.

medium for exchange in sparingly soluble aromatics. A series of experiments were performed with this salt to investigate the kinetics. The effect of hydrochloric acid concentration was studied in 50 mol % acetic acid

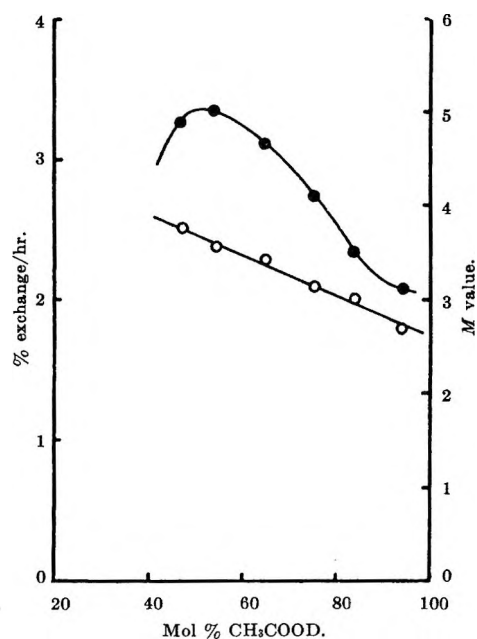


Figure 6. Effect of acetic acid concentration upon exchange rate for 0.015 M Na_2PtCl_4 and 0.01 M DCl at 80°: ○, M value curve; ●, exchange curve.

and the kinetics were compared with the effect of sodium chloride concentration (Figure 4).

It is seen that an inverse effect is due to the chloride ion concentration. Some hydrochloric acid is essential since precipitation of platinum occurs below a concentration of 0.02 M HCl. At this acid concentration, negligible exchange of protons in the methyl group of the acetic acid occurred within the reaction time, and the reverse technique (*i.e.*, the use of C_6D_6) which was previously utilized with K_2PtCl_4 was not necessary.

A further comparative study involving the dependence of relative rates upon the concentrations of Na_2PtCl_4 and benzene is given in Figure 5. In Figure 6 the change in rate of deuteration and multiple exchange is shown as a function of the acetic acid concentration, distributions being given in Table II. A concentration of 0.01 M HCl was used in this study and a maximum occurs in the exchange curve. This is due to the precipitation of platinum at low acetic acid concentrations since, once platinum precipitates, subsequent exchange is very slow.

The effect of hydrochloric acid concentration in acetic acid (98%) is given in Table III, the results indicating that a maximum in the exchange occurs at approximately 0.01 M sodium acetate (the base in acetic acid solutions). This corresponds to the point where visible amounts of platinum precipitate. Vapor phase chromatographic analysis indicated that no side reactions with the benzene were observed in the solutions where no precipitation occurred. However, in all reactions where platinum precipitated, chlorobenzene and biphenyl were formed. The possibility of subsequent heterogeneous exchange on the precipitated

Table II: Distribution of Deuterium in Benzene for Different Solvent Mixtures (See Figure 6)

Sample	Mol % of CH ₃ COOD	Distribution							<i>M</i> value
		<i>d</i> ₀	<i>d</i> ₁	<i>d</i> ₂	<i>d</i> ₃	<i>d</i> ₄	<i>d</i> ₅	<i>d</i> ₆	
A	46.3	84.8	1.95	2.05	2.35	2.50	3.05	3.35	3.76
B	53.9	83.8	2.2	2.3	2.6	2.7	3.2	3.1	3.53
C	64.8	84.1	2.6	2.65	2.75	2.8	2.95	2.25	3.41
D	75.5	84.7	2.9	2.8	2.8	2.65	2.45	1.65	3.11
E	84.0	86.0	3.2	2.8	2.6	2.3	1.95	1.15	3.01
F	94.1	86.7	3.65	2.85	2.5	2.0	1.55	0.75	2.69

Table III: Effect of Acidity in Glacial Acetic Acid on Benzene Exchange Using 0.02 *M* Na₂PtCl₄, for 4 Hr at 80°

Concn of acid or base	% D	Distribution						
		<i>d</i> ₀	<i>d</i> ₁	<i>d</i> ₂	<i>d</i> ₃	<i>d</i> ₄	<i>d</i> ₅	<i>d</i> ₆
0.10 <i>M</i> CH ₃ COONa	1.6	97.0	0.6	0.6	0.5	0.5	0.5	0.3
0.03 <i>M</i> CH ₃ COONa	2.6	94.4	1.4	1.2	1.1	0.9	0.6	0.3
0.01 <i>M</i> CH ₃ COONa	4.0	90.8	2.8	2.1	1.7	1.3	0.9	0.4
...	4.6	88.6	4.1	2.7	2.0	1.4	0.8	0.4
0.01 <i>M</i> HCl	4.3	88.6	4.3	2.7	2.0	1.3	0.8	0.3
0.03 <i>M</i> HCl	3.9	89.9	4.5	2.5	1.7	1.1	0.6	0.2
0.10 <i>M</i> HCl	2.6	93.3	2.7	1.9	1.3	0.7	0.3	0.1

catalyst was considered; however, both HCl and CH₃COOH strongly inhibit exchange on this self-activated platinum.

A kinetic comparison of a series of monosubstituted benzenes and two polycyclic aromatics is given in Table IV. It will be noted that the exchange rate is independent of the electronic nature of the substituent and the low voltage mass spectrometric distributions indicate significant steric hindrance. This series also illustrates the advantages of the *homogeneous* technique when compared with *heterogeneous* exchange.¹⁶ With naphthalene and other condensed polycyclics,¹⁷ the exchange is confined to the β -positions at this temperature owing to large steric effects at the remaining positions. In addition, the *M* value is unity, which contrasts markedly with *M* values of 3–4 for benzene and its derivatives. This would suggest that multiple exchange is hindered by bond fixation in condensed polycyclic aromatics.

Isotope Effect. To obtain information on the rate-determining step of the reaction, an isotope effect using recrystallized K₂PtCl₄ was performed. Two separate types of experiments were carried out, deuteration with C₆H₆ and dedeuteration with C₆D₆. Fractional abundances of exchanged C₆H₆ and C₆D₆ are given in Figure 7. It may be seen that there is a considerable change in the multiple exchange value for the forward and reverse exchange reactions. The isotope effect $k(\text{deuteration})/k(\text{dedeuteration})$ was calculated to be 1.65 ± 0.05 .

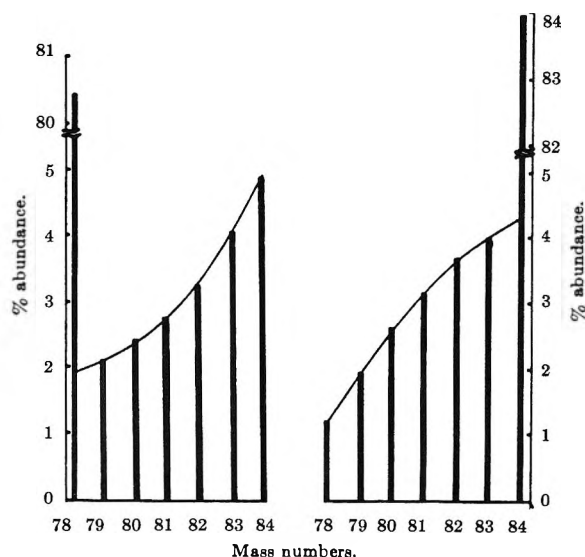


Figure 7. Distributions of deuterated products for C₆H₆ and C₆D₆, using 0.020 *M* K₂PtCl₄, 0.03 *M* HCl, and 1:1 acetic acid–water, for 7.5 hr at 75°.

Discussion

Acidities in Nonaqueous Media. From the foregoing results it is evident that the acidity of the solution strongly influences the performance of the platinum salts as catalysts for exchange. The concentration of acetic acid affects the solubility of benzene and the multiple exchange characteristics of the reaction. Hydrochloric acid concentration is critical to both stability of catalyst and exchange rate. An understanding of acidities in water–acetic acid solvents is initially required.

Acidities of hydrochloric acid in water–acetic acid mixtures have been investigated in a thorough study by Schwarzenbach and Stensby^{18a} over the complete range 0–100% acetic acid. A function^{18b} pwH (defined as $\text{pwH} = (-\log [\text{H}]) f_{\text{Cl}^-}$, where H is used to represent the total activity of the solvated proton and f_{Cl^-} is the total

(16) J. L. Garnett and W. A. Soilich, *Australian J. Chem.*, **14**, 441 (1961); **15**, 56 (1962).

(17) R. J. Hodges and J. L. Garnett, unpublished work.

(18) (a) G. Schwarzenbach and P. Stensby, *Helv. Chim. Acta*, **42**, 2343 (1959); (b) for the present paper to avoid confusion, pwH was chosen as a term to replace the $\text{pw}\oplus$ representation used by the original authors.^{18a}

Table IV: Exchange of Monosubstituted Benzenes and Naphthalene

Compound	Wt, g	Media for exchange ^a	Temp, °C	Ex-change time, hr	Distribution								% D
					<i>d</i> ₀	<i>d</i> ₁	<i>d</i> ₂	<i>d</i> ₃	<i>d</i> ₄	<i>d</i> ₅	<i>d</i> ₆		
Benzene	0.176	A	82	4	82.2	2.6	2.8	2.9	3.1	3.5	2.9	10.7 ^b	
Bromobenzene	0.300	A	82	4	82.6	4.6	5.8	6.8	7.3	
Toluene	0.173	A	82	4	84.6	4.1	4.4	4.8	1.1	0.7	0.4	4.7	
<i>t</i> -Butylbenzene	0.173	A	82	4	87.6	3.1	4.4	5.0	5.4 ^d	
Trifluorotoluene	0.238	A	80	3	92.8	1.95	1.95	3.85	3.4	
Benzene	0.088	B	75	2.3	87.8	1.65	1.65	1.85	2.05	2.40	2.70	7.8 ^c	
Biphenyl	0.100	B	75	2.3	83.0	3.0	4.0	5.5	1.7	1.3	1.5	5.0	
Naphthalene	0.100	B	75	2.3	75.3	20.4	3.3	0.6	3.6	

^a 2.0-ml amount of exchange media was used in each run. Solution A: CH₃COOD (1.00 mol), D₂O (1.00 mol), K₂PtCl₄ (1.48 × 10⁻³ mol), and DCl (1.48 × 10⁻³ mol). Solution B: CH₃COOD (1.00 mol), D₂O (0.50 mol) Na₂PtCl₄ (1.30 × 10⁻³ mol), and DCl (1.30 × 10⁻³ mol). ^b Theoretical equilibrium for benzene, 85.7%. ^c Theoretical equilibrium for benzene, 82.1%. ^d Calculated assuming exchange in the aromatic positions only.

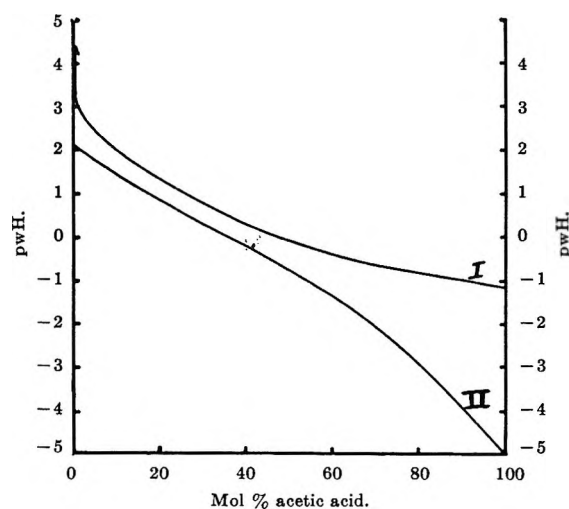


Figure 8. The variation of pwH as a function of acetic acid concentration. Curve I: 0.01 *m* CH₃COONa, 0.1 *m* (CH₃)₄N⁺Cl⁻. Curve II: 0.01 *m* H⁺ClO₄⁻, 0.1 *m* (CH₃)₄N⁺Cl⁻.

activity of the chloride ion) was used to compare acidities in such mixtures. pwH is numerically similar to pH in aqueous solution. Figure 8 illustrates the changes in pwH for an acid and a base in solutions as the mole ratio of acetic acid is increased. The upper curve is that of 0.01 *M* NaAc + 0.1 *M* (CH₃)₄N⁺Cl⁻ and the lower curve that of 0.01 *M* HCl + 0.1 *M* (CH₃)₄N⁺Cl⁻.

The stability of PtCl₄²⁻ under exchange conditions was found to be markedly dependent upon these acid concentrations in aqueous solutions, 4 *M* HCl being necessary. Now the mean activity coefficient of hydrogen ions in 4 *M* HCl is 1.76;¹⁹ hence the pH is -0.85 ≈ -1. For 50 mol % acetic acid in H₂O, a pwH of -1 occurs at a concentration of 0.01 *M* HCl and, in glacial acetic acid, pwH is -1 when the concentration in sodium acetate is 0.01 *M* (Figure 8). The point coinciding with the decomposition of PtCl₄²⁻ under exchange conditions appears in three solvent mixtures at approximately the same pwH value. It is thus reasonable to

assume that decomposition of the PtCl₄²⁻ occurs through some solvolysis product, the formation of which is inhibited when the pwH value is lower than -1.

Acid concentrations where the pwH value is well below -1 should also be avoided. In aqueous acetic acid solutions competitive complex formation with the catalyst is apparent between the chloride ion and the benzene (Figure 4). Although less competition occurs in glacial acetic acid (Table III), high acidities will produce exchange in the methyl group of the acetic acid¹⁷ and will limit severely the amount of deuteration possible. This change in the role of the hydrochloric acid is probably due to the fact that glacial acetic acid has a lower dielectric constant and dissociation is small. Above 2 *M* HCl in 1:1 molar CH₃COOD-D₂O, no further decrease in rate is observed (Figure 4), possibly also due to a limited dissociation of the HCl and again exchange in the methyl group is considerable.

The rate of exchange and the multiple exchange value (*M*) are quite different in the present homogeneous metal-catalyzed system than in exchange induced by electrophilic displacement, *i.e.*, attack on an aromatic compound by D⁺ species²⁰ where *M* values of unity are expected and observed. No acid-induced exchange at pwH -1 was observed within the reaction times of this study and acid exchange in benzene was slower by a factor of 50 when 4.6 *M* HCl was used in 50 mol % acetic acid.

Existence of a π-Complex Intermediate. Stepwise exchange in a molecule occurs when only one deuterium atom enters the hydrocarbon after each interaction with the catalyst. Multiple exchange is a process whereby more than one hydrogen atom is exchanged within one completed reaction cycle. A consequence of multiple exchange is that deuterium is not randomly distributed

(19) W. M. Latimer, "Oxidation Potentials," 2nd ed, Prentice-Hall, Inc., New York, N. Y., 1952.

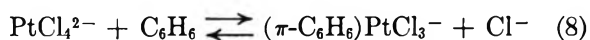
(20) W. M. Lauer, G. W. Matson, and G. Stedman, *J. Am. Chem. Soc.*, **80**, 6437 (1958).

in the reaction product. With aromatic compounds multiple exchange can be due to strong π -complex formation. Since the multiple exchange value of the present reaction is high, this would indicate the possible role of π complex intermediates.

From Figure 1 it is noted that the exchange is catalyzed by the square-planar platinum(II) chlorocomplex but not by the octahedral platinum(IV) complex. Square-planar transition metal salts have been used for many analogous reactions. Cramer, *et al.*,⁶ reduced chloroplatinic acid with an excess of stannous chloride for the hydrogenation of ethylene in methanol solution and found that the rate of hydrogenation of the higher olefins paralleled the ability of the olefin to π -complex with the platinum. Palladium(II) complexes are active catalysts for the isomerization of olefins²¹ and a π -allylic mechanism has been postulated to account for the observed reactivities. The results of Figures 4 and 5 show that the exchange is inversely proportional to $[\text{Cl}^-]$ and directly proportional to (PtCl_4^{2-}) . As the percentage exchange is a measure of the relative rate of reaction, then the rate of exchange is also first order with respect to benzene (when curve is corrected for approach to equilibrium). Thus the exchange rate follows the kinetics

$$k_{\text{ex}} \propto \frac{[\text{PtCl}_4^{2-}][\text{C}_6\text{H}_6]}{[\text{Cl}^-]} \quad (7)$$

A plausible interpretation of these kinetics involves the formation of an equilibrium π -complex according to the equation



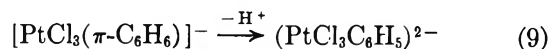
and the exchange rate would then be proportional to the concentration of this complex.

Significance of M Value. Since benzene possesses an M value well above unity ($M = 3-4$, Table II), this would imply that multiple exchange processes predominate over stepwise deuteration during the time that one benzene molecule is complexed with the inorganic chloride. Thus either a simultaneous replacement of the protons occurs when the benzene is π -complexed or the π -complexed benzene is converted to an activated σ complex where stepwise exchange occurs. A number of consecutive π - σ conversion processes would then account for the high M value even though each exchange involves a stepwise mechanism.

Studies on the monosubstituted benzenes (Table IV) indicate that the exchange is independent of the electronic nature of the substituent. Shatenstein²² points out that a vigorous electrophilic catalyst will reduce selectivity in replacement, and the distribution of the *meta* and *para* isomers will be close to statistical. This has been observed for the exchange of bromobenzene.¹⁷ In addition, activating and deactivating substituents become less important to the rate. This closely parallels the kinetics observed in the present exchange.

Thus multiple electrophilic attack of the Pt^{II} species on the already π -complexed aromatic would explain the relatively high M value.

The Exchange Reaction. The invariance of exchange rate observed for the series of monosubstituted benzenes may also be satisfactorily interpreted if one assumes that the electrophilic attack on the aromatic is not the rate-controlling step. In addition, severe steric hindrance of the *ortho* positions in the monosubstituted benzenes and the α position in naphthalene (Table IV) suggests that the electrophile is very large. This is consistent with the concept of a sterically hindered elimination of a proton from a π -complexed aromatic to give a σ -bonded platinum complex.



A plausible alternative to this mechanism involves ligand-substitution reactions in platinum(II) square-planar complexes. Very recently, the displacement of C_6H_5 in *trans*- $\text{Pt}(\text{PEt}_3)_2(\text{C}_6\text{H}_5)_2$ by Cl^- has been reported.²³ The substitution was carried out in acidified methanol solution and the mechanism proposed involved the rapid preequilibration with H^+ and Cl^- to give a six-coordinated hydrido complex, followed by a slow elimination reaction of the σ -bonded benzene and rearrangement to *trans*- $\text{Pt}(\text{PEt}_3)_2\text{ClC}_6\text{H}_5$. The rate was proportional to $[\text{H}^+]$ but not to $[\text{Cl}^-]$. This mechanism would only involve stepwise exchange as the starting materials are prepared by Grignard reactions or by use of phenyllithium.²⁴ As stepwise exchange is not observed in the present reaction for benzene derivatives, an intermediate π complex must also be involved. Falk and Halpern²⁵ have proposed a similar mechanism involving a six-coordinated species for the H exchange in *trans*- $\text{PtHCl}(\text{PEt}_3)_2$, and kinetics follow the equation

$$\frac{-d[\text{HPtCl}(\text{PEt}_3)_2]}{dt} = (K_1 + K_2[\text{Cl}^-])[\text{D}^+][\text{HPtCl}(\text{PEt}_3)_2] \quad (11)$$

This compound, however, is quite inactive for exchange in benzene under the present conditions.

The kinetics of the present study are independent of $[\text{H}^+]$ and inversely proportional to $[\text{Cl}^-]$, and the M value is not altered by either HCl or NaCl (Figure 4).

(21) M. B. Sparke, L. Turner, and A. J. M. Wenham, *J. Catalysis*, **4**, 332 (1965).

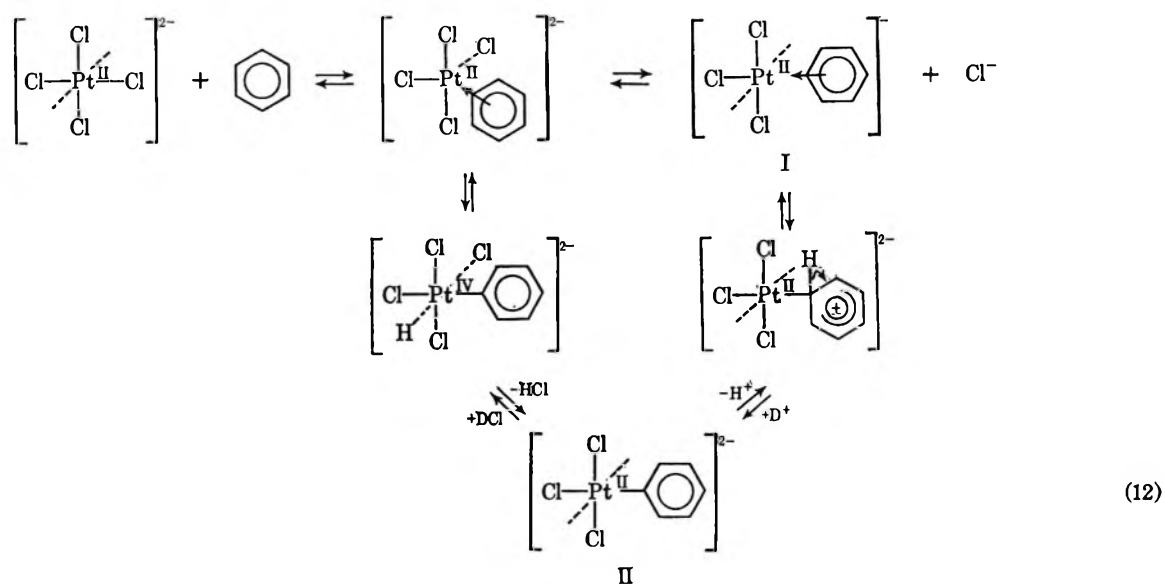
(22) A. I. Shatenstein, "Isotopic Exchange and Replacement of Hydrogens in Organic Compounds," Consultants Bureau, New York, N. Y., 1962, p 262.

(23) U. Belluco, U. Croatto, P. Uguagliati, and R. Pietropaolo, *Inorg. Chem.*, **6**, 718 (1967).

(24) J. Chatt and B. L. Shaw, *J. Chem. Soc.*, 4020 (1959).

(25) C. D. Falk and J. Halpern, *J. Am. Chem. Soc.*, **87**, 3003, 3523 (1965).

The kinetics, however, do not preclude a mechanism involving hydrido intermediates. The results merely indicate that complete dissociation direct from a σ -complex does not occur. A rearrangement back to the π complex is the preferred step and is not rate determining. The reduction in exchange rate, due to chloride ion, is apparently incurred in the preliminary formation of the π -complex intermediate. The exchange step may involve either a reversible electrophilic displacement of a proton from the π -bonded aromatic or a reversible rearrangement of the π -bonded complex to a six-coordinated hydrido complex with the subsequent exchange involving the hydride group. Further evidence pertaining to the proposed mechanisms (eq 12) will now be discussed.



Mechanism of π -Complex Formation. A small isotope effect is observed in the deuteration of benzene $k(\text{deuteration})/k(\text{dedeuteration}) = 1.65 \pm 0.05$. It may be seen from the distribution (Figure 7) that there is a considerable difference in the M value of reaction. Anderson and Kembal's¹⁵ derivation of the M value does not include a consideration of the benzene molecules that initially form π complexes and then return to the parent benzene without deuteration. Thus a correction factor is necessary to account for the results of the present study. From Figure 7 it may be seen that a smooth curve through the corrected percentage abundances (d_1 to d_6) can be extrapolated reasonably accurately to the d_0 peak. This amount is assumed to represent the percentage of benzene- d_0 that was originally π -complexed but did not deuterate. The revised distributions are presented in Table V. It is apparent that the direction of exchange does not appreciably affect the amount of benzene complexed (I) in the first step of the reaction. The predominant isotope effect of the exchange process is thus incurred in subsequent steps of the exchange mechanism. The origin of this

isotope effect is uncertain; although the exchange step is fast, the relative bond strength of the C-D and C-H bonds may result in a preference to multiple exchange with the C-H bonds.

A similar treatment of the results of Figure 6 and Table II indicates that the mole percentage of acetic acid does not alter the amount of π -complex intermediate formed. The revised distributions are summarized in Table VI and it is apparent that with the exception of sample A (where some Pt precipitated owing to low acidity) the uncomplexed benzene remains relatively constant over a wide range of acetic acid concentrations. The reduction in the exchange most likely occurs because of a lower concentration of deuterium in the solvation sphere of the platinum-benzene complex result-

ing in a lower M value. The fact that no solvent effect is observed in the π -complex formation is consistent with other substitution reactions involving square-planar platinum complexes.²⁶ The generally accepted

Table V: Corrected Distribution of Figure 7^a

Compound	% benzene- d_0	Cor (Figure 7)	% benzene not complexed	% benzene complexed
C_6H_6	80.4	1.9	78.5	21.5
C_6D_6	83.9	4.3	79.6	20.4

^a Correction applied for molecules which π complex but do not exchange.

mechanism for substitution reactions²⁷ is *via* a five-coordinated intermediate with the aromatic as the

(26) U. Belluco, A. Orio, and M. Martelli, *Inorg. Chem.*, **5**, 1370 (1966).

(27) C. H. Langford and H. B. Gray, "Ligand Substitution Processes," W. A. Benjamin, Inc., New York, N. Y., 1965, Chapter 2.

entering group in this special case. The rate-determining step is the formation of this five coordinated species for many substitution reactions.²⁷ Aprotic solvents possessing a strong coordinating nature do have a very significant effect on the rate of substitution²⁷ and this has been observed in the present reaction. For example, dimethyl sulfoxide in small concentrations is quite toxic to the exchange, apparently owing to preferential coordination.

Table VI: Corrected Distribution of Table II^a

Sample	% benzene- <i>d</i> ₀	Cor	% benzene not complexed	% benzene complexed
A	84.8	1.8	83.0	17.0
B	83.8	2.2	81.6	18.4
C	84.1	2.5	81.6	18.4
D	84.7	3.0	81.7	18.3
E	86.0	3.8	82.2	17.8
F	86.7	4.8	81.9	18.1

^a Corrections similar to those of Table V.

The inverse effect of chloride ions could be interpreted as a competing reaction for substitution in the square-planar platinum. It must also be noted that the dissociation of the π complex is slow and is independent of the chloride ion concentration since there is no change in *M* value (Figure 4).

Nature of the π Complex. The data represented in Figure 3 may also be extrapolated back to *d*₀ to overcome the problems of differences in *M* values. Revised distributions are summarized in Table VII. Using this technique, an apparent activation energy for the complex formation is calculated to be 28.1 kcal/mol. The over-all activation energy of deuteration is 25.7 kcal and it is apparent that the exchange step has a considerably lower activation energy. The displacement reaction of phenyl groups by chloride ions would not be expected to be rate determining, and Belluco, *et al.*,²³ have obtained an *E*_A of 10.6 kcal/mol for the displacement of phenyl groups in *trans*-Pt(PEt₃)₂Ph₂.

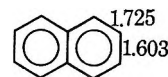
At this stage little conclusive evidence is available about the nature of the intermediate π complex.

Table VII: Corrected Distributions of Figure 3^a

Temp, °C	Exchange rate, % D/hr	<i>M</i>	% benzene- <i>d</i> ₀	Cor (Figure 3)	% benzene complexed	Rate of benzene complexed, %/hr
60.0	0.1096	4.00	94.38	0.61	6.23	0.182
70.0	0.3345	3.82	94.05	0.78	6.73	0.601
79.6	0.930	3.46	93.63	1.11	7.48	1.86
88.7	2.41	3.26	93.12	1.63	8.51	5.46
100.0	7.24	2.96	92.46	2.24	9.78	18.9

^a Corrections similar to those of Table V.

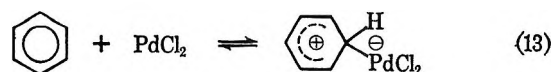
Ruthenium(II) complexes where the benzene is π -bonded through only two double bonds have recently been reported.²⁸ The possibility of loss of aromatic delocalization energy in the present system must also be considered as the activation energy is relatively high (namely, 28.1 kcal/mol) for the π -complex formation. Bond fixation in naphthalene occurs more readily than in benzene and a π -bonded species analogous to the ruthenium complex could be expected for naphthalene and platinum(II). However, results show that at 80° stepwise exchange occurs in the β position only (Table IV). This suggests that in naphthalene (III) the π complex is associated with only one bond of the molecule. The bond order²⁹ of the 1-2 bond is considerably higher than that of the 2-3 bond and a π complex with the 1-2 bond would be more likely to occur. Because of steric hindrance involving the α position (shown for a large number of polycyclic aromatics), multiple exchange would then always be confined to the one β position and could not be observed.



III

This study suggests that the π complex is somewhat olefinic in character, analogous to the already well-known π olefinplatinum complexes, and it has been found that olefins do poison the catalyst for exchange. In benzene, there would be a considerably larger loss of delocalization energy than in naphthalene; however, overlap of the π orbitals with the platinum will reduce the necessary activation energy and this type of complex must also be considered.

Further support for the proposed mechanism is provided by van Helden and Verberg³⁰ in a study of the conversion of benzene to biphenyl using PdCl₂ in glacial acetic acid. The reaction proceeded only in the presence of sodium acetate, and the rate of coupling of substituted aromatics showed little dependence on the electronic nature of the substituent. Large steric hindrance of the *ortho* positions also was observed in the series studied. The results are analogous to the present reaction and were explained by assuming the rate-determining step to be the formation of a complex with the PdCl₂ (eq 13) as in normal electrophilic aromatic substitution.



The authors suggested that subsequent reaction with acetate ions led to dimerization *via* a π -cyclohexadienyl-

(28) G. Winkhaus and H. Singer, *J. Organometal. Chem.* (Amsterdam), **7**, 487 (1967).

(29) C. A. Coulson, R. Daudel, and J. M. Robertson, *Proc. Roy. Soc. (London)*, **A207**, 306 (1951).

(30) R. van Helden and G. Verberg, *Rec. Trav. Chim.*, **84**, 1263 (1965).

palladium chloride complex. Davidson and Triggs³¹ have also studied this coupling reaction but preferred the explanation that σ -phenylpalladium(II) complexes were involved as intermediates in the reaction.

In the present study, where reduction of the platinum(II) was not prevented by acidity, analysis of the deuterated byproducts (chlorobenzene and biphenyl) indicated that the deuterium was also incorporated in the *ortho* positions.¹⁷ This is in contrast with the direct deuteration of these substances under conditions where the catalyst is stable; steric hindrance in the *ortho* position is very pronounced. With platinum therefore, the coupling reaction in a deuterated solvent at low acidity is preceded by several exchange cycles and this indicates that π complexes are formed prior to electrophilic attack leading to substitution or dimerization. This effect is also observed with the platinum(IV) reduction to platinum(II) (Table I).

In conclusion, the mechanism envisaged (eq 12) could involve either of two pathways once the π complex is obtained. The σ complex (II) could be formed by

either rearrangement to an octahedral Pt^{IV} complex or electrophilic attack upon the aromatic. The π -complex intermediate (I) would be formed by either pathway and is the aromatic equivalent of Zeise's salt $KPtCl_3 \cdot C_2H_4$. The kinetics of formation indicate that Cl^- ions compete with the benzene in the formation of the complex but do not increase the rate of dissociation as there is no observed variation in M value. This π complex may involve all six π electrons; however, an olefinic π complex cannot be discounted on the evidence available. At this time, it is not possible to distinguish between the mechanisms.

Acknowledgment. The authors thank the Australian Institute of Nuclear Science and Engineering and the Australian Research Grants Committee for assistance. Acknowledgment is also made to the donors of the Petroleum Research Fund administered by the American Chemical Society for support of this research.

(31) J. M. Davidson and C. Triggs, *Chem. Ind. (London)*, 457 (1966)

The Electronic Properties of Aluminum Oxide and the Chemisorption of Water, Hydrogen, and Oxygen

by S. Khoobiar,¹ J. L. Carter, and P. J. Lucchesi

Esso Research and Engineering Company, Linden, New Jersey (Received November 2, 1967)

A method is described for measuring the electronic properties of a polycrystalline Al_2O_3 over a wide range of temperatures. It has been found that adsorbed surface impurities dominate the low-frequency dielectric constant measurements and that at high frequency the bulk properties dominate. The conductivity increases upon chemisorption of H_2O , O_2 , or H_2 and upon chemisorption H_2 dissociates and donates electrons to the Al_2O_3 , whereas O_2 accepts electrons from the Al_2O_3 .

Oxides such as Al_2O_3 play a key role in industrial catalysis, either alone or as supports for metals. Although it is generally agreed that a study of the electronic properties of catalytic oxides can give much insight into their catalytic properties, such studies are very difficult to make over a wide range of conditions. On the other hand, it is necessary to cover a wide range of conditions in order to obtain useful new information with polycrystalline systems such as Al_2O_3 . We present in this paper a study of polycrystalline Al_2O_3 covering a range of conditions that to our knowledge has not been reported previously.^{2,3}

The equations used in the paper were previously

derived and applied to mixed semiconductor oxides⁴ and nonstoichiometric semiconductor oxides.⁵ In polycrystalline alumina the surface to bulk ratio is 10^5 – 10^6 times as great as the surface to bulk ratio for a single crystal. Since the forbidden energy gap is of the order of 9 eV (*vide infra*), the Debye length is

- (1) Halcon International, Little Ferry, N. J.
- (2) (a) S. Levy and M. Folman, *J. Phys. Chem.*, **67**, 1278 (1963);
(b) J. F. Garcia de la Banda, *J. Catalysis*, **1**, 136 (1962).
- (3) J. M. Thorp, *Trans. Faraday Soc.*, **55**, 442 (1959).
- (4) G. H. Yonker, *J. Phys. Chem. Solids*, **9**, 165 (1959).
- (5) J. H. Becker and H. P. R. Fredrikse, *J. Appl. Phys.*, **31**, 1, 447 (1962).

greater than the linear dimension of the crystallites. The effects of adsorbed surface species therefore extend throughout the "bulk" of the solid. For this reason we assume that the same equations that have been derived for bulk electronic properties hold for this work. This assumption has also been made by others.⁶

Introduction

In this section, we shall review a few well-known equations⁷ as derived for single crystals in order to set the background for presenting the data. If n is the density of electrons in the conduction band, N_a^- the density of acceptor centers that are ionized, P the density of holes in the valence band, and N_a^+ the density of ionized donor centers

$$n + N_a^- = P + N_a^+ \quad (1)$$

Also, the energy gap, temperature, and carrier densities are related by

$$\text{n-type } \begin{matrix} n > p \\ N_d > N_a \end{matrix} \quad n = N_c \exp\left[\frac{(-E_c - E_f)}{kT}\right] \quad (2)$$

$$\text{p-type } \begin{matrix} p > n \\ N_a > N_d \end{matrix} \quad p = N_v \exp\left[\frac{-E_f - E_v}{kT}\right] \quad (3)$$

intrinsic $p > n$

$$n = p = (\text{const}) \exp\left[\frac{-(E_c - E_v)}{2kT}\right] \quad (4)$$

In eq 3 and 4, E_f refers to Fermi energy, E_c the energy level of the conduction band, E_v the energy level of the valence band, and N_c and N_v , respectively, to the density of states in the conduction and valence bands.

The thermoelectric power, Q , is given by

$$Q = \frac{Q_n \sigma_n + Q_p \sigma_p}{\sigma} \quad (5)$$

where the subscript n refers to the electron contribution, and p refers to the contribution from holes. The symbol σ refers to conductivity and $\sigma = \sigma_n + \sigma_p$.

Since Q_n is a negative quantity by convention, Q is positive when $Q_p \sigma_p > Q_n \sigma_n$ (p-type semiconductor), and Q is negative when $Q_p \sigma_p < Q_n \sigma_n$ (n-type semiconductor). Also

$$Q_n = \frac{-k}{e} \left[A_n + \frac{E_{fn}}{kT} \right] \quad (6)$$

and

$$Q_p = \frac{k}{e} \left[A_p + \frac{E_{fp}}{kT} \right] \quad (7)$$

In eq 6 and 7, e refers to the electronic charge, A is the scattering factor for electrons and holes, and $E_{fn} = E_f - E_c$; $E_{fp} = E_f - E_v$. From these equations

$$\frac{E_{fn}}{kT} = \ln \frac{N_c}{n} \quad (8)$$

$$\frac{E_{fp}}{kT} = \ln \frac{N_v}{p}$$

We now define $\alpha = \sigma_p/\sigma_n$, and $b = \mu_n/\mu_p$ where the symbol μ refers to mobility. Combining these definitions with the foregoing equations gives

$$\frac{2e}{k} Q = \epsilon' \frac{(\alpha - 1)}{(\alpha + 1)} + \delta - \ln \alpha \quad (9)$$

where

$$\epsilon' = \frac{E_c - E_v}{kT} + A_n + A_p$$

and

$$\delta = A_p - A_n + \ln \frac{N_v}{N_c b}$$

The foregoing equations can also be written in the following form, at temperatures low enough to prevent all the impurities from ionizing.

$$\text{n-type } \frac{n(N_a + n)}{N_d - N_a - n} = N_c \exp\left[\frac{-(E_c - E_d)}{kT}\right] \quad (10)$$

$$\text{p-type } \frac{p(N_d + p)}{N_a - N_d - p} = N_v \exp\left[\frac{-(E_a - E_v)}{kT}\right] \quad (11)$$

for $N_a > n$, these reduce to

$$n = N_c \frac{N_d - N_a}{N_a} \exp\left[\frac{-(E_c - E_d)}{kT}\right] \quad (12)$$

and for $N_d > p$

$$p = N_v \frac{N_a - N_d}{N_d} \exp\left[\frac{-(E_a - E_v)}{kT}\right] \quad (13)$$

Experimental Section

The special cell used in these studies is shown in Figure 1. The powder under investigation is pressed into the annulus between the two stainless steel concentric cylinders, which are used as the electrodes, at a pressure of 100,000 psi. This high pressure is sufficient to provide good grain to grain contact as well as electrode to sample contact.⁸ The surface area of the sample was measured after pressing and was found to be unchanged. The density of the specimen was calculated from its weight and volume. The dimensions of the cylindrical specimen are 1 mm thick

(6) J. Yahia, *Phys. Rev.*, **130**, 5 (1963).

(7) N. B. Hannay, "Semiconductors," Reinhold Publishing Corp., New York, N. Y., 1960.

(8) J. T. Richardson, private communication.

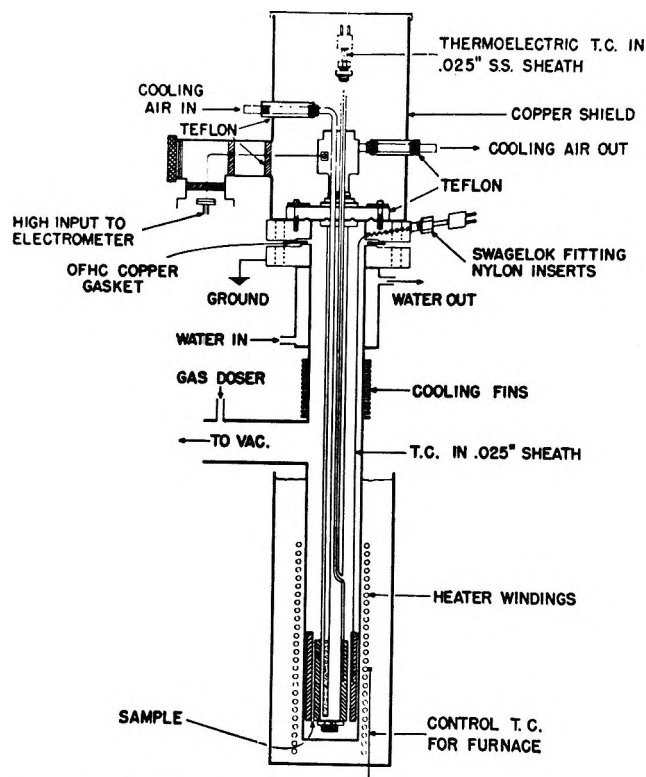


Figure 1. Cross section of the cell.

by 50 mm long with an i.d. of 22 mm. The outside electrode is grounded and the center electrode is floated above ground by Teflon insulators which have a greater resistance to ground than the sample does. As can be seen from Figure 1, the "high input" is bolted directly to the electrometer and completely shielded by copper to prevent any movement of the lead wires and eliminate any stray pickup.

To make the dc conductance measurements, the method involving voltage drop through a known resistor is used. A 64-V battery is used in this procedure and since the sample has a thickness of 1 mm, the effective voltage is 640 V/cm. For the ac measurements (dielectric constant and conductivity) the "high" lead and the grounded lead are connected directly to the terminals of the capacitance bridge and readings are taken at the desired frequencies. For the thermoelectric power measurements the "high" is connected directly to the electrometer and completely shielded as previously described. The cooling air to the center electrode is turned on and when the desired ΔT is reached the air is turned off. The measurements of ΔE vs. ΔT are then made as the center electrode warms up to the starting temperature. The absolute temperature of both electrodes is also measured at these points. These measurements may be made either under vacuum or in the presence of adsorbed gases.

A summary of the measurements that can be made with the above equipment and the range of experimental conditions that can be studied are given in Table I.

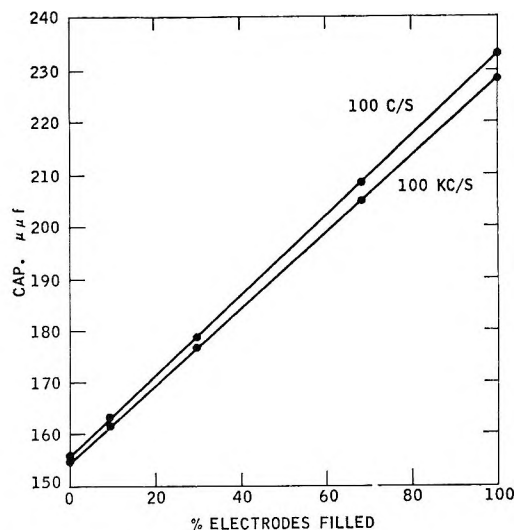


Figure 2. Determination of cell blank.

Properties of Al_2O_3

1. *Dielectric Properties.* The alumina was prepared by heating β -trihydrate alumina, which was obtained from the Davison Chemical Co., for 4 hr at 600° in flowing nitrogen. This alumina gave the characteristic X-ray diffraction pattern of η -alumina⁹ and had a BET surface area of $295 \text{ m}^2/\text{g}$. In order to measure a blank for the leads and electrodes, the overall capacitance of the system was measured at different frequencies as a function of the per cent of the cell filled with Al_2O_3 . All samples were degassed at 150° and 10^{-7} mm, and all measurements were made at 150° . Figure 2 summarizes the results. The measurements at frequencies between 100 cps and 100 kcps all fall between the two lines shown. The straight lines obtained as a function of the per cent of electrodes filled extrapolate to $154.5 \pm 0.5 \mu\text{f}$. From the data

$$C = C_0 E' W + B \quad (14)$$

where W is the extent of filling of the cell by the sample in %, E' is the dielectric constant of the sample, B is the "blank" capacitance, and C_0 is the capacitance per unit volume when air is the dielectric. From the slope at $W = 100\%$ we obtain, using eq 14 and the known value of C_0 (8.6×10^{-14}), $E' = 8.5$ for η - Al_2O_3 .

As an independent check on this value of E' , we can use the equation

$$E' = \frac{C_s}{1 + D^2} \frac{\ln r}{2\pi C_0 L} \quad (15)$$

which applies to a cylinder of length L and ratio r of outer to inner radius. C_s is the series capacitance

(9) J. W. Newsome, H. W. Heiser, A. S. Russell, and H. C. Stumpf, "Alumina Properties," The Aluminum Company of America, Pittsburgh, Pa., 1960.

Table I: Summary of Measurements Made with Conductivity Equipment

	Condition	Produced by	Measured with
T , temperature	77–1000°K	Liquid N ₂ and electrical heater	Iron–constantan thermocouple and precision potentiometer
P , pressure	10 ⁻⁸ mm, atmospheric	Fore and ion pump	Ion pump gauge, thermocouple gauge, Hg manometer
Gases added	Isotherm	BET system	Hg manometer and cathetometer
R_{dc} (dc resistance)	10 ² –10 ¹⁸ ohms		Vibron electrometer
C_s (ac series capacitance)	1–1000 $\mu\mu\text{F}$ at 100 cps to 5×10^6 cps	...	General Radio 716 capacitance bridge and tuned null detector
D , dissipation factor	0–55% at 100 cps to 5×10^6 cps	...	716 capacitance bridge and tuned null detector
ΔT , temperature difference	10–60°	Air flow into inside electrode	ΔT directly measured by precision potentiometer
Q , thermoelectric power	1 mV–1 V	Temperature difference	Vibron electrometer
Q , thermoelectric power	1 μV –10 V	Temperature difference	Honeywell microvoltmeter

and D is the dissipation factor, the term $1 + D^2$ connecting series capacitance to parallel capacitance. From actual measurements of C_s and D , we obtain in our system a value $E' = 2.4$. However, eq 15 assumes a uniformly fused dielectric material, not a porous one. The actual capacity of the porous sample will be lower than that of the nonporous sample by the ratio of the density of porous Al₂O₃ to that of fused Al₂O₃. This ratio is $3.9/1.12 = 3.4$. We should multiply the value obtained from (15) by 3.4, which gives $E' = 8.2$, in good agreement with the value 8.5 quoted above, and with the literature values of 8.2 to 8.8.¹⁰

It is worth noting that these results with porous Al₂O₃ indicate the density of the sample in our apparatus is uniform, and the measurements are reproducible. Similar measurements in our apparatus using porous SiO₂ gave a value of $E' = 4.6$, which compares with $E' = 4.3$ reported for fused SiO₂ under similar conditions.¹¹

2. *Degassing of Al₂O₃—the Role of H₂O.* The sample was degassed at 150, 300, 400, 500, and 600° to a pressure of 10⁻⁷ mm. R_{dc} , C_s , and D were measured at the temperature of degassing and then at temperatures lower than the degassing temperature. From these measurements, the E' was evaluated using eq 15 and the density correction discussed earlier. In addition to E' , these measurements provide values of $E'/D = E''$ and of

$$R_{dc} \text{ (specific)} = R_{dc} \text{ (measured)} \left[\frac{2\pi L}{3.4 \ln r} \right] \quad (16)$$

$$R_{ac} \text{ (specific)} = \frac{L}{2\pi f C_0 E''} \quad (17)$$

where in eq 17 f denotes frequency.

Figure 3 summarizes the dependence of the conductivity on frequency at different degassing temperatures. It is well known that the surface of Al₂O₃ is covered with hydroxyl groups¹² and that these hydroxyl groups are progressively removed by evacuation at the temperatures used in this study. It is clear that as these hydroxyl groups are removed the conductivity falls sharply, with the low-frequency values dropping by almost two orders of magnitude.

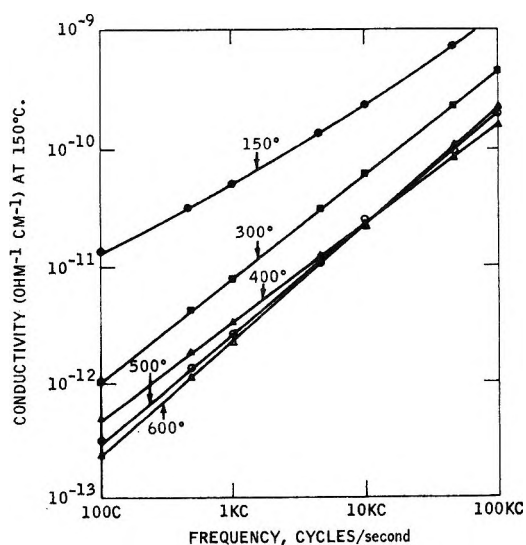


Figure 3. Conductivity (measured at 150°) vs. frequency for η -Al₂O₃ as a function of the outgassing temperature.

(10) "American Institute of Physics Handbook," McGraw-Hill Book Co., Inc., New York, N. Y., 1957.

(11) "Handbook of Chemistry and Physics," 45th ed, Chemical Rubber Publishing Co., Cleveland, Ohio, 1964.

(12) J. B. Peri and R. B. Hannan, *J. Phys. Chem.*, **64**, 1526 (1960).

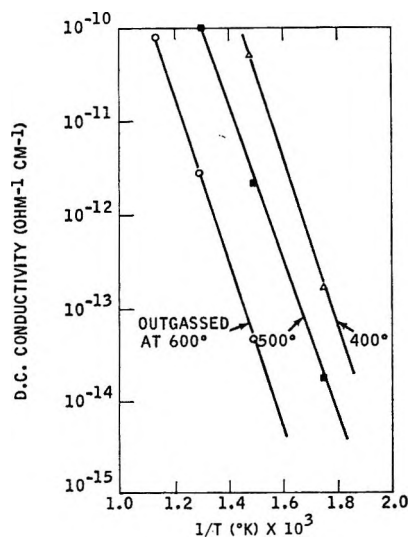


Figure 4. The dc conductivity of η - Al_2O_3 vs. reciprocal sample temperature, as a function of outgassing temperature.

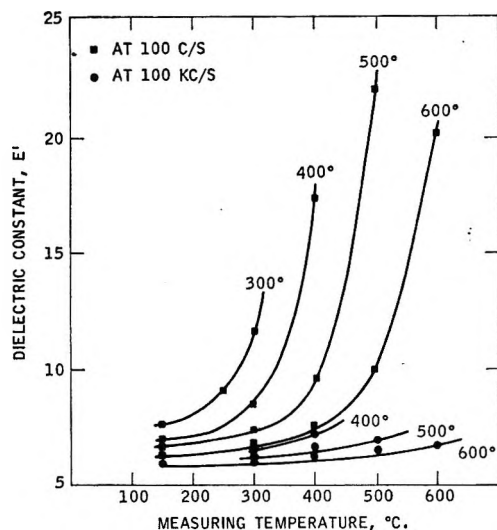


Figure 5. Dielectric constant of η - Al_2O_3 vs. measuring temperature, as a function of the outgassing temperature: ■, 100 cps; ●, 100 kc/s.

Figure 4 shows a plot of dc conductivity against $1/T$ for samples degassed at different temperatures. From eq 10-13, if degassing only removed impurities (H_2O and OH) but did not change the nature of the impurities present, only the quantity in the pre-exponential part of the equations would change. The temperature dependence of the conductivity would not change. This is what is observed, since in Figure 4 a set of nearly parallel lines is obtained from the plot of conductivity vs. $1/T$.

Figure 5 gives the variation of E' with temperature at different degassing temperatures and different frequencies. The data obtained in these degassing experiments can be rationalized with a model for polycrystalline Al_2O_3 in which the surface properties predominate. These, in turn, are to a large extent

determined by "impurities" in the form of hydroxyl groups. At higher temperatures, under vacuum, these are removed and the conductivity decreases.

The surface region can be considered as a region containing polar "solvent" species in a fairly rigid structure. These species (OH groups) contribute to a dielectric constant that changes with temperature only at lower frequencies. At higher temperatures, the surface is affected in at least two important ways. The acceptor impurities are removed to some extent, probably desorbing as H_2O . Also the solid structure which holds the dipoles becomes less rigid and the impurities become more mobile. In every case the low frequency E' increases sharply as the measuring temperature approaches the outgassing temperature. This contributes to a rather unusual effect—an increase of dielectric constant with increasing temperature. However, this phenomenon is quite similar to the variation of the E' of ice near the melting point¹³ and also similar to the E' of solid H_2S near its melting point. This is thought to represent the "frozen in" dipoles becoming mobile enough to permit orientation.

It is interesting to note that these effects alone would lead us to expect a rather large difference between the catalytic properties of Al_2O_3 at higher temperatures compared with lower temperatures, especially for reactions involving ionic intermediates.

The Chemisorption of H_2 and O_2 on Al_2O_3

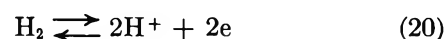
From the basic equations (10-13), we can derive

$$n = N_c (p_{\text{H}_2})^{1/\gamma} \exp \left[\frac{-(E_c - E_d)}{kT} \right] \quad (18)$$

$$p = \frac{1}{N_c} (p_{\text{H}_2})^{-1/\gamma} \exp \left[\frac{-E_d - E_v}{kT} \right] \quad (19)$$

In these equations, p_{H_2} refers to the hydrogen partial pressure at chemisorption equilibrium and γ is an integer. Equilibrium was attained at each pressure before recording the conductivity and the thermoelectric power values. Reversibility with respect to the gas pressure was also achieved; *i.e.*, data obtained at low pressure following a high-pressure point agree with points obtained in a steadily increasing pressure pattern. From the data on the increase of conductivity, Figure 6, with pressure it is apparent that the number of charge carriers after chemisorption is much greater than before; therefore, it is approximately true that the final number of charge carriers is equal to the charge transferred from the adsorbate to the alumina.

If, for example, the chemisorption of H_2 proceeds by the mechanism



(13) C. Kittel, "Introduction to Solid State Physics," 2nd ed, John Wiley and Sons, Inc., New York, N. Y., 1960.

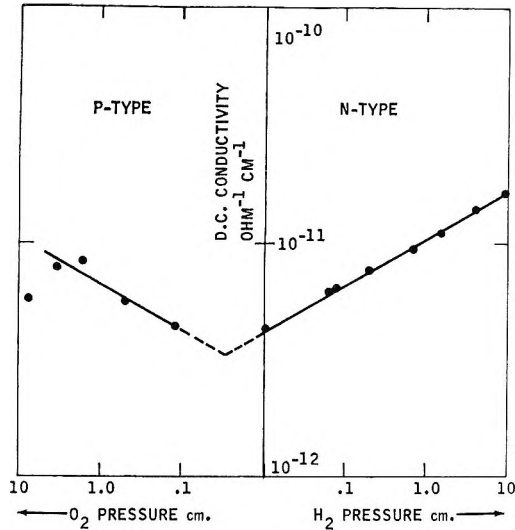


Figure 6. The dc conductivity of $\eta\text{-Al}_2\text{O}_3$ vs. O_2 and H_2 pressure measured at 600° .

then $e \approx \text{H}^+ \approx K e q (p_{\text{H}_2})^{1/4}$ and the value of $\gamma = 4$. From the definition of $\alpha = \sigma_p / \sigma_n$ and from (18) and (19), we derive

$$\alpha_{\text{H}_2} \cong \text{constant} \times (p_{\text{H}_2})^{-2/\gamma} \tag{21}$$

At constant temperature

$$\frac{d \ln \alpha_{\text{H}_2}}{d \ln p_{\text{H}_2}} = \frac{-2}{\gamma} \tag{22}$$

If σ_i refers to intrinsic conductivity, i.e., $\sigma_i = en(\mu_n + \mu_p) = ep(\mu_n + \mu_p)$, and $b = \mu_n / \mu_p$

$$\frac{\sigma}{\sigma_i} = \frac{b^{1/2}(\alpha + 1)}{(b + 1)\alpha^{1/2}} \tag{23}$$

the minimum conductivity will occur when $\alpha = 1$, so then

$$\frac{\sigma_m}{\sigma_i} = \frac{2b^{1/2}}{(b + 1)} \tag{24}$$

In general, from (23) and (24)

$$\frac{\sigma}{\sigma_m} = \frac{\alpha + 1}{2(\alpha)^{1/2}}$$

or

$$\frac{d(\ln \sigma / \sigma_m)}{d \ln \alpha} = \mp 1/2 \text{ for } \begin{cases} \alpha \gg 1 \\ \alpha \ll 1 \end{cases} \tag{25}$$

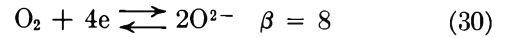
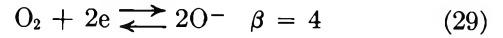
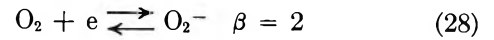
Combining with eq 22 gives

$$\frac{d \ln \sigma / \sigma_m}{d \ln p_{\text{H}_2}} = \frac{-1}{\gamma} \tag{26}$$

In the case of the chemisorption of O_2 , we obtain

$$\frac{d \ln \sigma / \sigma_m}{d \ln P_{\text{O}_2}} = \frac{1}{\beta} \tag{27}$$

where the value of β depends on the chemisorption mechanism as



Integration of eq 26 and 27 will yield

$$\ln \alpha_{\text{H}_2} = \text{constant} - \frac{2}{\gamma} \ln p_{\text{H}_2} \tag{31}$$

$$\ln \alpha_{\text{O}_2} = \text{constant} + \frac{2}{\beta} \ln p_{\text{O}_2} \tag{32}$$

To anticipate our results, the experimental data (Figure 6) gave $\beta = 5$ and $\gamma = 3.9$.

From eq 9 we obtain the variation of Q with α . The values of ϵ' and δ in eq 9 can be estimated from the maximum and minimum values of Q in Figure 7.

$$\frac{2e}{k}(Q_{\text{max}} - Q_{\text{min}}) \cong 2(\epsilon' - 1) - 2 \ln 2(\epsilon' - 1) \tag{33}$$

$$\frac{2e}{k}(Q_{\text{max}} + Q_{\text{min}}) \cong 2\delta \tag{34}$$

For our experiments, $\epsilon' \cong 128kT$ and $\delta \cong 16kT$ (Figure 7).

Figure 7 is a plot of theoretical eq 9 and experimental data. Equations 31 and 32 were used for the scale of Figure 7 abscissa to relate $\ln \alpha_{\text{H}_2}$, $\ln \alpha_{\text{O}_2}$ to $\ln p_{\text{H}_2}$ and $\ln p_{\text{O}_2}$. For the experiments involving H_2 and O_2 chemisorption, the Al_2O_3 was degassed at 600° and 10^{-7} mm. It was then treated with O_2 at various pressures. After reevacuation at 600° , the sample was treated with H_2 at 600° . Measurements were made of σ_{dc} , E' , and Q .

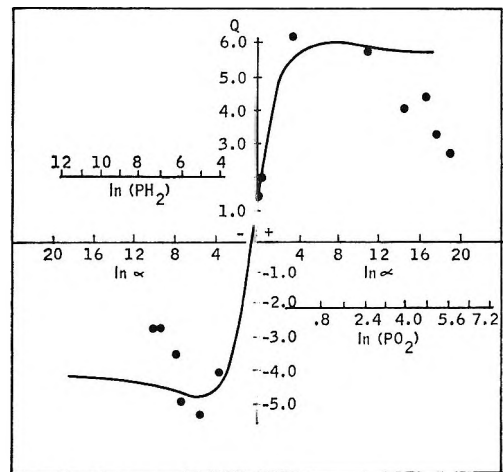
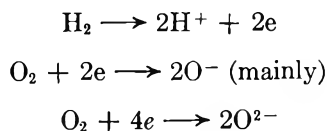


Figure 7. Thermoelectric power (Q) for $\eta\text{-Al}_2\text{O}_3$ at 600° as a function of H_2 and O_2 pressure. Solid line is theoretical (abscissa, $\ln \alpha$). The points are experimental (abscissa, $\ln P_{\text{O}_2}$, $\ln P_{\text{H}_2}$). $Q = \text{mV}/^\circ\text{C}$; pressure = $\text{cm} \times 10^{-2}$.

We reproduce in Figure 6 the change in σ_{dc} following changes in O_2 or H_2 pressures. We obtain from the data of Figure 6 and eq 26 and 27, $\gamma = 3.9$ and $\beta = 5.0$. These values favor the following chemisorption mechanism for the sample of Al_2O_3 used in this work.



We reproduce in Figure 7 the variation of Q with H_2 and O_2 equilibrium partial pressure. The experimental data check the form of the equation predicted from eq 9 fairly well. It was recognized at the outset that the shape of the curve, with respect to the theoretical, and the magnitude of the effect would be the important considerations. It was considered that the position of the curve, relative to the plus-minus axis, would be extremely difficult to reproduce. Experimentally, it was found that we could reproduce the difference between the maximum and minimum values of Q as well as the shape of the curve.

We observe from Figure 7 the same effects evident from measurements of conductivity, namely that η - Al_2O_3 used in this work is a p-type conductor rendered n-type by the chemisorption of H_2 at 600° . The data in Figure 7 were found to be reproducible using the same sample of Al_2O_3 . However, a different specimen prepared from the same batch of Al_2O_3 did *not* always give the effect observed in Figure 7, *i.e.*, the change from p- to n-type conductivity upon chemisorption of H_2 . The shape of the curve and the magnitude of the effect was always reproducible, however, and the same conclusions are drawn, the only difference being that the Q did not become negative when H_2 was added.

From the data of Figure 7 and eq 33 and 34, we derive

$$\begin{aligned} Q_{\max} &= 4.8 \text{ mV}/^\circ\text{C} \\ Q_{\min} &= -5.1 \text{ mV}/^\circ\text{C} \\ E' &= 128kT \\ \delta &= 16kT \end{aligned}$$

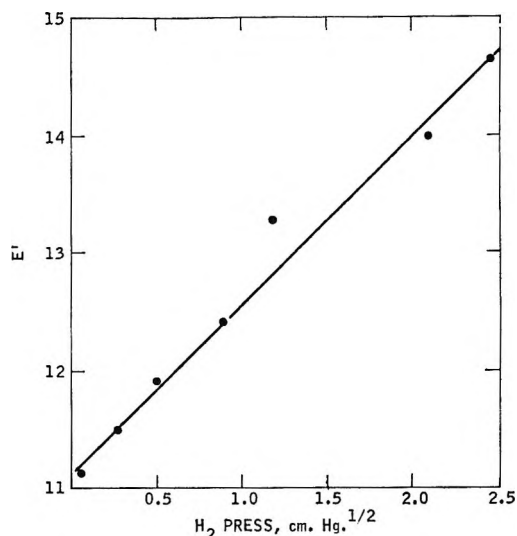


Figure 8. Dielectric constant of η - Al_2O_3 vs. square root of H_2 pressure measured at 600° .

The energy gap between conduction and valence band for this sample of η - Al_2O_3 has the very high value 9.6 eV. This compares with 9.3 reported for Al_2O_3 by Harrop and Creamer.¹⁴ Figure 8 summarizes an interesting plot of E' and P_{H_2} , which is in excellent agreement with theory for the proposed mechanism of hydrogen chemisorption.

In summary, the system described in this paper can accurately measure the electronic properties of powdered materials, which are normally considered insulators, over a range of frequencies and temperatures not before available. This system has been applied to the study of polycrystalline Al_2O_3 . For this catalytic oxide, it is found that the impurities adsorbed on the surface dominate the low-frequency dielectric constant as indicated in Figure 5. At high frequencies, the surface impurities are unable to follow the field, and bulk properties become more important. The dc conductivity is increased by chemisorption of H_2 or O_2 . Upon chemisorption, H_2 dissociates and donates electrons to the Al_2O_3 , whereas O_2 accepts electrons from the Al_2O_3 .

(14) P. J. Harrop and R. H. Creamer, *Br. J. Appl. Phys.*, **14**, 335 (1963).

Tracer Studies of the Isomerization of Cyclopropane

over a Deuterated Zeolite Catalyst¹

by B. H. Bartley,² H. W. Habgood, and Z. M. George

Research Council of Alberta, Edmonton, Alberta, Canada (Received November 3, 1967)

The isomerization of cyclopropane over sodium Y zeolite was investigated using a chromatographic pulse technique and with the protonic acid sites on the catalyst maintained in a deuterated form by the presence of a constant low partial pressure of D₂O in the helium carrier gas. The deuterium content of the product propylene, unreacted cyclopropane, and that of a propylene slug separately injected and passed through the catalyst were determined. The proposed reaction scheme allows for consecutive and parallel first-order reaction steps involving exchange, isomerization without exchange, and isomerization with exchange. Expressions derived for the resultant concentrations of propylene-*d*₀ and cyclopropane-*d*₀ and -*d*₁ permitted evaluation of the rate constants. The results showed that H-D exchange occurs in the isomerization step as well as by separate exchange reactions of cyclopropane and propylene, but that in the isomerization step, about 26% of the reaction also occurs without exchange. Separate experiments with cyclopropane-*d*₆ and H₂O-wet catalyst showed an isotope effect of 1.5 associated with the catalyst hydrogen and no isotope effect associated with the cyclopropane hydrogen. It is concluded that both exchange of cyclopropane and isomerization proceed *via* the same nonclassical protonated cyclic carbonium ion and that the isomerization step further involves an intramolecular hydrogen transfer.

Introduction

The isomerization of cyclopropane to propylene is catalyzed by various acidic oxides and also by crystalline zeolites.³⁻⁹ Roberts³ examined a number of acidic oxides; Hall and coworkers⁴⁻⁶ studied this reaction over a silica-alumina catalyst; and Bassett and Habgood⁷ and Habgood and George⁹ worked with various cationic forms of zeolites X and Y.

The results of these previous studies indicate that the surface reaction at low pressure is first order with no side reactions. Some complications may arise with very active catalysts owing to subsequent polymerization or coking of the propylene product. The results of Bassett and Habgood⁷ and of Habgood and George⁹ showed that negligible irreversible adsorption of reactants or products was found over most group Ia and IIa zeolite catalysts, although Hall and coworkers found extensive irreversible adsorption of the first slugs of cyclopropane passed over silica-alumina. The previous work from this laboratory, in particular the acceleration of the reaction by small traces of water, supported the original suggestion of Roberts³ pointing toward protonic or Brønsted acid sites as the active catalytic centers. Although Larson, Gerberich, and Hall⁵ had found evidence favoring Lewis sites, the most recent results of Gerberich, Hightower, and Hall^{10,11} based on measurements with methyl- and ethylcyclopropanes have supported the Brønsted mechanism.

Thus the isomerization of cyclopropane to propylene has possible applications as a test reaction for the measurement of Brønsted acidity of catalysts. The present study is concerned with elucidating the mech-

anism of the isomerization reaction by means of isotopic-tracer experiments to follow the incorporation of deuterium from the catalyst into the cyclopropane and the product propylene.

Sodium Y zeolite was chosen as a catalyst having moderate catalytic activity and good kinetic behavior. The catalytic activity is markedly increased by the presence of small amounts of water.⁹ All of the catalyst acidity was kept in the Brønsted form by keeping the sodium Y zeolite slightly hydrated with a constant partial pressure of D₂O in the helium carrier gas. Under these conditions, any Lewis acidity should be converted to Brønsted acidity.

This work is an extension of the preliminary measurements reported by Habgood and George⁹ and, like

(1) Contribution No. 406 from the Research Council of Alberta. Presented at the Second Canadian Symposium on Catalysis, Hamilton, Ontario, June 1967.

(2) RCA Postdoctoral Fellow 1966-1967.

(3) R. M. Roberts, *J. Phys. Chem.*, **63**, 1400 (1959).

(4) W. K. Hall, J. G. Larson, and H. R. Gerberich, *J. Amer. Chem. Soc.*, **85**, 3711 (1963).

(5) J. G. Larson, H. R. Gerberich, and W. K. Hall, *ibid.*, **87**, 1880 (1965).

(6) W. K. Hall, F. E. Lutinski, and H. R. Gerberich, *J. Catal.*, **3**, 512 (1964).

(7) D. W. Bassett and H. W. Habgood, *J. Phys. Chem.*, **64**, 769 (1960).

(8) I. Tadao and G. L. Osberg, *A.I.Ch.E. J.*, **11**, 279 (1965).

(9) H. W. Habgood and Z. M. George, *Proc. Soc. Chem. Ind. Conf. Mol. Sieves*, in press.

(10) H. R. Gerberich, J. W. Hightower, and W. K. Hall, *J. Catal.*, **8**, 391 (1967).

(11) J. W. Hightower and W. K. Hall, *Amer. Chem. Soc. Div. Petrol. Chem. Preprints*, **12** (3), 191 (1967); *J. Amer. Chem. Soc.*, **90**, 851 (1968).

those measurements, has used the gas chromatographic pulse technique.

Theoretical Section

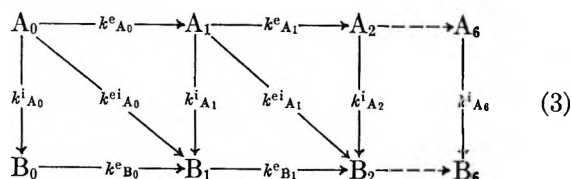
Considering first the conversion of cyclopropane (A) to propylene (B) by an irreversible first-order surface reaction, the isomerization rate constant, k^i , may, in the usual fashion, be written as

$$k^i = \frac{1}{t_A} \ln \frac{1}{1-x} \quad (1)$$

where t_A is the contact time and x is the fractional conversion. In a microcatalytic experiment in which a discrete pulse of reactant is passed through the catalyst column, the contact time is the net retention time of the reactant on the catalyst, or in terms of the net retention volume and carrier-gas flow rate, V_R/F . The fractional conversion x may be expressed as $[B]/[A_0^0]$, where $[B]$ is the amount of propylene formed and $[A_0^0]$ is the amount of cyclopropane injected. By rearrangement, eq 1 can be expressed in the form

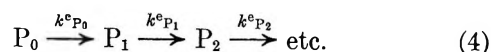
$$[B] = [A_0^0](1 - e^{-k^i t_A}) \quad (2)$$

If we now consider the possible reactions that may occur when cyclopropane- d_0 is passed over a deuterated catalyst which may exchange deuterium with both cyclopropane and propylene, these reactions may be written as follows.



where A denotes cyclopropane and B denotes propylene, with subscripts giving the number of deuterium atoms in each. Each rate constant, k , has a subscript indicating the reactant for that particular reaction and a superscript describing the reaction as one of exchange (e), isomerization without exchange (i), or isomerization with exchange (ei). If the catalyst is maintained in a fully deuterated condition, the reverse exchange reactions, *e.g.*, $A_1 \rightarrow A_0$, may be considered negligible. The isomerization reactions are for practical purposes thermodynamically irreversible and are all assumed to be first order. Reactions involving a double incorporation of deuterium in a single step are assumed absent.

To study the exchange reactions of propylene, propylene- d_0 may be passed through the catalyst and the exchange reaction sequence is



which is identical with the bottom sequence of reactions 3 but written with different symbols to avoid confusion in the resultant integral equations.

As indicated by reaction scheme 3, the observed deuteration of propylene formed by isomerization may be the result of deuteration of the cyclopropane prior to isomerization, deuteration occurring during isomerization, deuteration of the propylene after isomerization, or a combination of all three. In deriving equations for the product distribution from a single pulse of injected cyclopropane, we must make allowance for the different retention times of cyclopropane and propylene in the catalyst column. Any chromatographic band develops a Gaussian profile within a column as a result of various band-broadening effects. If these effects are neglected, in other words if the cyclopropane pulse is assumed to travel through the column without any increase in band width and if the band of the product propylene is taken as the sum of incremental pulses of similar width formed along the full length of the column, then the following equations may be derived for the concentrations (or amounts, since first-order kinetics are assumed) of the various species emerging from the column.

$$[A_0] = [A_0^0]e^{-k_{A_0}t_A} \quad (5)$$

$$[B_0] = \frac{k^i_{A_0}t_A[A_0^0]}{k_{A_0}t_A - k^e_{B_0}t_B} [e^{-k^e_{B_0}t_B} - e^{-k_{A_0}t_A}] \quad (6)$$

$$[A_1] = \frac{k^e_{A_0}[A_0^0]}{k_{A_0} - k_{A_1}} [e^{-k_{A_1}t_A} - e^{-k_{A_0}t_A}] \quad (7)$$

$$[P_0] = [P_0^0]e^{-k^e_{P_0}t_P} \quad (8)$$

$[A_0^0]$ and $[P_0^0]$ are the concentrations of cyclopropane and of propylene injected into the catalyst column and

$$k_{A_0} = k^e_{A_0} + k^i_{A_0} + k^{ei}_{A_0} \quad (9)$$

$$k_{A_1} = k^e_{A_1} + k^i_{A_1} + k^{ei}_{A_1} \quad (10)$$

The contact times t_A and t_B are the net retention times of cyclopropane and propylene.

Equation 8 relates to the exchange of propylene on the catalyst and may be used with eq 6 through the identities

$$k^e_{B_0} \equiv k^e_{P_0} \quad (11)$$

$$k^e_{B_1} \equiv k^e_{P_1} \quad (12)$$

$$t_B \equiv t_P \quad (13)$$

Additional equations may be written for the concentrations of further isotopic species in the reaction scheme, but the use of these more complex equations would require a higher level of accuracy than that attained in the present measurements. Equations 5 and 8 for $[A_0]$ and $[P_0]$ are ordinary first-order rate equations and their derivations are straightforward. Equation 7 for $[A_1]$ is a combination of two first-order rate equations. The net rate of formation of A_1 is

$$\frac{d[A_1]}{dt} = k^e_{A_0}[A_0] - k_{A_1}[A_1] \quad (14)$$

which, on substitution of eq 5 for $[A_0]$, becomes

$$\frac{d[A_1]}{dt} = k_{A_0}^e [A_0^0] e^{-k_{A_0} t} - k_{A_1} [A_1] \quad (15)$$

Provided that k_{A_0} is not equal to k_{A_1} , the solution to eq 15 is eq 7. In our reaction scheme we would not expect k_{A_1} and k_{A_0} to be equal because of the different numbers of deuterium atoms in A_0 and A_1 . In the case that k_{A_1} is equal to k_{A_0} , the solution to eq 15 has the form

$$[A_1] = k_{A_0}^e t_{A_1} [A_0^0] e^{-k_{A_1} t_{A_1}} \quad (16)$$

The derivation of eq 6 for $[B_0]$ is somewhat more complex as a result of the continuous formation of propylene along the catalyst column and of the different retention times for propylene and cyclopropane. We must consider the production of B_0 from A_0 according to $k_{A_0}^i$, which occurs all along the column as the band of A passes through, and the disappearance of B_0 according to $k_{B_0}^e$, as long as the B_0 remains in the column. Let us first consider one small element of B_0 , $\delta[B_0]^0$, that is formed in the catalyst column during the interval Δt at time t and distance y along the column, where t varies from 0 to t_A and y from 0 to 1 during the passage of A along the column. The amount of A_0 at this time is given by the first-order rate law as $[A_0^0] e^{-k_{A_0} t}$. Hence the amount of B_0 formed in this interval Δt is

$$\delta[B_0]^0 = k_{A_0}^i [A_0^0] e^{-k_{A_0} t} \Delta t \quad (17)$$

The propylene B_0 then continues on through the reactor and decreases by exchange according to

$$\frac{d(\delta[B_0])}{d\tau} = -k_{B_0}^e \delta[B_0] \quad (18)$$

where τ is the time from the formation of this particular element of B_0 and the total residence time, τ_{\max} , is obtained from the relation

$$\frac{t_B - \tau_{\max}}{t_B} = y = \frac{t}{t_A} \quad (19)$$

Hence the amount of B_0 remaining at the column exit from $\delta[B_0]^0$ is given by

$$\delta[B_0] = \delta[B_0]^0 e^{-k_{B_0}^e t_B (1 - (t/t_A))} \quad (20)$$

To obtain the total amount of B_0 leaving the column, we must add all of the incremental amounts arising from isomerization of A_0 over the full length of the column

$$\int_0^{[B_0]} \delta[B_0] = k_{A_0}^i [A_0^0] e^{-k_{B_0}^e t_B} \int_0^{t_A} e^{-(k_{A_0} - k_{B_0}^e (t_B/t_A)) t} dt \quad (21)$$

which becomes eq 6.

The quantities that are experimentally measurable are the retention times t_A and t_B , the amounts of cyclopropane and propylene leaving the reactor (the sum of

which is equal to $[A_0^0]$, and the amounts of A and B species, as determined from the measured conversions and the mass spectrometric analyses of the cyclopropane and propylene collected. Knowing $[A_0^0]$, $[A_0]$, and t_A , the rate constant for the disappearance of A_0 , k_{A_0} , can be determined using eq 5. From the observed exchange of a propylene slug separately injected at the same temperature, the rate constant for exchange of propylene- d_0 , $k_{B_0}^e$, can be determined by eq 8. Substituting these values of k_{A_0} and $k_{B_0}^e$ in eq 6, the rate constant for the isomerization of A_0 without exchange, $k_{A_0}^i$, can be determined. Knowing k_{A_0} and $k_{A_0}^i$, we can determine the sum of $k_{A_0}^e$ and $k_{A_0}^{ei}$ from eq 9, but to determine these two rate constants individually is not possible by eq 5-8 alone. The rate constant for exchange of A_0 , $k_{A_0}^e$, occurs in eq 7 but along with the additional unknown k_{A_1} . Equations to solve for k_{A_1} would introduce further unknowns. For the whole kinetic scheme there are 14 equations involving 25 rate constants; in addition, we have eq 1 referring to the rate constant k^i . Hence, in order to determine the rate constants even for the first few reactions in the scheme, some assumption must be made concerning relations among the rate constants for the various isotopic species.

The assumption we have made is that the over-all rate constant for isomerization, that is, the chromatographically determined rate constant k^i defined by eq 1 is equal to the sum of the rate constants of any single species for isomerization with and without exchange. That is

$$k^i = k_{A_0}^i + k_{A_0}^{ei} = k_{A_1}^i + k_{A_1}^{ei} = \dots = k_{A_n}^i \quad (22)$$

Evidence to support this assumption is presented below. Thus with k^i determined from the chromatographic peak areas and $k_{A_0}^i$ evaluated as described in the preceding paragraph, we can determine $k_{A_0}^{ei}$. By subtracting k^i from k_{A_0} , we obtain $k_{A_0}^e$.

Experimental Section

The gas-chromatographic microcatalytic-reactor system was similar to that used previously.^{7,9} The helium carrier gas was purified by passage through a quartz diffusion cell (Electron Technology, Inc., Kearny, N. J.) and provision was made for passing the helium through a saturator to attain a constant partial pressure of D_2O (or, in a few experiments, of H_2O). The saturator consisted of a U tube that was packed with clean, dry Chromosorb-P firebrick, was baked out at 500° for 2 days in flowing dry helium, was cooled to room temperature, and was evacuated; D_2O or H_2O was injected onto the firebrick through a rubber septum located on a side arm above the firebrick. The side arm was then sealed off and helium was passed through the saturator for a short while to distribute the D_2O or H_2O evenly over the firebrick. The firebrick will carry up to 35% of D_2O without appearing wet. The temperature of

the saturator was kept at 0° giving, with allowance for pressure drop, an average vapor pressure over the catalyst of 2.8 torr for D₂O or 3.6 torr for H₂O. The normal range of carrier-gas flow rates was 20–50 ml/min.

A 10-g sample of sodium Y zeolite supplied by the Linde Division of Union Carbide Corp. (Lot SK-40-51-31) was treated with 1 l. of 1 M NaCl at 70° overnight, with vigorous stirring. The material was then washed with distilled water until it was free of Cl⁻. It was left at 100° overnight, pelletized, crushed, and sieved to 20–40 mesh. The sample used in the experiments had a weight of 0.40 g calculated on a fully dehydrated basis and had the formula Na_{0.96}Ca_{0.006}AlO₂·2.39SiO₂. The treatment with sodium chloride had reduced the calcium content from 0.6 to 0.1%.

The catalyst was activated by slow heating in flowing helium to 500°, followed by treatment with oxygen at 500°, as described in an earlier paper.⁹ There was no apparent loss of crystallinity during the course of the measurements, as indicated by the unchanged rectilinear character of low-temperature nitrogen-adsorption isotherms.

Prior to any measurements, the catalyst was equilibrated at a temperature around 200° with D₂O by passing wet helium through the catalyst column for a sufficient time to achieve equilibrium coverage.⁹ The helium was maintained wet by passage through the saturator for all measurements.

The experiments were carried out over the temperature range 200–400°. Normally about 0.5 hr was allowed after each change in temperature; this time was sufficient to give reproducible results, although possibly not complete reequilibration.⁹ From previous frontal chromatographic measurement of adsorbed H₂O, the D₂O adsorbed at equilibrium on the catalyst surface was estimated as ranging from 2.5 to 0.5 molecules/zeolite large cavity over the temperature range 205–350°.

The reactions were carried out by injecting a slug of cyclopropane-*d*₀ (3 ml at 10 torr) by means of a set of fast-acting metal valves. Over this catalyst of relatively low reactivity there was no change in conversion with successive slugs of cyclopropane. The retention volumes of propylene and of cyclopropane could not always be measured directly under the experimental conditions of this investigation; they were accordingly estimated by extrapolation from measurements made at lower temperatures. These retention volumes corresponded to maximum concentrations of adsorbed cyclopropane at the injection partial pressure of 10 torr of 0.02 molecule/large cavity at 205° and 0.003 molecule at 350°.

The products of reaction were collected in a liquid nitrogen cooled trap for 30 min and then flashed onto the analytical column (20 ft × 0.25 in., 20% squalane on Chromosorb at 60°). The product peaks separated

by gas chromatography were collected separately in break-seal tubes for mass spectrometric analysis using 70-V ionizing electrons. The cracking patterns for cyclopropane-*d*₀, propylene-*d*₀, propylene-*d*₁, propylene-*d*₂, and propylene-*d*₃ were determined experimentally. The cracking patterns for the deuterated cyclopropanes were calculated assuming a CH bond breaks twice as easily as a CD bond. This assumption also gave good agreement between observed and calculated cracking patterns for the propylenes. The flow rates were chosen to give relatively low conversions of cyclopropane to propylene and this also gave relatively small amounts of multiply deuterated compounds. The deuterium distributions in propylene and in unreacted cyclopropane were determined by comparing the spectra of the standards against the spectra of the unknown and obtaining the best fit for the C₃ fragments.

Results

The various reactions of kinetic scheme 3 were studied by injecting slugs of cyclopropane-*d*₀ and of propylene-*d*₀ over the deuterated catalyst. The experimental conditions, measured conversions, and isotopic compositions are summarized in Table I. Knowing the peak areas and the isotopic compositions of the cyclopropane and propylene peaks, the various exchange and isomerization rate constants were evaluated as described above and are plotted in Figure 1. The precision of the values for $k_{A_0}^e$ is less than for the other rate constants because $k_{A_0}^e$ is the difference of the two quantities k_{A_0} and k^i and will be influenced by the errors in each. The activation energies for the various reactions

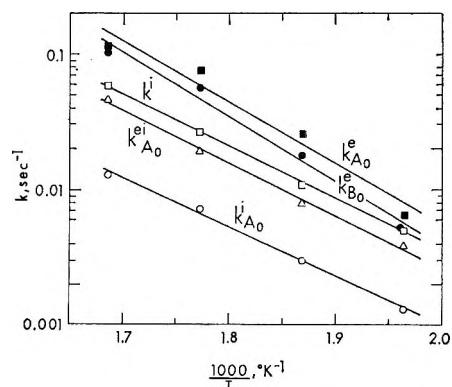


Figure 1. Arrhenius plots of the rate constants for the various exchange and isomerization reactions of cyclopropane over sodium Y zeolite according to scheme 3. There was an error in calculating the $k_{A_0}^e$'s shown in this figure. The correct values in order of increasing temperature are 0.0116, 0.0365, 0.102, and 0.172; the corresponding activation energy is 20 kcal/mol. The rate constants $k_{A_0}^e$ were also calculated directly from the observed conversion to A₁ using eq 7 with the assumption that $k_{A_1} = k_{A_0} - 1/6k_{A_0}^e$ (the fraction 1/6 is the statistically expected decrease in the rate constant for exchange of A as the result of introducing one deuterium among the six exchangeable hydrogens) to give the values 0.0114, 0.0343, 0.095, and 0.146, respectively.

Table I: Reaction of Cyclopropane- d_0 and Propylene- d_0 Over Deuterated Sodium Y Zeolite

Temp. °C	Contact time, sec		Con- version, %	Re- actant	Isotopic composition of products, %							
	t_A	t_B			Cyclopropane (A)				Propylene (B)			
					d_0	d_1	d_2	d_3	d_0	d_1	d_2	d_3
236	13.0	20.1	6.5	A	86.0	13.6	0.5	0.3	22.3	62.7	10.3	2.9
		20.1		B					90.4	9.2	0.6	0.1
262	8.3	11.2	8.6	A	73.9	23.1	3.0	0.4	21.6	58.0	15.0	4.2
		11.2		B					81.9	13.6	3.9	0.5
291	3.9	4.7	9.7	A	67.4	27.6	4.8	0.7	19.8	53.8	12.6	12.0
		4.7		B					76.9	20.5	2.5	0.2
320	3.0	3.2	15.7	A	60.5	31.2	7.4	1.2	14.6	55.8	24.2	4.4
		3.2		B					72.6	23.4	3.9	0.2

of A_0 and B_0 are listed in Table II. The fraction of isomerization of A_0 proceeding without exchange, $k^i_{A_0}/(k^i_{A_0} + k^{ei}_{A_0})$, is given in Table III. In addition to the results shown here, two preliminary sets of measurements were carried out using the same catalyst sample and gave essentially the same results.

A separate series of experiments was carried out to compare the isomerization rate constants, k^i , for the reactions of cyclopropane- d_0 and of cyclopropane- d_6 over the D_2O -wet catalyst. No isotopic analyses were made on the products; the rate constants were calculated by eq 2 from the cyclopropane and propylene peak areas. A larger sample (2 g) from the same lot of catalyst was

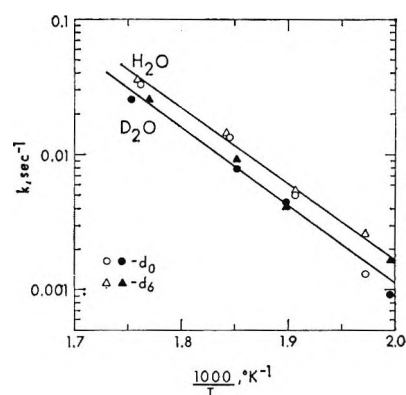
Table II: Activation Energies for Individual Reactions in Cyclopropane Isomerization According to Reaction Scheme 3

Activation energy, kcal/mol	Rate constant				
	$k^e_{A_0}$	$k^i_{A_0}$	$k^{ei}_{A_0}$	k^i	$k^e_{B_0}$
	21	17	18	18	22

Table III: Proportion of Isomerization of Cyclopropane- d_0 over Deuterated Catalyst Occurring Without Exchange

Temp, °C	$k^i_{A_0}/(k^i_{A_0} + k^{ei}_{A_0})$
236	0.26
262	0.28
291	0.28
320	0.22
	Av 0.26

used here and this permitted direct measurement of cyclopropane retention volumes under reaction conditions. Cyclopropane- d_0 and cyclopropane- d_6 had the same retention volumes and they were also the same on the D_2O -wet and on the H_2O -wet catalyst. The rate constants for isomerization on the D_2O -wet catalyst are shown as the lower line of Figure 2 and show no difference within experimental error between A_0 and A_6 . This is taken as support for the assumption of eq


Figure 2. Rate constants for the isomerization of cyclopropane- d_0 and cyclopropane- d_6 over the H_2O - and the D_2O -wet form of the sodium Y zeolite.

22 that the rate constant for the isomerization of each isotopic species of cyclopropane, considered without regard to accompanying exchange, is equal to that for every other species and to that obtained chromatographically from the injection of cyclopropane- d_0 . In other words, there is no kinetic isotope effect for isomerization associated with the cyclopropane hydrogen. (As will be shown below, an isotope effect within the molecule may contribute to the proportions of different products.)

The upper line of Figure 2 shows the results of a similar experiment with the same catalyst equilibrated with H_2O . Again, no significant difference was found in reactivity between cyclopropane- d_0 and cyclopropane- d_6 , but these rate constants with the H_2O -wet catalyst are about 1.5 times greater than those for the deuterated form of the catalyst. A small contribution to this greater reactivity in the presence of H_2O may arise from the higher partial pressure of water vapor,⁹ but it is likely that most of the difference represents a kinetic isotope effect associated with the catalyst hydrogen. Larson, Gerberich, and Hall⁵ in experiments in which cyclopropane- d_0 was isomerized over the same silica-alumina catalyst, first in the deuterated form and then in the hydrogen form, found no difference in rate but, as they pointed out, protonation of the active sites

during passage of the slug could obscure a possible isotope effect in the catalyst hydrogen. In the same study with silica-alumina catalyst they found, in experiments involving coisomerization of cyclopropane- d_0 and $-d_6$, an inverse isotope effect of k_{d_0}/k_{d_6} equal to 0.85. This is in contrast to our finding with the zeolite catalyst of no detectable isotope effect associated with the cyclopropane hydrogen.

The activation energy (24 kcal/mol) obtained with this second sample of catalyst is significantly higher than that for the first sample from the same lot, as given by the data in Figure 1. There is no obvious reason for this difference which is at variance with the previous results for sodium X.⁹

An attempt was made to determine the possible extent of irreversible adsorption of cyclopropane and propylene on the catalyst. This was done by comparing the chromatographic peak areas for samples sent through the catalyst column with those for samples by-passing the catalyst. By measuring the areas for several slugs in succession, alternating slugs through and by-passing the catalyst and plotting the area as a function of slug number, it was possible to obtain a greater precision than from single measurements. This procedure also allowed correction for the drop in sample pressure due to withdrawal from the sample reservoir; for no irreversible adsorption all points fell on a straight line of a slight negative slope. The chromatographic measurements were, of course, corrected for any small changes in flow rate. Where reaction occurred, the comparison was of the total area of cyclopropane plus propylene with the by-passing cyclopropane.

At 210° and a flow rate giving negligible conversion, there was no detectable irreversible adsorption of cyclopropane from a sample pressure of 100 torr.

Several tests were carried out at 335° and a flow rate giving about 40% conversion, *i.e.*, toward the upper limit of the temperature range of the experiments. With a cyclopropane sample pressure of 10 torr, no irreversible adsorption was detected, but at a sample pressure of 100 torr, about 12% of the material was not recovered. The loss seemed to be in the propylene fraction and this was confirmed by injection of propylene slugs which showed marked irreversible adsorption.

Irreversible adsorption of propylene is not unexpected and probably indicates some polymerization on the catalyst. Because any polymerization would be a higher order reaction, these effects would be most noticeable at higher pressures and (possibly) lower temperatures.

Hall and coworkers have raised the possibility that the Brønsted acidity of a catalyst may be the result of an interaction between hydrocarbon residue and Lewis acid centers. Although our experiments were carried out in the presence of water to provide the maximum concentration of Brønsted acid sites, we did attempt to place a limit on the possible extent of such coke for-

mation under limiting low-pressure conditions. This was done in an experiment using a 0.79-g catalyst sample and a small slug of propylene, 3 ml at 1 torr. At 236° there was no significant difference in peak areas of propylene through the catalyst and by-passing the catalyst. Taking the measurement uncertainty as 2% of the sample size, this corresponds to about 2×10^{15} molecules. The catalyst sample contained 2.9×10^{20} large cavities. Consequently, the maximum concentration of chemisorbed propylene was 1 molecule/ 1.5×10^5 large cavities. Similar results were also obtained for experiments with dry sodium Y catalyst.

Any irreversible adsorption, in addition to possibly altering the nature of the catalytic sites on the surface, will also interfere with the measurement of the degree of conversion. The calculated rate constant will be low if part of the propylene product is not detected.

Deviations in kinetics may also occur if the partial pressure of cyclopropane is high enough to extend into the nonlinear region of the adsorption isotherm. The adsorption equilibrium coefficient K will vary along the length of the column as the pressure within the pulse decreases. The observed retention volume will decrease with increasing sample pressure and the reaction will not be first order with respect to cyclopropane partial pressure (a plot of $\ln 1/(1-x)$ vs. $1/F^\circ$ will depart from linearity). The best test for such an effect is to compare the conversion for cyclopropane samples of different partial pressures. Such a test at 315° confirmed first-order behavior to pressures above 10 torr, although noticeable decreases in conversion and retention volume were found at 100 torr.¹²

Discussion

The principal experimental results may be summarized as follows.

(i) Exchange with catalyst deuterium may occur simultaneously with the isomerization of cyclopropane as well as by separate reactions of the cyclopropane and propylene.

(ii) There is a normal hydrogen-deuterium kinetic-isotope effect associated with the catalyst hydrogen.

(iii) There is no kinetic-isotope effect associated with the cyclopropane hydrogen.

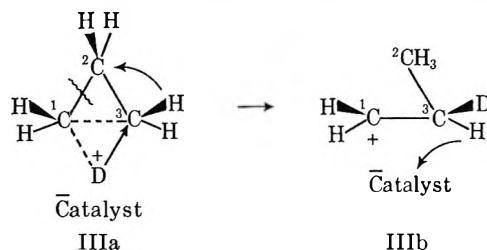
(iv) The activation energies for isomerization and for hydrogen-deuterium exchange of cyclopropane are similar.

(v) During the isomerization reaction over deuterated catalyst, the proportion of isomerization occurring without exchange is relatively high (26%).

Conclusion v differs from the conclusions of Hightower and Hall¹¹ with silica-alumina catalyst. They carried out coisomerization experiments in which an

(12) J. W. Hightower and W. K. Hall (submitted for publication in *J. Phys. Chem.*) have described marked departures from first-order behavior for cyclopropane isomerization over silica-alumina at higher reaction pressures and lower reaction temperatures than those investigated here.

a proton which migrates to C-2 with simultaneous breaking of the 1-2 bond and rearrangement of charges to give IIIb. This intermediate is the same primary



propyl cation as in the first mechanism but with the deuterium on the middle carbon rather than on the methyl carbon and with the ion in a different steric configuration on the surface. A deuterium or hydrogen from the middle carbon then returns to the catalyst to give propylene. Without any isotope effect, the degree of deuteration would be 50%; the observed 74% degree of deuteration could arise from an isotope effect of 2.8 or from some rearrangement of the primary to the secondary propyl cation before propylene is released.

This second mechanism predicts that the deuterium involved in the isomerization-exchange reaction will be located on the middle carbon atom, as opposed to location in the methyl group according to the first mechanism. These two suggested alternatives might be distinguished on the basis of the location of the deuterium atom in the product propylene, but it might be difficult to separate the effects of exchange during reaction $A_0 \rightarrow B_1$ from the random deuteration that would occur in propylene formed by the route $A_0 \rightarrow A_1 \rightarrow B_1$ and the deuteration in positions 1 and 3 in propylene formed *via* $A_0 \rightarrow B_0 \rightarrow B_1$.

Both of the postulated mechanisms for step c involve an intramolecular hydrogen transfer. The generally unstable nature of primary carbonium ions would suggest that the separate species depicted as IIa and b and IIIa and b probably should be considered as transitory stages rather than distinct intermediate configurations.

Baird and Aboderin concluded, in their experiments on the solvolysis of cyclopropane in solution, that there was complete mixing of the added deuterium by rapid rearrangements within the nonclassical carbonium ion. On the catalyst surface, the strong forces of adsorption may well act to inhibit such reactions. Silver¹⁴ and Skell and Starer¹⁵ found that reactions in solution that proceeded *via* a primary propyl cation gave about 10%

of cyclopropane in addition to propylene. This is probably further evidence for the particularly high reactivity of the primary cation. It is unlikely that we could detect any small degree of reclosing of the ring to re-form cyclopropane.

The exchange of propylene over the deuterated catalyst probably occurs *via* the secondary propyl cation $\text{CH}_3\text{CH}^+\text{CH}_2\text{D}$ to give a mixture of propylene- d_0 , - $1d_1$, and - $3d_1$. This mechanism was supported by the observed absence of exchange on C-2 in experiments in which propylene- $2d_1$ was passed over H_2O -wet catalyst.

It has already been pointed out that our results differ somewhat from those of Hall and coworkers^{5,10,11} for cyclopropane and alkyl cyclopropanes on silica-alumina with regard to isotope effects and the extent of exchange accompanying isomerization. Their conclusions agree with ours, to the extent of proposing the cyclic nonclassical carbonium ion as the common intermediate in both isomerization and exchange. For the ring-opening step, however, their results are consistent with the more usual mode of deprotonation of an intermediate *n*-propyl cation—and of secondary alkyl cations in the case of substituted cyclopropanes—to form olefins without the need for intramolecular hydrogen transfer. With alkyl cyclopropanes, the inherently greater stability of secondary, relative to primary, carbonium ions may allow time for the necessary steric rearrangement on the catalyst surface. We hope to investigate the degree of deuteration resulting from the isomerization of methylcyclopropane in our system.

In our experiments the presence of Brønsted sites on the surface seems adequately explained by either residual acidic OH groups on the zeolite or by interaction of the adsorbed water with strong cationic or Lewis acid centers. There was no positive evidence of sites associated with adsorbed hydrocarbon residues as suggested by Hightower and Hall¹¹ for silica-alumina, but our observations do not rule out such a possibility with more active zeolite catalysts in the absence of water.

Acknowledgments. We thank Dr. W. K. Hall of the Mellon Institute for a number of useful discussions and for providing us with prepublication copies of ref 10 and 12 and the final version of ref 11. Technical assistance was provided by J. Mendiuk.

(14) M. S. Silver, *J. Amer. Chem. Soc.*, **82**, 2971 (1960).

(15) P. S. Skell and I. Starer, *ibid.*, **82**, 2971 (1960).

The Vaporization of Ytterbium Dicarbide

John M. Haschke and Harry A. Eick

Department of Chemistry, Michigan State University, East Lansing, Michigan 48823 (Received November 3, 1967)

Samples of ytterbium dicarbide and ytterbium sesquicarbide have been prepared by direct reaction of the elements in sealed tantalum bombs. The vaporization of the dicarbide according to the reaction $\text{YbC}_2(\text{s}) \rightarrow \text{Yb}(\text{g}) + 2\text{C}(\text{s})$ has been studied by the target collection Knudsen effusion technique over the temperature range 1100–1550°K. An X-ray fluorescence method for analysis of the condensed effusate has been developed. Second- and third-law results are reported, and the $\Delta H_{f,298}^\circ$ of $\text{YbC}_2(\text{s})$ has been determined to be -18.0 ± 1.0 kcal/gfw.

Introduction

Current interest in the vaporization behavior and thermodynamics of lanthanide and alkaline earth dicarbides is evidenced by the number of investigations recently reported. Aside from recent descriptions of the samarium,¹ gadolinium,² and cerium³ dicarbide systems, extensive reviews of the thermodynamics of both the alkaline earth⁴ and lanthanide⁵ dicarbides have appeared in conjunction with newly obtained results.

The vaporization behavior of lanthanide dicarbides appears to fall into two classes—one having only metal vapor in equilibrium with the condensed phase and the other having both the metal vapor and the gaseous metal dicarbide as equilibrium species. The lanthanide metals which commonly exhibit the trivalent oxidation state always exhibit dicarbide vapor species. Together with the alkaline earth dicarbides, both europium⁶ and samarium⁷ dicarbides exhibit only gaseous metal as significant equilibrium vapor species and consequently vaporize according to the reaction



Europium and samarium, like the alkaline earth metals, exhibit an oxidation state of +2. With the anticipation that ytterbium, which is also divalent, would behave similarly, the vaporization of the dicarbide was studied by the target collection Knudsen effusion technique.

In an attempt to obtain better agreement between second- and third-law values of $\Delta H_{f,298}^\circ$ for reaction 1 and to find the source of a slight temperature trend in a preliminary third-law heat, a complete repetition of the measurements was undertaken and constitutes essentially a second independent determination. The analytical procedure used for determining the amount of effusate condensed, the sticking coefficient, the vapor pressure in equilibrium with the dicarbide on the metal-rich side of the $\text{YbC}_{2.00}$ composition, and the procedure used in temperature measurement have, therefore, been examined carefully.

Experimental Section

Preparative Methods. Ytterbium dicarbide was prepared by an adaptation of the technique employed by Spedding, *et al.*⁸ Samples were prepared from mixtures of ytterbium metal (Research Chemicals, Inc., Phoenix, Ariz.; 99.9%) and CP graphite (Fisher Scientific Co., Pittsburgh, Pa.) which had been outgassed previously under vacuum at 1800°. The reactants were sealed by heliarc welding into previously outgassed tantalum bombs made from 6.35- or 9.52-mm seamless tantalum tubing. Samples were prepared with stoichiometries of YbC_x , where $1.5 \leq x \leq 2.2$. To effect reaction, the bombs were heated by induction for 3–6 hr at 1300–1500° for compositions where $x \geq 2$, and at 1000–1300° for those where $1.5 \leq x \leq 2$. Since helium sealed into the bombs promoted rupture and subsequent loss of metal vapor, samples were packed tightly into the tubes and the remaining volume was eliminated by crimping the tube flat prior to sealing.

Analytical Methods. The products were analyzed chemically for metal content by ignition of the oxalate to the sesquioxide⁹ and for unbound graphite which precipitated when the samples were acidified with dilute HCl. X-Ray powder diffraction patterns of the polycrystalline phases were obtained with 114.59-mm Debye-Scherrer cameras using copper $K\alpha$ radiation ($\lambda_{\text{vac}} 1.54050 \text{ \AA}$). Samples were handled in a helium-

(1) H. A. Eick, J. M. Haschke, and P. A. Pilato, IUPAC Thermodynamik Symposium, Heidelberg, Sept 1967.

(2) C. L. Hoening, N. D. Stout, and P. C. Nordine, *J. Am. Ceram. Soc.*, **50**, 385 (1967).

(3) P. Winchel and N. L. Baldwin, General Atomics GA Project 109, John Hopkins Laboratory Report, San Diego, Calif., 1967.

(4) J. Cuthbert, R. L. Faircloth, R. H. Flowers, and F. C. Pummery, *Proc. Brit. Ceram. Soc.*, **8**, 155 (1967).

(5) R. L. Faircloth, R. H. Flowers, and F. C. Pummery, United Kingdom Atomic Energy Authority Research Group Report AERE-R 5480, 1967.

(6) R. E. Gebelt and H. A. Eick, *J. Chem. Phys.*, **44**, 2872 (1966).

(7) P. A. Pilato and H. A. Eick, 152nd National Meeting of the American Chemical Society, New York, N. Y., Sept 1966.

(8) F. H. Spedding, K. Gschneidner, and A. H. Daane, *J. Am. Chem. Soc.*, **80**, 4499 (1958).

(9) L. A. Sarver and P. H. Brinton, *ibid.*, **49**, 943 (1927).

filled glove box and stored under vacuum to prevent hydrolysis.

The vaporization mode of ytterbium dicarbide was investigated mass spectrometrically with a Bendix time-of-flight mass spectrometer, Model 12-107. All species emanating from a molybdenum Knudsen cell heated by electron bombardment were subject to analysis with both a high (70 eV) and a low (10 eV) energy ionizing electron beam in the temperature range 1280–1485°.

Target Collection. The effusion apparatus used for the target collection work is essentially that described by Ackermann.¹⁰ The Pyrex and Vycor system was evacuated to residual pressures of 10^{-5} – 10^{-6} torr. Aluminum targets, which previously had been cleaned with abrasive, washed, and subjected to background count with the X-ray fluorescence spectrometer, were stacked in a liquid nitrogen cooled holder and exposed to the effusate for measured time intervals. To minimize the effects of changes in the fluorescence spectrometer, all targets were accompanied in both background and postexposure counting with an unexposed control target. To ensure reproducible geometry in analysis, the fraction of effusate analyzed was not determined by a knife edge on the target holder but by a knife-edged insert placed inside the rim of the target during analysis. The effective perpendicular distance from orifice to target was obtained by adding the distance from crucible to target rim, as measured with a cathetometer, to the distance from the rim to the target face. Targets were exposed at both successively increasing and decreasing temperatures.

Temperature measurements were made with an NBS-calibrated Leeds and Northrup disappearing-filament type of pyrometer by sighting *via* a prism and window into a blackbody hole drilled into the bottom of the Knudsen cell. After exposure of the targets, the holder was replaced by an optical window and the temperatures of the orifice and blackbody hole were checked over the temperature range. Temperatures were corrected for prism and window absorbance, which was measured with a standard lamp.

Knudsen cells with knife-edged orifices of both high-density graphite and molybdenum were used in the vaporization experiments. Molybdenum cell orifice areas of 58.0×10^{-4} , 20.8×10^{-4} , and 7.06×10^{-4} cm² were determined both by planimeter measurements of micrographic photographs and by microscope measurements of the circular orifices viewed over an American Optical Co. micrometer slide calibrated in 0.01-mm divisions. The cylindrical cells (internal height = internal diameter = 0.795 cm) were charged with 0.3–0.4-g samples.

One vaporization experiment with a metal-rich sample (Yb_2C_3 – YbC_2) was conducted at a constant temperature of 928°. Targets were exposed at se-

lected times to observe the behavior of the Yb pressure as the YbC_2 stoichiometry was approached.

Since an oxide coat on the aluminum targets might affect the sticking ability of ytterbium vapor, a series of experiments was conducted to check the sticking coefficient. Aluminum targets mounted in the vacuum system were coated with gold by vapor deposition from a Knudsen source at 1400°. Targets with an average coating of 8 mg of gold were obtained and exposed to the dicarbide effusate as described previously. The composition study described above and this sticking coefficient investigation were performed with an analytical calibration different from that used for the other data.

X-Ray Fluorescence. X-Ray fluorescence analysis was employed for determination of the amount of effusate collected. A Siemens Kristalloflex-IV generator and fluorescence attachment, with LiF analyzing crystal, tungsten tube, and proportional counter were used in initial measurements, while a Norelco generator and Siemens water-cooled scintillation counter were employed in later measurements. The sample holder was modified to accommodate the 2.54-cm o.d. aluminum targets used in the collection apparatus. Standard curves which allowed analysis of 0.5–10- μg quantities of effusate were obtained for ytterbium $L\alpha_1$ radiation by weighing a standard ytterbium solution onto precounted targets¹¹ and scanning the region $2\theta = 48.85$ – 49.35° in 4-min preset counts. The initial standard curve (sensitivity equals (662 counts/ μg)/4 min) was obtained by integration of detected radiation, while the second (sensitivity equals (274 counts/ μg)/4 min) was obtained by discrimination, *i.e.*, the maximization of ytterbium to background radiation. The 3–7- μg quantities of effusate collected per target were analyzable to $\pm 0.2 \mu\text{g}$ by this procedure.

Results

Both analytical and X-ray powder diffraction results substantiate the presence of ytterbium dicarbide. The reaction products from stoichiometries YbC_x , with $x \geq 2$, produced the dicarbide phase or dicarbide plus graphite. The invariant X-ray powder diffraction patterns which were indexable on tetragonal symmetry yielded lattice parameters which agree to within $\pm 0.01 \text{ \AA}$ with those reported previously.⁸ Faint spurious X-ray diffraction lines were observed occasionally in dicarbide preparations. Analytical results for the crystallographically pure dicarbide samples used in the vaporization experiments, together with standard deviations, are: ytterbium from oxalate ignition, $87.4 \pm 0.6 \text{ wt } \%$ (calcd 87.8); bound carbon, $12.6 \pm 0.5 \text{ wt } \%$ (calcd 12.2). The products

(10) R. J. Ackermann, U. S. Atomic Energy Commission Report ANL-5482, 1955.

(11) J. M. Haschke, R. L. Seiver, and H. A. Eick, submitted for publication.

from reaction of stoichiometry YbC_x , with $1.5 \leq x \leq 2$, produced a mixture of two phases: one the golden dicarbide and the other a silver-gray phase. At the Yb_2C_3 stoichiometry, the presence of dicarbide was not detectable in the X-ray powder diffraction pattern. Elemental analysis of the silver-gray phase yields: ytterbium by ignition to the sesquioxide, 90.3 ± 0.2 wt % (calcd for Yb_2C_3 , 90.58); bound carbon, 9.7 ± 0.2 wt % (calcd 9.42); unbound carbon, 0.0 wt %.

The only detectable equilibrium vapor species emanating from a Knudsen source charged with dicarbide was gaseous ytterbium. The sensitivity of the mass spectrometer allowed detection of partial pressures of 10^{-8} atm; thus the equilibrium ratio $\text{YbC}_2(\text{g})/\text{Yb}(\text{g}) < 10^{-5}$.

The high-density graphite Knudsen cells proved unsuitable for equilibrium studies since the ytterbium diffused rapidly through them. X-Ray fluorescence analysis of graphite samples bored from the exterior of the crucibles indicated a high concentration of this element. No difficulties were encountered with the molybdenum cells.

The equilibrium pressure above the Yb_2C_3 - YbC_2 two-phase region was found at 928° to be ten times that above the dicarbide-graphite two-phase region. The metal pressure in equilibrium with the sesquicarbide remained essentially constant with time before decreasing sharply to that in equilibrium with the dicarbide. Debye-Scherrer X-ray powder diffraction patterns of the sample indicated complete conversion to the dicarbide, which when vaporized to 50% metal depletion exhibited no detectable change in pressure.

By comparison with collection on gold, the sticking coefficient of ytterbium on aluminum is unity. Figure 1 (*cf.* runs 21B (Al) and 22B (Au)) indicates the coincidence of aluminum and gold data for two successive vaporization experiments with the same Knudsen cell. These data are also indicative of the precision attainable with the X-ray fluorescence analytical technique.

The equilibrium vapor pressure of ytterbium has been determined in seven vaporization experiments over the temperature range 825 – 1275° . A graph of $\log P_{\text{Yb}}$ vs. $1/T$ is presented in Figure 1. The linear least-squares equation describing the 61 data points in the temperature region 1100 – 1550°K is

$$2.303 R \log P_{\text{Yb}(\text{atm})} = [(-50,890 \pm 640)/T] + (18.98 \pm 0.50)$$

From this equation, the following thermodynamic data, together with their standard deviations, are calculated for reaction 1: $\Delta H^\circ_{1325} = 50.89 \pm 0.64$ kcal/gfw; $\Delta S^\circ_{1325} = 18.98 \pm 0.50$ eu. These second-law values have been corrected to 298°K by use of published heat content and entropy data¹²⁻¹⁴ and the

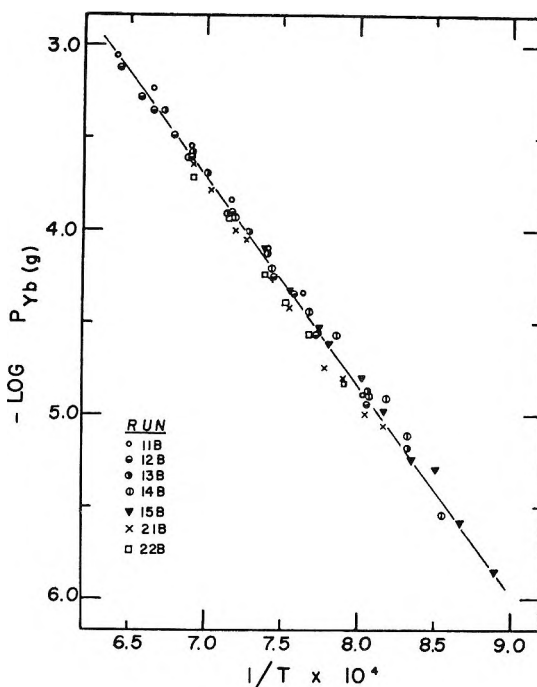


Figure 1. Equilibrium pressure of ytterbium vapor over ytterbium dicarbide.

following assumptions. The heat content of YbC_2 was assumed to be that of CaC_2 minus ΔH_{trans} for the tetragonal to cubic conversion (1.33 kcal/gfw)¹⁵ occurring at 720°K . Although the analogous tetragonal to cubic transition is observed for most of the lanthanide dicarbides, no such transition occurs in the ytterbium case.¹⁶ Krikorian, *et al.*, observed "some change of structure" between 700 and 1000° during slow heating in a high-temperature X-ray diffraction apparatus. X-Ray powder diffraction patterns for the dicarbide before and after vaporization experiments, however, imply that tetragonal dicarbide is the equilibrium phase as no change occurred in the sample during vaporization. The results of this data reduction, with the listed error indicating the composite of standard deviation and estimated error in thermodynamic values are: $\Delta H^\circ_{298} = 54.3 \pm 1.0$ kcal/gfw; $\Delta S^\circ_{298} = 24.9 \pm 1.2$ eu; $\Delta G^\circ_{298} = 46.9 \pm 1.0$ kcal/gfw. The value of ΔH°_{298} has been combined with the heat and free energy of formation of gaseous Yb at 298°K .^{12,17,18}

(12) R. Hultgren, R. L. Orr, P. D. Anderson, and K. K. Kelley, "Selected Values of Thermodynamic Properties of Metals and Alloys," John Wiley and Sons, New York, N. Y., 1963.

(13) D. R. Stull and G. C. Sinke, "Thermodynamic Properties of the Elements," Advances in Chemistry Series, No. 18, American Chemical Society, Washington, D. C., 1956.

(14) K. K. Kelley, Bureau of Mines Bulletin 584, U. S. Government Printing Office, Washington, D. C., 1960.

(15) G. E. More, *Ind. Eng. Chem.*, **35**, 1292 (1943).

(16) N. H. Krikorian, T. C. Wallace, and M. G. Bowman, Proceedings, Colloque International Sur les Derives Semimetallique du Centre National de la Recherche Scientifique et Université du Paris, Orsay, 1965.

to obtain: $\Delta H_f^\circ_{298}(\text{YbC}_2(\text{s})) = -18.0 \pm 1.0$ kcal/gfw; $\Delta G_f^\circ_{298}(\text{YbC}_2(\text{s})) = -18.6 \pm 1.2$ kcal/gfw. The entropy of ytterbium dicarbide has also been determined from ΔS°_{298} and Stull and Sinke's entropy values¹³ to be $S^\circ_{298}(\text{YbC}_2(\text{s})) = 19.2 \pm 1.4$ eu.

A third-law ΔH°_{298} has been calculated for reaction 1 using free energy functions approximated for $\text{YbC}_2(\text{s})$ ^{14,18-22} as follows: $\text{fef}_{\text{YbC}_2(\text{s})} = \text{fef}_{\text{CaC}_2(\text{s})} - \text{fef}_{\text{Ca}(\text{s})} + \text{fef}_{\text{Yb}(\text{s})}$. To eliminate the effects of the tetragonal to cubic transition, $\text{fef}_{\text{CaC}_2(\text{s})}$ was calculated as follows: $\text{fef}_{\text{CaC}_2(\text{s})} = (H^\circ_T - H^\circ_{298} - \Delta H^\circ_{\text{trans}})/[T - (S^\circ_T - \Delta S^\circ_{\text{trans}})]$, where $\Delta H^\circ_{\text{trans}} = 1.33$ kcal/gfw and $\Delta S^\circ_{\text{trans}} = 1.84$ eu.¹⁵ Published free energy functions for gaseous ytterbium and graphite^{12,13} were combined with the value computed for $\text{YbC}_2(\text{s})$ to obtain values of Δfef for reaction 1. The third-law average $\Delta H^\circ_{298} = 52.15 \pm 0.42$, which, when combined with estimated errors in free energy functions, gives $\Delta H^\circ_{298} = 52.2 \pm 1.2$ kcal/gfw.

This third-law ΔH°_{298} shows no apparent temperature trend; however, a third-law treatment based on free energy functions derived for $\text{YbC}_2(\text{s})$ using $\text{CaC}_2(\text{s})$ values uncorrected for enthalpy and entropy of transition had a definite temperature trend of 1.5-2.0 kcal/gfw.

Discussion

Some metal dicarbides, *e.g.*, uranium dicarbide,²³ exhibit variation of composition with temperature. However, the composition of alkaline earth and most lanthanide dicarbides³ is apparently invariant. An exception may be the europium species which some workers have been unable to prepare²⁴ and for which Gebelt and Eick indicated a composition of $\text{EuC}_{1.87}$.⁶ However, Cuthbert, *et al.*,⁹ prepared $\text{EuC}_{2.00}$ *in situ* in an effusion cell by heating until the europium pressure became constant. The present investigation established that both $\text{YbC}_{2.00}$ and $\text{YbC}_{1.50}$ represent stable phases in the ytterbium-carbon system. The existence of a Yb_2C_3 phase proposed previously⁸ has been confirmed both analytically and crystallographically, but it is not isostructural with the previously characterized sesquicarbides. Although the lanthanide and alkaline earth dicarbides have many similarities, the M_2C_3 phase has been reported for the lanthanides, but not for the alkaline earths. Apparently, its existence requires the presence of a trivalent metal ion. The occasional presence of faint diffraction lines in dicarbide preparations indicates either the existence of other graphite-rich phases or the reaction of the sample with the tantalum container.

That equilibrium between ytterbium vapor, the dicarbide, and graphite is achieved very rapidly without any apparent diffusion problems is indicated by the ease of ytterbium diffusion through the graphite Knudsen cells. Other evidences that the system reaches equilibrium quickly are both the lack of orifice

effects in a sevenfold variation of orifice area and the coincidence of the pressure data collected at both ascending and descending temperatures. Although no weight loss data were obtained and a value cannot be calculated, the effective vaporization coefficient seems close to unity.

The presence of an oxide coat on the aluminum metal apparently does not affect the sticking ability of an effusing metal vapor. The results of recent investigations of metal surfaces by low-energy electron diffraction²⁵ imply that oxygen is absorbed rapidly on clean metal surfaces, and, therefore, an aluminum oxide or a gold surface with absorbed oxygen might possess similar sticking capacities for effusing metal vapor. The sticking coefficients of nitrogen on tungsten have been measured as a function of temperature, and the sticking probability and capacity were found to be increased greatly as substrate temperature decreased.²⁶ In light of these considerations, the sticking coefficient of ytterbium vapor on a liquid nitrogen cooled metal target is probably equal to, or at least very close to, unity.

The X-ray fluorescence technique which is readily applicable to all elements with $Z > 19$ has proved to be a useful method for quantitatively analyzing the effusate collected by Knudsen effusion without transfer of the effusate from the target. The combined vapor pressure data in Figure 1, representing two essentially independent measurements, show excellent agreement. Second-law enthalpy data, *i.e.*, relative pressures, may be obtained readily by the fluorescence technique without analytical standardization for the spectrometer.

The usefulness of the third-law enthalpy calculation has been reiterated by the present experiment. Preliminary results (*cf.* runs 11B-15B, Figure 1) from second-law ($\Delta H^\circ_{298} = 56.1$ kcal/gfw) and third-law ($\Delta H^\circ_{298} = 50.3$ kcal/gfw) calculations were not in good agreement, and a temperature trend was evident in the third-law data. From third-law considerations, error

(17) C. E. Habermann and A. H. Daane, *J. Chem. Phys.*, **41**, 2818 (1964).

(18) J. R. Berg, F. H. Spedding, and A. H. Daane, U. S. Atomic Energy Commission Report IS 327, 1961.

(19) K. K. Kelley and E. G. King, Bureau of Mines Bulletin 592, U. S. Government Printing Office, Washington, D. C., 1961.

(20) B. C. Gerstein, J. Mullaly, E. Phillips, R. E. Miller, and F. H. Spedding, *J. Chem. Phys.*, **41**, 883 (1964).

(21) O. V. Lounasmaa, *Phys. Rev.*, **143**, 399 (1966).

(22) O. V. Lounasmaa, *ibid.*, **129**, 2460 (1963).

(23) E. K. Storms, U. S. Atomic Energy Commission Report, LA-DC-6952, 1965.

(24) A. L. Bowman, N. H. Krikorian, G. P. Arnold, T. C. Wallace, and N. G. Nereson, Proceedings of the 6th Rare Earth Conference, Gatlinburg, Tenn., 1967.

(25) H. E. Farnsworth and H. H. Madden, "Solid Surfaces and the Solid-Gas Interface," Advances in Chemistry Series, No. 33, American Chemical Society, Washington, D. C., 1961.

(26) G. Ehrlich, *J. Chem. Phys.*, **34**, 29 (1961).

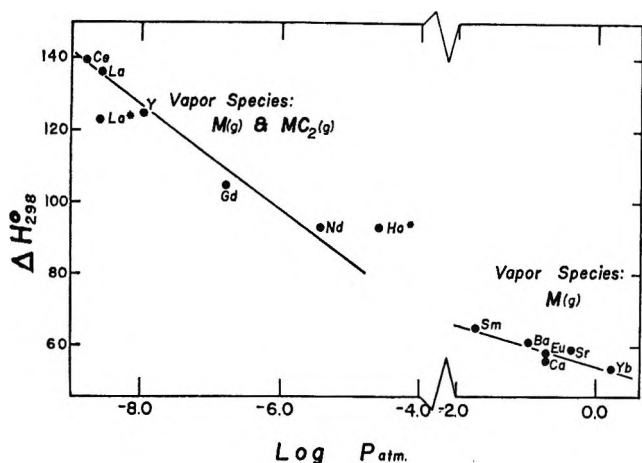


Figure 2. Correlation of ΔH°_{298} of $MC_2(s) \rightarrow M(g) + 2C(s)$ with vapor pressure of M at $1500^\circ K$.

could arise from: (a) inaccuracy in measurement of absolute pressures (*i.e.*, analytical error or sticking problems), (b) systematic error in temperature measurements, or (c) error in the f_{ef} approximation for reaction 1. The reexamination of experimental parameters eliminated possibilities (a) and (b) and indicated that free energy functions were in error. Elimination of the temperature trend by deletion of ΔH and ΔS for the tetragonal to cubic transition from the CaC_2 data reemphasizes that, although errors in third-law calculations from free energy functions containing small enthalpy errors are small, those arising from small entropy errors are often large.

A consideration of the high-temperature behavior of the lanthanide dicarbides indicates two modes of vaporization. Those elements which normally exhibit only the +3 or +4 oxidation state—lanthanum, neodymium, gadolinium, ytterbium, and cerium^{5,27-29}—have been observed to vaporize under equilibrium conditions to both the gaseous element and gaseous dicarbide. However, those lanthanides exhibiting the +2 oxidation state and the alkaline earths yield,^{4-7,30} within detection limits, only the gaseous metal. Holmium dicarbide³¹ has also been studied, but the effusate was not examined mass spectrometrically.

The enthalpies observed for reaction 1, which is a common but often competitive process with the vaporization of dicarbide species, indicate clearly a difference between the +2 and +3 type species. Literature values for the enthalpies, obtained for reaction 1 for both types and corrected to $298^\circ K$, appear in Figure 2.^{1,3-6,27-31} The enthalpies of the +3 types, measured at a median temperature of approximately $2200^\circ K$, are higher than those collected for the +2 type dicarbides obtained in a temperature range approximately 1000° lower.

It is interesting to speculate why the enthalpies of vaporization vary so markedly with apparent oxidation number and why the dicarbides apparently fall

into two classes based upon mode, temperature, and enthalpy of vaporization. An examination of the physical properties of the elements in question indicates a marked difference in their vapor pressures. The metal dicarbides which vaporize at low temperatures principally to the elements have high metal vapor pressures. On the other hand, those which vaporize at higher temperatures to both species have low metal vapor pressures. Figure 2 shows a correlation between the enthalpy of vaporization for reaction 1 and the vapor pressure of the metal at $1500^\circ K$.^{12,17,32} The enthalpies again fall into two distinct groups, but even more unusual is the apparently linear relationship existing within each set. Kinetic or mechanistic implications are unobtainable from equilibrium thermodynamic data, but the correlation of ΔH°_{298} , which is actually a measure of change in dicarbide decomposition pressure with the metal vapor pressure, may imply that free metal is involved in the vaporization mechanism. In other words, the activity of metal in equilibrium with the dicarbide is related directly to the activity of the free metal at a given temperature.

As Cuthbert, *et al.*, have noted,⁴ some correlation is also observed between ΔH°_{298} and the ratio of $MC_2(g)/M(g)$. At the higher values of ΔH°_{298} , the ratio approaches unity while at the lower values, it approaches zero. Some examples of $MC_2(g)/M(g)$ ratios for various M 's which are observed to decrease almost in order with decreasing ΔH°_{298} (Figure 2) are: Ce, 0.8³ or 0.77;³³ La, 0.96;³⁴ Y, 0.95;²⁹ Nd, 0.2;³⁵ Sm, ≤ 0.003 ;⁴ Eu, 0.01;⁶ and Yb, < 0.00001 . The cerium case is unique, as $CeC_4(g)/Ce(g) = 0.2$;^{3,33} $MC_4(g)$ is not a significant contributor to the other equilibria. As is to be expected, vaporization by the dicarbide mode obviously becomes more competitive with increasing temperature.

The two lines in Figure 2 may prove useful in predicting and evaluating ΔH°_{298} values for lanthanide dicarbides and in approximating the ratio of $MC_2(g)/M(g)$ in the equilibrium vapor. The values of

(27) D. D. Jackson, R. G. Bedford, and G. W. Barton, Jr., U. S. Atomic Energy Commission Report UCRL 7362-T, 1963.

(28) D. D. Jackson, G. W. Barton, O. H. Krikorian, and R. S. Newberry, IAEA Symposium on Thermodynamics of Nuclear Materials, International Atomic Energy Authority, 1962.

(29) G. DeMaria, M. Guido, L. Malaspina, and B. Pesce, *J. Chem. Phys.*, **43**, 4449 (1965).

(30) R. H. Flowers and E. G. Rauh, *J. Inorg. Nucl. Chem.*, **28**, 1355 (1965).

(31) G. F. Wakefield, A. H. Daane, and F. H. Spedding, 4th Rare Earth Conference, Phoenix, Ariz., 1964.

(32) F. H. Spedding, J. J. Hanak, and A. H. Daane, *Trans. AIME*, **212**, 379 (1961).

(33) G. Balducci, A. Capalbi, G. DeMaria, and M. Guido, *J. Chem. Phys.*, **43**, 2136 (1965).

(34) W. A. Chupka, J. Berkowitz, C. F. Giese, and M. G. Inghram, *J. Phys. Chem.*, **62**, 611 (1958).

(35) G. DeMaria, G. Balducci, A. Capalbi, and M. Guido, Meeting on Thermodynamics of Ceramic Systems, London, 1966.

ΔH°_{298} for lanthanum⁵ and holmium³¹ appearing with asterisks in Figure 2 are questionable if a linear relationship actually exists. Obviously, the holmium case should be reinvestigated, since the high enthalpy and the previously noted correlation of $MC_2(g)/M(g)$ indicate that gaseous holmium dicarbide should be a significant vapor species. It is also interesting to

speculate concerning ΔH°_{298} for thulium which has a $\log P = -2.2$ at 1500°K.

Acknowledgment. The support of the U. S. Atomic Energy Commission (COO-716-031) and the assistance of P. A. Pilato in the mass spectrometric analyses are acknowledged gratefully.

Radical Production by γ Irradiation of 3-Methylpentane, Methyltetrahydrofuran, and Methylcyclohexane Glasses at 77°K with and without Alkyl Halide Solutes¹

by Miriam Shirom and John E. Willard

Department of Chemistry, University of Wisconsin, Madison, Wisconsin 53706 (Received November 3, 1967)

The yield of free radicals from the γ irradiation of 3-methylpentane (3MP) at 77°K ($G = 1.6$) is not changed by photobleaching of the trapped electrons or by the presence of electron scavengers (except as the latter cause H abstraction by hot processes). This indicates that solvent radicals cannot be formed by neutralization of solvent ions by trapped or scavengeable electrons. The G values for radicals produced by the $RX + e^- \rightarrow R + X^-$ reaction from ten organic halides in 3MP glass increase with increasing halide concentration up to ca. 0.8 mol %, above which they remain constant, at ca. 1.1, indicating that this is the yield of electrons able to escape recombination with the parent ion. Trapped methyl radicals formed by dissociative electron capture by methyl halides in 3MP glass do not decay by abstracting hydrogen from the solvent. Hot methyl radicals formed by dissociative electron capture by CH_3I in 3MP glass abstract hydrogen to form CH_4 , with $G(CH_4) = 0.3$. $G(C_2H_6)$ for the analogous reaction of ethyl halides in 3MP or MTHF is 0.15. Photobleaching of the intense electron signal produced by γ irradiation of methyltetrahydrofuran (MTHF) glass does not change the concentration of the free radical present in the system. The G values for dissociative electron capture by alkyl halides in MTHF and methylcyclohexane (MCH) glasses increase with alkyl halide concentration to plateau values qualitatively similar to the results in 3MP glass.

Introduction

Trapped free radicals and trapped electrons, observable by esr, are formed by the γ radiolysis of organic glasses at 77°K.² When dilute alkyl halides are present in the glass, alkyl radicals formed by dissociative electron attachment ($RX + e^- \rightarrow R + X^-$) are also observed.^{3,4} The work reported here answers the following questions concerning the radiation chemistry of such hydrocarbon matrices. (1) Is the yield of 3-methylpentyl radicals from the radiolysis of 3-methylpentane (3MP) glass decreased by electron scavengers which decrease the possibility of reactions such as $RH + e^- \rightarrow R + H$? Is it increased by photobleaching of trapped electrons in the glass? (2) Are 3MP radicals produced by attack of CH_3 or C_2H_5 radicals on 3MP during decay of these radicals in a glassy 3MP matrix? (3) What concentration of alkyl halide is required to capture all available electrons produced in the radiolysis of 3MP, 2-methyltetrahydrofuran (MTHF), and methyl-

cyclohexane (MCH) glasses? (4) What is the maximum $G(e^-)$ value in 3MP glass, as indicated by the yields of dissociative electron capture? (5) What are the relative cross sections for dissociative capture by different alkyl halides as determined from competitive capture experiments?

The yields of dissociative electron capture by alkyl halides in 3MP glass increase in the sequence $RI < RBr < RCl^3$ when the electrons are produced by photoionization of tetramethyl-*p*-phenylenediamine (TMPD).

(1) This work was supported in part by the U. S. Atomic Energy Commission (Contract AT (11-1)-32) and by the W. F. Vilas Trust of the University of Wisconsin, Madison, Wis.

(2) (a) W. H. Hamill in "Radical Ions," L. Kevan, Ed., John Wiley and Sons, Inc., New York, N. Y., in press; (b) J. E. Willard in "Fundamentals of Radiation Chemistry," P. Ausloos, Ed., John Wiley and Sons, Inc., New York, N. Y., in press.

(3) R. F. C. Claridge and J. E. Willard, *J. Amer. Chem. Soc.*, **87**, 4992 (1965).

(4) D. W. Skelly, R. G. Hayes, and W. H. Hamill, *J. Chem. Phys.*, **43**, 2795 (1965).

This is the opposite of the sequence found in the γ radiolysis of aqueous⁵ and organic liquid solutions.⁶ It has been suggested that the difference may be caused by complexing of the halides by the TMPD.³ It was, therefore, of interest to determine the relative yields from the different halides in 3MP glass by a method capable of producing electrons in the absence of TMPD.

Experimental Section

Reagents. Phillips pure grade 3MP was purified by passing through a 6-ft column of freshly activated (200°) silica gel. Subsequent fractional distillation did not alter the results obtained. MTHF (stabilized with hydroquinone) was shaken with aqueous NaOH, washed with water, dried with MgSO₄, further purified by preparative gas chromatography, and distilled repeatedly through P₂O₅ on the vacuum line. MCH from the Aldrich Chemical Co. was passed through freshly activated silica gel, followed by drying with P₂O₅ on the vacuum line.

Eastman White Label CH₃I and C₂H₅I were passed through silica gel and fractionally distilled or used as received. *n*-C₃H₇Br, *n*-C₄H₉Br, *n*-C₄H₉Cl, and *sec*-C₄H₉Br (all Eastman White Label) were stirred with H₂SO₄, washed with aqueous NaHCO₃ and with H₂O, and further purified by preparative gas chromatography. Matheson CH₃Cl, CH₃Br, and C₂H₅Cl, Mallinckrodt analytical grade CCl₄ and CHCl₃, and Fisher Certified reagent CH₂Cl₂ were used as received.

Sample Preparation and Measurement. Samples containing CH₃Cl, CH₃Br, or C₂H₅Cl were prepared by condensing metered amounts of the vapor onto 3MP, MTHF, or MCH on the vacuum line. Other alkyl halides were pipetted into the solvent to form the desired concentration. All samples (0.3 ml) were degassed by freeze-pump-thaw cycles and distilled through P₂O₅ on the vacuum line into 3-mm i.d. Suprasil tubes, which were sealed off for esr examination. In the preparation of samples of pure 3MP, MTHF, or MCH, considerable vapor was pumped off with the sample in the liquid state to ensure removal of CO₂.

Irradiations were done at 77°K under liquid nitrogen for 5 min at a dose rate of 2×10^{18} eV g⁻¹ min⁻¹ using Co⁶⁰ γ rays and the samples were then transferred under liquid nitrogen to a Varian-type liquid-nitrogen dewar, positioned in the cavity of a Varian 4500 spectrometer equipped with 100-kc modulation and Fieldial. The spectrometer output was recorded either as the first derivative of the esr signal, or, with the aid of an integrator, as the esr absorption curve.

Analyses for CH₄ and C₂H₆ were made by gas chromatography. In some cases a glass ampoule in which the sample was irradiated was broken in the carrier gas at the inlet of the chromatography column. In others, the volatile gases were separated from the sample with the

aid of a Toepler pump and cold traps and were admitted to the carrier gas through a by-pass injection cell.

Determination of *G* Values. The radical yields are proportional to the areas under the esr absorption curves, after corrections for small differences in the diameter of the esr tubes (calibrated by comparing the signals from different tubes filled from the same solution of galvinoxyl in benzene) and for variations in the sensitivity of the spectrometer (monitored by a pitch or galvinoxyl sample). All samples were sufficiently large to extend above and below the region of sensitivity of the cavity. Measurements for use in determining *G* values were done at microwave powers demonstrated to be below the onset of saturation.

Areas under the absorption curves, recorded with the aid of the integrator, were determined by weighing. The area per unpaired spin was determined from spectra of samples containing known concentrations of galvinoxyl⁷ in benzene. These could not be used at 77°K because fractional crystallization caused inhomogeneous distribution of the galvinoxyl through the regions of different sensitivity of the cavity. Stable samples of galvinoxyl in dry KCl and in glucose gave 4 ± 0.2 as the ratio of the area of the esr absorption curves at 77°K to those at room temperature, as predicted from the Boltzmann relation. Two samples of known concentration of diphenylpicrylhydrazyl (DPPH) in benzene gave esr absorption curve areas per spin within $\pm 10\%$ of the average from galvinoxyl.

The methods used for distinguishing the *G* values of different radicals in a mixture will be described with the results. Where error limits are given, these are the maximum spread observed in a number of determinations.

Results

Electron Capture as a Function of Alkyl Halide Concentration. The dotted line of Figure 1A shows the six-line esr spectrum of 3-methylpentyl radical in a sample of pure 3MP glass at 77°K, after γ irradiation at 77°K and decay of the electron signal. When 1 mol % ethyl chloride, bromide, or iodide is present in the 3MP, the 12-line ethyl radical spectrum (solid line of Figure 1A) resulting from dissociative electron attachment (C₂H₅X + e⁻ → C₂H₅ + X⁻) is superimposed on the 3-methylpentyl signal. A plot of the height of the ethyl radical spectrum as a function of concentration of ethyl iodide (Figure 2) shows that some 20% of the electrons are captured by as little as 0.04 mol % of halide, 50% by 0.1 mol %, and nearly all by about 0.8

(5) A. Sgutka, J. K. Thomas, S. Gordon, and E. J. Hart, *J. Phys. Chem.*, **69**, 289 (1965).

(6) (a) R. R. Williams, Jr., and W. H. Hamill, *Radiat. Res.*, **1**, 158 (1954); (b) P. R. Geissler and J. E. Willard, *J. Amer. Chem. Soc.*, **84**, 4627 (1962).

(7) G. M. Coppinger, *ibid.*, **79**, 501 (1957).

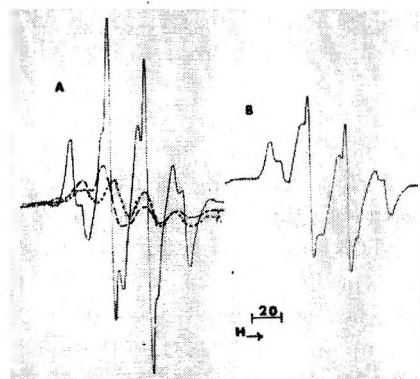


Figure 1. Electron spin resonance spectra of γ -irradiated 3MP glasses at 77°K: (A) solid line, 1 mol % C_2H_5I in 3MP; dotted line, pure 3MP; dashed line, 0.39 mol % CCl_4 in 3MP; (B) 1 mol % C_2H_5I plus 0.39 mol % CCl_4 in 3MP. All samples were measured at the same gain, modulation, amplitude, and power and received the same γ dose.

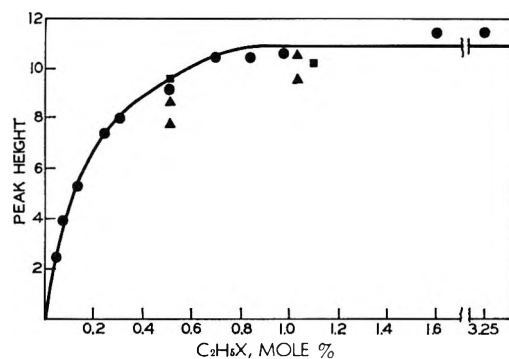


Figure 2. Ethyl radical concentration (arbitrary units) as a function of ethyl halide concentration in γ -irradiated 3MP at 77°K: ●, C_2H_5I ; ▲, C_2H_5Br ; ■, C_2H_5Cl .

mol %. Points for C_2H_5Cl and C_2H_5Br fall on the same curve.

Analogous data for solutions of ethyl iodide in γ -irradiated MCH glass at 77°K indicate that complete scavenging of electrons is also achieved at about 1 mol % in this solvent. A somewhat higher concentration, *i.e.*, about 2 mol %, is required in MTHF (Figure 3).

G Values of 3-Methylpentyl Radicals with and without Alkyl Halides Present. The *G* value for the production of 3-methylpentyl radicals by irradiation of pure 3MP at 77°K is 1.6 ± 0.3 . Except for the yield of the $R + 3MP \rightarrow RH + 3MP\cdot$ reaction from hot R radicals produced by the $RI + e^- \rightarrow R + I^-$ reaction, this yield is not altered by the presence of 1 mol % alkyl halide in the 3MP glass during γ irradiation or by the subsequent decay of the trapped R radicals, trapped electrons, or other metastable species known to be produced.^{2,8-10}

The areas under esr absorption curves, such as those of Figure 4A and B, for γ -irradiated samples of pure 3MP and of 3MP containing 1 mol % C_2H_5I become identical within the experimental error, when allowed

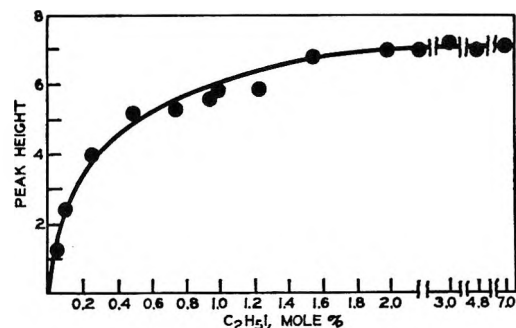


Figure 3. Ethyl radical concentration (arbitrary units) as a function of C_2H_5I concentration in γ -irradiated MTHF at 77°K.

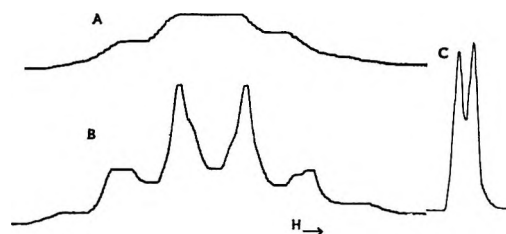


Figure 4. Electron spin resonance absorption curves: (A) 3MP radical from pure 3MP at 77°K, (B) C_2H_5 from 1 mol % C_2H_5I in 3MP at 77°K, (C) $4.2 \times 10^{-3} M$ galvinoxyl in benzene at 300°K.

to stand until the C_2H_5 radicals have all decayed (48 hr). For 3MP containing 1 mol of CH_3I , the remaining 3MP radical concentration after the decay of the CH_3 is higher by about 25%, attributable to H abstraction by hot CH_3 radicals.

Absence of H abstraction during the decay of CH_3 radicals is also demonstrated by observing the first-derivative esr spectrum of γ -irradiated 3MP glass containing 1 mol % CH_3I at a gain such that the two peaks on the extremes of the six-line 3-methylpentyl spectrum are readily measurable, while the initial height of the central lines of the methyl radical signal is far off scale. Under these conditions the height of the 3-methylpentyl lines does not change detectably over 2.5 hr, during which time the CH_3 -radical signal (half-life 16 min) decays completely.

G Values of Dissociative Electron Capture in 3MP. With the fact established that *G*(3-methylpentyl radicals) for 3MP glass at 77°K is independent of the presence of alkyl halides (except for hot-radical reactions induced by dissociative electron capture), $G(RX + e^- \rightarrow R + X^-)$ could be obtained from the difference between the areas under the esr absorption curve of γ -irradiated pure 3MP (Figure 4A) and the

(8) K. Tsuji, H. Yoshida, and K. Hayashi, *J. Chem. Phys.*, **46**, 810 (1967).

(9) M. Shirom, R. F. C. Claridge, and J. E. Willard, *ibid.*, **47**, 286 (1967).

(10) (a) R. F. C. Claridge and J. E. Willard, *J. Amer. Chem. Soc.*, **89**, 510 (1967); (b) J. Mittal and W. H. Hamill, *ibid.*, in press.

absorption curve of 3MP containing alkyl halide (Figure 4B). This was done for 1 mol % C_2H_5Cl , C_2H_5Br , C_2H_5I , $n-C_3H_7Br$, $n-C_4H_9Cl$, $n-C_4H_9Br$, $sec-C_4H_9Br$, CCl_4 , $CHCl_3$, and CH_2Cl_2 . Each of the compounds gave the same G for radical production from the halide, 1.1 ± 0.2 [taking $G(3MP)$ as 1.6], implying that the same population of electrons can be captured by any one of the halides and that the probability that dissociation will accompany electron capture in 3MP at 77°K is the same for each. In these determinations the total radical yield with added halide is equal for the different alkyl halides regardless of the extent of hot-radical reaction, since each solute radical lost by hot reaction produces a solvent radical.

The yields of methyl radical, from 3MP glasses containing CH_3Cl , CH_3Br , and CH_3I , were identical (as shown from measurements of peak heights), and the G values for the sum of CH_3 and 3MP radicals (corrected for the rapid decay of CH_3) were equivalent to the corresponding values obtained for the higher alkyl halides.

Radical Formation in MTHF. The esr signal observed from γ -irradiated MTHF glass was similar to that reported earlier.¹¹ At low esr powers it included the intense singlet attributable to trapped electrons superimposed on the free-radical signal. When the singlet was photobleached without removing the sample from the cavity, the intensity of the free-radical lines was unchanged within the accuracy of measurement ($\pm 2\%$), indicating that the neutralization process does not produce new radicals, consistent with the findings of Dainton and coworkers^{11a} but contrary to the report of Smith and Pieroni.^{11b}

Relative Electron Capture Cross Sections of Alkyl Halides. Competitive capture experiments with two alkyl halides present together in the same glass during irradiation have been used to determine relative electron capture cross sections. When esr detection is used, such experiments are limited to pairs of alkyl halides whose radicals are sufficiently different from each other in shape of signal or lifetime so that they can be distinguished. The central lines of the C_2H_5 signal (Figure 1A) are prominent compared to those of equal concentrations of 3MP radicals and of the CH_2Cl , $CHCl_2$, and CCl_3 radicals. We have irradiated solutions of 1 mol % C_2H_5I in 3MP glass containing concentrations of 0.2–0.4 mol % CCl_4 , $CHCl_3$, or CH_2Cl_2 . In each case three other samples were irradiated simultaneously: (1) pure 3MP, (2) 3MP containing 1 mol % C_2H_5I , (3) 3MP containing the same concentration of chloromethane used in the mixed sample. The four esr spectra were of the type shown in Figure 1. The relative electron-capture cross sections of the C_2H_5I and chloromethane were calculated from the relative heights of the low-field central line of the C_2H_5 signal, after subtracting from it the height of the signal at the same field from the sample containing only 3MP

plus chloromethane. Assuming that the corrected heights, G_{Et}^0 for C_2H_5 in 3MP and G_{Et} for C_2H_5 in the sample containing chloromethane, were proportional to the yields of ethyl radicals in the samples, the relationship $1/G_{Et} = 1/G_{Et}^0 + 1/G_{Et}^0(G_{Ch}/G_{Et})([Ch]/[Et])$ yielded the ratio G_{Ch}/G_{Et} of the electron-capture cross section of the chloromethyl molecule to that of ethyl iodide. It is to be noted that $G_{Et} = G_{Et}^0 - G_{Ch}$ and $G_{Ch}/G_{Et} = G_{Ch}[Ch]/(G_{Ch}[Ch] + G_{Et}[Et])$, where G_{Ch} is the yield of the chloromethyl radicals in the mixture. The ratio of cross sections $C_2H_5I:CH_2Cl_2:CHCl_3:CCl_4$ found is 1:1.3:2.0:2.6, with the estimated error being about $\pm 20\%$.

Hot-Radical Reactions Following Dissociative Electron Capture. It has been reported¹⁰ that $G(CH_4)$, which is 0.06 for the γ irradiation of pure 3MP at 77°K, increases to 0.56 when 0.65 mol % CH_3I is present. When 1 mol % of the electron-scavenger CCl_4 is present with the CH_3I , $G(CH_4)$ is 0.08. These results are consistent with the conclusion that CH_3 radicals produced by the $CH_3I + e^- \rightarrow CH_3 + I^-$ reaction form CH_4 by hot reaction, at the time of the dissociative process, or by thermal reaction when the matrix is subsequently warmed. Other work¹² has shown that CH_4 formation in similar systems must be by hot reaction at 77°K rather than on warmup.

In the present work, methane analyses following γ irradiation of 1 mol % CH_3I in 3MP confirm the earlier evidence that CH_4 is produced by reaction of hot CH_3 radicals. The absolute yields obtained are somewhat lower, *i.e.*, $G(CH_4)$ from pure 3MP = *ca.* 0.04 and the increase in $G(CH_4)$ in the presence of CH_3I = *ca.* 0.3. Consistent with the fact that the CH_4 must be formed by the $CH_3 + C_6H_{14} \rightarrow CH_4 + C_6H_{13}$ reaction, the average G for C_6H_{13} production is higher in the presence of CH_3I than that from pure 3MP, the two values being 2.0 ± 0.2 and 1.6 ± 0.3 , respectively.

$G(C_2H_6)$ from the γ irradiation of 1 mol % C_2H_5I in 3MP at 77°K is *ca.* 0.26, while that from pure 3MP is 0.13, indicating that G for abstraction of H from 3MP by hot C_2H_5 radicals from dissociative capture is about 0.13. A similar G is obtained for the reaction of the hot ethyl radicals to form C_2H_6 in a MTHF matrix. The ratios of $CH_4:CH_3$ and $C_2H_6:C_2H_5$ formed by the dissociative capture processes in 3MP are about 0.6 and 0.16, respectively, consistent with the conclusion that the energy available following dissociative capture is more effectively used for reaction in the case of methyl than ethyl radicals. Determinations¹² using the photoionization of 0.05 mol % TMPD as the source of electrons in 3MP glass containing 1 mol % RCl have given the ratios $CH_4:CH_3 = 3.8$, $C_2H_6:C_2H_5 = 1.7$, and $C_3H_8:C_3H_7 = 0.28$. These are of

(11) (a) F. S. Dainton, J. P. Keene, T. J. Kemp, G. A. Salmon, and J. Teply, *Proc. Chem. Soc.*, 265 (1964); (b) D. R. Smith and T. J. Pieroni, *Can. J. Chem.*, **43**, 2141 (1965).

(12) W. G. French and J. E. Willard, unpublished data.

interest because they again show decreasing reactivity with increasing complexity of the radicals and because they indicate that the ratio of alkane to radical depends upon the source of the electron.

In a study of the photolysis of CH_3I in hydrocarbon matrices at 4°K ,¹³ the production of CH_4 has been attributed to the energy of relaxation of the CH_3 radical from the tetrahedral state, in which it is produced, to the planar state.

Half-Lives. Methyl radicals produced by dissociative capture during the photoionization of TMPD in 3MP containing methyl halides at 77°K decay by 90% or more by a pure first-order process, with a half-life of about 16 min. The present work shows that CH_3 radicals produced by γ irradiation of similar glasses in the absence of TMPD have the same decay characteristics. In γ -irradiated MTHF- CH_3X matrices at 77°K , the first 70% of the decay of methyl radicals is also pure first order, while the half-life is less than in 3MP (ca. 10 min). Ethyl radicals show "composite" first-order¹⁴ decay in both 3MP and MTHF at 77°K . The time required for 25% decay of the radicals present immediately after irradiation in 3MP is about 3 hr in 3MP and 20 min in MTHF. It is of interest that the composite first-order decay of trapped electrons in 3MP at 77°K , as observed by esr, has a much shorter initial half-time, measured starting 4 min after the end of irradiation (10–20 min), than the corresponding decay in MTHF or MCH (several hours). The half-life of electrons in 3MP at 72°K is several hours. The effects of matrix and temperature on the decay properties of radicals and electrons are under continuing investigation.

Discussion

The data presented in this paper are informative with respect to the mechanisms of formation of radicals in γ -irradiated hydrocarbon glasses, the extent to which electrons escape geminate recombination in these glasses, the relative electron-capture cross sections of alkyl halides in such matrices, and the characteristics of the dissociative capture process in γ -irradiated matrices as compared to matrices where the electrons are produced by photoionization of TMPD.

The value of 1.1 for $G(\text{R})$ from the $\text{RX} + \text{e}^- \rightarrow \text{R} + \text{X}^-$ process in 3MP at 77°K , when RX is present at a concentration on the plateau of Figure 2, represents the maximum yield of electrons which can escape geminate recombination.^{15,16} The absolute value is subject to an uncertainty of several tenths of a G unit because of the lack of precision in determination of the areas of esr absorption curves, but it appears to be higher than the G values for trapped electrons in pure 3MP glass determined from the intensity of their infrared¹⁷ or esr⁸ absorption spectra. The latter measurements have given values of 0.8 and 0.5, respectively, also with rather broad error limits. These values are to

be compared with the values of 0.1–0.2¹⁸ for escape of electrons from geminate recombination in liquid hydrocarbons, as determined by electrical conductivity measurements and the value of $G(\text{C}_2\text{H}_5) = 6.7$ for radical production from 1.2 mol % $\text{C}_2\text{H}_5\text{I}$ in liquid hexane at 300°K .^{6b} The latter value presumably includes radical formation by the $\text{C}_2\text{H}_5\text{I} + \text{H} \rightarrow \text{C}_2\text{H}_5 + \text{HI}$ process, which is probably precluded by activation energy considerations at 77°K .

A question of considerable interest is whether the $\text{C}_6\text{H}_{14}^+$ ions formed by ionizing radiation in 3MP: (a) are stable, (b) allow positive charge to migrate by electron transfer from a C_6H_{14} molecule with formation of a new $\text{C}_6\text{H}_{14}^+$ ion, (c) allow positive charge to transfer by proton transfer of the type $\text{C}_6\text{H}_{14}^+ + \text{C}_6\text{H}_{14} \rightarrow \text{C}_6\text{H}_{13} + \text{C}_6\text{H}_{15}^+$. There is substantial experimental evidence, based on the use of positive charge scavengers, that positive charge does migrate.²

The present work shows that the neutralization of those electrons which escape geminate recombination does not produce new C_6H_{13} radicals, *i.e.*, does not occur by the $\text{C}_6\text{H}_{14}^+ + \text{e}^- \rightarrow \text{C}_6\text{H}_{13} + \text{H}$ process, which is often invoked as a dominant radical-production mechanism. This suggests, though it does not prove, that the predominant positive ion in a γ -irradiated 3MP matrix is $\text{C}_6\text{H}_{16}^+$ and that the C_6H_{13} radicals observed result from the proton-transfer mechanism. These radicals are $\text{CH}_3\text{CHCH}(\text{CH}_3)\text{CH}_2\text{CH}_3$, resulting from removal of a secondary hydrogen from 3MP.¹⁹

The fact that the pure first-order decay of trapped CH_3 radicals produced by dissociative electron capture by CH_3X in 3MP at 77°K cannot be ascribed to abstraction of hydrogen from the solvent has been discussed earlier.³ It is confirmed by the absence of growth of C_6H_{13} radicals during decay of solute radicals in the present work. It is of importance, by contrast,

(13) C. D. Bass and G. C. Pimentel, *J. Amer. Chem. Soc.*, **83**, 3754 (1961).

(14) We use the term "pure" first-order decay for a process for which a plot of $\log C$ vs. t gives a straight line, and "composite" first-order decay for processes for which this plot is not linear but for which plots of C vs. t for samples which have received different doses are superimposable after normalization for the dose.

(15) A value of $G(\text{e}^- \text{ capture}) = 1.6$ deduced from the maximum optical absorption produced by the presence of biphenyl^{2,18} is ambiguous and probably high because both the biphenyl anion and cation may contribute to this absorption. Assurance that one radical is formed per each electron captured by an RX molecule and that nondissociative capture to form RX^- does not occur is given by the fact that all of the ten alkyl halides tested gave the same value of $G(\text{R})$. If nondissociative capture occurred, it would be expected to vary from one type of halide to another.

(16) T. P. Guarino and W. H. Hamill, *J. Amer. Chem. Soc.*, **86**, 777 (1964).

(17) D. W. Skelly and W. H. Hamill, *J. Chem. Phys.*, **44**, 2891 (1966).

(18) (a) A. Hummel and A. O. Allen, *ibid.*, **44**, 3426 (1966); (b) F. R. Freeman and J. M. Fayadh, *ibid.*, **43**, 86 (1965).

(19) D. Henderson and J. E. Willard, unpublished data. The conclusion comes from a comparison of the esr spectrum of the radicals in γ -irradiated 3MP glass with the esr spectra of the radicals produced by radiolysis of each of the possible 3-methylpentyl iodides and chlorides.

that C_6H_{13} radicals are formed by attack by hot alkyl radicals on 3MP at the time of their birth by dissociative capture.

The production of radicals from alkyl halides by dissociative electron capture in γ -irradiated 3MP glass matrices, reported here, differs in two significant ways from the similar production using electrons from the photoionization of TMPD in similar matrices. Whereas the quantum yields from the TMPD method de-

crease in the order $RCl > RBr > RI$, the three types of halides give identical yields by γ radiolysis. This is consistent with the hypothesis that the order observed with TMPD is conditioned by complexing with the TMPD. The other difference is that the ratio of hot reaction of the radicals, to form alkane, to radical trapping is much higher by the TMPD method than in γ radiolysis. This is as yet unexplained but may also be dependent on complexing.

Intrinsic Mobilities and Independent Fluxes in Multicomponent Isothermal Diffusion. I. Simple Darken Systems

by P. C. Carman

National Chemical Research Laboratory, South African Council for Scientific and Industrial Research, Pretoria, South Africa (Received November 6, 1967)

Darken diffusion in an s -component system is characterized by independent diffusive fluxes, whereas in experimental measurements, only $s - 1$ fluxes are independent. By applying the methods of nonequilibrium thermodynamics, the relationships between Darken coefficients and experimental coefficients have been derived. It is also shown that the R_{ik} coefficients obtained in the inverted form of the phenomenological equations when only $s - 1$ fluxes are independent have no significance for Darken diffusion. The use of an intrinsic mobility for each diffusing species is sufficient for Darken diffusion. The introduction of intrinsic diffusion coefficients, in systems where $s > 2$, only leads to a multiplicity of meaningless quantities, and is, therefore, unnecessary and confusing. Part I deals with systems in which there are no interactions of the components. Data for two ternary systems of this type are discussed, but there are, in fact, no data at present which can be used for a critical discussion of Darken diffusion in ternary systems.

Introduction

Darken's theory¹ of isothermal diffusion is based on the assumption that diffusive transport for each species i is determined by the simple relationship

$$v_i^0 = J_i^0/c_i = -q_i \nabla \mu_i \quad (1)$$

where J_i^0 (mol/sec cm²) is the diffusive flux, relative to a properly chosen reference frame; c_i (mol/ml) is the concentration; v_i^0 is the corresponding diffusive velocity; and μ_i is the molar chemical potential. The gradient $-\nabla \mu_i$ has the dimensions of a virtual mechanical force acting on 1 mol of i , so that the coefficient q_i is an intrinsic mobility or diffusive velocity per unit force. It is characteristic for the species i and, while it can and does vary with composition, it is not affected by the diffusive velocities of other components. Thus in a simple system of s components, *i.e.*, one in which the components do not dissociate, associate, or form compounds, there are s independent mobilities and hence s independent fluxes.

For binary systems, the relationship between the two intrinsic mobilities and the experimental interdiffusion coefficient is well-known and has been applied successfully to metallic solid solutions.^{1,2} In the case of liquids, Darken's theory has been shown to be at least approximately valid for a number of nearly ideal non-electrolyte systems. Further, in a number of decidedly nonideal systems, experimental data can be accounted for by the appearance of association polymers and of compounds, so that the number of intrinsic mobilities involved exceeds two.³

The objective of the present paper is to establish the relationships between intrinsic mobilities and experimental coefficients for multicomponent systems, with

(1) L. S. Darken, *Trans. Amer. Inst. Mining Met. Eng.*, **175**, 184 (1948).

(2) (a) W. Seith and A. Kottmann, *Angew. Chem.*, **64**, 376 (1952); (b) H. W. Mead and C. E. Birchenall, *J. Metals*, **9**, 874 (1957); (c) J. E. Reynolds, B. L. Averbach, and M. Cohen, *Acta Met.*, **5**, 29 (1957); (d) J. R. Manning, *Phys. Rev.*, **116**, 69 (1959).

(3) P. C. Carman, *J. Phys. Chem.*, **71**, 2565 (1967).

special reference to ternary systems. Part I deals with simple Darken systems, in which only s intrinsic mobilities are involved, while part II covers cases where interactions of various kinds must be taken into account.

Phenomenological Relationships

According to nonequilibrium thermodynamics, if the superscript x denotes any reference frame, the corresponding flux is given by

$$J_i^x = \sum_{k=1}^s L_{ik}^x X_k^x \quad (2)$$

in which the phenomenological coefficients L_{ik}^x conform to the Onsager reciprocal relation

$$L_{ki}^x = L_{ik}^x \quad (3)$$

i.e., the square $s \times s$ matrix $||L_{ik}^x||$ is symmetric. The X_k^x are conjugate forces, conforming to the relationship

$$\sigma T = \sum_{i=1}^s J_i^x X_i^x \quad (4)$$

where σ is the rate of change of local entropy with time and T is the local absolute temperature. The simplest conjugate force for diffusion is $-\nabla\mu_i$, and, as a system at uniform temperature and pressure is in mechanical equilibrium, the same force can be used for all reference frames in isothermal diffusion,⁴ *i.e.*, the superscript can be dropped in

$$X_i^x = X_i = -\nabla\mu_i \quad (5)$$

Only $s - 1$ forces are independent, as they are subject to the Gibbs–Duhem relation

$$\sum_{i=1}^s c_i X_i = -\sum_{i=1}^s c_i \nabla\mu_i = 0 \quad (6)$$

In all current discussions of multicomponent diffusion, it is assumed that the reference frame is fixed by some mean diffusive velocity or by the velocity of one of the components r .^{4,5} The corresponding fluxes are thus interrelated by the general expression

$$\sum_{i=1}^s \alpha_i^x J_i^x = 0 \quad (7)$$

where the weighting factors α_i^x are subject to the condition

$$\sum_{i=1}^s \alpha_i^x c_i = 1 \quad (8)$$

so that only $s - 1$ fluxes are independent. Thus if J_i^V refers to a volume-fixed frame, J_i^M to a mass-fixed frame, J_i^N to a number-fixed frame, and J_i^r to a frame fixed by component r

$$\alpha_i^V = \bar{V}_i, \alpha_i^M = M_i / \sum_{i=1}^s c_i M_i, \alpha_i^N = N_i / c_i, \alpha_i^r = \delta_{ir} / c_r \quad (9)$$

where \bar{V}_i is the partial molal volume of i , M_i is its molecular weight, N_i is its mole fraction, and δ_{ir} is the Kronecker δ (unity for $i = r$, and zero otherwise).

As shown by Hooyman and de Groot,⁶ the effect of eq 7 is to limit the number of independent coefficients L_{ik}^x

$$\sum_{k=1}^s \alpha_i^x L_{ik}^x = 0 \quad (10)$$

for all values of i . Together with eq 3, this means that there are only $1/2s(s - 1)$ independent coefficients, *i.e.*, one in a binary system and three in a ternary system.

From the viewpoint of diffusion theory, the various reference frames cannot all be equivalent, since they correspond to different velocities. In experimental measurements, a cell-fixed frame applies, and this corresponds to a volume-fixed frame, if small effects due to volume changes on mixing are neglected. This does not necessarily mean, however, that L_{ik}^V coefficients have a greater physical significance. It is often convenient, particularly in dilute systems, to choose a preponderant component r , the "solvent," as reference frame, the transformation of L_{ik}^x coefficients to L_{ik}^r coefficients being effected by the simple equation

$$L_{ik}^r = L_{ik}^x - \frac{c_k}{c_r} L_{ir}^x - \frac{c_i}{c_r} L_{kr}^x + \frac{c_i c_k}{c_r^2} L_{rr}^x \quad (11)$$

This is quite general and can be equally applied, for instance, to transform from one reference component to another.

Darken's theory does not specify a particular reference frame. It merely assumes that the true random-walk mechanism giving rise to diffusion is such that each component has an independent flux and that the reference frame is so chosen that no diffusion-generated bulk flow takes place relative to it. Darken fluxes J_i^0 are thus not subject to eq 7 and Darken coefficients L_{ik}^0 are not restricted by eq 10; *e.g.*, in a binary system, there are at least two and possibly three independent L_{ik}^0 coefficients. In the simple Darken systems discussed in this paper, all cross coefficients, L_{ik}^0 ($k \neq i$), are zero, so that

$$J_i^0 = L_{ii}^0 X_i \quad (12)$$

where

$$L_{ii}^0 = c_i q_i \quad (13)$$

On any other reference frame, nonzero, symmetric cross coefficients appear. Thus, for instance, if eq 11 is used to calculate L_{ik}^r , we obtain

(4) S. R. de Groot and P. Mazur, "Non-Equilibrium Thermodynamics," North-Holland Publishing Co., Amsterdam, 1962.

(5) D. D. Fitts, "Non-Equilibrium Thermodynamics," McGraw-Hill Book Co., Inc., New York, N. Y., 1962.

(6) G. J. Hooyman and S. R. de Groot, *Physica*, **21**, 73 (1955).

$$L_{ik}^r = \delta_{ik}L_{ii}^0 + \frac{c_i c_k}{c_r^2} L_{rr}^2 \quad (i \neq r, k \neq r) \quad (14)$$

The mere existence of such coefficients as L_{12}^r in a ternary system, therefore, does not necessarily mean that they have any physical significance. In a Darken system, they are a trivial result of the choice of reference frame.

Before turning to the relationship to diffusion coefficients, inverted phenomenological equations must be dealt with briefly, as they figure largely in many current discussions.

Inverted Phenomenological Equations

When eq 7 limits the number of independent fluxes to $s - 1$, an inverted form of eq 2 cannot be obtained directly, since, owing to eq 10, the $s \times s$ matrix $\|L_{ik}^z\|$ is singular. However, by transforming to an r -component fixed frame, giving

$$J_i^r = \sum_{k=1}^s L_{ik}^r X_k \quad (i \neq r, k \neq r) \quad (15)$$

the inverted form

$$X_i = \sum_{k=1}^s R_{ik} J_k^r \quad (i \neq r, k \neq r) \quad (16)$$

can be obtained, in which the matrix $\|R_{ik}\|$ is the inverse of the nonsingular, symmetric $(s - 1) \times (s - 1)$ matrix $\|L_{ik}^r\|$. By substituting $J_k^r = J_k^z - (c_k/c_r)J_r^z$ and defining R_{ir} coefficients by

$$\sum_{k=1}^s R_{ik} c_k = 0 \quad (17)$$

we obtain

$$X_i = \sum_{k=1}^s R_{ik} J_k^z \quad (18)$$

This is the only inverted form obtainable for eq 2 when there are $s - 1$ independent fluxes, with eq 17 serving as comparable restriction upon R_{ik} coefficients to eq 10 upon L_{ik}^z .

No superscript is necessary for R_{ik} , since v_k^r is a relative velocity and so is reference frame independent. This has led to the widely adopted viewpoint that R_{ik} coefficients are simpler and have greater physical significance than L_{ik}^z coefficients. By using eq 17, eq 18 can be transformed to

$$X_i = \sum_{k=1}^s R_{ik} c_k (v_k^z - v_i^z) \quad (19)$$

i.e., the total resistance to diffusion is made up of terms containing R_{ik} and the relative velocity $v_k^z - v_i^z$. Thus nonequilibrium thermodynamics appears to support theories of diffusion based on the viewpoint that R_{ik} represents a friction coefficient for the relative diffusive velocity of i and k components.⁷⁻¹⁰ It is difficult to controvert this when only $s - 1$ fluxes are independent.

In Darken's theory, however, there are s independent fluxes and eq 10 does not apply, so that the matrix $\|L_{ik}^0\|$ is nonsingular and has an inverse $\|R_{ik}^0\|$. In the simple Darken equation (eq 12), this is particularly obvious, since we have merely

$$X_i = R_{ii}^0 J_i^0 \quad (20)$$

where

$$R_{ii}^0 = 1/L_{ii}^0 = 1/c_i q_i \quad (21)$$

It is possible to obtain the form of eq 18, but the R_{ik} obtained then appear as complicated expressions of R_{jj}^0 and have clearly no physical meaning. Thus in the simplest case of a binary system, there is only one independent parameter, R_{12} , but two independent Darken parameters, R_{11}^0 and R_{22}^0 , the two cases being related by

$$R_{12} = -\frac{c_1}{c_2} R_{11}^0 = -\frac{c_2}{c_1} R_{22}^0 = -\frac{c_1 c_2 R_{11}^0 R_{22}^0}{c_1^2 R_{11}^0 + c_2^2 R_{22}^0}$$

Relationship between Phenomenological and Diffusion Coefficients

Experimental data are based on concentration gradients and hence expressed as diffusion coefficients. The simple form of Fick's law

$$J_i^z = -D_i^z \nabla c_i \quad (22)$$

is only possible when there is a single independent concentration gradient, *i.e.*, (a) in binary systems and (b) in self-diffusion. Binary systems give the interdiffusion coefficient $D_1^V = D_2^V = D_{12}$. The self-diffusion coefficient D_i^* can be obtained by producing a concentration gradient of labeled i in any system, provided concentration gradients of total i and of all other components are zero. According to Darken, as labeled and unlabeled molecules have the same properties and environment, they have equal mobilities, so that D_i^* gives a direct measurement of mobility

$$D_i^* = q_i RT \quad (23)$$

When $s > 2$, there are $s - 1$ independent concentration gradients, so that eq 22 must be replaced by the more general form

$$J_i^z = -\sum_{k=1}^s {}^r \mathcal{D}_{ik}^z \nabla c_k \quad (i \neq r, k \neq r) \quad (24)$$

The left-hand superscript denotes the fact that a reference component must be chosen, whose concentration gradient does not appear in eq 24, so that there are s possible sets of ${}^r \mathcal{D}_{ik}^z$ coefficients. In each set there are $(s - 1)^2$ coefficients, as ${}^r \mathcal{D}_{ik}^z \neq {}^r \mathcal{D}_{ki}^z$ and there are $s - 1$ independent fluxes, each with $s - 1$ coefficients.

(7) R. W. Laity, *J. Phys. Chem.*, **63**, 80 (1959).

(8) S. Ljunggren, *Trans. Roy. Inst. Technol. Stockholm*, **172**, 1 (1961).

(9) R. J. Bearman, *J. Phys. Chem.*, **65**, 1961 (1961).

(10) P. J. Dunlop, *ibid.*, **68**, 26 (1964).

The script form is used to ensure that D_{12} cannot be confused with ${}^r\mathcal{D}_{12}^V$. Strictly, D_{12} should be written as $D_1^V = {}^2\mathcal{D}_{11}^V$ or as $D_2^V = {}^1\mathcal{D}_{22}^V$, but this is unnecessarily elaborate for binary systems.

In dilute solutions, the "solvent" is the obvious choice as reference component, but, when the whole range of compositions is covered, it may not be advisable to keep to the same component when it is present in only trace proportions.

Taking the case of a ternary system as the one of most interest, experiment gives the coefficients ${}^3\mathcal{D}_{11}^V$, ${}^3\mathcal{D}_{12}^V$, ${}^3\mathcal{D}_{21}^V$, and ${}^3\mathcal{D}_{22}^V$, if component 3 is used as reference. These can be transformed to the r -component-fixed frame, *i.e.*, to \mathcal{D}_{ik}^r (the left-hand superscript is superfluous here), and these in turn can be transformed to L_{11}^r , L_{12}^r , L_{21}^r , and L_{22}^r , in which the equality $L_{12}^r = L_{21}^r$ is an indication of the accuracy of the data employed. Alternatively, ${}^3\mathcal{D}_{ik}^V$ can be transformed to L_{ik}^V and L_{ik}^r obtained by use of eq 11. The procedures for the foregoing transformations have been well discussed and need not be repeated here.^{4,5,11-13}

Then, from eq 13 and 14, if Darken's theory applies

$$\left. \begin{aligned} L_{11}^r &= c_1q_1 + \left(\frac{c_1^2}{c_3}q_3\right) \\ L_{22}^r &= c_2q_2 + \left(\frac{c_2^2}{c_3}q_3\right) \\ L_{12}^r &= \frac{c_1c_2}{c_3}q_3 \end{aligned} \right\} \quad (25)$$

In order to check the validity of eq 25, it is necessary to evaluate q_i , preferably by self-diffusion measurements and the use of eq 23. At present, however, no data exist on self-diffusion in ternary systems, so that it is only possible, where viscosities are available, to make estimates from the value of q_i in pure component i and to correct for the relative viscosity of the solution.

It will be noted from eq 25 that, if $c_2 = 0$, we have a binary system, for which

$$L_{11}^r = \frac{c_1}{c_3}(c_3q_1 + c_1q_3)$$

It can be simply shown

$$L_{11}^r = \frac{D_{13}}{RT} \frac{c_1}{c_3} \frac{\partial \ln c_1}{\partial \ln a_1}$$

where a_i is the thermodynamic activity of i . Thus

$$\begin{aligned} D_{13} &= RT\bar{V}_3 \frac{\partial \ln a_1}{\partial \ln c_1} (c_3q_1 + c_1q_3) \\ &= RT \frac{\partial \ln a_1}{\partial \ln N_1} (N_3q_1 + N_1q_3) \\ &= \frac{\partial \ln a_1}{\partial \ln N_1} (N_3D_1^* + N_1D_3^*) \end{aligned}$$

where N_i is mole fraction of i . These are the equations derived by Darken and others for binary Darken systems.^{1,14,15} In the Hartley-Crank method,¹⁵ viscosity corrected values of q_i are used instead of D_i^*/RT .

Intrinsic Diffusion Coefficients

For binary systems, both Darken¹ and Hartley and Crank¹⁵ introduced the concept of intrinsic diffusion coefficients D_i^0 by comparing the Fick equation

$$J_i^0 = -D_i^0 \nabla c_i \quad (i = 1, 2) \quad (26)$$

with eq 1. This is feasible in binary systems, since we can write

$$D_i^0 = c_i q_i \frac{\partial \mu_i}{\partial c_i} \quad (27)$$

and so obtain a simple and unequivocal relationship between D_i^0 and q_i .

Such is not the case in multicomponent systems, since μ_i is determined not only by c_i but by $s - 1$ independent concentrations, so that

$$\nabla \mu_i = \sum_{k=1}^s \left(\frac{\partial \mu_i}{\partial c_k} \right) \nabla c_k \quad (i \neq r, k \neq r) \quad (28)$$

In this, ${}^r(\partial \mu_i / \partial c_k)$ stands for differentiation of μ_i when only c_k and c_r are varied. It will be denoted by ${}^r\mu_{ik}$, where the superscript indicates that a different set of differentials is obtained for each choice of reference component r . Thus, eq 1 becomes

$$J_i^0 = -c_i q_i \sum_{k=1}^s {}^r\mu_{ik} \nabla c_k \quad (i \neq r, k \neq r) \quad (29)$$

from which, by comparing with eq 24, it can be seen that the simplest modified definition of an intrinsic diffusion coefficient would be

$${}^r\mathcal{D}_{ik}^0 = c_i q_i {}^r\mu_{ik} \quad (i \neq r, k \neq r) \quad (30)$$

In other words, there are $(s - 1)^2$ such coefficients for each intrinsic mobility, most of which would be cross coefficients which would have no physical meaning, since no cross terms appear in Darken's equation. As intrinsic mobilities have a definite meaning and the concept of intrinsic diffusion coefficients adds nothing of theoretical or practical value, it is best dropped.

Application to Ternary Systems

The only data covering a complete range of compositions in ternary systems are those of Toor and coworkers.^{16,17} In the first system studied, toluene-chloro-

(11) D. G. Miller, *J. Phys. Chem.*, **63**, 570 (1959).

(12) P. J. Dunlop and L. J. Gosting, *ibid.*, **63**, 86 (1959).

(13) J. G. Kirkwood, *et al.*, *J. Chem. Phys.*, **33**, 1505 (1960).

(14) P. C. Carman and L. H. Stein, *Trans. Faraday Soc.*, **52**, 619 (1956).

(15) G. S. Hartley and J. Crank, *ibid.*, **45**, 801 (1949).

(16) J. K. Burchard and H. L. Toor, *J. Phys. Chem.*, **66**, 2015 (1962).

benzene-bromobenzene at 30°,¹⁶ it was found that, within the fairly wide limits of experimental error, all ${}^r\mathcal{D}_{ik}^V$ coefficients were zero for $k \neq i$, and ${}^r\mathcal{D}_{11}^V = {}^r\mathcal{D}_{22}^V = {}^r\mathcal{D}_{33}^V = D^V$, whatever the reference component r used. This is a highly specialized system, in which all molar volumes and, presumably, partial molar volumes are approximately equal and, as all three binary systems are nearly ideal, the same can be assumed for the ternary mixtures. Under these conditions

$$\nabla\mu_i = RT\nabla \ln c_i$$

Consequently,

$$\begin{aligned} J_i^V &= -D^V\nabla c_i \\ &= -\frac{c_i D^V}{RT}\nabla\mu_i \end{aligned}$$

so that

$$L_{ii}^V = \frac{c_i D^V}{RT}$$

and cross terms are zero. It follows that, if component 3 is used for reference

$$L_{11}^r = \frac{c_1 D^V}{RT} \left(1 + \frac{c_1}{c_3} \right)$$

$$L_{12}^r = \frac{c_1 c_2 D^V}{RT}$$

$$L_{22}^r = \frac{c_2 D^V}{RT} \left(1 + \frac{c_2}{c_3} \right)$$

This, from eq 25, if diffusion is determined by intrinsic mobilities

$$q_1 = q_2 = q_3 = D^V/RT$$

In other words, the single coefficient D^V is only possible if the three components are so similar that, in addition to equal molar volumes and formation of ideal solutions, each has approximately the same intrinsic mobility in a given composition. It follows that self-diffusion coefficients for all three components should be equal to one another and to D^V . The only opportunity for testing this with self-diffusion data at present is in limiting solutions in bromobenzene. The limiting binary interdiffusion coefficients approach an approximately common value, namely, 1.41×10^{-5} cm²/sec for toluene and 1.36×10^{-5} cm²/sec for chlorobenzene, and this should equal the self-diffusion coefficient for bromobenzene. The only value available for the latter is 1.15×10^{-5} cm²/sec at 20°,¹⁸ which, corrected to 30° by multiplying by the inverse ratio of the viscosities, gives a value of 1.32×10^{-5} cm²/sec. Within the experimental errors and the approximations involved, the three values are in reasonable agreement.

If the main variable affecting D^V is the viscosity, then D^V_η should be almost independent of composition. A comparison of the three limiting values in Table I

Table I: Values of D^V_η for Limiting Compositions

Limiting composition	Limiting $D^V \times 10^5$	η , cP, at 30°	$D^V_\eta \times 10^5$
Pure bromobenzene	1.36	0.98	1.33
Pure chlorobenzene	1.78	0.69	1.23
Pure toluene	2.31	0.53	1.22

Table II: Data for Four Compositions in Methanol (1)-1-Propanol (3)-Isobutyl Alcohol (2) System^a

100c ₁	0.719	0.366	0.364	1.708
100c ₂	0.379	0.159	0.748	0.161
100c ₃	0.466	0.922	0.198	0.199
N ₁	0.460	0.253	0.278	0.825
N ₂	0.242	0.110	0.573	0.078
${}^3\mathcal{D}_{11}^V \times 10^5$	1.04	0.909	0.765	1.505
${}^3\mathcal{D}_{12}^V \times 10^5$	0.032	0.030	0.027	0.211
${}^3\mathcal{D}_{21}^V \times 10^5$	-0.023	-0.009	-0.039	-0.004
${}^3\mathcal{D}_{22}^V \times 10^5$	0.875	0.721	0.624	1.383
$\mathcal{D}_{11}^r \times 10^5$	1.87	1.096	1.418	8.50
$\mathcal{D}_{12}^r \times 10^5$	1.72	0.389	1.462	15.9
$\mathcal{D}_{21}^r \times 10^5$	0.410	0.072	1.323	0.66
$\mathcal{D}_{22}^r \times 10^5$	1.764	0.879	3.58	2.86
$L_{11}^r RT \times 10^7$	1.84	0.463	0.725	24.4
$L_{12}^r RT \times 10^7$	0.518	0.049	0.885	2.06
$L_{21}^r RT \times 10^7$	0.535	0.048	0.895	2.05
$L_{22}^r RT \times 10^7$	0.605	0.136	2.26	0.415
$q_1 RT \times 10^5$	1.17	0.96	0.80	1.5
$q_2 RT \times 10^5$	0.85	0.72	0.58	1.38
$q_3 RT \times 10^5$	0.92	0.77	0.65	1.49

^a c_i in mol/cm³, ${}^r\mathcal{D}_{ik}^r$ and $q_i RT$ in cm²/sec, and $L_{ik}^r RT$ in mol/cm sec.

shows that variations of D^V_η are relatively small.

Shuck and Toor¹⁷ have measured ${}^3\mathcal{D}_{11}^V$, ${}^3\mathcal{D}_{12}^V$, ${}^3\mathcal{D}_{21}^V$, and ${}^3\mathcal{D}_{22}^V$ for four compositions in the methanol-1-propanol-isobutyl alcohol system at 30°, where methanol is component 1, isobutyl alcohol is component 2, and 1-propanol is the reference component, $r = 3$. This can be regarded as an approximately ideal system, so that

$$\nabla\mu_i \simeq RT\nabla \ln N_i$$

but, as molar volumes are not even approximately equal, $\nabla \ln N_i \neq \Delta \ln c_i$. In fact, we can write

$${}^r\mu_{ik} \simeq \frac{RT}{c_i} \left[\delta_{ik} - N_i + \left(\frac{\bar{V}_k}{\bar{V}_r} N_i \right) \right] \quad (i \neq r, k \neq r) \quad (31)$$

On the assumption of ideality, Shuck and Toor have shown that L_{ik}^V coefficients obey the Onsager reciprocal relation within the limits of experimental error. In Table II, the course of calculation followed has been

(17) F. O. Shuck and H. L. Toor, *J. Phys. Chem.*, **67**, 540 (1963).

(18) L. Miller and P. C. Carman, *Trans. Faraday Soc.*, **55**, 1831 (1959).

to transform ${}^3\mathcal{D}_{ik}^V$ coefficients to \mathcal{D}_{ik}^r coefficients and these in turn to L_{ik}^r coefficients. It can be seen that L_{12}^r and L_{21}^r are in good agreement.

As neither self-diffusion coefficients nor viscosities are available, a direct check on eq 25 is not possible. The procedure adopted in Table II, therefore, has been to use eq 25 to calculate q_1 , q_2 , and q_3 from the L_{ik}^r coefficients for the four ternary compositions studied and to see whether they show consistent behavior. The values for the limiting case of the pure components are given in Table III for comparison. In the case of a pure component such as methanol, q_2 and q_3 are determined from the limiting values of the binary inter-diffusion coefficients of isobutyl alcohol and of 1-propanol in methanol as given by Shuck and Toor, while q_1 is given by the self-diffusion coefficient of pure methanol.¹⁹ No value for the self-diffusion of isobutyl alcohol is available.

Table III: Limiting Mobilities^a and Viscosities for Methanol (1), Isobutyl Alcohol (2), and 1-Propanol (3)

	Methanol	Iso- butyl alcohol	1-Propanol
$q_1 RT \times 10^6$	2.46	0.59	0.80
$q_2 RT \times 10^6$	1.84	?	0.58
$q_3 RT \times 10^6$	1.97	0.40	0.73
η (30°), cP	0.51	2.81	1.72

^a $q_i RT$ in cm²/sec.

It is to be noted that (i) in the three pure alcohols, the values of q_i are in the inverse order of the viscosities and are in fact roughly proportional to $1/\eta^{0.85}$; (ii) $q_1 > q_3 > q_2$ for all compositions, as would be expected from the relative molecular sizes; and (iii) variations with composition are in accord with expectation, *e.g.*, a high methanol content should correspond to relatively low viscosities and correspondingly high mobilities, as is actually found.

The acetone–benzene–carbon tetrachloride system studied by Cullinan and Toor²⁰ is decidedly nonideal and, as ternary activity data are lacking, phenomenological coefficients cannot be obtained. Even if they were available, however, discussion of this system would properly belong to part II, as at least the acetone–carbon tetrachloride system does not conform to a simple binary Darken system. The results in the binary system can be explained if dimerization of the acetone is assumed.

Apart from the work of Toor and coworkers, diffusion measurements and full thermodynamic data are available for several aqueous ternary systems, though, as the solutes are solids, their range of concentrations is limited by solubility and other considerations to a relatively small part of the total composition range. All of these, however, involve the interactions dealt with in part II and will be discussed there.

(19) J. R. Partington, R. F. Hudson, and K. W. Bagnall, *Nature*, **169**, 583 (1952).

(20) H. T. Cullinan and H. L. Toor, *J. Phys. Chem.*, **69**, 3941 (1965)

Intrinsic Mobilities and Independent Fluxes in Multicomponent

Isothermal Diffusion. II. Complex Darken Systems

by P. C. Carman

National Chemical Research Laboratory, South African Council for Scientific and Industrial Research, Pretoria, South Africa (Received November 6, 1967)

The Darken theory has been applied to the available diffusion data in ternary systems for which accurate thermodynamic data are available. These are aqueous systems in which allowance has to be made for dimerization, hydration, compound formation, and electrolytic dissociation. Calculations are limited by the necessity to derive mobilities by use of viscosity corrections, but agreement between calculated and observed values of L_{ik}^r is shown to be good.

Introduction

There is considerable evidence that, in many non-ideal binary systems, Darken's theory is applicable if account is taken of various interactions of the components. Thus for certain binary nonelectrolyte systems for which self-diffusion coefficients were available, it was shown recently¹ that the relationship between these and the corresponding interdiffusion coefficients could be accounted for by the formation of association polymers or of compounds. Similar relationships have been established in concentrated aqueous solutions of strong electrolytes if hydration of ions is assumed.² In several other cases, where it has only been possible to estimate intrinsic mobilities by viscosity corrections to limiting values, as in the Hartley-Crank³ equation, similar conclusions have been reached both for nonelectrolytes^{4,5} and for 1:1 electrolytes.⁶

Exactly the same considerations can be applied to multicomponent systems. The essential feature of the Darken theory is that, owing to various types of interaction in a system of s components, the number of diffusing species exceeds s , but each one has an intrinsic mobility and is governed by the equation

$$J_i^0 = c_i q_i X_i \quad (1)$$

where $X_i = -\nabla\mu_i$. Each additional species, however, is governed by an equilibrium condition and, in the case of electrolytic dissociation, by a condition of electrical neutrality, so that the number of independent species is still s . Consequently, diffusion can be expressed in terms of s independent total fluxes of the original s components, their total concentrations, and their corresponding potential gradients. For any component involved in such an interaction, however, the corresponding phenomenological equation is no longer

$$J_i^0 = L_{ii}^0 X_i = -c_i q_i \nabla\mu_i \quad (2)$$

but becomes

$$J_i^0 = \sum_{k=1}^s L_{ik}^0 X_k \quad (3)$$

where the L_{ik}^0 can be quite complex functions of concentrations and intrinsic mobilities.

The number of possible forms which eq 3 can take is too varied to make a generalized treatment useful, so that the procedure adopted here will be to illustrate the principles involved by specific cases, based upon existing data for ternary systems. With regard to such application, eq 3 is subject to the same analysis as used in part I; *i.e.*, L_{ik}^r is calculated from experimental data and compared with values calculated from

$$L_{ik}^r = L_{ik}^0 - \frac{c_i}{c_r} L_{kr}^0 - \frac{c_k}{c_r} L_{ir}^0 + \frac{c_i c_k}{c_r^2} L_{rr}^0 \quad (4)$$

which is obtained from eq 11 of part I. It only reduces to eq 14 of part I in simple Darken systems, where L_{kr}^0 and L_{ir}^0 are zero.

In the following, all ternary systems have been discussed for which both diffusion coefficients and accurate measurements of thermodynamic activities are available, so that values of L_{ik}^r (obsd) can be derived. It is convenient to deal first with nonelectrolyte systems and then with those containing electrolytes.

Urea-Sucrose-Water System at 25°

In the binary urea-water system, it has been shown that thermodynamical activities up to 4 mol/l. can be explained on the assumption that dimerization takes place and that monomer and dimer form ideal solu-

- (1) P. C. Carman, *J. Phys. Chem.*, **71**, 2565 (1967).
- (2) J. Tamás and K. Újszászy, *Acta Chim. Acad. Sci. Hung.*, **49**, 377 (1966).
- (3) G. S. Hartley and J. Crank, *Trans. Faraday Soc.*, **45**, 801 (1949).
- (4) D. K. Anderson, *Dissertation Abstr.*, **21**, 1388 (1961).
- (5) D. K. Anderson and A. L. Babb, *J. Phys. Chem.*, **65**, 1281 (1961).
- (6) R. A. Robinson and R. H. Stokes, "Electrolyte Solutions," 2nd ed, Butterworths and Co., Ltd., London, 1959, pp 329-331.

tions.^{7,8} Interdiffusion and self-diffusion data over the same range are consistent with Darken's theory if it is assumed that the dimer mobility is about 0.7 monomer mobility and that mobilities vary with $\eta_r^{-0.9}$, where η_r is relative viscosity.^{7,9} Similarly, for the sucrose-water system, both thermodynamical activities and diffusion data can be accounted for, up to 1.5 mol/l., by assuming that all sucrose molecules are hydrated with five molecules of water and form ideal solutions.¹ Ellerton and Dunlop⁸ have shown that thermodynamical activities of urea-sucrose-water solutions up to 1 mol of solute/kg of water can be explained by combining the foregoing assumptions with the further assumption that urea can form a complex with hydrated sucrose molecules. It is of interest, therefore, to examine the diffusion data of the same workers¹⁰ on a solution containing 0.5 mol of solute/l. The equations derived represent a rather general case, which can be reduced to simpler forms when fewer interactions are encountered.

The subscripts 1, 2, and 3 refer to total urea, sucrose, and water, respectively, and higher numbers refer to the actual diffusing species; *i.e.*, 4-6 for monomeric, unhydrated components, 7 for urea dimer, 8 for hydrated sucrose, and 9 for urea-sucrose hydrate. Then eq 1 applies for J_i^0 when $i > 3$ and we have to derive eq 3 for both i and $k < 4$. If all sucrose molecules are uniformly hydrated with h molecules of water, where in this case $h = 5$, and a fraction α of uncombined urea exists as monomer

$$c_1 = c_4 + 2c_7 + c_9; \quad c_4 = \alpha(c_1 - c_9) \quad (5)$$

$$c_2 = c_8 + c_9; \quad c_5 = 0 \quad (6)$$

$$c_3 = c_6 + hc_2 \quad (7)$$

The various equilibria correspond to

$$X_1 = X_4; \quad X_2 = X_5; \quad X_3 = X_6 \quad (8)$$

$$X_7 = 2X_4 = 2X_1 \quad (9)$$

$$X_8 = X_5 + hX_6 = X_2 + hX_3 \quad (10)$$

$$X_9 = X_4 + X_8 = X_1 + X_2 + hX_3 \quad (11)$$

where the flux J_1^0 is given by

$$\begin{aligned} J_1^0 &= J_4^0 + 2J_7^0 + J_9^0 \\ &= c_4q_4X_4 + 2c_7q_7X_7 + c_9q_9X_9 \\ &= (c_4q_4 + 4c_7q_7 + c_9q_9)X_1 + c_9q_9X_2 + c_9q_9hX_3 \end{aligned}$$

To simplify the evaluation of q_7 and q_9 , it will be assumed in the following that dimer mobility $q_7 \simeq 0.7q_4$ and that the addition of urea to hydrated sucrose makes a negligible difference to sucrose mobility; *i.e.*, $q_9 \simeq q_8$. Thus

$$\begin{aligned} J_1^0 &= [(c_1 - c_9)(1.4 - 0.4\alpha)q_4 + c_9q_8] \times \\ &\quad X_1 + c_9q_8X_2 + hc_9q_8X_3 \quad (12) \end{aligned}$$

Similarly

$$\begin{aligned} J_2^0 &= J_8^0 + J_9^0 \\ &= c_9q_8X_1 + c_2q_8X_2 + hc_2q_8X_3 \quad (13) \end{aligned}$$

$$\begin{aligned} J_3^0 &= J_6^0 + hJ_2^0 \\ &= hc_9q_8X_1 + hc_2q_8X_2 + \\ &\quad [(c_8 - hc_2)q_6 + h^2c_2q_8]X_3 \quad (14) \end{aligned}$$

It can be seen that eq 12-14 correspond to eq 3 and that $L_{ik}^0 = L_{ki}^0$. Thus

$$\left. \begin{aligned} L_{11}^0 &= (c_1 - c_9)(1.4 - 0.4\alpha)q_4 + c_9q_8 \\ L_{22}^0 &= c_2q_8 \\ L_{33}^0 &= (c_3 - hc_2)q_6 + h^2c_2q_8 \\ L_{12}^0 &= c_4q_8 = L_{21}^0 \\ L_{13}^0 &= hc_9q_8 = L_{31}^0 \\ L_{23}^0 &= hc_2q_8 = L_{32}^0 \end{aligned} \right\} \quad (15)$$

Substituting in eq 4 for $r = 3$, corresponding values for L_{ik}^r are obtained.

Ellerton and Dunlop⁸ give the equilibrium constant for urea dimer as 1.8 and for urea-sucrose hydrate as 13.0, in terms of true mole fractions. From these, it can be calculated that

$$c_1 = c_2 = 0.5 \times 10^{-3}, \quad c_3 = 48.2 \times 10^{-3}$$

$$c_9 = 0.055 \times 10^{-3}, \quad \alpha = 0.97$$

For 0.5 mol of sucrose/l., in absence of urea, the relative viscosity is 1.62 and the self-diffusion coefficients of sucrose and water are, respectively, 0.374×10^{-5} and 1.53×10^{-5} cm²/sec.¹¹ As 0.5 mol of urea/l. only increases the viscosity of water by 2%, its effect will be neglected and the foregoing values will be used for η_r , q_8RT , and q_6RT , respectively. The limiting diffusion coefficient of urea in water is 1.382×10^{-5} cm²/sec, so that, in accord with the binary system, it is assumed that

$$q_4RT \simeq 1.382\eta_r^{-0.9} \times 10^{-5} \quad (16)$$

In Table I, calculated values of L_{ik}^0 and of L_{ik}^r are given, and the latter are compared with those obtained from transformation of the experimental diffusion coefficients. The values for L_{22}^r agree very well, while the agreement for L_{11}^r is poorer. This is not unexpected, since q_8 is not subject to a large viscosity correction, while the reverse is true for q_4 . Most important, L_{12}^0 is equal to c_9q_8 , *i.e.*, a positive term depending on the formation of urea-sucrose hydrate, and this is the dominant term in L_{12}^r , so that the good agreement between the calculated value of L_{12}^r and observed

(7) R. H. Stokes, *J. Phys. Chem.*, **69**, 4012 (1965).

(8) H. D. Ellerton and P. J. Dunlop, *ibid.*, **70**, 1831 (1966).

(9) P. C. Carman, *ibid.*, **70**, 3355 (1966).

(10) H. D. Ellerton and P. J. Dunlop, *ibid.*, **71**, 1538 (1967).

(11) R. R. Irani and A. W. Adamson, *ibid.*, **62**, 1517 (1958).

values of L_{12}^r and L_{21}^r is of particular significance. It is nearer to the latter, which is the more accurate according to the estimated errors given by Ellerton and Dunlop.¹⁰

Table I: Urea (1)-Sucrose (2)-Water (3) System at 25°^a

Quantity	Calcd value × 10 ⁶	Quantity	Value × 10 ⁶	
			Calcd	Obsd
$L_{11}^0 RT$	4.27	$L_{11}^r RT$	4.32	4.77
$L_{22}^0 RT$	1.87	$L_{12}^r RT$	0.18	0.25
$L_{33}^0 RT$	787	$L_{21}^r RT$		0.19
$L_{12}^0 RT$	0.206	$L_{22}^r RT$	1.76	1.77
$L_{13}^0 RT$	1.03			
$L_{23}^0 RT$	9.35			

^a $L_{ik}^0 RT$ and $L_{ik}^r RT$ in mol/cm sec.

Mannitol (1)-Sucrose (2)-Water (3) System at 25°

Ellerton and Dunlop¹² also investigated four compositions in this system up to a maximum of 0.5 mol/l. of each solute. As there is no reason to assume dimerization of mannitol or combination between mannitol and sucrose from thermodynamic activities and there is little evidence that mannitol forms hydrated molecules, this should be a simpler system to study, since c_7 and c_8 are zero and $c_4 = c_1$ and $c_8 = c_2$. In absence of self-diffusion data, however, it is extremely difficult to arrive at useful estimates of the various mobilities. Taking the case of 0.5 mol/l. of each solute, we have relative viscosities of 1.62 for sucrose alone, 1.30 for mannitol alone, and no less than 2.274 for both, so that large viscosity corrections are necessary for both components. Mills and Ellerton¹³ measured diffusion coefficients for traces of sucrose in mannitol solutions, and these vary approximately with $\eta_r^{-0.9}$, but the effect of sucrose concentration upon self-diffusion coefficients of sucrose in sucrose solutions is complex¹¹ and the variation is nearer to $\eta_r^{-0.7}$ over the range of interest here. Similarly, for traces of mannitol in sucrose solutions,¹³ the variation corresponds to $\eta_r^{-0.9}$, but binary diffusion coefficients for mannitol-water obtained by Dunlop¹⁴ correspond more nearly to $\eta_r^{-0.75}$. Obviously, viscosity corrections can only be very approximate and, for the ternary compositions under consideration, a common factor of $\eta_r^{-0.8}$ has been adopted for all components, giving

$$q_4 RT \simeq 0.666 \eta_r^{-0.8} \times 10^{-5} \quad (17)$$

$$q_8 RT \simeq 0.523 \eta_r^{-0.8} \times 10^{-5} \quad (18)$$

$$q_6 RT \simeq 2.5 \eta_r^{-0.8} \times 10^{-5} \quad (19)$$

Equation 19 will be used for water in most of the following systems, as this seems to be fairly widely applicable. It is based on a self-diffusion coefficient of 2.5×10^{-5} cm²/sec for pure water at 25°.

Comparison of the resulting values of L_{11}^r and L_{22}^r in Table II with those obtained from experimental diffusion coefficients shows that they agree well within the

Table II: Mannitol (1)-Sucrose (2)-Water (3) System at 25°

$10^6 c_1$	0.25	0.5	0.25	0.5
$10^6 c_2$	0.25	0.25	0.5	0.5
$10^6 c_3$	51.0	49.4	47.8	46.1
η_r	1.45	1.684	1.921	2.274
Calcd value × 10 ⁹				
$L_{11}^0 RT$	1.24	2.19	0.985	1.725
$L_{22}^0 RT$	0.97	0.86	1.545	1.355
$L_{33}^0 RT$	946	814	708	598
$L_{33}^r RT$	4.85	4.30	7.73	6.78
$L_{11}^r RT$	1.26	2.27	1.00	1.80
$L_{12}^r RT$	-0.003
$L_{22}^r RT$	0.95	0.84	1.46	1.28
Obsd value × 10 ⁹				
$L_{11}^r RT$	1.24	2.30	0.99	1.69
$L_{12}^r RT$	0.062	0.083	0.110	0.191
$L_{21}^r RT$	0.045	0.074	0.076	0.137
$L_{22}^r RT$	0.96	0.84	1.59	1.33

uncertainties of the viscosity correction. The least satisfactory aspect from the viewpoint of Darken theory is that experimental L_{12}^r and L_{21}^r coefficients have definite positive values and are, in fact, comparable with the value for the urea-sucrose-water system, although there is no reason to assume that mannitol and sucrose form a complex. The calculated value is zero or very slightly negative.

Electrolytes

Owing to electrolytic dissociation, all electrolytes must be regarded as giving complex Darken systems. Presence of a single fully dissociated electrolyte or any number of such electrolytes with a common ion raises the number of diffusing species to $s + 1$ in a system of s components, but the condition of electrical neutrality ensures that the number of independent species is still s . Diffusion can thus be expressed once again in terms of s independent fluxes corresponding to the s undissociated components. When electrolytic dissociation is not complete, undissociated molecules, intermediate ions such as HSO_4^- , and ion pairs add to the number of diffusing species, but each is subject to an equilibrium, so that the number of independent fluxes remains unchanged.

Darken's theory is particularly fitted for application to electrolytes, since it has always been customary to describe ionic transport in terms of ionic mobilities. As usually discussed, the solvent is employed as

(12) H. D. Ellerton and P. J. Dunlop, *J. Phys. Chem.*, **71**, 1291 (1967).

(13) R. Mills and H. D. Ellerton, *ibid.*, **70**, 4089 (1966).

(14) P. J. Dunlop, *ibid.*, **69**, 4276 (1965).

reference frame, but this arbitrary choice of one component cannot have fundamental meaning for concentrated solutions. It is a short step, therefore, to use of intrinsic mobilities on the Darken reference frame, for which all s components have independent fluxes. In the Hartley-Crank form, this is the approach used by Robinson and Stokes for concentrated binary solutions.¹⁵

For an ion i with a valence z_i , eq 1 is applicable, provided that X_i is the total potential gradient, *i.e.*

$$X_i = -[\nabla\mu_i + (z_iEF \times 10^7)] \quad (20)$$

where $\nabla\mu_i$ is the true molar chemical potential gradient, F is the faraday in coulombs, and E is an electrical field in volts per centimeter. In a conductivity experiment, $\nabla\mu_i$ is zero and E is the externally applied field, so that the limiting mobility q_i^0 at infinite dilution is given by the limiting equivalent conductivity, λ_i^0

$$q_i^0 = \frac{\lambda_i^0}{|z_i|F^2} \times 10^{-7} \quad (21)$$

where $|z_i|$ is the numerical value of z_i and the flux for $E = 1$ is equal to $c_i\lambda_i^0/F$. In diffusion, an internal electrical field is set up due to differential mobilities of the ions present, but it is not necessary to know its value, as it is eliminated from the expressions for flux of total electrolytes present by applying the condition of electrical neutrality.

Calculation of Ionic Mobilities

Strictly speaking, even with use of eq 20 for X_i , eq 1 is not applicable to electrolytes, since it does not incorporate corrections for electrophoresis and relaxation. In the following sections, however, these corrections have been ignored and eq 1 is assumed, with ionic mobilities q_i calculated by applying a viscosity correction to q_i^0 .

Some justification for this is required. In the first place, all calculations involving these corrections are very complex and, even in the simplest case of a single 1:1 electrolyte, valid approximations can be made only up to molalities of about 0.02, which is far below the level of any concentration thus far studied in ternary diffusion. In the case of electrolytic conductivity, to which most attention has been given, the trend of the calculations indicates that any attempt to extrapolate the approximations well beyond their valid limits is liable to give corrections which are much too large and even of the wrong sign. Second, while the corrections play a large part in conductivity, their effect upon ordinary diffusion coefficients is relatively small. Consequently, equivalent conductivities at finite concentrations cannot be used to determine ionic mobilities for diffusion at those concentrations, and there is much more reason for dropping the corrections altogether for diffusion.

Thus for a single electrolyte, there is no relaxation

correction, and the electrophoretic correction is very small as long as the ions concerned do not differ too much in mobility; *e.g.*, for NaCl, the correction does not exceed 2% up to a molality of 4.0, even assuming that the approximation used is valid so far above the correct limit of 0.02. The true electrophoretic correction is probably much smaller. When the highly mobile hydrogen ion is present, much larger electrophoretic corrections are to be expected, which could decrease the calculated diffusion coefficient by several per cent, so that neglect of the correction in this case is probably not justified.

In ternary systems containing more than two kinds of ion, relaxation effects can be present, but there is evidence that they are not large for most common ions at the electrolyte concentrations of interest here. If only a trace of an ion is diffused in a supporting electrolyte, electrophoretic effects are absent, and calculations for limiting dilutions of the supporting electrolyte indicate that very large relaxation effects are to be expected. If this were true, it would mean that the self-diffusion coefficient for an ion in a given composition would give a completely misleading indication of its mobility for ordinary diffusion, since the large relaxation corrections would not be comparable. In actual measurements for Na⁺, K⁺, and Cl⁻, however, little indication of relaxation effects appeared,^{16,17} since the tracer diffusion coefficients were primarily affected by viscosity and, in fact, were approximately proportional to η_r^{-1} at concentrations of supporting electrolyte up to molarities of 4.0. For these ions, therefore, it seems reasonable to neglect relaxation and to assume that mobilities can be determined (a) by applying viscosity corrections or (b) from self-diffusion measurements, just as in the case of nonelectrolytes. The rapid-moving hydrogen ion was once more an exception, as it showed a rapid decrease of the tracer diffusion coefficient for very small concentrations of supporting electrolyte and continued to decrease more rapidly than expected from the viscosity at higher concentrations. It must be assumed that relaxation cannot be ignored in this case.

NaCl (1)-Mannitol (2)-Water (3) System at 25°

Diffusion in this system has been studied by Dunlop¹⁴ at relatively high concentrations. Consistent with nonelectrolyte systems already discussed, species 1-3 denote the components above, while the higher numbers denote additional species. In this case, 4 and 5 denote Na⁺ and Cl⁻, the electrolyte being assumed fully dissociated, and hydration for the moment will be disregarded. In eq 3, there are no cross coefficients,

(15) See ref 6, p 327.

(16) J. H. Wang, *J. Phys. Chem.*, **58**, 686 (1954).

(17) See ref 6, p 317.

Table III: NaCl (1)-Mannitol (2)-Water (3) System at 25°

	Binary			Ternary			
	1.5	3.0	...	1.5	3.0	1.5	3.0
$10^9 c_1$	1.5	3.0	...	1.5	3.0	1.5	3.0
$10^9 c_2$	0.75	0.2	0.2	0.75	0.75
$10^9 c_3$	53.8	52.1	50.5	52.5	50.6	48.7	46.8
η_r	1.15	1.37	1.49	1.28	1.55	1.77	2.08
Calcd value $\times 10^9$							
$L_{11}^0 RT$	10.5	17.6	...	9.66	16.3	7.26	12.5
$L_{22}^0 RT$	3.63	1.09	0.94	3.15	2.78
$L_{33}^0 RT$	1210	1010	910	1070	890	770	650
$L_{11}^r RT$	11.4	20.6	...	10.5	19.4	8.0	15.2
$L_{12}^r RT$	0.12	0.21	0.37	0.67
$L_{22}^r RT$	3.83	1.11	0.95	3.33	2.95
Obsd value $\times 10^9$							
$L_{11}^r RT$	10.8	18.1	...	10.1	17.3	7.9	13.7
$L_{12}^r RT$	0.19	0.26	0.43	0.88
$L_{21}^r RT$	0.16	0.24	0.38	0.83
$L_{22}^r RT$	3.99	1.11	0.89	3.27	2.78

but the effective mobility q_1 for NaCl is a function of the mobilities for Na^+ and Cl^- , *i.e.*

$$q_1 = \frac{q_4 q_5}{q_4 + q_5} \quad (22)$$

This corresponds to the well-known Nernst-Hartley relationship for diffusion of single electrolytes and thus need not be derived here. To obtain estimates for q_4 and q_5 at 25°, we have (i) measurements of self-diffusion coefficients of Na^+ and Cl^- up to high concentrations of NaCl,^{16,17} which, at the concentrations of interest here, show variations, respectively, of a little less and a little more than η_r^{-1} ; and (ii) a measurement of limiting equivalent conductivities of Na^+ and Cl^- in 10% mannitol¹⁸ which both correspond more nearly to $\eta_r^{-0.8}$. In Table III, for presence of both solutes, a variation with $\eta_r^{-0.9}$ has been assumed, *i.e.*

$$q_1 RT = \frac{RT \eta_r^{-0.9}}{F^2} \left(\frac{\lambda_4^0 \lambda_5^0}{\lambda_4^0 + \lambda_5^0} \times 10^{-7} \right) \quad (23)$$

$$= 0.805 \eta_r^{-0.9} \times 10^{-5} \quad (24)$$

Equation 17, with q_2 instead of q_4 , can be used for mannitol mobility, and eq 19, with q_3 instead of q_5 , can be used for water mobility. The latter is in accord with measurements of self-diffusion coefficients of water in concentrated NaCl solutions,^{16,19} since these vary approximately with $\eta_r^{-0.8}$.

In Table III, the coefficients for the binary compositions 1.5 and 3 mol/l. of NaCl and 0.75 mol/l. of mannitol are included, the former being calculated in this case with q_1 proportional to η_r^{-1} . This corresponds to the Hartley-Crank calculation carried out by Robinson and Stokes,⁶ and, in accord with them, the calculated values of L_{11}^r are too high. To reach agreement, hydration to the extent of about 1 molecule of water/molecule of NaCl had to be postulated. In the

ternary system, the calculated values also tend to be high, presumably for the same reason. Agreement of calculated and observed values of L_{22}^r is reasonably good throughout. Calculated values of L_{12}^r are consistently lower than observed values. The difference in this relatively small cross term is perhaps not unreasonable in the light of possibilities of experimental error and of the use of relative viscosities to estimate mobilities but it is also to be noted that it could be readily accounted for if only a small fraction of the mannitol were bound to, say, some of the sodium ions. As NaCl and mannitol are mutually "salted-in" this is a distinct possibility.

KCl (1)-Glycine (2)-Water (3) System at 25°

As this ternary system has been studied only up to 0.5 mol/l. of each solute,²⁰ it will be discussed very briefly. For binary glycine-water systems, data for interdiffusion,²¹ self-diffusion of glycine,²² relative viscosity, and thermodynamic activity²³ up to 2 mol/l. are available. Since KCl up to 0.5 mol/l. makes no appreciable change in the viscosity of water, viscosities of the ternary mixtures are assumed to be affected by glycine alone, and, as the limiting equivalent conductivities of K^+ and Cl^- in various aqueous solutions of nonelectrolytes¹⁸ vary approximately with $\eta_r^{-0.8}$, q_1 is assumed to be given by

(18) B. J. Steel, J. M. Stokes, and R. H. Stokes, *J. Phys. Chem.*, **62**, 1514 (1958).

(19) D. W. McCall and D. C. Douglass, *ibid.*, **69**, 2001 (1965).

(20) L. A. Woolf, D. G. Miller, and L. J. Gosting, *J. Amer. Chem. Soc.*, **84**, 317 (1962).

(21) H. D. Ellerton, G. Reinfelds, D. E. Mulcahy, and P. J. Dunlop, *J. Phys. Chem.*, **68**, 403 (1964).

(22) J. H. Wang, *J. Amer. Chem. Soc.*, **75**, 2777 (1953).

(23) H. D. Ellerton, G. Reinfelds, D. E. Mulcahy, and P. J. Dunlop, *J. Phys. Chem.*, **68**, 398 (1964).

$$q_1RT = 0.977\eta_r^{-0.8} \times 10^{-5} \quad (25)$$

From the variation of the self-diffusion coefficient of glycine in the binary system, the same viscosity factor is applied, *i.e.*

$$q_2RT = 1.061\eta_r^{-0.8} \times 10^{-5} \quad (26)$$

Equation 19 with q_3 replacing q_6 is used for water mobility in absence of other evidence.

Table IV: KCl (1)–Glycine (2)–Water (3) System at 25°

	Binary		Ternary
	1-2	2-3	
10^3c_1	0.50	...	0.50
10^3c_2	...	0.50	0.50
10^3c_3	54.5	54.2	53.4
η_r	1.00	1.076	1.076
Calcd value $\times 10^9$			
L_{11}^0RT	4.99	...	4.70
L_{22}^0RT	...	5.01	5.01
L_{33}^0RT	1360	1280	1260
L_{11}^rRT	5.10	...	4.81
L_{12}^rRT	0.11
L_{22}^rRT	...	5.12	5.12
Obsd value $\times 10^9$			
L_{11}^rRT	5.19	...	4.82
L_{12}^rRT	0.15
L_{21}^rRT	0.19
L_{22}^rRT	...	5.32	5.22

In Table IV, only the highest concentration in the ternary system is presented, as there are no further points of interest for the lower concentrations. The table also includes the binary values for 0.5 mol/l. of KCl and of glycine. It can be seen that the calculated and observed values of L_{11}^r and L_{22}^r are in reasonable agreement. The calculated value of L_{12}^r is decidedly too small, but it is a very small coefficient and Woolf, Miller, and Gosting²⁰ have pointed out that L_{12}^r and L_{21}^r (exptl) are only correct within a few parts in the second figure after the decimal point.

NaCl (1)–KCl (2)–H₂O (3) System at 25°

The general relationships between ion mobilities and phenomenological coefficients for two electrolytes with a common ion in a ternary system have been presented by Wendt,²⁴ and the specialized forms adopted by his equations in this and the following system will be employed here. The only difference in treatment is that his coefficients are referred to the solvent reference frame, whereas the same coefficients are here used with the Darken reference frame. Thus L_{ik}^0 is calculated by his equation for L_{ik}^r and the true L_{ik}^r is obtained from eq 4. If 4, 5, and 6 refer to Na⁺, K⁺, and Cl⁻, respectively, assuming complete dissociation, then

$$c_4 = c_1; \quad c_5 = c_2; \quad c_6 = c_1 + c_2 \quad (27)$$

and

$$L_{11}^0 = c_4q_4(c_5q_5 + c_6q_6) / \sum_{k=4}^6 c_kq_k \quad (28)$$

$$L_{12}^0 = -c_4q_4c_5q_5 / \sum_{k=4}^6 c_kq_k \quad (29)$$

$$L_{22}^0 = c_5q_5(c_4q_4 + c_6q_6) / \sum_{k=4}^6 c_kq_k \quad (30)$$

Thus in this case, not only are L_{11}^0 and L_{22}^0 relatively complex functions of mobility and concentration, but also there is a rather large negative cross coefficient.

As noted earlier, self-diffusion coefficients of Na⁺ and of Cl⁻ in NaCl solutions vary approximately with η_r^{-1} , so that it has been assumed that, in a solution containing ions only, q_4 , q_5 , and q_6 are given by

$$q_i = \frac{\lambda_i^0}{\eta_r |z_i| F^2} \times 10^{-7} \quad (31)$$

As in the previous systems, the mobility of water is assumed to vary with $\eta_r^{-0.8}$. Relative viscosities were estimated from the data of Ruby and Kawai.²⁵

In Table V, experimental values of L_{ik}^r are those calculated by Miller²⁶ from the data of Dunlop and Gosting²⁷ and of Dunlop.²⁸ The agreement between calculated and observed values of L_{ik}^r is remarkably good throughout the table. Only at the highest concentration is the calculated value of L_{11}^r for NaCl definitely too large. This is in accord with the binary NaCl–H₂O system in Table III, where it was attributed to hydration.

Na₂SO₄ (1)–H₂SO₄ (2)–H₂O (3) System at 25°

Diffusion measurements in this system have been given by Wendt²⁹ and L_{ik}^r values in Table VI are taken from his paper. Calculations in this case are subject to great uncertainties since, apart from the ions Na⁺ (4), H⁺ (5), and SO₄²⁻ (6) for the fully dissociated electrolytes, it is necessary to consider HSO₄⁻ (7) and possibly also NaSO₄⁻ and even Na₂SO₄ and H₂SO₄. If only the first four are assumed to be present, then application of Wendt's general equations²⁴ to obtain L_{ik}^0 gives eq 32–34.

$$L_{11}^0 = \frac{1}{4}c_4q_4(c_5q_5 + 4c_6q_6 + c_7q_7) / \sum_{k=4}^7 z_k^2 c_kq_k \quad (32)$$

$$L_{12}^0 = -\frac{1}{4}c_4q_4(c_5q_5 - c_7q_7) / \sum_{k=4}^7 z_k^2 c_kq_k \quad (33)$$

$$L_{22}^0 = [c_5q_5c_7q_7 + \frac{1}{4}(c_5q_5 + c_7q_7) \times (c_4q_4 + 4c_6q_6)] / \sum_{k=4}^7 z_k^2 c_kq_k \quad (34)$$

(24) R. P. Wendt, *J. Phys. Chem.*, **69**, 1227 (1965).

(25) C. E. Ruby and J. Kawai, *J. Amer. Chem. Soc.*, **48**, 1119 (1926).

(26) D. G. Miller, *J. Phys. Chem.*, **69**, 3374 (1965).

(27) P. J. Dunlop and L. J. Gosting, *ibid.*, **61**, 215 (1957)

(28) P. J. Dunlop, *ibid.*, **63**, 612 (1959).

(29) R. P. Wendt, *ibid.*, **66**, 1279 (1962).

Table V: NaCl (1)-KCl (2)-H₂O (3) System at 25°

10^3c_1	0.25	0.50	0.25	0.50	1.50
10^3c_2	0.25	0.25	0.50	0.50	1.50
10^3c_3	54.7	54.4	54.3	54.0	51.1
η_r	1.021	1.045	1.021	1.045	1.19
Calcd value $\times 10^9$					
L_{11}^0RT	2.68	4.78	2.89	5.20	13.73
L_{12}^0RT	-0.87	-1.16	-1.13	-1.69	-4.51
L_{22}^0RT	3.53	3.78	6.27	6.87	18.12
L_{33}^0RT	1350	1310	1330	1310	1110
L_{11}^rRT	2.71	4.89	2.92	5.31	14.69
L_{12}^rRT	-0.84	-1.11	-1.08	-1.58	-3.55
L_{22}^rRT	3.56	3.81	6.38	6.98	19.08
Obsd value $\times 10^9$					
L_{11}^rRT	2.61	4.78	2.81	5.14	13.34
L_{12}^rRT	-0.76	-1.04	-1.00	-1.53	-4.07
L_{21}^rRT	-0.74	-1.02	-0.98	-1.47	-3.81
L_{22}^rRT	3.50	3.82	6.37	6.98	18.96

Table VI: Na₂SO₄ (1)-H₂SO₄ (2)-H₂O (3) System at 25°

	Binary				Ternary			
	0.5	1.0	0.5	1.0	0.5	1.0
10^3c_1	0.5	1.0	0.5	1.0	0.5	1.0
10^3c_2	0.5	1.0	0.5	0.5	1.0	1.0
10^3c_3	54.8	54.0	54.4	53.3	53.5	52.6	52.4	51.3
10^3c_7	0.37	0.70	0.55	0.63	0.90	1.10
10^3c_4	1.0	2.0	1.0	2.0	1.0	2.0
10^3c_5	0.63	1.30	0.45	0.37	1.10	0.90
10^3c_6	0.5	1.0	0.13	0.30	0.45	0.87	0.60	0.90
η_r	1.23	1.55	1.09	1.19	1.28	1.59	1.39	1.69
Calcd value $\times 10^9$								
L_{11}^0RT	1.66	2.64	2.18	3.19	2.19	3.30
L_{12}^0RT	-1.09	-1.01	-1.41	-1.65
L_{22}^0RT	5.1	9.2	6.32	5.76	11.0	10.3
L_{33}^0RT	1170	950	1280	1160	1090	910	1000	840
L_{11}^rRT	1.76	2.97	2.28	3.35	2.37	3.62
L_{12}^rRT	-0.99	-0.85	-1.23	-1.33
L_{22}^rRT	5.2	9.6	6.42	5.92	11.2	10.6
Obsd value $\times 10^9$								
L_{11}^rRT	2.10	3.66	2.36	4.00	2.32	3.87
L_{12}^rRT	-0.65	-0.61	-0.75	-1.04
L_{21}^rRT	-0.54	-0.56	-0.64	-1.31
L_{22}^rRT	4.35	7.25	5.36	4.65	8.69	7.88

where z_k is the valence of ion k and

$$c_4 = 2c_1; \quad c_5 = 2c_2 - c_7; \quad c_6 = c_1 + c_2 - c_7 \quad (35)$$

Thus the first step in application of these equations is to determine the concentration of HSO₄⁻, c_7 . In Table VI, the work of Baes³⁰ has been used, but, as practically every composition in this table considerably exceeds the maximum ionic strength for which the bisulfate ion dissociation quotients of Baes are valid, the estimates for c_7 must be very approximate.

As in the previous system, it has been assumed that ionic mobilities are proportional to η_r^{-1} , while water mobilities are again assumed to vary with $\eta_r^{-0.8}$. As

viscosities are large, viscosity corrections must be regarded as a major source of error.

Apart from the ternary compositions, Wendt also measured diffusion coefficients for four binary compositions and these are also included in Table VI. The thermodynamic data for calculation of L_{ii}^r (obsd) for the binary systems were obtained from Robinson and Stokes.³¹ It is to be noted that, in the case of Na₂SO₄, these are decidedly higher than the calculated values of L_{11}^r . Since ion-pair formation to give NaSO₄⁻ is

(30) C. F. Baes, *J. Amer. Chem. Soc.*, **79**, 5611 (1957).

(31) See ref 6, pp 477, 501.

extremely likely to be considerable at the concentrations studied and would tend to give much higher calculated values, this is the most likely reason for the discrepancy. Unfortunately, as no independent mode of estimating the proportion of NaSO_4^- is available, a corrected value cannot be calculated. In the case of the binary H_2SO_4 solutions, the opposite effect is found, *i.e.*, calculated values of L_{22}^r are too large. Here we have the extremely fast-moving hydrogen ion, with the result that electrophoretic corrections cannot be left out of account. An approximate calculation showed that $L_{22}^0(\text{calcd})$ could be reduced by as much as 9% from this cause. Hydration also leads to lower calculated values, and the further assumption of 3–4 mol of water/mol of H_2SO_4 would suffice to bring calculated and observed values of L_{22}^r into agreement.

When we turn to the ternary systems, it is found that agreement between calculated and observed values of L_{11}^r is much better than in simple Na_2SO_4 solutions, presumably because formation of NaSO_4^- is suppressed. The largest difference, as should be expected, is for the 2:1 ratio of $\text{Na}_2\text{SO}_4:\text{H}_2\text{SO}_4$. The difference between observed and calculated values of L_{22}^r remains much the same as for the binary system, as is to be expected if interionic effects and hydration are responsible. The values of L_{12}^r are strongly negative, as predicted, and calculated and observed values agree reasonably well, when it is borne in mind that the many possibilities of error have most effect on this coefficient.

In brief, the complexities of this system scarcely permit a close agreement between calculated and observed values, but the fact that the ternary system is highly consistent with the binary systems and raises no new problems provides strong reasons for regarding these as Darken systems.

Discussion

Though diffusion measurements have been carried out in a number of other ternary systems, the foregoing sections cover all the cases where accurate thermodynamic data are available over the concentration range of the diffusion experiments. To date, the main application of such data has been to calculate the corresponding experimental phenomenological coefficients and to demonstrate the validity of the Onsager reciprocal relation. It has been shown here that the data can be interpreted very satisfactorily in terms of Darken diffusion and correlate well with the corresponding binary systems.

In all cases, agreement of calculated and observed values of L_{11}^r and L_{22}^r is within reasonable limits. The agreement for L_{12}^r is not so good in general, but this is a relatively small term which must bear a large burden of accumulated errors in measurement and in approximating assumptions. This may be sufficient to account for discrepancies, but it is perhaps significant that the error tends to be almost invariably in one direction;

i.e., the calculated value is somewhat more negative or less positive than the observed one. This may mean that Darken diffusion, which is indicative of a jump mechanism,¹ is not able to give a complete description of diffusion in the various systems studied.

Unfortunately, mobilities have had to be calculated by applying viscosity corrections which are open to considerable uncertainty, especially when relative viscosities are large. At present, there are no data at all for self-diffusion coefficients in ternary systems, although such measurements are essential to test the view that Darken diffusion predominates for the systems discussed here.

Acknowledgment. I wish to thank Mr. S. J. van der Walt for relative viscosity determinations in the NaCl -mannitol- H_2O system and Mr. D. J. Strydom for the same in the Na_2SO_4 - H_2SO_4 - H_2O system.

Addendum

Miller³² has recently published a series of papers on the determination of solvent-fixed phenomenological coefficients, l_{ij} , for individual ions in aqueous solutions of electrolytes. It is of interest to note the relationship between these coefficients and coefficients used here. In, for example, the NaCl - KCl - H_2O system, it was assumed that $L_{44}^0 = c_4q_4$, $L_{55}^0 = c_5q_5$, and $L_{66}^0 = c_6q_6$ for the individual ions, with zero cross coefficients, and these were used to derive L_{11}^0 , L_{12}^0 , and L_{22}^0 for the whole salts and then L_{11}^r , etc., for a solvent fixed frame. An alternative procedure is to transform ionic coefficients first to a solvent-fixed frame, giving the l_{ij} coefficients of Miller, and then to use these to derive L_{11}^r , etc., the final result being the same as before.

The important feature of Miller's work is that l_{ij} coefficients are calculated from experimental data and thus are open to theoretical interpretation. He finds that cross coefficients are definitely not zero. This can arise in various ways, the first being the transformation to a solvent-fixed frame, for instance

$$l_{45} = \frac{c_4c_5}{c_3^2} L_{33}^0$$

Again, if electrophoretic and relaxation corrections are introduced, nonzero ionic cross terms L_{ij}^0 result, and these also appear in the l_{ij} . Hydration of ions does not produce ionic cross terms, L_{ij}^0 , but does affect l_{ij} cross terms on transformation to a solvent-fixed frame. Finally, partial dissociation or ion-pair formation has a profound effect.

Miller's emphasis on l_{ij} coefficients and hence on ionic mobilities is wholly in accord with Darken systems. He does not favor R_{ij} coefficients. His choice

(32) D. G. Miller, *J. Phys. Chem.*, **70**, 2639 (1966); **71**, 616, 3588 (1967).

of a solvent-fixed frame is based on sound practical reasons, but it is an arbitrary choice of one reference component and becomes more unrealistic from a theo-

retical viewpoint as concentrations increase. The significant coefficients are L_{ij}^0 coefficients for a Darken reference frame.

Electron Spin Resonance of Nitrogen Dioxide in Frozen Solutions¹

by B. H. J. Bielski, J. J. Freeman, and J. M. Gebicki

Chemistry Department, Brookhaven National Laboratory, Upton, New York 11973 (Received November 6, 1967)

The electron spin resonance of nitrogen dioxide trapped in frozen nitromethane, chloroform, carbon tetrachloride, and water were studied over a wide range of temperatures. In all solvents a triplet spectrum observed near -100° split into many lines when the temperature was raised. Simultaneously, the hyperfine splitting constant due to interaction of the unpaired electron with the N¹⁴ magnetic moment decreased from 55 to about 12 G. The multiline spectra were interpreted in terms of an interaction between NO₂ and N₂O₄.

Introduction

A number of attempts have been made to study the esr spectrum of the paramagnetic nitrogen dioxide and several accounts have appeared of the observation of triplet absorption spectra, characteristic of the interaction of the unpaired electron and N¹⁴ magnetic moments.²⁻⁴ The isotropic component of the hyperfine splitting constant was found to be 54.6–57.8 g for NO₂ trapped in inert gas matrices at 4°K. Extension of these studies to solutions of NO₂ did not produce consistent results. Holm, *et al.*,⁵ measured a line width of 155 G for NO₂ in pure dinitrogen tetroxide at room temperature, which increased on dilution with carbon tetrachloride to 227 G. In carbon disulfide, Bird, *et al.*,³ recorded a fully resolved NO₂ triplet with a splitting constant of 107 G. This was about twice as large as the splitting observed for NO₂ trapped in inert matrices or in ice. Further attempts to repeat and extend these studies to solutions of NO₂ in carbon tetrachloride, chloroform, nitromethane, and dinitrogen tetroxide yielded only broad singlets.⁴ On cooling, all signals disappeared because of rapid dimerization of the NO₂.

This paper reports results of esr studies of frozen solutions of NO₂ in water, nitromethane, chloroform, and carbon tetrachloride. In order to overcome the difficulties associated with dimerization on cooling, modified techniques were used to introduce NO₂ into the solvents. In one method, dilute solutions of nitromethane were frozen at boiling nitrogen temperature and irradiated with ultraviolet light. During photolysis, methyl and NO₂ free radicals were released and trapped in the matrix.⁶ The methyl radicals were then removed by annealing so that the behavior of NO₂ alone

could be studied. In a second method, mixing of cooled solvent and solid N₂O₄ also resulted in the trapping of NO₂. Except at very low temperatures, similar esr spectra were obtained with solutions prepared by either technique.

Experimental Section

Analytical grade chloroform, carbon tetrachloride, and nitromethane were distilled over a 30-plate column. Water and heavy water (99.7% deuterated) were purified by triple distillation from acid dichromate and alkaline permanganate, while deuterated chloroform (Merck, Sharp and Dohm, Ltd.) was used directly. The concentration of nitromethane in these solvents was varied between 0.05 and 1.0 M. A small sample of the solution was sealed in a 2-mm i.d. quartz tube and irradiated at boiling nitrogen temperature with light from a GE BH-6 high-pressure mercury arc lamp for periods between 0.5 and 2 hr. In initial experiments the light was filtered through a Corning No. 7-59 uv filter (transmission peak at 3600 Å), which passed uv

(1) Research performed under the auspices of the U. S. Atomic Energy Commission. Part of this work was presented at the Sixth Australian Spectroscopy Conference, Brisbane, 1967.

(2) (a) J. G. Castle, Jr., and R. Behringer, *Phys. Rev.*, **80**, 114 (1950); (b) C. K. Jen, S. N. Foner, E. L. Cochran, and V. A. Bowers, *ibid.*, **112**, 1169 (1958); (c) J. B. Farmer, D. A. Hutchinson, and C. A. McDowell, Fifth International Symposium on Free Radicals, Uppsala, 1961, 44-1.

(3) G. R. Bird, J. C. Baird, and R. B. Williams, *J. Chem. Phys.*, **28**, 738 (1958).

(4) P. W. Atkins, N. Keen, and M. C. R. Symons, *J. Chem. Soc.*, 2873 (1962).

(5) C. H. Holm, W. H. Thurston, H. M. McConnell, and N. Davidson, *Bull. Amer. Phys. Soc., Ser. II*, 397 (1956).

(6) B. H. J. Bielski and R. B. Timmons, *J. Phys. Chem.*, **68**, 347 (1964).

light in the wavelength region corresponding to the onset of the first strong absorption band of nitromethane. Since identical esr spectra were obtained with solutions irradiated with unfiltered light, the use of the filter was omitted in later studies.

In some experiments frozen dinitrogen tetroxide and cold solvent were mixed at a low temperature. A portion of the resulting slurry was then transferred to a cooled quartz tube and sealed for esr studies. No attempt was made to exclude air or moisture from the system, but the operations were performed as rapidly as possible.

The esr measurements were carried out in a Varian spectrometer Model V4500 equipped with a 12-in. magnet, 100-Kc field modulation, and a variable-temperature accessory. The first derivative of the absorption spectrum was recorded. The g values were measured by direct comparison with the singlet of 1,1-diphenyl-2-picrylhydrazyl (DPPH), $g = 2.0036$.

Results

Water, heavy water, carbon tetrachloride, chloroform, deuterated chloroform, and nitromethane were used as solvents. Both the photolyzed frozen solutions of nitromethane and the cold mixtures of dinitrogen tetroxide and solvent gave esr spectra. Except at low temperatures, the method used to introduce the paramagnetic species into the matrix did not affect the appearance of the spectrum. At -180° , samples prepared with N_2O_4 showed only a broad singlet absorption.

In all solvents, at -180° the spectra of photolyzed nitromethane solutions consisted of a poorly resolved set of asymmetric lines. By analogy with an earlier study of NO_2 in solid nitromethane and in carbon tetrachloride,¹⁶ the spectra were identified as superimposed absorptions of the methyl and NO_2 free radicals. On warming, the signal due to the methyl radicals disappeared between -140 and -120° and a characteristic NO_2 triplet remained (Figure 1A). The average splitting of the triplet in all matrices studied was about 55 G.

In all solvents, the triplet split further on warming, the number of absorption lines and their intensities varying with temperature and the nature of the matrix. Although the best resolved hyperfine spectra were observed close to the melting point of each matrix, the rapid disappearance of the signal at that point caused difficulties in recording. All signal was lost when the matrix was allowed to melt.

The best resolved spectra were recorded with NO_2 trapped in nitromethane and in chloroform. The sequence of spectra recorded in nitromethane at different temperatures is shown in Figure 1. At -60° the triplet recorded at -110° split into nine symmetrical lines separated by 5.3 G (Figure 1B). These were further split on warming to give a 15-line spectrum (Figure 1C).

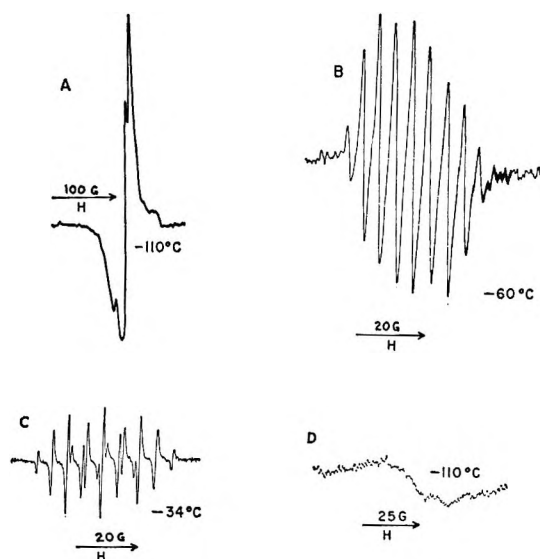


Figure 1. Effect of matrix temperature on the esr spectrum of NO_2 trapped in nitromethane: A–C, change on steady warming; D, spectrum after recooling from -34° .

On recooling to -110° , instead of the original triplet, a broad unresolved spectrum was recorded (Figure 1D). In chloroform the esr absorption of NO_2 underwent similar changes, except that the intermediate nine-line spectrum was not observed. Also, because of the differences in the melting points of these solvents, the final

Table I: Features of the Electron Spin Resonance Spectra of NO_2 in Frozen Solutions

Solvent	Melting point of solvent, $^\circ C$	Sample temp, $^\circ C$	Number of peaks	Splitting constant, G	g value
CH_3NO_2	-29.0	-94	3	ca. 57.5	2.0035
		-60	9	5.3 ± 0.3	
		-34	15	12.2 ± 0.2 5.3 ± 0.3	
$CHCl_3$	-63.5	-102	3	ca. 56.0	2.0058
		-68	15	12.6 ± 0.3 5.6 ± 0.3	
H_2O	0.0	-102	3	ca. 57.35	2.0086
D_2O		-32	7	6.8 ± 0.6	
CCl_4	-22.8	-80	3	ca. 55.0	2.0038
		-42	27		

Table II: Relative Line Intensity Distributions in the Electron Spin Resonance Spectra of NO_2 in $CHCl_3$ at -68° and CH_3NO_2 at -34°

Solvent	Line number							
	1	2	3	4	5	6	7	8
	15	14	13	12	11	10	9	
$CHCl_3$	1.5	4.4	6.7	1.2	3.6	4.4	1.1	7.6
CH_3NO_2	2.3	5.1	7.1	1.5	4.6	4.4	1.0	7.7

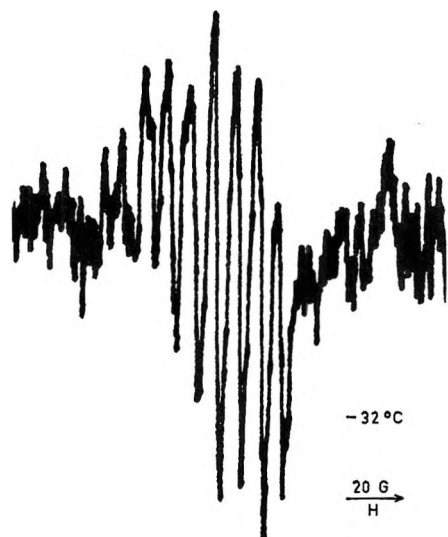


Figure 2. Electron spin resonance spectrum of NO₂ in water.

15-line spectrum was recorded at about -70° . The slight differences in the line intensities and splitting constants observed in the two solvents were within the experimental error (see Tables I and II). The substitution of deuterated chloroform for chloroform did not affect the spectrum.

The esr signals of NO₂ in water and in heavy water were identical. The spectra were difficult to record because the signal disappeared rapidly even at -25° . Figure 2 shows a typical noisy seven-line spectrum recorded in ice at -30° . In carbon tetrachloride the original triplet split at -48° into six groups of lines, each consisting of several unresolved components. At least 27 lines were observed at -42° (Figure 3). Table I summarizes the main features of the esr spectra of NO₂ in the various solvents used.

Discussion

The esr triplets observed with annealed photolyzed solutions of nitromethane suggest that the absorption was due to the interaction of magnetic moments of an unpaired electron and a single N¹⁴ nucleus. The identification of the molecular species containing the nitrogen atom is aided by an earlier study of the esr spectra of photolyzed pure nitromethane and nitromethane dissolved in carbon tetrachloride.⁶ Bielski and Timmons presented in their investigation evidence that the triplet observed at low temperatures after the removal of methyl radicals is due to the presence of NO₂ in solid matrix. Further, although resolution of the triplet is far from satisfactory (Figure 1A), the observed isotropic hyperfine constant of about 56 G agrees with values measured for NO₂ in other systems.⁷ In contrast with observations made by Atkins, *et al.*,⁴ with NO₂ trapped in ice at 77°K, no anisotropy was seen at low temperatures in the solvents used in this study. Poor resolution of the triplets may partly account for this apparent disagreement.

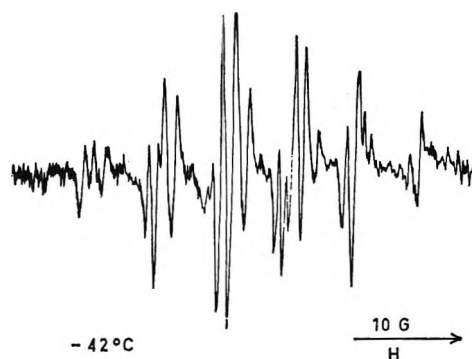


Figure 3. Electron spin resonance spectrum of NO₂ in carbon tetrachloride.

The possibility of a contribution to the esr signals by methyl free radicals, once the matrix was kept for several minutes near -100° , can be dismissed. The lifetime of this radical is known to be quite short in frozen solutions and the esr spectra were similar, whether the NO₂ was produced by photolysis of nitromethane or by the equilibrium dissociation of N₂O₄.

Since prolonged photolysis of nitromethane might result in the formation of some nitric oxide, which has a paramagnetic $^2\pi_{1/2}$ state, the esr spectra of deaerated carbon tetrachloride and water saturated with NO (up to $3 \times 10^{-3} M$) were investigated between -180° and room temperature. Only weak, broad singlets were observed at low temperatures, unlike any of the spectra obtained with photolyzed solutions of nitromethane.

In all systems studied, the triplets characteristic of NO₂ trapped at low temperature showed additional hyperfine splitting when the matrix was allowed to warm up. Such splitting could arise from coupling of spin of the unpaired electron to rotational moments of the NO₂, from radical-matrix or from radical-radical interactions. Although spin-rotational coupling has been observed with NO₂ in the gas phase,^{2a} it is not possible to postulate the existence of rotational states in the various matrices investigated which could account for the observed esr absorption. The possibility of interaction between the electron and solvent nuclei was ruled out by experiments in which substitution of deuterated analogs of chloroform and water failed to affect the esr spectra. Contribution of lattice site effects is probably negligible, except for solutions in CCl₄ where the hyperfine interaction may have an anisotropic component. Both glassy and polycrystalline matrices were investigated and the spectra of trapped NO₂ did not depend to any observable degree on the orientation of solvent molecules.

The absence of radical-radical interaction was indicated by two observations: the independence of the esr absorption of the concentration of trapped NO₂,

(7) See P. W. Atkins, N. Keen, and M. C. R. Symons, ref 3, for a summary of earlier results.

and the nature of the multiline spectra. If the matrix prevented dimerization of NO_2 while allowing interaction of the unpaired electron with two nitrogen nuclei, in the absence of anisotropy the spectrum should consist of five lines with relative intensities 1:2:3:2:1. No such spectra were seen.

The only other interactions which might account for the observed absorption are between NO_2 and other stable molecules also trapped in the matrix. In photolyzed solutions, ethane, nitromethane, and dinitrogen tetroxide molecules may be present in considerable quantities. Only N_2O_4 has to be considered in solutions prepared by mixing this compound with the cold solvent. Since the nature of the multiline spectra was independent of the method used to introduce NO_2 into the matrix, interaction with N_2O_4 is the one most likely to account for the observed spectra. It should follow that in all solvents studied the paramagnetic species responsible for the esr absorption should be the same. A more detailed examination of the spectra supports this conclusion.

The best resolved and most symmetrical spectra were obtained in nitromethane and in chloroform about 5° below the melting point of the solution (Figure 1C). Data listed in Tables I and II show that these 15-line spectra differed only slightly in the relative line intensity distributions. The three most prominent lines (numbers 3, 8, and 13) were in the ratio 1:1:1 and they can be assigned to interaction with one N^{14} nucleus. Comparison of the splitting constant for this coupling ($a^{\text{N}} = 12.4$ G) with the value measured for NO_2 triplets at low temperatures ($a^{\text{N}} = \text{about } 55$ G) indicates that a considerable delocalization of the unpaired electron took place on warming. In addition to this narrowing, each line of the triplet split into a quintet, whose lines were separated, on the average, by 5.4 G. The line intensities within the quintets were slightly different in the two solvents: in nitromethane the ratios were 1.0:2.3:3.9:2.3:1.0, and in chloroform the ratios were 1.0:3.3:5.7:3.4:1.0.

This analysis suggests that near the melting point of these two matrices the unpaired electron interacts with three nitrogen nuclei of which two are equivalent. Figure 4 shows a 15-line spectrum together with a line reconstruction based on this suggestion. One nitrogen atom is in the NO_2 molecule on which the single electron is largely localized and the two equivalent nitrogen nuclei belong to a N_2O_4 molecule. This suggests that even in the frozen solutions the NO_2 has sufficient translational freedom to dimerize to some extent. The average line intensities for the quintets are not in the ideal ratio of 1:2:3:2:1, but the discrepancy is probably not significant.

While this explanation appears to account for the 15-line spectra observed in nitromethane and chloroform, it also affords an understanding of the intermediate 9-line spectrum in nitromethane (Figure 1B). If it

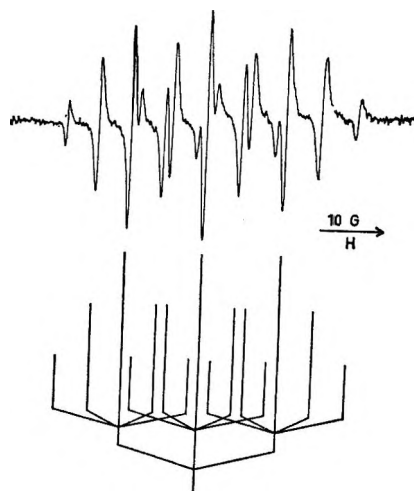


Figure 4. A 15-line esr spectrum of NO_2 . The line reconstruction assumes interaction with one N^{14} nucleus, producing a splitting of 12.2 G, and two equivalent N^{14} nuclei, producing a splitting of 5.3 G.

is assumed that at lower temperatures some of the closely spaced lines of the 15-line spectra cannot be resolved, the intensities of these lines can be added to produce a 9-line spectrum, as shown in Table III. The resultant intensities compare well with values obtained from the experimental spectrum.

Table III: Relative Line Intensities in Nitromethane

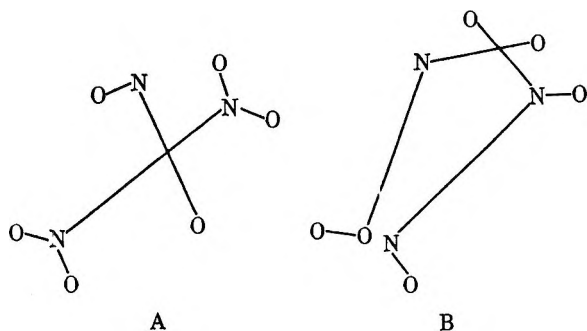
Temp = -60° (Total no. of lines, 9)		Temp = -34° (Total no. of lines, 15)	
Line	Relative intensity	Line	Relative Intensity
1	1.0	1	1.0
2	3.1	2	2.2
3	3.8	3 + 4	3.8
4	4.0	5 + 6	4.0
5	4.0	7 + 8 + 9	4.3
6	3.6	10 + 11	4.0
7	3.1	12 + 13	3.8
8	2.0	14	2.2
9	1.0	15	1.0

In water and in heavy water great difficulty was encountered with the resolution of spectra of NO_2 . Although below -80° these systems behaved similarly to solutions of NO_2 in organic solvents, there was rapid loss of signal at higher temperatures. It was, therefore, necessary to warm the aqueous samples rapidly to between -50 and 40° , where the triplets split further. Loss of signal was observed in spectra recorded with fresh samples in the downfield and in the upfield directions, suggesting a true time-dependent decay of intensity. The best resolved spectra consisted of seven lines with an average intensity distribution of 1.6:3.1:3.4:3.5:2.6:1.6:1.0 and a splitting constant of 6.8 G. The asymmetry of the spectrum probably arises from

a decrease in the concentration of paramagnetic molecules during the period of recording. It is likely that this spectrum corresponds to the nine-line spectrum in nitromethane, with the two outermost absorption lines obscured by background noise.

The multiline esr spectrum of NO₂ in carbon tetrachloride could not be interpreted in terms of NO₂-N₂O₄ interaction. In this solvent the N¹⁴ triplet split into six groups of poorly resolved lines at -48°. Attempts to obtain better resolution at higher temperatures were not successful.

The most probable stabilizing force in the NO₂-N₂O₄ complex is an electrostatic interaction between the O atoms of the NO₂ and the N atoms of the N₂O₄ molecule. Two configurations allow the closest approach of these atoms and are, therefore, the most likely: in one, the plane of the NO₂ bisects the N-N bond of N₂O₄, so that each of the O atoms of the dioxide lies an equal distance from the N atoms of N₂O₄ (A). In the



other configuration, the N-N bond lies in the plane of the NO₂ molecule (B). In calculating the potential energy of the systems, it was assumed that in any given

molecule each O atom carried one half of the net charge of the N atom and the magnitudes of the charges were assumed to be different in the two interacting species. No values were assigned to the net charges.

The distance between O atoms in NO₂ is 2.202 Å. This value is based on an N-O distance of 1.188 Å and bond angle of 134°4'.⁸ Using the value of 1.75 Å for the N-N bond length in N₂O₄⁹ it can be shown that the parallel configuration (B) has lower potential energy. Experimental estimations of this energy have not been made, but apparently the interaction stabilization is not sufficient for the complex to survive the melting of the matrix.

The existence of the proposed complex would help to explain several observed phenomena. Figure 1 shows that once the complex was formed, then on recooling only a broad, weak singlet absorption was recorded instead of the usual triplet. This singlet probably corresponds to an envelope of unresolved 15 absorption lines. It is also apparent that an NO₂ molecule can complex with only one molecule of N₂O₄ and thus the esr spectrum should be independent of the concentration of N₂O₄ and of the nature of the matrix. It should, however, depend strongly on temperature, because freedom of NO₂ to dimerize is a prerequisite of complex formation. This was found to be the case. The absence of any residual triplet spectrum from uncomplexed NO₂ at higher temperatures suggests that on warming virtually every monomer molecule either dimerizes or complexes with a dimer already present in the matrix.

(8) P. Gray and A. D. Yoffe, *Chem. Rev.*, **55**, 1069 (1955).

(9) M. Green and J. W. Linnett, *Trans. Faraday Soc.*, **57**, 10 (1961).

Energy Transfer in Thermal Methyl Isocyanide Isomerization.

Dilution Effects at Low Pressure^{1a}

by Y. N. Lin^{1b} and B. S. Rabinovitch

Department of Chemistry, University of Washington, Seattle, Washington 98105 (Received November 9, 1967)

The effect of three inert gases, helium, ethane, and pentene-1, on the rate of activation and reaction of methyl isocyanide in the low-pressure region at 280.5° has been examined. A study of the variation of the relative collision efficiency $\beta_0(D)$ of these gases, as compared with the parent substrate, has been made as a function of dilution over the range $D = 0-\infty$. The predicted decrease of $\beta_0(D)$ with increasing dilution is observed. The variation is qualitatively correct in magnitude and increases as expected on going from the quasi-strong collider, pentene-1, to the weaker collider, helium. The measurements can in principle provide information about the nature of the collisional transition probability model(s) involved and the values of relative collision cross sections of inert molecules to substrate molecules. The present measurements are not sufficiently precise to permit full exploitation of this aspect but can be taken to suggest that a stepladder model fits best for pentene-1 and ethane, and an exponential model for helium. The average value of the energy decrement per collision experienced by the isocyanide molecule is of the order of 1.0, >5.0, and >6.0 kcal mole⁻¹ for helium, ethane, and pentene-1, respectively.

Introduction

In thermal unimolecular reaction systems the relative collisional efficiency of an inert bath molecule, β , may be measured by the effect on the rate produced by added inert gas as compared to the effect produced by the addition of substrate molecules. The quantity acquires more fundamental significance if the comparison in question is made in terms of the specific collision rates of the reactant gas molecules with added inert or added parent substrate species.² The nature of the relative collision efficiency and various alternative phrasings of its definition, whose aptness depends on the experimental conditions, have recently been examined in detail.³ It has been shown that relative efficiency depends on the degree of dilution of substrate by inert gas, D , and on the region of falloff concerned; the latter may be specified in terms of the magnitude of the specific collision rate of the substrate molecules, ω , in the gas (mixture) in question.

Relative efficiency at any dilution D takes on its simplest aspect as $\omega \rightarrow 0$, corresponding to the "low-pressure" region of a unimolecular reaction; alternative definitions of β as differential quantities, $\beta_0(D)$ and $\beta_0'(D)$, and as integral quantities, $\bar{\beta}_0(D)$ and $\bar{\beta}_0'(D)$, all become equivalent as $D \rightarrow \infty$; also, the distinctions between comparisons of substrate and bath molecule efficiencies at equal values, or increments, of specific collision rates (primed quantities) and comparisons of collision rate at equal values, or increments, of specific reaction rates (unprimed quantities) disappear for $\omega \rightarrow 0$.^{3b} These quantities have been fully defined by TR³ and all of them need not be repeated here. $\beta_0(D)$ connotes the ratio of the specific collision rate of substrate molecules with the added

inert bath molecules in question (and corresponding to dilution D) relative to the increment in specific collision rate in the pure substrate system required to produce the same increase in the specific rate of transport of substrate molecules above the critical threshold energy E_0 for reaction. The predicted variation of efficiency over the range $\beta_0(0)$ to $\beta_0(\infty)$ has been verified experimentally in the methyl isocyanide isomerization system with added helium inert bath molecules:⁴ $\text{CH}_3\text{NC} \xrightarrow{\text{He}} \text{CH}_3\text{CN}$. Helium is the weakest collider known for this system.⁵ In the present paper, the work on helium is amplified and the study is extended to the more efficient inert species, ethane and pentene-1.

Experimental Section

The sources and purification of methyl isocyanide and helium have been described.⁵ Ethane and pentene-1 were Phillips Petroleum Co. research grade and were free of any interfering impurities.

The apparatus, procedure, and chemical analysis followed the earlier work. The reactor was a 12-l. Pyrex bulb closed by a Springham valve and was heated in an air furnace. Temperature was regulated by a proportional controller and was measured with

(1) (a) This work was supported by the National Science Foundation. (b) Abstracted from a Ph.D. thesis to be presented by Y. N. Lin which should be consulted for further details.

(2) (a) H. S. Johnston, *J. Am. Chem. Soc.*, **75**, 1567 (1953); (b) D. J. Wilson and H. S. Johnston, *ibid.*, **75**, 5763 (1953); (c) M. Volpe and H. S. Johnston, *ibid.*, **78**, 3909 (1956).

(3) (a) D. C. Tardy and B. S. Rabinovitch, *J. Chem. Phys.*, **45**, 3720 (1966); (b) *ibid.*, **48**, 1282 (1968), called TR.

(4) B. S. Rabinovitch, D. C. Tardy, and Y. N. Lin, *J. Phys. Chem.*, **71**, 1549 (1967).

(5) F. J. Fletcher, B. S. Rabinovitch, K. W. Watkins, and D. J. Locker, *ibid.*, **70**, 2823 (1966).

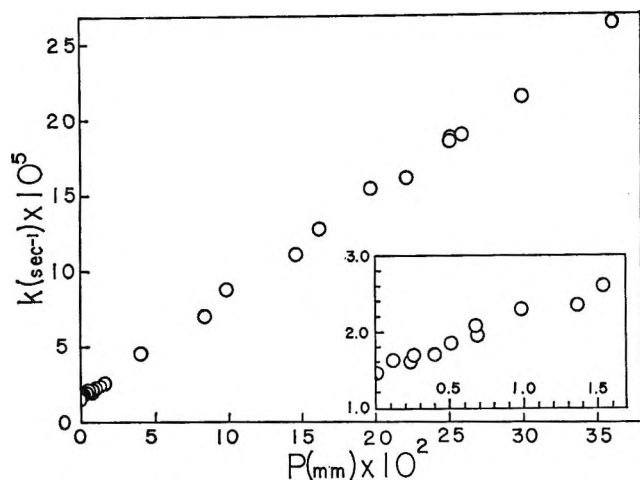


Figure 1. Variation of k_0 with methyl isocyanide dilution by pentene-1 at 553.5°K.

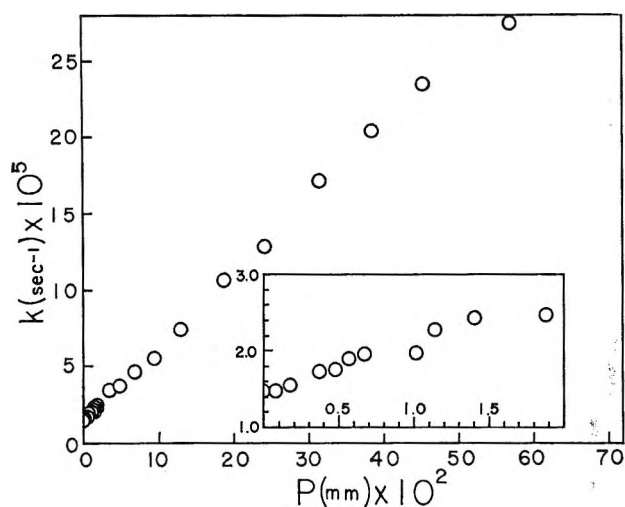


Figure 2. Variation of k_0 with methyl isocyanide dilution by ethane at 553.5°K.

Plots of k_0 vs. p_{inert} are given in Figures 1–3 for each of the inert gases. In the course of measuring the rates of isomerization at low dilutions, *i.e.*, small amounts of inert addend, the rate of isomerization of the pure substrate was determined repeatedly at the standard pressure.^{1b} The average of ten measurements, $k_0 = 1.46 (\pm 0.03) \times 10^{-5} \text{ sec}^{-1}$ at $p_{\text{CH}_3\text{NC}} = 1.16 \times 10^{-2}$ mm, was adopted as the intercept value at $p_{\text{inert}} = 0$; the parenthetical quantity is the standard deviation of the average.

The bimolecular activation rate constant of the parent methyl isocyanide, obtained from the slope of the plot of k_0 vs. $p_{\text{CH}_3\text{NC}}$, has been given as⁵ $k_{\text{CH}_3\text{NC}}^a = 96.0 \times 10^{-5} \text{ mm}^{-1} \text{ sec}^{-1}$. (A possibly more accurate value determined here is $98.0 \times 10^{-5} \text{ mm}^{-1} \text{ sec}^{-1}$.) The k_0 intercept at zero substrate pressure is $0.3 \times 10^{-5} \text{ sec}^{-1}$ rather than 0.1×10^{-5} as suggested earlier.⁵ The plot is a straight line in the second-order region of pressure. For helium addend, a similar plot of

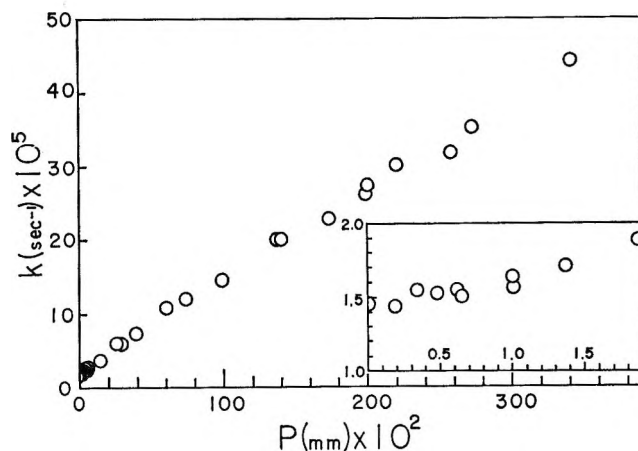


Figure 3. Variation of k_0 with methyl isocyanide dilution by helium at 553.5°K.

k_0 vs. p_{He} is a curve. The slope at relative concentrations of added inert to substrate of $\sim 300:1$ corresponds effectively to the condition of infinite dilution; the ratio of this slope to that for the parent substrate, converted to a collision basis, gives $\beta_0(\infty)$. In fact, the high-pressure helium plot corresponds effectively to the high pressure limit at relative concentrations above 85:1. The plot should be linear in this region and therefore the slope of the curve can be most accurately determined for the high-pressure condition.

The limiting low-pressure slope is more difficultly determined, owing both to scatter in the data and to the fact that the magnitude of the slope varies continuously in this region. The following procedure was adopted for its evaluation. Starting at some very low pressure of addend where minimal statistical requirements were satisfied, the slope of the data, treated as a straight line, was determined by least squares with use of the fixed intercept $k_0 = 1.46 \times 10^{-5} \text{ sec}^{-1}$. Successive data points were added one by one and the slopes were redetermined. The procedure was continued for the helium system up to a $p_{\text{He}}:p_{\text{CH}_3\text{NC}}$ ratio of $\sim 2:1$. Actually, since the relative efficiency per collision of He at zero dilution is ~ 0.25 , the effective upper collision ratio corresponds only to 0.5:1 and is still in the lower dilution range. An average slope determined from data at inert gas pressures (collisional dilutions) from 0 to p_{He} corresponds approximately to the value of the slope for the collisional dilution that obtains at $p_{\text{He}}/2$. This value was extrapolated to zero pressure on the basis of both stepladder and exponential transition probability models, with use of the families of theoretical dilution curves given in Figure 1a and b of Tardy and Rabinovitch;^{3b} from that theoretical curve whose value of $\beta_0(D_{p/2})$ was equal to the experimental value, the value of $\beta_0(0)$ could be read.⁶ This was repeated at each value of $D_{p/2}$. A similar procedure was followed for the two other diluents. The results are summarized

Table II: Summary of Low-Dilution Experimental Values of $\beta_0(0)$ Derived from Linear Least-Squares Fit

Dilution ($p_{\text{inert}}/p_{\text{CH}_3\text{NC}}$)	$10^4 k_{\text{M}}$, $\text{mm}^{-1} \text{sec}^{-1}$	β_p	β_{μ^a}	$\beta_0(D_{p/2})^b$	$\beta_0(0)$ (SL) ^c (extrap)	$\beta_0(0)$ (exp) ^c (extrap)	
Pentene (M_1)							
0-0.240	84.6	0.881	0.990	0.792	0.80	0.792	
0-0.254	86.9	0.905	1.017	0.813	0.82	0.813	
0-0.393	70.2	0.730	0.821	0.657	0.69	0.660	
0-0.500	74.1	0.772	0.868	0.695	0.72	0.700	
0-0.668	83.6	0.870	0.978	0.783	0.80	0.790	
0-0.680	78.4	0.817	0.919	0.735	0.76	0.740	
0-0.980	83.1	0.865	0.972	0.777	0.81	0.780	
0-1.35	74.4	0.775	0.870	0.696	0.75	0.700	
					Av	0.77	0.75
Ethane (M_2)							
0-0.363	72.0	0.750	0.690	0.765	0.77	0.77	
0-0.477	65.6	0.683	0.628	0.697	0.72	0.70	
0-0.560	72.6	0.755	0.695	0.771	0.79	0.77	
0-0.666	73.3	0.764	0.702	0.780	0.80	0.78	
0-1.01	61.8	0.645	0.593	0.659	0.71	0.67	
0-1.14	65.3	0.680	0.625	0.695	0.75	0.71	
0-1.40	66.5	0.693	0.638	0.709	0.77	0.71	
0-1.88	60.1	0.626	0.576	0.640	0.70	0.65	
					Av	0.75	0.71
He (M_3)							
0-0.345	18.5	0.193	0.0815	0.208	0.240	0.218	
0-0.478	17.7	0.184	0.0777	0.199	0.230	0.212	
0-0.624	16.1	0.168	0.0710	0.182	0.225	0.195	
0-0.648	12.7	0.133	0.0561	0.144	0.185	0.160	
0-0.996	15.5	0.161	0.0680	0.174	0.230	0.200	
0-1.02	14.0	0.146	0.0616	0.158	0.210	0.183	
0-1.37	16.5	0.172	0.0725	0.186	0.265	0.212	
0-1.88	20.2	0.211	0.0890	0.228	0.325	0.248	
					Av	0.238	0.204

^a $(\mu_{\text{AM}_1}/\mu_{\text{AA}})^{1/2} = 1.124$; $(\mu_{\text{AM}_2}/\mu_{\text{AA}})^{1/2} = 0.920$; $(\mu_{\text{AM}_3}/\mu_{\text{AA}})^{1/2} = 0.422$. ^b $s_{\text{AA}^2}/s_{\text{AM}_1^2} = 0.800$; $s_{\text{AA}^2}/s_{\text{AM}_2^2} = 1.11$; $s_{\text{AA}^2}/s_{\text{AM}_3^2} = 2.56$. The values are based on: $\sigma_{\text{A}} = 4.47 \text{ \AA}$; $\sigma_{\text{M}_1} = 5.70 \text{ \AA}$; $\sigma_{\text{AM}_1} = 5.09 \text{ \AA}$; $\sigma_{\text{M}_2} = 4.42 \text{ \AA}$; $\sigma_{\text{AM}_2} = 4.45 \text{ \AA}$; $\sigma_{\text{M}_3} = 2.56 \text{ \AA}$; $\sigma_{\text{AM}_3} = 3.52 \text{ \AA}$. $\epsilon_{\text{A}}/k = 380^\circ\text{K}$; $\epsilon_{\text{M}_1}/k = 310^\circ\text{K}$; $\epsilon_{\text{AM}_1}/k = 343.5^\circ\text{K}$; $\epsilon_{\text{M}_2}/k = 230^\circ\text{K}$; $\epsilon_{\text{AM}_2}/k = 296^\circ\text{K}$; $\epsilon_{\text{M}_3}/k = 10.2^\circ\text{K}$; $\epsilon_{\text{AM}_3}/k = 62^\circ\text{K}$. $\Omega_{\text{AA}^2,2^*} = 1.330$; $\Omega_{\text{AM}_1^2,2^*} = 1.270$; $\Omega_{\text{AM}_2^2,2^*} = 1.204$; $\Omega_{\text{AM}_3^2,2^*} = 0.839$. $s_{\text{AA}} = 5.15$; $s_{\text{AM}_1} = 5.75$; $s_{\text{AM}_2} = 4.88$; $s_{\text{AM}_3} = 3.22 \text{ \AA}$. Values of σ and $\Omega^{2,2}$ from J. O. Hirschfelder, C. F. Curtiss, and R. B. Bird, "Molecular Theory of Gases and Liquids," John Wiley and Sons, Inc., New York, N. Y., 1954. ^c SL = stepladder model; exp = exponential model.

in Table II. The extrapolation was only a modest one so that the sense of the experimental values is little affected by any uncertainty in the procedure, as may be seen from Table III.

Discussion

Dependence of $\beta_0(D)$ on D . It has been shown by TR that plots of $\beta_0(D)$ vs. dilution of substrate by the weak collider give a family of curves, each curve corresponding to a different value of E' . E' was defined as the ratio $\langle \Delta E \rangle / \langle E^+ \rangle$, where $\langle \Delta E \rangle$ is the average energy removed from the hot molecule by the inert gas per collision, and $\langle E^+ \rangle$ is the average excess energy of the reacting molecules above the critical energy E_0 as calculated from the Boltzmann distribution, *i.e.*, for the strong collision case.⁷ A separate family of curves may be calculated for any assumed model of the collisional transition probability

distribution. TR discussed two such families corresponding to extremes of model types—the stepladder and exponential models (their Figure 1a and b). The dispersion of the values $\beta_0(0)$ and $\beta_0(\infty)$ decreases with increasing efficiency of the inert activators as E' increases. For a strong collider, the ratio $\beta_0(0)$ and $\beta_0(\infty)$ approaches its lower limit of unity. For a given substrate at fixed temperature, $\langle E^+ \rangle$ is fixed and the collisional efficiency depends on $\langle \Delta E \rangle$. Above some value of E' which depends upon dilution and corresponds very roughly to (a range of) $\beta_0(D)$ values around 0.1, the exponential model is less ef-

(6) Interpolation was made as necessary in Figures 1a and b of TR. The curve in question corresponds to a value of E , that is not necessarily the same as that which correlates with the experimental value of $\beta_0(\infty)$.

(7) Note that the equilibrium assumption for energy levels below E_0 holds under strong collision conditions.

Table III: Comparison of Experimental and Theoretical Dependence of Rate on Dilution

"Infinite" dilution range (p_M/p_{CH_3NC})	$10^3 k^a_M$, $mm^{-1} sec^{-1}$	β_p	β_μ	$\beta_0(\infty)$	$\beta_0(0)$, stepladder		$\beta_0(0)(SL)/\beta_0(\infty)$, stepladder		$\beta_0(0)$, exponential		$\beta_0(0)(exptl)/\beta_0(\infty)$, exponential	
					Found	Theoret	Found	Theoret	Found	Theoret	Found	Theoret
Pentene-1												
7-30	67.8	0.71	0.80	0.64 ^a	0.77 ^a	0.75 ^a	1.20	1.17	0.75 ^a	0.67 ^a	1.17	1.05
				0.98 ^{b,c}	1.15 ^b	1.00 ^b	1.17	1.02	1.15 ^b	0.98	1.17	1.00
Ethane												
11-50	45.0	0.47	0.43	0.48 ^a	0.75 ^a	0.62 ^a	1.56	1.29	0.71 ^a	0.55 ^a	1.48	1.15
				0.69 ^{b,c}	1.00 ^b	0.78 ^b	1.45	1.13	1.00 ^b	0.71 ^b	1.45	1.03
Helium												
85-300	11.3	0.118	0.050	0.127 ^a	0.238 ^a	0.289 ^a	1.87	2.28	0.204 ^a	0.215 ^a	1.61	1.69
				0.165 ^{b,c}	0.298 ^b	0.340 ^b	1.81	2.06	0.264 ^b	0.255 ^b	1.60	1.55

^a Values based on the cross sections adopted in Table II including $\sigma_{CH_3NC} = 4.47 \text{ \AA}$. ^b Values based on $\sigma_{CH_3NC} = 6.76 \text{ \AA}$, with σ_M and ϵ/k values as in Table II. ^c These are considered to be the most reliable values for $\beta_0(\infty)$.

ficient than the stepladder model. For $D > 0$, this relationship is inverted when E' , or $\beta_0(D)$, is less than this value.

The order of decreasing efficiencies of the inert gases is pentene-1, ethane, and helium. We wish first to examine qualitatively the agreement of the experimental results with the theory. In order to do so, the relative collision cross section must be known for the inert gases and the substrate. To this point we have handled the data in the conventional way by assuming values of the relevant molecular diameters, s . The values elected are the same as those used in ref 5, which were based⁸ on the Lennard-Jones constants, where $\sigma_A = 4.47 \text{ \AA}$ for methyl isocyanide and $\sigma_M = 4.42$ and 2.56 \AA for ethane and helium, respectively; also $\sigma_M = 5.70 \text{ \AA}$ for pentene-1. The experimental ratios of $\beta_0(0)/\beta_0(\infty)$ (where the experimental values of $\beta_0(0)$ were extrapolated from the low-dilution efficiencies in the manner described earlier) are given in Table III. These values and ratios may be compared in Table III (all quantities superscripted *a*) with the theoretical predictions based on the same assumed cross sections and the experimental value of $\beta_0(\infty)$. The latter fixes the theoretical value of $\beta_0(0)$ as shown in Figure 4 which is found from TR. The individual $\beta_0(0)$ and $\beta_0(\infty)$ values are given in Table III along with the theoretical ratios. The qualitative correspondence of the data and theory is correct in that pentene-1 which is the most efficient gas has the least value of the ratio $\beta_0(0)/\beta_0(\infty)$, while helium which is the least efficient gas has the largest value of the ratio; ethane is intermediate. In addition, the semi-quantitative agreement of the various sets of numbers is also satisfactory. The agreement, for what it is worth, is somewhat better for the stepladder (SL) model for pentene-1 and ethane, and for the exponential (exp) model for helium (the latter conclusion revises the early indications⁴). This behavior con-

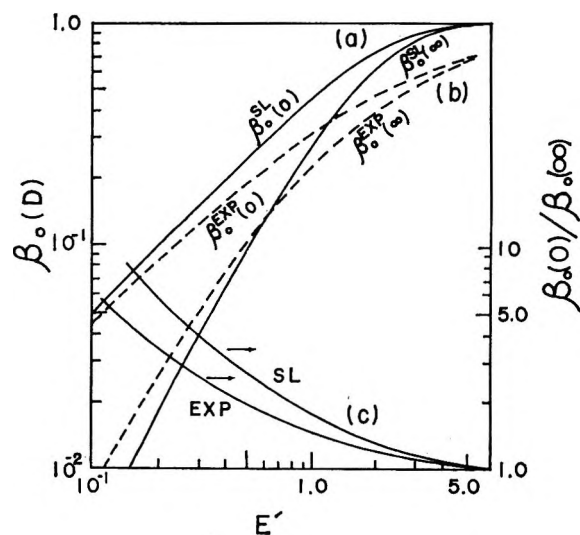


Figure 4. Plots of $\beta_0(D)$ at zero dilution ($\beta_0(0) = \gamma_p$) and infinite dilution ($\beta_0(\infty) = \gamma_N(\infty) \gamma_p$) for (a) a stepladder model and (b) an exponential model; (c) the ratio of $\beta_0(0)/\beta_0(\infty)$ (i.e., $1/\gamma_N(\infty)$) as a function of E' for both stepladder and exponential models. This figure is derived from TR.

forms to that found in earlier work from this laboratory which employed a different technique for the study of energy transfer in another system.⁹

If the data plotted in Figures 1-3 were sufficiently accurate, then the correct probability model could be deduced with confidence from the observed and predicted behavior. Unfortunately this is not the case here. We proceed below to examine this matter in another light and note that any lack of agreement be-

(8) J. O. Hirschfelder, C. F. Curtiss, and R. B. Bird, "Molecular Theory of Gases and Liquids," John Wiley and Sons, Inc., New York, N. Y., 1954.

(9) G. Kohlmaier and B. S. Rabinovitch, *J. Chem. Phys.*, **38**, 1692, 1709 (1963); see also D. W. Setser, B. S. Rabinovitch, and J. W. Simons, *ibid.*, **40**, 1751 (1965); **41**, 800 (1965).

Table IV: Smoothed Experimental Values of β and γ Parameters as a Function of Dilution^a

Dilution p_M/p_A	$\beta_0(D)$	γ_P^{SL}	$\gamma_N^{SL(D)}$		Dilution, p_M/p_A	$\beta_0(D)$	γ_P^{EXP}	$\gamma_N^{EXP(D)}$	
			Exptl	Theoret				Exptl	Theoret
Ethane					Helium				
0	1.0	1.0	1.0	1.0	0	0.29	0.29	1.0	1.0
0.1	1.0	1.0	1.0	0.99	0.1	0.28	0.29	0.97	0.98
0.25	1.0	1.0	1.0	0.99	0.25	0.27	0.28	0.96	0.94
0.50	1.0	1.0	1.0	0.98	0.50	0.25	0.27	0.93	0.91
1.0 ^b	0.98	1.0	0.98	0.95	1.0 ^c	0.23	0.27	0.85	0.86
1.5	0.96	1.0	0.96	0.93	1.5	0.21	0.26	0.81	0.82
11-50	0.69	0.78	0.88	0.88	85-300	0.165	0.26	0.65	0.65
Pentene-1									
7-30	1.0	1.0	1.0	1.0					

^a $\sigma_A = 6.76 \text{ \AA}$ was used throughout the table. ^b Corresponds to 1.48:1 on a collision basis. ^c Corresponds to 1.40:1 on a collision basis.

tween the experimental and theoretical ratios of Table III means that $\beta_0(\infty)$ and $\beta_0(D_{p/2})$ do not correspond to precisely the same value of E' : based on $\sigma_{CH_3NC} = 4.47 \text{ \AA}$ and $\beta_0(D_{p/2})$, E' is 2.10 (SL) and >4.5 (exp) for pentene-1, 2.0 (SL) and >4.0 (exp) for ethane, and 0.49 (SL) and 0.53 (exp) for helium; from $\beta_0(\infty)$ the corresponding E' values are 1.95 (SL) and 4.2 (exp) for pentene-1, 1.49 (SL) and 2.55 (exp) for ethane, and 0.59 (SL) and 0.58 (exp) for helium (note that^{3a} $\langle \Delta E \rangle = 1.35E'$ kcal mole⁻¹ at 280°). It is this matter which we now examine.

The ratio of $\beta_0(0)/\beta_0(\infty)$ is a function of E' ; values of E' deduced from the observed ratio with use of Figure 4c depend on the assumed collision model but are independent of a knowledge of collision diameters which cancel. These values of E' may be used to check the consistency of the data as follows. A value of $\beta_0(\infty)$ is found from E' with use of Figure 4a. The relative collision cross sections are then determined from the relation $\beta_0(\infty) = \beta_\mu(\infty)(s_{AA}/s_{AM})^2$, where s is related to the Lennard-Jones parameter σ through⁸ $s^2 = \sigma^2\Omega^{2.2}(T^*)$ where T^* is a reduced parameter. With the newly determined relative value of s_{AA}^2 and s_{AM}^2 , $\beta_0(D_{p/2})$ is recalculated from the data and then extrapolated to $\beta_0(0)$ as before so that a new ratio $\beta_0(0)/\beta_0(\infty)$ is found. This provides a way to adjust E' and σ_{AM} values mutually by iteration of the procedure. Two iterations are all that are required for convergence of E' and the s^2 ratio to constant values which reconcile these parameters. This iteration procedure was applied to the data for all three gases. The iterated values of σ_M agreed best with those in the literature¹⁰ when an SL model was used for pentene-1 and ethane and an exp model for helium and agreed very poorly for the alternative models.^{1b}

Alternative Value of σ_A . It is of interest to find the values of s_M , i.e., of σ_M , that correspond to two particular values of σ_A . One of these is the quantity 4.47 \AA previously adopted. The second is the value

6.76 \AA whose relevance may be clarified by the following digression.

It has been found¹⁰ that higher (C_4 and above) n -alkanes may have unit deactivation efficiency. Use of the alkane diameters given by Hirschfelder, Curtiss, and Bird⁸ leads to a Lennard-Jones σ value for methyl isocyanide of 6.76 \AA . Values of $\beta_0(\infty)$ and $\beta_0(0)$ and their ratios have been recalculated with use of this quantity but with retention of unchanged values of the inert gases collision diameters. The results are superscripted b in Table III; since the efficiencies based on these cross sections exceed or are very close to unity for pentene-1, and for ethane at low dilutions, the extrapolation to zero dilution is negligible and $\beta_0(0)$ is the same for both the SL and exp models. Again, pentene-1 gives the smallest value of the β ratio and helium the largest. The qualitative and semiquantitative agreement with the theory is good. The iteration procedure again supports the SL model for the alkanes and exp model for He,^{1b} and these values in Table III are considered to provide the best experimental estimates.

γ_N and γ_P . In the second-order region $\beta_0(D)$ can be factored as^{3,4} $\beta_0(D) = \gamma_N(D)\gamma_P$, where $\gamma_P, \gamma_N(D) < 1$. γ_P is the relative rate of weak-collisional activation of an equilibrium set of populations compared to the corresponding strong-collisional rate; thus γ_P is a statement concerning average weak-collisional activation inefficiency. $\gamma_N(D)$ is the relative rate of weak-collisional activation for a steady-state set of populations relative to the corresponding rate for equilibrium populations, at certain dilution; it provides a measure of the average effective population depletion at levels below the critical threshold. At limiting low dilution of substrate by small amounts of inert addend, $\gamma_N \rightarrow 1$ since equilibrium populations prevail and $\beta_0(0) \rightarrow \gamma_P$.

(10) B. S. Rabinovitch, Y. N. Lin, S. C. Chan, and K. W. Watkins, *J. Phys. Chem.*, **71**, 3715 (1967).

Table V: Collection of E' Values for Various Treatments of the Data

Basis	Pentene-1				Ethane				Helium			
	4.47 Å		6.76 Å		4.47 Å		6.76 Å		4.47 Å		6.76 Å	
	SL	Exp	SL	Exp	SL	Exp	SL	Exp	SL	Exp	SL	Exp
$\beta_0(\infty)$	1.95	4.20	>4.5	>4.5	1.49	2.55	>4.0	>4.0	0.59	0.58	0.70	0.72
$\beta_0(D_{p/2})$	2.10	>4.5	>4.0	>5.0	2.02	>4.0	>4.0	>4.5	0.49	0.53	0.62	0.75
$\beta_0(0)/\beta_0(\infty)$	1.9		2.1		1.14		1.28		0.80	0.65	0.84	0.62

The experimental data were smoothed and "experimental" values of γ_P and $\gamma_N(D)$ were found as follows. At each of several dilutions, the experimental value of $\beta_0(D)$ was extrapolated to zero dilution in the manner described earlier in connection with the construction of Table II; the value of $\beta_0(D)$ thus found is γ_P ; then the corresponding experimental value $\gamma_N(D)$ is given by $\gamma_N(D) = \beta_0(D)/\gamma_P$. "Theoretical" values of γ_P and $\gamma_N(D)$ were also obtained as a function of dilution by finding E' from the experimental value of $\beta_0(\infty)$ and then reading the theoretical curves shown in Figure 2 of TR. This treatment was made for all possible cases^{1b} but only the most relevant are given in Table IV. γ_P is roughly independent of dilution at low D as required in theory. The agreement between the experimental and theoretical values of $\gamma_N(D)$ is good in general.

Values of E' . The various assumptions and treatment applied to the data lead to varying estimates of

E' . These are summarized in Table V. Despite the variability of the treatments, the qualitative and semi-quantitative consistency of the estimates of E' is evident. Even the most inaccurate values of the ratio $\beta_0(0)/\beta_0(\infty)$, obtained for ethane, or the uncertainty in σ_A does not disguise the deduced order of magnitude of E' . The optimum estimates are those shown in boldface. They correspond to values of $\langle \Delta E \rangle$ in kcal mole⁻¹ which are, for pentene-1, >6.0 (SL); for ethane, >5.0 (SL); and for helium, 1.0 (exp).

It would be desirable to study dilution effects in systems having greater intrinsic accuracy than isocyanides; nonetheless, the present study illustrates one aspect of the refinements that can be made in future studies of energy transfer by inert gases in thermal unimolecular systems.

Acknowledgment. We wish to thank Dr. D. C. Tardy for his stimulating interest in this work.

Photodecomposition of Solid Metal Azides

by V. R. Pai Verneker¹

Explosives Laboratory, Feltman Research Laboratories, Picatinny Arsenal, Dover, New Jersey 07801
(Received November 13, 1967)

Study is made of the general characteristics of the photodecomposition of metal azides (NaN_3 , KN_3 , BaN_6 , AgN_3 , and PbN_6). Rates of gas evolution from azides irradiated with light of different wavelengths are plotted against the time of irradiation. It is shown that photolysis of NaN_3 , BaN_6 , and AgN_3 leads to the formation of nitride, whereas photolysis of KN_3 and PbN_6 does not lead to nitride formation. Further, the nitrides are shown to decompose with light of long wavelength. The acceleration in the photolytic rate of metal azides in the later stages of decomposition is attributed to (1) the photodecomposition of the metal nitride, if it is formed, and (2) to the photoionization of metal atoms, if light of sufficient energy is present. The photoemission of electrons from the metal serves to explain why the initial photolytic rate does not go to zero but decelerates to a constant minimum value.

Introduction

The interest in the photochemical decomposition of metal azides arises from the fact that it forms an attractive point of entry into the field of radiation-induced reactions in solids and further gives us an insight as to why some metal azides are explosive whereas others are not. Evidence for this is found in the wealth of information resulting from the photolytic studies of azides.²⁻¹⁴ The photodecomposition behavior of these materials varies widely from sample to sample and is very dependent on the method of preparation, age of the sample, the method of storage, and the impurities present.^{4,13,14} However, despite these difficulties it is possible to study the general features of photodecomposition by following the gas evolution as a result of irradiation. Jacobs, Sheppard, and Tompkins¹¹ studied the photochemical decomposition of NaN_3 , KN_3 , SrN_6 , and BaN_6 . Their results can be summarized as follows. The general features of the time dependence of the rate of photolysis at constant intensity are (1) an initial deceleratory reaction, followed by (2) an acceleratory phase to the reaction, leading to (3) a constant rate of photolysis. In NaN_3 , process 2 is absent: in the other three azides, its appearance was shown to depend critically on the energy of the incident photons (photons of wavelength shorter than 2537 Å). Absorption spectra of NaN_3 and KN_3 are very similar and so the divergence in the behavior of NaN_3 from the rest of the azides is possibly attributable to topochemical features. The increase in the rate of gas evolution, which occurs in the later stages of decomposition, is not present in all metal azides. The object of the present study was to investigate the conditions for the appearance of this latter feature in the decomposition behavior.

Experimental Section

Materials. Sodium, potassium, and barium azides were prepared by passing hydrazoic acid gas through

aqueous solutions of their respective carbonates and precipitating by the addition of acetone. In one set of experiments the carbonates were of reagent grade quality and in another set of experiments they were of spectroscopic grade.

Lead azide was prepared by passing hydrazoic acid gas through an aqueous solution of lead nitrite, the latter solution being prepared by passing nitrous oxides through a suspension of lead oxide in water. Reagent grade and spectroscopic grade lead oxides were used as alternatives. Lead azide was also prepared by the reaction of sodium azide with lead acetate.

Silver azide was prepared by the reaction of sodium azide with silver nitrate. Barium nitride was also required to investigate the effect of light on this decomposition product, and samples were obtained from K & K Laboratories Inc., New York, N. Y.

(1) Address correspondence to the author at Research Institute for Advanced Studies, Baltimore, Md. 21227.

(2) (a) P. W. M. Jacobs and F. C. Tompkins, *Proc. Roy. Soc. (London)*, **A215**, 254 (1952); (b) J. G. Dodd, *J. Chem. Phys.*, **35**, 1815 (1961).

(3) W. E. Garner and J. Maggs, *Proc. Roy. Soc. (London)*, **A172**, 299 (1939).

(4) J. A. N. Thomas and F. C. Tompkins, *ibid.*, **A209**, 550 (1951).

(5) P. W. M. Jacobs, F. C. Tompkins, and D. A. Young, *Discussions Faraday Soc.*, **28**, 234 (1959).

(6) B. E. Bartellete, F. C. Tompkins, and D. A. Young, *Proc. Roy. Soc. (London)*, **A246**, 197 (1958).

(7) S. K. Deb and A. D. Yoffe, *ibid.*, **A256**, 514 (1960).

(8) S. K. Deb and A. D. Yoffe, *ibid.*, **A256**, 528 (1960).

(9) P. Gray and T. C. Weddington, *Chem. Ind. (London)*, 1555 (1955).

(10) P. W. M. Jacobs, F. C. Tompkins, and V. R. Pai Verneker, *J. Phys. Chem.*, **66**, 1113 (1962).

(11) P. W. M. Jacobs, J. G. Sheppard, and F. C. Tompkins, Fifth International Symposium on Reactivity of Solids, Munich, 1964, p RS-45.

(12) P. W. M. Jacobs and A. R. T. Kurishy, *J. Chem. Soc.*, 911, 4723 (1964).

(13) V. R. Pai Verneker and A. C. Forsyth, *J. Phys. Chem.*, **71**, 3736 (1967).

(14) P. W. M. Jacobs and A. R. T. Kureishy, *Can. J. Chem.*, **44**, 703 (1966).

Apparatus. In the photodecomposition apparatus, the azide was spread on the bottom of a transparent silica cell with a flat window at the top. The cell was connected to a vacuum line consisting of a trap immersed in liquid nitrogen, a standard volume flask, an Alphatron vacuum gauge, a second trap, a vacuum valve, a diffusion pump, a third trap, a second Alphatron gauge, a fourth trap, a McLeod gauge, a second valve which separated the line from a second diffusion pump, and a mechanical pump. With this sequence of components the nitrogen evolution rate could be measured either on the first Alphatron gauge (*i.e.*, "a static system") with the first valve closed or on the second Alphatron gauge with the first valve open and the second valve closed (*i.e.*, the so called "dynamic system"). In the second method, the evolved gas was continuously removed from the vicinity of the sample thus maintaining a pressure of less than 10^{-6} mm during photolysis. The temperature of the azide was measured with a copper-constantan thermocouple which was embedded in the sample.

As will be shown later, three wavelength ranges were of interest.

1. *Wavelengths Shorter than 2000 Å.* These wavelengths are present in the radiations from a low-pressure mercury lamp and they were filtered out by insertion of a water filter in the beam. By comparing two photolytic runs, one with the water filter and the other without the water filter, the effect of light of wavelength shorter than 2000 Å on the decomposition could be studied.

2. *Wavelengths Centered about the Mercury Resonance Line at 2537 Å.* These wavelengths were selected from the spectrum of a high-pressure mercury lamp by the use of an interference filter.

3. *Wavelengths Longer than 3000 Å.* These were obtained from a high-pressure mercury lamp with the use of appropriate dye filters such as CS7-54 (without the filters the high-pressure lamp provides some intensity in the 2000–3000-Å region, in addition to the longer wavelength).

Tests were made to determine whether the appropriate metal nitride was present in the decomposition products. Irradiated samples were dissolved in water and tested colorimetrically for ammonia using Nessler's reagent. The results of the tests for the presence of the nitride were checked at different temperatures and found to be independent of the temperature.

Results and Discussion

The general features of the rate-time plot for any particular azide were not affected by (1) any variations in the impurity content of the different preparations of the same azide and (2) the method of collecting the gas, *i.e.*, "static" or "dynamic."

Figure 1A shows the rate of nitrogen evolution from barium azide as a function of the time of irradiation

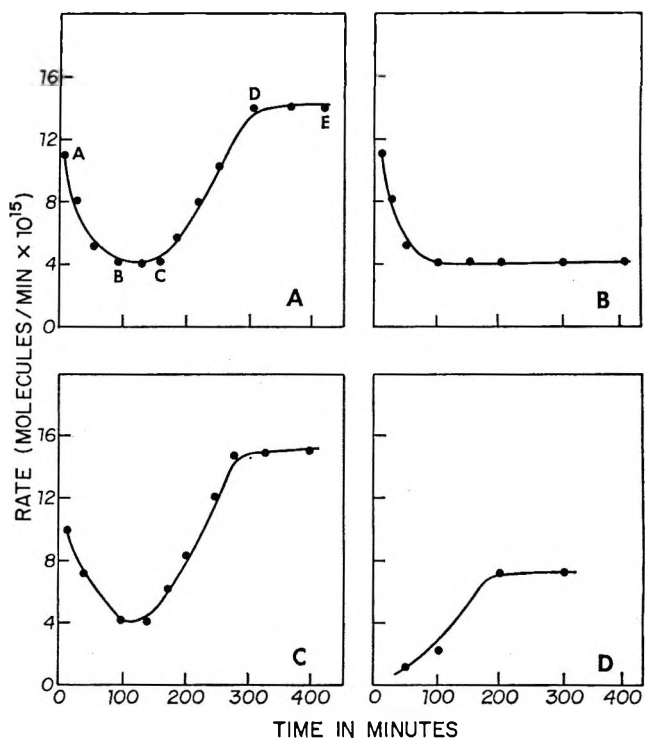


Figure 1. Photolysis of barium azide using light of wavelength: A, 1849 + 2537 Å; B, 2537 Å; C, ranging essentially from 2000 to 3000 Å; D, of barium nitride with light of wavelength ranging essentially from 2000 to 3000 Å.

with light of wavelengths 1849 + 2537 Å. For a fresh salt the rate falls off, reaches a minimum, and then rises to attain a constant rate. Figure 1B shows a similar plot for a different sample which was irradiated with light of wavelength 2537 Å. The acceleratory portion CDE in Figure 1A is absent in Figure 1B. The high-pressure mercury lamp was always used with a water filter, and Figure 1C shows a plot obtained when light of wavelength ranging essentially from 2000 to 3000 Å was used as the radiation source. The general features of the plot are similar to those in Figure 1A.

After each experiment, the irradiated barium azide was dissolved in water and tested for ammonia using Nessler's reagent and a colorimeter. A significant amount of NH_3 was found in all cases indicating the formation of barium nitride during irradiation.

Barium nitride, Ba_3N_2 , was next exposed to radiations of wavelength ranging essentially from 2000 to 3000 Å and the results clearly show that photolysis occurs with an accelerating rate. (Figure 1D).

Figures 2A and 2B present plots of the rate of nitrogen evolution from fresh samples of potassium azide *vs.* time of irradiation, using different radiation sources (*i.e.*, different wavelengths). In all cases, the rate decreased to a minimum and then increased to a constant value. Tests for NH_3 (nitride formation) were negative.

Figures 3A, 3B, 3C, and 3D show similar plots for sodium azide. Because NaN_3 is reported to undergo a phase transition at 19°, these experiments were done at

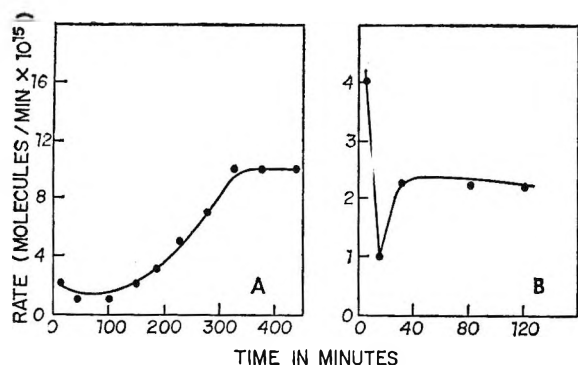


Figure 2. Photolysis of KN_3 using: A, light of wavelength ranging essentially from 2000 to 3000 Å; B, light of wavelength 2537 Å alone.

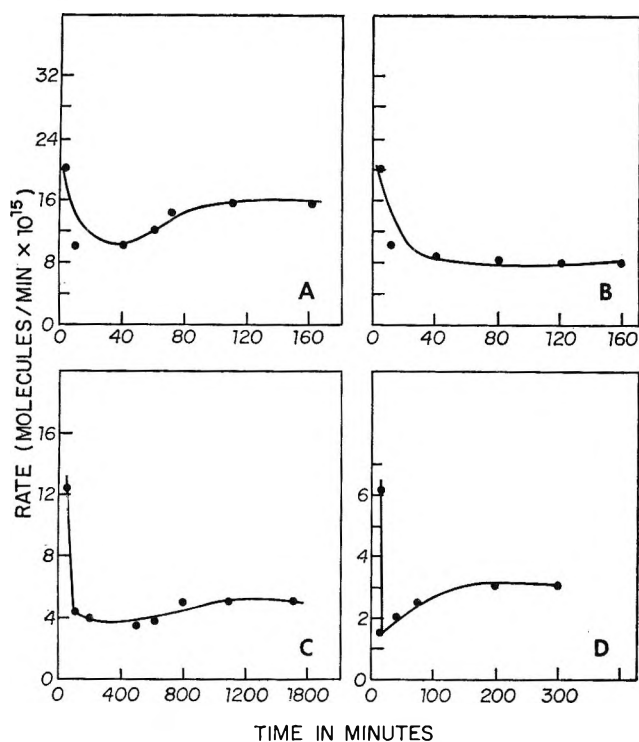


Figure 3. Photolysis of NaN_3 using light of wavelength: A, 1849 + 2537 Å; B, 2537 Å; C, ranging essentially from 2000 to 3000 Å; D, in the range 2400-3000 Å.

4 and 30°. The general characteristics remained unchanged. Light of wavelength 2537 Å alone (Figure 3B) did not bring about the acceleration in the decomposition rate which was seen if light of wavelength 1849 + 2537 Å (Figure 3A), 2000-3000 Å (Figure 3C), or 2400-3000 Å (Figure 3D) was used. In all cases tests for nitride were positive.

Silver azide irradiated with light of wavelength 1849-2537 Å did not show the acceleration in the decomposition rate (Figure 4A). However, irradiation with light of wavelength ranging essentially from 2000 to 3000 Å produced a pronounced acceleration (Figure 4B). Tests for nitride were positive.

In the case of lead azide (Figures 5A and 5B) no

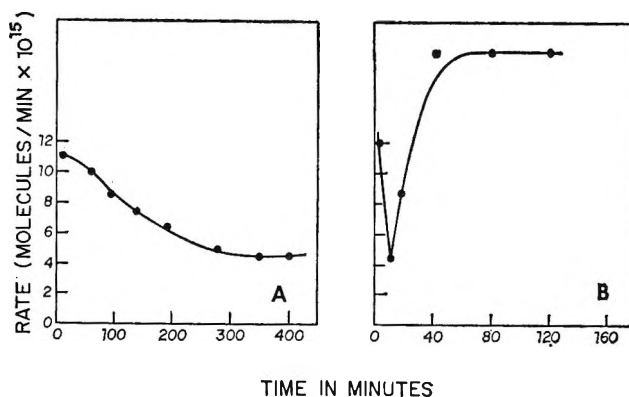


Figure 4. Photolysis of AgN_3 using light of wavelength: A, 1849 + 2537 Å; B, ranging essentially from 2000 to 3000 Å.

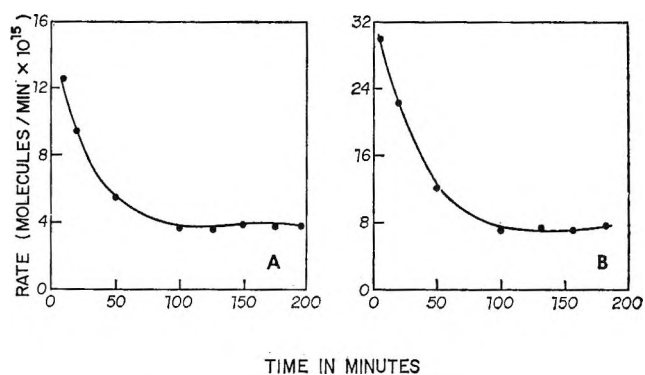


Figure 5. Photolysis of PbN_6 using light of wavelength: A, 1849 + 2537 Å; B, ranging essentially from 2000 to 3000 Å.

acceleration was observed no matter what wavelength was used. Tests for nitride were negative. Table I summarizes the foregoing results for the different azides.

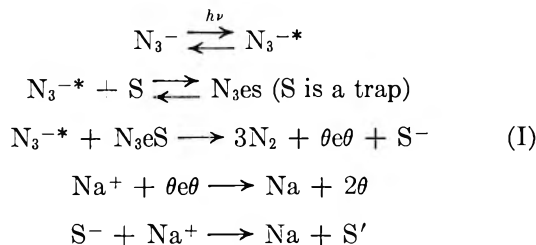
The common feature of the photolytic decomposition of NaN_3 , KN_3 , BaN_6 , AgN_3 , and PbN_6 is that when irradiated with the above sources, the rate of gas evolution initially decreases to a minimum value. The

Table I: Correlation of the Acceleratory Region in the Rate-Time Plot with (1) Ionization Potential and (2) Nitride Formation^a

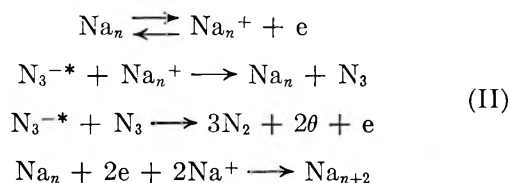
Metal azides	Nitride formation	Rate increase for irradiation with light of indicated wavelength			Ionization potential of metal atom, Å
		2537 Å	2537 + 1849 Å	2000-3000 Å ^b	
KN_3	A	P	P	P	2870
NaN_3	P	A	P	P	2420
BaN_6	P	A	P	P	2390
AgN_3	P	A	A	P	1650
PbN_6	A	A	A	A	1680

^a P, present; A, absent. ^b Essentially.

decrease in the photolytic rate may be caused by the gradual consumption of defects (initially present) which are helpful to the reaction. Jacobs, *et al.*,¹⁰ have suggested that these defects are either impurity ions or crystal imperfections, such as anion vacancies or jogs in dislocations. The rate of the gas evolution, based on this model suggested by Jacobs, *et al.*,¹⁰ ought to decrease, but as the reaction proceeds metal atoms are produced leading to the formation of metal specks



where S is a trap, e an electron, N_3^{-*} exciton, θ anion vacancy, and S' is another trap. (S' is not the same as S, as it is associated with two Na atoms and two anion vacancies whereas S has a normal crystal lattice environment of cations and anions.) Continuous repetition of this process leads to the formation of a metal nucleus. A second process now comes into operation originating from the photoemission of electrons from the metal.



where Na_n represents a metal speck. This model, proposed by Jacobs, *et al.*,¹⁴ was put forward to explain why the photolytic rate of KN_3 , after an initial deceleration, increases to attain a constant value. Jacobs, *et al.*,¹¹ did not observe any acceleration in the photodecomposition of NaN_3 and they ascribed it to topochemical features. Our results show that when NaN_3 , KN_3 , and BaN_6 are irradiated by light of wavelength $1849 + 2537 \text{ \AA}$, we do observe an acceleration after the initial deceleration. These results could well be explained on the model proposed by Jacobs, *et al.*¹⁴ However, under similar conditions $\alpha\text{-PbN}_6$ (Figure 5A) and AgN_3 (Figure 4A) do not show any acceleration. The work functions of all these metals (Pb, Ag, Ba, Na, and K) are such that light of wavelength 1849 \AA is sufficient to start process II, *i.e.*, photoemission of electrons from the metal. Therefore, the acceleration in the rate-time plot cannot be attributed to process II. One can, however, say that process II does occur and accounts for the fact that the photolytic rate does not go to zero but decelerates to a constant minimum value. This explains our results on $\alpha\text{-PbN}_6$ and AgN_3 .

Now if one brings in the idea of ionization potential (energy to remove an electron from an atom) instead of work function (energy to remove an electron from a metal) and considers Na_n in process II as a speck of Na atoms which has not attained metallic character, then one can see from Table I that light of wavelength 1849 \AA is sufficient to ionize Na, K, and Ba atoms but is not sufficient to ionize Pb and Ag atoms. Further, light of wavelength 2537 \AA alone is enough to ionize K atoms and one would therefore expect an acceleration in KN_3 even when irradiated with 2537-\AA radiation alone. This is precisely what our results show (Figure 2B). In short, whereas the Jacobs model of work function¹⁴ explains why the photolytic rate does not go to zero as the defects are consumed, one has to bring in the concept of ionization potential to explain why Na, K, and Ba azides show an acceleration and Pb and Ag azides do not. However, it should be borne in mind that the ionization potentials listed in Table I are for the metals in a vacuum, and these will change depending on the dielectric constant of the material.

When irradiated with light of wavelength ranging essentially from 2000 to 3000 \AA , an acceleration occurs in the decomposition rates of all those azides which form nitride. It is concluded that light of longer wavelength decomposes the nitride which is formed. This is substantiated by our results on the decomposition of barium nitride by irradiating with light from a high-pressure lamp with water filter. It is, however, not yet possible to explain why light of shorter wavelength does not decompose the nitride formed during the reaction. Perhaps the absorption coefficient of light of short wavelength is much greater for azides than for nitrides and the azides shield the nitrides from this light, but this is a speculation and subject to additional investigation.

In conclusion, it can be stated that the common feature of the photolytic decomposition of NaN_3 , KN_3 , BaN_6 , AgN_3 , and PbN_6 is that when photolyzed, the rate of gas evolution initially decreases to a minimum value. The decrease in photolytic rate seems to be caused by the gradual consumption of defects (initially present) which are helpful to the reaction. The photolytic rate ought to decrease to zero as these defects are completely used up; however, as the reaction proceeds, metallic specks are produced and these in turn initiate a second process, based on the photoemission of electrons from the metal, which keeps the photolytic process going. After reaching the minimum value those azides which form nitride as a photodecomposition product show an acceleration in the photolytic rate. This acceleration is caused by the photodecomposition of the nitride. All azides can show an acceleration in their photolytic rate if light capable of photoionizing the metal atoms (formed during photolysis) is used as a photolyzing source.

The Viscosity of Molten Bismuth-Bismuth Halide Solutions¹

by Jordan D. Kellner

Atomics International, A Division of North American Rockwell Corporation, Canoga Park, California 91304
(Received November 15, 1967)

The viscosities of solutions of bismuth in BiBr₃ and in BiCl₃ were measured by a capillary technique up to 600°. When compared to the data for the iodide reported earlier, the viscosity is greatest for the iodide solutions and least for the chloride solutions. The Arrhenius coefficients are greatest for the chloride system and least for the iodides and increase with decreasing temperature for the chloride and bromide solutions. These results are shown to be consistent with the "free-volume" model of transport in ionic melts.

Introduction

In a previous paper,² the viscosities of Bi-BiI₃ solutions were measured at temperatures ranging from 400 to 500°. The consolute temperature of 458° in this system made it possible to measure the viscosities of all compositions with Pyrex capillary cells. In this paper the work is extended to include the bismuth-bismuth bromide system above the consolute temperature of 538°, across the entire composition range. The bismuth-bismuth chloride system was studied only up to 30 mol % metal and 600° because of its high consolute temperature (780°).

Experimental Section

The bismuth halides used were obtained commercially and distilled twice under about 0.25 atm of oxygen. These salts and the purified bismuth² were handled only under dry argon.

The technique is identical with that reported previously.² The cells were constructed of quartz so that temperatures above the consolute temperature (538°) in the bromide system could be reached. Due to the high pressures (~10 atm) generated at 600°, heavy-walled quartz (4 mm) was used. The tungsten to quartz compression seals used were similar to those described by Grantham and Yosim.³ The cell was calibrated at room temperature with 10% glycerine-water solution, double-distilled water, heptane, acetone, and ether. In all calibrations a straight line was obtained when η/ρ , the ratio of the viscosity to the density, was plotted *vs.* time.

Only three different cells were used in all the determinations, one of them for about 75% of the compositions studied. The calibration curves were checked before each run, and virtually no changes were noted. The corrections that must be applied for the difference in temperature of unknown and standard liquid were less than the estimated error and were not applied.

Results and Discussion

The viscosities of Bi-BiBr₃ solutions containing 0, 15, 30, 45, 50, 60, and 80 mol % Bi and BiCl₃ solutions

containing 0, 15, and 30 mol % Bi were determined at temperatures ranging from 220 to 600°. Higher concentrations of metal in BiCl₃ were not run because of the limited solubility of the metal in the salt at these temperatures. The viscosity of pure bismuth could not be determined with this apparatus because of the very low value of the kinematic viscosity ($\eta/\rho = 0.12$ cSt at 500°). The flow velocity of bismuth through the capillaries used was great enough to cause turbulent flow with a resultant scatter in the data. Therefore, the literature value⁴ for the viscosity of pure bismuth was used.

The kinematic viscosities calculated from the calibration equation were combined with density data to obtain the viscosity values. Up to 40 mol % Bi, the data of Keneshea and Cubicciotti⁵ for the densities of chloride and bromide solutions were used. The densities of more concentrated solutions were obtained by interpolation using a value at 70 mol % for the bromide⁶ and a value for bismuth.⁷ The viscosities are shown in Table I for the bromide system and in Table II for the chloride. Figure 1 shows the values for the three pure halides. A smooth curve was drawn through a plot of time of flow *vs.* temperature for each solution, and the time of flow at 10° intervals from the smoothed curve was used to calculate the viscosity data. The standard deviation of the measured flow time from the smooth curves was 0.06 sec for flow times of about 40-100 sec. Based on this factor and an estimated error in temperature measurement, the data are estimated to be accurate to within 2%. The data obtained for the Bi-BiCl₃ solutions and for pure BiCl₃ are lower by more than a factor of 10 than those given

(1) This work was supported by the Research Division of the U. S. Atomic Energy Commission.

(2) J. D. Kellner, *J. Phys. Chem.*, **71**, 3254 (1967).

(3) L. F. Grantham and S. J. Yosim, *J. Chem. Phys.*, **38**, 1671 (1963).

(4) F. Sauerwald and K. Topler, *Z. Anorg. Chem.*, **157**, 177 (1926).

(5) (a) F. J. Keneshea and D. Cubicciotti, *J. Phys. Chem.*, **62**, 843 (1958); (b) *ibid.*, **63**, 1472 (1959).

(6) L. E. Topol and F. Y. Lieu, *ibid.*, **68**, 851 (1964).

(7) E. Gebhardt and K. Kostlin, *Z. Metallk.*, **48**, 601 (1957).

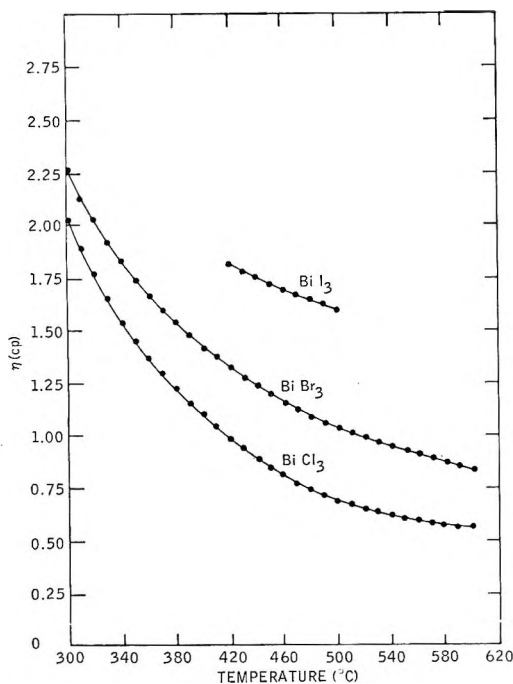


Figure 1. Viscosity vs. temperature for the pure salts BiCl_3 , BiBr_3 , and BiI_3 .

by Aten⁸ in 1909. Since Aten's temperature coefficients are nearly the same as those of the present work, one can only suggest that the units Aten called "absolute units" are really decipoises instead of poises.

At any particular temperature the viscosity of the pure salt increases as the size of the anion increases (see Figure 1). This dependence of the viscosity on the anion size is observed⁹ in most metal halides. This sequence is reasonable in view of the fact that the viscosity of the melt depends mainly on the mobility of the largest ion in contrast to electrical conductivity where the smallest ion is more important.

The usual Arrhenius equation

$$\eta = Ae^{E/RT} \quad (1)$$

was used to calculate an "Arrhenius coefficient," E , of viscosity. The values of the Arrhenius coefficient which have been called in the literature and in the previous paper "apparent activation energy" are shown in Table III for the three bismuth halide systems. The $\ln \eta$ vs. $1/T$ plots for the three pure salts are shown in Figure 2. The "Arrhenius coefficient" of viscosity is greatest for the smallest anion, Cl^- and least for the largest anion, I^- .

The viscosity isotherms as a function of composition for the metal solution of the bromide and chloride systems are shown in Figures 3 and 4. Most of the isotherms in Figure 3 could not be completed because an immiscibility gap is present at that temperature and composition. The isotherms in Figure 4 end at 30 mol % because of the high consolute temperature in this system; however, it seems likely from the similarity of

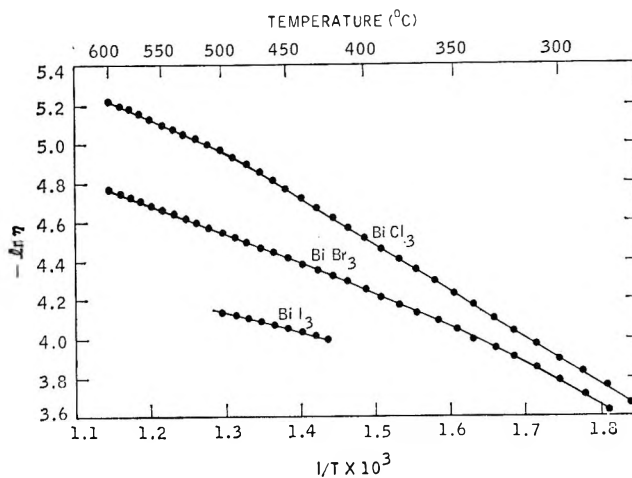


Figure 2. Plots of \ln viscosity vs. $1/T$ for BiCl_3 , BiBr_3 , and BiI_3 .

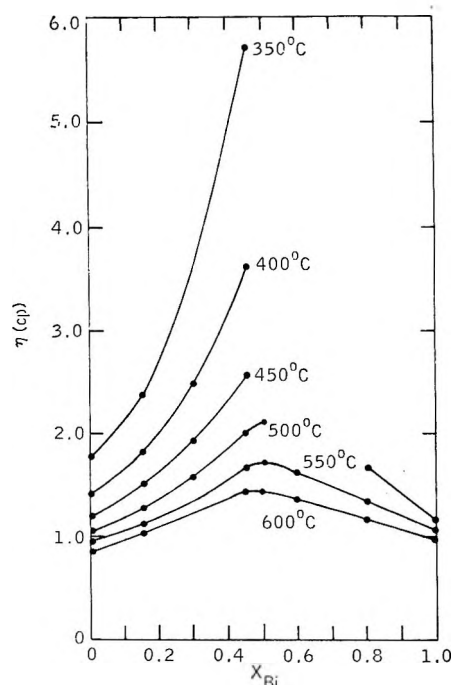


Figure 3. Viscosity isotherms for the Bi-BiBr_3 system.

the isotherms for the three halides that a maximum would be found for the chloride isotherms if the melts were studied at a high enough temperature. The maxima appear at about the same composition in the bromide system and in the iodide system reported earlier.²

The $\ln \eta$ vs. $1/T$ plots for the metal solution of the bromide and chloride systems are shown in Figures 5 and 6. One can see in Table III that generally, the "Arrhenius coefficient" of viscosity increases with added metal, reaching a maximum at 50% in the iodide

(8) A. H. W. Aten, *Z. Physik. Chem.*, **66**, 641 (1909).

(9) G. J. Janz, A. T. Ward, and R. D. Reeves, "Molten Salt Data," Technical Bulletin Series, Rensselaer Polytechnic Institute, Troy, N. Y., 1964.

Table I: The Viscosity of Bi-BiBr₃ Solutions

Temp, °C	Viscosity, cP						
	0% Bi	15%	30%	45%	50%	60%	80%
600	0.845	1.04		1.47	1.49	1.38	1.20
590	0.862	1.06		1.51	1.52	1.41	1.22
580	0.880	1.08		1.54	1.58	1.47	1.25
570	0.892	1.09		1.59	1.61	1.51	1.27
560	0.919	1.11		1.63	1.67	1.58	1.31
550	0.935	1.13		1.68	1.73	1.63	1.35
540	0.956	1.16		1.74	1.76	1.70	1.38
530	0.979	1.18		1.80	1.81	1.75	1.44
520	1.00	1.22		1.87	1.89		
510	1.03	1.25		1.95	1.99		
500	1.06	1.29	1.60	2.03	2.13		
490	1.08	1.32	1.66	2.12	2.39		
480	1.11	1.36	1.73	2.22	2.68		
470	1.14	1.41	1.79	2.32	2.97		
460	1.16	1.45	1.88	2.44	3.22		
450	1.20	1.50	1.95	2.56	3.47		
440	1.24	1.55	2.04	2.73	3.71		
430	1.27	1.60	2.14	2.89	3.97		
420	1.31	1.66	2.24	3.10	4.24		
410	1.36	1.72	2.37	3.28	4.49		
400	1.41	1.80	2.49	3.62	4.72		
390	1.47	1.89		3.88	5.09		
380	1.54	2.00		4.19	5.51		
370	1.60	2.12		4.47	5.94		
360	1.66	2.24		5.00	6.36		
350	1.75	2.40		5.72	7.15		
340	1.83			6.51	8.24		
330	1.92			7.27	9.81		
320	2.02			8.23	11.4		
310	2.13			9.31	13.0		
300	2.28			11.06	14.6		
290	2.45			12.91			
280	2.66			14.81			

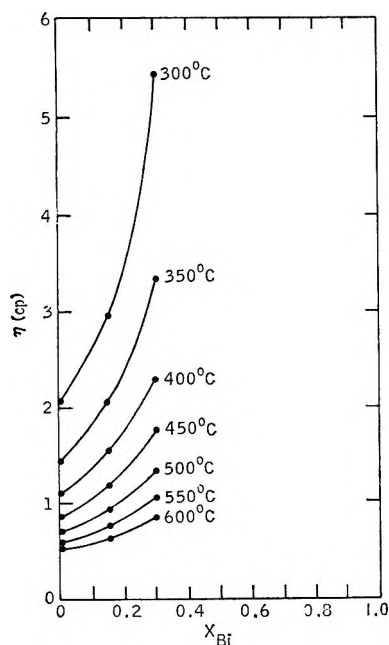


Figure 4. Viscosity isotherms for the Bi-BiCl₃ system.

and 60% in the bromide. There is a small increase in the coefficient at low temperatures for all the solutions studied.

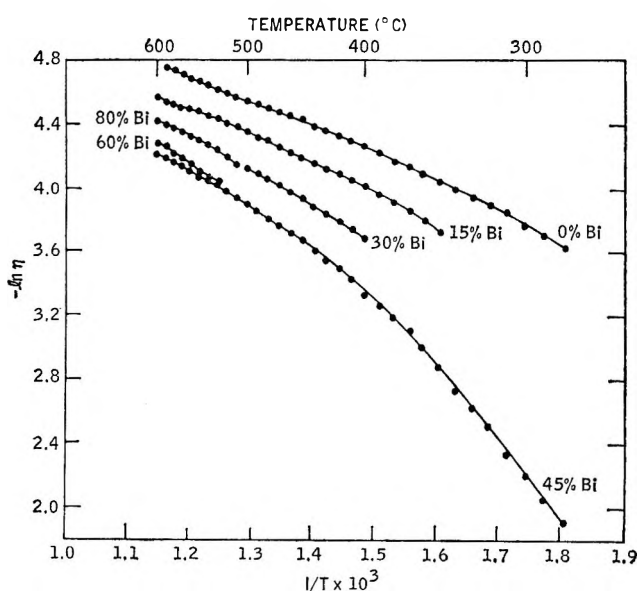
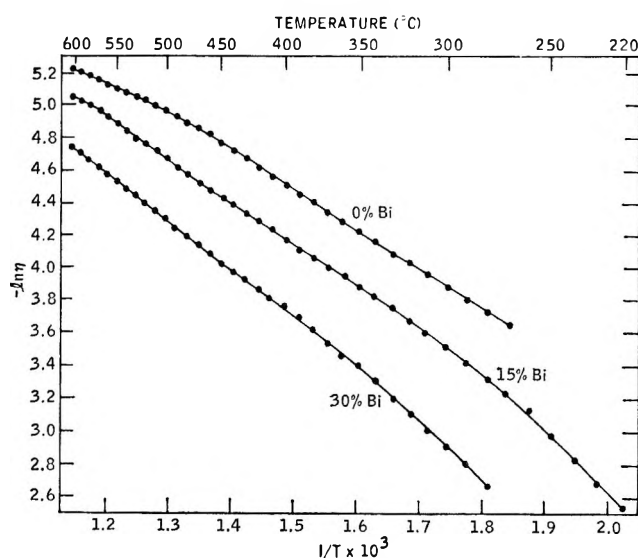
The iodide data were interpreted according to the "hole" theory of viscosity in the previous paper.² This model pictures viscous flow as consisting of two steps. First a suitable hole forms from the free volume available to the melt and then the "flow unit" breaks away from its neighbors and enters this space. If one of these processes dominates the other, then "Arrhenius behavior" is observed; *i.e.*, eq 1 holds. The iodide melts can be considered to be "free volume limited," in that the rate-determining step in the flow process is the formation of a hole. The maximum in the isotherm is caused by a diminution in the free volume as metal is added, the free volume reaching a minimum at about 50 mol % Bi. However, the fact that the iodide melts follow the Arrhenius equation is probably a result of the narrow temperature range of the data (~400–500°). In the chloride and bromide cases where the temperature range is greater than 300°, the temperature

Table II: The Viscosity of Bi-BiCl₃ Solutions

Temp. °C	Viscosity, cP		
	0%	15%	30%
600	0.539	0.642	0.879
590	0.552	0.656	0.907
580	0.562	0.674	0.944
570	0.573	0.692	0.984
560	0.592	0.721	1.03
550	0.606	0.753	1.07
540	0.620	0.787	1.12
530	0.637	0.820	1.17
520	0.655	0.854	1.22
510	0.672	0.892	1.28
500	0.693	0.930	1.35
490	0.718	0.979	1.43
480	0.743	1.03	1.50
470	0.771	1.08	1.59
460	0.807	1.13	1.68
450	0.843	1.18	1.78
440	0.897	1.25	1.87
430	0.937	1.31	1.97
420	0.985	1.38	2.08
410	1.04	1.46	2.19
400	1.10	1.55	2.31
390	1.16	1.64	2.49
380	1.22	1.73	2.67
370	1.29	1.83	2.94
360	1.37	1.93	3.14
350	1.46	2.05	3.34
340	1.54	2.19	3.64
330	1.66	2.33	3.99
320	1.77	2.52	4.41
310	1.90	2.73	4.85
300	2.05	2.95	5.43
290	2.20	3.24	6.02
280	2.36	3.56	6.77
270	2.59	3.93	
260		4.42	
250		5.07	
240		5.86	
230		6.77	
220		7.96	

Table III: Arrhenius Coefficient of Viscosity (kcal/mol)

X _{Bi}	Temperature range, °C		
	300-400	400-500	500-600
Bi-BiI ₃			
0		1.72	
0.15		2.04	
0.30		2.08	
0.45		4.79	
0.50		6.53	
0.55		6.45	
0.60		5.56	
0.70		1.35	
1.00		1.84	
Bi-BiBr ₃			
0	3.68	2.98	2.98
0.15	4.78	3.44	3.01
0.30		4.57	
0.45	8.40	5.62	3.79
0.50	10.8		3.90
0.60			4.70
0.80			4.26
1.00	1.30	1.84	2.21
Bi-BiCl ₃			
0	4.8	4.8	3.4
0.15	7.7 ^a	5.2	5.2
0.30	6.97	5.75	5.75

^a 220-300°**Figure 5.** Plots of \ln viscosity vs. $1/T$ for the Bi-BiBr₃ system. (The 50% data were omitted for clarity.)**Figure 6.** Plots of \ln viscosity vs. $1/T$ for the Bi-BiCl₃ system.

coefficient of viscosity is dependent on temperature (see Table III). Also, the Batchinski equation is not followed in the bromide and chloride cases, whereas it is followed in the iodide system. However, if a short 100° range is chosen, then the Batchinski equation holds equally well in all three systems. The increase in Arrhenius coefficient may be due to the equilibrium that exists at low temperatures in the chloride and bromide systems between the monomer subhalide BiX

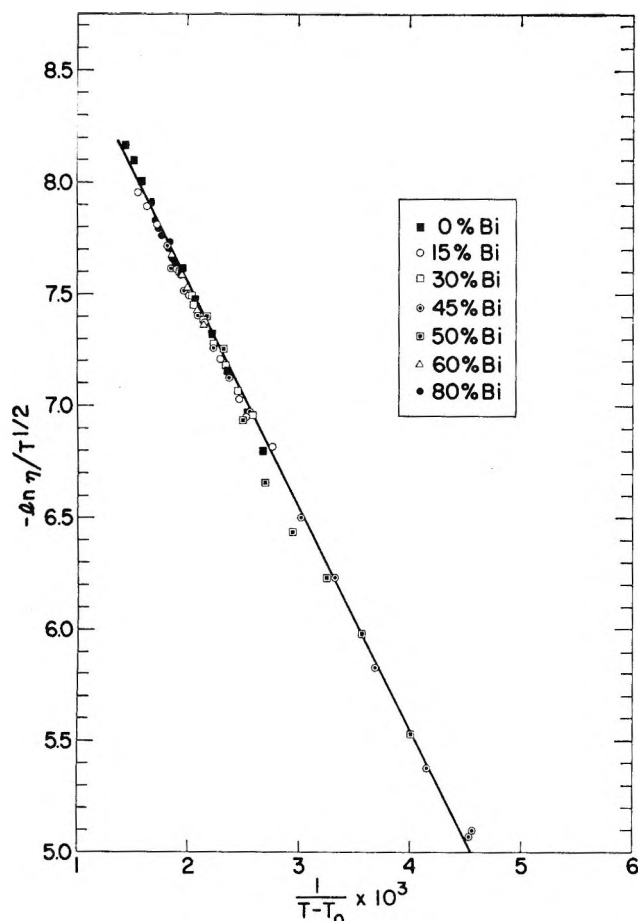


Figure 7. Plot of $\ln \eta/T^{1/2}$ vs. $1/(T - T_0)$ for the Bi-BiBr₃ system.

and polymeric form, probably (BiX)₄.¹⁰ In the past, an increase in the Arrhenius coefficient at low temperatures was taken to be caused by complexing. However, it is of interest to see how the data fit the free-volume model of Cohen and Turnbull.¹¹ These authors derive the following expression which is similar to an empirical equation used earlier by Doolittle¹² for the diffusion coefficient, D , in a fluid of hard spheres

$$D = ga^*u \exp(-\gamma v^*/v_f) \quad (2)$$

where g is a geometric factor, a^* is approximately equal to the molecular diameter, u is the gas kinetic velocity, γ is a factor between $1/2$ and 1 to correct for overlap of free volume, v^* is the minimum hole volume necessary for a migration to occur, and v_f is the free volume. Hogenboom, Webb, and Dixon¹³ point out that the viscosity relation, using the Stokes-Einstein equation and eq 2, should be

$$\ln \eta/T^{1/2} = \ln A + \frac{B}{v_f} \quad (3)$$

where B is γv^* . As pointed out by Barlow, Lamb, and Matheson,¹⁴ this equation is equivalent to

$$\ln \eta/T^{1/2} = \ln A + \frac{K}{T - T_0} \quad (4)$$

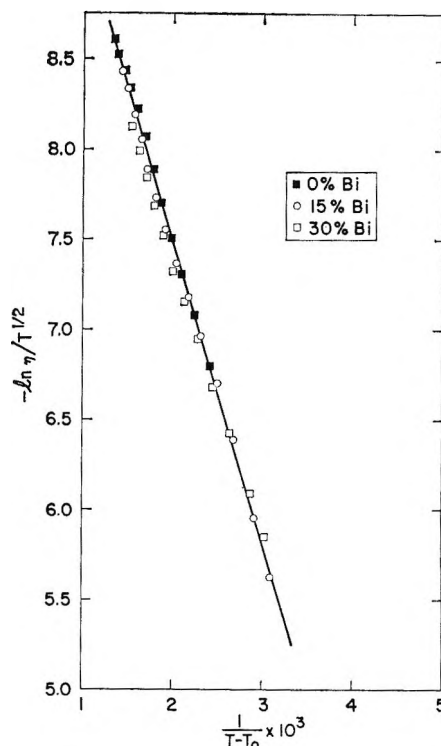


Figure 8. Plot of $\ln \eta/T^{1/2}$ vs. $1/(T - T_0)$ for the Bi-BiCl₃ system.

where $K = \gamma v^*/\alpha \bar{v}$, α being the thermal expansivity, and \bar{v} the mean molecular volume. Equation 4 follows if the specific volume is a linear function of the temperature and if all liquid expansion appears as an increase in free volume. Equation 4 has been used empirically for many years to describe the viscous behavior of liquids.

In Figures 7 and 8, $\ln \eta/T^{1/2}$ plotted vs. $1/(T - T_0)$ is shown for the bromide and chloride systems. These lines were obtained by a computer program in which $\ln \eta/T^{1/2}$ and T for each composition were given, and K , T_0 , and $\ln A$ were determined. The values for these quantities for each composition studied are shown in Table IV. It seems remarkable, as Figures 7 and 8 show, that all the data for all compositions of each halide fall on the same straight line. However, until there is some independent way to calculate these quantities from structural parameters, eq 4 must be considered as merely a three-parameter fit for the data, which would be expected to be better than a two-parameter equation. Nevertheless, the fact that the constants K and $\ln A$ are the same for all the com-

(10) (a) L. E. Topol, S. J. Yosim, and R. A. Osteryoung, *J. Phys. Chem.*, **65**, 1511 (1961); (b) L. E. Topol and R. A. Osteryoung, *ibid.*, **66**, 1587 (1962).

(11) M. H. Cohen and D. Turnbull, *J. Chem. Phys.*, **31**, 1164 (1959).

(12) A. K. Doolittle, *J. Appl. Phys.*, **22**, 1471 (1951).

(13) D. L. Hogenboom, W. Webb, and J. A. Dixon, *J. Chem. Phys.*, **46**, 2586 (1967).

(14) A. J. Barlow, J. Lamb, and A. J. Matheson, *Proc. Roy. Soc. (London)*, **A292**, B22 (1966).

Table IV: Values of the Constants in Eq 4

	$\ln A$	K	T_0 , °K	$A \times 10^4$
B:Br ₃	-9.72	1086	180	0.60
15% Bi	-9.53	1008	228	0.72
30% Bi	-9.56	1017	286	0.71
45% Bi	-9.52	1006	332	0.73
50% Bi	-9.50	1000	353	0.75
60% Bi	-9.50	1000	333	0.75
80% Bi	-9.51	1000	283	0.74
BiCl ₃	-10.97	1740	127	0.17
15% Bi	-10.98	1703	171	0.17
30% Bi	-10.93	1752	224	0.18
BiI ₃	(-8.65) ^a	(561) ^a	(310)	(1.7) ^a
15% Bi			(320)	
30% Bi			(360)	
45% Bi			(380)	
50% Bi			(400)	
55% Bi			(400)	
60% Bi			(400)	
70% Bi			(365)	

^a Average values for all compositions.

positions that contain the same anion is suggestive that T_0 does indeed have a physical meaning, *i.e.*, the temperature at which the free volume disappears.

The iodide system is not plotted because the short range of values for $\ln \eta/T^{1/2}$ makes the choice of T_0 almost arbitrary. However, if one does choose values of T_0 for the iodide melts, to force the data for all

compositions to be on the same line, then this line will have a smaller K value, a smaller A value, and intersect the other two curves within a region common to all three systems. The parameters K , $\ln A$, and T_0 are given for the iodide system in Table IV in parentheses to emphasize that they are approximate. These three lines have a common intersection because each line contains some points that correspond to a composition of 100% bismuth, and the viscosity of pure bismuth at these temperatures would give $\ln \eta/T^{1/2}$ values of between -7.5 and -7.8.

According to the Cohen-Turnbull equation (eq 2), and the Stokes-Einstein relation, A in eq 3 is proportional to $m^{3/2}/a^2$, where m is molecular weight and a is ionic diameter. Thus, A should increase in the order Cl, Br, I as is shown to be the case in Table IV. Since at a temperature T , the viscosity is dependent only on A , K , and $T - T_0$ in eq 4, and for all solutions containing the same anion, K and A are the same, the differences in viscosity are due to the term $(T - T_0)$. This term is proportional to free volume and goes through a minimum as the bismuth concentration increases causing the viscosity to go through a maximum.

This picture is consistent with the minimum in free volume found in the iodide system at 55 mole %² and with the fact that the molar volume isotherms show negative deviations from ideality for all three systems.

Acknowledgment. The author is indebted to Mr. Alex Nickols for the computer calculations.

Infrared Spectral Evidence for Trihalomethyl lithium and -sodium Compounds in Solid Argon

by Lester Andrews and T. Granville Carver

Chemistry Department and Center for Advanced Studies, University of Virginia, Charlottesville, Virginia 22901
(Received November 16, 1967)

The matrix reaction of alkali metal atoms and perbromochloromethanes produces the trihalomethyl radical followed by a secondary reaction of metal atoms with CX_3 to yield a sufficient concentration of the trihalomethyl alkali metal compounds for infrared spectral study. Use of the five perbromochloromethane precursors with lithium-6, lithium-7, and sodium verifies the molecular identity. Assignments to the antisymmetric carbon-halogen stretching frequencies are 521 and 462 cm^{-1} for the chlorine and bromine species, respectively, while the lithium-6 stretching frequencies are 437 and 391 cm^{-1} , respectively, for the chlorine and bromine molecules. The carbon-halogen frequencies lead to markedly lower force constants than calculated for the carbon tetrahalides which suggests that the CX_3 group has a significant amount of anionic character.

Introduction

There has been a great deal of recent research activity on α -haloalkyllithium compounds or carbenoids.¹ Kobrich² has reviewed the chemistry and mechanisms of carbenoid reactions. The reactions of trichloromethyl lithium were first thought to go through the carbene intermediate,³ but later work suggested that the intermediate in reactions of carbenoids is a "carbene-salt complex"^{4,5} in contrast to proposed mechanisms using the carbenoid structure itself as the intermediate.^{1,2,6}

We have announced the infrared detection of the trichloromethyl radical^{7,8} in solid argon using the matrix reaction of lithium and carbon tetrachloride. In the case of reactions of lithium atoms with methyl halides to produce the methyl radical,^{9,10} subsequent reaction of lithium atoms with methyl radicals gives methyl lithium¹¹ isolated as the monomer. Thus, the lithium-tetrahalomethane study yields trihalomethyl lithium in an argon matrix at 15°K for spectral study. This technique provides a unique opportunity for spectroscopic observations of carbenoids since these compounds decompose exothermally^{4,5} at temperatures near -70°. The infrared spectra of the trihalomethyl lithium and sodium compounds should provide information about the bonding and structure of these chemically interesting species.

Experimental Section

The 15°K refrigeration system, lithium atom source, experimental technique, chemicals, and purification procedures have been described in detail in earlier publications.^{8,12} Samples of tetrahalomethane in argon ($Ar/CX_4 = {}^{200}/_1$ to ${}^{600}/_1$) were simultaneously deposited with an atomic beam of lithium ($Li/CX_4 \approx 1/2$ to $3/1$) on a CsI window maintained at 15°K.

Infrared spectra were recorded on a Beckman IR-12 filter-grating spectrophotometer in the 200-4000- cm^{-1} region. Frequency accuracy is ± 1 cm^{-1} and spectral slit widths were 0.8 cm^{-1} at 900 cm^{-1} , 0.9 cm^{-1} at 700 cm^{-1} , and 2.1 cm^{-1} at 500 cm^{-1} .

Results

Perbromochloromethane Precursors. In the earlier work with CCl_4 ⁸ and CBr_4 ,¹² absorptions labeled M and L in the 375-525- cm^{-1} spectral region were observed to increase in intensity relative to absorptions owing to the trihalomethyl radical when the lithium concentration was increased. The bands L showed a definite lithium isotopic shift and a shift to longer wavelength as bromine successively replaced chlorine in the parent material. Table I lists the absorptions M and L for the perbromochloromethane and ⁷Li and ⁶Li parent materials. In several CCl_4 experiments, the relative intensities of the M and L bands remained approximately constant.

Figure 1 contrasts spectra in the 370-590- cm^{-1} spectral region for all of the perbromochloromethane

- (1) G. L. Closs and R. A. Moss, *J. Am. Chem. Soc.*, **86**, 4042 (1964).
- (2) G. Kobrich, *Angew. Chem. Intern. Ed.*, **6**, 41 (1967).
- (3) W. T. Miller, Jr., and C. S. Y. Kim, *J. Am. Chem. Soc.*, **81**, 5008 (1959).
- (4) D. F. Hoeg, D. I. Lusk, and A. L. Crumbliss, *ibid.*, **87**, 4147 (1965).
- (5) G. L. Closs and L. E. Closs, *Angew. Chem.*, **74**, 431 (1962).
- (6) W. T. Miller, Jr., and D. M. Whalen, *J. Am. Chem. Soc.*, **86**, 2089 (1964).
- (7) L. Andrews, *J. Phys. Chem.*, **71**, 2761 (1967).
- (8) L. Andrews, *J. Chem. Phys.*, **48**, 972 (1968).
- (9) W. L. S. Andrews and G. C. Pimentel, *ibid.*, **44**, 2527 (1966).
- (10) L. Andrews and G. C. Pimentel, *ibid.*, **47**, 3637 (1967).
- (11) L. Andrews, *ibid.*, **47**, 4834 (1967).
- (12) L. Andrews and T. G. Carver, *ibid.*, in press.

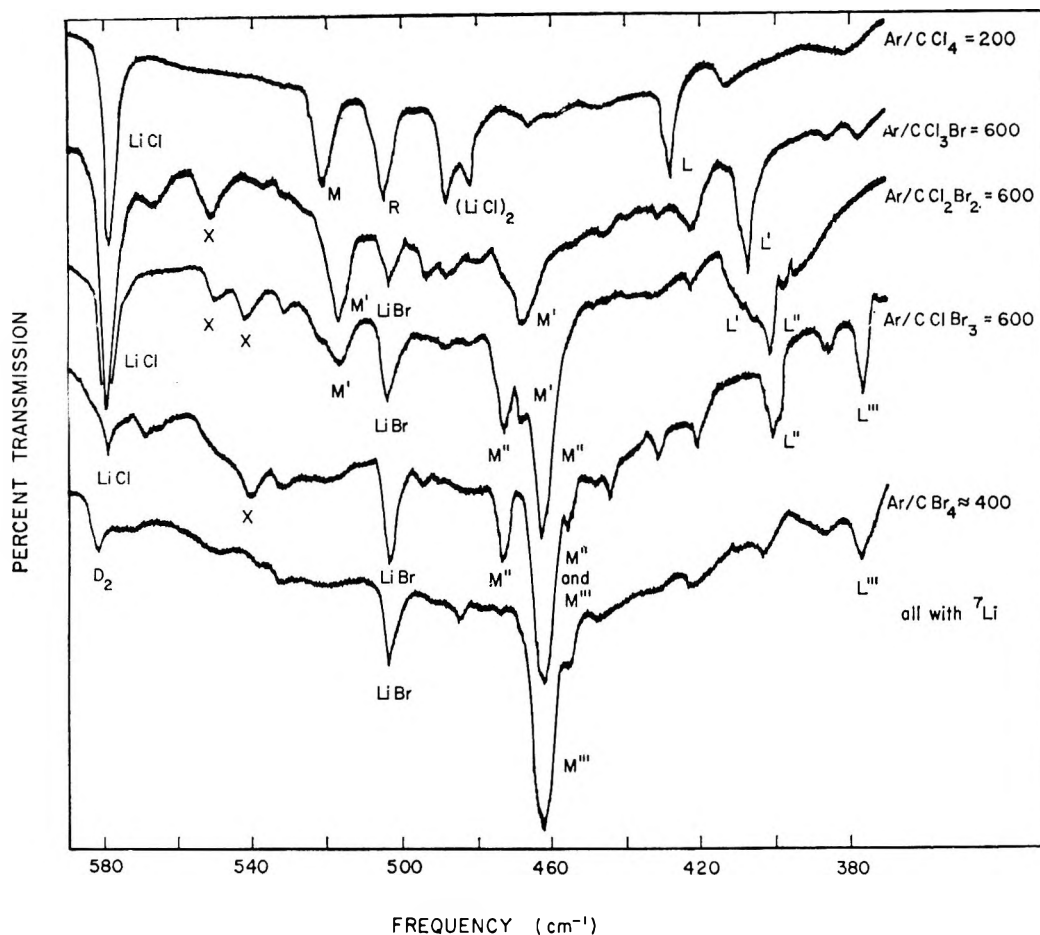


Figure 1. Infrared spectra recorded in the 370–590-cm⁻¹ spectral region for samples of CCl₄, CCl₃Br, CCl₂Br₂, CClBr₃, and CBr₄ in argon deposited with lithium-7 at 15°K.

Table I: Absorptions M and L for All Parent Materials Used

Parents	M band, cm ⁻¹	L band, cm ⁻¹
⁶ Li, CCl ₄	521	437
⁷ Li, CCl ₄	521	429
⁶ Li, CCl ₃ Br	517, 468	410
⁷ Li, CCl ₃ Br	518, 469	407
⁷ Li, CCl ₂ Br ₂	518, 473, 468, ^a 463	407, ^a 401
⁶ Li, CClBr ₃	473, 463	404, 391
⁷ Li, CClBr ₃	473, 463	401, 377
⁶ Li, CBr ₄	462	391
⁷ Li, CBr ₄	462	377

^a Shoulder.

parents deposited with ⁷Li. LiCl and LiBr absorptions are noted. The number of primes on the M and L labels indicates the number of bromine atoms present in the species which will be discussed below.

When CBr₄ is deposited with an equimolar mixture of ⁶Li and ⁷Li, the L band becomes a doublet with the same ⁶Li and ⁷Li components, 391 and 377 cm⁻¹, respectively, observed when the pure isotopic lithium metal was used. Experiments using the 51% ¹³C-enriched CCl₄ sample with ⁷Li show that the L bands be-

comes a doublet with components at 729 and 723 cm⁻¹, while with ⁶Li the L band broadens and shifts 2 cm⁻¹ to longer wavelengths from the 437-cm⁻¹ frequency observed using natural CCl₄.

Upon warming of the deposited sample to 45°K and recooling to 15°K, the M and L bands decrease in intensity to about half of their original value while absorptions of dihalocarbene^{13,14} disappear completely and trihalomethyl radicals^{8,12} decrease less than one-fourth of their original intensity. These data show that the M and L absorptions are due to a species different from the dihalocarbenes and the trihalomethyl radicals.

Variation of Alkali Metal. Figure 2 illustrates spectra recorded for experiments using sodium with the five perbromochloromethane precursors. Although the same M absorptions within ±1 cm⁻¹ were observed using Na as Table I lists for the Li parent, no sodium counterpart of the band L was observed. The M absorptions were markedly more intense relative to the trihalomethyl radical and dihalocarbene absorptions

(13) L. Andrews, *J. Chem. Phys.*, in press.

(14) L. Andrews and T. G. Carver, *ibid.*, in press.

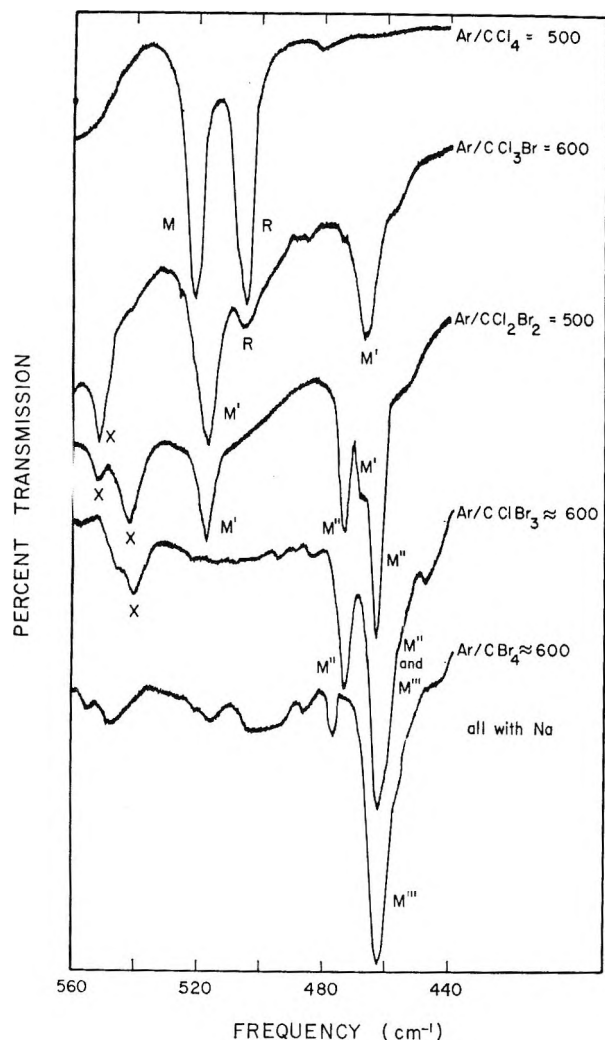


Figure 2. Infrared spectra recorded in the 440–560-cm⁻¹ spectral region for samples of the five perbromochloromethanes in argon deposited with sodium at 15°K.

for the Na parent than for Li, which shows that the M absorber must be still a third molecular species.

Figure 3 contrasts spectra recorded for experiments using ⁶Li, Na, and K with CCl₄. The band labeled M is at 521.0 ± 0.5 cm⁻¹ for the three alkali metals, while the R band shifts from 506 to 505 to 507 cm⁻¹ as the alkali metal atomic weight increases. The last spectrum recorded for the 51% carbon-13-enriched CCl₄ sample with potassium shows a triplet structure with components at 521, 506, and 496 cm⁻¹. The same enriched CCl₄ sample deposited with sodium yields a triplet whose components absorb at 521, 505, and 495 cm⁻¹.

Discussion

The purpose of this publication is to identify absorptions which can be assigned to the trihalomethyl alkali metal compounds and to examine these data with regard to structure, vibrational potential function, and bonding in these species.

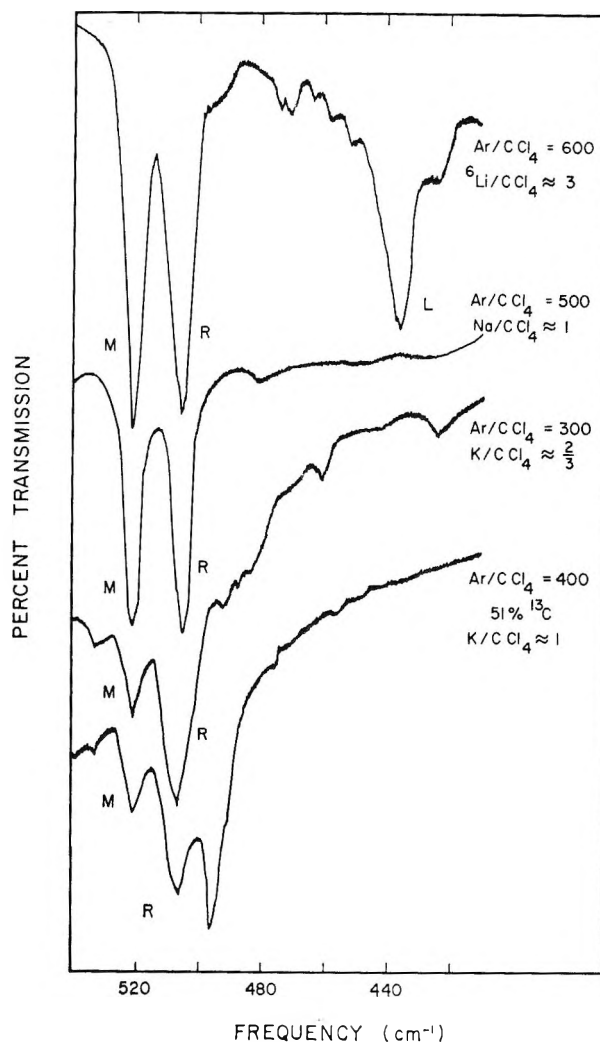


Figure 3. Infrared spectra recorded in the 420–540-cm⁻¹ spectral region contrasting the effect of different alkali metal atoms deposited with CCl₄ in argon at 15°K.

Species M Identity. Since the M and L absorptions maintain approximately constant relative intensities as concentrations of Li and CCl₄ are varied, they are assigned to the same molecular species. The band L doublet in the equimolar lithium isotope experiment shows that species M contains a single lithium atom and suggests that its sodium counterpart likely contains a single sodium atom. The band L in the carbon-13-enriched CCl₄ experiments is shifted to lower frequency which indicates that carbon is present in species M.

The spectra illustrated in Figures 1 and 2 show four different sets of M absorptions noted M, M', M'', M''', where the primes note the number of bromine atoms in species M. Single M (521 cm⁻¹) and M''' (462 cm⁻¹) absorptions are observed in the CCl₄ and CBr₄ experiments, respectively, but when the CCl₃Br and CClBr₃ precursors are used, additional M' (517 and 468 cm⁻¹) and M'' (473 and 463 cm⁻¹) bands are recorded. These same M' and M'' absorptions are observed in the CCl₂Br₂ experiments, which suggests

that the M and M''' bands are doubly degenerate and that the M' and M'' bands result when this degeneracy is broken by mixing bromine with chlorine atoms in species M. The same frequency pattern is observed for the doubly degenerate antisymmetric carbon-halogen stretching vibration in the series of radicals⁸ CCl₃, CCl₂Br, CClBr₂, and CBr₃ and their haloform¹⁵ counterparts. In the experiments using the three mixed perbromochloromethanes, two different trihalomethyl radicals⁸ are produced and their subsequent reaction produces two different trihalomethyl-lithium or -sodium compounds, which is shown in Figures 1 and 2 by the appearance of two different M (and L) species in the CCl₂Br₂ and CClBr₃ experiments.¹⁶

The fact that four different degrees of chlorine-bromine substitution exist for the species M indicates that three equivalent halogens are present in the M absorber. The presence of carbon is verified by the observed carbon-13 isotopic shifts. Three equivalent halogens imply that species M contains a single carbon atom.

Thus, species M has the formula CX₃Li and is isolated as the monomer, whereas in the sodium experiments, the formula CX₃Na is implied, both presumably with the C_{3v} structure.

Species M Vibrational Assignment. The band L for the trichloromethyl-lithium compounds shows a lithium isotopic shift from 437 to 429 cm⁻¹ which suggests that this vibration involves the lithium atom while the carbon-13 shift shows that the carbon atom participates in the vibration. However, the calculated lithium isotope shift (21 cm⁻¹) assuming a C-Li diatomic molecule is larger than observed which indicates that the vibration is not a pure C-Li stretch so it must partially involve the halogen atoms. This is reasonable in view of the fact that the symmetric halogen stretching mode is expected in this region, and it has the same a₁ symmetry as the lithium stretch in the C_{3v} point group. The band L appears to be nondegenerate on mixing of chlorine and bromine atoms and is assigned to the symmetric stretching mode involving primarily the lithium and carbon atoms, but also the halogen atoms. No assignment is made to the pure C-X symmetric stretching vibration.

In the preceding section we showed that the M and M''' bands are doubly degenerate and that the M' and M'' bands result when this degeneracy is broken by mixing of chlorine and bromine atoms. Thus, the M bands are assigned to the doubly degenerate antisymmetric carbon-halogen stretching vibrations of the C_{3v} species.

The absorption labeled R in Figures 1-3 has the same intensity as the M band using Li and Na parents, but its intensity increases markedly over the M band using K. The behavior in the K experiment suggests that the band R is not a fundamental vibration

due to species M unless the K atom perturbs the vibration significantly differently than does Li or Na. No bromine counterpart of the absorption R was observed. The R band could be the symmetric C-Cl stretch expected in the 400-550-cm⁻¹ region which might be perturbed and made more intense by the K atom. However, a more likely possibility is that the band R is a combination band in Fermi resonance with the band M, since such resonance occurs for ν_3 and $\nu_1 + \nu_4$ for CCl₄ but not for CBr₄.

No other absorptions were observed which could be assigned to bending vibrations of species M owing to their very low intensity and the long wavelength limit of our spectrophotometer.

The bands labeled X in the CCl₃Br and CClBr₃ spectra in Figures 1 and 2 were both observed in the CCl₂Br₂ spectra. No CCl₄ or CBr₄ counterparts of the X bands were detected, so no assignment is made.

Species M Force-Constant Calculations. For the C_{3v} geometry for species M, the antisymmetric C-X stretch (ϵ) is the highest frequency in its symmetry class. Using symmetry coordinates, one can factor out the antisymmetric stretching coordinate using Wilson's separation of high and low frequencies.¹⁷ For normal-coordinate calculations we need to estimate the X-C-X bond angle. Since the CX₃ part of species M has a large amount of anionic character, we consider the isoelectronic species NX₃. However, the Cl-N-Cl bond angle for NCl₃ is not known so we use the value of 100° which is near the F-N-F bond angle¹⁸ of 102° in NF₃. Such calculations give $F_r - F_{rr} = 1.26$ mdyne/Å for CCl₃Li and 1.14 mdyne/Å for CBr₃Li (and their sodium counterparts, since the same halogen stretching frequencies were observed).

The ¹³C counterpart of the 521-cm⁻¹ band M in the CCl₄ experiment is calculated to be at 505 cm⁻¹ which coincides with the R absorption. However, if the bands M and R are in Fermi resonance, normal-coordinate calculations could not correctly predict the observed carbon-13 shift. Fermi resonance would shift band M to higher frequency while its carbon-13 counterpart would be displaced to lower frequency since the combination band R lies between the band M frequencies for both carbon isotopes and is expected to show little carbon-13 shift. This is the case for ν_3 and $\nu_1 + \nu_4$ of ¹²CCl₄ and ¹³CCl₄ where the carbon-12 and carbon-13 fundamental frequencies are shifted apart by Fermi resonance with the intermediate combination bands. Normal-coordinate calculations for

(15) G. Herzberg, "Infrared and Raman Spectra," D. Van Nostrand Co., Inc., New York, N. Y., 1945.

(16) No detectable amount of LiCCl₃ was produced in the Li-CCl₂Br reaction possibly owing to the fact that the Li-CCl₃ reaction may favor the carbene product relative to the trihalomethyl-lithium compound product more than the Li-CCl₂Br reaction.

(17) E. B. Wilson, Jr., *J. Chem. Phys.*, **9**, 76 (1941).

(18) J. Sheridan and W. Gordy, *Phys. Rev.*, **79**, 513 (1950).

ν_3 (788 cm^{-1}) of $^{12}\text{CCl}_4$ predict ν_3 of $^{13}\text{CCl}_4$ to be 764 cm^{-1} whereas the observed value is 751 cm^{-1} .

Using the C-Li diatomic assumption, for lack of sufficient data prevents a more sophisticated approach, the lithium stretching force constant is calculated to be 0.45 $\text{mdyn}/\text{\AA}$ for CCl_3^6Li and 0.48 $\text{mdyn}/\text{\AA}$ for CCl_3^7Li . The lack of agreement in these two force constants suggests that the vibrational mode involves the chlorine atoms.

Conclusions

The infrared spectra of the trihalomethyl alkali metal compounds are of interest insofar as they provide information on the structure, vibrational potential function, and bonding in these species.

Structure. Observation of a doubly degenerate vibration for the perchloro and perbromo species clearly indicates the presence of threefold symmetry. Presumably the species belong to the C_{3v} point group. This rules out the possibility of the "carbene-salt complex"^{4,5} structure for the molecule, but, of course, it cannot preclude this complex as a reaction intermediate.

Potential Constants. A large number of calculations show that the stretch-stretch interaction force constants for chloro and bromocarbon species are small, around 0.30 $\text{mdyn}/\text{\AA}$. Using this reasonable estimated value for F_{rr} and the calculated values of $F_r - F_{rr}$, we determine $F_{C-Cl} = 1.56 \pm 0.2$ $\text{mdyn}/\text{\AA}$ for CCl_3M and $G_{C-Br} = 1.44 \pm 0.2$ $\text{mdyn}/\text{\AA}$ for CBr_3M . These values are somewhat lower than their tetrahalomethane counterparts as is shown in Table II.

The force constant calculated for the lithium stretching mode is near 0.5 $\text{mdyn}/\text{\AA}$, which compares to 0.8 $\text{mdyn}/\text{\AA}$ found¹¹ for F_{C-Li} of CH_3Li . Since the CX_3Li force constant is based on a vibrational frequency which also involves the halogen atoms, we hesitate to attach any significance to the comparison of the CH_3Li and CX_3Li lithium stretching force constants.

Bonding. Table II also compares stretching force constants for several anions and their neutral counter-

Table II: Stretching Force Constants ($\text{mdyn}/\text{\AA}$) for Anionic Species and Their Neutral Counterparts

CH_4	CCl_4	CBr_4	GeCl_4	SnCl_4	SnBr_4
5.05 ^a	3.08 ^c	2.45 ^d	2.72 ^e	2.50 ^e	2.02 ^e
CH_3Li	CCl_3Li	CBr_3Li	GeCl_3^-	SnCl_3^-	SnBr_3^-
4.32 ^b	1.56	1.44	1.09 ^f	1.18 ^g	1.06 ^g

^a J. L. Duncan and I. M. Mills, *Spectrochim. Acta*, **20**, 523 (1964). ^b Reference 11. ^c Reference 8. ^d Reference 12. ^e Frequencies from K. Nakamoto, "Infrared Spectra of Inorganic and Coordination Compounds," John Wiley and Sons, Inc., New York, N. Y., 1963. ^f Frequencies from M. L. Delwaille, *Compt. Rend.*, **228**, 1585 (1949). ^g Frequencies from L. A. Woodward and M. J. Taylor, *J. Chem. Soc.*, 407 (1962).

parts calculated using the separation of frequencies. An X-M-X bond angle of 100° was assumed for the anions since the isoelectronic PCl_3 molecule¹⁹ has a bond angle near this value. The force constants for the three anions are noticeably lower than those for the neutral species, which is expected since repulsions caused by an additional electron present in the anion are not counterbalanced by the attractions of an equal number of protons as in a neutral molecule. The anion force constants are about half of those for their neutral counterparts, the same relationship observed for CX_3Li and CX_4 . This comparison suggests that CX_3Li is highly ionic, much more so than CH_3Li whose force constant is near 85% of that for methane. We expect CX_3Li to be more ionic than CH_3Li since the CX_3 group stabilizes negative charge better than the CH_3 group.

Since the same antisymmetric carbon-halogen frequencies were observed for the Li and Na compounds, the same amount of anionic character in the CX_3 group is implied. This is not too surprising in view of the almost identical electronegativities of lithium and sodium.

(19) P. Kisliuk and C. H. Townes, *J. Chem. Phys.*, **18**, 1109 (1950).

Dielectric Study of the Hydration of Cyclohexylamine in Benzene

by M. Duane Gregory,^{1a} Harold E. Affsprung,^{1b} and Sherril D. Christian

Department of Chemistry, University of Oklahoma, Norman, Oklahoma 73069 (Received November 16, 1967)

Measurements have been made of the dielectric constant of solutions of water in benzene, cyclohexylamine (CHA) in benzene, and the ternary system H₂O and CHA in benzene. From the dielectric data and results of a previous distribution study of the hydration of CHA in benzene,² dipole moments of CHA, H₂O, and CHA·H₂O (1.33, 1.76, and 2.82 D, respectively) were calculated. The present results support the conclusion of the previous investigation that hydrates of the amine dimer or higher polymers are not present in significant concentrations.

Introduction

Previously, we reported a study of the hydration of cyclohexylamine (CHA) in benzene solution.² Water solubility and partition data were interpreted as indicating that the primary hydrated species is the amine monomer monohydrate. We report here measurements of the dielectric constant of solutions of CHA in benzene at nearly unit water activity. The results support the conclusions of the previous hydration study and permit calculation of the dipole moments of water, CHA, and the 1:1 amine hydrate in benzene.

Experimental Section

Dielectric constants were determined with the Kahl Dipolmeter DMO1, which operates on the superposition (beat) method at approximately 2.0 Mc. A Sola constant voltage transformer was used to maintain a stable current source. A DFL-1 cell (range 1.8 to 3.4 dielectric constant) with a capacity of 30 ml was used for all measurements. The cell was maintained at 25.00 ± 0.02° by means of a Haake constant temperature circulator Model F. Solutions were equilibrated in a 25° temperature bath and transferred to the cell with a 50-ml syringe. The tip of the syringe could be inserted to the bottom of the cell, so that during the time required to introduce a sample very little air entered the cell. The cell was washed with anhydrous ether and flushed with dry nitrogen before adding samples. Solutions were not introduced into the cell until the "dry" cell reading reached a reproducible value.

CHA was purified as before,² and solutions of CHA in benzene were stored in vapor contact with P₂O₅ prior to use. The benzene was washed with concentrated H₂SO₄ until no brown coloration appeared. It was then washed with 20% NaOH and finally H₂O before being distilled over CaH₂. Concentrations of CHA (0.05–0.5 M) were determined by pH titration with a Beckman Zeromatic II pH meter. Solutions of water in benzene were prepared by equilibrating pure benzene with sulfuric acid and calcium chloride solu-

tions of known water activity. The calcium chloride solutions were distributed directly with benzene, whereas the sulfuric acid solutions were allowed to equilibrate with benzene by vapor contact, using the isopiestic equilibrators described previously.³ Water concentrations were determined with a Beckman KF-3 Aquameter; water concentrations ranged from 0.005 to 0.0350 M. Ternary mixtures of CHA, water, and benzene were prepared by partitioning CHA between benzene and water. Since very little benzene and CHA are present at equilibrium in the water-rich phase, it was assumed that the water activity is equal to unity in these systems.

Results

Figures 1 and 2 show data obtained for the two-component systems, CHA–benzene and water–benzene. It appears that the dielectric constant, ϵ varies linearly with the formal concentration of solute in both systems. The results were analyzed by using a form of the Clausius–Mosotti equation⁴ suitable for treating dielectric data for dilute solutions of polar solute molecules in a nonpolar solvent

$$\epsilon = n_m^2 + 4\pi f_A((n_m^2 + 2)\mu/3)^2/3kT$$

where n_m is the refractive index of the pure solvent (1.5 for benzene at 25°), μ is the dipole moment of the solute, and f_A is the concentration of the solute. From the slopes of the straight lines in Figures 1 and 2 (0.216 and 0.376 M⁻¹), the dipole moments of CHA and water are calculated to be 1.33 and 1.76 D, respectively. These values compare well with literature values 1.33⁵ and 1.34 D⁶ for CHA and 1.71,^{7a} 1.72,^{7b} and 1.835 D⁸ for water in benzene.

(1) (a) Abstracted in part from the Ph. D. dissertation of M. Duane Gregory, University of Oklahoma, Norman, Okla., 1969; (b) Deceased August 5, 1967.

(2) M. D. Gregory, S. D. Christian, and H. E. Affsprung, *J. Phys. Chem.*, **71**, 2283 (1967).

(3) S. D. Christian, H. E. Affsprung, J. R. Johnson, and J. D. Worley, *J. Chem. Educ.*, **40**, 419 (1963).

(4) L. Onsager, *J. Am. Chem. Soc.*, **58**, 1486 (1936).

(5) G. L. Lewis and C. P. Smyth, *ibid.*, **61**, 3067 (1939).

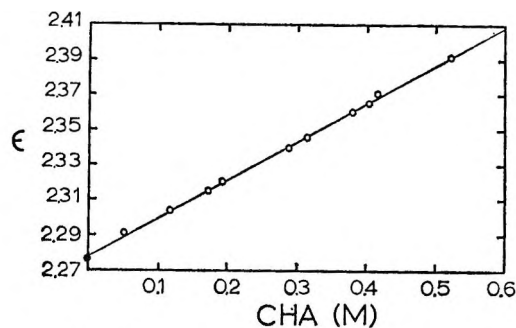


Figure 1. Dielectric constant of CHA-benzene system at 25°.

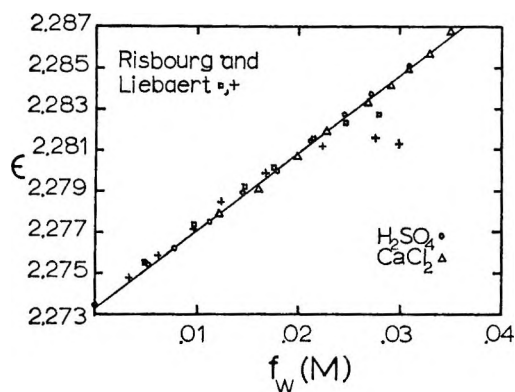
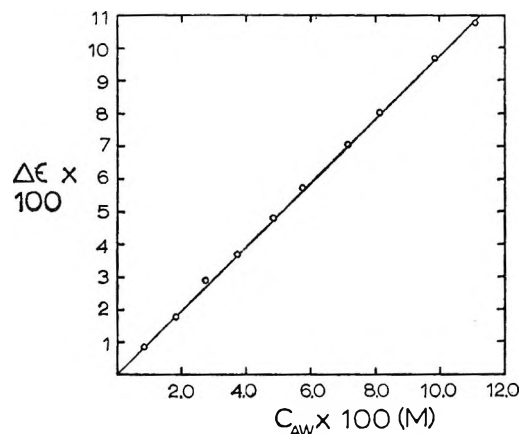


Figure 2. Dielectric constant of water-benzene system at 25°.

The dipole moment of the CHA monohydrate was determined by applying a method similar to that described in a previous publication from this laboratory.⁹ The concentrations of the amine monomer, water monomer, and amine monomer monohydrate were calculated from values of the equilibrium constant for hydrate formation² (6.74 l./mole at 25°) and the known solubility of water in benzene at 25° (0.0350 M). Since the water activity, and hence the concentration of the free water molecules in benzene, is virtually constant, the increase in the dielectric constant of ternary mixtures with increase in amine concentration at constant water activity may be attributed to only two species, the CHA monomer and CHA·H₂O. From the calculated CHA monomer concentration and the data in Figure 1, the contribution of free CHA molecules to the increase in dielectric constant may be computed and subtracted from the observed increase in dielectric constant attributable to both amine species. The difference, $\Delta\epsilon$, is assumed to be contributed solely by the species CHA·H₂O; $\Delta\epsilon$ is plotted against C_{AW} , the calculated concentration of CHA·H₂O, in Figure 3. From the slope of the curve, 0.971 M⁻¹, a dipole moment of the complex of 2.82 D may be calculated.

Discussion

It is worthwhile considering how the presence of species other than the 1:1 hydrate will influence the dependence of $\Delta\epsilon$ on solute concentration. From

Figure 3. Contribution of CHA·H₂O to the total dielectric constant at 25°.

measurements of the distribution ratios of a polar solute between water and an organic solvent and the solubility of water in solutions of the solute at various water activities, the important quantity Δf_w can be obtained as a function of a_w and f_A . (Δf_w is defined as the increase in formal solubility of water at a given a_w owing to the presence of the dissolved polar solute.) If only the 1:1 hydrate is present, as seems to be indicated by the previous study of the hydration of cyclohexylamine,² Δf_w will be equal to C_{AW} . In this case, the value of the dipole moment of AW can be inferred directly from the slope of a plot of $\Delta\epsilon$ vs. Δf_w (equivalent to Figure 3) without use of a numerical value of the hydrate formation constant.

If several different hydrates of the monomer of the polar solute are present, the ratio $\Delta\epsilon/\Delta f_w$ is given by

$$\frac{\alpha_{11}K_{11}C_A C_W + \alpha_{12}K_{12}C_A C_W^2 + \dots}{K_{11}C_A C_W + 2K_{12}C_A C_W^2 + \dots}$$

where C_A and C_W are concentrations of uncomplexed (monomeric) polar solute and water, respectively; K_{11} , K_{12} , ... are formation constants for the monomer monohydrate, monomer dihydrate, ...; and α_{11} , α_{12} , ... are proportionality constants between the concentrations of the individual hydrated species and the increment in dielectric constant contributed by these species. Since C_A is present to the first power in each term in the numerator and denominator, the ratio $\Delta\epsilon/\Delta f_w$ is constant at a fixed water activity. Thus, in spite of the fact that a number of distinct hydrates of the monomer are present, a plot of $\Delta\epsilon$ vs. Δf_w will be linear.

On the other hand, if a hydrate of the dimer (or

(6) M. Aroney and R. J. W. Le Fèvre, *J. Chem. Soc.*, 3600 (1960).

(7) (a) J. W. Williams, *Physik Z.*, 29, 204 (1928); (b) J. W. Williams, *J. Am. Chem. Soc.*, 52, 1838 (1930).

(8) A. Risbourg and R. Liebaert, *Compt. Rend.*, 264C, 237 (1967).

(9) T. F. Lin, S. D. Christian, and H. E. Affsprung, *J. Phys. Chem.*, 71, 1133 (1967).

other polymeric species of the polar solute) is present in addition to hydrates of the monomer, curvature is expected in a plot of $\Delta\epsilon$ vs. Δf_w . For example, if only the 1:1 and 2:1 hydrates exist

$$\frac{\Delta\epsilon}{\Delta f_w} = \frac{\alpha_{11}K_{11}C_A C_w + \alpha_{21}K_{21}C_A^2 C_w}{K_{11}C_A C_w + K_{21}C_A^2 C_w} = \frac{\alpha_{11}K_{11} + \alpha_{21}K_{21}C_A}{K_{11} + K_{21}C_A}$$

and except in the unique case where $\alpha_{11} = \alpha_{21}$, the ratio will depend upon C_A , and hence upon Δf_w . Therefore, the linearity of the plot in Figure 3 is consistent with the conclusion of the previous report that hydrates of polymeric amine species are not present in significant concentrations, although the dielectric results at unit water activity do not by themselves preclude the possibility that polyhydrates of the amine monomer exist.

As mentioned in the previous section, values of dipole moment given here for the monomers of CHA and water in benzene are in reasonable agreement with literature values. However, the data in Figure 2 for water in benzene do not agree with the results of Risbourg and Liebaert⁸ for water concentrations greater than about 0.02 *M* (included in Figure 2). These authors noted that the dielectric constant increases less rapidly for a given increment in water concentration at the higher water activities, and from the curving over of the plot of $\Delta\epsilon/\epsilon$ vs. f_w , they attempted to calculate polymerization constants for water in benzene. We have been unable to detect the negative curvature reported by Risbourg and Liebaert, although the dielectric data recorded in Figure 2 cover a range of concentrations extending all the way to saturation of benzene by water. Possibly the observed curvature resulted from the method used by these workers to prepare their samples; water was apparently added directly to benzene, and the heterogeneous mixture was warmed several degrees above room temperature, with shaking, to promote dissolution of the water. We have been unsuccessful in preparing homogeneous solutions of water in benzene using this method. For example, if approximately half as much water as is required for saturation is added to pure, anhydrous benzene, vigorous shaking for over 24 hr does not cause all the water to dissolve. On the other hand, it has been demonstrated that isothermal equilibration of pure benzene with water solutions of known activity (either directly by distribution of the two phases or by vapor phase equilibration) does lead to the attainment of equilibrium within 8 to 10 hr.³ We believe the slowness of attainment of equilibrium in experiments in which water is added directly to pure benzene is due to the very small surface area of the water droplets in comparison with the interfacial areas of the organic and aqueous

solutions employed in the equilibration methods utilized in the present study. Our conclusion that water is essentially monomeric in benzene is in agreement with results of recent isopiestic and vapor pressure studies of water-benzene mixtures.^{10,11}

The calculated dipole moment of CHA·H₂O (2.82 D) is similar in magnitude to moments reported for other hydrogen-bonded complexes of amines with hydroxylic proton donors. Table I gives values of the dipole moments of some amine complexes taken from the literature.¹²⁻¹⁷

Table I

Complex	μ, D	Ref
Triethylamine- <i>n</i> -butyl alcohol	2.34	12, 13
Triethylamine- <i>t</i> -butyl alcohol	2.24	12, 13
Triethylamine-chloroform	2.07	14
Pyridine-phenol	3.44	15
Pyridine- <i>n</i> -butyl alcohol	3.37	16
Triethylamine-pyrrole	3.10	17

A reasonable model for the CHA-water complex is shown in Figure 4. The dipole of the amine is assumed to be directed along the N···H-O axis, and it is supposed that the water molecule is free to rotate about this axis. If no charge separation were to occur on formation of the hydrogen bond, this model would lead to a predicted value of the dipole moment of the complex of 2.40 D, computed from vector addition of the values of dipole moment of the monomers of amine and water. We conclude that the difference between the observed and computed dipole moment of the complex (0.4 D) is due to charge separation. In this connection, it may be noted that results of a similar study of the 1:1 hydrate of acetone in 1,2-dichloroethane led to the conclusion that the complex dipole moment was practically equal to that computed from vector addition of the dipole moments of monomeric water and acetone.⁹

Several authors have proposed that a charge separation occurs when an amine bonds to a proton donor.^{12,18-20}

(10) S. D. Christian, H. E. Affsprung, and J. R. Johnson, *J. Chem. Soc.*, 1896 (1963).

(11) W. L. Masterton and M. C. Gendrano, *J. Phys. Chem.*, **70**, 2895 (1966).

(12) J. W. Smith, *J. Chim. Phys.*, **61**, 125 (1964).

(13) A. H. Boud and J. W. Smith, *J. Chem. Soc.*, 4507 (1956).

(14) C. F. Jumper and B. B. Howard, *J. Phys. Chem.*, **70**, 588 (1966).

(15) R. J. Bishop and L. E. Sutton, *J. Chem. Soc., Suppl.*, 6100 (1964).

(16) D. Cleverdon, G. B. Collins, and J. W. Smith, *J. Chem. Soc.*, 4499 (1956).

(17) D. Bertin and H. Lumbroso, *Compt. Rend.*, **263C**, 181 (1966).

(18) T. Zeegers-Huyskens, *Spectrochim. Acta*, **21**, 221 (1965).

(19) R. A. Heacock and L. Marion, *Can. J. Chem.*, **34**, 1782 (1956).

(20) G. C. Pimentel and C. H. Sederholm, *J. Chem. Phys.*, **24**, 639 (1956).

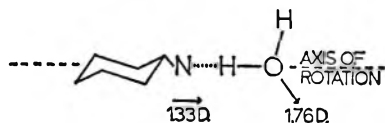


Figure 4. Model of the $\text{CHA} \cdot \text{H}_2\text{O}$ complex.

Infrared spectra and dielectric data have been the primary methods utilized in these studies. In many cases an apparent enhancement of the dipole moment of the complex over that which is calculated from an appropriate model is found. Zeegers-Huyskens¹⁸ used infrared spectral measurements to investigate the interaction of *n*-propylamine with proton donors having aqueous $\text{p}K_a$ values ranging from 16 to 0.8. She concluded that for donors having $\text{p}K_a$ values of 9 or less, charge separation significantly alters the appearance of the $\text{O}-\text{H} \cdots \text{N}$ and $\text{N}-\text{H}$ stretch bands. The $\text{O}-\text{H} \cdots \text{N}$ band disappears in compounds with $\text{p}K_a < 9$ and a large band appears in the region 2750–2500 cm^{-1} . This new band was attributed to the $\text{N}-\text{H}^+ \cdots \text{O}$ stretching vibration. Smith¹² and Jumper and Howard¹⁴ have used the dielectric method to investigate the dipole moments of hydrogen-bonded complexes. They report dipole enhancements of amine complexes ranging from 0.4 D for weak proton donors to 6 D for donors with very low $\text{p}K_a$ values. Hulett, Pegg, and Sutton²¹ report enhancements of 1.00, 1.26, and 0.91 D for trimethylamine complexed with phenol, *p*-chlorophenol, and *p*-cresol, respectively, in cyclohexane. Smith and coworkers^{13,16} have determined

the dipole enhancement of the complexes formed by triethylamine and pyridine with *n*- and *t*-butyl alcohol. They concluded that the enhancement in the triethylamine complexes is greater than that in the pyridine complexes by 0.18 and 0.25 D for the *n*- and *t*-butyl alcohol complexes, respectively.

The dielectric method should be more widely applied than it presently is in inferring the geometry and charge distribution of complexes, but in our opinion reasonable conclusions can be drawn only if equilibrium constants and stoichiometries of association reactions are known from spectral or classical studies before attempts are made to interpret dielectric results. The technique utilized in the present investigation simplifies the interpretation of data, inasmuch as the concentration of one of the reactive species (the water monomer) is held constant in the ternary system. This makes it possible to infer the contribution of the associated species to the dielectric constant of the solution with a minimum of calculation.

Acknowledgment. The authors are indebted to the Office of Saline Water for a grant (GS-14-01-0001-1315) in support of this research. M. D. G. wishes to express his appreciation for a Public Health Service Fellowship (5-F1-GM-30, 419-03) from the National Institute of General Medical Sciences. The authors also wish to thank Dr. F. Kohler for his interest and helpful suggestions.

(21) J. R. Hulett, J. A. Pegg, and L. E. Sutton, *J. Chem. Soc.*, 3901 (1955).

Studies of Membrane Phenomena. VI. Further Study of Volume Flow

by Y. Kobatake, M. Yuasa, and H. Fujita

Department of Polymer Science, Osaka University, Toyonaka, Japan (Received November 16, 1967)

Volume flows (J_v) of aqueous solutions of KCl and LiCl through oxidized collodion membranes were measured under the condition in which either pressure difference Δp or electric potential difference $\Delta\zeta$ was applied externally across the membrane, and for each system the electroosmotic coefficient ω_{12} defined by $-L(J_v/\Delta\zeta)_{\Delta p=0}$ and the hydraulic coefficient ω_{22} defined by $-L(J_v/\Delta p)_{\Delta\zeta=0}$ (where L is the effective thickness of the membrane) were calculated from these data as functions of the concentration of the external electrolyte solution. Expressions for these phenomenological coefficients were derived on the basis of the thermodynamics of irreversible processes in conjunction with an approximate hydrodynamic equation for the movement of the local center of mass. They showed that both ω_{12} and ω_{22} are composed of two parts, one associated with the movement of individual ions relative to the local center of mass and the other with the mass flow. The former term in each coefficient was estimated approximately using our previous assumptions for the mobilities and activities of mobile ions in charged membranes. Comparison with the experimentally determined values of ω_{12} and ω_{22} indicated that the contribution of this term to either coefficient was essentially negligible. Thus for the membrane-electrolyte systems studied the observed volume flows can be argued to have consisted mainly of the mass flow. The observed values of the electroosmotic coefficient approached a nonzero value even at the limit of high electrolyte concentration and, on the average, accorded well with those derived from osmosis data in a previous part of this series.

Introduction

Part V of this series¹ dealt with the volume flow of liquid which occurs in the system where an ionizable membrane separates bulk solutions of a 1:1 electrolyte of different concentrations. The consideration was confined to the case where neither hydrostatic pressure nor electric field is applied externally across the membrane. Moreover, it was assumed that the system is maintained at a constant temperature. The present paper considers the volume flow occurring under the condition that there are no gradients of concentration and temperature between the bulk solutions but they are subject to externally applied differences in pressure and electric potential. In doing this, emphasis is placed on taking the movement of the local center of mass explicitly into account, with the interest in obtaining relations which allow the contributions of mass flow to electroosmotic and pressure flows to be evaluated. With respect to this point, the present study may be differentiated from those of previous authors²⁻⁶ who concerned themselves with these flow processes. Application of the theory is made to data which are obtained with oxidized collodion membranes over wide ranges of concentration of aqueous KCl and LiCl.

Theoretical Section

The system considered is the same as in part V, except that here the concentrations of the bulk solutions on both sides of the membrane are taken to be equal (denoted by C in moles/cc). The electric potential and pressure differences applied externally across the membrane are denoted by $\Delta\zeta$ and Δp , respectively. It is assumed, as before, that the flow of

water (denoted by subscript w) and those of cation and anion (designated by subscripts $+$ and $-$) occur, on the average, only in the direction (x) perpendicular to the membrane surfaces. Considerations below are restricted to the system which is in the steady state.

Then, according to the thermodynamics of irreversible processes, the electric current density I and the volume flow J_v , both relative to the frame fixed to the membrane, are represented by⁷

$$I = -\sum_{j,k} e_j (L_{jk})_m \left[e_k \frac{d\zeta}{dx} + \left(\bar{V}_k - \frac{M_k}{M_w} \bar{V}_w \right) \frac{dp}{dx} \right] + \sum_j e_j C_j U_m \quad (1)$$

$$J_v = -\sum_{j,k} \left(\bar{V}_j - \frac{M_j}{M_w} \bar{V}_w \right) (L_{jk})_m \times \left[e_k \frac{d\zeta}{dx} + \left(\bar{V}_k - \frac{M_k}{M_w} \bar{V}_w \right) \frac{dp}{dx} \right] + U_m \quad (2)$$

Here $(L_{jk})_m$ ($k, j = +, -$) are the mass-fixed phenomenological coefficients and obey the Onsager reciprocal relation $(L_{+-})_m = (L_{-+})_m$; e_j , \bar{V}_j , C_j , and M_j are the

(1) Y. Toyoshima, Y. Kobatake, and H. Fujita, *Trans. Faraday Soc.*, **63**, 2828 (1967).

(2) D. Mackay and P. Meares, *ibid.*, **55**, 1221 (1959).

(3) C. W. Carr, R. McClintock, and K. Sollner, *J. Electrochem. Soc.*, **109**, 251 (1962).

(4) N. Lakshminarayanaiah and V. Subrahmanyam, *J. Polymer Sci.*, **A2**, 4491 (1964).

(5) J. H. B. George and R. A. Courant, *J. Phys. Chem.*, **71**, 246 (1967).

(6) J. Greyson, *ibid.*, **71**, 259 (1967).

(7) S. R. deGroot and P. Mazur, "Non-Equilibrium Thermodynamics," North-Holland Publishing Co., Amsterdam, 1962, p 423.

molar electric charge, partial molar volume, concentration in moles/cc, and molar weight of species j (w , $+$, $-$); U_m is the velocity of the local center of mass; ζ is the local electric potential; and p is the local pressure. Neglecting, as before, interacting flows between different ion species and introducing the mass-fixed ionic mobilities, u_+ and u_- , in terms of the coefficients $(L_{++})_m$ and $(L_{--})_m$, eq 1 and 2 are transformed to give

$$I = -(u_+C_+ + u_-C_-)F\frac{d\zeta}{dx} - (\bar{V}_+^*u_+C_+ - \bar{V}_-^*u_-C_-)\frac{dp}{dx} + (e_+C_+ + e_-C_-)U_m \quad (3)$$

$$J_v = -(\bar{V}_+^*u_+C_+ - \bar{V}_-^*u_-C_-)\frac{d\zeta}{dx} - \frac{1}{F}(\bar{V}_+^*u_+C_+ + \bar{V}_-^*u_-C_-)\frac{dp}{dx} + U_m \quad (4)$$

where \bar{V}_k^* ($k = +, -$) stands for

$$V_k^* = V_k - \frac{M_k}{M_w} \bar{V}_w \quad (5)$$

and F is the Faraday constant.

In part V we set the last term on the right-hand side of eq 3 equal to FXU_m , since formally the condition of electric neutrality requires $e_+C_+ + e_-C_- = FX$. Here X represents the density of electric charges fixed on the polyelectrolyte molecules constituting the membrane and is expressed in equiv/cc of membrane phase. However, this assignment assumes that all excess counterions, *i.e.*, those dissociated from the membrane skeletons, are carried by mass flow. In reality, only a fraction of them may migrate with mass flow and contribute to the flow of electricity, since the electrostatic interaction of the membrane polyions tends to immobilize part of the counterions in their vicinity. Thus it is more appropriate to write the last term in eq 3 as $F\psi XU_m$, where ψ is a dimensionless parameter to represent the fraction of X that can be conveyed by mass flow.

Following the argument given in part V, the steady-state value of U_m may be represented by the approximate hydrodynamic equation

$$U_m = -k\frac{dp}{dx} - k(e_+C_+ + e_-C_-)\frac{d\zeta}{dx} \quad (6)$$

where k is a constant which may depend on the fluidity of solvent as well as the compactness and other structural characteristics of the membrane. Formal application of the condition of electric neutrality again requires setting the term $e_+C_+ + e_-C_-$ in this equation equal to FX . However, physically, this term represents the number density of excess counterions which can transmit the external electric force acting on them to their surrounding liquid medium. We assume here that such "effective" counterions are

ones which can migrate with mass flow. If this is the case, the term $e_+C_+ + e_-C_-$ in eq 6 may also be written $F\psi X$, with the dimensionless parameter ψ introduced above.

With these assignments to $e_+C_+ + e_-C_-$ in eq 3 and 6, substitution of eq 6 into eq 3 and 4, followed by integration of the resulting equations over the membrane thickness (L) under the steady-state condition ($dI/dx = 0$ and $dJ_v/dx = 0$), gives

$$I = -\omega_{11}(\Delta\zeta/L) - \omega_{12}(\Delta p/L) \quad (7)$$

$$J_v = -\omega_{21}(\Delta\zeta/L) - \omega_{22}(\Delta p/L) \quad (8)$$

where the coefficients ω_{ij} ($i, j = +, -$) are represented by

$$\omega_{11} = (u_+C_+ + u_-C_-)F + kF^2(\psi X)^2 \quad (9)$$

$$\omega_{12} = \omega_{21} = (\bar{V}_+^*u_+C_+ - \bar{V}_-^*u_-C_-) + kF\psi X \quad (10)$$

$$\omega_{22} = (\bar{V}_+^*u_+C_+ - \bar{V}_-^*u_-C_-)(1/F) + k \quad (11)$$

It should be noted that, in deriving eq 7 and 8, the parameter ψ may not be treated as independent of ion concentrations.

The result that $\omega_{12} = \omega_{21}$ indicated by eq 10 is the familiar Saxèn relation.⁸ Tracing back the above development, we find that this relation is a consequence of our assumption made above for the term $e_+C_+ + e_-C_-$ in eq 3 and 6. The ample experimental evidence so far reported⁹ on the Saxèn relation may be taken as a justification of this assumption.

All ω_{ij} are composed of two terms. The first term in each coefficient refers to the movement of individual ions relative to the local center of mass and may not vanish even when the charge density of the membrane is diminished. On the other hand, the second term is associated with the mass flow caused by gradients of pressure and electric potential, and depends on the charge density and structural details of the membrane as well as the fluidity of solvent.

From eq 7 it follows that

$$\omega_{11} = -L(I/\Delta\zeta)_{\Delta p=0} = L/r \quad (12)$$

where r is the electrical resistance of the membrane per unit area in the absence of pressure gradient (and of concentration gradient as well). Since this quantity has been studied separately in part III,¹⁰ no further comment on ω_{11} is made below.

From eq 8, we obtain

$$\omega_{12}/\omega_{11} = (J_v/I)_{\Delta p=0} \quad (13)$$

which may be combined with eq 12 to give

$$\omega_{12} = L(J_v/Ir)_{\Delta p=0} = [J_v/(\Delta\zeta/L)]_{\Delta p=0} \quad (14)$$

(8) U. Saxèn, *Ann. Physik*, **47**, 46 (1892).

(9) D. G. Miller, *Chem. Rev.*, **60**, 15 (1960).

(10) Y. Toyoshima, M. Yuasa, Y. Kobatake, and H. Fujita, *Trans. Faraday Soc.*, **63**, 2803 (1967).

This indicates that ω_{12} is the volume flow produced by an electric field of unit strength in the absence of pressure gradient (and of concentration gradient as well). Thus this coefficient may be termed the electroosmotic coefficient of a given system.

Finally, it also follows from eq 8 that

$$\omega_{22} = -[J_v/(\Delta p/L)]_{\Delta \zeta=0} \quad (15)$$

which indicates that ω_{22} is the volume flow produced when the membrane is subject to unit pressure gradient in the absence of electric potential gradient (and of concentration gradient as well). Thus with the larger ω_{22} , the membrane is more permeable to liquid under a pressure gradient. Hence we may term ω_{22} the hydraulic permeability of a given membrane.

Equations 12, 14, and 15 tell how the coefficients ω_{11} , ω_{12} , and ω_{22} can be determined from experiment. For instance, ω_{12} can be obtained by measuring J_v (volume of liquid transferred through 1 cm² of the membrane in 1 sec) as a function of $\Delta \zeta/L$ (electric potential gradient) under the condition where there exists no difference of hydrostatic pressure (and of concentration) across the membrane, followed by evaluating the slope of J_v against $\Delta \zeta/L$. In practice, first J_v may be measured as a function of electric current density I , and then the slope of J_v vs. I may be multiplied by the value of L/r which can be determined from a separate resistance measurement conducted under the same experimental conditions.

Once data for ω_{1j} are obtained in this way, we can proceed to examine the relative contributions of the two terms comprising each coefficient. The experiment described below was undertaken to obtain data relevant for this purpose.

Experimental Section

Two oxidized collodion membranes numbered 2 and 3 in part V, together with one newly oxidized collodion membrane numbered 4, were chosen for the present measurements. For each of these membranes, data

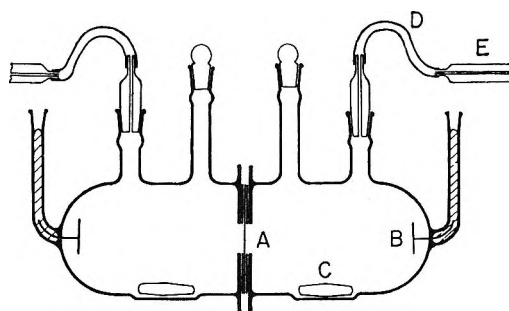


Figure 1. Schematic diagram of the cell used for measurements of the volume flows, $(J_v/I)_{\Delta p=0}$ and $(J/\Delta p)_{I=0}$: A, membrane; B, Ag-AgCl plate electrode; C, stirrer; D, Teflon tubing; E, capillary.

were taken over wide ranges of C of KCl and LiCl. Table I summarizes pertinent characteristics of these membrane-electrolyte pairs.

Before use, each membrane was thoroughly conditioned with a concentrated solution of a given electrolyte, following the procedure described in part III.¹⁰

Figure 1 shows a schematic diagram of the cell used. The bulk solutions of equal concentration C on both sides of the membrane were stirred vigorously by a pair of magnetic stirrers in order to maintain them uniform in composition. The cell was immersed in a water bath thermostatted at $30 \pm 0.02^\circ$, and moreover, the entire system was placed in an air bath of 30° . Great care was taken to prevent the solution from leaking out of the cell and joint portions.

The solution in the cell was led to two horizontally mounted capillaries of uniform bore through Teflon tubing, and the movement of the liquid meniscus in one of them was followed as a function of time by a travelling microscope. In every case treated, plots of the distance travelled by the liquid meniscus against time became accurately linear after some interval of time from the start of a particular run. The slope of this linear portion multiplied by a factor λ^{-1} ($=S_c/S_m$) was taken as the steady-state value of J_v under given experimental conditions. Here S_c denotes the cross section of either capillary and S_m the effective area of the membrane.

Electric current was delivered to the cell from a battery through a pair of Ag-AgCl electrodes mounted as shown in Figure 1, and its strength was measured with a microammeter connected in series. During the measurement at a given electric current, the two capillaries were held at an equal level so as to obtain the condition $\Delta p = 0$. At any concentration of the external solution, plots of J_v against I were accurately linear over the range of I studied (0–20 mA/cm²).

Pressure difference Δp was applied across the membrane by shifting one of the capillaries relative to the other in the vertical direction. The distance between them was measured accurately by means of a cathetometer. Δp was varied in the range from 0 to 20 cm in

Table I: Some Characteristics of Membrane-Electrolyte Pairs Studied

Mem-brane	Elec-trolyte	$\phi^X \times 10^2$, equiv/l.	α^b
2	KCl	1.20 ^a	0.50
	LiCl	1.31	0.37
3	KCl	1.91 ^a	0.50
	LiCl	1.97	0.37
4	KCl	1.70 ^c	0.50
	LiCl	1.70	0.37

^a Taken from Table I of part III. ^b $\alpha = u_+^0/(u_+^0 + u_-^0)$, taken from Table I of part IV. ^c Actually, the values of ϕ^X for membrane 4 determined from membrane potential data by the method described in part IV.

water, and in this range J_v increased linearly with Δp . The measurements were made under the condition of no electric current being delivered to the cell. Therefore, the resulting data for J_v did not exactly correspond to the absence of potential gradient across the membrane, but must have contained a contribution from the so-called streaming potential. However, as shown in the Appendix, this effect was negligibly small in the membrane-electrolyte systems studied. Thus, in the presentation below, data obtained under $I = 0$ are simply taken as those corresponding to the condition $\Delta\zeta = 0$.

Results and Discussion

Hydraulic Permeability. Figure 2 plots data for $\omega_{22}/L (= -(J_v/\Delta p)_{\Delta\zeta=0})$ on membranes 3 and 4 as a function of $\log C$. One can conclude from this graph that ω_{22}/L is essentially independent not only of the species and concentration of electrolyte but also of the charge density of the membrane. The average value of the plotted data is indicated by a horizontal line and yields $8.2 \times 10^{-11} \text{ cm}^3 \text{ dyne}^{-1} \text{ sec}^{-1}$. All membranes examined had essentially the same thickness of about 0.05 cm. Hence ω_{22} for the systems studied was about $4.1 \times 10^{-12} \text{ cm}^4 \text{ dyne}^{-1} \text{ sec}^{-1}$ on the average.

Our problem now is to estimate the contributions of the first and second terms of eq 11 to this experimental value of ω_{22} . To this end, we invoke our previous assumptions¹ for the mobilities and activity coefficients of mobile ions in charged membranes, together with the Donnan equilibrium between the membrane phase and the external salt solution. Then it is shown that the first term in question is represented by

$$\begin{aligned} \bar{V}_+^{*2}u_+C_+ + \bar{V}_-^{*2}u_-C_- = \\ (\Lambda_0/2)[\bar{V}_+^{*2}\alpha + \bar{V}_-^{*2}(1-\alpha)]Z(C,\phi X) + \\ (\Lambda_0/2)[\bar{V}_+^{*2}\alpha - \bar{V}_-^{*2}(1-\alpha)](\phi X) \end{aligned} \quad (16)$$

where

$$Z(C,\phi X) = (4C^2 + \phi^2 X^2)^{1/2} \quad (17)$$

$$\Lambda_0 = u_+^0 + u_-^0 \quad (18)$$

$$\alpha = u_+^0/(u_+^0 + u_-^0) \quad (19)$$

and u_+^0 and u_-^0 are the mobilities of cation and anion species in polyelectrolyte-free solution. In deriving eq 16, it has been assumed, in conformity to our previous finding with oxidized collodion membranes, that the thermodynamically effective charge density of the membrane, ϕX , and the hydrodynamically effective one, $\phi'X$, have the same value;^{10,11} for the meaning of these effective charges the reader is referred to part III of this series. Actually, this assumption need not be introduced, but it is pertinent for the present purpose.

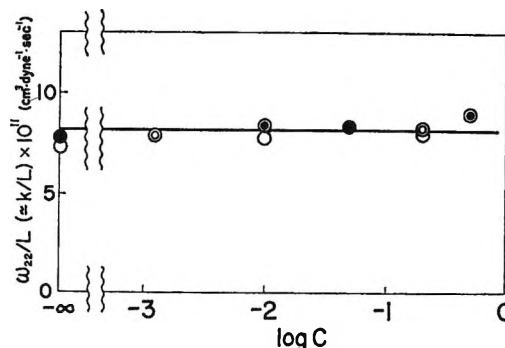


Figure 2. Plots of ω_{22}/L against $\log C$ for membranes 3 and 4 with KCl, LiCl, and distilled water: \circ , membrane 3 with KCl; \bullet , membrane 3 with LiCl; \odot , membrane 4 with KCl; \odot , membrane 4 with LiCl; C is expressed in moles/l.

For KCl, $\alpha = 0.5$, so eq 16 is simplified to

$$\begin{aligned} \bar{V}_+^{*2}u_+C_+ + \bar{V}_-^{*2}u_-C_- = (\Lambda_0/4)[(\bar{V}_+^{*2} + \\ \bar{V}_-^{*2})Z(C,\phi X) + (\bar{V}_+^{*2} - \bar{V}_-^{*2})(\phi X)] \end{aligned} \quad (20)$$

In order to evaluate the right-hand side of this equation, the values of \bar{V} for K^+ and Cl^- must be known. Unfortunately, these are not experimentally accessible quantities. Therefore, we estimate them in terms of the Stokes radii of individual ions using the relation

$$\bar{V}_i = (4\pi N_A/3)r_i^3 \quad (21)$$

where N_A is the Avogadro number and r_i is the Stokes radius of ion species i . Using literature values for r_{K^+} and r_{Cl^-} ,¹² we obtain $\bar{V}_{K^+} = 19.5 \text{ cc/mole}$ and $\bar{V}_{Cl^-} = 18.2 \text{ cc/mole}$. Hence, with \bar{V}_w being taken as 18.1 cc/mole

$$\bar{V}_{K^+}^* = -19.6 \text{ cc/mole}; \quad \bar{V}_{Cl^-}^* = -17.3 \text{ cc/mole}$$

Introduction of these values, together with $\Lambda_0 F = 122 \text{ cm}^2 \text{ ohm}^{-1} \text{ equiv}^{-1}$ for KCl in water at 30° ¹³ and $\phi X = 2 \times 10^{-5} \text{ equiv/cc}$ for membrane 2-KCl (see Table I), into eq 20 gives $4.4 \times 10^{-16} \text{ cm}^4 \text{ dyne}^{-1} \text{ sec}^{-1}$ for $\bar{V}_+^{*2}u_+C_+ + \bar{V}_-^{*2}u_-C_-$ at $C = 1 \text{ mole/l}$. This value is negligibly small compared with the experimental value of ω_{22} . Similar results are deduced at other values of C as well as for other pairs of membrane and electrolyte treated. Therefore we can conclude that for the present systems the contribution of the first term of eq 11 to the observed hydraulic permeability was negligible. Thus Figure 2 may be taken as representing the values of k/L for these systems, and a value of $8.2 \times 10^{-11} \text{ cm}^3 \text{ dyne}^{-1} \text{ sec}^{-1}$ can be assigned to their average.

Electroosmotic Coefficient. Figure 3 shows that ex-

(11) Y. Toyoshima, Y. Kobatake, and H. Fujita, *Trans. Faraday Soc.*, **63**, 2814 (1967).

(12) H. S. Harned and B. B. Owen, "The Physical Chemistry of Electrolyte Solutions," Reinhold Publishing Corp., New York, N. Y., 1957, p 217.

(13) "Landolt-Börnstein Tabellen," II-7, 6th ed, Springer, Berlin, Göttingen, and Heidelberg, 1960, pp 54, 88.

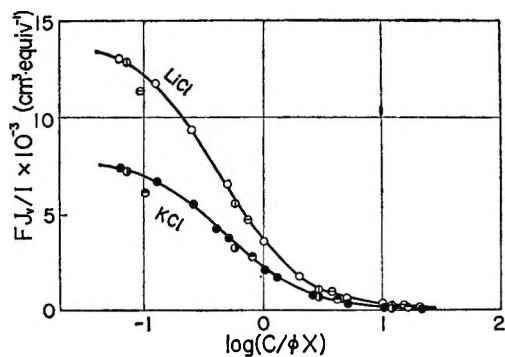


Figure 3. Plots of $F(J_v/I)_{\Delta p=0}$ against the reduced concentration $C/\phi X$ for membranes 2, 3, and 4 with KCl and LiCl: ●, membrane 2 with KCl; ●, membrane 3 with KCl; ●, membrane 4 with KCl; ○, membrane 2 with LiCl; ○, membrane 3 with LiCl; ○, membrane 4 with LiCl.

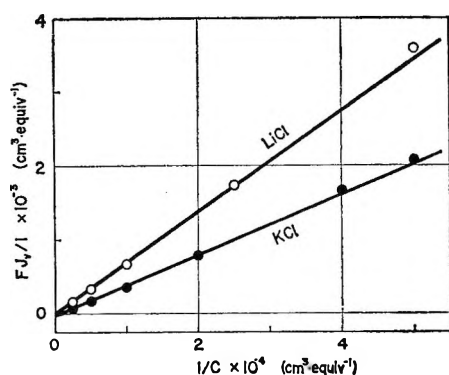


Figure 4. Plots of $F(J_v/I)_{\Delta p=0}$ against $1/C$ for membrane 3 with KCl and LiCl: ●, KCl; ○, LiCl.

perimental values of $F(J_v/I)_{\Delta p=0}$ for membranes of different charge density in solutions of either KCl or LiCl collect to a single composite curve when plotted against a reduced concentration defined by $C/\phi X$. Here the necessary values for ϕX have been taken from Table I. In Figure 4 is shown the behavior of $F(J_v/I)_{\Delta p=0}$ in the region of high salt concentration for membrane 3 in KCl and LiCl. It is interesting to see the plotted points for a given system follow a straight line over a remarkably wide range of C^{-1} and the line nearly passes through the coordinate origin.

The data of Figure 3 can be transformed to those of $-(J_v/\Delta \zeta)_{\Delta p=0}$, *i.e.*, ω_{12}/L according to eq 14, provided that electric resistance data r for these membrane-electrolyte systems are available. Actually, such data have been obtained in part III for membranes 2 and 3, but not yet for membrane 4. Therefore, in this paper, we present ω_{12}/L only for the former two membranes. The results are shown in Figures 5 and 6. In deriving these curves, use was made of smoothed data for both $(J_v/I)_{\Delta p=0}$ and r , since the measurements of these quantities had not been performed at exactly identical values of C .

The order of magnitude of the first term on the right-hand side of eq 10 may be estimated by the same

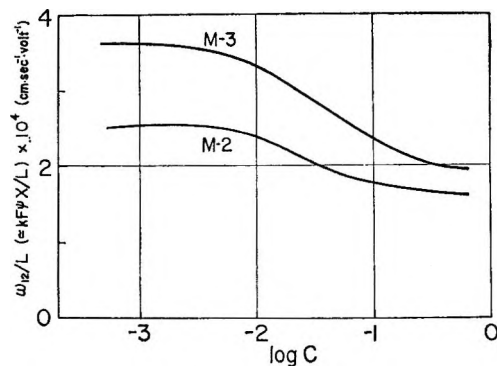


Figure 5. ω_{12}/L as a function of $\log C$ for membrane 2 with KCl. M-2 and M-3 refer to membranes 2 and 3. C is expressed in moles/l.

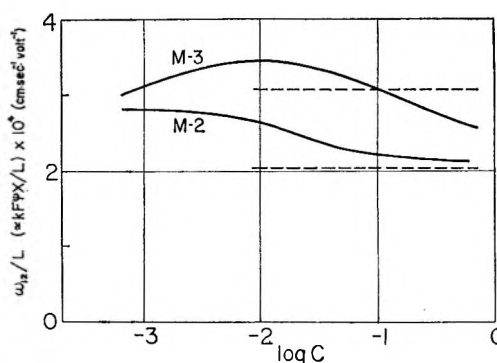


Figure 6. ω_{12}/L as a function of $\log C$ for membranes 2 and 3 with LiCl. Dashed lines represent values of ω_{12}/L for the same membrane-electrolyte systems calculated from osmosis data obtained in part V. C is expressed in moles/l.

method as has been used for the first term of eq 11. It can be shown that for the systems studied here this term is also quite small compared with the observed values of ω_{12} , but the difference is not as extreme as has been found in the case of ω_{22} . For example, for membrane 2 in KCl at 30° this term is about $-1.7 \times 10^{-6} \text{ cm}^2 \text{ sec}^{-1} \text{ V}^{-1}$ at $C = 1 \text{ mole/l.}$ and thus amounts to be nearly 10% of the observed value of ω_{12} . However, its contribution diminishes monotonically as C is lowered. Thus at $C = 0.1 \text{ mole/l.}$ it becomes only about 2% of the observed ω_{12} . From this consideration one may conclude that for the present systems the electroosmotic coefficient ω_{12} is practically equal to $kF\psi X$, the second term of eq 10, except in the region of high salt concentration. In other words, the curves shown in Figures 5 and 6 may be taken as representing the dependence of ψX on concentration C except in such a region of C . Two features of them may be pointed out here. One is that the indicated dependence of ψX on C is not appreciable in any of the four systems shown, and the other is that ψX appears to level off a nonzero value in the limit of high concentration. This latter behavior does not accord with a recent theory of Kobatake and Fujita¹⁴ and of Manning,¹⁵

which predicts that a quantity equivalent to our $kF\psi X$ approaches zero with $C^{-1/2}$ as C is increased.

Comparison with Previous Results. As has been demonstrated in part V, it is possible to evaluate a parameter K_p defined by

$$K_p = \sigma kRT/L \quad (22)$$

from measurements of volume flows caused under concentration gradients. Here R is the gas constant, T is the absolute temperature, σ is the reflection factor which represents permeability of the membrane surface to small ions, and k and L have the same meaning as those defined above. The values of K_p determined in part V with membranes 2 and 3 were nearly independent of electrolyte species and the membrane's charge density and, on the average, yielded a value of 8.7×10^{-1} cm/sec. Introducing this, with the k/L value determined above (8.2×10^{-11} cm³ dyne⁻¹ sec⁻¹) and $T = 303^\circ\text{K}$, into eq 22 gives $\sigma \simeq 0.4$. This indicates that our membrane surfaces were partially leaky to small ions.

It was also shown in part V that if ψ is assumed to be constant, a parameter K_e defined by

$$K_e = kRT\psi X/L \quad (23)$$

can be evaluated from volume flow data obtained in the presence of concentration gradients. We insert the K_e values determined in part V for membrane 2-LiCl and membrane 3-LiCl into this equation, together with the k/L value indicated above. The results are

$$\psi X = 2.5 \times 10^{-6} \text{ equiv/cc (for membrane 2-LiCl)}$$

$$\psi X = 3.9 \times 10^{-6} \text{ equiv/cc (for membrane 3-LiCl)}$$

which are only about $1/5$ the corresponding values of ϕX (see Table I).

The values of $kF\psi X/L$ recalculated from these ψX and k/L are shown by dashed lines in Figure 6. It can be seen that they are quite consistent with the corresponding data (solid curves) derived from the present electroosmotic measurements. No such comparison between the present and previous results was attempted with respect to KCl solutions, since K_e for membranes 2 and 3 with KCl had to be left undetermined in our previous experiment.

Concluding Remarks

This study has demonstrated for oxidized collodion

membrane-1:1 electrolyte systems that the volume flow under either pressure gradient or electric potential gradient is mainly brought about by the movement of the local center of mass, *i.e.*, the so-called mass flow. Specifically, in the case of pressure flow, the mass flow almost entirely dominated the transport of liquid, whereas, in the case of electroosmotic flow, a small portion of the volume flow stemmed from the opposite movement of cation and anion species relative to the local center of mass when the concentration of the external solution was relatively high. Mathematically expressed, the first term on the right-hand side of eq 11 was negligible, but the first term of eq 10 was not necessarily negligible at high concentrations. As far as we are aware, none of the previous authors has estimated the relative contributions of the first and second terms in the expression for either hydraulic coefficient or electroosmotic coefficient. Therefore, it is too early to generalize the above arguments on our particular membrane-electrolyte systems. Nevertheless, we wish to point out that, in general, no satisfactory interpretation of volume flow data might be made unless the effect of mass flow is taken properly into consideration.

Appendix

Referring to eq 7 and 8, $(J_v/\Delta p)_{I=0}$ can be expressed by

$$(J_v/\Delta p)_{I=0} = [(\omega_{12}^2/\omega_{11}) - \omega_{22}]L^{-1} \quad (A1)$$

Introducing eq 13, 14, and 15 transforms eq A1 to

$$(J_v/\Delta p)_{I=0} = -[(J_v/I)(J_v/Ir)]_{\Delta p=0} + (J_v/\Delta p)_{\Delta \zeta=0} \quad (A2)$$

As found from Figure 3, the maximum value of $(J_v/I)_{\Delta p=0}$ is 7.5×10^{-2} cm³ coulomb⁻¹ for membranes 2 and 3 in KCl, while the maximum value of $(J_v/Ir)_{\Delta p=0}$ read off Figure 5 is 3.75×10^{-4} cm sec⁻¹ V⁻¹. Therefore, the first term on the right-hand side of eq A2 is about 3×10^{-6} cm⁴ sec⁻¹ coulomb⁻¹ V⁻¹ = 3×10^{-13} cm³ dyne⁻¹ sec⁻¹, which is less than 1% of the observed value of $-(J_v/\Delta p)_{I=0}$ (8.2×10^{-11} cm³ dyne⁻¹ sec⁻¹). Thus $(J_v/\Delta p)_{I=0}$ may be equated to $(J_v/\Delta p)_{\Delta \zeta=0}$, as far as the present systems are concerned.

(14) Y. Kobatake and H. Fujita, *J. Chem. Phys.*, **40**, 2212 (1964).

(15) G. S. Manning, *ibid.*, **46**, 4976 (1967).

Apparent Molal Volumes of Ammonium Chloride and Some Symmetrical Tetraalkylammonium Chlorides at Various Temperatures

by Frank J. Millero and W. Drost-Hansen

Contribution No. 909 from the Institute of Marine Sciences, University of Miami, Miami, Florida 33149
(Received November 16, 1967)

The apparent molal volumes, ϕ_v 's, of (0.05 *m*) NH_4Cl , Me_4NCl , Et_4NCl , $n\text{-Pr}_4\text{NCl}$, and $n\text{-Bu}_4\text{NCl}$ have been determined at one-degree intervals from 20 to 40° from precision density measurements. The apparent molal expansibilities, ϕ_E 's, have been calculated from the ϕ_v values at various temperatures and have been equated to the infinite dilution molal expansibility, \bar{E}^0 . The \bar{E}^0 values of the R_4NCl 's are not a linear function of molecular weight of the cation, R_4N^+ . The \bar{E}^0 of NH_4Cl is low, apparently due to the ability of the NH_4^+ ion to form an "icelike" species in solution. The \bar{E}^0 's of Pr_4NCl and Bu_4NCl appear to be high compared to the lower molecular weight R_4NCl 's. This nonlinear behavior is interpreted as being due to expansibility changes in the structure of water caused by the R_4N^+ cations, $\bar{E}^0(\text{struct})$. This structural effect decreases as the temperature increases and increases as the size of R_4N^+ increases. The similarity of \bar{V}^0 properties of R_4N^+ cations and the aliphatic alcohols is discussed, and it is postulated that the abnormal properties of R_4N^+ salts may be normal for solutes able to cause hydrophobic bonding.

Introduction

This study is a continuation of a program¹ of measuring the apparent molal volumes of aqueous salt solutions at various temperatures. Interest in the symmetrical tetraalkylammonium salts stems from the abnormal behavior of ϕ_v , the apparent molal volume found by other workers.²⁻¹¹ Also, since these large symmetrical cations are not hydrated in the normal sense (*i.e.*, electrostrictive hydration), we hoped to determine the absolute expansibility of the Cl^- ion by a method similar to that used by Conway, *et al.*,^{5,6} in determining the absolute \bar{V}^0 of Cl^- ion.

Precision density measurements were made on dilute solutions (0.05 *m*) of NH_4Cl , Me_4NCl , Et_4NCl , $n\text{-Pr}_4\text{NCl}$, and $n\text{-Bu}_4\text{NCl}$ at one-degree intervals from 20 to 40°. The apparent molal volume, ϕ_v , and apparent molal expansibility, ϕ_E , have been calculated from the density data.

Experimental Section

NH_4Cl used was reagent grade Baker Analyzed. All the tetraalkylammonium chlorides were obtained from Eastman Organic Chemicals. All the salts were purified by several recrystallizations according to the methods listed by Conway, *et al.*⁵ Each salt was dried *in vacuo* for at least 1 week before use. The solutions were made by weight with degassed, doubly distilled water.

The magnetic float densitometer used to make the density measurements has been described elsewhere.¹² The constant-temperature bath in which the densitometer is submersed was controlled to $\pm 0.001^\circ$ with a Hallikainen regulator.

Results

The densities of the various solutions have been measured at 1° intervals from 20 to 40°. The densities of the solutions were fit to equations of the form

$$d_{\text{soln}} = A + Bt + Ct^2 + Dt^3 \quad (1)$$

The constants for this equation are listed in Table I along with the root-mean-square (rms) deviations. The thermal expansion coefficient, $\alpha_{\text{soln}} = -(\partial d_{\text{soln}}/\partial t)1/d_{\text{soln}}$, of the solutions can be calculated from

$$\alpha_{\text{soln}} = -(B + 2Ct + 3Dt^2)/d_{\text{soln}} \quad (2)$$

The apparent molal volumes listed in Table II were calculated from the equation

$$\phi_v = \frac{1000\Delta d_{\text{soln}}}{d_{\text{H}_2\text{O}}d_{\text{soln}}m} + \frac{M}{d_{\text{soln}}} \quad (3)$$

(1) F. J. Millero and W. Drost-Hansen, presented at the 154th National Meeting of the American Chemical Society, Chicago, Ill., Sept, 1967.

(2) W. Y. Wen and S. Saito, *J. Phys. Chem.*, **68**, 2639 (1964).

(3) W. Y. Wen and S. Saito, *ibid.*, **69**, 3569 (1965).

(4) W. Y. Wen and K. Nara, *ibid.*, **71**, 3907 (1967).

(5) B. E. Conway, R. E. Verrall, and J. E. Desnoyers, *Trans. Faraday Soc.*, **62**, 2738 (1966).

(6) B. E. Conway, R. E. Verrall, and J. E. Desnoyers, *Z. Phys. Chem. (Leipzig)*, **230**, 157 (1965).

(7) B. E. Conway and R. E. Verrall, *J. Phys. Chem.*, **70**, 3952 (1966); **70**, 3961 (1966).

(8) J. E. Desnoyers and M. Arel, *Can. J. Chem.*, **45**, 359 (1967).

(9) F. Franks and H. T. Smith, *Trans. Faraday Soc.*, **63**, 2586 (1967).

(10) H. E. Wirth, *J. Phys. Chem.*, **71**, 2922 (1967).

(11) L. G. Hepler, J. M. Stokes, and R. H. Stokes, *Trans. Faraday Soc.*, **61**, 20 (1965).

(12) F. J. Millero, *Rev. Sci. Instrum.*, **38**, 1441 (1967).

Table I: Constants for Density Equation

Salt	A, g/ml	10 ⁴ B, g/ml deg	-10 ⁴ C, g/ml deg ²	10 ⁸ D, g/ml deg ²	Rms dev, ppm
NH ₄ Cl	1.001355	26.171	6.5780	2.4349	0.4
Me ₄ NCl	1.000385	17.652	6.3473	2.1656	1.2
Et ₄ NCl	1.000145	28.121	6.6932	2.5212	1.0
n-Pr ₄ NCl	0.999879	25.061	6.6391	2.4989	1.5
n-Bu ₄ NCl	0.999312	44.662	7.4151	3.3222	0.9

from the apparent molal volumes; they are listed in Table II. The average ϕ_E at 25 and 30° and the average deviation from the mean are compiled in Table IV; also listed are the results of other workers^{2,9} for comparison. Since ϕ_E is not strongly dependent upon concentration⁹ and the measurements were made on dilute solutions, we have equated ϕ_E with \bar{E}^0 , the partial molal expansibility at infinite dilution. The difference between ϕ_E and the true value of \bar{E}^0 is well

Table II: Apparent Molal Volume and Apparent Molal Expansibility of NH₄Cl and Some Symmetrical Tetraalkylammonium Chlorides at Various Temperatures^a

Temp, °C	—NH ₄ Cl (0.06970 m)—		—Me ₄ NCl (0.05268 m)—		—Et ₄ NCl (0.05369 m)—		—n-Pr ₄ NCl (0.05042 m)—		—n-Bu ₄ NCl (0.05341 m)—	
	ϕ_V	ϕ_E	ϕ_V	ϕ_E	ϕ_V	ϕ_E	ϕ_V	ϕ_E	ϕ_V	ϕ_E
20	36.156	0.018	107.15	0.06	166.04	0.07	228.45	0.13	292.31	0.17
21	36.174	0.019	107.21	0.06	166.11	0.12	228.58	0.14	292.48	0.19
22	36.193	0.019	107.27	0.12	166.23	0.11	228.72	0.09	292.67	0.22
23	36.212	0.019	107.39	0.12	166.34	0.08	228.81	0.16	292.89	0.23
24	36.231	0.005	107.51	0.07	166.42	0.08	228.97	0.16	293.12	0.19
25	36.236	0.033	107.58	0.05	166.50	0.12	229.13	0.10	293.31	0.20
26	36.269	0.006	107.63	0.10	166.62	0.08	229.23	0.13	293.51	0.23
27	36.275	0.034	107.73	0.05	166.70	0.12	229.36	0.21	293.74	0.24
28	36.309	0.005	107.78	0.11	166.82	0.09	229.57	0.12	293.98	0.29
29	36.314	0.020	107.89	0.05	166.91	0.13	229.69	0.18	294.27	0.26
30	36.334	0.021	107.94	0.17	167.04	0.12	229.87	0.13	294.53	0.27
31	36.335	0.020	108.11	0.11	167.16	0.19	230.00	0.12	294.80	0.27
32	36.375	0.021	108.22	0.01	167.35	0.07	230.12	0.17	295.07	0.27
33	36.396	0.035	108.23	0.13	167.42	0.17	230.29	0.21	295.34	0.26
34	36.431	0.021	108.36	0.10	167.59	0.12	230.50	0.16	295.60	0.26
35	36.452	0.022	108.46	0.09	167.71	0.10	230.66	0.14	295.86	0.29
36	36.474	0.021	108.55	0.14	167.81	0.17	230.80	0.17	296.15	0.28
37	36.495	0.022	108.69	0.08	167.98	0.14	230.97	0.13	296.43	0.29
38	36.517	0.021	108.77	0.11	168.12	0.14	231.10	0.21	296.72	0.25
39	36.538	0.022	108.88	0.16	168.26	0.14	231.31	0.21	296.97	0.22
40	36.560		109.02		168.40		231.52		297.19	

^a ϕ_V is given in milliliters per mole, and ϕ_E is given in milliliters per mole per degree.

Table III: Apparent Molal Volume of NH₄Cl and Some Symmetrical Tetraalkylammonium Chlorides at 25°

Salt	Molality	ϕ_V , ml/mol		Ref
		Our value	Lit. value	
NH ₄ Cl	0.06970	36.24	36.36	14
Me ₄ NCl	0.05268	107.58	107.69	5
Et ₄ NCl	0.05369	166.50	166.57	5
n-Pr ₄ NCl	0.05042	229.3	232.06	5
n-Bu ₄ NCl	0.05341	293.31	292.83	5

The densities of water used in these calculations were taken from Tilton and Taylor's work.¹³ The results at 25° can be compared to other workers^{6,14} by using the equation

$$\phi_V = \phi_V^0 + S\sqrt{c} + bc \quad (4)$$

This comparison is shown in Table III. The apparent molal expansibilities $\phi_E = \partial\phi/\partial tV$ can be calculated

within the experimental error (± 0.03 ml/mol deg); thus equating ϕ_E and \bar{E}^0 is justifiable.

Discussion of Results

Recently, various workers^{6,15-17} have attempted to divide the partial molal volume of ions at infinite dilution into two contributions

$$\bar{V}^0(\text{ion}) = \bar{V}^0(\text{int}) + \bar{V}^0(\text{elect}) \quad (5)$$

where $\bar{V}^0(\text{int})$ is the intrinsic volume of the ion plus the volume due to void space and $\bar{V}^0(\text{elect})$ is the decrease in volume due to electrostriction. For ions that have strong structural effects on water (e.g., Li⁺, F⁻, Be²⁺,

- (13) L. W. Tilton and J. K. Taylor, *J. Res. Nat. Bur. Stand.*, **18**, 205 (1937).
- (14) B. B. Owen and S. R. Brinkley, *Chem. Rev.*, **29**, 461 (1941).
- (15) L. Hepler, *J. Phys. Chem.*, **61**, 1426 (1957).
- (16) P. Mukerjee, *ibid.*, **65**, 740 (1961).
- (17) E. Glueckauf, *Trans. Faraday Soc.*, **61**, 914 (1965).

Table IV: Apparent Molal Expansibility of NH_4Cl and Some Symmetrical Tetraalkylammonium Chlorides

Salt	ϕ_E , ml/mol deg			Ref
	25°	35°	Other workers ^a	
NH_4Cl	0.018 ± 0.007	0.023 ± 0.003	...	
Me_4NCl	0.079 ± 0.028	0.108 ± 0.030	0.11 (15°)	9
Et_4NCl	0.100 ± 0.020	0.136 ± 0.027	0.13 (15°)	9
$n\text{-Pr}_4\text{NCl}$	0.141 ± 0.027	0.166 ± 0.029	0.14 (15°)	9
$n\text{-Bu}_4\text{NCl}$	0.223 ± 0.028	0.266 ± 0.015	0.25 (15°), 0.24 (25°)	9, 2

^a These values are for tetraalkylammonium bromides; however, since $\bar{E}^0(\text{Cl}^-) \sim \bar{E}^0(\text{Br}^-)$ the comparison is justified.

and Mg^{2+})^{17,18} another term, \bar{V}^0 (struct), must be added to eq 5.

$$\bar{V}^0(\text{ion}) = \bar{V}^0(\text{int}) + \bar{V}^0(\text{elect}) + \bar{V}^0(\text{struct}) \quad (6)$$

Since the term $\bar{V}^0(\text{int})$ is large for most ions compared to the other terms of eq 6, it is difficult to separate the individual terms of $\bar{V}^0(\text{ion})$.

If one differentiates eq 6 with respect to temperature, the partial molal expansibility of an ion at infinite dilution, $\bar{E}^0(\text{ion})$, is given by the equation

$$\bar{E}^0(\text{ion}) = \bar{E}^0(\text{int}) + \bar{E}^0(\text{elect}) + \bar{E}^0(\text{struct}) \quad (7)$$

where $\bar{E}^0(\text{int})$ is the expansibility due to void space (since the intrinsic size of the ion can be assumed to be independent of temperature), $\bar{E}^0(\text{elect})$ is the expansibility due to electrostriction (solute-solvent interactions), and $\bar{E}^0(\text{struct})$ is the expansibility due to structural changes in water. Since the large R_4N^+ ions have little or no electrostriction ($\bar{V}^0(\text{elect}) \sim 0$ and $\bar{E}^0(\text{elect}) \sim 0$), it was of interest to determine whether $\bar{E}^0(\text{ion})$ for R_4N^+ could be related to some function of these ions, for instance $\bar{V}^0(\text{ion})$ and a general relationship for $\bar{E}^0(\text{ion})$ for other ions could be inferred. It has been shown by others^{5,6,19} that \bar{V}^0 of R_4N^+ halides is a linear function of the molecular weight of the cation^{5,6} and $\bar{V}^0(\text{R}_4\text{N}^+)$ is a linear function of the radius cubed.¹⁹ From the linear function of $\bar{V}^0(\text{R}_4\text{N}^+)$ halides, others^{5,6} have been successful in determining the absolute \bar{V}^0 of Cl^- , Br^- , and I^- (by plotting $\bar{V}^0(\text{R}_4\text{N}^+)$ halides *vs.* the molecular weight of the cation and extrapolating to zero) or $\bar{V}^0(\text{H}^+)$, that agree within experimental error with those calculated by other methods.²⁰

From the results of \bar{E}^0 of the R_4NCl 's at 25° (Figure 1), it can be clearly seen that a linear relation is not obtained when one plots $\bar{E}^0(\text{R}_4\text{NCl})$ *vs.* the molecular weight of the cation, R_4N^+ . A smooth curve is obtained with the \bar{E}^0 of Pr_4NCl and Bu_4NCl appearing to be high compared to the lower molecular weight, R_4NCl 's. At 30°, however, a linear relation is obtained for Me_4NCl , Et_4NCl , and Pr_4NCl with \bar{E}^0 of Bu_4NCl appearing to be high. The high values of \bar{E}^0 of Pr_4NCl and Bu_4NCl at 25° indicates that the structural term, $\bar{E}^0(\text{struct})$, is causing a larger value for \bar{E}^0 than expected

by comparison with the lower molecular weight R_4NCl 's. The \bar{E}^0 results at 30° indicate that $\bar{E}^0(\text{struct})$ decreases with temperature with only Bu_4NCl appearing to be high. $\bar{E}^0(\text{struct})$ disappears as the temperature is increased and increases as the size of the R_4N^+ increases. Although Pr_4N^+ and Bu_4N^+ chlorides clearly show the structural term, $\bar{E}^0(\text{struct})$, this does not mean that the effect is not important for the lower molecular weight R_4N^+ salts (especially at lower temperatures). The low \bar{E}^0 of NH_4Cl is apparently due to the ability of NH_4^+ to form an "icelike" structure which has a negative expansibility similar to water below 4° (or ice becoming liquid at 0°).

It should be noted that the adiabatic molal compressibility, $\bar{K}^0 = -(\partial \bar{V}^0 / \partial P)_V$, behavior of the R_4N^+ bromides and chlorides⁷ is similar to the \bar{E}^0 behavior. The \bar{K}^0 of the R_4N^+ salts are generally higher (less negative) than \bar{K}^0 of salts, and \bar{K}^0 decreases (\bar{V}^0 increases) as $\bar{V}^0(\text{R}_4\text{N}^+)$ becomes larger. Although a linear increase in \bar{K}^0 was not found for all the R_4N^+ ions⁷ (as for \bar{E}^0 for our measurements), it does appear that \bar{K}^0 of Pr_4N^+ and Bu_4N^+ is small (\bar{V}^0 is larger) compared to Me_4N^+ and Et_4N^+ . The high value for \bar{E}^0 and \bar{K}^0 for Pr_4N^+ and Bu_4N^+ compared to the other R_4N^+ cations suggests that $\bar{V}^0(\text{struct})$ for the R_4N^+ cations is negative. Since the structural effects disappear as the temperature or pressure is increased, this negative contribution is reduced causing \bar{E}^0 and \bar{K}^0 of Pr_4N^+ and Bu_4N^+ to appear high.

Further evidence for $\bar{V}^0(\text{struct})$ having a negative value for the R_4N^+ cations can be shown by comparing the \bar{V}^0 of R_4N^+ cations with the aliphatic alcohols and other ions. First, if one calculates $\bar{V}^0(\text{R}_4\text{N}^+)$ from radii obtained from molecular models, one obtains a value that is smaller than the measured value.⁹ This difference increases in magnitude with increasing ionic size. For simple ions, where this effect is due to electrostriction, the reverse is true^{6,16,17} (*i.e.*, $\bar{V}^0(\text{elect})$ decreases with increasing ionic radius). This behavior is similar, however, to that observed for the aliphatic

(18) F. J. Millero, *J. Phys. Chem.*, **71**, 4567 (1967).

(19) R. Zana and E. Yeager, *ibid.*, **71**, 4241 (1967).

(20) For comparison of $\bar{V}^0(\text{H}^+)$ obtained by various methods, see P. Mukerjee, *ibid.*, **70**, 270 (1966).

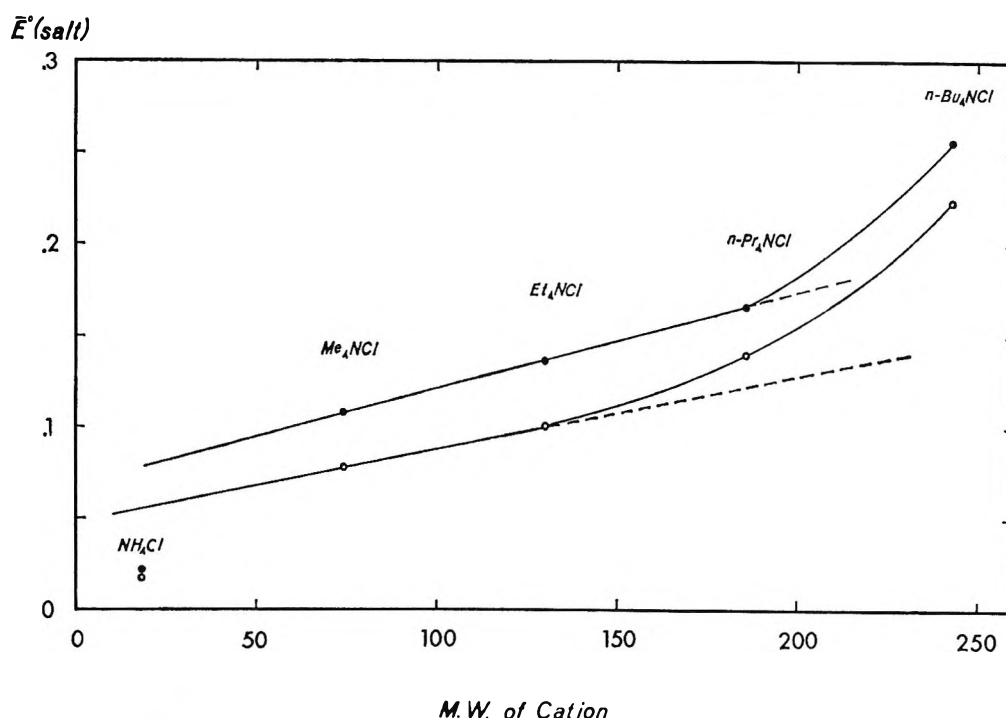


Figure 1. Molal expansibility, \bar{E}^0 , of NH_4Cl and some R_4NCl salts vs. molecular weights of cations at 35° (solid circles) and 25° (open circles).

alcohols.²¹ Second, when one plots $\bar{V}^0(\text{R}_4\text{N}^+)$ cations vs. r^3 (the crystal radius), a slope of 2.3 is obtained.¹⁹ This slope is lower than the theoretical value of 2.52 ($4\pi N/3$) and also the value obtained for other ions (4.75).¹⁹ Thus the \bar{V}^0 of the R_4N^+ is lower than expected from comparison to other ions. Since $\bar{V}^0(\text{elect})$ is very small or zero for the R_4N^+ cations (with the exception of Me_4N^+), the low value of \bar{V}^0 can be attributed to $\bar{V}^0(\text{struct})$ being negative. The $\bar{V}^0(\text{Me}_4\text{N}^+)$ is lower when compared to the higher molecular weight R_4N^+ cations, indicating that this cation has a negative contribution due to electrostriction, $\bar{V}^0(\text{elect})$.¹⁹ This is in agreement with Kay and Evans' conductance and viscosity B -coefficient studies.²²

The similarity of the \bar{V}^0 behavior of the R_4N^+ cations with the behavior observed for the aliphatic alcohols (ROH) can also be demonstrated as follows.

1. The \bar{E}^0 of the R_4N^+ salts increase with increasing temperature (Table IV) in a manner similar to the behavior of aliphatic alcohols (MeOH, EtOH, PrOH, BuOH, PeOH, *i*-BuOH, and *sec*-BuOH).^{23,24} The \bar{E}^0 's of electrolytes (salts), however, decrease with increasing temperature.^{25,26}

2. Comparison of the \bar{E}^0 of R_4N^+ cations and aliphatic alcohols²³ (shown in Figure 2 at 30°) indicates that a common line is obtained when plotted vs. \bar{V}^0 , with the exception of Bu_4N^+ . Since $\bar{E}^0(\text{elect})$ is very small or zero for the R_4N^+ cations and the alcohols, the \bar{E}^0 of these solutes can be attributed to $\bar{E}^0(\text{int})$ and $\bar{E}^0(\text{struct})$. It appears that $\bar{E}^0(\text{int})$ is proportional to \bar{V}^0 and as the volume increases $\bar{E}^0(\text{struct})$ becomes impor-

tant. The apparent deviation of the Bu_4N^+ cation compared to the other solutes may be real or due to a gradual increase of $\bar{E}^0(\text{struct})$. From the comparison between electrolyte and nonelectrolyte, \bar{V}^0 behavior as a function of temperature, one might postulate that the $\bar{V}^0(\text{R}_4\text{N}^+)$ salts increase with increasing temperature like nonelectrolytes and do not go through a maximum near 40 – 60° like other electrolytes.^{27–29} From the recent measurements,³⁰ it appears that up to 65° the \bar{V}^0 of the R_4NBr salts do not go through a maximum.

As mentioned in the Introduction, we hoped to obtain the absolute expansibility of the Cl^- ion, $\bar{E}^0(\text{Cl}^-)$, by plotting $\bar{E}^0(\text{R}_4\text{NCl})$ vs. the molecular weight of the cation and extrapolating to zero. Although the linearity does not exist for all the R_4NCl salts, it is possible to estimate $\bar{E}^0(\text{Cl}^-) = 0.048$ ml/mol deg at

- (21) F. Franks and D. J. G. Iv \ddot{e} s, *Quart. Rev. (London)*, **21**, 1 (1966).
 (22) R. L. Kay and D. F. Evans, *J. Phys. Chem.*, **70**, 2325 (1966).
 (23) M. E. Friedman and H. A. Scheraga, *J. Phys. Chem.*, **69**, 2795 (1965).
 (24) D. M. Alexander, *J. Chem. Eng. Data*, **24**, 252 (1959).
 (25) R. E. Gibson and O. H. Loeffler, *J. Amer. Chem. Soc.*, **63**, 443 (1941).
 (26) H. S. Harned and B. B. Owen, "The Physical Chemistry of Electrolytic Solutions," 3rd ed, ACS Monograph No. 137, Reinhold Publishing Corp., New York, N. Y., 1958.
 (27) A. J. Ellis, *Chem. Commun.*, **21**, 802 (1966).
 (28) A. J. Ellis, *J. Chem. Soc.*, 1579 (1966).
 (29) A. J. Ellis, *ibid.*, 660 (1967).
 (30) S. Schiavo, B. Scrosati, and A. Tommasini, *Ric. Sci.*, **37**, 211 (1967).

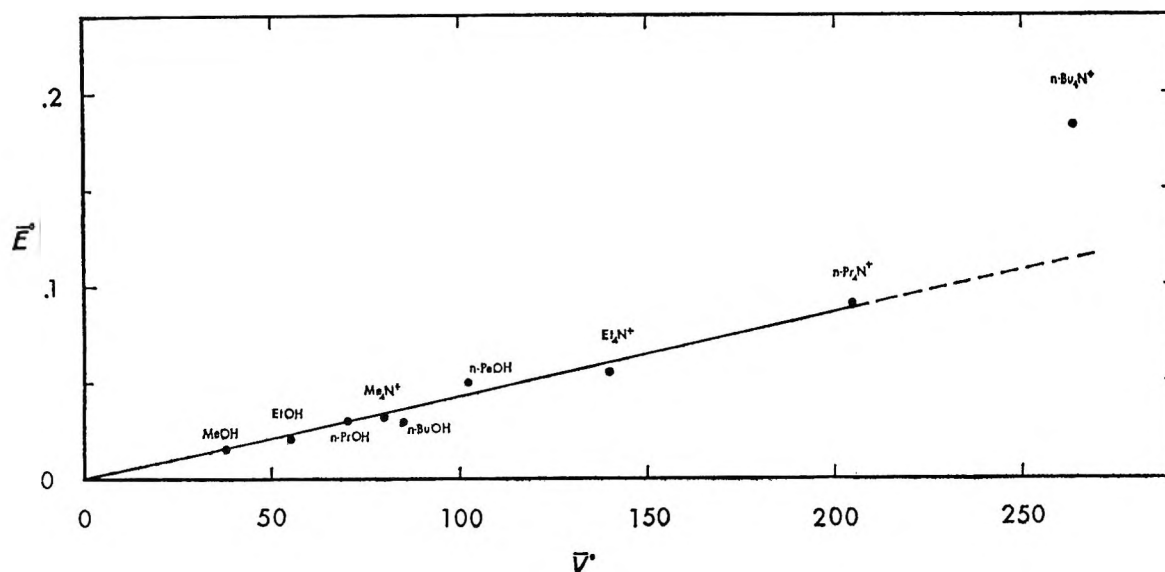


Figure 2. Molal expansibility, \bar{E}^0 , of R_4N^+ cations and ROH alcohols (M. E. Friedman and H. A. Scheraga, *J. Phys. Chem.*, **69**, 3795 (1965)) vs. \bar{V}^0 or R_4N^+ cations and ROH alcohols at 30°.

25° using the results for Me₃NCl and EtNCl. Using the $\bar{E}^0(\text{HCl}) = 0.034$ ml/mol deg²⁶ at 25°, $\bar{E}^0(\text{H}^+) = -0.014$ ml/mol deg. From the $\bar{V}^0(\text{R}_4\text{NBr})^9$ at 5 and 25°, it is possible to calculate $\bar{V}^0(\text{Br}^-) = 30.32$ and 31.02 ml/mol, respectively, by the method of Conway, *et al.*^{5,6} From these two values of $\bar{V}^0(\text{Br}^-)$, the absolute $\bar{E}^0(\text{Br}^-) = 0.035$ ml/mol deg can be calculated. Using $\bar{E}^0(\text{KBr}) = 0.060$,¹ $\bar{E}^0(\text{KCl}) = 0.069$,¹ and $\bar{E}^0(\text{HCl}) = 0.034$ ml/mol deg,²⁶ $\bar{E}^0(\text{H}^+)$ is found to be equal to 0.010. Thus, $E_0(\text{H}^+)$ is between -0.010 and -0.014 ml/mol deg; *i.e.*, $\bar{E}^0(\text{H}^+)$ is small and negative. From the recent measurements of \bar{V}^0 of $R_4\text{NBr}$ salts over a wide range of temperatures (15–65°),³⁰ we obtain a value for $\bar{E}^0(\text{H}^+)$ within these limits at 25°, although the experiments were not made in very dilute solutions nor with the precision of Franks and Smith's work.⁹ To adjust the $\bar{E}^0(\text{ions})$ (listed in our previous paper¹) to the average $\bar{E}^0(\text{H}^+)$, 0.012 should be added to the anions and subtracted from the cations.

Using the absolute $\bar{V}^0(\text{Br}^-) = 31.02$, $\bar{V}^0(\text{KCl}) = 26.89$,³¹ $\bar{V}^0(\text{KBr}) = 33.73$ ⁸ and $\bar{V}^0(\text{HCl}) = 17.82$ ml/mol,³² one obtains $\bar{V}^0(\text{H}^+) = -6.19$ ml/mol at 25°. This value is lower than that obtained by others;²⁰ however, this may be due to the negative $\bar{V}^0(\text{struct})$ of the R_4N^+ ions, which increases in magnitude as the size of the R_4N^+ increases (the negative contribution of $\bar{V}^0(\text{struct})$ for the R_4N^+ salts would cause the value of $\bar{V}^0(\text{halide})$ to be larger than the true absolute value and this would likewise give a value for $\bar{V}^0(\text{H}^+)$ that is lower than that obtained by others).²⁰

Previous studies seem to indicate that the R_4N^+ salts strongly influence the structure of water.^{2–11} The negative deviations of \bar{V}^0 from the limiting law and the other thermodynamic anomalies of the R_4N^+ salts have been attributed to ion pairing,^{10,11,33–35} hydrophobic bonding,³⁶ "iceberg effect,"³⁷ micelle for-

mation,³⁸ salting-in effects,^{8,39} and induced cation-cation interactions.^{2–4,9} Franks and Smith⁹ have recently discussed these various explanations and suggested that induced cation-cation interaction is the preferred explanation. This cation-cation interaction presumably is due to the overlapping of extensive hydration structures and not directly caused by coulombic interactions. Since the measurements described in this paper were not made as a function of concentration, we cannot use our results to discuss the solute-solute interactions of the R_4N^+ salts. From the similarity of the \bar{V}^0 properties of R_4N^+ cations with the aliphatic alcohols at infinite dilution, it appears that the apparent abnormal properties of the R_4N^+ cations may, in fact, be normal for solutes that can cause hydrophobic bonding.⁴ Presently there are no theoretical means of estimating the limiting slope (ϕ_V vs. c) for nonelectrolytes and, furthermore, very few measurements have been made of nonelectrolytes in dilute solutions with the accuracy of the present study.

In our future work we plan to measure the ϕ_V of electrolytes and nonelectrolytes as a function of concentration and temperature (over a large range, 0–100°) with hopes of obtaining a better understanding of solute-solvent, solute-solute, and solvent-solvent interactions in aqueous solution.

(31) F. Vaslow, *J. Phys. Chem.*, **70**, 2286 (1966).

(32) L. A. Dunn, *Trans. Faraday Soc.*, **62**, 2348 (1966).

(33) R. M. Diamond, *J. Phys. Chem.*, **67**, 2513 (1963).

(34) B. J. Levien, *Aust. J. Chem.*, **18**, 1161 (1965).

(35) R. L. Kay and D. F. Evans, *J. Phys. Chem.*, **70**, 366 (1966).

(36) F. Franks and H. T. Smith, *ibid.*, **68**, 3581 (1964).

(37) H. S. Frank and W. Y. Wen, *Discussions Faraday Soc.*, **24**, 133 (1957).

(38) S. Lindenbaum and G. E. Boyd, *J. Phys. Chem.*, **68**, 911 (1964).

(39) B. E. Conway and R. E. Verrall, *ibid.*, **70**, 1473 (1966).

Acknowledgment. The authors wish to thank Dr. R. L. Key for his helpful comments and suggestions and Dr. F. Franks who made his manuscript available to us

prior to publications. The authors wish to acknowledge the support of the Office of Saline Water for this study.

The Electrical Conductivity of Aqueous Tetraalkylammonium Halide Solutions under Hydrostatic Pressure

by R. A. Horne and R. P. Young

Arthur D. Little, Inc., Cambridge, Massachusetts 00214 (Received November 20, 1967)

The electrical conductivities of 0.10 *M* aqueous solutions of the salts $R_4N^+A^-$, where R is CH_3 , C_2H_5 , C_3H_7 , $n-C_4H_9$, and $n-C_5H_{11}$ and A^- is Cl^- , Br^- , and I^- , have been measured at 4 and 25° over the pressure range 1 atm to 4000 kg/cm². The results of these measurements support the viewpoints that (1) the hydrophobic hydration atmospheres of these ions are fundamentally different from the coulombic hydration envelopes surrounding "normal" ions such as the alkali metal cations, in particular being much more stable with respect to hydrostatic pressure, and (2) cation-cation interactions are important in solutions of the larger ions in this series.

Introduction

In order to account for certain properties of liquid water and aqueous solutions, Wicke¹ has proposed that, in addition to the "free" or monomeric water and the flickering, H-bonded Frank-Wen clusters, there exists a "third state" which he postulates consists of dimers, trimers, tetramers, etc., even though such small aggregates were specifically discounted in Nemethy and Scheraga's² quantitative development of the Frank-Wen³ theory. Similarly, in order to account for certain interface phenomena, we have been obliged to postulate a "third state" which we have called simply the β structure to distinguish it from the α structure of the Frank-Wen clusters and the hydration atmospheres of normal ions.^{4,5} This β structure, which is largely present at interfaces, is less susceptible to destruction by the application of hydrostatic pressure than is the α structure of the Frank-Wen clusters.⁵

The solution properties of the tetraalkylammonium ions have long been recognized as being different from those of "normal" cations such as the alkali metal ions, and Wicke¹ also discussed this "hydration of the second kind." These ions are heavily hydrated and powerfully enhance the structure of the water surrounding them as reflected in their very large viscosity *B* coefficients, ranging from +0.10 for $(CH_3)_4N^+$ to almost +0.90 for $(C_3H_7)_4N^+$ as compared to about +0.14 for Li^+ , the strongest structure maker of the alkali metal cations.⁶ A comparison of the dependence of the *B*

coefficients on ionic radius of the tetraalkylammonium ions with that of the alkali metal cations (Figure 1) illustrates that the hydration of the two families of cations are profoundly different, the former exhibits hydrophobic—the latter, coulombic hydration.⁷ We have further proposed that the structure of the hydrophobic hydration of the tetraalkylammonium ions is the β form.^{4,5} Inasmuch as the β form is more stable with respect to temperature than the α form, the Walden products for the tetraalkylammonium cations are notably more invariant with respect to temperature.^{8,9}

(1) E. Wicke, *Angew. Chem.*, **5**, 106 (1966).

(2) G. Nemethy and H. A. Scheraga, *J. Chem. Phys.*, **36**, 3382, 3401 (1962).

(3) H. S. Frank and W. Y. Wen, *Discussions Faraday Soc.*, **24**, 133 (1957).

(4) R. A. Horne, "The Structural Forms of Liquid Water at Interfaces and Near Biopolymers," Technical Report No. 22, Arthur D. Little, Inc., May 31, 1966; Office of Naval Research Contract No. Nonr-4424(00).

(5) R. A. Horne, A. F. Day, R. P. Young, and N. T. Yu, "Interfacial Water Structure: The Electrical Conductivity of Aqueous Electrolyte Permeated Particulate Solids under Hydrostatic Pressure," Technical Report No. 23, Arthur D. Little, Inc., Sept 30, 1966; Office of Naval Research Contract No. Nonr-4424(00); *Electrochim. Acta*, in press.

(6) R. L. Kay, T. Vituccio, C. Zawoyski, and D. F. Evans, *J. Phys. Chem.*, **70**, 2336 (1966).

(7) R. A. Horne, "Hydrophobic Hydration," Technical Report No. 25, Arthur D. Little, Inc., Sept 30, 1966; Office of Naval Research Contract No. Nonr-4424(00).

(8) R. A. Robinson and R. H. Stokes, "Electrolyte Solutions," 2nd ed, Butterworth and Co. Ltd., London, 1959.

(9) R. L. Kay and D. F. Evans, *J. Phys. Chem.*, **70**, 2325 (1966).

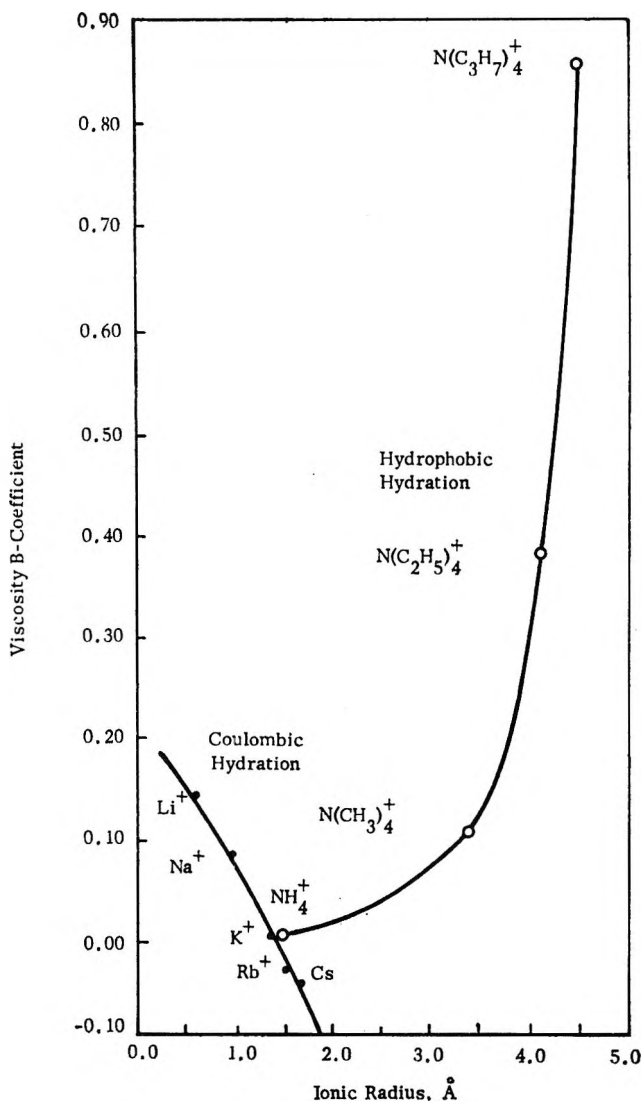


Figure 1. The dependence of the water-structure-altering properties of cations on their radii (from ref 7).

The persistence of the anomalous minimum in the isothermal compressibility of pure water to higher pressures⁹⁻¹¹ and conductance measurements at high pressure^{5,2} indicate that the β structure is also much more stable with respect to the application of hydrostatic pressure than the α structure; thus the hydration of the tetraalkylammonium cations should be more stable under pressure and their electrical conductivity should exhibit a smaller pressure dependency than that of the coulombically hydrated alkali metal cations. The conductance of solutions of the latter ions, due to the reduction of their effective hydrated ionic radii by the application of hydrostatic pressure, increases more rapidly with increasing pressure than one would expect on the basis of viscosity and volume changes.¹³⁻¹⁷ The purpose of the present study was to investigate experimentally the foregoing prediction.

Experimental Section

The apparatus and procedures for measuring the

electrical conductivities of aqueous electrolytic solutions under pressure have been described previously.¹⁸ The conductivity cell used was of a capillary type. In the cases of the highly hygroscopic salts, 0.10 *M* solutions were prepared by dilution of Volhard analyzed approximately 0.2 *M* solutions.

Results

Measured values of the specific conductances of 0.10 *M* aqueous solutions of the tetraalkylammonium halides at 1 atm and 4 and 25° are listed in Table I. Although good data are available for very dilute solutions, for example from the study of Evans and Kay,¹⁹ surprisingly enough there are very few data in the literature on more concentrated solutions that can be compared with the present results.

Table I: Specific Conductances ($\text{ohm}^{-1} \text{cm}^{-1}$) of 0.10 *M* Aqueous Solutions of the Tetraalkylammonium Halides at 1 Atm

	4°	25°
(CH ₃) ₄ NCl	0.00584	0.009693
(C ₂ H ₅) ₄ NCl	0.004956	0.008410
(<i>n</i> -C ₄ H ₉) ₄ NCl	0.003377	0.005856
(CH ₃) ₄ NBr	0.005877	0.009701
(C ₂ H ₅) ₄ NBr	0.004996	0.008380
(<i>n</i> -C ₃ H ₇) ₄ NBr	0.004306	0.007369
(<i>n</i> -C ₄ H ₉) ₄ NBr	0.003875	0.006621
(<i>n</i> -C ₅ H ₁₁) ₄ NBr	0.003656	0.006367
(CH ₃) ₄ NI	0.005721	0.009454
(C ₂ H ₅) ₄ NI	0.00473	0.00828
(<i>n</i> -C ₃ H ₇) ₄ NI	0.00402	0.00687

Figure 2 shows the variation of the relative specific conductance, $\kappa_p/\kappa_{1 \text{ atm}}$, with pressure of a 0.10 *M* KCl solution at $25.31 \pm 0.02^\circ$ and a 0.10 *M* NH₄Cl solution at $25.28 \pm 0.03^\circ$. The values for the two electrolytes are very similar and in agreement with earlier published data for 0.10 *M* KCl at 24.94° .²⁰ Also shown in Figure 2 (dashed line) is the relative conductance expected on the basis of solvent viscosity and specific volume changes only, $\eta_{1 \text{ atm}}^0 V_{1 \text{ atm}}^0 / \eta_p^0 V_p^0$ in the absence of pressure-induced dehydration of the ions.

(10) N. E. Dorsey, "Properties of Ordinary Water-Substance," Reinhold Publishing Corp., New York, N. Y., 1940.

(11) G. S. Kell and E. Whalley, *Phil. Trans. Roy. Soc. (London)*, **A258**, 565 (1965).

(12) R. A. Horne and R. P. Young, *J. Phys. Chem.*, **72**, 376 (1968).

(13) W. A. Zisman, *Phys. Rev.*, **39**, 151 (1932).

(14) R. A. Horne, *Nature*, **200**, 418 (1963).

(15) R. A. Horne, *Water Resources Res.*, **1**, 263 (1965).

(16) R. A. Horne, R. A. Courant, and D. S. Johnson, *Electrochim. Acta.*, **11**, 987 (1966).

(17) R. A. Horne, *Advan. High Pressure Res.*, in press.

(18) R. A. Horne and G. R. Frysinger, *J. Geophys. Res.*, **68**, 1967 (1963).

(19) D. F. Evans and R. L. Kay, *J. Phys. Chem.*, **70**, 360 (1966).

(20) R. A. Horne and R. A. Courant, *J. Chem. Soc.*, 3548 (1964).

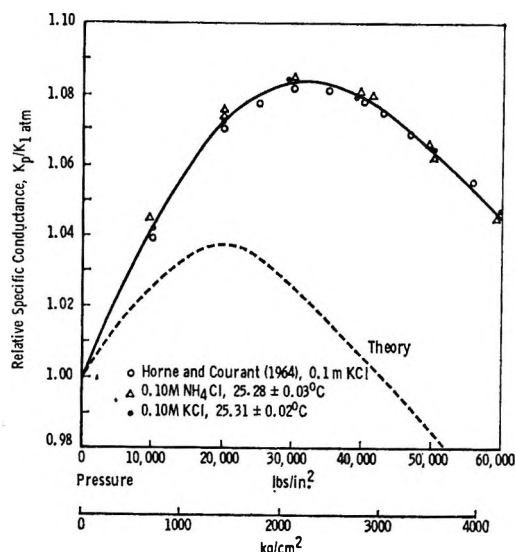


Figure 2. Pressure dependence of the relative specific conductances of KCl and NH_4Cl solutions.

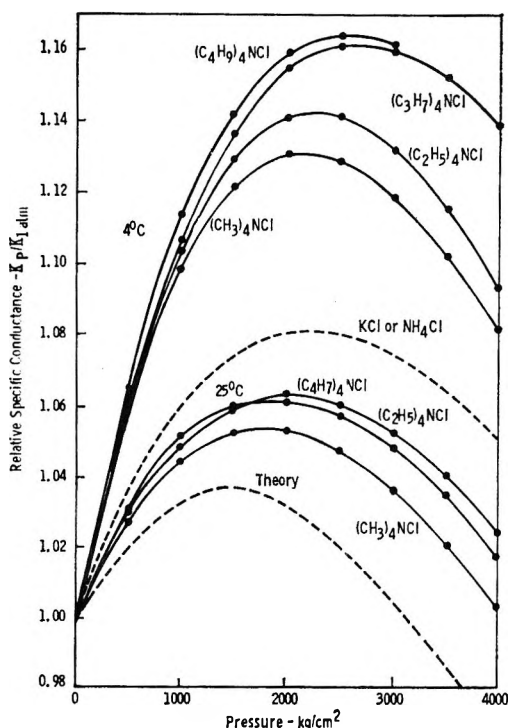


Figure 3. Pressure dependence of the relative conductance of 0.10 *M* aqueous solutions of tetraalkylammonium chloride solutions at 4 and 25°C.

Figures 3–5 show the pressure dependence of the relative conductance of 0.10 *M* aqueous solutions of the tetraalkylammonium chlorides, bromides, and iodides, respectively. For purposes of comparison, the KCl– NH_4Cl and theoretical curves are repeated in these figures as dashed lines.

Discussion

Figures 3–5, generally speaking, exhibit the predicted approach of $\kappa_p/\kappa_{1 \text{ atm}}$ vs. P of the tetraalkylammonium

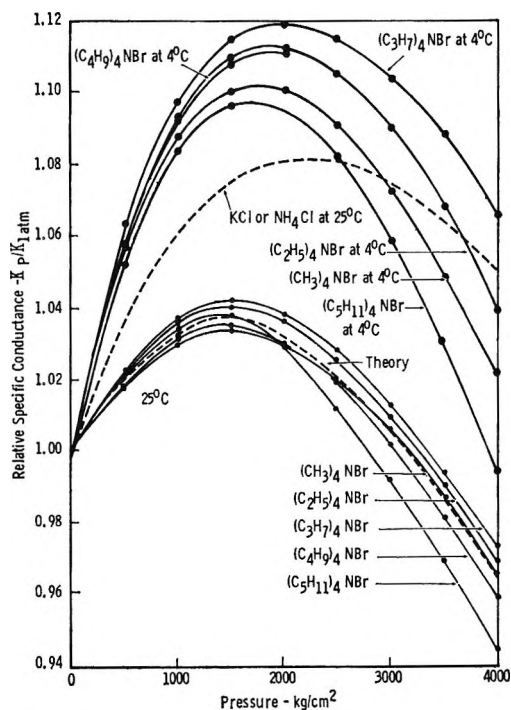


Figure 4. Pressure dependence of the relative conductance of 0.10 *M* aqueous solutions of tetraalkylammonium bromide solutions at 4 and 25°C.

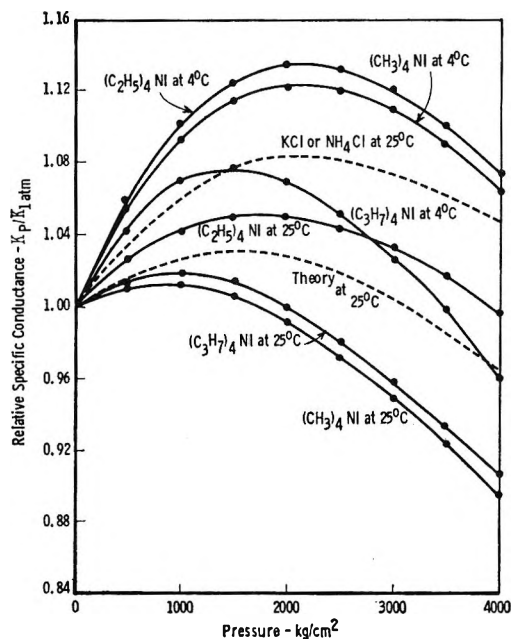


Figure 5. Pressure dependence of the relative conductance of 0.10 *M* aqueous solutions of tetraalkylammonium iodide solutions at 4 and 25°C.

ion to the theoretical curve indicating that, as expected, the β structure or hydrophobic hydration atmosphere surrounding these ions is much more stable with respect to pressure than the α structure or coulombic hydration atmosphere surrounding “normal” cations and that, as a consequence, there is relatively little pressure dehy-

dration of these ions, especially for the larger members of the series.

However, in addition to the predicted behavior, these figures show two phenomena that were quite unexpected: the series of curves are irregular in the sense of not being simply in the order of increasing size of R in R_4N^+ , and in the case of larger R^+ and/or the iodides, some of the observed curves actually fall *below* the theoretical curve; that is to say, the solutions are less conductive than they should be. These irregularities came as such a surprise that a number of the experiments were repeated, but these checks indicated that the irregularities are real. While the viscosity B coefficients form a simple series $(C_3H_7)_4N^+ > (C_2H_5)_4N^+ > (CH_3)_4N^+$ (Figure 1), $\kappa_p/\kappa_{1\text{ atm}}$ appears to go through a maximum for $(C_3H_7)_4N^+$ in the case of the bromides and for $(C_2H_5)_4N^+$ in the case of the iodides. Although there is a regular sequence in the case of the chlorides, $(C_4H_9)_4N^+ > (C_3H_7)_4N^+ > (C_2H_5)_4N^+ > (CH_3)_4N^+$, it is exactly the opposite of the order we might expect; that is to say, the ion with the least hydrophobic character, $(CH_3)_4N^+$, does *not* fall furthest away from the theoretical curve *nor* does the ion with the most hydrophobic least coulombic character fall closest. The causes of this unexpected turn of affairs is certainly not clear at the present time. Possibly the role of the anion must be taken into consideration, inasmuch as the anion appears to be capable of changing the order. Similar reversals of order and differences between chlorides and bromides and iodides were uncovered by Lindenbaum and Boyd²¹ in their investigation of the osmotic and activity coefficients for aqueous solutions of the symmetrical tetraalkylammonium halides. They suggest that water-structure making by the cations is the dominant effect for the chlorides, but in the case of the bromides and iodides, water-structure-enforced ion pairing (see below) becomes more important. Subsequently, however, the very regular behavior of the thermodynamics of solution of these salts led Lindenbaum²² to question the relative importance of such explanations in terms of water structure, yet still later Wood, *et al.*,²³ returned to structural concepts in order to account the observed heats of dilution of the tetraalkylammonium fluorides. Although, as a consequence of careful and intensive study, we now have many pieces of the puzzle, no clear picture has emerged, and the best we can do at the present time is to conclude weakly that these are very complex systems, that the water structure within them admits of alteration in at least several ways, quite probably simultaneously, and that solute-solute interactions play an important role as well.

The maximum for $(C_3H_7)_4N^+$ or $(C_2H_5)_4N^+$ is not quite so unexplicable and is not without precedent. For example, the tetra-*n*-butylammonium and tetraisoamylammonium salts appear to be exceptional in that they, unlike their sister cations in the series, are

capable of forming "higher" hydrates.^{12,24} Evidently the β -structured hydrophobic hydration sheath is a sort of geodesic dome, possibly a multilayer one, and for a given set of bond lengths, stretchabilities, and bendabilities such a structure can enclose certain sized volumes more readily and with greater stability than others. If such is the case, a volume corresponding to $(C_2H_5)_4N^+$ or $(C_3H_7)_4N^+$ is evidently particularly awkward for the encompassing water structure while a volume corresponding to $(n-C_4H_9)_4N^+$ is particularly convenient.

In the case of "normal," *i.e.*, coulombically hydrated, electrolytes such as $MgSO_4$ ²⁵ or H_2SO_4 ²⁶ the dissociation into ionic species increases with increasing pressure as a consequence of the volume decrease arising from the electrostriction of the nearby water. It should be cautioned, however, that it is specious to argue therefrom that the application of hydrostatic pressure should stabilize rather than destroy ionic hydration²⁷ inasmuch as the electrostricted region comprises only a small part of the total hydration atmosphere ion.^{17,28,29} The observed volume change upon ion formation is

$$|\Delta V_{H_2O,B}| + |\Delta V_{H_2O,E}| - |\Delta V_{H_2O,C}|$$

where the subscripts B, E, and C indicate the Frank-Wen structure-broken region, the electrostricted region, and the local Frank-Wen cluster region, respectively, and not simply

$$|\Delta V_{H_2O,E}|$$

This more detailed picture of the hydration atmosphere of cations casts considerable doubt on the meaningfulness of hydration numbers determined from compressibilities.³⁰

In sharp contrast to "normal" electrolytes, in the case of the tetraalkylammonium halides, especially for the larger cations *and* anions, there appear to be ion *association* processes which are accompanied by a volume decrease. The exact nature of these associations requires further clarification. Wen and Saito,³¹ on the basis of their partial molal volume studies, have proposed that there is a "structural salting in" of the larger

(21) S. Lindenbaum and G. E. Boyd, *J. Phys. Chem.*, **68**, 911 (1964).

(22) S. Lindenbaum, *ibid.*, **70**, 814 (1966).

(23) R. H. Wood, H. L. Anderson, J. D. Beck, J. R. France, W. E. de Vry, and L. J. Soltzberg, *ibid.*, **71**, 2149 (1967).

(24) D. L. Fowler, W. V. Loebenstein, D. B. Pall, and C. A. Kraus, *J. Am. Chem. Soc.*, **62**, 1140 (1940).

(25) F. H. Fisher, *J. Phys. Chem.*, **66**, 1607 (1962).

(26) R. A. Horne, R. A. Courant, and G. R. Frysinger, *J. Chem. Soc.*, 1515 (1964).

(27) Reference 9, footnote 37

(28) R. A. Horne and J. D. Birkett, *Electrochim. Acta*, **12**, 1153 (1967).

(29) R. A. Horne, "Electrostriction and the Dehydration of Ions Under Pressure," Technical Report No. 26, Arthur D. Little, Inc., Nov 30, 1966; Office of Naval Research, Contract No. Nonr-4424(00).

(30) D. S. Allam and W. H. Lee, *J. Chem. Soc.*, 426 (1966).

(31) W. Y. Wen and S. Saito, *J. Phys. Chem.*, **68**, 2639 (1964).

Table II: Arrhenius Activation Energies of Electrical Conductance (in kcal/mole) at 13°

	Pressure									
	1 atm	500	1000	1500	2000	2500	3000	3500	4000	4500
KCl	3.76	3.59	3.43	3.40	3.29	3.23	3.24	3.27	3.28	3.30
(CH ₃) ₄ NCl	4.01	3.77	3.60	3.51	3.45	3.43	3.41	3.35	3.43	3.48
(C ₂ H ₅) ₄ NCl	4.13	3.90	3.76	3.63	3.57	3.53	3.53	3.55	3.59	3.60
(C ₄ H ₉) ₄ NCl	4.30	4.03	3.83	3.71	3.63	3.58
(CH ₃) ₄ NBr	3.92	3.65	3.51	3.43	3.39	3.39	3.42	3.45	3.49	3.54
(C ₂ H ₅) ₄ NBr	4.04	3.79	3.62	3.54	3.49	3.46	3.44	3.46	3.49	3.52
(<i>n</i> -C ₃ H ₇) ₄ NBr	4.20	3.90	3.75	3.67	3.61	3.57	3.52	3.49	3.49	3.55
(<i>n</i> -C ₄ H ₉) ₄ NBr	4.18	3.95	3.73	3.65	3.59
(<i>n</i> -C ₃ H ₇) ₄ NBr	4.33	4.10	3.95	3.87	3.83	3.80	3.83	3.86	3.43	4.02
(CH ₃) ₄ NI	3.92	3.60	3.33	3.13	2.97	2.84	2.72	2.64	2.56	2.51
(C ₂ H ₅) ₄ NI	4.40	4.16	3.96	3.85	3.79	3.76	3.76	3.77	3.81	3.87
(<i>n</i> -C ₃ H ₇) ₄ NI	4.19	3.95	3.81	3.71	3.66	3.65	3.65	3.68	3.71	3.74

tetraalkylammonium cations. Wood, *et al.*,³² have similarly found evidence for cation-cation interactions in their heats of dilution data, and Frank³³ has represented the processes as a sort of merger of the hydration cages of two cations to form a combined species accompanied by an over-all volume decrease. Our own and equivalent view of the interaction is that it represents an example of hydrophobic bonding, that, in order to minimize the perturbation of water structure caused by the weakly coulombic, strongly hydrophobic solutes, the water minimizes their volume by forcing them into one another's arms. The effect is the more pronounced the greater the hydrophobic character of the solute and is affected also by the water-structure-altering properties of the anion present. Inasmuch as the interaction gives rise to an over-all volume decrease, the application of hydrostatic pressure favors the ion-association process even though pressure is, in general, a water-structure-breaking variable, both locally and in bulk. Thus the observed tendency of $\kappa_p/\kappa_{1 \text{ atm}}$ *vs.* P to fall below the theoretical curve, especially in the case of the iodides of the higher tetraalkylammonium cations, can be interpreted as further evidence supporting the theory of cation-cation interactions in these systems.

In our earlier studies we have found the Arrhenius activation energy, E_a , to be a useful property in investigating the mechanism of solvent and solute transport processes in aqueous solution.¹⁶ Values of E_a (calculated from the 4 and 25° conductances to give an average value at 13°, remembering that in aqueous solutions E_a is *not* independent of temperature) are listed in Table II and plotted as a function of pressure in Figure 6. Generally speaking, E_a increases with the increasing size of the cation, although (*n*-C₃H₇)₄N⁺ may be an exception to the rule. No clear trend on the dependence on anion size is evident. The values of E_a are reliable to within about 5%. Earlier we reported that E_a of electrical conductance *vs.* P goes through a minimum for aqueous solutions of strong 1:1 salts such as KCl^{34,35} and the same phenomenon in the case of the tetraalkyl-

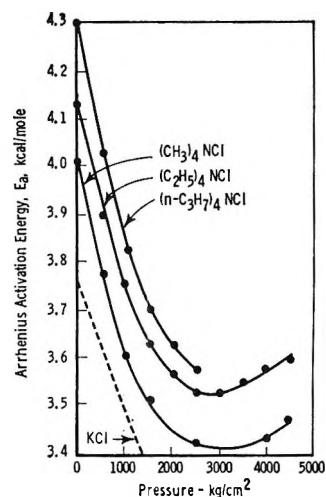


Figure 6. The pressure dependence of the Arrhenius activation energy of electrical conductance.

ammonium salts is exemplified in Figure 6. To repeat, the structure of the coulombic hydration of K⁺ is presumably quite different from the structure of the hydrophobic-hydration envelope of R₄N⁺; therefore, the similarity of the curves for K⁺ and R₄N⁺ in Figure 6 implies that the minima arise from structural changes in the bulk water rather than in the local water structure near the ions. However, if such is the case, then it is surprising that these minima do not tend to flatten out as the ratio of bulk to local water is decreased by increasing the electrolyte concentration or as the structure of the bulk water is loosened by increasing the temperatures.³⁶

Acknowledgment. This work was supported by the Office of Naval Research.

(32) R. H. Wood, H. L. Anderson, J. D. Beck, J. R. France, W. E. de Vry, and L. J. Soltzberg, *J. Phys. Chem.*, **71**, 2149 (1967).

(33) H. S. Frank, *Z. Physik. Chem.*, **228**, 367 (1965).

(34) R. A. Horne, B. R. Myers, and G. R. Frynsinger, *J. Chem. Phys.*, **39**, 2666 (1963).

(35) R. A. Horne and R. P. Young, *J. Phys. Chem.*, **71**, 3824 (1967).

The Thermal Stability of Hydroxyl Groups in Decationated Zeolites X and Y

by Jan B. Uytterhoeven, P. Jacobs, K. Makay, and R. Schoonheydt

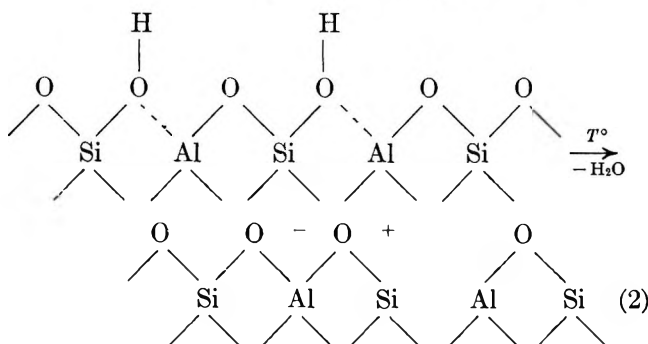
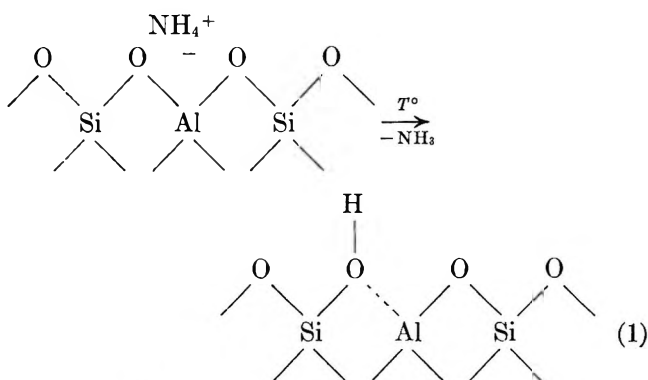
Laboratorium voor Oppervlaktescheikunde, Instituut voor de wetenschappen van de aardbodem, Heverlee, Belgium

Accepted and Transmitted by The Faraday Society (November 23, 1967)

A detailed study has been made of the influence of different degrees of decationation and of two different pretreatments, flash heating and slow heating, on the thermal stability of the OH groups. The absorption coefficient of the OH bands at 3650 and 3550 cm^{-1} in the infrared spectra of decationated molecular sieves type X and Y were determined. The variation in intensity of the OH bands made it possible to follow quantitatively and selectively the dehydroxylation of the two kinds of OH groups. Thermogravimetric determinations confirmed the data obtained from ir analysis. The following assignments have been given to the two OH bands. The 3650- cm^{-1} band is attributed to OH groups located on oxygens forming the bridge between adjacent cuboctahedra. The 3550- cm^{-1} band is assigned to hydroxyls located on six-membered rings of oxygen ions in the cuboctahedron. The 3650- cm^{-1} band is more stable than the 3550- cm^{-1} band and this is explained in terms of differences in dissociation energy. An higher proportion of protons is located at the bridge oxygens after flash than after slow heating. The flash pretreatment gives, therefore, more stable samples. The difference in thermal stability between X and Y samples is discussed on the basis of migration of protons over the oxygen framework.

Introduction

Structural OH groups are created in the framework of synthetic faujasites X and Y by a process called decationation. This process consists of replacing the exchangeable ions by NH_4^+ ions and subsequent heating. In a first step below 300° the ammonium ions decompose into NH_3 and protons, which enter the lattice to form OH groups. In a second step dehydroxylation takes place. Following Uytterhoeven, Christner, and Hall,¹ these reactions may be represented by



These reactions may overlap.

Outgassing at about 500°, a pretreatment frequently adopted by previous workers,²⁻⁴ produces samples completely free of NH_3 but in most cases also partially dehydroxylated. The term decationation is used to denote the over-all activation process, including the NH_4^+ exchange and heating to temperatures at which NH_3 is completely removed and some dehydroxylation takes place. Hence, it does not give an accurate definition of the state and properties of the samples that underwent such a pretreatment. For a more precise definition we refer to reaction 1 as deammoniation and to reaction 2 as dehydroxylation.

The decationated zeolites X and Y have been studied by several authors using ir spectroscopy. The OH stretching region between 3800 and 3500 cm^{-1} has received particular attention.^{1,4-8}

The bands observed at 3750 and 3695 cm^{-1} are due to silica gel like impurities⁴ and to water molecules associated with residual Na^+ ions,⁹ respectively, and are not further discussed in this work. The typical bands introduced by decationation are located around 3650 and 3550 cm^{-1} .¹ Although the occurrence of

(1) J. B. Uytterhoeven, L. G. Christner, and W. K. Hall, *J. Phys. Chem.*, **69**, 2117 (1965).

(2) P. B. Venuto, L. A. Hamilton, P. S. Landis, and T. J. Wise, *J. Catalysis*, **4**, 81 (1966).

(3) P. B. Venuto, L. A. Hamilton, and P. S. Landis, *ibid.*, **5**, 484 (1966).

(4) C. L. Angell and P. C. Schaffer, *J. Phys. Chem.*, **69**, 3463 (1965).

(5) J. L. White, A. N. Jelli, J. M. André, and J. J. Fripiat, *Trans. Faraday Soc.*, **63**, 461 (1967).

(6) P. E. Eberly, Jr., *J. Phys. Chem.*, **71**, 1717 (1967).

(7) B. V. Liengme and W. K. Hall, *Trans. Faraday Soc.*, **62**, 3229 (1966).

(8) T. H. Hughes and H. M. White, *J. Phys. Chem.*, **71**, 2192 (1967).

(9) J. B. Uytterhoeven, B. V. Liengme, R. Schoonheydt, and W. K. Hall, submitted for publication.

these bands has been observed by all previous workers, there are minor differences in the reported frequencies. The extreme values of the frequencies are 3670 and 3640 cm^{-1} ^{3,8} for the high-frequency (HF) and 3570 and 3540 cm^{-1} for the low-frequency (LF) band.^{1,4,5} In order to simplify the discussion, the notations HF band and LF band will be used in this work instead of the real frequencies. In the present instance the HF band occurred at 3650 cm^{-1} while the LF one was observed at 3550 cm^{-1} .

Uytterhoeven, Christner, and Hall¹ considered the HF band as the main OH band and concluded, from the occurrence of two bands, that the hydroxyls are located in two distinct environments. Several authors^{4,8} have suggested that the LF band might be due to neighboring OH groups interacting by hydrogen bonding. From the consideration of a scale model of the zeolite, this type of interaction seems not probable.¹

White, Jelli, André, and Fripiat⁵ have studied the change in intensity of the HF and LF bands on physical adsorption of several inert gases. The intensity of the HF band gradually decreased when such gases as N₂, Ar, Kr, O₂, and CH₄ were adsorbed. A concomitant development of an additional band was observed at a lower wave number, which was dependent on the nature of the adsorbed gas. On the other hand, the LF band remained unaffected during the adsorption process. Taking into account that only the large zeolitic cages were accessible to these gases, White, *et al.*,⁵ concluded that the OH groups responsible for the HF band were located in the large cavities, whereas the OH groups which gave rise to the LF band were situated inside the cuboctahedron. The same authors explained the presence of two distinct bands by a bathochromic effect of an electrostatic origin.

Decationated zeolites, especially of the Y type, are very active catalysts for hydrocarbon cracking. Some authors^{2,3} have postulated that the OH groups are the active sites for acid catalysis. Others¹⁰ have considered that the tricoordinated aluminum generated by dehydroxylation might act as a Lewis-type acid.

Decationation also decreases the thermal stability of these zeolites, and structure collapse accompanies dehydroxylation.

For these reasons, the dehydroxylation of X- and Y-type zeolites containing different amounts of NH₄⁺ ions has been studied by following the changes in intensity of the HF and LF bands as a function of temperature. As this would require a knowledge of the absorption coefficients for each band, these quantities have also been determined.

Experimental Section

Materials. Samples of the zeolites in the Na⁺ form were obtained from the Linde Co.; lot no. 1340080 was an X-type zeolite (SK 20) and lot no. 51-35 was a Y-type zeolite (SK 40). The Al/Na ratio was 1.02 for

X and practically 1 for the Y sample as received. Samples containing different proportions of exchangeable NH₄⁺ ions were obtained by stirring the material, as received, with a solution of ammonium acetate of varying strengths, centrifuging, and decanting the supernatant solution. Excess electrolyte was removed by repeated washing with distilled water. The samples were dried in an electric oven kept at 50° to minimize losses of NH₄⁺ ions by decomposition. However, even at this temperature, some NH₄⁺ ions were lost, more so from the X than from the Y samples. The samples were analyzed for Al and Na content, and the degree of decationation was calculated from the difference between these two quantities. The analytical data are presented in Table I.

Table I: Analytical Data

Sam- ples ^a	Al ³⁺ , mg-atom	Na ⁺ , mg- atom	Na ⁺ ions per unit cell	"Deca- tionated" sites, mequiv/g	Deg of deca- tiona- tion, % ^b
X ₄₀	6.96	4.07	50.07	2.89	41.5
X ₇₅	7.52	1.81	20.6	5.71	75.9
Y ₅₀	4.70	2.52	30.15	2.08	49.5
Y ₉₀	5.08	0.50	5.32	4.58	90.1

^a The subscripts to the symbols X and Y refer to the approximate degree of decationation. ^b The degree of decationation was calculated from the ratio $100(\text{Al} - \text{Na})/\text{Al}$.

Prior to any analytical or spectroscopic determinations, the different samples were stored in a desiccator over a saturated NH₄Cl solution so as to obtain material of a constant and well-defined water content. All of the results are expressed on the basis of the weight after calcination at 1000°.

Instrumentation. The spectroscopic work was performed in a Pyrex cell fitted with CaF₂ windows and very similar to that used by Eberly.⁶ The sample could be heated, *in vacuo*, to any desired temperature between room temperature and 500° in the spectrophotometer itself. The temperature of the film was measured by a chromel-alumel thermocouple attached to the stainless steel sample holder. In a side arm of the cell NH₃ gas, previously purified by vacuum distillation, was stored in a 150-ml flask fitted with a small mercury manometer. By means of a calibrated volume (3.81 ml) measured amounts of NH₃ gas could be introduced into the cell and allowed to adsorb on the film. The volume of the cell was kept as small as possible (approximately 200 ml) so as to favor complete adsorption.

The zeolite samples without binder were pressed into a film between two steel plates (maximum load 200

(10) J. Turkevich, F. Nozaki, and D. N. Stamires, *Proc. Intern. Congr. Catalysis, 3rd, Amsterdam, 1965*, 1, 586 (1965).

kg/cm² of film). Films approximately 2 × 3 cm were used, the weight and area of which were carefully measured. Average film thickness was 4 mg/cm².

Determination of the Absorption Coefficient. The absorption coefficient was first determined in an indirect way by NH₃ adsorption, on films previously deammoniated by heating to 300° under vacuum for 1 hr. Known amounts of NH₃ were then introduced into the cell. After each adsorption the OH spectrum was recorded and the area of the OH bands was determined by graphical integration. The decrease in intensity of the OH bands (ΔA) was a linear function of the amount of NH₃ adsorbed per cm² of film (N), according to Beer's law adapted for work on solid films: $\Delta A = kN$. On the assumption that one OH disappeared for every molecule of NH₃ adsorbed, the absorption coefficient of the OH groups was calculated from the slope of this line. This procedure is only valid if all of the ammonia introduced is adsorbed by the film. Determination of an adsorption isotherm for NH₃ showed that this was the case in these experiments.

As the HF and LF bands have very different coefficients, the X₄₀ sample was prepared. The ir spectrum of this sample shows only the HF band, the absorption coefficient of which was determined as described. Assuming that this coefficient was applicable to the HF band in all of the other samples, we could estimate the amount of NH₃ consumed by reaction with OH groups of the HF band. After deduction of this quantity from the total amount of NH₃ introduced, the adsorption coefficient of the LF band could be calculated for any other sample having both the HF and LF bands. To take into account the scatter of the experimental points, several runs were carried out for each sample. After normalization for film thickness, a statistical treatment of the data allowed the calculation of the absorption coefficient using the least-square method as described for ir work by Baumann.¹¹

The coefficients obtained in this manner are evidently apparent values as their magnitude depends on the instruments and the experimental conditions used. The spectra were obtained using a Beckman IR 12 grating spectrophotometer, which was set so as to obtain 70% transmission in single beam at 2800 cm⁻¹. Slit openings of up to 5 times the standard slit were needed corresponding to a spectral slit of less than 10% of the half-width of the narrowest band. The spectra were recorded in absorbance units at a speed of 40 cm⁻¹/min and a chart speed of 2 in./100 cm⁻¹.

The coefficients so obtained are: k_{HF} assumed the same in all samples, 68.155 cm² μmole⁻¹; k_{LF} in X₇₅, 40.3 cm² μmole⁻¹; k_{LF} in Y₉₀ and Y₅₀, 32.6 cm² μmole⁻¹.

The difference in k_{LF} between X and Y is probably due to the difference in particle size of the samples. The Y samples were submitted to a fractionation procedure as described by Angell and Schaffer⁴ and only the fine fraction was used for this study. Scattering

losses were therefore minimized and a good base line could be adopted. On the other hand, the X sample was coarse grained as the material could not be satisfactorily fractionated. A loss of intensity by scattering occurred in the OH stretching region and hence the adoption of a base line tangential to the extremes of the peak may have introduced a systematic deviation. For the HF band, however, the difference was not important as this band was narrow and a good base line could be drawn.

The absorption coefficients for the HF and LF bands obtained from ir analyses were checked by direct thermogravimetric measurements. The dehydroxylation of the different zeolites as a function of temperature was followed on samples pressed into films using a Cahn electrobalance, Type RH, under vacuum. In a parallel set of experiments the change in intensity of the OH bands as a function of temperature was recorded, using conditions similar to those adopted in the thermogravimetric experiments. From ir analyses it was concluded that above 300° the weight loss could be accounted for by dehydroxylation alone. Combining the weight loss and the decrease in band intensity for treatments above 300° the absorption coefficient could be calculated as in the NH₃ adsorption experiments. The correspondence between the coefficients calculated by the two methods was better than 10%. The values obtained by NH₃ adsorption are used throughout this work, as they are the statistical average of a great number of experiments.

Sample Treatment for Thermal Stability Studies. The influence of two different vacuum pretreatments was studied. In the "flash pretreatment" the samples were first outgassed at room temperature for a few hours to remove hydration water, after which it was very rapidly (10 min) heated to 300° to cause a quantitative deammoniation. In the "isothermal step" or IS method the sample was heated slowly. After a preliminary room-temperature outgassing, the temperature was raised gradually to about 80° and maintained at this level for 1 hr. The sample was then cooled and a spectrum was taken. Outgassing was resumed in the same way passing through several isothermal steps. The change in hydroxyl content as a function of these two pretreatment conditions was followed thermogravimetrically and by quantitative ir spectroscopy up to a temperature limit of 500°. In the IS method there was a difference between ir spectroscopy and thermogravimetry: in the first case the temperature was raised, without intermittent cooling, as soon as a constant weight was obtained on each isothermal step. The thermogravimetric analysis gave only the total amount of hydroxyls removed, while the ir method allowed a distinction to

(11) R. P. Baumann, "Absorption Spectroscopy," John Wiley and Sons, Inc., New York, N. Y., 1962.

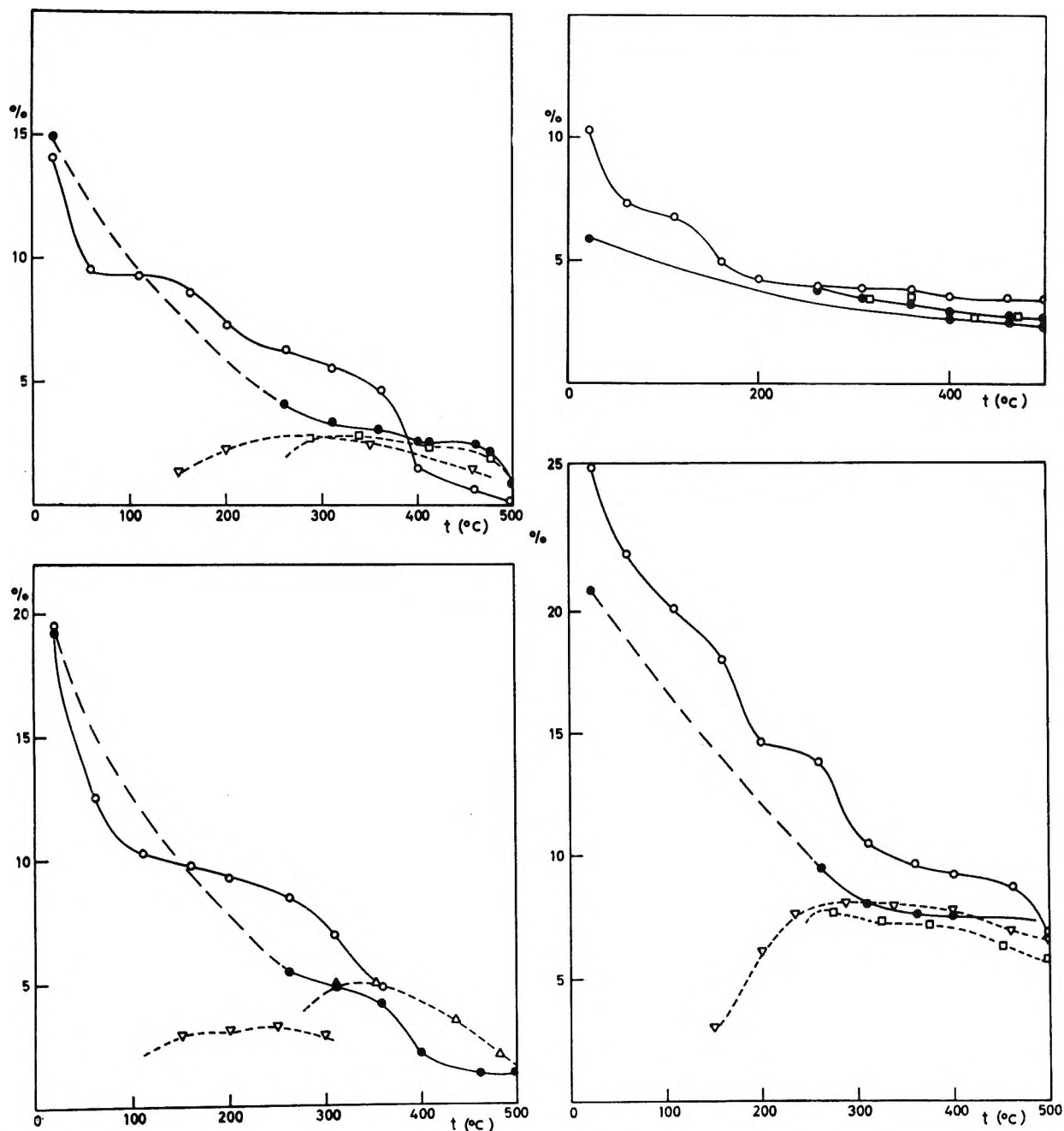


Figure 1. Content in volatile products as a function of temperature: obtained by thermogravimetry: \circ , IS pretreatment; \bullet , flash pretreatment; obtained by ir spectroscopy: \square or Δ , IS pretreatment; ∇ , flash pretreatment. Data are for the samples X₄₀ (upper left), X₇₅ (lower left), Y₅₀ (upper right), and Y₉₀ (lower right).

be made between the OH's responsible for the HF and for the LF bands.

Results

Figure 1 shows the content of volatile components (NH₃ and/or OH) of the different samples as a function of temperature. The results are expressed as a fraction (per cent) of the final weight after calcination. The evolution of the OH concentration measured by ir spectroscopy is plotted on the same graph. The ir spectra show that NH₃ is quantitatively removed at 260° for the X samples and at 300° for the Y samples.

It can be seen from Figure 1 that the OH contents calculated by ir analyses show a shallow maximum, whereas the thermogravimetric curves reach a more or less constant level around these temperatures. Further, at about 300° the thermogravimetric curve coincides with the OH content calculated from ir measurements, confirming the validity of the absorption coefficient determination.

In the thermogravimetric experiments, flash and IS desorption gave two distinct curves. Below a certain limit the weight loss on flash desorption is a little higher than on IS desorption at corresponding temperatures.

Table II: Degree of Dehydroxylation, Ratio of the Intensity of the LF to the HF Bands (LF/HF), and Distribution of OH's in the Unit Cell Calculated from the Ir Spectra

Sample	T_{\max} , °C	% dehydroxn at T_{\max}	% dehydroxn at 500°	LF/HF at T_{\max}	LF/HF at 500°	OH/unit cell at T_{\max} in the HF band	OH/unit cell at T_{\max} in the LF band
X ₄₀ Flash	330	39	68	21.9	...
IS	280	39	76
X ₇₅ Flash	365	49	82	1.35	...	25	8
IS	250	66	92	3.28
Y ₅₀ Flash	360	0	35	1.56	1.29	9.7	15.1
IS	300	0	35
Y ₉₀ Flash	290	0	27	3.10	2.53	11.9	36.9
IS	275	0	16	3.88	2.93	10.0	38.8

^a Temperature at which the intensity of the OH bands was maximum.

Flash desorption has, however, a pronounced stabilizing effect and retards the dehydroxylation at higher temperature. Except for the very stable Y₅₀ sample, the curves show a sudden drop in OH content. The temperature at which this occurs is lower for X than for Y samples and is shifted upward for lower degrees of decationation. This drop in OH content occurs at higher temperatures for flashed samples than for IS pretreated samples, the delay being of approximately 100°. For the X samples complete dehydroxylation was attained at 500° at which temperature the Y₉₀ IS only started to dehydroxylate. The Pyrex apparatus, however, did not allow investigations to be carried out at temperatures above 500°.

Figure 2 shows the total OH content and the amount of OH's involved in the HF and LF bands as calculated from the ir spectra. The data are expressed in milliequivalents of OH per g of zeolite dried at 1000° and also in per cent of the maximum theoretical OH content calculated from chemical analysis. The per cent scale applies only to the total amount of OH groups.

It is evident again that the X samples are less stable than the Y, as can be deduced from the OH contents after pretreatment at 500°. Further, there was considerable overlap between the deammoniation and dehydroxylation reactions in the case of the X samples. Even at 300° the OH content is considerably lower than the theoretical maximum value indicating that considerable dehydroxylation has taken place. On the other hand, the Y samples did not show appreciable dehydroxylation after pretreatment at 300°.

It is clear from the curves in Figure 2 that the OH groups involved in the LF bands are less stable than the OH's of the HF band. This is less apparent for the X samples: the X₄₀ sample has indeed no LF band, and the X₇₅ is very unstable. For the two Y samples, the dehydroxylation affected only the LF band, and in the temperature range below 500°, the HF band remained unaltered. For the different samples studied, the temperature at which the OH content is at a maximum (T_{\max}), the per cent dehydroxylation at that tempera-

ture and at 500°, and also the ratio of the intensities of the LF to the HF band are summarized in Table II. The data in this table are obtained from ir measurements. A comparison of the data in Table II accentuate the difference between flash and IS treatment. Flash pretreatment retards the dehydroxylation process. For stable samples like Y₅₀ and Y₉₀ the difference is less important than for the unstable X samples. The decrease in the LF/HF ratios at higher temperatures also supports the preferential dehydroxylation of the LF sites.

Discussion

A great deal of experimental evidence supports the hypothesis that the two distinct OH vibration bands correspond to different locations of the OH groups in the lattice.^{1,5} The relative intensity of the HF and LF bands is indeed very different for X and Y zeolites and depends on the degree of NH₄⁺ exchange. Hence some relation must exist between the different ion-exchange sites and the location of the hydroxyls. Until recently, the well-known classification of ion-exchange sites by Breck¹² was the only basis for discussing the location of the exchangeable ions. This classification was based on X-ray work on hydrated zeolites. Recently, new X-ray work on dehydrated synthetic faujasites was published by Eulenberger, Shoemaker, and Keil.¹³ The two systems have in common that a majority of exchangeable ions, up to 32 per unit cell, are located on the free six-membered rings of oxygens of the cuboctahedra, adjacent to the big cavity or "supercage." The two systems agree also on the location of some cations up to a maximum of 16 per unit cell in the hexagonal prisms forming the link between cuboctahedra. The rest of the cations could not be located by X-ray diffraction on hydrated samples. Breck postulated that they were located along the walls of the big cavity but did not further define their position. However, Eulen-

(12) D. W. Breck, *J. Chem. Educ.*, **41**, 678 (1964).

(13) G. R. Eulenberger, D. P. Shoemaker, and J. G. Keil, *J. Phys. Chem.*, **71**, 1812 (1967).

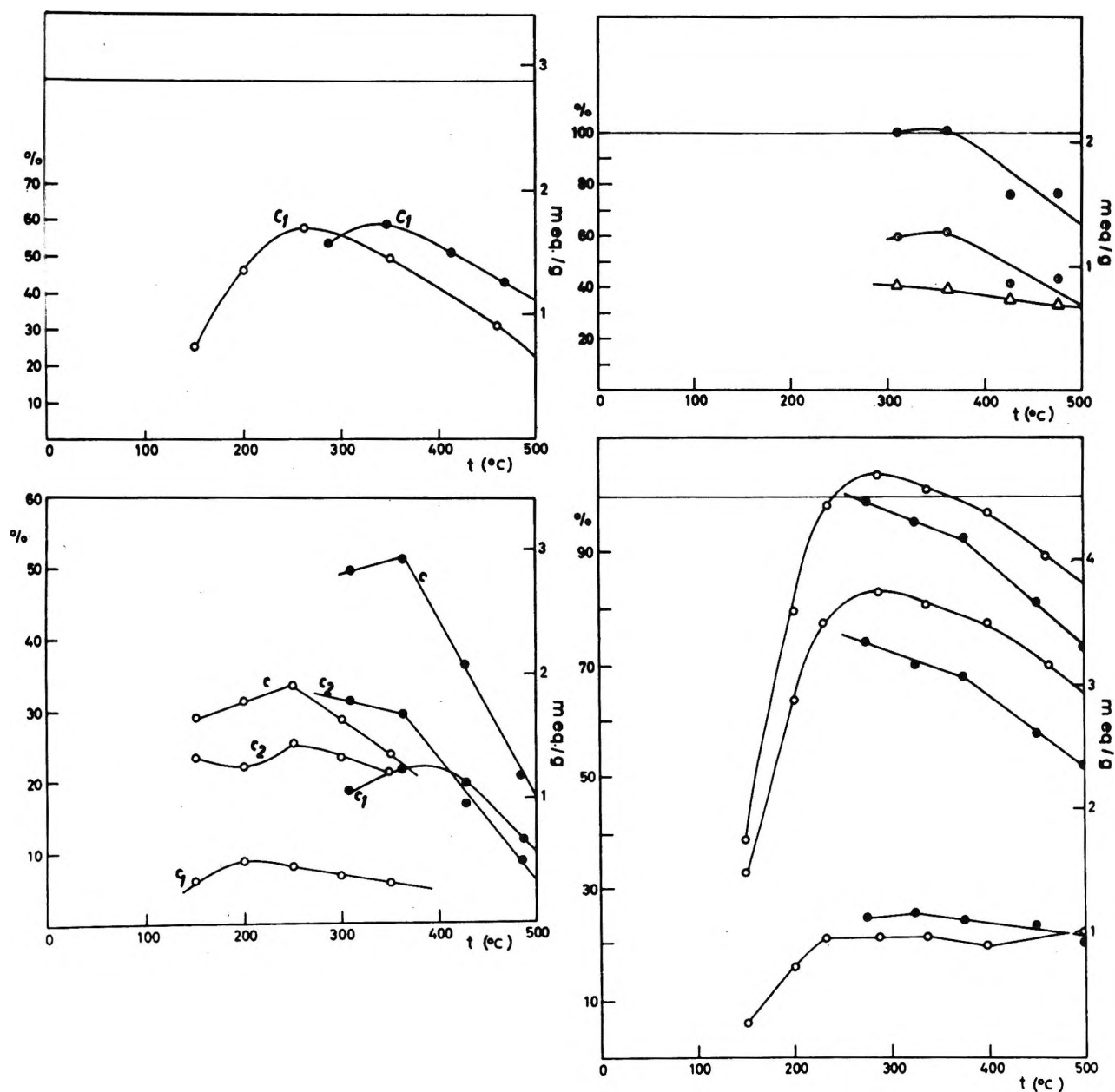


Figure 2. Total OH content and content in OH groups involved in the HF and LF bands, calculated from the ir spectra: upper left, X_{40} : ●, flash; ○, IS; lower left, X_{75} : ●, flash; ○, IS; C = total OH; C_1 = OH groups of the HF band; C_2 = OH groups of the LF band; upper right, Y_{50} : ●, total OH content; Δ, OH groups of the HF band; ○, OH groups of the LF band; lower right, Y_{30} : ●, flash pretreatment; ○, IS; two upper curves, total OH content; two middle curves, OH groups of the LF band; two lower curves, OH groups of the HF band.

berger, *et al.*,¹³ presented evidence that in dehydrated samples the cations in excess of the two well-defined sites were located inside the cuboctahedron on the six-membered rings of oxygens. The work of Eulenberger, *et al.*, was performed on type-Y zeolite in the Na^+ , K^+ , and Ag^+ forms, and no X-ray data on decationated samples have so far been published. In Eulenberger's sample, with 57 exchangeable ions per unit cell, only 19 Na^+ ions are located inside the cuboctahedron. In view of these findings, dehydrated X zeolites would also have their exchangeable ions in excess of the two well-defined sites, inside the cuboctahedra, and not in the

supercage as postulated by Breck. As the number of ions inside the cuboctahedron increases, some six-membered rings of oxygens would carry two cations, one being inside the cuboctahedron and the other either inside the big cavity or inside the hexagonal prism. We shall refer to such six-membered rings as doubly occupied.

The lack of experimental data on the position of the unexchanged Na^+ ions in decationated zeolites makes a discussion of a possible relationship between the location of OH groups and ion-exchange sites somewhat difficult. On the basis of Sherry's work¹⁴ on ion exchange, how-

ever, we may assume that the first ions to exchange with NH_4^+ would be located in the most accessible sites, that is, inside the big cavity. At the temperature of deammoniation (300°), the protons and the residual Na ions are known to migrate.¹⁵ It is thought that each time a six-membered ring of oxygens is liberated by decomposition of an ammonium ion, an Na^+ ion tends to migrate from a doubly occupied six-membered ring inside the cuboctahedron toward this liberated ring.

All of these considerations lead us to envisage two distinct OH locations. The first, responsible for the HF band, is on the oxygens forming the hexagonal prism between cuboctahedra, referred to as "bridge oxygens." The second location is on "ring oxygens" belonging to six-membered rings of oxygens forming the cuboctahedra. OH groups formed on ring oxygens are responsible for the LF band. Consideration of a structural model of faujasite reveals that there are 96 bridge oxygens and 384 ring oxygens per unit cell and that there is no other type of oxygens besides these two. This explains the observation that there are no more than two OH bands in the IR spectra of deammoniated zeolites.

The assignments of the HF band to hydroxyls on bridge oxygens and of the LF band to hydroxyls on ring oxygens is further supported by the following observations.

(1) In the X_{40} sample the number of Na^+ ions is sufficient to occupy all of the available six-membered rings so that no empty six-membered rings are available. There are indeed (Table I) 50 residual Na^+ ions per unit cell. If we assume that Pauling's rule on the electrical neutrality in crystals applies in this case, the protons liberated during the deammoniation cannot go on a ring oxygen as long as this ring is occupied by an Na^+ ion. The fixation of the proton to a bridge oxygen fits best the rule of Pauling. This explains the observation that the X_{40} sample has only a strong HF band and no LF band.

(2) The excess of exchangeable ions with respect to the exchange sites of types I and III in Eulenberger's notation¹³ is higher in X than in Y samples. The HF band is therefore more intense in the decationated X than in the Y samples. This is seen in Table II when the population of OH groups on bridge oxygens (HF) per unit cell is considered.

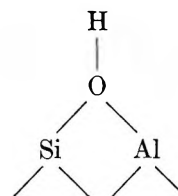
(3) Consideration of the relative population of the HF and LF band after deammoniation at 300° , for samples having different degrees of decationation, further indicates that the HF band is close to its maximum intensity before the LF band starts to develop (Table II, columns 7 and 8).

Other arguments in favor of this assignment are found in the literature.^{1,7,8} It is well known that the deammoniation is a reversible reaction and that the two OH bands disappear when NH_3 is re-adsorbed.¹ When

bigger molecules are adsorbed, the reaction with the OH groups of the LF band is hindered. Liengme and Hall⁷ reported that the HF band disappeared completely by adsorption of pyridine whereas the intensity of the LF band was only slightly diminished. Hughes and White,⁸ adsorbing pyridine at an elevated temperature (250°), have observed a complete reaction of the OH groups of the HF band with pyridine while the LF band remained unaltered. With piperidine the reaction went to completion with both kinds of OH groups. This is understood on the basis of our assignment of the OH bands. The protons will occupy on the oxygens the sp^3 orbitals which are not used for bonding with the Si and Al ions in the framework. Each oxygen has two free orbitals. Consideration of a scale model leads to the conclusion that the free orbitals on the bridge oxygens are directed into the big cavity. The OH groups formed on these oxygens, responsible for the HF band, are accessible to all reacting molecules which can enter the big cavity. Four different orientations of the free orbitals are possible on the ring oxygens, but only one is in such a direction that it is accessible from the big cavity, one is more or less oriented into the hexagonal prism, and the other two are oriented inside the cuboctahedron.

Pyridine and piperidine are both excluded from the inside of the cuboctahedron: this explains the incomplete reaction in the case of pyridine. The ability of piperidine to react with the total amount of OH groups on ring oxygens, in spite of the sterical hindrance, must be related to its higher affinity for protons: piperidine is a much stronger base than pyridine. This can only be understood if we take in account the mobility of the protons in the zeolite structure. The activation energy of migration of the protons is approximately 5 kcal.¹⁵ As compared to pyridine the lone pair of electrons on the nitrogen of piperidine exerts its influence further from the nitrogen. Hence, piperidine could influence the migration of the protons toward a free orbital on a ring oxygen in such a position that reaction with piperidine can take place.

The site where the OH group is located in deammoniated zeolites may be schematically represented by



Although a formal bond between oxygen and aluminum is not required to ensure electrical neutrality, it is needed to fulfil the coordination requirement of the

(14) H. S. Sherry, *J. Phys. Chem.*, **70**, 1158 (1966).

(15) J. B. Uytterhoeven, R. Schoonheydt, and J. J. Fripiat, International Symposium on Reaction Mechanisms of Inorganic Solids, The Chemical Society, London, 1966, Abstract 5-2.

aluminum. The influence of the aluminum ion weakens the force constant between the oxygen and the proton, and this explains the lowering in frequency as compared to Si-OH groups in silica, alumina, and silicoalumina gels.¹ The observation that OH groups on bridge oxygens absorb at a different frequency than OH groups on ring oxygens is probably due to local differences in the electrical potential throughout the structure as suggested by White, *et al.*⁵ As the hexagonal prisms between cuboctahedra constitute zones of higher density in the structure, it is probable that the potential in the vicinity of the bridge oxygens is different from that existing near the ring oxygens. The treatment given to this problem by White, *et al.*,⁵ is correct, but more precise data on the potential at specific points in the structure and on the residual charge on the protons are desirable.

These considerations invalidate the hypothesis that the lowering of the wave numbers of the OH stretching bands in zeolites, as compared to free SiOH groups in silica, is due to hydrogen bonding. Hughes and White⁸ postulated that the 3550-cm⁻¹ band was due to an OH at a highly accessible O₁-type oxygen, hydrogen-bonded to an O₄ oxygen. According to Eulenberger, *et al.*,¹³ the distance between these oxygens is 2.67 Å in a sodium Y zeolite. Referring to Pimentel and McClellan,¹⁶ Hughes and White concluded that this distance was very close to the O-H...O distance of 2.83-2.91 Å necessary to cause a frequency shift of 100-200 cm⁻¹. Our main objection to this argument is that O₄ and O₁ are oxygens belonging to the same tetrahedron.

Considering the orientation of the orbitals on oxygen, it is very unlikely that hydrogen bonding occurs between an OH and an oxygen belonging to a same tetrahedron. The correlation between O-H...O distance and frequency shift referred to by Hughes and White is valid only for "straight" hydrogen bonds and certainly does not apply to the kind of hydrogen bonds invoked by these authors. The shortest distance between framework oxygen, not belonging to the same tetrahedron, which could be considered for possible O-H...O bonding is approximately 3.7 Å,¹⁷ an improbably long distance for hydrogen bonding to occur.

Following Coggeshall¹⁸ we may estimate the dissociation energy of the hydroxyl groups which gave rise to the HF and LF bands. The values so obtained are of the order of 105 kcal mole⁻¹ for the HF band and 101 kcal mole⁻¹ for the LF band. This difference in dissociation energy explains the difference in thermal stability between the two kinds of hydroxyls.

The stabilizing effect of flash activation is understood on the basis of the different distribution of the OH groups over the LF and HF bands (Table II). The comparison is difficult for the X samples, because of the

considerable dehydroxylation which had occurred. For the Y₉₀ sample more hydroxyls are located on the less stable ring oxygens after IS pretreatment than after flash desorption. Therefore the flash pretreatment gives higher stability. Because high temperatures are very rapidly attained in the flash operation, migration of the exchangeable ions, including NH₄⁺, may be important before the NH₄⁺ ions decompose.

The NH₄⁺ ions are located only in the big cavities. During their migration from one six-membered ring of oxygens (exchange site I) to another, they are obliged to go over square faces of oxygens. Upon flash desorption the decomposition of the NH₄⁺ ions could be retarded because of a certain pressure of NH₃ realized in the pore system. Therefore a higher proportion of NH₄⁺ ions will decompose at the square faces, where the bridge oxygens are situated. Hence a higher proportion of the protons react with bridge oxygens upon flash than upon IS deammoniation.

The difference in stability between X and Y zeolites cannot be wholly understood on the basis of higher concentration of hydroxyls. Although the stability increases with lower degree of decationation, the X samples with lower hydroxyl contents are still less stable than the thoroughly decationated Y, as can be deduced from a comparison of the X₄₀ and Y₉₀ samples (Table II). From electrical neutrality considerations, the most probable sites for the location of the protons are the oxygens coordinated to an Al³⁺ ion. In X samples, nearly all of the oxygens are shared between an aluminum-bearing and a silicon-bearing tetrahedron and each oxygen is a possible site for proton fixation. In Y zeolites approximately one-third of the oxygens are shared between two silicon-bearing tetrahedra, and these oxygens must have a lower affinity for protons. The migration of protons must therefore be easier in X zeolites, and hence the probability of encounter between two protons on the same oxygen, the initial step of the dehydroxylation, must be higher in X than in Y zeolites. This explains the difference in thermal stability between these two types.

Acknowledgment. We are indebted to Professor J. J. Fripiat, University of Louvain, for the use of the infrared spectrophotometer and other equipment, and for many fruitful discussions. We thank the NFWO (Belgium) for financial support and for a Research Grant to R. Schoonheydt. The gift of samples of the zeolite by the Linde Co. is gratefully acknowledged.

(16) G. C. Pimentel and A. L. McClellan, "The Hydrogen Bond," W. H. Freeman, San Francisco, Calif., 1960, pp 95-96.

(17) W. H. Baur, *Am. Mineralogist*, **49**, 697 (1964).

(18) N. D. Coggeshall, *J. Chem. Phys.*, **18**, 978 (1950).

Spectrophotometric Identification of γ -Radiolytic Intermediates in a New Halogenic Glassy Matrix¹

by A. Grimison and G. A. Simpson

*Puerto Rico Nuclear Center² and Chemistry and Physics Departments, University of Puerto Rico, Río Piedras, Puerto Rico
(Received November 28, 1967)*

The absorption spectra, dose dependence, and character of the intermediates produced by γ radiolysis at 77°K of a 50:50 vol % mixture of Freon-11 (CCl₃F) and Freon-114B2 (CF₂BrCF₂Br) have been determined. Color centers are formed at 330 and 585 m μ which can be bleached by light of suitable wavelengths and which are assigned to cationic species. The stabilization of other cationic intermediates by this matrix is demonstrated by the detection of intermediates of several heterocyclic additives. Identification of the following cations and their λ_{\max} has been made: thiophene (830, 320 m μ), pyrrole (800 m μ), and pyridine (380 m μ).

Hamill^{3,4} has discussed the usefulness of some halogenic matrices for isolation and spectrophotometric identification of radiolytic intermediates at 77 °K. The matrices discussed, carbon tetrachloride and *n*- or *sec*-butyl chloride, are either opaque or form cracked glasses at liquid nitrogen temperatures. Measurements of the absorption spectra of these matrices require the use of short path lengths. Therefore, high concentration of reactant and high doses may be required to produce detectable spectra of radiolytic intermediates. These limitations can be avoided if a more transparent glassy matrix could be used which retains the electron trapping and positive hole stabilization characteristics of the opaque solvents.^{3,4}

Sandorfy⁵ has discovered that a 50:50 vol % mixture of Freon-11 (CCl₃F) and Freon-114B2 (CF₂BrCF₂Br) forms a stable, clear glass at 77°K suitable for spectroscopic studies. This matrix is transparent up to 3-cm path length throughout the entire visible region to 2700 m μ and is translucent for path lengths up to 20 cm.

The spectroscopic properties of the intermediates produced by radiolysis in this Freon mixture (FM) have been determined. The ability of this matrix to stabilize the intermediates produced by radiolysis of some dissolved heterocyclic compounds has also been investigated and is reported here.

Experimental Section

The apparatus used to determine absorption spectra at 77°K with the Beckman DK1A spectrophotometer is shown in Figure 1. A brass dewar holder⁶ permits reproducible positioning of a rectangular quartz dewar in the sample beam of the spectrophotometer. The rectangular quartz dewar⁷ has been used previously for luminescence studies but has never been described. It consists of General Electric lamp glass No. 204 square drawn quartz tubes attached concentrically by a ring seal and fused to quartz plates at the

bottom. This design was preferred to that described by Farhataziz and Dyne⁸ for reasons of lower signal noise from nitrogen bubbles and flexibility in cell-path length. Optical cells of 1 \times 1 cm² Spectracil tubing or up to 2.4-cm Pyrex Lollipop cells could be used. Most of the spectrophotometric data reported here were obtained through the use of this apparatus in the Beckman DK1A. However, spectra of the individual components, which form opaque films, were usually determined in an H. S. Martin and Co. "cold-finger" dewar, having an optical path of 1.6 mm, using the Cary-14 spectrophotometer. All spectra were determined in times ranging from 5 min to 2 hr after irradiation.

E. I. duPont or Matheson Freons were used after purification. Freon-11 was recrystallized twice at 77°K, retaining the liquor after half the material had solidified. Freon-114B2 was distilled twice, retaining a middle portion. The purification procedures were checked by glpc analysis. Methyltetrahydrofuran (Eastman Organic Chemicals, Co.) was passed over alumina under a nitrogen atmosphere and then transferred under vacuum to a flask containing a sodium-potassium alloy and stored until needed. N,N,N',N'-tetramethyl-*p*-phenylenediamine (TMPD) was liberated

(1) Presented in part at the "March" Meeting of the American Physical Society, Chicago, Ill., March, 1967; A. Grimison and G. A. Simpson, *Bull. Amer. Phys. Soc.*, **12**, 423 (1967).

(2) Puerto Rico Nuclear Center is operated by the University of Puerto Rico for the U. S. Atomic Energy Commission under Contract No. AT-(40-1)-1833.

(3) T. Shida and W. H. Hamill, *J. Chem. Phys.*, **44**, 2369 (1966).

(4) T. Shida and W. H. Hamill, *ibid.*, **44**, 4372 (1966).

(5) C. Sandorfy, *Can. Spectry*, **10**, 85 (1965).

(6) A scaled line diagram of the dewar holder and quartz cell is available in a Puerto Rico Nuclear Center Publication PRNC No. 88, Río Piedras, Puerto Rico, 1966.

(7) K. Funabashi, P. J. Herley, and M. Burton, *J. Chem. Phys.*, **43**, 3939 (1965).

(8) Farhataziz and P. J. Dyne, AECL No. 2113, Atomic Energy of Canada Ltd., Chalk River, Ont., 1964.

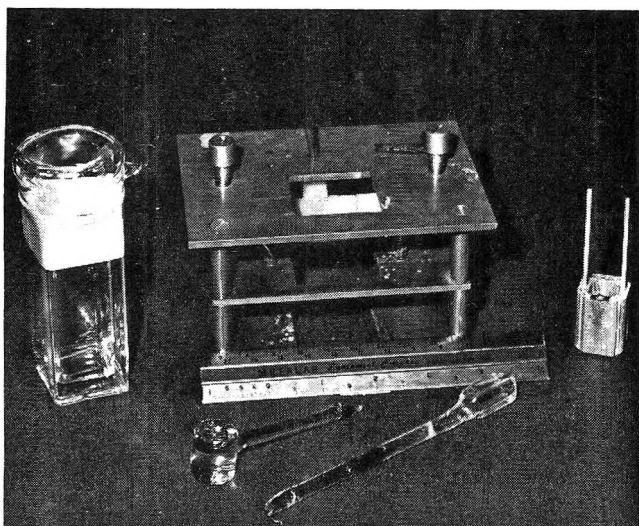


Figure 1. Optical equipment used with Beckman DK1A spectrophotometer. Figure shows square quartz dewar, dewar holder, square quartz cells, cell holder, and Pyrex Lollipop cell.

from its dihydrochloride by addition of NaOH and then was extracted with 3-methylpentane. The solution was evaporated and the solid was sublimed and was stored in the dark until the preparation of solutions. Re-sublimation was performed if discoloration occurred on standing. All other reagents were of the highest commercial purity and were distilled or sublimed prior to sample preparation.

Degassed solutions of the indicated molar concentration were prepared by conventional vacuum techniques using the required volume of FM which had been dried over molecular sieve (Type 3X) while under vacuum.

The dose rate was estimated using the Fricke dosimeter (the density of FM being 2.61 ± 0.06 g/cc at 77°K) in the optical cell in a dewar containing water.

Optical bleaching was performed with a 250-W Sylvania quartz iodine lamp, using Corning color filters transmitting wavelengths greater than $460\text{ m}\mu$ (CS No. 3-71) or greater than $650\text{ m}\mu$ (CS No. 2-64). Photolysis of TMPD was effected by 10-min exposure of a sample ($10^{-3} M$) to an Osram HBO 500 lamp.

Results and Discussion

Upon γ irradiation, a deep violet color is produced in the FM. The associated spectrum is shown in Figure 2, together with the effect of bleaching with wavelengths greater than $460\text{ m}\mu$. The FM bands at 330 and $585\text{ m}\mu$ are destroyed on bleaching. After bleaching there remains a broad absorption band, having λ_{max} at $600\text{ m}\mu$, which is unaffected by further bleaching. Absorption at wavelengths less than $270\text{ m}\mu$ could not be determined, owing to the solvent cutoff, but the absorption between 270 and $300\text{ m}\mu$ increases on bleaching. No other new absorption bands are produced. The variation of the optical density at $585\text{ m}\mu$ with total dose, and with the extent of

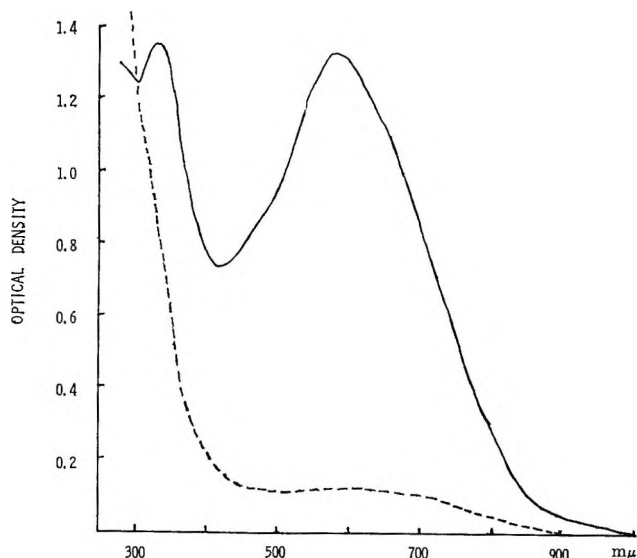


Figure 2. Absorption of doubly purified irradiated 50:50 vol% mixture of Freon-11 and Freon-114B2 at 77°K : —, after irradiation (1.6×10^{22} eV/l.); ---, after 20-min photobleaching.

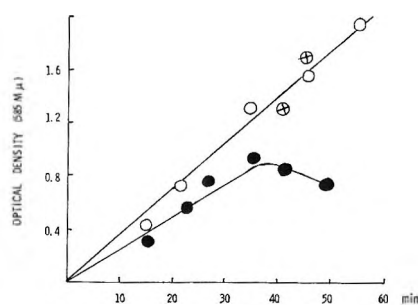


Figure 3. Optical density of irradiated 50:50 vol% mixtures of Freon-11 and Freon-114B2 at $585\text{ m}\mu$ vs. time of γ irradiation at 4.7×10^{20} eV/l. min and 77°K : ●, E. I. Du Pont Co. reagents; ○, doubly purified reagents (Freon-11, recrystallization; Freon-114B2, distillation); ⊕, triply purified reagents.

purification of the FM, is presented in Figure 3. This shows the $585\text{ m}\mu$ absorption to be a linear function of the dose and insensitive to further purification after two initial purification steps. The bands in irradiated FM are relatively stable, no obvious time dependence being observed for times up to 2 hr. The efficiency of production of the $585\text{-m}\mu$ band can be expressed as the product of the yield per 100 eV and the extinction coefficient. The value obtained from the slope of the curve in Figure 3 for purified FM and the dose rate is $G\epsilon = 4.5 \times 10^3 M^{-1} \text{ cm}^{-1}$ (molecules/100 eV).

Bleaching the sample with light of wavelengths greater than $650\text{ m}\mu$, and thus into the tail of $585\text{-m}\mu$ band, produces only a decrease in the $585\text{-m}\mu$ band. This indicates that the color centers at 330 and $585\text{ m}\mu$ are associated with distinct entities and that the $330\text{-m}\mu$ band extends into the region $460\text{--}650\text{ m}\mu$. Variation

of the FM composition results in a variation in both the relative intensities and positions of the 330- and 585- $m\mu$ bands. The absorption bands produced on γ radiolysis of the separate components at 77°K were, therefore, determined, although aerated cells then had to be used, as distinct from the FM irradiations. For Freon-11, maxima are produced at 310 and at 535 $m\mu$, with a shoulder at 600 $m\mu$. For Freon-114B2 a maximum is produced at 360 $m\mu$. These absorption bands were also decreased on bleaching. These results show that the color centers in the FM are similar to, but not identical with, the color centers observed in the separate components.

Irradiation of a 0.15 vol % solution of the FM in glassy MTHF at 77°K results in the trapped electron band of MTHF at 1200 $m\mu$ being decreased by 78% relative to the pure solvent. This indicates that the FM is very efficient in scavenging electrons. However, the bleachable bands cannot be assigned to species resulting from simple electron attachment to the FM. This was demonstrated by the photolysis of a solution of TMPD in the FM, as a source of low-energy electrons. This photolysis produced the well-known absorption of the Wursters blue cation but produced no additional absorption resembling that observed in γ -irradiated FM.

In order to test the possibility that the color centers observed in the FM are cationic in nature, an attempt was made to observe positive charge transfer on photostimulation. A solution of TMPD in the FM was γ -irradiated so as to produce both FM color centers and TMPD cation absorption, but under conditions where a considerable concentration of TMPD neutral molecule remained. This sample was subsequently bleached with light of wavelengths greater than 460 $m\mu$, so that only the overlapping FM color centers and TMPD cation absorptions were excited. Since the TMPD cation⁹ itself is inert to photostimulation, a photostimulated positive-charge migration from the FM color center to TMPD neutral molecule should cause a decrease in the FM color center and an increase in the TMPD cation absorption. The results are shown in Figure 4. These results are consistent with a decrease in the underlying FM absorption and a concomitant increase in the TMPD cation absorption. Using the known relative optical densities of FM⁺ absorption at 585 and 630 $m\mu$ and that of TMPD⁺ in the absence of any FM⁺ absorption, the spectrum in Figure 4 can be resolved into its components. Thus it is determined that FM⁺ has an optical density of 0.25 at 585 $m\mu$ before bleaching and that TMPD⁺ has 1.16 and 1.57 OD units at the same wavelengths before and after bleaching, respectively. Under the conditions of the bleaching experiment, both the 585- and 330- $m\mu$ bands are completely removed in the absence of any additive. If it is assumed that only the positive species giving rise to the 585- $m\mu$ band react and that

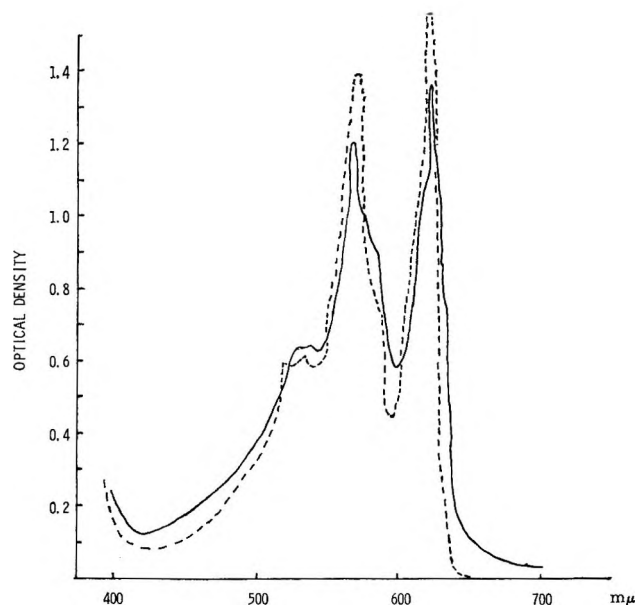


Figure 4. Absorption spectrum of irradiated N,N,N',N' -tetramethyl-*p*-phenylenediamine ($10^{-2} M$ in FM at 77°K, dose rate = 4.7×10^{20} eV/l. min): —, after 10-min irradiation; ---, after 10-min bleach ($\lambda > 460 m\mu$).

all of those species are effective in causing an increase in the TMPD⁺ absorption, then a value of $\epsilon_{585} = 1.2 \times 10^4 M^{-1} cm^{-1}$ is obtained using $\epsilon = 1.93 \times 10^4 M^{-1} cm^{-1}$ for TMPD⁺ at 585 $m\mu$.⁹ This value may be high since the migration of cations associated with the 330- $m\mu$ band contributes to the TMPD⁺ increase and since there is, presumably, some inefficiency in the charge-transfer process. The value may be compared with that obtained from the oscillator-strength equation,¹⁰ using the approximation $f = 4.32 \times 10^{-9} \epsilon_{\max} \Delta\nu_{1/2}$. The value of $\Delta\nu_{1/2} = 0.80 \times 10^4 cm^{-1}$ is determined from the $\lambda_{1/2}$ values of 450 and 750 $m\mu$. Assuming an $f = 1$ gives the value of $\epsilon_{585} = 2.9 \times 10^4 M^{-1} cm^{-1}$, which is approximately twice the earlier value and provides a rough corroboration of the order of magnitude. Now use of the value of $\epsilon_{585} = 1.2 \times 10^4$ and the $G\epsilon$ value indicates that the efficiency of production of the 585- $m\mu$ FM species by radiation is greater than 0.4/100 eV.

The shifts observed in the λ_{\max} of the cation bands in the components and in FM suggests that the transitions associated with these cations are not restricted to isolated entities such as CCl_3F^+ and $CF_2BrCF_2Br^+$. The transitions may involve a participation of the solvent environment with these cations *via* electron exchange.

On the addition of small amounts ($\sim 10^{-2} M$) of various heterocyclic compounds to the FM and subsequent γ irradiation, the yield of the solvent bands decreased and new absorptions were produced. The

(9) W. C. Meyer and A. C. Albrecht, *J. Phys. Chem.*, **66**, 1168 (1962).

(10) R. S. Mulliken, *J. Chem. Phys.*, **7**, 14 (1939).

Table I: Effects of Heterocyclic Additives on γ -Irradiated FM at 77°K

Solute	Concn, <i>M</i>	λ_{\max} (solute intermediate), <i>m</i> μ	OD ^a (585 <i>m</i> μ)	OD _{solute} ^a (λ_{\max})	Change in heterocyclic band on bleaching solvent band
None	1.00
Furan	4.6×10^{-2}	1000, 710	0.17	0.30, 1.00	Decrease, form λ_{\max} 500 <i>m</i> μ
Thiophene	4.2×10^{-2}	830, 320	0.11	0.14, 0.65	Increase, form λ_{\max} 530 <i>m</i> μ
Pyrrole	2.9×10^{-2}	800	0.39	1.77	Increase
Imidazole	Saturated	580	1.40	1.40	Decrease
Pyridine	5.1×10^{-3}	380	0.72	1.60	Increase
Pyrimidine	2.2×10^{-1}	650	0.32	0.45	Decrease
Pyrazine	1.3×10^{-1}	650	0.23	0.52	Decrease
Pyridazine	2.2×10^{-2}	475 sh, 380 sh	0.29	0.43, 0.40	Decrease

^a 1.3×10^{22} -eV/l. dose.

results of these experiments are shown in Table I. It is not probable that the solutes can compete effectively with the FM itself for electron trapping, so that negative intermediates of solutes are not expected in a halogen matrix. The results suggest that competition for positive-charge formation in the matrix has occurred and that new cationic intermediates¹¹ are produced. The necessary and sufficient test for the existence of a cationic intermediate of an additive must be that not only does the additive depress the FM⁺ absorption, but also that on bleaching the FM⁺ absorption an increase in the absorption of the intermediates is produced.

Pyrrole, thiophene, and pyridine exhibit new absorption maxima as indicated, which increase on bleaching the solvent band. These absorptions are, therefore, assigned to cation intermediates of pyrrole, thiophene, and pyridine. A preliminary Pariser-Parr-Pople SCF calculation¹² using optimized parameters for the appropriate neutral molecule yielded transition energies of 1.2 and 3.2 eV for the pyrrole and pyridine radical cations, respectively, against the above experimental values of 1.5 and 3.3 eV for the absorptions assigned to cationic species.

For the other additives, an assignment cannot be made as readily. For imidazole, pyrimidine, pyridazine, and pyrazine, the contribution of the intermediate is uncertain, owing to overlap with the FM color centers. The solute intermediate absorptions decrease on bleaching, but the maxima can be obtained

by suitable bleaching experiments, since the FM color centers disappear more readily. It is not certain whether imidazole gives an absorption maximum at 585 *m* μ or enhances the FM absorption at 585 *m* μ , since no residual absorption is obtained on bleaching. Furan also shows a decrease in the absorption of the intermediate on bleaching, but a new maximum is formed at 500 *m* μ . (The absorption of irradiated thiophene, which increases on bleaching, also exhibits a new maximum at 530 *m* μ). A possible explanation of the decreases observed on bleaching intermediates from furan, imidazole, pyrimidine, pyrazine, and pyridazine is that these intermediates are photolytically unstable. The nature of these species is being further investigated.

The glassy FM matrix is recommended for use in isolating γ -radiolytic intermediates because of its superior transmission properties and its ability to trap electrons irreversibly, to trap positive charges reversibly, and to stabilize cationic intermediates.

Acknowledgment. The authors wish to thank Professor C. Sandorfy for suggesting this matrix and Professor W. H. Hamill for much helpful discussion. This work was supported by a grant from the USAEC Division of Biology and Medicine.

(11) These experiments cannot distinguish between a cation that is the direct result of the competition for positive-charge formation or an intermediate whose precursor is the primary cationic intermediate. For convenience the term cationic intermediates is used here.

(12) A. Grimison, unpublished results.

The Radiolysis of Cyclohexane in the Presence of Deuterated Olefins.

The Involvement of the Olefins in Hydrogen Formation¹

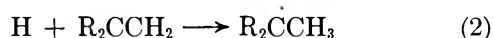
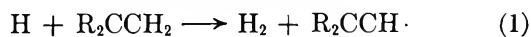
by M. G. Robinson and G. R. Freeman

Department of Chemistry, University of Alberta, Edmonton, Canada (Received November 28, 1967)

The hydrogen yields from the radiolysis of cyclohexane solutions containing low concentrations of deuterated olefins (C₃-C₇) have been measured. The presence of significant amounts of HD and D₂ in the products confirms an earlier suggestion that the olefins participate in hydrogen formation as well as acting as inhibitors. However, it is mainly the alkyl groups of the fully deuterated olefins that are involved in HD formation. A small amount of molecular D₂ elimination occurs from the olefinic carbons. The addition of ethanol to a solution of C₃D₆ in cyclohexane reduced the yields of HD and D₂ by the same proportionate amounts. The results are explained by ionic reactions. There is no clear-cut evidence for the occurrence of hydrogen atom scavenging.

Introduction

Hydrogen atoms have frequently been proposed²⁻⁹ as being the reactive precursors of the molecular hydrogen formed in the radiolysis of liquid alkanes. In an investigation⁵ of the effect of structurally different olefins on the radiolysis of *n*-hexane, the decrease in yield of hydrogen was attributed to scavenging of hydrogen atoms by the olefin. From a kinetic treatment of the results, it was concluded that hydrogen atom abstraction from the olefin R₂CCH₂ occurred, reaction 1, as well as hydrogen atom addition, reaction 2. The ratio of hydrogen abstraction to hydrogen



addition, k_1/k_2 , was found to be ~ 0.3 for olefins having the structures RCHCH₂ and R₂CCH₂. Furthermore, the evidence purported to show that the hydrogen abstraction occurred mainly from the olefinic carbons (*e.g.*, reaction 1).

These conclusions seemed surprising in view of the fact that the dissociation energies of the C-H bonds on the olefinic carbons are considerably greater than those of C-H bonds in alkyl groups in the olefins.¹⁰ Also, there is no clear-cut evidence for the interaction of hydrogen atoms with olefins in the condensed-phase radiolysis of alkanes. The evidence for such interactions involves kinetic plots based on a mechanism that has been shown not to be unique.¹¹ It was, therefore, decided to check the above conclusions by using olefins suitably labeled with deuterium.

Experimental Section

Fisher Spectroanalyzed cyclohexane was thoroughly degassed, taking care to remove carbon dioxide. Phillips research grade propylene was purified by distillation and freeze-pump-thaw cycles in a vacuum

system. The deuterated olefins, from Merck Sharp and Dohme, were similarly deaerated before use. Benzene-free ethanol (Reliance Chemical Co.) was purified as reported elsewhere.¹²

The nmr spectrum of CD₃CHCH₂ indicated less than 0.1% of isotopic scrambling. That of hept-1-ene-1,1,2-*d*₃ showed 10% scrambling of —CD=CD₂ and —CH=CD₂, while C₃D₆ was shown to contain 99% D. The samples were prepared by standard vacuum techniques.

Most samples consisted of 2.0 ml of liquid in 2.5-ml cells. They were irradiated in a ⁶⁰Co Gammacell-220 at 23°. The dose rate was 5×10^{17} eV/ml min and the doses given were in the range 2×10^{18} to 2×10^{19} eV/ml.

For hept-1-ene-1,1,2-*d*₃, 4.0-ml aliquots of standard solutions (0.05–1 mol %) in cyclohexane were thoroughly degassed and distilled into 4.5-ml cells. These samples were given doses of 9×10^{18} eV/ml.

Gaseous products that were volatile at 77°K were collected by vacuum distillation and measured in a McLeod-Toepler apparatus. The isotopic composition of the mixture was determined by using a CEC(21-614)

- (1) The work was partly supported by The Defense Research Board of Canada.
- (2) G. E. Adams, J. H. Baxendale, and R. D. Sedgewick, *J. Phys. Chem.*, **63**, 854 (1959).
- (3) G. R. Freeman, *Can. J. Chem.*, **38**, 1043 (1960).
- (4) T. J. Hardwick, *J. Phys. Chem.*, **64**, 1623 (1960).
- (5) T. J. Hardwick, *ibid.*, **66**, 291 (1962).
- (6) T. J. Hardwick, *ibid.*, **66**, 1611 (1962).
- (7) S. Z. Toma and W. H. Hamill, *J. Amer. Chem. Soc.*, **86**, 1478 (1964).
- (8) J. Y. Yang and I. Marcus, *J. Chem. Phys.*, **42**, 3315 (1965).
- (9) R. A. Holroyd, *J. Phys. Chem.*, **70**, 1341 (1966).
- (10) J. A. Kerr, *Chem. Rev.*, **66**, 465 (1966).
- (11) M. G. Robinson and G. R. Freeman, *J. Chem. Phys.*, in press.
- (12) J. C. Russell and G. R. Freeman, *J. Phys. Chem.*, **71**, 755 (1967).

mass spectrometer. The instrument was calibrated with standard mixtures of H_2 , HD, and D_2 , the relative proportions of which were in the ranges found experimentally in the irradiated samples.

Results

The deuterated olefins used were: CH_3CDCD_2 , CD_3CHCH_2 , C_3D_6 , $(CD_3)_2CCH_2$, $(CD_3)_2CCD_2$, and $CH_3(CH_2)_4CDCD_2$. The yields of HD and D_2 from solutions of these olefins in cyclohexane are shown in Figure 1. The HD yield depends greatly on the position of deuterium substitution on the olefin.

Very small yields of D_2 were produced from solutions containing C_3D_6 , CH_3CDCD_2 , $(CD_3)_2CCD_2$, and $CH_3(CH_2)_4CDCD_2$, and the $G(D_2)$ vs. olefin concentration curves were identical (Figure 1); $G(D_2) = 0.005$ at 1 mol % olefin. A somewhat smaller amount of D_2 was formed from $(CD_3)_2CCH_2$ (Figure 1) and no D_2 could be observed ($G(D_2) < 0.001$) from solutions of CD_3CHCH_2 . It appears that the D_2 is formed mainly by ejection from the olefinic carbons of excited olefin molecules or ions.

The decrease in hydrogen yield, $\Delta G(H_2)$, caused by a given concentration of olefin varied somewhat from olefin to olefin, but the $G(H_2)$ vs. olefin concentration curves were all similar to that reported earlier for the cyclohexane solutions of C_3H_6 and C_3D_6 .¹¹ What is more important, the value of $G(HD)/\Delta G(H_2)$ was independent of concentration for a given olefin, but varied greatly from one olefin to another (Table I).

Table I: Ratio of the HD Yield to the Decrease in the H_2 Yield

Olefin	No. of samples	Concn range, mol %	$G(HD)/\Delta G(H_2)$
CH_3CDCD_2	8	0.038-1.09	0.010 ± 0.002^a
CD_3CHCH_2	10	0.072-1.20	0.051 ± 0.003
C_3H_6	4	0.20-1.86	0.067 ± 0.003
$CH_3(CH_2)_4CDCD_2$	7	0.11-1.05	0.018 ± 0.003
$(CD_3)_2CCH_2$	8	0.055-1.16	0.062 ± 0.004
$(CD_3)_2CCD_2$	6	0.046-1.14	0.081 ± 0.004

^a The deviations were random and no trend was noticeable.

The value of this ratio varied from 0.01 for CH_3CDCD_2 to 0.08 for $(CD_3)_2CCD_2$. Examination of the table leads to the conclusion that most of the HD is formed by the reaction of a hydrogen precursor from cyclohexane with the alkyl group of the olefin.

In cyclohexane that contained 1.86 mol % C_3D_6 , the addition of ethanol suppressed the yields of both HD and D_2 by equal proportionate amounts, while the total hydrogen yield remained virtually unchanged (Figure 2).

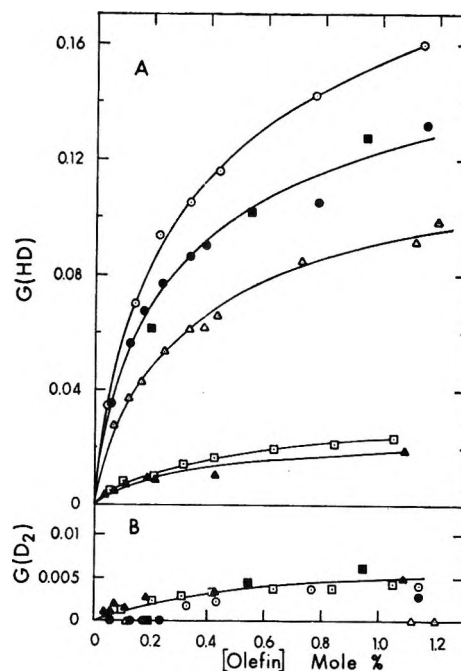


Figure 1. Yields of HD and D_2 from cyclohexane solutions containing various deuterated olefins (A, HD; B, D_2): \circ , $(CD_3)_2CCD_2$; \bullet , $(CD_3)_2CCH_2$; \blacksquare , C_3D_6 ; Δ , CD_3CHCH_2 ; \square , $CH_3(CH_2)_4CDCD_2$; \blacktriangle , CH_3CDCD_2 .

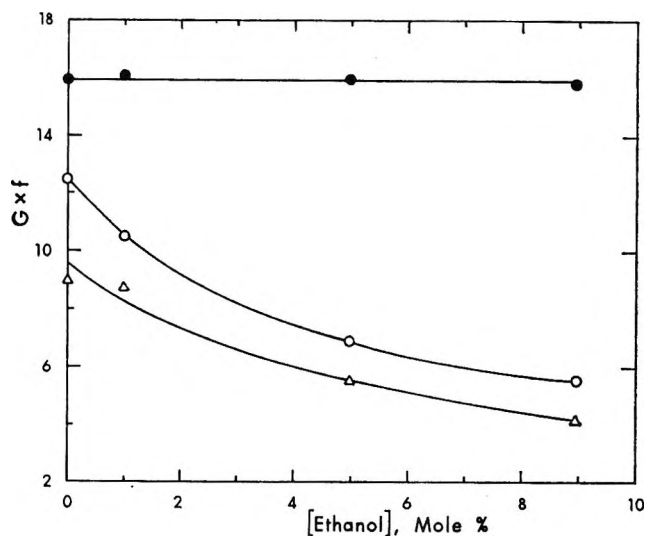


Figure 2. Yields of H_2 (\bullet), HD (\circ), and D_2 (Δ) from cyclohexane solutions containing 1.86 mol % propylene- d_6 , as a function of added ethanol concentration. $f = 5$ for H_2 , 100 for HD, and 1000 for D_2 .

Discussion

The formation of HD and D_2 from the present solutions supports the earlier conclusion⁶ that olefins enter into hydrogen-forming reactions. However, the results in Table I contradict the suggestion that "hydrogen abstraction" occurs mainly from the olefinic carbons.⁵ Comparison of the values of $G(HD)/\Delta G(H_2)$ for the solutions containing CH_3CDCD_2 ,

CD_3CHCH_2 , and C_3D_6 shows that about $1/6$ of the abstraction occurs from the olefinic carbons and that $5/6$ occurs from the methyl group. The contributions of the olefinic groups in the larger olefins to hydrogen formation are likewise small (Table I).

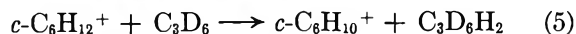
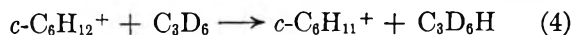
The D_2 is formed mainly by molecular ejection from the olefinic carbons of excited olefin molecules or ions.

If HD were formed mainly by hydrogen atom abstraction, for example

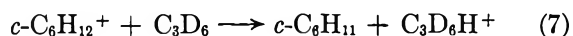
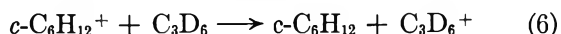


then the addition of ethanol to the solution should have had little effect on the HD yield. However, not only did ethanol reduce the HD yield but it also reduced the D_2 yield by the same proportionate amount (Figure 2). Ethanol reacts with positive ions in cyclohexane under irradiation,¹³ so it appears that both HD and D_2 have positive-ion precursors in the present systems.

The donation of H and H_2 by alkane ions to olefin molecules, *e.g.*, reactions 4 and 5, has been shown to occur in both the gas^{14,15} and liquid¹⁶ phases. Although these reactions help to explain the decrease in



the hydrogen yield, they cannot explain the appearance of HD and D_2 in the products. The yields of HD from all of the deuterated olefin solutions and the yields of D_2 from the $>\text{C}=\text{D}_2$ olefins are too great to be explained by a direct radiolysis effect. Some other reaction, such as electron abstraction or proton donation, must also occur in these solutions



Neutralization of ions such as those formed in reactions 6 and 7 could explain the formation of both HD and D_2 . The formation of HD and of D_2 each has several possible routes and speculation about them is not worthwhile here.

It has been demonstrated by kinetic analysis that the decrease in hydrogen yield that occurs when propylene is added to cyclohexane can be attributed mainly to either hydrogen atom scavenging or to electron scavenging, but the latter process offers a somewhat better explanation of the over-all results.¹¹ The fact that monoolefins do not have positive electron affinities in the gas phase does not mean that olefins will

not "associate" with electrons in alkane solutions.¹¹ Positive-ion reactions such as reactions 6 and 7 doubtless occur in the same solutions.

When scavengers that react either with positive ions or with electrons, but not with both, are used, suppression of the hydrogen yield is almost an order of magnitude more sensitive to electron-scavenger concentration^{17,18} than to positive-ion-scavenger concentration.^{13,19} This is probably due, at least in part, to greater mobilities of solvated electrons than of positive ions in these liquids.¹⁹ However, the scavenging of the electrons reduces the mobility of the negative species and increases the lifetimes of the positive ions, thereby increasing their probability of being scavenged.^{16,19} The correlation of $G(\text{HD})$ with $\Delta G(\text{H}_2)$ in the present systems can, therefore, be explained if the olefins react with both positive ions and electrons. This would also explain why, within experimental error, $G(\text{H}_2)$ was independent of ethanol concentration while $G(\text{HD})$ and $G(\text{D}_2)$ decreased in the experiments recorded in Figure 2. The neutralization of an alcohol oxonium ion by an olefin anion apparently does not yield more hydrogen than does the corresponding neutralization of a hydrocarbon cation.

Hardwick's⁵ ratios, $k(\text{abstraction})/k(\text{addition})$, are equivalent to the present ratios $G(\text{HD})/\Delta G(\text{H}_2)$ for the fully deuterated olefins. The value of 0.08 for $(\text{CD}_2)_2\text{CCD}_2$ is much smaller than Hardwick's value of 0.3 for undeuterated olefins of this structural type.⁵ This difference is probably due to an isotope effect in the formation of hydrogen from the olefins. Isotope effects of this magnitude have previously been observed in systems containing olefins.²⁰⁻²³

(13) J. W. Buchanan and F. Williams, *J. Chem. Phys.*, **44**, 4377 (1966).

(14) P. Ausloos and S. G. Lias, *ibid.*, **43**, 127 (1965).

(15) F. P. Abramson and J. H. Futrell, *J. Phys. Chem.*, **71**, 1233 (1967).

(16) (a) P. Ausloos, A. A. Scala, and S. G. Lias, *J. Amer. Chem. Soc.*, **88**, 1583 (1966); (b) P. Ausloos, A. A. Scala, and S. G. Lias, *ibid.*, **89**, 3677 (1967).

(17) G. Scholes and M. Simic, *Nature*, **202**, 895 (1964).

(18) S. Sato, R. Yugeta, K. Shinsaka, and T. Terao, *Bull. Chem. Soc. Jap.*, **39**, 156 (1966).

(19) G. R. Freeman, *J. Chem. Phys.*, **46**, 2822 (1967).

(20) E. G. Spittler, S. J. P. Jordon, L. M. Dorfman, and M. C. Sauer, Jr., *J. Phys. Chem.*, **67**, 2235 (1963).

(21) B. R. Wakeford and G. R. Freeman, *ibid.*, **68**, 3214 (1964).

(22) J. Y. Yang and I. Marcus, *J. Chem. Phys.*, **43**, 1585 (1965).

(23) The value $G(\text{H}_2) = 0.80$ was measured for each of the pure liquids C_3H_6 and $1\text{-C}_4\text{H}_8$ irradiated at 0° . Pure C_3D_6 gave $G(\text{D}_2) = 0.42$. The over-all isotope effect $G(\text{H}_2)/G(\text{D}_2) = 1.9$ for propylene agrees with that observed in cyclohexene.²¹

The Mechanism of Radiation-Induced Luminescence from Scintillators in Cyclohexane

by Robert R. Hentz and Ronald J. Knight

Department of Chemistry and the Radiation Laboratory,¹ University of Notre Dame, Notre Dame, Indiana 46556
(Received November 30, 1967)

The radiation-induced luminescence from scintillators (*p*-terphenyl and 2,5-diphenyl-1,3,4-oxadiazole) was studied in deaerated cyclohexane solutions containing an electron scavenger. The scavengers SF₆, N₂O, CO₂, C₂H₅Br, *n*-C₃H₇Cl, and benzyl acetate were used. A study also was made of the effect of these solutes and the scintillators on nitrogen yields obtained in radiolysis of cyclohexane solutions of N₂O. Over the concentration ranges studied with γ radiation, the six solutes have no effect on the intensity of luminescence produced by uv excitation of the scintillators. However, all six solutes do quench scintillator luminescence produced by γ irradiation of the cyclohexane solutions and in a manner very similar to the effect of the electron scavengers and scintillators on N₂ yields from the γ -irradiated N₂O solutions. Relative specific rates of electron capture are calculated using a model for radiation-induced ionic reactions in liquids of low dielectric constant; values obtained from the luminescence-quenching and N₂O-protection studies are compared. It is concluded that radiation-induced scintillator luminescence in cyclohexane is explicable in terms of a sequence of ionic reactions. The scintillator captures electrons and positive charge in competition with recombination of the sibling cation-electron pairs produced in the solvent. Scintillator excitation occurs in the neutralization of a scintillator anion by a solvent or scintillator cation and in the neutralization of a scintillator cation by an electron.

Introduction

Studies of radiation-induced luminescence from scintillators in various solvents have shown that different mechanisms are involved in aromatic and alkane solvents.² In the case of benzene solutions, *e.g.*, it has been established that scintillator excitation occurs *via* energy transfer from the ¹B_{2u} state of the solvent to the scintillator.³ However, in cyclohexane solutions the mechanism of scintillator excitation has not been established although a number of mechanisms have been suggested: (1) energy transfer from an excited cyclohexane molecule,⁴ (2) charge transfer from a solvent cation and subsequent neutralization,⁵⁻⁷ and (3) non-localized deposition of energy followed by preferential localization in the scintillator.^{6,7}

Burton² recently has reviewed evidence against the participation of excited cyclohexane molecules in the sensitization of scintillator luminescence. From the absence of structure in the absorption spectrum of cyclohexane,⁸ it was inferred that the lifetime of the excited state is less than 10⁻¹¹ sec; measurement of decay times of scintillator luminescence in X-irradiated cyclohexane solutions gives $\tau < 0.3 \times 10^{-9}$ sec for the lifetime of excited cyclohexane in the liquid phase.⁵ By combination of $\tau < 0.3 \times 10^{-9}$ sec with Q' values⁹ and γ' values,⁶ specific rates are obtained of $k > 10^{12} M^{-1} \text{sec}^{-1}$ and $k > 3 \times 10^{11} M^{-1} \text{sec}^{-1}$ for excitation transfer to scintillators and for quenching of a cyclohexane excited state by CCl₄, respectively. Because such specific rates are considerably greater than the maximum value expected for an excitation-transfer process ($\sim 5 \times 10^{10}$

$M^{-1} \text{sec}^{-1}$), it was argued² that a mechanism involving excitation transfer is untenable.

Much recent work¹⁰⁻¹³ indicates that ionic processes play a significant role in the radiation chemistry of alkanes. Such work suggests that ionic processes may play an important role in the radiation-induced luminescence of scintillators in alkane solutions. The usual scintillators qualify as scavengers of electrons and of positive charge (by charge transfer from solvent cations). Thus, luminescence may be a consequence of the neutralization of scintillator cations and anions. To test such a mechanism, the radiation-induced luminescence of scintillators has been studied in cyclohex-

(1) The Radiation Laboratory of the University of Notre Dame is operated under contract with the U. S. Atomic Energy Commission. This is AEC Document No. COO-38-582.

(2) M. Burton, *Mol. Cryst.*, in press, provides a recent review of the data and arguments with references to the pertinent literature.

(3) S. Lipsky and M. Burton, *J. Chem. Phys.*, **31**, 1221 (1959).

(4) V. Laor and A. Weinreb, *ibid.*, **43**, 1565 (1965).

(5) M. Burton, A. Ghosh, and J. Yguerabide, *Radiation Res. Suppl.*, **2**, 462 (1960).

(6) C. R. Mullin, M. A. Dillon, and M. Burton, *J. Chem. Phys.*, **40**, 3053 (1964).

(7) M. Burton, *Discussions Faraday Soc.*, **36**, 7 (1963).

(8) L. W. Pickett, M. Muntz, and E. M. McPherson, *J. Am. Chem. Soc.*, **73**, 4862 (1951).

(9) M. Burton, M. A. Dillon, C. R. Mullin, and R. Rein, *J. Chem. Phys.*, **44**, 2236 (1964).

(10) G. Scholes and M. Simic, *Nature*, **202**, 895 (1964).

(11) F. Williams, *J. Am. Chem. Soc.*, **86**, 3954 (1964); J. W. Buchanan and F. Williams, *J. Chem. Phys.*, **44**, 4377 (1966).

(12) P. J. Dyne, *Can. J. Chem.*, **43**, 1080 (1965).

(13) G. R. Freeman, *J. Chem. Phys.*, **46**, 2822 (1967).

ane solutions containing a solute previously characterized as an electron scavenger; six such solutes were used. For comparison, a study was made of the effect of these same solutes and of the scintillators on nitrogen yields obtained in radiolysis of cyclohexane solutions of the electron scavenger N_2O .¹⁰ Correlations were sought between the kinetic parameters of luminescence quenching and N_2O protection.

Experimental Section

Materials. Fisher Spectrograde cyclohexane was passed through a 5-ft column of silica gel, subjected to two partial freezings, dried over sodium, and distilled from sodium with a Nester-Faust spinning-band column; only the middle fraction was used, which contained negligible amounts of unsaturated impurities ($<10^{-4} M$) as shown by both ultraviolet spectrophotometry and gas chromatography with a flame-ionization detector. Scintillation grade *p*-terphenyl (PTP) from Eastman Organic Chemicals was recrystallized twice from benzene. The following chemicals were used as received: scintillation grade 2,5-diphenyl-1,3,4-oxadiazole (PPD) from K and K Laboratories, puriss grade benzyl acetate from Aldrich Chemical Co., ethyl bromide from Columbia Organic Chemicals, and Eastman Red Label *n*-propyl chloride.

Matheson Co. N_2O and SF_6 were passed through NaOH pellets and stored on the vacuum line. These gases and CO_2 , obtained from Air Reduction, were purified on the vacuum line just prior to sample preparation. Air was removed by pumping on the gas condensed in a trap at 77°K; water was retained in the trap as it was allowed to warm from 77 to 193°K, and the more volatile gases distilled into another trap at 77°K. This procedure was repeated several times.

Procedures. Solutions (10 ml) were pipetted into 78 ± 2 -ml vessels which consisted of a 50-ml Pyrex flask fitted with a side arm for connection to the vacuum line, a break-seal, and a tube of 12 cm length and 1.6 cm diameter in which the solution was irradiated. The solutions were degassed by at least four cycles of freeze (77°K), pump, and thaw. Such gaseous solutes as N_2O , SF_6 , and CO_2 were added by condensation of the desired amount onto the sample at 77°K; the amount of gas was determined by measurement of the pressure (with a calibrated Series 17477 Consolidated Vacuum Corp. gauge) in a 380-ml volume at room temperature. The cells were sealed and those containing gases were shaken thoroughly and allowed to stand overnight prior to irradiation. The concentration of a gas in solution was calculated from the known amount of gas in the vessel, the volumes of vessel and solution, and the following Ostwald solubility coefficients: $\beta(N_2O)^{14} = 2.62$ at 23°, $\beta(SF_6)^{15} = 1.22$ at 25°, and $\beta(CO_2)^{16} = 1.72$ at 25°.

Solutions were irradiated at room temperature in the Notre Dame 10-kc ^{60}Co facility at a dose rate to the

Fricke dosimeter solution, based on $G(Fe^{3+}) = 15.6$, of 1.51×10^{18} eV $g^{-1} min^{-1}$. Dose to the cyclohexane solutions was determined by correction for the electron density of the solution relative to that of the dosimeter. After irradiation, N_2 and H_2 were removed by three cycles of freeze (77°K), pump, and thaw using a Toepler pump to collect the gas in a closed loop for subsequent injection into a gas chromatograph. Separation of the gases was achieved with a 0.25-in. \times 5-ft column packed with activated 30–60 mesh 5A molecular sieve and operated at room temperature with helium as carrier gas; a Gow-Mac 9677 matched-thermistor detector was used. Calibrations were made with each series of analyses by injection of known amounts of pure gas measured in calibrated volumes of the Toepler pump.

The apparatus and procedure for measurement of relative luminescence intensities from γ -irradiated scintillator solutions have been described;¹⁷ 20-ml samples were prepared in 35 ± 1 ml cylindrical vessels by the procedure described for preparation of solutions for radiolysis. Relative luminescence intensities from uv-excited scintillator solutions were measured with a Cary spectrophotometer fitted with a fluorescence attachment;¹⁸ ~ 4 -ml samples were prepared, as previously described, in quartz cells 1 cm square and ~ 6 cm in length. A Cary Model 14-R was used for absorption spectrophotometry.

Results

On the basis of preliminary investigations, the following six electron scavengers were chosen for study as quenchers of the radiation-induced luminescence of scintillators in cyclohexane: SF_6 ,¹⁹ N_2O ,^{10,20} CO_2 ,²¹ C_2H_5Br ,²² *n*- C_3H_7Cl ,^{22,23} and benzyl acetate.^{22–24} Over the concentration ranges studied with γ excitation, the six solutes have no effect on the intensity of luminescence produced by direct excitation of PTP or PPD at 3130 Å. However, all six solutes do quench scintillator luminescence produced by γ irradiation of the de-aerated cyclohexane solutions. This quenching effect

(14) S. Sato, R. Yugeta, K. Shinsaka, and T. Terao, *Bull. Chem. Soc. Japan*, **39**, 156 (1966).

(15) G. Archer and J. H. Hildebrand, *J. Phys. Chem.*, **67**, 1830 (1963).

(16) J. Gjaldbaeck, *Acta Chem. Scand.*, **7**, 534 (1953).

(17) M. Burton, P. J. Berry, and S. Lipsky, *J. Chim. Phys.*, **52**, 657 (1955).

(18) M. A. Dillon and M. Burton, "Pulse Radiolysis," Academic Press, London, 1965, p 260.

(19) R. N. Compton, L. G. Christophorou, G. S. Hurst, and P. W. Reinhardt, *J. Chem. Phys.*, **45**, 4634 (1966); B. H. Mahan and C. E. Young, *ibid.*, **44**, 2192 (1966).

(20) R. K. Curran and R. E. Fox, *ibid.*, **34**, 1590 (1961); G. J. Schulz, *ibid.*, **34**, 1778 (1961).

(21) P. M. Johnson and A. C. Albrecht, *ibid.*, **44**, 1845 (1966).

(22) J. P. Guarino, M. R. Ronayne, and W. H. Hamill, *Radiation Res.*, **17**, 379 (1962).

(23) L. J. Forrestal and W. H. Hamill, *J. Amer. Chem. Soc.*, **83**, 1535 (1961).

(24) J. A. Ward and W. H. Hamill, *ibid.*, **87**, 1853 (1965).

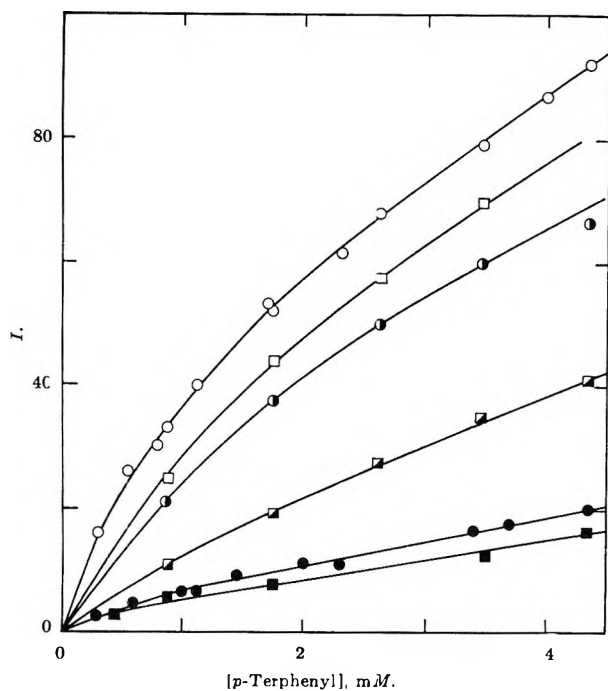


Figure 1. The effect of N_2O and benzyl acetate on the radiation-induced luminescence from *p*-terphenyl in deaerated cyclohexane solutions: \circ , *p*-terphenyl alone; \bullet , $5 \times 10^{-3} M N_2O$; \circ , $0.12 M N_2O$; \square , $10^{-3} M$ benzyl acetate; \blacksquare , $7 \times 10^{-2} M$ benzyl acetate; \blacksquare , $0.28 M$ benzyl acetate.

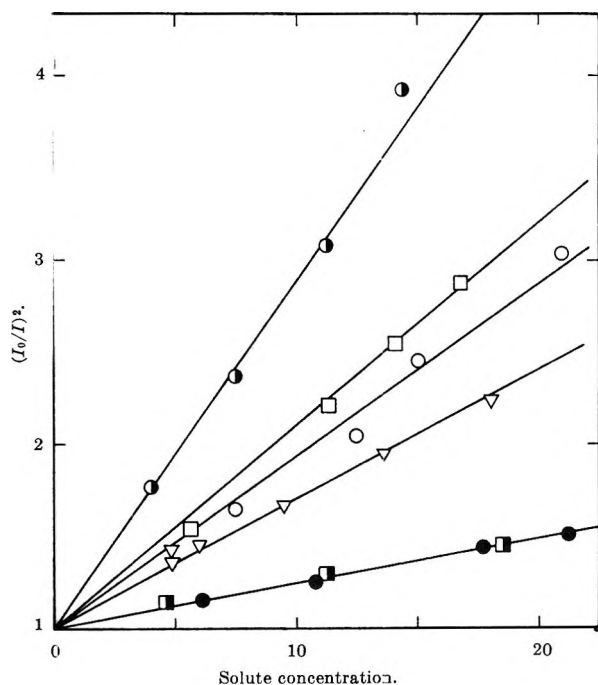


Figure 2. Dependence of $(I_0/I)^2$ on the concentration of an electron scavenger (units are 4 mM for $n\text{-C}_3\text{H}_7\text{Cl}$ and mM for the other solutes) in γ irradiation of deaerated solutions of $10^{-2} M$ PPD in cyclohexane: \bullet , SF_6 ; \square , benzyl acetate; \circ , $\text{C}_2\text{H}_5\text{Br}$; ∇ , N_2O ; \bullet , CO_2 ; \blacksquare , $n\text{-C}_3\text{H}_7\text{Cl}$.

is illustrated in Figure 1 by plots of relative luminescence intensity, I (I_0 for solutions without quencher), vs. concentration of PTP for solutions containing dif-

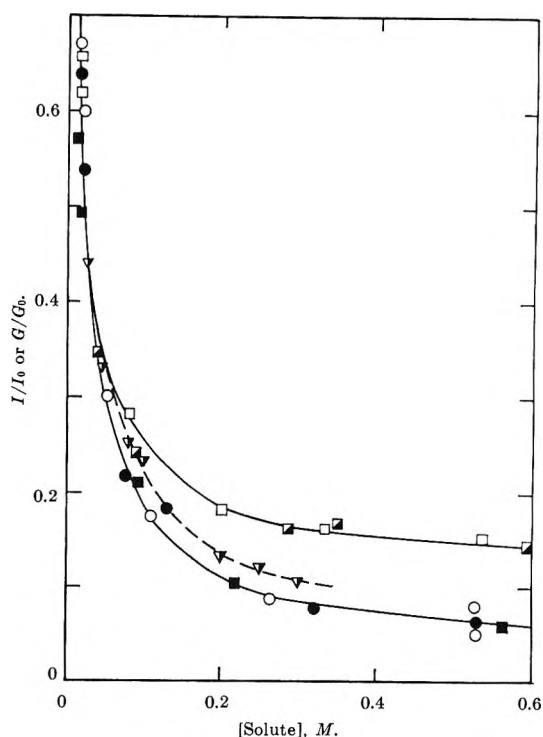


Figure 3. The effect, in deaerated cyclohexane, of high concentrations of an electron scavenger on nitrogen yields from $10^{-2} M N_2O$ solutions (solid symbols) and on luminescence from $10^{-2} M$ PPD solutions (open symbols) and $3.5 \times 10^{-3} M$ PTP solutions (partially filled symbols): \square , benzyl acetate; \circ , $\text{C}_2\text{H}_5\text{Br}$; ∇ , N_2O .

ferent concentrations of N_2O or benzyl acetate. In Figure 2, results obtained for low concentrations of each of the six solutes in $10^{-2} M$ PPD solutions are plotted as $(I_0/I)^2$ vs. scavenger concentration; similar plots were obtained for PTP solutions with each of the four solutes studied— SF_6 , N_2O , $\text{C}_2\text{H}_5\text{Br}$, and benzyl acetate. The significance of such a plot is considered in the Discussion. Results obtained at higher scavenger concentrations in PPD and PTP solutions are shown in Figure 3.

The reaction of hydrated electrons with N_2O to produce nitrogen is fast, $k^{25} = 5.6 \times 10^9 M^{-1} \text{ sec}^{-1}$, whereas the corresponding reaction of H with N_2O is comparatively slow, $k^{26} = 10^5 M^{-1} \text{ sec}^{-1}$. Such considerations have led to the use of N_2O as a scavenger for electrons produced in the γ irradiation of hydrocarbons.^{10,14} Use of N_2O has the virtue that an easily measured product is formed in the electron scavenging reaction; however, interpretation of the N_2 yields involves certain complications which are considered in the Discussion. In Figure 4, nitrogen yields obtained at low concentrations of each of six solutes in $10^{-2} M N_2O$ solutions are plotted as $(G_0/G)^2$ vs. concentration of the added solute; G and G_0 denote the

(25) J. P. Keene, *Radiation Res.*, **22**, 1 (1964); E. J. Hart and E. M. Fielden, *Advances in Chemistry Series*, No. 50, American Chemical Society, Washington, D. C., 1965, p 253.

(26) G. Czapski and J. Jortner, *Nature*, **188**, 50 (1960).

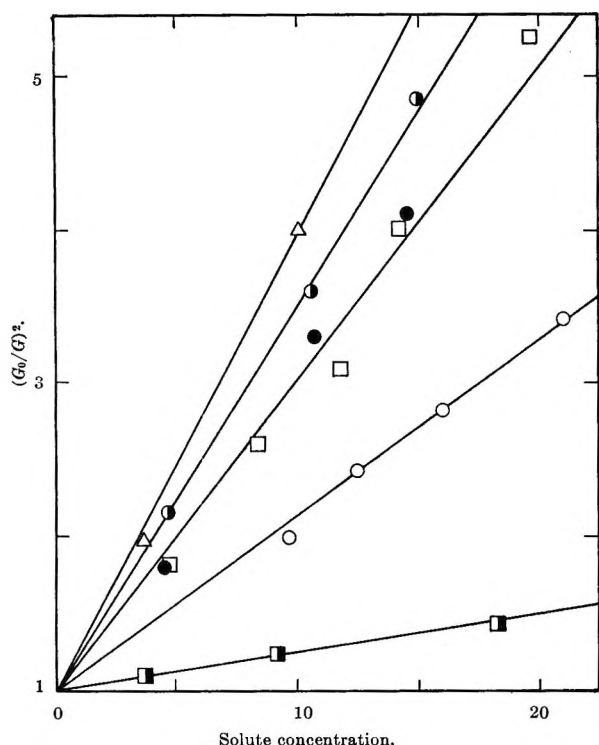


Figure 4. Dependence of $(G_0/G)^2$ on the concentration of an electron scavenger or scintillator (units are 4 mM for $n\text{-C}_3\text{H}_7\text{Cl}$ and mM for the other solutes) in γ irradiation of deaerated solutions of $10^{-2} M \text{N}_2\text{O}$ in cyclohexane: Δ , PPD; \bullet , SF_6 ; \bullet , CO_2 ; \square , benzyl acetate; \circ , $\text{C}_2\text{H}_5\text{Br}$; \blacksquare , $n\text{-C}_3\text{H}_7\text{Cl}$.

100-eV yields of N_2 from N_2O solutions with and without added solute, respectively. Similar plots were obtained with PTP as solute at lower N_2O concentrations. Results obtained at higher concentrations of the added solutes in $10^{-2} M \text{N}_2\text{O}$ solutions are shown in Figure 3. At $10^{-2} M \text{N}_2\text{O}$, a value of $G_0 = 1.7$ was obtained which was independent of dose up to at least $1.1 \times 10^{20} \text{ eV ml}^{-1}$; all yields were determined at doses of $5.6 \times 10^{19} \text{ eV ml}^{-1}$ or less.

Discussion

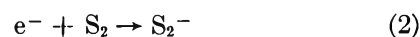
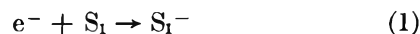
Nitrogen-Yield Suppression. In recent years, a useful model has been emerging for interpretation of the behavior of ionic species produced by high-energy radiation in liquids of low dielectric constant.^{11-13,27} The general features of such a model are as follows. Electrons having a wide range of initial energies (from essentially zero to values of $\sim 1 \text{ MeV}$ in most cases) are generated in the liquid by high-energy radiation; such electrons lose their energy to the medium and are thermalized at various distances, related to their initial energies, from their sibling cations. Thus, a distribution function exists which gives the fraction of sibling cation-electron pairs for which the separation at thermalization lies between r and $r + dr$; such a function is represented by $F_r' dr$. Under the influence of their mutual Coulombic fields (the complications associated with spurs of more than one ion pair being

ignored), sibling ion pairs have a probability of recombination given by $1 - f_r$ (in which f_r represents the escape probability²⁸), and a characteristic lifetime for recombination which can be represented as the reciprocal of a specific rate k_r ; *i.e.*, those sibling ion pairs that recombine can be treated as excited molecules with a specific rate of decay k_r . From electrical-conductivity measurements that give $G_{fi} = 0.1$ for free ion pairs²⁹ (that escape recombination) and using an estimated $G_i \approx 3$ for total ion pairs,¹¹⁻¹³ a value of $\sim 97\%$ is calculated for the percentage of all sibling cation-electron pairs that recombine.

With the general model presented, it is possible to derive an equation for G_0/G in a solution in which two scavengers, S_1 and S_2 , compete for the electrons and scavenging by S_1 gives a measured product with yields of G_0 and G in the absence and presence of S_2 , respectively. Thus

$$G = G_{fi} [k_1 S_1 / (k_1 S_1 + k_2 S_2)] + G_i \int_0^\infty [k_1 S_1 / (k_r + k_1 S_1 + k_2 S_2)] F_r' dr \quad (\text{I})$$

in which $F_r' = F_r'(1 - f_r)$, S denotes molarity of the scavenger, and k_1 and k_2 are specific rates of the reactions



It is assumed that scavenger concentrations are large enough to preclude combination of *free* electrons and cations at the dose rate used. Because

$$\frac{\int_0^\infty [k_1 S_1 / (k_r + k_1 S_1 + k_2 S_2)] F_r' dr}{\int_0^\infty [(k_1 S_1 + k_2 S_2) / (k_r + k_1 S_1 + k_2 S_2)] F_r' dr} = \frac{k_1 S_1}{k_1 S_1 + k_2 S_2} \quad (\text{II})$$

eq I can be rewritten as

$$G = G_i k_1 S_1 / (k_1 S_1 + k_2 S_2) \quad (\text{III})$$

in which

$$G_i = G_{fi} + G_i \int_0^\infty [(k_1 S_1 + k_2 S_2) / (k_r + k_1 S_1 + k_2 S_2)] F_r' dr$$

Use of the empirical result^{11,30} (valid at low scavenger

(27) A. Hummel and A. O. Allen, *J. Chem. Phys.*, **46**, 1602 (1967).

(28) L. Onsager, *Phys. Rev.*, **54**, 554 (1938), gives $f_r = \exp(-e^2 / \epsilon k T r)$, in which e is the charge on the electron and ϵ is the dielectric constant.

(29) A. O. Allen and A. Hummel, *Discussions Faraday Soc.*, **36**, 95 (1963); G. R. Freeman, *J. Chem. Phys.*, **39**, 988 (1963).

(30) A. A. Scala, S. G. Lias, and P. Ausloos, *J. Amer. Chem. Soc.*, **88**, 5701 (1966); P. Ausloos, A. A. Scala, and S. G. Lias, *ibid.*, **89**, 3677 (1967).

concentrations) that $G_0 = a(k_1S_1)^{1/2}$ and $G_t = a(k_1S_1 + k_2S_2)^{1/2}$ gives

$$(G_0/G)^2 = 1 + k_2S_2/k_1S_1 \quad (\text{IV})$$

The results obtained (cf. Figure 4) conform reasonably well to eq IV. Such conformity is not considered a confirmation of the model; the results conform about as well to a Stern-Volmer plot. If applicability of eq IV to the results for $10^{-2}M$ N_2O solutions is assumed, specific rates for $e^- + S$ can be calculated relative to $k(e^- + N_2O) = 1$. Such k values are presented in Table I.

Table I: Values of $k(e^- + S)$ for Various Solutes Relative to $k(e^- + N_2O) = 1$

Solute	$k(e^- + S)$		
	N_2O^a	PPD ^a	PTP ^a
PPD	2.9	1.4	..
SF ₆	2.5	2.7	2.3
CO ₂	2.0	0.34	..
Benzyl acetate	2.0	1.6	1.7
C ₂ H ₅ Br	1.1	1.3	1.1
PTP	1.0	..	1.8
<i>n</i> -C ₇ H ₇ Cl	0.062	0.084	..

^a The column headed N_2O gives values obtained from results on the suppression of $G(N_2)$ in N_2O solutions; the columns headed PPD and PTP give values obtained from the results on luminescence quenching in PPD and PTP solutions, respectively.

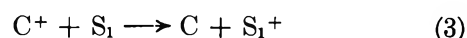
The value of G/G_0 is about 0.06 at 0.6 M of either C₂H₅Br or benzyl acetate (cf. Figure 3), which corresponds to $G = 0.1$ ($G_0 = 1.7$). If essentially all electrons are scavenged at 0.6 M of a good scavenger,¹³ and assuming that each electron scavenged by N_2O gives ~ 1.6 molecules of N_2 ,^{31,32} $G = 1.6 G_t k_1 S_1 / (k_1 S_1 + k_2 S_2)$. For $G_t = 3$, $S_1 = 10^{-2} M$, and $S_2 = 0.6 M$, values of G equal to 0.07 and 0.04 are calculated for C₂H₅Br and benzyl acetate, respectively, using the relative specific rates of Table I; thus, the mechanism indicates that processes other than electron scavenging make little or no contribution to the measured $G = 0.1$ at 0.6 M S_2 .

Luminescence Quenching. As shown in Figures 1-3, electron scavengers quench radiation-induced scintillator luminescence in cyclohexane solutions in a manner very similar to the effect of such scavengers and the scintillators on N_2 yields from irradiated cyclohexane solutions of N_2O . Such a similarity suggests that a common precursor, namely the electron, is involved in scintillator luminescence and formation of N_2 from N_2O .

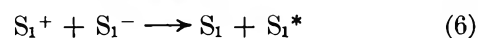
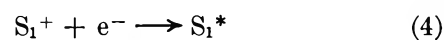
There is evidence for the formation of both aromatic cations and anions, including those of PTP, in irradiated nonpolar glasses at 77°K^{33,34} and in cyclohexane at room temperature.³⁵ Arai and Dorfman³⁶ report $k = 7.2 \times 10^9 M^{-1} \text{sec}^{-1}$ for reaction of PTP

with the solvated electron in ethanol. Consequently, aromatic scintillators (I.P. = 8-9 eV) should scavenge both electrons, as indicated by the effect of PTP and PPD in N_2O solutions (Figure 4), and positive charge in irradiated cyclohexane (I.P. = 9.88 eV). There is also abundant evidence that charge neutralization processes involving aromatic cations or anions or both (produced by photoionization,³⁷ high-energy irradiation,^{34,38} electrochemically,³⁹ or chemically⁴⁰) give rise to luminescence. Therefore, the general ionic model, which was used for interpretation of N_2 yield suppression by electron scavengers in irradiated N_2O solutions, can be applied plausibly to the quenching of radiation-induced scintillator luminescence by electron scavengers in cyclohexane solutions.

Scintillator ions are formed in reactions 1 and 3



in which C denotes cyclohexane and S_1 is now the scintillator. As in the case of N_2O , reaction 1 competes with the recombination at a specific rate k_r of sibling cation-electron pairs and scavenges all free electrons ($\sim 3\%$ of the total). However, reaction 3 (in addition to scavenging all free solvent cations) is in competition with either the recombination of sibling cation-electron pairs at a specific rate k_r or the recombination of sibling cation-scavenged electron(anion) pairs at a specific rate k_r' ; *i.e.*, account is taken of the possibility that an electron and anion may have appreciably different mobilities whereas those of C^+ and S_1^+ are essentially equal. Scintillator luminescence, then, may be a consequence of one or more of the reactions 4-6.



Thus, luminescence is quenched by an electron scavenger S_2 whose product anion is such as to preclude luminescence in any of the possible charge-neutralization processes.

(31) See Table VII of R. R. Hentz, D. B. Peterson, S. B. Srivastava, H. F. Barzynski, and M. Burton, *J. Phys. Chem.*, **70**, 2362 (1966).

(32) J. M. Warman, *Nature*, **213**, 381 (1967).

(33) J. P. Guarino and W. H. Hamill, *J. Amer. Chem. Soc.*, **86**, 777 (1964); N. Christodouleas and W. H. Hamill, *ibid.*, **86**, 5413 (1964); T. Shida and W. H. Hamill, *J. Chem. Phys.*, **44**, 2375 (1966).

(34) B. Brocklehurst and R. D. Russell, *Nature*, **213**, 65 (1967).

(35) G. Scholes, M. Simic, G. E. Adams, and J. W. Boag, *ibid.*, **204**, 1187 (1964); J. P. Keene, E. J. Land, and A. J. Swallow, *J. Amer. Chem. Soc.*, **87**, 5284 (1965).

(36) S. Arai and L. M. Dorfman, *J. Chem. Phys.*, **41**, 2190 (1964).

(37) G. N. Lewis and D. Lipkin, *J. Amer. Chem. Soc.*, **64**, 2801 (1942); W. M. McClain and A. C. Albrecht, *J. Chem. Phys.*, **43**, 465 (1965).

(38) D. W. Skelly and W. H. Hamill, *ibid.*, **43**, 3497 (1965).

(39) E. A. Chandross and J. W. Longworth, *J. Amer. Chem. Soc.*, **87**, 3259 (1965); K. S. V. Santhanam and A. J. Bard, *ibid.*, **87**, 139 (1965).

(40) E. A. Chandross and F. I. Sonntag, *ibid.*, **86**, 3179 (1964); A. Weller and K. Zachariasse, *J. Chem. Phys.*, **46**, 4984 (1967).

An equation analogous to eq I can be derived for the luminescence yield, G (proportional to I), in the presence of electron scavenger S_2

$$G = \frac{G_t k_1 S_1 \beta_6}{k_1 S_1 + k_2 S_2} + G_t \int_0^\infty \left[\left(\frac{k_3 S_1}{k_r + k_3 S_1} \right) \times \left(\frac{k_r \beta_4}{k_r + k_1 S_1 + k_2 S_2} \right) + \left(\frac{k_1 S_1}{k_r + k_1 S_1 + k_2 S_2} \right) \times \left(\frac{k_r' \beta_5 + k_3 S_1 \beta_6}{k_r' + k_3 S_1} \right) \right] F_r dr \quad (\text{V})$$

in which β represents the probability that the neutralization process gives rise to luminescence. The equation for G_0 is obtained when $S_2 = 0$.

There are three cases in which eq V can be converted into eq VI

$$(G_0/G)^2 = (I_0/I)^2 = 1 + k_2 S_2 / k_1 S_1 \quad (\text{VI})$$

by the procedure used in conversion of eq I into eq IV; case A: $\beta_5 = 0$, $\beta_4 = \beta_6$, $k_r = k_r'$, $k_1 = k_3$; case B: $\beta_4 = 0$, $\beta_5 = \beta_6$; case C: $\beta_4 = \beta_5 = \beta_6$ and

$$[k_3 S_1 / (k_r + k_3 S_1)] [k_r / (k_r + k_1 S_1 + k_2 S_2)] \ll [k_1 S_1 / (k_r + k_1 S_1 + k_2 S_2)] \quad (\text{VII})$$

There is some evidence that $k_1 \approx 10 k_3^{13,41}$ and that $k_r' \ll k_r^{13,30}$. Thus, the conditions of case A probably are not satisfied. The condition of case B that $\beta_4 = 0$ seems very improbable. However, the condition of case C expressed in eq VII becomes $k_r / (k_r + k_3 S_1) \ll 10$ for $k_1 \approx 10 k_3$; *i.e.*, case C can provide a plausible basis for rationalization of the results in terms of eq VI.

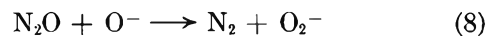
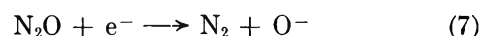
All things considered, perhaps it is somewhat surprising that the luminescence-quenching results conform reasonably well to eq VI (*cf.* Figure 2). Again, such conformity is not considered a confirmation of the model; the results conform about as well to a Stern-Volmer plot. Assuming the applicability of eq VI to the results, values of $k(e^- + S)$ relative to $k(e^- + N_2O) = 1$ can be calculated; such values are presented in Table I for both PPD and PTP solutions.

A value for the yield of electrons scavenged by $10^{-2} M$ PPD when $S_2 = 0$ may be estimated as $G_0 \approx 1$.^{13,31} The yield of electrons scavenged by $10^{-2} M$ PPD with $0.6 M$ S_2 present, assuming that essentially all electrons are being scavenged, is $G = G_t k_1 S_1 / (k_1 S_1 + k_2 S_2)$. Thus, for $G_t = 3$, $S_1 = 10^{-2} M$, and $S_2 = 0.6 M$, values of $G/G_0 \approx 0.05$ are calculated for both C_2H_5Br and benzyl acetate, using the relative specific rates in Table I for PPD solutions. Such calculated values are to be compared with measured values of I/I_0 (*cf.* Figure 3) equal to 0.06 and 0.14 for $0.6 M$ C_2H_5Br and benzyl acetate, respectively. The comparison for C_2H_5Br clearly indicates little or no contribution to scintillator luminescence from processes other than the postulated ionic processes; smallness of the apparent discrepancy in $0.6 M$ benzyl

acetate does not merit speculation on possible causes.

Comparison and Conclusions. The kinetics, in cyclohexane solutions, of radiation-induced scintillator luminescence and its quenching by electron scavengers are obviously quite complex; consequently, it is considered unlikely that the relative specific rates given in Table I have any precise quantitative significance; such values are presented as a basis for comparison of the results obtained in N_2O , PPD, and PTP solutions and for whatever insights they may provide into the specific mechanisms.

Agreement between the values given in Table I for each of the solutes SF_6 , benzyl acetate, C_2H_5Br , and $n-C_3H_7Cl$ is about as good as one could reasonably expect. The disagreement between relative specific rates obtained for CO_2 may be rationalized in terms of a secondary effect in the N_2O solutions. Such an interpretation grants validity to the value of k obtained for CO_2 by study of luminescence quenching in the PPD solutions. The interpretation of N_2 yields in the use of N_2O as an electron scavenger seems to require some kind of two-step process, *e.g.*



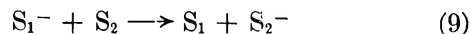
Thus, $G(N_2)$ is greater than $-\Delta G(H_2)$ in cyclohexane solutions¹⁰ and is greater than the yield of scavenged electrons, both in cyclohexane (as determined by comparison with other electron scavengers³¹) and in the gas phase.³² Consequently, if CO_2 competes with N_2O for O^- as well as for the electron, the larger specific rates in N_2O solutions are understandable. Warman³² has obtained evidence for a competition between N_2O and CO_2 for O^- in the gas phase. The rationalization suggested can be tested by use, in place of N_2O , of some other electron scavenger which gives an easily measured product in a less ambiguous manner.

The anomalies evident in values of k obtained for PPD and PTP are not readily understandable. It should be noted that for all solutes other than the scintillators themselves, the values of k given in Table I for the scintillator solutions involve a ratio of slopes. Thus, there may be some cancellation of deviations from eq VI in these cases such that there is fair agreement with the values obtained directly from slopes in the N_2O solutions, in which case eq IV follows more directly. Consequently, the discordant k values of PPD and PTP, only obtainable directly from the slopes, suggest that quenching of scintillator luminescence is too complicated to be represented by eq VI, perhaps because the conditions for conversion of eq V to VI are not satisfied.

Regardless of any shortcomings of the kinetic analyses of luminescence quenching and N_2 -yield sup-

(41) Compare, *e.g.*, the results for electron scavengers in ref 31 with results for cation scavengers in ref 11 and 30.

pression, it seems clear that radiation-induced scintillator luminescence in cyclohexane is largely, perhaps entirely, explicable in terms of the ionic reactions 1-6. It is also noteworthy that reactions of the type⁴²



apparently are not significant in a liquid of low di-

electric constant; *e.g.*, compare the value of $k(SF_6)/k(N_2O)$ in Table I with the corresponding value of 200 obtained in a gas-phase competition study,⁴² in which reaction 9 (with N_2O as S_1 and SF_6 as S_2) was invoked for explanation of the large value.

(42) W. J. Holtzlander and G. R. Freeman, *J. Phys. Chem.*, **71**, 2562 (1967).

Recoil-Tritium Reactions in the Solid Phase: Absolute Yields and Phase Effects

by Michael Menzinger and Richard Wolfgang

*Departments of Chemistry, Yale University, New Haven, Connecticut and University of Colorado, Boulder, Colorado
(Received November 30, 1967)*

A method for determining the absolute yields of recoil-tritium reactions in the solid phase is described. First results of this technique confirm that phase effects play only a minor part in hot hydrogen atom reactions—a situation very different from that for hot halogens. It appears that while caging effects are important in halogen atom reactions, they are not usually significant for atomic hydrogen.

Introduction

In this paper, we report on a simple method for the determination of absolute yields of products formed by reactions of recoil tritium in the solid phase. Results of this technique provide a definitive measure of the importance of phase effects in hot-hydrogen reactions.

The ability to obtain, in absolute terms, the yields of products formed in gas-phase reactions of recoil tritium has been of great importance in developing models of hot-hydrogen reactions. By contrast, results on recoil-tritium interactions in the condensed phase have usually been expressed relative to the yield of some product which is arbitrarily taken as unity. Such relative yields are useful but obviously do not lend themselves to quantitative comparisons of reactivity between different reactants and under various conditions.

The effect of phase on the reactions of recoil tritium is an example of a problem which requires absolute-yield data as a basis for a definitive answer. Relative-yield patterns have suggested that there is little phase dependence of hot-hydrogen reactions.¹ This conclusion is in striking contrast to the situation for hot halogens but must remain tentative until quantitatively tested by absolute-yield measurements.

Recoil tritium for gas-phase studies has usually been generated using the ${}^3\text{He}(n,p)\text{T}$ reaction.^{1a} Calculations of the total tritium produced using the cross section of this process and the neutron flux are generally inaccurate owing to uncertain knowledge of the latter quantity.² For this reason, monitor samples are usu-

ally employed. These contain a substance which will react with all the tritium, whether hot or thermal, to give volatile products. Comparison with the total activity in the monitor, after appropriate normalization for amounts of ${}^3\text{He}$, etc., then provides a basis for estimating absolute yields with any given reagent irradiated under identical conditions. Corrections for tritium lost by recoiling into the walls are often necessary.^{3,4}

The most generally used gas-phase monitor is the *n*-butane- ${}^3\text{He}$ system developed by Rosenberg.^{5,6} Butane reacts with hot tritium to yield labeled butane, lower hydrocarbons, and hydrogen. Tritium reaching thermal energies will also react to form HT, provided that the system has been carefully purified of scavenger substances, such as O_2 . As no polymeric products are produced, virtually all the activity appears in volatile form. The stopping power of butane is relatively high, and thus by use of moderate ampoule volumes and pres-

(1) (a) R. Wolfgang, *Progr. Reaction Kinetics*, **3**, 97 (1965); (b) E. K. C. Lee and F. S. Rowland, *J. Amer. Chem. Soc.*, **84**, 3085 (1962).

(2) Quoted neutron fluxes are mostly too unreliable ($\pm 20\%$) to be used for absolute-yield calculations. Furthermore, irradiation vials^{1b} often contain neutron-absorbing substances which change the actual flux to which the sample is exposed.

(3) P. J. Estrup, Ph.D. Thesis, Yale University, New Haven, Conn., 1959.

(4) W. Argersinger, *J. Phys. Chem.*, **67**, 976 (1963).

(5) A. H. Rosenberg and R. Wolfgang, *J. Chem. Phys.*, **41**, 2159 (1964).

(6) A. H. Rosenberg, Ph.D. Thesis, Yale University, New Haven, Conn., 1964.

tures, corrections for tritium recoiling into the walls are negligible or small.

Recoil tritium for condensed-phase studies is generally produced by the ${}^6\text{Li}(n,\alpha)\text{T}$ reaction.^{1a} A lithium salt is intimately but heterogeneously mixed with the other reagent. Some of the tritium is lost by recoil into the salt. This loss is difficult to estimate and to reproduce in different reagent systems. For this reason, yields from such experiments have been expressed only in relative terms.

Recoil loss into the lithium salt could be virtually eliminated by using samples containing only a small fraction of salt, in granules smaller than the recoil range (4.3 μ).⁷ However, this method is subject to a further possible uncertainty, in that the product may be adsorbed on the crystal surface.⁸ For this reason, we decided to develop a technique for solids which employed ${}^3\text{He}$ as a tritium source.

A solid film of reagent is frozen onto the walls of a quartz irradiation vessel which is then filled with a low pressure of ${}^3\text{He}$. Since the range of the recoil tritium (100 cm at typical He pressures⁶) is much greater than the thickness of gas, all of it reaches the reagent. Provided the reagent film is thick, compared to the recoil range (~ 0.22 mg/cm² in hydrocarbons⁶), all of the tritium stops in the reagent and has the chance to react there.

If all products of both hot and thermal tritium reactions with the reagent are volatile, the entire activity may be recovered and the sample is "self-monitoring." If this is not the case, or if there is doubt, a separate monitor, irradiated identically, may be used. This could be a standard butane (or other aliphatic hydrocarbon) gas monitor. Alternatively, a frozen-film sample of butane, pentane, or cyclohexane may be used, since this work shows these systems to provide 100% recovery of the tritium.

Experimental Section

Materials Used. The ${}^3\text{He}$ (Monsanto Research Corp.) was purified by passing it through activated charcoal at liquid nitrogen temperature.⁶ Phillips 66 research grade *n*-butane, *n*-pentane, and cyclohexane, and Matheson Corp. research grade oxygen were used without further purification.

Filling and Irradiation. Cylindrical quartz ampoules, 2 cm in diameter and 4 cm long, were used as the sample containers. The filling procedure has been described elsewhere.^{5,6} Sufficient hydrocarbon was used to provide an average film thickness of at least twice the tritium range.

Special attention was paid to the freezing of the hydrocarbon onto the ampoule walls. The validity of our monitoring method is dependent on the hydrocarbon film having no thin spots through which the tritium might recoil. The sealed vial was heated with

an air gun to vaporize the sample and was immersed in liquid nitrogen, which was vigorously stirred in order to ensure uniform cooling of the container.

This procedure was repeated until the hydrocarbon film appeared to coat the entire interior surface of the vial, as judged by visual inspection.

The vial was then quickly packed in Dry Ice and irradiated for 60 sec in the pneumatic tube of the Brookhaven graphite reactor under a neutron flux of approximately 10^{13} neutrons/cm² sec.

Analysis. The samples were allowed to vaporize, and the vials were broken under vacuum. Assay was by radio gas chromatography described elsewhere.^{5,6}

A rough calculation showed that recoil losses were expected to be small for the gaseous samples. The data do in fact bear out this expectation. Consequently, no recoil-loss correction was applied.

Results and Discussion

Efficiency of Solid-Film Monitoring. Table I shows the efficiency of activity recovery of hydrocarbons irradiated under various conditions. The gaseous, unscavenged butane system, previously found to give complete tritium recovery,^{5,6} is taken as monitor and assigned 100% efficiency. As expected, gaseous pentane and cyclohexane also yield essentially all the tritium in volatile measurable form. In the presence of oxygen, recovery is reduced reflecting the percentage of tritium which reaches thermal energies. This tritium yields oxygenated nonvolatile species instead of forming HT by a low-energy abstraction process.

For the solid butane, pentane, and cyclohexane, recoveries are within $\pm 3.9\%$ of 100%. This confirms that the film-irradiation technique of solids makes all the tritium, within experimental error, available for reaction. It also establishes that these systems are effectively self-monitoring and could be used as monitors for other reagents.

Phase Effects in Recoil Tritium Reactions. Table II shows the product distribution of the three hydrocarbons studied in both gas and solid phases. In the unscavenged samples, absolute activities given are based on self-monitoring by each sample. Yields from oxygen-scavenged systems are based on a gaseous butane monitor. These results are in good agreement with earlier work on the same systems in the gas phase.^{9,10}

(7) G. Friedlander, J. W. Kennedy, and J. M. Miller, "Nuclear and Radiochemistry," 2nd ed, John Wiley and Sons, New York, N. Y., 1964, p 95.

(8) Lithium salts are slightly soluble in alcohols, ketones, and related compounds. Such homogeneous systems could give absolute yields. Work of this nature has been reported: W. J. Hoff and F. S. Rowland, *J. Amer. Chem. Soc.*, **79**, 4867 (1957). However, since no accurate monitoring procedure was used, the absolute yields found were of rather low precision.

(9) D. Urch and R. Wolfgang, *J. Amer. Chem. Soc.*, **83**, 2982 (1961).

(10) J. K. Garland, Ph.D. Thesis, University of Kansas, Lawrence, Kan., 1963.

Table I: Tritium Recovery Determined by Gas- and Solid-Phase Self-Monitoring^a

Sample	Phase	Reagent	pV (hydro-carbon)	pV (³ He)	pV (O ₂)	Tritium recovered, %
BX2	Gas	<i>n</i> -Butane	1310	12.7	0	(100.0)
BX4	Gas	<i>n</i> -Butane	1340	12.5	19.5	72.9
BX6	Gas	<i>n</i> -Pentane	415	8.1	0	98.3
BX5	Gas	<i>n</i> -Pentane	676	12.2	19.5	76.7
BX10	Gas	Cyclohexane	160	13.1	0	102.1
BX11	Gas	Cyclohexane	190	19.1	0	96.5
BX14	Gas	Cyclohexane	232	12.0	17.8	72.2
BX3	Solid	<i>n</i> -Butane	720	8.5	0	100.6
BX18	Solid	<i>n</i> -Butane	430	11.8	0	99.4
BX8	Solid	<i>n</i> -Pentane	415	7.7	0	101.5
BX9	Solid	Cyclohexane	400	7.3	0	104.4
BX13	Solid	Cyclohexane	315	4.6	0	90.3
BX16	Solid	Cyclohexane	430	5.3	0	98.3
BX17	Solid	Cyclohexane	385	9.5	0	101.0

^a pV units given in cm³ (cm Hg). The ampoule volume is approximately 12 cm³.

Table II: Comparison of Absolute Yields of Individual Products between Gas and Solid Phases

	<i>n</i> -Butane ^{a,b}			<i>n</i> -Pentane ^{a,b}			Cyclohexane ^{a,b}		
	Gas		Solid	Gas		Solid	Gas		Solid
	Scavenged	Un-scavenged		Scavenged	Un-scavenged		Scavenged	Un-scavenged	
HT + CH ₂ T	47.4	67.8	63.6	48.4	67.7	62.0	48.3	76.0	75.2
C ₂ H ₅ T	0.8	1.5	3.1	2.4	2.9	2.3	0	1.25	0
C ₂ H ₃ T	0.7	1.3	0.35	0.6	0.8	1.1	1.3	2.6	0
C ₃ T products	0.7	1.8	2.1	1.2	1.9	2.1	nd ^c	nd	nd
C ₄ T products	23.3	28.14	30.6	0.8	0.9	1.5	nd	nd	nd
<i>n</i> -Pentane- <i>t</i>				23.3	26.4	31.0	nd	nd	nd
<i>n</i> -Hexane- <i>t</i>							0.4	0.56	1.8
<i>n</i> -Hexane-1- <i>t</i>							0.7	0.61	2.2
Cyclohexane- <i>t</i>							21.5	19.0	20.8

^a All yields are based on 100% recovery of tritium in unscavenged *n*-butane sample (see Table I). Yields in scavenged runs determined on the basis of using unscavenged *n*-butane identically irradiated. ^b The individual product yields represent averages from the runs listed in Table I. ^c The abbreviation nd stands for not determined.

It should be kept in mind that the unscavenged yields represent both hot and thermal reactions. Hot processes alone are represented by the scavenged samples. As expected and noted previously, thermal reactions are reflected primarily in increased yields of HT in the unscavenged samples.¹

The phase effect between gas and solid is seen to be of only minor importance. What differences there are seem to reflect the more rapid collisional deexcitation in the solid phase. An example is the absence of C₂ molecules from solid cyclohexane. These are presumably formed by the unimolecular decay of highly excited C₆ entities formed by direct hot reactions. In the solid phase, these energetic primary products lose energy by collision instead of by decomposition.

The confirmation that phase effects are not important in hot-hydrogen reactions means that experiments in the solid phase can be used as a basis for understanding the primary atom-molecule interaction. This is of im-

portance in connection with recent beam studies on hot hydrogen in which solid targets are employed.¹¹

If caging by the crystal lattice were important, yields would increase in the solid owing to the trapping of tritium in the vicinity of radicals produced in a prior bond-breaking collision. The results show that caging is at most of minor importance in the dominant hot hydrogen atom reactions. This is not surprising, since as has been suggested previously,¹ hydrogen atoms are probably small enough to escape from the crystal cage.

The lack of large phase effects in hot hydrogen atom reactions contrasts dramatically with the situation presented by hot-halogen reactions. In the latter case, major yields from interactions with organic molecules change by as much as fivefold between gas and solid.^{12,13}

(11) M. Menzinger and R. Wolfgang, *J. Amer. Chem. Soc.*, **89**, 5992 (1967).

Photochemical studies of halogen molecules¹⁴ indicate caging of halogen atoms to be quite effective. This probably accounts for the strong phase dependence found in their reaction as hot atoms. Conversely, the early finding of Bodenstein,¹⁵ that there is no gas-liquid phase effect in the photolysis of HI, supports our conclusion that caging of hydrogen atoms tends to be unimportant.

Acknowledgment. This work was supported by the U. S. Atomic Energy Commission.

(12) J. C. W. Chien and J. E. Willard, *J. Am. Chem. Soc.*, **75**, 6160 (1953).

(13) J. E. Willard, "Effects of Nuclear Transformations," Vol. I, AEC, Vienna, 1961.

(14) J. Franck and E. Rabinowitsch, *Trans. Faraday Soc.*, **30**, 120 (1934).

(15) As quoted by G. Kornfeld in the discussion to ref 14.

Extension of the "Band Model" to the Inner-Sphere Mechanism of Electron-Transfer Reactions

by I. Ruff

L. Eötvös University, Institute of Inorganic and Analytical Chemistry, Budapest, Hungary

Accepted and Transmitted by The Faraday Society (December 1, 1966)

The band model, suggested for interpreting the kinetic behavior of outer-sphere electron-transfer reactions, has been modified for the inner-sphere mechanism. The bridging ligand of the binuclear activated complex can be a favored electron transporter, reducing the height of the energy barrier by its oxidation-reduction potential and the barrier width by its complex-formation ability. Because of these phenomena, the entropy of activation increases, resulting in a catalytic effect. In addition to this, the bridging ligand can reduce the activation energy, if the formation enthalpy of the binuclear complex is larger than the energy of electrostatic repulsion between the reactant ions. Such types of catalytic effects of halogenide ions have been interpreted and the entropies of activation have been calculated. Good agreement has been shown between the theoretical and experimental results.

1. Introduction

In earlier papers¹⁻⁴ a new model has been suggested to calculate the kinetic parameters of oxidation-reduction and electron-exchange reactions, assuming an indirect electron-transfer mechanism. For the reactions considered in those works, it could be expected that the reactants approach each other, at most, up to the first coordination sphere in the activated complex. This requirement is satisfied at first by so-called "substitution inert" ions having a regular or nearly regular octahedral coordination sphere.⁵ Namely, the ions of "substitution labile" complexes are able to form temporarily a binuclear complex without an appreciable increase of the activation energy: *i.e.*, an activated complex can be formed in which the first coordination spheres of the two ions penetrate.

It has been proved experimentally that electron-transfer reactions proceed by these two types of mechanisms (*cf.* reviews^{6,7}). They are usually quoted as the "outer-sphere" and the "inner-sphere" mechanism.

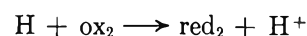
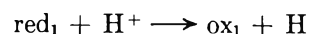
2. The Model

The model suggested, which has been shown to be in good agreement with the experimental results for reactions proceeding by the outer-sphere mechanism,^{1,2} is the following.

It has been assumed that the reaction takes place either by *electron* transfer, in a narrower sense, with the aid of the intermediate reaction



as follows



(1) I. Ruff, *J. Phys. Chem.*, **69**, 3183 (1965).

(2) I. Ruff, *Acta Chim. Acad. Sci. Hung.*, **47**, 241 (1966).

(3) I. Ruff, *ibid.*, **47**, 255 (1966).

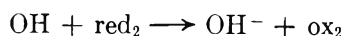
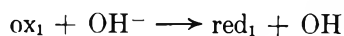
(4) I. Ruff, *ibid.*, **52**, 364 (1967).

(5) D. R. Stranks and R. G. Wilkins, *Chem. Rev.*, **57**, 743 (1957).

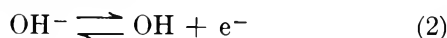
(6) H. Taube, *Proc. R. A. Welch Found. Conf. Chem. Res.*, **6**, 7 (1962).

(7) I. Ruff, *Kem. Kozl.*, **26**, 73 (1966).

or by *hole* transfer



i.e., the intermediate process is



The Bohr radius of the electron belonging to the hydroxonium radical (H_3O) and that of the hole in the hydroxyl radical (OH) has been estimated by a simple approximation.⁴ This value is about 40 Å. Such a greatly extended wave function gives the possibility of considering the electron or hole to be a practically delocalized "free" particle like the charge carriers of semiconductors.

It has been shown that the energy of the electron of the H_3O radical, OH^- ion, and the reactants can be calculated using the corresponding normal oxidation-reduction potentials. Taking such energy conditions into account, the energy barrier of the electron-transfer reaction can be given as shown in Figure 1. Here the delocalized levels of H_3O and OH^- are marked by the long horizontal lines. In the equilibrium state, the upper level is practically unoccupied and the lower one is occupied. The energy ranges, lying below and above these, are unimportant for us, hence unoccupied and occupied states, respectively, cannot exist here, since their existence would result in the decomposition of the water because of the spontaneous transitions. The levels of reactants (electron donor and acceptor) may exist only between these two energy limits.

The electron should overcome the rectangular potential barrier (dotted line) to accomplish one step of an electron transfer. This can happen either by ac-

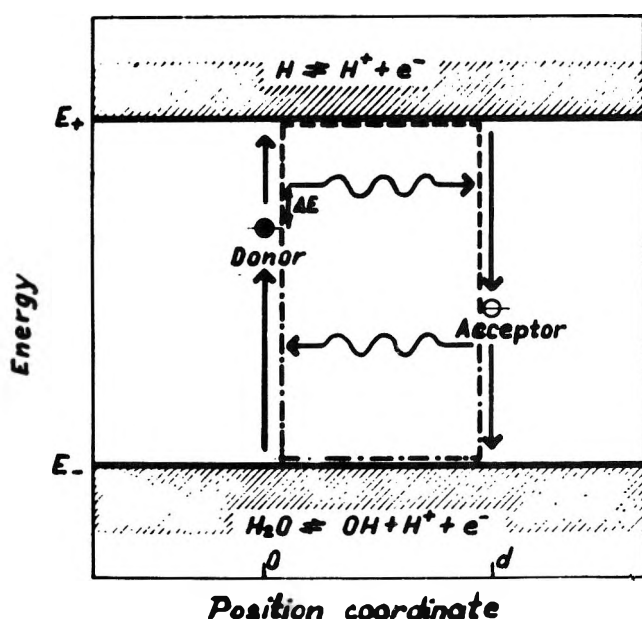


Figure 1.

cepting higher energy values than the height of the barrier and forming an H_3O , or by the tunnel effect possessing lower energy than the barrier height. The activation energy is determined by the Franck-Condon restriction and, in the first case, by the barrier height.

The hole transfer is quite similar, but everything happens in just the opposite direction and the barrier height is given by the lower energy limit and the unoccupied reactant level (hole donor).

Thus the reaction rate observed macroscopically is one of the four possible paths: namely, which has the smallest free-energy change of activation, *i.e.*, the fastest one.

Figure 1 is very similar to the well-known band system of the semiconductors (conduction, forbidden, and valence band) both by its shape and meaning. Due to this similarity, this model will be called the "band model." (There is a marked difference, of course: the H_3O and OH levels are imperfection states too, not like the conduction and valence bands in semiconductors.)

3. Theoretical Equations

It has been shown⁴ that the entropy of activation can be calculated by the equations

$$\Delta S^\ddagger = \Delta S^\ddagger_e + \Delta S^\ddagger_i + \Delta S^\ddagger_t - R \quad (3)$$

where

$$\Delta S^\ddagger_e = R \ln p_e \quad (4)$$

$$\Delta S^\ddagger_i = R \sum_i \ln p_i \quad (5)$$

and

$$\Delta S^\ddagger_t = -2R \ln c_* \quad (6)$$

Here p_e is the transition probability of the electron, p_i is the probability of satisfaction of the i th configuration requirement of the activated complex (ΔS^\ddagger_i represents what part of the collisions takes the place of a good orientation), and c_* is the so-called normalized concentration: *i.e.*, at this concentration the average distance between the reactants in solution is equal to the distance d between the reactants in the activated complex

$$c_* = (d^3 N_A \times 10^{-3})^{-1} \quad (7)$$

where N_A is the Avogadro number. ΔS^\ddagger_t represents the entropy due to the change in the degrees of freedom of translation.

In the case of *transfer above the barrier*, the activation energy is

$$\Delta E \geq U \quad (8)$$

where U is the barrier height (see Figure 1), but then we have

$$p_e = 1 \quad (9)$$

if the reactants situate inside of the effectivity space of one H₃O or OH radical. Considering their mentioned Bohr radii, this means that the reactants should approach each other at least to about 80 Å. Thus on the basis of eq 6

$$\Delta S^\ddagger_t = +23 \text{ eu} \quad (10)$$

Since we are speaking of the outer-sphere mechanism, the reactants can be considered to be of spherical symmetry, *i.e.*, for the collision there is no configurational restriction. Thus we have

$$\Delta S^\ddagger_i = 0 \quad (11)$$

(Here the term "collision" means that the two species are just at the distance, d , required by the activated complex.) Thus using eq 3, it can be written

$$\Delta S^\ddagger = 21 \text{ eu} \quad (12)$$

In the case of the tunnel effect^{1,2} the fastest path corresponds to the minimal d . For the outer-sphere mechanism, this occurs probably by the penetration of the second coordination spheres. Thus d is about 9.4 Å, from which it follows that

$$\Delta S^\ddagger_t \cong 0 \quad (13)$$

On the basis of the Gamow equation

$$p_e = \exp\left(-\frac{4\pi}{h}d\sqrt{2m(U - \Delta E)}\right) \quad (14)$$

where h is the Planck constant and m is the mass of the electron. Thus the total entropy of activation is

$$\Delta S^\ddagger = -R\frac{4\pi}{h}d\sqrt{2m(U - \Delta E)} - R \quad (15)$$

since eq 11 is valid in this case too.

In the case of transition metal ions, the activation energy is given by

$$\Delta E = (10Dq)_{\text{ox}} - (10Dq)_{\text{red}} \quad (16)$$

where the terms of the right-hand side are the crystal-field splittings of the (electron or hole) donor ion in its oxidized and reduced state, respectively. Equation 16 arises from approaching the ligand-electron repulsion energy by Van Vleck's treatment.⁸ This energy is needed to preform the environment of the ion to be left by the electron or hole, as it is required by the Franck-Condon principle, *i.e.*, to "push" the ligands toward the central ion.

4. Energy Barrier for the Inner-Sphere Mechanism

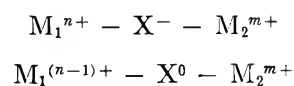
In the case of the inner-sphere mechanism, the electron transfer is preceded by the formation of binuclear complex of the configuration



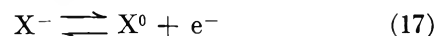
Unlike the outer-sphere mechanism, now the energy barrier is determined by the properties of the ligand L

and metal ions M_1^{n+} and M_2^{m+} . Though the wave function of L is much more localized than that of the hydrogen or hydroxyl ion, it will still be able to transport the electron, since here the distance between the initial and final position of the electron is smaller. Applying the usual expression, L functions as a bridge for the electron.

If L is a halide ion, the binuclear complexes before and after the excitation of the hole, respectively, are



Thus the intermediate reaction is



Similar to the hydroxyl ion, the halide ion can play a part in the hole transfer, since this later intermediates the transfer by an electron-donation process followed by an electron-capture process. Using the approximations of the previous papers,¹⁻⁴ the relative energy of the hole of X^0 could be taken into consideration by the normal oxidation-reduction potential with respect to eq 17, and that of the electron and hole of the metal ions can be calculated also by the corresponding normal oxidation-reduction potentials.

Thus the energy barrier is altered, as seen in Figure 2. It can be seen that the same possibilities can be taken into account as for outer-sphere electron-transfer: *i.e.*, (i) electron and hole transfer is possible; (ii) both can take place either by tunneling or by the transfer above the barrier. The essential difference is that in this case the barrier height of the hole-transfer reaction is not determined by the energy limit E_- , but by E_z , if

$$E_z > E_- \quad (18)$$

If $E_z < E_-$, the hydroxyl ions intermediate the reaction, since they can affect even when they are not situating just between the reactants, being their wave functions much more extended.

Similarly, it is possible for a suitable bridging ligand to catalyze the electron-transfer path reducing the actual barrier height.

In this case, it acts as an acceptor for an electron from the reducing agent. It must be a stronger oxidizing agent than the hydroxonium ion is. The bridging ligand was usually a halide ion in the investigated cases; later the treatment will be limited only to these.

This does not mean, however, that the electron-transfer path has been excluded because the halides are catalyzers for the hole transfer. If the reactants are able to form a binuclear activated complex, the

(8) F. H. Van Vleck, *J. Chem. Phys.*, **3**, 803, 807 (1935).

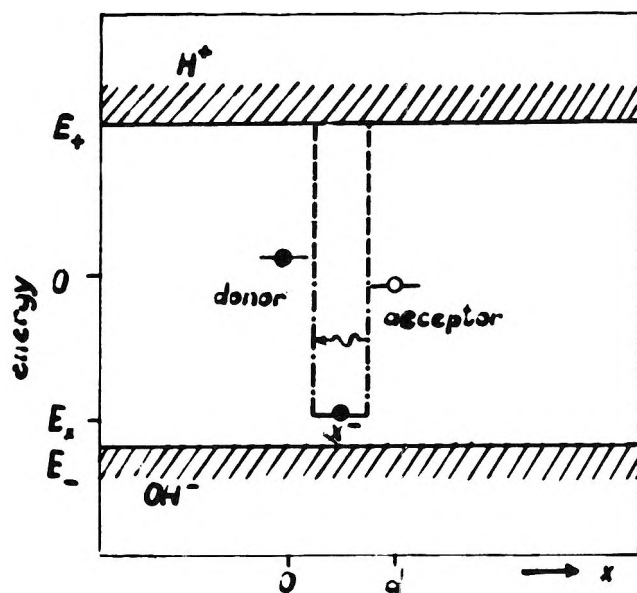


Figure 2.

electron transfer through the H_3O radical is favored as well, since the barrier width is decreased.

5. The Entropy of Activation

The entropy of activation can be calculated making use of eq 3-6 in this case too. This requires the determination of d and U .

(i) The distance between the reactants in the activated complex is

$$d = r_n + r_m + 2r_L \quad (19)$$

where r_n and r_m are the ionic radii of M^{n+} and M^{m+} , respectively, while r_L is that of the ligand. The radius of the metal ion is markedly influenced by complex formation; no large error is made, however, when about 0.5 \AA is assumed.

In Table I the calculated d values are shown using the ionic radii of the halide ions being in octahedral

Table I

X^-	$r_L, \text{ \AA}$	$e^0, \text{ V}$	$d, \text{ \AA}$	$\Delta S^\ddagger, \text{ eu}$
F^-	1.36	-4.0	3.72	-9.8
Cl^-	1.81	-2.3	4.62	-7.2
Br^-	1.95	-1.8	4.90	-6.5
I^-	2.16	-1.2	5.32	-5.5

coordination. In the fifth column the values of ΔS^\ddagger are given which have been calculated by applying eq 6 and 7.

(ii) The probability of tunnelling can be determined with respect to eq 14 by the former d values and by one of the equations

$$U = E_0 - E_x \quad (20)$$

$$U = E_0 - E_- \quad (21)$$

and

$$U = E_+ - E_0 \quad (22)$$

where E_0 is the energy corresponding to the normal oxidation-reduction potential of the appropriate donor. The suitable equation should be chosen among eq 20-22 depending upon whether the reaction is assumed to be hole transfer with $E_x > E_-$ or $E_x < E_-$, or electron transfer. Among these entropy values, the favored one is that which results in the smallest ΔF^\ddagger , since the reaction proceeds *via* this pathway.

The application of eq 20 requires the knowledge of the normal oxidation-reduction potential due to the equilibrium described by eq 17. As this contains halogen atoms, the potential cannot be observed experimentally. It can be calculated, however, on the basis of standard free-energy values,⁹ assuming the hydration energy of halogen atoms to be zero. This seems to be a close approximation because the hydration energies of X_2 molecules are only 3-5 kcal/mol (0.1-0.2 eV), too. The calculated normal oxidation-reduction potentials are given in the third column of Table I.

If the composition of the donor ion is ML_6X , or ML_4X_2 , where L is NH_3 or H_2O , the normal potential due to ML_6 has been used which does not essentially differ from the value corresponding to the mixed complexes.¹⁰

The values of ΔS^\ddagger , calculated in this way, have been summarized in the third column of Table II for some reactions studied experimentally. In these calculations the observed activation energy has been applied for the value of ΔE . Namely, the correctness of the relations, obtained for the entropy of activation, can be controlled without using the theoretical ΔE values which could not easily be calculated. In addition, no new approximations and errors are introduced by this treatment.

(iii) For the outer-sphere mechanism, the ΔS^\ddagger_1 part of activation entropy, arising from the oriented collision, should not be taken into account, since the reactants can be considered, in close approximation, to be of spherical symmetry. That is not the case, however, for the binuclear activated complex, because the bridging ligand occupies usually only one or two places in the coordination sphere of the reactants. At the other places there are other ligands unable to form a bridge. Thus the probability should be also considered which is due to the suitable spacial orientation.

The ideal orientation in the activated complex is the linear arrangement of the two metal ions and the halide

(9) W. M. Latimer, "Oxidation Potentials," Prentice-Hall, Inc., New York, N. Y., 1952.

(10) F. Basolo and R. G. Pearson, "Mechanism of Inorganic Reactions," John Wiley and Sons, Inc., New York, N. Y., 1958, p 318.

Table II

No.	Activated complex ^a	ΔS^\ddagger_e , eu	$\Delta S^\ddagger_{\text{calcd}}$, eu	$\Delta S^\ddagger_{\text{obsd}}$, eu
Electron-Transfer Reactions				
1	Cr(II)-F-Cr(III)(NH ₃) ₅	-8.0	-23	-30 ^b
2	Cr(II)-Cl-Cr(III)(NH ₃) ₅	-10.3	-23	-23 ^b
3	Cr(II)-Cl-Co(III)(NH ₃) ₅	-9.4	-22	-25 ^c
4	Eu(II)-Cl-Co(III)(NH ₃) ₅	-11.3	-24	-30 ^d
5	Eu(II)-Br-Co(III)(NH ₃) ₅	-12.1	-24	-32 ^d
6	V(II)-Cl-Co(III)(NH ₃) ₅	-10.3	-23	-20 ^c
Hole-Transfer Reactions				
7	V(II)-Br-Co(III)(NH ₃) ₅	-11.4	-23	-22 ^d
8	Fe(II)-Cl-Fe(III)	-10.1	-23	-24 ^e
9	Fe(II)-Cl-Fe(III)Cl	-9.8	-21	-20 ^e
10	Fe(II)-F-Fe(III)	-10.1	-25	-21 ^f
11	Fe(II)-F-Fe(III)F	-9.8	-24	-22 ^f

^a The H₂O ligands have been omitted. ^b H. Taube, *Proc. R. A. Welch Found. Conf. Chem. Res.*, **6**, 7 (1962). ^c A. Zwinkel and H. Taube, *J. Amer. Chem. Soc.*, **83**, 793 (1961). ^d J. P. Candlin, J. Halpern, and D. L. Trimm, *ibid.*, **86**, 1019 (1964). ^e J. Silverman and R. W. Dodson, *J. Phys. Chem.*, **56**, 846 (1952). ^f J. Hudis and A. C. Wahl, *J. Amer. Chem. Soc.*, **75**, 4153 (1953).

ion. It cannot be determined *a priori* how this configurational restriction is rigorous: *i.e.*, to what extent the metal-halide-metal angle might deviate from 180°. It seems to be acceptable, however, that the configuration is "good" as far as the metal-metal line passes nearer to the nucleus of the halide than to the center of another ligand.

For reactant ions ML₅X such positions take place of a probability of 1/6, while for ML₄X₂ ions this value is 1/3. This gives -3.6 and -2.2 eu, respectively, for ΔS^\ddagger_i .

In the fourth and fifth columns of Table II the observed values of the activation entropy are compared with the calculated over-all ones using eq 3. Considering the approximations and the average errors of the observed entropy of activation, an agreement within ± 5 eu can be regarded as a good one.

On the basis of the good fit obtained in most cases, it can be concluded that the basic assumption of the theory seems to be right: *i.e.*, the band model is able to explain the entropy of activation of inner-sphere electron-transfer reactions.

Thus the catalytic effect of the halide ions arises from two reasons with respect to the entropy of activation: (i) *the barrier width is decreased* by the formation of the binuclear complex; (ii) *the barrier height is decreased* for the hole when the halide can be oxidized more easily than the hydroxyl ion.

It can be seen in Tables I-II that the first effect appears for every halide ion, while the second is expected only for Cl⁻, Br⁻, and I⁻ and, at first, is expected for systems favoring the hole-transfer path ($E_0 < -0.1$ V).

The data of Table II are interesting, from the point of view that the calculated as well as the observed values do not show any trend; all of them are about -20 eu. In the case of the theoretical data this is the result owing to an inner compensation. Namely, the larger d value causes an increase of ΔS^\ddagger_t and a decrease of ΔS^\ddagger_o and *vice versa*. This confirms the applicability of the band model, since the same assumed energy conditions predicted properly a change of activation entropy from -40 up to +20 eu for the outer-sphere mechanism.¹⁻⁴

6. The Activation Energy

In the case of the outer-sphere mechanism, the relatively large distance between the reactants gave the possibility of neglecting the electrostatic interactions. In this way the total activation energy could be explained by the Franck-Condon restriction. For the inner-sphere mechanism, however, the formation free energy of the binuclear complex and the electrostatic interactions should be taken into account, in addition to this. It can be expected, in general, that the latter one enhances the activation energy, while the former one can enhance as well as reduce it, depending on the individual properties of the reactants.

It can be seen that the problem is rather complicated to endeavor to obtain quantitative theoretical results. It is probable, however, that the main part of the activation energy is the result of the Franck-Condon restriction. This can be seen in Table III, where the activation energies of the inner-sphere transfers listed in Table II are compared with those of the outer-sphere transfers having the same donor. A catalytic

Table III

No.	Donor process	ΔE , kcal/mol		
		Calcd	Outer sphere ^e	Inner sphere
1	Cr(II) → Cr(III)	9.5	...	13.4
2				11.1
3				14.7
4	En(II) → En(III)	...	9.0 ^a	5.0
5				4.7
6	V(II) → V(III)	13.2	13.2 ^b	14.1
7	Co(III)(NH ₃) ₆ → Co(II)(NH ₃) ₅	...	13.5 ^c	9.1
8	Fe(III) → Fe(II)	9.5	9.9 ^d	8.8
9				10.0
10				9.1
11				9.5

^a Obtained for electrode reaction: J. E. B. Randles and K. W. Somerton, *Trans. Faraday Soc.*, **48**, 937 (1952). ^b K. V. Krishnamurthy and A. C. Wahl, *J. Amer. Chem. Soc.*, **80**, 5921 (1958). ^c N. S. Biradar, D. R. Stranks, M. S. Vaidhya, G. J. Weston, and D. J. Simpson, *Trans. Faraday Soc.*, **55**, 1268 (1959). ^d J. Silverman and R. W. Dodson, *J. Phys. Chem.*, **56**, 846 (1952). ^e The data in this column refer to isotopic electron-exchange reactions.

effect owing to the decrease in activation energy can be observed only in the case of reactions 4, 5, 7, 8, and 10, but for the other reactions no catalysis of this type appears. Thus, in the latter case, the acceleration arises from the increase in the entropy of activation only: *i.e.*, either the electrostatic repulsion and the free-energy change of the complex formation have no marked effect or they are opposite and compensate each other.

As can be concluded from the present treatment, the electrostatic and polarization interactions are not the most important effects, unlike in the theories of Eyring and coworkers,¹¹ Libby,¹² and Marcus,¹³ which, there-

fore, do not seem to be easily extendable to the inner-sphere mechanism. On the other hand, this model does not contain such complicated parameters and computing processes as the conjugation theory^{14,15} does.

(11) R. J. Marcus, R. J. Zwolinsky, and H. Eyring, *J. Phys. Chem.*, **58**, 432 (1954).

(12) W. F. Libby, *ibid.*, **56**, 863 (1952).

(13) R. A. Marcus, *J. Chem. Phys.*, **24**, 966 (1956); **26**, 867 (1957); *Disc. Faraday Soc.*, **29**, 21 (1960); *J. Phys. Chem.*, **67**, 853 (1963).

(14) J. Halpern and L. E. Orgel, *Discussions Faraday Soc.*, **29**, 32 (1960).

(15) P. V. Manning, R. C. Jarnagin, and M. Silver, *J. Phys. Chem.*, **68**, 265 (1964).

Light-Induced Proton Ejection and Electron Transfer in the Zinc Tetraphenylporphin-Benzoquinone System

by Kenneth P. Quinlan

Photochemistry Section, Energetics Branch, Space Physics Laboratory, A. F. Cambridge Research Laboratories, L. G. Hanscom Field, Bedford, Massachusetts 01730 (Received December 6, 1967)

Excitation of zinc tetraphenylporphin in the presence of *p*-benzoquinone activates a reversible proton ejection and an electron transfer attended by the formation of the benzosemiquinone ion radical. The reaction is slightly quenched by air and inhibited by large concentrations of benzoquinone. The results are similar to those found with the chlorophyll-benzoquinone system.

Introduction

In a recent communication,¹ the chlorophylls were shown to eject a proton during the light-activated single-electron transfer with *p*-benzoquinone. Possible sources of the origin of the proton from chlorophyll based upon previous work^{2,3} are the methine and the C-10 positions. A study of the zinc tetraphenylporphin (ZnTPP)-benzoquinone system offered an opportunity to see whether the presence of hydrogens at these particular sites is necessary for proton ejection.

Two additional significant observations were also noted in the study of the chlorophyll-benzoquinone system. Proton ejection was in the same apparent proton-activity range whether air was present or not,¹ and high concentrations of benzoquinone inhibited proton ejection.⁴ Results are presented in the present paper to show that the light-induced reaction between zinc tetraphenylporphin and benzoquinone is slightly quenched by air and inhibited by large concentrations of benzoquinone.

Experimental Section

The zinc $\alpha,\beta,\gamma,\delta$ -tetraphenylporphin was kindly supplied by G. Sherman of Brandeis University. It was further purified by chromatography on a column of a mixture of magnesia and Hy-Flo Super Cel using the method of Seely and Calvin.⁵ Benzoquinone was purified by sublimation. Methanol was Baker Analyzed reagent spectrophotometric grade. Dimethylformamide was purified by distillation from calcium hydride under vacuum.

The method of measuring the apparent pH values of the solutions has recently been described.⁶ In the

(1) K. P. Quinlan and E. Fujimori, *J. Phys. Chem.*, **71**, 4154 (1967).

(2) R. C. Dougherty, H. H. Strain, and J. J. Katz, *J. Amer. Chem. Soc.*, **87**, 104 (1965).

(3) R. B. Woodward and V. Skaric, *ibid.*, **83**, 4676 (1961).

(4) K. P. Quinlan, unpublished results. Electron spin resonance studies of the same system in dimethylformamide showed a large decrease in the esr signal with increasing amounts of *p*-benzoquinone.

(5) G. R. Seely and M. Calvin, *J. Chem. Phys.*, **23**, 1068 (1955).

(6) K. P. Quinlan and E. Fujimori, *Photochem. Photobiol.*, **6**, 665 (1967).

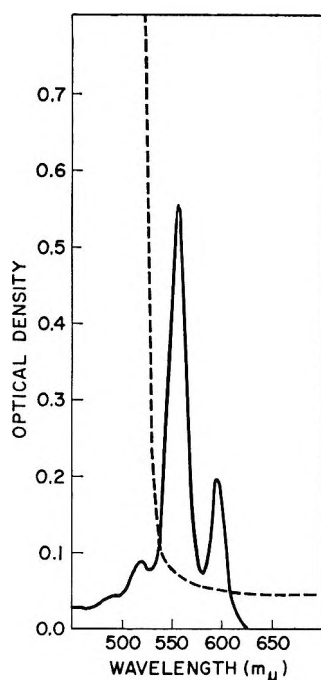


Figure 1. Absorption spectra of $2.88 \times 10^{-5} M$ zinc tetraphenylporphyrin in methanol, —, and the CS3-69 filter, - - -.

present study, the solutions were irradiated with a 500-W projection lamp setup consisting of a collimating lens, a Corning CS3-69 filter, a 1-cm heat filter of 0.05% copper sulfate, and a 7-cm filter of distilled water. The light intensity was 3.5×10^4 ergs/cm² sec.

The epr spectra were obtained with a Varian V-4502 spectrometer utilizing 100-kc modulation. The samples were irradiated with light from a 1-kW projection lamp. The light was passed through a 1-cm heat filter of 0.05% copper sulfate and the CS3-69 filter.

The test solutions were prepared at the time of determination. Air-free systems were obtained by flushing with nitrogen which was previously scrubbed with either alkaline pyrogallol or chromous chloride solutions. Methanol was used directly for systems studied in the presence of air.

The adsorption spectrum of ZnTPP in methanol and the CS3-69 filter is shown in Figure 1.

Results and Discussion

Figure 2 shows the esr spectra of the ZnTPP-benzoquinone system in the presence and absence of air when ZnTPP is excited with light. The figure illustrates the characteristic five-line spectrum of the *p*-benzosemiquinone formed in the deaerated system as a result of an electron transfer from the ZnTPP. Benzoquinone in methanol gives a diminutive signal but is in no way affected by yellow light. The small light-induced signal obtained at a modulation amplitude of 7.0 g in the presence of air indicates that there is an interaction between the ZnTPP and benzoquinone.

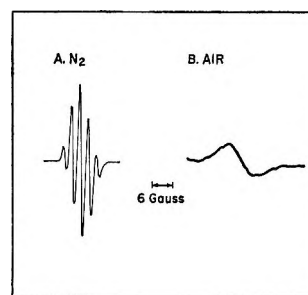


Figure 2. Effect of air on the light-induced esr spectra of the zinc tetraphenylporphyrin-*p*-benzoquinone system in methanol: A, air free ($1.8 \times 10^{-4} M$ ZnTPP and $1.5 \times 10^{-3} M$ quinone); B, air ($1.8 \times 10^{-4} M$ ZnTPP and $1.3 \times 10^{-3} M$ quinone).

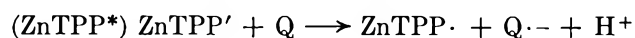
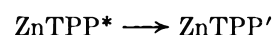
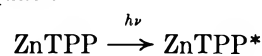
The decrease in signal height may be because of an interaction of oxygen with the formed radicals. No signal is observed when ZnTPP is excited alone in methanol, whether methanol is air free or not.

Proton ejection accompanying electron transfer for the ZnTPP-benzoquinone system in methanol is illustrated by the typical results shown in Figure 3. Similar observations were also noted in aqueous dimethylformamide solutions. Figure 3 shows that no change in apparent pH is observed when either ZnTPP or quinone is irradiated with yellow light. Table I shows the results of a series of measurements performed in the absence and presence of air. In each case, proton ejection was observed in the presence of air. These results are similar to the chlorophyll system where proton ejection is observed in the presence of air. These values were calculated using $pK = 16.77$ for the autoprotolysis constant of methanol, and it was assumed that there was no buffering action.

Table I: Effect of Quinone Concentration on Proton Ejection from the Zinc Tetraphenylporphyrin-Benzoquinone System in Methanol

ZnTPP concn, <i>M</i>	Quinone concn, <i>M</i>	—Apparent proton ejection, <i>M</i> —	
		Deaerated	Aerated
2.88×10^{-5}	2.3×10^{-5}	4.0×10^{-10}	2.0×10^{-11}
2.88×10^{-5}	6.8×10^{-4}	4.2×10^{-10}	2.7×10^{-10}
2.88×10^{-5}	1.2×10^{-3}	1.0×10^{-9}	6.0×10^{-10}
2.88×10^{-5}	6.6×10^{-3}	5.1×10^{-10}	3.3×10^{-10}
2.88×10^{-5}	2.0×10^{-2}	2.7×10^{-10}	2.1×10^{-10}
2.88×10^{-5}	2.0×10^{-1}	No ejection	No ejection

The above results can be summarized by the following simplified equations



(7) E. J. King, "Acid-Base Equilibria," The Macmillan Co., New York, N. Y., 1965, p 298.

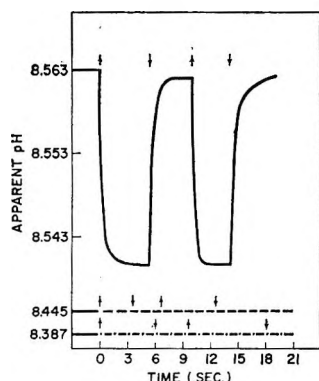


Figure 3. Proton ejection from the zinc tetraphenylporphyrin-*p*-benzoquinone system in aerated methanol (upward arrows represent light on; downward arrows represent light off): —, zinc tetraphenylporphyrin ($2.88 \times 10^{-6} M$) and *p*-benzoquinone ($6.6 \times 10^{-3} M$); - - - -, ZnTPP ($2.88 \times 10^{-6} M$); - - - -, quinone ($1.4 \times 10^{-3} M$).

where ZnTPP* and ZnTPP' are the excited singlet and triplet state of ZnTPP. In the presence of air, quinone and oxygen compete for the excited states of ZnTPP. This is shown by the small decrease in proton ejection in aerated solutions. The triplet state of ZnTPP and its quenching have been studied by Pekkarinen and Linschitz.⁸

The above results show that neither the methine nor the C-10 hydrogen is necessary for proton ejection. Comparison of the chlorophylls and ZnTPP indicates that no specific type of hydrogen is required for proton ejection from porphyrins during light-activated electron

transfer. These conclusions are based upon the assumption that the solvent plays no role in proton ejection.

A study of the effect of quinone concentration on proton ejection is shown in Table I. The results illustrate that an optimum concentration of quinone exists for maximum proton ejection. Proton ejection decreases as the quinone concentration increases beyond this point. At a concentration of $2 \times 10^{-1} M$ quinone, proton ejection is no longer detected. A solution containing $1.8 \times 10^{-4} M$ ZnTPP with $1.9 \times 10^{-1} M$ quinone in air-free methanol exhibited no light-induced esr signal. Evstigneev and coworkers⁹ also showed in their photopotential study of the chlorophyll-benzoquinone system that a high concentration of quinone reduced the magnitude of the photopotential. These results indicate that the interaction between chlorophyll or ZnTPP with benzoquinone cannot be simply restricted to an electron-transfer process.

The results reported in the present paper not only substantiate those obtained with the chlorophyll system, but also may shed light on the mechanism of the electron-transfer process in photosynthesis.

Acknowledgment. The author wishes to thank Dr. E. Fujimori for many helpful discussions.

(8) L. Pekkarinen and H. Linschitz, *J. Amer. Chem. Soc.*, **82**, 2407, 2411 (1960).

(9) V. B. Evstigneev, V. A. Gavrilova, and N. A. Sadovnikova, *Biokhimiya*, **31**, 1229 (1966).

Flash Photolysis Study of Sulfite, Thiocyanate, and Thiosulfate Ions in Solution

by L. Dogliotti and E. Hayon

*Pioneering Research Laboratory, U. S. Army Natick Laboratories, Natick, Massachusetts 01760
(Received December 14, 1967)*

The primary photolytic processes, as observed by the technique of flash photolysis, were studied for the sulfur polyvalent anions SO_3^{2-} , CNS^- , and $\text{S}_2\text{O}_3^{2-}$ in aqueous solution. Sulfite ions were found to produce two transient species, resulting from the primary photolytic process: $\text{SO}_3^{2-} \cdot \text{H}_2\text{O} \xrightarrow{h\nu} \text{SO}_3^- + e_{\text{aq}}^-$. A short-lived species apparently formed by the addition of e_{aq}^- to sulfite ions and tentatively assigned to HSO_3^{2-} (λ_{max} 720 $\text{m}\mu$) decays by first-order process, $k = (1.9 \pm 0.3) \times 10^4 \text{ sec}^{-1}$, and a longer lived species assigned to SO_3^- ($\lambda_{\text{max}} \sim 275 \text{ m}\mu$) decays by second-order process, $2k/\epsilon = 1.5 \times 10^6$ at 275 $\text{m}\mu$. Thiocyanate ions decompose on photolysis by at least two processes: $\text{CNS}^- \cdot \text{H}_2\text{O} \xrightarrow{h\nu} \text{CNS} + e_{\text{aq}}^-$ and $\text{CNS}^- \xrightarrow{h\nu} \text{CN}^- + \text{S}$. A transient spectrum, due to $(\text{CNS})_2^-$ radical anions, was found absorbing at λ_{max} 485 $\text{m}\mu$, with species decaying by a first-order process in air-free solutions and by a second-order process in the presence of oxygen. Thiosulfate ions decompose on photolysis by two processes: $\text{S}_2\text{O}_3^{2-} \cdot \text{H}_2\text{O} \xrightarrow{h\nu} \text{S}_2\text{O}_3^- + e_{\text{aq}}^-$ and $\text{S}_2\text{O}_3^{2-} \cdot \text{H}_2\text{O} \xrightarrow{h\nu} \text{S}_2\text{O}_2^- + \text{OH}^- + \text{OH}^-$. The OH radicals produced react with $\text{S}_2\text{O}_3^{2-}$ to form S_2O_3^- radicals. A transient optical spectrum with a λ_{max} 380 $\text{m}\mu$ assigned to S_2O_3^- decays by a second-order process in the absence of O_2 and by a first-order process in the presence of O_2 . S_2O_2^- has a $\lambda_{\text{max}} \sim 280 \text{ m}\mu$ and decays by a second-order process in the presence or absence of oxygen. The CTTS absorption bands of the three sulfur anions have been determined. The esr spectra of the radicals produced on uv irradiation of SO_3^{2-} , CNS^- , and $\text{S}_2\text{O}_3^{2-}$ ices at 77°K are given.

The ultraviolet absorption spectra of the sulfur polyvalent anions SO_3^{2-} , CNS^- , and $\text{S}_2\text{O}_3^{2-}$ are known, but, except for thiosulfate anions, their absorption spectra have not been characterized and their photochemistry has not been studied for many years.

Albu and Goldfinger¹ examined the absorption spectrum of the sulfite ion on the basis of the Franck-Haber theory of the electron-affinity spectrum of ions and showed that the SO_3^{2-} spectrum has a long wavelength limit of 2660 Å and corresponds to the process $\text{SO}_3^{2-} \cdot \text{H}_2\text{O} \xrightarrow{h\nu} \text{SO}_3^- + \text{H} + \text{OH}^-$. Haber and Wansbrough-Jones² studied the photochemistry of sulfite ions in the absence of oxygen and postulated the reactions $\text{H} + \text{H} \rightarrow \text{H}_2$ and $\text{SO}_3^- + \text{SO}_3^- \rightarrow \text{S}_2\text{O}_6^{2-}$ taking place under their experimental conditions. However, they found the quantum yield of dithionate to be 0.07 at pH 7.0 and suggested the possibility of the "back reaction" $\text{SO}_3^- + \text{H} \rightarrow \text{HSO}_3^-$ occurring. Bäckström³ studied the effects of inhibitors, particularly alcohols, on the photochemical oxidation of sulfite ions in solution.

Thiocyanate ions were found⁴ to decompose with light in the wavelength range 1800–3000 Å with the formation of sulfur. The reaction was postulated to be reversed in the dark. Matheson, *et al.*,⁵ found evidence for the formation of solvated electrons in the flash photolysis of aqueous solutions of CNS^- ions, and Gusarsky and Treinin⁶ interpreted the absorption band of thiocyanate ions at $\sim 220 \text{ m}\mu$ as due to a charge-transfer-to-solvent (CTTS) spectra.

The spectrum of $\text{S}_2\text{O}_3^{2-}$ in solution has an intense absorption peak at about 215 $\text{m}\mu$ ^{7,8} and has been assigned to a CTTS type of excitation.^{8–10} The limiting (maximum) quantum yield of decomposition of the CTTS band was found¹⁰ to be <0.1 in the presence of electron scavengers in solution.

In this work, the results on the flash-photolysis study of sulfite, thiocyanate, and thiosulfate anions in aqueous solution is presented. The primary photochemical processes occurring in these systems are discussed and the optical absorption spectra of the short-lived transients are identified.

Experimental Section

The flash-photolysis lamps and setup used in this work have been described elsewhere.¹¹ Total flash

- (1) H. W. Albu and P. Goldfinger, *Z. Phys. Chem.*, **16B**, 338 (1932).
- (2) F. Haber and O. H. Wansbrough-Jones, *ibid.*, **18B**, 103 (1932).
- (3) H. Bäckström, *J. Amer. Chem. Soc.*, **49**, 1460 (1927); *Z. Phys. Chem.*, **25B**, 122 (1934).
- (4) K. Jablczynski and H. Jablczynska, *Rocz. Chem.*, **10**, 579 (1930); *Bull. Soc. Chim. France*, **49**, 877 (1931).
- (5) M. S. Matheson, W. A. Mulac, and J. Rabani, *J. Phys. Chem.*, **67**, 2613 (1963).
- (6) E. Gusarsky and A. Treinin, *ibid.*, **69**, 3176 (1965).
- (7) A. D. Autrey and R. E. Connick, *J. Amer. Chem. Soc.*, **73**, 1842 (1951).
- (8) M. Smith and M. C. R. Symons, *J. Chem. Phys.*, **25**, 1074 (1956).
- (9) D. P. Ames and J. Willard, *J. Amer. Chem. Soc.*, **75**, 3267 (1953); W. S. Fyfe, *J. Chem. Phys.*, **37**, 1894 (1962).
- (10) R. Sperling and A. Treinin, *J. Phys. Chem.*, **68**, 897 (1964).

energies of 1800 J were used with a duration at "1/e time" of 5 μsec and a total flash duration of 70 μsec . A Bausch and Lomb grating monochromator with gratings blazed in the uv, visible, and near-ir regions were used. An EMI 9558QB photomultiplier tube was employed throughout this work. The optical absorption spectra of the transient species produced were obtained by the point-by-point method.

Solutions were prepared just previous to irradiation using water purified by triple distillation, radiolysis, and photolysis.¹² Reagents used were the best research grade supplied by Baker and Adamson and Mallinckrodt, and they were used without further

Results and Discussion

Photolysis of Sulfite Ions. All the work reported below was carried out in $10^{-2} M$ Na_2SO_3 solutions. The flash photolysis of sodium sulfite in aqueous solution gave rise to the formation of a transient species absorbing strongly in the wavelength region 350–1000 $m\mu$, see Figure 1, with a λ_{max} at about 720 $m\mu$. Except for variations in the amount of transient produced, the same optical spectrum was obtained at all sulfite ion concentrations studied up to $10^{-1} M$. Similarly, the same transient was formed in the presence or absence of oxygen (Figure 1). This broad absorption spectrum, with a peak at about 720 $m\mu$, was found to be due to

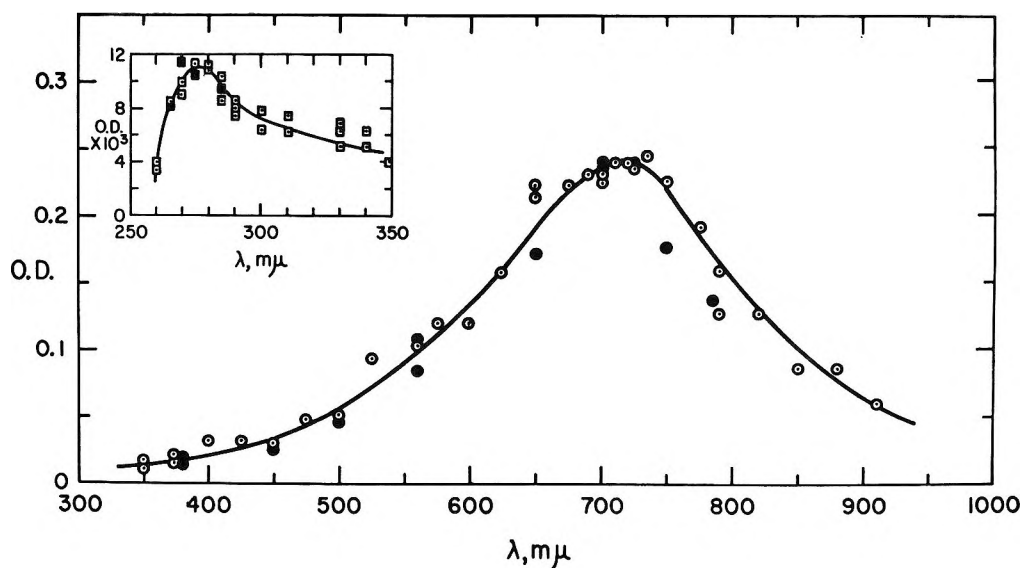


Figure 1. Transient absorption spectra produced on flash photolysis of $10^{-2} M$ Na_2SO_3 at pH 6.0, in N_2 -saturated (\circ) and in air-saturated (\bullet) solution. Optical density measured in 20-cm optical cells, 25 μsec after start of flash. Inset: longer lived transient measured in N_2 -saturated (\square) and air-saturated (\blacksquare) solutions 300 μsec after start of flash.

purification. Solutions were deaerated, using pre-purified nitrogen, by the syringe technique or by using a bubbler with a wide glass frit at the bottom of a cylindrical vessel under continuous N_2 gas flow conditions. The concentration of the solutes used in this investigation was kept to a minimum to reduce "inner-filter" effects but sufficient to obtain enough transient. Furthermore, since sulfur was produced in the photolysis of the three anions studied, it was essential to keep its concentration down to a minimum to avoid interference with the transmission of the monitoring light beam through the optical cell.

The esr spectra were recorded with a Varian V-4500 X-band spectrometer with 100-kc/sec modulation and a 9-in. electromagnet equipped with the Fielddial. A dual cavity was usually used together with a double recorder. The irradiated sample was placed in one cavity and in the other a KCl-pitch sample was used. All spectra were measured at 77°K, even those that were annealed at higher temperatures.

one single species which decays by a first-order process (see Table I). The decay rate of the transient was found to be the same in the presence or absence of oxygen, in neutral solution or at pH 12.0, with an average decay constant $k = 1.9 \pm (0.3 \times 10^4) \text{ sec}^{-1}$. On flashing a $10^{-2} M$ Na_2SO_3 solution saturated with N_2O gas, no transient was found absorbing in the wavelength region 500–800 $m\mu$.

A second transient species was observed on photolysis of $10^{-2} M$ SO_3^{2-} ions in N_2 -, N_2O -, and air-saturated solutions, absorbing in the wavelength region 250–380 $m\mu$, with a maximum absorption peak at about 275 $m\mu$; see Figure 1. This intermediate absorbs considerably less than the species with λ_{max} 720 $m\mu$, is longer lived, with a half-life of a few milliseconds, and decays by a second-order process; see Table I.

(11) L. Dogliotti and E. Hayon, *J. Phys. Chem.*, **71**, 2511 (1967). M. Langmuir and E. Hayon, *ibid.*, **71**, 3808 (1967).

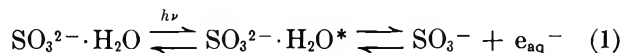
(12) E. Hayon, *Trans. Faraday Soc.*, **60**, 1059 (1964).

Table I: Rate Constants for the Decay of Transients Produced on Flash Photolysis of $10^{-2} M$ Na_2SO_3

Transient	System	pH	λ , $m\mu$	Decay rate ^a
HSO_3^{2-}	N_2 satd	Neutral	375	$k = 2.0 \times 10^4 \text{ sec}^{-1}$
HSO_3^{2-}	N_2 satd	Neutral	575	$k = 1.7 \times 10^4 \text{ sec}^{-1}$
HSO_3^{2-}	N_2 satd	Neutral	675	$k = 1.8 \times 10^4 \text{ sec}^{-1}$
HSO_3^{2-}	N_2 satd	Neutral	700	$k = 1.9 \times 10^4 \text{ sec}^{-1}$
HSO_3^{2-}	Air satd	Neutral	375	$k = 2.0 \times 10^4 \text{ sec}^{-1}$
HSO_3^{2-}	Air satd	Neutral	650	$k = 2.1 \times 10^4 \text{ sec}^{-1}$
HSO_3^{2-}	Air satd	Neutral	675	$k = 1.7 \times 10^4 \text{ sec}^{-1}$
HSO_3^{2-}	N_2 satd	11.9	650	$k = 1.4 \times 10^4 \text{ sec}^{-1}$
HSO_3^{2-}	$5 \times 10^{-4} M$ ethanol, air satd	Neutral	650	$k = 2.2 \times 10^4 \text{ sec}^{-1}$
SO_3^-	N_2 satd	Neutral	275	$2k/\epsilon = 1.5 \times 10^6$
SO_3^-	N_2 satd	Neutral	280	$2k/\epsilon = 1.5 \times 10^6$
SO_3^-	N_2 satd	Neutral	290	$2k/\epsilon = 1.6 \times 10^6$
SO_3^-	Air satd	Neutral	270	$2k/\epsilon = 1.7 \times 10^6$
SO_3^-	Air satd	Neutral	275	$2k/\epsilon = 1.3 \times 10^6$
SO_3^-	Air satd	Neutral	280	$2k/\epsilon = 1.9 \times 10^6$

^a Deviation is $\pm 15\%$.

The above experimental observations are explained on the basis that the main primary photolytic process resulting from the absorption of light by SO_3^{2-} ions is due to a CTTS transition, leading to the formation of SO_3^- radical anions and solvated electrons, according to



While the release of electrons from the spectroscopic excited state of sulfite ions can account and explain the results obtained by this flash-photolysis technique, one cannot exclude other photolytic processes which may be occurring simultaneously but which do not give rise to observable absorbing species under the conditions of our experiments. This is also true of the other systems described below.

The electron released in reaction 1 is considered to form an adduct with sulfite ions, giving an intermediate which is tentatively assigned to HSO_3^{2-}



The species with $\lambda_{\text{max}} 720 m\mu$ is assigned to the HSO_3^{2-} radical anion and the species with $\lambda_{\text{max}} \sim 275 m\mu$ is assigned to the SO_3^- radical anion. These assignments have been made taking into consideration the following facts and observations. The HSO_3^{2-} transient with $\lambda_{\text{max}} 720 m\mu$ is not formed on photolysis of SO_3^{2-} in presence of $2 \times 10^{-2} M$ N_2O . This is explained on the basis of a kinetic competition between reaction 2 and



with $k_3 = 5.6 \times 10^9 M^{-1} \text{ sec}^{-1}$.¹³ Under these experimental conditions ($10^{-2} M$ SO_3^{2-} and $2 \times 10^{-2} M$ N_2O at neutral pH), all the electrons have reacted

with N_2O according to reaction 3. The slow-decaying transient absorbing with $\lambda_{\text{max}} \sim 275 m\mu$ was still observed in N_2O solutions, indicating that e_{aq}^- is not involved in its formation.

Addition of H^+ ions, to convert e_{aq}^- to H atoms, where $k_4 = 2.3 \times 10^{10} M^{-1} \text{ sec}^{-1}$ ¹³ was found



not to be feasible. Franck-Haber's theory predicts that the corresponding electron-affinity spectrum of the bisulfite ion should be 1.5–2.0 eV to the shorter wavelength side of that of the sulfite ion. In agreement with this prediction, no absorption by the bisulfite ion was found at $\lambda > 2250 \text{ \AA}$, and no transient species were produced on flash photolysis of $10^{-2} M$ sodium bisulfite or $10^{-2} M$ sodium sulfite at pH 1.1–2.0, in air or N_2 -saturated solutions.

Instead of using H^+ ions as an electron scavenger, nitrate ions were added to a $10^{-2} M$ SO_3^{2-} solution. In N_2 -saturated solution containing $2 \times 10^{-4} M$ KNO_3 , no transient was observed at $720 m\mu$. However, using lower concentrations of NO_3^- ions, it was possible to form some HSO_3^{2-} and observe its decay. At $720 m\mu$, the transient was found to decay by a pseudo-first-order process dependent on $[\text{NO}_3^-]$, from which a $k(\text{HSO}_3^{2-} + \text{NO}_3^-) \simeq 10^9 M^{-1} \text{ sec}^{-1}$ was calculated. In addition, from the competition between reaction 2 and $k(e_{\text{aq}}^- + \text{NO}_3^-)$, it was estimated that $k(e_{\text{aq}}^- + \text{SO}_3^{2-}) \leq 2 \times 10^6 M^{-1} \text{ sec}^{-1}$.

Pulse radiolysis of aqueous solutions of sulfite ions was examined by Adams, *et al.*^{14,15} In a first pub-

(13) M. Anbar and P. Neta, *Int. J. Appl. Radiat. Isotopes*, **18**, 493 (1967).

(14) G. E. Adams, J. W. Boag, and B. D. Michael, *Proc. Chem. Soc.*, 411 (1964).

lication¹⁴ a transient spectrum with $\lambda_{\text{max}} \approx 350 \text{ m}\mu$ was reported on irradiation of neutral aqueous solutions in the presence of oxygen. This spectrum was suggested to be formed from the reaction $\text{OH}^- + \text{SO}_3^{2-} \rightarrow \text{SO}_3^- + \text{OH}^-$ and was assigned to the SO_3^- radical. In a later work, Adams, *et al.*,¹⁵ found no transient on pulse radiolysis of 0.5 M sulfite ions in presence of $2 \times 10^{-2} \text{ M N}_2\text{O}$ gas. In the presence of oxygen, they now observed a transient with an absorption maximum at 750 m μ but with no transient peaking at $\sim 350 \text{ m}\mu$, indicating that the transient has a reducing species (e_{aq}^- or O_2^-) as a precursor.

Their later results¹⁵ are in accord with the results presented above for the species absorbing at 720 m μ in the flash photolysis of SO_3^{2-} ions. The difference in λ_{max} is thought to be due to the use¹⁵ of flash spectrography in deriving the absorption spectrum of the transient.

Since $k(\text{e}^- + \text{O}_2 \rightarrow \text{O}_2^-) = 1.9 \times 10^{10} \text{ M}^{-1} \text{ sec}^{-1}$ and $k(\text{e}^- + \text{SO}_3^{2-})$ was estimated as $\leq 2 \times 10^{-6} \text{ M}^{-1} \text{ sec}^{-1}$, all the electrons produced in reaction 1 must react with oxygen under the experimental conditions described above. The formation of the transient on photolysis of air-saturated solutions is then probably the result of the reaction $\text{O}_2^- + \text{SO}_3^{2-} \xrightarrow{\text{H}_2\text{O}} \text{HSO}_3^{2-} + \text{OH}^- + \text{O}_2$.

The assignment of the slow-decay species, with $\lambda_{\text{max}} \sim 275 \text{ m}\mu$, to the SO_3^- radical anion was based on the following premises. Since the transient with $\lambda_{\text{max}} 720 \text{ m}\mu$ is formed as the result of the reaction of e_{aq}^- with SO_3^{2-} , the SO_3^- radical produced in the primary photolytic process could well account for the observed absorption spectrum in the uv region. In addition, the OD at 270 m μ was found to increase from 0.012 to 0.025 in air- or N_2 -saturated solutions compared to N_2O -saturated solutions. This doubling of the amount of SO_3^- radical formed is explained on the basis of reaction 3 followed by $\text{OH}^- + \text{SO}_3^{2-} \rightarrow \text{SO}_3^- + \text{OH}^-$. This observation provides strong support for the proposed main primary process taking place in the photolysis of sulfite ions, *viz.* reaction 1.

The examination¹⁶ of the esr spectrum produced on uv irradiation of $10^{-2} \text{ M Na}_2\text{SO}_3$ ices at 77°K showed a singlet with an isotropic g factor very close to 2.000 (see Figure 2a). The sulfite ice was colorless after uv irradiation, and the esr single line was found to disappear on thermal annealing of the ice to about -70° . Chantry, *et al.*,¹⁷ have observed the optical and esr spectra of SO_3^- radicals produced on γ irradiation of single crystals of sodium dithionate, sulfamic acid, and potassium sulfamate. The esr spectrum reported¹⁷ is a single line with an isotropic g factor of 2.004 due to $^{32}\text{SO}_3^-$ radicals. They also found a uv absorption at 270 and 240 m μ and concluded that the 270-m μ band is due to SO_3^- radicals. More recently, Gromov and Morton¹⁸ have observed the esr spectrum of SO_3^-

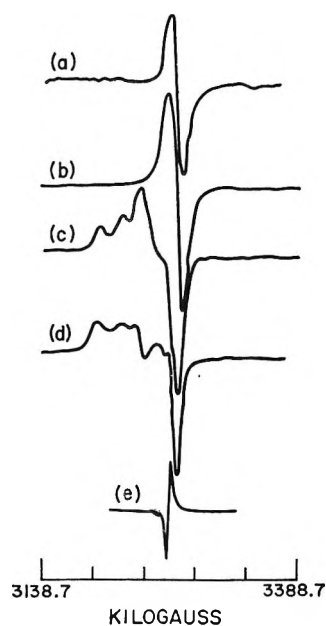


Figure 2. Electron spin resonance spectra of trapped radicals produced on uv irradiation at 77°K: (a) $10^{-2} \text{ M Na}_2\text{SO}_3$, colorless, radical disappears at -70° ; (b) $10^{-2} \text{ M NaHSO}_3$, purple-violet, radical and color disappear at -75° ; (c) 10^{-2} M KCNS , red, radical and color disappear at -95° ; (d) $10^{-2} \text{ M Na}_2\text{S}_2\text{O}_3$, yellow, radical and color disappear at -60° ; (e) pitch sample.

formed from γ irradiation of K_2SO_4 crystals and found the principal values of the g tensors of the radical to be in good agreement with those reported by Chantry, *et al.*¹⁷ These observations strongly support the assignment given above for the optical absorption spectrum and the esr spectrum of the SO_3^- radical produced in the photolysis of sulfite ions.

On uv irradiation of $10^{-2} \text{ M NaHSO}_3$ ices in the absence of oxygen, the sample turned purple-violet and gave rise to an esr singlet shown in Figure 2b. On annealing to -75° , both the coloration and the esr signal disappeared. The color would appear to indicate that the esr singlet corresponds to the transient species with $\lambda_{\text{max}} 720 \text{ m}\mu$. However, no transients are formed on photolysis of HSO_3^- ions at room temperature, and a different esr signal was observed on uv irradiation of SO_3^{2-} ices (Figure 2a). No clear explanation is presently available to account for this observation.

Carbonate ions have been used¹⁹ to derive relative rate constants for the reaction of OH radicals with a number of solutes in the pulse radiolysis of aqueous systems. By following the decrease in optical density

(15) G. E. Adams, J. W. Boag, and B. D. Michael, *Trans. Faraday Soc.*, **61**, 1674 (1965).

(16) Electron spin resonance spectra were measured by A. O. King of this laboratory.

(17) G. W. Chantry, A. Horsfield, J. R. Morton, J. R. Rowlands, and D. H. Whiffen, *Mol. Phys.*, **5**, 233 (1962).

(18) V. V. Gromov and J. R. Morton, *Can. J. Chem.*, **44**, 527 (1966).

(19) G. E. Adams and J. W. Boag, *Proc. Chem. Soc.*, 112 (1964).

at 6000 Å for the CO_3^- radical in the presence of, say, sulfite ions, the rate constant $k(\text{OH} + \text{SO}_3^{2-})$ was determined. We have added carbonate ions to nitrogen and nitrous oxide saturated $10^{-2} M \text{SO}_3^{2-}$ solutions and followed the transient at 500 $m\mu$, at which wavelength the $\epsilon_{\text{HSO}_3^-} \ll \epsilon_{\text{CO}_3^-}$. By analysis of the decay curves and the "initial" optical densities, it was concluded that CO_3^- radicals react with SO_3^{2-} ions and that HSO_3^{2-} reacted with either CO_3^- , and/or CO_3^{2-} ions. This is an example of the error that can be made in studying reactions of OH radicals by the above method, without an analysis of the decay rates and a complete knowledge of the absorption spectra of all the radicals produced in the system under study.

Photolysis of Thiocyanate Ions. The flash photolysis of potassium thiocyanate in aqueous solution showed the presence of a transient species, having reddish color and absorbing in the wavelength region 350–650 $m\mu$. The intermediate formed, with a maximum at 485 $m\mu$, was the same in the presence or absence of oxygen. At concentrations above $3-5 \times 10^{-4} M$ thiocyanate ions, a turbidity was noticeable on flashing the solution, and in 10^{-3} to $10^{-2} M \text{CNS}^-$ ions, the formation of sulfur masked the presence of transient absorbing species and gave rise to a strong smell of H_2S . All the work to be described below was carried out in $10^{-4} M \text{KCNS}$ solutions, prepared freshly just previous to photolysis.

Figure 3 shows the absorption spectrum of the radical produced on flash photolysis of $10^{-4} M \text{CNS}^-$ in nitrogen-saturated solution at pH 6.0. A weak absorption was found down to 260 $m\mu$ which appeared to have a decay rate similar to the species absorbing at 485 $m\mu$, but due to the small optical density of the transient it was not possible to measure the decay rate with accuracy.

The transient optical spectrum observed is considered

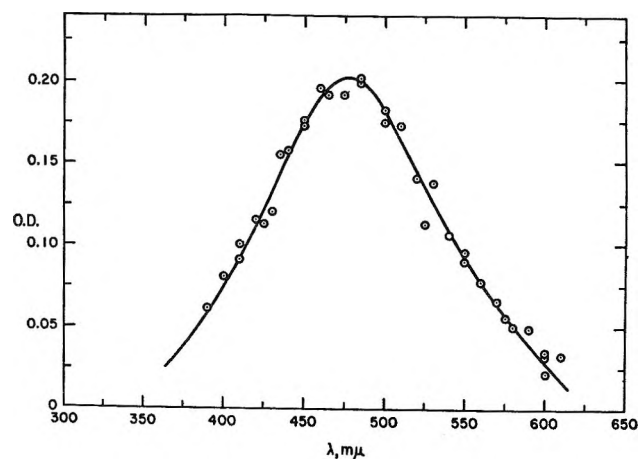
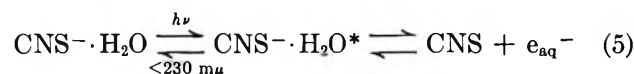


Figure 3. Transient absorption spectrum produced on flash photolysis of N_2 -saturated, $10^{-4} M \text{KCNS}$ at pH 6.0. Optical density measured in 20-cm optical cells, 80 μsec after start of flash.

to be due to the thiocyanate radical anion, produced during the photolysis of CNS^- ions in its CTTS absorption band



While thiocyanate ions absorb light up to about 270 $m\mu$, no transient with λ_{max} 485 $m\mu$ was formed at any $[\text{CNS}^-]$ used when a 20% acetic acid filter solution (cutoff 237 $m\mu$) was placed between the flash tube and the optical cell. From a change in filter solutions used, it was established that the CTTS band of thiocyanate ions lies below about 2300 Å. Further support for reaction 5 was obtained on flashing a $10^{-4} M \text{KCNS}$ solution saturated with N_2O gas. Under these conditions, the initial OD at 485 $m\mu$ increased from 0.042 to 0.080, *i.e.*, was approximately doubled. This is explained by the sequence of reactions 3 and 6.

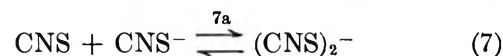


On flash photolysis of N_2O -saturated $10^{-4} M \text{KCNS}$ solution in the presence of 0.1 M ethanol, the amount of transient was the same as that produced in N_2 -saturated solutions of CNS^- and ethanol. This is explained as due to the competition between reaction 6 and



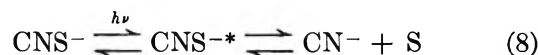
with all the OH radicals reacting with ethanol under these experimental conditions.

A similar transient has been observed in the pulse radiolysis of aqueous thiocyanate solutions²⁰ and has recently been definitely assigned to the $(\text{CNS})_2^-$ radical anion by Baxendale and Stott²¹ with $k_6 = 2 \times$



$10^{10} M^{-1} \text{sec}^{-1}$, $k_{7a} = 6.6 \times 10^9 M^{-1} \text{sec}^{-1}$, and $\epsilon_{500} = 7 \times 10^3 M^{-1} \text{cm}^{-1}$.²¹ Under our experimental conditions, it can be assumed that all the CNS radicals are present as $(\text{CNS})_2^-$.

In addition to the primary process 5, one must propose another reaction to explain the formation on photolysis (in presence or absence of acetic acid filter) of sulfur and H_2S in the system. Furthermore, this reaction must be independent of N_2O and take place in the presence of acetic acid filter; that is to say, this other photolytic process should not be limited to the CTTS wavelength band of CNS^- ions. Reaction 8 is proposed to take place. The dependence of the forma-



(20) G. E. Adams, J. W. Boag, J. Curren, and B. D. Michael, "Pulse Radiolysis," M. Ebert, J. P. Keene, A. J. Swallow, and J. H. Baxendale, Ed., Academic Press London, 1965.

(21) J. H. Baxendale and D. A. Stott, *Proc. Chem. Soc.*, 699 (1967).

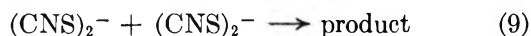
Table II: Rate Constants for the Decay of Transient Species Produced on Flash Photolysis of KCNS in Aqueous Solution

System	pH	λ , $m\mu$	Decay order	Decay rate
$10^{-4} M$, N_2 satd	6.0	480	First	$k = 3.0 \pm (1.5 \times 10^3) \text{ sec}^{-1}$
$10^{-4} M$, N_2 satd	6.0	550	First	$k = 2.5 \pm (1.0 \times 10^3) \text{ sec}^{-1}$
$2.5 \times 10^{-5} M$, N_2 satd	6.0	485	First	$k = 3.0 \pm (1.0 \times 10^3) \text{ sec}^{-1}$
$2 \times 10^{-4} M$, N_2 satd	6.0	485	First	$k = 2.8 \pm (1.2 \times 10^3) \text{ sec}^{-1}$
$10^{-4} M$, N_2 satd	0.75	485	First	$k = 2.0 \pm (1.0 \times 10^3) \text{ sec}^{-1}$
$10^{-4} M$, N_2 satd	11.9	485	Second	$2k/\epsilon = 8.9 \pm (3.0 \times 10^6)$
$10^{-4} M$, air satd	6.0	485	Second	$2k/\epsilon = 2.4 \pm (0.6 \times 10^6)$
$2.5 \times 10^{-5} M$, air satd	6.0	485	Second	$2k/\epsilon = 1.6 \pm (0.6 \times 10^6)$
$10^{-4} M$, air satd	11.9	485	Second	$2k/\epsilon = 7 \pm (2 \times 10^6)$
$(2.5-20) \times 10^{-4} M$, N_2O satd	6.0	485	First	$k = 2.0 \pm (1.0 \times 10^3) \text{ sec}^{-1}$
$10^{-4} M$, N_2O satd	11.9	485	First	$k = 2.8 \pm (0.6 \times 10^3) \text{ sec}^{-1}$
$10^{-4} M$, N_2O satd	1.0	485	First	$k = 2.6 \pm (1.0 \times 10^3) \text{ sec}^{-1}$
$10^{-4} M$, 0.1 methanol, N_2 satd	6.0	485	First	$k = 6.0 \pm (2.0 \times 10^3) \text{ sec}^{-1}$
$10^{-4} M$, 10^{-3} to $10^{-4} M$ allyl alcohol, N_2 satd	6.0	485	First	$k = 2.9 \pm (0.7 \times 10^3) \text{ sec}^{-1}$
$10^{-4} M$, $10^{-3} M$ allyl alcohol, air satd	6.0	485	First	$k = 3.7 \times 10^3 \text{ sec}^{-1}$

tion of sulfur and H_2S on CNS^- ion concentration could be explained in part due to reactions of the type $\text{S} + \text{CNS}^- \rightarrow \text{CN}^- + \text{S}_2$. Addition of allyl alcohol, a possible scavenger for sulfur, was found to reduce the initial amount of transient produced on flashing, not to affect the decay rate of the transient at $485 m\mu$, and to essentially eliminate the turbidity caused by the formation of sulfur in reaction 7. Similar results have been found independently by Luria and Treinin.²²

The decay rate of the transient produced on photolysis of CNS^- ions in nitrogen-saturated neutral and acidic solution was found to be a fairly good first-order decay at wavelength 400–600 $m\mu$ and was found to be independent of CNS^- ion concentration from 2.5×10^{-5} to $2 \times 10^{-4} M$; see Table II. The decay could still, however, be a pseudo-first-order decay. The decay is also first order in neutral, acid, or alkaline solutions saturated with N_2O gas. In presence of oxygen, however, the decay rate is a fairly good second order with $2k/\epsilon = 2.0 \pm (0.6 \times 10^6)$. In air-saturated $10^{-4} M \text{ CNS}^-$ at pH 1.0 and 1.8, decay of the transient at $485 m\mu$ cannot be established, since it is an equally good first-order decay ($k = 4.2 \times 10^3 \text{ sec}^{-1}$).

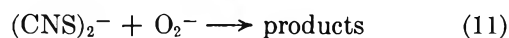
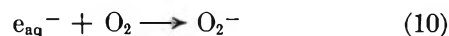
Adams, *et al.*,²⁰ have found in pulse-radiolysis work that in neutral solutions in the presence or absence of oxygen, $(\text{CNS})_2^-$ decays by a second-order process with $2k_9 = 2.9 \times 10^9 M^{-1} \text{ sec}^{-1}$, taking $\epsilon_{500} = 7.1 \times 10^3 M^{-1} \text{ cm}^{-1}$.



In acid solutions in the presence of oxygen, they found²⁰ a more complex decay kinetics for the transient absorbing at $500 m\mu$.

No explanation is presently available to explain

the difference in decay of apparently the same species $(\text{CNS})_2^-$ produced in flash-photolysis and pulse-radiolysis experiments. The second-order decay obtained in flash photolysis in presence of oxygen could be due to the reactions



From the results obtained, it would appear that there are at least two simultaneous primary processes occurring during the photolysis of thiocyanate ions with light of wavelength above about 2000 \AA : a spectroscopic excited state at $\lambda < 230 m\mu$ originating from a CTTS transition and leading to the ejection of an electron (reaction 5), and probably a $\pi^* \leftarrow \eta$ transition involving the no-bonding electron on the sulfur atom (reaction 8).

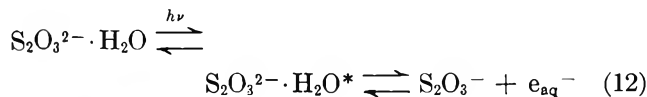
The esr spectrum of $10^{-2} M$ KCNS ices irradiated with uv light was determined and is shown in Figure 2c. The sample was found to be red on photolysis, in keeping with the expected absorption spectrum of thiocyanate radicals. On annealing to -95° the red disappeared as well as the esr absorption signal.

Photolysis of Thiosulfate Ions. The optical absorption spectra of two transient species have been observed in the flash photolysis of sodium thiosulfate in aqueous solution: a "short-lived" intermediate A absorbing in the region 340–450 $m\mu$ with $\lambda_{\text{max}} \sim 380 m\mu$ and a "long-lived" intermediate B absorbing from about 220 $m\mu$ to 400 $m\mu$ with $\lambda_{\text{max}} \sim 280 m\mu$ (see Figure 4). Transients A and B were shown to be formed in the pres-

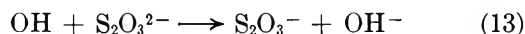
(22) M. Luria and A. Treinin, *J. Phys. Chem.*, in press.

ence or absence of oxygen and, except for variation in the amount of transients produced, at various concentrations of thiosulfate up to $10^{-2} M$ $\text{Na}_2\text{S}_2\text{O}_3$. The same transient absorption spectra were also observed in acid, neutral, and alkaline aqueous solutions. Unless stated otherwise, all the work reported below was carried out in $10^{-3} M$ $\text{Na}_2\text{S}_2\text{O}_3$ solutions.

Transient A was shown to be produced from the photoionization of thiosulfate ions and is assigned to



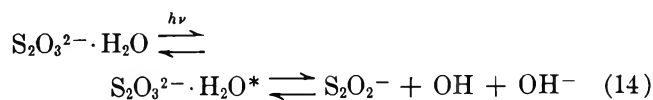
the S_2O_3^- radical anion produced by the photolysis of $\text{S}_2\text{O}_3^{2-}$ in the CTTS absorption band. On flashing a neutral $10^{-3} M$ $\text{Na}_2\text{S}_2\text{O}_3$ solution saturated with N_2O gas ($\sim 2 \times 10^{-2} M$ N_2O), the amount of transient A produced at λ 380 $m\mu$ increased by only 50% (see below) compared to a solution saturated with N_2 gas or air. The increase is due to reaction 3 followed by reaction 13 taking place. On flashing a neutral 10^{-3}



M $\text{Na}_2\text{S}_2\text{O}_3$ solutions containing up to $10^{-1} M$ ethanol in the presence or absence of $2 \times 10^{-2} M$ N_2O , the amount of transient produced was found to be decreased by about 50% compared to a N_2 - or air-saturated $\text{S}_2\text{O}_3^{2-}$ solution free of ethanol.

Transient B, with $\lambda_{\text{max}} \sim 280 m\mu$, was found to be formed by a second independent primary photolytic process. Thus it was found that whereas the optical density at 380 $m\mu$ of S_2O_3^- radical increased by $\sim 50\%$ in the presence of $2 \times 10^{-2} M$ N_2O , the optical density of transient B at 280 $m\mu$ remained the same in N_2O -, N_2 -, or air-saturated solutions. Furthermore, the use of filters to cut off the light output emitted from the flash lamps supports an independent mechanism leading to the formation of transient B. Use of 20% acetic acid filter (cutoff at $\sim 237 m\mu$) was found to reduce $\text{OD}_{380 m\mu}$ by about 0.5, whereas $\text{OD}_{280 m\mu}$ was reduced by 80%. Similarly, using a filter solution with ϵ cutoff at $\sim 215 m\mu$ almost eliminated transient B but reduced transient A to about 20%. It would hence appear that the peak of the CTTS absorption band of $\text{S}_2\text{O}_3^{2-}$ ions lies mainly above 210 $m\mu$, while the absorption band giving rise to transient B is below about 215 $m\mu$. These results seem to be in agreement with the conclusions reached by Sperling and Treinin¹⁰ on their study of the electronic absorption spectrum of $\text{S}_2\text{O}_3^{2-}$ ions. They have assigned the band giving rise to transient B in this work to the allowed $\pi^* \leftarrow \eta$ transition involving the no-bonding electrons on the oxygen atoms.

It is suggested, on the basis of the results mentioned above, that transient B is the S_2O_2^- radical anion and that it is produced as a result of a break of the S-O bond in $\text{S}_2\text{O}_3^{2-}$



Reaction 14 is supported by the results mentioned above in presence of ethanol and N_2O . Thus addition of N_2O should increase the formation of S_2O_3^- by only 50% compared to N_2 -saturated solutions, since S_2O_3^- is produced in the primary reaction 12, then from reaction 14 followed by 13 and finally from reaction 3 followed by 13. Similarly, addition of ethanol removes the OH radicals produced in reaction 14 due to reaction 6a taking place. This, therefore, results in a 50% decrease in the amount of S_2O_3^- formed. It would appear that under the conditions of our experiments, the quantum yields of reactions 12 and 14 are equal within 10–20%. The radical S_2O_2^- is not produced as a result of the decay of S_2O_3^- radicals, since, as indicated above, its formation appears to be unrelated to the amount of S_2O_3^- radicals produced.

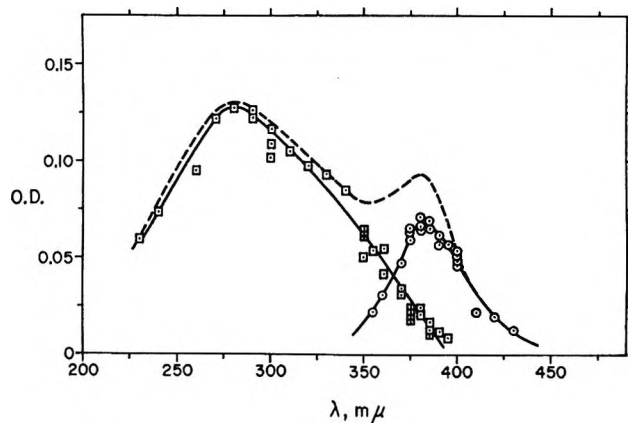
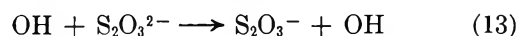


Figure 4. Transient absorption spectra produced on flash photolysis of aerated $10^{-3} M$ $\text{Na}_2\text{S}_2\text{O}_3$: ---, optical density of both transients measured 100 μsec after start of flash; ○, short-lived transient S_2O_3^- measured at 100 μsec after start of flash; ◻, long-lived transient S_2O_2^- measured at 2 msec after start of flash.

Pulse-radiolysis study of aqueous solutions of thiosulfate ions was found¹⁵ to form a transient absorption with $\lambda_{\text{max}} \sim 375 m\mu$ very similar to the short-lived transient produced in the flash photolysis of $\text{S}_2\text{O}_3^{2-}$ ions and assigned to S_2O_3^- radicals. The transient observed in pulse radiolysis was shown¹⁵ to result from the reaction of OH radicals with $\text{S}_2\text{O}_3^{2-}$



and an $\epsilon_{375} = 1.72 \times 10^3 M^{-1} \text{cm}^{-1}$ was reported.

S_2O_3^- radical anions formed under flash-photolysis conditions were found to decay in neutral and alkaline solutions in the absence of oxygen by a second-order process (see Table III), with $2k/\epsilon \simeq 4 \times 10^6$ at 380 $m\mu$. Taking the value of $\epsilon_{380} = 1.72 \times 10^3 M^{-1} \text{cm}^{-1}$ reported by Adams, *et al.*,¹⁵ one obtains a value

Table III: Rate Constants for the Decay of Transient Species Produced on Flash Photolysis of $10^{-3} M \text{Na}_2\text{S}_2\text{O}_3$ in Aqueous Solution

Transient	System	pH	λ , $m\mu$	Decay order	Decay rate
S_2O_3^-	N_2 satd	Neutral	380	Second	$2k/\epsilon = 4.1 \pm (1.0 \times 10^6)$ or $2k = 7.1 \pm (1.8 \times 10^9) M^{-1} \text{sec}^{-1}$
S_2O_3^-	N_2 satd ^a	Neutral	380	Second	$2k/\epsilon = 3.7 \pm (1.0 \times 10^6)$ or $2k = 6.4 \pm (1.6 \times 10^9) M^{-1} \text{sec}^{-1}$
S_2O_3^-	Air satd	Neutral	380	First	$k = 3.0 \pm (1.5 \times 10^3) \text{sec}^{-1}$
S_2O_3^-	Air satd	Neutral	400	First	$k = 3.3 \pm (1.0 \times 10^3) \text{sec}^{-1}$
S_2O_3^-	N_2 satd	10.9	380	Second	$2k/\epsilon = 4.6 \pm (1.0 \times 10^6)$ or $2k = 7.9 \pm (2.6 \times 10^9) M^{-1} \text{sec}^{-1}$
S_2O_3^-	Air satd	10.9	380	First	$k = 2.4 \pm (1.0 \times 10^3) \text{sec}^{-1}$
S_2O_3^-	10^{-3} to $2 \times 10^{-2} M$ methanol, N_2 satd	Neutral	380	Second	$2k/\epsilon = 3.2 \pm (1.0 \times 10^6)$ or $2k = 5.5 \pm (2.0 \times 10^9) M^{-1} \text{sec}^{-1}$
S_2O_3^-	10^{-3} to $2 \times 10^{-2} M$ ethanol, air satd	Neutral	380	First	$k = 2.4 \pm (1.0 \times 10^3) \text{sec}^{-1}$
S_2O_3^-	$10^{-3} M \text{Na}_2\text{CO}_3$	Neutral	380	First	$k = 3.0 \pm (0.5 \times 10^3) \text{sec}^{-1}$
S_2O_3^-	$10^{-3} M$ allyl alcohol, N_2 satd	Neutral	380	First	$k = 2.6 \pm (1.0 \times 10^3) \text{sec}^{-1}$
S_2O_2^-	N_2 satd	Neutral	270	Second	$2k/\epsilon = 4.4 \times (1.5 \times 10^4)$
S_2O_2^-	N_2 satd ^a	Neutral	270	Second	$2k/\epsilon = 4.0 \pm (1.5 \times 10^4)$
S_2O_2^-	Air satd	Neutral	270	Second	$2k/\epsilon = 5.7 \pm (2.0 \times 10^4)$
S_2O_2^-	N_2 satd	10.9	270	Second	$2k/\epsilon = 1.5 \pm (1.0 \times 10^6)$
S_2O_2^-	Air satd	10.9	270	Second	$2k/\epsilon = 2.0 \pm (1.5 \times 10^6)$
S_2O_2^-	10^{-3} to $10^{-1} M$ methanol, air satd	Neutral	270	Second	$2k/\epsilon = 6.0 \pm (2.0 \times 10^4)$
S_2O_2^-	10^{-3} to $10^{-1} M$ ethanol, N_2 satd	Neutral	270	Second	$2k/\epsilon = 4.0 \pm (2.0 \times 10^4)$
S_2C_2^-	$10^{-3} M$ allyl alcohol, N_2 satd	Neutral	270	Second	$2k/\epsilon = 2.0 \pm (1.0 \times 10^4)$

^a Acetic acid (20%) filter (cutoff 237 $m\mu$).

of $2k = 7.1 \pm (2.5 \times 10^9) M^{-1} \text{sec}^{-1}$. No decay order or decay rate has been reported in the pulse-radiolysis work.¹⁵ The bimolecular decay of S_2O_3^- radicals may form tetrathionate, $\text{S}_4\text{O}_6^{2-}$, a well known and relatively stable salt. In the presence of oxygen, S_2O_3^- appears to decay by a pseudo-first-order process dependent on oxygen concentration. The decay reactions taking place in presence of O_2 have not been studied in detail. Addition of ethanol, carbonate ions, or allyl alcohol does not seem to affect the decay rate of S_2O_3^- radicals; see Table III.

The S_2O_2^- transient, with $\lambda_{\text{max}} \sim 280 m\mu$, was found to decay by a second-order process, Table III, apparently independent of the presence or absence of O_2 , ethanol, and allyl alcohol.

The observation of sulfur and H_2S on flashing and the determination of these products plus sulfite ions in the photochemical decomposition of thiosulfate ions¹⁰ could, in part, result from the decay of the S_2O_2^- and S_2O_3^- radical anions. Other photolytic processes (e.g., $\text{S}_2\text{O}_3^{2-} \xrightarrow{h\nu} \text{SO}_3^- + \text{S}^-$) cannot be excluded at present. Although $k(e^- + \text{S}_2\text{O}_3^{2-}) =$

$6 \times 10^8 M^{-1} \text{sec}^{-1}$, no transient species produced from this reaction has been observed. Hydrated electrons could, however, react with thiosulfate ions to form HS (eventually giving H_2S) and SO_3^{2-} ions.

The esr spectrum of $10^{-2} M \text{Na}_2\text{S}_2\text{O}_3$ ices exposed to uv light was measured at 77°K and is shown in Figure 2d. The sample was yellow on photolysis, in agreement with the expected absorption spectrum of S_2O_3^- radicals. On thermal annealing to -60° , the faint yellow color, as well as the esr absorption signal, disappeared. Morton²³ has irradiated with γ rays single crystals of $\text{Na}_2\text{S}_2\text{O}_3 \cdot 5\text{H}_2\text{O}$ and examined them with an esr spectrometer. He found the presence of two singlets due to two radicals: one brown and assigned to S_2O_2^- and the other tentatively assigned to S_2O_3^- . On the basis of the flash-photolysis results obtained above, it is suggested that the colored less stable radical observed by Morton could be due to S_2O_3^- and the more stable colorless radical to S_2O_2^- . This is exactly a reversal of the assignments given by him.

(23) J. R. Morton, *Can. J. Chem.*, **43**, 1948 (1965).

NOTES

Structural Features of Some Water

n-Alkylamine Complexes

by J. J. Fripiat, A. Léonard, and E. Mendelovici

Laboratoire de Physico-Chimie Minérale, Institut des Sciences de la Terre, Heverlee, Louvain, Belgium

Accepted and Transmitted by The Faraday Society (June 5, 1967)

The structures of primary *n*-alkylamines derivatives and complexes have already been largely studied. Some 30 years ago, Hendricks^{1,2} and Wyckoff³ described the crystalline solids obtained by precipitating RNH₂HX derivatives in alcoholic solutions, X is any halogen, but most often Cl, and R is an aliphatic chain with 12 carbon atoms or less. All these crystals belong to the tetragonal system and are characterized by the same *a* parameter of 5.18 Å. The unit cell contains 2 alkyl chains oriented along the *c* direction and the basal spacing increases by 2.1 Å/CH₂ unit. The explanation of such an increase has raised a long discussion between Hendricks^{1,2,4} and Müller^{5,6} about the C-C-O angle in the aliphatic chain.

The intercalation of amines into the expanding lattice of montmorillonites has been studied by numerous workers, but it will not be referred to in this paper. Recently, Walker and Hawthorne⁷ attempted to obtain structural information on the complexes formed from primary *n*-alkylamines and nickel cyanide. They consist of alternating monolayers of amine and cyanide. The alkyl chains stand away from the plane of the cyanide layers and may show "solid-like" or "liquid-like" characteristics. The nitrogen of an amine molecule is keyed into the cyanide surface. Methyl keying into the opposite surface is exhibited by the solid complexes. Assuming a thickness of 3.2 Å for the Ni(CN)₂ layer and an angle of 50° between the aliphatic chain and the nickel cyanide plane, the increase of the basal reflections along the *c* axis may be accounted for.

During a study of amine intercalation mechanisms between silicate layers, it was found, accidentally, in our laboratory that the absorption of relatively small amounts of water by liquid alkylamines led to a remarkable organized structure characterized by sharp X-ray reflections. This is very easily demonstrated for liquid primary *n*-alkylamines poured into a specimen holder provided for recording the X-ray diffraction spectra of liquids. After a few minutes of contact with atmospheric moisture, strong X-ray reflections

appear, as shown later. We felt it interesting to report briefly these observations for the use of those involved in the study of the crystalline organization of liquids or in the study of organomineral complexes.

Experimental Section

Pure *n*-butyl-, *n*-hexyl-, and *n*-octylamines supplied by Fluka (Switzerland) were used as received. A few milliliters of these amines was introduced into a liquid-specimen holder closed by a Mylar window and fitting the usual Philips goniometer. For water contents of about 10%, at least within the surface layers, sharp X-ray diffraction patterns were obtained as shown in Figure 1, for *n*-hexyl-² and *n*-octylamine.¹

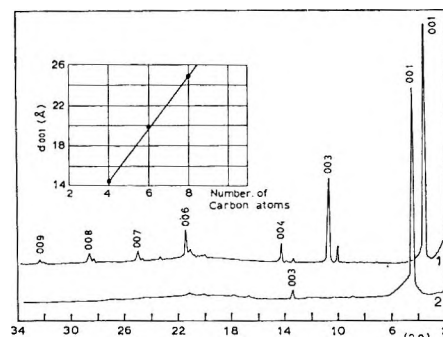


Figure 1. X-Ray diffraction pattern observed for the *n*-octyl-¹ and *n*-hexylamine² complexed with water: Cu K α radiation; 40 kV, 20 mA; rate meter, 64. The insert shows the variation of the *d*(001) spacing with respect to the number of carbon atoms in the chain.

In the absence of water or with pure frozen amines, no reflection was observed. The 001 reflections allow one to compute the *c* spacings: their variation against the number of carbon atoms is shown in the insert of Figure 1. The increase in the 001 basal spacings (Å) obeys the linear relationship

$$d_{(001)} = 4.20 + 2.59n_c$$

where n_c is the number of carbon atoms in the alkyl chain.

Discussion

In order to explain this relationship, different models allowing, or not allowing, for the presence of water

- (1) S. B. Hendricks, *Z. Kristallogr.*, **67**, 106 (1928).
- (2) S. B. Hendricks, *ibid.*, **68**, 189 (1928).
- (3) R. W. G. Wyckoff, *ibid.*, **74**, 25 (1930).
- (4) S. B. Hendricks, *ibid.*, **74**, 29 (1930).
- (5) A. Müller, *Proc. Roy. Soc. (London)*, **A120**, 437 (1928).
- (6) A. Müller, *Trans. Faraday Soc.*, **25**, 417 (1929).
- (7) G. F. Walker and D. G. Hawthorne, *ibid.*, **63**, 166 (1967).

molecules have been examined. Actually, the best fitting model consists of two chains standing up and connected to one another by a water molecule. It must be assumed that the terminal CH_3 groups are keying into the opposite methyl surfaces of adjacent layers. The observed basal spacings are then almost exactly equal to those computed by assuming a C-C bond length of 1.542 Å, a tetrahedral C-C-C angle of $109^\circ 28'$, a C-N bond length of 1.47 Å, a C-C-N angle of 110° , all these parameters being taken from Pauling⁸ and Sutton.⁹ The O-H...N hydrogen bond length is 2.80 Å, in agreement with Pimentel and McClellan,¹⁰ while the usual H-O-H angle of $104^\circ 45'$ was maintained. The absence of heavy atoms in the chain as well as the weakness of the $hk0$ reflections precludes any defined conclusions about the complete structure of these amine-water liquid complexes.

(8) L. Pauling, "The Nature of the Chemical Bond," Cornell University Press, Ithaca, N. Y., 1948, p 167.

(9) L. E. Sutton, "Tables of Interatomic Distances and Configuration in Molecules and Ions, Special Publication No. 11, The Chemical Society, London, 1958, p M174.

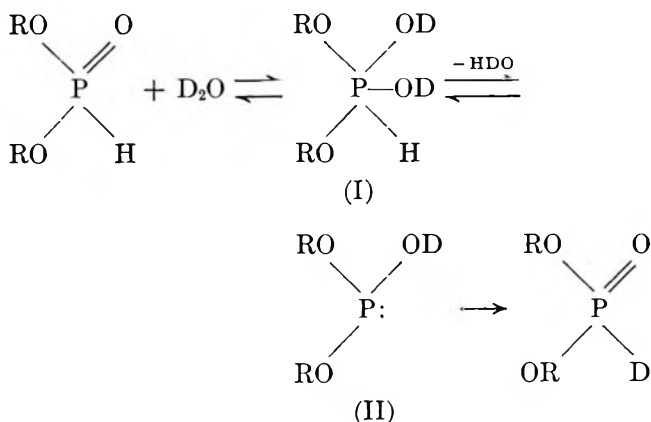
(10) G. C. Pimentel and A. L. McClellan, "Hydrogen Bond," Freeman and Co., London, 1960, p 289.

Isotopic Oxygen Exchange and Hydrolysis in Dialkylphosphonates

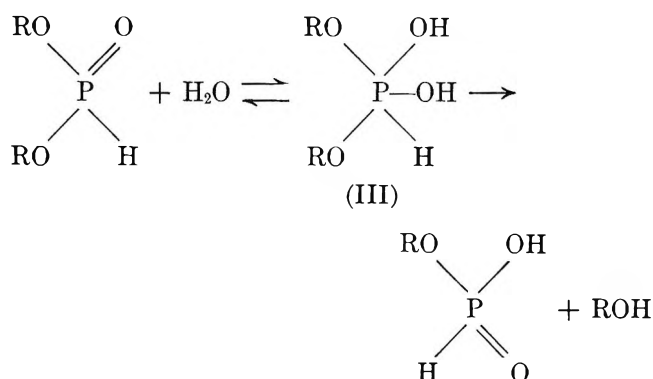
by David Samuel and Brian L. Silver

Isotope Department, Weizmann Institute of Science, Rehovoth, Israel
 Accepted and Transmitted by The Faraday Society (June 21, 1967)

The phosphorus-bonded hydrogen in dialkylphosphonates has been shown¹⁻⁴ to undergo exchange with the deuterium in solvent D_2O . This isotopic exchange is both acid and base catalyzed. A possible mechanism for the acid-catalyzed reaction is the addition of water to form a pentacovalent intermediate (I) containing two equivalent hydroxyl groups which could then lose



water to form the phosphite form (II) from which the deuterated phosphonate is produced by accepting a proton. If the two deuterio groups of (I) are equivalent (although this is not necessarily so), then, since there will be an equal change of either group being lost, the above mechanism could also serve as a path for the isotopic exchange of oxygen between dialkylphosphonates and solvent water. It is therefore of interest to ascertain whether isotopic oxygen exchange occurs at a comparable rate with isotopic hydrogen exchange. The rate of oxygen exchange is also of importance in considering the acid- and base-catalyzed hydrolysis of dialkylphosphonates,⁵ since in principle hydrolysis may also involve the addition of water to form a pentacovalent intermediate which then breaks down to give the hydrolysis products



If the first step is reversible and the two hydroxyl groups of (III) are equivalent, a pathway is available for the isotopic exchange of oxygen between dialkyl phosphonates and water which is analogous to the exchange found by Bender⁶ in the hydrolysis of carboxylic acid esters. We have, therefore, determined whether oxygen exchange between substrate and solvent occurs (a) during the acid- and base-catalyzed hydrolysis of dialkylphosphonates and (b) during the isotopic exchange of hydrogen in dialkylphosphonates. We have also determined the position of bond fission during the hydrolysis of these compounds using ^{18}O as tracer.

Experimental Section

Materials. Water enriched in ^{18}O was obtained from the Separation Plant of this Institute. Dialkylphosphonates were prepared from phosphorus trichloride and the appropriate alcohol⁷ and were fractionally distilled twice before use. Monoalkylphosphonates were made by adding 0.1 mole of sodium hydroxide in water to an aqueous solution of 0.1 mole of dialkyl-

- (1) P. R. Hammond, *J. Chem. Soc.*, 1365 (1962).
- (2) Z. Luz and B. L. Silver, *J. Amer. Chem. Soc.*, **83**, 4518 (1961).
- (3) B. L. Silver and Z. Luz, *ibid.*, **84**, 1091 (1962).
- (4) Z. Luz and B. L. Silver, *ibid.*, **84**, 1095 (1962).
- (5) P. Nylen, *Svensk Kem. Tidsskr.*, **49**, 79 (1937).
- (6) M. Bender, *J. Amer. Chem. Soc.*, **73**, 1626 (1951).
- (7) H. McCombie, B. C. Saunders, and G. J. Stacie, *J. Chem. Soc.*, 380 (1945).

phosphonate and removing the solvent by lyophilization.

Isotopic Oxygen Analysis. All analyses were by the method of Anbar and Guttman.⁸

Oxygen Exchange. Di-*n*-propylphosphonate was chosen for study since it has the advantage of being readily salted out of aqueous solution, thus facilitating its separation from the reaction mixture. Di-*n*-propylphosphonate (1 ml) was dissolved in aqueous solutions of HCl or NaOH (6 ml) in ¹⁸O-enriched water. The hydrolysis of dialkylphosphonates in strong base is very rapid. Consequently, only enough NaOH solution was added to hydrolyze 50% of the phosphonate. The remaining unhydrolyzed substrate was recovered from the reaction solution immediately. In acid medium, samples of the reaction solution were removed at measured times and the phosphonate was salted out by the addition of sodium chloride. The upper layer (phosphonate) was removed with a pipet, dissolved in normal water (5 ml), and immediately salted out again. This procedure was repeated and the phosphonate was then dissolved in dry dioxane (20 ml) and dried over Linde molecular sieve 4A for 16–18 hr. The residual phosphonate was left on the high-vacuum system for a further 4–5 hr and analyzed for its oxygen-18. Samples of phosphonate were recovered from the reaction mixture until a time corresponding to at least the half-life for the hydrogen exchange. To check that no exchange occurred during the isolation procedure, a sample of diethylphosphonate-¹⁸O (1.0 ml) in wet ether (25 ml) was dried overnight with Linde molecular sieve (5 g) and then isolated and analyzed for ¹⁸O as described above. There was no significant difference in ¹⁸O content of the phosphonate before and after the isolation procedure, the excess atomic percentage of ¹⁸O being, respectively, 74.8 and 73.9%.

Bond Fission. Alkyl phosphonates (5–10 g) were dissolved in aqueous solutions of HCl or NaOH (120 ml) in ¹⁸O-enriched water. After refluxing for 1 hr, the alcohol was isolated by distilling the reaction mixtures through a vacuum-jacketed Vigreux column (30 × 0.5 cm). In the case of dimethylphosphonate, the first fraction was methanol which was refractionated in a microcolumn (10 × 0.5 cm), the middle fraction (bp 64.5°) being taken for isotopic analysis. In the case of diethylphosphonate, the azeotrope of ethanol and water was collected (bp 78–81°), dried with two successive batches of Linde molecular sieve, and distilled in a microcolumn.

Results

Exchange. The results of the oxygen exchange experiments with di-*n*-propylphosphonate are given in Table

Table I: Oxygen Exchange in Di-*n*-propylphosphonate (Temp 22 ± 1°)

Solvent	Time, hr	Excess atom % ¹⁸ O in solvent	Excess atom % ¹⁸ O in recovered substrate
HCl, 1 N	0.02	8.81	0.004
	1	8.81	0.002
	2	8.81	0.003
	3	8.81	0.007
HCl, 0.5 N	1	3.45	0.011
HCl, 5.0 N	0.15	3.28	0.010
NaOH, 1.0 N	...	2.7	0.007

Table II: Position of Bond Fission in the Hydrolysis of Alkylphosphonates

Phosphonate	Solvent	Excess atom % ¹⁸ O in solvent H ₂ O	Excess atom % ¹⁸ O in recovered alcohol	% P-O bond fission
Diethyl	HCl, 1 N	1.90	0.030	98
	NaOH, 2.5 N	1.93	0.020	99
Dimethyl	HCl, 1 N	5.08	0.050	99
	NaOH, 2.5 N	3.55	0.007	100

I. From Table I it may be seen that no oxygen exchange occurs between phosphonates and solvent water for the stated reaction times (which correspond to at least one half-life of the acid-catalyzed hydrolysis⁹ and 5–10 half-lives of the acid-catalyzed hydrogen exchange^{1–4}).

Bond Fission. The results are given in Table II. The results show that in the hydrolysis of dimethyl- and diethylphosphonates in both acid and basic solution, the bond between phosphorus and oxygen is broken in every case (P-O-R). The isotopic results confirm the observation by Gerrard⁹ that in the hydrolysis of optical active di-*sec*-octylphosphonate the alcohol retains its optical activity. Since hydrolysis is complete under the experimental conditions, the results imply P-O bond fission in the hydrolysis of the monoalkyl phosphonates.

The lack of observable oxygen exchange is very strong evidence against a mechanism involving addition of water in the hydrolysis and hydrogen exchange of the compounds studied.

(8) M. Anbar and S. Guttman, *J. Appl. Radiation Isotopes*, **3**, 233 (1959).

(9) W. Gerrard, W. J. Green, and R. A. Nutkins, *J. Chem. Soc.*, 4076 (1952).

The Exchange Reaction of Pentafluoroethyl Iodide with Iodine

by C. Grygorcewicz and G. S. Laurence

Department of Physical Chemistry, University of Adelaide,
Adelaide, South Australia

Accepted and Transmitted by The Faraday Society
(July 14, 1967)

The exchange reactions of iodine with alkyl iodides are largely heterogeneous in the gas phase, but the exchange with trifluoromethyl iodide is homogeneous.¹ We report here similar measurements on the iodine-pentafluoroethyl iodide system, which is also homogeneous.

The procedure for the exchange experiments was identical with that previously described.¹ C₂F₅I, from Columbia Organic Chemicals Inc., was fractionally distilled before use. Known amounts of C₂F₅I (0.5–5 cm pressure) and ¹³¹I-labeled I₂ (10⁻² to 10⁻¹ mm) were sealed in the reaction vessel and heated to the required temperature. For the photochemical experiments, the reaction vessel was illuminated with 5461 Å of light from a medium-pressure mercury lamp. The progress of the exchange was followed without opening the reaction vessel. Measurements of the ¹³¹I activity with a scintillation counter, first of the total cell contents and then of the C₂F₅I after condensing the I₂ into a side arm at -48°, enabled the fraction exchange to be calculated. Separation of the C₂F₅I and I₂ is ~99% complete under these conditions. The C₂F₅I pressure was always much greater than the I₂ pressure, so that the fraction exchange $F = \frac{^{131}\text{I activity in C}_2\text{F}_5\text{I}}{\text{total } ^{131}\text{I activity in mixture}}$. The rate of exchange under these conditions is

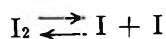
$$R_{\text{ex}} = \frac{-2[\text{I}_2] \ln(1 - F)}{t}$$

Results and Discussion

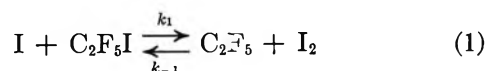
In the range from 120 to 170°, the thermal exchange rate was independent of the surface-to-volume ratio of the reaction vessel and the reaction is homogeneous. The rate of the thermal exchange was measured as a function of C₂F₅I concentration (1–4 × 10⁻⁶ mol/cm³) and I₂ concentration (3–13 × 10⁻⁹ mol/cm³) at 140°. The rate expression for the thermal exchange is

$$R_{\text{ex}} = k_e[\text{C}_2\text{F}_5\text{I}][\text{I}_2]^{1/2}$$

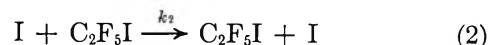
This rate expression corresponds to the reaction sequence



(equilibrium constant, K) followed by abstraction



or direct substitution



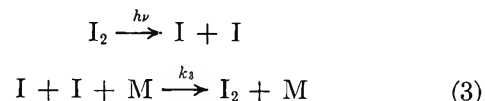
Reactions 1 and 2 lead to identical rate expressions and

$$k_e = (k_1 + k_2) K^{1/2}$$

The over-all activation energy of k_e is 31.6 ± 0.8 kcal/mol, and from the known values of K^2

$$k_1 + k_2 = 10^{10.0} \exp[-13,500 \pm 800/RT] \text{ l. mol}^{-1} \text{ sec}^{-1}$$

When the iodine atoms are generated photochemically, the reaction sequence is



followed by reactions 1 or 2 or both. Experimentally, the photochemical exchange rate is proportional both to the square root of the absorbed light intensity over an intensity range of 25 to 1 and to the C₂F₅I concentration in the range 1.5–12 × 10⁻⁶ mol/cm³. The rate of photochemical exchange given by the suggested reaction sequence is

$$R_{\text{ex}} = (k_1 + k_2)(I_{\text{abs}}/k_3)^{1/2}[\text{C}_2\text{F}_5\text{I}]^{1/2}$$

where I_{abs} is the rate of light absorption and $[\text{M}]$ is equivalent to $[\text{C}_2\text{F}_5\text{I}]$ under the experimental conditions where $[\text{C}_2\text{F}_5\text{I}] \gg [\text{I}_2]$. The observed rate law is

$$R_{\text{ex}} = k\phi(I_{\text{abs}})^{1/2}(\text{C}_2\text{F}_5\text{I})$$

suggesting that the iodine atom recombination step is, in fact, second order under our experimental conditions. A similar second-order dependence of the iodine atom recombination rate was observed for the photochemical exchange of iodine and CF₃I.

The activation energy for the photochemical exchange was measured over the range 70–140° and is 14.5 ± 0.8 kcal/mol. The activation energy for exchange $E_{\text{ex}} = E_{1,2} - \frac{1}{2}E_3$. E_3 is not known, but it is probably between 0 and -2 kcal/mol by analogy with the value in the presence of CH₃I and C₂H₅I.³ The difference between the values of E_{ex} for thermal (13.5 kcal/mol) and photochemical (14.5 kcal/mol) exchange may reflect a value of E_3 of ~-2 kcal/mol, but the level of significance is low.

The exchange of I₂ and CF₃I was interpreted as proceeding by abstraction rather than substitution from a comparison of the Arrhenius parameters for exchange

(1) G. S. Laurence, *Trans. Faraday Soc.*, **63**, 1155 (1967).

(2) W. H. Evans, T. R. Munson, and D. D. Wagman, *J. Res. Nat. Bur. Std.*, **55**, 147 (1955)

(3) R. Engleman and N. R. Davidson, *J. Amer. Chem. Soc.*, **82**, 4770 (1960).

and abstraction.¹ From the exchange between I₂ and CF₃I¹

$$k(\text{exchange}) = 10^{9.7} \exp[-15,800 \pm 700/RT] \text{ l. mol}^{-1} \text{ sec}^{-1}$$

while other kinetic studies⁴ lead to

$$k(\text{abstraction}) = 10^{10.6} \exp[-17,600/RT] \text{ l. mol}^{-1} \text{ sec}^{-1}$$

The activation energy for abstraction, 17.6 kcal/mol, is consistent with the recent determination of the heat of formation of CF₃I.⁵ The smaller values for the Arrhenius parameters for the exchange could imply that at least part of the exchange proceeds by direct substitution with a lower energy of activation (in the exchange of iodine with alkyl iodides in the liquid phase, the rates of abstraction and substitution are similar^{6,7}). However, the results were not sufficiently precise to establish this with any certainty, and the present results do not suggest that direct substitution is important in these systems.

If the exchange of I₂ with C₂F₅I takes place exclusively by abstraction, $k_1 = 10^{10.0} \exp[-13,500 \pm 800/RT] \text{ l. mol}^{-1} \text{ sec}^{-1}$ and the bond dissociation energy $D(\text{C}_2\text{F}_5\text{-I}) = E_1 - E_{-1} + D(\text{I-I})$. For the reaction of CF₃ radicals and I₂, E_{-1} is zero⁸ and is probably zero for C₂F₅ radicals also. We calculate that $D(\text{C}_2\text{F}_5\text{-I})$ is 49.6 ± 0.8 kcal/mol. This is some 4 kcal/mol less than $D(\text{CF}_3\text{-I})$ and this difference is about equal to that between $D(\text{CH}_3\text{-I})$ and $D(\text{C}_2\text{H}_5\text{-I})$.^{9,10} The frequency factor of k_1 , $1 \times 10^{10} \text{ l. mol}^{-1} \text{ sec}^{-1}$ is of the same order as that for the I₂-CF₃I system and is normal for halogen atom reactions of this type. For the similar abstraction reactions with CH₃I, C₂H₅I, and C₃H₇I, the frequency factors are 2.5×10^{11} , 4.2×10^{11} , and $1.1 \times 10^{11} \text{ l. mol}^{-1} \text{ sec}^{-1}$ respectively^{11,12} and are greater than the collision frequencies, suggesting a relatively loose transition state. It would seem that this is not a characteristic of the reactions of iodine atoms with fluorinated iodides.

Acknowledgments. This work was supported in part by a grant from the Australian Institute of Nuclear Science and Engineering.

(4) R. K. Boyd, E. W. Downs, J. S. Gow, and C. Horrex, *J. Phys. Chem.*, **67**, 719 (1963).

(5) C. A. Goy, A. Lorl, and H. O. Pritchard, *ibid.*, **71**, 1086 (1967).

(6) R. A. Herrmann and R. M. Noyes, *J. Amer. Chem. Soc.*, **78**, 5764 (1956).

(7) J. E. Bujake, M. W. T. Pratt, and R. M. Noyes, *ibid.*, **83**, 1547 (1961).

(8) J. C. Amphlett and E. Whittle, *Trans. Faraday Soc.*, **62**, 1662 (1966).

(9) J. A. Kerr, *Chem. Rev.*, **66**, 465 (1966).

(10) In ref 1, the value of $D(\text{CF}_3\text{-I})$ from the exchange results is given as 51.5 kcal/mol. From the photochemical activation energy, $D(\text{CF}_3\text{-I})$ is 52.0 ± 0.8 kcal/mol, in slightly better agreement with the value of 53.5 kcal/mol obtained from the data of ref 4 and 5.

(11) J. H. Sullivan, *J. Phys. Chem.*, **65**, 722 (1961).

(12) M. C. Flowers and S. W. Benson, *J. Chem. Phys.*, **38**, 882 (1962).

The Rate of Reaction of Active Nitrogen with Perfluorobutene-2

by N. Madhavan and W. E. Jones

Department of Chemistry, Dalhousie University, Halifax, Nova Scotia, Canada (Received July 14, 1967)

The reactions of active nitrogen with hydrocarbons and their derivatives have been studied by many workers. However, no studies have been reported of reactions with completely fluorinated hydrocarbons. We have found that when perfluorobutene-2 is admitted to a stream of active nitrogen, a bright red flame is produced. This flame is similar to that found in the hydrocarbon-active nitrogen reactions but appears slightly more intense. The flame lends itself readily to determination of the rate constant of the reaction by the diffusion-flame technique first developed by Hartel and Polanyi¹ and applied to the reaction of active nitrogen and ethylene by Greenblatt and Winkler.²

By this method, perfluorobutene-2 is allowed to escape through a small jet and diffuses into a stream of active nitrogen. At steady-state conditions, the partial pressure of active nitrogen is constant throughout the reaction space and drops to zero at the jet. Under these conditions, the rate constant may be expressed identically as obtained by Hartel and Polanyi¹ as

$$k = \frac{(\ln p_f/p_0)^2 D}{d^2/4 p_N}$$

where p_f and p_0 are the partial pressures of perfluorobutene-2 at the jet and at the edge of the flame, respectively; p_N is the partial pressure of nitrogen atoms; d is the diameter of the flame; and D is the diffusion coefficient of perfluorobutene-2 into the gas mixture.

Experimental Section

Perfluorobutene-2, ethylene, propylene, and nitric oxide were obtained from Matheson of Canada, Ltd., and purified by bulb to bulb distillation. Nitric oxide was further purified by condensation in and evaporation from caroxite. Gas chromatographic analysis indicated that the perfluorobutene-2 contained 98% *trans* and 2% *cis* isomers with no impurities. Purified nitrogen from Canadian Liquid Air Corp. was further purified by passage through a column of heated copper at 400° and through a liquid nitrogen trap. The nitrogen was activated either by a glow discharge excited by a 125-W microwave unit operating at 2450 MHz or by a condensed electric discharge.

The reaction was studied in a fast-flow system simi-

(1) H. v. Hartel and M. Polanyi, *Z. Phys. Chem. (Leipzig)*, **B11**, 97 (1930).

(2) J. H. Greenblatt and C. A. Winkler, *Can. J. Res.*, **B27**, 732 (1949).

lar to that described by Levy and Winkler.³ The major difference was the type of reaction vessel, which for the present experiments was made from Pyrex tubing of 60 mm i.d. and 45 cm length. The reactants were admitted to the active-nitrogen stream in the center of this reaction vessel from a jet of 1.5-mm diameter. The flow of the fluorocarbon or hydrocarbon was adjusted until a spherical diffusion flame was obtained. This flame was photographed in a darkened room with a scale attached to the reaction vessel. This allowed the flame diameter to be determined within an error of $\pm 2\%$.

The various partial pressures required for calculation of the rate constants were obtained from the total pressure of the gas mixture and the individual flow rates. The flow rate of perfluorobutene was determined by means of gas chromatography. A quantity of the gas was trapped directly following a measurement and under the conditions of the measurement. Quantitative determination of the amount of gas was made on a 1.5-m column of silica gel coated with 3% squalane. The limiting pressure or pressure of the reactant at the edge of the flame was obtained by reducing the reactant flow rate until the small reaction flame was practically indistinguishable from the yellow background of active nitrogen.

The concentration of nitrogen atoms was measured by the NO gas titration technique.^{4,5} The flow rates of NO, N₂, and the hydrocarbons were determined by evacuation of a known volume through the capillary flow meter.

A knowledge of the molecular diameters of the diffusing gases was required for the evaluation of D .⁶ The values of 3.75, 7.4, 3.5, and 5.8 Å for the molecular diameters of nitrogen, perfluorobutene-2, ethylene, and propylene, respectively, were used. The diameter of molecular nitrogen rather than atomic nitrogen has been used, since the amount dissociated is only a small percentage of the total flow in both the microwave and condensed discharges. The diameter of perfluorobutene-2 was obtained from viscosity measurements by comparison of its flow time through a fine capillary with that of gases of known viscosities. The other diameters were obtained from the literature.

Results and Discussion

Rate measurements of the reaction of perfluorobutene-2 with active nitrogen produced both in the condensed discharge and microwave discharge were made for several flow rates of fluorocarbon. In order to check the accuracy of the equipment and measurements, the reactions of ethylene and propylene with active nitrogen produced in the condensed discharge were also studied. The values determined for the various parameters necessary for the calculation of the rate constants and the rate constants are given in Table I.

Table I: Experimental Data for the Calculation of k^a

$10^3 p_f^b$ torr	$10^3 p_0$ torr	$10^3 p_N$ torr	d cm	$10^{-3} k$ torr ⁻¹ sec ⁻¹	$10^{-10} k$ cc mol ⁻¹ sec ⁻¹
N + C ₂ H ₄ , Condensed Discharge (Temp = 313°K, $D = 97.4$ cm ² sec ⁻¹)					
2.70	0.162	122	5.15	0.95	1.9
2.70	0.162	122	5.84	0.74	1.5
2.70	0.162	122	5.35	0.63	1.2
N + C ₃ H ₈ , Condensed Discharge (Temp = 313°K, $D = 48.3$ cm ² sec ⁻¹)					
1.76	0.171	122	2.54	1.3	2.5
1.76	0.171	122	2.41	1.5	2.9
1.76	0.171	122	2.80	1.1	2.2
N + C ₄ F ₈ -2, Condensed Discharge (Temp = 313°K, $D = 29.8$ cm ² sec ⁻¹)					
2.20	0.162	122	2.30	1.3	2.5
2.43	0.162	122	2.03	1.5	3.4
4.32	0.162	121	2.29	1.1	3.9
N + C ₄ F ₈ -2, Microwave Discharge (Temp = 298°K, $D = 27.4$ cm ² sec ⁻¹)					
1.6	0.12	19	3.71	2.8	5.2
1.6	0.12	19	4.37	2.0	3.7
1.6	0.12	19	4.39	2.0	3.7
0.6	0.04	19	3.00	4.6	8.5

^a N₂ flow rate, 187×10^{-6} mol sec⁻¹; N flow rate, 13.5×10^{-6} mol sec⁻¹ for condensed discharge; N flow rate, 2.0×10^{-6} mol sec⁻¹ for microwave discharge; total pressure, 1.75 torr. ^b p_f indicates partial pressure of hydrocarbons or fluorocarbon where appropriate. ^c All temperatures are $\pm 3^\circ$.

A comparison of the average rate constants determined in this work with those found by other studies for the active nitrogen-hydrocarbon reactions are given in Table II. It can be seen from the values tabulated that the measurements of the present work agree well within the accuracy of the technique. Also listed in Table II are the average values obtained for the rate of the active nitrogen-perfluorobutene reaction.

The measurement of the flame diameters is rather difficult, since the flames do not normally have a sharp cutoff in intensity near their edges. This was especially true of the hydrocarbons, since their flames tended to be somewhat diffuse and nonspherical. The fluorocarbon flame, however, was much better suited to diffusion-flame measurements. It was easily obtained in a near-perfect spherical shape with a relatively sharp cutoff. An example of such a flame is shown in Figure 1.

For the active nitrogen-ethylene reaction, the original

- (3) E. M. Levy and C. A. Winkler, *Can. J. Chem.*, **40**, 686 (1962).
- (4) (a) A. A. Westenberg and N. de Hass, *J. Chem. Phys.*, **40**, 3087 (1964); (b) L. Elias, *ibid.*, **42**, 4311 (1965).
- (5) J. T. Herron, *J. Phys. Chem.*, **69**, 2736 (1965).
- (6) J. O. Hirschfelder, C. F. Curtiss, and R. B. Bird, "Molecular Theory of Gases and Liquids," 2nd ed, John Wiley and Sons, Inc., New York, N. Y., p 14.

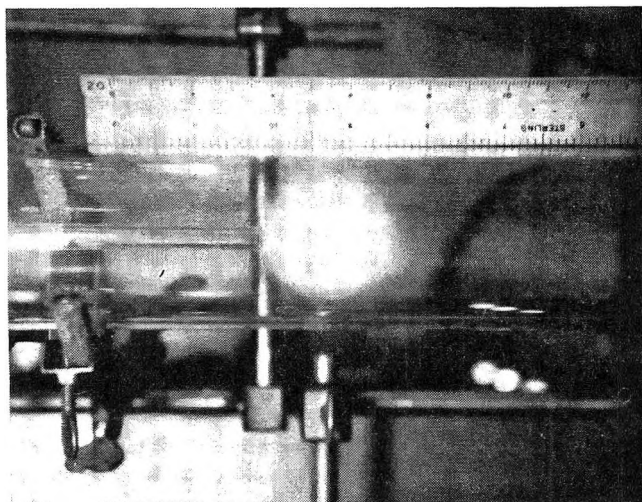


Figure 1. An example of the spherical flames produced by the reaction of perfluorobutene with active nitrogen produced in the microwave discharge.

measurement of the rate, which was made by diffusion-flame technique gave values of 1.45×10^{10} and 2.29×10^{10} at 298°K .² These values do not disagree markedly with recent measurements, as shown in Table II.

Table II: Comparison of Average Values of k with Known Values

Reaction	k (av present work), $\text{cc mol}^{-1} \text{sec}^{-1}$	k (previous work), $\text{cc mol}^{-1} \text{sec}^{-1}$	Ref
$\text{N} + \text{C}_2\text{H}_4$	1.5×10^{10} (313°)	1.0×10^{10} (340°)	<i>a</i>
		0.54×10^{10} (318°)	<i>b</i>
$\text{N} + \text{C}_3\text{H}_6$	2.5×10^{10} (313°)	1.9×10^{10} (340°)	<i>a</i>
		1.4×10^{10} (338°)	<i>b</i>
$\text{N} + \text{C}_4\text{H}_8-1$		2.0×10^{10} (340°)	<i>a</i>
$\text{N} + \text{C}_4\text{F}_8-2$	$3.3 \pm 1 \times 10^{10}$ (condensed discharge)		
	$5.3 \pm 2 \times 10^{10}$ (microwave discharge)		

^a J. T. Herron, *J. Phys. Chem.*, **70**, 2803 (1966). ^b G. Paraskevopoulos and C. A. Winkler, *ibid.*, **71**, 947 (1967).

Provided then that the flame produced in the reaction of active nitrogen with perfluorobutene-2 is representative of the reaction, it is probable that the rate constants calculated here represent closely the true rate of the reaction.

Acknowledgment. We wish to acknowledge financial support for this investigation by the National Research Council of Canada through a grant in aid of research. We also wish to thank the Isaak Walton Killam Memorial Scholarship Fund at Dalhousie for a scholarship to N. M.

The Variation of Partial Molar Volume of Some Tetraalkylammonium Iodides with Temperature in Aqueous Solutions¹

by Ram Gopal and Mohd. Aslam Siddiqi²

Department of Chemistry, Lucknow University,
Lucknow, U. P., India (Received August 4, 1967)

In order to investigate the nature of solute-solvent interaction of tetraalkylammonium ions (R_4N^+) in aqueous solutions, the partial molar volumes of some halides of these ions have been determined recently.^{3,4} From a study of the Walden product and the viscosity of the aqueous solutions of these salts, Kay and his associates^{5,6} have ascribed to the Me_4N^+ ion (also to the Et_4N^+ ion to some extent) a structure-breaking and to the other larger R_4N^+ ions a structure-promoting nature. The work on the heats of mixing of aqueous solutions⁷ and on the entropy changes⁸ also support these conclusions. In contrast, Allam and Lee⁹ have reported the Me_4N^+ and the Et_4N^+ ions to be appreciably solvated, which implies structure promotion of some kind by these ions. Solvation of the Me_4N^+ ion in aqueous solutions has already been suggested sometime ago.¹⁰ It may be noted that similar conclusion (*i.e.*, the solvation of all the R_4N^+ ions including Me_4N^+ and Et_4N^+) could be drawn from the theory of structure promotion in water by R_4N^+ ions, advanced by Frank and Evans¹¹ and confirmed from numerous investigations.

From this brief review, it appears that the difference in behavior of Me_4N^+ and the other larger R_4N^+ ions requires further investigation in order to clarify the dual nature of the smaller R_4N^+ ions, in contrast to the structure promotion only of the larger ones.

The variation of partial molar volume of electrolytes with temperature in aqueous solutions has been employed to study solute-solvent interaction by many workers;¹²⁻¹⁶ probably it is the simplest thermodynamical property to measure. The behavior of R_4N^+ ions,

- (1) Work supported by the CSIR, India.
- (2) Junior Research Fellow, CSIR, India.
- (3) W. Y. Wen and S. Saito, *J. Phys. Chem.*, **68**, 2639 (1964).
- (4) B. E. Conway, *et al.*, *Trans. Faraday Soc.*, **62**, 2738 (1966).
- (5) R. L. Kay and D. F. Evans, *J. Phys. Chem.*, **70**, 2325 (1966).
- (6) R. L. Kay, *et al.*, *ibid.*, **70**, 2336 (1966).
- (7) R. H. Wood and H. L. Anderson, *ibid.*, **71**, 1871 (1967).
- (8) G. E. Boyd, *et al.*, *ibid.*, **71**, 573 (1967).
- (9) D. S. Allam and W. H. Lee, *J. Chem. Soc., A*, 426 (1966).
- (10) E. R. Nightingale, Jr., *J. Phys. Chem.*, **63**, 1381 (1959).
- (11) H. S. Frank and M. W. Evans, *J. Chem. Phys.*, **13**, 507 (1945).
- (12) W. R. Bousefield and T. M. Lowery, *Trans. Faraday Soc.*, **6**, 85 (1910).
- (13) W. Geffecken, *Z. Phys. Chem.*, **A155**, 1 (1931).
- (14) A. F. Scott, *J. Phys. Chem.*, **35**, 2315 (1931).
- (15) O. Redlich and H. Klinger, *Monatsh.*, **65**, 137 (1934).
- (16) A. J. Ellis, *J. Chem. Soc., A*, 1582 (1966).

from this point of view, does not appear to have been investigated in detail³ up to this time. It may be remarked that for the common alkali metal halides, the limiting partial molar volume, \bar{V}_0 , first increases with rise in temperature,¹²⁻¹⁶ attains a maximum value near about 60° in most cases and around 40° in lithium chloride, and finally decreases on further increase in temperature. This property of some R_4NI , in aqueous solutions, has been investigated in the present communication with a hope to obtain some further insight into the R_4N^+ ion-water interaction in general and more specially into the behavior of the smallest Me_4N^+ ion.

Experimental Section

R_4NI salts were purified in the usual manner as given in ref 4. Conductivity water was used for making solutions in all the experiments. Density was measured with a dilatometer of about 30-ml capacity, the stem of which was graduated in 0.01 ml (graduation with a certificate A for accuracy from VEB Glaswerke, Stutzerbach, Thüringen, Germany) so that the volume could be read with ease up to 0.003 ml with a magnifying lens within an error not exceeding ± 0.002 ml. The temperature of the thermostat was regulated to within $\pm 0.02^\circ$ in the lower temperature range and $\pm 0.05^\circ$ in the higher temperature range. The dilatometer was calibrated with conductivity water and the accuracy of measurements was checked with some liquids of known accurate densities (reproducibility within $\pm 0.02\%$). While performing the experiments, it was found desirable to seal the dilatometer at the top so that it could be completely immersed in the oil of the thermostat and thus the condensation of water vapor in the upper parts of the capillary was avoided. A small ballast bulb was blown in the upper ungraduated capillary to avoid any appreciable pressure development in the sealed dilatometer at higher temperatures.

From the density data, the apparent molar volume, \bar{V} , was calculated from the equation $\bar{V} = [1000(d_0 - d)]/cd_0 + (M/d_0)$. The terms used have their usual significance. The limiting partial molar volume, \bar{V}_0 , was obtained from the usual extrapolation of the \bar{V} vs. \sqrt{C} curve, as required by Masson's equation

$$\bar{V} = \bar{V}_0 + S_V \sqrt{C}$$

Table I

Temp. °C	\bar{V}_0 , in ml/mol			
	Me_4NI	Et_4NI	Pr_4NI	Bu_4NI
25	125.7	185.5	250.9	312.2
30	126.5	186.3	252.4	314.0
40	127.2	187.4	254.0	318.5
50	128.7	189.1	256.4	322.5
60	130.2	191.1	258.8	327.5
70	131.9	194.3	262.6	335.5
80	134.0	198.7	266.8	347.0

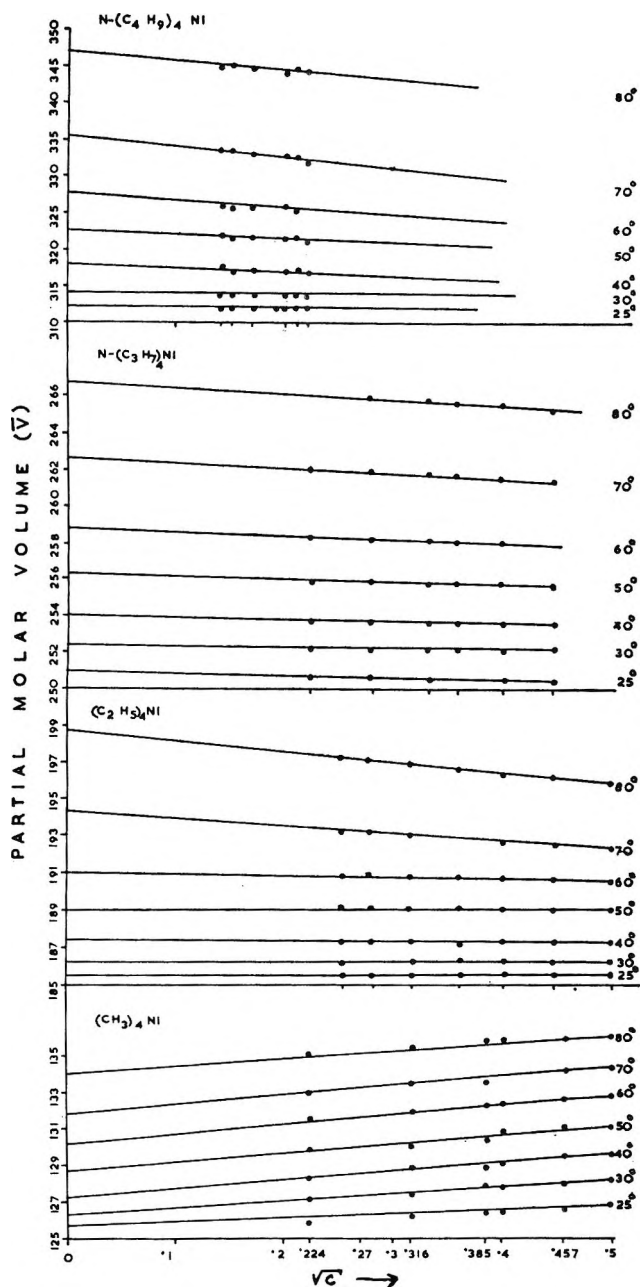


Figure 1. The partial molar volumes of some tetraalkylammonium iodides in aqueous solution at different temperatures.

The plots for different R_4NI salts, at different temperatures, are given in Figure 1.

As may be seen from Figure 1, the plots appear to be linear in all cases at all temperatures within the concentration range studied. The values of \bar{V}_0 ,¹⁷ obtained

(17) Anomalous behavior in \bar{V} vs. \sqrt{C} curves in the very dilute region has been reported (cf. B. E. Conway, *et al.*, *Trans. Faraday Soc.*, **62**, 2738 (1966)); also see O. Redlich and D. M. Meyer, *Chem. Rev.*, **64**, 221 (1964)) for R_4NBr and R_4NCl . However, \bar{V}_0 , obtained from extrapolation from higher concentrations³ and from the lower concentrations, do not differ appreciably. We, therefore, feel that the values of \bar{V}_0 of R_4NI , obtained by us, are reasonably correct. Considering $\bar{V}_0(I^-) = 35.5$ ml. at 25°, \bar{V}_0^+ , for the various R_4N^+ ions obtained in the present investigation is $\bar{V}_0(Me_4N^+) = 90.2$, $\bar{V}_0(Et_4N^+) = 150.0$, $\bar{V}_0(Pr_4N^+) = 215.4$, and $\bar{V}_0(Bu_4N^+) = 276.7$ ml, which compare with respective values 89.1, 149.6, 215.4, and 277.3 ml, given by Wen and Saito,³ very well.

for the first four members of R_4NI salts, at different temperatures, are given in Table I. Other higher members could not be studied owing to solubility restrictions.

Discussion

It may be noticed from Figure 1 that the slopes of \bar{V} vs. \sqrt{C} curves, except for Me_4MI and, at lower temperatures, for Et_4NI , are negative at all temperatures, as has already been reported by other workers^{3,4} at 25°. The concentration dependence of \bar{V} of R_4NX (X being a halide) salts has been well discussed by earlier workers and need not be examined here any further (except for Me_4NI which will be taken up later), especially because the study of the temperature dependence of \bar{V}_0 is the

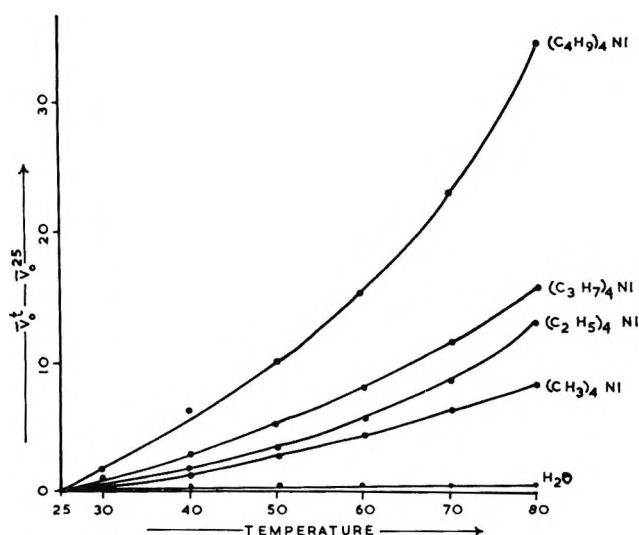


Figure 2. The temperature dependence of the partial molar volume of some tetraalkylammonium iodides.

immediate object of the present study. Plots of \bar{V}_0 (from Table I) against temperature for different R_4NI salts are given in Figure 2, in which $\bar{V}_0^t - \bar{V}_0^{25}$ is plotted against the temperature, t , so as to bring the curves for all the R_4NI salts and for water on the same chart, in order to get a better comparative idea of the variation of \bar{V}_0 with temperature in all the cases.

It may be noted that \bar{V}_0 increases with the rise in temperature in all cases including water. The larger the R_4N^+ ion is, the larger the temperature coefficient $d\bar{V}_0/dt$ is. Further, $d\bar{V}_0/dt$, for the same R_4NI salt, increases with the rise in temperature and the greater this increase is, the larger the R_4N^+ ion is; even Me_4N^+ ion and water are no exceptions. These observations can be explained by the structure-promotion effect of the R_4N^+ ions, in general, on the surrounding water medium, as has been suggested by Frank and his associates.^{11,18} Although some modifications to the original concept of Frank have been suggested,^{3,19} the general essential feature of the hypothesis, namely, the apparent structure promotion, is recognized by all

workers. The promoted or enhanced structure has been assumed to be tetrahedral or icelike^{11,18} although it has been questioned by many workers.²⁰⁻²⁵ The results of this investigation, summarized earlier, indicate that the alkyl chains of R_4N^+ ions, in general, promote structure²⁶ in water, but the structure appears to be the close-packed type which would involve contraction of the system during formation. On heating, this structure would break down, leading to the expansion of the system. The larger the ion, *i.e.*, the longer the alkyl chains are, the greater the structure promotion of the close-packed type and the larger the value of $d\bar{V}_0/dt$ will be. The icelike or tetrahedral structure promotion appears to be completely ruled out, since it would lead both to expansion of the system during formation and to contraction on melting; this would imply that $d\bar{V}_0/dt$, in a solution of R_4N^+ ions, should be even less than that of pure water, if not negative, which is certainly not the case, as is clear from Figure 2. Thus these experiments appear to provide a very convincing piece of evidence for the structure promotion by R_4N^+ ions and against the "iceberg" or tetrahedral structure of Frank and his associates.

Me_4N^+ ion is unique and deserves separate consideration. First, the positive slope of \bar{V} vs. \sqrt{C} curves indicates a similarity of ion-solvent interaction in solutions of Me_4N^+ and the common classical cations like alkali metal ions. As indicated in the opening paragraph, Me_4N^+ ion has been assumed to be a structure breaker⁵⁻⁸ and, at the same time, appreciably solvated.^{9,10} This behavior is again somewhat similar to the alkali metal ions which are structure breakers as well as solvated, the net result being dependent on the relative amounts of these two effects present in a particular ion. Owing to a comparatively smaller size as compared to other larger R_4N^+ ions, the Me_4N^+ ion is likely to give rise to appreciable ion-solvent dipolar interaction,³ leading to some electrostatic solvation. This automatically would involve a rearrangement of water molecules around the solvated ionic sphere, resulting in some structure breaking, as is the case in the common classical ions.²⁷ Also, there would be some structure promotion, over and above the electrostatic

(18) H. S. Frank and W. Y. Wen, *Discussions Faraday Soc.*, **24**, 136 (1957).

(19) R. M. Diamond, *J. Phys. Chem.*, **67**, 2513 (1963).

(20) J. Koefoed, *Discussions Faraday Soc.*, **24**, 216 (1957).

(21) D. D. Eley, *ibid.*, **24**, 218 (1957); *Trans. Faraday Soc.*, **35**, 1421 (1939).

(22) F. A. Bovey, *Nature*, **192**, 324 (1961).

(23) R. A. Pierotti, *J. Phys. Chem.*, **69**, 281 (1965).

(24) K. J. Mysels, *J. Amer. Chem. Soc.*, **86**, 3503 (1964).

(25) R. Gopal and A. K. Rastogi, *J. Indian Chem. Soc.*, **43**, 269 (1966).

(26) The iodide ion, I^- , is believed to be a structure breaker in water, so the R_4N^+ ions alone should be much stronger structure promoters than is indicated by the net structure promotion by R_4NI salts.

(27) Compare H. S. Frank and M. W. Evans, *J. Chem. Phys.*, **13**, 507 (1945).

solvation, owing to the four CH_3 groups which will induce some hydrophobic solvation.²⁸ The existence of some close-packed structure formation in the vicinity of the Me_4N^+ ion is indicated by the larger values of $d\bar{V}_0/dt$ for Me_4NI ²⁹ solutions as compared to that for pure water (Figure 2).

Acknowledgment. Financial assistance from the Society of Sigma Xi and the RESA for buying R_4NI salts is gratefully acknowledged.

(28) Compare R. Gopal and A. K. Rastogi, *J. Indian Chem. Soc.*, **43**, 269 (1966). If the Me_4N^+ ion is to fall in line with other R_4N^+ ions, the contraction in volume because of "hydrophobic" solvation should be about 5 ml rather than 16.3 ml, which indicates some other solvation as well.

(29) Compare ref 26. The structure-breaking nature of the I^- ion necessitates the Me_4N^+ ion to be a better structure promoter than is indicated by $d\bar{V}_0/dt$ values, which give the net effect of the Me_4NI salt. The structure-breaking nature, as indicated by non-equilibrium properties like conductance and viscosity, must be due to the "thawed region"²⁷ around the ion, due to electrostatic solvation.

Temperature Coefficients of Protein

Partial Volumes

by Henry B. Bull and Keith Breese

Biochemistry Department, University of Iowa, Iowa City, Iowa 52240
(Received August 17, 1967)

Partial specific volumes of proteins have been measured on numerous occasions largely in connection with sedimentation studies usually by one of three techniques: pycnometry, magnetic floats, and density gradient columns. More recently, Hunter¹ has devised a diver method suitable for small volumes of solution.

Information concerning the temperature coefficients of the partial volumes of proteins is limited, and we have attempted to extend our knowledge of this subject. We have adapted the specific gravity balance for this purpose.

Methods and Materials

A brass rod about 1.3 cm in diameter and about 9.5 cm long was rounded at the ends, a small hook embedded in one end, and the whole gold plated. One pan of a Sartorius analytical balance was removed and the plummet suspended from the unoccupied arm by means of a constantan wire 0.0071 cm in diameter. The balance could be read to 0.1 mg and estimated to 0.01 mg. The balance sat on a sturdy low table, the bottom of which was enclosed except for a front door. The constantan wire extended through the floor of the balance and through the top of the table. The solution whose density was to be measured was held in a 60-ml test tube sealed in a jacket through which water at the desired temperature was circulated at a brisk rate. The

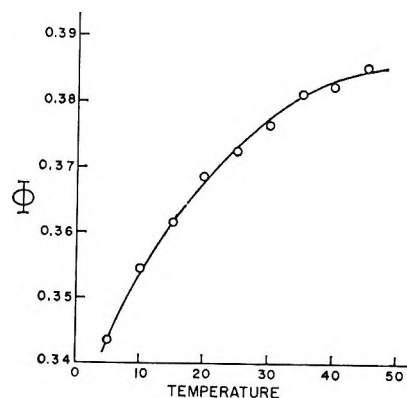


Figure 1. Plot of the apparent partial specific volume of KCl against temperature for a 1.0004 wt % solution of KCl.

temperature was held within 0.01° of a given setting and was read with a set of Brooklyn thermometers calibrated by the National Bureau of Standards. The test tube and jacket were in the cabinet beneath the table.

The plummet was weighed in air and, without disturbing the plummet, about 40 ml of the solution was run into the test tube such that the plummet was completely immersed and weighed at a series of temperatures extending from 5 to 45° . The volume of the plummet as a function of temperature was calculated from the measured buoyancy and the density of freshly boiled distilled water.² The volume of the plummet increased linearly with temperature. The average of five determinations of the density of a KCl solution containing 0.900034 g/100 g of solution was 1.001948 at 28.00° with a standard deviation of the mean of 0.93×10^{-6} . Hunter¹ gave 1.001954 for the density of a KCl solution of this concentration and temperature, and the value she interpolated from the "International Critical Tables" was 1.001952.

The apparent partial specific volume of the solute has been calculated by the expression

$$\Phi = \frac{1 - W_1 V_1}{W_2} \quad (1)$$

where W_1 and W_2 are the weights of solvent and solute, respectively, in 1 ml of solution and V_1 is the specific volume of water all at the experimental temperature. Figure 1 shows a plot of the partial specific volume of KCl.

The specific gravity balance requires, in principle, a surface tension correction if the calibrating liquid and the experimental solutions have different surface tensions; the suspending wire passes through the surface. The film pressures of the protein solutions used would be expected to be about 28 dyn/cm,³ corresponding to a

(1) M. J. Hunter, *J. Phys. Chem.*, **70**, 3285 (1966).

(2) H. S. Harned and B. B. Owen, "The Physical Chemistry of Electrolytic Solutions," 3rd ed, Reinhold Publishing Corp., New York, N. Y., 1958.

(3) S. Ghosh and H. B. Bull, *Biochim. Biophys. Acta*, **66**, 150 (1963).

buoyancy correction of about 0.6 mg for a wire 0.0071 cm in diameter. The constantan wire was, however, poorly wet both by water and by the protein solutions. We have attempted to estimate the surface tension effect by suspending 10 short sections of the suspension wire from a Lucite platform. The wires were well separated from each other and extended vertically in water. The water was replaced by 5% solutions of the proteins and the platform again reweighed. There was a gain of 0.87 mg per wire in going from air to water. As compared with the weight with the wires in water, there was a gain of 0.08 mg per wire in the methemoglobin solution, 0.34 mg per wire in the bovine serum albumin solution, and a loss of 0.03 mg per wire of the egg albumin solution. Thus it appears both the methemoglobin and the bovine serum albumin solutions wet the wires better than did water. If the surface tension correction be applied to the calculated partial specific volume of bovine serum albumin at 25°, the calculated value of 0.7376 is reduced to 0.7371. We have refrained from applying the surface tension corrections.

Since brass weights were used, there is no air buoyancy correction to be made to the air weight of the plummet. Upon immersion, the air buoyancy due to the plummet disappears and a corresponding air buoyancy of the weights appears. Since the correction applies both to the water calibration as well as to the experimental solutions, the correction tends to cancel, but not quite; it becomes a second-order correction. Air buoyancy corrections have been applied to all of our results.

The three proteins investigated were egg albumin, bovine methemoglobin, and bovine serum albumin. Egg albumin was crystallized and recrystallized twice from fresh hen eggs by the method of Kekwick and Cannan.⁴ Bovine oxyhemoglobin was crystallized and

recrystallized in the cold from red cell hemolysates using cold ethanol. Crystalline bovine serum albumin was from Sigma Chemical Co. The proteins were exhaustively dialyzed against water and then passed through mixed-ion-exchange columns. The oxyhemoglobin and serum albumin were lyophilized. During lyophilization, the oxyhemoglobin was quantitatively converted into methemoglobin as shown by its absorption spectrum from 500 to 600 m μ .

Dissolved air was removed from the protein solutions by applying a vacuum after they had been warmed to about 35°. Protein concentrations were determined on the solutions after the completion of the density measurements, by drying weighed aliquots of the solutions in a vacuum oven at 105° for 24 hr.

About 2, 5, and 10% solutions of egg albumin, about 5 and 10% solutions of methemoglobin, and about 5% solution of bovine serum albumin were used. In agreement with the conclusions of Dayhoff, Perlmann, and MacInnes,⁵ no dependence of the apparent partial specific volumes on protein concentration could be detected; accordingly, we have averaged our results from the different concentrations, and these are reported in Figure 2. The fact that the apparent partial specific volumes are independent of protein concentration means that the values given are actually partial specific volumes.

Results and Conclusions

The apparent partial specific volume of KCl as a function of temperature is not an essential part of this report, but since we have this information on hand, we are including it. Figure 1 shows a volume-temperature plot for a solution containing 0.010004 g of KCl/g of solution. As can be seen, the relation is not linear, and over part of the plot, the slope is large. At 20° the slope is 11.3×10^{-4} ml/deg.

Shown in Figure 2 are plots of the apparent partial specific volumes of bovine serum albumin, of egg albumin, and of bovine methemoglobin as a function of the temperature. The plots are linear up to 30 or 35°, but above these temperatures the slopes decrease significantly. For the linear portions, the slope of bovine serum albumin is 4.70×10^{-4} ml/deg, for egg albumin 4.27×10^{-4} ml/deg, and for bovine methemoglobin 4.07×10^{-4} ml/deg. The apparent partial specific volumes at 25° are: bovine serum albumin, 0.7376; egg albumin, 0.7477; methemoglobin, 0.7583.

Our value for the apparent partial specific volume of bovine serum albumin at 25° is significantly higher than that given by Hunter (0.7348).¹ It is also larger than that reported by Dayhoff, Perlmann, and MacInnes (0.7343).⁵ We notice, however, that Charlwood⁶

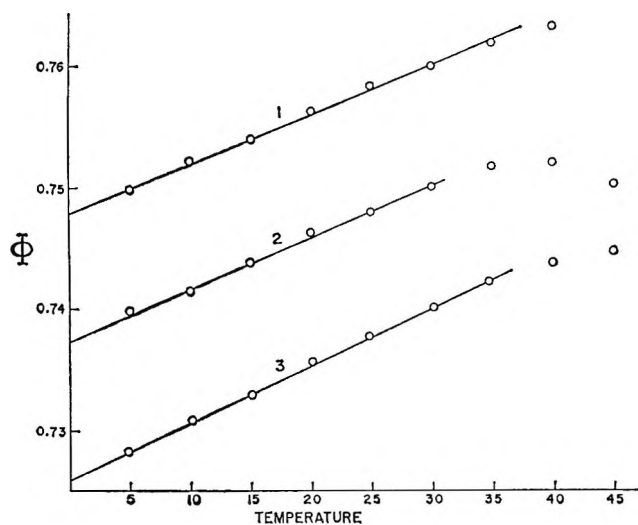


Figure 2. Plots of the apparent partial specific volumes of proteins against temperature: curve 1, bovine methemoglobin; curve 2 egg albumin; curve 3, bovine serum albumin.

(4) R. A. Kekwick and R. K. Cannan, *Biochem. J.*, **30**, 227 (1936).

(5) M. O. Dayhoff, G. E. Perlmann, and D. A. MacInnes, *J. Am. Chem. Soc.*, **74**, 2515 (1952).

(6) P. A. Charlwood, *ibid.*, **79**, 776 (1957).

finds the partial specific volume of this protein depends both on the sample lot and on the environment of the protein. For example, he reports a value of 0.7381 obtained after dialysis against water at pH 4.9 and one of 0.7357 for dialysis at pH 5.1. Failure to dry the protein leads, as pointed out by Hunter,¹ to a larger calculated partial specific volume. It does not appear, however, that our differences can be reconciled on the basis of water removal from the protein.

The situation in respect to the temperature coefficient of the apparent partial specific volume of bovine serum albumin is even more disturbing. Our coefficient of 4.70×10^{-4} ml/deg is indeed significantly different from the one reported by Hunter of 3.65×10^{-4} . As Hunter remarks, the temperature coefficient does not depend on protein concentration, and, accordingly, the extent of moisture removal from the protein should be unimportant. We are unable to account for the difference between our thermal coefficient and hers.

Our value of 0.7477 for the apparent partial specific volume of egg albumin at 25° compares favorably with that reported by Dayhoff, Perlmann, and MacInnes⁵ of 0.7481.

We have been unable to find a literature value for the apparent partial specific volume of bovine methemoglobin.

It appears likely that the thermal coefficient of the apparent partial specific volume reflects the thermal expansion of the protein as well as the release of water of hydration with increasing temperature.

Acknowledgment. We wish to thank Dr. Carl S. Vestling for the loan of the Sartorius balance. This research was supported by a grant from the Division of Molecular Biology, National Science Foundation.

Studies of the Solvent Effects on the Chemical Shifts in Nuclear Magnetic Resonance Spectroscopy. V. A Model for the Benzene Solutions of Polar Molecules¹

by Taku Matsuo

*Department of Organic Synthesis, Faculty of Engineering, Kyushu University, Hakozaki, Fukuoka-Shi, Japan
(Received September 13, 1967)*

Anomalous large solvent shifts of proton signals in nmr spectra of polar molecules in the benzene solutions have been reported by many authors. Ronayne and Williams recently proposed general principles to be used in predicting the directions and the relative magnitudes of the benzene-induced solvent shifts.² It is

suggested in that paper that benzene solvent molecule, an able π -electron donor, will solvate the electron-deficient site of each local dipole in a solute molecule, probably in a transient 1:1 association. The concept of single 1:1 association with a specific conformation is very attractive to organic chemists. It should be noted, however, that the interaction energy is only a few kilocalories per mole,³⁻⁶ as Ronayne and Williams admitted. This is close to the translational energy of molecules at the room temperature. The interactions in this energy region have been generally considered as due to van der Waals forces. Since van der Waals forces are known to be additive, one should expect that a solute molecule may be interacting with several surrounding molecules at the same time. Then it is rather difficult to believe that the time-averaged environments are always represented by the single 1:1 interaction between the solvent benzene molecule and each electron-deficient site of the solute. In fact, some of the observed values for the benzene-induced shifts are too large to be explained as being due to the formation of the 1:1 complex with a reasonable conformation at the electron-deficient site of each local dipole. For example, the benzene-induced shifts for the completely complexed species have frequently been observed to exceed 2 ppm.⁵⁻⁷ On the basis of Johnson and Bovey's calculation,⁸ the values are considered to be reasonable only if the solute protons are at about 2.6 Å directly above (or below) the plane of a benzene ring. In order to satisfy this condition, the C-H bonds of the solute molecules are required to be approximately perpendicular to the plane of the benzene molecule. Ronayne and Williams suggest that noncoplanar conformations are expected of the 1:1 association where the simple coulombic interactions between the π electrons and the local dipole of the solute molecule play major roles. The present author believes that such conformations are very unlikely in the association between benzene and rather strong π acceptors, like maleic anhydride⁶ and *p*-nitrobenzaldehyde.⁵ Even though the charge-transfer forces are not as important, the interacting molecules are very likely to take almost parallel conformation where the attractions due to the dipole-induced dipole interaction and the dispersion interaction will be certainly larger than otherwise. In this case, the solute protons may be at least 3.5 Å apart from the plane of the benzene molecule. The shielding

(1) Contribution No. 140 from the Department of Organic Synthesis, Faculty of Engineering, Kyushu University, Fukuoka, Japan.

(2) J. Ronayne and D. H. Williams, *J. Chem. Soc., B*, 540 (1967).

(3) J. H. Bowie, J. Ronayne, and D. H. Williams, *ibid.*, 785 (1966).

(4) Y. Nakayama and T. Matsuo, *J. Chem. Soc. Jap., Ind. Chem. Sect.*, 69, 1925 (1966).

(5) R. E. Klinck and J. B. Stothers, *Can. J. Chem.*, 44, 37 (1966).

(6) T. Matsuo, *ibid.*, 45, 1825 (1967).

(7) T. Matsuo and Y. Koderu, *J. Phys. Chem.*, 70, 4087 (1966).

(8) C. E. Johnson, Jr., and F. A. Bovey, *J. Chem. Phys.*, 29, 1012 (1958).

effect of the benzene ring current does not exceed 1.2 ppm at this distance.

The author here would like to propose a more general model in which van der Waals forces play major roles.⁹ Since van der Waals forces are additive, more than one solvent molecule may simultaneously but independently interact with a solute molecule. Then the large solvent shifts may be explained as being due to the cumulative effect of these clustering molecules. As to the study of weak charge-transfer complexes by the optical methods, Dewar and Thompson have warned that one should not overlook the role of general van der Waals forces in the molecular associations.¹⁰ The same thing could be said about the molecular interactions detected by nmr spectroscopy. Since van der Waals forces are due to the electronic perturbations of the nearby molecules,¹⁰ the strength of the interactions depends on the mutual orientations of the participating molecules. The energy of interaction due to van der Waals forces is generally obtained by taking an average over-all orientations for the molecules at relatively long distances. In the case of spectroscopic problems, however, the application of this simple procedure may not be adequate because the molecules at the closest positions play very important roles. At the closest distance, where the van der Waals radii of the constituent atoms come into contact with each other, the two molecules may be oriented so that a maximum attraction is achieved as a whole. The situation may be defined as an associated state. The associated solvent molecule will exchange with the bulk solvent at an extremely rapid rate, as Ronayne and Williams suggest.² Since the chemical shifts are measured from an internal standard, the effect of bulk solvent may be much smaller than those of the associated solvent molecule. In addition to the simple coulombic forces, the importance of hydrogen bonding, charge-transfer forces, dipole-induced dipole attractions (including dispersion interactions),⁹ and multipole interactions¹¹ should be strongly emphasized in the discussion of the associated states. The stronger the joint attraction due to these forces is, the longer the lifetime of the associated state will be. Then the mode of interaction will depend on the nature of the chemical bond in the solute molecule. If the solute molecule has any polar (or easily polarizable) group, there will be several solvent molecules associated with the functional group. In the neighborhood of a nonpolar, saturated bond, on the other hand, the interaction will be very small and the lifetime of the associated state, if it exists, may be extremely short. In order to achieve strong mutual attractions, the solute and the solvent molecules are required to take specific orientations with respect to each other. The orientations of benzene molecules with respect to the functional group of a solute molecule may be qualitatively estimated on the basis of the benzene-induced shifts which have been reported on

the various polar molecules.² At the sites close to the positive end of a polar group, the benzene molecule appears to take an orientation such that the π -electron cloud approaches the positive center as much as possible.^{2,9} In the neighborhood of the negative end of the polar group, on the other hand, the ring protons of benzene molecule seem to be directed toward the negative center.¹² These associations should be independent of each other, because the attractions are due to van der Waals forces. In a time average, the solvent molecules associated with the polar group, as a whole, will extend anisotropic shielding effects on the protons close to the functional group. The cumulative shielding effect ($\Delta\sigma$) on a proton may be given by the equation

$$\Delta\sigma = \frac{1}{T_a} \sum_{i=1}^n s_i \tau_i \quad (1)$$

where s_i , either positive or negative, is the shielding effect due to the benzene molecule at the site i and τ_i is the mean life of the associated state. The average interval (T_a) between the instants when the solute molecule encounters with benzene molecules may be a function of the mole fraction of benzene and the rate of exchange between the bulk and the associated species. The number of the relevant association sites is denoted by n . Since the association as described above is one of the thermodynamic processes, the mean life, τ_i , may be given in a form such as

$$\tau_i \sim f_i \exp(-E_i/RT) \quad (2)$$

where f_i and E_i are the frequency factor and the energy required for breaking the association. For a given functional group, the values of E_i for the relevant association sites may be more or less the same. At a constant temperature, T_a will be inversely proportional to the mole fraction of benzene. Then the benzene-induced shift is expected to show a linear increase with the mole fraction of benzene, as has been observed in many cases. Thus the benzene-induced shift ($\Delta\sigma$) will behave as if it is due to the formation of a 1:1 complex.

In the above discussion, it is taken for granted that the number of sites (n) may be larger than 2, even if the solute molecule contains a single functional group. Ronayne and Williams, on the other hand, suggest the possibility of multiple associations only in the case of polyfunctional solute molecules. In the Ronayne-Williams model, all the benzene-induced shifts for

(9) Y. Ichikawa and T. Matsuo, *Bull. Chem. Soc. Jap.*, **40**, 2030 (1967).

(10) M. J. S. Dewar and C. C. Thompson, Jr., *Tetrahedron, Suppl.*, **7**, 97 (1966).

(11) The author is grateful to N. Nakagawa at the University of Electrocommunications for suggesting the possible contribution of this factor.

(12) T. Schaefer and W. G. Schneider, *J. Chem. Phys.*, **32**, 1218 (1960).

various protons near a polar group are assumed to be ascribable to a single complexing benzene molecule. The condition will be fulfilled only if the attraction force is almost saturated by the interaction with a single benzene molecule. This is not valid in the case of van der Waals forces. If one insists on the 1:1 complex model, then it is very likely that he may be led to the idea of forces and conformations of the complex which may not be close to the true nature of molecular interactions in liquid media. Certainly, this is not a desirable situation, even though the model is proposed only to explain successfully the nmr solvent effect. Here, the present author suggests that the benzene-induced shifts should be generally explained as being due to the benzene molecules at several association sites around a solute molecule. The detail of this clustering model, such as the number and the conformations of these representative benzene molecules, are to be worked out further in future.

On the Kihara Core Model for Polar Molecules

by T. S. Storvick

Department of Chemical Engineering, University of Missouri, Columbia, Missouri

and T. H. Spurling

Department of Chemistry, University of Tasmania, Hobart, Tasmania, Australia (Received September 25, 1967)

Suh and Storvick¹ recently demonstrated that the Kihara² core potential, modified by the addition of a point dipole acting at the center of the core, correlated the second virial coefficients of a number of polar gases more successfully than the simpler Stockmayer³ model. Certain features of their derivation of the expression for the second virial coefficient for the model were unsatisfactory, and here we present a corrected derivation.

Assume that a permanent point dipole of strength μ is embedded at the geometric center of the core of the molecule. The orientation of the dipole within the core does not depend on the shape of the core but is assumed to be fixed for any molecular species. The core can be any convex body with a nonzero volume and we define a radius, a , which is the radius of a sphere having a volume equal to the volume of the convex body.

The potential function may now be written

$$U = 4\epsilon \left[\left(\frac{\rho_0}{\rho} \right)^{12} - \left(\frac{\rho_0}{\rho} \right)^6 \right] + \frac{\mu^2}{(\rho + 2a)^3} \times (2 \cos \theta_1 \cos \theta_2 + \sin \theta_1 \sin \theta_2 \cos (\phi_1 + \phi_2)) \quad (1)$$

in which ρ is the shortest distance between cores, and the nonorientational part of the potential has a minimum value of ϵ and is equal to zero when $\rho = \rho_0$. The angles θ_1 , θ_2 , ϕ_1 , and ϕ_2 are as defined by Buckingham and Pople.⁴

Following Kihara,² the second virial coefficient for the potential is given by

$$B(T) = \frac{N}{8\pi} \int_0^\infty (\rho^2 d\rho + A\rho d\rho + Bd\rho) \int_0^\pi \sin \theta_1 d\theta_1 \times \int_0^{2\pi} d\phi_1 \int_0^\pi \sin \theta_2 d\theta_2 \int_0^{2\pi} d\phi_2 \times \left[1 - \exp\left(\frac{-U}{kT}\right) \right] + V_0 + \frac{1}{4\pi} M_0 S_0 \quad (2)$$

where $A = M_0/\pi$, $B = (1/2\pi)[S_0 + (1/4\pi)M_0^2]$, and V_0 , M_0 , and S_0 are the volume, curvature, and surface area, respectively, of the core. For simplicity, we will now consider the core to be a sphere with radius a , so that $V_0 = 4/3 \pi a^3$, $M_0 = 4\pi a$, and $S_0 = 4\pi a^2$.

If eq 1 is substituted into eq 2 and the term $1/(\rho + 2a)^3$ is expanded in a binomial series, the expression can be integrated by the method of Buckingham and Pople.⁴ The final result (valid if $\rho_0 > 2a$) is

$$B(T) = \sum_{d=0}^2 b_d \left[y^{-2} (H_{12+d}(y) - 1/2 H_{6+d}(y)) - \frac{3-d}{d} \sum_{n=1}^{\infty} \tau^{2n} y^{4n-4} \left(\frac{n!}{2^{n+1}(2n+1)!} \right)^2 \times \left(\sum_{t=0}^n \frac{(2t)!}{(t!)^2} \right) \sum_{p=0}^{\infty} \frac{(6n)!}{p!(6n-p)!} \left(-\frac{2a}{\rho_0} \right) \times H_{6n+d+p}(y) \right] + b_3 \quad (3)$$

where $\tau = \mu^2/\rho_0^3 \epsilon$, $y = 2(\epsilon/kT)^{1/2}$, $b_0 = 2/3 \pi N \rho_0^3$, $b_1 = 4\pi a \rho_0^2 N$, $b_2 = 8\pi a^2 \rho_0 N$, $b_3 = 16/3 \pi a^2 N$, and

$$H_k(y) = y^{27-k/6} \sum_{m=0}^{\infty} \Gamma\left(\frac{6m+k-3}{12}\right) \frac{y^m}{m!}$$

This expression reduces to the expression for the second virial coefficient for the Lennard-Jones⁵ 12-6 potential if $a = 0$, $\mu = 0$; for the Kihara² core potential if $\mu = 0$; and for the Stockmayer³ potential if $a = 0$. Furthermore, the equation given by Suh and Storvick¹ (their eq 13) is this expression with the n series truncated at the $H_6(y)$ term.

(1) K. W. Suh and T. S. Storvick, *J. Phys. Chem.*, **71**, 1450 (1967).

(2) T. Kihara, *Rev. Mod. Phys.*, **25**, 831 (1953).

(3) W. H. Stockmayer, *J. Chem. Phys.*, **9**, 398 (1941).

(4) A. D. Buckingham and J. A. Pople, *Trans. Faraday Soc.*, **51**, 1173 (1955).

(5) J. E. Lennard-Jones, *Proc. Roy. Soc. (London)*, **A196**, 463 (1924).

Crystal Field Energy Levels for Various Symmetries

by Steven T. Spees, Jr.,¹ Jayarama R. Perumareddi,²
and Arthur W. Adamson

Department of Chemistry, University of Southern California,
Los Angeles, California 90007 (Received November 20, 1967)

The one-electron, d-orbital, crystal field energy levels for various symmetries have already been derived.³ (See also Appendix.) Except for the octahedral case which can be expressed in terms of only one radial parameter, all the others can be expressed in terms of two parameters

$$\langle \rho_2(r) \rangle = eq \int \frac{R(r)^2 r^4}{R^3} dr$$

and

$$\langle \rho_4(r) \rangle = eq \int \frac{R(r)^2 r^6}{R^5} dr$$

where e and q are the electronic charge and the point charge of the ligand, respectively, $R(r)$ is the radial function of the d orbital, and r and R are the electronic radius and the ligand distance from the central metal atom, respectively. For the octahedron, only the quartic parameter occurs and is usually expressed in terms of the well-known Dq parameter by the relation $1/6 \langle \rho_4(r) \rangle = Dq$. We show in Figures 1, 2, 3, and 4 the variation of the crystal-field d-orbital energy levels as the ratio $\rho = \langle \rho_2(r) \rangle / \langle \rho_4(r) \rangle$ is varied

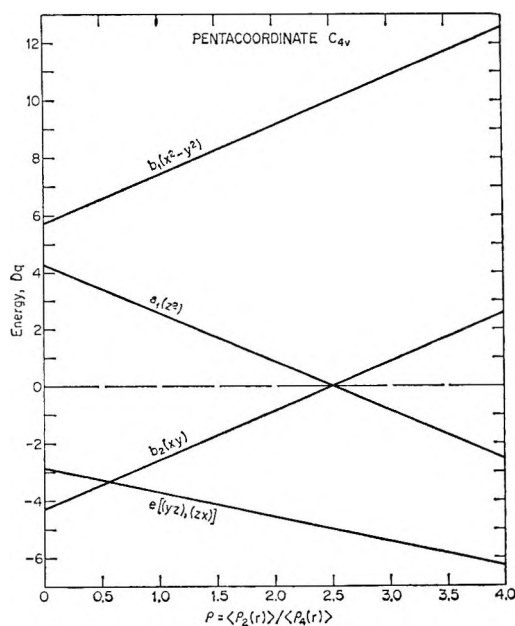


Figure 1. Plot of the one-electron d-orbital energy levels vs. the ratio of the radial parameters $\langle \rho_2(r) \rangle$ and $\langle \rho_4(r) \rangle$ in a five-coordinated complex of C_{4v} symmetry (square pyramid).

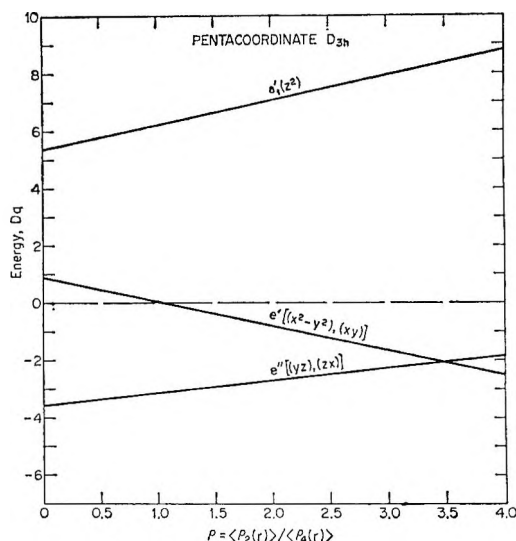


Figure 2. Plot of the one-electron d-orbital energy levels vs. the ratio of the radial parameters $\langle \rho_2(r) \rangle$ and $\langle \rho_4(r) \rangle$ in a five-coordinated complex of D_{3h} symmetry (trigonal bipyramid).

from 0 to 4. Basolo and Pearson⁴ and subsequently Hush⁵ have used $\rho = 2$. There is not much experimental evidence upon which to base a reasonable value for the ratio, ρ . Although the theoretical evaluation by use of Slater orbitals and Hartree-Fock functions for the radial part of the functions seem to give a high value such as 2 or more,⁶ the experimental evidence provided mainly by Piper and his coworkers⁷ in their studies on copper spectra points to a value of 0.9 or less. This ratio may not be a constant, but it may vary from one transition metal system to another, or, even for the same system, from one type of ligand to another. A comparison of the d-orbital energy levels is given in Table I for ρ equal to 1 and 2.

The principal purpose of this note is to point out that in addition to all other approximations and pitfalls involved in discussions of CFSE's, one should be aware

(1) Department of Chemistry, Michigan State University, East Lansing, Mich. 48823.

(2) Department of Chemistry, Florida Atlantic University, Boca Raton, Fla. 33432.

(3) (a) C. J. Ballhausen, *Kgl. Danske Videnskab. Selskab. Mat-Fys. Medd.*, **29**, No. 4 (1954); (b) C. J. Ballhausen and C. K. Jorgensen, *ibid.*, **29**, No. 14 (1955); see also ref 5. (c) A generalized treatment of electrostatic potentials and d-orbital energy levels for various possible symmetries is given in "Geometry, Color, and Magnetism: The Ti(III) and Cu(II) Systems and Their Relatives," by A. D. Liehr. These lecture notes are available upon request from Mellon Institute, Pittsburgh, Pa. 15213.

(4) F. Basolo and R. G. Pearson, "Mechanisms of Inorganic Reactions," 2nd ed, John Wiley and Sons, Inc., New York, N. Y., 1967, Chapters 2 and 3.

(5) N. S. Hush, *Australian J. Chem.*, **15**, 378 (1962).

(6) (a) S. Koide and M. H. L. Pryce, *Phil. Mag.*, **3**, 607 (1958); (b) H. A. Weakliem, *J. Chem. Phys.*, **36**, 2117 (1962); (c) T. S. Piper and R. L. Carlin, *ibid.*, **33**, 1208 (1960); (d) J. P. Perumareddi, unpublished results.

(7) (a) A. G. Karipides and T. S. Piper, *Inorg. Chem.*, **1**, 970 (1962); (b) W. E. Hatfield and T. S. Piper, *ibid.*, **3**, 841 (1964); (c) R. A. D. Wentworth and T. S. Piper, *ibid.*, **4**, 709 (1965).

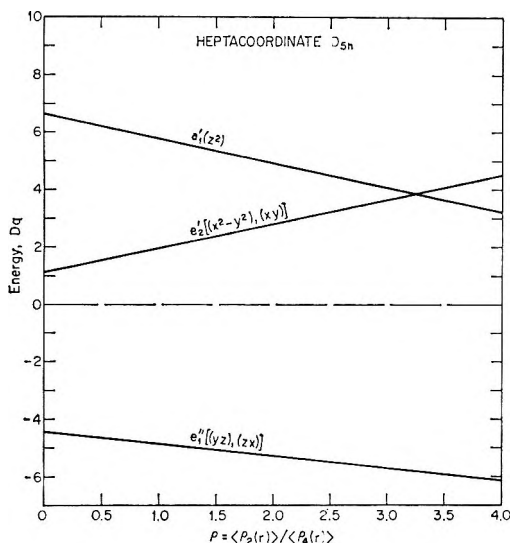


Figure 3. Plot of the one-electron d-orbital energy levels vs. the ratio of the radial parameters $\langle \rho_2(r) \rangle$ and $\langle \rho_4(r) \rangle$ in a seven coordinated complex of D_{5h} symmetry (pentagonal bipyramid).

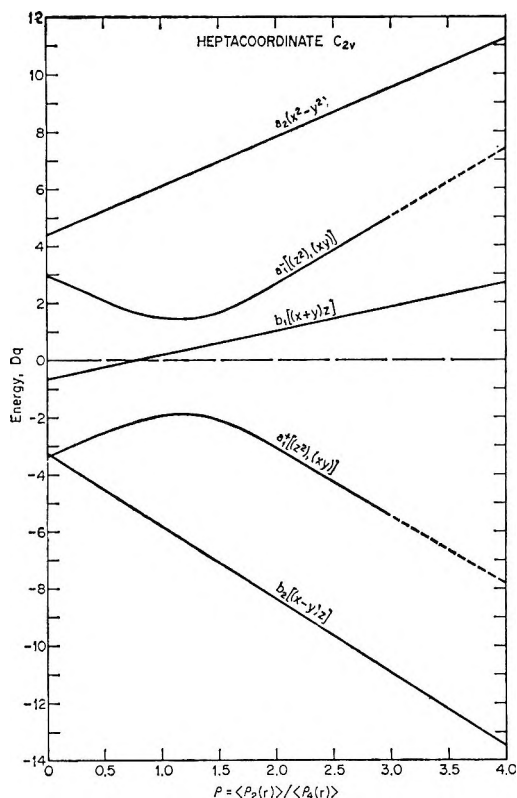


Figure 4. Plot of the one-electron d-orbital energy levels vs. the ratio of the radial parameters $\langle \rho_2(r) \rangle$ and $\langle \rho_4(r) \rangle$ in a seven-coordinated complex of C_{2v} symmetry (trapezoidal octahedron).

that a ratio of $\rho_2(r)/\rho_4(r)$ may be an additional variable. We do not believe that this has been explicitly discussed previously. This variation will be considered in a discussion of activation energies for the substitution reactions of inorganic complexes in a paper submitted by the authors for publication.

Table I: Comparison of the d-Orbital Energy Levels in Various Symmetries When ρ , the Ratio of the Radial Parameters, Is Given the Values 1 and 2

Symmetry	d orbitals	Energy in units of Dq	
		$\langle \rho_2(r) \rangle = 2\langle \rho_4(r) \rangle$	$\langle \rho_2(r) \rangle = \langle \rho_4(r) \rangle$
C_{4v}	$(x^2 - y^2)$	9.14	7.43
	(z^2)	0.86	2.57
	(xy)	-0.86	-2.57
	$(yz), (zx)$	-4.57	-3.71
D_{3h}	(z^2)	7.07	6.21
	$(x^2 - y^2), (xy)$	-0.82	0.04
	$(yz), (zx)$	-2.72	-3.14
D_{6h}	(z^2)	4.93	5.79
	$(x^2 - y^2), (xy)$	2.82	1.96
	$(yz), (zx)$	-5.28	-4.86
C_{2v}	$(x^2 - y^2)$	7.81	6.10
	$(z^2, xy)^-$	2.65	1.48
	$(x + y)z$	1.02	0.16
	$(z^2, xy)^+$	-3.09	-1.92
	$(x - y)z$	-8.38	-5.81

Acknowledgment. J. R. P. wishes to acknowledge helpful discussions with Dr. Andrew D. Liehr. We thank Mr. G. B. Arnold and Mr. J. F. Benes of the Mellon Institute Research Drafting Department for their assistance in drawing the figures. Most of this work was completed while S. T. Spees was at the University of Minnesota and J. R. Perumareddi was at the Mellon Institute and was supported in part by the National Science Foundation.

Appendix

Electrostatic Potentials and Crystal Field Matrix Elements

(i) Pentacoordinate C_{4v} Geometry (Square Pyramid). If one assumes a point charge, q , for ligands, the potential V when expanded in terms of spherical harmonics (retaining only those terms which give rise to nonzero matrix elements within the d manifold) takes the form

$$V = eq \left[5\sqrt{4\pi} Y_0^0 + \sqrt{\frac{4\pi}{5}} Y_2^0 \{ -2\rho_2(r) + \rho_2'(r) \} + \sqrt{\frac{4\pi}{9}} Y_4^0 \{ \frac{3}{2}\rho_4(r) + \rho_4'(r) \} + \sqrt{\frac{4\pi}{9}} Y_4^{4c} \left\{ \sqrt{\frac{35}{2}} \rho_4(r) \right\} \right] \quad (2a)$$

$$= eq \left[5\sqrt{4\pi} Y_0^0 - \sqrt{\frac{4\pi}{5}} \rho_2(r) Y_2^0 + \sqrt{\frac{4\pi}{9}} \rho_4(r) \left\{ \frac{5}{2} Y_4^0 + \frac{\sqrt{35}}{2} Y_4^{4c} \right\} \right] \quad (\text{if } \rho_n(r) = \rho_n'(r)) \quad (2b)$$

In the above, Y_4^{4c} is the cosine combination of Y_4^4 and Y_4^{-4} harmonics. The $\rho_n(r)$ defined for the ligands in the xy plane is given by $\rho_n(r) = r^n/R^{n+1}$ and correspondingly $\rho_n'(r) = r^n/R'^{n+1}$ for the axial ligand, where r is the radius of the electronic charge, e , and R and R' are the ligand distances from the central metal atom.

Use of the products of spherical harmonics⁸ gives the following crystal field matrix elements for the d orbitals (we shall use in the present and following cases the potential with $\rho_n(r) = \rho_n'(r)$)

$$\begin{aligned} \langle (x^2 - y^2) | V | (x^2 - y^2) \rangle &= \frac{2}{7} \langle \rho_2(r) \rangle + \frac{20}{21} \langle \rho_4(r) \rangle \\ \langle (z^2) | V | (z^2) \rangle &= -\frac{2}{7} \langle \rho_2(r) \rangle + \frac{5}{7} \langle \rho_4(r) \rangle \\ \langle (xy) | V | (xy) \rangle &= \frac{2}{7} \langle \rho_2(r) \rangle - \frac{5}{7} \langle \rho_4(r) \rangle \\ \langle (yz) | V | (yz) \rangle &= -\frac{1}{7} \langle \rho_2(r) \rangle - \frac{10}{21} \langle \rho_4(r) \rangle \\ \langle (zx) | V | (zx) \rangle &= -\frac{1}{7} \langle \rho_2(r) \rangle - \frac{10}{21} \langle \rho_4(r) \rangle \end{aligned} \quad (3)$$

and all other elements are zero. The $\langle \rho_n(r) \rangle$, which are regarded as parameters, are the average values of the n th power of the electronic radius, r , multiplied by the factor (eq/R^{n+1}) .

After substituting a proper relation between $\langle \rho_2(r) \rangle$ and $\langle \rho_4(r) \rangle$ and equating $1/6 \langle \rho_4(r) \rangle$ to Dq , we find the correspondence with the octahedral case desired.

(ii) *Pentacoordinate D_{3h} Geometry (Trigonal Bipyramid)*

$$\begin{aligned} V &= eq \left[5\sqrt{4\pi} Y_0^0 + \sqrt{\frac{4\pi}{5}} Y_2^0 \left\{ -\frac{3}{2} \rho_2(r) + 2\rho_2'(r) \right\} + \sqrt{\frac{4\pi}{9}} Y_4^0 \left\{ \frac{9}{8} \rho_4(r) + 2\rho_4'(r) \right\} \right] \quad (4a) \\ &= eq \left[5\sqrt{4\pi} Y_0^0 + \frac{1}{2} \sqrt{\frac{4\pi}{5}} \rho_2(r) Y_2^0 + \frac{25}{8} \sqrt{\frac{4\pi}{9}} \rho_4(r) Y_4^0 \right] \quad (\text{if } \rho_n(r) = \rho_n'(r)) \quad (4b) \end{aligned}$$

where the $\rho_n(r)$ are for the ligands in the xy plane and $\rho_n'(r)$ for the axial ligands.

The one electron d-orbital crystal-field energies are with the potential $\rho_n(r) = \rho_n'(r)$

$$\begin{aligned} \langle (z^2) | V | (z^2) \rangle &= \frac{1}{7} \langle \rho_2(r) \rangle + \frac{25}{28} \langle \rho_4(r) \rangle \\ \langle (x^2 - y^2) | V | (x^2 - y^2) \rangle &= -\frac{1}{7} \langle \rho_2(r) \rangle + \frac{25}{168} \langle \rho_4(r) \rangle \\ \langle (xy) | V | (xy) \rangle &= \frac{1}{7} \langle \rho_2(r) \rangle - \frac{25}{168} \langle \rho_4(r) \rangle \\ \langle (yz) | V | (yz) \rangle &= -\frac{1}{14} \langle \rho_2(r) \rangle - \frac{25}{42} \langle \rho_4(r) \rangle \\ \langle (zx) | V | (zx) \rangle &= -\frac{1}{14} \langle \rho_2(r) \rangle - \frac{25}{42} \langle \rho_4(r) \rangle \end{aligned} \quad (5)$$

and all others are zero.

(iii) *Heptacoordinate D_{3h} Geometry (Pentagonal Bipyramid)*

$$\begin{aligned} V &= eq \left[7\sqrt{4\pi} Y_0^0 + \sqrt{\frac{4\pi}{5}} Y_2^0 \left\{ -\frac{5}{2} \rho_2(r) + 2\rho_2'(r) \right\} + \sqrt{\frac{4\pi}{9}} Y_4^0 \left\{ \frac{15}{8} \rho_4(r) + 2\rho_4'(r) \right\} \right] \quad (6a) \\ &= eq \left[7\sqrt{4\pi} Y_0^0 - \frac{1}{2} \sqrt{\frac{4\pi}{5}} \rho_2(r) Y_2^0 + \frac{31}{8} \sqrt{\frac{4\pi}{9}} \rho_4(r) Y_4^0 \right] \quad (\text{if } \rho_n(r) = \rho_n'(r)) \quad (6b) \end{aligned}$$

where the primed $\rho_n(r)$ are for the axial ligands and the nonprimed are for the five ligands in the xy plane. The d-orbital energies are (when $\rho_n(r) = \rho_n'(r)$)

$$\begin{aligned} \langle (z^2) | V | (z^2) \rangle &= -\frac{1}{7} \langle \rho_2(r) \rangle + \frac{31}{28} \langle \rho_4(r) \rangle \\ \langle (x^2 - y^2) | V | (x^2 - y^2) \rangle &= \frac{1}{7} \langle \rho_2(r) \rangle + \frac{31}{168} \langle \rho_4(r) \rangle \\ \langle (xy) | V | (xy) \rangle &= \frac{1}{7} \langle \rho_2(r) \rangle - \frac{31}{168} \langle \rho_4(r) \rangle \\ \langle (yz) | V | (yz) \rangle &= -\frac{1}{14} \langle \rho_2(r) \rangle - \frac{31}{42} \langle \rho_4(r) \rangle \\ \langle (zx) | V | (zx) \rangle &= -\frac{1}{14} \langle \rho_2(r) \rangle - \frac{31}{42} \langle \rho_4(r) \rangle \end{aligned} \quad (7)$$

and all others are zero.

(iv) *Heptacoordinate C_{2v} Geometry (Trapezoidal Octahedron)*

$$\begin{aligned} V &= eq \left[7\sqrt{4\pi} Y_0^0 + \sqrt{\frac{4\pi}{5}} Y_2^0 \left\{ -\rho_2(r) \right\} + \sqrt{\frac{4\pi}{5}} Y_2^{2s} \left\{ \frac{2}{\sqrt{3}} \rho_2'(r) \right\} + \sqrt{\frac{4\pi}{9}} Y_4^0 \left\{ \frac{5}{2} \rho_4(r) - \frac{7}{9} \rho_4'(r) \right\} + \sqrt{\frac{4\pi}{9}} Y_4^{2s} \left\{ \frac{4\sqrt{5}}{9} \rho_4'(r) \right\} + \sqrt{\frac{4\pi}{9}} Y_4^{4c} \left\{ \frac{\sqrt{35}}{2} \rho_4(r) - \frac{\sqrt{35}}{9} \rho_4'(r) \right\} \right] \quad (8a) \\ &= eq \left[7\sqrt{4\pi} Y_0^0 + \sqrt{\frac{4\pi}{5}} \rho_2(r) Y_2^0 \left\{ -Y_2^0 + \frac{2}{\sqrt{3}} Y_2^{2s} \right\} + \sqrt{\frac{4\pi}{9}} \rho_4(r) \left\{ \frac{31}{18} Y_4^0 + \frac{4}{9} \sqrt{5} Y_4^{2s} + \frac{7\sqrt{35}}{18} Y_4^{4c} \right\} \right] \quad (\text{if } \rho_n(r) = \rho_n'(r)) \quad (8b) \end{aligned}$$

where it is supposed that five of the ligands occupy the five corners of an octahedron at a distance R from the central metal atom (forming the square pyramid) and the remaining two ligands are at a distance R' in the $(x + y)z$ plane or $(x - y)z$ plane with an angle of β , the tetrahedral angle. By assuming all ligands are at the same distance, R , we arrive at the following energies for the various d orbitals.

(8) It is very convenient to use Table A21 in J. S. Griffith, "The Theory of Transition Metal Ions," Cambridge University Press, London, 1961.

$$\begin{aligned}
 \langle (x^2 - y^2) | V | (x^2 - y^2) \rangle &= \frac{2}{7} \langle \rho_2(r) \rangle + \frac{46}{63} \langle \rho_4(r) \rangle \\
 \langle (z^2) | V | (z^2) \rangle &= -\frac{2}{7} \langle \rho_2(r) \rangle + \frac{31}{63} \langle \rho_4(r) \rangle \\
 \langle (xy) | V | (xy) \rangle &= \frac{2}{7} \langle \rho_2(r) \rangle - \frac{107}{189} \langle \rho_4(r) \rangle \\
 \langle (yz) | V | (yz) \rangle \\
 \langle (zx) | V | (zx) \rangle \} &= -\frac{1}{7} \langle \rho_2(r) \rangle - \frac{62}{189} \langle \rho_4(r) \rangle \\
 \langle (z^2) | V | (xy) \rangle \\
 \langle (xy) | V | (z^2) \rangle \} &= -\frac{4}{7\sqrt{3}} \langle \rho_2(r) \rangle + \frac{20}{63\sqrt{3}} \langle \rho_4(r) \rangle \\
 \langle (yz) | V | (zx) \rangle \\
 \langle (zx) | V | (yz) \rangle \} &= \frac{2}{7} \langle \rho_2(r) \rangle + \frac{40}{189} \langle \rho_4(r) \rangle \quad (9)
 \end{aligned}$$

and all others zero.

We notice in this case two nonvanishing nondiagonal matrix elements, which give rise to configuration interaction. The configuration interaction of the (yz) and (xz) orbitals is just that needed to mix them into the properly symmetrized combinations $1/\sqrt{2}[(xz) \pm (yz)]$ which are written in the text for simplicity $(x \pm y)z$. Then

$$\begin{aligned}
 \langle (x + y)z | V | (x + y)z \rangle &= \frac{1}{7} \langle \rho_2(r) \rangle - \frac{22}{189} \langle \rho_4(r) \rangle \\
 \langle (x - y)z | V | (x - y)z \rangle &= -\frac{3}{7} \langle \rho_2(r) \rangle - \frac{102}{189} \langle \rho_4(r) \rangle
 \end{aligned}$$

The configuration interaction of the (z^2) and (xy) orbitals is the usual type between two states of the same overall symmetry. So, by assuming equal mixing of the states, we solve the 2×2 secular determinant and denote the orbital with higher energy as $(z^2, xy)^-$ and the one with lower energy $(z^2, xy)^+$ (see also ref 5).

It may be pointed out that neglecting the presence of Y_0^0 terms and putting $\rho_n'(r) = 0$ in eq 2a, 4a, 6a, and 8a, which is equivalent to removing the corresponding ligands to infinity, there result the potentials, respectively, for a four-coordinated complex of square planar geometry (D_{4h}), a tricordinate complex of trigonal planar geometry (D_{3h}), a five-coordinated complex of pentagonal planar geometry (D_{5h}), and a five-coordinated complex of square pyramidal geometry (C_{4v}).

Estimation of the High-Temperature Entropy of Solids by the Entropy Correspondence Principle¹

by J. G. Eberhart and E. N. Gruetter

Sandia Laboratory, Albuquerque, New Mexico 87115
(Received October 5, 1967)

In recent years, Cobble and Criss²⁻⁴ have developed an entropy correspondence principle, which relates the

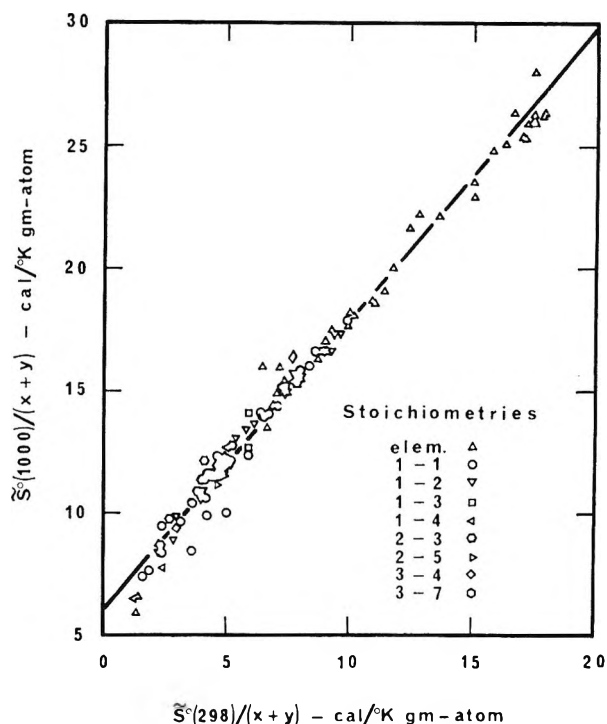


Figure 1. Entropy correlation for 298 and 1000°K.

standard partial molar entropy at one temperature, $S^o(T_2)$, to that at another temperature, $S^o(T_1)$, for a series of aqueous ions of similar charge and type (*i.e.*, simple ions, oxy anions, and acid oxy anions). The relationship between the partial molar entropies at two temperatures is linear and can be written in the form

$$S^o(T_2) = a(T_2, T_1) + b(T_2, T_1)S^o(T_1) \quad (1)$$

where the intercept and the slope depend on the two temperatures selected for the correlation and the ionic type. The relationship has been used to estimate partial molar entropies at elevated temperatures from room-temperature values.

The absolute entropies of solid metals and compounds at room temperature and above are examined in this note and are found to obey a similar linear relationship.

Table I: Coefficients in the Entropy Correspondence Equation

$T, ^\circ K$	$a(T, 298),$ cal/deg g-atom	$b(T, 298)$
298	0.00	1.000
500	2.92	1.038
1000	6.86	1.105
1500	9.38	1.141

(1) This work was supported by the U. S. Atomic Energy Commission.

(2) C. M. Criss and J. W. Cobble, *J. Am. Chem. Soc.*, **86**, 5385 (1964).

(3) J. W. Cobble, *Science*, **152**, 1479 (1966).

(4) J. W. Cobble, *Ann. Rev. Phys. Chem.*, **17**, 15 (1966).

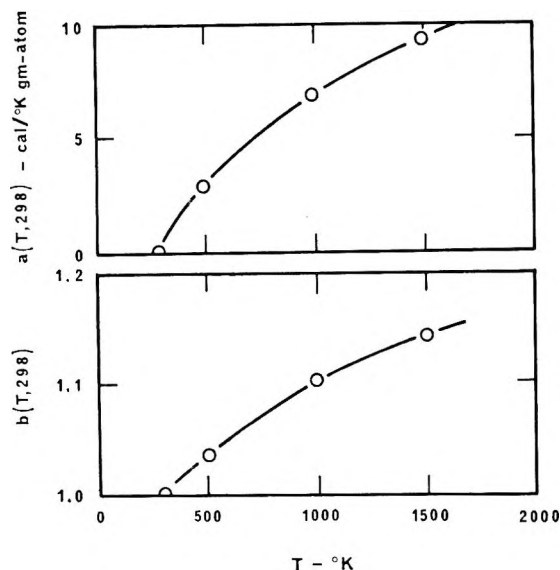


Figure 2. Intercept and slope for the linear correlation between entropy at 298°K and that at higher temperatures.

For reasons to be stated shortly, entropies will be given for Avogadro's number of atoms, *i.e.*, on a gram-atom basis. If \bar{S}° is the standard molar entropy of the compound A_xB_y , then $\bar{S}^\circ/(x+y)$ is the entropy per gram-atom. Using experimentally determined entropies taken from various tabulations of thermodynamic properties,⁵⁻⁷ plots were made of $\bar{S}^\circ(298)/(x+y)$ vs. $\bar{S}^\circ(500)/(x+y)$, $\bar{S}^\circ(1000)/(x+y)$, and $\bar{S}^\circ(1500)/(x+y)$. A typical result is shown in Figure 1 with entropies at 298 and 1000°K. It was found that solid compounds of all stoichiometries and solid elements obey the same linear entropy correspondence relationship

$$\frac{\bar{S}^\circ(T_2)}{x+y} = a'(T_2, T_1) + b(T_2, T_1) \frac{\bar{S}^\circ(T_1)}{x+y} \quad (2)$$

where, in the specific case of elementary substances, $x = 1$ and $y = 0$. The legend in Figure 1, which lists the values of x and y in the compounds, shows the wide variety of stoichiometries satisfying the relationship. The chemical types included in the plot are elementary metals and nonmetals, intermetallic compounds, and halides, oxides, carbides, and nitrides of metals. As can be inferred from eq 2, if molar entropies are used directly in the correlation, a different intercept, $(x+y)a$, is obtained for stoichiometries of each $x+y$ value.

Least-squares values of the intercept and slope in eq 2 were calculated for a fixed lower temperature of 298°K and upper temperatures of $T = 500, 1000, \text{ and } 1500^\circ\text{K}$. Table I shows the values of $a(T, 298)$ and $b(T, 298)$ at these upper temperatures. Plots of $a(T, 298)$ and $b(T, 298)$ vs. T in Figure 2 show that the slope and intercept of the linear correlation increase smoothly with the upper temperature.

The relationship shown in eq 2 permits the estimation

of high-temperature entropies from a low-temperature value and an empirically determined intercept and slope characteristic of the two temperatures.

From the relationships $\bar{S}^\circ(T)/(x+y) = a(T, 298) + b(T, 298)[\bar{S}^\circ(298)/(x+y)]$ and $C_p = T(\partial S/\partial T)_p$, it also follows that $\bar{C}_p^\circ(T)/(x+y) = \alpha(T, 298) + \beta(T, 298)[\bar{S}^\circ(298)/(x+y)]$, where $\alpha(T, 298) = da(T, 298)/d \ln T$ and $\beta(T, 298) = db(T, 298)/d \ln T$. Thus the entropy correspondence equation can also be used to estimate heat capacities at an upper temperature from entropies at a lower temperature.

(5) "JANAF Thermochemical Tables," The Dow Chemical Co., Midland, Mich., 1967.

(6) D. R. Stull and G. C. Sinke, "Thermodynamic Properties of the Elements," American Chemical Society, Washington, D. C., 1956.

(7) C. E. Wicks and F. E. Block, "Thermodynamic Properties of 65 Elements—Their Oxides, Halides, Carbides, and Nitrides," Bureau of Mines Bulletin 605, U. S. Government Printing Office, Washington, D. C., 1963.

On the Reaction Complex of the $C_3H_6^+ - C_3H_6$ Ion-Molecule Reaction

by Fred P. Abramson¹ and Jean H. Futrell²

Aerospace Research Laboratories, Office of Aerospace Research,
Wright-Patterson Air Force Base, Ohio 45433
(Received October 12, 1967)

In an earlier publication,³ we discussed ion-molecule reactions in olefin systems and suggested a classification scheme which is based on the concept of different types of intermediate complexes (*e.g.*, "loose" and "tight" complexes) being involved in particle-transfer, condensation, and molecular ion reactions. In particular, a difference between $C \cdots H \cdots C$ and $C \cdots C$ bonded complexes was proposed. Very similar ideas were put forward by Lampe, Franklin, and Field in a review article on ion-molecule reaction kinetics.⁴ Whenever the reaction complex is stoichiometrically equivalent to a stable ionic species, these authors suggested that an intimately bonded complex would be formed and that its dissociation products would resemble the unimolecular dissociation products of that ionic species. For example, they noted that the products of ion-molecule reactions of acetylene and ethylene molecular ions corresponded to the major mass spectral fragmentation peaks of certain C_4 hydrocarbons.⁵ Although they

(1) Consolidated Electrodynamics Corporation, Monrovia, Calif. 91017.

(2) Department of Chemistry, University of Utah, Salt Lake City, Utah 84112.

(3) F. P. Abramson and J. H. Futrell, *J. Phys. Chem.*, in press.

(4) F. W. Lampe, J. L. Franklin, and F. H. Field, *Progr. Reaction Kinetics*, **1**, 67 (1961).

(5) J. L. Franklin, F. H. Field, and F. W. Lampe, *Advan. Mass Spectry.*, **1**, 308 (1959).

correlated their results with 50-eV spectra, they suggested that the actual proportions of secondary ions resulting from such a complex should be similar to the relative intensities of fragment ions formed from molecules of the same atomic composition at low electron energy. Fuchs has also attempted a correlation of 50-eV mass spectra with ion-molecule reaction products in the butene and propene systems,⁶ and his findings will be discussed in relation to our results.

Following the suggestion of Franklin, *et al.*,^{4,5} we have determined the low energy electron impact mass spectra of various C₆H₁₂ hydrocarbons and their variation with electron energy with hope of correlating these patterns with the reaction products of the C₃H₆⁺-C₃H₆ reaction. We shall compare the results with the product distribution reported previously,³ restricting ourselves to those reactions which appear to proceed *via* a C-C bonded intermediate complex.

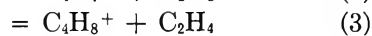
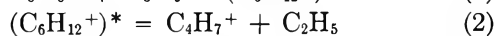
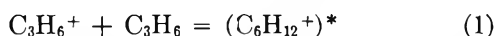
Experimental Section

The low-voltage mass spectra were obtained on a Consolidated Electro Dynamics Corp. Model 21-103C mass spectrometer equipped with an electron multiplier detector. Ionizing currents of 0.2 μA were used, and the anode potential was reduced to 4.5 V. The repeller potential was fixed at 6.3 V (field strength 25 V/cm), and the spectra were scanned electrostatically at various electron energies.

All chemicals used were obtained from the Chemical Samples Co. or from Matheson Coleman and Bell. All were of stated purity of 99% or better and were used without further purification.

Results and Discussion

The reactions which we are considering are



Using available thermochemical data,^{7,8} we estimate that reaction 2 is 0-4 kcal/mole exothermic; that reaction 3 is exothermic by 3-15 kcal/mole, depending on structure of the C₄H₈⁺ product; and that reaction 4 is exothermic by about 2 kcal/mole, all values being calculated for ground state ions. The exothermicity of reaction 4 is based upon a value for Δ*H*_f(C₅H₉⁺) = 199 kcal/mole, obtained from the following considerations. We find the appearance potential of C₅H₉⁺ to be lower than that for C₄H₈⁺ from cyclohexane by about 0.1 eV. We have also noted that the C₄H₈⁺ ion in cyclohexane reacts as 1-butene ions.⁹ Combining this information with the spectroscopic ionization potential of 1-butene¹⁰ and other required thermochemical quantities, we deduce that 199 ± 3 kcal/mole should be assigned to Δ*H*_f(C₅H₉⁺). All of these reactions are therefore exothermic and represent the competitive breakdown paths anticipated for the (C₆H₁₂⁻)^{*} complex.

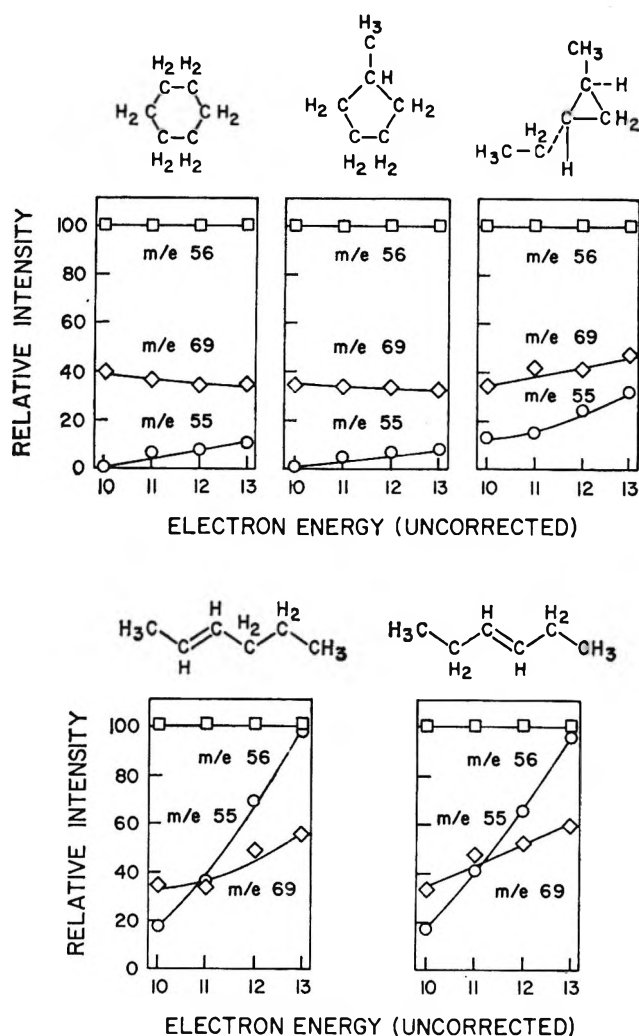


Figure 1. Clastograms for principal fragment ions produced by electron impact of selected C₆H₁₂ isomers.

In the present work, we have measured the low-energy mass spectra of the following compounds: cyclohexane, methylcyclopentane, 1-hexene, *trans*-2-hexene, *trans*-3-hexene, 2-methyl-1-pentene, *trans*-2-methyl-2-pentene, 3-methyl-1-pentene, 4-methyl-1-pentene, 2,3-dimethyl-1-butene, 2,3-dimethyl-2-butene, 3,3-dimethyl-1-butene, and *trans*-1-methyl-2-ethylcyclopropane. This, of course, does not represent an exhaustive list of possible C₆H₁₂ isomers. If we assume methyl arrangements do not occur in the interaction of C₃H₆⁺ with C₃H₆, the list includes (with the exception of the dimethyl cyclobutanes) all of the anticipated possible intermediates which are commercially available. Other butenes were considered because their

(6) R. Fuchs, *Z. Naturforsch.*, **16a**, 1026 (1961).

(7) F. H. Field and J. L. Franklin, "Electron Impact Phenomena," Academic Press, New York, N. Y., 1957.

(8) "Handbook of Chemistry and Physics," 45th ed, The Chemical Rubber Publishing Company, Cleveland, Ohio, 1964.

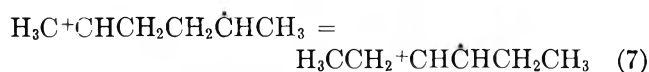
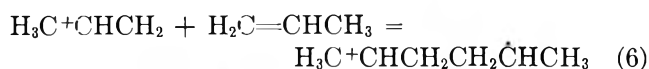
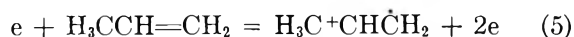
(9) F. P. Abramson and J. H. Futrell, *J. Phys. Chem.*, **71**, 3791 (1967).

(10) K. Watanabe, T. Nakayama, and J. Mottl, *J. Quart. Spectry. Radiative Transfer*, **2**, 369 (1962).

mass spectra¹¹ included prominent fragment ions from the dissociation reactions (2-4). Since the tabulated mass spectra of the *cis-trans* isomers exhibit very similar fragmentation patterns, the *trans* isomers were uniformly selected for the present investigation. The relative intensities of the ions of interest, m/e 55, 56, and 69, and their variation with electron energy for five of these compounds are presented in Figure 1 with the data normalized to the intensity of m/e 56 = 100. The cyclopropane and the hexenes are shown because they were the only compounds whose low-electron energy spectra approximated the ion-molecule reaction product distribution. The other compounds and the reasons for including them in Figure 1 will be discussed subsequently.

We have previously reported³ that the distribution of products from the reaction of $C_3H_6^+$ with propylene is m/e 55 = 53, m/e 56 = 100, and m/e 69 = 62, normalized in the same fashion as the data of Figure 1, in agreement with the data of several workers who have examined this system. A comparison with Figure 1 suggests that the best fit is obtained with the distribution of ions from 3-hexene fragmentation. The agreement is not exact, but no other of the compounds studied (except for the 2-hexene and the cyclopropane derivative) approached this degree of similarity. The mass spectrum of 3-hexene produced by electron impact by electrons a few volts above the ionization potential is very close to the required distribution. We therefore tentatively conclude that the reaction intermediate may be represented as a quasi-3-hexene structure, although the close similarity of the 2-hexene and 3-hexene low-voltage spectra preclude a clear-cut decision between these isomers.

One can write the following mechanism for the formation of 3-hexene from the reaction of $C_3H_6^+$ with C_3H_6



Reaction 5 is one way of representing the ionized propylene molecule-ion, which is likely formed by removal of one of the π electrons. It is perhaps equally plausible to represent it as a structure with the charge on the terminal carbon, and we represent the ion as indicated above only because the present work provided no evidence for the 2-methylpentene structure for the ion-molecule reaction complex. Reaction 7 yielding the required 3-hexene structure is plausible, since appearance potential measurements indicate that it is the most stable of the linear hexene ions.^{7,8}

Fuchs' results are interesting because he reached the same conclusion⁶ regarding the probable structure of

the $(C_6H_{12}^+)^*$ intermediate despite several incorrect assumptions. While he recognized that a given ion in the secondary spectrum may be produced by several of the primary ions, he nevertheless assigned the total cross section for producing the secondary ion to the primary ion of lowest appearance potential leading to that product ion. Consequently, although $C_4H_7^+$ is produced primarily by $C_3H_5^+$ and only to a lesser extent by $C_3H_6^+$,³ the entire cross section for producing $C_4H_7^+$ was ascribed to the molecule-ion, $C_3H_6^+$, the precursor ion of lowest appearance potential. In addition, rather than comparing low-voltage spectra (which more nearly approximate the energy content of the reaction intermediate) with the product spectrum from his ion-molecule reaction study, he compared them to the spectra of the hexenes at 50 eV. Finally, he made no allowance in his considerations for those reactions which apparently proceed *via* loose complexes.³ He noted that the overall product spectrum exhibits a strong resemblance to the 50-eV mass spectrum of 2- or 3-hexene and concluded that this was the structure of the reaction complex. Although this was a quite logical deduction based upon the data available and even now appears to have been correct, it must be regarded as fortuitous.

We have also included in Figure 1 our spectra of cyclohexane and methylcyclopentane to facilitate comparison with an interesting recent result obtained by Gordon, Doepker, and Ausloos.¹² They reported that, in the photolysis of propylene vapor at 1236 Å, the ion-molecule reaction intermediate, $C_6H_{12}^+$, undergoes an H_2 -transfer reaction with the substrate propylene. It had previously been shown that this reaction occurs only for cycloalkane ions with rings containing at least five carbons.^{13,14} Their logical deduction was therefore that the reaction intermediate must be either the cyclohexane or methylcyclopentane ion. Our results in Figure 1, from which we deduce that the 3-hexene ion is the most probable structure, appear to exclude these cycloalkane structures as the intermediate for the $C_3H_6^+ - C_3H_6$ reaction in the mass spectrometric experiments. It is also of interest to note that neither our results nor those of Gordon, Doepker, and Ausloos support the low-temperature radiation chemical result that 1-hexene is the major dimer product¹⁵ from the propylene molecular ion reaction in radiolysis. In all three cases experimental conditions were necessarily quite different, and it appears that these perturbations alter the nature of the product ultimately formed from the reaction intermediate.

(11) American Petroleum Institute Project No. 44, "Catalog of Mass Spectral Data," Texas A&M University, College Station, Texas.

(12) R. Gordon, R. Doepker, and P. Ausloos, *J. Chem. Phys.*, **44**, 3733 (1966).

(13) P. Ausloos and S. G. Lias, *ibid.*, **43**, 127 (1965).

(14) F. P. Abramson and J. H. Futrell, *J. Phys. Chem.*, **71**, 1233 (1967).

(15) C. D. Wagner, *Tetrahedron*, **14**, 164 (1961).

Electron Paramagnetic Resonance Spectra of the Naphthacene Trianion and the 5,12-Naphthacenequinone Anion Radicals

by Eddie T. Seo,

Physical Research Center, TRW Systems Group, TRW Inc.,
Redondo Beach, California 90278

John M. Fritsch,

Central Research Department, Monsanto Company,
St. Louis, Missouri 63141

and Robert F. Nelson¹

Department of Chemistry, Sacramento State College,
Sacramento, California 95819 (Received September 14, 1967)

Möbius and Plato have reported the electron paramagnetic resonance spectrum of a species obtained by electrochemical reduction of naphthacene in acetonitrile at -2.5 V *vs. sce.*² They have assigned this spectrum to the trianion radical of naphthacene. We, and other workers,³ have observed that this spectrum is obtained with unusual ease, especially in solutions that have not been carefully deoxygenated. This observation and previous experience with the electrochemical reduction of aromatic hydrocarbons led us to suspect that the naphthacene trianion radical was actually the anion radical of 5,12-naphthacenequinone. We have electrochemically generated both the hydrocarbon trianion and quinone anion radicals and recorded their respective spectra.

The epr spectrum obtained from naphthacene under the conditions described by Möbius and Plato and that obtained from 5,12-naphthacenequinone in acetonitrile appear to be identical (Figure 1 and ref 2). We repeated the experiment of Möbius and Plato involving the *in situ* electrolysis of naphthacene in not too carefully deaerated acetonitrile at -2.5 V *vs. sce.* The spectrum obtained was somewhat broadened, but obviously identical with that of Möbius and Plato and with that of the quinone. The quinone spectrum shown in Figure 1 was generated at -1.2 V and the same spectrum persists at -2.5 V because the electrochemical formation of the dianion is also reversible (an appreciable radical concentration is maintained by the dianion-parent radical equilibrium). In Figure 1, the total width of the naphthacenequinone anion spectrum is about 5.2 G with line widths of about 0.17 G. The corresponding values found by Möbius and Plato are 5.3 and 0.195 G. The spectrum can be interpreted, although not essential to the present argument, in terms of the naphthacenequinone anion. The coupling constants are listed in Table I; splittings for the various positions are tentatively assigned with the aid of McLachlan calculations⁴ The lack of any additional outside hyperfine lines and the approximate

Table I: Proton Hyperfine Coupling Constants for the 5,12-Naphthacenequinone Monoanion^a

Positions	Coupling constants, G	
	Exptl	Calcd
2, 3	0.71 ± 0.03	1.06
6, 11	0.71 ± 0.03	0.80
8, 9	0.37 ± 0.02	0.30
1, 4	0.37 ± 0.02	0.23
7, 10	0.37 ± 0.02	0.04

^a Calculated constants were obtained through the McLachlan procedure using $a_H = 23.7\rho c^7$ (M. Karplus and G. K. Fraenkel, *J. Chem. Phys.*, **35**, 1312 (1960)), $\lambda = 1.2$, $\alpha_o = \alpha_c + 1.26\beta_{cc}$, and $\beta_{c-o} = 1.55\beta_{cc}$ (J. Gendell, J. H. Freed, and G. K. Fraenkel, *ibid.*, **37**, 2832 (1962)).

equality of the two large calculated couplings make any other interpretation unlikely.

Protonation of naphthacene dianion in solution to form 5,12-dihydronaphthacene has been proposed recently.⁵⁻⁷ Hoijtink has suggested that the radical obtained by Möbius and Plato may be the monoanion radical of dihydronaphthacene.⁸ In fact, cyclic voltammetry experiments show that naphthacene first undergoes a reversible one-electron reduction step, followed by a second one-electron reduction step which exhibits no reverse anodic peak, even at a scan rate of 1000 V/min.⁹ The electrochemical reduction of 5,12-dihydronaphthacene was, therefore, investigated. The dihydronaphthacene was reducible at -2.2 V *vs. sce.* but *in situ* electrolysis in the epr spectrometer cavity at -2.5 V *vs. sce.* produced no radical species. Therefore, the possibility that the spectrum obtained by Möbius and Plato was due to the 5,12-dihydronaphthacene anion radical seems remote.

The origin of the quinone could be from either or both of two sources. Commercial samples of naphthacene were found to contain small quantities of naphthacenequinone which was probably formed by air oxidation of the hydrocarbon as noted previously.¹⁰ In fact, one can obtain an appreciable signal due to the quinone anion radical by electrolyzing a sample of the hydrocarbon at about -0.9 V. This potential is sufficient to reduce the quinone but not the hydrocarbon. If one then steps the potential to -1.2 V, the relatively weak quinone signal is swamped out by that of the naphthacene anion radical. The quinone reduction could barely be discerned on a cyclic polarogram of naph-

- (1) To whom correspondence should be directed.
- (2) K. Möbius and M. Plato, *Z. Naturforsch.*, **19a**, 1240 (1964).
- (3) W. C. Landgraf, Varian Associates, private communication.
- (4) A. D. McLachlan, *Mol. Phys.*, **3**, 233 (1960).
- (5) N. H. Velthorst and G. J. Hoijtink, *J. Am. Chem. Soc.*, **87**, 4529 (1965).
- (6) N. H. Velthorst and G. J. Hoijtink, *ibid.*, **89**, 209 (1967).
- (7) I. Bergman, "Polarography 1964," Vol. II, G. J. Hills, Ed., Interscience Publishers, Inc., New York, N. Y., 1966, p 925.
- (8) G. J. Hoijtink, *Z. Physik. Chem. (Frankfurt)*, **45**, 248 (1965).
- (9) R. F. Nelson, unpublished data.

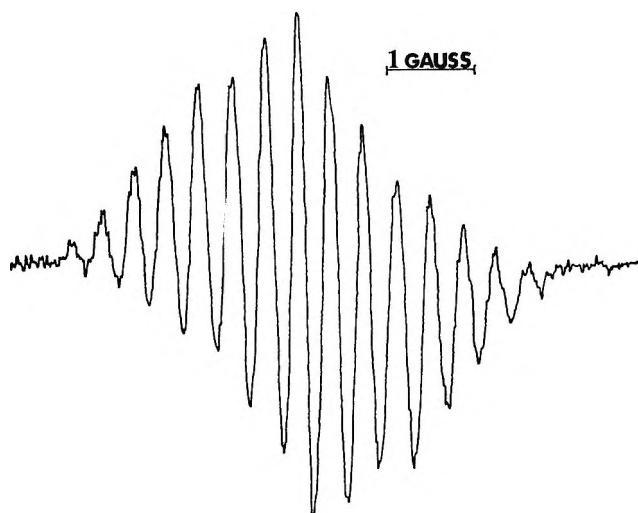


Figure 1. Epr spectrum of the 5,12-naphthacenequinone monoanion in acetonitrile. The radical was generated at -1.2 V vs. sce.

thacene in acetonitrile. However, this wave grew in magnitude when the potential sweep was carried out to a value sufficient for the reduction of the hydrocarbon to its dianion. It appears, therefore, that the quinone is being formed by a chemical reaction which follows the generation of the naphthacene dianion. Both sources are probably contributing to the presence of naphthacenequinone anion radical when one electrolyzes at -2.5 V.

Experimental Section

The 5,12-naphthacenequinone was prepared by oxidizing naphthacene (K and K Laboratories) with peracetic acid.¹⁰ The quinone was chromatographed on neutral alumina with benzene and then recrystallized from benzene. The quinone was also prepared by condensing $\alpha, \alpha', \alpha', \alpha'$ -tetrabromo-*o*-xylene (Aldrich) with 1,4-naphthoquinone (Eastman White Label).¹¹ The 5,12-dihydronaphthacene (Chemical Procurement Laboratories) and the naphthacene (J. Hinton, vacuum sublimed) were used as received.

The electrochemical techniques and instrumentation, as well as the purification procedures for acetonitrile and the supporting electrolyte (tetraethylammonium perchlorate), have been described.¹² The supporting electrolyte concentration was 0.1 *F* in all experiments. The epr spectrometer was a Varian Associates V-4500 with 100-kHz field modulation and Fieldial attachment.

Acknowledgments. The authors wish to thank Professor R. N. Adams of The University of Kansas for his assistance. Much of the reported work was performed in his laboratory. We also wish to thank Mr. Terry A. Miller for discussions and assistance.

(10) A. A. Lamola, W. G. Herkstroetter, J. C. Dalton, and G. S. Hammond, *J. Chem. Phys.*, **42**, 1715 (1965).

(11) M. P. Cava, A. A. Deana, and K. Muth, *J. Am. Chem. Soc.*, **81**, 6418 (1959).

(12) E. T. Seo, R. F. Nelson, J. M. Fritsch, L. S. Marcoux, D. W. Leedy, and R. N. Adams, *ibid.*, **88**, 3498 (1966).

COMMUNICATIONS TO THE EDITOR

Comment on "Electron Paramagnetic Resonance Spectra of the Naphthacene Trianion and the 5,12-Naphthacenequinone Anion Radicals"

Sir: In their paper, Seo, Fritsch, and Nelson¹ have given a reinterpretation of a spectrum which was originally assigned by us to the trinegative ion of naphthacene.² Since the observed spectrum neither shows any hfs lines with a characteristic group formation nor allows a definite determination of the total width due to the insufficient signal-to-noise ratio, any assignment is principally somewhat hypothetical, but lastly, "Hypothesen sind Netze: nur der wird fangen, der auswirft" (NOVALIS).

Nevertheless, we agree with the new interpretation of Seo, *et al.*, as being the most probable one. In addition

to their reasoning, the *g* factor of the radical species in question which we have measured to be $g_{\text{exptl}} = 2.00417$ further confirms their assumption, as *g* factors around 2.004 are typical for quinones.³ For the particular anion radical of 5,12-naphthacenequinone, we have furthermore calculated the theoretical *g* factor by using the linear relationship between the *g* factor and the sum of the spin densities on the oxygen atoms established by Brown.³ His method has been modified for McLachlan type calculations using the MO parameters cited by Seo, *et al.*¹ The result of our calculation is $g_{\text{theoret}} = 2.00408$, which is in good agreement with the

(1) E. T. Seo, J. M. Fritsch, and R. F. Nelson, *J. Phys. Chem.*, **72**, 1829 (1968).

(2) K. Möbius and M. Plato, *Z. Naturforsch.*, **19a**, 1240 (1964).

(3) H. W. Brown in W. Low, "Paramagnetic Resonance," Vol. II, Academic Press, New York, N. Y., 1963, p 704.

measured value. This high a g factor seems to be another argument against Hoijsink's suggestion⁴ that the spectrum in question might be due to the 5,12-dihydronaphthacene mononegative ion.

We would like to present a slightly different hfs analysis of the spectrum of the 5,12-quinone anion radical which appears to be in better agreement both with the observed intensity distribution and with the splitting constants predicted by McLachlan's MO method. Our proposed set of hfs constants is: $a_{2,3} = 1.11$; $a_{6,11} = 0.74$; $a_{8,9} = a_{1,4} = 0.37$; $a_{7,10} < 0.1$ Oe. These values give the following intensity ratios of the 15 lines: 1:4:8:14:22:28:33:36:33, etc. The analysis of Seo, *et al.*, gives 1:6:19:44:81:122:155:168:155, etc., requiring a much higher increase of intensity toward the center of the spectrum than is being observed. Specifically, if we regard the second, third, and fourth outmost lines (the intensity of the first line cannot be determined exactly because of noise) we have the experimental ratios of 1:2:3, whereas the analysis of Seo, *et al.*, would require about 1:3:7. Apart from this discrepancy the achieved signal-to-noise ratio would prohibit the observation of the outmost line in their analysis. Our proposed analysis, however, fits the observed spectrum in all details.

In the course of the electrochemical reduction of naphthacene and at an improved signal-to-noise ratio, one can observe an additional epr spectrum beside that of the 5,12-quinone monoanion. This spectrum has a noticeably higher g factor (2.00464) and consists of a quintet and a subsequent septet splitting, which can be assigned to four equivalent protons and two different pairs of protons with the following respective constants: $a_1 = 2.98$; $a_2 = 0.75$; $a_3 = 0.35$ Oe. The higher g factor indicates that this radical is possibly a further oxidation product of the 5,12-quinone. This assumption seems to be supported by the observation that a considerable increase of the spectrum intensity is obtained on the expense of the 5,12-quinone spectrum by purging oxygen into the solution during the electrochemical reduction process. The fact that the total width (14.10 Oe) of the new spectrum is considerably larger than that of the 5,12-quinone is not necessarily a contradiction to our assumption, since a similar effect has been observed in the case of an oxidation product of anthraquinone.⁵ The specific form of the new radical cannot easily be determined on account of the many possible structures from which even protonated forms cannot be excluded.

If, for instance, protonation has occurred at the 3,14 positions of the 5,12-quinone, the observed hfs splittings and g factor could also be attributed to the keto form of this radical anion, as in this case, neglecting hyperconjugation, the spin density is restricted to a π system identical with that of 1,4-naphthoquinone the epr spectrum of which is well known.⁶ The observed large splitting would have to be assigned to the

four methylene protons on account of hyperconjugative coupling. As $\rho_4 \approx 0.1$,⁶ this assumption leads to the correct order of magnitude for Q_{C-H} .

(4) G. J. Hoijsink, *Z. Phys. Chem. (Frankfurt)*, **45**, 248 (1965).

(5) U. Deffner and E. Brunner, *ibid.*, **51**, 290 (1966).

(6) E. W. Stone and A. H. Maki, *J. Chem. Phys.*, **36**, 1944 (1962).

II. PHYSIKALISCHES INSTITUT
FREIE UNIVERSITÄT BERLIN
BERLIN 33, GERMANY

K. MÖBIUS

AEG-FORSCHUNGSINSTITUT
FRANKFURT(M)-NIEDERRAD, GERMANY

M. PLATO

RECEIVED NOVEMBER 13, 1967

The Complete Macroscopic Characteristic of Isothermal Diffusion in Binary Systems of Neutral Components

Sir: Fick's law gives only one mutual diffusion coefficient D^v , in the volume-fixed frame of reference, if diffusion in a binary system is investigated in the traditional way.¹ Two intrinsic diffusion coefficients, D_1 and D_2 , can be introduced if the flow of the convection-fixed frame of reference is known.^{1,2} Further, two self-diffusion coefficients, D_1^* and D_2^* , can be determined.

Recently,^{3,4} since many experimental results in binary systems are available for discussion,⁵⁻¹¹ the relation among these five coefficients has been widely discussed. In many cases a clear discrepancy between the experimental values and Darken's equation has been observed.^{3,4} To explain this discrepancy, the formation of association polymers was recently assumed.⁴

We discuss diffusion in binary neutral systems by linear nonequilibrium thermodynamics.^{12,13} The flows can be represented in a convection-fixed frame of refer-

(1) J. Crank, "Mathematics of Diffusion," Oxford University Press, Oxford, 1956.

(2) L. S. Darken, *Trans. AIME*, **175**, 184 (1948).

(3) L. E. Trimble, D. Finn, and A. Gosgara, Jr., *Acta Met.*, **13**, 501 (1965).

(4) P. C. Carman, *J. Phys. Chem.*, **71**, 2565 (1967).

(5) D. K. Anderson, J. R. Hall, and A. L. Babb, *ibid.*, **62**, 404 (1958).

(6) R. R. Irani and A. W. Adamson, *ibid.*, **62**, 1517 (1958).

(7) L. Miller and P. C. Carman, *Trans. Faraday Soc.*, **55**, 1831 (1959).

(8) P. C. Carman and L. Miller, *ibid.*, **55**, 1838 (1959).

(9) A. P. Hardt, D. K. Anderson, R. Rathbun, B. W. Mar, and A. L. Babb, *J. Phys. Chem.*, **63**, 2059 (1959).

(10) A. L. Van Geet and A. W. Adamson, *ibid.*, **68**, 238 (1964).

(11) D. W. McCall and D. C. Douglass, *ibid.*, **71**, 987 (1967).

(12) S. R. de Groot and P. Mazur, "Non-equilibrium Thermodynamics," Amsterdam, N. Y., 1962.

(13) R. Haase, "Thermodynamik der Irreversiblen Prozesse," Darmstadt, 1963.

ence as was done in solid alloys^{14,15} and liquid electrolyte solutions.^{16,17}

In a neutral binary system, due to the Onsager relation, the three phenomenological coefficients L_{11} , L_{22} , and L_{12} are independent. They can be expressed by measurable quantities as

$$L_{ii} = \frac{c_i D_i^*}{RT} \quad (i = 1, 2) \quad (1)$$

$$L_{12} = \frac{c(D_{\text{Darken}}^{\vee} - D^{\vee})}{2RT} \frac{d \ln a_1}{d \ln N_1} \quad (2)$$

where

$$D_{\text{Darken}}^{\vee} = (N_2 D_1^* + N_1 D_2^*) \frac{d \ln a_1}{d \ln N_1} \quad (3)$$

and c_i , N_i , and a_i denote molar concentration, molar fraction, and activity, respectively, $c = c_1 + c_2$, R is the universal gas constant, and T is the absolute temperature.

Equation 3 is fulfilled only if the cross coefficient L_{12} , corresponding to the diffusional interaction between both components, is zero. This approximation was indirectly taken into account in Darken's derivation.² Therefore, the discrepancies from eq 3 can appear as a result of a nonvanishing cross coefficient L_{12} without the necessity of attributing it to compound formation. From eq 1, 2, and 3 it can be seen that a complete macroscopic description of diffusion in binary neutral systems requires the knowledge of three independent measurable quantities D^{\vee} , D_1^* , and D_2^* which only under the conditions $L_{12} = 0$ are interrelated by Darken's eq 3. The intrinsic diffusion coefficients D_i can be calculated as

$$D_i = D_i^* \frac{d \ln a_i}{d \ln c_i} + \frac{D^{\vee} - D_{\text{Darken}}^{\vee}}{2(1 - c_i v_i)} \quad (i = 1, 2) \quad (4)$$

where v_i denotes the partial molar volume. Again, only if L_{12} equals zero does the second right-hand-side term vanish and eq 4 simplifies to the form already derived by Darken.² This treatment also enables one to calculate the velocity of the convection-fixed frame of reference. It can also be shown that in the self-diffusion measurements one really measures flows in the convection-fixed frame of reference.

To illustrate the thermodynamic treatment presented above, we show in Figure 1 the three independent phenomenological coefficients as functions of molar fractions for the acetone-chloroform system at 25° for which the discrepancy from Darken's equation was recently discussed on the basis of compound formation.⁴

From Figure 1 it is seen that for the system considered, the cross coefficient L_{12} cannot be neglected. Therefore, Darken's equation (*i.e.*, eq 3) cannot be fulfilled. In other words, the previous discrepancy

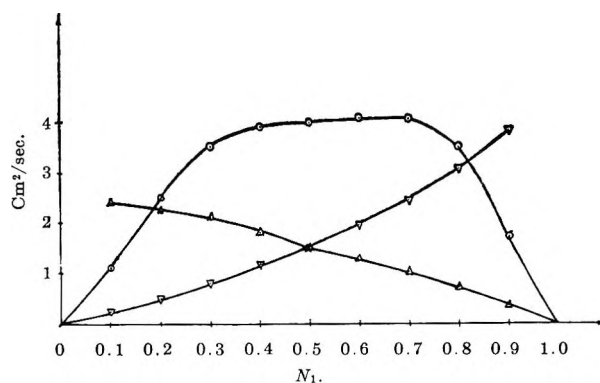


Figure 1. The phenomenological coefficients as a function of molar fraction for the acetone-chloroform system at 25°: ▽, $L_{11}(RT/c) \times 10^5$; △, $L_{22}(RT/c) \times 10^5$; ○, $L_{12}(RT/c) \times 10^5$.

in the discussed system can be explained without any explicit assumption concerning compound formation.

Any binary nonreacting system composed of neutral components can be treated in a similar way, giving the maximum information available from the linear non-equilibrium thermodynamics. The derivation of the present and further relations as well as other applications will be published later.

(14) B. Baranowski and A. S. Cukrowski, *Bull. Acad. Polon. Sci. Ser. Sci. Chim.*, **10**, 135 (1962).

(15) B. Baranowski and A. S. Cukrowski, *Arch. Hutnictwa*, **9**, 31 (1964).

(16) B. Baranowski and A. S. Cukrowski, *Z. Physik. Chem.*, **228**, 292 (1965).

(17) A. S. Cukrowski and B. Baranowski, *ibid.*, in press.

INSTITUTE OF PHYSICAL CHEMISTRY
POLISH ACADEMY OF SCIENCES
WARSAW, POLAND

BOGDAN BARANOWSKI

INSTITUTE OF BASIC
TECHNICAL PROBLEMS
POLISH ACADEMY OF SCIENCES
WARSAW, POLAND

ANDRZEJ S. CUKROWSKI

ACCEPTED AND TRANSMITTED BY THE FARADAY SOCIETY
(NOVEMBER 7, 1967)

Electron Spin Resonance of

Perfluorocyclobutanone Ketyl.

Long-Range Fluorine Coupling

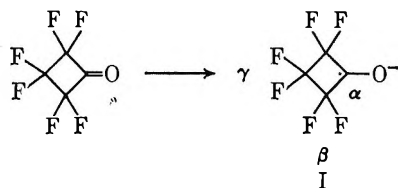
Sir: Recent work on hexafluoroacetone ketyl¹ has been extended to include a study of the ketyl of hexafluorocyclobutanone.² It was hoped that the cyclic

(1) E. G. Janzen and J. L. Gerlock, *J. Phys. Chem.*, **71**, 4577 (1967).

(2) D. C. England, *J. Am. Chem. Soc.*, **83**, 2205 (1961). We are grateful to C. G. Krespan and D. C. England of E. I. DuPont de Nemours and Co. for providing us with a generous sample of hexafluorocyclobutanone.

ketyl might provide information about the angular dependence of the β -fluorine coupling.^{3,4}

Hexafluorocyclobutanone ketyl (I) is obtained by electrolytic reduction in dry, nitrogen purged acetonitrile, at 0.2 V vs. saturated aqueous calomel electrode.⁵



The esr spectrum consists of a major pentet due to four equivalent fluorines, $A^F = 82.9 \pm 0.3$ G, which shows well-resolved second-order splitting. The second-order pentet is split into 1:2:1 triplets by two additional fluorines, $A^F = 37.33 \pm 0.22$ G.^{6a}

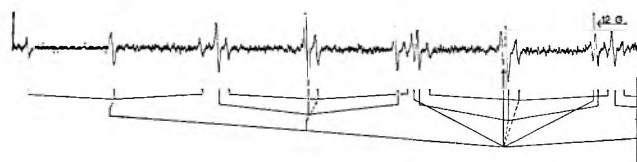
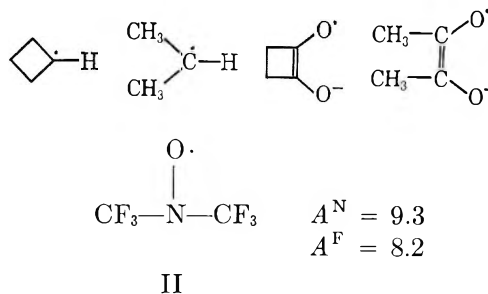


Figure 1. Esr spectrum of hexafluorocyclobutanone ketyl in acetonitrile. The high-field half of the spectrum, center line indicated by arrow, is shown. Scan rate is 10.5 G/min.

Figure 1 shows somewhat more than $3/5$ of the high-field side of the spectrum. The reconstruction was obtained by superimposing a triplet of 37.3 G on the second-order spectrum which in turn was predicted from values given by Fessenden⁷ for four equivalent nuclei ($I = 1/2$).⁸⁻¹⁰ Lines within the second-order multiplets comply with the predicted spacings and intensities.¹¹ (Some variation in intensities exists due to fluctuations in radical concentration.) It should be noted that although second-order splitting in the triplet structure might be anticipated ($[37.3/82.9]^2 \times 2.04 = 0.41$ G), careful inspection of four complete scans of the same spectrum did not reveal evidence for second-order splitting from the two additional fluorines.¹²

The 83-G coupling is assigned to the four β -fluorines and the 37-G coupling to the two γ -fluorines. The second-order splitting found in the perfluorocyclic ketyl established complete equivalence of the β -fluorines, which means the radical must have an essentially planar structure, at least on the esr time scale.¹³ The dihedral angle for the β -fluorines is thus 25–30°. Since the apparent dihedral angle for the freely rotating trifluoromethyl groups in hexafluoroacetone ketyl¹ is 45°¹⁴ where $A^F = 34.7$ G, the magnitude of β -fluorine coupling apparently increases between 30 and 45° as the dihedral angle decreases; *i.e.*, the direction of angular dependence of β -fluorine coupling appears to be the same as found for β -hydrogen coupling. Thus the ratio

of β -fluorine coupling in hexafluorocyclobutanone ketyl to hexafluoroacetone ketyl ($78/33 = 1.82$) is close to the same ratio of β -hydrogen coupling in cyclobutyl¹⁰ and 2-propyl¹⁰ radicals ($36.7/24.7 = 1.47$) and cyclobutane semidione and *cis*-2,3-butane semidione radical anions¹⁵ ($13.9/6.9 = 1.5$).¹⁶⁻¹⁹



(3) β -Hydrogen coupling is dependent on the dihedral angle:⁴ $A^H = B_{op} + (B \cos^2 \theta)p$. The dihedral angle in ketyls is the angle between the β -hydrogen- or fluorine-carbon bond and the p_z orbital of the carbonyl carbon.

(4) H. C. Heller and H. M. McConnell, *J. Chem. Phys.*, **32**, 1535 (1960).

(5) Tetraethylammonium perchlorate was used as supporting electrolyte. The experimental methods have been described in ref 1 and E. G. Janzen and J. L. Gerlock, *J. Am. Chem. Soc.*, **89**, 4902 (1967).

(6) Error is average deviation (a) from 26 measurements, (b) from 15 measurements including six intensity "2" peaks.

(7) R. W. Fessenden, *J. Chem. Phys.*, **37**, 747 (1962).

(8) This procedure gives the correct line positions for similar second-order spectra: *e.g.*, pyracene cation,⁹ ethyl,^{7,10} cyclobutyl,¹⁰ and cyclopentyl¹¹ radicals.

(9) E. DeBoer and E. L. Mackor, *Mol. Phys.*, **5**, 493 (1962).

(10) R. W. Fessenden and R. H. Schuler, *J. Chem. Phys.*, **39**, 2147 (1963).

(11) Lettering the major pentet branches A–E starting from high-field, line positions in gauss from the center line are

A	B	C	D	E
201.21	119.61	37.65	-47.06	-130.23
	115.47	35.45	-50.95	
		31.30		
		0.00		
164.14	82.17	-1.87	-83.79	-167.71
	78.32	-6.22	-87.69	
		-37.52		
126.54	44.69	-39.72	-121.06	-204.19
	40.63	-43.53	-125.17	

(12) Two possibilities arise: (a) second-order splitting in the triplet does not exist, or (b) second-order splitting exists but is not resolved. For case (a) a three-line multiplet with equal line widths and a 1:2:1 intensity ratio is expected; in case (b) normally the center line should be broader than the outer lines and the intensity ratio should approach 1:1:1. The average line width (measured from maximum to minimum of first derivative curve) is 1.23 ± 0.07 G^{6b} with no line width alternation evident. The average peak height ratio (measured from maximum to minimum) is 1:1.94 \pm 0.2:1 from 15 measurements.⁶

(13) The same conclusions were reached with the cyclobutyl radical:¹⁰ $A^H = 21.20$; $A^H = 36.66$; $A^H = 1.12$ G.

(14) E. W. Stone and A. H. Maki, *J. Chem. Phys.*, **37**, 1326 (1962).

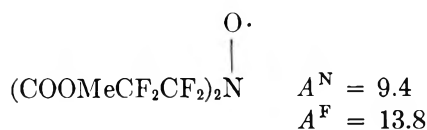
(15) G. A. Russell, E. T. Strom, E. R. Talaty, K. Y. Chang, R. D. Stephens, and M. G. Young, *Rec. Chem. Progr.*, **27**, 3 (1966).

(16) In the following pairs of nitroxides the β -fluorine coupling increases with increased substitution.¹⁷⁻¹⁹

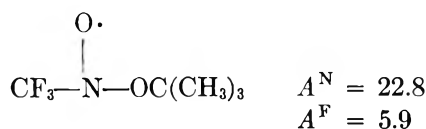
(17) W. D. Blackely and R. R. Reinhard, *J. Am. Chem. Soc.*, **87**, 802 (1965).

(18) E. T. Strom and A. L. Blumh, *Chem. Commun.*, 115 (1966), and private communications with E. T. Strom.

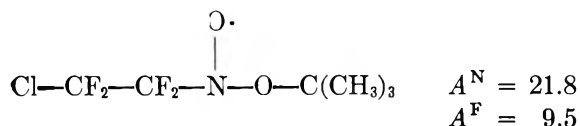
(19) J. L. Gerlock and E. G. Janzen, *J. Am. Chem. Soc.*, in press.



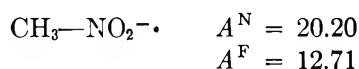
III



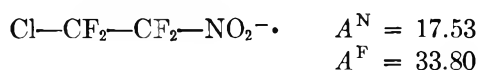
IV



V



VI



VII

Because the dihedral angle for the β -fluorines is greater than 45° in III and V¹² (and VII¹⁸), it has been suggested that maximum fluorine coupling may occur when $\theta = 90^\circ$.¹² Available data in fact suggest that minimum fluorine coupling may occur at some angle between 0 and 90° ; an increase in this angle in either direction may lead to an increase in fluorine coupling.

γ -Fluorine coupling in I is usually large compared to γ -coupling in other radicals; e.g., $A^{\text{H}} = 1.12$ G for cyclobutyl¹⁰ radical and $A^{\text{F}} = 1.88$ G for V.¹⁸ This may be due to p - π interaction between the γ -fluorines and the carbonyl p orbital.²⁰

Although the γ -fluorine coupling observed should be large enough to make second-order coupling detectable, none was found. Rationale for lack of second-order γ -coupling can be found in any mechanism which causes the γ -fluorines not to be completely equivalent. Since the β -fluorines are completely equivalent, the γ -fluorines alone must be experiencing time-dependent perturbations or the γ -fluorine coupling is more sensitive to small perturbations than the β -fluorine coupling. As a source of the perturbation, rapidly exchanging solvent and/or ion complexes or very small planarity fluctuations of the cyclobutane ring²¹ can be suggested. A special case of second-order coupling arises when two nuclei ($I = 1/2$) have equal coupling of opposite sign.⁷ In this case an apparent first order 1:2:1 triplet is predicted. Since an opposite sign for the two γ -fluorine couplings is inconsistent with usual hyperfine

coupling mechanisms, this interpretation seems less probable.

(20) Fluorine p - π interaction has been previously proposed for β -fluorine coupling¹⁸ (P. J. Scheidler and J. R. Bolton, *J. Am. Chem. Soc.*, **88**, 371 (1966)).

(21) The second-order splitting obtained from a cyclic radical having rapidly exchanging conformations is shown in Figure 33, ref 10.

Acknowledgment. This work was supported by AFOSR(SRC)-OAR U. S. A. F. Grant No. 1069-66.

DEPARTMENT OF CHEMISTRY
THE UNIVERSITY OF GEORGIA
ATHENS, GEORGIA 30601

JOHN L. GERLOCK
EDWARD G. JANZEN

RECEIVED DECEMBER 26, 1967

Comments on "Gibbs Equation for Polyelectrolyte Adsorption," by D. K. Chattoraj

Sir: In a recent paper, Chattoraj¹ suggested an equation for the adsorption of polyelectrolytes in the presence of salt with a common ion. His erroneous substitution for the electrochemical potential of individual ions in the Gibbs equation and his definition of surface excess led him to reach incorrect conclusions.

In this criticism we shall constrain ourselves only to the most fundamental points. Equation 2 given by Chattoraj

$$-d\gamma = \Gamma_p d\bar{\mu}_p + \Gamma_{\text{Me}^+} d\bar{\mu}_{\text{Me}^+} + \Gamma_{\text{X}^-} d\bar{\mu}_{\text{X}^-}$$

is correct only if the $\bar{\mu}_i$'s are the respective electrochemical potentials.² In this equation Γ stands for surface excess, $\bar{\mu}$ for the electrochemical potential, and subscripts p , Me^+ and X^- stand for polyelectrolyte, cation, and anion, respectively. For adsorption of polyacids on a polarized surface, the Gibbs equation assumes the form³

$$-d\gamma = \Gamma_p d\mu_p + \Gamma_{\text{X}^-} d\mu_{\text{X}^-} + q dE_{\text{Me}^+} \quad (1)$$

where μ_p and μ_{X^-} are the chemical potentials of the neutral polyelectrolyte and salt, and the surface charge density q divided by the charge of the electron is balanced by the surface excess of the ionic components $\Gamma_{\text{Me}^+} - \Gamma_{\text{X}^-}$ and $-\nu\Gamma_p$; ν is the charge of the polyacid molecule.

For a nonpolarized surface, the last term of eq 1 vanishes leaving an expression which can be obtained directly from Chattoraj's eq 2. However, his eq 3

$$-d\gamma = \Gamma_p \frac{dC_p}{C_p} kT \left[1 + \frac{\Gamma_{\text{Me}^+}}{\Gamma_p} \frac{C_p}{C_{\text{Me}^+}} \frac{dC_{\text{Me}^+}}{dC_p} \right]$$

(1) D. K. Chattoraj, *J. Phys. Chem.*, **70**, 3743 (1966).

(2) R. Parsons and M. A. V. Devanathan, *Trans. Faraday Soc.*, **49**, 404 (1953).

(3) I. R. Miller and A. Katchalsky in "Proceedings of the 4th International Congress on Surface Active Substances," Vol. II, "Physics and Physical Chemistry of Surface Active Substances," J. Th. G. Overbeek, Ed., Gordon and Breach Scientific Publications, New York, N. Y., 1967, p 275.

and his eq 7

$$\frac{-d\gamma}{d \ln C_r} = \Gamma_p kT \left[1 + \frac{\nu^2}{\nu + C_s/C_p} \right]$$

obtained by his erroneous substitution, for the electrochemical potentials, are incorrect. In these equations C designates bulk concentration.

The expressions obtained in ref 3 for the variation of the surface tension with polymer and salt concentration are

$$-\frac{1}{kT} \left(\frac{d\gamma}{d \ln C_p} \right)_{C_s} = \Gamma_p \left(1 + \frac{\nu^2 \phi_p^2 C_p}{\nu \phi_p C_p + C_s} \right) + \Gamma_{X^-} \frac{\nu \phi_p C_p}{C_s + \nu \phi_p C_p} \quad (2)$$

$$-\frac{1}{kT} \left(\frac{d\gamma}{d \ln C_s} \right)_{C_p} = \Gamma_p \frac{\nu \phi_p C_s}{C_s + \nu \phi_p C_p} + \Gamma_{X^-} \left(1 + \frac{C_s}{C_s + \nu \phi_p C_p} \right) \quad (3)$$

where ϕ_p is the osmotic factor of the polyelectrolyte measured in the absence of salt.⁴ In the derivation of eq 2 and 3 the experimentally justified additivity rule⁵ given in eq 4 and 5 was employed for expressing the chemical potentials of the neutral polyelectrolyte and the neutral salt in the mixed polyelectrolyte solution.

$$d\mu_p = kT d \ln C_p (\nu \phi_p C_p + C_s)^{\nu \phi_p} \quad (4)$$

$$d\mu_s = kT d \ln C_s (\nu \phi_p C_p + C_s) \quad (5)$$

In the corresponding expressions for the chemical potentials used by Chattoraj, the important osmotic factor which varies usually between 0.1 and 0.5 is missing. For a salt-free solution eq 7 of Chattoraj reduces to $-d\gamma/d \ln C_p = kT\Gamma(1 + \nu)$, whereas our eq 2 assume the form $-d\gamma/d \ln C_p = kT\Gamma(1 + \phi_p \nu)$. Experimentally, one can never achieve "ideal" polyelectrolyte solutions where the osmotic factors and activity coefficients would approach unity.

The more serious error follows from eq 10 of his paper which postulates $\Gamma_{X^-} > 0$. The Boltzmann distribution presented in Chattoraj's eq 11 and 18 imply proportionality between the concentrations in the bulk and the corresponding surface excess. His replacement of surface excess by surface concentrations excludes the possibility for the surface excess to be negative.

The requirement for $\Gamma_{X^-} < 0$ if X^- is not surface active follows from the Donnan equilibrium which can be written as

$$C_s(C_s + \nu \phi_p C_p) = \left(C_s + \frac{\Gamma_{X^-}}{\delta} \right) \left(C_s + \nu \phi_p C_p + \frac{\Gamma_{X^-} + \nu \phi_p \Gamma_p}{\delta} \right) \quad (6)$$

It is evident from eq 6 that for any arbitrary thickness δ of the surface phase, Γ_{X^-} is negative if Γ_p is positive

and if the osmotic factor in the surface ϕ_p^σ equals that in the bulk.

It will be shown in a forthcoming publication⁶ that the negative surface excess of the co-ion may result in no change of surface tension despite strong polyelectrolyte adsorption.

(4) Z. Alexandrowicz, *J. Polymer Sci.*, **56**, 97 (1962).

(5) Z. Alexandrowicz and A. Katchalsky, *ibid.*, **A1**, 323 (1963).

(6) M. A. Frommer and I. R. Miller, submitted to *J. Phys. Chem.*

POLYMER DEPARTMENT
WEIZMANN INSTITUTE OF SCIENCE
REHOVOTH, ISRAEL

I. R. MILLER

HYDRONAUTICS ISRAEL LTD.
REHOVOTH, ISRAEL

M. A. FROMMER

RECEIVED OCTOBER 11, 1967

Reply to the Comments on "Gibbs Equation for Polyelectrolyte Adsorption"

Sir: Recently, Miller and Frommer¹ have criticized the use of the Gibbs equation (2) in deducing our expression for the kT coefficient in the case of the polyelectrolyte adsorption.² In our treatment for the adsorption of RNa_ν in the presence of $NaCl$, the implicit assumption is that the surface like the bulk behaves as a distinct macrophase. The phase concept of the liquid surface has been discussed by Guggenheim.³ At distribution equilibrium between two such phases, it is legitimate to write³

$$\mu_{RN_{a\nu}}^S = \mu_{RN_{a\nu}} \quad (22)$$

$$\mu_{NaCl}^S = \mu_{NaCl} \quad (23)$$

Here μ_i^S and μ_i stand for the chemical potentials of the i th component in the surface and bulk phases, respectively. As in the case of the nonelectrolytes,^{3,4} we can obtain the Gibbs relation for the present case in the form

$$-d\gamma = d\pi = n_{RN_{a\nu}} d\mu_{RN_{a\nu}} + n_{NaCl} d\mu_{NaCl} \quad (24)$$

Let us now assume that the polyelectrolyte concentration in each phase is ideally dilute and both RNa_ν and $NaCl$ are completely dissociated so that $n_{RN_{a\nu}}$ and n_{NaCl} become equal to n_R and n_{Cl^-} , respectively. Further, the bulk chemical potentials of the electrolytes can be written in the usual forms

$$\mu_{RN_{a\nu}} = \mu_R + \nu \mu_{Na^+} \quad (25)$$

$$\mu_{NaCl} = \mu_{Na^+} + \mu_{Cl^-} \quad (26)$$

(1) I. R. Miller and M. A. Frommer, *J. Phys. Chem.*, **72**, 1834 (1968).

(2) D. K. Chattoraj, *ibid.*, **70**, 3743 (1966).

(3) E. A. Guggenheim, "Thermodynamics," North-Holland Publishing Co., Amsterdam, 1950, pp 46, 345, 367.

(4) J. T. Davies and E. K. Rideal, "Interfacial Phenomena," Academic Press Inc., New York, N. Y., 1961, p 197.

Differentiating (25) and (26) and combining the results with (24) we will obtain (27) after replacing ν by Z .

$$-d\gamma = n_R d\mu_R + (Zn_R + n_{Cl^-}) d\mu_{Na^+} + n_{Cl^-} d\mu_{Cl^-} \quad (27)$$

Combining this equation with relation 8 for the electro-neutrality, we obtain directly eq 2. If we treat the equilibrium between the two phases in this way, the use of the electrochemical potentials for the species concerned seems to be unnecessary.³ In the previous treatments given by Guggenheim,³ Van den Tempel,⁵ and others⁴ on the Gibbs equation for the adsorption of electrolytes at air-water or oil-water interfaces, the use of electrochemical potential is also similarly avoided. However, the Gibbs equation in terms of the electrochemical potentials of the ions, as given by Miller, *et al.*,¹ will also lead to eq 2 if it is properly combined with our eq 8 for the electroneutrality.

Miller and Frommer¹ put extra importance to the negative sign for n_{Cl^-} since the component NaCl or the species Cl^- are really surface deficit quantities. Our another basic assumption is that both the surface and bulk phases are macroscopically electroneutral so that

$$ZC_R + C_{Cl^-} = C_{Na^+} \quad (4)$$

$$ZC_R^S + C_{Cl^-}^S = C_{Na^+}^S \quad (28)$$

Subtracting (4) from (28), we find

$$Z(C_R^S - C_R) + (C_{Cl^-}^S - C_{Cl^-}) = (C_{Na^+}^S - C_{Na^+}) \quad (29)$$

The bracketed terms are the surface excess quantities (per unit volume) and for constant macroscopic thickness of the dilute surface solution, electroneutrality eq 8 remains valid. There is no additional necessity³ of using negative sign for n_{NaCl} or n_{Cl^-} , but if the negative sign for these quantities is used in eq 24, 27, and 29, we will still obtain relation 2. The only difference is that the neglected term $n_{Cl^-} d\mu_{Cl^-}$ becomes negative.

We can, therefore, derive eq 9 without any difficulty, but if n_{Cl^-} in (8) is to be replaced by $-n_{Cl^-}$, from sign consideration, the term $1 - (n_{Cl^-}/n_{Na^+})$ in (9) will become $1 + (n_{Cl^-}/n_{Na^+})$. The kT coefficient will always be given by the relation

$$m' = 1 + \frac{Z^2}{Z + xf(\psi)} \quad (30)$$

Using the Boltzmann equations for the ions, we have initially calculated² $f(\psi)$ to be equal to $1 - e^{-2\epsilon\psi/kT}$. Subsequently using integrated forms of the Boltzmann equation,⁶ the potential function is shown⁷ to be equal to $1 - e^{-\epsilon\psi/2kT}$. Miller and Frommer¹ have, however, opined that

$$\frac{n_{Cl^-}}{n_{Na^+}} = \frac{C_{Cl^-}^S - C_{Cl^-}}{C_{Na^+}^S - C_{Na^+}} = \frac{C}{ZC_R + C} \frac{\frac{C_{Cl^-}^S}{C} - 1}{\frac{C_{Na^+}^S}{C} - 1} \quad (31)$$

so that using again the Boltzmann equation, we find

$$\frac{n_{Cl^-}}{n_{Na^+}} = \frac{C}{ZC_R + C} \frac{e^{-\epsilon\psi/kT} - 1}{e^{\epsilon\psi/kT} - 1} = -\frac{C}{ZC_R + C} e^{-\epsilon\psi/kT} \quad (32)$$

It seems that the negative sign of n_{Cl^-} is involved in (32). Considering this sign also in eq 9, we find $f(\psi)$ is equal to $1 - e^{-\epsilon\psi/kT}$, so that m' will be independent of potential when $\psi > 60$ mV. However, if both the numerator and denominator of the ratio $[(e^{-\epsilon\psi/kT} - 1)dx]/[(e^{\epsilon\psi/kT} - 1)dx]$ in eq 32 are integrated between the limits zero to infinity as before,⁶ n_{Cl^-}/n_{Na^+} will be equal to $-(C/ZC_R + C)e^{-\epsilon\psi/2kT}$ and combining this result with (9), we will again find $f(\psi)$ to be equal to $1 - e^{-\epsilon\psi/2kT}$. Using the integrated form of the Boltzmann equation, the revised value of m' for the adsorption of $R_\nu N_\nu$ in the presence of $X_\nu M_\nu$ is given by (33) instead of (19).

$$m' = 1 + \frac{z - \nu +}{Z_+ \nu_+ + Z_+ \nu_+ x \frac{e^{Z_+ \nu_+ \psi/2kT} + e^{-Z_+ \nu_+ \psi/2kT} - 2}{e^{Z_+ \nu_+ \psi/2kT} - 1}} \quad (33)$$

Let us now examine the proposed Gibbs equation given by Miller and Frommer¹ (see eq 2 of their paper) which according to our own convention assumes the form

$$-d\gamma = n_R \frac{dC_R}{C_R} kT \left[1 + \frac{Z^2 \phi_p^2 C_R}{Z \phi_p C_R + C} + \frac{n_{Cl^-}}{n_R} \frac{Z \phi_p C_R}{Z \phi_p C_R + C} \right] \quad (34)$$

In the absence of NaCl in the surface phase ($n_{Cl^-} = 0$) and putting ϕ_p equal to unity, it will be noticed that the kT coefficient can be expressed by the same equation (7) of ours. Similarly in the presence of both NaCl and RNa_ν in the surface phase, our eq 30 will be obtained from the combination of eq 8 and 34 with the desired forms of the Boltzmann equations for the distribution of sodium and chloride ions.

It is admitted that the Gibbs equation obtained by us is valid for the adsorption of small polyions (*e.g.*, sodium sebacate) and rigid or flexible macro-ions (*e.g.*, proteins, sodium polyacrylate) under a strictly ideal situation. For nonideal solution, it has recently been shown⁸ that

$$m' = \xi \left[1 + \frac{Z^2 \phi}{Z + xf(\psi)} \right] \quad (35)$$

where

$$\xi = 1 + Z \frac{d \ln f_{\pm}}{d \ln C_R} \quad (36)$$

(5) M. Van den Tempel, *Rec. Trav. Chim.*, **72**, 419 (1953).

(6) B. H. Bijsterbosch and H. J. van den Hul, *J. Phys. Chem.*, **71**, 1169 (1967).

(7) D. K. Chattoraj, *ibid.*, **71**, 3709 (1967).

(8) D. K. Chattoraj, *J. Colloid Interface Sci.*, in press.

$$\phi = \frac{1}{\xi} \left(1 + \frac{1}{Z} \frac{d \ln f_{\pm}}{d \ln C_{Na^+}} \right) \quad (37)$$

f_{\pm} stands for the mean activity coefficient. For small ions, the Debye-Hückel expression for f_{\pm} is used for the solution of ξ and ϕ . For the case of long-chain polyelectrolytes, the use of the Katchalsky equation⁹ for the mean activity coefficient has been recommended by us. Even at infinite dilution of the macro-ions, ξ and ϕ may have effective contribution due to the segment-segment interaction and other factors. The nonideality in the equation given by Miller and Frommer is taken care of by the factor ϕ_p .

As pointed out in our paper,² the flexible polyelectrolyte at higher concentration binds a considerable amount of counterions. The extent of such counterion binding in the surface and bulk phases is expected to be significantly different. Neither our equation nor that given by Miller, *et al.*, can take full account of this complex situation. The applicability of the Gibbs equation for such a case will be discussed in our subsequent calculation.

(9) J. Bockris, Ed., "Modern Aspects of Electrochemistry," Butterworth and Co., Inc., Washington, D. C., 1954, pp 18-20.

CHEMISTRY DEPARTMENT
JADAVPUR UNIVERSITY
CALCUTTA 32, INDIA

D. K. CHATTORAJ

RECEIVED NOVEMBER 27, 1967

Hydrogen-Bonded Dimers and the 2.86- μ Band in Alcohols

Sir: Fletcher and Heller¹ have recently reported evidence for only monomers and two tetramers (linear and cyclic) when 1-octanol self-associates in *n*-decane. A major point of their paper is an admonition against making *a priori* decisions as to the stoichiometry of the self-association and designing the mathematical analysis for this stoichiometry. These authors found a plot of absorbance at 1.405 μ (7117 cm^{-1}) (free OH stretching overtone) *vs.* absorbance at 1.528 μ (6544 cm^{-1}) to be linear over a wide range of temperature and concentration showing that the 1.528- μ band is not due to an OH...OH dimer. Taking the 1.528- μ band as an overtone of the 2.86- μ band customarily assigned to dimers² casts doubt on the reliability of work where the 2.86- μ band furnished the major evidence that dimerization was occurring. We concur in the admonition of Fletcher and Heller on the dangers of *a priori* assignments of association stoichiometry. In addition, it seems clear that the 1.528- μ band in the 1-octanol-*n*-decane system is not due to an OH...OH dimer. However, the assignment of the 1.528- μ band as an overtone of a 2.86- μ band might possibly be in error, and the apparent absence of dimer in the 1-

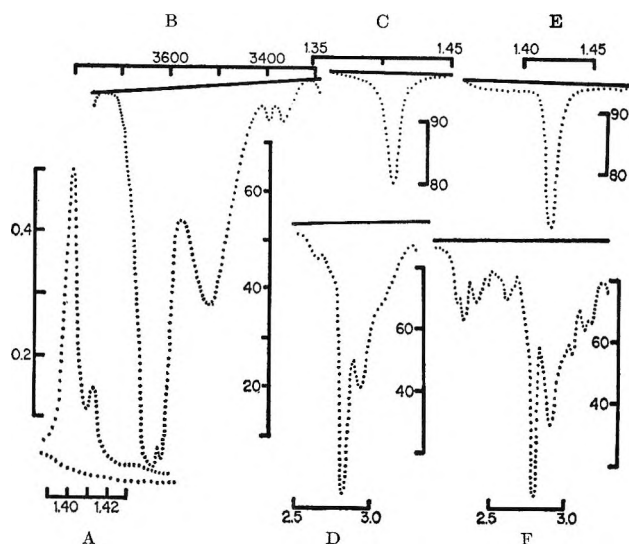


Figure 1. Spectra of free OH stretching overtone bands near 7100 cm^{-1} and OH stretching fundamental bands near 3500 cm^{-1} (2.86 μ) for the three systems methanol (MeOH), *t*-butanol (*t*-BuOH), and di-*t*-butylcarbinol (DTBC) in carbon tetrachloride solution. All spectra were recorded as per cent transmission (except DTBC band near 7100 as absorbance) *vs.* linear wavelength (except DTBC band near 3500 cm^{-1} as linear cm^{-1}) using the following instruments: MeOH and *t*-BuOH, 7100- cm^{-1} bands on Beckman DK-2, 3500- cm^{-1} bands on Baird 4-55; DTBC, 7100- cm^{-1} band on Cary 14R, 3500 cm^{-1} band on Perkin-Elmer 221PG. Additional details of the individual spectra are: A, DTBC 0.073 *m*, 10°, 2.0-cm quartz cell; B, DTBC 0.073 *m*, 10°, 1.0-cm quartz cell; C, MeOH 0.049 *M*, 25°, 1.0-cm quartz cell; D, MeOH 0.049 *M*, 25°, 1.1-cm rock salt cell; E, *t*-BuOH 0.063 *M*, 25°, 1.0-cm quartz cell; F, *t*-BuOH 0.063 *M*, 25°, 1.1-cm rock salt cell. The solvent *vs.* solvent curves are shown as solid lines (dotted for A). For D and F alternate calculations using a corrected background obtained by assuming the free OH stretching band near 3650 cm^{-1} to be symmetrical gave the same conclusions as shown in Table II. For A, the small peak at lower frequency ($\sim 1.41 \mu$) is always present in DTBC and its absorbance relative to the main peak is unaltered over a 40° temperature range.

octanol-*n*-decane system might not result for other alcohols in other solvents.

Table I lists the absorbance per unit path length (cm^{-1}) for the free OH stretching overtone band near 7100 cm^{-1} and the OH stretching fundamental near 3500 cm^{-1} (2.86 μ) for the three systems methanol (MeOH), *t*-butanol (*t*-BuOH), di-*t*-butylcarbinol (DTBC)- CCl_4 at several temperatures. Figure 1 shows representative spectra. Plots of absorbance near 7100 cm^{-1} *vs.* absorbance near 3500 cm^{-1} give parabolic curves consistent with dimerization in all cases. For methanol and *t*-butanol the situation is complicated by a band at 3350 cm^{-1} which appears at the higher concentrations in Table I and overlaps the 3500- cm^{-1} band. In the 7100- cm^{-1} region there are no overlap difficulties for any of the alcohols. For

- (1) A. N. Fletcher and C. Heller, *J. Phys. Chem.*, **71**, 3742 (1967).
- (2) U. Liddell and E. D. Becker, *Spectrochim. Acta*, **10**, 70 (1957).

Table I: Absorbance per Unit Path Length for 7100- and 3500-Cm⁻¹ Bands

Concn. ^a <i>M</i>	<i>A</i> ₇₁₀₀ , cm ⁻¹ ^b			<i>A</i> ₃₅₀₀ , cm ⁻¹ ^c		
	11°	25°	56°	11°	25°	56°
	MeOH-CCl ₄					
0.020	0.03793			0.08941		
0.025	0.04683	0.04635		0.1353	0.1045	
0.049	0.08884	0.08884		0.4291 ^d	0.3212	
0.074	0.1203	0.1316	0.1230	0.8518 ^d	0.7346 ^d	0.4337
0.098		0.1599	0.1632		1.104 ^d	0.6917
0.147			0.2313			1.399 ^d
	<i>t</i> -BuOH-CCl ₄					
0.021	0.04357	0.04333		0.08197	0.05621	
0.032	0.06434	0.06385	0.06198	0.1707	0.1208	0.05586
0.042	0.08493	0.08493	0.08243	0.2804	0.1989	0.1150
0.063	0.1219	0.1248	0.1219	0.6402 ^d	0.4188	0.2412
0.105		0.1970	0.1970		1.074 ^d	0.6455
0.210			0.3613			2.008 ^d
	DTBC-CCl ₄					
Concn. <i>m</i>	10°	20°		10°	20°	
0.042	0.136	0.137		0.1225	0.106	
0.053	0.171	0.173		0.174	0.165	
0.054	0.173	0.175		0.193	0.171	
0.063	0.203	0.206		0.276	0.256	
0.073	0.234	0.237		0.336	0.284	
0.078	0.252	0.255		0.375	0.350	
0.089	0.285	0.289		0.485	0.428	
0.105	0.338	0.341		0.682	0.631	

^a The concentrations for MeOH and *t*-BuOH are given for 25°. Multiplication of these concentrations by 1.017 and 0.9617 will give concentrations at 11 and 56°, respectively. ^b The measurements for MeOH and *t*-BuOH were made in 10- and 1-cm cells. For DTBC, 2- and 5-cm cells were used at 10 and 20°, respectively. ^c The measurements for MeOH and *t*-BuOH were made in 1.10-, 0.935-, and 0.0772-cm cells. For DTBC, a 1-cm cell was used. ^d Cases where 3350-cm⁻¹ band appears to overlap 3500-cm⁻¹ band.

DTBC no new bands occur in the fundamental OH stretching region up to 3.0 *m* since steric factors cause the self-association to terminate at the species responsible for the 3500-cm⁻¹ band.³ The 3651-cm⁻¹ free OH band and the 3523-cm⁻¹ band for DTBC do not overlap at the concentrations in Table I. Complete deuteration of the OH group in DTBC reveals no absorbance other than OH stretching in the region 3700–3300 cm⁻¹. There seems to be little chance that the DTBC absorbance values in Table I are in error due to unrecognized contributions in addition to the OH-containing species responsible for the band.

The constancy of A_{3500}/A_{7100}^n with changing concentration for a particular value of *n* identifies the stoichiometry between the species causing the 7100- and 3500-cm⁻¹ bands since A_{3500}/A_{7100}^n is proportional to the overall equilibrium constant, K_n , for $nM \rightleftharpoons Mn$ (if several structures for *Mn* occur, K_n is the sum of the K 's for the individual structures). Table II lists the average value of A_{3500}/A_{7100}^n over the concentrations in Table I for $n = 1, 2, 3$ as well as the 90% confidence probable error in this average⁴ and the percentage of the average given by the 90% confidence probable error. The criterion of this percentage as a minimum assigns the 3500-cm⁻¹ band to a dimer in each case.⁵

Two factors which could conceivably affect the constancy of A_{3500}/A_{7100}^n sufficiently to cause an erroneous

(3) L. K. Patterson and R. M. Hammaker, *Spectrochim. Acta*, **23**, 2333 (1967).

(4) H. A. Laitinen, "Chemical Analysis," McGraw-Hill Book Co., Inc., New York, N. Y., 1960, pp 546, 547.

(5) Since dimerization is strongly indicated, it is tempting to use A_{3500}/A_{7100}^n values in Table II to calculate ΔH° for dimer formation. This calculation assumes that the absorption coefficients for all bands are temperature independent so that a $\ln K$ vs. $1/T$ plot is faithfully reproduced by a $\ln (A_{3500}/A_{7100}^n)$ vs. $1/T$ plot. However, the data for these systems indicate that this assumption is not justified and that ΔH° deduced from a $\ln (A_{3500}/A_{7100}^n)$ vs. $1/T$ plot may be seriously in error.

Measurements in dilute solution where there is no band near 3500 cm⁻¹ (2.86 μ) show that the absorption coefficients of the bands in the 7100-cm⁻¹ region for all three alcohols decrease with increasing temperature after correction for the variation of solution density with temperature. Absorption coefficients for the 3500-cm⁻¹ region bands, although not directly measurable, can be obtained either by a least-squares technique (ref 3) or using a dimer concentration estimated by subtraction of the monomer concentration calculated from the 7100-cm⁻¹ band absorbance and the absorption coefficient for the 7100-cm⁻¹ band (measured in dilute solution where there is no band near 3500 cm⁻¹) from the stoichiometric alcohol concentration. In any case, the dimer absorption coefficient increases with increasing temperature. Unfortunately, the precision of these determinations often leaves something to be desired. However, these temperature variations of absorption coefficients are capable of changing ΔH° by more than a factor of 2 from the result of a $\ln (A_{3500}/A_{7100}^n)$ vs. $1/T$ plot. (The values in Table II give $\Delta H^\circ = -3.3, -4.0,$ and -2.1 for MeOH, *t*-BuOH, and DTBC, respectively. Introduction of the temperature dependence of the absorption coefficient changes ΔH° to $-7.1, -6.5,$ and -3.8 for MeOH, *t*-BuOH, and DTBC, respectively. All values are in kcal/mole.)

Table II: Average Values for A_{3500}/A_{7100}

	MeOH-CCl ₄								
	11°			25°			56°		
	<i>n</i> = 1	<i>n</i> = 2	<i>n</i> = 3	<i>n</i> = 1	<i>n</i> = 2	<i>n</i> = 3	<i>n</i> = 1	<i>n</i> = 2	<i>n</i> = 3
Average value for A_{3500}/A_{7100}	4.29	59.3	1014	4.59	43.7	525	4.60	26.9	168
Probable error ^a	2.28	3.64	564	2.10	3.5	366	1.79	2.1	82
(PE/AVG) ^b × 100%	51	6	56	46	8	70	39	8	49

	<i>t</i> -BuOH-CCl ₄								
	11°			25°			56°		
	<i>n</i> = 1	<i>n</i> = 2	<i>n</i> = 3	<i>n</i> = 1	<i>n</i> = 2	<i>n</i> = 3	<i>n</i> = 1	<i>n</i> = 2	<i>n</i> = 3
Average value for A_{3500}/A_{7100}	3.27	41.6	611	2.87	28.2	367	2.62	15.9	140
Probable error ^a	1.70	2.4	329	1.55	1.3	208	1.78	0.9	77
(PE/AVG) ^b × 100%	52	6	54	54	5	57	68	6	55

	DTBC-CCl ₄					
	10°			20°		
	<i>n</i> = 1	<i>n</i> = 2	<i>n</i> = 3	<i>n</i> = 1	<i>n</i> = 2	<i>n</i> = 3
Average value for A_{3500}/A_{7100}	1.38	6.21	30.2	1.23	5.46	26.3
Probable error ^a	0.37	0.33	10.2	0.21	0.19	5.4
(PE/AVG) ^b × 100%	27	5	34	17	4	20

^a Calculated at the 90% confidence level. ^b Probable error/average.

choice of *n* are activity coefficients and contributions to the monomer band by the free end groups of linear associated species. The low concentrations of alcohol and the small percentage of total alcohol present as the species causing the 3500 cm⁻¹ make interference from these sources seem unlikely.

The work of Fletcher and Heller serves as a warning that the assignment of the 3500-cm⁻¹ (2.86-μ) band should be carefully considered for each system studied. However, it appears that an OH···OH dimer (cyclic or linear or both) is responsible for the 3500-cm⁻¹ (2.86-μ) band for the systems treated here

Acknowledgments. R. M. C. and S. L. R. acknowledge the support of the NSF Undergraduate Research Participation Program, and P. E. R. acknowledges the support of an NSF Summer Fellowship for Teaching Assistants.

DEPARTMENT OF CHEMISTRY
KANSAS STATE UNIVERSITY
MANHATTAN, KANSAS 66502

R. M. HAMMAKER
ROBERT M. CLEGG
LARRY K. PATTERSON
PAUL E. RIDER
STEVEN L. ROCK

RECEIVED DECEMBER 18, 1967

The Alcohol Self-Association Dimer and the Absorption Band(s) near 1.53 μm

Sir: The communication of Hammaker, *et al.*,¹ is the first direct evidence of a second-order relationship between an alcohol monomer absorption band and the

2.86-μm band. We have made a similar evaluation for methanol in carbon tetrachloride and collaborate the findings of Hammaker, *et al.* (curve AA in Figure 1). The evidence now clearly indicates that the 2.86-μm (2.82 μm for methanol in CCl₄) band is indeed due to the self-association dimer. These results would then suggest that the first-overtone region between the monomer and the cyclic tetramer bands should also show a second-order relationship for methanol in carbon tetrachloride in contrast to the first-order relationship that we found for 1-octanol in *n*-decane.²

In Figure 2 it can be seen that for methanol in carbon tetrachloride, two definite peaks can be found near 1.53 μm, one at 1.515 and the other at 1.535 μm. The relative absorbance of these two peaks remains constant and they show a first-order relationship (curve CC in Figure 1) to the monomer absorbance independent of temperature when measured in the same manner as our previous paper.² When measured from the zero absorbance line (curve BB, Figure 2), an approximate first-order relationship is seen until the tetramer becomes predominant. Even with dimer absorbance per unit length as high as 1.0 cm⁻¹ in the fundamental, the formation of a measurable second-order peak in the first-overtone region is not observed. We thus conclude that the 1.53-μm band(s) is not an overtone of the 2.86-μm band. It is also not due to an alcohol-solvent interaction as its wavelength is no

(1) R. M. Hammaker, R. M. Clegg, L. K. Patterson, P. E. Rider, and S. L. Rock, *J. Phys. Chem.*, **72**, 1837 (1968).

(2) A. N. Fletcher and C. A. Heller, *ibid.*, **71**, 3742 (1967).

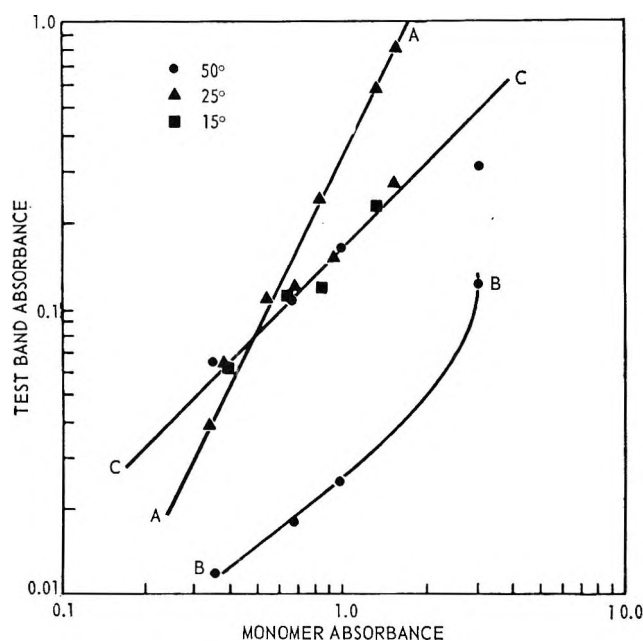


Figure 1. Absorption characteristics of test bands for methanol in carbon tetrachloride. Curve AA: concentration from 0.017 to 0.1 M , 1-cm cell, test absorbance measured at 2.82- μm peak, monomer band was $1/10$ of indicated absorbance value, line is second order. Curve BB: concentration from 0.05 to 0.4 M , 5-cm cell, test absorbance at 1.535 μm peak measured from zero absorbance line. Curve CC: concentration from 0.05 to 0.4 M , 5-cm cell, test absorbance at 1.535- μm peak measured from absorbance at 1.57 μm , line is first order. Monomer measured from 1.41- μm peak to zero absorbance line for all three curves with carbon tetrachloride in reference cell. Measurements were performed on a Beckman DK-2.

more dependent upon the solvent than is the monomer band (curves AA-CC in Figure 2).

In light of the present evidence we believe that the absorption bands near 1.53 μm for methanol are due to combination bands of the O-H and C-H fundamental stretching modes. Combination of the two fundamental C-H stretching modes at 3.37 and 3.48 μm with the O-H at 2.75 μm results in

$$2967 + 3636 = 6603 \text{ cm}^{-1} (1.512 \mu\text{m}) \quad (1)$$

$$2873 + 3633 = 6506 \text{ cm}^{-1} (1.536 \mu\text{m}) \quad (2)$$

which correspond exactly to the observed wavelengths for methanol within the wavelength accuracy of the Beckman DK-2.

It thus appears that in our previous study of the first overtone we could not have detected a dimer band (assuming these results for methanol in carbon tetrachloride are directly relatable to 1-octanol in n -decane). The major question is whether the dimer exists in quantities sufficient to affect material-balance equations. This point is essential since studies for the determination of tetramer equilibrium quotients would be affected if significant quantities of the dimer

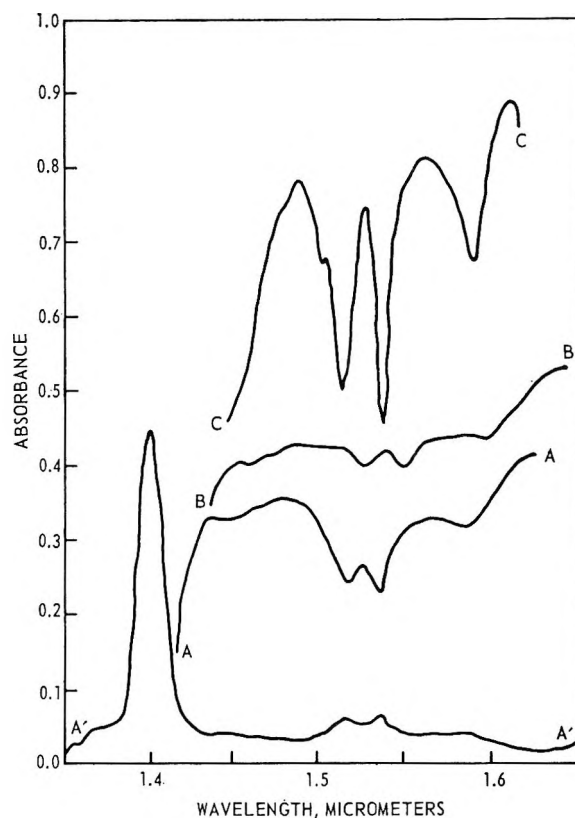


Figure 2. Absorption characteristics of methanol near 1.53 μm . Curve A'A': methanol in n -decane at 60°, 5-cm cell, 0-1 absorbance scale. Curve AA: methanol in n -decane at 60°, 5-cm cell, 75-125% transmission scale. Curve BB: 0.25 M methanol in toluene at 30°, 1-cm cell, 75-125% transmission scale. Curve CC: 0.16 M methanol in carbon tetrachloride at 50°, 5-cm cell, 90-100% transmission scale. All temperatures are nominal and all spectra were obtained with the corresponding solvent and cell in the reference beam.

are present. An answer to this question can be found in the experimental results of Hammaker, *et al.*

At low concentrations where the monomer is the predominant species, the apparent molar absorptivity, E_1 , is equal to the real molar absorptivity, ϵ_1

$$E_1 = A_1/C_0 \quad (3)$$

$$E_1 = \epsilon_1 \quad (C_0 = C_1) \quad (4)$$

A_1 is the monomer absorbance per unit length, C_0 is the total molar concentration of added alcohol, and C_1 is the monomer concentration. At high alcohol concentrations, eq 4 will no longer be valid due to the presence of self-association polymers. Thus a decrease in E_1 with increasing alcohol concentrations indicates the region where the polymer buildup is sufficient to affect the material-balance equations, *i.e.*, where $C_1 \neq C_0$. The data of Hammaker, *et al.*, for methanol and *t*-butanol show a decrease in the apparent molar absorptivity *only* at the concentrations where they indicate possible interference with the dimer absorbance by the higher-order polymer peak. Consequently,

Table I: Calculation of the Molar Absorptivity of the Monomer of Di-*t*-butyl Carbinol in Carbon Tetrachloride at 20°

Concn			Monomer molar absorptivities	
Total alcohol <i>m</i>	<i>M</i>	Dimer ^a <i>M</i>	ϵ_1 , uncor ^b	ϵ_1 , cor ^c
0.042	0.0665	0.0004	2.06	2.09
0.053	0.0839	0.0006	2.06	2.09
0.054	0.0854	0.0007	2.05	2.07
0.063	0.0995	0.0010	2.07	2.11
0.073	0.115	0.0012	2.07	2.10
0.078	0.123	0.0014	2.08	2.13
0.089	0.140	0.0018	2.07	2.11
0.105	0.165	0.0026	2.07	2.13
			Av 2.07 ±	2.10 ±
			0.01	0.02

^a Calculated from the absorbance at 3500 cm⁻¹ given by Hammaker, *et al.*,¹ using the molar absorptivity reported by Patterson and Hammaker.³ ^b Using the absorbance values reported by Hammaker, *et al.*, divided by the total molar concentration of the alcohol. ^c Using the absorbance values reported by Hammaker, *et al.*, divided by the total molar concentration of the alcohol less twice the molar concentration of the dimer.

these data do not show any evidence that the dimer is in sufficient concentration so as to affect the material-balance equation in spite of the high absorbance values found for the dimer at 2.86 μm. Their data for di-*t*-butyl carbinol (DTBC) are even more conclusive since the tetramer is not formed with this compound due to steric hindrance. We have evaluated their data in Table I. Even with absorbance per unit length values as high as 0.6, their data show no change in ϵ_1 . With DTBC it is possible to calculate the dimer concentration either directly by the equilibrium quotient or through the use of molar absorptivities reported by Patterson and Hammaker.³ Using the dimer concentration "correction" causes a perceivable trend in the molar absorptivity in Table I which suggests that the dimer equilibrium quotient of Patterson and Hammaker is too large.

A probable source of error in the calculated dimer concentrations is indicated by the molar absorptivity of DTBC being a function of the temperature.¹ Swenson⁴ has presented very convincing evidence that deviations of the molar absorptivity with temperature are due to appreciable amounts of the alcohol existing in the head space above the solution. This causes the calculated concentrations to be too high. These concentration errors would affect the dimer equilibrium study of DTBC performed by Patterson and Hammaker and could explain erroneous equilibrium quotients and molar absorptivities.

Since the molar absorptivity should not change with temperature,^{4,6} the "corrections" to ΔH performed by Hammaker, *et al.*, should not be made. We consider that the "uncorrected" ΔH values are correct. Since

these $-\Delta H$ values are below 5 kcal/mole,^{2,6} we interpret them as indicating that the dimer is acyclic (linear) with a single hydrogen bond.

The present evidence now supports the following facts about alcohol self-association. (1) The tetramer is the predominant polymer for unhindered alcohols.² (2) An acyclic dimer can be seen at 2.86 μm (3500 cm⁻¹),¹ but its concentration is sufficiently low so that it can usually be ignored in material-balance equations. (3) The dimer overtone band is not readily seen. (4) The alcohol band(s) near 1.53 μm (6536 cm⁻¹) are due to a combination of O-H and C-H stretch modes of the monomer.

(3) L. K. Patterson and R. M. Hammaker, *Spectrochim. Acta*, **23A**, 2333 (1967).

(4) C. A. Swenson, *J. Phys. Chem.*, **71**, 3108 (1967).

(5) K. H. Illinger and D. E. Freeman, *J. Mol. Spectry.*, **9**, 191 (1962).

(6) H. C. Van Ness, J. Van Winkle, H. H. Richtol, and H. B. Hollinger, *J. Phys. Chem.*, **71**, 1483 (1967).

CHEMISTRY DIVISION
RESEARCH DEPARTMENT
NAVAL WEAPONS CENTER
CHINA LAKE, CALIFORNIA 93555

AARON N. FLETCHER
CARL A. HELLER

RECEIVED JANUARY 22, 1968

A Criticism of the Term "Hydrophobic Bond"

Sir: The term "hydrophobic bond,"¹ that has come into use in the literature of polymers, seems to me to be inappropriate for two reasons. One, the alkyl groups of two polymer chains are not forced together by phobia for water. Dupré,² as long ago as 1869, pointed out that the excess of the sum of the surface tensions of two immiscible liquids over their interfacial tension is a measure of their work of adhesion: $W = \gamma_1 + \gamma_2 - \gamma_{1,2}$. Harkins and Cheng,³ in 1921, revived this concept and published values for adhesion between water and a number of other liquids. In the case of water and octane, for example, they give $W = 72.80 + 21.77 - 50.81 = 43.76$ ergs cm⁻². Furthermore, the energy of evaporating a mole of *n*-butane from its solution at 1 atm and 25° is 5.46 kcal, greater than it is from its own pure liquid at the boiling point,⁴ 4.81 kcal. This represents attraction, not phobia. Ice is wet by octane. The fact that octane is nearly insoluble in water is merely the result of the fact that this attraction is not strong enough to penetrate the high cohesion of water.

(1) For a clear statement of the term, see G. Némethy and H. A. Scheraga, *J. Phys. Chem.*, **66**, 1773 (1962).

(2) A. Dupré, "Theorie Mechanique de la Chaleur," Paris, 1869, p 1869.

(3) W. D. Harkins and Y. C. Cheng, *J. Am. Chem. Soc.*, **43**, 35 (1921).

(4) Data from a paper on solutions of inert gases in water, to be published in Debye Memorial number of *J. Amer. Chem. Soc.*

The noun, bond, seems likewise inappropriate because the attraction between the alkyl groups of two polymer chains has none of the characteristics that distinguish chemical bonds from van der Waals forces. Any "simple multiple proportions" between such groups result from regularities in the structures of the two chains, not from any valence forces between alkyl groups. The alkyl chains in micelles of soap are not bonded together by phobia for surrounding water; they stick together just as strongly in absence of water.

Major workers in this field are surely well aware of the fact that there is no true bond between alkyl groups of adjacent polymer chains, and are moreover competent to calculate the thermodynamic quantities involved in the interaction between such chains; why, then, should a terminology continue in use that misleads some into thinking that the "hydrophobic bond" represents a special concept that must be mastered in order to deal with these systems? Why not speak simply of alkyl interaction free energy, energy, or entropy? I do not find it necessary to invent "fluorophobic bonds" in order to handle the thermodynamics of the limited solubility of heptane in perfluorohexane.

I thank Némethy, Scheraga, and Kautzmann for kindly replying in some detail to my request for their views on this matter. However, I do not agree with their statement that "... hydrocarbons actually prefer a nonpolar environment to being surrounded by water." I say rather that molecules of water "prefer" to be hydrogen-bonded together rather than separate to admit alkanes. In order for these to dissolve, a large amount of water must be present per mole of alkane in order to supply sufficient entropy to offset the unfavorable balance of *attractive* energies.

Gilbert Lewis during a seminar responded to a graduate student who had contradicted him saying, "That is an impertinent remark, but it is also pertinent." It is in the latter sense only that I offer the above criticism.

DEPARTMENT OF CHEMISTRY
UNIVERSITY OF CALIFORNIA
BERKELEY, CALIFORNIA 94720

JOEL H. HILDEBRAND

RECEIVED JANUARY 18, 1968

Comments on the Communication "A Criticism of the Term 'Hydrophobic Bond'"

by Joel H. Hildebrand

Sir: Hildebrand's discussion¹ of the nature of the forces of interaction governing the solubility of hydrocarbons is incomplete. It is certainly true, as he states, that van der Waals interactions in themselves are on the balance favorable between the two sub-

stances, and that they therefore would actually favor mixing. As it was noted repeatedly before,²⁻⁴ this is indicated by a direct calculation of the relevant energies of interaction, just as it is shown by the data cited by Hildebrand.¹ However, the net free energy of solution, which determines solubility, is dominated by a large negative, *i.e.*, unfavorable excess entropy term.²⁻⁵ It has been shown²⁻⁵ that this entropy term arises owing to changes in the state of water and has to be attributed to increased ordering of water molecules, *i.e.*, to an increase in hydrogen bonding. As a result, in spite of the favorable interaction energies, the free energy of solution is positive. This can be expressed by saying that, in over-all terms, *i.e.*, in ΔF° , hydrocarbons actually prefer a nonpolar environment to being surrounded by water. This is implied in the use of the adjective "hydrophobic."

Because the source of immiscibility is an entropy factor, the water-hydrocarbon system differs qualitatively, and in a unique manner from most systems of low miscibility. Thus the interactions in this system do represent a special concept.

We do not wish to argue about the matter of nomenclature. However, it should be pointed out that the criticism of the use of the term "bond" in the present context, where it does not refer to a chemical bond but to a loose association, has been recognized repeatedly by various workers in the past, too. Nevertheless, the term "hydrophobic bond" has proven to be useful as shown by its frequent occurrence in recent physical, chemical, and biochemical nomenclature.

- (1) J. H. Hildebrand, *J. Phys. Chem.*, **72**, 1841 (1968).
- (2) W. Kautzmann, *Advan. Protein Chem.*, **14**, 1 (1959).
- (3) G. Némethy and H. A. Scheraga, *J. Phys. Chem.*, **66**, 1773 (1962).
- (4) G. Némethy, *Angew. Chem., Int. Ed.*, **6**, 195 (1967).
- (5) H. S. Frank and M. J. Evans, *J. Chem. Phys.*, **13**, 507 (1945).

THE ROCKEFELLER UNIVERSITY
NEW YORK, NEW YORK 10021

GEORGE NÉMETHY

DEPARTMENT OF CHEMISTRY
CORNELL UNIVERSITY
ITHACA, NEW YORK 14850

HAROLD A. SCHERAGA

DEPARTMENT OF CHEMISTRY
PRINCETON UNIVERSITY
PRINCETON, NEW JERSEY 08540

WALTER KAUTZMANN

RECEIVED FEBRUARY 17, 1968

The Internal Pressure of Simple Liquids

Sir: Any general theory of the liquid state must involve expressions for the interaction potentials between the molecules, thermal energy, and volume. Much progress is being made in this field, but the expressions obtained are generally complex and difficult to handle. For many purposes it is, therefore,

convenient to employ simpler, semiempirical models which can provide a useful description of experimental results together with some insight into molecular processes.

One such group of theories which is being found increasingly useful in describing the properties of liquids such as viscosity and PVT properties is those associated with the concept of free volume. Recently,¹ it has been found possible to combine together some free-volume concepts with the van der Waals equation to provide certain relations applicable to PVT behavior at low or moderate volumes. Naturally these relations give slightly different results to those obtained by other treatments, so that it is of interest to consider them in relation to the most discriminating experimental data.

It now appears that some suitable results are provided by the work of Bianchi, *et al.*,² and Turturro.³ They measured the quantity

$$\left(\frac{d \ln P_i}{dT}\right)_v$$

$$\begin{aligned} \frac{1}{P_i} \left(\frac{dP_i}{dT}\right) &= \frac{\left(\frac{V - V_0}{BR} + \frac{2\beta_0}{\alpha}\right)^{-2} \left[\frac{V - V_0}{BR} + \frac{2\beta_0}{\alpha} + \frac{2\beta_0 T}{\alpha^2} \left(\frac{d\alpha}{dT}\right)_v\right] - \left(\frac{dP}{dT}\right)_v}{T \left(\frac{V - V_0}{BR} + \frac{2\beta_0}{\alpha}\right)^{-1} - P} \\ &= \frac{1}{T} \left(\frac{\alpha}{\beta_T}\right) \left[\frac{\beta_T}{\alpha} + \frac{2\beta_0 T}{\alpha^2} \left(\frac{d\alpha}{dT}\right)_v\right] - \left(\frac{dP}{dT}\right)_v / \left(\frac{T\alpha}{\beta_T} - P\right) \end{aligned} \quad (\text{A})$$

where P_i , the internal pressure, is given by the usual equation

$$P_i = \left(\frac{dU}{dV}\right)_T = T \left(\frac{dP}{dT}\right)_v - P$$

Bianchi carried out direct measurements of $(dP/dT)_v$ on several liquids over a temperature range of 20–60° and as a result values of $(d \ln P_i/dT)_v$ were obtained to an accuracy estimated at $\pm 10\%$.

In his discussion of this quantity, Bianchi² starts from the concept that the intermolecular energy U can be represented by a term of the type a/V^n , *i.e.*, that it is dependent on volume only. From this he concludes that $(d \ln P_i/dT)_v$ should be zero. To a certain extent their results confirm this conclusion in that the value of $(d \ln P_i/dT)_v$ is very small, but the experiments also show that it is actually negative and quite measurable.

We shall now consider this result in relation to the van der Waals equation as applied to liquids. Starting from the conventional van der Waals equation

$$\left(P + \frac{a}{V^2}\right)(V - V_0) = RT$$

we first substitute P_i for a/V^2 and secondly introduce a

constant B in front of P to correspond with the fact that more than three degrees of freedom interact with volume in a typical liquid. The equation then becomes

$$\frac{\beta_T}{\alpha} = \frac{V - V_0}{BR}$$

This equation is then further modified for use at low volumes and high pressure by introducing the concept of a "molecular compressibility" β_0 . When this is done we obtain, as explained in ref 1, the approximate relation

$$\frac{\beta_T}{\alpha} = \frac{(V - V_0)}{BR} + \frac{2\beta_0}{\alpha}$$

where α is the coefficient of thermal expansion, β_T is the coefficient of isothermal compressibility, V is the volume, V_0 is the assumed molar volume at 0°K, β_0 is the isothermal compressibility of the close-packed molecules at 0°K, B is a constant related to the external degree of freedom of the molecule, and R is the gas constant.

It can be shown (eq A) that putting $(dP/dT)_v = \alpha/\beta_T$, we obtain, when P is small compared with $T\alpha/\beta_T$

$$\left(\frac{d \ln P_i}{dT}\right)_v = \frac{2\beta_0}{\alpha\beta_T} \left(\frac{d\alpha}{dT}\right)_v \quad (\text{I})$$

This equation may then be tested by using available PVT data to provide α , β_T , and $(d\alpha/\alpha T)_v$ at low pressures and then calculating β_0 . These may then be compared with values obtained by other means.

Measurements for $(d \ln P_i/dT)_v$ for carbon tetrachloride and benzene were published by Bianchi, *et al.*,² and values for *n*-octane and acetone were provided by Turturro.³ In carrying through the calculation according to eq I, it is essential to use the values for α , β_T and $(d\alpha/dT)_v$ which relate to the average volumes used in the $(d \ln P_i/dT)_v$ measurements.

No great accuracy can be claimed for the quantity $(d\alpha/dT)_v$, but smooth curves of α against T (constant v) with a negative slope were obtained, and $(d\alpha/dT)_v$ was given by the slope at the relevant

(1) R. N. Haward, *Trans. Faraday Soc.*, **62**, 828 (1966).

(2) U. Bianchi, G. Agalio, and A. Turturro, *J. Phys. Chem.*, **69**, 4392 (1965).

(3) A. Turturro, private communications.

Table I: The Estimation of 0°K compressibility (β_0) from Eq I

Liquid	Temp, °C	$(d \ln P_i/dT)_v$, °K ⁻¹	$(d\alpha/dT)_v$, °K ⁻²	β_0 , cm ² /dyne (this paper)	β_0 , cm ² /dyne ^a (ref 1)	β_0 , cm ² /dyne (adiabatic) ^d (ref 4)
Benzene ^a	41	-0.52×10^{-3}	4.4×10^{-6}	9×10^{-12}		11.9×10^{-12}
<i>n</i> -Octane ^b	45	-0.93×10^{-3}	5.9×10^{-6}	8×10^{-12}	4.6×10^{-12}	
Carbon tetra- chloride ^c	38.4	-0.46×10^{-3}	7.5×10^{-6}	3.2×10^{-12}		14.9×10^{-12}
Acetone ^d	32.5	-0.36×10^{-3}	1.6×10^{-6}	15×10^{-12}	8.3×10^{-12}	12.7×10^{-12}

^a Data from R. E. Gibson and J. F. Kincaid, *J. Amer. Chem. Soc.*, **60**, 513 (1938). The Tait equation with their constants was used for interpolation where necessary. ^b Data of H. M. Eduljee, D. M. Newitt, and K. E. Weale, *J. Chem. Soc.*, 3086 (1951). Tait equation used as above. ^c Data from R. E. Gibson and O. H. Loeffler, *J. Amer. Chem. Soc.*, **63**, 898 (1941) (as above). ^d Data from International Critical Tables, Vol. III, interpolated by computed cubic equation. Difficulty was found in fitting these results either to a Tait or Huggles equation.

temperature. The results obtained are given in Table I.

The results obtained here may be conveniently compared with those given in ref 1 and by Kudryavtsev and Samgina,⁴ whose modulus is, however, adiabatic and not isothermal. In view of the several approximations and of the rather crude model used, the agreement between the results seems reasonable. Differences from the results of Kudryavtsev cannot be due to their use of an adiabatic measurement since they generally obtained higher values of β_0 . In the case of acetone and octane the lower value given by the van der Waals equation¹ is probably due to use of high pressure (5000–7000 atm) at the point where the equation is applied to determine β_0 . (This is calculated from the intercept where $V = V_0$.) Bridgman's measurements at very high pressures (10,000–40,000 atm)⁵ certainly indicate that β_0 must be nonlinear with pressure over a wide range.

Recently, studies of the effect of pressure on viscosity have also led to proposals that the molar volume at 0°K has a finite compressibility.^{6,7} Hogenboom, *et al.*,⁷ have proposed that V_0 for an *n*-C(15) alkane should be assigned a compressibility equivalent to that of the solid near the melting point, *i.e.*, $\beta_0 25 \times 10^{12}$. This value is higher than any proposed here, but the compressibility of the solid may well be above that of the smaller molar volume at 0°K since it does contain some free space. Nevertheless, the higher figure agrees with the requirements of the viscosity theories.

However, the fact that a value of β_0 of the right order can be obtained by this method does suggest that the approach used may have some validity. Physically speaking, it appears that U is not a specific function of V . As the temperature rises at constant volume, so does the total pressure on the molecules. In this way the occupied volume is reduced and some elastic energy is stored.

Acknowledgment. The authors wish to thank Dr. A. Turturro of the Institute di Chimica Industriale,

Universita, Genova, Italy, for his assistance in carrying out this work.

- (4) B. B. Kudryavtsev and G. A. Samgina, *Russ. J. Phys. Chem.*, **39**, 476 (1965).
 (5) P. W. Bridgman, *Proc. Am. Acad. Arts Sci.*, **76**, 72 (1948).
 (6) A. J. Matheson, *J. Chem. Phys.*, **44**, 695 (1966).
 (7) D. L. Hogenboom, W. Webb, and A. J. Dixon, *ibid.*, **46**, 2586 (1967).

DEPARTMENT OF POLYMER AND FIBRE SCIENCE R. N. HAWARD
 THE UNIVERSITY OF MANCHESTER INSTITUTE B. M. PARKER
 OF SCIENCE AND TECHNOLOGY
 MANCHESTER 1, ENGLAND

RECEIVED FEBRUARY 7, 1968

Comment on "Quantum Theoretical Treatment of Equilibrium Chemical Rate Processes"

Sir: In a recent Note under the above title, Yao and Zwolinski¹ proposed a modified formulation of transition state theory in which the usual kT/h term in the expression for the rate constant is replaced by $\bar{\nu} e^{-h\nu/2kT} / (1 - e^{-h\nu/kT})$, equivalent to multiplying it by the factor $(h\bar{\nu}/2kT) / \sinh(h\nu/2kT)$, in which $\bar{\nu}$ is the frequency of passage across the barrier and ν is the absolute magnitude of the imaginary frequency $i\nu$ of a harmonic oscillator corresponding to an inverted parabolic potential along the reaction path. Their approach is similar in some respects to that used by us² in which the kT/h term is multiplied by the factor $(h\nu/2kT) / \sinh(h\nu/2kT)$.

In both cases the correction factor derives from the extraction from the statistical mechanical expression for the equilibrium constant of a partition function Q_s^{\ddagger} corresponding to motion in the reaction coordinate. However, whereas our expression² gives the

- (1) S. J. Yao and B. J. Zwolinski, *J. Phys. Chem.*, **72**, 373 (1968).
 (2) D. J. Le Roy, B. A. Ridley, and K. A. Quickert, Faraday Society Discussion on the Molecular Dynamics of the Chemical Reactions of Gases, Toronto, 1967.

Wigner³ correction $[1 + \frac{1}{24}(h\nu/kT)^2]$ for small values of ν , the expression derived by Yao and Zwolinski¹ takes the form $[1 - \frac{1}{24}(h\nu/kT)^2]$, corresponding to "tunneling factors" less than unity.

The error in their treatment originates in the formulation of the Hamiltonian. They set the potential energy equal to zero at the origin and assume that the kinetic energy, as well as the potential energy, is therefore negative. They then write the Hamiltonian in the form

$$H^\pm = -p^2/2\mu^\pm - fq^2/2 \quad (1)$$

where $f = -f^\pm > 0$.

Now if H is the Hamiltonian for a regular harmonic oscillator, then

$$\hat{H}\psi = E\psi \quad (2)$$

and the eigenvalues are given by $(n + \frac{1}{2})h\nu$. However, if we multiply (2) on both sides by -1 to give

$$-\hat{H}\psi = -E\psi = \hat{H}^\pm\psi \quad (3)$$

we have not thereby formulated the Schroedinger equation for the entirely different problem of a particle subject to a negative force constant. Yao and Zwolinski's conclusion that the eigenvalues for the case of the inverted parabola are given by $E^\pm = -(n + \frac{1}{2})h\nu$, and their subsequent deductions from this, are therefore untenable.

Actually, the correct Schroedinger equation for an inverted parabolic potential is

$$\frac{d^2\psi}{dq^2} + \frac{8\pi^2\mu^\pm}{h^2}(E + 2\pi^2\mu^\pm\nu^2q^2)\psi = 0 \quad (4)$$

where $\nu = 1/2\pi(f/\mu^\pm)^{1/2}$. This equation can be solved if we define a new variable $\nu^* = i\nu$ whereby (4) becomes

$$\frac{d^2\psi}{dq^2} + \frac{8\pi^2\mu^\pm}{h^2}(E - 2\pi^2\mu^\pm\nu^{*2}q^2)\psi = 0$$

with complex energy eigenvalues $E^* = (n + \frac{1}{2})h\nu i$, belonging to the Normal operator \hat{H}^* which is not Hermitian.

(3) E. P. Wigner, *Z. Physik. Chem.*, **19B**, 203 (1932).

LASH MILLER CHEMICAL LABORATORIES
UNIVERSITY OF TORONTO
TORONTO, ONTARIO, CANADA

B. A. RIDLEY
K. A. QUICKERT
D. J. LE ROY

RECEIVED FEBRUARY 9, 1968

Reply to "Comment on 'Quantum Theoretical Treatment of Equilibrium Chemical Rate Processes'"

Sir: From at least two points of view, namely, rate processes in condensed systems and reactions of radicals in the gas phase, the nature and magnitude of the "temperature-independent factor" is still in an un-

satisfactory state. In a recent Note,¹ the authors assumed that the unusual degree of freedom along the reaction coordinate is assumed to be a *stationary* harmonic vibration oscillation in an *inverted parabolic potential*. Ridley, Quickert, and Le Roy² took exception to our treatment.

For a bounded or stationary oscillation, the Virial Theorem requires that the kinetic energy and the potential energy must be of the same sign for *this inverted parabolic potential*. Since the potential energy for an inverted parabolic potential is negative, the kinetic energy as well as the total energy of this inverted H. O. must be negative. The solution for the *energy-reversed* H. O. becomes straightforward and the eigenvalues are found to be $E_n^\pm = -(n + \frac{1}{2})h\nu$, where ν is real. This energy-reversed oscillator is physically realizable since it satisfies the Schroedinger equation.

From the potential energy surface point of view and rate theory, we admit that we have erroneously introduced the negative energy oscillator into this treatment; however, our final expression eq 15, ref 1, although improperly derived, has certain desirable features in situations where, $\bar{\nu} \neq \nu \neq i\nu^\pm$.

(1) S. J. Yao and B. J. Zwolinski, *J. Phys. Chem.*, **72**, 373 (1968).

(2) B. A. Ridley, K. A. Quickert, and D. J. Le Roy, *ibid.*, **72**, 1844 (1968).

THERMODYNAMICS RESEARCH CENTER
TEXAS A&M UNIVERSITY
COLLEGE STATION, TEXAS

S. J. YAO
B. J. ZWOLINSKI

RECEIVED MARCH 22, 1968

The Primary Isotope Effect for the Replacement of H vs. D by Energetic Tritium Atoms

Sir: Variations in reaction yields from isotopic molecules, involving several kinds of isotope effects, have been observed for many energetic tritium atom reactions.¹⁻⁵ Direct measurement of the primary isotope effect for the replacement of H or D by energetic T, as in (1),⁶ has not been reported, since all

(1) H. C. Jurgeleit and R. Wolfgang, *J. Amer. Chem. Soc.*, **85**, 1057 (1963).

(2) E. K. C. Lee and F. S. Rowland, *ibid.*, **85**, 2907 (1963).

(3) R. Wolfgang, *Progr. Reaction Kinetics*, **3**, 97 (1965).

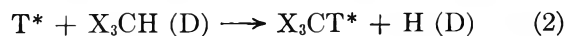
(4) E. K. C. Lee, G. Miller, and F. S. Rowland, *J. Amer. Chem. Soc.*, **87**, 190 (1965).

(5) E. K. C. Lee, J. W. Root, and F. S. Rowland, "Chemical Effects of Nuclear Transformations," Vol. 1, International Atomic Energy Agency, Vienna, 1965, p 5.

(6) Possible primary isotope effects involving the substitution of H*, D*, and T*, which we shall designate as primary *substitution* isotope effects, have not yet been measured for energetic hydrogen atom species. Energetic H* or D* from nuclear recoil are some factors of 10 beyond present levels of detection. Comparisons should be feasible for photochemical sources but have not yet been made: R. M. Martin and J. E. Willard [*J. Chem. Phys.*, **40**, 3007 (1964)] have given total yields for D* + CH₄ and H* + CD₄, representing a summation of primary substitution, primary replacement, and secondary substitution isotope effects.



previous experiments have also involved simultaneous isotopic variation in R. Thus, the substitution of T-for-H *vs.* T-for-D in CH₄-CD₄ mixtures involves possible secondary isotope effects from bond formation with CH₃ *vs.* CD₃ in addition to the primary replacement of H *vs.* D;⁵ the existence of an appreciably higher yield of CH₃T from CH₃F than of CD₃T from CD₃F (1.21 ± 0.04) illustrates that secondary isotope effects upon energetic substitution reactions can be quite substantial.⁴ We have now performed a direct measurement of the primary replacement isotope effect for H *vs.* D through measurements with CHX₃ and CDX₃ as in (2), in which the X groups are iden-



tical, and the only isotopic variant is the H *vs.* D in the tertiary position. The chief experimental problem, that of normalization of the tritium flux for comparison of two molecules, is readily solved through the measurement of T* reactions with X as an intramolecular monitor for the energetic tritium atom flux.

Our experiments have involved recoil tritium irradiation of various isotopic isobutanes, isolation of the tritium-labeled isobutane from other radioactive products, and then measurement of the fraction of the tritium in the tertiary position in each molecule. Comparisons of the relative yields in tertiary *vs.* primary positions for (CH₃)₃CH *vs.* (CH₃)₃CD and for (CD₃)₃CH *vs.* (CD₃)₃CD furnish two separate estimates of the primary replacement isotope effect. The measurements have been carried out for irradiations in both gas and liquid phases, with the results shown in Table I. While the data show a marked phase effect in all samples, all measurements show a consistent primary replacement isotope effect of ~1.25.

The original specific activity of isobutane-*t* was calculated from the consecutive measurement of the radioactivity and thermal conductivity response of

the isobutane peak from a radio gas chromatograph.⁷ The tertiary-T was similarly measured after complete exchange of primary-T by washing the isobutane with sulfuric acid.^{8,9} Separate tests established that tertiary-T exchange was negligible under conditions permitting complete exchange (>99.9%) of the primary-T in isobutane.¹⁰⁻¹²

The smaller mass of the H atom furnishes less inertial resistance to the oncoming energetic T atom than does the D atom, and the H atom can be set into more rapid motion in the initial stages of collision. (A free H atom struck by an energetic tritium atom would recoil with 25% greater velocity and 22% less kinetic energy than for the corresponding collision of free D with an energetic T atom.) While the final energy and velocity of an atom freed in a substitution reaction will depend upon the detailed interactions during the entire reaction,¹³ the primary replacement isotope effect probably reflects chiefly the initial ease of displacement of the H and D atoms. Our measurements are most valid for correlation with hydrogen replacement isotope effects for other systems with three heavy substituents on the central carbon atom, and may not apply directly to molecules such as methane for which rapid relaxation of additional substituents may be intimately involved in the detailed reaction. The overall substitution isotope effect in CH₄ *vs.* CD₄ (1.33 ± 0.04)⁵ presumably includes an additional contribution from the relatively greater rate of relaxation of CH₃ than for CD₃.⁵

The comparison of the relative activities of the tertiary and primary positions of isobutane has been used earlier as a test of the possible steric effect of methyl substituents upon the substitution reaction.^{9,11,14} The phase differences observed in our experiments make it difficult to estimate the magnitude of such substituent effects without a precise explanation of the origin of the phase differences themselves. Alternate postulates, without clear preference, can be suggested as: (a) the gas-phase results represent a

Table I: Primary Replacement Isotope Effect for Recoil Tritium Reactions with Isotopic Isobutanes

Compound	Gas phase ^a		Liquid phase ^b	
	R ^c	Isotope effect ^d	R	Isotope effect
(CH ₃) ₃ CH	0.87	1.26 ± 0.04	0.75	1.23 ± 0.06
(CH ₃) ₃ CD	0.69		0.61	
(CD ₃) ₃ CH	1.20	1.25 ± 0.04	0.99	1.27 ± 0.06
(CD ₃) ₃ CD	0.97, 0.95		0.78	

^a Sample contents: 2 cm of ³He, 6 cm of O₂, 70 cm of isobutane.

^b Sample contents: LiF, 10 mole % butadiene, isobutane.

^c R = (tritium activity per tertiary C-H or C-D bond)/(tritium activity per primary C-H or C-D bond); estimated error: ±2% (gas), ±3% (liquid). ^d Isotope effect = R_{tert. H}/R_{tert. D} for molecules with the same isotopic content in the primary position.

(7) J. K. Lee, E. K. C. Lee, B. Musgrave, Y.-N. Tang, J. W. Root, and F. S. Rowland, *Anal. Chem.*, **34**, 741 (1962).

(8) J. W. Otvos, D. P. Stevenson, C. D. Wagner, and O. Beeck, *J. Amer. Chem. Soc.*, **73**, 5741 (1951).

(9) A. Odell, A. Rosenberg, R. Fink, and R. Wolfgang, *J. Chem. Phys.*, **40**, 3730 (1964).

(10) Only small variations were found in the exchange rates for different isotopic isobutanes, and these caused no difficulties in the exchange of primary-T without appreciable loss of tertiary-T.

(11) A. Rosenberg, Ph.D. Thesis, Yale University, 1964.

(12) Attempts to use these techniques for study of the intramolecular distribution of tritium in isobutane-*t* from the reactions of 2.8 eV T* + (CH₃)₃CH have been unsuccessful so far because of a rapid bromine-photocatalyzed exchange of TBr with the tertiary position of isobutane.

(13) The energy deposition following T-for-H in *c*-C₄H₈ is essentially the same as that following T-for-D in *c*-C₄D₈. (Unpublished experiments by A. Hosaka and F. S. Rowland.)

(14) The value for tertiary/primary in *i*-C₄H₁₀ of 0.79 ± 0.04 (gas phase) reported in ref 9 is in semiquantitative agreement with the corresponding value of 0.87 ± 0.02 in Table I, although outside the limits of error of each.

perturbation of the more-correct liquid-phase results by isotope effects in rates of secondary decomposition reactions; or (b) the liquid phase results indicate a condensed phase limitation upon the motions necessary for completion of some substitution reactions in the tertiary position. In any event, the primary replacement isotope effect is independent of phase, and thereby of the choice between these alternate mechanisms.

(15) This research has been supported by AEC Contract No. AT-(11-1)-34, Agreement No. 126.

DEPARTMENT OF CHEMISTRY¹⁵
UNIVERSITY OF CALIFORNIA
IRVINE, CALIFORNIA 92664

THOMAS SMAIL
F. S. ROWLAND

RECEIVED FEBRUARY 20, 1968

Bidimensional Condensation in Adsorbed Layers

Sir: In a paper to appear,¹ we have derived formulas expressing the logarithm of the ratio of the vapor pressure of the adsorbate $P^{(\infty)}$ to the transition pressure in an adsorbed film $P^{(n)}$ and its first derivative as a function of the inverse absolute temperature. In the case

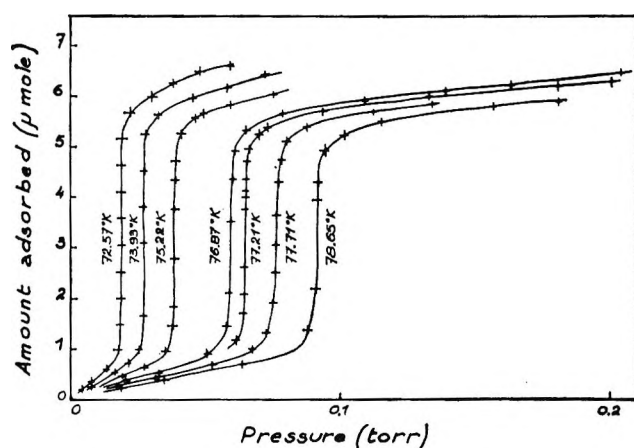


Figure 1. Adsorption isotherms of krypton on nickel chloride.

of a bidimensional condensation in the n th layer, we write

$$\log \frac{P^{(\infty)}}{P^{(n)}} = \frac{u^{(\infty)} - u^{(n)}}{RT} - \frac{1}{R}(s^{(\infty)} - s^{(n)}) \quad (1)$$

and

$$d\left(\log \frac{P^{(\infty)}}{P^{(n)}}\right) / d\left(\frac{1}{T}\right) = \frac{u^{(\infty)} - u^{(n)}}{R} \quad (2)$$

With an appropriate thermodynamic definition of the adsorbed layer, $u^{(n)}$ and $s^{(n)}$ constitute approximate values of the molar energy and entropy of the outer condensed layer; $u^{(\infty)}$ and $s^{(\infty)}$ represent the same quantities relative to the outer layer of the solid adsorbate.

Formula 1 differs from that of Singleton and Halsey^{2,3} by the addition of the entropic term $-1/R(s^{(\infty)} - s^{(n)})$. In this preliminary report on our experimental work, we wish to show the importance of this term.

We have studied the adsorption of krypton and xenon on a certain number of halides having a layer-like structure, namely NiCl_2 , CoCl_2 , FeCl_2 , CdCl_2 , CdBr_2 , CdI_2 , and PbI_2 . The results reported here concern only the condensation of the first layer of krypton on the basal face of these substrates: typical isotherms for nickel chloride are plotted in Figure 1. The coefficients of the regression lines (eq 1) are determined by least-squares analysis. Thus the ratio $P^{(\infty)}/P^{(1)}$ can be split into its energetic and entropic contributions. The results thus obtained are given in Table I, which also contains the crystallographic parameter a of the hexagonal or pseudo-hexagonal lattices of the adsorbents and, for comparison, the diameter of the krypton atom (distance between two krypton atoms in the (111) plane of the fcc solid krypton).

From these data two conclusions can be drawn. First, the entropic term of formula 1 may be as im-

- (1) Y. Larher, *J. Chim. Phys.*, in press.
- (2) J. H. Singleton and G. D. Halsey, *Can. J. Chem.*, **33**, 184 (1955).
- (3) L. J. Slutsky and G. D. Halsey in "Physical Chemistry, An Advanced Treatise," E. H. Eyring, D. Anderson, and W. Jost, Ed., Academic Press, New York, N. Y., 1966.

Table I: Respective Contributions of Energy and Entropy to the Ratio $P^{(\infty)}/P^{(1)}$ of the Vapor Pressure of the Adsorbate to the Condensation Pressure of the First Layer of Krypton on Different Adsorbents

Adsorbent	Temp, °K	$\frac{P^{(\infty)}}{P^{(1)}}$	Energetic contribution to $P^{(\infty)}/P^{(1)}$	Entropic contribution to $P^{(\infty)}/P^{(1)}$	a of the adsorbent, Å	Diameter of the krypton atom, Å
NiCl_2	75.69	26.9	5.13	5.25	3.543	
CoCl_2	75.34	22.4	4.78	4.68	3.544	
FeCl_2	75.13	19.4	4.85	4.00	3.579	
CdCl_2	82.52	21.3	9.20	2.32	3.854	4.07
CdBr_2	88.44	35.7	26.9	1.325	3.95	
CdI_2	88.35	53.1	41.8	1.27	4.24	
PbI_2	88.52	38.2	12.45	3.07	4.555	

portant as the energetic one: it is certainly not to be neglected *a priori*. Secondly, there is clearly a correlation between the quantities ($u^{(1)} - u^{(\infty)}$) and ($s^{(1)} - s^{(\infty)}$) on the one hand, the compatibility of the lattices of the adsorbent and adsorbate on the other (of course energies are comparable only for adsorbents with the same anion). A high compatibility of the lattices favors a high value of the energy difference ($u^{(\infty)} - u^{(1)}$) and a low value of the entropy difference ($s^{(1)} - s^{(\infty)}$). Such results are quantitatively satisfying and can be used for a deeper understanding of the molecular structure of the adsorbed phase.

In the cases studied here, there is a rough cancelling

of the effects of the energetic and entropic terms on the ratio $P^{(\infty)}/P^{(1)}$, so that the application of the Singleton-Halsey formula would have hidden the structural information contained in the experimental results. We conclude that a cautious attitude toward approximate molecular theories of adsorption, particularly those underestimating the role of entropy, is at least sometimes worthwhile.

SERVICE DE CHIMIE PHYSIQUE
C.E.N. SACLAY
GIF S/YVETTE, FRANCE

Y. LARHER

ACCEPTED AND TRANSMITTED BY THE FARADAY SOCIETY

(NOVEMBER 28, 1967)